

Proceedings of the Tenth International Conference on Permafrost

Salekhard, Yamal-Nenets Autonomous District, Russia
June 25–29, 2012

**TENTH
INTERNATIONAL
CONFERENCE
ON PERMAFROST**



**VOLUME 2:
TRANSLATIONS
OF RUSSIAN
CONTRIBUTIONS**

Edited by Academician Vladimir P. Melnikov
and Co-Editors Dmitry S. Drozdov and Vladimir E. Romanovsky

Salekhard
2012

Organizers



General-partner



Partners



Tenth International Conference on Permafrost

Proceedings of the Tenth International Conference on Permafrost
Salekhard, Yamal-Nenets Autonomous District, Russia
June 25–29, 2012

**Tenth International
Conference on Permafrost**

Volume 2: Translations of Russian Contributions

**Edited by Academician Vladimir P. Melnikov
and Co-Editors Dmitry S. Drozdov and Vladimir E. Romanovsky**

**The Northern Publisher
Salekhard
2012**

Tenth International Conference on Permafrost
Volume 2: Translations of Russian Contributions
Edited by Academician Vladimir P. Melnikov
and Co-Editors Dmitry S. Drozdov and Vladimir E. Romanovsky

© 2012

The State Enterprise of the Yamal-Nenets Autonomous District
The Northern Publisher (Severnoye Izdatelstvo)
All rights reserved.

Printed in Russia

Elmer E. Rasmuson Library Cataloging in Publication Data

International Conference on Permafrost (10th : 2012 :
Salekhard, Yamal-Nenets Autonomous District, Russia)

Tenth International Conference on Permafrost :

Resources and Risks of Permafrost Areas in a Changing World /

edited by Kenneth M. Hinkel [v.1], Vladimir P. Melnikov [v.2, 3].

Salekhard, Russia: The Northern Publisher; Tyumen, Russia: Pechatnik; Ekaterinburg,

Russia: Fort Dialog-Iset, 2012, 5 v. : ill., maps, cm.

Includes bibliographical references and index.

June 25-29,2012.

Contents: vol.1. International contributions - vol.2. Translations of Russian contribution - vol.3. Russian contribution -
vol.4. Extended Abstracts - vol.5. Extended Abstracts in Russian.

1. Permafrost-Congresses. 2. Frozen ground-Congresses.

I. Title. II. Hinkel, Kenneth M. III. Melnikov, Vladimir P.

Cover Design: The Northern Publisher

GB641.I6.2012

УДК 551.34; 502.3; 624.139

ББК 26.3

Д 37

ISBN 978-5-905911-01-9 (v.1)

ISBN 978-5-905911-02-6 (v.2)

ISBN 978-5-9961-0510-6 (v.3,5)

ISBN 978-5-91128-050-5 (v.4/1)

ISBN 978-5-91128-052-9 (v.4/2)

Production Editor: Thomas Alton (Fairbanks, Alaska)

Melnikov, P.I. (ed.). 2012. *Tenth International Conference on Permafrost. Vol. 2: Translations of Russian Contributions*. Co-edited by D.S. Drozdov and V.E. Romanovsky. The Northern Publisher, Salekhard, Russia, 569 pp.

Contents

Welcoming Remarks	xi
Preface	xii
Acknowledgments	xii
Russian Associate Editors and Reviewers	xiii
North American Readers	xiv
Permafrost Conditions in the Polar Regions of Mars	1
O.N. Abramenko, V.S. Isaev, Ix.A. Komarov	
Changes in Geocryological Conditions along the Reconstructed Salekhard-Nadym Railway	7
N.S. Aleksandrova	
Cryogenic Deformations in the Late Cenozoic Deposits of the Tunka Depression in the Baikal Rift Zone	13
S.V. Alekseev, L.P. Alekseeva, A.M. Kononov	
Mercury Content from the Tunguska Meteorite Craters and in Some Siberian Towns	19
V.A. Alekseev, N.G. Alekseeva, L.N. Luchsheva, V.V. Kopeykin, L.G. Pelehan, V.A. Rukavishnikov, V.A. Chechin, V.V. Krivulin	
Cryogenic Strata of Gas-Bearing Structures of Northern Western Siberia: Look to the Future	25
Yu.B. Badu	
Cryogenic Processes along Linear Structures	31
N.P. Bosikov	
Biological Properties of Bacteria Isolated from Permafrost in Central Yakutia	35
A.V. Brouchkov, A.M. Peterson, E.V. Glinska, G.I. Griva, V.E. Repin	
$\delta^{18}\text{O}$ Variations in Late Holocene Ice-Wedges and Winter Air Temperature Variability in the Yamal Peninsula, Russia, and in Adventdalen, Svalbard	41
N.A. Budantseva, A.K. Vasilchuk, A.M. Zemsikova, Yu.N. Chizhova, Yu.K. Vasilchuk, H.H. Christiansen	
Mathematical Simulation of Ground Freezing with the Visualization of Cryogenic Structure under Formation	47
V.G. Cheverev, E.V. Safronov	
Radiocarbon Chronology and Dynamics of Palsas in the Russian European North	51
Ju.N. Chizhova, A.C. Vasil'chuk, N.A. Budantseva, Yu.K. Vasil'chuk	
Temperature Dependence of the Equilibrium Pore Water Content in Gas Hydrate Contained Sediments	57
E.M. Chuvilin, V.A. Istomin	
Construction in the Cryolithozone Using Innovative Systems of Foundation Soil Thermal Stabilization	61
G.M. Dolgikh, S.N. Okunev, S.N. Strizhkov	
Permafrost Monitoring of Southern Tundra Landscapes in the Russian European North and West Siberia	65
D.S. Drozdov, G.V. Malkova, N.G. Ukraintseva, Yu.V. Korostelev	
Specific Features of Cryogenic Soil Formation in Western Yakutia	71
A.G. Dyagileva	
Contribution of Thawing Permafrost and Ground Ice to the Water Balance of Young Thermokarst Lakes in Central Yakutia	75
A.N. Fedorov, P.P. Gavriliev, P.Ya. Konstantinov, T. Hiyama, Y. Iijima, G. Iwahana	
Rock Glaciers and Permafrost Gravitational Formations of the Kolyma Upland	81
A.A. Galanin	
The Method of a Short Cylindrical Probe in Thermophysical Studies of the Bases of Dams Belonging to Northern Hydroelectric Complexes	87
R.I. Gavriliev	
Environmental Hazards of the Coastal Plains on Northern Yakutia	93
A.V. Gavrilov, E.I. Pizhankova, A.Yu. Derevyagin, A.B. Chizhov	
Main Features of Urban Pedogenesis in Permafrost Areas (Case of Yakutsk City)	97
A.Yu. Germogenova	
Critical Coefficients of Stress Intensity of Frozen Soils with Natural Structure	103
S.G. Gevorkyan	

Interaction between Pile and Freezing of Frost-Susceptible Soil with Time (Taking into Account Phase Change).....	107
P.A. Gorbachev	
Physical and Mechanical Processes in Cryogenic Formations Associated with Temperature Change	111
J.B. Gorelik	
The Change of Geotechnical–Geocryological Parameters of Permafrost Foundations in the Western Sector of Russia’s Cryolithozone by 2050	117
V.I. Grebenets, A.V. Kislov, D.G. Shmelev	
The Study of Exogenic Permafrost-Related Geological Processes along the Yuzhno-Russkoe-Beregovoe Road.....	123
A.A. Gubarkov, M.V. Andreeva, E.M. Elantsev, A.V. Khomutov	
Coding of Ground Type during Geotechnical Site Investigations in Permafrost Regions.....	129
A.V. Iospa, A.A. Popova, V.I. Aksenov, G.I. Klinova	
Main Types and Causes of Deformations on Railways and Roads in the Norilsk Industrial District	133
V. Isakov	
Glacial Topography of the Northwestern Part of the Putorana Plateau	137
E.N. Ivanova-Efimova	
Implementation of Mathematical Landscape Morphology Methods for Estimating Risk of Damage to Linear Engineering Structures due to Thermokarst Processes	141
V.N. Kapralova, A.S. Viktorov	
The Transition Layer in Permafrost-Affected Soils, Northeast European Russia.....	145
D. Kaverin, G. Mazhitova, A. Pastukhov, F. Rivkin	
Ice Volume Estimates in the Bolshezemelskiy Artesian Basin Permafrost.....	149
V.Z. Khilimonyuk, E.N. Ospennikov, S.N. Buldovich, E.I. Gorshkov	
Environmental and Geological Problems of Subarctic Territories and Possible Solutions	153
V.Z. Khilimonyuk, A.V. Broushkov, S.I. Grebenkin	
Assessment of Landslide Geohazards in Typical Tundra of Central Yamal	157
A.V. Khomutov	
Heat and Mass Transfer in Water-Saturated Ceramics with Macro Inclusions of Ice.....	163
V.S. Kolunin, A.V. Kolunin, A.D. Pisarev	
Method for Estimating Properties of Cryopegs from the Yamal Peninsula	169
I.A. Komarov, N.V. Kiyashko	
Cryogenic Risks and Railroad Resources in Permafrost Regions.....	175
V.G. Kondratyev	
Experimental Study of Isotope Composition of Bound Water	181
V.N. Konishchev, V.V. Rogov, V.N. Golubev, S.A. Sokratov	
The Use of Sites with a Dense Network of Thaw Tubes to Monitor the Thickness of the Seasonally Thawed Layer in Central Yakutia	185
P.Ya. Konstantinov, A.N. Fedorov, I.S. Ugarov, R.N. Argunov, Y. Iijima	
Evaluation of the Ground Ice Content Based on Data from the NOAA Satellite: The Case of the Western Coast of the Yamal Peninsula, Russia.....	189
S.G. Kornienko	
Phytomass Reserves and Characteristics within the Active Layer of the Forest-Tundra Bog Ecosystem	195
N.P. Kosykh	
Impact of Thawing on Ground Deformation	199
P.I. Kotov	
Ground Ice in the Cryolithozone, Yamal Peninsula.....	205
L.N. Kritsuk	
Problematic Aspects of the Study and Exploration of the Arctic Cryolithozone	211
V.S. Krupoderov, V.A. Dubrovin	
Geotechnical Solutions for Slope Stabilization Along the Amur Highway Characterized by Permafrost Degradation of Road Embankments	215
S.A. Kudryavtsev, T.Yu. Valtseva, R.G. Michailin, Yu.B. Berestyani	
Providing the Optimal Temperature for Underground Plant Seed Storage in Permafrost.....	221
G.P. Kuzmin, V.N. Panin	

Impact of Mineral Composition on Heat-Conducting Properties of Frozen Volcanic Ashes from Kamchatka	225
E.P. Kuznetsova, R.G. Motenko	
Modeling of Active Layer and Runoff: A Case Study from Small Watersheds, Kolyma Water Balance Station.....	231
L. Lebedeva, O. Semenova	
Gradient of Seasonal Thaw Depth along the Yamal Transect	237
M.O. Leibman, A.V. Khomutov, P.T. Orekhov, O.V. Khitun, H. Epstein, G. Frost, D.A. Walker	
Deposits of Gas Hydrates as a Potential Source of Mercury on the Continental Slope and Shelf in Northeast Sakhalin.....	243
L.N. Luchsheva, A.I. Obzhairov, A.S. Astakhov	
GIS-based Assessment of Contemporary Climate and Permafrost Changes in Northern Russia.....	247
G.V. Malkova, A.V. Pavlov	
The Dynamics of Seasonal Soil Freezing in Central Russia.....	253
A. Maslakov, V. Grebenets, D. Ablyazina, D. Shmelev, A. Radosteva, V. Pastukhov, V. Antonov, A. Bykovskiy, G. Gavrilov, A. Gorbatyuk, D. Mandzhiev, P. Melnik, A. Saveleva, A. Smirnov, G. Khmelnitskiy, A. Shpuntova, G. Kraev, D.A. Streletskiy	
The Salinity of Cryogenic Quaternary Deposits in the Yenisey North.....	259
A.G. Matyukhin, I.D. Streletskaya	
Stability and Growth of Gas Hydrates at Pressures below Ice-Hydrate-Gas Equilibrium	263
V.P. Melnikov, A.N. Nesterov, A.M. Reshetnikov, V.A. Istomin	
A Technological Approach to Minimize Problems of Thermal Erosion During Development of Yamal Gas-Condensate Deposits	267
S.P. Mesyats, N.N. Melnikov	
Impact of Oil Pollution on the Depth and Cryogenic Structure of the Seasonally Frozen Layer at Samotlor Field, West Siberia.....	271
E.S. Miklyayeva, V.A. Soldatov	
Design of Reliable Bases and Foundations in Permafrost Regions	275
M.A. Minkin, O.A. Potapova	
Impact of Permafrost Degradation on Northern Taiga Ecosystems in Western Siberia.....	281
N.G. Moskalenko	
Long-Term Temperature Regime of the Northeast European Permafrost Region During Contemporary Climate Warming	287
N.G. Oberman	
Quaternary Deposits and Geocryological Conditions of Gydan Bay Coast of the Kara Sea	293
G.E. Oblogov, I.D. Streletskaya, A.A. Vasiliev, E.A. Gusev, H.A. Arslanov	
Thermal Monitoring of Ground Temperature Stabilization Systems	297
S.N. Okunev, G.M. Dolgikh, S.N. Strizhkov, N.A. Skorbilin	
Permafrost Structures and Deformations in Quaternary Sediments of West Yamal Peninsula	303
O.L. Opokina, E.A. Slagoda, A.I. Bazhenov	
Territorial Biospheric Resources of the Bolshezemelskaya Tundra Cryolithozone under Intensive Exploration of Hydrocarbon Deposits	309
G.G. Osadchaya, T.Yu. Zengina	
Thermophysical Properties of Moss Cover and its Influence on the Thermal Regime of the Ground, Spitsbergen Archipelago.....	313
N.I. Osokin, A.V. Sosnovskiy	
Separation of Mobile Forms of Chemical Elements during the Formation of Segregated Ice.....	317
V.E. Ostroumov	
Influence of “Landscape Position Marginality Degree” on the Intensity of Dangerous Processes	323
E. Panchenko	
Preventive Localization of Adverse Exogenous Geological Processes in the Cryolithozone.....	329
V.V. Pendin, T.P. Dubina, O.S. Ovsyannikova, S.D. Ganova	
Gas Shows in the Permafrost of the Bovanenkovo Gas-Bearing Structure	333
E.E. Podborny	
Effects of Solid Microparticles on Grinding of Ice	339
L.S. Podenko, N.S. Molokitina	

Climate Change, Frost Action, and Permafrost-Related Processes in the Northern Taiga Region of West Siberia.....	343
O.E. Ponomareva, A.G. Gravis, N.M. Berdnikov, T.A. Blyakharchuk	
Ice Energy as a Model of Activity of Exogenic Geological Processes	349
V.L. Poznanin	
Evaluation of Landscape Conditions for Environmental Management in the Discontinuous Permafrost Subzone (Bolshezemelskaya Tundra)	353
A.M. Rocheva	
Observations of Microorganisms in Segregated Ice Using Methods of Electron Microscopy	357
V.V. Rogov, A.N. Kurchatova	
Solution to a Series of Problems of Frozen Ground Mechanics Using Time-Analogy Methods	361
L.T. Roman	
Changes in the Areas of Thermokarst Lakes in the Territory of the Bovanenkovo Field (Yamal) over the Last 20 Years.....	367
G.S. Sannikov	
Estimate of Engineering Characteristics of Runoff under Conditions of Limited Data on Hydrometeorological Observations, Northeastern Russia.....	371
O.M. Semenova, L.S. Lebedeva, I.N. Beldiman	
Stressed-Deformed State of Trenchless Polyethylene Pipelines Installed at Negative Temperatures	377
A.A. Serebrennikov, I.G. Lavrov, D.A. Serebrennikov	
Identification, Diagnostics, and Ranking of Geocryological Hazards for Long-Distance Pipelines and Other Linear Structures.....	381
D.O. Sergeev, J.V. Khalilova, G.Z. Perlshtein, A.N. Khimenkov, E.M. Makaricheva, A.N. Ugarov	
Water in the Form of Spatially Ordered Droplets Near the Vapor-Water Boundary	385
A.V. Shavlov, V.A. Dzhumandzhi, S.N. Romanyuk	
Glaciation of Siberia as Viewed from the Position of Earth Cryology: Glaciers as a Component of the Cryolithozone	389
V.S. Sheynkman	
Composition of Water-Soluble Salts in Late Cenozoic Deposits, Northeast Yakutia.....	395
D.G. Shmelev	
Features of Pleistocene-Holocene Permafrost History of the Western and Eastern Sectors of the Russian Arctic and Subarctic	401
N.A. Shpolyanskaya	
Forecast of Air Temperature Change in Yakutia to the Middle of the Twenty-First Century.....	407
Yu.B. Skachkov, L.G. Neradovskiy	
The Impact of Development and Fire on the Thermal State of Permafrost, Central Yakutia	411
P.N. Skryabin, S.P. Varlamov	
Structure and Composition of Complex Massive Ice Bodies in Late Pleistocene-Holocene Sediments of the Marre-Sale Cape, West Yamal	415
E.A. Slagoda, O.L. Opokina, A.N. Kurchatova, V.V. Rogov	
Some Astronomical Problems of the Cryosphere Evolution	421
I.I. Smulskiy	
Proof of the Glacier Origin of Tabular Massive Ice.....	427
V.I. Solomatin, N.G. Belova	
The Ice Complex of Western Taymyr.....	433
I.D. Streletskaya, A.A. Vasilev	
Changes in Surface Area of Thermokarst Lakes on the Basis of Satellite Images	439
T.V. Tarasenko, V.I. Kravtsova	
Calculation of Frost Heave Tangential Stress with Regard to the Deformability of a Pile Shaft.....	445
Z.G. Ter-Martirosyan, P.A. Gorbachev	
Permafrost Conditions Associated with the Railroad Bridge Crossing of the Shchuchya River, Southern Yamal Peninsula.....	449
S.N. Titkov	

Permafrost and Landscapes of the Russian European North in the Twenty-First Century	453
N.V. Tumel	
The Possibilities of Industrial Development of Natural Resources on Permafrost-Affected Bog Landscapes and Peatlands of the Bolshezemelskaya Tundra	459
N.V. Tumel, G.G. Osadchaya	
Terrain Indicator Approach and Results for Permafrost Studies	463
N.G. Ukraintseva, D.S. Drozdov, Y.V. Korostelev, T.A. Korobova	
The Role of Cryogenic Head in the Formation of Repetitive Wedge Ice and Long-Term Frost Heave	469
A.A. Urban	
Large-Scale Mapping of Cryogenic Landscapes in the West Siberian Northern Taiga	475
E.V. Ustinova	
Thermal State of the Upper Horizons of the Permafrost in Central Yakutia	481
S.P. Varlamov, Yu.B. Skachkov, P.N. Skryabin, N.I. Shender	
Pollen and Spores as Indicators of the Origin of Massive Ice	487
A.C. Vasil'chuk, Yu.K. Vasil'chuk	
Classification of Tabular Massive Ice Bodies	493
Yu.K. Vasil'chuk	
Onshore and Offshore Permafrost in the Kara Sea	499
A.A. Vasiliev, P.V. Rekant	
Interannual Dynamics of Seasonal Thaw Depths of the Kenkeme-Lena Landscapes	503
I.S. Vasiliev	
Assessment of the Corrosiveness of Permafrost Landscapes	509
M.A. Velikotskiy, V.P. Marakhtanov	
Geocryological Programs for Specialist Training at Zabaikalsky State University	513
A.G. Verkhoturov	
Models of Mathematical Landscape Morphology in Cryolithozone Research	517
A.S. Viktorov, V.N. Kapralova, T.V. Orlov	
Composite Cast-in-Drilled Hole Piles in Frozen Soils, Magadan	523
V.P. Vlasov	
Interpretation of Natural Permafrost-Related Geomorphic Processes and Landforms in the Bovanenkovo Hydrocarbon Field on the West Coast of the Yamal Peninsula	527
A.A. Yermak, E.A. Slagoda, I.R. Idrisov	
Phytoindicators of Landslide Disturbances in the Central Yamal	531
K.A. Yermokhina, E.G. Myalo	
Changes in the State of Frozen Ground in the Course of Long-term Operation of the Yakutsk Combined Heat and Power (YCHP) Plant	537
S.I. Zabolotnik, P.S. Zabolotnik	
Evaluation of Critical Ecological Situations in the Tyumen Northern Cryolithozone under Economic Development	543
L.I. Zotova, S.Yu. Dedyusova	
Author Index	549
Subject Index Volume 1	551
Subject Index Volume 2	553

Welcoming Remarks

I am honored to welcome the participants to the Tenth International Conference on Permafrost—TICOP.

This conference marks a milestone for permafrost research in many ways. First, obviously, because it is already the tenth time the permafrost community has met to present and exchange knowledge on science and engineering. Ten is a large number when one considers how recently the term “permafrost” was coined; it is also a very small number in light of the growing awareness of permafrost’s overwhelming relevance to the Earth climate system.

Second, TICOP is significant because forty years have passed since the conference was last held in Russia. The last one was in Yakutsk in 1973. It is the Russian Federation’s honor to have been given the assignment to organize the conference once again, this time in Salekhard in the Yamal-Nenets Autonomous District.

Third, and lastly, this conference is important because permafrost science and engineering has entered a new era with an explosion of the number of papers published and the rapid transformation of permafrost research into an increasingly multi- and interdisciplinary endeavor.

Permafrost science and engineering has managed to transcend scientific and engineering disciplines to answer and develop new scientific questions relevant to the entire Earth climate system. This, in return, has prompted an incredible awareness about permafrost in an increasing number of scientific communities that traditionally were uninvolved with it. Additionally, the media, decision-makers, activists, teachers, and of course the general public have grasped the issue in one way or another.

A simple search on the internet shows that not one day passes without a news item appearing in reference to permafrost. Permafrost thaw and its consequences form the bulk of this growing interest. The threats to northern and mountain infrastructure, the destabilization of thawing

permafrost coasts, the increased microbial breakdown of subsurface organic matter leading to the release of carbon dioxide and methane, and the seeping of methane stored as gas hydrates all have huge potential consequences for inhabitants of permafrost regions and beyond. Therefore, the need for international collaboration is more pressing than ever.

In this context, the Tenth International Conference on Permafrost, held in Salekhard in June 2012, takes place at the right time and in the right place (i.e., on permafrost). With more than 350 presentations, more than 200 papers published in the proceedings, and more than 600 expected participants, TICOP will open the floor to the presentation and discussion of the newest results in permafrost research and engineering. The conclusions that will stem from the conference will crystallize the state of the art. They will highlight the importance of permafrost research and engineering for areas at risk, and they will focus on the consequences of permafrost thaw for the Earth climate system.

On behalf of the International Permafrost Association, I would like to congratulate the local organizers of the conference. They have put together an excellent program with a variety of scientific sessions and social events that will allow the participants to understand what it takes to live on warming permafrost. They have made a special effort to involve young researchers from all over the world, and they have awarded 150 of them with a stipend covering the registration, accommodations, and travel to the conference.

I wish all of you an excellent conference filled with the exchange of knowledge, exciting results, and many fruitful discussions with colleagues and old and new friends.

— Hans-Wolfgang Hubberten, President,
International Permafrost Association

Preface

Since the Second International Conference on Permafrost, held in 1973 in Yakutsk, permafrost science and engineering has witnessed the ever-increasing need for new knowledge and understanding, within Russia and the Former Soviet Union and throughout the international cold regions communities. The Tenth International Conference on Permafrost, held in Salekhard, provides the venue for the exchange of current information and knowledge concerning the dynamics of permafrost regions, their roles in global change, and challenges for development and environmental protection.

At its June 2010 meeting, the Council of the International Permafrost Association approved the preparation of proceedings of peer-reviewed papers for the Tenth International Conference on Permafrost. The resulting two-volume

proceedings are the result of a collaborative effort between the U.S. Permafrost Association and the Russian Organizing Committees. Many of the review and production procedures and software that were developed for the Ninth International Conference on Permafrost were utilized. Volume 1 contains the English language papers, and Volume 2 the English translations of Russian papers; all were submitted electronically by autumn 2011. A total of 82 papers from 13 countries are presented in Volume 1. Volume 2 contains 107 Russian papers that were reviewed and translated in Russia, and subsequently read and edited in North America. A companion volume of approximately 370, two-page Extended Abstracts from 15 countries was prepared by the Russian organizers.

Acknowledgments

The International Permafrost Association and the Russian organizers of the Tenth International Conference on Permafrost acknowledge the many individuals and sponsoring organizations that made the production of these two volumes possible. The Governor of Yamal-Nenets Autonomous District, Dmitry N. Kobylking, and Vice-governor Aleksander V. Mazharov, as co-chairs of the local TICOP Committee, provided support and advice throughout the conference organizational process. They were ably assisted by staff members Aleksey Titovskiy and Irina Voronova. Members of the Earth Cryosphere Institute, Siberian Branch of the Russian Academy of Science (SB RAS), and Anna Kurchatova and Sergey Turenko of Tyumen State Oil and Gas University all provided guidance and important administrative services in the preparation and publication processes. The U.S. Permafrost Association (USPA) provided administrative assistance for the editing and final camera-ready layout.

Review of the Russian papers was coordinated by the senior co-editor Dmitry Drodzdov. Translation of the Russian papers was coordinated by Irina Voronova, Salekhard, and performed by a team from the Translation Laboratory, Fedorov Institute for Translation and Interpretation, St. Petersburg University. Each translated paper was read by either a Russian-English speaking permafrost specialist residing in North America and/or by several other specialists in the U.S. The purpose was to improve the translation of terminology and to produce a more readable text. However, considering the limited time available, some text may not be easily understood. If a question arises, the reader is referred to the

original Russian text that is published in a separate TICOP volume. Some titles of papers were edited and some keywords were added or deleted in order to maintain consistency between papers.

Readers included Mikhail Kanevskij, Yuri Shur, Vladimir Romanovsky, and Ben Abbott, University of Alaska Fairbanks; Nikolay Shiklomanov and Dmitry Streletskiy, George Washington University; Vladimir Roujanski, EBA Canada; Kevin Bjella, Cold Regions Research and Engineering Laboratory, Fairbanks; and Jerry Brown, Woods Hole, MA. Final editing and preparation of the camera-ready copy of both volumes were completed in Fairbanks, Alaska, by Tom Alton, copy editor, using Microsoft Word and Adobe InDesign.

The resources of the U.S. Permafrost Association based in Fairbanks, Alaska, were provided through GW Scientific and the expertise of Engineering and Environmental Internet Solutions (EEI), and particularly Gary Whitton. The International Arctic Research Center, University of Alaska Fairbanks (UAF), provided logistical support for copy editor Tom Alton. Two major sponsors helped defer U.S. costs for the preparation of the proceedings: BP and Arctic Foundations, Anchorage. Funds for the publication of both volumes were provided by the government of the Yamal-Nenets Autonomous District.

— Jerry Brown, Volume Coordinator,
U.S. Permafrost Association

Russian Associate Editors and Reviewers

Abramov A.A.	Institute of Physicochemical and Biological Problems in Soil Science (RAS)
Aksenov V.I.	Open Joint Stock Company «Fundamentproekt»
Alekseeva O.I.	Melnikov Permafrost Institute (SB RAS)
Badu Yu.B.	Lomonosov Moscow State University
Baulin V.V.	Lomonosov Moscow State University
Buldovich C.N.	Lomonosov Moscow State University
Vasiliev A.A.	Earth Cryosphere Institute (SB RAS)
Vasilchuk A.K.	Lomonosov Moscow State University
Volokhov S.S.	Lomonosov Moscow State University
Gal'chenko V.F.	Vinogradsky Institute of Microbiology (RAS)
Gilichinsky D.A.	Institute of Physicochemical and Biological Problems in Soil Science (RAS)
Golitsyn M.S.	All-Russian Research Institute of Hydrogeology and Engineering Geology (VSEGINGEO)
Gubin S.V.	Institute of Physicochemical and Biological Problems in Soil Science (RAS)
Drozdov D.S.	Earth Cryosphere Institute (SB RAS)
Iospa A.A.	Open Joint Stock Company «Fundamentproekt»
Kaplina T.N.	PNIIS
Klinova G.I.	Open Joint Stock Company «Fundamentproekt»
Komarov I.A.	Lomonosov Moscow State University
Konischev V.N.	Lomonosov Moscow State University
Kochurov B.I.	“Kamertone” Publishes Ltd
Kritsuk L.N.	All-Russian Research Institute of Hydrogeology and Engineering Geology (VSEGINGEO)
Kuznetsova I.L.	Open Joint Stock Company «Fundamentproekt»
Kuzmin G.P.	Melnikov Permafrost Institute (SB RAS)
Kunitsky V.V.	Melnikov Permafrost Institute (SB RAS)
Kurchatova A.N.	Earth Cryosphere Institute (SB RAS)
Kutvitskaya N.B.	Open Joint Stock Company «Fundamentproekt»
Kutuzov S.S.	Institute of Geography (RAS)
Lavrentiev I.I.	Institute of Geography (RAS)
Leibman M.O.	Earth Cryosphere Institute (SB RAS)
Maximova L.N.	Lomonosov Moscow State University
Malkova G.V.	Earth Cryosphere Institute (SB RAS)
Merzliakov V.P.	Sergeev Institute of Environmental Geoscience (RAS)
Moskalenko N.G.	Earth Cryosphere Institute (B RAS)
Oberman N.G.	MIREKO Mining Geological Company
Osadchaya G.G.	Institute of Management, Information and Business
Ospennikov E.N.	Lomonosov Moscow State University
Ostroumov V.E.	Institute of Physicochemical and Biological Problems in Soil Science (RAS)
Pavlov A.V.	Earth Cryosphere Institute (SB RAS)
Perlshein G.Z.	Sergeev Institute of Environmental Geoscience (RAS)
Razumov S.O.	Melnikov Permafrost Institute (SB RAS)
Rivkin F.M.	Open Joint Stock Company «Fundamentproekt»
Rogov V.V.	Lomonosov Moscow State University
Roman L.T.	Lomonosov Moscow State University
Romanovskii N.N.	Lomonosov Moscow State University
Sergeev D.O.	Sergeev Institute of Environmental Geoscience (RAS)
Slagoda E.A.	Earth Cryosphere Institute (SB RAS)
Solomatn V.I.	Lomonosov Moscow State University
Streletskaya I.D.	Lomonosov Moscow State University
Sukhodolsky S.E.	PNIIS
Titkov S.N.	PNIIS
Ukrainitseva N/G.	Earth Cryosphere Institute (SB RAS)
Fedorov-Davydov	D.G. Institute of Physicochemical and Biological Problems in Soil Science (RAS)
Fedoseeva V.I.	Melnikov Permafrost Institute (SB RAS)
Fotiev S.M.	Earth Cryosphere Institute (SB RAS)
Khrustalev L.N.	Lomonosov Moscow State University
Cheverev V.G.	Lomonosov Moscow State University
Chuvikin E.M.	Lomonosov Moscow State University
Shamanova I.I.	PNIIS

Shepelev V.V. Melnikov Permafrost Institute (SB RAS)
Shesternev D.M. Melnikov Permafrost Institute (SB RAS)
Yakushev V.S. Gazprom VNIIGAZ

North American Readers

Abbott, B. University of Alaska Fairbanks
Brown, J. Woods Hole, MA
Bjella, K. Cold Regions Research and Engineering Laboratory, Fairbanks
Kanevskij, M. University of Alaska Fairbanks
Romanovsky, V. University of Alaska Fairbanks
Roujanski, V. EBA Canada
Shiklomanov, N. George Washington University
Streletskiy, D. George Washington University
Shur, Y. University of Alaska Fairbanks

Permafrost Conditions in the Polar Regions of Mars

O.N. Abramenko, V.S. Isaev, I.A. Komarov

Lomonosov Moscow State University, Faculty of Geology, Geocryological Department, Moscow, Russia

Abstract

Reported are recent data on the thickness, composition, and structure of the polar ice caps of Mars. The time and space patterns and variation amplitudes have been estimated for the radiation budget and mean monthly temperatures of the ground surface on a spatial grid of polar Mars.

Keywords: Mars; radiation heat budget; permafrost conditions; polar deposits.

Introduction

The ample body of recent evidence has considerably enlarged and dramatically changed the views of the atmosphere, climate, and surface of Mars, which is becoming the principal target of many research projects. With the available data of climate monitoring, the information on any point of the planet can be almost as precise as that for planet Earth. Thus the knowledge of Mars has been raised from hypotheses up to a qualitatively new level.

Background

Obviously, the Mars polar ice caps, which control the particular high-latitude landscape patterns, provide irrefutable proof of the existence of permafrost. The ice caps are often called perennial or residual, as they persist throughout the summer season (after the seasonal CO₂ snow cover disappears). These are Mars's largest permafrost-glacial structures, with stepped surfaces cut by concentric scarps and V-shaped valleys that twist spiralwise around the cap center in a vortex-like feature (Fig. 1).

The south and north polar caps may extend to 50°S or 50°N, respectively, depending on the season or seasonal change. As the caps retreat in spring in the respective hemispheres, there emerge different landforms of the planet's surface: polygons, dunes, and others.

The polar deposits consist of CO₂ and H₂O ice up to 3700 m thick, according to data from the Mars Express satellite.

As a result of spring thawing, the atmospheric pressure increases substantially and drives large masses of gas to the opposite hemisphere, with a wind speed of 10 to 40 m/s, or sometimes as high as 100 m/s.

The ice sheets lie over a heavily cratered old surface in the southern hemisphere and upon a smoother terrain in the north. The deposits of several kilometers in thickness result from long-term accumulation of volatiles (in the form of ice) and mineral substrate (dust). The residual, perennial caps must be composed mostly of H₂O ice, judging by the temperature regime. Viking-2 infrared radiation spectrometry of the Mars surface shows that the north polar cap and the adjacent area is never colder than 203 K (-70°C) in the summer season, implying that the existence of CO₂ and gas hydrates at that time is unlikely.

Currently the north ice cap covers a much larger area than the southern one (1000 km and 300 km across, respectively) and is commensurate with the Greenland ice sheet (Kieffer et al. 1992). The difference is due to the perihelion position

of Mars (the closest approach to the sun) during the summer of the southern hemisphere, whereby the latter receives more sunlight than the northern cap. The relative amounts of incoming sunlight in the polar regions are controlled jointly by the precession cycles of the orbital perihelion (72 kyr) and the planet's spin axis (175 kyr) (Kieffer et al. 1992).

The dome-shaped caps of thick ice and dust layers are reasonably assumed to be plastic under long-lasting loads. However, it remains unclear whether plastic strain may exist in the polar ice sheets because ice loses its plasticity at temperatures below -70°C as a result of lattice change. The flow point of this ice (the minimum load at which ice begins to flow) is extremely high compared to the normal ice while the relaxation time is much longer than in the ice of the coldest Antarctic regions.

However, the material is likely to have experienced plastic deformation given the great thickness of the ice caps (a few kilometers), their old age (hundreds of million years), and temperature rise with depth. Successive deposition apparently increased the stress in the overlying layers while plastic strain grew correspondingly, bringing the material to irreversible progressive flow. The ice-rich layers below may have been extruded and flowed off into the cap's periphery. The spread of material was possibly uneven over the caps due to local variations in thickness and ice contents of the deposits, in the underlying surface topography, and climate-driven temperature change.

Mars differs from the Earth in the presence of CO₂ ice and in the pressure and temperature of the solid-gas equilibrium, the latter being dependent on the annual balance of the absorbed and outgoing solar heat. The amount of CO₂ ice can be inferred from atmospheric pressures and temperatures. Calculations using Viking Orbiter records show that 75 ± 12

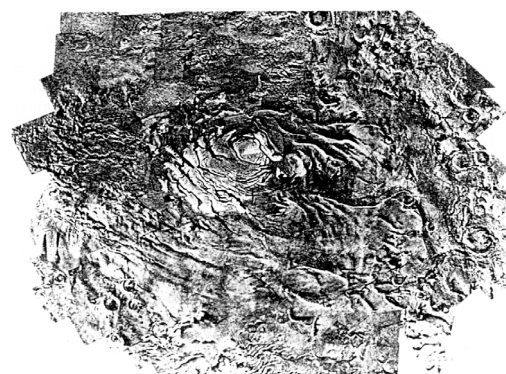


Figure 1. North polar ice cap of Mars. A mosaic of photographs, after Kieffer et al. (1992).

and 110 ± 7 g/cm² CO₂ is deposited as icing within the polar caps in the north and south, respectively (Malin & Edgett 2001), more in the south where the winter season is longer. On the average, about 25% of the whole atmosphere is recycled in the seasonal ice caps, which influences strongly the wind circulation.

The two poles differ in the amount of seasonal CO₂ sublimation, partly because of a difference in albedo. The sublimation is more efficient in the darker northern cap than in the southern hemisphere. The albedo may depend partly on the amount and distribution of dust, but explaining any difference solely by dust forcing is ambiguous.

The most striking difference in CO₂ sublimation at the two poles is in residual ice that persists in the southern cap for at least several seasons. The possibility of H₂O storage in the polar ice caps has important implications for the composition of the layered deposits likely containing abundant water ice. It is quite difficult to obtain a synthetic pattern of water reserves by correlating data on water vapor and surface processes. As it was calculated in 1990, from 1 to $8 \cdot 10^{-2}$ g/cm² ice can be sublimated for a summer season within the north polar cap (Yokohata et al. 2002). Thus H₂O vapor rising from the cap must bear a component of regolith moisture. Then it was concluded that the atmospheric transport of moisture hardly may be sufficient to recharge the ice cap, and the northern cap may thus lose a considerable amount of H₂O ice. However, one should be rather cautious about postulating the moisture deficit since there is inconsistency in different mechanisms of transport and the role of moisture in the regolith.

A large amount of water vapor can accumulate also outside the polar regions, in areas of ancient ice in dark and "warmer" exposed layered deposits. This fact should be taken into account in budget estimates, because although the ice cap sublimation provides most of the observed water vapor in the atmosphere, the latter cannot return that moisture to the ice cap during the winter season. More control on the H₂O ice budget may come from local redistribution of water and from chemical weathering (Yokohata et al. 2002). Despite the fact that the layered deposits have temperatures much below the water freezing point, fine ice grains can be locally coated with thin water films. This effect on account of insolation has been recorded on the equatorward sides of V-shaped valleys with a low albedo.

Persistent dust makes the Martian atmosphere relatively low transparent and yellowish. Dust is transported by frequent dust storms which have been observed historically as yellow clouds or occasionally as a continuous yellow veil wrapping the whole planet (Kieffer et al. 1992).

The stratigraphy of the Mars polar regions is rather intricate but leads to some classification of units that are (1) layered deposits and adjacent ice and (2) areas on the periphery of the layered deposits (Tanaka & Scott 1987). The north and south polar layered deposits are much more similar than their surrounding areas. The layered deposits lie over a basal plain surface, which is older and more heavily cratered in the south but younger and smoother in the north. Residual ice lies over layered deposits at both poles.

Assessment of Permafrost Conditions

Methods for studying radiation heat budget in the Mars polar regions

The time and spatial patterns of the surface radiation heat budget components in the polar regions of Mars, as well as the temperature patterns of the ground surface and near-surface atmosphere, were investigated using the Global Mars Climate Database produced jointly by Laboratoire de Météorologie Dynamique du CNRS (LMD, Paris) and Atmospheric, Oceanic and Planetary Physics, Department of Physics (AOPP, Oxford University, Oxford, England). The database is a system of search and calculation providing information on climate parameters at any user-specified time and place (point or area), with a selected stepsize from the Mars surface. The database has a calculation subroutine and a friendly interface, the information being presented as maps or spreadsheets. On this basis, more than 50 maps and tables have been compiled by processing the data on a spatial grid for the coordinates 90°, 86.2°, 82.5°, 78.8°, 75° N and S; 135°, 90°, 45°, 0° W; and 45°, 90°, 135°, 180° E. The data include annual cycles of the radiative fluxes (solar and thermal IR) on the ground and at the top of the atmosphere, absorbed and outgoing radiation, and mean monthly surface temperatures.

Turbulent heat transfer was found as the surface-air temperature difference (according to GMCD), at a minimum height of 5 m above the ground surface, multiplied by the heat transfer coefficient. The latter was assumed to be 2–5 W/(m²×K) based on laboratory data for the terrestrial conditions of 6 mbar and temperatures typical of the Mars high latitudes. The heat spent for sublimation (ablation) of CO₂ or H₂O ices was evaluated from GMCD-derived mean annual rates of the process. The CO₂ and H₂O ice sublimation heat was assumed to be 572 and 2816 kJ/kg, respectively, estimated with regard to the temperature dependence. The heat flux from the ground to the ice was calculated from mean annual temperature gradients in the near-surface CO₂ or H₂O ices and the temperature dependence of their thermal conductivities known from the literature.

Estimates of the radiation budget components in the Mars polar regions

The north polar ice cap receives no sunlight in the winter season. The IR radiative flux of the atmosphere varies from 1.55 to 2.75 W/m² and that of the ground surface from 19.2 to 25.6 W/m²; the radiation ratio is 0.85. In the late winter-early spring, the atmospheric density is 0.019 kg/m³, which has been the minimum value over the entire period of observations. As spring comes, the total solar irradiance (TSI) is 200 W/m², scattered radiation becomes 120 W/m², and the air and ground infrared fluxes grow, respectively, to 4.25 W/m² and 27.4 W/m², while the radiation ratio remains at 0.85; the atmospheric density increases gradually to 0.0315 kg/m³. In summer the insolation is the maximum, TSI increases to 320 W/m², the scattered component to 102 W/m², and the infrared components of the atmosphere and the surface become as high as 17.2–25.0 W/m² and 90–190 W/m², respectively; the density increases slowly to 0.0315 kg/m³. In the fall, the polar night comes and CO₂ begins to precipitate. The amount of CO₂ in the cap

reaches 64 kg/m^3 . The radiation components decrease: TSI to 110 W/m^2 , scattered radiation to 56 W/m^2 , and the air and ground infrared radiation to $2\text{--}5.2$ and $22.5\text{--}40.5 \text{ W/m}^2$, respectively; the radiation ratio becomes $0.825\text{--}0.945$, and the density decreases to 0.024 kg/m^3 . The latitude-dependent variations are very prominent as the air and ground infrared radiative fluxes, as well as the outgoing and absorbed components, increase toward the equator. The longitude-dependent changes in the radiation components may be due to variations in topography and thickness of the polar deposits, as well as to surface slope variations in the northern hemisphere.

In the southern hemisphere, incoming sunlight is zero in the summer season. The atmosphere and the surface IR fluxes are, respectively, $0.8\text{--}2$ and 15.4 W/m^2 , and the radiation ratio is $0.80\text{--}0.86$. The atmospheric density is the minimum in the latest winter-earliest spring ($0.0122\text{--}0.0178 \text{ kg/m}^3$). As the fall comes, the amount of insolation changes, TSI becomes 240 W/m^2 , the scattered component reaches 150 W/m^2 , and the IR components are $3.1\text{--}4.5 \text{ W/m}^2$ for the atmosphere and $23.1\text{--}26.3 \text{ W/m}^2$ for the ground; the density increases gradually to 0.0535 kg/m^3 . In winter, the position of the planet in the perihelion provides maximum sunlight, and TSI is as high as 420 W/m^2 , the scattered radiation is 150 W/m^2 , and the infrared components grow to $27\text{--}41 \text{ W/m}^2$ (atmosphere) and $110\text{--}260 \text{ W/m}^2$ (ground). The atmospheric density likewise reaches its maximum (0.098 kg/m^3). The polar night comes again with spring, and the radiation components decrease; TSI decreases to 92 W/m^2 , scattered radiation is as low as 48 W/m^2 , and the infrared components reduce to $1.55\text{--}3.65$ and $21\text{--}33 \text{ W/m}^2$ (air and ground, respectively); the radiation ratio is $0.85\text{--}0.88$, and the atmospheric density is $0.014\text{--}0.018 \text{ kg/m}^3$. The latitude zoning in the southern hemisphere is similar to that in the northern one, and the longitudinal variations are likewise produced by differences in elevation and slope.

The albedo data are reported as annual means for the limitations imposed by the available database. The mean annual albedo values range from 0.1 to 0.52 , the maximum being characteristic of the polar regions.

The annual sums of outgoing radiation are from 414 to 750 W/m^2 in the northern cap and from 532 to 840 W/m^2 in the south. The annual sum of absorbed radiation ranges from 658 to 2016 W/m^2 in the south and between 702 and 1539 W/m^2 in the north (Abramenko et al. 2011).

Generally, the Martian climate patterns are as complicated as the terrestrial ones, being controlled by latitudinal zoning and the heat budget. The climate depends on weather conditions in the warm and cold seasons as a result of intricate processes of radiation exchange and heat-and-mass transfer in the system 'ground surface—atmosphere—cosmic space.' All of these processes are jointly reflected in the ground temperature as an integrative indicator. Some part of incoming sunlight goes back to the space being reflected from clouds and backscattered by molecules in the atmosphere; some part is absorbed by the clouds and the atmosphere. The remaining heat reaches the surface and consists of a normal beam and scattered larger components. The largest part of the radiation is absorbed by the surface and only a minor part is scattered. The short-period radiation absorbed by the atmosphere and the ground surface is transformed into the

long-period one and drive thermal processes: condensation and sublimation of CO_2 and H_2O , turbulent heat transfer, heat transport by atmospheric circulation and vortices. When moving from west to east and from north to south and back, air overcomes various regional heterogeneities in the planetary shell and either gains or loses energy. The atmosphere receives heat reflected from the surface as air moves over the ice caps in the summer season and, on the contrary, loses the stored energy outside the polar regions. The reason is in the continuous "drying" of the atmosphere in winter when air turbulence decreases with less incoming radiation. This results from precipitation of CO_2 , which neither sublimates nor recharges the atmospheric energy resources.

Mean annual, seasonal, and diurnal temperatures of the ground surface and their variations

The mean ground surface temperature in the insolated part of Mars at an average distance from the sun is -43°C , and that averaged over latitudes and seasons is -63°C . Like on the Earth, the Mars ground temperatures vary as a function of latitude and orography and have diurnal and seasonal cycles with greater contrasts than in the terrestrial temperatures. The amplitude of diurnal temperature variations on the equator reaches $\sim 100^\circ$. The ground is $30\text{--}50^\circ$ warmer than the atmosphere at 5 m above the surface in the day time and is $5\text{--}7^\circ$ colder in the night.

Mid-latitude seasons in the northern and southern hemispheres have different temperature regimes because of the orbit ellipticity.

In the same way as in the terrestrial high latitudes, the sun does not set in summer and does not rise in winter in the Mars polar regions. Therefore, the ground temperatures are maximum in summer and minimum in winter. The summer and winter ground temperatures vary, respectively, from -63° to -58°C and from -138° to -128°C in the northern polar region; the respective ranges in the south are from -43° to -38°C and from -143° to -133°C (Komarov et al. 2004).

It is noteworthy that Mars, with its low-density atmosphere, cannot hold back the heat that comes to the surface in the daytime and, hence, a great amount of heat escapes to space in the dark time (night and polar night). This is the reason for large diurnal temperature variations. In the most favorable conditions, in summer daytime, air may be as warm as 293 K (MCDB) in the insolated half of the planet, but frost in winter nights may reach 148 K . The lowest temperature at the southern ice cap is 113 K , the average being 155 K , which is approximately the freezing point of carbon dioxide at the atmospheric pressure on the Mars surface. The lowest temperature of the northern cap is 148 K .

It is important that, unlike the Earth, the Mars surface temperature is due mostly to beam solar heat rather than atmospheric heat transport seeking to balance temperature contrasts. As a result, the temperature may locally (on steep slopes exposed to the sun) reach or even slightly exceed 273 K , while the mean of the north ice cap periphery (at 82° N) in the early summer is 235 K ($L_s = 90^\circ$).

The two hemispheres on Mars differ in durations of the warm and cold seasons and in temperatures controlled by their approaches to the Sun; winters in the southern hemisphere are longer and colder while summers are shorter

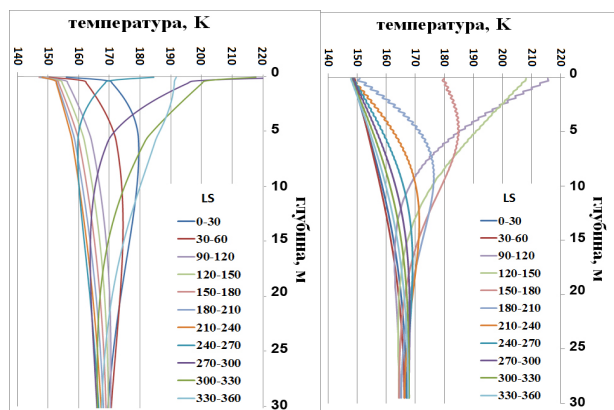


Figure 2. Monthly mean temperatures in the southern (left) and northern (right) polar ice caps along 180°. LS are solar longitudes corresponding to months of the Martian year.

but warmer. Another feature of the cold season (autumn and winter, $L_s=210-300^\circ$) is dust storms and related climate change, which show up in the dynamics of ice cap thickness.

Generally, the mean daily temperatures vary over the year from 143.0 K to 272.7 K at the south polar cap and from 147.4 K to 251.0 K in the north.

The temperature regime of the uppermost northern ice cap, where H_2O ice locally predominates, was modeled using the *HeatMars* program for a one-layer subsurface (Pustovoit 2005). Similar modeling for the southern ice cap, which rather fits a two-layer model and is seasonally dominated by CO_2 ice on the surface, was with the *Teplo* (“Heat”) software (Khrustalev et al. 1994) (Fig. 2). The heat capacities of H_2O and CO_2 ices in the Martian conditions were obtained from reference books.

The abrupt temperature change at the depth 25 cm (left) is due to the two-layer structure with CO_2 snow lying over H_2O ice. The line colors correspond to the months of the Martian year.

Thermal conductivities were calculated from known values of heat inertia and heat capacity. The active layer thicknesses in the southern and northern ice caps were estimated to be 12 to 14 m and 24 to 26 m, respectively.

Structure and stratigraphy of polar deposits

From insufficient instrumental resolution, it is difficult to estimate the total thickness of the polar deposits while studying the topography of the top and underlying surfaces. According to Dzurisin & Blasius (1975), the polar deposits are 4–6 km thick in the north cap and 1–2 km thick in the southern one. With reference to these estimates, Malin (1986) concluded that the northern deposits reach their maximum of 5 km along a ridge at about $87^\circ N$ and are 2 km thick on average. The most recent maps of the ground surface contours confirm the average thickness of polar deposits in the north to be 2 km. Thickness for the southern polar deposits is more difficult to estimate from the surface contours because of an impact basin below, but a 2-km thickness appears to be a reasonable value. Layered deposits locally lie under residual ice and are seasonally overlain by frozen CO_2 .

Residual ice over the northern and southern polar layered deposits has different distribution patterns and, at least for

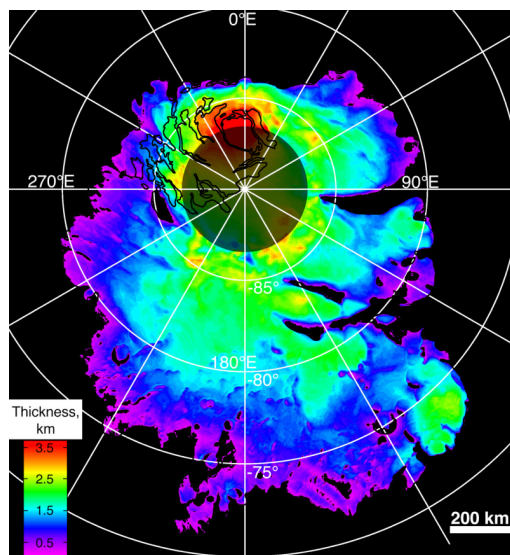


Figure 3. Thickness of the southern ice cap according to MARSIS radar records.

several recent years, differs also in composition. Perennial ice covers the polar deposits almost completely in the north but only partly in the south. In the southern cap it is $2-3^\circ$ offset from the pole. Local ice patterns on both poles are controlled by, among other factors, the surface slope; the slopes that are exposed to the sun have more chance to become free from ice.

According to Viking 1 and 2 records, the northern residual ice consists of frozen H_2O , which provides saturation of atmospheric water vapor in the summer season. The ice albedo there, with regard to the presence of minor amounts of dust and other dark-colored detrital material, is about 0.43. The situation is more complex at the southern pole, where residual ice has consisted of CO_2 at least in the recent years, and the temperatures have been much below the sublimation point of H_2O ice.

The exact thickness of the north polar residual ice remains unknown. It would be pointless to discuss separately the thickness of this ice, not knowing whether it may penetrate into the layered deposits below. The available thermal data indicate that the northern cap consists of pure residual ice and give no evidence of dust or rock matter. The southern residual ice, however, differs rather markedly from compacted sedimentary material.

The seasonal caps of frozen CO_2 spread far outside the layered deposits and reach several tens of grams per square centimeter for a winter. The ice caps grow and reduce seasonally every year, but topographic features can change within a year. Seasonal ice in the north is thinner than that in the south, possibly because the surface is smoother.

Three more stratigraphic units lie near or upon the surface described above. They are a zone of coarse clastic material in the north, dunes on both poles, and different plain-land complexes in the south. These units are difficult to classify, except for the distinct morphology of the dunes. The most recent MARSIS radar data from the Mars Express indicate the thicknesses of the northern and southern ice caps to be, respectively, 2 and 3.7 km (Fig. 3).

Conclusions

At present, the surface area of ice in the north polar cap of Mars is much larger than that of the southern cap: 1000 km and 300 km across, respectively. The size difference between the two caps is due to the fact that Mars is currently in the perihelion (and hence closest to the sun) during the summer season of its southern hemisphere. Heavy dust storms that are frequent in the polar regions produce layered deposits. According to records of the MARSIS radar (Mars Express), the thicknesses of the northern ice cap is 2 km and of the southern ice cap is 3.7 km. The minimum annual variations of the surface height at both caps are 10 cm, with a quasi-linear latitudinal tendency of a maximum CO₂ deposition of 4 cm per degree latitude. Unlike the Earth, the Martian ice caps contain CO₂ ice and deposits of dust storms besides water ice. The mathematically estimated active layer thicknesses in the southern and northern ice caps are 12 to 14 m and 24 to 26 m, respectively.

References

- Abramenko, O.N., Komarov, I.A., & Isaev, V.S. 2011. The radiation heat budget of the Antarctic and Mars polar regions: comparative analysis. *Kriosfera Zemli* 15 (4): 53-55.
- Dzurisin, D. & Blasius, K. 1975. Topography of the polar layered deposits of Mars. *J. Geophys. Res Letters* 80 (23): 3286-3306.
- Khrustalev, L.N., Emeliyanov, N.V., Pustovoit, G.P., & Yakovlev, S.V. 1994. *Teplo* software for simulating thermal interaction of engineering structures with permafrost soils. Certificate No. 940281, RosAPO.
- Kieffer, H.H., Jakosky, B.M., Snyder, C.W., & Matthews, M.S. (eds.). 1992. *Mars*. University of Arizona Press, Tucson.
- Komarov, I.A., Isaev, V.S., & Abramenko, O.N. 2004. Characters of changes in thermophysical parameters of the Martian polygonal terrains in dependence from their geographic position. *Vernadsky-Brown Microsymposium* 40, October 11-13, 2004, Abstract # ms 044, CD-ROM, Moscow, Russia.
- Malin, M.C. 1986. Density of Martian north polar layered deposits: Implications for composition. *Geophys. Res. Letters* 13 (5), 444-447.
- Malin M.C. & Edgett, K.S. 2001. Mars Global Surveyor Mars Orbiter Camera: Interplanetary cruise through primary mission. *J. Geophys. Res.* 106 (10): 23,429-23,570.
- Pustovoit, G.P. 2005. *HeatMars* software for calculating temperature fields in the near-surface layers of Mars. *Proc. 3rd Conf. of Geocryologists of Russia*. Book 4. Moscow University, 345-350.
- Tanaka, K.L. & Scott, D.H. 1987. Geologic map of the polar regions of Mars: *U.S. Geological Survey Miscellaneous Investigations Series* Map I-1802-C, scale 1:15,000,000.
- The Mars Climate Database. <http://www-mars.lmd.jussieu.fr>.
- Yokohata, T., Odaka, M., & Kuramoto, K. 2002. Role of H₂O and CO₂ ices in Martian climate changes. *Icarus* 159.

Changes in Geocryological Conditions along the Reconstructed Salekhard-Nadym Railway

N.S. Aleksandrova

Faculty of Geography, Department of Cryolithology and Glaciology, Lomonosov Moscow State University, Moscow, Russia

Abstract

Conditions for the reconstructed Salekhard-Nadym railway are presented. The predominant types of natural territorial complexes (terrain types) and permafrost-related geohazardous processes were identified. Conditions at three study sites were evaluated. Numerical modeling of changes in the thermal regime for the typical railway route sections was completed using the Teplo software.

Keywords: geocryological conditions; change forecast; railway; Western Siberia.

Introduction

Active economic development in the North of Russia's European territory and Western Siberia began more than 70 years ago. New cities (Vorkuta, Norilsk, and others) were rapidly built, and mineral resources were intensively explored. The creation of the transportation infrastructure system, which was supposed to connect the emerging cities to the discovered mineral deposits, immediately became a necessity. Primary attention in this respect was paid to railway transportation.

Construction of transportation infrastructure in Western Siberia is now becoming even more critical due to a new stage of the region's economic development. The Northern Sea Route exists on paper only, and air transport and winter roads cannot cope with large volumes of cargo in the region. Therefore, the demand for railway transport is growing, and the Salekhard-Nadym railway is one of the main lines that could partially solve the transportation problem of the region.

The occurrence of permafrost complicates economic activity and certainly affects construction and operation of the railway. Engineering-geocryological (permafrost) conditions along the road are characterized by the presence of discontinuous permafrost, with continuous or layered vertical structures (i.e., possible sequence of thawed and frozen sediment layers). The permafrost thickness varies from several tens to hundreds of meters. The permafrost is characterized by a wide range of ground temperatures and ice contents and highly variable active layer depths. Geocryological characteristics are closely interrelated, and there is a relationship between climate and lithology, terrain features, and the type of vegetative cover. This relationship results in a variability of permafrost landscape conditions in the region.

The purpose of this study is to evaluate the impact of geocryological conditions on reconstruction of the Salekhard-Nadym railway within the sporadic and discontinuous cryolithozone of Western Siberia.

Physiographic Setting

The Salekhard-Nadym transpolar railway is located in the northern part of the West Siberian Plain, south of the Ob

Bay. The railway starts on the right bank of the Ob River, runs along the right bank of the Poluy River, and crosses the Nadym River near the Town of Stary Nadym (Fig. 1).

The terrain in the area is represented by a slightly dissected, gently undulating plain with elevations ranging from 10 to 80 m. There are many permanent and temporary watercourses and peatlands (Trofimov & Kashperyuk 1989). The climate is subarctic with cold winters and chilly summers; the mean annual air temperature is -5.8°C in the town of Salekhard and -5.2°C in the town of Nadym (SNiP 23.01-99 2000). The railway route parallels the boundary between two natural zones – the forest-tundra and the northern taiga (Gvozdetskiy & Mikhailov 1978). The

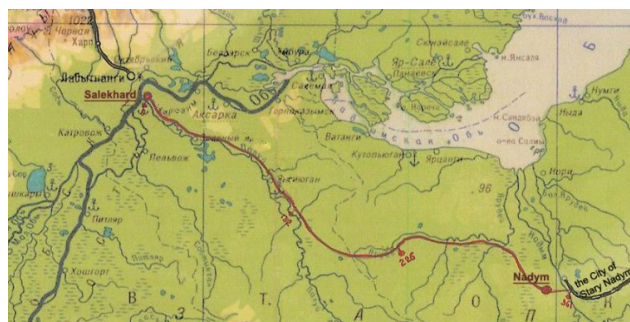


Figure 1. Location of the Salekhard-Nadym railway (<http://www.lgt.ru>).

Table 1. Geocryological zones within the railway construction corridor.

Region	Ground temperature, $^{\circ}\text{C}$	Thickness, m *	Perma-frost distribution type	Lithology	Cryogenic geomorphic processes and landforms
Ust-Ob	-0.1...3	80	Sporadic	sand, silt, clayey silt	Thermal erosion, frost mounds
Ob-Nadym	~ 1	40	Discontinuous (mainly in peatlands)	sand, silt, clayey silt	Thermokarst, Pingos, Frost blisters
Nadym	-0.5...1.5	50-70		sand	Frost mounds

* Note: The vertical structure of the permafrost interval is mainly two-layered; Thickness of the upper permafrost layer is presented.

Table 2. Proportion of different natural territorial complex types along the Salekhard-Nadym railway route on a percentage basis (based on the total route length).

No	Type of natural territorial complex	%
1	Watersheds (m, gmIIsh)	3.3
2	Bedrock slope highly dissected by erosion (ravines, gullies, river and creek valleys (mIIIkz, g,mIIIzr)	52.7
3	Fluvial terraces (Lacustrine-fluvial complex a-(aIII-IV, bIV)	18.7
4	Major river floodplains (Yarudey, Poluy, Nadym; aIV, bIV)	18.2
5	Minor stream valleys (aIV)	7

railway crosses three geocryological (permafrost) regions identified on the basis of geocryological zoning (Trofimov, Baulin & Vasilchuk 1989, Table 1).

The Salekhard-Nadym railway is located on various landscape-permafrost conditions that define the complexity of its design, construction, and operation. Numerous water courses require construction of multiple drainage control structures such as culverts, bridges, and water-diversion structures (excavations, etc.).

The landscape-permafrost conditions of the road are represented by five natural territorial complex types (terrain types) with different types of vegetative cover (Table 2).

Permafrost (mainly “warm”) occurs sporadically along the railway route. Permafrost within the first natural territorial complex type is confined to peatlands on the watersheds and to shrub-tundra adjoining it. Permafrost was encountered underlying the grass-moss tundra and sparse larch-birch forest on the high floodplain of the Poluy River. Permafrost is also found in peatlands, within the grass-moss tundra which covers shallow bedrock slopes, in small stream valleys with variable vegetation types (a mixed type, birch forest, moss tundra), and at forested sites within fluvial terraces of the Nadym River.

Methods

Technogenic impact causes additional spatial and time variability of the complex multicomponent system of permafrost conditions. In the course of railway construction, this variability takes place mainly through the change in thermal exchange at the ground surface due to the erection of embankments of various heights.

Calculations of the change in the ground thermal regime were completed with the Teplo (Warmth) software developed by Professor L.N. Khrustalev and his solution of the non-steady thermal conductivity problem with regard to Stephan’s condition and a moving phase boundary. The climatic trend is assumed on the basis of the Salekhard weather station data analysis: the mean annual air temperature increase by 0.04°C per annum (Pavlov & Malkova 2005). Redistribution of the snow cover along the embankment slopes was also taken into account. The prevailing southwestern winds during winter lead to the increase of the snow accumulation at the leeward (northern) side of the embankment.

The data on ground temperature change was obtained

Table 3. Study sites.

No	Type of natural territorial complex	Sediments		Vegetation	% of the total route length
		Origin (unit)	Composition		
1	Watersheds	m,gmIIsh	Clayey silt	shrub tundra	2.4
2	Shallow bedrock slope highly dissected by erosion (ravines, gullies, river and creek valleys)	mIIIkz, g,mIIIzr	Silty fine sand, clayey silt	middle-density and middle-size birch forest	29.8
3	Floodplain of the Poluy River, widespread peatlands	aIV, bIV, laIII-IV	peat, clayey silt, sand	grass-moss tundra	3.1

for three study sites with the calculation interval of 10, 20, and 30 years. The climatic parameters for all profiles were obtained from the Salekhard weather station.

The study sites were selected based on the ratio between the length of the natural territorial complex traversed by the railway and the total length of the railway. These sites are located at different geomorphic levels (i.e., from watersheds being the highest to floodplains being the lowest). The presence of permafrost within a natural territorial complex was a criterion of a study site selection (Table 3).

Description of the Study Sites

Study Site No. 1 is located within the Poluy River and the Yarudey River watershed. The ground temperature profile is shown in Figure 2. The vegetative community is represented by the shrub tundra. These landscape-permafrost conditions are observed within 3% of the railway. The fact that the railway does not cross the sediments of this age anywhere else and that it is the most elevated area is a unique feature of this site.

Study Site No. 2 is located on the shallow bedrock slope (near the edge of the Poluy River valley) and is heavily dissected by erosion with numerous ravines, gullies, and creek and river valleys. Birch forest is the most widespread vegetation type at the site (29.8%). Temperature distribution with depth is similar to Site No. 1 (Fig. 2).

Study Site No. 3 is located on the Poluy River floodplain, which is covered by expansive muskegs. The vegetative community of the site is the grass-moss tundra. The ground temperature was measured on Oct. 6, 2008 (Fig. 2). The railway route crosses the floodplain several times.

Results

The forecast of ground temperature regime was completed for the proposed railway route, which will be closely parallel to the existing abandoned railway (i.e., the so-called “dead road”).

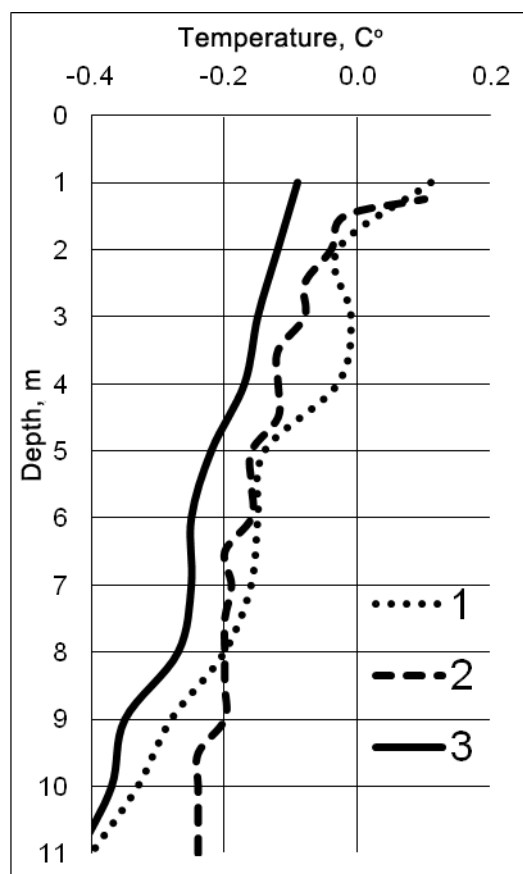


Figure 2. Temperature measurements at three study sites (Site No.1, measurement date April 30, 2008; Site No.2, Sept. 18, 2008; Site No.3, Oct. 6, 2008).

The present state of the “dead road” allows us to evaluate challenges associated with the railway operation in this region. It should be noted that not everything that happened to the railway bed, the rail-sleeper grating and the drainage control structures, should be expected to apply to the proposed railway construction, since the “dead road” embankment was not always raised to the design elevation, and the “dead road” was never operational.

The “dead road” condition was described by Lengiprotrans OJSC in 2008.

The main processes associated with the deformation (or complete failure) of the railway bed involve drainage control structures, water diversion, surface differential settlement and subsidence, embankment erosion features, earthflows, etc.

The following two types of surface instability can be identified in the study area: first, differential settlement (or subsidence), which results in abrupt change in the surface morphology; and second, uniform settlement of the railway bed. These two types developed almost everywhere along the railway. They are a dominant process among other geohazardous processes (erosion, earthflow, etc.).

The most recent site investigations along the railway showed that differential settlement/subsidence or uniform settlement developed within every section of the “dead road” of more than 500 m in length.

Most of the sites characterized by uniform settlement of the railway bed are observed in areas underlain by permafrost. The railway bed study showed that along railway sections where the embankment height exceeds 2

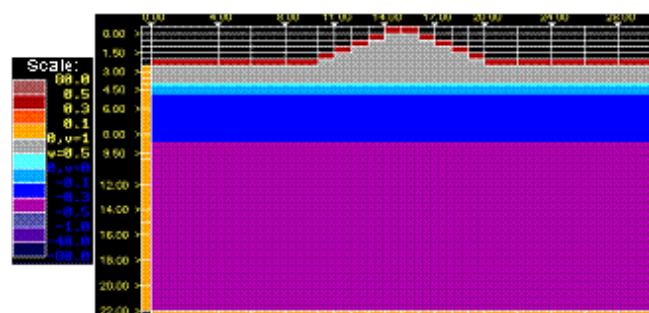


Figure 3. Initial temperature field distribution (measurement date April 30, 2008).

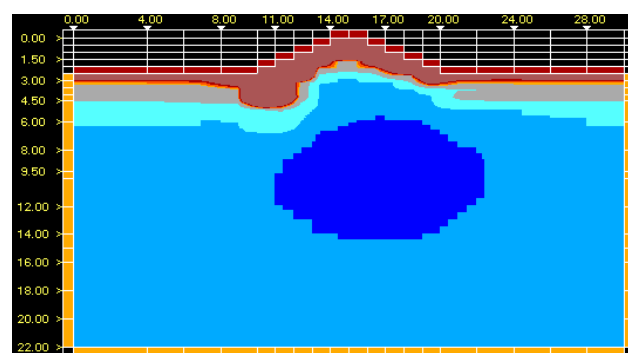


Figure 4. Ground temperature distribution 10 years after the embankment construction (as of October 1 when the thaw depth is maximum).

m (there are almost no such sites left today) the permafrost thermal regime is practically stable. This is not observed in lower embankments. These conditions are associated with various processes occurring in or near the embankment, such as different extent of snow accumulation and cycles of freezing-thawing.

The uniform settlement of the railway bed is observed in all natural territorial complexes, but it is the most widespread within peatlands.

Differential settlement (or subsidence) of the ground surface occurs locally within sites underlain by thawing ice-rich permafrost.

Washout and complete failure of the embankment occurs mainly in the zones where the route goes along floodplains of the large rivers (Poluy and Yarudey). This does not occur within floodplains of small streams.

Almost all railway bed and facility deformations are associated with the decline of the bearing capacity of the foundation soils, which, in turn, occurs due to the change in ground temperature regime.

Study Site No. 1. Permafrost along Profile 1 is “warm”; the ground temperature does not exceed -0.5°C and, thus, permafrost there is the most unstable.

The following assumptions were made for computer simulation purposes along this profile: the embankment height is 1.99 m and the fill used for the embankment construction was thawed (Fig. 3). According to the computation results, a noticeable increase in ground temperature by $0.2\text{--}0.3^{\circ}\text{C}$ is expected throughout the territory in 10 years. Permafrost will become even more unstable. The ground temperature will be -0.1°C along most of the profile length. The coldest

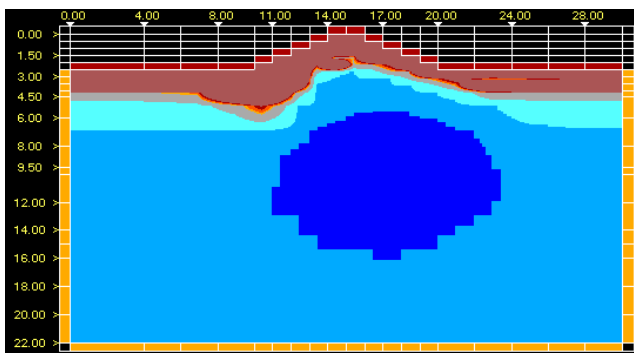


Figure 5. Ground temperature distribution 30 years after embankment construction (as of October 1 when the thaw depth is maximum).

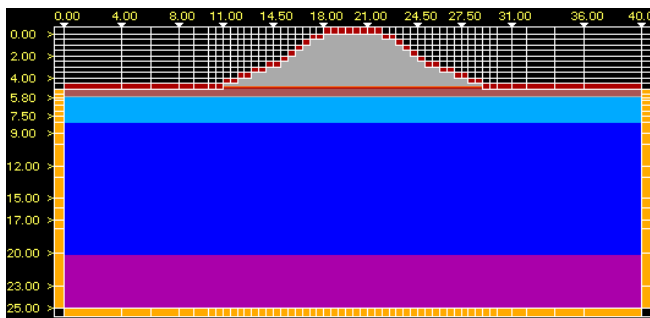


Figure 6. Initial temperature field distribution (temperature measurement date Sept. 18, 2008).

zone will be located at some depth under the embankment. Its temperature will be -0.1 to -0.3°C . A thaw bulb associated with the warming effect of snow cover will develop from the northern side (the left side of the profile).

Similar conditions will be observed 20 years later; however, the core with the lowest temperatures under the embankment will slightly increase in size. This is associated with the cooling effect of the railway bed because it is the railway bed, not the ground, where all positive heat transfer occurs. The thaw bulb at the left side will increase.

In the 30th year after embankment construction, the ground temperature will remain close to 0°C (Fig. 5). The thawing trends will continue on both sides. The colder core will begin to decrease in size due to the temperature increase in the overlying layers.

On the whole, it is possible to say that with this trend of climate change, permafrost within the natural territorial complexes of this type will degrade completely in the coming several decades. The bearing capacity of the ground will decrease several times, which will adversely influence operation of the railway bed.

Study Site No. 2. This study site differs from other study sites in the vertical distribution of ground temperatures. At Study Site No. 2, ground temperature colder than -0.2°C is found only below the depth of 6 m (Fig. 6). Ground temperatures were measured in boreholes at different times (April 30, 2008 and Sept. 18, 2008). The ground temperatures at the depth of zero annual amplitude (10 m) are higher than those at Study Site No. 1. The embankment height at this site is 5.13 m, as per the design. A colder zone will develop below the embankment (with ground temperature colder than -0.5°C , Fig. 7) ten years after the

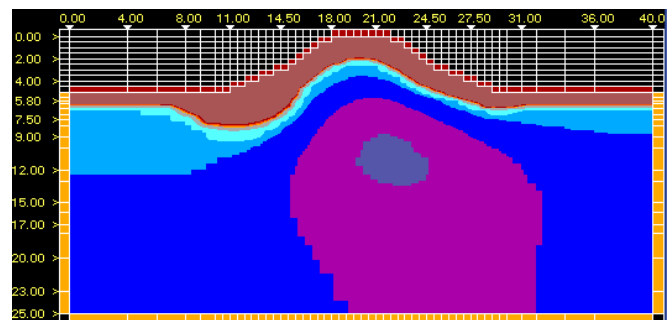


Figure 7. Ground temperature distribution 10 years after the embankment erection (as of October 1 when thaw depth is maximum).

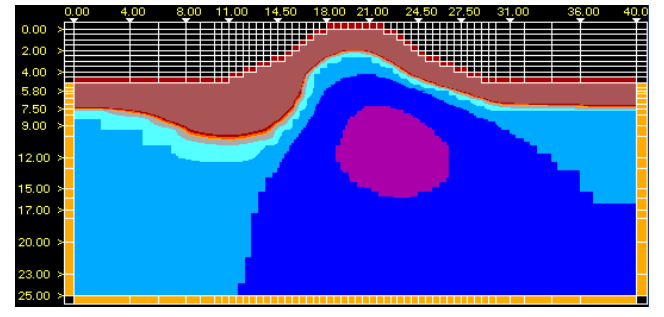


Figure 8. Ground temperature distribution 30 years after the embankment erection (October 1 when thaw depth is maximum).

embankment construction, similar to Study Site No. 1.

The embankment fill will freeze to a depth of approximately 7 m, and this condition will remain even until October 1 when the thaw depth is at its maximum. This will have a generally positive effect on the stability of the embankment foundation. The ground temperature at a depth below 15 m will increase by several tenths of a degree. A thaw bulb will develop at the northern slope and it will be larger in size. This is associated with the composition of sediments (very fine silty sand, and in the first case the soil consists of clayey silt). An unfavorable trend of general temperature increase will be observed after 20 years. The zone under the embankment will decrease significantly, and thawing will intensify on the slopes. The “heat” wave will reach the depth of 20 m (0.1°C instead of -0.3 ... -0.4°C observed initially). Ground warming will continue in the same way also into the 30th year of operation. Thawing will exceed 5 m on the left slope (Fig. 8).

It should be noted that in the case of the higher embankment (Study Site No. 2) the warming will occur more slowly than in the case of the lower embankment (Study Site No. 1).

Study Site No. 3. This site is the coldest. It is the only site with ground temperature lower than -0.4°C . It is composed of clayey silt underlain by fine-grained sand of approximately 8 m in thickness. At the end of the fall of 2008 (Sept. 19, 2008), the active layer was 2.7 m thick (Fig. 9). The ground temperature at the depth of zero annual amplitude was -0.3°C . The embankment height was 2.81 m, as per the design.

A general increase in ground temperature up to -0.1°C will be observed ten years after the beginning of the railway operation (Fig. 10). The active layer on the left embankment

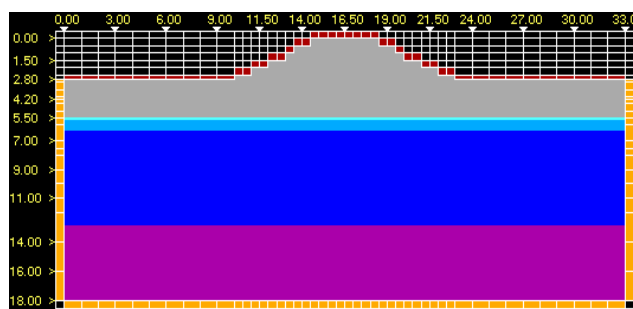


Figure 9. Initial temperature field distribution (temperature measurement date Sept. 18, 2008).

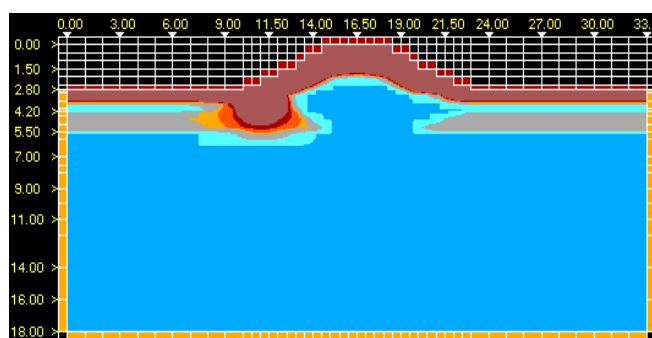


Figure 10. Ground temperature distribution 10 years after the embankment erection (as of October 1 when thaw depth is maximum).

slope is more than 3 m thick. As at the other study sites, the temperature decrease to 0.1°C will be noted under the embankment centerline. Permafrost is very unstable.

Twenty years later, a significant core of cooling will develop under the embankment, with the temperature in the center lower than -0.5°C . The temperature along most of the section decreased as well. It can be stated that favorable conditions for the strengthening of the soil foundation soil (lowering of ground temperature) emerge at this embankment height. Thirty years later, the trend of ground cooling under the railway bed will continue. The thaw bulb will spread out outside the embankment (Fig. 11).

In conclusion, it can be noted that permafrost will strengthen only at Study Site No. 3. This is associated with the lithology and the height of the embankment. An unfavorable situation will develop at Study Site No. 1, where permafrost degradation will occur despite the fact that this site is underlain by clayey silt. Study Site No. 2 will have a trend identical to the trend at Study Site No. 1 after 30 years. The difference occurs because Study Site No. 2 is composed of coarser sediments (sand), which intensifies thawing, but the embankment height (more than 5 m) is favorable for producing additional ground cooling.

Conclusions

The proposed railway crosses five natural territorial complex types: watersheds, shallow bedrock slopes, fluvial terraces, major river floodplains, and small stream valleys. Permafrost (mainly “warm”) is found in the form of patches along the railway route. Permafrost within the first natural territorial complex type occurs in peatland on the watershed and within the adjacent shrub tundra. Permafrost was

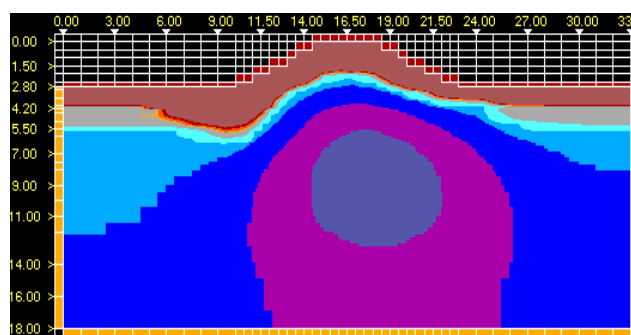


Figure 11. Ground temperature distribution 30 years after the embankment erection (as of October 1 when thaw depth is maximum).

encountered within the high floodplain of the Poluy River under the sparse larch-birch forest and grass-moss (moss) tundra. Permafrost is also found in peatlands and grass-moss tundra within the shallow bedrock slopes and in the small stream valleys with variable vegetation types (mixed, birch forest, moss tundra), and within the fluvial terrace of the Nadym River underlying forested areas.

The dire condition of the existing railway bed is mainly associated with thaw flow processes and destructive action of floodwaters. However, the most hazardous process is the ubiquitous railway bed settlement and subsidence. There are various mechanisms for the instability of the railway bed surface. Gradual uniform settlement and abrupt differential settlement, or subsidence, of the railway bed surface are observed along the railway route. The latter developed at sites with failed water drainage facilities (culverts, etc.).

The ground temperature regime forecast showed an increase in the active layer depth near the embankment slopes, which is associated with the increased thickness of the snow cover (from the southern side) and, consequently, with the warming effect the snow has on ground temperatures. The embankment height is also an important factor determining the ground temperature regime in the future. A general increase in ground temperatures occurs in the low-height embankments (2 m, Study Site No. 1). In higher embankments (5 m high at Study Site No. 2), permafrost strengthens during the first ten years of the railway operation. However, warming of the embankment begins after 10 years due to the fact that the ground is fine-grained and the cold core under the embankment thaws as a result of the increase in the active layer depth on the embankment slopes. Study Site No. 3 with the embankment height of 2.7 m is characterized by the most favorable conditions for permafrost strengthening.

In conclusion, considering the complexity of the permafrost terrain conditions, it is necessary to carry out special initial measures for thawing and compaction of patches of the warm perennally frozen soils, as well as additional cooling of the embankment base in places where permafrost preservation is assumed. This significantly complicates railway construction and operation.

Acknowledgments

This work is based on the generalization of available published materials for the study area and reports by

Lengiprotrans OJSC provided by S.N. Titkov of the Production and Scientific-Research Institute for Engineering Research in Construction and V.I. Voytsekhovskaya, the chief specialist of the Engineering Geology Department of Lengiprotrans OJSC. It is also based on Internet sources and quantitative calculation methods using Teplo software.

The author would like to thank the faculty of the Cryolithology and Glaciology Department, including V.I. Grebents, for his assistance, S.N. Titkov, and V.I. Voitsekhovskaya for the materials provided.

References

- Construction norms and regulations. Construction climatology. SNiP 23.01-99. 2000, 68 pp.
- Gvozdetskiy, N.A. & Mikhailov, N.I. 1978. *Physical Geography of the USSR. Asian part*. Moscow, Mysl, , 572 pp.
- Pavlov, A.V. & Malkova, G.V. 2009. Small-scale mapping of modern ground temperature change trends in the north of Russia. *Kriosfera Zemli* 13 (no 4): 32–39.
- Trofimov, V.T., Baulin, V.V., & Vasilchuk, Yu. K. 1989. Geocryological zoning of the West-Siberian platform. In *Geocryology of the USSR Western Siberia* / Moscow, Nedra, pp. 159-162.
- Trofimov, V.T. & Kashperiyuk, P.I. 1989. Orography, in *Geocryology of the USSR Western Siberia*. Moscow, Nedra, pp. 38-40.

Cryogenic Deformations in the Late Cenozoic Deposits of the Tunka Depression in the Baikal Rift Zone

S.V. Alekseev, L.P. Alekseeva, A.M. Kononov
Institute of the Earth's Crust, SB RAS, Irkutsk, Russia

Abstract

Sections of the late Cenozoic alluvial deposits, which were exposed in the slope faces of fluvial terraces in the Tunka depression, are presented. Deformations in layered sediments and topsoil layers are characterized. The cryogenic mechanism of the development of the deformation structures in unconsolidated sediments is substantiated based on analysis of well-known publications and results of our own field studies.

Keywords: cryoturbations; deformation structures; freeze-thaw cycles; frost heave; involutions; Tunka depression.

Introduction

The problem of the development of deformation structures in unconsolidated sediments attracts the attention of specialists in various fields. Development of involutions can be caused by various processes. One of the possible mechanisms of their formation is a cryogenic one (Artyushkov 1965, Kostyaev, 1965, Dylík & Maarleveld 1967, Romanovskiy 1977, Shilts 1978, Washburn 1988, Dijkmans 1989, Ershov 1990, Vandenberghe 1992, Hinkel 1993, Murton & French 1993, French 2007, Fundamentals of Geocryology 1996, Paik & Lee 1998; Swanson et al. 1999, Harris et al. 2000, Melnikov & Spesivtsev 2000, Murton et al. 2000, Murton & Bateman 2007, French & Demitroff 2001, French et al. 2003, Lemcke 2001, Lemcke & Nelson 2004, Van Vliet-Lanoë 1991, Van Vliet-Lanoë et al. 2004, Ghysels et al. 2006, Dillon & Sorenson 2007, Kovács et al. 2007, Ogino et al. 2007, Ewertowski 2009, French et al. 2009 et al.). According to these publications, permafrost and cold climate are the most important conditions for the formation of involutions in periglacial regions. The most important mechanisms of the unconsolidated sediment deformation include differential frost heave, varying freezing rates of saturated soils, cryohydrostatic pressure, multiple recurrence of freeze-thaw cycles, and a set of other factors including flat topography, soils prone to frost heave, layers of higher density above layers of lower density, water saturation of soils during autumn freeze-thaw period, and lack of snow and vegetation covers.

The authors of this paper studied cryogenic deformations in the Late Cenozoic unconsolidated deposits exposed in the Tunka depression in the Baikal rift zone and propose possible mechanisms of their formation.

Study Area

The Tunka depression is one of the intermountain basins of the Baikal type that are part of the Baikal rift zone and are infilled with a thick layer of Cenozoic deposits. Its maximum width is slightly more than 30 km and its length is up to 60 km. Elevations of the depression bottom at the edge of Irkut River, which longitudinally crosses the depression from west to east, are 700–780 m. All the depressions of the Tunka rift are filled with a thick layer (more than 2.5 km) of Cenozoic volcanogenic sedimentary deposits. Late

Cenozoic sedimentation occurred during the period of active tectonic movements (rise of mountain ranges and sinking of depressions) as well as global climate changes (Logachev 1958).

The Pleistocene-Holocene cryogenic epoch (1.9 to 2.0 million years ago) was characterized by severe climate (cryochrons) and a relatively warm climate (termochrons). A characteristic feature of the epoch is a multiple recurrence of long-term permafrost aggradation and permafrost degradation. This is most evident in the structures of the Southern geocryological zone. The most important factor of the Pleistocene history of the Tunka rift was its mountain glaciation. In the Late Pleistocene, many glaciers of the Tunka range advanced down to the foothills and formed terminal moraine complexes and various glacial landforms.

The thickness of the Tunka depression Quaternary deposits is approximately 500 m. The deposits consist of alluvial, delluvial, glacial, fluvio-glacial, eolian, and to a less extent lacustrine formations. All Quaternary deposits are divided into three lithological complexes: cobble and pebble (proluvium), sand (alluvium and eolian deposits), and surface loess (subaerial sandy silt and clayey silt and clayey silt and clay formations with varying silt content). Deformation structures are confined to the surface complex deposits forming the upper parts of fluvial terraces.

Permafrost distribution within the depression is sporadic (Fig. 1). Permafrost is found locally within bogs, floodplains, and lower terraces composed of sand and silt, clayey silt, and within peatlands. Permafrost is up to 40 m thick. The permafrost table is rarely found at a depth lower

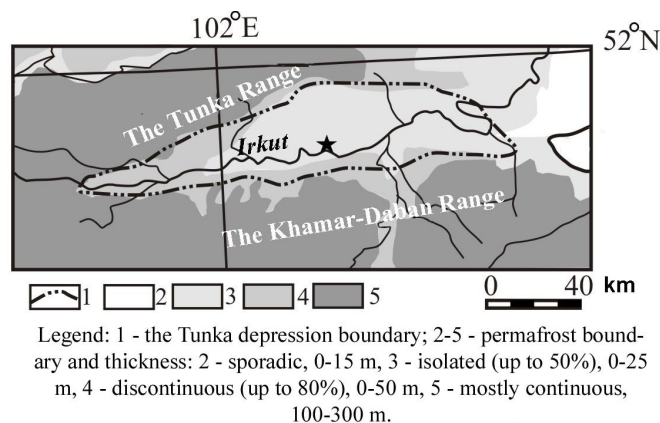


Figure 1. Permafrost distribution map for the Tunka depression and the surrounding mountains (asterisk - the studied section locations).

than 20 m depth. The permafrost temperature is high: from -0.2 to -1°C. Active layer depth is 0.8–1.5 m in peatlands and 2.5–3.0 m in sandy and clayey soils. Seasonal freezing layer depth is up to 1 m. The permafrost ice content is high, since the volumetric water content is 25–40% (Leshchikov, 1978). The thickness of the ground temperature annual fluctuations layer does not exceed 8–10 m. In the active layer, the temperature gradient reaches 5°C per 1 m, which is favorable for soil frost cracking development when combined with shallow snow thickness.

Permafrost-related processes and landforms are widespread. They include frost heave mounds up to 1.5 m high, frost cracking, thermokarst, icing formation, and patterned ground.

Results and Discussion

Cryogenic deformations of various forms were recognized in the reference sections. Classic vein structures were exposed in the Irkut River terrace slope (Fig. 2 a, b). The veins consist

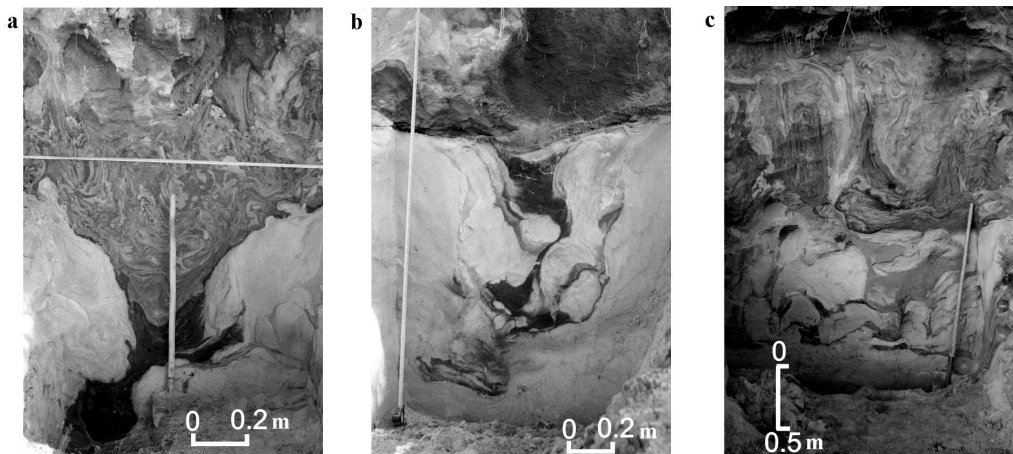
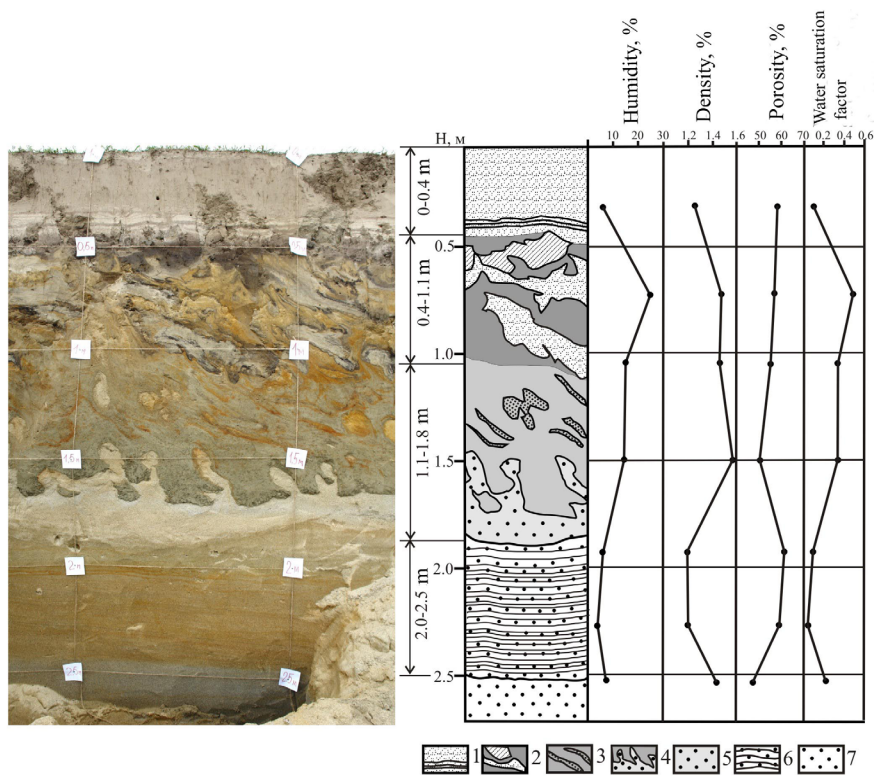


Figure 2. Cryogenic deformations (left bank of the Irkut River): a and b – pseudomorphs of ice wedges, c – cryoturbations.



Legend: 1 - gray very fine sand, at the bottom – fissile light-gray sand, does not roll; 2 - mostly yellow coarse-silt sand with light-gray fine sand and buried soil bands; 3 - mostly greenish-gray very fine sand with numerous ochreous coarse-silt sand cross-beds; 4 - drop-shaped deformations: light-gray coarse sand from the bottom horizon penetrated up into greenish-gray silt sand; 5 - light-gray coarse sand; 6 - horizontally bedded yellow medium-coarse sand; 7 - bluish-gray medium-coarse sand.

Figure 3. Deformations in the alluvial deposits of the Irkut River (right bank slope near Nugan village). On the right is a schematic section with the physical properties characteristics of soils at various depths.

of gray clayey silt with an admixture of oxidized clayey silt, fine sand, and sometimes clay and clayey silt. In the lower and middle parts of the veins there is a large amount of black soil indicative of increased content of organic material. Enclosing sediments include light gray, bedded medium, and coarse fluvial sands which are sometimes ferruginized. These are clear signs that make it possible to qualify these formations as pseudomorphs after ice wedges were found: vein shaped (wedge shaped in this case); traces of overlying deposits collapse into the cavity left by the melting of the wedge ice; deformation of the enclosing sediments at the joint with the vein bodies; presence of air bubbles (which indicates the melting of segregation ice inclusions); and section structural particularities—occurrence of denser sediments (silty sandy loams and clayey silty loams) over the less dense ones (sands).

As a rule, in the upper part (0.5–1.5 m) of the studied sections, 1–1.2 m thick cryoturbated horizons are clearly visible (Fig. 2c). The chaotic and incoherent movement of ground-mass produced by cycles of freeze-thaw resulted in the formation of strata where fine light yellow and yellow sands of varying grain size, gray plastic clayey silts, peat mixed with mineral soil, often with detritus admixtures, buried soil, and thin layers of clayey silts were crumpled and folded.

The structure of the section exposed in the Irkut River terrace slope near the Nugan village is of particular interest (Fig. 3).

The section consists of three parts. The top overlying bench (0–0.4 m) is composed of gray, fine-grained sands. In the bottom bench there are thin layers of lighter sand. The bottom deposits are not flexible and not disturbed. The horizon, which is second from the top, is intensely deformed to the depth of 1.8 m by multiple freeze-thaw processes. It is composed of sands. The upper part is composed mostly of coarse yellow sands with numerous pockets of either fine light gray sand or dark buried soil. The lower part is composed of very fine, greenish gray sand with narrow oblique streaks of yellow (ochreous) coarse sand. The small difference of density, porosity, particle size distribution of deposits (Fig. 4), and special variations in vegetation on the surface predetermined the differential frost heave of these heterogeneous deposits. In more water-

logged interbeds enriched in fine fraction, the processes of ice segregation and frost heave lead to the evolution of active cryoturbation formation.

At the very bottom of the second horizon at the depth of 1.4 m from the surface, drop-shaped and wrinkled folds 30–40 cm thick were found. The joint pattern is very clear because of the difference in the color of sediments. The formation of such a wave-like surface between the upper layer of fine sand and the bottom layer of coarse sand occurred during the bottom deposits multiple freeze-thaw as a result of thawed soil plastic flow due to varying density and moisture content. The gray coarse sand when exposed to subzero temperature froze faster than water-logged and denser overlying greenish gray fine sand that is enriched in fine fraction. The emerging segregation ice resulted in heaving the bottom layer sand into the upper layer, which had not yet frozen. The process resulted in the formation of drop-shaped structures. The heave process intensified because of the density inversion; since the sands in the upper layer are heavier than those of the bottom layer, they were heaving the bottom layer sands up and attempting to take their place. While the subsequent thawing caused the plastic movement of thawed soil, the wave-like surface formation continued.

The physical nature of numerous folds formation (convective instability deformations) in the Quaternary and older deposits was already discovered in the 1960s (Artyushkov 1965, Kostyaev 1965). Experimentally, the possibility of such an insolation-like deformations-forming mechanism was proved in the course of ice-saturated permafrost thaw simulation (Harris et al. 2000) as well as in the course of laboratory simulations of periglacial involutions generated by the annual freeze-thaw of the layered soils with reverse density (Ogino and Matsuoka 2007).

The third, lower part of the section penetrated to the depth of 2.7 m. It is composed of horizontally stratified undeformed yellow and bluish-gray, washed coarse sands without organic matter, which indicates a stable sedimentation process and the absence of adverse external influence.

Thus we can say with confidence that the active layer thickness at this part of the Irkut River valley did not exceed 1.8 m, at least during the Holocene.

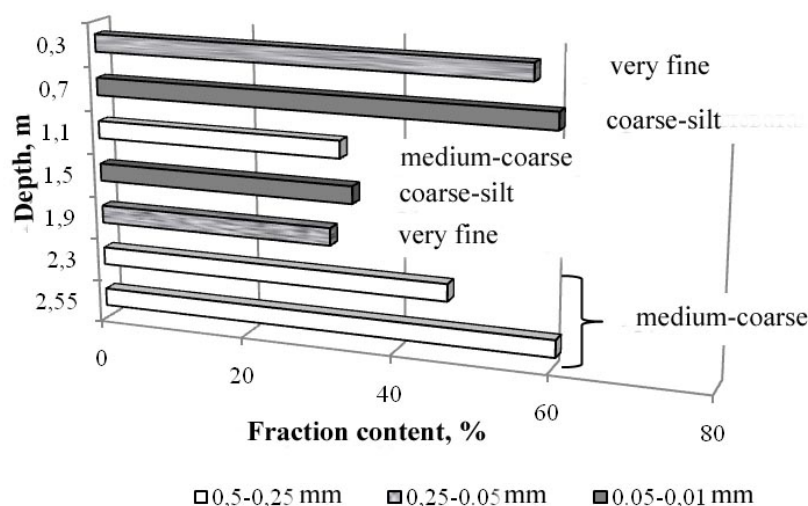


Figure 4. Distribution of soil fractions in the section exposed in the right bank slope of the Irkut River near Nugan village.

Conclusions

Since the Tunka depression is located in the sporadic permafrost area and the upper part of the geological section is subject to periodic impact of the freeze-thaw processes, an unambiguous conclusion about the cryogenic origin of deformation structures in the Irkut River can be made. The presence of cryoturbation groundmass approximately to the depth of 1.8 m signifies the influence of temperature changes resulting in the plastic deformation of the deposits. The freezing of the section caused segregative ice formation and bottom deposit heave. During the thawing of the deposits, the sedimentary displacement and mixing of the material continued. The lack of deformation pattern homogeneity in the upper (chaotic pattern) and the bottom (clear, drop-shaped pattern) parts of the cryoturbation horizon is most likely to be caused by the differences in the physical properties of the sediments (moisture, facies composition, plasticity, and density) as well as temperature conditions of the seasonally frozen soils and permafrost.

It should be noted that the convective deformations in loose deposits are widespread outside the permafrost area as well. The nature of the deformations is largely determined by the general history of the evolution of geological structures. For example, high seismic activity of the Tunka depression (the estimated magnitude of paleo-events often reaches values of 6.5 and higher) can result in the superposition of loose deposit deformations caused by earthquakes and multiple freeze-thaw processes. In this regard, the development of criteria to unambiguously determine the nature of cryogenic or other deformations is essential for paleogeographic, paleoclimatic, paleogeocryological, and paleogeoseismological reconstructions.

Acknowledgments

The authors are grateful to the group of tectonic physicists who took part in the cooperative field works and discussions on the results: A.S. Gladkov (Ph.D.), O.V. Lunina, (Ph.D.), and A.V. Andreev (Ph.D. student).

References

- Artyushkov, E.V. 1965. Convective deformations formation in poorly lithified sedimentary rocks. *Izv. AN SSSR, ser. geol.* 12: 79-101.
- Kostyaev, A.G. 1965. On differences in permafrost and convective (diagenetic) structures in Quaternary sediments. *Ground ice* - Moscow, izd-vo MGU, 2: 159-171.
- Leshchikov, F.N. 1978. Permafrost in Angara and the Baikal region. Novosibirsk, Nauka, 141 pp.
- Logachev, N.A. 1958. Cenozoic continental deposits of the Baikal type depressions. *Izv. AN SSSR, seriya geol.*, pp. 18-29.
- Melnikov, V.P. & Spesivtsev, V.I. 2000. Cryogenic formations in the Earth lithosphere (graphic version). Novosibirsk: NITs OIGGM SO RAN, izd-vo SO RAN, 343 pp.
- Fundamentals of Geocryology. Part 2. *Lithogenetic geocryology 1996*. Under the editorship of E.D. Ershov, Moscow, izd-vo MGU, 339 pp.
- French, H.M., Demitroff, M., Streletskiy, D.A., Forman, S.L., Godzik, Ya., Konishchev, V.N., Rogov, V.V., & Lebedeva-Verba, M.P. 2009. Late Pleistocene permafrost occurrence in Pine Barrens in southern New Jersey in the USA. *Cryosphere of the Earth XIII*, 3: 17-28.
- Dijkmans, J.W.A. 1989. Frost wedges in an eolian sand sheet near Søndre Strømfjord, W. Greenland and their paleoenvironmental implications. *Zeitschrift für Geomorphologie N.F.* 33: 339-353.
- Dillon, J.S. & Sorenson, C.J. 2007. Relict Cryopedogenic Features in Soils with Secondary Carbonate Horizons, Western Wyoming, USA. *Permafrost and Periglac. Process.* 18: 285-299.
- Dylik, J. & Maarleveld, G.C. 1967. Frost cracks, frost fissures and related polygons: a summary of the literature of the past decade. *Mededelingen van de Geologische Stichting, Nieuwe Serie* 18: 7-21.
- Ewertowski, M. 2009. Ice-wedge Pseudomorphs and Frost-cracking Structures in Sediments, Central-West Poland Weichselian. *Permafrost and Periglac. Process.* 20: 316-330.
- French, H.M. 2007. *The Periglacial Environment* (3rd ed). John Wiley & Sons Ltd, England.
- French, H.M. & Demitroff, M. 2001. Cold-climate origin of the enclosed depressions and wetlands ('spungs') of the Pine Barrens, southern New Jersey, USA. *Permafrost and Periglac. Process.* 12: 337-350.
- French, H.M., Demitroff, M., & Forman, S.L. 2003. Evidence for Late-Pleistocene permafrost in the New Jersey Pine Barrens (latitude 39°N), Eastern USA. *Permafrost and Periglac. Process.* 14: 259-274.
- Ghysels, G. & Heyse, I. 2006. Composite-wedge Pseudomorphs in Flanders, Belgium. *Permafrost and Periglac. Process.* 17: 145-161.
- Harris, C., Murton, J.B. & Davies, M.C.R. 2000. Soft-sediment deformation during thawing of ice-rich soils: results of scaled centrifuge modelling experiments. *Sedimentology* 47: 687-700.
- Hinkel, K.M. 1993. Are soil tongues in northeastern Indiana periglacial relics or active fingering zones? *Quaternary Research* 39: 75-83.
- Kovács, J., Fábíán, S.Á., Schweitzer, F., & Varga, G. 2007. A Relict Sand-wedge Polygon Site in North-central Hungary. *Permafrost and Periglac. Process.* 18: 379-384.
- Lemcke, M.D. 2001. *The Origin and Paleoclimatic Significance of Sediment-Filled Wedges in Northern Delaware*. University of Delaware: Newark, Delaware, 142 pp.
- Lemcke, M.D. & Nelson, F.E. 2004. Cryogenic Sediment-Filled Wedges, Northern Delaware, USA. *Permafrost and Periglac. Process.* 15: 319-326.
- Murton, J.B. & French, H.M. 1993. Thermokarst involutions, Summer Island, Pleistocene Mackenzie Delta, western Canadian Arctic. *Permafrost and Periglac. Process.* 4: 217-229.
- Murton, J.B., Worsley, P., & Gozdzik, J. 2000. Sand veins and wedges in cold aeolian environments. *Quaternary Science Reviews* 19: 899-922.
- Murton, J.B. & Bateman, M.D. 2007. Syngenetic Sand

- Veins and Anti-Syngenetic Sand Wedges, Tuktoyaktuk Coastlands, Western Arctic Canada. *Permafrost and Periglac. Process.* 18: 33-47.
- Ogino, Y. & Matsuoka, N. 2007. Involutions Resulting from Annual Freeze–Thaw Cycles: a Laboratory Simulation Based on Observations in Northeastern Japan. *Permafrost and Periglac. Process.* 18: 323-335.
- Paik, I.S. & Lee, Y.I. 1998. Desiccation cracks in vertic paleosols of the Cretaceous Hasandong Formation, Korea: genesis and paleoenvironment. *Sedimentary Geology* 119: 161-179.
- Shilts, W.W. 1978. Nature and genesis of mudboils, central Keewatin, Canada. *Canadian Journal of Earth Sciences* 15(7), 1053-1068.
- Swanson, D.K., Ping, C-L., & Michaelson, G.J. 1999. Diapirism in Soils due to Thaw of Ice-Rich Material near the Permafrost Table. *Permafrost and Periglac. Process.* 10: 349-367.
- Van Vliet-Lanoë, B. 1991. Differential frost heave, load casting and convection: converging mechanisms, a discussion of the origin of cryoturbations. *Permafrost and Periglac. Process.* 2: 123-139.
- Van Vliet-Lanoë, B., Magyari, A., & Meilliez, F. 2004. Distinguishing between tectonic and periglacial deformations of quaternary continental deposits in Europe. *Global and Planetary Change* 43: 103-127.
- Vandenbergh, J. 1992. Cryoturbations: a sediment structural analysis. *Permafrost and Periglac. Process.* 3: 343-352.
- Walters, J.C. 1978. Polygonal patterned ground in central New Jersey. *Quaternary Research* 10: 42-54.
- Washburn, A.L. 1988. World of cold. *Geocryological researches*. Moscow, Progress, 384 pp.

Mercury Content from the Tunguska Meteorite Craters and in Some Siberian Towns

V.A. Alekseev^{1,2}, N.G. Alekseeva^{1,2}, L.N. Luchsheva^{1,2}, V.V. Kopeykin^{1,2}, L.G. Pelehan^{1,2}, V.A. Rukavishnikov^{3,4},
V.A. Chechin^{3,4}, V.V. Krivulin⁵

¹Troitsk Institute for Innovation and Fusion Research (TRINITI), Troitsk, Moscow Region, Russia

²Pushkov Institute of Terrestrial Magnetism, Ionosphere and Radio Wave Propagation (IZMIRAN), Troitsk, Moscow Region, Russia

³Vavilov Institute for the History of Science and Technology of the RAN

⁴Lebedev Physical Institute, Moscow, Russia

⁵Joint Stock Company "Conversion & Dwelling"

Abstract

This paper presents the results of research into mercury concentrations in the samples taken from three craters located in the explosion epicenter of the Tunguska meteorite. In 2009 and 2010, several expeditions were conducted using ground-penetrating radar to study the structures of 40 craters. Boreholes were drilled at seven craters. Mercury content in samples obtained during drilling was evaluated. Data on mercury content at natural sites of other regions of Siberia are provided for comparison.

Keywords: craters; geochemical anomaly; ground-penetrating radar; mercury; permafrost; thermokarst; Tunguska meteorite.

Introduction

In 1927, L.A. Kulik was the first to discover a huge blowdown of trees (Fig. 1) at the Stony Tunguska River and suggest that it was a result of the impact of an enormous meteorite (Kulik 1939).

The total area of the forest fall is about 2125 m². Numerous rounded craters were revealed near the radial center of the tree fall. Our research was conducted in the vicinity of the epicenter of the explosion between the Northern and the Southern swamp (Fig. 2). This is a wavy and swampy watershed surface covered with a coniferous forest and sparse forests. Craters of a complicated genesis occur in the swamps. Some scientists think that these craters are a result of permafrost thermokarst.

The research conducted by L.A. Kulik did not give the desired results (Kulik 1939, Krinov 1949), as the expedition did not have modern geophysical equipment. It is believed that the disturbance of the environment after the Tunguska meteorite explosion in the atmosphere activated regional thermokarst that could smooth out the impact on permafrost.

Later research shifted to the study of fine-dispersed fraction, and the examination of the Tunguska meteorite craters was discontinued (Vasilev 2004).

V.A. Alekseev supposed that fine-dispersed particles can be formed in microfractures of a comet as a result of the pressure growth arising when a comet enters the Earth's atmosphere (Alekseev 1998). These particles are located in tree resin and can be found, along with large elements, in impact craters.

The region of the paleo-volcano in the Tunguska meteorite explosion epicenter contains many volcanogenic structures the fractures of which serve as channels for the transfer of deep-deposited substance to the Earth's surface, especially during earthquakes (Alekseev, Alekseeva 2005). The geochemical anomaly in moss layers of 1908–1910 was reliably detected but its genesis was not determined.

Extraterrestrial substance can be accompanied by gases and aerosols—products of degassing of a deep-seated magma chamber. The 1908 impact of the explosion wave and of high temperature during the impact of the Tunguska meteorite caused short-lived vaporization of some volume of these products and their condensation on the surface and sublayer.

Our interest in mercury is based on the fact that we consider mercury to be an indicator of deep degassing of the Earth. Therefore, mercury will help to shed light on the genesis of craters. Mercury has different forms that are formed at high temperatures and represent their indicators. In our opinion, the analysis of mercury forms represents the

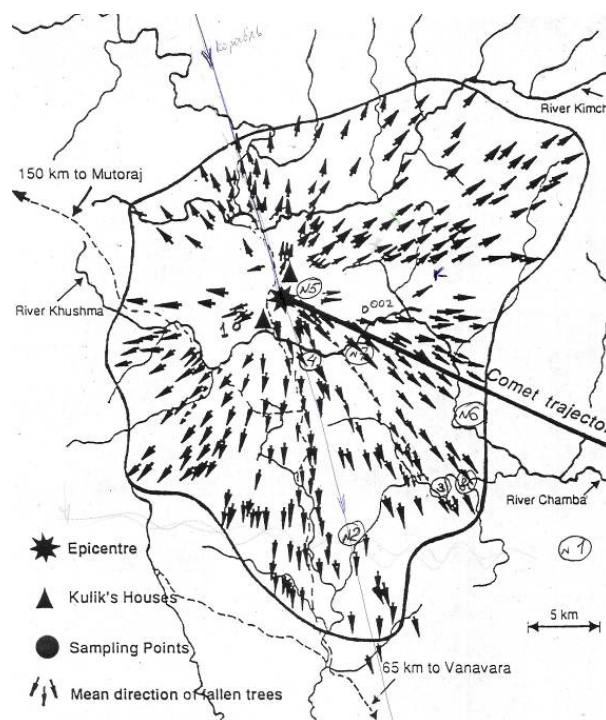


Figure 1. Map of forest blowdown.



Figure 2 Satellite image of the region of the Tunguska meteorite impact. The circle – Suslov's crater; the square – the First and the Second craters; the green color – taiga; the pinkish color – swamps and swampy sparse forests with thermokarst pits.



Figure 3. Appearance of Suslov's crater.



Figure 4. Appearance of the First crater.

most suitable method for studying the supposed location of the comet elements on the Earth and for studying the formation of craters resulting from the collision of the comet elements with the ground.

The average mercury content in soils of West Siberia is 20–30 ng/g with the range of fluctuations from 10 to 1500 ng/g. The Clarke for mercury in the Earth's crust is 30 ng/g, and its occupational exposure limit for soils is 2100 ng/g.

Anthropogenic contamination of the environment with mercury is characterized by similarly high mercury content (mainly in the sorbed form) over rather vast areas. Natural sources of mercury are found locally. They are characterized by a highly non-uniform distribution of mercury concentrations, and a significant amount of mercury is represented in high-temperature mineral forms.

Our research in the Gorny Altai region and in the Polar Urals showed a wide range of mercury values. There were field regions with very high mercury concentrations of up to 2–9 µg/g, but in general mercury was represented at background concentrations.

Objective

During the expeditions in July of 2009 and 2010, we studied the craters in the zone of the Tunguska meteorite impact (Alekseev et al. 2011). The internal structures of craters down to the depth of 20 m were examined with the "Losa" ground-penetrating radar. The craters selected as impact-generated preserved their form owing to permafrost and have a shape of a cone intersecting the swamp down



Figure 5. Appearance of the Second crater.

to the depth of about 15 m. After the explosion and the fall of the fragments that disturbed permafrost, thermokarst processes began.

About 40 craters were found and surveyed at the 2 km x 0.5 km site between the Northern and the Southern swamps. They were distinguished by abnormal morphology and the appearance of peat hills. According to our observations, the surface level inside the craters is generally lower by 1–4 m than that of the surrounding area. Craters were found in the forest and on mountain slopes.

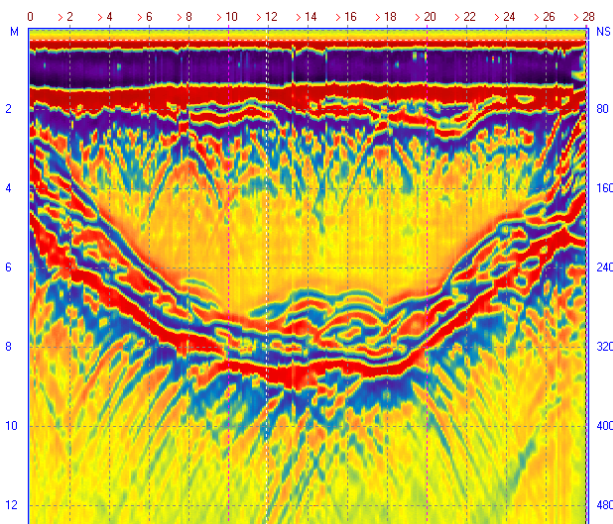


Figure 6. Radargram of Suslov's crater.

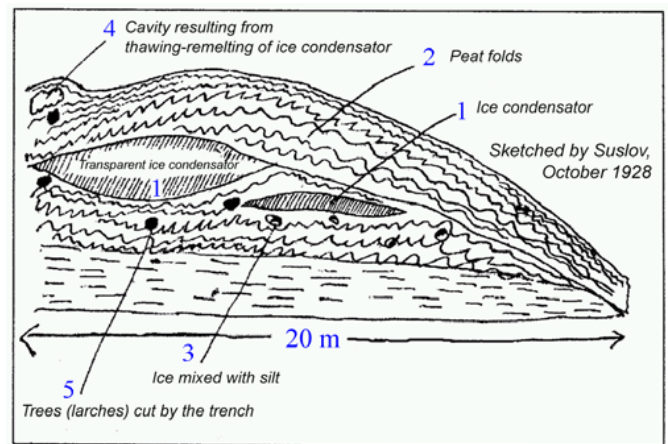
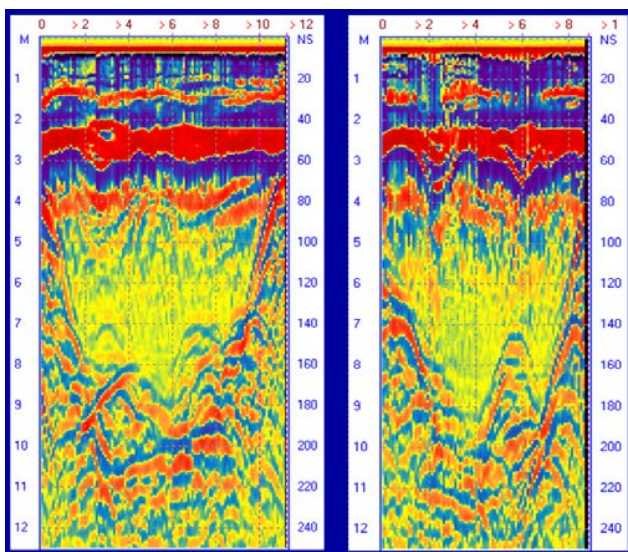


Figure 9. Suslov's sketch (October 1928) of the wall of the trench dug for water drainage out of Suslov's crater: 1 – ice body; 2 – peat folds; 3 – ice mixed with silt; 4 – cavity at the place of a thawed ice body; 5 – tree trunks cut by the trench (larch).



Figures 7 and 8. Radargrams of the First and the Second craters.

We analyzed the occurrence of mercury using the samples collected after drilling the craters that were initially studied with the ground-penetrating radar during the expeditions of 2009 and 2010 (Suslov's crater and the First and the Second craters according to our designation). Photos of craters are presented in Figures 3, 4, and 5, and the radargrams are given in Figures 6, 7, and 8.

Suslov's crater, located almost at the center of the fall, is the crater that received most of L.A. Kulik's attention. In 1928, Kulik's expedition dug a trench from Suslov's crater toward the lowland for water drainage. Suslov sketched a section of the crater's side (Fig. 9) (Kandyba 1998).

“At the depth of 1.5 m from the surface the diggers came across two relatively fresh larch trunks. These trunks lay slantwise, their tops were raised at the angle of 25 and 37 degrees to the horizontal and directed towards the southeast at the azimuths of 125 and 150 degrees. Clean ice lenses were found under both trunks. The survey showed that both trees died, being alive – they were not dead trees.” Kulik's expedition included swamp specialist L.V. Shumilova. According to her conclusions, the crater age calculated

by peat annual layers was 21 years. This indicates that the crater was formed in 1908, the year of the catastrophe (Kandyba 1998).

Permafrost preserved all possible traces of the impact of the Tunguska Cosmic Body and its constituents. Comprehensive research of the craters, their genesis, chemistry, and their isotopy layers will make it possible to clarify the nature of the Tunguska Cosmic Body, the greatest enigma of the 20th century. Meanwhile, it is necessary to take account of the continuous karst processes in the permafrost zone (Kudryavtsev 1978, Maslov et al. 2005).

Methods

Mercury analyzer RA-915+ was used to measure mercury concentrations. This analyzer was part of an analytical complex making it possible to conduct quick selective measurements of mercury concentrations in atmospheric air, gas flows, and in liquid and solid samples. The opto-electronic circuit of the analyzer ensures an ultra-low detection limit of mercury in the mode of direct measurements. The method is based on the atomic absorption spectrometry with Zeeman correction of non-selective absorption. Multi-pass cell increases measure sensitivity. Zeeman correction of non-selective absorption ensures high accuracy of measurements irrespective of disturbing factors such as dust, humidity, aerosols, absorbing vapors, and gases.

The analytical complex comprises: 1) Analyzer «RA-915+»; 2) Attachment «RP-91» to determine mercury content in water solutions by cold vapor method; 3) Attachment «RP-91S» to directly determine by the pyrolysis method mercury content in soil, rocks, bottom deposits, and samples with a small amount of organic substances. Analysis of samples with complex matrix by the pyrolysis method does not require preliminary preparation of samples. The complex is designed for operation in laboratory and field conditions.

The analytical complex ensures the unrivaled low limit of mercury detection in the air in the mode of continuous measurements (without preliminary accumulation on

Table 1. Operational parameters of attachment RP-91 to analyzer RA-915+.

Analyzed object	Solid samples (soil)
Detection limit	1.0 µg/kg
Maximum sample weight	0.4 g
Continuous operation time	8 hours
Analyzer weight	7.5 kg
Attachment weight	5.5 kg
Voltage	220 V
Self-contained supply	RA-915+ — 6/14 V
Power consumption	RP-91S — 250 Watt
Current frequency	50 Hz

Table 2. Content, ng/g, and forms of mercury in samples from Suslov's crater and the Second crater.

Horizon, m	Sample description	Suslov's crater	The Second crater	Mercury forms
Surface	Moss	68	–	FS
Lowered edge	Soddy soil	42	–	FS US IF OS SG
Upper layer	soil	26	–	FS
2 m	Soddy soil	19, 23	–	FS
2.5 m	Clay	11	–	FS HTF SG
3 m	Clay g	11	12	FS+SP
4.3 m	Drab clay	–	17	SP+FS+US
4.4 m	clay	–	9	FS+SP+US
5.2 m	clay (a) sand (b)	–	3 2	SP+FS+US SP+FS+US
5.4 m	Yellow silt	–	6	FS+SP+CS
6.5 m	Clay	15	–	FS SP US CS
7.1 m	Drab clay	–	12	FS+US+CS

Abbreviations in Table 2:

- FS – physically sorbed form of mercury
- US – low-temperature form of mercury in an unbound state
- IF – high-temperature isomorphous form of mercury
- OS – forms of mercury connected with organic substances
- HTF – high-temperature form of mercury.

sorbents): 2 ng/m³ at one-second averaging of a signal and 0.3 ng/m³ at thirty-second averaging of a signal. It has a wide dynamic range: 2–20,000 ng/m³ in the continuous mode and 5,000–200,000 ng/m³ in the high concentrations mode. The relative error limit is 20%. This method enables operation in field conditions using internal batteries. There is a possibility of measuring the mercury content in the atmospheric air from mobile carriers.

Mercury analyzer RA-915+ complete with attachment RP-91S is used for direct determination of mercury content in soil, rocks, bottom deposits, and samples with a small share of organic substance with the help of the pyrolysis method.

Table 3. Mercury concentrations (ng/g) in soils and in vegetation of 4 populated points of Siberia.

FS form of mercury	Vanavara	Chamdalsk	Surgut	Novosibirsk
Soil	22	14	13	18
Moss	27 fresh 34 old	31 fresh 50 old	21	–
Fresh pine needles	9	8	20	17
Old pine needles	36	26	25	33

Attachment RP-91S is intended for thermal destruction of a sample and for transition of mercury from a bound state to an atomic one with the subsequent determination of the amount of emitted mercury by analyzer RA-915+ (Table 1).

Mercury analyzer RA-915+ complete with attachment RP-91S is used in ecology and sanitary science for express-analysis of complex objects. In geological and geochemical studies, it is used for examination of natural and anthropogenic cycles of mercury as well as for determination of mercury content in soils, rocks, and ores.

Results

X-ray diffraction analysis of two soil samples was performed. The first subsurface sample found in the clay fraction had the following content: plagioclase Ca₂NaAlSi₃O₈, potassium feldspar KAlSi₃O₈, pyroxene Ca(Mg,Fe)[Si₂O₆], and possibly argillaceous minerals. Samples of crystalline powder included plagioclase Ca₂NaAlSi₃O₈, potassium feldspar KAlSi₃O₈, pyroxene Ca(Mg,Fe)[Si₂O₆], serpentine Mg₃(Si₂O₅)(OH), apatite Ca₅(PO₄)₃F and argillaceous minerals (montmorillonite).

The most detailed analysis was devoted to mercury content in these particles and other ground samples.

The results showed that mercury content in samples 1, 2, and 3 from the First crater is 1 ng/g. The samples are represented by black sand. Despite extremely low mercury weight content, sample 3 revealed an isomorphous mercury form of the highest temperature. It can be assumed that the soils in this place were subjected to some severe impact that caused evaporation of the major portion of mercury and there mainly remained only its high-temperature and the most stable form.

Mercury content in samples of the Second crater are H 4 m – 18 ng/g, H 4.4 m – 10 ng/g, and H 5 m – 8 ng/g. Samples are represented by argillaceous minerals. The color of the H 4 m clay is dark-yellow and other varieties are yellow. The mercury content level in the soils of the Second crater is significantly higher than that in the First crater, although it is considerably lower than Clarke of mercury (45 ng/g, according to N.A. Ozerova). The samples of the Second crater are characterized by a significant content of mercury in the sulfide form and especially in isomorphous form. The soils in the area of this crater were probably exposed to a smaller impact than the ground of the First crater (Table 2).

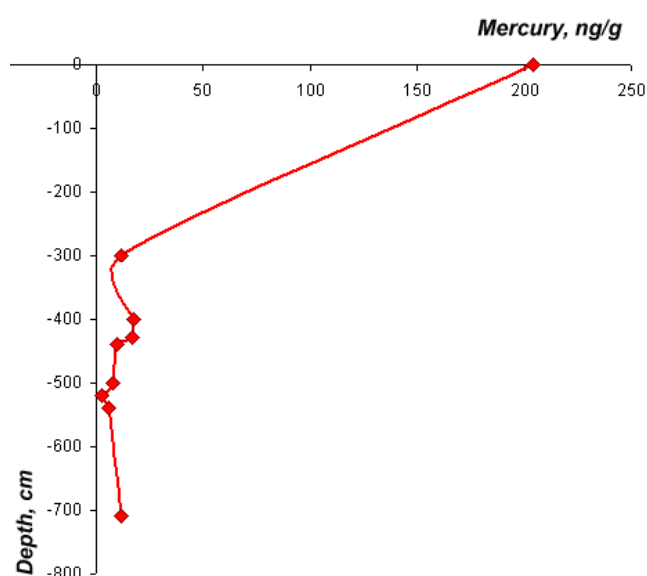


Figure 10. Vertical profile of mercury distribution in soil deposits of borehole No. 2 (the Second crater). Horizontal axis – mercury content, ng/g; vertical axis – depth, cm.

The isomorphous form of mercury occurs rather seldom. There arise difficulties in the course of identification of this mercury form. Normally, concentrations of isomorphous mercury are 1 to 3 levels lower than those of the sorbed mercury form. It is also difficult to link it to a particular mineral, as only a limited quantity of minerals containing isomorphous mercury was studied experimentally. Its release temperature can vary from 450 to 1000°C. If the mineral composition of a sample is known, it can be considered with much certainty that the particular mineral contains isomorphous mercury. Isomorphous mercury can be contained in barite and magnetite.

Table 3 presents mercury concentrations in soils of different towns of Siberia.

Rapid enrichment of the moss surface layer with mercury near the epicenter of the Tunguska explosion can be explained by the proximity to an active fault from which emanations of mercury and other elements and gases intensely emit into the atmosphere. Mosses are good concentrators of mercury and of other metals, and they capture mercury from the surface air.

Another reason can be a discharge of mercury from the underlying ground because of a high-temperature impact occurring somewhere nearby a crater, which preserved soil humus in the surface layer (prevented humus from being burned into ash). More detailed information can be obtained with the help of an areal survey in this region with sampling of surface and underlying soils to find out where the contamination comes out, using a testing grid with points located at rather small intervals from each other. There must be complete certainty that this is not anthropogenic contamination with mercury.

Figure 10 presents a graph of mercury concentration change with depth in the Second crater. For comparison, the mercury concentration in the background region at the distance of 100 m from Suslov's crater is given, and it equals 200 ng/g.

The appearance of the curves of mercury adsorption and of pyrolyzate content in a cell can indicate that the major portion of mercury in the surface layer exists in a sorbed form. However, some portion of it is tightly bound with organics and therefore forms several peaks in a high-temperature zone.

In a standard sample, mercury is in a sorbed form.

Conclusions

- 1) Mercury concentrations in the Tunguska meteorite craters are low and below the Clarke values.
- 2) The mercury content in the black sand samples of the First crater is 1 ng/g.
- 3) Sample No. 3 from the First crater contains the isomorphous form of mercury with the highest temperature.
- 4) The ground was possibly exposed to thermal impact; the major portion of mercury evaporated and the high-temperature form of mercury that is the most stable remained.
- 5) The mercury content in the samples of the Second crater is 8-18 ng/g.
- 6) Mercury is present in sulfides and particularly in an isomorphous form.
- 7) The ground in the area of this crater was probably exposed to a smaller thermal impact than the ground of the First crater.
- 8) The enrichment of surface mosses with mercury can be explained by the proximity to the active fault. Mosses are good sorbing agents. Discharge of mercury from underlying ground is possible as a result of a high-temperature impact.
- 9) The comparison of mercury concentrations in the craters of the Tunguska explosion epicenter with its concentrations in soils and vegetation of Siberian populated points (Table 5) indicates contamination of the air with mercury, as soils and plants are good sorbing agents and indicators of this process.
- 10) The peculiarities of mercury distribution in the ground of craters and in other populated points of Siberia indirectly testify to the cosmogenic nature of the Tunguska explosion.

Acknowledgments

The authors express their gratitude to the following: Academician of RAS, A.M. Cherepashchuk, for continued support and assistance; Professor of Tomsk University, G.F. Plekhanov, for constructive discussion of the issue; the Director of Sternberg Astronomical Institute (Moscow State University); the management of the Department of Environmental Protection of Ministry of Natural Resources of the Russian Federation; the director of the Tunguska Reserve, L.N. Logunova, and the Reserve's employees for support in conducting the expeditions; the Director of Conversion & Dwelling OJSC, V.V. Krivulin, for sponsoring the purchase of the equipment; the Organizing Committee of the Tenth International Conference on Permafrost (TICOP) for the attention to our research and assistance in preparing this paper.

References

- Alekseev, V.A. 1998. New aspects of the Tunguska meteorite problem. *Planetary Space Sci.*, 40 (nos. 2/3): 169-177.
- Alekseev, V.A. & Alekseeva, N.G. 2005 *Particularities of the problem of the Tunguska body*, "Asteroid-Comet Hazard – 2005", St. Petersburg.
- Alekseev, V.A., Alekseeva, N.G., & Kopeykin, V.V. 2011. Results of georadar and hydrogenic studies of impact-generated craters of the Tunguska meteorite in 2009 and 2010. *Optics of atmosphere and ocean*, 12: 1105-1107.
- Kandyba, Yu.L. 1998. *Tragedy of the Tunguska meteorite* – Krasnoyarsk: Izd. Siberian Fund "Tunguska Space Phenomenon", 416 pp.
- Krinov, E.L. 1949. *Tunguska meteorite* M.: AN SSSR, 196 pp.
- Kudryavtsev, V.A. (ed.). 1978. *General Geocryology* M.: Izd-vo IGU, 1978, 464 pp.
- Kulik, L.A. 1939. Data on the Tunguska meteorite. DAN SSSR, *Novaya Seriya* 11 (no. 8): 520-524.
- Maslov, A.D. et al. 2005. *Geocryology basics*, Ukhta: In-t upravl., inf. i biznesa, 176 pp.
- Vasilev, N.V. 2004. *Tunguska meteorite. A space phenomenon of the summer of 1908*. M.: NP ID Russkaya Panorama, 372 pp.

Cryogenic Strata of Gas-Bearing Structures of Northern Western Siberia: Look to the Future

Yu.B. Badu

*Faculty of Geography, Lomonosov Moscow State University, Cryolithology and Glaciology Department,
Moscow, Russia*

Abstract

Summarizing the results of long-term research, the author concludes that the cryogenic stratum in northern West Siberia is a single Middle and Late Neopleistocene and Holocene cryogenic formation related to continuous cycles of transgression-regression in the Polar Basin under conditions of severe cyclic climate change. The cryogenic stratum of northern Yamal is divided by the author into stratigraphic units clearly correlating with the schemes of G.I. Lazukov, V.A. Zubakov, and I.D. Danilov. The structure and state of the cryogenic stratum reflect the features of permafrost formation in the strata of gas-bearing structures.

Keywords: cryogenic stratum; gas-bearing structure; permafrost formation; permafrost thickness; subaquatic freezing.

Introduction

The preliminary stratigraphic correlation of the sections of Quaternary deposits on the Yamal, Gydan, and Tazovsky peninsulas and the elaboration of the local stratigraphic section (Podborny & Badu 2011) were performed to develop a detailed cryostratigraphic description of the cryogenic stratum.

The dome type of permafrost was identified for the first time by Dubikov (1980, 2002) and was studied by Baulin (1985), Romanovskii (1993), and others. They discovered that the gas-bearing dome has a heat effect on the position of the bottom of the cryogenic stratum, and they developed the first hypotheses regarding the state of the cryogenic stratum.

Cryogenic Stratum

The composition and structure of Cenozoic deposits in West Siberia are defined by the marine sedimentation regime and the development of neotectonic gas-bearing structures during the whole of the Mesozoic. The thermal state of this area during the Pleistocene and the Holocene was determined by the radiation and heat balance of the "atmosphere-hydrosphere-lithosphere" system. This is the main reason for the formation and development of the cryogenic stratum in subaquatic bottom deposits of a shallow shelf and in the subaerial conditions of the drying of the exposed sea floor.

The upper and lower boundaries of the cryogenic stratum are defined by the position of the 0°C isotherm. The frozen ice-bearing part of the stratum is limited from below by the T_{bf} isotherm (i.e., the initial ground freezing temperature). The horizon of negative-temperature cryotic ground is located below this. It does not contain ice inclusions due to the high salt content reducing its freezing temperature and onset temperature for ice formation.

Thick gas-bearing structures with their high temperature and pressure bed at the base of the cryogenic stratum are at the depth below 400–500 m.

Gas-bearing Structure

The gas-bearing structure is a neotectonic formation of the lithosphere. In the geological section, the Cenozoic unconsolidated sediments cover the Late Cretaceous

compacted sediments that overlie the productive gas-bearing structure of the Early Cretaceous.

Geological history

According to the geologists of the Cryos Scientific and Technical Firm, the formation of structures began in the Late-Cretaceous time as marine sedimentation. Neotectonic movements were activated in the Oligocene, when some structures of the Paleogene deposits were brought to the surface and exposed to denudation. The dome parts of the structures were reworked more intensively, the Paleogene deposits were re-deposited completely, and the Cretaceous deposits were re-deposited partially. The lower layers of Paleogene deposits were usually preserved at the limbs of the structures. At the end of the Oligocene and in the Neogene, the intensity of neotectonic movements decreased significantly. Their direction abruptly changed at the Late Pliocene and the Quaternary stages of development. The territory settled and was flooded with the waters of the Yamal transgression. This point of view is well known. Moreover, it was revealed in the process of the study of the geological sections of the Kharasavey, Bovanenkovo, Arctic, Novy Port, and other structures (Badu 2006, 2011b) that the Quaternary deposits with angular and stratigraphic unconformity overlie Cretaceous and Paleogene sediments. The roof of the latter gradually rises to the central and the axial parts of the Tazovskiy and the Gydan peninsulas. The transgressive part in the section of the Quaternary deposits is composed of sediments of the Poluy suite. In sections of some structures, the thickness of sediments of the Yamal series is slightly reduced due to the decrease in thickness of the stratum of the Salekhard suite. This is explained by the fact that the sediments of the Kazantsev suite were deposited on its eroded roof with unconformity after short-term drainage of occasional sites starting in the beginning of the Late Neopleistocene (Fig. 1).

The Salekhard suite deposits, which form the cover on the plains of the Yamal watershed divide, are the main key horizon of the marine stratum, the age of which is assumed to be the Middle Neopleistocene (Badu 2006, 2011b).

The Third, Second, and First Marine terraces were formed during the Neopleistocene at the eroded surface of the Kazantsev deposits along the coasts of the peninsula. The

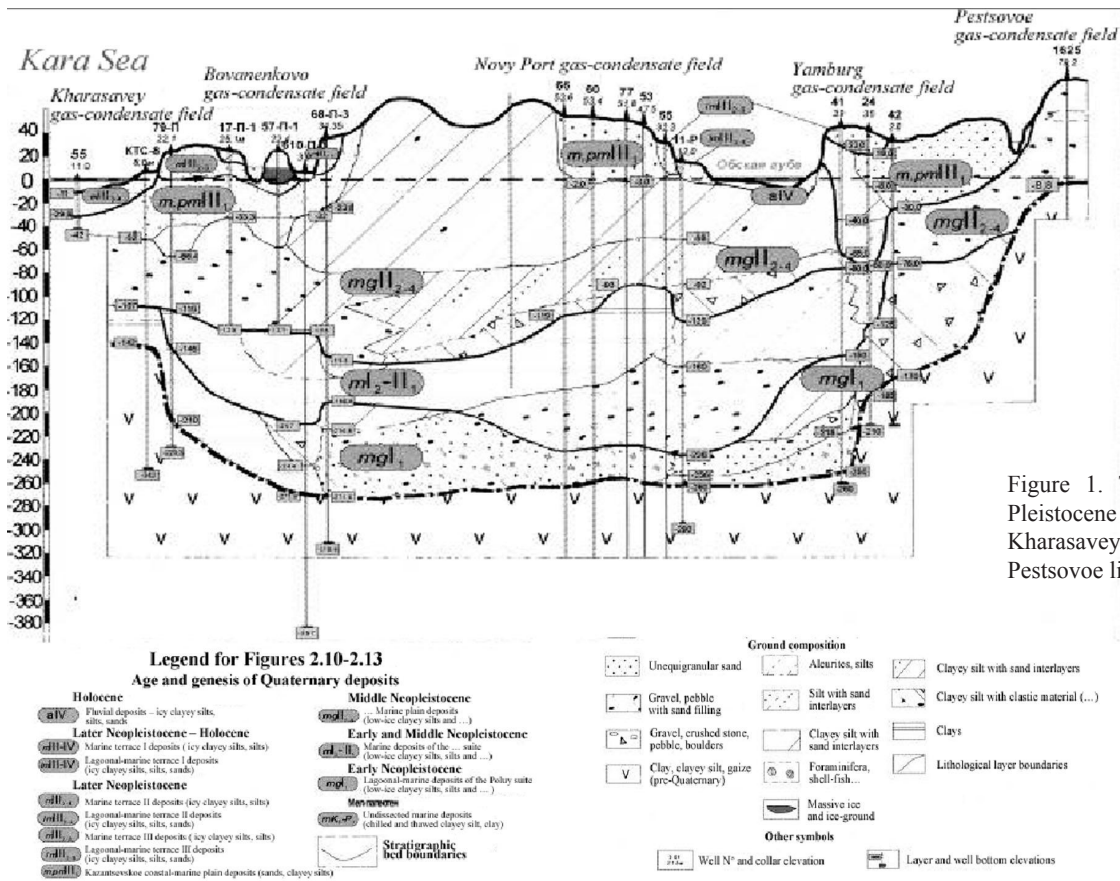


Figure 1. The section of the Pleistocene stratum along the Kharasavey – Novy Port – Pestsovoe line.

central part of Yamal, the south of Tazovskiy, and the axial part of Gydan during this period were already drained, and the cryogenic stratum was under formation in these areas. Sedimentation of the fluvial deposits of river beds and floodplains and their freezing started from the Sartan age and continued through the Holocene until present.

The end of the Middle Neopleistocene is associated with completion of marine shelf sedimentation. Marine sedimentation ended in the Late Neopleistocene during the epochs shorter than the previous ones. The freezing of the deposits accumulated during the Early and the Middle Neopleistocene until the beginning of the Late Neopleistocene and noticeably changed the state of the soil stratum. The modern terrain and soil conditions were in many ways formed by the Holocene events (uplift of the Polar Basin level, denudation and re-deposition of soils, climatic changes), but mostly by the active freezing of the soil stratum in its subaerial and subaquatic parts. The whole sedimentation history during the Late Neopleistocene was directly connected with syngenetic and epigenetic freezing. Data on cryogenic structure and ice content of the identified layers were reported in the descriptions of sections of gas-bearing structures (Badu 2006, 2011b).

Permafrost formation

The cryogenic stratum in the northern West Siberian platform is a single stratum formed in the Middle and Late Neopleistocene and the Holocene. It was formed during continuously alternating cycles of transgression-regression of the Polar Basin under conditions of cyclic changes of the severe climate. The Pleistocene cycle of the cryogenic

stratum formation has regional specifics of permafrost formation (Badu 1978, 2006, 2010, Trofimov, Badu & Dubikov 1980).

The rates of epigenetic freezing of deep soil horizons slow down within gas-bearing structures because the endogenous heat flow from below reduces the value of the temperature gradient which causes water migration to the freezing front. Segregated ice formation is also complicated by high salt content in soils.

The centers of gas-bearing domes are usually located at the depth of at least 400 m. Nonetheless, such bedding of a thick geologic body with high thermal capacity significantly influences the position of the 0°C isotherm (Fig. 2) and the bottom of the frozen ice-bearing stratum of soil (Fig. 3).

The 0°C isotherm depth is smaller above the highest part of the dome, and permafrost thickness above the dome decreases by 20–30% compared to the peripheral part of the gas-bearing dome. The volume of the hard frozen and plastic frozen parts of the cryogenic stratum is reduced above the gas-bearing structure.

The differences in freezing depths and permafrost thicknesses were noted (Badu 2011a) in the sections:

- with Late Neopleistocene marine terraces, where a part of the dome is located below the marine water area (130–180 m);
- the marine water area (90–110 m);
- with the Holocene floodplain and the shallow bedding of the gas-bearing dome (160–180 m);

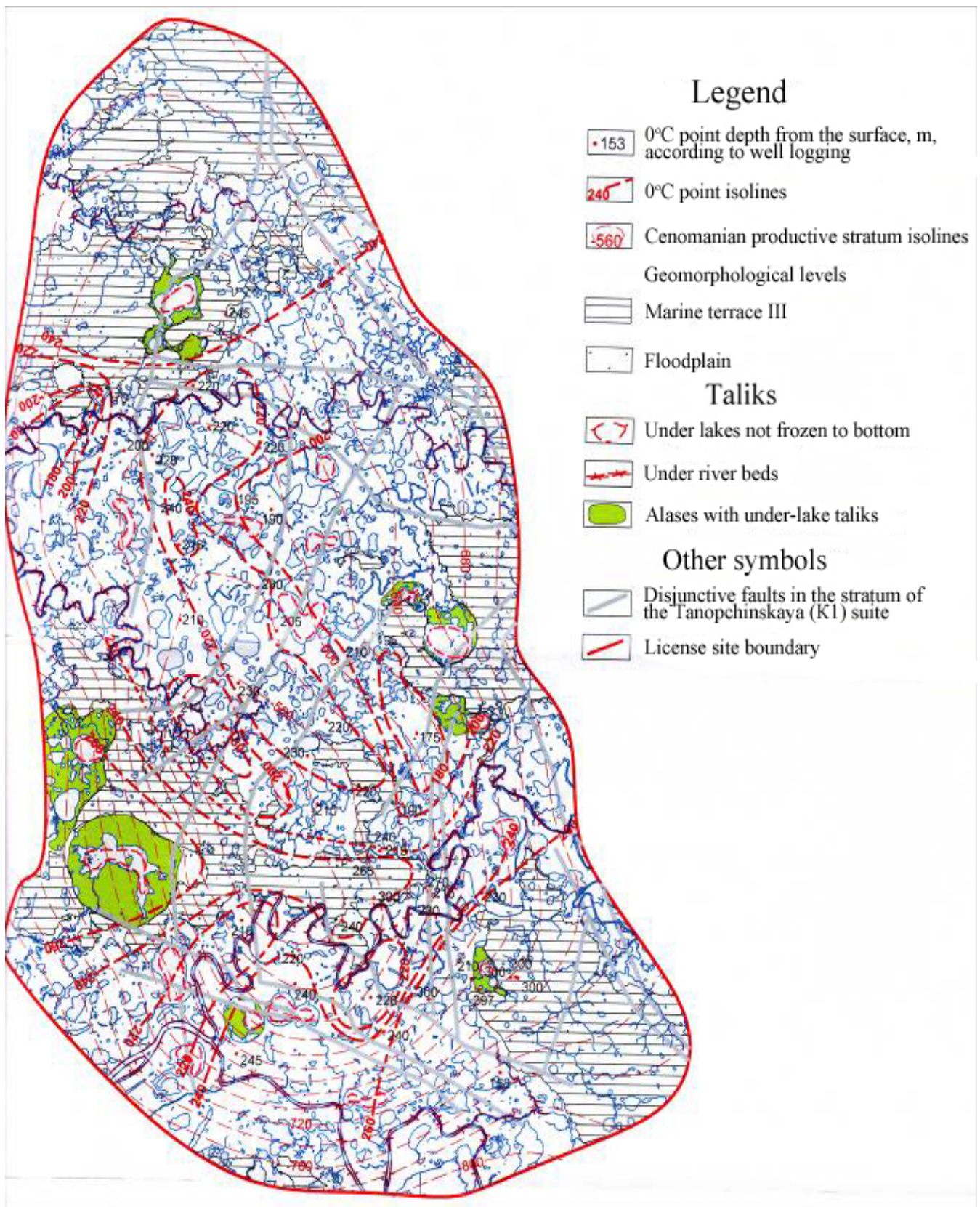


Figure 2. Thickness of the cryogenic stratum of the Bovanenkovo structure.

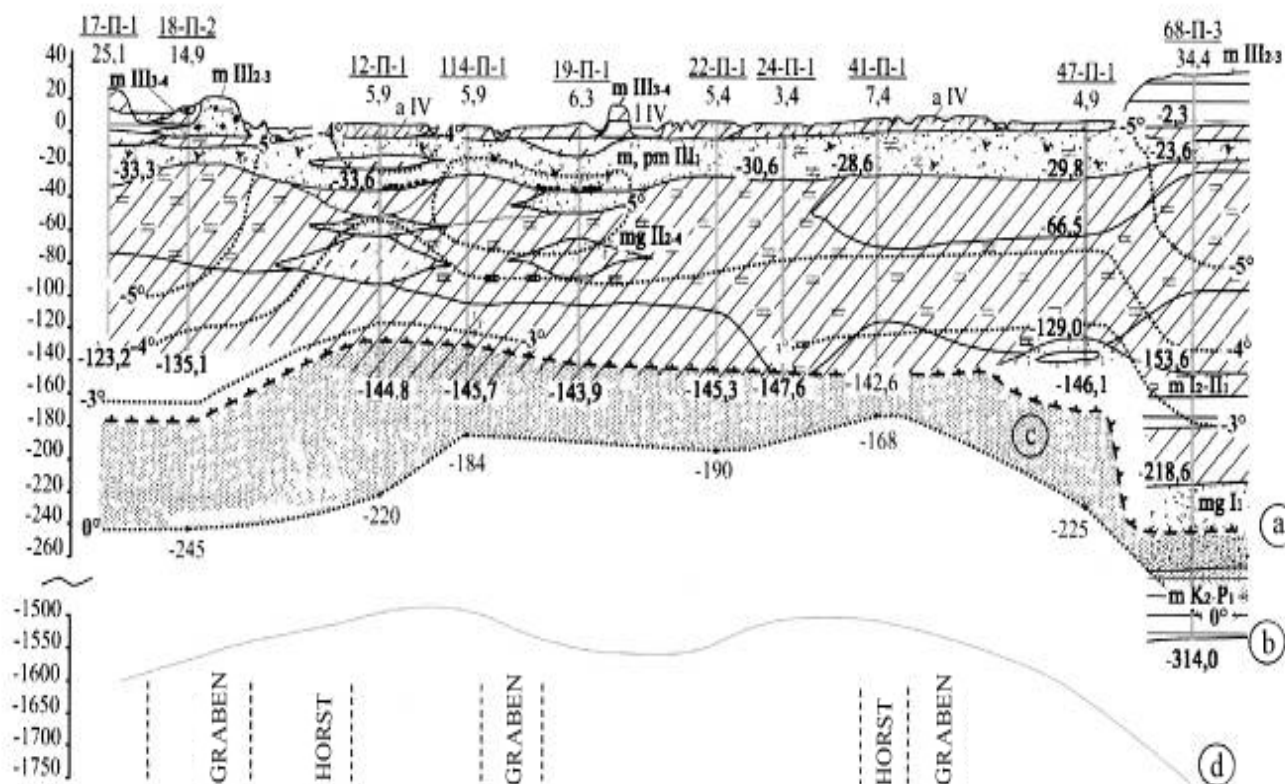


Figure 3. Cryogenic stratum of the Bovanenkovo structure along its western steepest slope on the line of intersection (from NW to SE) of the gas-bearing dome. a – bottom of permafrost (at $T_c < T_{bf}$); b – bottom of cryogenic stratum with depth positions of the 0°C isotherm; c – chilled soils (at $T_c > T_{bf}$); d – roof of the productive bed with assumed zones of disjunctive faults in the deposits of the Tanopchinskaya suite (K_{1br}).

- on the watershed divide areas of Yamal, where the duration of the subaerial freezing period is maximum, and the Paleogene deposits with a different type of pore water mineralization are located close to the surface above the dome (180–220 m);
- on the eastern coast of the Yamal and Tazovskiy peninsulas with lagoon and fluvial types of the Late Neopleistocene and Holocene sedimentation (200–220 m).

Permafrost thicknesses at the western and the eastern Yamal coasts are associated with the marine and the lagoon type of sedimentation and, respectively, with major or minor salinity of sediments. They are also associated with different freezing conditions of deep-water and shallow-water deposits in the regressing open sea basin and in the shallowing semi-closed lagoon (bays, gulfs). Permafrost thickness is less in the marine strata of the western Yamal coast and is greater at its eastern coast. The 0°C isotherm depths also vary from 250–280 m to 400–430 m.

The temperature field of the cryogenic stratum of gas-bearing structures is not homogeneous in local cryo-anomalies either. It is defined by the climatic and landscape interaction in the upper 10 to 20 m part of the permafrost section. In the middle part (40–70 m) it is defined by climatic temperature variations of the Holocene optimum and the

Late Holocene cooling. In the lower part (100–300 m), it is defined by long-term Late Neopleistocene temperature variations distorted by the heat flow of gas domes.

The following assumption was suggested (Badu 2006, 2011a): the more migration and autochthonous gas in the hydrated form is bound under and inside its hard frozen cover in low-temperature cryogenic strata of gas-bearing structures, the more bodies of tabular massive ice are contained in the cover, and the rarer are the cryopegs in the top part of the section.

There are fewer obstacles to gas migration to the surface in “warmer” permafrost. The gas concentrates more in the stratum of plastic frozen soils where it is bound in the gas-hydrate state. The conditions for accumulation of autochthonous gas associated with the decomposition of large quantities of organic matter are the most favorable in such strata. Cryopegs are pressed out by freezing and constrained in the stratum by hard frozen soils that are widely developed in the top 40 to 50 m part of such strata. However, they are also found at the depth below 100–120 m, where the difference between the low freezing point of high-mineralized pore water and the high negative temperature of the frozen (plastic frozen) or the chilled stratum is significant.

It was known (Baulin 1985, Romanovskiy 1993, and others) that the closer the dome is to the surface, the more active its thermal impact on the bottom of the cryogenic stratum. Now it is detected that more heat is emitted in a number of structures above horsts (in the productive stratum) and the diffusing gas, which expands adiabatically and chills and freezes the ground above grabens and downthrusts. The geologists of the Cryos Scientific and Technical Firm reported gas occurrences in the same places of the stratum during the drilling of assessment wells (Podborny & Badu 2011).

The following processes and phenomena are observed in river valleys located above the dome of gas-bearing structures: the widening of the floodplain area due to thermal erosion; accelerated growth of syngenetic ice wedges; the mineralization of fluvial river-bed sediments in the lower and the middle river reaches; thermokarst activation in ice-rich floodplain fluvial deposits (Badu 2006).

The top part of the stratum was frozen synchronously with sedimentation. Ice-rich deposits were formed here in different lithological and facial conditions. The lower part of the stratum was frozen epigenetically after the denudation of its most ice-rich part. However, the primary vertical distribution of segregated ice, which formed in the corresponding cold period, is preserved in the epigenetic part of the section. It is not associated with the current thermal state of the middle part of permafrost in some sections because the frozen sediments had low moisture content and high salinity.

Permafrost formation in the saline bottom sediments of the shelf is determined by heat exchange in the water-seabed system. But the formation of the cryogenic stratum with gas-hydrate ice-ground and tabular massive ice bodies above gas-bearing structures is complicated by the freezing of host sediments due to the adiabatic expansion of diffusing gas.

As a result of the activation of neotectonic movements, the thixotropic and unfrozen soils already chilled below 0°C at the dome limbs experienced dynamic stresses of underwater landslides and were being folded. Also, folded tabular massive ice bodies formed in conformable layers of spontaneously freezing host sediments as a result of stress discharge in the water chilled to the negative temperatures close to the freezing point.

Therefore, during the transfer from the subaquatic regime to the subaerial one the main features of subaquatic permafrost formation are preserved in the stratum whose freezing continues after the sea bed is exposed.

Ice and ground-ice formations in the subaquatic syngenetic permafrost are reported in some sections (Badu 2011). They were formed in the saline water-saturated bottom soils. They do not look similar to subaerial permafrost forms, either in the composition of host sediments or in the method of freezing or in the ice formation type.

The explanation for this assumption is as follows: Marine sediments in the top part of the section were deposited at negative sea water temperatures, the freezing point of which is -1.7 to -1.8°C. This is associated with high content of easily soluble salt that hinders ice formation in the pore solution. Moreover, sandy soils with high content

of silt particles and micaceous minerals have thixotropic properties. Thixotropic soils retain a lot of interfacial water with a lower initial freezing temperature than that of free water. Upper horizons of sediments are water-saturated, but thixotropic bonds prevent their flowing at insignificant inclination of the bottom surface. Gradual water and salt re-distribution occurs in the stratum of chilled sediments. Sediments get compacted under the impact of ground pressure; pore moisture is pressed out to the surface or the most coarse-grained layers, and salts are concentrated in the lower horizon of the stratum.

Liquefied marine sediments can flow even at 1–2° angles and are retained only due to thixotropic structural bonds. Not only neotectonic shocks or large sea waves passing at the surface, but also a simple increase of the layer's inclination angle above the critical value (i.e., at least 2–3°) can lead to the destruction of thixotropic structure. In this case the sediment strata no less than 15 m thick are placed into movement and folding. It is noted in a significant number of the Northern Yamal and Gydan sections that dislocations are confined to the limbs of neotectonic structures.

Sediment deformation at the underwater coastal slope is the immediate cause of ice formation and their transfer to the frozen state. Free and demineralized water is emitted during the destruction of the thixotropic ground mass. Its initial freezing temperature grows step-wise, and the water becomes over-chilled. The most significant accumulations of the pressed-out free water are formed in fold hinges, mainly in sandy sediments or at lithological boundaries. By its structure, this ice is similar to injected ice; it contains suspended mineral material, chaotically oriented inclusions of frozen soil, and multiple air bubbles of a rounded shape. These indicators reflect a step-wise stress relief and dynamic (forced) intrusion of free water masses into the deposits. However, in comparison with injected ice, they hardly destroy the lithological stratification and bed conformably with deformed layers. Moreover, the water pressed out directly from host deposits and frozen at the same place is concentrated at lithological boundaries. It forms clean amorphous glass-like ice without mineral inclusions or gas bubbles. Two ice types usually replace each other along the layers and are separated from each other by a clear contact. Individual ice inter-layers and minor lenses are frequently found in sandy deposits. They are the result of the same press-out free water.

The subaquatic freezing of bottom deposits is accompanied by the phenomena characteristic of marine conditions. Step-wise change of properties leads to the spontaneous freezing of the plastically deformed stratum of deposits. Salts in marine sediments hinder water migration to the freezing front. Consequently, cryostructures are poorly developed. Ice formation occurs more intensively with moisture fixation in pore ice (structureless cryostructure without visible ice) and preserving the primary moisture distribution in chilled sediments. This was reflected in the regular distribution of the total moisture content and the volumetric visible ice content in horizons of fine-grained deposits and in the domination of incomplete reticulate cryostructures.

The identified cryolithological indicators confirm the hypothesis of marine subaquatic permafrost formation

developed by A.I. Popov. Sediment freezing occurred as a result of the folding-plicative deformation of the stratum of bottom sediments at the underwater coastal slope and free water emission from thixotropic chilled grounds. Fresh water is the first to emit from marine sediments in the process of deformation. It is immediately frozen in the negative temperature field, providing for a very quick freezing of deposit layers that are many meters thick.

According to the data of Popov (1984, 1991), Maslov (1985), Shpolyanskaya (1993, 1999, 2006), and Danilov (1978), this process is the main mechanism for syngenetic formation of tabular massive ice bodies in bottom marine sediments due to the fold deformations of their initially horizontal stratification. We referred to it as the plicative type of subaquatic syngenetic permafrost formation (Badu 2010).

This concept is opposite to the one assuming that permafrost during the Pleistocene was formed in subaerial conditions and was flooded and thawed during transgression periods.

The study of the structure and the composition of the cryogenic stratum and its ground ice features in gas-bearing structures provides a huge volume of indirect information on paleo-conditions of sedimentation, freezing, and the formation of segregated, wedge, and tabular massive ice. This information enables us to make an objective interpretation of permafrost formation in the Earth's crust. The reliability of paleo-reconstructions created on the basis of this information can only be assessed in the distant future.

References

- Badu, Yu.B. 1978. *Cryolithogenesis in conditions of the West-Siberian platform north*. Dissertation abstract. Moscow, Izd-vo MGU, 24 pp. (in Russian).
- Baulin, V.V. 1985. *Permafrost in Oil-gas Production Regions of the USSR*. Moscow, Izd-vo Nedra, 176 pp. (in Russian).
- Badu, Yu.B. 2006. Stratigraphy, micro-faunistic and mineralogical characteristics of deposits: *Cryosphere of oil, gas and condensate fields in the Yamal Peninsula*. Cryosphere of the Kharasavey gas-condensate field. St. Petersburg, Izd-vo Nedra, Vol. 1: 42–56 (in Russian).
- Badu, Yu.B. 2010. *Cryolithology* (textbook). Moscow, Knizhny dom Universitet, 528 pp. (in Russian).
- Badu, Yu.B. 2011a. Cryogenic strata of gas-bearing structures in the Western Siberia north: *Materialy IV konferentsii geokriologov Rossii*. M.V. Lomonosov Moscow State University. Moscow, Izd-vo Universitetskaya kniga, Vol. 2. (Part 5): 9–15 (in Russian).
- Badu, Yu.B. 2011b. Geological structure of the cryogenic stratum in the Western Siberia north. *Inzhenernaya geologiya*. June, 1, 2011 Moscow, PNIIS, pp. 40–55 (in Russian).
- Danilov, I.D. 1978. *The Pleistocene Subarctic Marine Plain*. Moscow, Izd-vo Mosk. un-ta, 198 pp. (in Russian).
- Dubikov, G.I. 2002. *Composition and Cryogenic Structure of Permafrost in Western Siberia*. Moscow, Izd-vo Geos, 246 pp. (in Russian).
- Maslov, A.D. 1985. Physical-mechanical and thermophysical properties of bottom deposits in the southeastern part of the Barents and the southwestern part of the Kara Seas. *Geotechnical Properties of the World Ocean deposits*. Leningrad. PGO Sevmorgeologiya, pp. 51–64 (in Russian).
- Melnikov, V.P., Fedorov, K.M., Volf, A.A., & Spesivtsev, V.A. 1998. Analysis of possible bottom ice heave formation scenario for the Pechora Sea shelf. *Kriosfera Zemli*. 2 (no. 4): 51–57 (in Russian).
- Podborny, E.E. & Badu, Yu.B. 2011. Correlation of Cenozoic deposits sections in northern Yamal: *Materialy IV Konferentsii Geokriologov Rossii*. M.V. Lomonosov Moscow State University. Moscow, Izd-vo Universitetskaya kniga, 2 (Part 5): 143–148 (in Russian).
- Popov, A.I. 1984. On dislocations and cryolithogenesis in the Northern Eurasia Pleistocene, *Vestnik MGU, Geografiya*, 3: 3–9 (in Russian).
- Popov, A.I. 1991. On the submarine type of cryodiagenesis: *Inzhenernaya geologiya* 6: 49–55 (in Russian).
- Romanovskii, N.N. 1993. *Principles of Cryolithogenesis of the Lithosphere*. Moscow, Izd-vo MGU, 335 pp. (in Russian).
- Shpolyanskaya, N.A. 1993. Convective nature of dislocations in the deposits with massive ice in the Western Siberia north. *Geoekologiya (Inzhenernaya Geologiya, Gidrogeologiya, Geokriologiya)* 1: 94–103 (in Russian).
- Shpolyanskaya, N.A. 1999. Cryogenic structure of dislocated strata with sheet ice as indicator of their genesis (Northern West Siberia). *Kriosfera Zemli* 4, (no. 4): 61–70 (in Russian).
- Shpolyanskaya, N.A., Streletskaya, I.D., & Surkov, A.V. 2006. Cryolithogenesis within the Arctic shelf (modern and ancient). *Kriosfera Zemli* 10 (no. 3): 49–60 (in Russian).
- Trofimov, V.T., Badu, Yu.B., & Dubikov, G.I. 1980. *Cryogenic Structure and Ice Content of Permafrost of the West-Siberian Platform* Moscow. Izd-vo MGU, 247 pp. (in Russian).

Cryogenic Processes along Linear Structures

N.P. Bosikov

Melnikov Permafrost Institute, SB RAS, Yakutsk, Russia

Abstract

This paper discusses the sources and peculiarities of thermokarst development along unpaved roads (paved across inter-alases) and electric-power transmission lines. It analyzes the degree of thermal erosion in Central Yakutia (West Siberia). It describes the structure of permafrost exposed to thermokarst and the nature of surface disturbance depending on the conditions of the territory's moisture conditions.

Keywords: alas; moistening; lake thermokarst; Lena-Amga interfluve; talik.

Introduction

A large network of unpaved roads, electric-power transmission lines, and other communications was built up across the Lena-Amga alas area in Central Yakutia. Many of them were made regardless of the occurrence of ice-rich permafrost. It is well known that ground ice is widespread over the inter-alases of the Abalakhskaya Plain located at the Lena-Amga interfluve. The volumetric content of ice reaches 30-40% of the total mass of the ground. The ice beds occur at the depth of 2.0–2.5 m from the surface. Due to the present moistening deficit, the development of lake thermokarst on the territory of Central Yakutia is insignificant. However, some areas display the emergence and development of this process (Bosikov 1977). Thermokarst depressions occur along the unpaved roads within the inter-alas plains of the Lena-Amga area and are the result of technogenic disturbance of the soil surface.

To establish the geographical reasons for the development of thermokarst lakes and to determine the rate of their expansion and deepening, we made observations along the unpaved roads of the Lena-Amga interfluve. The collected data allow us to identify the reason for the start and the end of the thermokarst process and to determine the rate at which it develops on disturbed landscapes located along linear structures.

Methods

We have been conducting observations of thermokarst development along the Maya-Beke unpaved road since 1973. Thermokarst depressions and lakes were morphometrically measured in the summer season. The lake depths were measured with an echo sounder. All relative heights and depressions were determined by leveling. When assessing the general moistening of the territory, we used the method suggested by A.V. Shnitnikov (1957). According to the method, the general moistening of the territory is expressed through conventional coefficient m , which represents the ratio of the mean multi-year sum of atmospheric precipitation to the mean summer temperature (May–September) for the same period of time.

Results of Observations and Discussion

The part of the Maya-Beke road selected for observation is located on an inter-alas area that contains permafrost with

thick wedge ice. The wedge ice beds at the depth of 2.0–2.5 m from the surface and its thickness reaches 10–15 m. Before the road was built, its area was occupied by dense forest vegetation. Road construction was initiated after the forest was cleared. According to the local inhabitants, the roadbed was constructed in 1962.

It is well known that a forest strip 15–20 m wide is initially cleared as a right of way across an inter-alas. Then the upper layers of ground are removed down to the depth of 0.5–1.0 m with a bulldozer in order to bank the road bed. The altered heat exchange at the ground surface initiates thermokarst development along the paved road because ice-rich permafrost thaws.

To establish the speed of thermokarst development along the Maya-Beke dirt road, we have been monitoring it since 1973. Geomorphologically, the observed part of the road is found at the flat non-drained inter-alas of the Abalakhskaya Plain.

As shown in Table 1, the soil surface is slightly lowered during the first 17 years following disturbance. As a rule, this process is observed on flat, non-drained areas of an inter-alas. The tops of ice wedges melt in the areas where meltwater and rainwater drain down the slope leading to the formation of depression-hillocky microrelief forms at the soil surface. Further, the ground ice ceases to thaw due to the growth of a protective layer above it (Shur 1998). For this reason, the thermokarst process stops as well.

In spring, water accumulates on the non-drained areas where the ground has subsided. For example, the water depth reached 1.5 m at a part of the Maya-Beke road in 1980 (see Table 1).

We monitored the development of thermokarst depressions under small water bodies located in the Yukechinskiy area located 10 km from the point described (Bosikov 1998). The observations indicated that the water accumulated at the concave areas of the land surface creates the conditions for thawing of ground ice (i.e., for the development of a thermokarst lake). It is well-known that this process is possible only when the water balance of the small lake is positive, and growth stops if there is no water.

Thawing under small water bodies is 1.5–2.0 times greater than in dry polygonal formations (Vasilev 1982). In summer we measured the temperature of water in intrapolygonal depressions. The water depth ranged between 0.8 and 1.0 m. The measurements were made three times a day: at 9 a.m., 1 p.m., and 9 p.m. At the same time, we measured the air temperature in the grassy vegetation.

Table 1. Morphometric parameters of the thermokarst lake in different years, m.

Year of monitoring	Lake depth	Depth of total land subsidence	Lake width	Lake length	Talik depth
1962	0	0	0	0	0
1973	0	0.5	0	0	0
1974	0	0.7	0	0	0
1975-79	0	1.2	0	0	1.0
1980	1.5	1.5	10.0	50+70	3.0
1990	1.0	2.0	12.0	60+80	3.5
1993	2.0	4.26	15.0	70+85	4.0
1995	2.0	4.30	15.0	75+85	4.5
2000	3.45	4.45	35	383	5.0
2001	3.50	4.58	35	384	5.5

The results indicated that the temperature sum is 5°C higher for sunny days and 10.2°C higher in cloudy days than the air temperature in the grassy vegetation. This allows us to conclude that the total thermal impact of a small water body on the underlying ground is much greater than the air impact on the land. Thus, in this area, the water accumulated in the depressions of the soil surface along unpaved roads initiates the active development of thermokarst.

When the water depth of a small lake reaches 1.5 m, thermokarst begins to intensively develop by melting of ground ice. Up until 2000, two separate, small lakes were present at the observed part of the Maya-Beke road (see Table 1). In 2000 the dam between them washed away, thus forming a single lake along the road.

As Table 1 shows, the ground subsided during the first 17 years due to the increase in the seasonal thawing and to the thawing of the tops of ice wedges. A thermokarst lake formed the next year when subsidence reached 1.2 m. It should be noted that thermokarst depressions are not filled with water in the years when moisture is insufficient. A protective layer develops over the ice-rich ground and the thermokarst process ceases. The depressions are filled with water during years with much water, which considerably increases the depth of seasonal thawing. When a lake has a water depth of 2.0 m, the ground ice beneath remains thawed all year round. A stable water regime of a thermokarst lake is maintained when the thawing reserve of ground ice is more than 35%. Thawing of such an amount of ground ice causes the self-development of a thermokarst lake, regardless of the hydrometeorological conditions of certain years. The self-development continues until the ground ice has essentially all melted.

Establishment of the lake regime in the Yukechinskiy area caused the talik under the lake to grow at a rate of 0.5 m per year. The data show that the ice-rich permafrost intensively thaws in Central Yakutia when water remains at the soil surface for an extended period of time.

In 1995, we made one-time measurements of the depth of thermokarst depressions along the Maya-Tabaga-Byuteydeekh road located on the Lena-Amga interfluvium. The cryogenic and geologic structure of this area does not differ from that of the Maya-Beke road. A total of 16 thermokarst depressions filled with small lakes were surveyed. All the

depressions are found at the water-logged area of the inter-alas plain. The depth of the depressions along the road varies from 4.6 to 6.41 m. These data show that thermokarst lakes develop along unpaved roads all over the territory of Central Yakutia.

The spatio-temporal analysis of thermokarst lake development revealed that the emergence and intensive expansion of thermokarst lakes coincide with the years of high moistening of the territory (i.e., when the lakes are full of water). It is established that thermokarst processes develop rhythmically (Bosikov 1989).

Massive wetting of the territory was observed in 1980 and 1994. As a result, a thermokarst process started and developed along unpaved roads of the region, specifically along the Maya-Beke road.

The reason for the drying of the catchment area of alases was related to forest cutting for electric-power transmission lines. The route observations revealed that the construction of electric-power transmission lines along the edge of alase depressions causes their catchment area to drain and dry up. Many alases dried up for this reason, although the weather conditions of those years contributed to the preservation of lakes.

The formation of hazardous ravines for the water pipeline was observed 2 km from Syrdakh Village. The formation of ravines was triggered by the water discharge from a water pipeline onto the slope of the alase depression, which is composed of silty clay loess with ground ice. The self-development of a ravine occurs after the ground ice is exposed. The depth and degree of thermal erosion depends on the intensity and length of the impact exerted by flowing water on frozen ground and on the composition of the flowing water.

Conclusions

- 1) The development of lake thermokarst along the unpaved roads across the non-drained, inter-alas plains is possible when the ground ice content is more than 35%.
- 2) After an unpaved road is built, the initial development of lake thermokarst lasts for decades under a dry climate.
- 3) The abundant development of lake thermokarst in the

territory of Central Yakutia was triggered by the rise of the general moistening of the territory.

- 4) The flow of melt- and rainwater blocked by unpaved roads leads to the formation of a small barrier lake and, further, to the development of thermokarst.
- 5) The cutting of forest strips in the catchment areas of alases for the construction of linear structures causes these depressions to dry up.

References

- Bosikov, N.P. 1977. The dynamics of levels and the development of alas lakes in Central Yakutia. *Izvestia VGO*, 109: 357-361.
- Bosikov, N.P. 1989. The intensity of plowed fields destruction within inter-alas landscapes. *Geography and Natural Resources* pp. 83-86.
- Bosikov, N.P. 1998. Wetness variability and dynamics of thermokarst processes Central Yakutia.. *Permafrost Seventh International Conference Proceedings*, Yellowknife, Canada, pp. 71-74.
- Shnitnikov, A.V. 1957. The variability of the general moistening of the mainlands of the Northern Hemisphere. *Zapiski GO SSSR. Nov. ser. M.L. Vol. 16.*, 337 pp.
- Shur, Yu.L. 1988. *The upper permafrost horizon and thermokarst*. Novosibirsk: Nauka, 212 pp.
- Vasilev, I.S. 1982. *The regularities of the seasonal thawing of grounds in Eastern Yakutia*. Novosibirsk: Nauka, 132 pp.

Biological Properties of Bacteria Isolated from Permafrost in Central Yakutia

A.V. Brouchkov

Lomonosov Moscow State University, Moscow, Russia

A.M. Peterson, E.V. Glinska

Chernyshevsky Saratov State University, Saratov, Russia

G.I. Griva

Tyumen Science Center, SB RAS, Tyumen, Russia

V.E. Repin

Institute of Chemical Biology and Fundamental Medicine, SB RAS, Novosibirsk, Russia

Abstract

Cultures of microorganisms have been isolated from Pliocene-aged permafrost at the Mamontova Gora (Mammoth Hill) outcrop in Yakutia. The culturable bacteria are few and exist in frozen ground as sporadic survived cells; no spores or colonies have been observed on microscopic examination of samples. The bacteria are quite low in taxonomic diversity. All isolated strains are Gram positive and have a limited set of properties.

Key words: bacteria; biochemical reactions; permafrost; relict microorganisms; taxonomic diversity.

Introduction

Permafrost is widespread on our planet and is locally as old as hundreds of thousands to millions of years. Frozen ground is a natural storage of the Earth's oldest microbial communities and a pool of ancient genes and biomolecules (Ashcroft 2000). Data on viable bacteria found in permafrost have many exciting implications for the evolution of microbial life (Repin 2008), biodiversity on the Earth (Brown et al. 2001), existence of life on other planets (Abyzov et al. 2006), and potential biogeochemical activity of permafrost (Johnson et al. 2007, Brouchkov et al. 2009). Another important factor is that frozen ground can store viable pathogenic microbes, and special mitigation measures have to be developed in case of their spontaneous liberation as a result of natural or man-caused thawing of permafrost (Repin et al. 2000). Furthermore, knowledge of the properties of relict microorganisms can provide clues to their tenacity. This study focuses on new biochemical features of bacteria isolated from permafrost at the Mamontova Gora (Mammoth Hill) site in Yakutia.

Sampling Site

Mamontova Gora (Russian for *Mammoth Hill*) is an outcrop of ancient permafrost striking for 12 km along the left bank of the Aldan River, 325 km upstream from its inflow into the Lena. This is a currently eroding remnant of the Aldan-Amga watershed composed of up to 80 m thick alluvium sequences of different ages. Sediments at the base of the exposed section, where samples were collected, are mostly sand with Neogene flora. The composition (Markov 1973) records deposition in the Middle Miocene (11–16 Ma). Permafrost is known to have existed in this part of Eurasia in the Early Pleistocene, 1.8–2 myr ago (Lazukov 1989), but paleoclimate reconstructions (Volkova & Kulkova 1988, Zubakov 1990) from spore-pollen, paleogeographic, and stratigraphic evidence predict steady cooling throughout the second half of the Neogene and an abrupt drop of mean

annual temperatures at the Late Miocene-Early Pliocene boundary (5.5 Ma).

Permafrost began forming in the area when the mean July air temperatures fell to +12 to +16°C and the mean January temperatures became as cold as -12 to -32°C in the Late Pliocene (3.5 Ma) (Bakulina & Spector 2000). The Mammoth Hill permafrost never thawed later in the geologic history, as one may infer from the absence of surface glaciation in the Quaternary. During the Pleistocene glaciation in eastern Eurasia and West Siberia, the area was likely free from ice sheets, which could have caused thawing of older permafrost (Arkhipov & Volkova 1994, Grichuk et al. 1987). The Neogene sediments apparently remained frozen throughout the Pleistocene during the colder continental (colder than present) and dry climate with low annual precipitation. The Neogene permafrost persisted even during the Holocene optimum, judging by the cryostructure of the upper Miocene and younger sediments. Late Cenozoic tectonic activity (Lazukov 1989) prevented the territory from flooding during transgressions and from related thawing of permafrost, which happened in the coastal plains of Yakutia. Therefore, permafrost at the site may be as old as 3–3.5 Ma.



Figure 1. Sampling site.

Table 1. Morphological and cultural features of isolated strains

Strains	Culturing, colonies	Morphology			
		Gram stain	Cell shape	Spores	Mobility
6	Medium, opaque, round, yellow, flat, smooth, glossy	+	Short rods with rounded ends	-	+
13 15 17 30	Medium, opaque, irregularly-shaped, colorless, flat, wrinkled, glossy	+	Short rods with rounded ends	+	+
14	Small, semi-transparent, round, colorless, flat, smooth, glossy	+	Short rods with rounded ends	-	+
20 27 40	Large, opaque, round, colorless, flat, smooth, matted	+	Long rods with truncated ends	+	+
29	Large, opaque, round, colorless, flat, wrinkled, matted	+	Short rods with rounded ends	+	+
32	Small, semi-transparent, round, colorless, flat, smooth, glossy	+	Irregularly-shaped short rods	-	+
33 37	Small, semi-transparent, round, colorless, flat, smooth, glossy	+	Short rods with truncated ends	-	+
34	Small, semi-transparent, round, orange, flat, smooth, glossy	+	Short rods with truncated ends	-	+
39	Small, opaque, round, colorless, flat, wrinkled, glossy	+	Irregularly-shaped short rods	-	+

The permafrost was sampled from the lower and middle parts of the most strongly eroded and recently slumped upright bluff walls (Fig. 1), at 15–30 m above the river level and 40–50 m below the ground surface. According to our observations, thermal erosion at the site reaches a rate of 4–5 m per year in the upper section and 1–1.5 m/yr in the middle section. Sampling was from depths 1–1.5 m below the active layer, which ruled out the presence of previously thawed sediments.

Paleo-microbiological studies often face a problem of contamination. In order to check whether extant microbiota or DNA could penetrate into the permafrost monolith samples, a special test was performed in which a solution of synthetic amplicon (1100 bp D-loop of mitochondrial DNA) was placed on the surface of a sample. The amplicon concentrations at different depths in the sample measured after three months of storage implied surface contamination to be very unlikely in the undisturbed frozen ground, at least at the storage conditions we applied.

Results

Neither vegetative cells nor spores have been found under microscopic examination of smears of thawed permafrost. Therefore, bacteria must be few or, possibly, tightly coherent with the substrate (Zvyagintsev 1987). SEM images of the samples show sporadic cells coated with polysaccharide/polypeptide films.

Visible growth of the incubated bacteria appeared on the third day. The bacteria exhibited weak growth on solid media (fishmeal hydrolysate (FH) agar), often being semi-transparent, and produced some turbidity in liquid media. Smears contained small and large cells, Gram-positive

asporous rods, and irregularly shaped Gram-positive cocci.

The cultures isolated from the Petri dishes and broths were plated in FH agar for obtaining colonies. The inoculated bacteria were cultured at 28 and 37°C for three days. Most of cultures did not grow on replica plating, while inoculation in pure culture yielded strain Nos. 6, 13, 14, 15. After the soil suspension was incubated for two weeks at room temperature, rod bacteria of different sizes and cocci emerged in Gram-stained smears. Growth in another test, in soil suspension incubated following the above procedure, was weak on the first day and profuse on the third day, in all culture media. Gram-positive rod bacteria appeared in the smears. Unlike the first test, most cultures showed visible growth on replica plating. Inoculation in pure culture gave strain Nos. 17, 20, 27, 29, 30, 32, 33, 34, 37, 39, 40. Thus bacteria surviving in permafrost are in a dormant state and need some time to resume reproduction.

Some strains shared similarity in culture and morphology patterns and were tentatively grouped on this basis (Table 1). Strains (Nos. 13, 15, 17, 30) that developed irregularly shaped colonies with glossy wrinkled surfaces in FH agar made the largest group, and formed short Gram-positive rods with rounded ends in smears. Another group included strains (Nos. 20, 27, 40) that grew as large round colonies with matted surfaces on agar. That group differed from the previous one in cell morphology; the bacteria looked like long spore-forming rods with truncated ends.

Strain 29 was morphologically similar to the second group of sporous bacteria but had different culturing properties (Table 1). The other strains were Gram-positive rods different in morphology or culture. Isolation of such an amount of microorganisms was possible because their

Table 2. Biochemical reactions of isolated strains

Strains	Catalase	Oxidase	Voges-Proskauer test	Citrate	Reduction of nitrates	Hydrolysis			Formation of acids from							Formation of			N ₂ Fixation
						Casein	Gelatin	Starch	Glucose	Mannitol	Arabinose	Xylose	Lactose	Mannose	Sorbitol	Ammonia	Indole	Hydrogen sulfide	
6	+	+	-	-	+	-	-	-	-	-	-	-	-	-	-	-	-	+	-
13	+	+	+	+	+	-	+	-	-	+	-	-	-	+	-	-	-	-	-
14	+	-	-	-	+	-	-	-	-	-	-	-	-	-	-	-	-	-	-
15	+	+	+	+	+	-	+	-	-	+	-	-	-	+	-	-	-	+	+
17	+	+	+	+	+	-	+	-	-	+	-	-	-	+	-	-	-	+	+
20	+	-	-	+	+	-	+	-	-	-	-	-	-	+	-	-	-	+	+
27	+	-	-	-	+	-	+	-	-	-	-	-	-	+	-	-	-	-	+
29	+	-	+	+	+	-	+	-	-	+	-	-	-	+	-	-	-	+	+
30	+	+	+	+	+	-	+	-	-	+	-	-	-	+	-	-	-	+	+
32	+	+	-	-	+	-	+	+	-	-	-	-	-	-	-	-	-	+	+
33	+	+	+	+	+	-	+	+	-	+	-	-	-	-	-	-	-	+	+
34	+	+	-	-	+	-	-	+	-	-	-	-	-	+	-	-	-	+	-
37	+	+	-	-	+	-	-	-	-	-	-	-	-	-	-	-	-	+	-
39	+	+	-	+	+	-	+	-	-	+	-	-	-	+	-	-	-	-	+
40	+	-	-	+	+	-	+	-	-	-	-	-	-	+	-	-	-	-	+

resting state (endospores) maintained their tenacity in extreme physicochemical conditions (Greenblatt et al. 1999, Nicholson et al. 2000). More questions arise about asporous bacteria. The mechanism responsible for multiple year-long survival of biological molecules, even in the resting state, remains unclear (Baker & Agard 1994, Jaenicke 1996, Levy & Miller 1998).

Most of strains were capable of anaerobic growth on fishmeal agar or on Hiss's culture medium (Medzhidov 2003). Some strains exhibited anaerobic growth only on fishmeal agar with 0.2% KNO₃, possibly, by nitrate respiration. Strain Nos. 13, 17, 29, 30, and 33 were incapable of anaerobic growth on any medium we used. However, the same strains may possibly develop in anoxic environments upon some other substrates.

All isolated microorganisms were catalase-positive, reduced nitrates to gases, and were caseinase-free. The results of other biochemical tests varied in different strains. The isolated strains were remarkable in low saccharolytic activity. As for the peptolitic activity, most of them demonstrated an ability to release hydrogen sulfide on peptone decomposition. Most bacterial isolates (10 out of 15) fixed atmospheric nitrogen and grew profusely on Ashby's nitrogen-free culture medium. The nitrogen fixation ability of microorganisms is important for their survival under conditions of nitrogen shortage.

Interestingly, the strains of group 1 all behaved in a similar way in biochemical reactions. Those of group 2 differed only in their ability to use citrate as a source of carbon and

in hydrogen sulfide production. Strain Nos. 33 and 37, being similar in culture and morphology, differed in biochemical activity.

Having investigated the resistance of the strains to different physicochemical factors, we found out that most bacteria grew equally well at temperatures from +8 to +43°C. Such a broad temperature range was observed for bacteria isolated from permafrost (Abyzov et al. 2004). The lower temperature limit for most of the strains was +8°C.

When incubated at +2°C for two months, the bacteria developed no visible colonies. In previous experiments of this kind (Katayma et al. 2007, Brouchkov et al. 2009), some isolates could grow even at -5°C. High temperatures (+43°C) inhibited growth in four strains. The bacteria isolated from permafrost differed markedly in temperature resistance. For instance, the optimal growth temperature for *Bacillus* sp., strain F, isolated from samples at the same Mammoth Hill site (Brouchkov et al. 2009) was +37°C, while strains from the Yakutian and Alaskan ice did not grow at +30°C (Katayma et al. 2007).

The presence of 6.5% NaCl in the medium inhibited growth in seven strains; at 10% NaCl, none of the analyzed strains showed any visible growth. The lower pH limit at which the isolates could grow was in the range from 5.0 to 6.0. Nine strains were resistant to high pH (11.0) (Table 3).

Comparison of the tolerance limits to different physicochemical factors showed that the strains of group 1 were similar while those of group 2 differed in tolerance to 6.5 % NaCl and 5.0 pH.

Table 3. Viability of isolated strains in extreme conditions

Strains	Growth at														
	+2°C	+8°C	+43°C	6.5%NaCl	10%NaCl	pH 4.0	pH 5.0	pH 5.5	pH 6	pH 8.5	pH 9.0	pH 10.0	pH10.5	pH 11.0	pH 12.0
6	-	+	+	+	-	-	-	+	+	+	+	-	-	-	-
13	-	+	+	+	-	-	+	+	+	+	+	+	+	+	-
14	-	+	-	-	-	-	-	-	+	+	+	-	-	-	-
15	-	+	+	+	-	-	+	+	+	+	+	+	+	+	-
17	-	+	+	+	-	-	+	+	+	+	+	+	+	+	-
20	-	+	+	-	-	-	-	+	+	+	+	+	+	+	-
27	-	+	+	-	-	-	-	+	+	+	+	+	+	+	-
29	-	+	+	+	-	-	+	+	+	+	+	+	+	+	-
30	-	+	+	+	-	-	+	+	+	+	+	+	+	+	-
32	-	+	-	-	-	-	+	+	+	-	-	-	-	-	-
33	-	+	+	+	-	-	-	+	+	+	+	+	+	+	-
34	-	-	-	-	-	-	-	+	+	+	+	-	-	-	-
37	-	+	-	-	-	-	-	-	+	+	+	-	-	-	-
39	-	-	+	-	-	-	-	-	+	+	+	-	-	-	-
40	-	+	+	+	-	-	+	+	+	+	+	+	+	+	-

Table 4. Antibiotic resistance of bacterial strains

Chemical groups of antibiotics	Antibiotic	Strains														
		6	13	14	15	17	20	27	29	30	33	37	39	40	47	
Aminoglycosides	Streptomycin	++	+	+	++	++	++	++	++	+	-	-	-	++	++	
	Neomycin	++	++	++	++	++	++	++	++	++	++	++	++	++	++	
Macrolides	Erythromycin	++	-	-	++	++	++	++	++	+	++	-	-	++	++	
	Oleandomycin	++	-	-	+	++	++	++	-	++	-	-	-	++	++	
Betalactams	Benzylpenicillin	++	++	-	++	++	+	-	++	++	++	-	-	-	-	
	Oxacillin	++	++	-	++	++	-	-	++	++	++	-	-	-	-	
	Carbenicillin	++	++	-	++	++	+	+	++	++	++	++	++	+	+	
Aromatic antibiotics	Levomycetin Chloramphenicol	-	-	-	-	-	-	+	-	-	-	-	-	-	-	

Note: -- resistant strains; + - moderately resistant strains; ++ - sensitive strains.

In other experiments, we studied antagonism of the strains against several test cultures (*E. coli* 113-13, *S. aureus* 209-P, *B. cereus* 8035). *E. coli* antagonism was observed in one strain (29). Strain Nos. 13, 15, 30, and 39 inhibited the growth of Gram-positive *S. aureus* and *B. cereus*; Nos. 17 and 33 were antagonistic to *B. cereus* while strain 37 stimulated its growth; strain 29 was active against *S. aureus*. Given that the species isolated from permafrost are mostly Gram-positive, the capability of the isolates to impede the growth of these bacteria makes them more competitive in their natural environment.

Strain Nos. 6, 15, 17, and 30 were sensitive to all antibiotics except chloramphenicol. Strain Nos. 14, 37, 39 showed the highest resistance. Neomycin caused a prominent

antibacterial effect on all isolates. Chloramphenicol showed weak antibacterial activity: only strain 27 was sensitive to it (Table 4).

The obtained data differ from those reported for microorganism isolated from Antarctic ice which demonstrated high antibiotic resistance (Andreeva et al., 2008). Possibly, this is because the Antarctic ice is younger than the Yakutian permafrost. Microorganisms from natural ice, though being taxonomically similar, differ in the range of antibiotic resistance as a function of isolation place, ages of samples, and possibility to interact with the extant organisms (Mindlin et al. 2008).

Conclusions

Permafrost from the Mammoth Hill outcrop contains viable microorganisms. Culturable bacteria are few and exist as sporadic survived cells. No colonies were observed on microscopic examination of soil samples.

The isolated organisms are of limited taxonomic diversity. Most of them turn out to be non-culturable and stop growing when inoculated into synthetic culture media. No dominant cultures have been revealed. All isolated strains are Gram positive and have a narrow scope of properties.

The Mammoth Hill isolates stand out in their capability of nitrogen fixation, sensitivity to antibiotics, weak antagonistic activity, and growth within broad ranges of temperatures, salinity, pH, and other extreme conditions.

The bacteria with the revealed biological properties, given the very fact of their ancient age, are obviously worth further investigation and may have good prospects for use in biotechnologies.

References

- Abyzov, S.S., Mitskevich, I.N., Poglazova, M.N., & Ivanov, M.V. 2004. Microbiological studies of the Antarctic ice sheet. *Transactions, S.N. Vinogradsky Institute of Microbiology* Issue 12, 7–28.
- Abyzov, S.S., Duxbury, N.S., & Bobin, N.E. 2006. Super-long anabiosis of ancient microorganisms in ice and terrestrial models for development of methods to search for life on Mars, Europa and other planetary bodies. *Advances in Space Research* 38 (6), 1191–1197.
- Andreeva, I.S. 2008. Natural reservoirs of multiple antibiotic resistance of microorganisms. In *Proc. IV Congress of the Russian Society of Biochemists and Molecular Biologists*. Novosibirsk, 11–15 May, p. 613 (in Russian).
- Arkhipov, S.A. & Volkova, V.S. 1994. *Pleistocene Geological History, Landscapes, and Climates of West Siberia*. NIC OIGGM SO RAN, Novosibirsk, 105 pp. (in Russian).
- Ashcroft, F., 2000. *Life at the Extremes*. Harper Collins, 326 pp.
- Baker, D. & Agard, D. 1994. Kinetics versus thermodynamics in protein folding. *Biochemistry* 33, 7505–7509.
- Bakulina, N.T. & Spektor, V.B. 2000. Paleoclimate reconstructions for the Neogene of Yakutia from spore-pollen data. In *Climate and Permafrost, Institute of Permafrost*, Maksimov G.N., Fedorov A.N. (Eds.), Yakutsk, pp. 21–32 (in Russian).
- Brinkmeyer, R., Knittel, K., & Jürgens, J. 2003. Diversity and structure of bacterial communities in Arctic versus Antarctic pack ice. *Appl. Environ. Microbiol.* 11, 6610–6619.
- Brown, M.V. & Bowman, J.P. 2001. A molecular phylogenetic survey of sea-ice microbial communities (SIMCO). *FEMS Microbiology Ecology* 35, 267–275.
- Brouchkov, A.V., Melnikov, V.P., Sukhovey, Yu.G., Griva, G.I., Repin, V.E., Kalenova, L.F., Brenner, E.V., Subbotin, A., Trofimova, Yu.B., Tanaka, M., Katayama, T., & Utsumi, M. 2009. Relict microorganisms of permafrost as possible objects of gerontology. *Uspekhi Georntologii*, 22 (2), 253–260.
- Greenblatt, C.L., Davis, A., & Clement, B.G. 1999. Diversity of microorganisms isolated from amber. *Microbial Ecology* 38, 58–68.
- Grichuk, V.P., Zelikson, E.M., & Borisova, O.K. 1987. *Reconstruction of Early Cenozoic climates from paleoflora*, in: *Earth's Climates in the Geological Past*, Nauka, Moscow, pp. 69–77 (in Russian).
- Griva, G.I. 2005. *Development of Gas Fields of Yamal: Geoenvironment Conditions*. Tomsk University, Tomsk, 330 pp. (in Russian).
- Jaenicke, R. 1996. Stability and folding of ultrastable proteins. In *Eye Lens Crystallins and Enzymes from Thermophiles* FASEB, 10, 84–92.
- Johnson, S.S., Hebsgaard, M.B., & Christensen, T.R. 2007. Ancient bacteria show evidence of DNA repair. *Proc. Natl. Acad. Sci. USA* 104, 14401–14405.
- Katayama, T., Tanaka, M., Moriizumi, J., & Brouchkov, A. 2007. Phylogenetic analysis of bacteria preserved in a permafrost ice wedge for 25000 years. *Appl. Environ. Microbiol.* 73 (7), 2360–2363.
- Lazukov, G.I. 1989. *The Pleistocene of the USSR Territory*. Vissaya Shkola, Moscow, 320 pp. (in Russian).
- Levy, M. & Miller, S.L. 1998. The stability of the RNA bases: *Implications for the origin of life*. *Biochemistry* 95 (14), 7933–7938.
- Markov, K.K. (ed.). 1973. *The Mammoth Hill Section of Recent Deposits*. Moscow University, Moscow, 198 pp. (in Russian).
- Medzhidov, M.M. 2003. *Microbiological Growth Media. A Handbook*. Meditsina, Moscow, 208 pp. (in Russian).
- Mindlin, S.Z. Soina, V.S., Petrova, M.A., & Gorlenko, Zh.M. 2008. Isolation of antibiotic resistance bacterial strains from Eastern Siberia permafrost sediments. *Journal of Genetics* 44, 27–34 (in Russian).
- Netrusov, A.I. (ed.). 2005. *Practical Training in Microbiology*. Akademiya, Moscow, 608 pp. (in Russian).
- Nicholson, W.L., Munakata, N., & Horneck, G. 2000. Resistance of Bacillus endospores to extreme terrestrial and extraterrestrial environments. *Microbiol. Mol. Biol.* 64, 548–572.
- Repin, V.E. 2008. Evolution patterns of bacteria. In *Evolution of Life during Abiotic Events of the Earth*. Rusinek, O.T., Fialkov, V.A. (Eds.). Izd. SO RAN, Novosibirsk, pp. 253–264 (in Russian).
- Repin, V., Gus'kov, A.A., & Belanov, E.F. 2000. Permafrost as a potential source for replenishing collections with pathogenic microorganisms. *Hydrological Science and Technology* 16 (1-4), 35 - 39.
- Volkova, V.S. & Kulkova, N.A. 1988. Quantitative estimate of some elements of Late Oligocene and Neogene climates. In *Palynology of the USSR*, Nauka, Novosibirsk, pp. 31–38 (in Russian).
- Zubakov, V.A. 1990. *Neogene Gbal Climate*. Gidrometeoizdat, Leningrad, 223 pp. (in Russian).
- Zvyagintsev, D.S. 1987. *Soils and Microorganisms*. Moscow University, Moscow, 256 pp. (in Russian).

$\delta^{18}\text{O}$ Variations in Late Holocene Ice-Wedges and Winter Air Temperature Variability in the Yamal Peninsula, Russia, and in Adventdalen, Svalbard

N.A. Budantseva, A.K. Vasilchuk, A.M. Zemskova, Yu.N. Chizhova, Yu.K. Vasilchuk
Lomonosov Moscow State University, Department of Geography and Geology, Moscow, Russia

H. H. Christiansen
The University of Svalbard (UNIS), Geology Department, Longyearbyen, Norway

Abstract

The content of stable oxygen isotopes in syngenetic Late Holocene ice-wedges located in the Erkutayakha River valley in Southern Yamal and in the Adventdalen Valley in Svalbard were investigated and compared. The variation of the $\delta^{18}\text{O}$ values did not exceed 2–3.5‰ in the ice-wedges of the two sites, which are 2000 km apart but located in different climatic areas. The isotope data of the ice-wedges enable reconstruction of the mean winter air temperature for the Late Holocene. The variability range corresponds to approximately 2.5°C. There is a correlation between isotope curves from the ice-wedge in the Adventdalen Valley and from glacier ice from the Lomonosov Plateau in Svalbard. This indicates the correspondence between the scale and the chronology of the change in the climatic conditions in the Late Holocene.

Keywords: stable oxygen isotopes; radiocarbon dating; Svalbard; Yamal.

Introduction

Here we present a study of Late Holocene ice-wedges from the Erkutayakha River valley in Southern Yamal and from the Adventdalen Valley in Svalbard. The main purposes of the study are to directly date the age of the ice-wedges; to investigate the content of stable oxygen isotopes in the ice of one ice-wedge in Svalbard and one from the Yamal Peninsula, Russia, which have common morphological and genetic characteristics; and to reconstruct the temperature conditions of the ice-wedge development.

Areas of Investigation of Ice-Wedges

Ice-wedges in the valley of the Erkutayakha River in Southern Yamal

Normally ice-wedge polygons are not clearly marked at the floodplains of the southern Yamal rivers, although ice-wedges are widespread there.

The climate of Southern Yamal is subarctic, with a long severe winter and a very short summer (not longer than 50–60 days). The warmest months of the year are July and August (the mean monthly temperature ranges from 5 to 7°C), while the coldest month is January and sometimes February (the mean temperature is from -22 to -24°C). The mean annual air temperature fluctuates between -8 and -10°C. Annual precipitation totals 400 mm, according to data of the Marresale meteorologic station.

The Holocene syngenetic floodplain containing wedge ice was investigated at the left bank of the Erkutayakha River in the summer of 1998 (68°11'18" N, 68°51'39" E) (Fig. 1).

The elevation of the floodplain surface (above the minor level of the river reaches 2.5–3 m). The polygons are more distinct in drier areas. Open frost cracks with the width of 5 mm are observed here. Brown peat is revealed in one of the bank outcrops.

Within the studied cross section, thickness of peat was 0.2 m. It contained stems and roots of plants. The peat

layer was underlain by 0.5-m-thick grey sand with massive cryostructure. Down to the depth of 1.5 m, very peaty and stratified sand occurred, mainly with massive cryostructure and lenses of segregated ice

An ice-wedge 0.8 m wide at the top was exposed down to 0.4 m. The ice was clear and contained no admixtures. Individual veins with widths up to 4–5 mm were observed in it.

Ice-wedges in the Adventdalen Valley in Svalbard

Ice-wedges are widespread in Svalbard, primarily in the lower parts of large sediment-filled valleys (e.g., in the Reindalen and Adventdalen valleys) (Matsuoka &

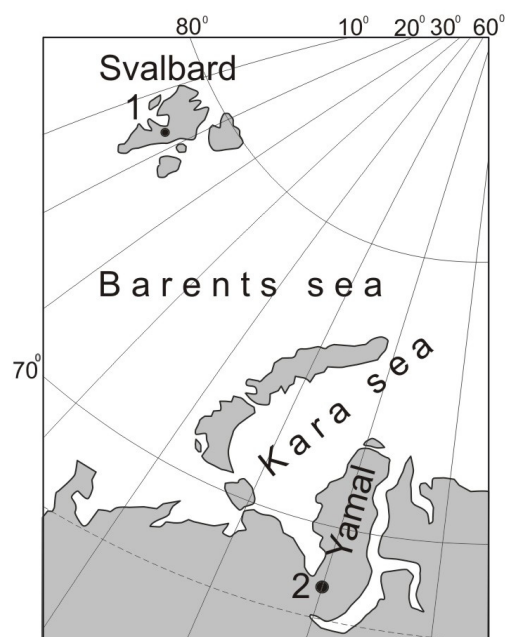


Figure 1. The location of the research areas. 1 - the valley of the Adventselva River in Svalbard, 2 - the valley of the Erkutayakha River on the Yamal Peninsula with polygonal (patterned) relief.

Hirakawa 1993, Christiansen 2005). The Adventdalen Valley is located in central Svalbard. It is a wide U-shaped valley, 3.5 km wide and 27 km long.

The climate of the area is polar, with about 190 mm of snow precipitation per year. The area is characterized by considerable temperature fluctuations during the winter period due to its maritime location. Strong winds from the east dominate in winter, causing shallow snow thickness, normally less than 1 m. Permafrost is continuous in the Adventdalen Valley, and it is up to about 100 m thick. The thickness of the seasonally thawed layer is about 95–100 cm (Christiansen 2005).

Ice-wedges are widespread in the valley. The study site (78° 12' 05" N, 15° 50' 04" E, 9 m a.s.l.) is located on the lower part of a large colluvial fan with a proximal loess cover. Elementary ice veins (2–3 mm wide on average) have been identified in open fissures at the beginning of summer, and they penetrate to the ice-wedge (Matsuoka & Hirakawa 1993). Each ice-wedge cracks and acquires a new annual vein on average once in 6–7 years (Matsuoka & Hirakawa 1993).

Frost cracking is normally active when the mean daily winter air temperature is below -15°C (Matsuoka & Hirakawa 1993). Christiansen (2005) made observations at the polygons in Adventdalen, where the mean annual ground temperature at the bottom of the active layer was about -6°C. According to her observations, frost cracking was particularly active when the mean daily air temperature dropped down to or below -20°C and remained at this level for some time while the ground temperature at the bottom of the active layer decreased to -15°C.

Methods

Samples of ice-wedges for isotope analysis from the Erkutayakha site were sampled according to a technique designed by Yu.K. Vasil'chuk (Vasil'chuk 1992, Vasil'chuk & Vasil'chuk 1996). This technique suggests detail sampling of ice along vertical and horizontal profiles. For isotope analysis from the Erkutayakha site, we selected 25 samples of ice from the upper part of the ice-wedge along a horizontal profile from the left to right sides of the wedge. The ice was sampled from blocks cut with an axe at different distances from the left side. Samples were filtered for control and analyzed in two laboratories. The most valid values are shown on an isotopic diagram (Fig. 2). Sixty-five samples of the ice-wedge were sampled from the Adventdalen site from the upper part of the ice-wedge along a horizontal profile using a chain saw. It was sawn long triangles from the top ice-wedge, exposed in trenches through the active layer at the end of summer.

The ice samples were kept frozen at -19.5°C and were analyzed in the laboratory at -5°C. All the ice sample fragments were described on a light table, photographed in the transmitted light, and further sawed up with a hand saw. The mineral admixtures were cleaned out of the samples with a scraper. Samples with a width from 0.7 to 2 cm were put into separate plastic bags. The sawed samples thawed at 7°C, and the obtained water was poured into containers of 50 ml.

The isotope composition of the Svalbard ice-wedge was determined one month after the sampling, using the Delta-V

mass spectrometer equipped with standard Gas Bench in the stable isotope laboratory of the Geography Department at the Lomonosov Moscow State University. When measuring $\delta^{18}\text{O}$, we balanced the analyzed samples with CO_2 during 24 hours. To calibrate the measurements, we utilized the international standard of the mean ocean water SMOW-V and the international laboratory standards of the IAEA, as well as of the isotope laboratory of the Austrian Institute of Technology.

The isotope composition of the Southern Yamal ice-wedge was determined by D. Rank and V. Papesch in the Arsenal Scientific Research Center in Vienna and by E. Soninnen in the isotope laboratory of the University of Helsinki.

Organic matter from the floodplain was radiocarbon-dated in the Geology Institute of RAS.

Results of Radiocarbon Dating of the Ice-Wedges ice in the Erkutayakha and Adventdalen Valleys

Radiocarbon dating revealed the young age of the ice wedge and host sediments in the Erkutayakha Valley. The age of the peat from the ground vein at the depth of 0.3 m made up 1000 ± 170 years (GIN-10632), while the concentrations of roots at the depth of 1.0 m were dated to be 1820 ± 80 years (GIN-10986). The similar age of 1820 ± 100 years (Hel-4492) was obtained in the radiocarbon laboratory of the University of Helsinki, which confirms the validity of the obtained dates.

These radiocarbon dates make it possible to evaluate the time and intensity of the accumulation of ice veins and the sediments containing them. The date of the ground vein (about 1000 years ago) most probably registers the period of active development of the peat vein and of the ice wedge after the transition of the surface to the stage of a high floodplain. Thus, considering that the date of 1800 years relates to the depth of 1.0 m, we assume that about 70–80 cm of sand accumulated for the period of not more than 800 years. We may assume that the ice veins most probably began to form in the period of accumulation of a very peaty sand (i.e., about 1800–2000 years ago). Then, due to the relatively short-term flooding of the area (between 1800 and 1000 years ago), there accumulated a horizon of the gray sand, while the development of veins was low active. They began to increasingly grow about 1000 years ago when the surface became dry again and acquired the regime of a high floodplain. In general, it may be stated that: 1) The sediments composing the upper 2–3 m of the floodplain's profile accumulated approximately 2000 years; 2) The surface of the high floodplain transitioned to the subaerial regime about 1000 years ago; 3) The wedge ice of the floodplain has the age of about 2000 years.

Organic material from the outer part of an ice-wedge in the Adventdalen Valley, close to the study site, was ^{14}C AMS dated to 2850–2955 cal. year BP (AAR-6674) (Jeppesen 2001). Two other ^{14}C AMS dates from 2.6 and 2.3 m below ice-wedge terrain in both sides of the Adventdalen valley gave ages of 2355–2720 cal. years BP (AAR-6672) and 3590–3695 cal. years BP (AAR-6673) (Jeppesen, 2001). Therefore, we assume that the studied ice wedge has an age of around 3000 years.

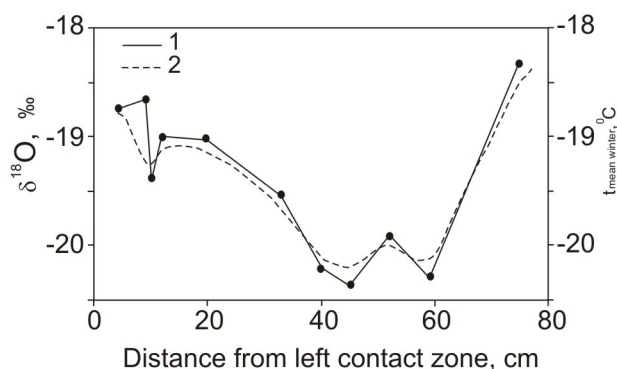


Figure 2. The $\delta^{18}\text{O}$ variations in the Late Holocene ice vein of the Erkutayakha River's valley: 1 – the $\delta^{18}\text{O}$ values; 2 – the mean winter air temperatures.

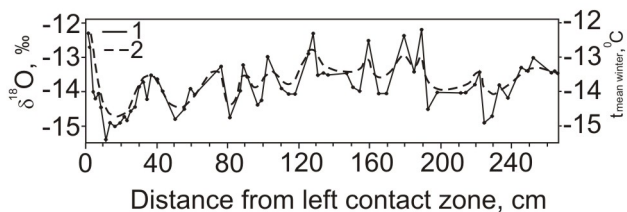


Figure 3. The $\delta^{18}\text{O}$ variations in the studied ice-wedge from the Adventdalen Valley: 1 – the $\delta^{18}\text{O}$ values; 2 – the mean winter air temperatures calculated according to Yu.K. Vasilchuk (1992, 1993) equation.

Variations of Stable Isotopes in the Wedge Ice

The $\delta^{18}\text{O}$ variations in the ice-wedge of the Erkutayakha River valley

The $\delta^{18}\text{O}$ values in the ice-wedge varied from -18.0 to -20.63‰ (Fig. 2), while in the segregated ice lenses of the floodplain ice-wedge host sediments varied from -15.01 to -19.76‰. There is good correlation between the isotope values obtained in the different laboratories used. The relatively narrow range of the $\delta^{18}\text{O}$ values; fluctuations indicates rather stable winter conditions at the time of ice-wedge development. The $\delta^{18}\text{O}$ values make up about -18‰ in the contemporary ice wedge in Southern Yamal.

For calculation of mean winter temperature, we have applied the equation of Yu.K. Vasilchuk (Vasilchuk 1992, 1993) connecting oxygen isotope values of ice-wedges and mean winter/January air temperatures:

$$T_{\text{mean winter}} = \delta^{18}\text{O}_{\text{ice-wedge}} (\pm 2^\circ\text{C}) \quad (1)$$

$$T_{\text{January}} = 1,5 \delta^{18}\text{O}_{\text{ice-wedge}} (\pm 3^\circ\text{C}) \quad (2)$$

The calculation shows that the mean winter air temperature in Southern Yamal during last 2000 years varied from -17 to -20°C (i.e., it was close to the contemporary one).

The $\delta^{18}\text{O}$ variations in the ice-wedge of the Adventdalen Valley

The $\delta^{18}\text{O}$ values in the ice-wedge we studied in Adventdalen range from -12.23‰ to -15.4‰ (Fig. 3).

According to earlier collected data from the ice-wedges of the Adventdalen Valley, the $\delta^{18}\text{O}$ values ranged from -11.5‰

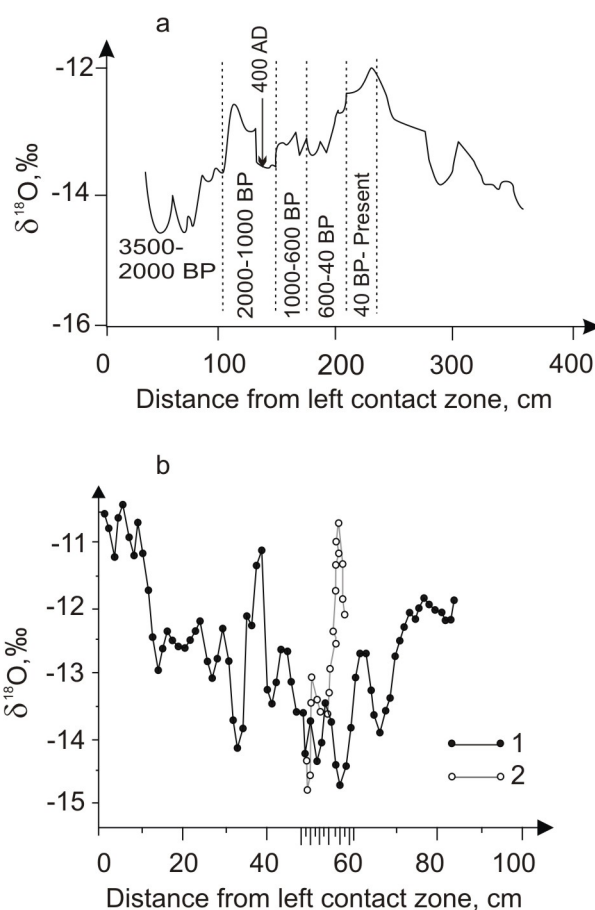


Figure 4. The $\delta^{18}\text{O}$ variations in the ice-wedges from the Adventdalen Valley a) from J.W. Jeppesen (2001) from close to the ice-wedge studied in this paper, b) from H. Vittinghus et al. (2008) 1 - lower ice-wedge profile, 2 - upper ice-wedge part.

to -15.5‰ (Jeppesen 2001) and from -10.5‰ to -14.8‰ (Vittinghus et al. 2008) (Fig. 4).

Evaluating the entire range of the $\delta^{18}\text{O}$ variations (3-5‰), we observe that the variations of the stable oxygen isotopes in the ice-wedges of the Adventdalen Valley are typical of the Holocene ice-wedges, which, as a rule, make up 3–4‰ (Vasilchuk 2006). The calculation of mean winter temperatures based on the equation of Yu.K. Vasilchuk (Vasilchuk 1992, 1993) shows that the mean winter air temperature in Adventdalen varied from -12° to -15°C (Fig. 3).

The correlation between ice-wedge isotope variation from the Yamal Peninsula and from Svalbard

The $\delta^{18}\text{O}$ values in the ice-wedge of the Erkutayakha River valley in southern Yamal vary within the range of 2.6‰: from -18.0 to -20.63‰. The $\delta^{18}\text{O}$ values in the ice-wedge from Adventdalen Valley vary by 3.2‰: from -12.23‰ to -15.4‰.

The isotope data indicate that the Svalbard winters are less severe (compare Fig. 2 and Fig. 3), but isotope variations are more expressed compared to the Yamal Peninsula (Fig. 5). We select for comparison two fragments of isotopic curves where we have found some coincidence of peaks.

The isotopic record very likely registers all the most severe winter conditions, while mild winters are only partly registered. As a rule, cracking and development of an annual

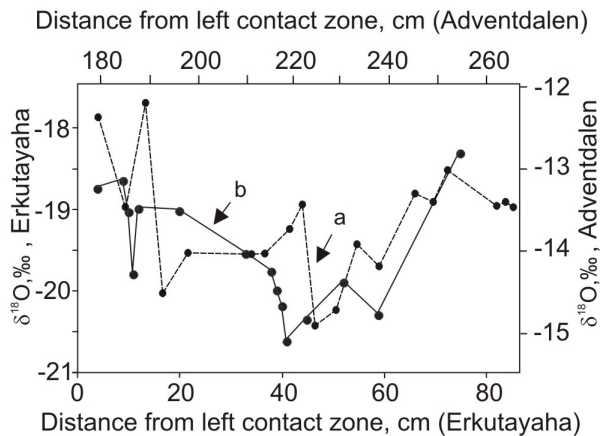


Figure 5. Comparison of the isotopic record fragments of the (a) ice wedge at the Adventselva River floodplain and (b) ice-wedge in the Erkutayakha River floodplain.

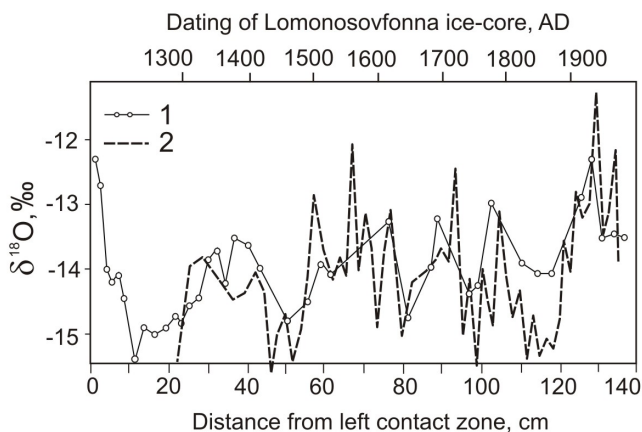


Figure 6. The comparison between the isotope curves of the ice-wedge in the Adventdalen Valley (1) and the glacial ice of the Lomonosov Plateau (2) (from Kotlyakov & Gordienko 1982).

ice vein occurs in severe winters. In mild winters, cracking occurs less often and ice veins form rarely, therefore the isotope diagrams may not register many mild winters.

Comparing the Isotope Data from the Ice-Wedges with Svalbard Glaciers

The ice-wedges that we studied at the floodplain of the Erkutayakha River valley in Southern Yamal and in the Adventdalen Valley in Svalbard are both most likely aged within the last 3000 years. Thus we can regard them as synchronous and chronologically comparable.

We compared the isotope curves of the ice veins with the isotope curve of the glacial ice of the Lomonosov Plateau in Svalbard obtained by V.M. Kotlyakov and F.G. Gordienko on the basis of the data collected by Ya.-M.K. Punning. The ice core from the borehole of the Lomonosov Plateau represents a nicely preserved ice stratigraphy from Svalbard (Kotlyakov & Gordienko 1982, Punning et al. 1987).

The drill core's base was dated to the 12th century. The glacial ice at the Lomonosov Plateau accumulated in the period comprising the second half of the accumulation stage of the ice-wedges studies here.

The comparison drawn between the Svalbard isotope curves of the ice-wedge and the ice core from the Lomonosov Plateau showed close ranges of the isotope content variation: $\delta^{18}\text{O}$ varied from -12.3‰ to -15.5‰ in the ice-wedge, while in the glacial ice it ranged from -11.3‰ to -15.5‰. The coincidence of some isotope peaks was also registered (Fig. 6).

Conclusions

- 1) Syngenetic ice-wedges are revealed in the upper profile part of the high floodplains in the valley of the Erkutayakha River in Southern Yamal and in the Adventdalen Valley in Svalbard. The ice-wedges developed during the Late Holocene, mainly within the last 3000 years, and continue to grow at present.
- 2) The close ranges of the isotope variations and the coincidence of the peaks of the Svalbard isotope curves of the ice-wedge as well as of the ice core testify to the correspondence between the scale and the chronology of the change in the climatic conditions of the given region for the last 3000 years.
- 3) The change of the $\delta^{18}\text{O}$ values for the last 3000 years that occurred in two ice-edge profiles is characterized with the close ranges of variations: the $\delta^{18}\text{O}$ values varied by 2.6‰ (from -18.0 to -20.63‰) in the Erkutayakha River valley of Southern Yamal; at the Adventdalen Valley the $\delta^{18}\text{O}$ values varied by 3.2‰ (from -12.23‰ to -15.4‰).
- 4) The isotopic records of the ice-wedges make it possible to reconstruct the mean winter air temperatures for the last 3000 years. The ranges of their variability were also close, and equal 2.5°C (from -18 to -20.5°C) in Southern Yamal and 3°C (from -12 to -15°C) in Svalbard.

Acknowledgments

The authors are grateful to A. Sinitsin, P. Valthard for the assistance in the field research. The research was partially financed by the Russian Foundation for Basic Research (grants 10-05-00986 and 11-05-01141) and by the Federal Agency. The University Centre in Svalbard is thanked for logistical assistance with the fieldwork in Svalbard.

References

- Christiansen, H.H. 2005. Thermal regime of ice-wedge cracking in Adventdalen, Svalbard. *Permafrost and Periglacial Processes* Vol. 16. Iss. 1: 87–98.
- Jeppesen, J.W. 2001. *Palaeoklimatiske indikatorer for central Spitsbergen, Svalbard. Eksemplificeret ved studier af iskiler og deres vaertssediment*. Master's thesis, University of Copenhagen. UNIS. Svalbard (in Danish).
- Kotlyakov, V.M. & Gordienko, F.G. 1982. *Isotopic and geochemical glaciology*. Leningrad. Gidrometeoizdat. 288 pp.
- Matsuoka, N. & Hirakawa, K. 1993. Critical polygon size for ice-wedge formation in Svalbard and Antarctica. *Permafrost. Sixth International Conference, Proceedings*. Vol. 1. Beijing, China. Wushan,

- Guangzhou: South China University of Technology Press: 449 – 454.
- Punning, J.-M., Vaikmäe, R., & Tøugu, K. 1987. Variations of $\delta^{18}\text{O}$ and Cl^- in the ice cores of Spitsbergen. *J. Phys. Colloques (VIIth Symposium on the Physics and Chemistry of Ice)*. Paris. Vol. 48. N C1.: 619–624.
- Vasil'chuk, Yu.K. 1993. Northern Asia cryolithozone evolution in Late Quaternary Permafrost. Sixth International Conference, Proceedings. Vol. 1. Beijing, China. South China University of Technology Press. Wushan, Guangzhou: 945–950.
- Vasil'chuk, Yu.K. 1992. *Oxygen isotope composition of ground ice (application to paleogeocryological reconstructions)*. Theoretical Problems Department. The Russian Academy of Sciences, Geological Faculty of Moscow University, Research Institute of Engineering Site Investigations. Moscow. Vol. 1, 420. Vol. 2; 264.
- Vasil'chuk, Yu.K. & Kotlyakov, V.M. 2000. *Principles of isotope geocryology and glaciology. A comprehensive textbook*. Moscow University Press, 616 pp.
- Vasil'chuk, Yu.K. 2006. *Ice Wedge: Heterocyclity, Heterogeneity, Heterochroneity*. Moscow University Press, 404 pp.
- Vasil'chuk, Yu.K., Budantseva, N.A., & Zemskova, A.M. 2011. $\delta^{18}\text{O}$ variation of Late Holocene ice wedges of Adventdalen, Svalbard. *Fourth Conference of Russian geocryologists*. Moscow State University. Moscow. Vol.1: 291-297.
- Vasil'chuk, Yu.K. & Vasil'chuk, A.C. 1996. Late Pleistocene oxygen isotope curves and radiocarbon dating for syngenetic ice-wedges. International Workshop on isotope-geochemical research in Baltic Region. Lohusalu, Estonia. Centre for Isotope Research. University Groningen. The Netherlands: 77–92.
- Vittinghus, H., Christiansen, H.H., Meyer, H., & Elberling, B. 2008. Hydrogen and oxygen isotope studies from an ice wedge in Svalbard permafrost. *Ninth International Conference, Extended Abstracts*. University of Alaska Fairbanks: 333–334.

Mathematical Simulation of Ground Freezing with the Visualization of Cryogenic Structure under Formation

V.G. Cheverev, E.V. Safronov

Lomonosov Moscow State University, Faculty of Geology, Department of Geocryology, Moscow, Russia

Abstract

A numerical solution of the mathematical model of freezing and frost heave of ground under varying conditions of heat and mass transfer with regard to moisture migration, thaw shrinkage, and the formation of a layered structure is discussed.

Keywords: cryogenic structure; freezing; grounds; mathematical simulation.

The published results of experimental studies of the parameters of moisture transfer in frozen, freezing, thawing, and thawed grounds (see references) provided the basis for the development of a theory of cryogenic moisture transfer and frost heave of freezing grounds that, given the determined mechanism of moisture transfer, can be more specifically called a “filtration-diffusion theory.”

The essence of the theory is as follows (Cheverev 2004).

Different categories of unfrozen water having physical-chemical connection with the mineral component of ground can, to various extents, take part in cryogenic moisture transfer. However, the major role is played by the osmotic category of unfrozen water in view of its highest specific content and its ability to transmit pore pressure. Therefore, the dominant mechanism in the formation of the driving forces of the cryogenic flow of moisture in freezing ground is the osmotic mechanism stemming from the existence of an electric double layer (EDL).

At the same time, chemically and physical-chemically adsorbed categories of unfrozen water as well as immobilized pore solution reduce the frost heave of freezing ground: adsorbed water, due to its insignificant quantity and low mobility; the water of intra-crystalline swelling, due to its non-participation in transit moisture flow; and pore solution, due to its competing interaction with a diffuse layer of cations and the non-presence of physical-chemical connection with the mineral skeleton.

As established experimentally, a layer of transit moisture transfer with virtually no moisture gradients, but with pore pressure gradients, is formed in the thawed zone in front of the moving freezing boundary during the ground freezing. The moisture content of this layer corresponds to the shrinkage limit, and the process of thaw shrinkage of freezing ground is caused by the formation of negative pore pressure in this zone. In the process of ground consolidation in front of the freezing boundary, the flow of water from an external source into the freezing zone emerges and gradually increases.

There is an excess of the initial moisture content over the moisture content of the shrinkage limit ($\Delta W = W_{\text{beg}} - W_{\text{shr}}$), which is related to the fact that moisture in freezing ground takes part in the formation of schlieren ice. A massive cryogenic structure of mineral layers and the content of unfrozen water are formed from the ground moisture content that corresponds to the shrinkage limit. Where the ground moisture content does not exceed the moisture content of

the shrinkage limit during ground freezing, frost heave deformations can occur only due to the increase of water volume in the process of water-ice phase transition. The emergence of an additional flow of water from an external source into the freezing zone means the transition from a closed system of moisture exchange to an open one. This is connected to the increase of frost heaving of freezing ground, which presents the greatest scientific and practical interest.

Under the conditions of quasi-steadiness of the freezing process, the deformation of frost heave due to the external flow of water depends on the hydraulic conductivity of ground (λ_w), the pressure gradient of cryogenic migration ($\text{grad}P_w = [-P_w(T) + P_{w0} + P_w(G)] / H_f$), and the duration of cryogenic migration, as expressed by the following equation:

$$\Delta H = 1.09 \tau_i \lambda_w [-P_w(T) + P_{w0} + P_w(G)] / H_f + 0.09 H_{\text{shr}} (W_{\text{beg}} - W_{\text{shr}}) + 1.09 H_f (W_{\text{shr}} - W_w) + K_{\text{str}} H_f + H_f (n - W_{\text{beg}}), \quad (1)$$

where H_f is the thickness of the frozen zone, W_{shr} is the volumetric moisture content of the ground shrinkage limit, H_{shr} is the thickness of the shrinkage zone, n is the ground porosity, W_w is the volumetric moisture content due to unfrozen water content, W_{beg} is the initial volumetric moisture content of ground, K_{str} is the coefficient of structural decompaction of frozen ground in the freezing zone that is a constituent of the temperature deformation coefficient of frozen ground, τ_i is the duration of the external water flow impact, $P_w(T)$ is the pressure (the potential) of unfrozen water at the boundary of segregated ice formation, P_{w0} is the pore pressure at the lower boundary of the thawed zone, $P_w(G)$ is the pressure in unfrozen water due to the static load upon the freezing ground, H_f is the total thickness of freezing ground.

In the case of freezing in a closed system the first term of the right part of the equation (1) will be omitted, and the equation will take the following form:

$$\Delta H = 0.09 H_{\text{shr}} (W_{\text{beg}} - W_{\text{shr}}) + 1.09 H_f (W_{\text{shr}} - W_w) + K_{\text{str}} H_f + H_f (n - W_{\text{beg}}). \quad (2)$$

Based on the obtained results, S.N. Buldovich and V.G. Cheverev developed a physical formulation and an approximate analytical solution of the problem of heat and mass transfer and ice formation in the thawed and frozen

zones of freezing ground (Ershov et al. 1999). The problem is solved for a layer of thawed ground with moisture content at the shrinkage limit. The layer freezes from the surface under conditions of an open system, that is, with unrestricted access of moisture at its base (the presence of a water-bearing stratum).

The main difference between this solution and the mathematical models in the scientific literature is the adoption of a one-to-one correspondence between the pressure gradient of unfrozen water and the temperature gradient in the frozen zone according to the relation (1.2.7) in the paper (Cheverev 2004). The intensity of migration flow of moisture in the frozen zone is as follows:

$$I_{wi} = \lambda_{wi}(T) \cdot K \cdot dT/dz \quad (3)$$

where $\lambda_{wi}(T)$ is the coefficient of hydraulic conductivity in the frozen zone of ground, m/h; K is the proportionality coefficient expressed in meters of water column per a degree of the temperature of frozen ground that equals 121 m/degree; dT/dz is the temperature gradient.

Hydraulic conductivity properties of frozen ground decrease sharply with the decrease of temperature. Therefore, as the migration flow moves into the frozen zone, the excess moisture freezes out. It takes part in the formation of ice inclusions and frost heaves in the frozen zone of ground. Transit moisture transfer from the area of feeding at the bottom of the freezing layer towards the freezing front takes place in the thawed zone. This occurs due to the difference of negative pressures corresponding to the moisture potentials both at the onset freezing temperature and the temperature at the phase boundary of thawed and frozen zones.

The intensity of moisture flow in the thawed zone equals to:

$$I_w = \lambda_w \cdot K \cdot (T_{beg} - T_f)/h - h_p \quad (4)$$

where λ_w is the coefficient of hydraulic conductivity of thawed ground; T_{beg} and T_f are the temperature of the beginning of ground freezing and the temperature at the front of freezing respectively; h is the depth of freezing; h_p is the size of the calculated area.

The problem is solved by the method of successive change of stationary states on the basis of the general heat balance of thawed and frozen zones.

Contrary to the traditional approach, the temperature distribution in the frozen zone is not taken as linear but is defined by a function that accounts for inner volumetric heat sources. In fact, in the frozen zone the heat release associated with the crystallization of the freezing out of migration moisture and, to a lesser extent, the release of volumetric heat of ground as its freezing take place. Thus the temperature gradients should increase along the heat flow movement toward a “cold” surface. The temperature curve is bent in this direction. The difference of the conductive heat flows on the “cold” surface and at the freezing front (at the side of the frozen zone) equals the total intensity of inner heat sources.

This approach accounts for the complicated direct and inverse relations between various components of heat and moisture transfers. For example, the increase of migration

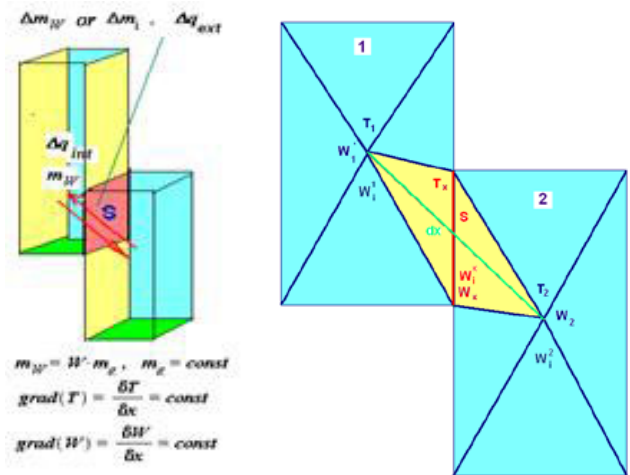


Figure 1. Heat and mass transfer between two contacting cells.

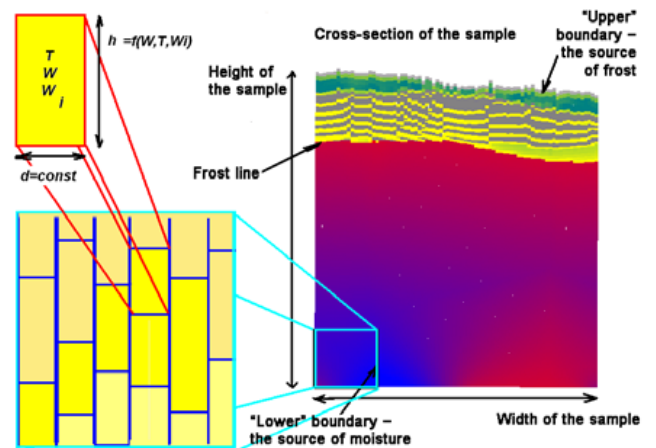


Figure 2. Network of cells in the numerical model. The process of the vertical deformation of a cell is shown. The width of the cell remains constant, while the height varies.

flow into the frozen zone will cause an additional bending of the temperature curve and, consequently, a decrease of the temperature gradient in the bottom part of the frozen zone. This leads to a drop in the flow intensity. In addition, the curvature increase of the temperature curve reduces the amount of freezing bound moisture, etc. Generally, a change in any component of heat and temperature transfers inevitably changes the temperature at the boundary of the thawed and frozen zones. This is the main value determining the extent of frost heave and moisture transfer between different zones.

Developing this solution, E.V. Safronov and V.G. Cheverev worked out a two-dimensional numerical model of ground freezing. In this model, the area of freezing ground was divided into a network of cells. Temperature, ice content, and moisture content were calculated for each cell and for each time unit based on the equations of heat and material balance.

The main conceptual issues of the model are as follows:

- 1) A ground section was taken as a research area. The section formed a semi-bounded surface, the upper boundary of which was the front of low temperatures, whereas the bottom boundary was the source of heat and moisture.

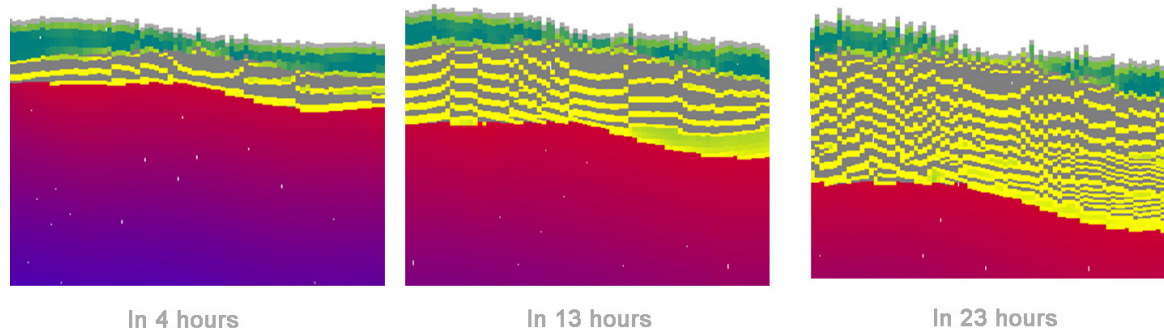


Figure 3. The formation of cryogenic structure of freezing kaolinite clay over time. The thawed zone is marked with red and blue. There is a gradation of moisture content at the transition from red to blue in the direction of the ground moisture increase. The ground with a moisture content of the shrinkage limit is depicted in red, and the yield point is depicted in blue. Ice layers are marked in gray, and frozen layers are marked in yellow-green with their ice content increasing from yellow to green.

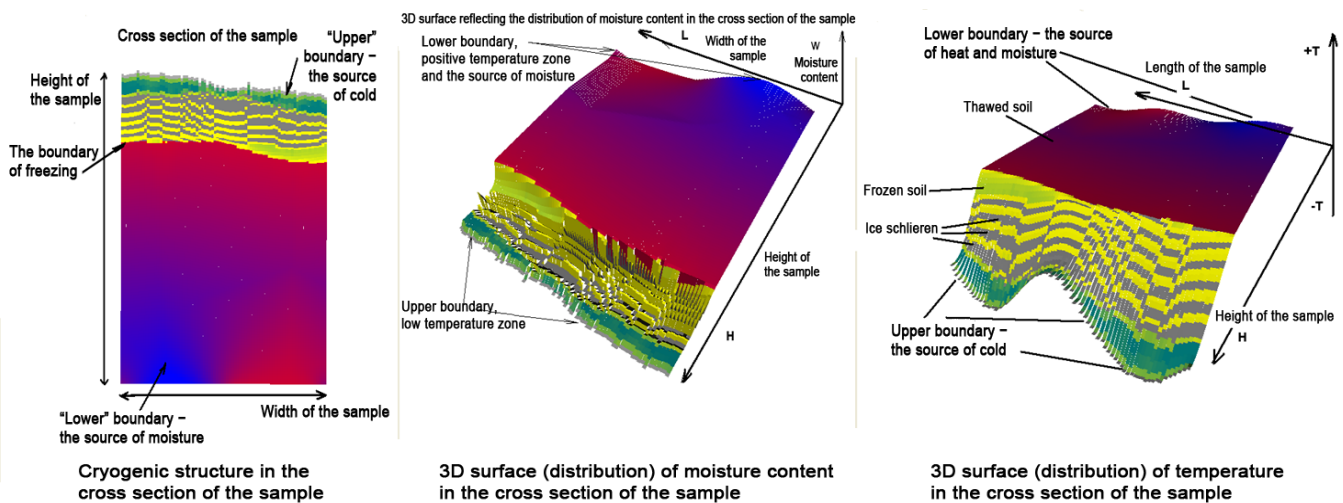


Figure 4. The distribution of temperature and moisture content during ground freezing.

- 2) Unrestricted and time-varying heat and moisture transfers were allowed at the boundary of the simulation area. The ground mass for each cell in the simulation area remained constant.
 - 3) All parameters of heat and mass transfer (i.e., the thermodynamic potential, heat capacity, thermal conductivity, and equilibrium content of fluid phase) are variable and depend on average values of moisture content, ice content, and temperature per cell volume for each cell of the numerical model.
 - 4) This model examines a change of steady-states at equal time intervals. That is, heat and moisture flows are assumed to be constant within a time unit. Temperature, moisture content, and ice content of the entire cell volume are also taken to be constant within this time unit. They are assumed equal to the average value in the volume. This also applies to all parameters of heat and mass transfer that depend on them (Fig. 1).
 - 5) The model allows for the vertical deformation of cells based on the changes of moisture and ice content in a cell. In this regard, the model allows for different moisture content in the thawed zone. It also considers the process of the thawed zone subsidence under the conditions of ice schlieren growth during freezing due to inner sources of moisture in the thawed zone. The change of the internal stress pattern of a cell due to the alteration of ground deformation is not yet considered (Fig. 2).
 - 6) The model examines the emergence of ice macro-schlieren from ice micro-schlieren and from ice-cement of the frozen zone. The increase of ice content above some critical point is the condition of the formation of ice macro-schlieren. It is assumed that there is a thermodynamic potential difference of the films of moisture on the surface of ice macro-schlieren and ice-cement, as well as of ice micro-schlieren due to the excess surface energy of micro-schlieren and ice-cement.
- The numerical model allows us to display the change in the cryogenic structure of the frozen zone in time under conditions of constant deformation of freezing ground. Figure 3 shows the cryogenic structure of freezing kaolinite clay implemented in the numerical model at different time intervals. Conditions of freezing (i.e., the values of heat and moisture flows) were chosen in advance as variable along the perimeter of the lower boundary (the thawed zone) and the upper boundary (the boundary of freezing), but as constant in time (Fig. 4).

Thus the following abilities of the model can be pointed out:

- 1) Establishment of the primary layered cryogenic structure in freezing ground and the prediction of its evolution in time.
- 2) Changing boundary conditions of heat and mass transfer along the volume of freezing ground and over time.
- 3) Establishment of the dynamics of shrinkage and frost heave of freezing ground.
- 4) Simulation of freezing of ground of random shape.
- 5) Simulation of heat and moisture transfers in freezing ground in contact with an engineering facility.

References

- Cheverev, V.G. 2004. *The nature of cryogenic properties of Moscow grounds*: Izdatelstvo Nauchny Mir, 234 pp.
- Cheverev, V.G. & Ershov, E.D., Magomedgadzhieva, M.A., & Vidyapin, I.Y. 1998. Results of physical simulation of frost heaving in grounds, *7 International Conference on Permafrost*. Canada, 145-149.
- Edlefsen, N.E. & Andersen, A.B. 1966. Thermodynamics of ground moisture. *Sbornik statey Termodinamika pochvennoy vlagi*. Leningrad: Gidrometeoizdat, 5-273.
- Ershov, E.D., Orlov, V.O., Buldovich, S.N., Medvedev, A.V., & Cheverev, V.G. 1999. Frost heave of grounds and its effect on structures. Ed: E.D. Ershov, *Osnovy geokriologii 5. Inzhenernaya geokriologiya*, Moscow: Izdatelstvo MGU, 109-133.
- Feldman, G.M. 1988. *Moisture movement in melted and frozen grounds*. Novosibirsk: Izdatelstvo Nauka, 257 pp.
- Goldshhteyn, M.N. 1948. The deformation of foundation beds and foundations of buildings and structures during freezing and thawing. *Trudy Vsesoyuznogo nauchno-issledovatel'skogo instituta zheleznodorozhnogo transporta 16*, Moscow, 212 pp.
- Grechishchev, S.E. 1979. Inter-phaze interactions in pore moisture and the thermo-rheological model of frozen ground. *Zhurnal Inzhenernaya geologiya 4*, Moscow: Izdatelstvo Nauka: 72-85.
- Orlov, V.O., Dubnov, Yu.D, & Merenkov, N.D. 1977. *Heaving of freezing grounds and its effect on structures foundations*. Leningrad: Stroyizdat, Leningradskoe otdelenie, 183 pp.

Radiocarbon Chronology and Dynamics of Palsas in the Russian European North

Ju.N. Chizhova, A.C. Vasil'chuk, N.A. Budantseva, Yu.K. Vasil'chuk
Lomonosov Moscow State University, Faculty of Geography, Moscow, Russia

Abstract

Palsas in frozen mires of the Russian European North (near Usa, Abez, Nikita, Eletskiy, and Khanovey settlements and the Bugry station) were studied and ^{14}C dated. During the Holocene, the paleodynamics of these palsas were not similar. Some of them actively grew even during the Holocene optimum. Their current state even within the same massif can be both degradational and stable and aggradational and pulsating.

Keywords: European North; Holocene; palsa; stratigraphy; radiocarbon age.

Introduction

Palsas (frost mounds of a maximum height of about 10 m with an icy core composed of peat or peat-overlying mineral deposits) are widely distributed in Northern Europe, Asia, and northern North America.

Palsas are one of the most prevalent forms of permafrost terrain. Most frequently they are found in districts with higher annual mean temperatures (about zero) in areas of continuous and sporadic permafrost, but they are also frequently found in colder continuous permafrost (Åkerman 1982, Washburn 1983, Vasil'chuk & Lakhtina 1986, Vasil'chuk & Vasil'chuk 1998, Vasil'chuk et al. 2008). They are almost always found in the northern regions where peatlands are present and are usually developed in areas with long winters and a thin snow cover.

The beginning of the formation of a palsa as a landform can be determined by radiocarbon dating of deposits formed at the time when the heave surface appeared above the water surface of the surrounding bog. The time of heave can be reliably determined by the identification of the deposits that were accumulated in the palsa stratigraphy during this initial period of heaving.

Recent studies have observed significant and relatively rapid changes in the distribution of permafrost and palsas during the second half of the 20th century and the beginning of the 21st century in Northern America and Europe. These changes showed a reduction of area occupied by palsas in arctic and subarctic peatlands, and are usually considered to have occurred in response to global climatic changes. At the same time, there are data revealing that the growth and dynamics of individual palsas are associated with local factors that influence the hydrology. These may include river channel migration, changes in lake configuration, and even the activity of beavers (Lewkowicz & Coultish 2004). There are data on the current growth of palsas and the range of expansion in both the south and the north of the cryolithozone (Vasil'chuk et al. 2008).

According to studies by Yu.K. Vasil'chuk, the mechanisms of palsa formation can be varied (Fig. 1). For some palsas, hummocks are formed in bogs during the development of vegetation. During freezing, the moisture is supplied to hummocks from all sides, and heave results. Freezing gradually penetrates deeper peat, clayey silt, and clay. During freezing, shrinkage of the ground surrounding the hummock takes place due to desiccation. On the contrary, the hummock continues to heave as a result of the supply of

additional water and moisture migration to the freezing front under conditions of negative temperatures and low long-term gradients. This leads to the formation of segregated ice schlieren. However, this is only one of the possible scenarios for palsa development. Palsa formation within depressions with high moisture content and active peat accumulation (Fig. 1a) is also very common. A combination of palsa formation mechanisms at the place of a hillock and in a depression can also be noted within a single palsa massif. Moreover, the ice content of a palsa formed in the moistened depression can be significantly higher than that of a palsa primary formed at the hummock (Fig. 1b).

Yu.K. Vasil'chuk (1983) carried out a detailed study of the ice content and cryogenic structure of palsas in the north of West Siberia near Azovy settlement. Based on those results, he noted that the total thickness of ice lenses is often 3–4 m less than the height of a palsa above the depressions.

Moreover, a great number of cavities and hollows with a total volume of up to 20% of the surrounding permafrost volume were found in ice-rich palsa sections. Similar cavities and hollows were earlier observed by N.G. Bobov (1960) in palsas of Central Yakutia. A.P. Gorbunov's observation (1967) is very valuable as well. He noted that intensive air (and even paper sheets) suction into a borehole occurred in the process of drilling one such palsa at the Tian Shan. This unambiguously indicates the presence of cavities with vacuum.

Radiocarbon Dating of Palsas

The authors obtained 75 new radiocarbon dates for the peat covering palsas in the Usa River basin of the Bolshezemelskaya tundra (near Usa, Abez, Nikita, Eletskiy, and Khanovey settlements and Bugry Station).

A palsa 3.2 m high (Fig. 2) near Bugry Station was selected for dating. The peat accumulation began here about 8.6 ka BP. Freezing began 2.3–2.1 ka BP, and this palsa was formed as a result.

Several palsas of various ages were studied in detail and dated near Usa settlement. A small palsa (height of 0.8 m, Fig. 2B a) was the youngest; the hypnum peat at the depth of 0.1 m is 140 years old. In the section of a palsa that is about 4 m high, the buck-bean valley peat at the depth of 0.8 m is 6.65 ka BP, and at the depth of 0.3 m the peat is 5.2 ka BP (Fig. 2B d). This palsa is the most ancient.

Radiocarbon dating of a 3-m-high palsa near Abez settlement was carried out on eight samples of peat taken

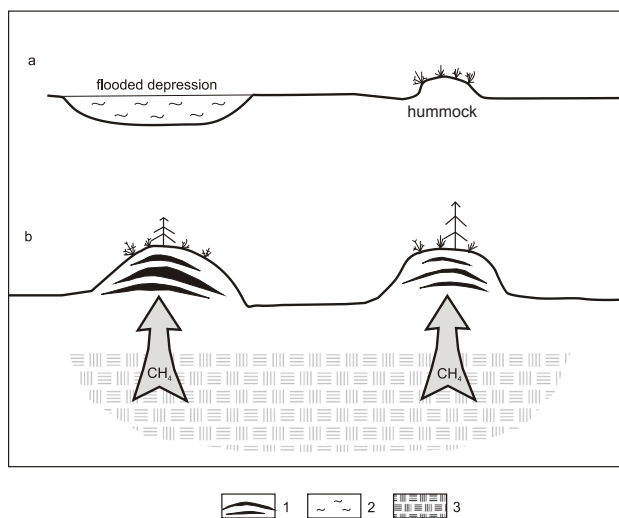


Figure 1. Scheme of palsa formation during heaving of the flooded depression and of the hummock, and further growth of palsa and their ice content with supply of methane from below that contribute to floatation of palsa. 1 – ice lenses, 2 – water, 3 – organic mass (the source of methane).

from the axial part. It showed that the accumulation of peat began there at 5.6 ka BP. The accumulation of peat ended at 2.7 ka BP, which was established by ^{14}C dating of transient moss-grass peat sampled from the depth of 0.1 m (Fig. 2C). Two similar radiocarbon dates were earlier obtained by Evseev (1976) from the base of the peat in a palsa near the same village (5.7 and 5.5 ka BP).

The transition from the peat formed 8.2–7.5 ka BP under conditions of a forest horsetail bog (within the depth interval 0.80–0.65 m) to the peat with a high content of wood remains (which probably indicates partial desiccation of the site) about 5.3 ka BP (Fig. 2D b). This is found at 0.65 m depth in the section of the 4.7-m-high palsa near Nikita settlement.

A palsa 3.5 m high (Fig. 2D c) was studied 1.5 km to the south of this settlement. Remains of a large bush and wood at the depth of 0.4–0.5 m was dated at 6.3–6.1 ka BP and indicate the subaerial conditions of peatland development.

A small 0.7-m-high palsa is composed of lowland peat (Fig. 2D a). It began to heave at 1.5 ka BP.

A 4-m-high palsa near Eletskaia settlement is covered by peat 1.15 m thick (Fig. 2E a). The wood-sedge peat from the depth of 0.3 m has an age 4.8 ka BP and represents the initiation of heaving. The second 3.5-m-high palsa is covered by peat about 1 m thick (Fig. 2E b). Massif drying as a result of heaving occurred at 7.42–7.12 ka BP.

A 2.5-m-high palsa (Fig. 2F) was dated near Khanovey settlement. Peat at the base started accumulating 8.8 ka BP. Remains of aquatic plants indicate that peat accumulation here occurred in eutrophic conditions. Peat from 0.6 and 0.5 m depths was dated at 8.5 and 7.5 ka BP, respectively. Peat in the depth range 0.3–0.1 m is much younger, between 3.75 and 3.85 ka BP. A recent date was obtained for the palsa's top.

Radiocarbon dating of three samples taken from the slope of this palsa demonstrated that the peat here is much younger than in its axial part and has an age of 2.9–2.8 ka BP. The peat thickness here does not exceed 0.25 m. Moreover, dating inversion is noted here (a date of 3.5 ka BP between 2.9 and 2.8 ka BP). This is a result of peat sliding

downward from the earlier formed palsa, or of filling of cavities formed during heaving. Younger ages from modern to 480 years were obtained for the palsa basis and for the flooded depression around it.

Radiocarbon dating allows us to state that palsa formation could occur in different Holocene periods (including the present), both in different geocryological zones and within a single massif. This is indicated by the changes in peat composition and its accumulation rate. This allowed us to reconstruct the initial events of heaving and palsa formation from different massifs (Fig. 2).

Dynamics of Palsa Development in the Holocene

It is assumed that the Holocene optimum covering about two thirds of the first half of the Holocene was a period of general permafrost degradation and decay of most palsas. But our research showed that this is not absolutely true.

H. Seppa and colleagues (Välliranta et al. 2010, Salonen et al. 2011) studied the changes in the woody vegetation during the Holocene at palsa massifs in the Bolshezemelskaya tundra and the Pechora River basin. They assume that the expansion of the natural areas of woody vegetation (spruce, birch) occurred in this region (currently located at the treeline and outside it) during the Holocene optimum. The vegetation grew here as isolated sparse forests since the beginning of the Holocene (Välliranta et al. 2010).

During the Holocene optimum, which is defined here between 8.0 and 3.5 ka BP, the summer mean temperature in tundra was 3°C higher than present (Salonen et al. 2011). Spruce forests were growing at that time around the Khariney Lake located 150 km to the north of the modern treeline. The temperature decreased about 3.5–2.5 ka BP, which led to an active aggradation of permafrost and intensive palsa growth, as well as wood vegetation extinction. The most ancient remains of the vegetation dated about 2.5 ka (Salonen et al. 2011).

Radiocarbon dating allowed us to define the beginning of heaving and the dynamics of palsas in the Holocene in the areas near the Bugry Station and Usa, Abez, Nikita, Eletskiy, and Khanovey settlements.

Calculations show that the heave processes within the areas are caused both by general climatic changes and local factors. Peat accumulation rate, periods of heaving, and the duration of the subaerial and the subaquatic phases can be different within the same massif.

Nonetheless, the stages of the intensification and relative decrease of heave processes can be identified based on the large amount of data. Permafrost did not degrade and, on the contrary, the formation of new palsas could begin during the Holocene optimum even within the southern part of the cryolithozone. Intensive peat accumulation as a result of high summer temperatures and the same winter severity (locally more severe than present) during the Holocene optimum were the main factors in this phenomenon, which at first glance can seem to be a geocryological contradiction.

The studied palsas are described in more detail below.

Bugry Station

It was found that at the initial stage the growth of a small palsa 0.8 m high near the Bugry station repeatedly ceased. It

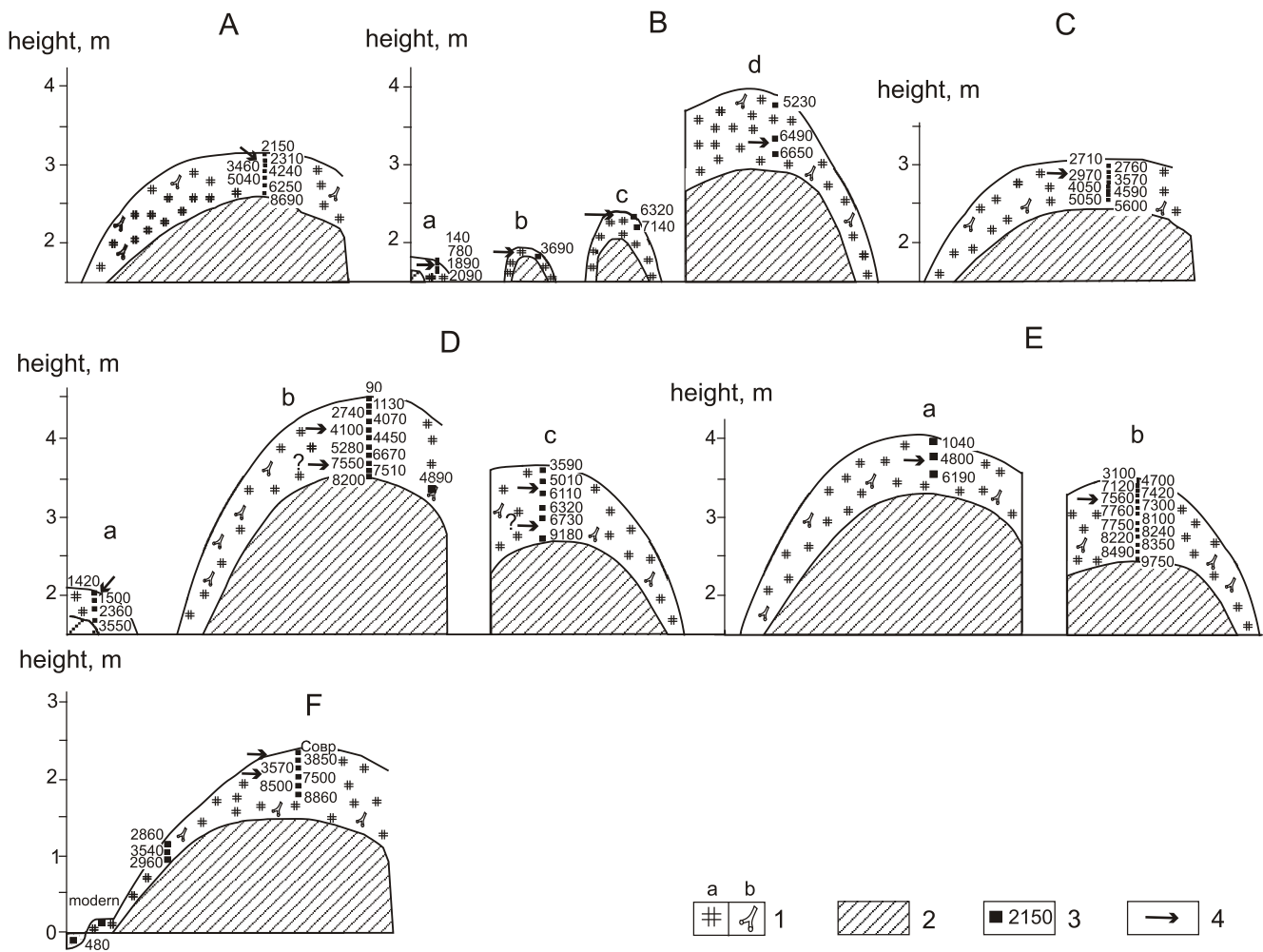


Figure 2. Radiocarbon dating of palsas in the Bolshezemelskaya tundra (Vasil'chuk et al. 2003, 2008): A – Bugry station, B – Usa settlement, C – Abez settlement, D – Nikita settlement, E – Eletskiy settlement, F – Khanovey settlement. 1 – peat (a) and tree branch (b), 2 – clayey silt, 3 – radiocarbon dates, 4 – heaving event.

was evidently formed during the past century, since the age of the sample from 0.1 m depth and that of the sedge-hypnum peat from the surface is approximately 140 years (Fig. 2A).

The formation of another palsa about 2 m high started not earlier than 3.7 ka BP. Since a sedge-hypnum peat bed is at the surface, it can be assumed that the heaving process was quite fast. This is associated with the fact that the high-bog peat did not have enough time to form. Since there is no lichen cover the palsa, it can be assumed that heaving occurred not long ago (within the past 100 years).

Change of sedge lowland peat 7.10 ka BP (at 0.5 m depth) to lowland buck-bean peat 6.32 ka BP is found in the section of a 2.5-m-high palsa. This indicates the activation process in the change of the water-mineral supply regime between 7.1 and 6.3 ka BP. According to radiocarbon dates and peat composition, heaving occurred here not earlier than 6 ka BP.

The formation of a palsa about 4 m high began not earlier than 6.5–6.0 ka BP. At the same time, the buck-bean lowland peat was replaced by the woody peat with residuals of pine, willow, and birch. The peat accumulation rate during the subaquatic phase was quite high at 0.06 cm/yr. According to the correlation of dates and the peat layer thickness, the transition to the subaquatic phase was completed about 5 ka BP. At that time peat accumulation and palsa growth ceased completely.

Usa Settlement

The heaving process near Usa settlement was most intensive after 6.5–6.0 ka BP. The palsa rose above the surface by 2–3 m. Some of the palsa formed at that time is beginning to decay. However, the active heaving process started again 3.7–2.1 ka BP and is still going on. The uplift of the younger palsa surface is 0.35–1.60 m (Fig. 3A).

Abez Settlement

The formation of a palsa near Abez settlement started about 2.7 ka BP. This is identified by a transition to the young (i.e., quickly freezing) transient moss and moss-grass peat with the remains of *scheuchzeria*, herbs and cowberry (Fig. 3B).

Nikita Settlement

The formation of a 4.7-m-high palsa near Nikita settlement started about 7.5 ka BP, according to replacement of the lowland bog peat by peat with high content of woody remains. This probably indicates partial site drying (Fig. 3C). Heaving took a long time, according to the peat accumulation rate. The transient phase was completed about 2.7 ka BP. Buck-bean (*Menyanthes trifoliata*), sedge (*Carex chordorrhiza*, *C. diandra*), and horsetail (*Equisetum*) remains are found at the depth of 0.25–0.35 m. This indicates the partial thawing and

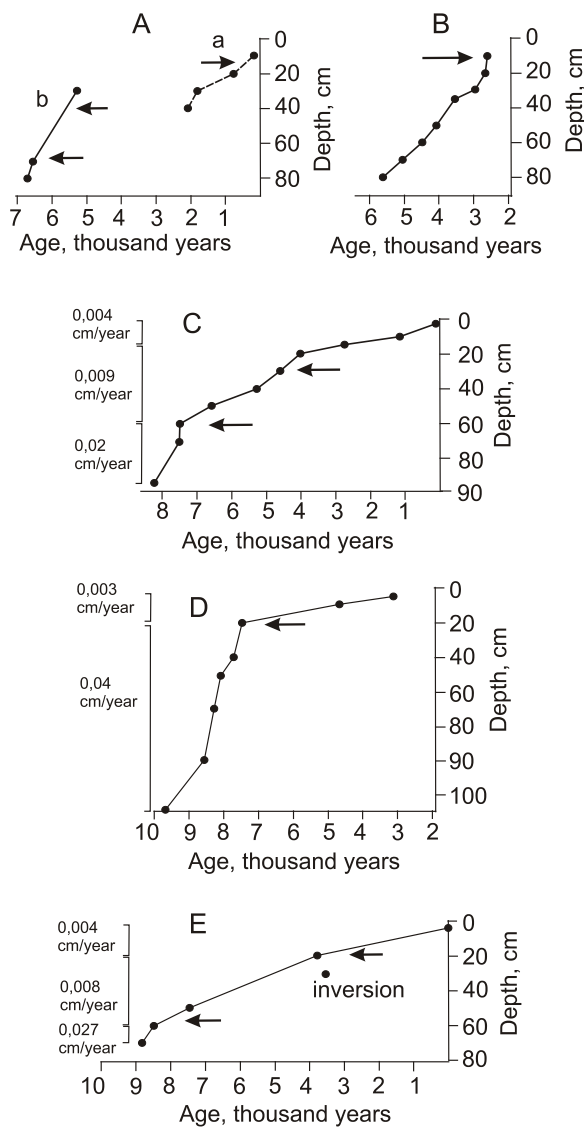


Figure 3. Assumed heave events (shown with arrows) and the rate of peat accumulation in palsas of the Bolshezemelskaya tundra: A – Usa settlement, B – Abez settlement, C – Nikita settlement, D – Eletskiy settlement, E – Khanovey settlement.

subsidence of the palsa about 4.5 ka BP. Later it recovered again and grew until reaching its current size. A 3.5-m-high palsa started forming about 6.7 ka BP. This is identified by replacement of black woody-horsetail near-bottom peat with remains of wood and large bushes.

Partial thawing of the palsa probably occurred about 5 ka BP, according to horsetail remains in the peat at the depth of 0.2–0.3 m. Then the palsa recovered again (not earlier than 3.6 ka BP). A 0.7-m-high palsa composed of peat accumulated in conditions of intensive flooding of the site began growing about 2.3 ka BP. This was defined by replacement of sedge lowland peat with sedge-hypnum peat containing buck-bean and herbs. The heave was extremely unstable; it evidently thawed and subsided repeatedly and it is most probable that only a low hillock or a hummock remained after the subsidence. Then it froze and heaved again. But after 1.5–1.4 ka BP this pulsating state was transformed to a more stable one.

Eletskiy Settlement

The beginning of heaving and termination of the subaquatic phase of palsa development was identified in the section of the 4-m-high palsa near Eletskiy settlement at a depth of 0.3 m, dated at 4.8 ka BP. The next subaerial phase lasted for about 5 ka.

The formation of a 3.5-m-high palsa evidently occurred at 7.5 ka BP. The rate of peat accumulation during the subaquatic phase was 0.27 m/ka (Fig. 3D). The peat accumulation rate during the subsequent subaerial phase was 0.08 m/ka. Sedge lowland-type peat is found on the palsa top. This can indicate a partial thawing of the palsa 4.7–3.1 ka BP.

It can be assumed that the heave process near Eletskiy settlement occurred most intensively about 7.7 ka BP, when the palsa grew by 3.0–3.4 m.

Khanovey Settlement

Dating of the peat from the palsa near Khanovey settlement showed a long gap in peat accumulation or a steep slowing down of the peat formation process between 7.5 and 3.5 ka BP. This testifies to the massif's freezing and the formation of a comparatively low palsa. Peat accumulation resumed for a short period about 3.5 ka BP. Since a recent date was received for the palsa top (the peat accumulation is still going on), it is evident that the palsa uplifted above the surface not long ago (Fig. 3E).

The distribution of radiocarbon dates in the palsa section (more ancient in the axial part and younger on the slope) demonstrated two important points. Firstly, this landform is properly identified as a palsa. It is not a residual that formed as a result of erosion of an initially flat peatland. The followers of the hypothesis of the erosional origin of palsa in this area agreed. It was also acknowledged by the researchers who recognized heaving as the main mechanism of palsa-like forms. They thought that in the Bolshezemelskaya tundra this process takes place in more southern areas, while the heave terrain forms that occurred in the North near Vorkuta, under the conditions of colder ground temperatures, were referred to as residual large-block forms generated as a result of erosion in frost cracks. Secondly, both the initial period of heaving 7.5 ka BP and the time of secondary additional heaving approximately 3.5–2.8 ka BP are clearly observed here. At the time of initial heaving, a small palsa several meters in diameter and probably no more than 1.0–1.5 m high was formed. At the time of secondary heaving, a palsa more than 3 m high and more than 45 m in diameter was formed from the initially small one. It covered the surrounding flooded depression where peat accumulation occurred 2.8 ka BP, but then stopped after heaving.

Usa River Valley

Palsa mires in Usa River valley developed in several stages. A 3.5- to 5.0-m-high palsa was formed 7–6 ka BP. The height of the peatland surfaces at that time reached 2.25–4.00 m. Smaller palsas were formed 3.5–2.0 ka BP. Their height was 0.35 m.

Conclusions

- 1) Palsas are found in the European North both in areas of continuous permafrost and in areas of discontinuous or sporadic permafrost.
- 2) The southern limit of palsa formation in the European North coincides with the southern permafrost boundary: it is approximately 67°50'N for the Kola Peninsula and southward from 66°20'N for the Bolshezemelskaya tundra. The northern limit reaches 68°10'N in the Nenets Autonomous Area and 67°30'–68°00'N in the Bolshezemelskaya tundra and extends far into the zone of cold continuous permafrost.
- 3) Permafrost did not always degrade and, on the contrary, the formation of new palsas could have begun during the Holocene optimum, even within the southern part of the cryolithozone. This occurred due to intensive peat accumulation as a result of high summer temperatures and winter severity during the Holocene optimum.
- 4) Some palsas have a cyclic development; thermokarst impacts the surface of earlier formed palsa, which leads to the abrasion and subsidence of some of them, and subsequent massif drainage is completed with the formation of a new palsa.

Acknowledgments

This work was completed with a partial support of the Russian Foundation for Basic Research (grants 10-05-00986 and 11-05-01141) and the Federal Agency of Science and Innovations (state contract 02.740.11.0337).

References

- Åkerman, H.J. 1982. Observations of palsas within the continuous permafrost zone in eastern Siberia and in Svalbard. *Geografisk Tidsskrift* No 82: 45-51.
- Bobov, N.G. 1960. Modern formation of palsa (permafrost heaves) in the Lena-Vilyuy interfluve. *Izvestiya AN SSSR. Ser. Geograficheskaya* No 5: 64-68 (in Russian).
- Evseev, V.P. 1976. Regularities of palsa (migrational frost heaves) distribution in the European part of the USSR and Western Siberia. *Cryolithology problems*. No 5: 95-159 (in Russian).
- Gorbunov, A.P. 1967. *Tian Shan permafrost*. Frunze: Ilim, 166 pp. (in Russian).
- Salonen, J.S., Seppä, H., Valiranta, M., Jones, V.J., Self, A., Heikkilä, M., Kultti, S., & Yang, H. 2011. The Holocene thermal maximum and late-Holocene cooling in the tundra of NE European Russia. *Quaternary Research*. V. 75. Iss. 4: 100-111.
- Seppälä, M. 2011. Synthesis of studies of palsa formation underlining the importance of local environmental and physical characteristics. *Quaternary Research* V. 75: 366-370.
- Välliranta, M., Kaakinen, A., Kuhry, P., Kultti, S., Salonen, J.S., & Seppä, H. 2010. Scattered late-glacial and early Holocene tree populations as dispersal nuclei for forest development in north-eastern European Russia. *Journal of Biogeography* V. 38. Iss. 5: 922-932.

- Vasil'chuk, Yu.K., Vasil'chuk, A.C., Sulerzhitsky, L.D. et al. 2003. Radiocarbon Chronology of palsa in the Bol'shaya Zemlya Tundra. *Doklady Earth Sciences* Vol.393, No.8: 1160-1164.
- Vasil'chuk Yu.K. & Vasil'chuk A.C. 1998. The ¹⁴C age of palsas in Northern Eurasia. *Radiocarbon*. V. 40. No 2: 895-904.
- Vasilchuk, Yu.K., Vasil'chuk, A.C., Budantseva, N.A., & Chizhova, Ju.N. 2008. *Palsa of frozen peat mires* / Ed.: Member of the Russian Academy of Natural Science, Prof. Yu.K. Vasil'chuk. Moscow University Press, 571 pp. (in Russian).
- Vasilchuk, Yu.K. & Lakhtina, O.V. 1986. *Palsas development in north of Western Siberia during Holocene. Permafrost ground formation and forecast of cryogene processes*. T.N. Kaplina (Ed). Moscow. Publ. House Nauka: 123-128 (in Russian).
- Vasilchuk, Yu.K. 1983. *About formation specific of palsas in the northern Western Siberia during Holocene. Natural conditions of Western Siberia*. Prof.A.I.Popov & Prof.V.T.Trofimov (Eds.). Moscow University publ.: 88-103 (in Russian).
- Washburn, A.L. 1983. Palsas and continuous permafrost. *Proceedings of the Fourth International Conference on Permafrost*, Fairbanks, Alaska, United States, July 17-22, 1983. Edited by Pewe T.L., Brown J. Fairbanks, Washington, D.C.: National Academy Press: 1372-1377.

Temperature Dependence of the Equilibrium Pore Water Content in Gas Hydrate Contained Sediments

Evgeny M. Chuvilin

Moscow State University, Moscow, Russia

Vladimir A. Istomin

VNIIGAZ, Moscow, Russia

Abstract

Analysis of sediment composition of saturated gas hydrates revealed that pore water does not completely transform into gas hydrates. The minimal possible amount of water in the sediment at fixed thermo-pressure conditions may be considered as equilibrium residual water (nonclathrated water), analogous to unfrozen water in frozen sediments. Experimental study of equilibrium for the “pore water in sediment – hydrate-forming gas – bulk gas hydrate” system allowed us to develop the technology for determination of nonclathrated water in sediments. On the basis of the proposed technique the experimental data of nonclathrated water content were obtained in different conditions. These data allow us to define the dependence of nonclathrated water content via pressure, temperatures, type of dispersed sediment, and hydrate-former (methane and carbon dioxide). A comparison of the behavior of nonclathrated water and unfrozen water is presented.

Keywords: equilibrium water content; gas hydrates; unfrozen water; nonclathrated water; sediment; ice.

Introduction

Experimental investigations and analysis of the phase composition of gas hydrate saturated sediments (Chuvilin et al. 2005) revealed that pore water in sediments is not fully converted into the gas hydrate phase at fixed temperature and pressure due to thermodynamic (pore distributions of disperse sediments leads to phase transition for a spectrum of temperatures) and kinetic (absence of direct gas-water contact during pore gas hydrate formation) factors. Thus the residual pore water in the disperse sediment samples can be subdivided into two essentially different types:

- 1) Pore water that cannot be converted into the hydrate phase at the considered temperature and pressure (this is an equilibrium part of liquid water at pore space).
- 2) Pore water that may be transformed into gas hydrate from a thermodynamic point of view, but such a process is not fully completed for kinetic reasons.

The equilibrium part of the pore water in sediments under consideration (in relation to bulk gas hydrate phase at given pressure and temperature) was called “nonclathrated water,” as analogous to “unfrozen water” in frozen sediments (Chuvilin et al. 2008, 2011).

Nonclathrated water (as well as unfrozen water) influences the physical and mechanical properties of sediments. Therefore, we need to develop an experimental method for detecting the amount of nonclathrated water in the samples.

Method of Determination of Nonclathrated Water within Sediments

The proposed technique for determination of the nonclathrated water content is based on measuring the equilibrium water content in a dried sediment plate placed in close contact with an ice plate under isothermal conditions of pressure that is created by a gas that will form the hydrate (Chuvilin et al. 2008, and Method for determination of pore water content in equilibrium with gas hydrate in dispersed

media). The technique is similar to the contact method for the unfrozen water estimate in geocryology.

It should be pointed out that according to our experimental data, the gas hydrates appear on the ice surface under these conditions. The three-phase equilibrium (pore water – gas – bulk gas hydrate) may be studied by this method due to the hydrate film covering the ice plate (Chuvilin et al. 2011). The technique includes preparation methods of sediment and ice plates for the experiment and data processing. Modeled sediments with well-known properties were used for test experiments: kaolinite clay and sand-clay mixes consisting of quartz sand with kaolinite or montmorillonite clay particles (Tables 1, 2).

Table 1. Granulometric composition of sediments.

Type of sediment	Particle size distribution/%		
	1-0.05 mm	0.05-0.001 mm	<0.001 mm
Quartz sand	94.8	3.1	2.1
Kaolinite clay	4.5	70.9	24.6
Montmorillonite clay	0.3	46.2	53.5

Table 2. Mineral composition and some properties of sediments.

Type of sediment	Mineral composition	ρ_s g/cm ³	S/%
Quartz sand	Quartz >90%	2.65	0.012
Kaolinite clay	Kaolinite 92% Quartz 6% Muscovite 2%	2.66	0.043
Montmorillonite clay	Montmorillonite 93.4% Andesite 2.9% Biotite 2.9% Calcite 0.8%	2.45	1.988

Most of the experiments were obtained on the kaolinite clay samples. During preparation of the sand-clay mixtures, the weight content of clay particles was set at 14, 25, and 40%. The air-dried sediment plates and ice plates were cooled in a cold room in temperatures from -8 to -10°C and while in contact under isothermal conditions. Each dried sediment plate was placed between two ice plates to form laminated cassettes.

The prepared ice-sediment cassette was placed into a special pressure chamber cooled to the experimental temperature. The experimental pressure chamber filled with the ice-sediment cassettes was pressurized at a negative temperature (-8 to -10°C). Then the chamber was evacuated and subsequently saturated with cool hydrate-forming gas (methane or CO_2). During methane pressurization, the initial gas pressure registered from 0.1 to 8.7 MPa and for CO_2 from 0.1 to 2.5 MPa. The pressure chamber containing the ice-sediment cassettes was placed into a cooling chamber with a constant negative temperature. The thermostat system used in these experiments allowed for maintaining a constant negative temperature in a pressure chamber with an accuracy of $\pm 0.2^{\circ}\text{C}$. The determination of nonclathrated water content in different model sediments and the estimation of gas-pressure influence on nonclathrated water content were carried out at -7.5°C .

During the experiment, the cooling chamber temperature remained constant and the pressure chamber pressure was fixed. As a rule, in the beginning of the experiment, pressure in the pressure chamber declined slightly because of hydrate formation on the ice plate surfaces.

At the end of the experiment, pressure was released and the pressure chamber was opened in the cold room. The sediment and ice plates (covered by hydrate under the pressure of hydrate-forming gas) were separated from each other. The equilibrium water content was determined using an electronic balance with an accuracy of 0.001 g. Determination of nonclathrated water content was replicated two or three times. During the experiment (14 days), the equilibrium water content was reached for all the sediment samples independent of their composition and experimental conditions (Chuvilin et al. 2011). All experiments are at thermodynamic equilibrium and the characterized nonclathrated water content was in a hydrate-containing medium. Determining the temperature effect on the change of nonclathrated water content in model sediments was carried out under the fixed gas pressure for methane-saturated samples of 4.3 to 4.1 MPa, and for CO_2 -saturated samples of 1.65 to 1.6 MPa. Under the given conditions, temperature influence was studied in methane- and CO_2 -saturated samples from -13 to $+4^{\circ}\text{C}$.

To extend this method for positive temperatures, we used ice-containing quartz sand plates instead of ice plates. Prepared cassettes made of plates of air-dried sediment and frozen sand were placed inside the pressure chamber and kept under pressure of hydrate-forming gas during 5 days at constant negative temperatures (-6 to -8°C). After part of the porous ice had transformed into hydrate, the temperature was stepwise (by 2 to 3°C) increased to 0°C within 1 to 2 days. After that, the experimental temperature was set and the pressure chamber was kept under experimental conditions from 7 to 10 days until equilibrium water content was

reached (the time depends on thermobarometric conditions and type of sediment). The chamber then was cooled to -6 to -8°C , pressure was released to the atmosphere, samples were recovered, and their gravimetric water content was determined. The content corresponded to nonclathrated water content at experimental positive temperature values.

The elaborated method allows determination of equilibrium water content (nonclathrated water) in sediments of different composition in a wide range of pressures and temperatures.

Experimental Data and Discussion

Based on the proposed method, a set of experiments was carried out to estimate the nonclathrated water at three-phase equilibrium conditions (gas-liquid water-bulk CH_4 or CO_2 hydrate) in model sediments.

Temperature influence

At fixed gas pressure, the nonclathrated water content in sediments depends on temperature. During a temperature rise, the maintenance of nonclathrated waters is increased in full analogy with unfrozen water behavior. In Figure 1, it is possible to see the changes of nonclathrated water content in methane-saturated kaolinite clay at fixed pressure of about 4.2 MPa (± 0.1 MPa). As follows from obtained data, the increase of equilibrium temperature from -10.6°C to 4°C led to the more than 2.5 times increase in nonclathrated water content. In comparison with unfrozen water, the maintenance of nonclathrated water in sediment is lower. This distinction increases with a rise in temperature, so at -10°C it was less than twice but at -3°C it was exceeded by three times.

Temperature dependence of nonclathrated water content for CO_2 -saturated sediments at a fixed gas pressure (1.6 MPa) is shown in Figure 2.

These data show that nonclathrated water content of hydrate-bearing sediments increases sharply at temperatures above 0°C and when approaching the equilibrium temperature.

Gas pressure influence

Figure 3 presents the results of nonclathrated water determinations in kaolinite clay, which was saturated by methane at pressure from 0.1 to 8.7 MPa and by CO_2 at pressure from 0.1 to 2.5 MPa and temperature of -7.5°C . As the experimental data show, the nonclathrated water content in kaolinite clay declines as the pressure increases. In the pressure range from 2 to 4 MPa, this decrease is very steep, virtually by two times. At a pressure increase of 4 to 8.7 MPa, the equilibrium water content reduction becomes negligible.

When pressure increased from 4.3 to 8.7 MPa, the nonclathrated water content decreased by only 0.35%. At pressure above 6 MPa, this decrease is not more than 0.1% (Fig. 3). The power type dependence has been obtained on nonclathrated water content via gas (methane) pressure for kaolinite clay.

The nonclathrated water from pressure in CO_2 -saturated sediment is similar to that in methane-saturated sediment; however, quantitatively they strongly differ. This is related to differences in the thermobaric conditions of hydrate CH_4 and CO_2 (Fig. 3). As seen from the obtained experimental

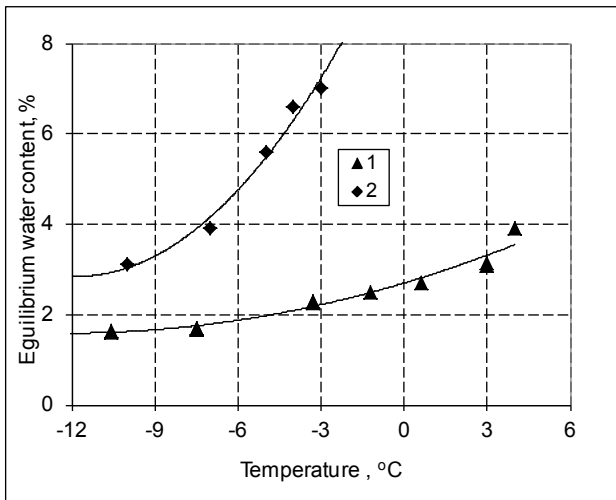


Figure 1. Temperature influence on equilibrium pore water content in kaolinite clay. 1- nonclathrated water content under methane pressure (pressure = 4.1 to 4.3 MPa); 2- unfrozen water content at atmospheric pressure.

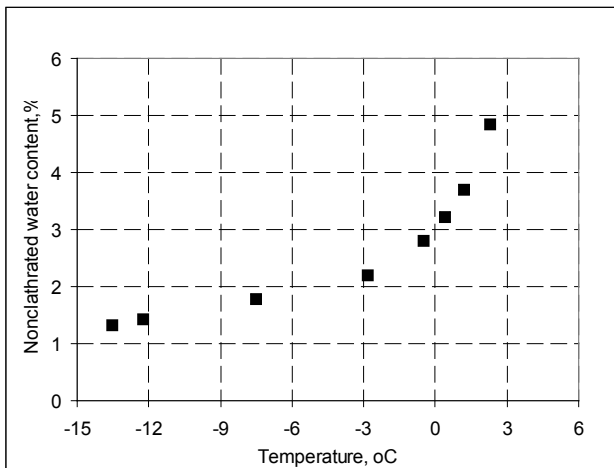


Figure 2. Temperature influence on nonclathrated water content in kaolinite clay under CO₂ gas pressure (pressure = 1.6 MPa).

data, nonclathrated water content in CO₂-saturated kaolinite clay declines under increasing pressure. In the pressure range of 0.9 to 1.6 MPa, this decrease is abrupt, virtually by two times. Then, at a pressure increase of 1.6 to 2.5 MPa, the equilibrium water content reduction becomes negligible. At a pressure above 1.6 MPa, this decrease is not more than 0.1%.

Sediment type influence

Nonclathrated water content dependence on pressure is determined mainly by dispersion and mineral composition of sediment.

The experiment on estimation of nonclathrated water content in sandy-clay mixtures showed that at the same content of clay particles but with different mineral composition, the nonclathrated water content may differ by one order of magnitude (Fig. 4).

In quartz sand with 25% kaolinite particles at CO₂ pressure of 1.6 MPa, the equilibrium liquid-phase content was about 0.4%. In the same conditions in sand samples with 25% montmorillonite particles, it was up to 4.4%. The sharp difference in nonclathrated water content may be explained by the energetic characteristics of clay additives, mainly

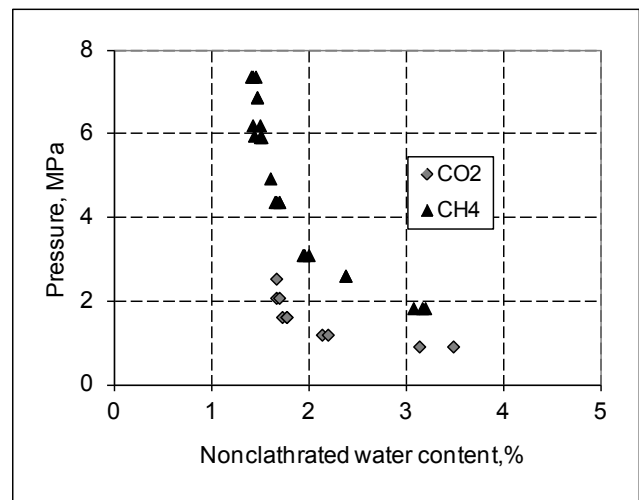


Figure 3. Change of nonclathrated water content depending on CO₂ and CH₄ gas pressure in kaolinite clay at -7.5°C.

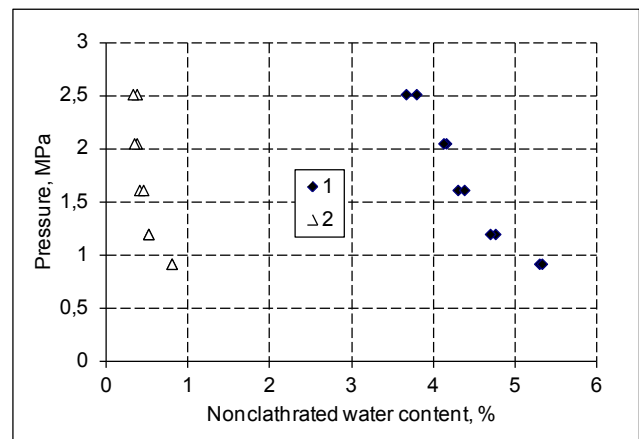


Figure 4. Change of nonclathrated water content depending on CO₂ pressure in modeled sediment samples at -7.5°C. 1- sand with 25% montmorillonite particles; 2- sand with 25% kaolinite particles.

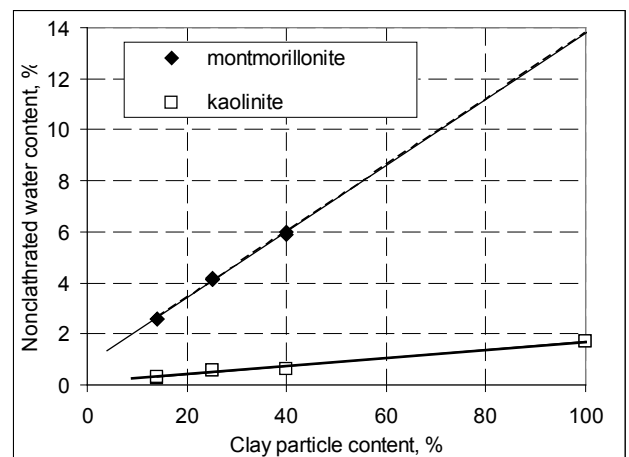


Figure 5. Influence of clay minerals on nonclathrated water content in methane-saturated sand samples (pressure of 4.1 to 4.4 MPa, and temperature of -7.5°C).

by the specific active area that determines the quantity of bound water. Considering the data about gas adsorption of nitrogen, the specific active surface for kaolinite clay was 12 m²/g, and the value of the outer specific active area for montmorillonite clay was equal to 70 m²/g.

The change in nonclathrated water content in sand samples with an increasing kaolinite or montmorillonite particles content at the fixed methane pressure of 4.1 to 4.4 MPa and at the temperature of -7.5°C is shown in Figure 5.

The experimental data show that nonclathrated water content in sediment samples linearly increases with the increase in the amount of clay. The nonclathrated water content increases more intensively in samples with montmorillonite clay. According to the obtained data, the nonclathrated water content can be estimated in montmorillonite clay of about 14%.

Conclusions

On the basis of developed experimental methods, we performed an experimental research investigation of equilibrium (nonclathrated) water content in sediments at three-phase equilibrium "pore water-gas-bulk hydrate." Nonclathrated water in gas hydrate containing sediments is analogous to unfrozen water in frozen sediments. It depends on temperature, pressure, type of the dispersed sediment, and hydrate-forming gas. At fixed pressure, the nonclathrated water, as well as of unfrozen water content in sediments, decreases with the decrease of temperature. However, quantitatively they differ significantly, and the difference increases with the increase of temperature. As a rule, unfrozen water content in sediments is higher than nonclathrated water content. With the increase of clay particles content in sediments, especially of montmorillonite particles, nonclathrated and unfrozen water content in sediments increases.

Pressure has a greater influence on nonclathrated water content than on unfrozen water content. Unlike unfrozen water, equilibrium water content in hydrate saturated sediments decreases with the increase of pressure. Under the influence of gas pressure, nonclathrated water "freezes out," turning into hydrate. Hydrate-forming gas has a significant influence on nonclathrated water content. Unlike unfrozen water, nonclathrated water content can exist not only under negative temperature, but also at temperatures above 0°C .

Acknowledgments

This research was done with the partial financial support of Schlumberger Moscow Research Center.

References

- Chuvilin, E.M., Kozlova, E.V., & Skolotneva, T.S. 2005. Experimental simulation of frozen hydrate-containing sediments formation. *Proceedings of the Fifth International Conference on Gas Hydrate. Thermodynamic Aspects*. Trondheim, Norway, V., pp. 1540-1547.
- Chuvilin, E., Guryeva, O., Istomin, V., & Safonov, S. 2008. Experimental method for determination of the residual equilibrium water content in hydrate-saturated natural sediments. *Proceedings of the 6th International Conference on Gas Hydrates (ICGH 2008)*, Vancouver, British Columbia, CANADA, July 6-10, 2008.
- Chuvilin, E.M., Istomin, V.A., & Safonov, S.S. 2011. Residual nonclathrated water in sediments in equilibrium with gas hydrate. Comparison with unfrozen water. *Cold Regions Science and Technology* 68: 68-73.

Construction in the Cryolithozone Using Innovative Systems of Foundation Soil Thermal Stabilization

G.M. Dolgikh, S.N. Okunev, S.N. Strizhkov

FundamentStroyArkos LLC Scientific and Production Association, Tyumen, Moscow

Abstract

Innovative construction experience of FundamentStroyArkos Scientific and Production Association (FSA) is presented. FSA's innovation and investment cycle includes research, design, production, installation, construction, quality control, quality assurance, and monitoring of foundation soil thermal stabilization systems. The economic efficiency of innovative engineering solutions and considerable actual economic benefits from their implementation in production are demonstrated in more than 300 projects.

Keywords: foundations; ground freezing; HNP and VNP systems; permafrost; thermal stabilization.

Permafrost, which is used as a foundation for construction of buildings and structures, underlies more than 60% of the Russian territory. Its extraordinary diversity and fragility cause considerable difficulties during the construction and operation of buildings and structures. Many structures are in critical condition even in the construction stage, despite the fact that permafrost itself is a reliable foundation (Fig. 1). FSA's construction and design experience in developing prospective foundation soil thermal stabilization systems is shown in Figure 2.

Problems arise with uncontrolled flow of heat and moisture, warming of foundation soils, and, as a consequence, transformation of permafrost into saturated soil mass that has no bearing capacity for the support of structural loads. Construction on permafrost requires large capital expenditures. However, even if the project budget is

adequate, natural and human-induced factors, which cause permafrost thermal degradation and subsequent loss of the foundation soil bearing capacity, are often underestimated. The situation is aggravated by global warming, which is characterized by an increase in mean annual near surface air temperatures of 0.2–2°C in the past decades and an increase in permafrost temperature of as much as 1°C. Further increases in air temperatures are predicted: 1.0–1.5°C by 2025, 2–4°C by 2050, and 4–8°C by 2100. Principles I and II of using permafrost as foundations are well-known. In addition, the following solutions are most frequently used in the design and construction: construction of crawl spaces or basements (with artificial ventilation, natural convection, and the use of suspension floors and crawl spaces in combination with soil thermal stabilization systems), as well as construction of on-grade floor foundations combined with the foundation



Figure 1. Examples of accidents and disasters.

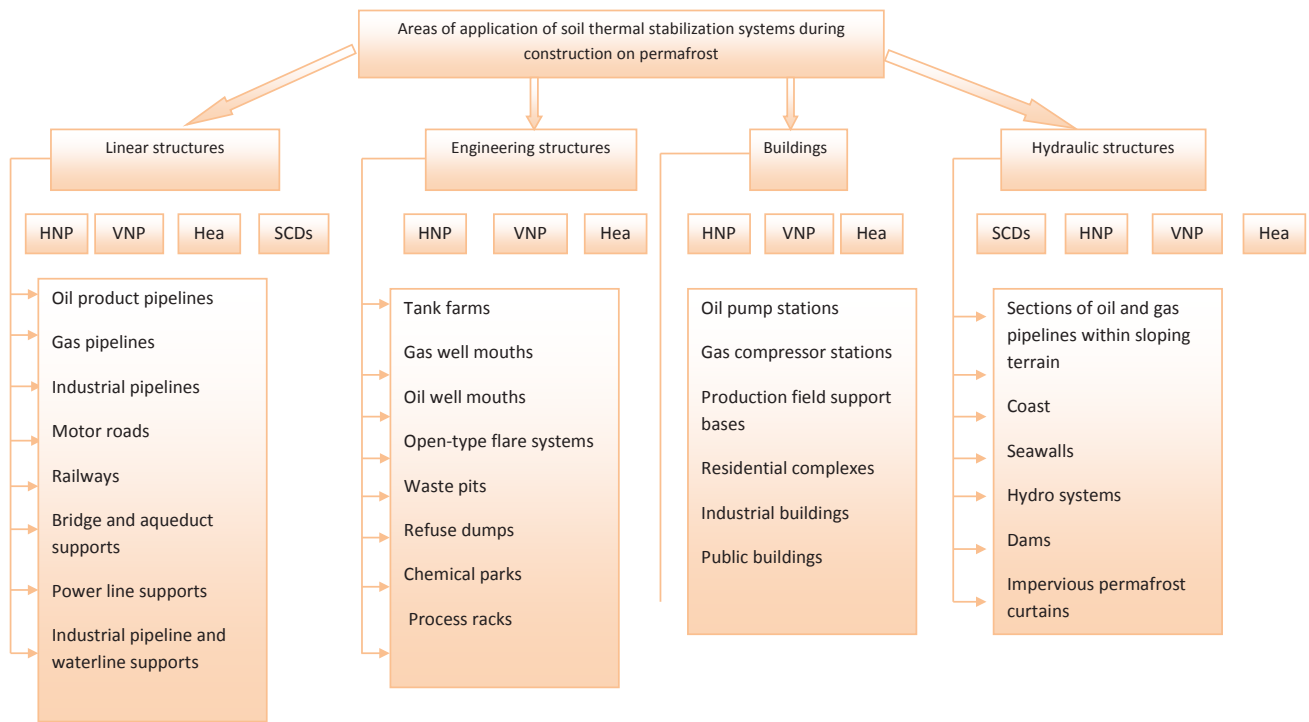


Figure 2. FSA's construction and design experience in developing prospective foundation soil thermal stabilization systems.

soil thermal stabilization systems. The extensive experience accumulated in the design and construction of buildings and structures on permafrost, including the innovative solutions by FSA, suggests that planning solutions using soil thermal stabilization systems are the most reliable, stable, and promising. Such foundations can support large buildings and structures with frames over 100 m.

Foundation soil thermal stabilization systems produced by FSA can be divided into three groups:

- HS, heat stabilizers: individual seasonal cooling devices (vertical, inclined, slightly-inclined).
- HNP, horizontal naturally operating pipe systems that consist of horizontal cooling and connecting pipes placed under insulation, a condenser unit, a circulation accelerator, and a hydraulic seal.
- VNP, vertical naturally operating pipe systems that consist of vertical cooling pipes, connecting pipes, a condenser unit, a circulation accelerator, and a hydraulic seal.

HS systems are used for thermal stabilization of pile foundations in a ventilated crawl space, as well as along the perimeter of a building. In addition, inclined HSs modifications are capable of cooling the foundation soils under large-frame buildings with on-grade floor foundations. The HNP and VNP systems are the most innovative engineering solutions. An HNP system enables reliable thermal stabilization of buildings with floor-on-grade foundations and crawl spaces or basements, with the frame width exceeding 100 m.

The VNP system is the most universal engineering solution. It allows soil thermal stabilization vertically (i.e., confined to the areas where pile foundations are located) and horizontally, and freezing of the uppermost layers of the ground, which serves as the base for shallow foundations, such as floor-on-grade foundations. The HNP and VNP systems provide considerable economic advantages by significantly reducing the cost of materials used for the

foundations and bases in the course of construction. But the main advantage of the HNP and VNP systems is that their use can significantly increase the width of buildings and structures (over 100 m). This, in turn, brings great economic benefits by reducing the length of the utility corridors. One of the ways to reduce the cost of construction and operation of structures on permafrost consists of the construction of buildings and structures with on-grade floors: the use of enlarged and block buildings with horizontal naturally operating pipe (HNP) systems. This paper shows the buildings and structures of the Samburgskoye Field gas processing facility where all the buildings and structures are built with the use of on-grade floor foundations and HNP systems. This allowed a 40% reduction in the cost of work and enabled completion of construction in only one year. The HNP systems of foundation soil freezing were first used to support facilities at the Sandybinskoye and Urengoy hydrocarbon fields. The system represents a passive hermetically sealed heat-transfer device that requires no power. It operates automatically in winter due to gravitational force and positive difference in temperatures between the ground and outside air.

The HNP system consists of two main elements:

- cooling tubes: the evaporator section located in the building foundation where it is used for the coolant circulation and the ground freezing;
- condenser section located above the ground surface and connected to the evaporator section. It is designed for the condensation of the coolant vapor and transfer of the coolant along the system by means of natural convection and gravity. The system's coolant is ammonia.

Experience accumulated during the first year of the system's operation shows that in some cases freezing of the foundation soils has to be faster at the initial stage of the construction and operation (i.e. at the time when it is necessary to reach immediately the design bearing capacity of the foundation base).

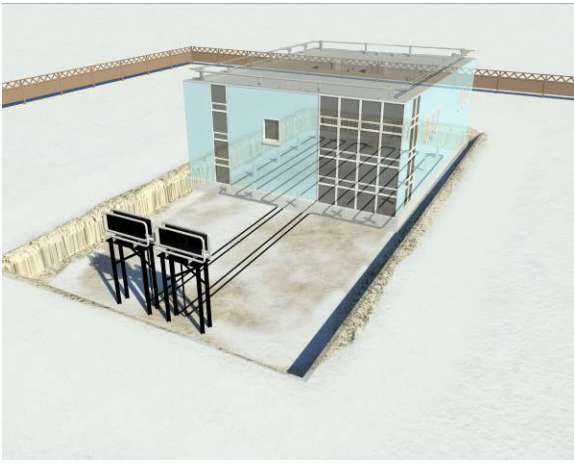


Figure 3. The HNP system includes horizontal cooling and connecting pipes placed under the insulation (underground portion) and the condenser unit (aboveground portion).

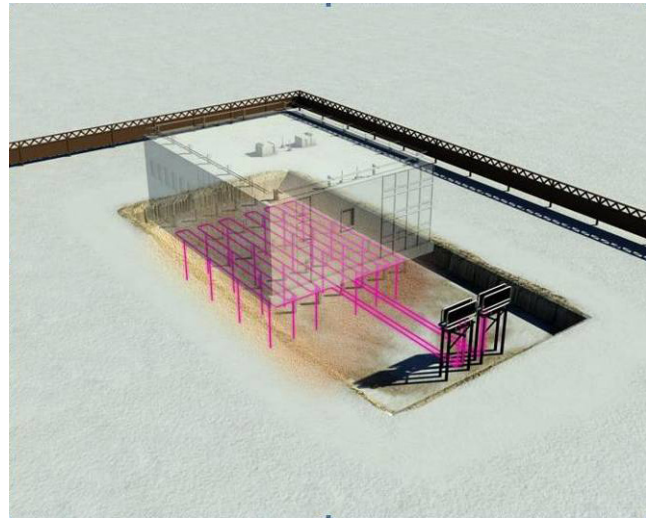


Figure 5. A VNP system includes vertical cooling pipes and connecting pipes (underground portion) and a condenser unit (aboveground portion).



Figure 4. Foundation soil thermal stabilization using the HNP system at a production building (116.2 x 66 m) in the Vankor Oil Field.



Figure 6. Foundation soil thermal stabilization with the VNP system at a production building in the Bovanenkovo Gas Condensate Field.

A Vertical Naturally Operating Pipe (VNP) system with vertical tubing extending downward into the ground and capable of delivering cold to the depth of 12–15 m was developed in order to promote faster freezing of the foundation soils at the initial stage of the construction and operation. The mass introduction of the HNP and VNP systems coincided with the construction of facilities at Yuzhno-Russkoye, Samburgskoye, Verkhnechonskoye, Vankor, Bovanenkovo, Nydinskoye, and Yuzhno-Khylchuyuskoye hydrocarbon fields. Another engineering solution, the individual heat stabilizers, is designed to freeze thawed soils and to chill frozen medium- to high-plasticity soils under buildings with or without ventilated basements, pipe racks, and other structures in order to increase their bearing capacity and to prevent frost heaving of piles. These devices include a tube protected by a solid metal casing, which is filled with coolant—either carbon dioxide or ammonia. The total length of a heat stabilizer ranges from 10 to 23 m.

The height of the aboveground condenser section with aluminum fins is up to 3 m, whereas the evaporator section of a heat stabilizer is embedded into the ground. This engineering solution proved to be crucial during the construction of the 548-km Vankor-Purpe oil pipeline. The pipeline route

runs across several landscape zones underlain by various types of perennially frozen soils. This includes ground ice and ice-cored frost mounds that form hills covered with a vegetative layer, organic turf, and shrubs. Design and construction of the pipeline in such terrain conditions was a serious challenge. Overall, 238 km of the pipeline, the northern portion, was built aboveground, whereas, the remaining 310 km of the pipeline, the southern portion, had to be built below ground. For the aboveground portion of the pipeline, FSA designed supports with heat stabilizers placed inside the piles. Overall, 38,000 units were installed in the northern aboveground portion of the pipeline, and more than 28,000 units were installed in the underground southern portion.

Apart from the oil and gas industry facilities, FSA's innovative engineering solutions were also tested during the construction of a precious metal ore processing factory in Khakandzha (Magadan Region) and at the dams in Yakutia: the Irelyakh dam on the Liendokit River, and a tailings retention dam of the Nyurba mining and processing complex. Several deep foundation Seasonally Cooling Devices (SCDs) were designed specifically for these projects. For example, a collector SCD was designed for the Liendokit River dam. It is connected through

Table 1. Technical and economic indicators demonstrating the advantages of new engineering solutions.

Name of venue	Cost of the foundation construction		Sum of cost reduction
	Ventilated basement	On-grade floors with an HNP system	
Samburgskoye Gas Field: Production building 18x105 m, Fire station 30x42 m	105.3	80.1	25.2
Economic benefit is 24%			
Khakandzhinskoye Gold-Silver Deposit: Gold processing plant (main building is 110x48 m, mill building 19x26 m, 7VST-1000)	296.2	203.3	92.9
Economic benefit is 31%			
Kharasaveiskoye Gas Condensate Field: Heated parking 54x72 m	132.8	93.7	35.5
Economic benefit is 27%			

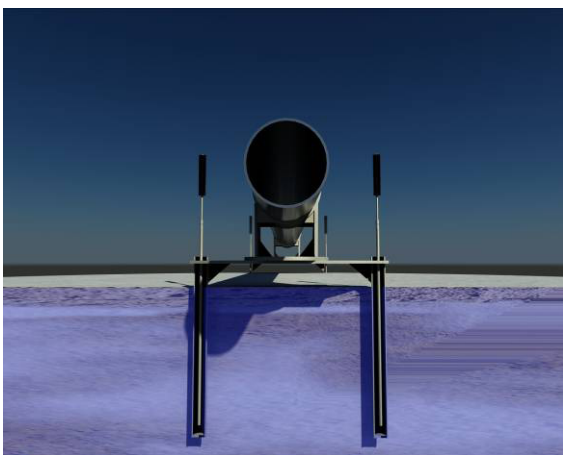


Figure 7. Individual heat stabilizers installed in conjunction with piles.



Figure 8. Vankor-Purpe oil pipeline.



Figure 9. Liendokit River dam. Nyurba mining and processing complex of AIROSA Company.



Figure 10. Liendokit River dam with deep foundation and a seasonally cooling device of a collector type.

a collector to the air cooling unit, in which the air cooling of the finned tubes is carried out by fans. Artificial air cooling of the finned tubes causes a significant increase in the heat exchange during very cold and calm periods which are typical of Yakutia. The cooling tube temperature drops down and almost reaches the ambient air temperature. Such a system is designed for intensive initial ground freezing and further sustainable maintenance of the artificially developed frost bulb in the ground.

The main technical and economic indicators that demonstrate the benefits of the new engineering solutions are given in Table 1.

All recently built facilities are continuously monitored and inspected. This includes geocryological monitoring. The ground temperature curves plotted as a result of the long-term geocryological monitoring indicate a fairly good correlation of the estimated, simulated, and actual values of the ground temperatures of the foundation soils. They also indicate a stable decrease in ground temperatures year after year with a well-defined negative trend. Results of the study are used in the design and construction of various structures on permafrost.

Permafrost Monitoring of Southern Tundra Landscapes in the Russian European North and West Siberia

D.S. Drozdov

Earth Cryosphere Institute, SB RAS, Tyumen, Moscow, Russia

Russian State Geological Prospecting University, MGRI – RSGPU, Moscow, Russia

G.V. Malkova, N.G. Ukraintseva, Yu.V. Korostelev

Earth Cryosphere Institute, SB RAS, Tyumen, Moscow, Russia

Abstract

The characteristics of permafrost, especially the thermal state of the active layer, depend on latitude and elevation and are generally controlled by climate and its contemporary changes in space and time. This paper is concerned with the results of active layer monitoring at two sites in the southern tundra in the zone of continuous permafrost in the Russian European North and in West Siberia. It is concerned with the inferred climate, landscape, lithology, and geomorphology controls of seasonal thaw depths and ground temperatures.

Keywords: permafrost temperature; seasonal thaw; southern tundra; active layer monitoring; climate change.

Introduction

The ground thermal regime is the principal target of permafrost monitoring (Pavlov 2008). Mean annual temperature and seasonal thaw depth are the basic parameters that record the state of the active layer (Grechishchev 1981) and the responses of permafrost to natural and technogenic effects. Their spatial and temporal variations depend on latitude and elevation and are subject to the influence of numerous local agents. Climates in similar landscapes generally become more severe in the eastern direction.

The temperature monitoring data are compared below for two areas located within large oil and gas provinces of the Russian European North (Bolvensky site in the Pechora River mouth, near Varandey) and in West Siberia (Urengoy site, near the gas production site in the northern Urengoy field, UKPG-15). Both sites belong to the zone of continuous permafrost within southern tundra (Fig. 1) and, being distant from engineering structures, record the undisturbed background permafrost settings. Monitoring at the two sites has been run as part of two international projects: Thermal State of Permafrost (TSP) and Circumpolar Active Layer Monitoring (CALM).

Ground temperatures at the Bolvensky station have been

logged for 28 years (1983–2011), and the monitoring of seasonal thaw depths began in 1999 at a specially equipped CALM site (Malkova 2010). At the Urengoy station, temperature logging has been done since 1975, and the CALM site has been in operation only since 2006 (Drozdov et al. 2010). Comparison of data from the two sites, which are geographically distant but have similar landscape, geological, and permafrost settings, provides clues to the current trends of the respective high-latitude territories.

Physiographic Background

Mean annual air temperatures in the Russian high latitudes show cyclic variations, almost synchronous at different weather stations. See Figure 2 for curves of mean annual, mean summer, and mean winter air temperatures at the two weather stations of Bolvensky (within the Bolvensky permafrost monitoring site) and Tazovsky (nearest to the Urengoy site).

The climate norm (mean annual air temperature T_a for the period 1961–1990) at the Bolvensky weather station is -4.7°C , and the mean over the past decade has risen to -3.1°C . At the Tazovsky station, the reference temperature for 1961–1990 is twice as low (-9.2°C) but the mean over the 2000–2010 period has likewise increased markedly to -7.7°C . The observed T_a difference between the two sites is fully due to winter means as the summer means are both about $+10^\circ\text{C}$. The sum of positive temperatures at the weather stations (and, respectively, at the sites of permafrost



Figure 1. Location map of Bolvensky and Urengoy permafrost monitoring sites. Color grades show continuous (1), sporadic (2), and patch (3) permafrost zones.

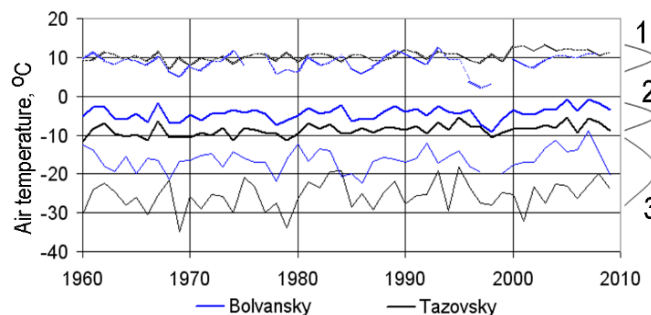


Figure 2. Annual and seasonal air temperature variations at the Bolvensky and Tazovsky weather stations. 1 – summer mean; 2 – annual mean; 3 – winter mean.

monitoring) is 30–35°C-month, which allows them to be assigned to the southern tundra subzone.

Snow thickness, another important factor for the ground thermal regime, is largely controlled by winds in the tundra. It is thus thinnest (10–20 cm) on hilltops and windward slopes and deepest (up to 1.5–2.0 m) in depressions and at the foot of hills. The density of snow varies during the cold season from 0.19 to 0.39 g/cm³, being 0.25–0.28 g/cm³ on average in different years.

With these thicknesses and densities, snow causes an insulating effect on the annual temperature fluctuations (distribution and variation in amplitude).

Site Description

The Bolvansky site is located on the southern side of the Pechora Gulf in the southern tundra subzone (Bolshaya Zemlya tundra in the European part of Russia) in a cumulative glacial-marine coastal plain with elevations of 20 to 50 m. This is an area of hilly topography dissected by ravines and depressions of limnic and drained lake basins. Permafrost there is continuous, with unfrozen lenses (taliks) beneath depressions. Ice contents are high (totaling up to 56% loam).

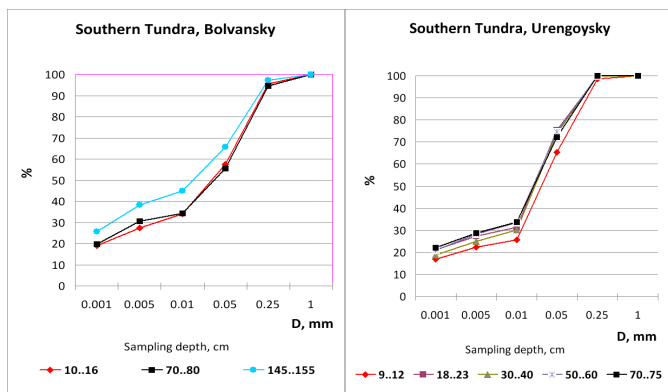


Figure 3. Grain sizes of surface sediments at the Bolvansky and Urengoy sites.

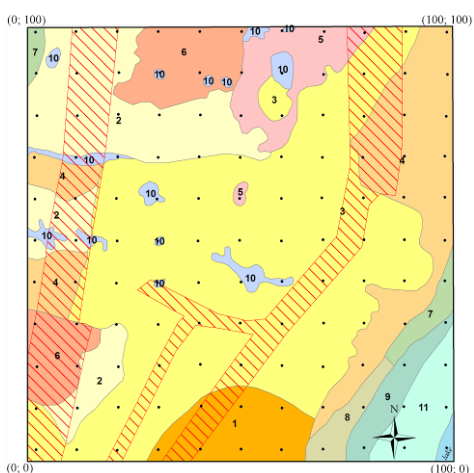


Figure 4. Landscape zoning at the Bovansky CALM site. Completed by N.G. Ukraintseva after Yu.N. Bochkarev.

The surface sediments consist of Upper Quaternary marine loamy sand and loam with inclusions of pebble underlain at depths 10 to 15 m by Middle Quaternary glacial-marine bouldery loam. Surface peat layers, from 1 to 5–7 m thick, occur in the head parts of valleys, in hill saddles, and in the bottoms of dry lake basins; the same is true of the locations of thick ice lenses.

The Urengoy (UKPG-15) site is located in the southern Taz Peninsula, on the left bank of the Khadutte River. It belongs to coastal plain III (III cumulative marine terrace) rising 30 to 40 m above the sea level, where low hills are separated by branching ravines. Unlike the Bolvansky site, there are few lakes. The surface sediments are silty loam with sand layers and lenses overlain with peat, up to 1 or 2 m thick. The permafrost there is ice-rich (total water is 60% in loam and 21–28% in sand) and continuous from the surface, almost without taliks.

The grain size distributions of surface sediments are very similar at both sites (Fig. 3), which is evidence of their genetic correlation. Large percentages of silt size grains result from intense frost weathering of the active layer.

Local ecosystems associated with different landscapes within the two CALM sites have been classified (at the level of landscape facies) and mapped to scale 1:5000 (Figs. 4 and 5). Maps of this kind, based on the landscape-indication approach, can be used as a basis for estimating local variations in lithology, water content, and active layer thickness. Local map modeling could also be done.

The two sites are similar also in landscape zoning patterns, with mostly hummocky tundra (sometimes with scarce patches) on drained low hilltops and shrubby tundra with dwarf birch (yernik) and willows on slopes. There are old tractor ruts at both sites and fresh fire traces at UKPG-15.

Monitoring of Seasonal Thaw Depth

Seasonally variable thaw depth of permafrost is the local parameter studied at uniform 100 x 100 m CALM sites with

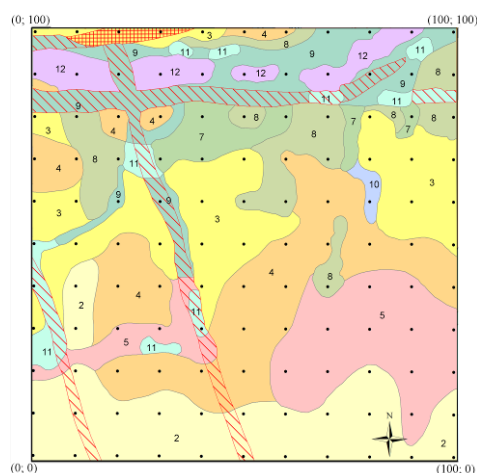


Figure 5. Landscape zoning at the Urengoy CALM site (UKPG-15). Compiled by N.G. Ukraintseva.



Legend to Figures 4 and 5: Tundra subzones (1-6): flat lichen (1), hummocky shrub-grass-moss-lichen (2), hummocky shrub-lichen (3), hummocky-tussock ledum-lichen (4), patchy willow-moss-lichen (5), patchy shrub-grass-moss-lichen (6); 7 – willow hill slopes; 8 – willow-yernik hill slopes; 9 – willow-yernik swampy ravines; 10 – ledum-moss-lichen swampy micro-ravines; 11 – grass-moss bogs; 12 – hummocks with willow and yernik; 13 – old ruts of off-road vehicles; 14 – burned-out places; 15 – grid nodes.

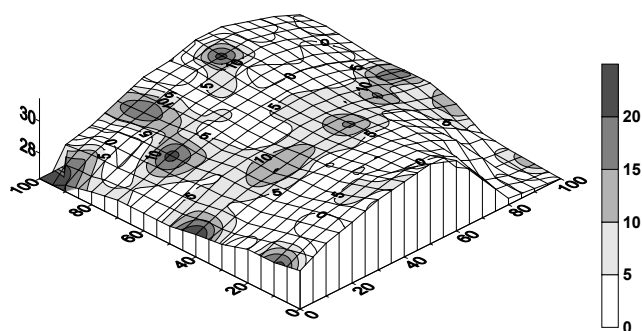


Figure 6. Peat thickness at Bolvansky site (5 cm on average).

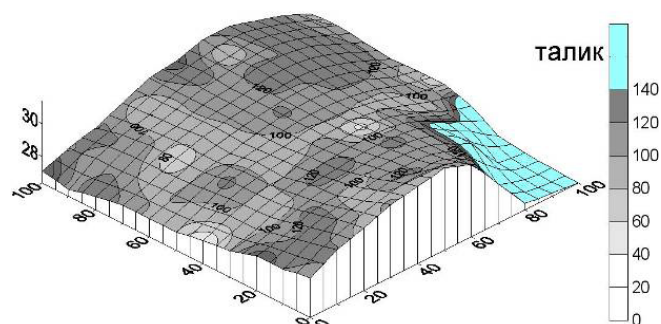


Figure 7. Thaw depth at Bolvansky site (average at each picket for 1999 through 2010).

data points at every 10 m (121 pickets). Thaw depths are measured at each picket with a metal probe, yearly at the end of the warm season or several times in a summer in some years. Besides the thaw depth measurements, there are other works, such as surface leveling and sampling of sediments, soils, and vegetation. The space and time variations of the measured parameters are estimated with the kriging technique using the Surfer software, as the CALM project implies.

In our view, however, the way of continual imaging (as isolines) employed in the CALM project is not quite reasonable. The changes of peat thickness, as well as thaw depth, more often have discrete patterns according to surface details, moisture, and vegetation mosaics in local geosystems. Therefore, it appears more appropriate to use rather a map of landscape facies as a contour line basis.

The CALM site at the Bolvansky monitoring station is located on the top of a low hill composed of loam, in a typical landscape. The peat thickness within the site varies from 1 to 22 cm, being 5 cm on average (Fig. 6).

The lithology of the active (seasonally thawing) layer and vegetation patterns are the most important controls of thaw depths. They are the shallowest depths (under 60 cm) within minor swampy ravines where peat is the thickest and vegetation consists of shrubs, mosses, and lichen (subzone 10). Thaw depths from 60 to 100 cm are common to hummocky shrub-grass moss-lichen, and ledum-lichen subzones (Nos. 2 and 4). The maximum depths of 100 to 140 cm correspond to hummocky shrub-lichen (No. 3) and patchy (Nos. 5 and 6) subzones (Figs. 4 and 7). Thaw depth variations for the observation period (1999–2010) have been under 15%.

A buried talik was discovered at the edge of a lake within the shrubby southeastern part of the site. The acoustically

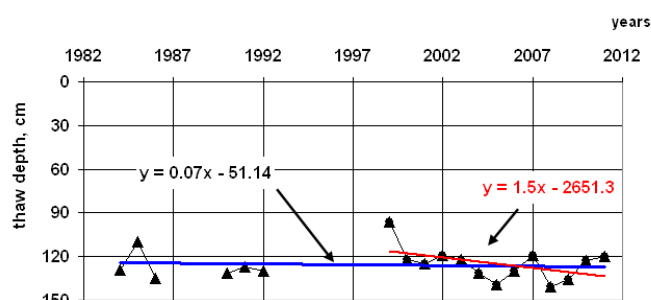


Figure 8. Average thaw depth variations at the Bolvansky site.

defined permafrost table lies there at depths 3.5 to 4 m. The lake depression accumulates thick snow, which prevents soil from winter freezing. This is an obvious medium-scale relief effect (besides the vegetation and micro-relief effects) on both thaw depth and permafrost table position.

Yearly variations in average thaw depths for 1999 through 2010 were as shown in Figure 8. The lowest values (90 cm) were measured in 1999 followed by a progressive increase to 120–130 cm until 2011, at a rate 1.5 cm/yr. However, the increasing thaw depth trend becomes almost cancelled out by data for the 1980s–1990s, when the summer air temperature was also rising (Fig. 2). So the growth rate over the total period was only 0.07 cm/yr. Note that yearly thaw depth variations are virtually independent of winter climate parameters but correlate closely with the summer ones (Malkova 2005), especially with thawing index (or DDT, degree-days of thawing) (Melnikov & Grechishchev 2002, Pavlov 2008).

The CALM site UKPG-15 within the Urengoy monitoring station is located on a hilltop gently dipping northward, in a grass-shrub-moss-lichen tundra landscape type with scarce patches. The peat thickness is from 4 to 10 cm (7 cm on average) and is generally inversely proportional to the thaw depth (Figs. 9 and 10).

The spatial variations of thaw depths and their correlation with landscape zoning at the Urengoy site have been portrayed in a series of discrete map models (Ukrainitseva et al. 2011).

The thaw depths at the UKPG-15 site are the largest (75–96 cm) within dominant landscape facies (Nos. 2–5) of grass-shrub-moss-lichen and lichen tundras (Figs. 5 and 11) and decrease to 60–78 cm in depressions and swampy shrubby ravines that accumulate much moisture (zones 7–12). Anthropogenic effects (healed old tractor ruts) increase thaw depths by a factor of 1.5 to 2, especially in places of localized surface run-off.

The two CALM sites of Bolvansky and Urengoy are very similar in general outlook, lithology, and active layer thickness (thaw depths). The similarity of summer temperature means between the two sites, according to data of nearby weather stations (Fig. 2), demonstrates again that the warm season climate parameters are the principal control of local permafrost patterns.

Thaw depth measurements alone can neither provide unambiguous evidence of permafrost stability under the contemporary climate change at specific sites nor show whether permafrost is beginning to degrade. More information in this respect comes from ground temperatures.

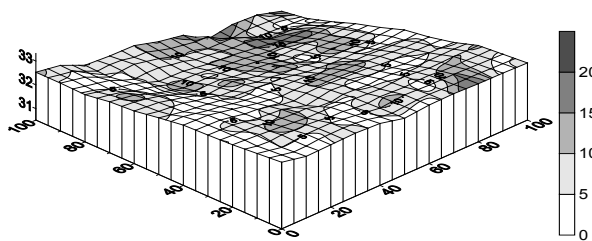


Figure 9. Peat thicknesses at the UKPG-15 site (7 cm on average).

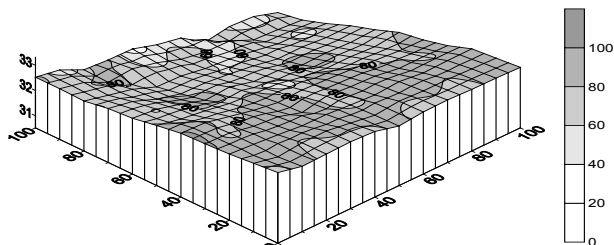


Figure 10. Thaw depths at the UKPG-15 site (average at every picket for 2006 through 2010).

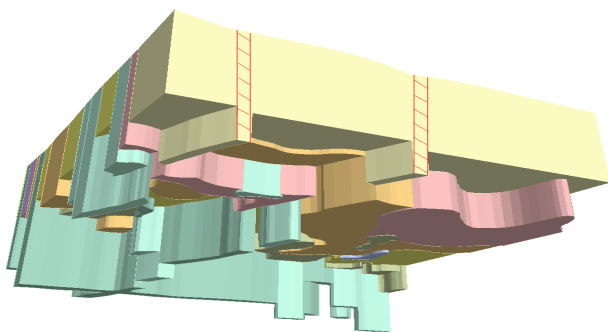


Figure 11. Thaw depths averaged over landscape subzones at the Urengoy (UKPG-15) CALM site. Narrow vertical bands of thawing anomalies correspond to linear man-caused effects (old ruts). Legend same as in Figures 4 and 5.

Ground Temperature Patterns

The monitoring of permafrost temperatures at the Bolvansky station in the Russian European North began in 1983. The space and time temperature patterns show prominent correlation with landscape zoning. The highest growth rates of mean annual ground temperatures (T_g) were observed in drained tundra areas of the coldest ground at the site (T_g -2.0...-2.3°C). Warming in those landscape conditions reached 0.5 to 0.8°C by 2011, at a mean long-term T_g trend of 0.03°C/yr (borehole 59, Fig. 12). The total ground warming within polygonal peatbogs (T_g -1.6°C) was slightly less: 0.6°C, at a rate of 0.02°C/yr (borehole 55, Fig. 12). Eroded lake edges and outliers composed of high-temperature permafrost (T_g -1.0...-1.2°C) are the least sensitive to climate change showing a T_g increase as low as 0.2–0.5°C at a rate of 0.01°C/yr (borehole 51, Fig. 12).

The air temperature (T_a) trend for the observation period has been 0.07°C/yr (Fig. 13) (i.e., 2 to 7 times as high as that of ground temperatures).

The temperature of the active layer is especially sensitive to climate change. Active layer temperatures were logged in borehole 59a at the center of the CALM site, in typical landscape conditions. The annual means from 1983 through

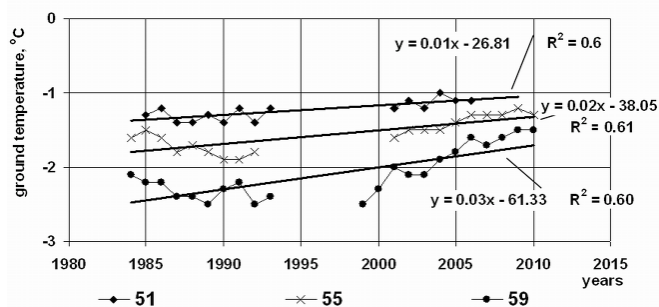


Figure 12. Time-dependent variations of mean annual ground temperature in different landscape subzones at the Bolvansky site. Borehole 59: typical tundra; borehole 55: degrading polygonal peatbog; borehole 51: drained tundra at lake edge.

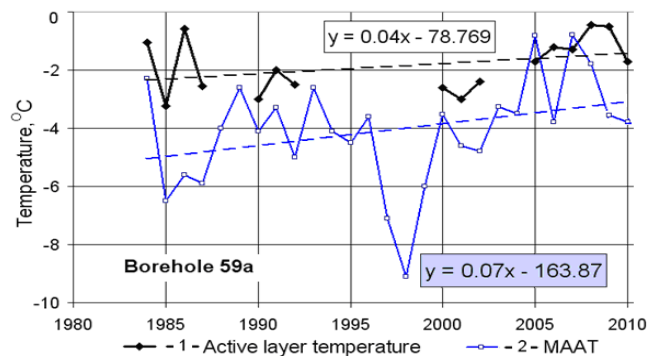


Figure 13. Mean annual temperatures of active (seasonally thawing) layer and air at the CALM site of Bolvansky permafrost monitoring station for 28 years.

2010 were in the range -3.5 to -0.4°C. The active layer temperature trends generally follow the air temperature patterns (T_a), though they have smaller amplitudes (Fig. 13).

The annual temperature means of the active layer have been -2 to -3°C in different years, which corresponds to a long-term steady trend, but some growth tendency has appeared since 2001. Before 2007, the active layer temperatures remained within -1...-2°C (semi-transitional thawing type). Then the atypically warm and snowy winter of 2007–2008 caused notable warming (-0.4°C) when the temperatures risked approaching 0°C (transitional thawing type) and prerequisites arose for detachment of the permafrost surface. However, the air temperature in 2009 was within the climate norm (-3.6°C), and the mean annual active layer temperature in 2010 again decreased markedly to become -1.7°C. The cold winter of 2010–2011 and the cool summer of 2011 have brought more stability to the active layer temperatures at the site.

The ground temperatures at the Urengoy (UKPG-15) station in northern West Siberia have been monitored since 1974 with two gaps (Fig. 14).

The temperature patterns in this drained and swampy watershed tundra are similar to those in tussock peatbogs of terrace I of the Khadutte River: T_g was -5.5...-6°C in 1974 but grew to -4.2...-4.7°C in 2010–2011 (i.e., warming reached ~1.5°C). The T_g warming rate has been ~0.04°C/yr at the respective air temperature trend ~0.06°C/yr (Vasiliev et al. 2008). The anomalous peak of air temperatures in 2007–2009 made still faster T_g warming rates (Drozdov et al. 2010). The only exception has been a rare landscape type of a south-looking steep slope of coastal terrace III

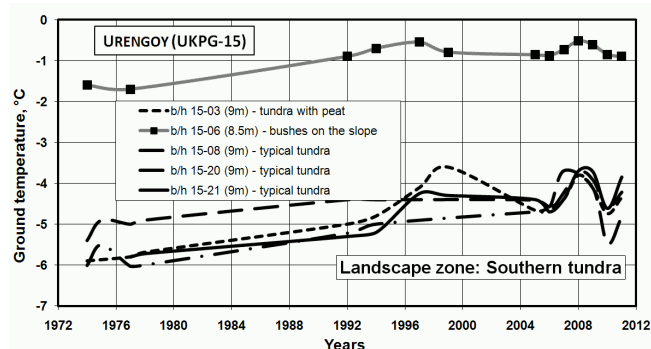


Figure 14. Typical patterns of mean annual ground temperatures in the tundra zone and in azonal willow-covered slopes (borehole15-06) at the Urengoy site (UKPG-15).

grown with thick and tall moss-grass willow shrubs, where permafrost temperatures were originally higher than in the surroundings (T_g -1.7°C in 1974) and the general warming was notably lower (less than 1°C) due to the buffer role of the shrubs.

Note that permafrost began to stop warming, following the respective tendency in air temperatures, much earlier than in the European North of Russia, already since the 1990s. Then the conditions became favorable for more southern plant species to migrate northward (e.g., young larches appeared in the southern tundra), but these conditions disappeared after several harsh winters in the early 2000s (DrozdoV et al. 2010).

Conclusions

The Bolvansky and Urengoy permafrost monitoring sites exist in similar geological, geomorphic, and landscape conditions. As for the climate factors that influence the temperatures and thaw depths of the active layer, the similarity is in summer air temperature means and snow accumulation.

The mean annual air temperature in northern West Siberia is 5°C lower than in the European North on account of harsher winters.

The thaw depths, being dependent primarily on air temperature summer means, are similar at both sites. The monitoring results show increasing thaw depths in drained areas of southern tundra for the past 10–12 years, but this tendency is cancelled out if the trends of the 1980s are taken into account.

Low annual and winter air temperature means in West Siberia cause severe permafrost conditions in tundra landscapes ($-4\dots-5^\circ\text{C}$), while in the European North they are within the range -1 to -2°C .

The climate warming rate in the two areas for the past three decades has been 0.06 to $0.07^\circ\text{C}/\text{yr}$. In the late 1990s there was a warm peak in West Siberia marked by appearance and then disappearance of trees in the southern tundra.

The general response of permafrost to climate warming consists of ground warming rates being the fastest in colder landscape zones and the slowest in the warmer ones.

The ground temperature trends in natural conditions are lower than the air trends by factors of 2 to 7 in the European North and only 1.5 to 2.5 in West Siberia.

Acknowledgements

This study was supported by grants 08-05-00421a, 08-05-00872a, 09-05-10030k, 10-05-10027k, 11-05-00544a, and 11-05-00084k from the Russian Foundation for Basic Research, as well as by NSF grants OPP-9732051 and OPP-0225603. It was carried out as part of integration research programs of the Presidium of the RAS Siberian Branch and as part of international projects TSP (Thermal State of Permafrost) of the University of Alaska Fairbanks and CALM (Circumpolar Active Layer Monitoring). Additional logistical support was provided by Gasprom Dobycha Urengoy Ltd. and Nenetsky nature reserve.

References

- DrozdoV, D.S., Ukraintseva, N.G., Tsarev, A.M., & Chekrygina, S.N. 2010. Changes of permafrost temperature field and geosystem state on Urengoy oil-gas-field territory during the last 35 years (1974–2008). *Kriosfera Zemli XIV* (1), 22–31.
- Grechishchev, C.E. (ed.). 1981. *Prediction of Physical and Geological Trends in Permafrost in High-Latitude Areas under Development: Methodological Guidelines*. VCEGINGEO, Moscow, 78 pp. (in Russian).
- Malkova, G.V. 2005. The effect of climate change on seasonal thaw depths (from monitoring results at the Bolvansky CALM site). In *Priority Lines in Research of Earth's Cryosphere*. Abstracts Intern. Conf., Pushchino, 25–28 May 2005, pp. 122–123.
- Malkova, G.V. 2010. Mean annual ground temperature monitoring on the steady-state station “Bolvansky”. *Kriosfera Zemli XIV* (3), 3–14.
- Melnikov, E.S. & Grechishchev, C.E. (eds.). 2002. *Permafrost and Development of Petroleum Provinces*. GEO, Moscow, 400 pp. (in Russian).
- Pavlov, A.V. 2008. *Monitoring of Permafrost*. GEO, Novosibirsk, 229 pp. (in Russian).
- Ukraintseva, N.G., DrozdoV, D.S., Popov, K.A., Matyshak, G.V., & Tsarev, A.M. 2011. Monitoring of permafrost, active layer, and landscape systems in forest-tundra and southern tundra of West Siberia. *Proc. 4th Workshop of Cryologists of Russia*, Moscow University. Book 2, Part 6. Dynamic Geocryology. Universitetskaya kniga, Moscow, pp. 334–341 (in Russian).
- Vasiliev, A.A., DrozdoV, D.S., & Moskalenko, N.G. 2008. Permafrost temperature dynamics of West Siberia in context of climate changes. *Kriosfera Zemli XII* (2), 10–18.

Specific Features of Cryogenic Soil Formation in Western Yakutia

A.G. Dyagileva

M. K. Ammosov North-Eastern Federal University, Institute of Applied Ecology of the North, Yakutsk, Russia

Abstract

One of the peculiarities of the process of soil formation in permafrost regions that distinguishes it from, among other things, geochemical weathering is the migration of microelements in permafrost soils. Three main types of cryogenic soils are described and sampled for distribution of microelements. In the extreme continental climate of Yakutia, soil formation is influenced by vegetative cover. The most important factor is the presence of the underlying permafrost horizon, which serves as an aquiclude and forms a suprapermafrost geochemical barrier.

Keywords: cryogenic soils; dry permafrost; ice-rich permafrost; microelements; thixotropic.

Background

Yakutia is located in the northeastern part of Siberia. It lies within four geographic zones: taiga forest (nearly 80% of the area), forest-tundra, tundra, and arctic desert.

The climate of Yakutia is severe and sharply continental. This is confirmed by the amplitude of average air temperature between the coldest and warmest months; the amplitude of 64.6°C does not occur anywhere else in the world. The annual amplitude of maximum and minimum air temperatures exceeds 101°C. The absolute value of the minimum temperature in the eastern mountain systems of troughs, basins, and other depressions is up to -70°C. The total duration of negative temperatures lasts from 6.5 to 9 months per year. With these climate parameters, the Republic has no analogues in the Northern Hemisphere.

Virtually all of the vast territory of Yakutia is affected by perennially frozen ground. Continuous permafrost is developed on most of the region, where it is interrupted only by local open taliks existing beneath the channels of large rivers and beneath large lakes. The average thickness of permafrost reaches 300 to 400 m, whereas in the Vilyuy River basin it reaches 1500 m; this is the greatest thickness of permafrost on Earth.

The vertical section of permafrost zone is very diverse within Yakutia. In its western areas, for instance, the permafrost zone is composed of two strata. The upper one is composed of ice-rich frozen ground. The lower one is composed of cryotic deposits with temperatures below 0°C containing mineralized ground waters with negative temperatures (cryopegs). The thickness of the upper stratum is 300–350 m, and the thickness of the lower stratum is much larger, reaching 600–900 m or more. In Western Yakutia, a third (middle) stratum is indicated. In places it is represented by frozen ground with no visible inclusions of ice or cryopegs. A subaqueous permafrost zone developed in the offshore coastal area of the arctic seas also generally has the two-strata structure.

The formation of thick permafrost in Northern Yakutia began about 2 million years ago. Then permafrost gradually spread throughout the territory of the Republic. Its formation was accompanied by intensive development of cryogenic processes such as frost cracking, formation of ice-wedge ice, polygonal relief with non-sorted circles, and the appearance of seasonal and perennial frost mounds (Integrated Atlas 2009).

Cryogenic Soils

Cryogenic soils are a group of soils of the tundra and northern taiga zones with pronounced cryoturbations in the soil profile that lead to deformation of genetic horizons. These soils are closely underlain by ice-rich permafrost with active manifestation of cryogenic mass transfer which determines the homogeneity of the soil profile and the presence of solid and dissolved organic matter throughout the mineral part of the profile. Many soils in this group are characterized by thixotropy, deformation, suprapermafrost gleization, and unsaturated surface horizons. The following types of soils are identified in this group: cryogenic gley soils, cryogenic homogeneous (non-gleyed), and cryogenic thixotropic (Desyatkin et al. 2009).

Cryogenic gley soils (hereafter soil types are named according to the soil classification by Elovskaya [1987]) are usually confined to lowlands. Here they are formed under the conditions of impeded drainage in deposits of silty clay and clay (more often represented by ancient alluvium) and in the continuous presence of an ice-rich horizon in the soil profile near the surface. Their surface consists of a moist litter layer of needles, leaves, lichens, and mosses. This is underlain by unconsolidated, dark-brown organic soil represented by peat or peaty-humus, followed by a gleyed mineral horizon with a notably greater degree of gleying in the suprapermafrost level. These soils are acidic or slightly acidic, less often they are alkaline when on carbonate parent materials. Organogenic horizons are not base-saturated and have high hydrolytic acidity. In mineral horizons, this activity is low. The content of organic matter in organic soils is significant. Organic matter is represented by coarse humus (mainly of moldy or humus-moldy nature). Very mobile fulvic humus penetrates the soil particles and sometimes accumulates in the suprapermafrost horizon. This is the most common type of soil in North and Northwestern Yakutia.

Table 1 is the description of the morphological structure of the profile of a typical cryogenic gley soil. The section is from the sparse larch forest of the Kolyma River basin.

Cryogenic homogeneous soils (non-gleyed), a soil type of hydromorphic non-gleyed formation, are usually confined to watersheds and their slopes. They are developed under sparse and moss-lichen larch forests and are formed on weathered bedrocks of various composition. Moss cover in the form of cushions of sphagnum peat or cryogenic hillocky microrelief is often well developed on the surface of cryogenic homogeneous

Table 1. Morphological structure of the profile of a typical cryogenic gley soil.

O/O2	0-10 cm	Light brown mosses becoming a slightly decayed, moist forest litter penetrated by plant roots. The transition is noticeable with smooth boundary.
A/T	10-18 cm	Brownish-dark-gray, organogenic, medium and strongly decayed vegetative debris, densely intertwined with plant roots (up to 1.5 cm), moist. Sharp transition in color and roots, slightly curved boundary.
Bg	18-34 cm	Dark-gray silty clay with a bluish tinge, structureless, consolidated, moist with flowage in the bottom part. Small patches of organic matter (diameter up to 3 mm). Overlies ice-rich permafrost.

Table 2. morphological structure of a profile of typical cryogenic homogeneous soils.

O	0-4 cm	The litter of leaves and needles. Transition is clear, the boundary is pocket-like.
AO	4-7(14) cm	Dark brown, crumbly, moist, organogenic. Soil is silt with some clay, fine clods. Transition is clear, the boundary is curvy.
Bcr	7 (1 4) – 35 cm	Brownish-gray with abundant rusty spots. Rare inclusions of pebbles of 1-3 cm in size; moist, silty clay, the top is powder-like, the bottom is platy, penetrated by roots. Does not react to HCl. Overlies permafrost with low ice content.

soils. A litter of considerable thickness (10–12 cm) of brown or dark-brown undecomposed peaty remains overlies the top part of the profile and is underlain by a dark organogenic horizon with an admixture of mineral fine-grained soil. Below is the mineral horizon of uniform brownish-gray color with clearly visible manifestations of cryogenic processes that overlie the permafrost. The mineral material, overlying the ice-rich permafrost, is structureless, mixed with granulated plant remains of varying degrees of decomposition, and saturated by brownish humic substance. The maximum depth of thawing is 50–65 cm. The entire soil profile is characterized by a relatively high content of humus. The humus composition is of a fulvic nature. The soils have a high absorption capacity. Depending on the underlying parent material, acidic unsaturated soils developed on acid materials occur, as well as saturated neutral or slightly alkaline soils developed on basic and carbonate materials. Based on particle size distribution, the soils are often silty clays; less often they are silts.

Table 2 is the description of the morphological structure of a profile of typical cryogenic homogeneous soils. The section is located in a larch forest of the Tyung River basin.

Cryogenic thixotropic soils usually occupy flat watersheds, gentle sloping hills, and terraced surfaces. They are developed on the weathered bedrocks, slope and

Table 3. morphological structure of a typical profile of cryogenic thixotropic soil.

O	0-6 cm	Live, moist moss cover. The lower part consists of weakly decomposed plant remains. Transition is clear, the boundary is smooth.
AO	6-15 cm	Dark-brown, organogenic, moist, loose, densely penetrated by roots. The transition is clear, the boundary is smooth.
Bcr	15-22 cm	Light gray with bluish tinge, moist, water seeps in from the pit walls. Thixotropic, structureless, sandy. The soil pit was immediately filled by a sand slump from the walls. Underlain by ice-rich permafrost.

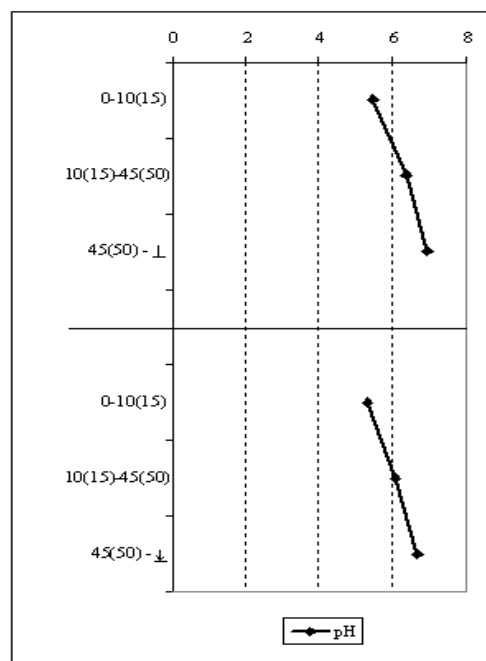


Figure 1. The acid-alkaline conditions (pH) of the active layer. Top: "ice-rich" permafrost; lower: "dry" permafrost.

glacial deposits of clayey texture under moss-lichen larch forests with a well-developed understory of dwarf birch, willow, ledum, swamp blueberry, and cowberry. Soils are characterized by pronounced cryogenic forms of microrelief such as pitted hillocks and polygonal fractures. Their profile is similar to cryogenic homogeneous soils. They are characterized by greater humidity and thixotropy. Cryogenic thixotropic soils are also characterized by acidic reaction as well as by very high hydrolytic acidity in the upper, coarse humus horizon due to the high content of slightly decomposed organic matter. Organic matter content and hydrolytic acidity are sharply reduced in the mineral part of the profile. Similarly, the distribution of nutrients decreases sharply along the profile. Their quantity in horizon A is very high, whereas it is very low in horizon Bcr. These are poor soils for agriculture, except for reindeer pastures.

Table 3 is the description of the morphological structure of a typical profile of cryogenic thixotropic soil. The section is located in the larch forest of the middle Tyung River.

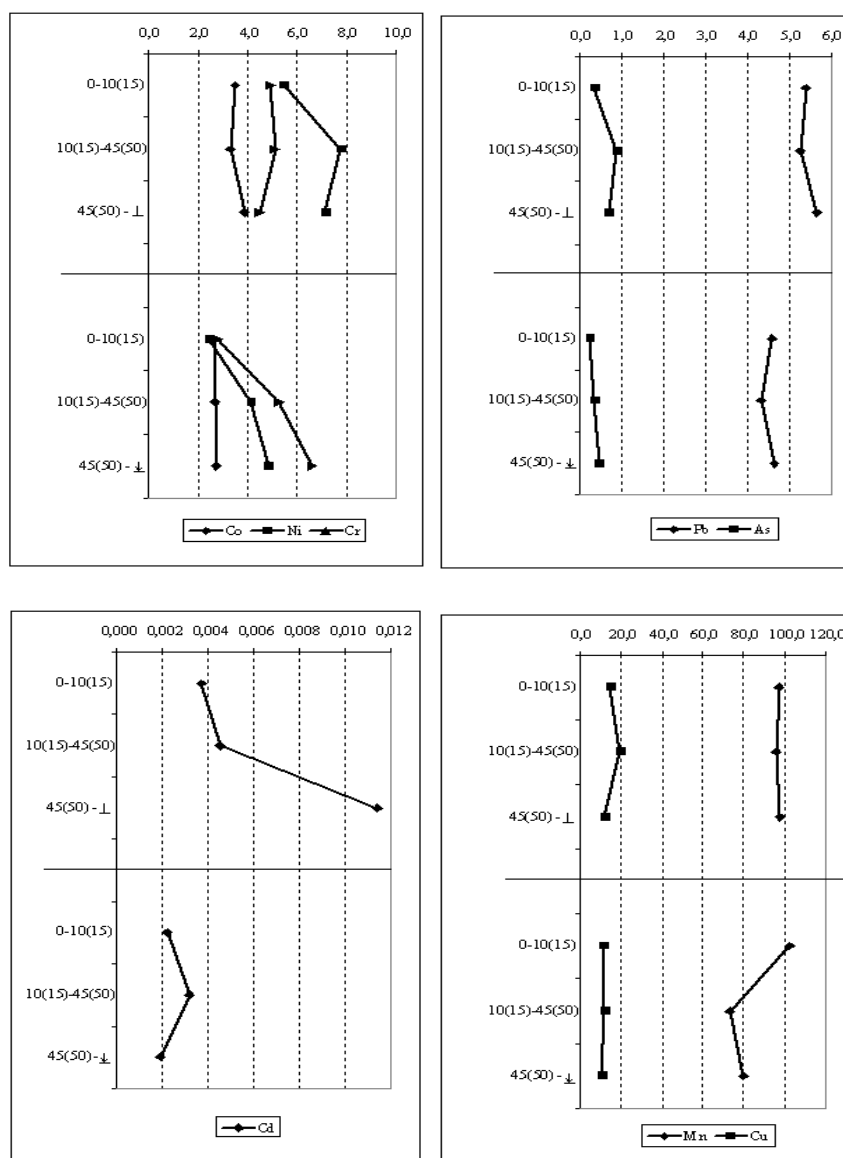


Figure 2. The content of mobile forms of microelements in cryogenic soils in the active layer; upper plots: “ice-rich” permafrost; lower plots: “dry” permafrost.

Objectives and Methods

The study of cryogenic soils was conducted in the Nakyn industrial area in Western Yakutia.

In the course of field observations, 13 soil profiles within the natural landscapes of the watershed of the Hannya-Nakyn interfluvium were examined. Of these, eight sections are characterized by ice-rich permafrost and five are characterized by dry permafrost. All soil sections were made with a sampling of 2x2 km, with morphological description and sampling from all genetic horizons.

All samples were air dried at room temperature, sieved through a sieve with a 1-mm mesh, and transferred to paper bags.

The following physical-chemical parameters were examined: the acid-alkaline conditions (pH) and the contents of mobile forms of microelements (Cr, Ni, Co, Mn, Pb, Cd, Cu, and As).

The acid-alkaline conditions (pH) are determined by the potentiometric method. Distilled water is poured on a 20-gm soil sample in the ratio of 1:2.5, and water and soil are

thoroughly mixed. The pH values are measured using pH-meter ANION 4100.

The measurement of the content of mobile forms of microelements is performed using atomic absorption spectrometry and a multi-channel gas analyzer MGA-915. A 0.1-gr soil sample is covered with 10 ml 1N HCl and is stirred on the rotator mixer for one hour. Suspensions are filtered through blue ribbon filter paper. The filtrate is analyzed by the MGA 915 with an automatic sample changer.

In order to trace the behavior of microelements in the cryogenic soils, an average soil profile model of microelements for “ice-rich” and “dry” permafrost was constructed. The following average depths of the soil profile models were adopted: 0–10(15); 10(15)–45(50); and 45(50)–permafrost, according to which the corresponding diagrams were drawn.

Results and Discussion

The pH values in cryogenic soils with “ice-rich” and “dry” permafrost in the soil profile regularly increase with depth from slightly acidic to neutral (5.3–6.9) (Fig. 1).

Different trends of migration and distribution of microelements throughout the soil profile are observed at equal pH values.

The accumulation of the majority of microelements is observed in the supraperafrost horizon where “dry” permafrost is present (Fig. 2). The reason for this is that the soil material is dry and represented mostly by silt with some clay (i.e., it has a low sorption capacity).

The accumulation of microelements in the mineral horizon of the soil profile is detected in soils with “ice-rich” permafrost. This profile is characterized by high moisture content (i.e., high sorption capacity) and heavier fractions of soil particles (silty clay, clay). These properties create anaerobic conditions that lead to gleying processes associated with high iron content. Therefore, Mn and Cu are present in this horizon, as these elements belong to the iron group.

Thus the properties of soil material determine the permafrost conditions.

Conclusions

In the course of this study, 13 soil profiles within the natural landscape of the Hannya-Nakyn interfluvium were examined. Among those studied, eight are characterized by “ice-rich” permafrost and five are characterized by “dry” permafrost.

Analytical studies determining acid-alkaline conditions (pH) and the content of mobile forms of microelements (Cr, Ni, Co, Mn, Pb, Cd, Cu, and As) were carried out.

The pH values in cryogenic soils with “ice-rich” and “dry” permafrost in soil profile regularly increase from slightly acidic to neutral (5.3 to 6.9).

The accumulation of the majority of microelements is observed in the supraperafrost horizon, where “dry” permafrost is present.

The accumulation of microelements in the mineral horizon of the soil profile is observed in soils with “ice-rich” permafrost.

Thus the properties of soil material determine the permafrost conditions.

References

- Desyatkin, R.V., Okoneshnikova, M.V., & Desyatkin, A.R. 2009. Soils of Yakutia. Ros. akad. nauk, Sib. otd-nie, Int Biol. problem Kriolitozony, Yakutsk, Bichik, 64 pp. (in Russian).
- Elovskaya, L.G. 1987. *Classification and diagnosis of Yakutia permafrost soils*. Yakutsk, YAF SO AN SSSR, 172 pp. (in Russian).
- Integrated Atlas of the Republic of Sakha (Yakutia). 2009. FGUP. Yakutsk Aerogeodetic Enterprise (in Russian).

Contribution of Thawing Permafrost and Ground Ice to the Water Balance of Young Thermokarst Lakes in Central Yakutia

A.N. Fedorov, P.P. Gavriliev, P.Ya. Konstantinov
Melnikov Permafrost Institute, SB RAS, Yakutsk, Russia

T. Hiyama
Research Institute for Humanity and Nature, Kyoto, Japan

Y. Iijima
Research Institute for Global Change, Yokosuka, Japan

G. Iwahana
Hokkaido University, Sapporo, Japan

Abstract

The main purpose of the work is to define the role of permafrost thawing in the water balance supply of young thermokarst lakes in Central Yakutia in conditions of modern climate change. The materials obtained at the Yukechi monitoring site of the SB RAS Melnikov Permafrost Institute near Yakutsk from 1992 to 2008 and the data of the Yakutsk weather station were used in this study. The calculations showed that under conditions of mass thermokarst activation in Central Yakutia, up to one-third of the water balance supply is provided by the melting of ground ice.

Keywords: Central Yakutia; climate change; ground ice; landscape; thermokarst; water balance.

Introduction

Starting in 1992, the Melnikov Permafrost Institute of the Siberian Branch of the Russia Academy of Sciences (SB RAS) monitored the dynamics of young thermokarst depressions at the Yukechi site located 50 km southeast of Yakutsk on the right bank of the Lena River. Initially, the main attention was directed to the study of the surface subsidence rates and the evolution of thermokarst landscapes (Fedorov et al. 1998, Fedorov & Konstantinov 2003, 2008).

The investigated thermokarst depressions are represented by young formations, and their occurrence is associated with anthropogenic activity. People have been living on and farming the land for a long time. Animal husbandry has been the main type of farming, but grubbing and land plowing were conducted as well. Mainly grain crops were planted in this area. Plowed sites were created in the 1930s with the beginning of total collectivization of small peasant farms. These were abandoned in the early 1960s due to the enlargement of small collective farms (Bosikov 1989).

Thermokarst subsidence was not yet defined in aerial photographs taken in 1944, but some inhomogeneity of the plowed land can already be observed in the 1952 aerial photographs. It can be assumed that thermokarst formation in plowed lands started at the end of the 1940s and the beginning of the 1950s, when the peak of ground temperature increase was observed in Central Yakutia. By the beginning of our monitoring in 1992, the relative depth of thermokarst depressions was about 2 m. The water depth in the deepest channels between high-centered polygons reached 0.8 m. In most locations the depth was 0.4–0.6 m.

The studied site is an alas landscape typical of Central Yakutia. The deposits are represented by an ice complex with ice wedges. Clayey silt and silt, sometimes with addi-

tion of dust particles and fine-grained sand inter-layers prevail in the composition of the upper Quaternary horizons. Ice wedges are developed within inter-alas areas throughout the territory. Ice wedges occur at a depth of 2–2.5 m. The width of the upper part of ice wedges varies from 1–1.5 to 2.5–3 m. The cross dimension of ground between ice wedges usually does not exceed 4–6 m in plan. According to Lachenbruch's classification (Lachenbruch 1962), the non-orthogonal patterned system prevails with intersections of thermal contraction cracks at 120°. The thickness of the Ice Complex is 20–25 m. The ground temperature at 10–15 m depth in the primary larch forest is -3°C, and at the grass-graminoid meadow it is -2°C. The seasonal thawing depth in these landscapes is 1.3 and 2 m, respectively.

The climate is extremely continental. The annual mean temperature in Yakutsk (the nearest weather station) is -10.2°C; the January mean temperature is -42.6°, and the July mean temperature -18.7°C. The amount of precipitation is 234 mm per annum (Scientific-applied reference aid... 1989). However, the annual mean air temperature increased by 3°C in the recent decades between 1966 and 2009 (Skachkov 2010).

Thermokarst activation is observed in Central Yakutia starting from the beginning of the 1990s. Melting-out of the upper ice wedge heads causes subsidence of the surface; thermokarst depressions become deeper and wider; thermokarst lakes are initiated (Fedorov & Konstantinov 2003, 2008). This process agrees quite well with ground temperature variability in Central Yakutia. Also, climatic conditions changed significantly during the recent two decades (Table 1). This could also serve as the reason for activation of the cryogenic processes.

Our monitoring of the Yukechi site between 1992 and 2010 shows that thermokarst development rates are quite intensive. For example, the average surface subsidence rates in the major observed thermokarst depressions were 5–10 cm per annum (Fig. 1). The maximum subsidence was about

Table 1. Deviations of the main climatic temperature characteristics from the mean value for 1961–2010 at the Yakutsk weather station.

Years	Annual mean air temperature deviation, °C	Freezing index deviation, degree/day	Thawing index deviation, degree/day
1961-1970	-1.1	-303	-106
1971-1980	-0.7	-253	-40
1981-1990	0	-21	-19
1991-2000	0.5	245	37
2001-2010	1.4	330	126

2 m in the absolute value; the water depth increased from 0.4–0.6 to 2–2.5 m. The area of deep, young thermokarst lakes became larger by 2.5 times (Fedorov & Konstantinov 2008). These changes began to influence the landscape structure (Fig. 2). We noted almost the same widening of minor thermokarst lakes in the area of Churapcha Village in Central Yakutia. Kravtsova & Bystrova (2010) noted the same changes in the Vilyuy River basin by means of satellite images.

The role of climatic-hydrological and water-balance processes in thermokarst formation is studied insufficiently in the permafrost zone and in particular for the areas of ice-complex development. This indicates the extreme importance of the study and evaluation of the water balance of growing thermokarst lakes under conditions of current climate changes. It also indicates the importance of the development of effective measures for control, rational use, and protection of water and land resources on this basis.

Data Sources and Methodology

The work was completed on the basis of data generalization from the comprehensive monitoring of cryogenic landscapes for the Yukechi site in Central Yakutia (1992–2008), and from relative estimates. The methods adopted in geocryology, hydrology, hydrogeology, and hydro-melioration were used for the calculations (Chistyakov 1964, Kudryavtsev et al. 1974, Pavlov 1975, Gavriliev & Mandarov 1976, Buslaev 1981, Gavriliev 1991, and others).

We used the following equation for the water balance of the young thermokarst lake to evaluate cryogenic landscape development and transformation trends. The equation takes into account climatic, geocryological, hydrogeological, hydrological, landscape, and other conditions and factors:

$$W_{ik} = (P_{pr} + W_{ic} + S_s + W_{sp} + C) - (E_o + E_{sn}) \quad (1)$$

where W_{ik} is water balance of the growing thermokarst lake; P_{pr} is amount of precipitation; W_{ic} is water from ice complex melting; S_s is surface runoff; W_{sp} is supra-permafrost runoff; C is condensation; E_o is evaporation from the water surface; E_{sn} is moisture evaporation from the snow surface.

The main water supply sources include atmospheric, surface and supra-permafrost runoffs, and permafrost

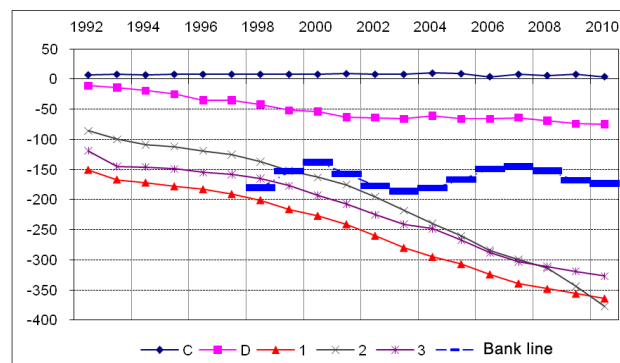


Figure 1. Surface subsidence (vertical axis in cm) dynamics at the Yukechi site, Site 2.

supply. Atmospheric supply was evaluated on the basis of the precipitation amount at the nearest Yakutsk weather station. Surface water runoff was based on methods of Chistyakov (1964) and Buslaev (1981). The runoff coefficient for Central Yakutia on average is 10–20% of the total precipitation volume. The supra-permafrost runoff is represented by an active layer water inflow from the area of the catchment basin. Permafrost is supplied with water through the melting of ice wedges and ground texture ice. The average volumetric ice content of these deposits is 0.5 and 0.2 for the specified ice varieties, respectively (Konstantinov 2000). The values given predetermine the major proportion of permafrost supply for the input part of the water balance of thermokarst water bodies.

According to Shepelev (2011), the value of condensation supply of suprapermafrost water in the pine forest on eolian sands in Central Yakutia is 8–10 mm during the warm period of the year. This is approximately 5–6% of the summer precipitation in the Yakutsk area.

In 2008 the catchment basin area of the thermokarst lake under study was 6775 m², and the lake water surface area was 3135 m² (i.e., the catchment basin area was almost twice as large as compared to the lake's area).

Evaporation from the water surface and evaporation from the snow surface are the main loss components of water balance. The evaporation power values E_o are defined through calculation methods and experimental methods with the use of the GGI-3000 evaporator. At the Melnikov Permafrost Institute stations, evaporation from the water surface is 202–403 mm for May–September in different years, whereas according to the Yakutsk weather station data it was 398–436 mm. According to calculations by the Gavriliev (1976) heat balance method, evaporation from the water surface in Yakutsk was 439 mm. Evaporation from the snow surface was studied in detail by Are (1976). On open sites it can vary from 7.5 to 26% (16% on average) from all snow cover.

Monitoring of bottom dynamics of the thermokarst depression (future lake) and the bank line (shoreline) in the lake was conducted by means of leveling of the entire thermokarst subsidence area with a 2 x 2 m grid and using as control a system of six benchmarks buried in permafrost to 3–4 m. Four benchmarks are represented by metal borehole conductor strings while two benchmarks are wooden. The measurements were completed in September 1992–1993 and 2008 during the maximum ground thawing period. Benchmark elevations remained



Figure 2. Landscape changes at the Yukechi, Site 2.

unchanged during almost 20 years. Monitoring of control points was conducted annually at the end of September in order to follow the subsidence of the bottom surface and lake level. The water surface level and area were surveyed regularly as well. In 1993, the thickness of talik under the thermokarst basin was 3 m, and in 2008 it was 6 m. The volume of water in 1998 and 2003 was calculated taking into account changes in the bank line of the thermokarst lake and the bottom subsidence. The calculation of the water volume and the water balance in the growing young thermokarst lake was completed every 5 years: in 1993, 1998, 2003, and 2008.

We calculated the water balance on the basis of the water volume in the lake. Regular measurements of subsidence, the thermokarst lake bottom surface, and the lake bank line dynamics allowed us to calculate the water volume for a specific period. The SURFER 8 software was used for the analysis of leveling results and the calculation of the required water area and the volume values for the lake (Fig. 3). For example, in 1993 the area of independent water bodies not connected with each other, at the water level -2.0 m, was 195 m^2 , and the water volume in these water bodies was 33.7 m^3 . In 1998, the lake gained a single contour, but independent high-center polygons formed islands in it. The bank line of the lake was at the level of -1.8 m, and the area was 957 m^2 ; the water volume was 340 m^3 . In 2003 the lake was wider

and deeper. The characteristics were as follows: bank line -1.86 m, area 1229 m^2 , and water volume 807 m^3 . By 2008, the lake changed completely after a number of rainy years; the water level grew to -1.52 m, the area increased to 3135 m^2 , and the volume reached 3503 m^3 .

Then the water volumes from precipitation that fell directly on the lake water surface and the water volumes from ground ice melting were calculated. The volume of the water evaporated from the lake was calculated with account of the evaporation value at the Yakutsk weather station. We did not divide the runoff into surface and supra-permafrost, and it was calculated as a remainder of the water balance equation. Moisture condensation as an input element does exist, and we do not have specific data for its calculation. For water balance calculation, we included it into the remainder together with the runoff

Results

Water Volume from Precipitation.

According to the nearest Yakutsk weather station data for 1993–2008, 239 mm of precipitation fell on average per annum, with the maximum value of 326 mm (2006) and the minimum value of 134 mm (2001). The water supply was estimated for the summer (May–September) and the winter (October–April) periods. Between 1994 and 1998, the total water supply increase taking into

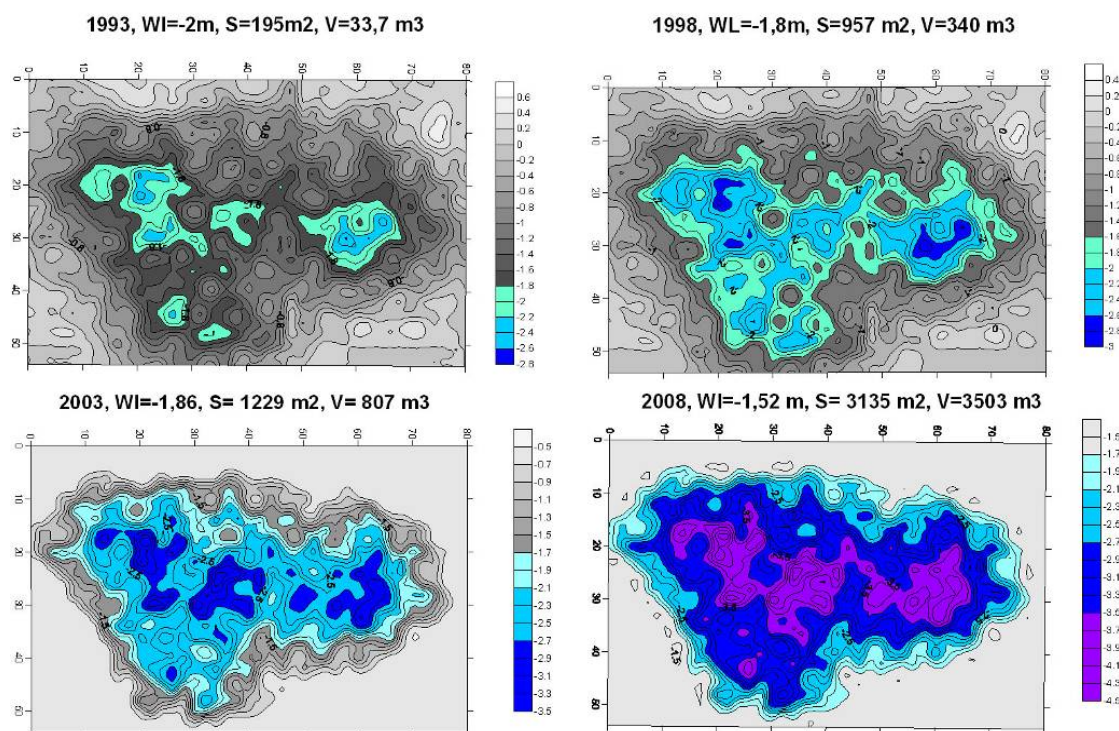


Figure 3. Size and water content changes in the young thermokarst lake at the Yukechi site.

account the change in annual lake area per thermokarst lake was 516.4 m³ in summer and 202.8 m³ in winter (excluding mean evaporation from the snow surface of 16% of winter precipitation). In 1999–2003, the water supply from precipitation was 900.8 m³ in summer and 358.0 m³ in winter, and in 2004–2008 it was 2266 m³ and 940.6 m³, respectively. Water supply changes by five-year periods were not that significant for the catchment basin area which decreased due to the lake area increase as compared to the lake alone.

Water losses from evaporation.

According to the Yakutsk weather station data for 1993–2008, the evaporation power was on average 0.36 m, with the maximum value being 0.39 m (1993) and the minimum value being 0.30 m (2000). Between 1994 and 1998, 1144.0 m³ of water evaporated from the lake that was changing in area; between 1998 and 2003 it was 2274.3 m³; and between 2004 and 2008 it was 4964.4 m³. While the total evaporation volumes during the first five-year periods were commensurable, the evaporation volumes became extremely notable with the significant increase of the total water supply and the lake widening.

Water volume from ice complex melting.

We calculated the water supply from ground ice melting under three different conditions: directly from under the lake, from the shallow-water area, and from the thermokarst depression slopes. Annually, 9.6 m³ (1993) to 440 m³ (2008) arrived directly from under the lake, the area of which varied from 195 m² in 1993 to 3135 m² in 2008. We conventionally assumed that the lake area of the previous year was the lake contour for the calculation of ice melting directly from under the lake. For example,

if the lake area in 1994 was 347 m² on average, we used 195 m² for calculation (the lake area in 1993). And the area difference was referred to the shallow-water zone.

The annual mean lake bottom subsidence according to our monitoring in 1994–1998 was 0.054 m; in 1999–2003 it was 0.136 m; and in 2004–2008 it was 0.176 m. Based on these values, we calculated that the ice complex with volumetric ice content 0.5 melted on average 0.1 m, 0.27 m, and 0.35 m during these years. These data were included in our calculations.

Water supply due to ground ice melting in the shallow-water zone was calculated independently. The subsidence rate in the shallow-water zone was 0.05 m per annum, like in the shallow lake between 1994 and 1998, and the annual ice complex melting was estimated as equal to 0.1 m.

Ground subsidence up to 0.02 m per annum occurs also on relatively steep slopes of the thermokarst depression. This was also taken into account in the water supply calculation due to the ice complex melting. We estimate the annual ice complex melting at these sites as equal to 0.04 m.

Water supply due to ice complex melting between 1994 and 1998 was 369 m³ of water, between 1999 and 2003 it was 903 m³, and between 2004 and 2008 it was 1834 m³ of water.

Water volume supplied by means of surface and supra-permafrost runoff, including condensation.

We did not calculate these data directly due to the known methodological difficulties. However, the available data on the water volume in the lake for specific time periods allowed us to calculate its quantity through the water balance equation. On residual principle, 417.0 m³

Table 2. Structure of water supply formation in the young thermokarst lake at the Yukechi site.

Years	Atmospheric precipitation per lake, m ³	Ground ice melting, m ³	Total runoff, m ³	Evaporation, m ³	Water volume in the lake, m ³
1994/1998	664.0	369.3	417.0	-1144.0	306.3
1999/2003	1272.3	902.8	566.2	-2274.3	467.0
2004/2008	2980.1	1833.8	2646.5	-4964.4	2496.0

Table 3. Structure of the input part of water balance in the young thermokarst lake.

Years	Surface part of water supply, m ³	Atmospheric precipitation per lake, %	Ground ice melting, %	Total runoff, %
1994/1998	1450.3	45.8	25.5	28.8
1999/2003	2741.3	46.4	32.9	20.7
2004/2008	7460.4	39.9	24.6	35.5

fell on the total runoff with condensation in conditions of all known water balance equation values in 1994–1998, 566.2 m³ in 1999–2003, and 2646.5 m³ in 2004–2008.

The catchment basin area was estimated on the basis of the field topographic survey in 2008. Taking into account the widening of the thermokarst lake, the catchment basin area varied from 9256 m² in 1993 to 6316 m² in 2008. In total, between 1994 and 1998 the water volume supplied to the catchment basin was 9689.6 m³, between 1999 and 2003 it was 8337.4 m³, and between 2004 and 2008 it was 8981.9 m³. Only 4.3% of this precipitation reached the lake in 1994–1998, 6.8% in 1999–2003, and 29.5% in 2004–2008. The earlier estimated runoff coefficient in Central Yakutia was 10–20% (Chistyakov 1964, Buslaev 1981). The anomalous runoff between 2004 and 2008 is primarily associated with the precipitation regime and the snow melt regime in spring (the increase of winter precipitation, anomalous autumn precipitation). These played a significant role in flooding of all Central Yakutia lakes in the studied period.

Conclusions

The produced calculations allowed us to evaluate the structure of water supply formation in the young thermokarst lake, the input and the output components, as well as the water balance during the specific time periods (Tables 2 and 3). The input part includes all sources: summer and winter precipitation, ground ice melting, and total runoff, including surface and supra-permafrost runoff together with condensation. There is no inflow of inter- and sub-permafrost waters due to the fact that the thaw basin is closed. The output part consists of water evaporation both in summer and spring. Water runoff from the lake is not included in the output part because this thermokarst lake does not have outflow. The water balance in the thermokarst lake is the input and the output ratio.

Therefore, the role of ground ice melt in the water balance formation in the young thermokarst lake in Central

Yakutia is quite significant and makes up to one-third of the whole input in the balance. This is also confirmed by morphological changes in the lakes. Both extension and deepening of young thermokarst lakes occur in Central Yakutia almost throughout the entire territory. Not really large-scale, but quite notable, permafrost landscape transformation occurs in conditions of modern climate changes with activation of cryogenic processes. During the recent 10–20 years, many open sites at the ice complex, earlier used as cultivated lands and pastures, became “bylars,” the primary form of thermokarst subsidence terrain.

Acknowledgments

This work was prepared in the framework of the RAS SB VI.63.2.3 project and under the auspices of the Institute for Humanity and Nature (RIHN), Kyoto, the Research Institute for Global Change (NHCP/RIGC/JAMSTEC), Yokosuka, and the Hokkaido University, Sapporo, Japan. We thank the employees of the Cryogenic Landscapes Laboratory of the RAS SB Melnikov Permafrost Institute: Drs. I.S. Vasilev, N.P. Bosikov, and A.N. Nikolaev, researchers P.V. Efremov, R.N. Argunov, and A.P. Kondakov for participation in the fieldwork during the many years.

References

- Are, A.L. 1976. Results of six-year snow evaporation monitoring in Central Yakutia. Regional and thermo-physical permafrost studies in Siberia. *Yakutsk* 126-131 (in Russian).
- Bosikov, N.P. 1989. Plough land destruction intensity within inter-alar landscapes. *Geography and natural resources* No.4:83-86 (in Russian).
- Buslaev, I.G. 1981. Heat and moisture provision and hydro-technical amelioration norms in Central Yakutia. *Yakutsk* 90 pp. (in Russian).
- Chistyakov, G.E. 1964. *Water resources of Yakutia rivers*. Moscow: Izd-vo AN SSSR, 256 pp. (in Russian).

- Fedorov, A.N. & Konstantinov, P.Y. 2003. Observations of surface dynamics with thermokarst initiation, Yukechi site, Central Yakutia. *Permafrost: Proceedings of the 8th International Conference on Permafrost* Vol. 1. Zurich, Switzerland, A.A.BALKEMA Publishers, 239-243.
- Fedorov, A.N. & Konstantinov, P.Y. 2008. Recent Changes in Ground Temperature and the Effect on Permafrost Landscapes in Central Yakutia. *Ninth International Conference on Permafrost*. Fairbanks, Institute of Northern Engineering, University of Alaska 1:433-438.
- Fedorov, A.N., Konstantinov, P.Y., Vassiliev, I.S., Bosikov, N.P., Torgovkin, Y.I., & Samsonova, V.V. 1998. Observations of permafrost-landscape dynamics related to anthropogenic disturbances, Yukechi study site, Central Yakutia. *PERMAFROST*. Seventh International Conference Proceedings. Yellowknife, Canada, 259-263.
- Gavrilev, P.P. 1991. Permafrost land amelioration in Yakutia. *Novosibirsk: Nauka, Sib. otdeleniye* 184 pp. (in Russian).
- Gavrilev, P.P. & Mandarov, A.A. 1976. Flood irrigation of meadows in Central Yakutia. *Novosibirsk: Nauka, Sib. otdeleniye*, 165 pp. (in Russian).
- Konstantinov, P.Y. 2000. Cryogeomorphological method for determination of relative ice-rich permafrost thawing settlement. *Kriosfera Zemli* Vol. IV, No. 4: 82-88 (in Russian).
- Kravtsova, V.I. & Bystrova, A.G. 2009. Change of thermokarst lake sizes in different parts of Russia for the recent 30 years. *Kriosfera Zemli* Vol. XIII, No. 2: 16-26 (in Russian).
- Kudryavtsev, V.A., Garagulya, L.S., Kondrateva, K.A., & Melamed, V.G. 1974. *Permafrost forecast bases for engineering-geological studies*. Moscow, Izd-vo MGU, 431 pp. (in Russian).
- Lachenbruch, A. 1962. Mechanics of thermal contraction cracks and ice-wedge polygons in permafrost. *Geol. Soc. Amer. Pap.*, No. 70: 68 pp.
- Pavlov, A.V. 1975. Ground and atmosphere heat exchange in northern and middle latitudes of the USSR territory. *Yakutsk* 302 pp. (in Russian).
- Scientific and applied reference aid on USSR climate. 1989. Series 3. Long-term data. Parts 1-6. Issue 24. Book 1. *Leningrad, Gydrometeoizdat*, 607 pp. (in Russian).
- Shepelev, V.V. 2011. Cryolithozonesuprapermafrost waters. *Novosibirsk, Akad. Izd-vo GEO*, 169 pp. (in Russian).
- Skachkov, U.B. Climatic parameters. Review of the modern climate and natural environment changes in the Republic of Sakha (Yakutia). *Yakutsk* 1-3 (in Russian).

Rock Glaciers and Permafrost Gravitational Formations of the Kolyma Upland

A.A. Galanin

Melnikov Permafrost Institute, SB RAS, Yakutsk, Russia

Abstract

Approximately 1160 formations that are morphologically similar to rock glaciers were identified based on remote mapping and field research in the ridges of Grand Rapids, Tumanskiy, Khasynskiy, and Del-Urenchen as well as in the Dukchinskiy and Kilganskiy Mountains. A map of the rock glaciers of the Kolyma Upland was compiled. Apart from cirque rock glaciers formed as a result of ablation, a large number of slope-associated, lobate-shaped formations were identified. These rock glaciers form in the zones of tectonic badland and in association with the active seismic-generating faults. The integration of the regional data on tephrochronology, lichenometry, pollen spectra, and radiocarbon dates allows us to preliminarily relate most of the active rock glaciers to the Late Holocene.

Keywords: Kolyma Upland; Neoglacial epoch; paleoseismic-dislocations; rock glaciers; landslides.

Introduction

Rock glaciers have been observed in many mountain structures of America, Europe, and Asia (Barch 1996, Gorbunov 2008 a,b,c). A considerable number of them (more than 6,000) were recently detected in the territory of northeastern Asia (Galanin 2009 a,b). At the same time, the rock glaciers of many mountain structures in this region remain poorly investigated. This is linked with the fact that large representative sites are remote and difficult to reach, the bodies of rock glaciers are difficult to excavate, and their age and flow rates are problematic to distinguish.

The investigation and mapping of the formation of rock glaciers are areas of considerable interest both fundamentally (Barch 1996) and practically (e.g., in the design of linear structures in mountain areas). Some rock glaciers of the Chukotsk Peninsula provide a source of high-quality construction gravel and are actively mined at present.

The primary target of this paper is to provide general characteristics of the geography and morphology of the rock glaciers of the Kolyma Upland, which still remain the least described in the literature. This paper is based on field studies at key sites and results of the areal interpretation of air and satellite photographs. The ages of the rock glaciers were estimated on the basis of methods tested earlier (Galanin 2009a, Galanin & Pakhomov 2010).

Rock glaciers began to form in the territory of the Kolyma Upland and adjacent areas relatively recently. A detailed review of their research history was reported separately (Galanin 2008). The fact that rock glaciers occur in North Priokhotie was mentioned by Titov (1976). He characterizes them as a form of colluvium, relatively rare and poorly studied in this region.

Rock glaciers were discovered in the North Priokhotie (in the territory of Khabarovskiy Region) by Bogachev et al. (1994), who distinguished several morphological types. The sizes of the identified formations range from several hundreds of square meters to 1.5 km², while their thickness varies from 5 to 30 m, occasionally up to 40 m. The front slopes have a steep gradient of up to 40°. The surfaces of rock glaciers are uneven with sinuous furrows, conical depressions, and ramparts from 0.5 to 10 m. The researchers

conclude that rock glaciers are widespread polygenetic phenomena that are closely interconnected with cryogenic slope structures and depend on the climatic and geological conditions of the territory.

The research history of the rock glaciers of the Kolyma Upland reached its most dramatic point in the 1990s, when tens and hundreds of these formations were remotely identified as seismic-induced landslides (paleoseismic-dislocations) and their “swarms” (Vazhenin 2000). This resulted in some speculative seismic forecasts and geodynamic constructions. This fact served as a reason for special research into the formation of rock glaciers in northeastern Asia that lasted for more than 10 years (Galanin 2009 a,b). One of its results was proof that the previous paleoseismic-geologic investigations were incorrect (Smirnov et al. 2001).

Meanwhile, some regions of northeastern Asia and the Kolyma Upland are actually located within the seismic belt of the Cherskiy, Koryaksko-Kamchatskiy, and Chukotskiy seismic zones. For instance, in some regions there were identified sporadic ground-ice formations of large size that exhibit strong morphological evidence of the recent seismo-tectonic deformations, including surface ruptures, detachments from the bed, and rock disintegration. They are often associated with large faults and seismic dislocations. We classified such morphologically abnormal rock glaciers as fault-associated rock glaciers. The most representative rock glaciers of this type were detected in North Priokhotie on the Koni Peninsula and on the Chukotsk Peninsula in the vicinity of the village of Providenie city (Galanin 2009a). At the same time, analysis of all the detected glacier-like formations (approximately 6,000) of northeast Asia (Galanin 2009b) did not indicate that they are spatially associated with the seismic lineaments of the current seismic zoning map (General Seismic Zoning – 97). For this reason, further research is required into the genesis of fault-associated and deformed ice-ground bodies that are morphologically similar to rock glaciers.

Rock Glacier Map of the Kolyma Upland

The method employed in the mapping of rock glaciers was described earlier (Galanin 2009b). The interpretation

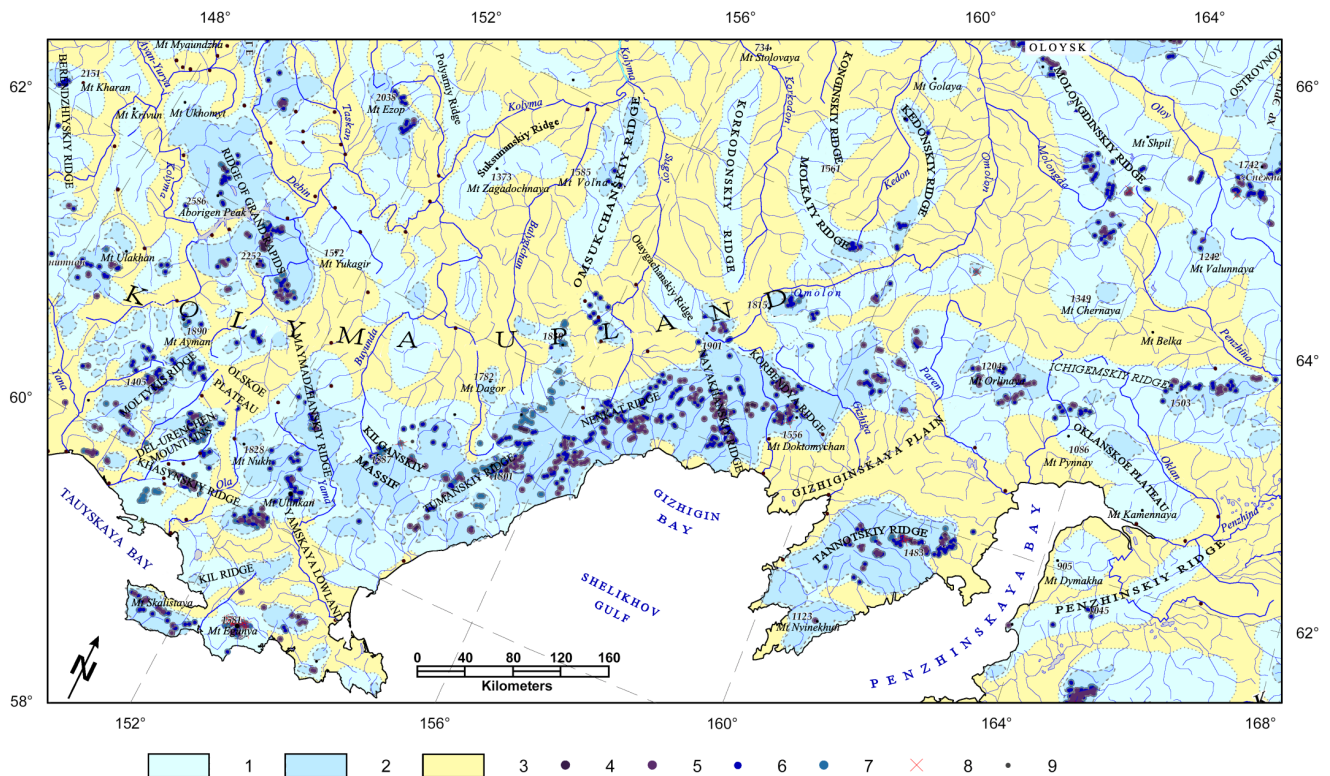


Figure 1. Rock glaciers of Kolyma Upland: 1 – areas of the first Late Pleistocene glaciation (Yermakovsko-Zyryan), 2 – areas of second Late Pleistocene glaciation (Early-Karginsky-Sartansky) 3 – areas not covered by late Pleistocene glaciations, 4–7 – rock glaciers and their paragenetic landforms: 4 – complex cirque-associated, 5 – simple cirque-associated, including inactive, 6 – lobate-shaped slope-associated; 7 – inactive, 8 – large seismic dislocations (disturbances) in association with abnormal and deformed rock glaciers, 9 – settlements.

of satellite photographs with resolution from 6 to 15 m made it possible to detect about 1160 sites on the territory of the Kolyma Upland that are morphologically similar to rock glaciers or develop in close association with them. Among them, about 550 formations were classified as slope-associated lobate-shaped type; 279 tongue-shaped and 24 complex rock glaciers were discovered within glacial cirques; 115 large snow and firn basins were identified; 82 rock glaciers were classified as inactive.

The mean density of rock glacier distribution makes up about 10 to 17 glaciers per 1000 km² and reaches its maximum values within the Okhotsk-Kolyma divide. Most of the investigated sites are associated with the upper parts of late glacial complexes of the Pleistocene-Holocene age. Complex rock glaciers (formations that are in transition to glaciers) occur rather rarely at the head of late glacial complexes as glacier forms and are found mainly in the axial parts of the Tumanskiy, Korbendya, and Tenianny Ridges (Fig. 1). Slope-associated rock glaciers including those associated with large faults and with the zones of tectonic badland occur most often.

The Ridge of Grand Rapids and the Bokhapchinskie Mountains

The massif of the Bolshoy Mandychan Mountain (2200 m a.s.l.) constitutes a part of the Grand Rapids Ridge and is associated with the mountain massif of the same name that adjoins the Bokhapchinskie Mountains. Sharply dissected alpine type of relief of stages 2–3 is widespread here with the maximum elevations ranging from 2000 to 2200 m a.s.l. and the relative heights reaching 1400 m. The largest late glacial

complex is found at the northern slope of the Mandychansky Massif. It extends over 12.5 km and belongs to the basin of Lake Gagar and the Maly Mandychan River (Fig. 2). The geomorphological map and description of the investigated area are published (Galanin & Pakhomov 2010).

The entire glacial complex is composed of large boulders and blocks of granite-porphyrines that form the core of the granitoid batholith of the Late Jura-Early Cretaceous age. Eight to ten stadial moraines that are separated from each other by lake basins, rock bars, or flat icing surfaces are distinguished. The latest generations of rock glaciers comprise active and inactive rock glaciers of different size and morphology that were identified at the head of Levada Creek (Figs. 2, 3).

The large cirque-valley rock glacier is associated with the left cirque of the multi-chambered cirque at the head of Levada Creek. Its length is about 2600 m and it developed from a cirque moraine. The abnormally deformed surface with ruptures in its continuity indicates that the frontal part (observation points 59, 60) underwent a rapid and catastrophic dislocation over the distance of approximately 1 km.

An inactive slope-associated rock glacier is found on the right side of Levada Creek at the height of 1070.3 m (observation point 56). It belongs to the polylobate type and is superimposed on the earlier stadial moraine rampart. It has a length of about 200 to 250 m and width of 1 km. The surface is composed of large granite blocks and has partly inverted mound-and-pit microrelief with ridges and lobes directed toward the valley thalweg. The gradient of the front slope is about 30°. The depressions have a discontinuous vegetation cover with dwarf pine and birch.

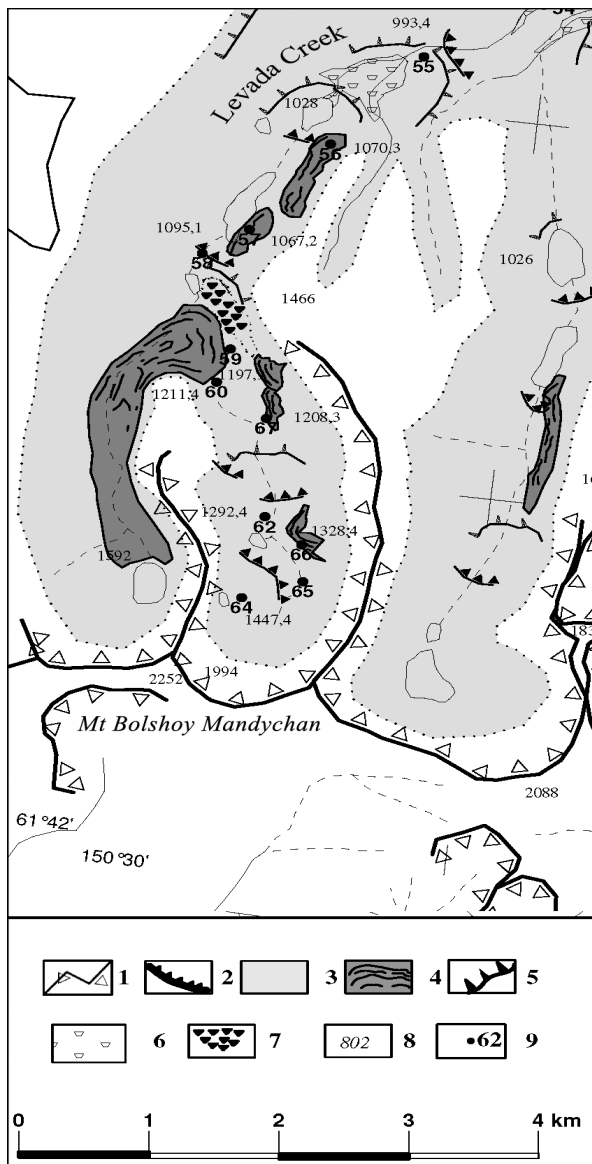


Figure 2. Rock glaciers in the head of the Mandychansky late glacial complex (Ridge of Grand Rapids): 1 – edges of glacial cirques, 2 – crossbars and rocky benches of the thalweg, 3 – the maximum limits of the Last Glaciation (Late Wisconsinian), 4 – rock glaciers, 5 – moraine edges, 6 – glacio-fluvial sediments, 7 – large block landslide of the cirque wall, 8 – elevation points, m a.s.l., 9 – sites of lichenometry and Schmidt Hammer Test data.

The age of the inactive rock glaciers in the basin of Levada Creek corresponds to the Early Holocene, while the age of the contemporary active generations is not more than 2000 to 2500 years BP (Galanin & Pakhomov 2010).

The Del-Urenchen Mountains

Another late glacial complex was studied at the area of Cycyn Creek (tributary of the Khasyn River), whose 6-km-long, sub-latitudinal valley is oriented along the fault and forms a system of multi-chambered cirques in the upper reaches of Cycyn Creek (Fig. 4).

Fragments of the numerous marginal channels indicate that the degradation of the last glaciation in this area underwent four stages and continued in the Holocene. A lateral moraine with buried ice remnants was formed at the left side of the creek at the end of deglaciation. A thick slope-associated

rock glacier of the polylobate type developed here in the Late Holocene.

This rock glacier called Karamkenskii is located 2.5 km northeast of the village of Karamken. The length of some of its lobes ranges from 100 to 150 m, while the general width is approximately 2 km. The surface is tilted toward the creek thalweg at an angle of about 10°. The front slope height ranges from 40 to 60 m, while its gradient is 35 to 40°.

Morphologically, the rock glacier is a narrow slope-associated surface that resembles a terrace and has a constantly renewing steep front slope. The surface has no soil and vegetative cover and is composed of large rock debris and gabbro-diorite boulders or, less often, of hornstones coming from the adjacent bedrock slope with the gradient of 45 to 50°. The surface is permanently located in the shade, which favors a large snow bank remaining at the base of the slope throughout the summer.

The microrelief is formed by hillocks and ridges with elevations from 3 to 8 m directed across the flow of the rock glacier. The largest blocks of rocks with a diameter up to 3.5–4 m are associated with the hillock tops. The vegetation covers less than 5% of the rock glacier surface.

The hillocks separated by oval and diamond-shaped basins with a depth of 2 to 2.5 m form a group of five curved ramparts positioned over one another.

According to the tephrochronologic data, the age of the rock glacier surface is 2700 years BP (Galanin et al. 2005). Lichenometry dating allowed us to estimate that the dynamic (minimum) age of this formation is up to 2000±400 years BP (Galanin & Glushkova 2006).

The 50-km-long sub-latitudinal *Khasynskiy Ridge* extends at a distance of 60 to 70 km from the coastline of the Okhotsk Sea. The maximum peak height reaches 1400 m a.s.l. The youngest glacial landforms and sediments are located in the axial part of the ridge. At the heads of the valleys, the complex multi-chambered cirques have steep and abrupt back walls.

The typologic late glacial complex was investigated in the basins of Shater and Bessi Creeks. Its geomorphological map and description have been reported (Galanin et al. 2005). Two small drop-shaped inactive rock glaciers composed of large blocks and rock debris were detected at the right side of the Bessi Creek valley at the height of about 600 m a.s.l. Their marginal slopes have a gradient of 25–30°. The surfaces of the rock glaciers are tilted slightly toward the thalweg and are covered with clumps of Siberian dwarf pine.

A 10-cm-thick horizon of volcanic ash dated about 2700 years BP was discovered at 10–15 cm depth in the sediments of the drained glacial lake at the head of the same valley. The lake probably existed for a short period of time adjacent to the front part of the tongue-shaped rock glacier that is currently in the inactive state. Its flattened surface is built of coarse-grained sediments and is completely devoid of soil and vegetation. The rock glacier length is approximately 400 m. No volcanic ash was found, which allows us to estimate the lower limit of its age. We link the rock glacier formation to the Neoglacial cooling of 2000 to 2500 years BP. The spore and pollen spectra revealed in the lake sediments confirm this supposition (Galanin et al. 2005).

Three zones were detected in the pollen diagram. Zone 1 (55–31 cm) has a high content of *Alnus* (up to 60%), *Betula*



Figure 3. Morphological features of the lobate slope-associated rock glacier at the head of Levada Creek (site 57, see Fig. 2): *a* – pitted surface of the active lobe, *b* – the thawing lobe at the cirque lake.

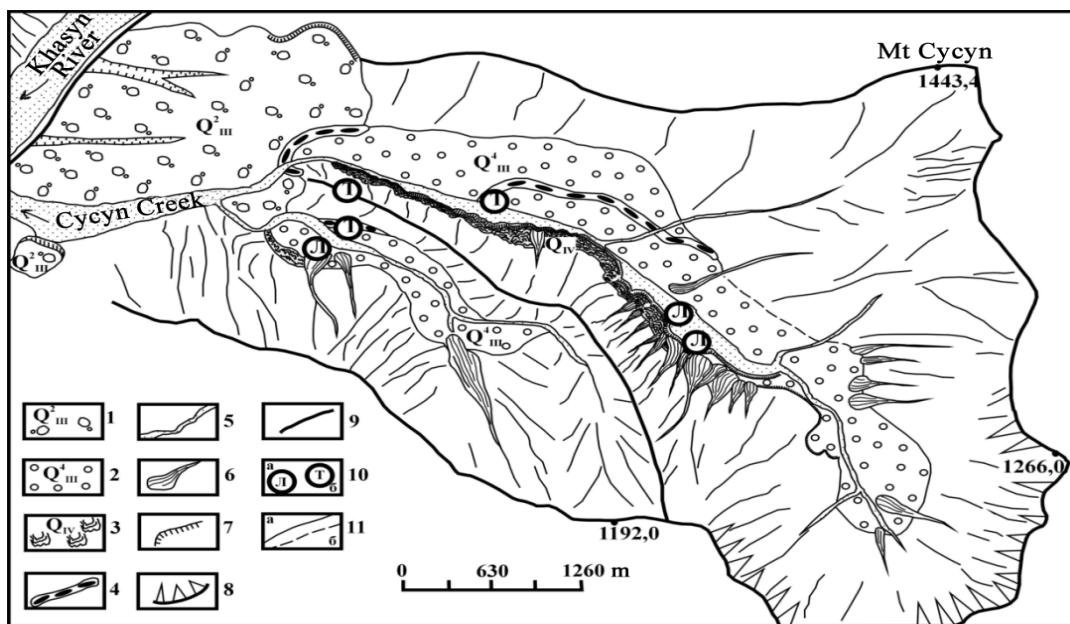


Figure 4. Geomorphological scheme of Karamkenskij rock glacier at the head of Cycyn Creek (Del-Urechen Ridge): 1 – Late Pleistocene moraine of the first stage (Early Wisconsinian); 2 – Late Pleistocene moraine of the second stage (Late Wisconsinian); 3 – slope-associated lobate-rock glaciers of the Holocene age; 4 – moraine crests; 5 – modern channel and floodplain; 6 – avalanche-debris flows; 7 – bluffs of the erosional channels; 8 – edges of cirques with bedrock outcrops; 9 – Cycyn Creek catchment area; 10 – sites of lichenometry dating (a) and tephrochronology locations on the surface and in soil sections (b); 11 – geomorphological boundaries: a – observed; b – supposed.

(shrub species, up to 12%), *Pinus Haploxyylon* (up to 15%), and a rich variety of herbs. It is related to the end of the Boreal and to the beginning of the Atlantic period according to the Blytt-Sernander classification.

Zone 2 (31–4 cm) corresponds to the coldest interval of the entire spectrum. This zone undergoes a decrease in the pollen of *Alnus* (down to 10%) and *Pinus Haploxyylon* (down to 2–10%). The correlation of the *Betula* sp. pollen is fluctuating between 5 and 20%, while the *Poaceae* content rapidly increases (up to 70%). *Botrychinaceae* predominates in the spore group (up to 250%).

The spectra of zone 3 (4–0 cm) are in good agreement with the contemporary type of vegetation cover of *Pinus Haploxyylon* (up to 40%), *Alnus* (up to 35%) and *Betula* (up to 8%). The pollen of *Cyperaceae*, *Artemisia*, *Ericales*, and

Brassicaceae except for *Poaceae* (up to 15%) is presented in small quantities. *Polypodiaceae* (up to 180%), *Spagnum* (up to 10%), and *Botrychinaceae* (up to 3%) constitute the spore content. The currently inactive rock glacier most probably formed within the interval of the second pollen zone at the end of the Atlantic period of the Late Holocene 2000 to 2500 years BP, which agrees well with the age of the indicator ash horizon.

The Tumanskiy Ridge

Five formations were detected by Sedov (1995) at the upper reaches of the Nyarka, Dyuken, Kalalaga, and Kananyga rivers in the mountains of the western coast of the Gizhinskaya Bay (the Tumanskiy Ridge). The author interpreted them as glaciers and named them Nyarka,



a



b

Figure 5. a – the frozen seismo-tectonic badland (area of the bedrock crushing) consisting of hastate debris of Triassic carbonaceous shales and sandstones at the head of Bezmyanniy (No-named) Creek (Kilganskiy Massif, 61°0.34'N, 153°50.23'E); b – the lens of congelation ice in the fractured bedrocks on the top of Juliet Hill cut by prospecting trench.

Dyukon, Okhotskiy, Sommitelny, and Koltsevoy. The length of the detected formations varies from 0.3 to 1.2 km, while their area ranges from 0.2 to 0.47 km². They are all found at the bottoms of glacial cirques of northern and northwestern aspect. The elevation of the firm lines fluctuates between 690 and 1500 m a.s.l., while the ablation area at three glaciers during the observations was covered with seasonal snow bank 30 to 50 cm thick. Under this snow cover, a 30-cm-thick layer of new ice was identified. The firm basin consists of a number of avalanche fans rising 3 to 5 m above the surface of the snow and firm fields. According to the given descriptions, the formations investigated by the author correspond more to complex rock glaciers of an ablation type with mixed nival and congelation alimentation.

The Kilganskiy Mountain Massif

Several abnormal (fault-associated rock glaciers) as well as several other ice and rock formations were studied within the Kilganskiy Mountain Massif in the western part of the Tumanskiy Ridge. The massive reticulated glaciation developed here in the Late Pleistocene, widely distributed through valleys and glacial facets and absent classic glacial cirques (Fig. 1).

Nearby the Julietta mine and at the head of the Kilgana River in the area of rugged medium mountains a great variety of frozen ice and rock formations and rock glaciers of slope-associated types were identified. Most often they are adjacent to either ruptures or glacial facets.

A specific row of forms that develop under dynamic seismo-tectonic activity, syngenetic freezing, and ice formation may be detected. These are tectonic wedges and outliers, seismo-tectonic badland (Fig. 5), and fault-associated rock glaciers. In paragenesis with these features, taluses, desorption, underwashing, snow, water and rock mudflows, and icings dynamically form within the same periglacial (permafrost) landscape.

The fault-associated rock glacier in the basin of Krasniy Creek is composed of small angular rock debris of Triassic sandstones and siltstones and belongs to the polylobate type. The thickness of the lobes in the frontal part makes up 10 to 15 m. Each lobe is sustained by a separate talus. The steep crumbling front slope transforms into a sub-horizontal area

40 to 50 m wide and 25 to 30 m long. Its back part is covered with a talus fan. The total width of the joined lobes of the rock glacier is approximately 300 m.

Conclusions

The research performed in the Kolyma Uplands detected a considerable number of rock glaciers of several morphogenetic types. It also revealed transitional formations of a mixed genesis with an unclear classification status. The resulting map of the rock glaciers of the Kolyma Uplands and the investigation of key typological sites make it possible to determine some specific features of the morphology, age, and geography of these formations in the study region.

Rock glaciers and transitional formations similar to these are widespread in water divide areas of mountain structures mainly within the range of a 200-km-long strip extending along the coast of the Okhotsk Sea and exposed to the active influence of Pacific monsoons. Most of the rock glaciers inherit the areas and the relic elements of the Late Pleistocene glacial relief and stratigraphically overlay the late-glacial complexes. This makes it possible to consider some rock glaciers as the final (Holocene) stage of deglaciation.

Another distinguished genetic type of rock glaciers (permafrost type) is linked with syngenetic freezing of thick sequences forming at the base of slopes by accumulation of coarse-grained sediments saturated with interstitial ice.

The available direct and indirect data on the age of rock glaciers indicate that the formation processes of cirque-associated and slope-associated rock glaciers were activated at the end of the Atlantic period.

Some of the currently active slope-associated rock glaciers are connected with synlithogenic (contemporary) freezing of the disintegrated coarse-grained sediments in the zones of active fault disintegration, and therefore they may give indirect information on the Holocene seismo-tectonic activity in the region. The structure and genesis of such formations are yet to be studied in more detail.

Acknowledgments

The investigation was carried out with the support of the Russian Foundation of Basic Research, project No. 11-05-0046-a.

References

- Barsch, D. 1996. *Rockglaciers: Indicators for the Present and Former Geoecology in High Mountain Environments*. Berlin, 331 pp.
- Bogachev, S.S., Shmatkov, V.A., & Kozlov, A.A. 1994. The rock glaciers of northern Khabarovskiy region. *Geografiya i prirodnye resursy* 2: 182-184 (in Russian).
- Galanin, A.A. & Glushkova, O.Yu. 2006. Glaciations, climate and vegetation of the Tauyskaya Bay region (North Priokhotie) in the Late Quaternary. *Geomorfologiya* 2: 50-61 (in Russian).
- Galanin, A.A. & Pakhomov, A.Yu. 2010. The experience in the application of the "Oniks 2.6.2." sclerometer to date the Mandychanskiy late glacial complex (the Cherskiy Ridge). *Geomorfologiya* 1: 16-25 (in Russian).
- Galanin, A.A. 2008. Rock glaciers: research history and contemporary notions. *Vestnik SVNTS DVO RAN* 3: 17-28 (in Russian).
- Galanin, A.A. 2009b. The rock glaciers of the north-east of Asia: mapping and geographical analysis. *Kriosfera Zemli* 4: 75-83 (in Russian).
- Galanin, A.A. 2009a. *The rock glaciers of the northeast of Russia: structure, genesis, age and geographical analysis*. Dissertation abstract of the Doctor of Sciences (geography). Magadan: SVKNII DVO RAN, 43 pp. (in Russian).
- Galanin, A.A., Glushkova, O.Yu., Smirnov, V.N., Pakhomov, A.Yu., Solomatkina, T.B., & Matrosova, T.V. 2005. The Neoglacial morpholithogenesis in the mountains of North Priokhotie. *Stranitsy chetvertichnoy istorii severo-vostochnoy Azii* Magadan: SVKNII DVO RAN, 40-61 (in Russian).
- Gorbunov, A.P. 2008a. The rock glaciers of the World: general review (report 1). *Kriosfera Zemli* 2: 65-74 (in Russian).
- Gorbunov, A.P. 2008b. The rock glaciers of the World: general review (report 2). *Kriosfera Zemli* 3: 58-68 (in Russian).
- Gorbunov, A.P. 2008c. The rock glaciers of the World: general review (report 3). *Kriosfera Zemli* 4: 14-23 (in Russian).
- Sedov, R.V. 1995. The glaciers and snow patch basins of the Okhotsk coast. *Materials of glaciological studies* 79. 139-144 (in Russian).
- Smirnov, V.N., Galanin, A.A., Glushkova, O.Yu. & Pakhomov, A.Yu. 2001. Pseudoseismodislocations in the mountains of Primagadanie. *Geomorfologiya* 2: 81-92 (in Russian).
- Titov, E.E. 1976. The main characteristics of the contemporary colluvial morphogenesis in the mountains of the North-East of the USSR. *Geomorfologiya* 2: 11-25 (in Russian).
- Vazhenin, B.P. 2000. *The principles, methods and results of the paleoseismogeologic investigations in the north-east of Russia*. Magadan: SVKNII DVO RAN, 206 pp. (in Russian).

The Method of a Short Cylindrical Probe in Thermophysical Studies of the Bases of Dams Belonging to Northern Hydroelectric Complexes

R.I. Gavrilov

Melnikov Permafrost Institute, SB RAS, Yakutsk, Russia

Abstract

Construction of northern dams usually involves the upper rock horizons in the zone of weathering and destruction. When conducting thermophysical studies of dam bases in this zone, probe methods are the only ones that can be employed. Among them, the method of a short cylindrical probe may be singled out due to the fact that it is practically convenient to insert such a probe into the mass of frozen ground and rocks under study. Utilizing this method, we investigated the coefficient of thermal conductivity of the rock mass at the dam bases of the Vilyuy Hydroelectric Complex-III (HEC-III) (carbonate rocks) and the Telmamskiy Hydroelectric Complex (HEC) at the Mamakan River (granite). This paper gives a brief description of the probe and reports the results of the research into the thermophysical properties of rocks in their natural conditions at the specified points.

Keywords: dam bases; rocks; short cylindrical probe; thermophysical properties.

Introduction

Dam construction in the northeastern regions of Russia is complicated by permafrost. All permafrost properties, including strength properties, depend greatly on temperature conditions. Therefore, when designing a dam located on permafrost, it is necessary to make thermal estimates that predict the interaction between the dam's structure and the surrounding rock mass. Such estimates require knowledge of the thermophysical characteristics of rocks in their natural setting.

The areas where northern dams are constructed are usually characterized by a complex geological structure, as they encompass the upper horizons of the weathering zone including the zones of fractured rock. The rock mass in the fractured zone is represented by an accumulation of small and large fragments, plates, and blocks of parent rocks filled with unequal content of ice and of fine-grained soils. The orientation of fragments and plates is different, ranging from horizontal to vertical.

The fractured and weathered zones are sometimes impossible to sample for laboratory determination of thermophysical properties. The only acceptable research method in this case is to measure thermophysical properties of the rock mass directly in mines and adits using a probe.

The probe method that has become the most widespread among the numerous ones discussed in the literature is the method of a cylindrical probe that has an infinite length ("probe-needle") and constant heating power. This probe is represented by a metal rod that contains a heater and a thermocouple temperature sensor. Theoretically, it reflects a linear heat source in an infinite body, and therefore it must be infinitely long. Practically, this condition is satisfied when the probe length exceeds its diameter by more than 30 times (Blackwell 1954). Even with such a ratio between the probe's dimensions, its insertion into the mass of frozen ground and rock encounters considerable technical difficulties, as it is practically impossible to make deep holes with ordinary drill bits in such hard materials. Generally, "probe-needles" are mainly applied to thawed ground. In this case,

they are simply stuck into the wall of a test pit without exerting much pressure on them.

Considering what was stated above, we suggest the method of a short cylindrical probe (Gavrilov 1984) to make field measurements of thermophysical properties of frozen ground and rock mass. Such a probe has a low ratio of length to diameter equaling five instead of thirty in the case of the "probe-needle." This renders it possible to use standard drill bits with carbide and diamond tips to drill holes in the rock mass for inserting a probe. Thus the method of a short cylindrical probe was developed as a practical need in order to make mass thermophysical measurements in geotechnical site investigations prior to the construction of large facilities on permafrost. Based on this method, over different periods of time, we carried out field measurements of thermophysical properties of rocks in the adits of the dam bases of the Vilyuy HEC-III (1979-1981) and of the Telmamskiy HEC at the Mamakan River (1985) (Fig. 1).

The experiments were performed in the mass of carbonate rocks at the Vilyuy HEC-III and in the granite mass at the Telmamskoe reservoir. Despite the extreme strength of the indicated rocks, the applied probes showed themselves to be the best advantage. They proved rather reliable in the ac-

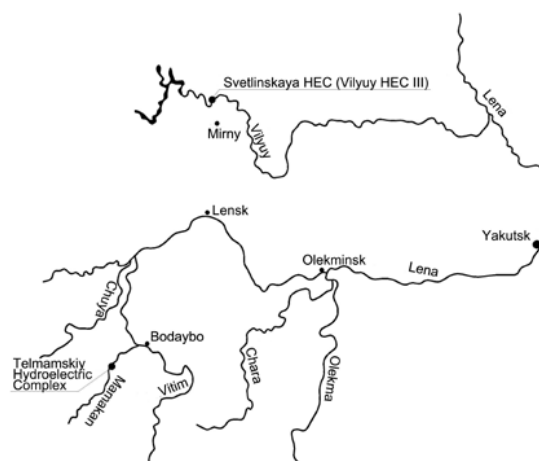


Figure 1. Map of sites under study.

curacy of measurements, simplicity of structure, and resistance to mechanical exposure. The present paper reports the results obtained in the research to illustrate the method of a short cylindrical probe under complicated geocryological conditions of investigations into the bases of northern dams. It should be noted that the early literature presented little information on permafrost and short probes. That is why the author thinks it necessary to briefly describe its main characteristics, focusing mainly on an explanation of the measurement method.

The Method of a Short Cylindrical Probe

If a short cylindrical heat source (a probe) of constant heating power Q is inserted into the wall of a semi-closed environment ($z>0$) with an insulated surface, then the excess temperature of the source (the probe) at the beginning of the coordinates ($r=0, z=0$) at the wall of the investigated object is described by the formula (Gavrilev 1984):

$$\mathcal{G}_\tau = \left(q_l / \pi R^2 \lambda \right) \int_0^R dz \int_0^R \left(r / \sqrt{r^2 + z^2} \right) \operatorname{erfc} \left(\sqrt{r^2 + z^2} / 2\sqrt{a\tau} \right) dz, \quad (1)$$

where $\mathcal{G}_\tau = t_\tau - t_c$ is the excess temperature of the heat source; t_τ is the temperature of the heat source at ($r=0, z=0$) at any point of time τ ; $q_l = Q/l$ is the heating power of the heat source per unit of its length l ; R is the probe radius; $r-z$ are the current spatial coordinates; λ and a are the coefficients of thermal conductivity and thermal diffusivity of the rock mass; $\operatorname{erfc} = 1 - \operatorname{erf}$; erf is the Gauss error function.

With higher time values when $\tau \geq (R^2 + l^2)/a$, formula (1) amounts with a sufficient degree of accuracy to the following asymptotic expression:

$$\mathcal{G}_\tau = \left(q_l / 2\pi\lambda \right) \left(A - l / \sqrt{\pi a \tau} \right), \quad (2)$$

where $A = l/R \left(\sqrt{1 + l^2/R^2} - l/R \right) + \ln \left(l/R + \sqrt{1 + l^2/R^2} \right)$ is the probe's constant.

Formula (2) is valid for any ratio l/R . However, we assume $R/l \leq 0,1$ in order to approximately estimate the series convergence of time when its subsequent components become extremely small. Then, with $\tau \geq l^2/a$, the difference between Formulas (1) and (2) does not exceed 2%.

Formula (2) suggests that if the observation data of the experiment \mathcal{G}_τ or Δn_τ are depicted as a graph of \mathcal{G}_τ (or Δn) against the parameter $1/\sqrt{\tau}$, we will have an asymptotic straight line (Fig. 2).

The points of the intersection of this straight line with the axes of ordinate and abscissa will respectively give \mathcal{G}_{cm} or Δn and $1/\sqrt{\tau_1}$ which may be used in the estimate of thermophysical properties. Based on the stationary increase of the probe temperature \mathcal{G}_{cm} , the coefficient of thermal conductivity is estimated:

$$\lambda = q_l A / 2\pi \mathcal{G}_{cm} \quad (3)$$

The coefficient of thermal diffusivity is determined according to the value $1/\sqrt{\tau_1}$

$$a = \left(l^2 / \pi A^2 \right) \left(1 / \sqrt{\tau_1} \right)^2 \quad (4)$$

The probe (Fig. 3) consists of a metal tube body (1) that

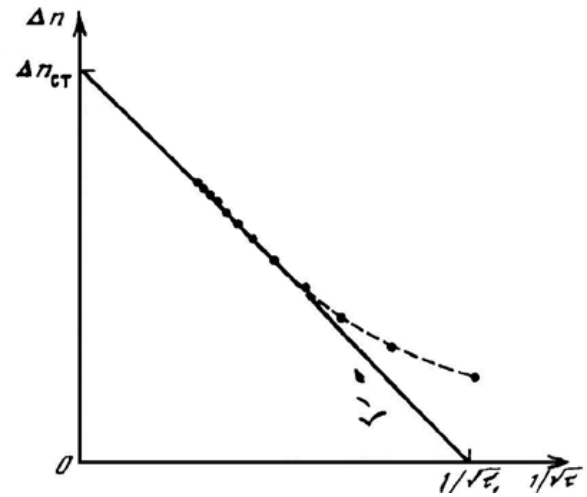


Figure 2. The graph of the galvanometer readings Δn (divisions) against the parameter $1/\sqrt{\tau} (\text{h}^{-1/2})$.

has an embedded electric heater (2). The “hot” thermocouple junction (3) is soldered to the center of the probe body at the base of its insulating handle (7), while the “cold” junction (4) is outside the probe. One end of the body is plugged, while the other is attached to cylindrical handle (7) made of material with a low coefficient of thermal conductivity (e.g., ebonite). The handle is equipped with a flexible attachment (6) of foam rubber that insulates the zone with the diameter of about 15–20 probe diameters from heat at the mass surface. Hole (8), which is inside the handle and through which the wires are pulled from the electric heater and from the thermocouple, is filled with waterproof substance (e.g., paraffin), while the hollow of body (1) is filled with substance of high thermal conductivity (e.g., fusible Wood’s metal). The probe size is determined based on the ratio: $l \geq 10R$, specifically $R=0,3$ and $l=3$ cm.

The thermocouple circuit is connected to a galvanometer (12). Heater (2) is included in the circuit with source of current (11), the rheostat (9), and switch (10).

Before making measurements, the probe is inserted into the examined mass (5) through a hole drilled in advance, while the “cold” thermocouple junction is positioned in the environment at a distance that excludes the thermal effect of the probe during the experiment (30–40 cm). To reduce the thermal resistance at the contact surface between the probe and the mass, the cavity is preliminarily filled with lubricant made of mud or technical petroleum jelly. The insertion of the probe presses the excess lubricant out of the cavity ensuring a good contact between the probe and the mass. It should be noted that the ratio of the probe dimensions indicated above makes it possible to utilize standard drill bits for drilling holes in the mass of frozen ground and rocks.

The thermophysical characteristics of the examined material are determined with the help of the suggested probe in the following way. After the insertion of the probe into the mass, researchers wait 20–30 minutes for the temperature field of the system to stabilize. At the same time, the stopwatch and the current of the probe heater are switched on. The direct current in the circuit of the probe heater is maintained with the help of a rheostat (9) during the experiment. After 30–40 minutes, the readings of the galvanometer n are measured over time intervals.

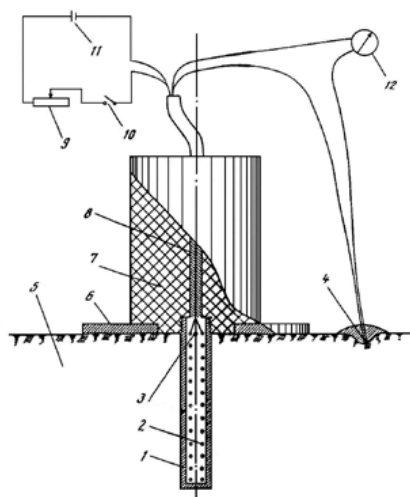


Figure 3. The structure of a short cylindrical probe.

Based on the acquired data, we construct a graph of Δn against the parameter value $1/\sqrt{\tau}$ (see Fig. 2). The value Δn is defined at the intersection of the straight line (obtained by drawing the asymptote of the experimental line) with the ordinate axis, while the value $1/\sqrt{\tau_1}$ is determined at the intersection of this straight line with the absciss axis.

According to formulas (3) and (4), the coefficients of thermal conductivity and thermal diffusivity are estimated. Formula (3) may be presented in the following way:

$$\lambda = BI^2 / \Delta n_{cm} \quad (5)$$

The error of the determination of thermophysical characteristics is estimated to be within $\pm 7\%$.

Results for the Coefficient of Thermal Conductivity of the Rock at Dam Bases

The Telmamskiy Hydroelectric Complex, Mamakan River

The bedrock in the area where the Telmamskiy HEC is constructed is mainly represented by granites and veins (pegmatites) that occupy up to 5% of the general rock volume. The thermal conductivity coefficient of the bedrock was measured both in the field (directly in the rock mass of the adit 1 by probing methods and in the laboratory in the drill cores obtained from boreholes 65, 81, and 110).

Adit 1 is located at the right bank of the Mamakan River at the absolute elevation of 319 m according to the III–III section representing the axis of the dam. The adit is buried into the bedrock mass down to 30 m and occupies a weathered layer (about 10 m from the river mouth). The rocks are in the frozen state. The mean temperature of the adit was approximately 2°C below zero during the research.

The field measurements of thermal conductivity coefficient of the granite mass in Adit 1 were made with the short cylindrical probes at 10 points. The holes for probes were drilled in the rock mass by the drill bits with diamond tips. We had only 4 drill bits that soon became worn in the granite mass, but we managed to take approximately 60 measurements in the granite mass and pegmatite veins during the field season. The probes were 6 mm in diameter and 30 mm in length, which corresponds to the sizes of the diamond

Table 1. The averaged values of the thermal conductivity coefficient of the rock mass in Adit 1 located in the dam base of the Telmamskiy HEC, Mamakan River.

Point No.	Height, m	The distance from the river estuary, m	$\lambda, \text{W}/(\text{m}^*\text{K})$	Rock description
1	1.0	5.8 (l)	2.91	Fine-grained, gray, biotite, massive, hard and fissured granite (description A)
2	1.0	4.8 (r)	3.00	Medium-grained, light gray, biotite, massive, very hard and slightly fissured granite (description B)
3	1.4	3.7 (r)	3.13	Pegmatite vein (description C)
4	0.6	7.2 (l)	2.90	Description A
5	1.2	9.5 (r)	2.97	Description B
6	1.2	13.1 (l)	2.45	Description A
7	0.8	14.4 (r)	3.09	Description B
8	1.1	20.0 (r)	2.90	Description B
9	1.1	20.9 (r)	2.76	Description B
10	1.0	18.8 (r)	2.88	Description C

Note: The letters in the brackets of the third column stand for: “l” - the left wall of the adit, “r” - the right wall of the adit.

drill bits. Table 1 shows the results gathered during field measurements of the thermal conductivity coefficient in the granite mass at the base of the Telmamskiy HEC dam.

Geologically, two types of granite are distinguished according to their formation phases: amphibole and biotite granites, and aplite-like granites. The texture of the first type is porphyritic due to the presence of phenocrysts of potassium feldspar, while its structure is massive and gneissoid. Amplitude-like granites are leucocratic, fine-grained grayish pink and pink granites of amplitude-like texture and massive structure that are characterized by low biotite content.

Our measurements did not reveal significant changes in the coefficient of thermal conductivity of granites depending on texture. According to the given data of numerous experiments in Adit 1, the thermal conductivity coefficient of granites and pegmatites fluctuated within a narrow range: from 2.76 to 3.13 $\text{W}/(\text{m}^*\text{K})$ making up 2.94 $\text{W}/(\text{m}^*\text{K})$ on average. This is apparently explained by the relatively constant mineralogical composition that includes plagioclase and oligoclase (40–70%), quartz (30–35%) and microcline (up to 20%) or amphibole (0.2–4.0%). A great influence on the coefficient of thermal conductivity of granites is made by the their biotite content, which sometimes reaches 40%, resulting in a decrease of the coefficient down to 2.47 $\text{W}/(\text{m}^*\text{K})$ (point 6 in Table 1).

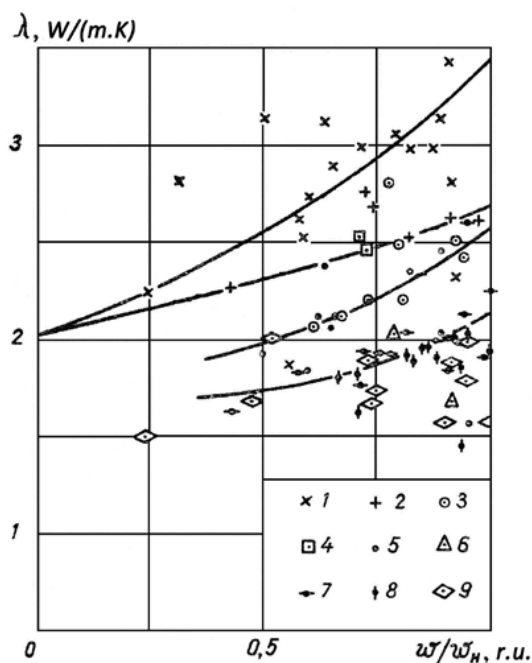


Figure 4. The thermal conductivity coefficient of the rock mass in Adit 1000 depending on the degree of moisture saturation for different rock types.

Pegmatites are characterized by rich content of microcline (60–80%). The rest of the minerals have the following composition in pegmatites: quartz, 20–30%; plagioclase and albite oligoclase, 10–20%; biotite, 1–2%; and muscovite, up to 5%. At the same time, the thermal conductivity coefficient of pegmatites is almost equal to that of granites ranging from 2.82 to 3.13 W/(m*K), with an average of 2.97 W/(m*K).

The results obtained by field measurements of the thermal conductivity coefficient for the granite mass in Adit 1 agree well with the results produced by the laboratory investigations into the drill cores obtained from the boreholes. According to the laboratory studies, the mean thermal conductivity of granites and pegmatites is 3.11 W/(m*K) with the mean values of the volume weight of the structure equaling 2.63 g/cm³ and the gravimetric moisture equaling 0.3%.

The Vilyuy HEC-III

The construction site of the Vilyuy HEC-III is located at the middle reaches of the Vilyuy River, 1.5–2 km above the mouth of the M. Botuobiya River. The area where the dam of the Vilyuy HEC-III is constructed is characterized by a complex geological structure. This structure contains the Upper Cambrian sedimentary rocks represented by two suites (Ilginskaya and Verkholsenskaya) and covered with an intrusive sheet of Triassic dolerites. Insufficiently strong marls and argillite clay are dominant as well as dense, very hard, thin-bedded, and massive limestone and dolomites. These rocks in their natural occurrence are interstratified, forming interbeds and members of varying thickness. The marls often contain gypsum crusts and veins that are differently oriented and have an irregular shape. All the rocks have fissures of different shape and direction most of which are filled with ice.

The field measurements of thermophysical properties of the rocks at the dam base of the Vilyuy HEC-III were carried out in Adits 1000 and 1001, which were made in the landslide sediments (Layer 12) at the slope on the left bank of the Vilyuy River. Approximately 150 measurements of thermal conductivity coefficient of rocks in their natural arrangement were made during the summers of 1979–80. At the same time, the moisture content and the volumetric weight of the rocks were measured in the adits. The mean temperature of the adits was 3°C below zero.

The measurements revealed that the rocks of the dam base in their natural occurrence are in the state of complete water saturation. However, the near-wall zone in the adits was somewhat dehydrated after it was drilled. The degree of moisture saturation of the rocks sometimes reaches only 0.3. This allowed us to draw a graph of the coefficient of thermal conductivity of rocks in their natural occurrence against the degree of moisture saturation $U=W/W_H$ (Fig. 4) (W – the current moisture content; W_H – saturation moisture).

Function $\lambda(U)$ is represented by a concave curve (i.e., as the degree of moisture saturation of the rocks increases, their coefficient of thermal conductivity increases), which is apparently explained by the developed network of micropores. The $\lambda(U)$ function curves presented in Figure 4 for the major rock types at the dam base of the Vilyuy HEC-III in Layer 12 under the negative temperature (about 3°C below zero) are approximated by the following electric ratio:

$$\lambda = D + KU^\delta \text{ when } 0,3 \leq U \leq 1, \quad (6)$$

where D , K and δ are empirical parameters for values of different rock types presented in Table 2.

Fissured rocks exhibit a low coefficient of thermal conductivity irrespective of their type (within the range from 1.5 to 2.0 W/(m*K)). They do not reveal any distinct dependence of the thermal conductivity coefficient on the degree of moisture saturation. This is perhaps linked to the fact that the coefficient of thermal conductivity of fissured rocks is influenced more by the size of air voids than by the air porosity when the pores are uniformly distributed in the rock volume.

Conclusions

The areas where northern dams are constructed are usually characterized by a complex geological structure, and the construction process usually involves the upper horizons in the zone of rock weathering and rock fracturing. The only acceptable research method in this case is to measure the thermophysical properties of the rock mass by probe methods directly in the mines and adits.

The method of a short cylindrical probe proved to be the most suitable probe method among the well-known ones that can be used to measure thermophysical properties of frozen ground mass and bedrock in mines and adits. It is accounted for by the practical convenience of its insertion into the examined mass of hard materials. The low ratio of the probe length to its diameter (equaling 5) makes it possible to apply standard drill bits with carbide and diamond tips to make holes for inserting the probe in a hard mass. The method of a short cylindrical probe demonstrated its

key advantages when employed under challenging field conditions. Such probes exhibit a sufficient degree of accuracy in measurements, are simple to use under harsh industrial conditions, and are rather resistant to mechanical exposure.

Short cylindrical probes were utilized in measurements of thermophysical properties of rocks in the adits of dam bases of the Vilyuy HEC-III (1979–1980) and the Telmamskiy HEC at the Mamakan River (1985). The total number of measurements taken in carbonate rocks of the Vilyuy HEC-III was 150. Sixty measurements were made in the granite mass at 10 points of the Telmamskiy HEC.

The measurements revealed that the granite mass is characterized by a steady coefficient of thermal conductivity fluctuating between 2.76 and 3.13 W/(m*K) and averaging 2.94 W/(m*K) when the volumetric weight of the structure equals 2.63 g/cm³ and the gravimetric moisture equals 0.3%. It is shown that the results obtained in the field studies are in good agreement with the values of thermal conductivity coefficient of granites (equaling 3.11 W/(m*K)) obtained in laboratory studies of the drilled borehole cores.

The field studies at the Vilyuy HEC-III comprise landslide sediments (Layer 12) of the weathered zone. It is established that the rocks of the dam base in their natural occurrence are in a state of complete water saturation. However, the near-wall zone of the adits proved to be in a somewhat drier state, which yielded a coefficient of thermal conductivity of rocks at the dam base depending on the degree of moisture saturation within the range from 0.3 to 1.0. Fissured rocks reveal a low coefficient of thermal conductivity irrespective of their type (within the range from 1.5 to 2.0 W/(m*K)) and do not show any distinct dependence on the degree of moisture saturation. This is explained by the fact that the size of pores plays a more considerable role in this case than the general volume of pores that are uniformly distributed in the volume of rock.

The research established that the method of a short cylindrical probe plays an important role in thermophysical studies of rocks at the base of northern dams by preserving their natural structure even though the rocks usually occur in the weathered or fractured zone of constituent bedrock.

References

- Blackwell, J.H. 1954. Transient flow methods for determination of thermal constants of insulating materials in bulk. *J. Appl. Phys.* 25: 137-144.
- Gavrilev, R.I. 1984. The method of a short cylindrical probe for determination of thermophysical properties of soils and rocks. *IFZh.* 17 (no. 5): 855-856.

Environmental Hazards on the Coastal Plains of Northern Yakutia

A.V. Gavrilov, E.I. Pizhankova, A.Yu. Derevyagin, A.B. Chizhov

Lomonosov Moscow State University, Laboratory of Geological Environmental Protection, Geology Department, Russia

Abstract

This paper presents the results of a study of modern permafrost-related hazards caused by climate variations on the coastal lowlands of Northern Yakutia. The study employed remote sensing data and shows that activation of hazardous processes is related to two factors. The first is the presence of a thick stratum of the ice-rich permafrost formed during a negative temperature trend in the Late Pleistocene. The second is a negative-to-positive temperature trend change during the transition from the Late Pleistocene to the Holocene, which triggered the destruction of ice-rich sediments. In some cases, this process has been active throughout the Holocene, intensifying during short warming-periods (coastal thermal erosion); in other cases, it was active exclusively during warm periods and under especially favorable conditions (within negative morphological structures—thermokarst and thermal erosion). The current climate warming, accompanied by a precipitation increase in Northeastern Yakutia, is related to this kind of warm period. It is caused by frequent severe floods in the negative morphological structure in the middle course of the Alazeya River. This has led to periodic flooding of vast areas including numerous villages. In the case of continuing warming, thermal erosion and local thermokarst caused by flooding may intensify these extremely hazardous destructive processes. Based upon aerial and satellite imagery obtained within a 50-year time span, the measured rate of coastal thermal erosion of the New Siberian Islands reaches 5 to 7 m per year.

Keywords: aerial imagery; climate variation; environmental hazard; ice complex; thermal erosion, thermokarst hazard.

Introduction

The coastal lowland plains of Northern Yakutia (Yana-Indigirka and Kolyma Lowlands) and the New Siberian Islands are among the very few permafrost areas where the traditional management of natural resources by native northern peoples dominates. Such land management does not lead to environmental degradation. However, natural processes, including permafrost-related hazards which lead to large-scale environmental changes, are widespread in this area. In these coastal lowlands, which are underlain by ice-rich permafrost, the natural environment (NE) is highly sensitive to climate change.

Long-period climate changes caused by variations in the Earth's orbit during the Late Pleistocene glaciation created favorable conditions for formation of the Ice Complex (IC) in the vast plain of the East Siberian Arctic. This plain covers an area from the edge of the shelf exposed at that time to the mountain ridges of the Verkhoyansk-Kolyma region, oriented latitudinally. The volumetric ice content of the IC deposits forming the upper 30–50 m of the accumulative coastal plain section is 70 to 95%. These deposits include particularly thick ice wedges.

The same long-period climate variations caused warming during the transition from the Late Pleistocene to the Holocene (13,000–9,000 years ago), which triggered the lake thermokarst. Deep (20–40 m) thermokarst depressions seriously affected the coastal plain. In the same period, a rise of sea level caused flooding of the coastal plain, which started with flooding of the major thaw lake basins. Within this period, which is short by geological standards (12,000–7,000 years ago), 70 to 90% of the plain stretching for 700 to 1000 km from north to south and for 2000 to more than 2500 km from east to west was flooded, forming the modern shelf seas: the Laptev, the East Siberian, and the Chukchi seas.

Thermokarst developed mainly within negative morphological structures (Romanovskiy et al. 1999, Gavrilov

2008). Within positive structures, the ice-rich coastal sediments were exposed to thermal erosion during the sea transgression. In the recent couple of centuries, coastal thermal erosion destroyed several islands composed of the IC in the Laptev Sea and in the East Siberian Sea.

Low-temperature, thick, ice-rich permafrost formed during the NE evolution in the Late Pleistocene/Holocene, and its ability to degrade under the influence of climate and sea-level variations, determine the present-day environmental situation. However, the periodic thermokarst and thermal erosion activation is due not to the long-period climate variations, but to short-period ones taking place during the long-period variations.

Methods

The study was performed using remote sensing materials. The study of the coastal dynamics of the New Siberian Islands was based on aerial and space images obtained over a 50-year time span. For this purpose, the multi-scale images of different years were accurately compared for the first time. The comparison was performed using software developed by ScanEx (ScanEx Image Processor 3.0). This software allows for the spatial transformation of heterogeneous data from different years without loss of image quality (pixel by pixel). The New Siberian Islands aerial photographs taken in 1951 were scanned in high resolution and superimposed onto the Landsat & ETM+ satellite images (SI) obtained in 2001. The software ensured accurate quantification of the coastal dynamics. Based on the SI panchromatic channel spatial resolution (15 m), the error of the coastal retreat rate estimates does not exceed 5–15% for the rate of 3 to 5 m per year over the 50-year interval between the surveys.

In addition to the materials mentioned above, the SI mosaics obtained from Google Earth.com and Kosmosnimki.ru were used to study the changes in the natural environment and permafrost-related hazards.

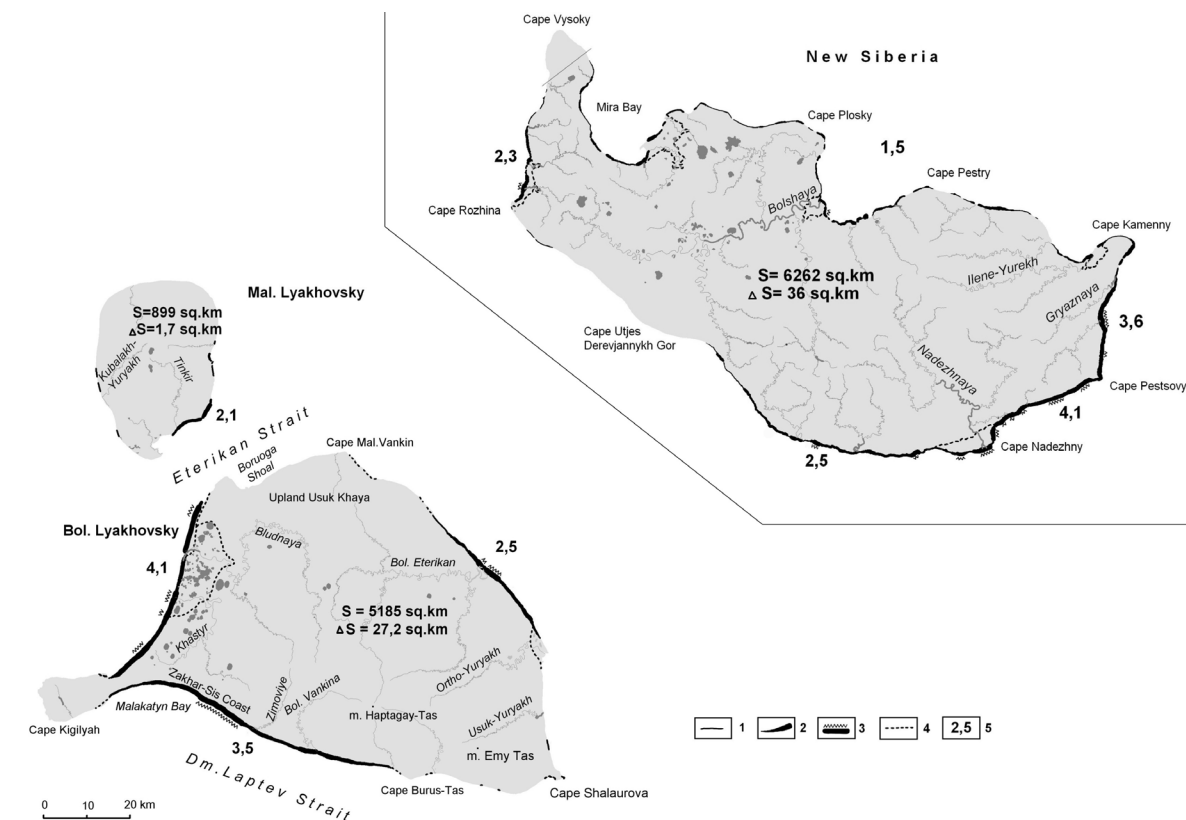


Figure 1. Rates of coastal retreat for the New Siberian Islands during 50 years: 1 – less than 1 m/year, 2 – from 1 to 5 m/year, 3 – over 5 m/year. 4 – marine and alluvial-marine terraces boundaries, 5 – average rates for retreating coastal segments, m per year.

Results and Discussion

Coastal geosystems are among the most dynamic of all geosystems. Their environmental significance is indicated by the study of the suggested liquefied natural gas transportation project from the western sector of the Arctic along the Northern Sea Route to Eastern Asia.

During the Holocene, the sea expanded onto the land primarily through negative morphological structures, which is reflected in the configuration of the modern coastline. The negative features are represented by gulfs, bays, and straits; positive ones are represented by islands, peninsulas, and capes. This process of sea transgression accompanied by thermal erosion of the ice-rich coastal sediments continues today. An example is the Chondon Graben, including a bay of the same name that is incised deeply into the land. In the area adjacent to the bay, bottoms of numerous thermokarst lakes are below sea level.

Coastal thermal erosion is most clearly evident in the disappearance of the islands composed of IC. The last of them (Figurin, Vasilevskiy, and Semenov islands) totally disappeared in the first half of the twentieth century. Currently on the brink of disappearance are Muostakh, Makar, and Shelonsky islands (Gavrilov 2008).

The study of the coastal dynamics of Big Lyakhovskiy and Little Lyakhovskiy islands using aerial and satellite images from 1951 and 2001 made it possible to measure the scale and the rate of change of coastline position along its entire length and to determine the area reduction (Fig. 1, Pizhankova & Dobrynina 2010). Comparison of these data with coastline landscape materials and climate data enabled

us to identify the major factors affecting the rate of thermal erosion, to classify the coasts on the basis of geological and geomorphological structure, and to obtain the quantitative parameters of thermal denudation of the coastal bluffs composed of the IC.

The study showed that 46% of the Big Lyakhovskiy Island coast, 21% of Little Lyakhovskiy Island coast, and 65% of New Siberian Islands coast are affected by thermal erosion. During the period from 1951 to 2001, the Big Lyakhovskiy Island area decreased by 27 km², the New Siberian Islands area by 36 km², and the Little Lyakhovskiy Island area by 2 km², which is 0.5, 0.6, and 0.2%, respectively, of the area of these islands. Coastal retreat rates can reach 5-7 m per year and rarely 10 m per year. Considering the short warm season duration at high latitudes, these rates should be considered catastrophic.

The factors influencing coastal dynamics can be divided into two main groups: (1) geological and geomorphological and (2) hydrological and climatic. The first group determines variations in the coastal retreat rates depending on the height of the coastal bluff; the structure of the coastal section determined by the tectonic features and the geological history; the depth and the offshore extent of the underwater slope; and the presence of shoals and tidal flats.

Hydrological and climate factors of the coastal thermal erosion include the ice-free period duration; sea currents; the strength and direction of winds and fetches; the sum of positive air temperatures; snow accumulation; and the radiation-thermal balance of the exposed surface of coastal bluffs. The analysis of aerial and satellite imagery and interpretation of measurements allows us to estimate



Figure 2. River flooding in the mouth of the Sloboda River (left tributary of the Alazeya River). Note the flooded meander lakes and gullies at the banks of Alazeya River. Google Earth.com. July 17, 2006.

the role of these factors in the coastal dynamics. The New Siberian Islands coastal retreat rates caused by the combined action of these factors as well as the average rates of thermal erosion for the retreating coastal parts are shown in Figure 1.

According to the reports of the Hydro-meteorological Center of Russia, the current sea-ice conditions in the arctic seas of Siberia have shown a significant decreasing trend in the area of ice cover. Considering these data, we can assume that the coastal retreat rates of the Eastern Arctic coast due to thermal erosion have increased in comparison with the studied period (1951–2001).

Arctic coastal bluffs that are composed of ice-rich sediments are among the geosystems that are most sensitive to contemporary changes in the natural environment. Other areas where the modern warming can cause hazardous natural processes are the negative morphological structures composed of sediments of ice and alas complexes that are formed in thaw lake basins. The high ice content of soils combined with the area of poor drainage conditions significantly increases the potential hazard for thermokarst. The area around the upper and middle courses of the Alazeya River, which is impounded by the Kisilyakh-tas ridge 500 km from the mouth of the river, is one of the areas where such a hazard is real. Here the initiation of thermal erosion and thermokarst was triggered by disastrous spring floods that continued during the entire warm period of the year. These floods have become more frequent since the 1990s. They are caused by climate warming as well as a long-term increase in winter and annual precipitation. The negative role of this hydrological process is enhanced by the occurrence of thick permafrost that prevents infiltration of flood waters.

The hydrological characteristics (river slope, stream cross-



Figure 3. Andryushkino village in mid-September 2007. Photo by I. Podgorny: <http://gp-russia.livejournal.com/1031258.html>.

section, and discharge capacity) of the Alazeya River, which determine the valley bottom and surrounding drainage area, are significantly worse than those of the adjacent Indigirka and Kolyma rivers. The winter precipitation increase (by 4–6% compared to the normal) caused deepening and expansion of the thermal erosional network linking numerous thermokarst lakes with the river. It also caused an annual spring water level increase in lakes, resulting in floods and the concentration of huge masses of water in the Alazeya River valley and in the mouths of its tributaries (Fig. 2).

The villages of Andryushkino, Argakhtakh, and Svatay are located in the zone considered to be hazardous because of flooding. In 2007, the flooding of Andryushkino lasted until the beginning of the winter season (Fig. 3). Frequent floods convinced the government of Yakutia of the need to take protective measures, including relocation of the settlements. Up to 80% of hayfields and reindeer pastures are also subject to long-term floods.

The area of prolonged flooding led to an increase in the active layer thickness from 0.6–0.75 m to 0.8–1.2 m (Gotovtsev et al. 2008). In Andryushkino village, the thaw depth reached 1.5 m. It triggered ground ice degradation and extensive local thaw settlement accompanied by formation of thermokarst ponds. The thaw settlement is particularly intense in the territory of Andryushkino village. River thermal erosion activity significantly increased everywhere. In Andryushkino village, the riverbank retreated by 50 m within a five-year period. The increase in solid flow leads to an even greater narrowing of the riverbed and reduction in its discharge capacity.

It should be emphasized that the activation of local thermokarst and thermal erosion in the middle course of the Alazeya River is a result of natural climate dynamics. Major transformation of the Yakutia coastal lowlands topography by widespread development of thermokarst was completed 9,000–8,000 years ago (Kaplina 1987). After this period, thermokarst activation in this region occurred repeatedly. This is indicated by numerous dates of late Holocene sections of alas peat bogs on the coastal plains of Northern Yakutia. Thus the warming periods causing thermokarst activation occurred repeatedly during the Holocene.

Moreover, the topography of alas plains, widespread on the coastal lowland, was formed not only by IC thermokarst, but also by the alas complex thermokarst, which occurred repeatedly. All alas plains without exception are located within the negative morphological structures (Romanovskiy et al. 1999, Gavrilov 2008).

Conclusions

- 1) Thick permafrost strata and their high volumetric ice-content in the upper horizons that may exceed 70% are the main features of the natural environment of the Northern Yakutia coastal lowlands. These conditions determine the high risk of permafrost-related hazards that affect the natural environment. The formation of such strata (IC) was associated with a negative temperature trend in the Late Pleistocene under the influence of climatic fluctuations caused by variations in the Earth's orbit.
- 2) Accumulation of the ice complex during the epoch of the transition of the climatic trend from negative to positive determined the activation of thermokarst and thermal erosion, which transformed the topography of the IC coastal plains. Most of the territory of the Late Pleistocene plain flooded during the Holocene sea transgression.
- 3) Thermokarst and thermal erosion determine the present-day environmental conditions as well. These processes occur during short-term warming periods (including the contemporary one) and, apparently, only in negative morphological structures. It is most probable that the thermal erosion of ice-rich coastal sediments evolved throughout the Holocene with the periods of activation related to short-term warming periods. Currently, the rate of coastal retreat reaches 5 to 7 m per year.
- 4) The local thermokarst in the Alazeya River valley can evolve if modern warming continues. Thermokarst was activated repeatedly in this area, as indicated by numerous late Holocene dates of alas peat bogs on the coastal plains of Northern Yakutia.
- 5) Catastrophic floods in the middle course of the Alazeya River are caused by modern climate change. The continuous permafrost extent prevents the infiltration of flood waters.

Acknowledgments

This study was partially funded by Grant RFBR 09-05-00594-a.

References

- Gavrilov, A.V. 2008. *Eastern Siberia Arctic Shelf Permafrost (The Current State and History of Development in Middle Pleistocene - Holocene)*. Author's abstract, Doctor of Sciences in Geology and Mineralogy, Moscow. p. 48 (in Russian).
- Gotovtsev, S.P., Nakhodkin, N.A., Baryshev, E.V., & Kopyrina, L.I. 2008. On causes of flooding of the villages in the Alazeya River basin. *Nauka i Tekhnika v Yakutii*, No. 2(15): 23-26 (in Russian).
- Kaplina, T.N. 1987. Permafrost Formation during the Late Cenozoic on Accumulation Plains of North-Eastern Asia. Author's abstract, Doctor of Sciences in Geology and Mineralogy, Yakutsk, IM SO AN SSSR, p. 41 (in Russian).
- Pizhankova, E.I. & Dobrynina, M.S. 2010. The dynamics of Lyakhovski Islands coastline (Results of satellite image interpretation). *Kriosfera Zemli* 14, (no. 4): 66-79 (in Russian).
- Romanovskiy, N.N., Gavrilov, A.V., Tumskoy, V.E., Grigor'ev, M.N., Hubberten, H.V., & Zigert, K. 1999. Thermokarst and its role in shaping the coastal zone of the Laptev Sea Shelf. *Kriosfera Zemli*, 3, (no. 3): 79 – 91 (in Russian).

Main Features of Urban Pedogenesis in Permafrost Areas (Case of Yakutsk City)

A.Yu. Germogenova

*Republican Agrochemical Research Station, Ministry of Agriculture of Sakha Republic (Yakutia)
State Institution*

Abstract

The properties of permafrost soils of Yakutsk and similar soils of neighboring areas are compared (TOC content, pH, electrical conductivity, and carbonate content). The influence of vegetation type, the position in mesorelief, and the elementary urban landscape type upon the distribution of soil properties with depth and their values in root zone are analyzed. It is shown that the relative variability of organic carbon and carbonates in urban soils is affected mostly by the type of elementary urban landscape and the type of ecosystem, whereas the attribution of soils to the form of mesorelief determines the character of change in more labile properties such as pH and electrical conductivity.

Keywords: permafrost soils; urban pedogenesis; urban soils; urbanization.

Introduction

Yakutsk, the largest city in Northeastern Russia, is located on the first and second terraces of the Lena River. This region is characterized by the presence of permafrost as well as extra-continental climate. The average annual temperature in the vicinity of Yakutsk is -9.3°C , the sum of growing degree days is $1578^{\circ}\text{C}\cdot\text{days}$, annual precipitation is 238 mm, and humidity factor is 0.4–0.5 (Elovskaya 1987). Being formed under these conditions, urban soils undergo specific changes that are not typical for soils of large cities in non-permafrost areas.

Different authors point out the following specific modifications of soils of large cities of European Russia in comparison with natural soils: enrichment in organic carbon, alkalization, salinization, increase in content of exchangeable calcium and magnesium on the soil adsorption complex (SAC) (Zelikov 1964, Obukhov & Lepneva 1990, Agarkova 1991, Stroganova 1998, State of... 2000). The main factor determining the nature of these transformations is the attribution of soil to a certain type of elementary urban landscape (Kasimova 1995). There are virtually no data on the urban soils in permafrost areas of Russia.

Modified surface horizons of soils in Yakutsk and their natural analogues were studied in order to investigate the changes of soil properties and regimes under the influence of urban pedogenesis. In order to do this, an assessment of urban soil modifications in different ecosystems (forests and grasslands) was carried out. Properties and regimes of soils formed on lower and higher forms of mesorelief were also studied, and the dependence of soil parameter changes on the type of land use or the attribution of the territory to different EUL (recreational, residential, and transportation) was determined. The organic carbon content, pH level, the content of soluble salts (estimated according to the electrical conductivity of water extract 1:2.5), and carbonate content were tested in the laboratory. In order to identify the dominant factor of modification of labile properties of the studied soils, the comparison of relative changes of average values and the coefficient of variation were performed for different soil properties.

Soils of the Yakutsk vicinity are characterized by high complexity due to this area's location on the terraces and in the floodplain of the Lena River. This complexity is also due partially to some features of the parent materials, the influence of permafrost, and related features of the hydrothermal regime. The soil cover consists of various types of alluvial soils and their evolutionary series. Chernozem-like, alluvial, and sod soils, as well as their variations, are presented in the places with grass vegetation on various elements of mesorelief. Elevated parts of terraces are occupied by forest ecosystems where permafrost pale soils have developed under the forest vegetation.

Permafrost, widely developed in the region, has a great influence on soil formation as an additional local factor. Both natural and urban soils are characterized by the occurrence of cryogenic features in their profiles. Morphologically, these features are reflected (1) in a specific permafrost soil structure, especially in the lower horizons, (2) in the presence of tongue-shaped humus and mineral horizons, as well as the features of the soil churning caused by cryoturbation processes, and (3) in morphologically visible suprapermafrost cryogenic accumulation of various chemical compounds in the form of spots, stripes, flows, etc. Permafrost soils are also characterized by specific soil regimes: temperature, water, salt, air, and nutrient regimes (Elovskaya 1987).

Results and Discussion

Modification of organic profile

Humus thickness in natural soils varies from 20 to 53 cm, and organic carbon content in upper horizons varies from 2.1 to 5.3% (prevailing values are 2.2 to 3.3%). In natural soils, all types of TOC distribution with depth were detected (Table 1). The soils underneath the pine forest (Section 1-1) are the richest in organic matter (5.3% in the upper horizon) having a shallow humus depth (19 cm) and regressive-accumulative type of TOC distribution over the section. Soils with 32–49 cm thick humus profile, with 2.1 to 3% of organic carbon content in the upper part, and with a uniform type of TOC distribution are forming under dry climate

conditions on meso-elevations on sands and sandy silts underneath dry-steppe meadows. Additional moisture in the soil profiles in lower terrain creates optimum conditions for humus formation. The thickness of horizons A+AB is 53–56 cm under an evenly accumulative type of TOC distribution and the TOC content in upper horizons of 3 to 4.5%.

In the cities, the humus status of soils changes ambiguously. We could detect a 0.1 to 0.3% increase in organic carbon accumulation in root zones, especially in the upper part, whereas the spatial irregularity of the parameter (variability) rises rather sharply (Table 2). Thus in comparison with natural analogues the soils of Yakutsk show only slight initial stages of the humus formation intensification. This is related to a moderate degree of human impact within a relatively small city. Yakutsk is a relatively young city (370 years old) with a low rate of emission load (low level of industrialization) and a low population of 268,000.

We can clearly trace the influence of the EUL type on the changes in organic carbon content in the upper horizons. For the forest soils of the recreational zone, the decrease in TOC content by 2.2% was observed. In the soils of city mini-parks, an increase in TOC content is significant (2.1%), whereas no noticeable changes were observed in roadside areas.

The increase in trend of TOC content in the root zone is traced in urban soils of grass ecosystems, which is related to the change of the herbaceous layer, the pollution by carbon-containing compounds, and direct human impact (Table 2).

The organic profile of soils of the meso-depressions are more affected by the city influence, whereas the soils of meso-elevations virtually do not react to the city “pressure.” The maximum accumulation and the spatial heterogeneity of organic carbon content in the soils of meso-depressions are associated with the upper 10–20 cm layer.

Thus the direction of the organic profile modification in the city depends on the type of vegetation and the type of EUL, whereas the intensity of this process depends on both the ecosystem type and the soil location in the mesorelief.

Effect of city conditions on the pH level and carbonate content in soils

The pH level of natural soils ranges from 6.8 to 8.3, increasing from the surface to the middle part of the soil profile (towards the horizons of the accumulation of CaCO_3) and decreasing below that. The carbonate content usually varies from 0.3 to 6.1%, but in some cases no carbonate accumulation was detected. The peculiarities of the water regime of soils in forest ecosystems (Section 1-1) make them less alkaline (pH 6.8 to 7.7) with minimum carbonates (0.3%) compared to the soils of grass ecosystems. The soils of the grass ecosystems located on meso-elevations have lower pH (7.2 to 7.8) than the soils located in meso-depressions (7.2 to 8.3). In the same landscapes, carbonates are accumulated in amounts of 0.9 to 1.6% and 1 to 6%, respectively.

CaCO_3 content in the profile of urban soils ranges from 1.0 to 4.3%, whereas pH ranges from 7.1 to 8.5 units. Maximum values are confined to the horizons of carbonates accumulation which are located in either the upper or the middle parts of the profile. Changes of CaCO_3 content and

pH level under the influence of the city impact are differently directed and are determined by the type of ecosystem, the initial condition of the soil, and mainly by the type of land-use or EUL.

In the soils of the recreational zone (Section 1), no changes of soil water pH were observed; however, the tendency of CaCO_3 migration was traced down the profile. Two factors contributed to this tendency. First, the characteristics of the ground water regime underneath the forested areas and the increasing active layer thickness due to the soil temperature increase in the city. Second, there was low atmotechnogenic (determined by interaction of the atmosphere with engineering structures) contamination of such landscapes by calcium-containing dust (Ecogeochemistry... 1995, State of... 2000). Lack of carbonates in the upper part of the soils underneath forest vegetation in cities located in the steppe zone has been mentioned by other authors (Bezuglova et al. 1997, Butova et al. 1977).

Opposite processes, whose direction depends on the type of land-use, occur in soils of grass ecosystems under urban impact. The changes in CaCO_3 content and pH level have not been detected in soils of city mini-parks, whereas the accumulation of carbonates in the upper horizons by 0.3–2.5% and pH increase by more than one unit have been registered in roadside soils. The main reason is the use of materials containing carbonates for road and building construction.

Only the statistically uncertain trend of alkalinization by 0.5 pH with a slight increase of the spatial variability and the tendency of the carbonate content to increase (from 0.4 to 0.6%) has been traced in the root zone of soil horizons under the influence of urban pedogenesis (Table 2). The most intense changes occur in the soils of roadside areas.

Forest soils show a more significant increase in pH and its spatial variability than soils in grass ecosystems (Table 2). Alkalinization of the upper horizons has been registered for the sections of soils located both on meso-elevations and in meso-depressions.

No changes in the carbonate content under the influence of urban pedogenesis have been observed in the root zone horizons of urban soils of grass ecosystems. As for the forest soils, the trend of increasing average value (by 0.4%) and spatial variability (by 30%) of carbonate content was clearly detected. These differences are due to the degree of anthropogenic impact (EUL type) and some changes in ground water regime characteristics of the areas with various kinds of vegetation. Urban soils of meso-elevations have a general tendency for an increase in carbonate content, whereas the soils of meso-depressions are characterized by downward migration due to changes in the hydrological regime.

Comparison of the relative changes in the pH average values and variability in the root zone horizons between urban soils and natural soils shows that the influence of the ecosystem type is insignificant, whereas the effect of the mesorelief form significantly affects the relative change of the spatial variability. Regarding the carbonate content, the roles of parameters are entirely opposite: the ecosystem type has the greatest influence, while the effect of mesorelief is less significant. In this case the main role is played by a particular type of EUL that the soil belongs to.

Table 1. Properties of the soils of Yakutsk and its vicinity (key sections).

EUL type	# of section	Soil type	Soil horizon	Depth, cm	pH, units	TOC, %	EC, mS/cm	CaCO ₃ , %
I-II terraces, forest ecosystems								
recreational (park)	1	permafrost pale gray transitional underneath a pine forest	A	5-10	7.3	3.1	0.43	-
			AB	10-22	7.5	0.3	0.13	-
			BCf	22-61	7.4	0.0	0.09	-
			C	61-98	8.4	0.0	0.20	0.91
natural analogue	1-1	permafrost pale gray transitional underneath a pine forest	A	1-19	7.3	5.3	0.62	-
			Bfg(Ca)	19-75	7.7	0.8	0.32	-
			C	75-105	6.8	0.1	0.08	-
Abandoned floodplain, meso-elevations, meadow ecosystems								
residential (mini-park)	2	permafrost meadow chernozem-like, shallow-modified	Au	0-10	7.5	3.9	1.65	-
			A	10-20	7.1	4.2	1.77	-
natural analogue	2-1	permafrost meadow chernozem-like (20-year-old)	A _p	0-29	7.2	2.1	0.05	-
			AB	29-49	7.4	1.4	0.04	-
			BC	49-60	7.7	-	0.04	-
			Cg	60-126	8.6	-	0.07	-
transportation (roadside area)	3	permafrost alluvial sod chernozem-like, shallow-modified	Au	0-10	7.9	2.3	0.24	2.55
			Au	10-20	8.1	1.8	0.19	1.01
	4	permafrost alluvial-sod, shallow-modified	A	4-14	7.4	2.2	0.16	-
			AC1	14-49	7.7	0.6	0.17	-
			AC2	49-65	8.5	0.4	0.46	-
			C	65-96	7.6	0.1	0.11	-
natural analogue	3,4-1	permafrost alluvial sod chernozem-like	A	0-32	7.4	2.4	0.18	-
			B1Ca	32-66	7.8	1.6	0.24	1.63
			B2	66-103	7.7	0.9	0.29	-
			C	103-107			0.38	-
	3,4-2	permafrost alluvial sod chernozem-like	A	2-15	7.3	2.3	0.24	-
AB	5-34	7.0	0.8	0.17	-			
BC	34-107	7.1	0.7	0.14	-			
Abandoned floodplain, meso-depressions, meadow ecosystems								
transportation (roadside area)	5	permafrost alluvial sod gleyey, shallow-modified	Ag	6-18	8.5	2.4	0.76	1.66
			ABg	18-32	8.5	2.0	0.47	4.27
			BCg	32-97	8.2	0.5	0.30	-
natural analogue	5-1	permafrost alluvial sod	A	3-30	7.3	3.0	0.44	0.71
			AB	30-53	7.4	1.6	0.36	-
			BC	53-98	7.2	1.0	0.34	-
residential (mini-park)	6	permafrost meadow chernozem-like salinized, shallow-modified	Au	0-10	7.1	6.7	8.85	-
			Au	10-20	7.4	6.8	0.97	-
natural analogue	6-1	permafrost meadow chernozem-like salinized	Adsa	0-4	7.2	4.5	12.6	2.30
			A sa	4-23	7.3	4.2	1.38	1.76
			AB ca,g	23-38	8.3	2.1	1.08	6.14
			B ca,g	38-56	7.6	1.6	1.11	5.64
			BC Ca,g	56-107	7.8	-	0.52	1.09
			Cg	107-160	7.6	-	0.66	-

Table 2. The influence of the main factors upon the change of urban soils properties in comparison with their analogues

Factor		TOC, %		pH, units		ES, mS/cm		CaCO ₃ , %	
		ΔX_{avr}	ΔCV	ΔX_{avr}	ΔCV	ΔX_{avr}	ΔCV	ΔX_{avr}	ΔCV
Urban pedogenesis		0.1	18	0.5		0.0	-80	0.2	
ecosystem type	forest	-2.2		0.9				0.4	125
	meadow	1.5					-71		
position in mesorelief	elevations							0.4	-92
	depressions	0.6	36			-1.4		-0.5	

Note: ΔX_{avr} – deviation from the mean value of the properties of urban soils in comparison with their natural analogues;
 ΔCV – deviation of the variation coefficient of the values of urban soil properties in comparison with natural soils;
 insignificant parameters are omitted.

The content of soluble salts in the city soils and their analogues

According to Elovskaya (1987) and Savvinov (1989), saline soils are widespread in the valley of the Lena River. The causes of salinity are the following: dry and extra continental climate; the presence of permafrost, preventing sufficient leaching of salts out of the soil stratum; salinity of the parent material; and the general hollow topography.

Electrical conductivity in natural soils ranges from 0.04 to 12.6 mS/cm. Most of the soils belong to the category of non-saline (EC=0.2-0.8 mS/cm) ones. Strongly saline soil is only that in Section 6-1 in the upper level with electrical conductivity of 12.6 mS/cm, which is associated with the soil's position in the relief depression. The type of salinity is defined as the chloride-sulphate and sulphate-magnesium-calcium.

Most of Yakutsk soils are not saline: EC value ranges from 0.09 to 8.85 mS/cm (dominating values are 0.25-0.70 mS/cm). The changes of soluble salt content in urban soils in comparison with natural landscapes are determined by their initial characteristics, position in the relief, and EUL type.

The soils underneath forest vegetation (Section 1) are characterized by the trend of desalination of soluble salts (EC for a meter-thick test soil stratum was 0.32 to 0.62 mS/cm, whereas in the recreational area of the city it is 0.13 to 0.43 mS/cm). This is due to an increase in precipitation and the active layer thickness in urban areas. No significant changes can be detected in the accumulation of soluble salts in urban soils located on the meso-elevations of the relief. The most intensive downward migration of soluble salts was registered in the soils confined to low-relief elements. Urbanization can contribute to soil desalination in the case of an initially high salt content. Thus on the territory of a mini-park (Section 6) in the upper soil level, ES amounted to 8.85 mS/cm, whereas in the natural analogue it was 12.6 mS/cm. The electrical conductivity of roadside soils (Section 5) compared to the natural analogue increased from 0.44 to 0.76 mS/cm, which is due to increasing anthropogenic pressure on these EUL.

No significant changes in the content of soluble salts and its variability in the studied soil horizons of urban forest ecosystems were detected. In grass ecosystems, a general trend of desalination of the upper 10 cm of soil profile and the accumulation of soluble salts at the bottom of the root zone was registered. No significant changes in salt content

have been observed in the areas of meso-elevations in the root zone of soils. In soils of meso-depressions, soluble salts are moving into deeper soil horizons under the influence of downward flow of groundwater.

In general, a trend toward a reduction of the soluble salts content and desalination has been found in urban soils. The intensity of this process is determined by the topographic location and the initial soil salinity. EUL type has no significant importance.

Conclusions

In the soils of Yakutsk, the direction and extent of humus, carbonate, and salt content modification and the distribution of pH depend on the initial state of soils, their attribution to a certain EUL type, ecosystem, and the form of mesorelief.

The distribution of organic carbon, carbonates, EC, and pH values in soil profiles virtually do not change under conditions of low human impact, whereas under conditions of the increased impact a multi-directional modification is observed.

The type of elementary urban landscape plays a main role in producing changes in organic carbon content, pH level, and content of carbonates. Distribution of soluble salts under urban conditions is mostly affected by the location in mesorelief.

The most significant modification of soil properties was detected in the 0–20 cm layer. In contrast to the urban areas of the taiga zone, no proven changes in a number of soil properties have been observed in Yakutsk.

The attribution of soils to a certain type of ecosystem determines the maximum relative change in organic carbon and carbonate content in urban soils compared to natural soils, whereas their attribution to the mesorelief form determines the variability of the pH and EC values.

We suggest that in some areas of Yakutsk that have not experienced an intensive human impact, the "humidification" of landscapes is possible in contrast to "aridization," which has been observed in urban soils of the taiga zone.

Acknowledgments

We thank Dr. R.V. Desyatkin for assistance in organizing the field work and Dr. G.V. Stoma for assistance in preparing the paper.

References

- Agarkova, M.G. 1991. Ecological and genetic peculiarities of urban ecosystem soils. Abstract of candidate dissertation, Moscow. 26 pp. (in Russian).
- Bezuglova, O.S., Kryshchenko, V.S., Privalenko, V.V., & Gorbov, S.N. 1997. Peculiarities of soil cover of Rostov-on-Don urban landscape. *Problems of anthropogenic soil formation* Moscow 2: 203-205 (in Russian).
- Elovskaya, L.G. 1987. *Classification and diagnosis of Yakutia permafrost soils*. Yakutsk. 172 pp. (in Russian).
- Kasimova, N.S. (ed.). 1995. *Ecogeochemistry of urban landscapes*. Moscow: 336 pp. (in Russian).
- Obukhov, A.I. & Lepneva, O.M. 1990. Ecological effects of deicing agents on urban roads and measures to eliminate them. *Ecological studies in Moscow and Moscow region*. Moscow: 197-201 (in Russian).
- Savvinov, D.D. 1989. *Soils of Yakutia*. Yakutsk. 152 pp. (in Russian).
- State of planted vegetation in Moscow. 2000. Moscow: Prima-Press-M. 276 pp. (in Russian).
- Stroganova, M.N., Myagkova, A.D., & Prokofeva, T.V. 1998. Urban soils: Genesis, classification and functions. *Soil, city, ecology*. Moscow. pp. 15-108 (in Russian).
- Zelikov, V.D. 1964. Some materials for the characterization of soils of forest parks, city parks and streets of Moscow. *Izvestiya VUZov. Forest Magazine* No. 3. 28-32 (in Russian).

Critical Coefficients of Stress Intensity of Frozen Soils with Natural Structure

S.G. Gevorkyan

Fundamentproekt Open Joint-Stock Company, Moscow, Russia

Abstract

The results of experimental determinations of the critical stress intensity coefficients K_{IC} of frozen soils with natural structures are discussed in this paper. These coefficients were determined for the first time. The experiments were performed at different negative temperatures for soils with varying moisture contents.

Keywords: destruction; frozen soil; natural structure; stress intensity coefficient (SIC); thermal-contraction cracks; viscosity.

Introduction

Thermal-contraction cracking (or frost cracking) of frozen soil and the resultant formation of patterned ground are widely developed both in the permafrost area and in the zones of deep seasonal freezing of soils. This process, caused by thermal contraction of the ground massif as a result of chilling, is frequently responsible for damage to building foundations, underground reservoirs, road pavements, railroad cuts, slopes and embankments, earth dams, airfield pavements, pipelines, communication cables, and other structures.

Thermal-contraction cracking is particularly intensive under arctic climatic conditions. Thermal-contraction cracks frequently predetermine the basic features of landform development. They often trigger erosional and landslide processes and lead to deep ground freezing and irregular moisture distribution caused by changes in the hydrothermal regime of soil. The cracks contribute to denudation of unconsolidated soil from slopes because they serve as zones with especially intensive weathering. Thawing of wedge ice formed in thermal-contraction cracks may lead to active thermokarst or gully formation, and therefore may be hazardous to the stability of engineering structures.

Therefore, the need to study thermal-contraction cracking is closely associated with the impact of this process on engineering structures and its important geomorphic role.

Thermal-contraction cracking occurs as temperature stresses develop in the frozen ground as the temperature at the surface decreases. Cracking in the initially continuous (without any cracks) ground occurs if the temperature stresses in it reach the frozen ground tensile strength (Broek 1980, Grigoryan et al. 1987). The further propagation of thermal-contraction cracks into permafrost is defined by the stress concentration in the tip of the crack.

The stress intensity coefficient (SIC) is one of the important characteristics of the stress near the crack tip. If two bodies containing cracks have similar stress intensity coefficients, then the stress near the crack tips will be similar in both cases. According to Griffiths-Irwin's criterion, the crack starts developing when the stress intensity coefficient in the crack tip reaches some critical value (Broek 1980, Grigoryan et al. 1987). This value is a physical constant of the material and is called a critical stress intensity coefficient, or a coefficient of viscosity of destruction. The K_{IC} symbol is used to designate the critical SIC for ruptures.

The quantitative forecast of basic parameters of thermal-contraction cracking has gained more value due to the active economic development of the Arctic. These parameters include location of cracks, distances between cracks, and the depth of their penetration into permafrost. However, such forecast is impossible without the determination of strength characteristics of frozen ground, the K_{IC} value in particular.

Grechishchev, together with Aksyonov and Sheshin, previously defined the critical SIC K_{IC} based on remolded specimens of frozen soil (Grechishchev et al. 1980, 2000, Grechishchev & Sheshin 1971, 1974, Sheshin 1974, 1975). The critical SIC K_{IC} values for snow were given by Epifanov (2006), Epifanov & Yuriev (2006), and Epifanov & Osokin (2009, 2010). However, the critical SIC K_{IC} values for frozen soils with natural structure have not been defined so far.

We were the first to carry out an experimental study and to determine the critical SIC K_{IC} values for frozen soils with natural structures. Tests were performed on sand, sandy silt, silty clay, and clay at temperatures -1°C , -1.3°C , -3.5°C , -7.5°C , and -12.5°C (Gevorkyan 2011).

Methods

Frozen ground monoliths (cores) were sawed into disks 30 to 50 mm high for further specimen preparation and testing. Special samples for the laboratory determination of physical properties of soil were taken from each monolith.

We used the method of bending a two-point beam with a cut to determine the critical stress intensity coefficient (coefficient of viscosity of destruction coefficient). The method is based on the measuring of the force causing the destruction of the specimen. So we cut out small bars (parallelepipeds) from the discs of frozen ground to experimentally determine the critical stress intensity coefficients. For this purpose, the bars were sawed with a thin hacksaw blade from the frozen monoliths. Then these bars were finished with the help of an angle bar and a thin knife to ensure parallel planes and the correctness of the geometry of the produced parallelepipeds. Afterwards, a small cut several millimeters deep was made across one of the long parallelepipeds (Fig. 1).

All operations for specimen production were carried out at negative temperatures in specially equipped walk-in freezers.

The ANS device designed by Krivov (2009) was used as a test machine. The pressure was produced by a pneumatic

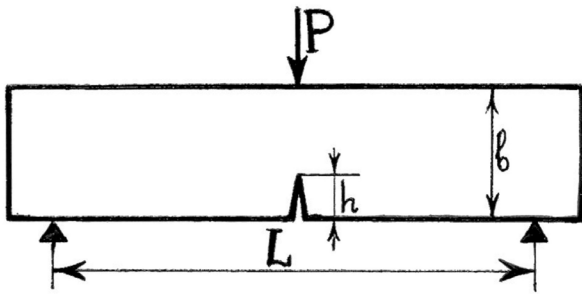


Figure 1. Scheme of specimen loading.

system controlled by a PC with special software. The technical capabilities of the ANS device and the stress control algorithms allowed us to set and maintain constant load within the range from 4 to 650 kg (the accuracy of the loading is 0.15 kg). This device allows us to monitor the specimens' deformations, load and temperature in the real-time mode. All test information is preserved in the computer.

Before the tests, the ANS device were placed into a walk-in freezer and kept there for at least 24 hours at the same negative temperature at which the tests were supposed to be performed.

Two supports 10 ± 1 mm high were placed under the specimens (bars) to conduct tests. The load was applied to a specimen via a metal roll 10 ± 1 mm in diameter, installed across the specimen at equal distances from the supports. A pneumatic system rod was connected to the loaded roll, and the load was smoothly increased until the specimen is destructed (Fig. 2).

Results and Discussion

We determined the critical SIC K_{IC} based on the tests results. Its value was estimated according to the following equation (Broek 1980):

$$K_I = \frac{PL}{ab^{1.5}} \cdot \left[2,9 \cdot \left(\frac{h}{b} \right)^{0,5} - 4,6 \cdot \left(\frac{h}{b} \right)^{1,5} + 21,8 \cdot \left(\frac{h}{b} \right)^{2,5} - 37,6 \cdot \left(\frac{h}{b} \right)^{3,5} + 38,7 \cdot \left(\frac{h}{b} \right)^{4,5} \right]$$

where P – breakdown load, L – distance between the axes of the supports, a – specimen (bar) width, b – specimen height, h – initial depth of the cut. We obtained 65 values of the critical SIC K_{IC} for frozen soils with natural structure for different temperatures and different moisture contents. These values are presented in our work (Gevorkyan 2011).

In general, we can make the following preliminary conclusions on the basis of the obtained results.

- 1) All other conditions being equal, the highest critical SIC K_{IC} value is typical of frozen sand, and the lowest critical SIC K_{IC} value is typical of frozen clay.
- 2) With temperature falling, the critical SIC K_{IC} value of all soils grows proportionally to the fourth root of the absolute value of the frozen ground temperature:

$$K_{IC} = C_0 \cdot \sqrt[4]{|T - T_{bf}|} \quad , \quad C_0 = const.$$

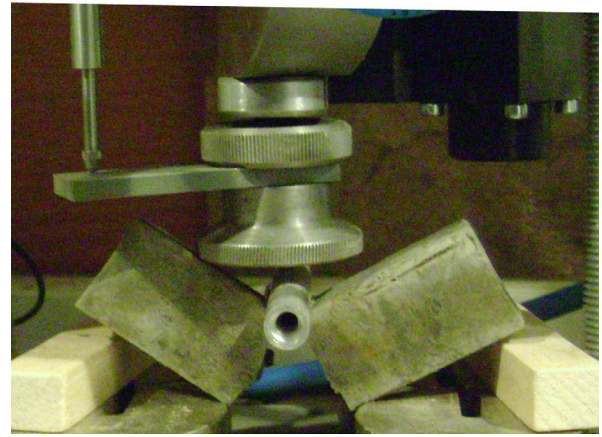


Figure 2. Destruction of specimen.

where T – ground temperature; T_{bf} – ground temperature at the beginning of freezing; the constant C_0 depends on the soil type and its total gravimetric moisture content W_{tot} .

According to our test data, this correlation is traced for sands and sandy silts, at least until the temperature T exceeds -12.5°C . The same dependence is observed for silty clays until the temperature T reaches -2.0°C . With further temperature decrease, the stress intensity coefficients K_{IC} of clayey silt quickly grow in a linear fashion (Figs. 3, 4).

We would like to note that, according to Grechishchev's and Sheshin's data obtained on remolded specimens, with the temperature decrease the critical SIC K_{IC} value grows proportionally to the square root of the absolute value of the frozen ground temperature. The following dependence is observed (Grechishchev et al. 1980, 2000, Grechishchev and Sheshin 1971, 1974):

$$K_{IC} = K_0 \cdot \sqrt{|T|} \quad , \quad K_0 = const,$$

where the constant K_0 is defined by soil properties.

- 3) The SIC K_{IC} value for all frozen soils significantly depends on the total gravimetric moisture content W_{tot} . All other conditions being equal, the less the ground moisture content, the lower the critical SIC K_{IC} value for this soil. In other words, with W_{tot} tending to zero, SIC K_{IC} tends to zero as well. There is always a specific value of the total moisture content W_{tot} (about 30 to 40%) depending on the ground temperature and type of soil, at which SIC K_{IC} of the frozen ground has the highest value for the given temperature. With the further increase in the total moisture content, the K_{IC} value gradually decreases, finally reaching the value equal to the critical SIC for pure ice at this temperature.
- 4) For comparison, according to Epifanov's data (Epifanov 2006), the critical SIC of fresh river ice at temperature $T = -15^\circ\text{C}$ makes about 0.104 to $0.105 \text{ MPa} \cdot \text{m}^{1/2}$, at $T = -17^\circ\text{C}$ the SIC $K_{IC} = 0.109 \text{ MPa} \cdot \text{m}^{1/2}$, and at $T = -24^\circ\text{C}$ the SIC K_{IC} is $0.145 \text{ MPa} \cdot \text{m}^{1/2}$. According to Grechishchev's data for uniform sandy silt (Grechishchev et al. 2000), $K_{IC} = 0.6 \text{ MPa} \cdot \text{m}^{1/2}$ at $T = -3^\circ\text{C}$, and $K_{IC} = 0.9 \text{ MPa} \cdot \text{m}^{1/2}$ at $T = -8^\circ\text{C}$. In this case, such slightly higher (in comparison with our data) values of K_{IC} coefficient can be explained by the fact that Grechishchev and his colleagues determined these coefficients based on the tests performed on artificially remolded specimens.

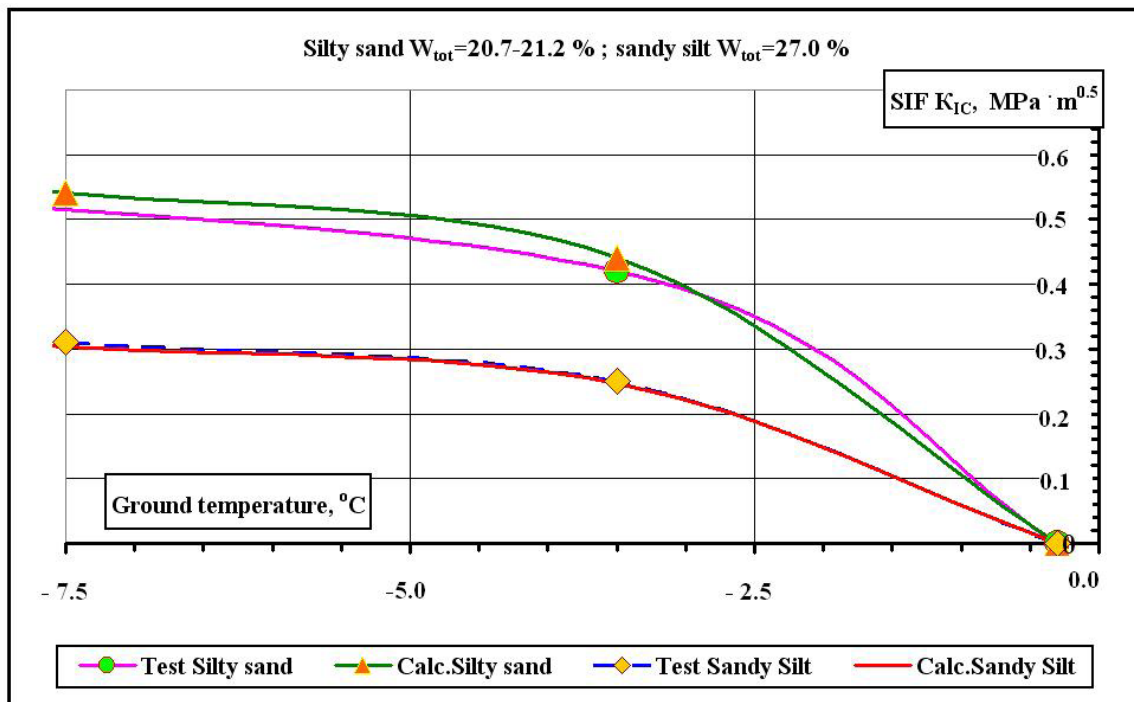


Figure 3. Dependence of stress intensity coefficients K_{IC} on temperature for silty sand and silt.

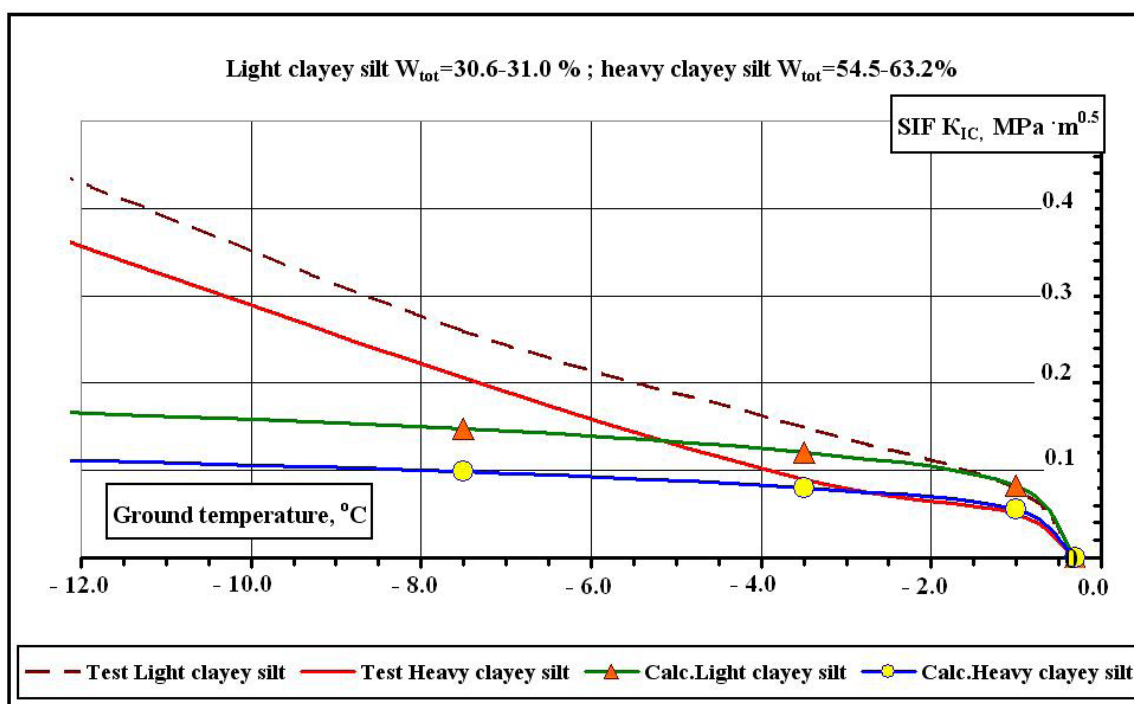


Figure 4. Dependence of stress intensity coefficients K_{IC} on temperature for silt with some clay and silty clay.

References

- Broek, D. 1980. *Fundamentals of destruction mechanics*. Moscow, Vysshaya shkola, 368 pp. (in Russian).
- Epifanov, V.P. & Osokin, N.I. 2009. Plastic flaw and break of snow cover on the mountain slope, Spitsbergen archipelago. *Kriosfera Zemli* Vol. XIII, No 2, pp. 82-93 (in Russian).
- Epifanov, V.P. & Osokin, N.I. 2010. Study of strength properties of snow cover on the mountain slope, Spitsbergen archipelago. *Kriosfera Zemli* Vol. XIV, No 1, pp. 81-91 (in Russian).
- Epifanov, V.P. & Yuriev, R.V. 2006. Viscosity of ice destruction. *Doklady Akademii nauk* Vol. 406, No 2, pp. 187-191 (in Russian).
- Epifanov, V.P. 2006. Fresh ice brittle rupture. *Materialy glyatsiologicheskikh issledovaniy* Edition 100, pp. 128-140 (in Russian).
- Gevorkyan, S.G. 2011. Values of critical stress intensity coefficient for frozen soils with natural structure. *Prostranstvo i vremya* No 4, pp. 157-162 (in Russian).
- Grechishchev, S.E. & Sheshin, Yu.B. 1971. Thermal deformation studies of frozen sandy silty soils in Central Yakutia. *Trudy VSEGINGEO* Edition 42, pp. 19-25 (in Russian).

- Grechishchev, S.E. & Sheshin, Yu.B. 1974. Experimental study of temperature stresses in frozen ground specimens. *Trudy VSEGINGEO* Edition 70, pp. 68-74 (in Russian).
- Grechishchev, S.E., Chistotinov, L.V., & Shur, Yu.L. 1980. *Cryogenic physical and geological processes and their forecast*. Moscow, Nedra, 384 pp. (in Russian).
- Grechishchev, S.E., Kazarnovskiy, V.D., Kretov, V.A., Aksyonov, V.I., & Sheshin, Yu.B. 2000. Thermorheological and contraction properties of frozen lumpy soils. *Kriosfera Zemli* Vol. IV, No 3, pp. 74-78 (in Russian).
- Grigoryan, S.S., Krass, M.S., Guseva, E.V., & Gevorkyan, S.G. 1987. *Quantitative theory of geocryological forecast*. Moscow, Izdatelstvo Moskovskogo universiteta, 268 pp. (in Russian).
- Krivov, D.N. 2009. *Deformation and destruction of frozen saline soils in the area of Bolshezemelskaya tundra*. Moscow: Izdatelstvo Moskovskogo universiteta, 25 pp. (in Russian).
- Sheshin, Yu.B. 1974. Some experimental data on frozen peat tensile strength and thermal-expansion coefficients. *Trudy VSEGINGEO* Edition 70, pp. 75-78 (in Russian).
- Sheshin, Yu.B. 1975. Some data on strength and deformation properties of frozen peat in Western Siberia in natural and laboratory conditions. *Trudy VSEGINGEO* Edition 87, pp. 118-122 (in Russian).

Interaction between Pile and Freezing of Frost-Susceptible Soil with Time (Taking into Account Phase Change)

P.A. Gorbachev

Moscow State University of Civil Engineering (National Research University), Moscow, Russia

Abstract

This paper describes the problem of the interaction between pile and frost-susceptible soil with time, taking into account variable freezing rate and viscosity. It is shown that these parameters significantly influence the values of tangential frost heave stress at the pile-soil interface and the value of the total heave force applied to the pile.

Keywords: foundation stability; freezing rate; pile; rheology; soil freezing; tangential frost heave stress; total heave force; viscosity.

General Considerations

A complex stress-strain state is created in the soil around the pile as a result of freezing of frost-susceptible soil. The cylindrical model was used to simulate pile-soil interaction. That model consists of a pile with diameter $2a$ embedded in a cylindrical domain of frost-susceptible soil with diameter $2b$ (Fig. 1).

To solve this problem, we assume that the pile is buried into unfrozen soil (below the seasonal frost depth) to the depth sufficient for frictional forces acting on the lateral surface of the pile to compensate for frost heave forces. Therefore, the pile is fixed because the total heave force N_{heave} is balanced by the restraining force N_{res} . As a result, for conditions of this particular problem, the equilibrium of frozen and unfrozen parts of the soil-pile domain can be considered separately (Fig. 1).

To model the freezing of the soil cylinder by approximate methods, the task of heat transfer should be solved taking into account phase changes during the freezing. By means of the calculation for different moments of time, the temperature distribution with depth of the domain (z coordinate) can be obtained.

The temperature distribution along the active layer depth is approximated by the linear dependence:

$$\theta(z, t) = \theta_1 \cdot \left(1 - \frac{z}{d_f(t)} \right), \quad (1)$$

where θ_1 – constant temperature at the ground surface; z –

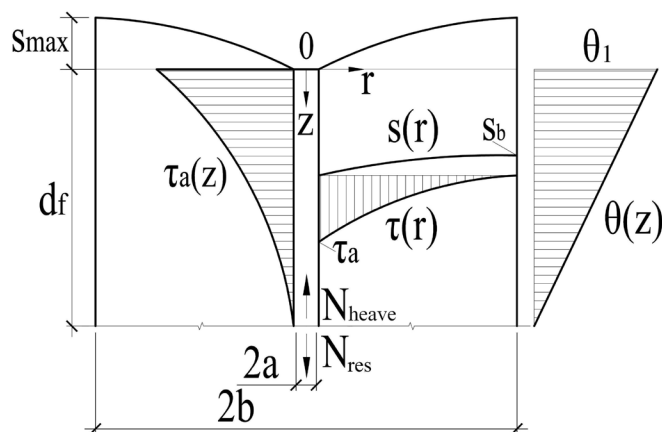


Figure 1. Geotechnical cylindrical model of the soil-pile domain and its main design parameters for the freezing front position at the maximum seasonal freezing depth.

current coordinate within the active layer; $d_f(t)$ – freezing front location coordinate, varying on the basis of the equation:

$$d_f(t) = \beta(t) \cdot \sqrt{t}, \quad (2)$$

where t – time in seconds; $\beta(t)$ – coefficient characterizing the rate of freezing front penetration into the ground. The definition of this coefficient is based on the solution of the heat transfer problem and is approximated with the function:

$$\beta(t) = \beta_0 \cdot e^{\frac{t}{\chi}}, \quad (3)$$

where β_0 – initial coefficient of the freezing rate; χ – coefficient which characterizes the rate of β change; β_0 and χ selection is based on the finite element solution of the heat transfer problem.

The dependences $d_f(t)$ for constant and variable $\beta(t)$ can be presented in the form of diagrams (Fig. 2).

The variable coefficient β significantly influences the function of the freezing front coordinate $d_f(t)$: Curve 2 grows more slowly than Curve 1 (Fig. 2). The freezing front penetration into the ground slows down due to additional energy consumption that is needed to overcome the ground water phase changes occurring in a certain temperature interval. This is the difference from the first case where all phase changes occur at a constant temperature. The uneven rate of freezing front propagation through the ground, which is taken into account by variable $\beta(t)$, significantly affects

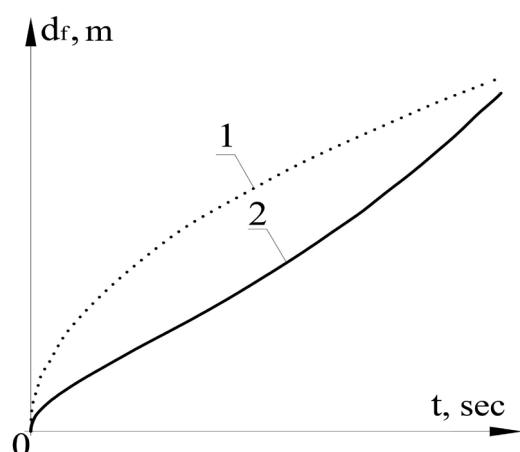


Figure 2. Position of the freezing front with time d_f for 1) constant coefficient β and 2) variable coefficient β .

the shape of the curves reflecting the heave rate of soil with time. This, in its turn, affects the change in the tangential uplift stress τ_a and the total heave force applied to the pile N_{heave} with time.

Major Relationships

Let us write down the rheological equation for frozen soil:

$$\dot{\gamma} = \frac{\tau - \tau^*}{\eta} + \frac{\dot{\tau}}{G}, \quad (4)$$

where $\dot{\gamma}, \dot{\tau}$ – shear strain rate and rate of tangential stress; τ, τ^* – current and maximum tangential stress values respectively; G – shear modulus; η – soil viscosity.

Only a viscous-plastic part of equation 4 is considered in this work. Consequently, the following equation is obtained:

$$\dot{\gamma} = \frac{\tau - \tau^*}{\eta} \quad (5)$$

The shear strain rate depending on the heave rate and the radius for the cylindrical model is the following (Ter-Martirosyan 2009):

$$\dot{\gamma} = \frac{ds}{dr} \quad (6)$$

As a first approximation, the tangential stress τ distribution along the radius r can be computed from:

$$\tau(r) = \tau_a \frac{(b-r)^2}{(b-a)^2}, \quad (7)$$

where τ_a – tangential stress at the pile-soil interface (at $r=a$; see Fig. 1); a, b - pile radius and outer radius of the cylindrical model (radius of influence of the pile) respectively; r - current radius value, and $r \in [a, b]$.

Setting 5 and 6 equal, and taking into account 7, we determine the differential equation for the soil heave rate. Its solution at $r=b$ is the following:

$$s_b = -\frac{b-a}{\eta} \left(\frac{\tau_a}{3} - \tau^* \right) \quad (8)$$

It is known that soil viscosity increases as temperature decreases. Based on the analysis of the test data (Roman 2002), the following expression for the approximation of the soil viscosity η dependence on the temperature θ is suggested:

$$\eta(\theta) = \eta_0 e^{k\theta} \quad (9)$$

where η_0 – initial viscosity; θ – temperature; k – coefficient of proportionality.

Substituting equation 9 into equation 8, one can obtain the expression for the soil heave rate in case of variable viscosity.

Now we can define the heave rate of the soil outside the pile impact zone. For this task, we assume that volumetric deformation due to conditions of compression ($\sigma_2 = \sigma_3$) is accompanied only by elastic strains, according to the equation:

$$\varepsilon_v = \varepsilon_1 = \frac{\sigma_1 + 2\sigma_3}{K} + 3\alpha\theta(z, t) \quad (10)$$

where ε_v – volumetric soil strain; σ_i – principal stress components ($i=1,2,3$); K – volumetric strain modulus; α – coefficient of linear soil expansion averaged for the temperature interval $|\theta_{en} - \theta_b|$ between the end and the beginning of frost heave. Let us assume for this problem that $\theta_b = 0, \theta_{en} = \theta_1; \theta(z, t)$ – temperature in a soil layer z defined with equation 1 for the moment of time t .

Since the volumetric strain modulus K of soil significantly increases in case of freezing, we assume that $(\sigma_1 + 2\sigma_3)/K \ll 3\alpha\theta(z, t)$. Consequently, equation 1 will be the following:

$$\varepsilon_1 = 3\alpha\theta(z, t) \quad (11)$$

Let us integrate equation 11 under the condition that the temperature varies in accordance with equation 1. The integration constant can be found with the help of the boundary condition: $s|_{z=0} = 0$. Consequently, we determine the dependence for $s(z, t)$:

$$s(z, t) = -\frac{3}{2} \alpha\theta_1 \cdot \frac{(d_f(t) - z)^2}{d_f(t)}. \quad (12)$$

Let us calculate the time derivative from equation 12 to determine the heave rate:

$$\dot{s}(t) = -\frac{3}{2} \alpha\theta_1 \cdot \frac{(\beta_o^2 \cdot e^{2t/\chi} \cdot t - z^2)^2}{\beta_o \cdot e^{t/\chi} \cdot \sqrt{t}} \cdot \left(\frac{1}{\chi} + \frac{1}{2 \cdot t} \right), \quad (13)$$

where $t > 0$.

Setting 13 and 8 equal, as a result of transformations we obtain $\tau_a(z, t)$:

$$\tau_a(z, t) = 3 \cdot \tau^* + \frac{9}{2} \cdot \frac{\eta}{b-a} \alpha\theta_1 \cdot \frac{(\beta_o^2 \cdot e^{2t/\chi} \cdot t - z^2)^2}{\beta_o \cdot e^{t/\chi} \cdot \sqrt{t}} \cdot \left(\frac{1}{\chi} + \frac{1}{2 \cdot t} \right), \quad (14)$$

where $t > 0$.

The total heave force acting on the pile is determined in accordance with the expression:

$$N_{heave} = 2\pi a \int_0^{d_f} \tau_a(z) dz \quad (15)$$

Substituting 14 into 15, as a result of integration we obtain the following:

$$N_{heave} = 2\pi a \left(3\tau^* \beta_o \cdot e^{t/\chi} \cdot \sqrt{t} + 3\beta_o^2 e^{2t/\chi} t \cdot \frac{\eta}{b-a} \alpha\theta_1 \cdot \left(\frac{1}{\chi} + \frac{1}{2t} \right) \right) \quad (16)$$

If $\beta = \text{const}$, equations 14 and 16 transform into the following (Gorbachev 2010):

$$\tau_a(z, t) = 3 \cdot \tau^* + \frac{9}{4} \cdot \frac{\eta}{b-a} \frac{\alpha}{\beta} \theta_1 \cdot \frac{(\beta^2 \cdot t - z^2)}{t\sqrt{t}} \quad (17)$$

$$N_{heave} = 2\pi a \left(3\tau^* \beta \cdot \sqrt{t} + \frac{3}{2} \frac{\eta}{b-a} \alpha\theta_1 \beta^2 \right) \quad (18)$$

It is sufficient to substitute 9 into 14 to take into account the dependence of soil viscosity on temperature. By integrating

Table 1. Initial data.

Parameter	η_0 , Pa sec	k	τ^* , Pa	α , 1/°C	$ \theta_1 $, °C	$ \theta_b $, °C	$ \theta_{en} $, °C	β_0	χ	a, m	b, m	d_p , m
Value	3.3×10^{11}	0.4	0	$2 \cdot 10^{-3}$	7.4	0	7.4	3.3×10^{-4}	7×10^6	0.2	1	2

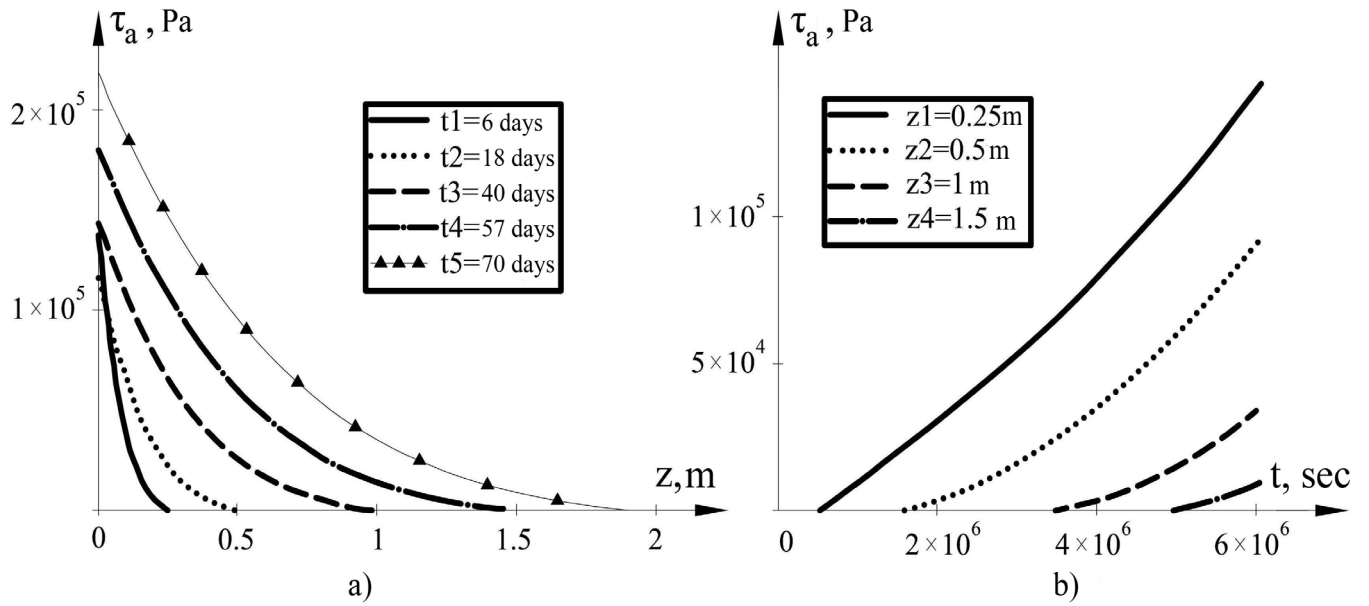


Figure 3. Tangential stress τ_a dependence ($\eta(\theta) \neq \text{const}$ and $\beta(t) \neq \text{const}$): a) on coordinate z for the fixed time moments t_1 to t_5 ; b) on time t for the points located at fixed depths z_1 to z_4 .

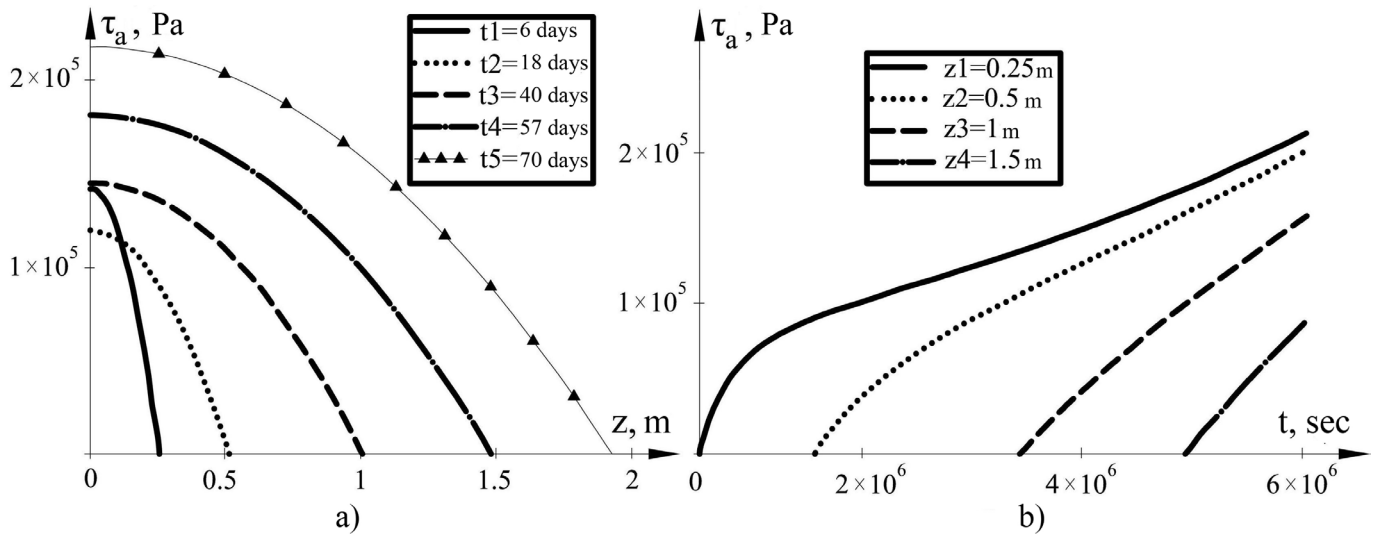


Figure 4. Tangential stress τ_a dependence ($\eta(\theta) = \text{const}$ and $\beta(t) \neq \text{const}$): a) on coordinate z for the fixed time moments t_1 to t_5 ; b) on time t for the points located at fixed depths z_1 to z_4 .

this expression along the coordinate z , we can obtain N_{heave} for the condition of variable viscosity. These dependences are not given due to their bulkiness.

Let us discuss the example illustrating the use of the obtained equations for the following initial data (Table 1).

The diagrams of tangential stress distribution with depth $\tau_a(z)$ for different moments of time and of tangential stress changes in time $\tau_a(t)$ for different depths are shown in Figure 3.

For comparison, similar diagrams are drawn for different conditions: 1) constant viscosity η and variable coefficient β ; and 2) constant η and β (Fig. 4 and Fig. 5, respectively)

Comparison of the diagrams in Figure 3a and Figure 4a allows us to see that the tangential stress τ_a decreases with z

less intensively in the case of constant viscosity $\eta(\theta)$ than in the case of variable viscosity $\eta(\theta)$. Lower viscosity values are observed at greater depths. Thus the soil at these depths undergoes lower stresses. Comparison of the diagrams with τ_a change in time for different z values (Figs. 3b, 4b) shows that stress increase, especially at initial stages, occurs more slowly when the variable viscosity is taken into consideration.

Let us compare the $\tau_a(z,t)$ curves at constant viscosity for the variable and the constant parameter β . In both cases tangential stress value τ_a decreases with depth z at various fixed moments of time (t_1 to t_5). However, the increase in τ_a value (Fig. 4a) occurs at the soil surface ($z=0$) in case of variable β , and the function τ_a at the soil surface decreases in

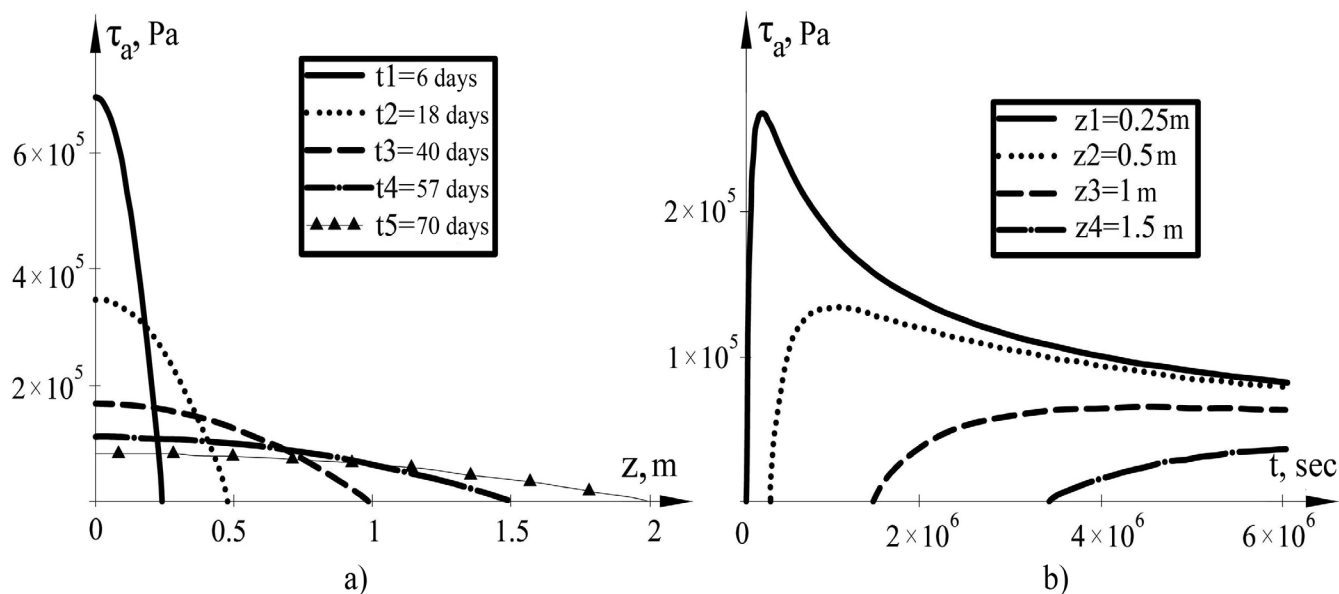


Figure 5. Tangential stress τ_a dependence ($\eta(\theta)=\text{const}$ and $\beta(t)=\text{const}$): a) on coordinate z for the fixed time moments t_1 to t_5 ; b) on time t for the points located at fixed depths z_1 to z_4 .

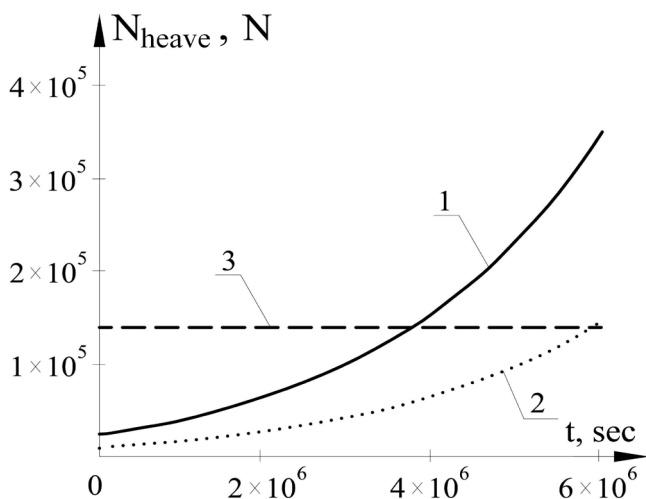


Figure 6. Total heave force N_{heave} time dependence for the cases: 1) $\beta(t)$ – variable and $\eta=\text{const}$; 2) $\beta(t)$ – variable and $\eta(\theta)$ – variable; 3) $\beta(t)=\text{const}$ and $\eta(\theta)=\text{const}$.

time in the case of constant β (Fig. 5a). At the same time, the areas under all curves $\tau_a(z)$ in Figure 5a are equal.

The tangential stress change in time also significantly depends on the parameter β . With variable $\beta(t)$, the tangential stress function continuously grows (Fig. 4b), while the curves in their shape follow the diagram for $d_f(t)$ (Fig. 2, Curve 2). With constant β , the function $\tau_a(z,t)$ increases in the points located close to the surface, passes through the extreme value, and then decreases (Fig. 5b, depths z_1 and z_2). At greater depths, the extreme value is leveled, and the function smoothly increases up to some particular value (Fig. 5b, depths z_3 and z_4).

According to the diagram $N_{\text{heave}}(t)$ (Fig. 6), the consideration of viscosity dependence η on temperature θ in the case of the variable coefficient β provides a noticeable reduction of the total heave force (in the example discussed, more than twice).

With the constant coefficient β , the total heave force is constant in time (see equation 18) and makes $N_{\text{heave}}=140$ kN (14.2t) in this case (Fig. 6, Curve 3). On the contrary, when

the freezing rate β is variable, the total heave force increases with time, similar to what can be observed in reality (Fig. 6, Curves 1 and 2).

Conclusions

- 1) Variations in the freezing rate parameter β significantly influence the soil heave rate and, consequently, the tangential heave stress τ_a variation with depth and with time. The total heave force grows with time when β is variable, and remains constant when $\beta=\text{const}$ (at $\tau^*=0$).
- 2) The consideration of variable viscosity η allows the reduction of the total heave force acting on the pile, because in this case the value of tangential stress decreases with depth more intensively, and the increase in τ_a with time at different depths occurs more slowly in comparison with the case when this parameter is constant.
- 3) Therefore, the variable soil viscosity η and the variable soil freezing rate parameter β should be taken into account in the analysis of stability of pile foundations affected by frost heave.

References

- Gorbachev, P.A. 2011. Interaction of a pile with freezing soil considering its rheological properties. In *Construction and formation of human environment: Collective works of the Fourteenth International Inter-University Scientific and Practical Conference of Young Scientists and Doctoral and Post-Doctoral Students*. Moscow: ASV, 563-567 (in Russian).
- Roman, L.T. 2007. *Permafrost mechanics*. Moscow: MAIK "Nauka/Interperiodika", 125 pp. (in Russian).
- Ter-Martirosyan, Z.G. 2009. *Soil mechanics*. Moscow: ASV, 461 pp. (in Russian).
- Tsytoich, N.A. 1973. *Mechanics of frozen soils (general and applied)*. Moscow: Vysshaya shkola, 445 pp. (in Russian).

Physical and Mechanical Processes in Cryogenic Formations Associated with Temperature Change

J.B. Gorelik

Earth Cryosphere Institute, SB RAS, Tyumen, Russia

Abstract

This paper describes the impact of internal stresses in the ground and deformation properties and the results and interpretation of the following problems: cryopeg mineralization; position of the lower boundary of schlieren ice beds in the permafrost masses; chemical composition of massive ice; and mechanisms of massive ice formation.

Keywords: cryopegs; deformations; freezing; injection ice; tabular massive ice; segregation ice; stresses.

Introduction

In the broadest approximation, purely thermo-physical terms can be employed to analyze and describe the state of water-saturated ground that is characterized by the balance between its thawed and frozen parts and to analyze the ground freezing and thawing processes. Such states and processes are inevitably accompanied by the change in the stress-deformed state of the ground, because significant power factors are concentrated near the phase change boundary where the water and ice densities are different. The solutions for a number of tasks can be significantly supplemented or changed considering the impact of this stress-deformed state. This report discusses specific examples that illustrate the correctness of this assertion.

Cryopeg Mineralization

The existence of cryopegs in permafrost sections can be associated with the specific mechanism of massive ice formation (Streletskaya & Leibman 2002), their mineralization, and the chemical composition of the solution, and taking into consideration the pore water genesis and the paleotemperature reconstruction of the conditions of permafrost formation (Fotiev 1997, Fotiev 1999). However, analysis of the change in brine concentration inside a cryopeg under the ambient temperature change occurs without regard to the deformability and strength properties of hosting permafrost. This can lead to certain errors in the obtained results. As an example, we will describe the cryopeg in the shape of a sphere with the radius R_0 at the initial negative temperature t_0 and the initial salt concentration C_0 . Let the ambient temperature fall to the value $t < t_0$. Part of the brine should freeze in the process, the solution concentration should increase, and the total volume of the system should increase as a result of the difference in density of water and ice. The main change of volume can occur only by means of the surrounding ground due to very low compressibility of water and ice. If the surrounding permafrost could not be deformed, then the liquid in the cryopeg would never freeze and the brine concentration would remain equal to the initial value. The new equilibrium state in such a rigid system is characterized only by the pressure increase inside the cryopeg. The opposite case to the one described above can be characterized by the probability of unlimited deformations of the host ground with the conditions of the pressure increase inside the cryopeg. A droplet of the brine

in ice (micro-cryopeg) can be its real analogue. Since the elastic limit of the ice is close to zero, its deformations are quite well described by the flow diagram of a very viscous incompressible liquid. In this case, with the temperature reduction described, the solution partially freezes and the salt concentration inside the cryopeg reaches a new equilibrium value C_t . This value is defined by traditional methods and without regard to the deformability of host ground. In this case the final equilibrium pressure value inside the cryopeg (droplet) will coincide with the initial one (Gorelik & Kolunin 2002).

In natural conditions cryopegs are present in permafrost (usually frozen sand) having deformation properties that are far from both cases described above. Below, the calculation results for elastic and elastic-plastic (the latter is more realistic) models of frozen sand deformation are given. The calculations are done with regard to the approaches described in the work (Gorelik & Kolunin 2002) and with the use of the methods discussed in the work (Sokolovskiy 1969). The required mechanical characteristics are taken from Tsytoich (1973) at corresponding temperatures. For the purpose of certainty, we will assume that the brine consists of the NaCl salt only; $C_0 = 35 \text{ kg/m}^3$; $t_0 = -1.9^\circ \text{C}$; $t = -7^\circ \text{C}$; R_0 is random. The traditional methods will give a new concentration value $C_t \approx 110 \text{ kg/m}^3$ in this case. We will obtain the following in the case of elastic deformation of sand: $C_t \approx 40.5 \text{ kg/m}^3$; $p_t \approx 5.99 \cdot 10^7 \text{ Pa}$ (599 atm); $R_t \approx 0.95 R_0$. Here, p_t , R_t are new equilibrium values of pressure inside the cryopeg and its radius (correspond to temperature $t = -7^\circ \text{C}$). We will obtain the following in the case of elastic-plastic behavior of frozen sand: $C_t \approx 76.0 \text{ kg/m}^3$; $p_t \approx 2.94 \cdot 10^7 \text{ Pa}$ (294 atm); $R_t \approx 0.78 R_0$. In both cases, the concentrations differ significantly from the value obtained with the usual method. Attention should be paid to extremely high values of internal pressure in the cryopeg. When a cryopeg is intersected by wells, the pressure should be quite quickly released until the values close to the hydrostatic value at this depth are achieved. Blowouts can occur at the well collar at the initial moment of intersection. The water level should be established close to the ground surface in the case of a quite high R_t .

The example given assumes the unlimited length of the ground mass in all directions. The deeper the cryopeg, the more real is this assumption. The probability of stress discharge at the surface should manifest itself while approaching the ground surface: the closer to the surface, the more accurate the calculation with the regular method.

The deformation properties of permafrost should be taken into account at least for the cases where the radius of the plastic zone R_p is smaller than the cryopeg bedding depth. In the example given, $R_p \approx 2.85 R_0$. Assuming that $R_0 = 5$ m, this should be taken into account starting from the depth of about 14 m.

It should be noted that in addition to chlorides, the chemical composition of cryopegs in the Yamal Peninsula contains also sulfates, bicarbonates, iron compounds, etc. Their mineralization can reach 150 g/l. The methodology for estimating the phase and water-ion composition in such cryopegs is given in the literature (Komarov & Volkov 2007, Komarov & Mironenko 2010).

Lower Boundary of the Ice Bed in Permafrost Mass

Laboratory tests (Biermans et al. 1978, Konrad & Morgenstern 1982, Radd & Oertle 1973) and theoretical investigations (Gorelik & Kolunin 2002) show that there is a minimal value for the external load on the schlieren ice given set temperature conditions for freezing a ground specimen. The ice segregation process ceases when this value is achieved. When the external load exceeds this minimal value, schlieren ice melting occurs under the same temperature conditions. It should be noted that this statement is true and was validated also for the specimen with a rigid, undeformable skeleton. Consequently, the cessation of the schlieren growth is associated with the effect of the load limit on the schlieren above a specific value, but not with the ground skeleton compaction. The latter, in the author's opinion, is incorrectly presented in some works. The fact that schlieren formation hardly occurs in intensively compacted grounds, even without external load, is most likely associated with the fact that the inter-particle relations emerging in the ground skeleton under these conditions become so significant in value that they eliminate its rupture (with the set temperature conditions) required for schlieren formation. In this context, the adhesive power effect is equivalent to the external load effect.

The investigation's results briefly discussed here by the author allowed us to obtain the correlation that links the limit depth L_p at which the existence of schlieren ice is still possible in the permafrost mass with its freezing temperature t_p (at the mass surface it is equal to the annual mean temperature), and the geothermic gradient value in the thawed zone G and the pressure from the overlying weight of the stratum (Gorelik & Kolunin 2002). The present version takes into account the ground salinity; only the main salinity component $NaCl$ is taken into account hereinafter:

$$L = \frac{-(t_p + \varepsilon \cdot C_w \cdot R_\mu \cdot T_0^2 / \mu \cdot \kappa \cdot \rho_w)}{(\lambda_u \cdot G / \lambda_f + g \cdot T_0 \cdot (\rho_s - \rho_w) / \kappa \cdot \rho_w)} \quad (1)$$

where: λ_u , λ_f is the ground heat conductivity coefficients for the thawed and the frozen states; ρ_s is the frozen ground density; g is the acceleration of gravity; μ is the molecular weight of salt ($kg/kmole$); $R_\mu = 8317$ J/kg kmole gas constant; C_w salt concentration in pore moisture at the depth L_p referred to its liquid phase kg/m^3 ; $\varepsilon \approx 2$ is the non-dimensional coefficient for the salt $NaCl$. The calculation

procedure is complicated if other salts in the solution are taken into account. Consequently, this case should be described specifically. In addition to the direct calculation of the value L_p , equation 1 can be useful for the reconstruction of the paleotemperature t_p on the basis of the actual data of the permafrost section. To do this, t_p should be expressed from (1) and calculations should be made based on the actual data. These data referred to the same section, although sparse, and are presented in independent works. We will use the results of the work (Dubikov et al. 1984) that gives the required data on well KTS-8 located on the second marine terrace of Cape Kharasavey, where the permafrost thickness is about 170 m; thickness of ground with negative temperature is about 250 m: $L_p \approx 166$ m; $G \approx 0.04$ degr/m; $C_w \approx 30$ kg/m³; $\rho_y \approx 2000$ kg/m³. Salinity, in addition to the concentration member in (1), also influences the relation of the thermal conductivity coefficients. This relation is above one as compared to non-salty grounds. It can be estimated based on the results of Ershov (1984) and Loseva et al. (1990) $\lambda_u / \lambda_f \approx 1.2$. The calculation gives the following: $t_p = -11.4^\circ C$. This value exceeds by 0.4–1.6 degrees the values for marine terraces with the current permafrost thickness 275–350 m, and by 3.7 degrees the values for plain sites with permafrost thickness 450 m, which were obtained by means of the solution of the inverse problem in the course of simulation of the permafrost formation process in different cooling epochs for the northern districts of West Siberia (Baulin & Chekhovskiy 1983). However, the proposed method is significantly more simple and can be recommended for the preliminary estimate of paleotemperature.

Chemical Composition of Tabular Massive Ice

The clarification of the mechanism of massive ice formation in a number of studies is based on the comparison of the total mineralization and the chemical composition of ice with analogous parameters from different water sources and pore solutions in host deposits (Dubikov 1982, Fotiev 2003). Such analysis is based on two suppositions. The first supposition is that in the process of ice formation the "fixation of the components of the initial water solution occurs" (Dubikov 1982: 33). The second supposition is not clearly formulated. However, it is assumed that the chemical composition of the salt solution in the ice of currently existing beds is very close to the composition of the solution from which it was formed. Nonetheless, it is known (Hoekstra et al. 1965, Harrison 1965, Kingeri & Gudnau 1966, Jones 1973) that brine drops in ice move under the impact of the imposed temperature gradient toward the higher temperature. This process is also interesting in terms of marine-ice demineralization dynamics (Tsurikov 1976). The velocity of this movement v_d is proportional to the imposed gradient: $v_d = s G_i$. In this expression G_i is the temperature gradient, and the coefficient s depends on the brine composition and the temperature at the point where the drop is located and makes $5 \cdot 10^{-11}$; $2 \cdot 10^{-10}$; $2 \cdot 10^{-9}$; $m^2/deg \cdot sec$ at temperatures -9, -4, and $-0.2^\circ C$, respectively (for the salt $NaCl$). Taking into account the assumed age of the beds, which is approximately 100,000 years (Fotiev 2003), it is easy to obtain the thickness of ice that should be free from brine admixtures in the current period at the minimal values

of the gradient $G_i \approx 0.03 \text{ degr/m}$. We will obtain 4.7, 19, and 180 m, respectively, for the temperature values given above. Since the overwhelming majority of ice beds are confined to the upper 50 m stratum (Dubikov 2002), the value of the effective gradients can exceed the given one. The reasons for this are seasonal and long-term mean temperature variations play a significant role here. The gradients in the warmest periods have the greatest impact under these circumstances. Ice mass desalination can occur during the period not exceeding ten thousand years under favorable thermal conditions.

If, for the purpose of simplification, we assume that there are no mineral admixtures inside the ice mass on which solution drops could adsorb, in the majority of cases the initial solution captured at the moment of ice formation should be removed from this mass before the beginning of studies. It can be replaced by the solution having a different composition from the side of the ice bed contact with the host ground. The salts that transformed to a solid state (hydrocarbonates, sulfates) within the ice as a result of the change in thermal conditions can be an exception. Although the authors of the study (Hoekstra et al. 1965) observed the movement of the solid salt *KCl* at temperatures below the eutectic point, Tsurikov (1976) concluded that this movement can be neglected on the basis of the actual data analysis concerning the demineralization of marine ice. He refers to this to explain the increased hydrocarbonate content in marine ice formed from demineralized sea water. The freezing temperature of such demineralized water exceeds the solidification point of hydrocarbonates forming it. However, the abovementioned author notes that hydrocarbonates also are actually contained in the ice for the case of freezing of the sea water of regular composition. The latter fact is not taken into account in the methodology for determination of salt composition in marine ice under the conditions of temperature reduction. That is based on the experimental investigations of V.V. Ringer and K.E. Gitterman “who assumed that the eutectic point of the calcium carbonate is -1.9°C , i.e., it is very close to the freezing point of the ocean water with salinity 35 g/l. If such water is freezing, the calcium carbonate should crystallize together with ice. Therefore, no carbonate ions should be present in the brine. That is why both authors did not include carbonates in the number of dissoluble salts for the preparation of artificial sea water...” (Tsurikov 1976: 14).

Since the ice-hosting deposits were formed in the coastal part of the demineralized sea basin (Fotiev 2003), the increased content of hydrocarbonates in the ice as compared to other salts cannot testify to the demineralized nature of the source of ice formation in the light of the abovementioned discussions. Therefore, both abovementioned suppositions are correct only during a relatively short time after ice formation. In the course of time, their salt composition should change significantly as compared to the initial composition of the solution. This degree of the change should be proportional to the salinity of the initial solution. With regard to salt adsorption on mineral admixtures, this easily explains the following fact: “...the solution from clean ice usually has the hydrocarbonate calcium composition, and the chemical composition of the solution from the ice-rich soil is chloride-sodium” (Streletskaya & Leibman 2002: 16).

In addition, we present important facts connected with the movement of a brine drop in the ice as observed in experiments. They can be useful for further study of the salt composition of massive ice. The velocity of drop movement increases with the increase of the molecular weight of the dissolved salt and does not depend on the drop radius (Hoekstra et al. 1965). This velocity increases by orders of magnitude with the temperature approaching 0°C (at the points of drop location), while the drop's size grows (Harrison 1965). The explanation of these facts requires taking into account the deformability of ice as a viscous body (Gorelik & Kolunin 2002). The movement velocity of solid particles in the ice is inversely proportional to their radius (Römken & Miller 1973, Gorelik & Kolunin 2002), and for sand particles it is by several orders of magnitude lower than the velocity of liquid drops of the solution at identical temperature gradients. The external pressure on the ice evidently has some specific impact on the movement velocity of inclusions. Radd & Oertle (1973) note that the movement of clay particles in the ice toward its warm front became visually noticeable after a load was applied to the specimen.

Mechanisms of Tabular Massive Ice Formation

The problem of formation mechanisms of massive ice is still debatable. These mechanisms are divided into two groups: one is based on the constitutional (inter-ground) mechanism, and the other is based on the primarily over-ground origin and consequent burial. Only inter-ground mechanisms of massive ice formation are discussed below. The segregation and injection mechanism is considered to be the most substantiated today. The segregation and injection mechanism, according to G.I. Dubikov (2002), actually means separate participation of the segregation and injection mechanisms either at different freezing stages of the initially thawed ground mass or on its spatially separated parts within the same bed. However, the conditions that trigger both segregation and injection mechanisms have quite strict physical limitations that should be described in connection to real freezing conditions. The essence of the segregation and the injection mechanisms implies that the overlying stratum should continuously move upward in the process of ice bed formation (when freezing from above). In such a process, the pressure from below onto the bottom of the growing bed should be equal to the sum of σ stresses from the overlying ground weight (including the bed itself) and the bending stresses of the frozen stratum that occur as a result of its irregular deformation. The pressure developed from below at the bed bottom is significantly different in its nature for both mechanisms. Thick massive ice strata can be formed only in the conditions close to the stationary ones in the case of the segregation mechanism. This is possible only in an open system when the moisture supply to the ice formation front from the external source is possible. Moreover, two options are possible: with or without ice penetration into the pores of the thawed ground underlying the bed. In the former case, the bed growth occurs if there is a two-phase freezing zone below it (Ershov 1979, Rogov 2009). If the ice grows without the two-phase zone formation, the temperature at

the ice formation front t_i should exceed the temperature of ice penetration into the capillaries of the underlying porous medium t_f . This value can be defined experimentally as the ending temperature of ground thawing. Moreover, the liquid flow should be positive. It follows from these two conditions that the following inequality should be fulfilled for a stable ice growth:

$$\sigma - P_0 < 2 \cdot \sigma_{iw} / R \quad (2)$$

where P_0 is hydrostatic pressure in the supplying water body, $\sigma_{iw} = 3.3 \cdot 10^3 \text{ J/m}^2$ is ice-water surface stress coefficient, R is typical radius of capillaries in the ground underlying the growing ice.

According to the data of multiple observations within Yamal and Alaska, more than two-thirds of all massive ice beds are underlain by sand. This means that for $R \approx 10^{-5} \text{ m}$ and above, the right part of the correlation (2) numerically does not exceed $7 \cdot 10^3 \text{ Pa}$, while the value of the left part cannot be below 10^4 Pa if the thickness of the overlying grounds is at least one meter and if the water level in the external body is not above the ground surface. The formation of massive ice immediately at contact with underlying sand is impossible even in the near-surface ground layers. When there is no two-phase zone, the ice bed growth inside clays is still possible in the way that its bottom is separated from the sand with a thin clay-rich interlayer (e.g., several millimeters thick, so it is hard to see it in borehole core and outcrops). However, this possibility can hardly be fulfilled in reality. Firstly, the thawing temperature of water-saturated clay is very close to zero (Grechishchev 1980). Secondly, the change of the temperature t_i significantly depends on seasonal and climatic temperature fluctuations at the ground mass surface and on the water level fluctuations in the supply water body (Gorelik & Kolunin 2002). It is very possible that such fluctuations occurring during a long-term freezing cycle can cause the reduction of the temperature t_i below the value t_f with irreversible touching of sand by the ice formation front (and its freezing, which leads to the cessation of the migration supply and the ice bed growth). Thirdly, it is hard to imagine a long (tens of meters horizontally) clay-rich interlayer several millimeters thick with no breaks in the form of micro-cracks or folds through which the ice can penetrate into the underlying sand. Based on ideas similar to the ones given above, J. Mackay reached a conclusion as far back as 1979 on the impossibility of massive ice formation with the segregation mechanism (Mackay 1979). This conclusion cannot be changed by means of ice growth examination with a two-phase zone present below the ice formation front. This is because direct calculations of the zone's length for natural freezing conditions (the thickness of the overlying stratum is at least 2 m, the annual mean temperature of the ground mass surface does not exceed -5°C) show that this value cannot be below one meter (i.e., the ice bed should almost always be separated from underlying sands by quite a thick clay-rich interlayer). Therefore, the massive ice formation with the segregation mechanism is highly unlikely in the overwhelming majority of the cases observed.

On the other hand, V.V. Baulin with co-authors came to the conclusion that at the Yamal and the Gydan peninsulas "... the overwhelming majority of large ice formations in

marine and glacial-marine deposits have evident indicators of injection origin" (Baulin et al. 1967: 140). The laboratory simulation of ice accumulation for the injection supply mechanism (Gorelik 2009) shows that many peculiarities of the massive ice texture and composition can be explained based on the injection mechanism of their formation.

Acknowledgements

This work was conducted with the financial support of the Program of Fundamental Research of ESD RAS No 13.

References

- Baulin, V.V., Belopukhova, E.B., Dubikov, G.I., & Shmelev, L.M. 1967. *Geocryological conditions of the West-Siberian Lowlands*. Moscow, Nauka, 214 pp. (in Russian).
- Baulin, V.V. & Chekhovskiy, A.L. 1983. Paleogeographic Pleistocene reconstructions on the basis of permafrost thickness and structure investigation. *Problemy geokriologii*, Moscow, Nauka pp. 177-184 (in Russian).
- Biermans, M.B.G.M., Dijkema, K.M., & de Vries, D.A. 1978. Water movement in porous media towards an ice front. *J. Hydrology* 37: 137-148.
- Dubikov, G.I. 2002. Composition and cryogenic structure of permafrost in Western Siberia, Moscow: GEOS, 246 pp. (in Russian).
- Dubikov, G.I. 1982. Western Siberia massive ice and permafrost paragenesis. *Plastovye ldy kriolitozony*, Yakutsk, SB RAS USSR, pp. 24-42. (in Russian).
- Dubikov, G.I., Badu, Yu.B., & Ivanova, N.V. 1984. Composition and structure of permafrost in Western Yamal. *Laboratory and field permafrost and ice investigations*, Moscow, PNIIS, pp. 27-35 (in Russian).
- Ershov, E.D. 1979. *Moisture transfer and cryogenic structures in dispersed grounds*. Moscow, MGU, 214 pp. (in Russian).
- Ershov, E.D. (ed.). 1984. *Thermophysical ground properties*. Moscow, MGU, 204 pp. (in Russian).
- Fotiev, S.M. 1999. Hydrochemical method of ground paleotemperature estimate on the Arctic coast. *Kriosfera Zemli*, 3, (no. 2):40 – 65 (in Russian).
- Fotiev, S.M. 2003. Massive ice genesis in Yamal marine sediments. *Kriosfera Zemli* 7, (no. 1): 63–75 (in Russian).
- Fotiev, S.M. 1997. Regularities in formation of the ion-salt composition of the Yamal natural waters. *Kriosfera Zemli* 1 (no. 2): 29 – 35 (in Russian).
- Gorelik, J.B. 2009. Simulation of ice accumulation in freezing grounds in case of injected moisture supply. *Kriosfera Zemli* 13, (no. 3): 45 – 53 (in Russian).
- Gorelik, J.B. & Kolunin, V.S. 2002. *Physics and simulation of cryogenic processes in the lithosphere*, Novosibirsk, GEO, 318 pp. (in Russian).
- Grechishchev, S.E., Chistotinov, L.V., & Shur, Yu.L. *Cryogenic physical and geological processes and their forecast*. Moscow, Nedra, 383 pp. (in Russian).
- Harrison, J.D. 1965. Measurement of brine droplet migration in ice. *Journal Applied Physics* 36: 12, 3811-3815.

- Hoekstra, P., Osterkamp, T.E., & Weeks, W.F. 1965. The migration of liquid inclusions in single ice crystals. *Journal Geophysics Research* 70 (20): 5035-5041.
- Jones, D.R.H. 1973. The temperature-gradient migration of liquid droplets through ice. *Journal Crystal Growth* 20: 145-151.
- Kingeri, U.D. & Gudnau, U.H. 1966. *Brine migration in salty ice. Ice and snow*. Moscow, Mir, 214-225.
- Komarov, I.A. & Mironenko, M.V. 2010. Simulation of the water- ion composition for salty permafrost and cryopegs in thermobaric conditions change. Materials of the International Conference “Actual Trends in Applied Mathematics Development in Energetics and Infocomm Technologies”, Moscow: Izd-vo MG TU N.E. Bauman, pp. 23-29 (in Russian).
- Konrad, J.-M. & Morgenstern, N.R. 1982. Effects of applied pressure on freezing soils. *Can. Geotech. J.* 19, 4: 494-505.
- Loseva, S.G., Kharina, M.G., & Kuleshova, V.Yu. 1990. Salinity impact on water-physical and thermophysical ground properties. *Zasolennye merslye grunty kak osovaniya sooruzheniy*, Moscow, Nauka, pp. 24-33 (in Russian).
- Mackay, J.R. 1979. Pulsating pingos, Tuktoyaktuk Peninsula, N.W.T. *Canadian Journal Earth Science* 14 (2): 209-222.
- Radd, F.J. & Oertle, D.H. 1973. Experimental pressure studies of frost heave mechanisms and the growth-fusion behavior of ice. *Permafrost Proceedings* 2nd International Conference at Yakutsk, USSR, July 13-28 1973. Washington, D.C., National Academy of Sciences, pp. 377-384.
- Rogov, V.V. 2009. *Principles of Cryogenesis*, Novosibirsk, GEO, 204 pp. (in Russian).
- Römken, M.J.M. & Miller, R.D. 1973. Migration of mineral particles in ice with a temperature gradient. *J. Colloid Interface Sci.* 42 (1): 103-111.
- Sokolovskiy, V.V. 1969. *Plasticity theory*, Moscow, Vysshaya shkola, 608 pp. (in Russian).
- Streletskaya, I.D. & Leibman, M.O. 2002. Cryogeochemical Interrelation of sheet ice, cryopegs and their host sediments of Central Yamal. *Kriosfera Zemli* 6 (no.3):15-24 (in Russian).
- Thermal regime and water-ice composition forecast for salty grounds and cryopegs. 2007. Problems of construction on salty permafrost. *Epokha*, pp. 148-186 (in Russian).
- Tsurikov, V.L. 1976. *Liquid phase in marine ice*. Moscow, Nauka, 210 pp. (in Russian).
- Tsytoovich, N.A. 1973. *Permafrost mechanics*. Moscow, Vysshaya shkola, 447 pp. (in Russian).

The Change of Geotechnical–Geocryological Parameters of Permafrost Foundations in the Western Sector of Russia’s Cryolithozone by 2050

V.I. Grebenets, A.V. Kislov, D.G. Shmelev

Lomonosov Moscow State University, Faculty of Geography, Moscow, Russia

Abstract

A quantitative simulation of the changes in geocryological and geotechnical parameters for resource-rich cryolithozone regions was completed for the Bolshezemelskaya Tundra, in the north of West Siberia, and the lower reaches of the Yenisey River. The simulation was performed with regard to evaluations of climatic change based on a set of calculation results from eleven models. It was found that for these regions, the worsening of the permafrost-environmental situation and of the geotechnical settings will occur with the estimated non-linear trend of climate warming. The bearing capacity of permafrost foundations will be reduced, and the adverse impact of tangential forces of frost heave and the cryogenic weathering of underground structures will increase. The bearing capacity of existing permafrost foundations may decrease by 2–3 times by the middle of the twenty-first century. Economic development that is associated with the destruction of the protective role of vegetative topsoil covers will be affected. The failure of structures built on the principle of permafrost preservation will occur in more southern regions.

Keywords: bearing capacity; climate; cryolithozone; forecast; foundations, frost heave.

Introduction

Permafrost is one of the most sensitive components of the natural environment of the North. This is due to the fact that the stability of geoecological, geotechnical, and geocryological conditions is primarily defined by the thermal regime of permafrost. Permafrost frequently thaws as a result of surface temperature increase under the impact of global climatic changes or local technogenic effects. Thawing occurs in economically developed areas where naturally protecting moss and peat covers are destroyed during construction. This is accompanied by melting of ground ice, reduction of the bearing capacity of permafrost foundations, the activation of slope processes, landscape changes, and the increase of the seasonal thaw depth (i.e., the zones of active frost heave development and cryogenic weathering of underground structures). Permafrost dynamics (its state, temperature, bearing capacity, seasonal ground thawing, and the activation of cryogenic processes) in urbanized areas is defined by three main factors: 1) geocryological (characteristics and properties of permafrost in the natural state); 2) geotechnical (construction-operational characteristics, type of technogenic impact, intensity, and the area of this impact’s contact with permafrost); 3) time (duration of impact, climatic changes). These factors frequently have non-synchronous and differently directed effects of various scales, and this leads to mosaic-like changes in permafrost.

The stability of geotechnical-geocryological conditions, geoecological settings, and geotechnical medium is to a large extent associated with climatic trends. Permafrost temperature is increased with the trend of climate warming. Consequently, the following phenomena occur: reduction of the bearing capacity of permafrost foundations, an increase of seasonal thawing depths, and, therefore, an increase of the zone within which tangential forces of frost heave adversely influence support structures as a result of active layer freezing. The existing (quite unfavorable) situation with the construction and reliability of structures in the cryolithozone

can get significantly worse if the trend of climate warming in the northern regions of Russia exists through the next decades. This paper will discuss forecasts for changes in important geotechnical-geocryological parameters, such as the bearing capacity of permafrost foundations and tangential forces of frost heave that influence support structures due to active layer freezing.

Methods

Changes in geotechnical-permafrost conditions of the Bolshezemelskaya tundra, in the north of West Siberia, and in the lower reaches of the Yenisey River were simulated. These are the cryolithozone regions with the maximum resource potential and a high degree of development. Changes of the geotechnical and the geotechnical-geocryological situation by 2030 and 2050 were predicted. The simulation output data included the depth of the seasonally thawed layer (or the depth of seasonal freezing for the territory where permafrost will thaw as a result of climate warming), the temperature within the depth of the foundation, the value of the bearing capacity of a permafrost pile, and the value of tangential forces of frost heave affecting the supports.

The research territories were divided into polygons $2 \times 2^\circ$ in size. Zonal landscapes were defined within them. All design values were estimated for the centers of these polygons. The Bolshezemelskaya tundra was divided into 16 polygons, $54\text{--}60^\circ\text{E}$, $66\text{--}68^\circ\text{N}$, typical tundra, and $64\text{--}66^\circ\text{N}$, southern tundra, forest tundra, and northern taiga. In northwestern Siberia there were 45 polygons, $62\text{--}74^\circ\text{N}$, $62\text{--}80^\circ\text{E}$. The lower reaches of the Yenisey River included 25 polygons, $80\text{--}90^\circ\text{E}$, $62\text{--}74^\circ\text{N}$, northern taiga, forest tundra, southern tundra, and typical tundra.

Three types of ground were investigated for all territories: clayey silt, sand, and peat covering the mineral ground (sand or sandy silt/clayey silt ground depending on regional peculiarities). The Polar Urals and the western branches of the Putoran Tableland were excluded from the analysis because in these mountain regions the permafrost conditions

play quite a subordinate role in construction of foundations supported on bedrock.

The estimate of the change in climatic resources by the middle of the twenty-first century (2046–2065) was completed based on calculation results from eleven climatic air, ocean, and dry-land interaction models: CCSM3 (USA), CGCM3.1 (Canada), CNRM-CM3 (France), CSIRO-Mk3.0 (Australia), ECHAM5/MPI-OM (Germany), GFDL-CM2.0 (USA), GFDL-CM2.1 (USA), MIROC3.2 (Japan), MRI-CGCM2.3.2A (Japan), PCM (USA), and INM (Russia). These were for the A2 scenario of polluting emissions into the air reflecting the least favorable anthropogenic human impact on the environment from the ecological point of view (Kislov et al. 2008, Strategic Forecast... 2005). The years 1961–1990 were assumed to be the “baseline” period for change estimates in accordance with the recommendations of the World Meteorological Organization.

Input geocryological conditions represented individual values of active layer depth and temperature at the depth of zero annual amplitude for 2000 for each division and each type of permafrost (in addition to the physical characteristics noted above). The temperature change depended on the depth of geotechnical development as well as the thickness of the active layer estimated for polygon centers by means of a solution of one-dimensional, non-stationary heat conductivity problems (with regard to Stephens condition). This allowed for quantitative estimates of the change in bearing capacity and tangential forces of frost heave by 2030 and 2050 as a result of the occurrence of the estimated climate warming model; according to the methodology suggested in SNiP 2.02.04–88 (SNiP 1990).

The bearing capacity of a frozen reinforced concrete pile with a square section 30x30 cm buried up to 10 m from the surface and installed with drilled-shaft technology, was estimated as the object for each polygon. Such pile types are widely used in cryolithozone settlements. For example, more than half of all buildings and structures are erected on similar foundations in the towns of the Norilsk industrial district (tens of thousands of piles). Metal pile-pipes 219 mm in diameter, buried to a depth of 8 m, were selected for the assessment of the adverse impact of the tangential forces of frost heave that influence the supports of these structures. Such piles are widely used for aboveground placement of main gas pipelines in northwestern Siberia.

Results

Estimates for the thermal ground regimes and changes in bearing capacity were completed (Vyalov et al. 1993) for two options of climatic warming (trend 0.033°C/yr and 0.066°C/yr). They showed that the permafrost temperature in northwestern Siberia could increase by 0.1–3.3°C by the middle of the twenty-first century, depending on geological-geographical conditions. Taliks will occur in the southern districts.

The problem of changes in permafrost conditions for different climatic scenarios has remained the focus of geocryological investigations during the recent 15–20 years. The works of Khrustalev & Shumilishskii (1997) and Khrustalev & Davydova (2007) showed that changes of air temperature and snow accumulation conditions

significantly influence the bearing capacity of building bases and structures. It is assumed (Ershov 1997, Pavlov & Gravis 2000) that by 2050, an air temperature increase of 1–5°C, a ground temperature increase of 1–2°C, and a seasonal thaw layer depth increase of 10–40% will occur. Thawing of island permafrost in the southern cryolithozone regions is possible.

It is noted that climate warming has already led to an increase of permafrost temperature. Romanovskiy et al. (2010) estimate that permafrost temperature has, in general, increased by 0.5–2.0°C at the depth of zero annual amplitude during the recent 20–30 years for Russia’s cryolithozone. The range of ground temperature change for the Russian North is from 0.004 to 0.05°C/yr (Pavlov & Malkova 2009).

The response of permafrost to climate warming can be more complicated. It is possible that the protective role of vegetative covers will intensify with the increase in air temperature and the amount of summer precipitation. This can lead to the preservation and even strengthening of permafrost conditions. The ice-rich transient layer under the bottom of the seasonally thawed layer, which requires greater energy consumption for phase changes, can hinder permafrost thawing as well (Konishchev 2009). However, the forecast results given below are in reference to the urbanized medium or linear structure building zones (i.e., to the areas where the protective vegetative topsoil cover is actually destroyed in the process of construction).

Climate warming causes the development of trends in permafrost degradation:

- The bearing capacity of permafrost foundations falls. The freezing forces (i.e., the shear strength R_{af}) decrease with the increase of permafrost temperature, and the freezing area A_{af} declines with the increase of the seasonal thaw depth.
- The seasonal thaw depth d_{th} increases. The impact zone of tangential forces of frost heave occurring during its freezing period (second half of autumn to beginning of winter) becomes greater.
- An increase of precipitation, primarily of snow accumulation, causes slower freezing of the seasonally thawed layer and an increase of ice formation within the seasonally thawed layer. Moisture has enough time to migrate to the freezing front; schlieren cryogenic structures are formed in fine-grained varieties, causing the intensification of tangential forces of frost heave.

The change in main geotechnical-geocryological parameters due to climate warming in the western sector of the Russian cryolithozone is to a large extent associated with the cryolithological peculiarities of the area.

The calculation results for the change in geotechnical-geocryological parameters are given in the form of cartographic images in Figures 1–6.

Figures 1 and 2 show that a quite noticeable reduction from 5–8% to 20–25% of the bearing capacity of permafrost pile foundations will occur in the European Northeast. In the more southern part, permafrost will thaw in the geotechnical development zone (the upper 10 m), and failure of the structures will occur.

Meanwhile, the frost heave forces can grow by 30–100%. This all can lead to the development of deformations of existing buildings and structures. In 20–25 years this will

Bolshezemelskaya tundra. Change of the bearing capacity in 2000-2050

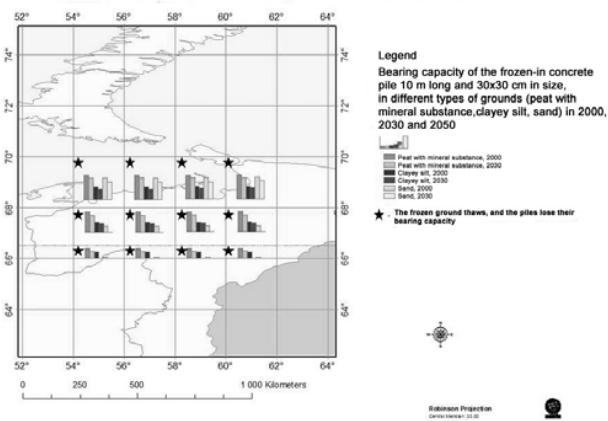


Figure 1. Change of the bearing capacity of a single typical permafrost pile with the climate warming trend preserved (2000–2050) in the Russian European North.

Bolshezemelskaya tundra. Change of frost heave tangential forces in 2000-2050

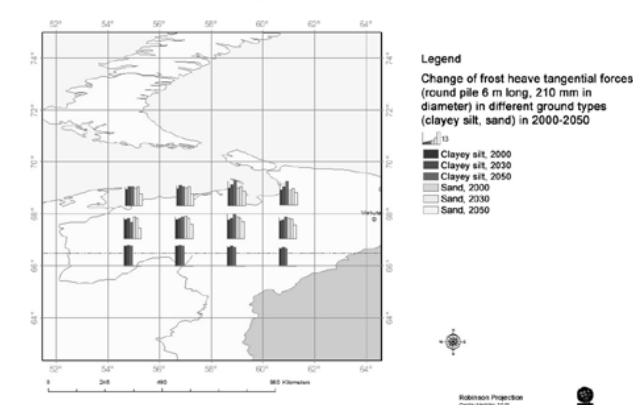


Figure 2. Increase of tangential forces of frost heave influencing the standard metal supports of aboveground structures with climate warming trend preserved (2000–2050) in the Russian European North.

also complicate the construction and operation of newly installed foundations. It will necessitate several measures, including:

- wider application of expensive pre-construction amelioration,
- installation of anti-filtration systems to a great depth in the process of drilling within the increasing seasonally thawed layer,
- an increase of the thickness of the filling layer under motor and rail roads,
- use of more expensive heat-insulating materials in the filling subgrade,
- installation of special protection against the “frost destruction” of the material of underground structures to a greater depth within the seasonally thawed layer.

Figures 3 and 4 clearly show that a significant worsening of the geotechnical-geocryological situation is possible for northwestern Siberia, and even a catastrophic worsening in the most developed gas production districts (Tazovskoe, Novy Urengoy, and Nadym) and oil production districts (Vankor). Possible effects include a reduction of the bearing capacity of foundations by many times and a noticeable

Western Siberia. Change of the bearing capacity in 2000-2050

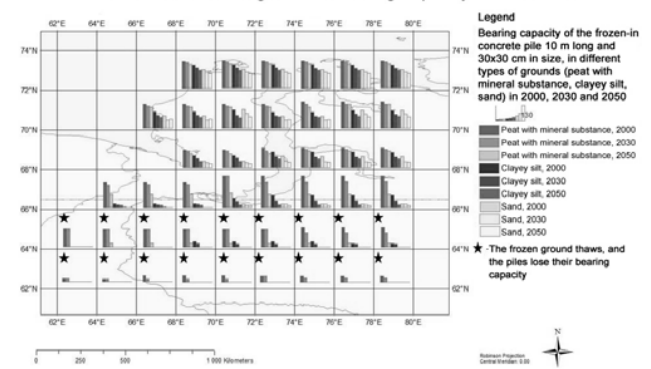


Figure 3. Change of the bearing capacity of a single typical permafrost pile with the climate warming trend preserved (2000–2050) in the West Siberian North.

Western Siberia. Change of frost heave tangential forces in 2000-2050

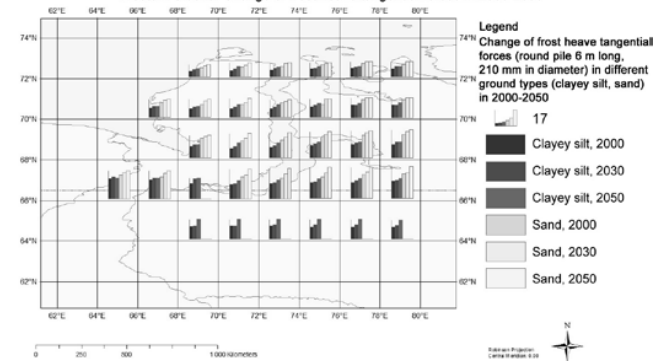


Figure 4. Increase of tangential forces of frost heave influencing the standard metal supports of aboveground structures with climate warming trend preserved (2000–2050) in the West Siberian North.

increase of the adverse impact on low-loaded frost heave supports. The geotechnical situation predicted for the nearest 20–40 years will worsen less in more northern regions (e.g., at the potential Bovanenkovo gas and condensate field and other regions located in northern Yamal). However, increases in the seasonal thaw depths in these regions can provoke an abrupt activation of thermokarst and thaw slumps, which will intensify the destruction of roads, pipelines, and other structures.

Figures 5 and 6 show that the change in geotechnical and geocryological parameters by 2030 and 2050 (should climate warming occur according to the forecast) will cause significant (mainly in the southern cryolithozone) worsening of the reliability of geotechnical bases in the Yenisey North. It should be noted that by 2030 permafrost will be preserved south of 68° only in ground peated from the surface, and it will almost disappear in the geotechnical development zone (the upper 10 m) by 2050. Consequently, the calculation of geotechnical parameters for these periods was not performed. However, a deep seasonal freezing depth will cause a sharp increase of tangential heave forces. The calculations show that the bearing capacity in the most northern districts can be reduced by 5–15% by 2030 and up to 30% by 2050. At the same time, it will, by 2050, be reduced by 30–40% in the peaty ground and by 2–3 times in sands and clayey silts in the Norilsk region. The tangential forces influencing the supports can increase by 20–30%

Lower reaches of the Yenisey River. Change of the bearing capacity in 2000-2050

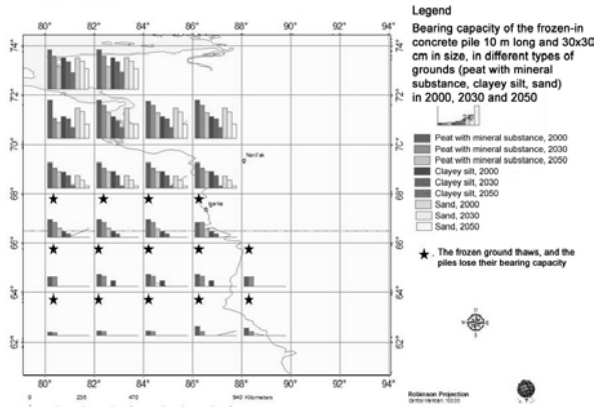


Figure 5. Change of the bearing capacity of a single typical permafrost pile with climate warming trend preserved (2000–2050) in the Yenisey North.



Figure 7. Deformation in the first housing estate of Igarka (July 2010) due to the reduction of bearing capacity of the permafrost piles.

Lower reaches of the Yenisey River. Change of frost heave tangential forces in 2000-2050

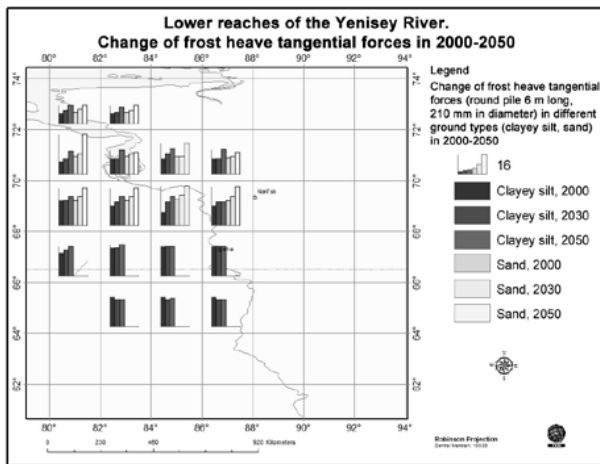


Figure 6. Increase of tangential forces of frost heave influencing the standard metal supports of aboveground structures with climate warming trend preserved (2000–2050) in the Yenisey North.



Figure 8. Housing at Laureatov Street in Norilsk. Irregular settlement of permafrost piles due to the warming and partial thawing of the surrounding permafrost, August 2009.

(maximum in silty sands) in the North by 2050 and by 1.5–2 times in the most southern regions.

In recent decades, the development of significant structural deformation is noted in many industrial regions and villages of the Far North (Kronik 2001, Grebenets 2003, Grebenets 2007). This is associated with the worsening of the geotechnical-geocryological situation. The most significant intensification of the deformation of structures is associated with a specific “warm” period during the recent 20 years and also with negative technogenic impacts (Figs. 7, 8).

Monitoring the stability of geotechnical systems in different permafrost regions shows that more than half of the industrial and municipal development areas currently have violations of geocryological and geocological conditions.

Discussion and Conclusions

Risks and damages caused by failures of structures on permafrost will increase by the middle of the 21st century as a result of climate warming in the western sector of Russia’s cryolithozone. This can become a serious social and economic problem. It can reduce the efficiency of the heat-energy, metallurgy, and lumber industries and lead to the

destruction of the transportation system, including the main pipelines in northwestern Siberia. This occurs at the time of a noticeable weakening of the requirements for monitoring the geotechnical-geocryological situation and the technical control of buildings and structures.

There are several reasons for deformations: 1) global or regional climate changes and unpredicted development of hazardous geotechnical-cryogenic processes under the impact of technogenesis or permafrost warming; 2) different errors and violations in the investigation, design, construction, and operation processes; 3) worsening of the socioeconomic situation in the northern regions.

It is evident that with climate warming in the studied cryolithozone regions, the risk to structures will increase. Risks and damages are caused by deformations of structures associated with irregular ground settling due to thawing or warming. The bearing capacity of permafrost foundations is reduced with ground heaving or foundation jacking and with the cryogenic destruction of the material of underground structures.

Noticeable winter warming during the recent 20–30 years in the western sector of Russia’s cryolithozone reduces the efficiency of various seasonal cooling units (cold ventilated cellars and channels, liquid and vapor-liquid heat units) that are applied for the preservation of foundations in the permafrost state. Should climate warming occur according to the forecast, the adverse effects of the reduction of the

bearing capacity of permafrost pile foundations and the increased impact of frost heave on pipeline supports cannot be neutralized by existing (already installed in-structure) geotechnical methods.

Numerous deformations of buildings and structures in the Far North could become a reason for depopulation and deferred development of the region.

A strategy of rational economic development of the cryolithozone should be worked out based on the estimate of the change of geocryological conditions under possible climate warming.

Acknowledgments

This work was completed with the support of the following programs: Support of Russia's Leading Scientific Schools, NSh – 3271.2010.5; CALM (NSF–OPP–0352958).

References

- Construction norms and rules. Bases and foundations on permafrost, 1990. SNiP 2.02.04–88, TsiTP Gosstroya SSSR, Moscow, 71 pp. (in Russian).
- Ershov, E.D. 1997. Permafrost degradation in case of possible global climate warming. *SOZh*, No 2, pp. 70–74 (in Russian).
- Grebenets, V.I. 2007. Deformation of structures in the cryolithozone in case of unpredicted changes of complex geotechnical–geocryological bases conditions *Inzhenernaya geologiya*, September, 17–20, 2007 (in Russian).
- Grebenets, V.I. 2003. Geocryological–geoecological problems occurring in urbanized territories in Northern Russia and methods for improvement and restoration of foundations. *Proc. of the Eighth International Conference on Permafrost*. Philips, M., Springman, S. & Arenson, L. (eds.) Zurich, pp. 3003–3009.
- Khrustalev, L.N. & Davydova, I.V. 2007. Climate warming forecast and its consideration for the evaluation of the buildings bases reliability on permafrost. *Kriosfera Zemli* 11 (no. 2): 68–75 (in Russian).
- Khrustalev, L.N. & Shumilishskii, M.V. 1997. Consideration of temperature variation in determining the bearing capacity of permafrost beds. *Osnovaniya, Fundamenti i Mekhanika Gruntov* 34(5): 24–26.
- Kislov, A.V., Evstigneev, V.M., Malkhazova, S.M., Sokolikhina, N.N., Surkova, G.V., Toropov, P.A., Chernyshev, A.V., & Chumachenko, A.N. 2008. *Forecast of climatic resource provision of the Eastern European plain in the warming conditions of the XXI century*. Moscow: Maks–Press. 292 pp. (in Russian).
- Konishchev, V.N. 2009. Permafrost response to climate warming. *Vestnik Mosk. Un–ta*, ser. 5. Geografiya, No 4, 10–19 (in Russian).
- Kronik, Ya.A. 2001. Accident rate and safety of natural–technogenic systems in the cryolithozone. *Materials of the Second Conference of Russia's Geocryologists, Vol. 4 Inzhenernaya Geokriologiya*, Moscow: Izd–vo MGU, pp. 138–147 (in Russian).
- Pavlov, A.V. & Gravis, G.F. 2000. Permafrost and modern climate. *Priroda*, No 4, 12–21 (in Russian).
- Pavlov, A.V. & Malkova, G.V. 2009. Small–scale mapping of current ground temperature change trends in the north of Russia. *Kriosfera Zemli* 13 (no.4): 32–39 (in Russian).
- Romanovskiy, V.E., Smith, S.L., & Christiansen, H.H. 2010. Permafrost Thermal State in the Polar Northern Hemisphere during the International Polar Year 2007–2009: a Synthesis. *Permafrost and Periglacial Processes* 21: 106–116.
- Strategic forecast of climate changes in the Russian Federation for the period till 2010–2015 and their impact on the branches of Russian economy*, 2005. Moscow: Rosgidromet, 28 pp. (in Russian).
- Vyalov, S.S., Fotieva, C.M., Gerasimov, A.S., & Zolotarev, A.I. 1993. Provision of permafrost bearing capacity in climate warming conditions. *Osnovaniya, Fundamenti i Mekhanika Gruntov* No. 6, 2–7 (in Russian).

The Study of Exogenic Permafrost-Related Geological Processes along the Yuzhno-Russkoe-Beregovoe Road

A.A. Gubarkov

Tyumen State Oil and Gas University, Tyumen, Russia

M.V. Andreeva, E.M. Elantsev, A.V. Khomutov

Earth Cryosphere Institute, SB RAS, Tyumen, Russia

Abstract

Monitoring of exogenic geological processes along the 68-km Yuzhno-Russkoe-Beregovoe (Pur-Tazovskoe watershed) road was conducted. Structures for erosion-control and water diversion, including culverts, were examined. Recently built structures for control of flooding, erosion, and thermal erosion within the road shoulders and the embankment slopes also were studied. This paper summarizes the efficiency of structures built in 2009 and presents observations of solifluction, thermokarst-related subsidence, and thermal erosion (denudation).

Keywords: culverts; embankments; erosion-control; exogenic geological processes; roadbed; thermal erosion.

Introduction

The Yuzhno-Russkoe-Beregovoe road is located in the zone of continuous permafrost. Site investigations, design, and construction of roads on permafrost include analysis of the geocryological conditions. Permafrost-related geological processes are responsible for the most unfavorable road construction and operational conditions. Construction on permafrost is referred to as the most complex (III and IV) categories (Aid... 1985, VSN-195-83, VSN 26-90). It is prohibited to cut unstable slopes composed of category III and IV soils prone to thaw settlement in order to avoid development of thaw flows, landslides, solifluction and thermokarst. When designing bridges and culverts, water diversion structures should be built to prevent backing up of runoff in the upper part of the structure, especially in areas where culverts are underlain by ice-rich soils (Manual... 1985).

Previous Studies

Information on geocryological conditions and the occurrence of exogenic geological processes, including permafrost-related ones, in the study area, is provided in several monographs (Ershov 1989, Baulin 1985). The Yuzhno-Russkoe-Beregovoe road was constructed in the Pur-Tazovskaya geocryological region (Gruzlov et al. 1989). The studied portion is located in the continuous permafrost zone, with permafrost temperatures ranging from -2°C to -4°C . The studied section of the road is divided into the western and eastern parts according to the drainage conditions, which, in many respects, determine the types of exogenic geological processes. The eastern part of the study area is characterized by poor drainage conditions. It is flooded in spring and partially flooded during summer and fall. Moreover, a large number of thermokarst lakes are located in the eastern part. The western part is heavily dissected by gullies and valleys of small and medium-size streams. It is less comparable to the eastern part, affected by thermokarst and muskeg formation.

Long-term geocryological monitoring results, which are available for adjacent territories, show that exogenic

geological processes have an impact on hydrocarbon field development in the region. Human-induced disturbances of the permafrost environment cause changes both in the geotechnical systems and in the adjacent natural complexes (Drozdov 2004, Moskalenko 2006, and others). It was determined that in the course of hydrocarbon field development, thermokarst and frost heave (i.e. permafrost-related geological processes and muskeg formation) are the main exogenic geological processes within the flat and poorly drained territories (Melnikova & Grechishcheva 2002, Ponomareva 2010). Erosion and thermal erosion actively develop within uneven terrain that has considerable slope inclinations and lengths, and in areas underlain by sandy and silty soils (Gubarkov et al. 2011).

Widespread hazardous exogenic geological processes in the region require regular monitoring. The monitoring results should be used for the development of control measures, design solutions, and construction of special structures that prevent or eliminate impacts of the hazardous exogenic geological processes. For example, depending on the type of water body, a specific type of control structure is selected to prevent hazardous impact of the water body on a geotechnical system.

Culverts, water diversion, and drainage structures

Water diversion channels and drainages are usually constructed in summer and autumn. Water diversion structures are designed to eliminate flooding of the construction objects by rain and melt waters (Manual... 1985). Minor artificial structures are installed in muskeg areas in order to avoid long-term ponding and spreading of muskeg over the adjacent dry areas. The structures are placed without calculations because it is hard to determine surface flow in muskegs. The structures are spaced at 300 to 500 m intervals, but there is at least one structure per each muskeg crossed (VSN-195-83). These measures also prevent development of slope processes and deforestation caused by flooding of the area. Protection of the road from gully erosion, landslides, and washout is provided by a complex of measures that include special grass planting combined with a series of geotechnical engineering measures (VSN 26-90).

Peat and peat-sand blends with grass planting, soils supported with cementing components (cement and oil), geotextiles, prefabricated gratings, concrete slabs, and other means are used for slope support. These means are stipulated in the corresponding standard documents of typical structures (VSN 26-90). The specific natural conditions of the construction area, slope flooding conditions, and the availability of local construction materials should be taken into account when selecting a slope support structure. The proposed support structure should ensure protection of the slope surface from erosion both in the course of road construction and during its operation, and provide for the minimum maintenance cost.

There are many slope reinforcement methods that utilize various materials. Volumetric geogrids are among the most widely developed and promising materials used in West Siberia. They consist of heat-welded polymer strips, which form a cellular structure (Matveev & Nemirovskiy 2006). For facilities being built in the northern part of West Siberia, frost resistance of the geogrids is very important. Frost resistance of the geogrids has been confirmed by more than 30 years of road operation in Alaska (Sannikov 2004). In 2000–2001, roads were constructed with the use of geogrids in the Zapolyarnoe gas field, based on foreign experience (Korobkov 2004). The slopes were reinforced by geogrids filled with a peat-sand blend, whereas drainage ditches and shoulders were reinforced by geogrids filled with crushed stone. Experience shows that geogrids successfully stabilize sliding and erosion processes caused by seasonal ground freezing and thawing (Chelobitchenko 2006).

Bridge crossings and culverts

The use of culverts on permanent or intermittent watercourses is allowed only if special icing control measures are provided. Bridges or structures with half-open cross-section are required for permanent or intermittent watercourses. They do not alter the thermal regime below stream channels and ensure non-pressure water flow. Conduits made of corrugated metal, at least 1.5 m in diameter, and steel pipes 1.42 m in diameter or in some cases 1.22 m in diameter can be used at stream crossings on regularly freezing watercourses with estimated flow rates of up to 30 m³/sec (VSN 26-90).

Research Methods

The methods of investigation for permafrost-related geological processes in the permafrost zone were developed by leading geocryologists (Grechishcheva 1979, Kudryavtsev et al. 1979, Methods... 1986, Pavlov 2008, and others). The methods of investigation of exogenic geological processes along linear structures are discussed in a number of publications (Korolev 2007, Pendin, 2009, and others). The monitoring of exogenic geological processes along roads included interpretation of the remote sensing materials and field studies. The remote sensing methods consisted of the interpretation of medium- and large-scale satellite imagery and aerial photography. Linear and aerial parameters of flooding, as well as characteristics of thermal erosion and thermal denudation were determined. In August 2009, field observations, characterization of key

sites, and measurements of morphological parameters of the hazardous exogenic geological processes and landforms were conducted along the Yuzno-Russkoe-Beregovoe road and in adjacent areas. The impact of exogenic geological processes on the road was documented. Types of processes and landforms were identified or reconstructed on the basis of indirect terrain indicators. Mitigation methods were selected. A comparative analysis of flooding zones along the road, which were identified in 2004–2007 and after the road upgrade in 2009, was conducted. The efficiency of erosion- and flood-control structures was evaluated. Two main tasks were solved at the fieldwork stage: 1) visual examination of the areas adjoining the road, both natural undisturbed terrain and human-disturbed areas; and 2) identification of sites along the road where hazardous exogenic geological processes develop.

Results and Discussion

Observations conducted in 2004–2009 and air photos taken in 2008 showed that the following exogenic geological and permafrost-related processes developed in the study area: seasonal and long-term frost heave, thermokarst, muskeg formation, and fluvial erosion. Most of the exogenic geological processes are inactive. No active slope processes with the ruptured vegetative-topsoil cover were observed in natural conditions during the 2009 monitoring period. Poor occurrence of slope and erosional processes in natural conditions of the Yuzhno-Russkoe field is the result of the widespread forest that protects the ground surface with well-developed, multi-layered covers, most importantly grass, moss, and lichen covers underlain by a thick peat layer. Though the area of research is located within the continuous permafrost zone, at the regional scale, permafrost is discontinuous, with open and closed taliks, and is characterized by a two-layered vertical structure. At the local scale, both permafrost degradation and permafrost aggradation are possible depending on the surface conditions. A total of 140 occurrences of hazardous exogenic geological processes (Table 1) were identified in 2004–2008 between 0.0 km and 68 km of the Yuzhno-Russkoe-Beregovoe road. Only 10 of the occurrences were still active in 2009. In 2004–2009, isolated occurrences of exogenic geological

Table 1. Number of the exogenic geological process occurrences and landforms documented in 2004–2009 between 0.0 km and 68 km of the road (between the Yuzhno-Russkoe oil-gas field and the Beregovoe gas-condensate field).

No	Exogenic geological process	2004-2008	2009
1	Erosion and thermal erosion	76	1
2	Solifluction and thaw slumping	18	1
3	Flooding	44	6
4	Frost heave and differential settlement	No accurate data	2
5	Thermal denudation	2	0



Figure 1. The 2009 construction of erosion- and landslide-control structures using geogrid.



Figure 2. Erosion-control structure with a geogrid filled with crushed stone. Photo taken in 2010.

processes were documented at 104 sites. At 16 sites, the processes formed paragenetic complexes consisting of a dominant process and one or several associated processes.

Thermal erosion was eliminated at all sites with special erosion-control structures made up of geogrid (Figs. 1, 2). In 2009, erosion in the form of a small recently formed gully was noted at one site only.

According to the results of the 2004–2007 investigations, widespread areas (several hundred meters across) of partial flooding (38) were mapped. Small areas of partial flooding (see Table 1) identified in 2009 did not exceed 10–20 m in length.

In 2009, active solifluction was observed at the base of a slope at one site in the form of a small lobate feature. In total, 18 features were observed. These features were associated with the process of solifluction and sliding of saturated soil within the road construction right-of-way. Solifluction was most actively developed during the construction period and the initial operational period prior to the road upgrade.

In 2009, differential frost heave and thaw settlement of the road embankment were observed at two small sites. Between 2004 and 2007, these processes were ubiquitous along the entire 68-km section of the road.

Thermal denudation processes were identified at two

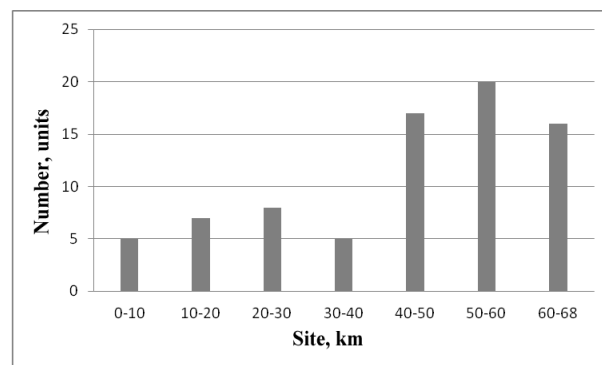


Figure 3. Erosion, thermal erosion, and talus and fluvial fans distribution along the Yuzhno-Russkoe-Beregovoe road.

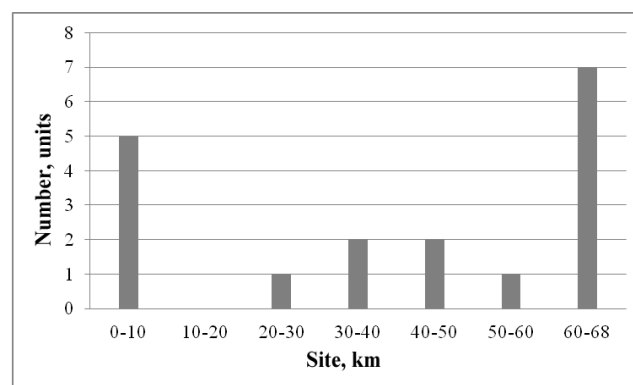


Figure 4. Distribution solifluction and thaw slumping on slopes adjoining the road.

sites composed of ice-rich soil. Thawing of ground ice and movement of the thawed soil downslope resulted in ground surface settlement up to 0.8 m across an area of several hundred square meters.

Analysis of monitoring results shows that erosion was the dominant exogenic geological process before 2009 (see Table 1). The previous monitoring results confirm that as well (2004–2008). By 2009, erosion was brought under control. Talus and fluvial fans that are widespread along the road indicate that erosion and thermal erosion are active prior to the road repair. The fans extend for hundreds and thousands of square meters. Erosion-control structures hundreds of meters long were installed upslope from fans. The number of erosion occurrences and associated erosion-control structures tends to increase from 0.0 km to 68 km on the road (Fig. 3).

The processes associated with the occurrence of solifluction and thaw slumping on slopes are the result of ground surface leveling during road construction. The increase in solifluction development and thaw slumping was influenced by the technogenic transformation of the ground surface. This transformation had an impact on the vegetative-topsoil cover, the active layer, and the uppermost permafrost layer. The area of slopes adjoining the road, where the works were completed, is an important factor as well. An increase in solifluction development occurs as a result of the removal of the vegetative-topsoil cover within large areas on the slopes. Widespread erosion and thermal erosion as well as slope undercutting by concentrated water flows were other factors for the increase in solifluction development. All occurrences

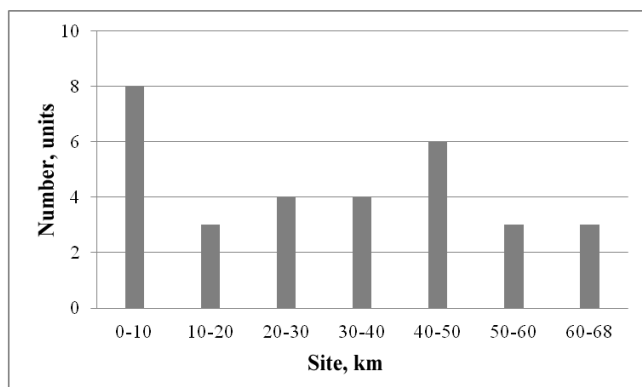


Figure 5. Distribution of flooded sites in 2004–2008 and culverts under the roadbed and along the road in 2009.

of solifluction and thaw slumping were observed at the surfaces underlain by ice-rich or saturated soils. These are usually slopes adjacent to the shoulders. Initial and re-occurring solifluction and thaw slumping-affected areas account for up to several thousand square meters at some work sites. In 2009, the slope processes were most active between 0.0 and 10 km and between 60 and 70 km on the road (Fig. 4). This is associated with soil lithology, ground ice content, and slope.

Large-diameter culverts were installed in the road embankment at 32 of 38 of the largest partially flooded sites that were identified in 2004–2007. At 6 more sites, drainage was promoted along the road in channels reinforced with geogrids and crushed stone. Consequently, backwaters were drained and the area dried out. Minor flooding zones (see Table 1) identified in 2009 did not exceed 10–20 m in length and did not pose any hazard to the road.

Only one partially flooded elongated area 280 m long remained in 2009 of formerly widespread partially flooded zones, each of which was several hundred meters long. The persistence of that last remaining flooded area is associated with the road crossing a muskeg located within an erosional-thermokarst valley. The shoulders are partially flooded due to the settlement of soil characterized by low bearing capacity, as well as high ground water level. Two more sites are characterized by regular flooding in spring and muskeg development in summer and autumn. Stunted and dead vegetation on the currently dry or drained surface at several sites along the road sites indicates former flooded conditions. Culverts were installed at 32 partially flooded sites. The surface of the sites is dry now, and no evidence of flooding was observed. The culvert distribution at the sites (Fig. 5) shows which sections of the road were mostly affected by flooding prior to drainage work in 2009. The muskeg portion of the road between 0.0 km and 10 km is the most flooded. At other sites, the distribution of flooded sites along the road is more regular.

The total number of culverts under the roadbed is shown in Figure 6. Elimination of possible flooding sites by means of culvert installation under the roadbed decreases from west to east. The terrain elevations on watersheds grow in this direction from 50–60 m to 60–80 m. The elevation amplitude between watersheds and water levels in river channels has the same trend (i.e. it changes from 20–30 m in the east to 30–40 m in the west). The number of culverts

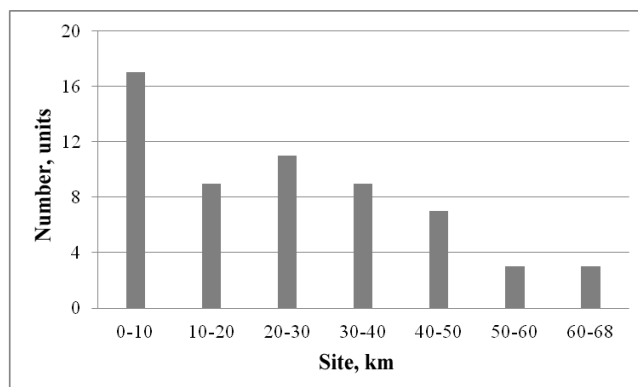


Figure 6. Culvert distribution under the roadbed.

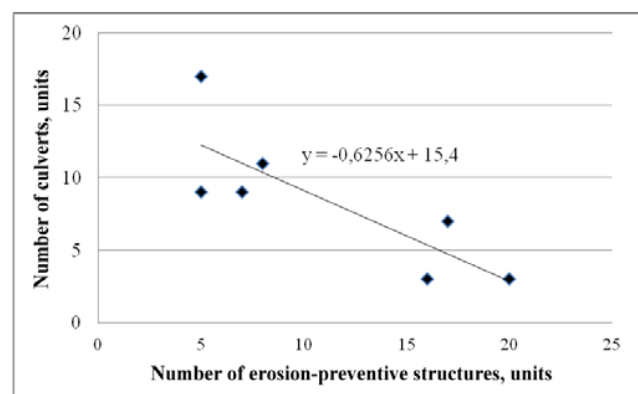


Figure 7. Dependence between culverts under (across) the motor roadbed and open erosion-preventive structures along it.

under the roadbed decreases westward with the increase of the number of deeply incised river and creek valleys. This is associated with an increase of the relief potential that improves drainage capabilities along the road and with subsequent runoff of water under bridge crossings.

The improvement of water runoff conditions along the motor road increases the potential of erosion and thermal erosion processes. Thermal erosion does not occur at partially flooded sites. The number of culverts under the roadbed in the case of flooding (Fig. 6) and the number of erosion-control structures (Fig. 3) at the sites with occurrences of thermal erosion are inversely proportional (Fig. 7).

A comparison can be made with natural conditions in the permafrost zone, where gully erosion (thermal erosion) and lake formation (thermokarst) are inversely proportional (Voskresenskiy 2001, Gubarkov 2009). An inversely proportional relationship between partial flooding (the analogue to lake formation) and human-induced gully erosion (the analogue to gully erosion) exists under the human-transformed conditions of the Yuzhno-Russkoe-Beregovoe road.

Conclusions

- 1) In 2004–2008, erosion and thermal erosion were the most prevalent hazardous geological processes along the Yuzhno-Russkoe-Beregovoe road. A sharp increase in erosion and thermal erosion occurred during construction of the road and at the beginning of its operation. From 5 to 20 erosion and thermal erosion

occurrences were identified for each 10-km section of the road in the form of gullies up to several hundred meters long. They are distributed in conformity with the terrain dissection associated with the depth of incision, the inclinations of river valley slopes, and the slope lengths.

- 2) The process of solifluction and slumping of the thixotropic soils was identified on the slopes adjoining the road. The distribution of this process has no clear spatial dependence associated with road construction. The increase in development of solifluction is influenced by the surface inclination and technogenic impact on the vegetative cover, topsoil, and on the properties of the thixotropic soils that often have high ice content.
- 3) In 2009, flooded areas were eliminated at all sites with the help of culverts installed in the road embankment. Erosion-control structures and culverts were also installed in ditches reinforced with geogrids.
- 4) In 2009, all occurrences of erosion and thermal erosion were eliminated. This should completely prevent their impact on the road in the future. Simultaneously the slopes adjoining the most erosion-prone sites were reinforced. This also averts the hazard of solifluction and sliding of thixotropic soils.
- 5) Exogenic geological processes characteristic of natural conditions exist in the human-transformed northern taiga. Erosion and thermal erosion are inversely proportional to lake development in natural conditions and with flooding in human-transformed conditions.

References

- Baulin, V.V. 1985. *Permafrost in oil-gas production regions of the USSR*. Moscow: Nedra, 176 pp. (in Russian).
- Chelobitchenko, S.A. 2007. *Calculation methodology and structural-process decisions for the roadbed on permafrost reinforced with volumetric geogratings*. Candidate of Sciences Dissertation. Moscow, 18 pp. (in Russian).
- Drozdov, D.S. 2004. *Information-cartographic modeling of natural-technogenic media in geocryology*: Author's abstract of the Doctor of Sciences (Geology and Mineralogy) dissertation. Tyumen, 49 pp. (in Russian).
- Ershov, E.D. (ed.). 1989. *USSR Geocryology. Western Siberia*. Moscow. Nedra, 454 pp. (in Russian).
- Grechishcheva, S.E. (ed.). 1979. *Methodological recommendations for stationary investigation of cryogenic physical-geological processes*. 1979. Moscow.: VSE-GENGEO, 72 pp. (in Russian).
- Gubarkov, A.A. 2009. *Interrelation of hydrological and cryogenic processes in minor river basins and at the Kara Region coast*: Candidate of Sciences Dissertation. Tyumen, 18 pp. (in Russian).
- Gubarkov, A.A., Aleshin, G.A., Idrisov, I.R. & Kirillov, A.V. 2011. Exogenous geological processes monitoring at the Zapolyarye - Novy Urengoy main gas pipeline. Tyumen, *Izvestiya vuzov. Neft i gaz*. No 3, 7-13 (in Russian).
- Khrustalev, L.N., Parmuzin, S.Yu., & Emelyanova L.V. 2011. *Northern infrastructure reliability in the changing climate conditions*. Moscow: Universitetskaya Kniga, 260 pp. (in Russian).
- Korobkov, N.F. 2004. *Erosion-preventive protection of embankment slopes and flanks in the cryolithozone with the use of geosynthetic gratings. The case of the Yamal-Nenets Autonomous District*: Candidate of Sciences Dissertation. Tyumen, 18 pp. (in Russian).
- Korolev, V.A. 2007. *Monitoring of geological, lithotechnical and ecological-geological systems*. Moscow.: KDU, 416 pp. (in Russian).
- Kudryavtsev, V.A., Garagulya, L.S., Kondrateva, K.A., Romanovskiy, N.N., Maksimova, L.N., & Chizhov, A.V. 1979. *Permafrost survey methodology*. Moscow: Izd-vo Mosk. un-ta, 359 pp. (in Russian).
- Manual to SNiP 2.05.07-85. Manual for design of railways and roads of industrial enterprises in permafrost areas. Matveev, S.A. & Nemirovskiy Yu.V. 2006. *Reinforced road structures: modeling and calculation*. Novosibirsk: Nauka, 336 pp. (in Russian).
- Melnikova, E.S. & Dubikova, G.I. (eds.). 1986. *Methods of regional geotechnical-geocryological investigations for plain territories*. Moscow: Nedra, 207 pp. (in Russian).
- Melnikova, E.S. & Grechishcheva, S.E. (eds.). 2002. *Permafrost and development of oil and gas fields*. Moscow.: Izd-vo GEOS, 402 pp. (in Russian).
- Moskalenko, N.G. (ed.). 2006. *Anthropogenic changes in ecosystems of the West-Siberian gas province*. Moscow: RASKhN, 358 pp. (in Russian).
- Pavlov, A.V. 2008. *Cryolithozone monitoring*. Novosibirsk: Izd-vo GEO, 229 pp.
- Pendin, V.V. & Ganova, D.S. 2009. *Geocological monitoring of the gas transport structures location area in the cryolithozone*. Moscow: Izd-vo PNIIS, 236 pp. (in Russian).
- Ponomareva, O.E. 2010. Nature-protecting zoning of the Nadym River basin (Western Siberia). *Kriosfera Zemli*, 14 (no. 2): 46-55 (in Russian).
- Sannikov, S.P. 2004. *Reinforcement of bearing layers of grounds and stone materials with volumetric geogratings*. Candidate of Sciences Dissertation. Tyumen, 18 pp. (in Russian).
- Voskresenskiy, K.S. 2001. *Modern terrain-forming processes on the plains of the Russian north*. Moscow: Izd-vo MGU, 263 pp. (in Russian).
- VSN 26-90. Instructions for design and construction of motor roads of the Western Siberia oil and gas fields (in Russian).
- VSN-195-83. Instructions for investigation and design of near-route motor roads in Siberian and Far East conditions (in Russian).

Coding of Ground Type during Geotechnical Site Investigations in Permafrost Regions

A.V. Iospa, A.A. Popova, V.I. Aksenov, G.I. Klinova
Fundamentproekt Open Joint-Stock Company, Moscow, Russia

Abstract

Coding (indexing) of frozen ground types is proposed in accordance with their physical properties. The coding is based on the state standard classification (GOST) and the results of long-term laboratory studies.

Keywords: engineering element; frozen ground; geological element; ground variety; ground properties.

Introduction

Engineering geological elements and specified ground elements are to be distinguished in the ground massif during the geotechnical site investigations for construction in accordance with the existing regulations (SP II-105097. Part I, GOST 20533-96) and based on the results of laboratory studies.

The engineering geological element (EGE) is the ground region that is characterized within each EGE by a complex of constant (uniform) indexes based on genesis, age, composition, structure, ground condition, or properties (or one of them). If an EGE is uniform in geological and genetic as well as lithologic and petrographical respect and contains a part of a section with the variability of composition, structure, and properties, then it can be divided into a number of elements (Trofimov 2005).

Calculated ground elements (CGE) are ground regions that are characterized by a specific physical and mathematical ground model of the “structure-base” system and a set of numerical values of physical and mathematical characteristics corresponding to this particular model.

The comparison of frozen ground properties by EGE is often regionally specific and predetermined not only by the genesis and the age of deposits, but also by the condition of their freezing (epigenetic or syngenetic). Therefore, an EGE-based frozen ground analysis for making engineering decisions can be difficult. A single EGE may combine a whole range of CGEs sharing certain physical and mechanical properties. In the same way, one CGE may be found in different EGEs.

Discussion

In practice, every geotechnical company uses its own system to determine an EGE. In the materials from most organizations that we deal with, EGEs are numbered in orderly fashion for each new object. They are given in order from the top to the bottom EGE 1, EGE 2, EGE 3, etc., or by the lithology, adding complementary alphabetic characters “a,” “m,” etc., for specific ground type (including frozen ground). Sometimes more complex numerical indexes are used.

As an example, in Table 1 we provide indexes that different geotechnical companies use for a range of ground varieties. They were applied in surveying at the same site (an areal and linear sites complex). The table demonstrates that the basic physical characteristics of the elements, distinguished

by different organizations, are similar. However, the coding of the elements differs, so a system of comparison of the elements is required to make unified design decisions.

With this approach, the synthesis and analysis of the results of the investigations are very difficult. This especially concerns the test results of the physical and mechanical properties of frozen ground. When different companies determine EGEs according to their own systems, engineering decision-making for construction becomes much more complicated. There are many cases when challenges arise even during the investigations conducted by only one company at the same site, since new ground types are determined in the course of more detailed surveys (passing the stages, feasibility study, working documentation), which changes the whole EGEs numeration.

In the early 2000s, when development of the previously explored oil and gas deposits commenced, our permafrost laboratory started receiving a large number of frozen ground undisturbed samples from the oil and gas facility construction sites in the Russian North. The laboratory was asked to determine the physical and mechanical properties of these samples. It was then that we had to face the problem of summarizing results of geotechnical site investigation. This was impossible to do without a unified coding system of ground types.

During geotechnical site investigations, grounds are to be classified in accordance with GOST 25100-95 (Grounds Classification). From our point of view, it is advisable to carry out the classification on the basis of this state standard. GOST 25100-95 provides types of each class of ground (rocks, soils, frozen) based on their physical properties (as well as some mechanical properties). EGEs and CGEs are formed based on the types of grounds or their total. We have developed a system that allows us to assign a personal classification code to each ground type, reflecting its type according to its particle size distribution, plastic limit, the presence of inclusions, plasticity index, salinity, peat content, ice content (for frozen ground), etc. This work resulted in a unified classification system for grounds common in the cryolithozone. It is based on the works of our colleague, engineer S.M. Miklyaev, and is supplemented by the results of the research carried out on multiple sites in the Far North.

In this paper, we present coding (indexing) of different ground types according to their physical properties, based on the State standard classification with a few additions based on the results of our research (Table 2).

We have been using this coding system for more than 10 years at oil and gas field development sites (Varandei,

Table 1. Comparison of the elements, distinguished by different surveying organizations at the same site.

Surveying organization	Element index	Total moisture $W_{tot}, \%$	Density $\rho, g/cm^3$	Total ice content I_{tot} u.f.	Ice content of inclusions I_{tot} u.f.	Organic matter content (O.M.), %	Salinity $D_{sal}, \%$
Fine sand with low ice content							
Company №1	EGE 13	19.0	1.97	0.35	-	-	>0.05
-----«----- №2	EGE 25	21.0	1.94	0.37	-	-	-
-----«----- №3	EGE 3a	17.0	1.86	0.26	-	-	-
-----«----- №4	EGE 2a	23.0	-	0.33	-	-	-
-----«----- №5	EGE 448	23.0	1.93	0.39	0	-	0
*	G.20.1	18.5-22.6	1.84-1.94	0.33-0.38	0	≤0.3	0.01
Sandy silt with low ice content							
Company №2	EGE 26	20.0	1.94	0.38	-	-	-
-----«----- №5	EGE 458	25.0	2.0	0.44	0.07	-	-
*	G.21.1	17.9-23.1	1.94-2.05	0.34-0.40	-	-	-
Heavy and light clayey silts, frozen, with low ice content							
Company №2	EGE 21	30.0	1.84	0.29	0.15	3.0	-
-----«----- №3	EGE 21.	27.0	1.91	0.21	0.1	-	-
-----«----- №5	EGE 209	35.3	1.79	0.14	0.02	-	-
*	G.29.33.1	16.0-36.5	1.68-2.10	0.15-0.33	≤0.2	≤3.0	≤0.06

* Ground laboratory and the frozen ground testing sector of “Fundamentproekt” Open Joint-Stock Company conducted tests at the sites of all geotechnical companies listed above. Characteristics obtained by “Fundamentproekt” are presented as intervals of specific values corresponding to all sites. Those of other organizations are presented only as estimated values.

Bovanenkovsky, Urengoy and Yamburg Oil and Gas Condensate Fields, etc.), at other industrial and civil construction projects (factory sites, power stations, roads, power lines, etc.), at the sites of third-party survey organizations (when “Fundamentproekt” performs a particular set of work, including frozen ground tests), and of course in our own research.

While working with this coding system, we faced the fact that visible ice inclusions are not observed in sands, because under natural conditions they usually have a massive cryogenic structure. That means their ice content, based on visible ice inclusions, equals zero. At the same time, sands can have different total moisture and ice content and, therefore, differ in physical and mechanical properties. This is what made separation (and indexing) of total ice content of sand, which is not covered by the contemporary state standard (GOST), also necessary. The classification is our proposal for distinguishing types of sands by the total ice content. It has been approved and included in the State standard. It should be noted that, at present, we do not use the classification of frozen ground based on temperature and strength properties (Table B.30 GOST 25100-95), because currently there are no clear quantitative criteria for distinguishing them.

Distinguishing sandy and silty varieties of clayey silts and sandy silts for practical purposes is carried out rarely, with the exception of special studies.

Below are examples of coding and a sequence of indexes distribution of typical dispersed frozen ground varieties:

- A.24.2 – seasonally thawed sandy silty loam (sandy, plastic);
- C.33.c – cooled clayey silty loam (heavy, silty, heavily saline);
- D.20.2 – frozen sand (fine, icy);
- D.29^b.a.2.1 - plastic frozen clayey silty loam (light, silty, slightly peaty, slightly saline, with low ice content).

Conclusion

The proposed classification scheme enables statistical processing of ground test results with consideration for the combination of their physical properties, formed in the process of cryolithogenesis with the distinction of calculated geological elements (Table 3).

The ground elements comparison system is essential in the process of developing the unified project decisions on the territory of permafrost. It is impossible without a unified indexing system of ground varieties, which we have proposed on the basis of GOST 25100-95 (Grounds Classification) and GOST 20522-96 (Grounds Methods of statistical processing of test results).

Table 2. Universal indexing of cryolithozone dispersed ground types, based on GOST 25100-95 Grounds Classification.

I. According to cryolithozone ground conditions

Index	Ground condition
A	active layer ground
B	thawed (non-frozen) ground
C	chilled ground
D	frozen ground

II. Name of ground according to granulometric composition (Grounds A, B, C, D, based on GOST 25100-95, according to Table B.10)

1	bouldery ground (blocky)
2-5	bouldery ground divided by the matrix composition according to Table B.10 (Note)
6	pebble/cobble ground (
7-10	pebble ground divided by the matrix composition according to Table B.10 (Note)
11	gravelly ground (gruss)
12-15	gravelly ground divided by the matrix composition according to Table B.10 (Note)
16	gravelly sand
17	sand with gravel
18 – 21	coarse sand to silty sand divided by the matrix composition according to Table B.10
22	gravelly sandy silt
23	sandy silt with gravel
24-25	24, 25 – sandy silt, divided by particle size distribution according to Table B.12
26	light gravelly clayey silt
27	light clayey silt with gravel
28, 29	light clayey silt divided by particle size distribution according to Table B.12
30	gravelly sand (gruss)
31	heavy clayey silt with gravel
32,33	24, 25 – heavy clayey silt divided by particle size distribution according to Table B.12
34	light gravelly clay
35	light clay with gravel
36,37	24, 25 – light clay divided by particle size distribution according to Table B.12
38	heavy gravelly clay
39	heavy clay with gravel
40	heavy clay (without gravel)
41	Organic silt
42	Organic clayey silt
43	Organic clay
44-46	peat divided by the degree of decomposition according to Table B.23

II. According to material composition according to the degree of salinity – lower case letter (Grounds D, C based on SP 11-114-2004, Table 6.7)

a	slightly saline
b	moderately saline
c	heavily saline

According to the degree of organic content – upper index (Grounds D, C based on SP 25100-95)

a, b, c, d	mixed with organic matter – heavily peaty clayey grounds and sands divided according to Table B.22
------------	--

III -1. According to ice content by visible ice inclusions (Frozen grounds (D) based on GOST 25100-95)

1-4	with low ice content - with very high ice content divided according to Table B.29
-----	---

III -2. According to hydrophysical properties (Thawed grounds (A, B) based on GOST 25100-95)

According to the degree of water saturation - coarse soils and sands

1-3	low degree of water saturation - water saturated separated coarse soils and sands according to Table B.17
-----	---

According to liquid condition - clayey soils

1-6	solid – fluid clayey silt and clays divided according to Table B.17
1-3	solid – fluid sandy silty loams divided according to Table B.17

Table 3. Summary table of physical and mechanical properties of frozen clayey silts at $T = -1^\circ$ (pipeline system «Zapolyarye – Pur-Pe», NPS-2).

Index	Ground name	Moisture W%*	Density ρ , kg/cm ³ *	Characteristic value	Estimated value	Number of definitions	Ground safety coefficient γ_g	Variation coefficient ν
331	Heavy and light clayey silts, frozen, with low ice content	$\frac{16.4-20.5}{17.8}$	$\frac{1.97-2.07}{2.03}$	estimated equivalent adhesion S_{eq}^p MPa (with consideration for transition coefficient)	0.290	39	1.03	0.18
		$\frac{14.2-32.0}{23.4}$	$\frac{1.91-2.48}{2.03}$	shear strength along the adfreeze plane with metal R_{af}^p MPa	0.066	10	1.06	0.16
		$\frac{15.8-18.1}{17.1}$	$\frac{2.00-2.16}{2.08}$	frozen ground compressibility coefficient ** $m_{f0.1-0.3}^n$, MPa ⁻¹	0.071	10	1.08	0.15
				frozen ground deformation modulus**, $E_{0.1-0.3}^n$, MPa	9.50	10	1.11	0.24
				initial freezing temperature T_{bf}^p °C	-0.4	38		

* - may differ, because grounds from different depths are chosen for different tests depending on the interaction between the foundation and foundation ground

** - in the range of normal pressure 0.1-0.3 MPa

References

- GOST 20522-96. Grounds. Methods of statistical processing of test results. 1996 *Moscow*: MNTKS, 26 pp.
- GOST 25100-95. Grounds. Classification. 1996 *Moscow*: MNTKS, 30 pp.
- SP 11-105-97 Engineering geological surveys in construction. Part I. General working rules 2000 *Moscow*: PNIIS Gosstroya Rossii, 45 pp.
- SP 11-105-97 Engineering geological surveys in construction. Part IV. Working rules in regions of permafrost distribution. 1999 *Moscow*: PNIIS Gosstroya Rossii, 60 pp.
- SP 11-114-2004 Engineering surveys on the continental shelf for construction of offshore oil-field structures. 2004 *Moscow*: PNIIS Gosstroya Rossii, 88 pp.
- Trofimov, V.T. (ed.). 2005 Ground studies. *Moscow*: *Izd-vo MGU*, 1024 pp.

Main Types and Causes of Deformations on Railways and Roads in the Norilsk Industrial District

V. Isakov

Lomonosov Moscow State University, Department of Cryolithology and Glaciology, Moscow, Russia

Abstract

The main types and causes of deformations of the road network in the Norilsk industrial district are discussed based on field observations and the study of published materials. The deformations are subdivided into major morphological types, and the explanation of their origin is given. It is discovered that underflooding, thermokarst, thermal erosion processes, and structural disadvantages of linear structures are the main reasons for deformations on railways and roads between Norilsk and Talnakh.

Keywords: cryolithozone; deformations; monitoring; Norilsk; roads; thermokarst.

Introduction

The Norilsk industrial district is one of the largest industrial complexes in the area of the cryolithozone. Railways and roads form the basis of the transportation system of the district. They connect large population areas, mineral mining and processing centers, and transportation sites including Norilsk, Talnakh, Kayerkan, Dudinka, and Alykel. The roads connecting the two largest populated cities and industrial centers, Norilsk and Talnakh, are the busiest. Roadbed and embankment deformations under the impact of cryogenic processes lead to the reduction of road capacity and operational safety.

The problem of stability of linear structures in this region has a long history. Nonetheless, the study of the underlying reasons for deformations has been insufficient, and therefore measures taken for the stabilization of roads do not produce the required results.

The author carried out a series of field and analytical investigations to determine the main causes of roadbed deformations in the Norilsk industrial district.

Study Area and Methodology

Environmental conditions of the region

The district is located within the Norilsk inter-mountain depression. The annual mean air temperature is -10.9°C . The vegetation is dominated by larch forests with small-leaved species (primarily, birch and alder). There are also locations (especially in the area of Norilsk and to the west of it) with exclusively dwarf-shrub and shrub vegetation. The deposits of the Valkovskaya lacustrine-fluvial terrace consisting of icy fine-grained sediments (mainly clayey silt and clay) with massive ground ice and a repeated network of ice wedges serve as a foundation for linear structures. The thickness of such deposits can reach several tens of meters. The mean annual ground temperature is usually within the range -3 to -5°C . Nonetheless, about 30% of the area is occupied by talik zones (Sheveleva & Khomichevskaya 1967). Alternation of thermokarst depressions and cryoplanation surfaces is the main feature of the terrain of the Valkovskaya terrace.

Railways and roads

The investigation was conducted within the oldest part of the railway in the Norilsk industrial complex, from

the Valek pier to Golikovo Station (the city boundary of Norilsk). This part was constructed in 1935 in a very short period. There were only 9 days between the date when the decision was made to build the railroad and the date when construction officially began. This obviously influenced the quality of the project decisions and the quality of the road construction. In the 1960s and 1970s, the route of the railway was straightened in order to increase the rail capacity (for the purpose of ore transportation from Talnakh). There are now two embankments of the railway, the operating one (straighter in plan) and the abandoned one (Fig. 1).

The modern Norilsk-Talnakh road with an asphalt cover was built in the 1960s and 1970s. Prior to that, an unpaved dirt road connected Norilsk with Valek Village and the village in the area of the future Talnakh city. The new paved road to Valek Village was mainly built along the old dirt road. The combined auto and railway bridge crossing the Norilskaya River was commissioned in 1963. The rail and motor road routes at the site from Golikovo Station to Valek Village are located at a significant distance from each other.

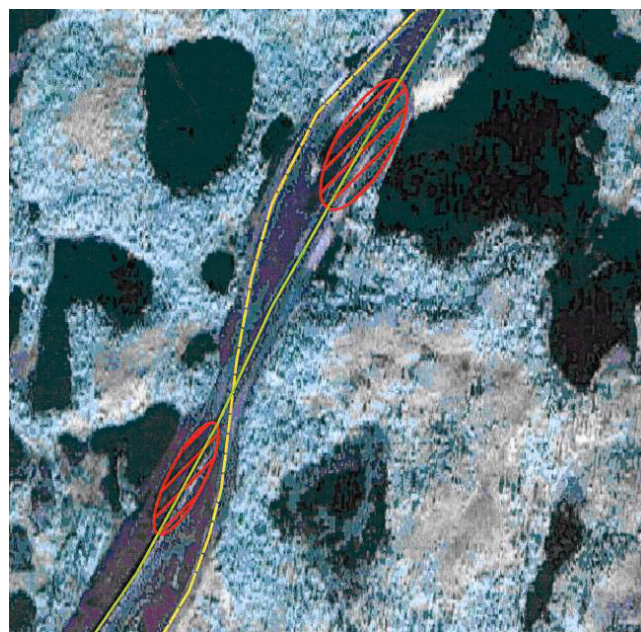


Figure 1. Corridor of the Norilsk-Talnakh railway at the Golikovo-Valek section. The embankment of the operating railway is marked in green and the abandoned embankment in yellow. The waterlogged sites formed after road straightening are hatched in red. Google image library.

The auto road and the railway are located within one corridor from the bridge crossing of the Norilskaya River to Talnakh.

Along the entire length, the railway and the auto road are constructed on embankments. The height of the embankment varies at different sites from slightly above 1 m to almost 20 m. The auto road embankment, as compared to the rail one, is significantly lower (4–6 m on average). Gravels with fine-grained soil filling (up to 30–40%) were used as material for the embankments. The water permeability of such ground is comparatively low; there is no cold air convection. The large width of embankments at the bottom reaches up to 60–80 m at some locations and leads to waterlogging near the embankment slopes.

Research methodology

Six km of rail and 18 km of auto roads connecting Norilsk and Talnakh were investigated in September 2010. The investigation included observations along transects, the study of satellite images, and the analysis of archive materials. The nature and scale of roadbed deformations were registered along transects, and the general state of the roadbed elements and the development of exogenic, including cryogenic, processes at the adjoining territories were evaluated. Satellite images were primarily used to determine the extent of waterlogged areas. The analysis of archive materials (mainly for the auto road) allowed us to evaluate the dynamics and the periodicity of deformations at different parts of the road. The layouts of the roadbed sites with especially hazardous deformations were prepared after the processing of materials obtained as a result of field observations and the analysis of satellite images. The reasons for the development of specific types of deformation were evaluated based on the generalization of the obtained materials and on the analysis of scientific literature.

Results and Discussion

Field observations show that deformation developed on at least 50% of the lengths of the auto and rail roadbeds. Deformations have different shapes and scales of occurrence. Those threatening safety were found approximately every 3 km. The main types of deformations of the investigated linear structures can be divided into the following groups: “long-wave longitudinal deformations,” which are regular changes of the longitudinal roadbed slopes in conformity with the natural terrain topography; local subsidence of the main embankment; deformations of the roadbed under low embankments; stepwise subsidence of the main embankment; and deformations associated with the changes of the angle of embankment slopes.

Long-wave longitudinal deformations

The formation of long-wave longitudinal deformations (Fig. 2) is evidently associated with the peculiarities of the interaction between high embankments and permafrost in foundation beds (bases). In particular, it is associated with the regularities of depression of the top of the permafrost depression at locations where the railway intersects thermokarst depressions and planation or residual surfaces. It is known (Lisitsyna et al. 1989) that the greater the cross-sectional height of the embankment, the higher the



Figure 2. Long-wave longitudinal deformation of the rail roadbed near the Valek crossing loop. Length of wave \approx 120 m.

temperature increase in its base, if other factors are held constant. The change of the embankment height moving from the depression to the residual surface can cause unevenness of the top of the permafrost in the embankment base and, as a result, lead to deformations at a scale comparable with the scale of the natural terrain change in the embankment base (Fig. 3).

Deformations of this type are most widely distributed within the study area. Their amplitudes range from several tens of centimeters to several meters; their lengths usually exceed 50 m and can reach hundreds of meters.

Long-wave longitudinal deformations are comparatively low-hazards because they form insignificant inclines. These cannot significantly influence safety. Nonetheless, such deformations can increase the wear of rails, force a reduction of operational speeds, and increase fuel consumption.

Local subsidence of the main embankment

The formation of local subsidence (Fig. 4) is mainly associated with the embankment crossing perennial or temporary rills and drained hollows. Rills can form local waterlogging zones near embankment slopes, and water can drain through the embankment body or the thawed ground under the embankment. The constant presence of local flood and drainage zones where the embankment crosses the valley bottom causes thawing and subsidence of the ground and the embankment. Local subsidence is usually up to several meters in length. The development of local subsidence with complex configuration was noted in the process of the investigation of the Norilsk-Talnakh auto road. It evidently repeats the shape of channels draining the local waterlogged zones. In terms of transportation safety, such local subsidence sites are more hazardous than long-wave deformations because they cause abrupt changes in the roadbed configuration at short fragments and intensively deform the roadbed. Local occurrences of subsidence are more characteristic of low (up to 10 m) embankments. This is associated with a higher shock-absorbing capacity of high embankments.

Deformations of the roadbed under low embankments

It is important to individually describe the problems of rail roadbed deformations at the zones of low (up to 2–4 m) embankments. The part of the low rail embankment

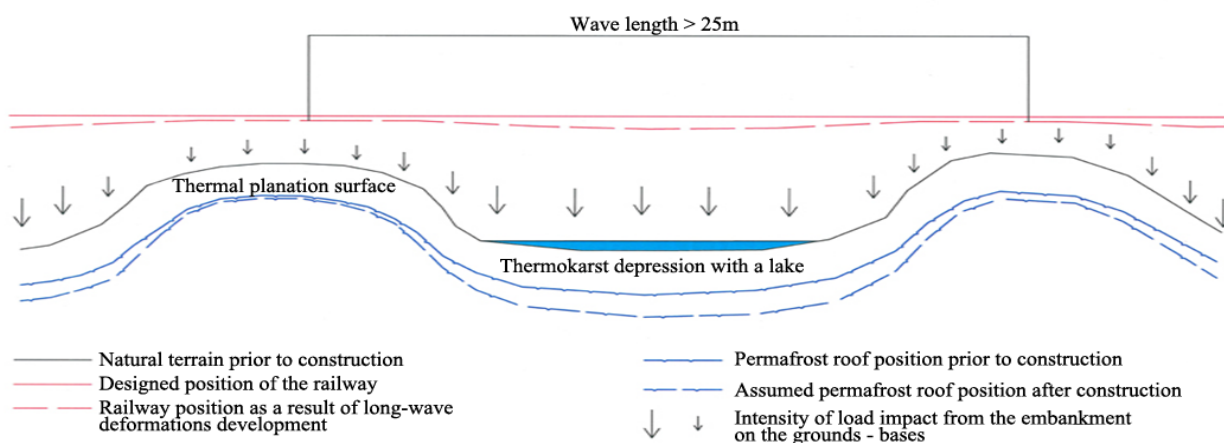


Figure 3. Diagram of long-wave longitudinal deformations.



Figure 4. Local subsidence formation on the Norilsk-Talnakh auto road.



Figure 5. Nature of deformations on the low embankment zone.

(0.7–3 m high) investigated between Golikovo Station and the Valek crossing loop is characterized by high intensity of both longitudinal and lateral deformations of the rail roadbed. These deformations have relatively low amplitudes (Fig. 5). A low height and a comparatively small area of the embankment lead to higher intensity of dynamic loads from passing trains as compared to high embankment zones. The observed intensive deformations are most probably associated with rheological processes, creep in particular, occurring in permafrost (Vyalov 1978) under the impact of dynamic loads. Permafrost thawing caused by waterlogging increased the likelihood of creep processes.

With such deformations, the speeds of transport movement are limited severely, frequently to very low speeds (10 km/h at the site under study). The rail and grating fails very quickly and requires replacement as a result of the stresses.

Deformations associated with the change in the angle of embankment slopes

The deformations associated with the change in the angle of embankment slopes are primarily formed as a result of embankment waterlogging and abrasion of thermokarst lake shores along the road route. The natural change of the position of thermokarst lakes (shore abrasion toward the dominating winds in particular) is evidently not taken into account in the design. Consequently, the embankment

bottom frequently goes directly into the lake, while thermal abrasion of natural and technogenic ground develops. Straightening of the railroad route at the Golikovo Station Valek site led to the formation of new waterlogging zones that are currently suffering intensive deformations (Fig. 6). Embankment waterlogging is accompanied by lowering of the permafrost surface. The permafrost surface is lowered by 1.5 m and more even under small lakes several tens of centimeters deep that are formed at the embankment base. This is two times higher than at the adjoining sites outside the waterlogging zone. Even greater depression of the permafrost surface can be expected in locations with larger lakes.

Permafrost thawing in the embankment base causes ground subsidence and, consequently, an increase of the slope steepness. This, in turn, leads to the intensification of the processes of erosion and mass movement of the embankment material (Fig. 6). Since the impact of waterlogging decreases with the increase in distance from the slope, differential permafrost thawing in the embankment base leads to lateral deformations. This causes curving of the rail track or cracking of the asphalt coating.

Stepwise settlement of the main embankment

Stepwise settlement of the main embankment site is another process associated with waterlogging and thermokarst.

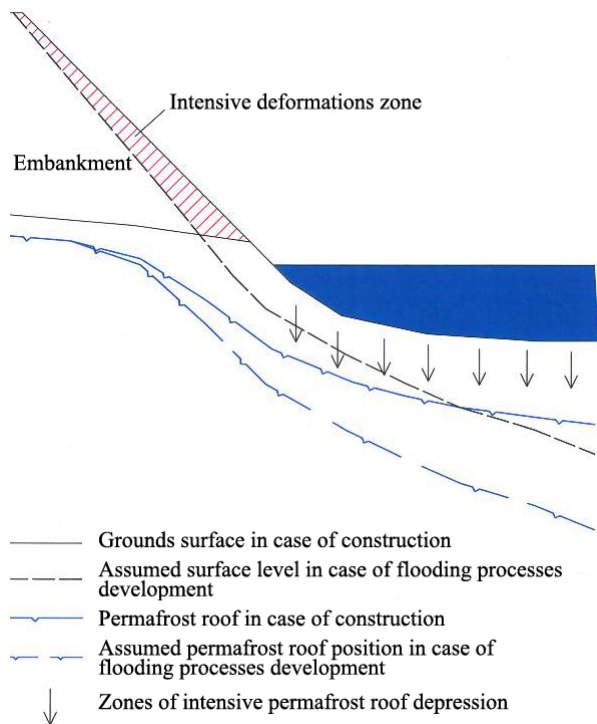


Figure 6. Development of deformations due to the increase of the embankment slope steepness as a result of waterlogging.

This process is most characteristic of the auto road sites waterlogged on one side only. The formation of deformations of such type is associated with the irregularity of permafrost thawing and settlement and with formation of asphalt “steps” (Fig. 7).

Such “steps” can frequently occupy a significant part of the embankment slopes. The difference in levels between “steps” can reach 5 cm. The stresses caused by differential embankment settlement lead to the formation of cracks in the asphalt coating and its intensive destruction. Complete destruction of the road coating can occur in case of the development of intensive deformations, as is shown in Figure 7.

Conclusions

The results of field investigations and their analysis show that the development of waterlogging, thermokarst, and thermal erosion processes is the main cause of road deformations within the study area. Both natural conditions of the region (widespread presence of ice-rich ground, poor drainage of the area, etc.) and structural disadvantages of linear structures (in particular, very limited presence and unsatisfactory work of the existing drainage structures) favor the activation of these processes. The comparison of the results of investigations conducted by the author with the previous findings shows that the development of deformations continues despite the fact that the roads have been operated already for several decades. For example, the number of Norilsk-Talnakh auto road locations with significant deformations grew by number and extent compared to 2006. A decrease of deformations is unlikely under the process of further operation. Their development will most likely continue.



Figure 7. Stepwise settlement of the main embankment site of the Norilsk-Talnakh auto road.

A detailed catalog of locations experiencing deformations was prepared based on the investigated results. It contains site references, brief descriptions, and layouts of deformations. This catalog aids in the preparation of a detailed program of geocryological monitoring and recommendations for roadbed stabilization.

Acknowledgments

The author would like to thank Dr. V.I. Grebents and Dr. A.G. Kerimov for their assistance in the organizational, methodological, and scientific support of this research.

References

- Lisitsina, O.M., Minaylov, G.P., Romanovskiy, N.N., & Parmuzin, S.Yu. 1989. Linear Construction. In *USSR Geocryology. Eastern Siberia and the Far East*. Moscow, Nedra, 452-457 (in Russian).
- Sheveleva, N.S. & Khomichevskaya, L.S. 1967. *Geocryological conditions of the Yenisey North*. Moscow, Nauka, 126 pp. (in Russian).
- Vyalov, S.S. 1978. *Rheological fundamentals of ground mechanics*. Moscow, Vysshaya shkola, 447 pp. (in Russian).

Glacial Topography of the Northwestern Part of the Putorana Plateau

E.N. Ivanova-Efimova
Moscow State University, Moscow, Russia

Abstract

Description and analysis of glacial topography on the Putorana Plateau based on satellite and aerial images are provided. Geographical zonation of the northwestern part of the Putorana Plateau based on the combination of geomorphological features and the distribution of snow and ice complexes is developed. The possibility of the existence of glaciers on the Putorana Plateau under conditions of modern occurrence is discussed. Planning of investigations in the area of the maximum spread of modern glaciation in the future is suggested.

Keywords: glacial topography; glaciers; Putorana Plateau.

Introduction

The Putorana Plateau is the highest part of the northwestern region of the Central Siberian Plateau. The maximum elevation of the plateau is a nameless mountain 1701 m high.

The existence of glaciers in the area is determined by several factors: negative mean annual temperature and low summer temperature accounting for solid precipitation and slight ablation in the warm period; increased accumulation of solid precipitation due to snow drifting and avalanche nourishment mainly on the northern and eastern slopes; the occurrence of solid precipitation at any season of the year; high elevation of the terrain as compared to the rest of the plateau; and, as a result, the interception of moisture-laden flows from the west. However, the elevation of the plateau is not sufficient for strong glaciation because a large part of it lies below the climatic snow line. The relief is dissected to a significant degree. There are considerable negative relief forms where snow tends to accumulate and persists in the shade for a long time.

There is no consensus among scientists concerning the boundaries of the Quaternary glaciation (Markov 1965, Grosswald 1999, Bolshiyakov 2006). However, they all agree on the fact that these boundaries used to be much greater than now. It can be stated that modern glaciation presents a regressive phase of one long cycle.

At present, the area of maximum glaciation is in the northwest of the plateau where 22 glaciers with an area of 2.54 km² are located, based on the catalog of USSR glaciers (Koryakin 1981), or 61 glaciers with an area of 7.1 km² (Sarana 2005). They occupy slopes and kars of mainly northern and eastern exposure. As can be seen from the presented information, all these glaciers are small.

A variety of glacial and fluvio-glacial relief forms confirm that large glaciers existed on the Putorana Plateau in the past. Such relief is found almost everywhere on the plateau.

Methodology

An interpretation of aerial photographs was made for the area of the most recent glaciation. The photographs were taken on July 31, 1987, and have the scale of 1:25,000. We also carried out the interpretation of satellite images of the area in the visible range. The images were of the same scale

and were taken in August of 2006–2008 with the resolution of 30 m/pixel. The major interpretation characteristics (shape, size, texture, color) were identified (Table 1), based on the combination of which sites were selected. Literature sources and topographic maps of the area were used as well. The MapInfo software was used to select sites and calculate their areas.

Topography of the Northwestern Part of the Putorana Plateau

The selected relief forms are presented in the geomorphological chart (Fig. 1). Tectonics was the main force that created the plateau's topography. Plateau-like forms as well as fractures were created. A large area is occupied by slopes of the first order. Most often, they are steep (10–25 degrees). On such slopes there are cirques where snow patches and glaciers are located, and these in turn feed the rivers. There are snow patches and glaciers in the cirques, mainly located in the southeastern part of the area. The slopes of the second order are dissected by pit-like hollows of a much smaller size (kars), which are extremely numerous. Kars have mainly northern and eastern exposure, and their formation is directly related to snow patches.

The topography created by ice accumulation activity of the glacier is represented by dumped moraines. They are found along the sides of trough valleys in the form of a lateral moraine, which is not always clearly visible. Asymmetry is observed as well; a moraine is found only at one side of the valley. Dumped moraines often occur at the bends of the valley; they are shorter and crescent-shaped. The end moraine is found only in the most western part of the area. It is eroded by the river. The moraine stands out through its shape and granular texture.

Relief forms created by fluvio-glacial processes are represented by two types of plains: hummocky-pitted and outwash ones. The formation of marshes takes place due to minor inclines and the presence of permafrost. Small lakes develop in the pits. The plains in the selected area are represented by depressions between larger massifs.

Topography created by gravitational processes is represented by two types of slopes: slump-talus and avalanche ones. Slump-talus slopes vary in steepness, which determines the rate of slope processes. Snow patches and glaciers are not located on very steep slopes, as they do not

Table 1. Interpretative characteristics and a brief description of nival-glacial systems and the elements of the relief.

Object / Site	Color	Texture	Shape	Size, km	Characterization
lava plateaus	gray-beige	granular	flat objects of irregular shape	length – about 5, width – 1.5-4	plateau-like, flattened plots
nival-glacial complexes	white	even-textured	rounded or elongated objects	along the long axis – 0.1-6.4	entire set of seasonal, perennial snow patches and glaciers in the photographs with area of more than 0.05 km ²
valleys with expressed troughs	green, yellowish	granular	elongated trapezoidal objects	length – 13-25, width – 1.5-4	parts of U-shaped valleys, the river flowing in such valleys originated in the cirque
nival-glacial slopes of the first order	light-gray, brown	with non-sorted circles	objects elongated along the edge of plateau-like sections, often with a wavy structure, in the concave parts – cirques	length – up to 14, width – 2	steep slopes with numerous cirques
nival-glacial slopes of the second order	black, brown, gray	with non-sorted circles	irregularly shaped	length – up to 10, width – 2	steep slopes with numerous kars, which are often filled with seasonal or permanent snow patches
moraine ridges and mounds	gray, brown, green	granular	elongated, ellipse-like objects, straight and curved	1.5-12.	lateral and end moraines
hummocky-pitted plains	green	with non-sorted circles	irregularly shaped	length – 4-5, width – 20-40	parts of valleys with hummocky-pitted topography, the area of hills about 0.25 km ² , shallow lakes
outwash plains	green	granular	irregularly shaped	width – more than 40, length – more than 5	low-angled parts of valleys with frequent meanders, former riverbeds, lakes
slump-talus very steep slopes	black, gray	longitudinally banded	objects extending along plateau-like sections	length – 8, width – 1-1.5	slopes steeper than 20 degrees
slump-talus, steep and of average steepness	black, brown, gray	granular	irregular shape	length – up to 14, width – 2	steep slopes without pronounced glacial transformation
slump-talus low-angled slopes	green, brown, gray	granular	objects of irregular shape with a slope less than 10 degrees	length – 5-13, width – 3-5	slopes without expressed glacial activity with gradient less than 10 degrees
avalanche slopes	gray, brown	transversely banded	objects elongated along the edge of plateau-like sections with a large number of avalanche channels	length – 10-12, width – 2	steep slopes with clearly expressed multiple erosions often filled with avalanche snow patches

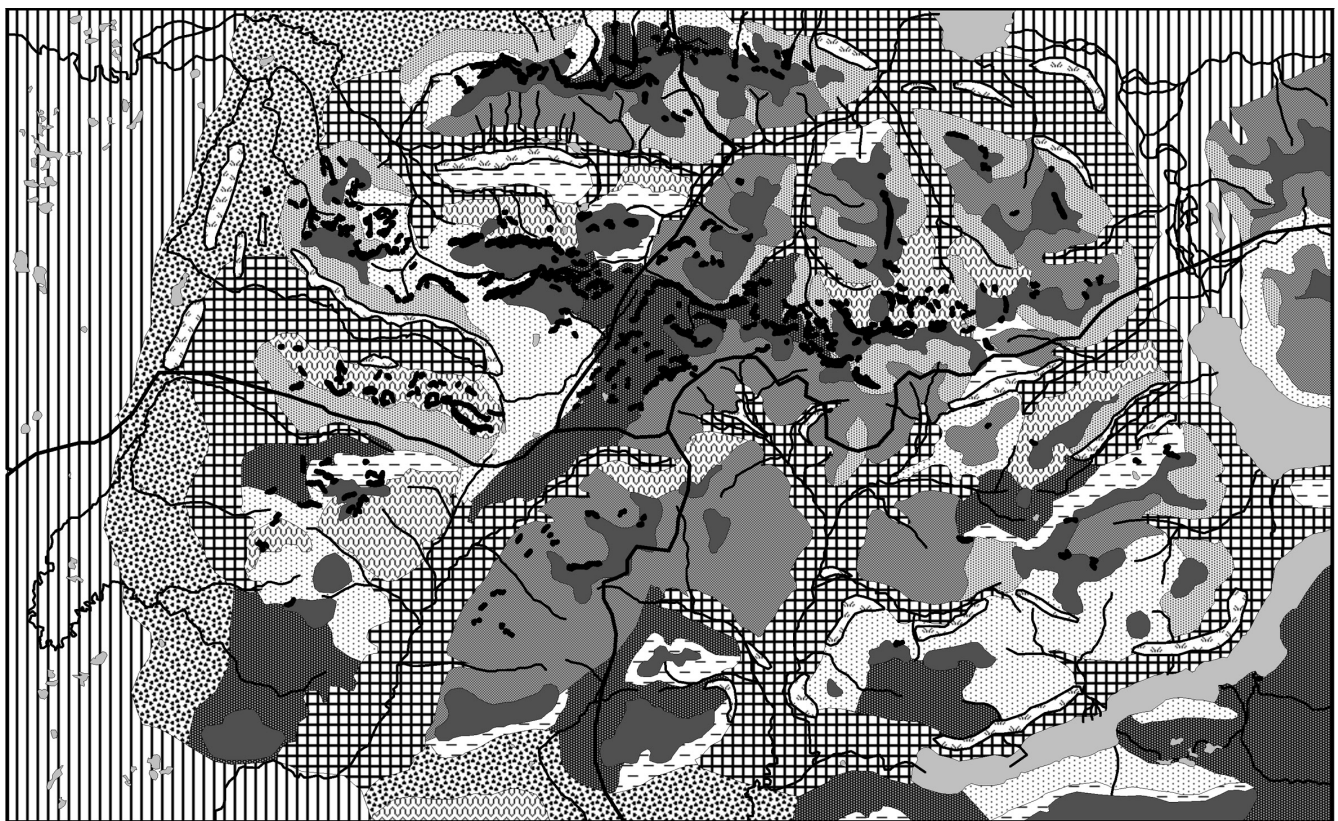
create conditions for the accumulation of snow. Avalanche slopes are marked by erosion trenches that create a special pattern. They are easily distinguished in the picture. Erosion trenches create conditions for the accumulation of avalanche snow. Such slopes are located on the periphery of the plots and on the slopes of southern exposure. Apparently, they are associated with strong thawing on the south side. Avalanches are frequent on these slopes.

The Putorana Plateau is located in the permafrost region, which is reflected in the topography. Permafrost-related processes are often superimposed on other processes or serve as their catalysts. For example, they act as suppliers of fragmentary material (frost crushing and weathering) on gravitational slopes. Solifluction terraces are sometimes found on turfed slopes. Besides, under the cover of moraine material, one can often find buried ice that gradually melts,

forming conical depressions. Frost cracking and heaving occur on the plains occupied by marshes. Therefore, the marshes have a hummocky nature. The average thickness of permafrost in the massif ranges up to 600 m. The Imangda River is too shallow for the formation of a large talik. In winter it freezes completely, and ice crust is formed in its wider parts. Basalts that predominantly compose the massif freeze stronger than unconsolidated fragmentary material. That is the reason for the formation of frozen rocks.

Geographical Demarcation of the Northwestern Part of the Putorana Plateau

We identified various relief forms for the chosen region. Some of them are of glacial origin. A number of zones were singled out based on the combination of all the features of



Scale 1:350 000 (1 cm = 3.5 km)

3,5 0 3,5 10,5 14,0 km

Legend:

- | | |
|---|--|
| 1. Relief forms created by tectonic vertical positive processes | 3. Relief forms created by gravitational processes |
| ■ lava plateaus | 3.1. slump-talus slopes: |
| 2. Relief forms created by glacial activity | a) ▨ very steep (more than 35 deg) |
| □ 2.1. nival-glacial processes | b) ▩ steep and of average steepness (35-10 deg) |
| ▧ 2.2. valleys with expressed troughs | c) ■ low-angled (less than 10 deg) |
| 2.2 Nival-glacial slopes: | ▨ 3.2. Avalanche slopes |
| ■ a) first order (dominated by cirques) | □ lakes — rivers |
| ▩ b) second order (dominated by kars) | — borders of geomorphologic regions |
| 2.3 Relief forms created by accumulative glacial activity | |
| ▨ dumped moraines | |
| 2.4. Relief forms created by fluvioglacial processes | |
| ▩ a) hummocky-pitted plains | |
| ▨ b) outwash plains | |

Figure 1. Geomorphological map of the northwestern part of the Putorana Plateau

the identified forms and on the location of snow patches and glaciers (Fig. 1). Their area is nearly identical (about 600 km²). This is the northwestern part or the area with the maximum spread of nival-glacial complexes. The northeastern area is an area with many nival-glacial systems occurring mainly in kars. The southwestern area is an area with a scattering of small nival-glacial complexes, a small number of kars, and mostly low-angled slopes; steep slopes have a southern exposure that does not create very favorable

conditions for glaciers. Moraine ridges are not expressed; these are the regions with the most developed plains. The southeastern area is an area that has a small number of snow patches but a large number of moraine ridges and cirques, which indicates glaciation occurring in the past. Snow patches and glaciers do not fully occupy the kars. There are certain forms of topography that could be formed only by large glaciers. This indicates a discrepancy between the relief forms and glaciation (Kalesnik 1963). Undoubtedly,

the glaciation here was much more extensive in the past than it is now.

The development of glaciation and the transition of the modern phase to the progressive one are possible on the Putorana Plateau under the conditions of a cyclical climate. This hypothesis is being tested.

Acknowledgments

We would like to express our gratitude for the help in writing and organizing this work to associate professors of the Department of Cryolithology and Glaciology of MSU: candidate of geological sciences N.A. Volodicheva, candidate of geological sciences V.V. Popovnin, and to senior research fellow and candidate of geological sciences D.A. Petrakov.

References

- Bolshiyaynov, D.Yu. 2006. *Passive glaciation of the Arctic*. St. Petersburg: AANII, 295 pp.
- Grosswald, M.G. 1999. *Eurasian hydrosphere catastrophes and Arctic glaciation. An essay in geomorphological analysis of continental paleohydrological systems*. Moscow: Nauchnyy mir, 115 pp.
- Kalesnik, S.V. 1963. *Glaciological essays*. Moscow: Geografiz., 552 pp.
- Markov, K.K., Lazukov, G.I., & Nikolaev, V.A. 1965. *The Quaternary Period*, vol. 1. The territory of the USSR. Moscow: Izd-vo MSU, 370 pp.
- Sarana, V.A. 2005. Glaciers on the Putorana Plateau. In *journal MGI*. Moscow: Vneshtorgizdat. Ed. pp. 200-214.
- Koryakin, V.S. 1981. *The catalog of the USSR glaciers*. The Putorana Plateau. Resources of the USSR surface waters, vol. 16. The Angara-Yenisei Region. Edition 1. Yenisei. Part 6. Leningrad.: GIMIZ, 46 pp.

Implementation of Mathematical Landscape Morphology Methods for Estimating Risk of Damage to Linear Engineering Structures due to Thermokarst Processes

V.N. Kapralova, A.S. Viktorov
Sergeev Institute of Environmental Geoscience, RAS, Moscow, Russia

Abstract

A method is suggested to estimate the risk of damage to engineering structures due to thermokarst processes with the help of mathematical landscape morphology methods. The assumptions that were used as the basis for modeling territories with thermokarst processes are presented and substantiated with experimental data. A series of images showing the distribution of thermokarst lakes were digitized to validate theoretical assumptions and results of mathematical analysis. The results show general correspondence between calculated and empirical data.

Keywords: landscape mathematical morphology; probability distribution; thermokarst dynamics; remote sensing; risk estimates.

Introduction

Assessment of risks associated with hazardous geological processes is one of the most challenging tasks of geology. It is especially important in the rapidly changing natural conditions of northern regions. Considerable research has been devoted to estimating risks of damages to engineering structures (Elkin 2004, Estimation and management..., 2003, Ragozin 2003). Statistical approaches of risk assessment are associated with difficulties related to the absence of long-term data and information required to develop reliable statistical relationships. Mathematical landscape morphology methods were suggested as another alternative approach to avoid this problem (Viktorov 1998). Mathematical landscape morphology is a branch of landscape science that studies quantitative principles of natural mosaic structures formed on the Earth's surface as well as methods of mathematical analysis of these mosaics.

This paper aims to develop a quantitative risk estimation procedure for linear objects by using mathematical landscape morphology methods.

Landscape pattern models are based on the use of mathematical dependences between geometrical characteristics of major landscape patterns.

The mathematical model of morphological structures of lacustrine thermokarst lowlands was developed within the mathematical landscape morphology principles and is based on the following suppositions (Viktorov 1998):

- 1) The process of formation of initial depressions is stochastic and independent. Initial thermokarst depressions formed simultaneously. The probability of formation of one depression in the area depends only on the area's size, with a much higher probability than the formation of several depressions.
- 2) The growth of thermokarst lakes by a thermo-abrasion process progresses independently in different lakes. It is directly proportional to heat accumulated in the lake and inversely proportional to the surface area of the lake basin below the water level.

These assumptions allow us to derive equations parameterizing territories affected by thermokarst processes (Viktorov 1998). The resulting equations include:

- probability distribution of the number of thermokarst

lakes (k) formed in a given area over given time (Poisson process)

$$P(k, t) = \frac{(\lambda ts)^k}{k!} e^{-\lambda ts}, \quad (1)$$

where λ is the average number of depressions forming in the unit area per unit time; s is size of the area; t is time.

- probability distribution of thermokarst lake radius change (Wiener random process with regard to diameters logarithms)

$$f_r(x) = \frac{1}{\sqrt{2\pi\alpha x}\sqrt{t}} e^{-\frac{(\ln x - \alpha t)^2}{2\sigma^2 t}}, \quad (2)$$

where α , σ is distribution parameters, t is age of lake.

Mathematical Model Implementation for Thermokarst in Lacustrine Lowlands

The model was tested over several regions. Test regions were selected based on morphological homogeneity and availability of remotely sensed data. The regions must be similar in terms of microstructure and background phototone as well as lake distribution and shape. Figure 1 shows satellite imagery of the selected regions:

- Sredneobskaya lowland in the Valoktayagun River valley (1);
- Inter-mountain valley in the western part of the Seward Peninsula (Alaska) (2);
- West Siberian Plain near the Pyakupur River (3, 5) and near the Vyngapur River (4).

All these regions consist of tundra plains underlain by middle-Duaternary alluvial sediments of various ice contents and are located on river terraces.

The model shows that at a particular moment of time lakes sizes should have a log normal distribution. Using specially developed "Vectorizator" software, we digitized the lakes in each selected region. The water surface contrasts quite well on images and is visually identifiable. As a result, digitizing allows us to make a binary representation of the image without loss of information on lake geometry. An operator identifies and outlines the lake boundary in the magnified image fragment in a semi-automatic mode.

Then the software automatically calculates with high

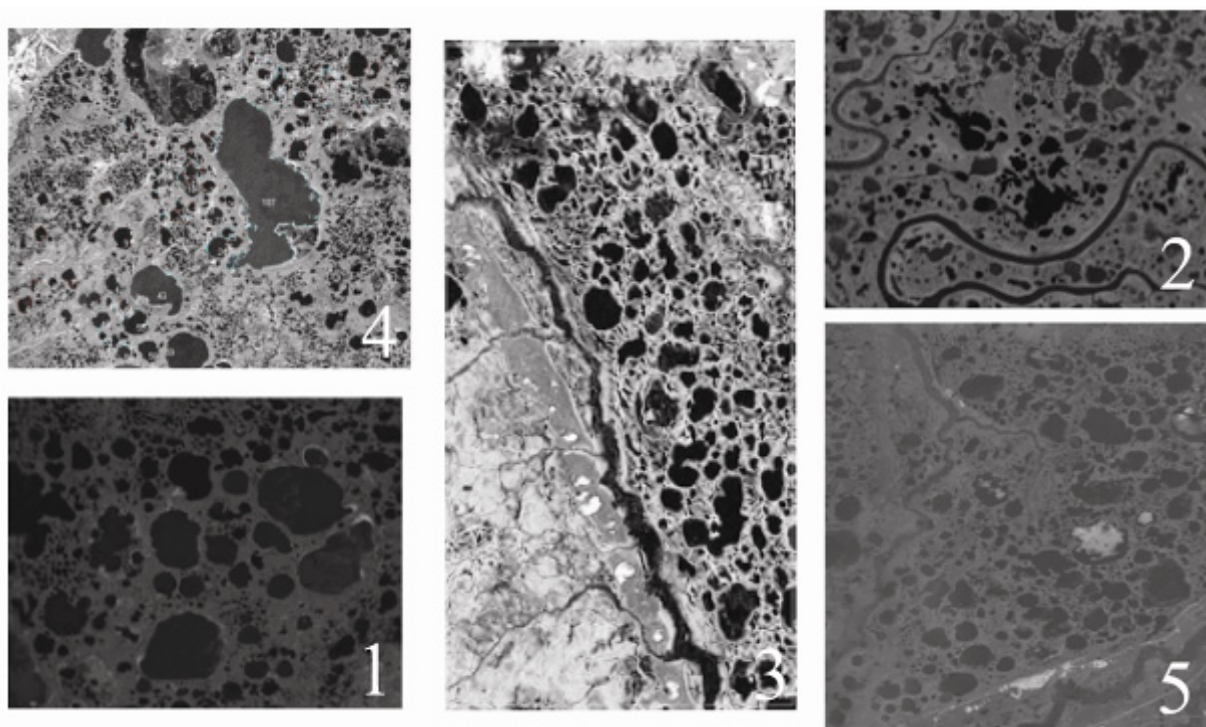


Figure 1. Satellite images of select test regions (see text for locations).

Table 1. Distribution parameters and their correspondence to log normal distribution for lake areas.

District	χ^2	number of degrees of freedom	χ^2 value at 0.95 significance level
District 1	13.80	5	11.07 (15.09)
District 2	5.60	5	11.07 (15.09)
District 3	4.02	4	9.49 (13.28)
District 4	6.49	4	9.49 (13.28)
District 5	3.91	5	9.49 (13.28)

precision the diameter, area, perimeter, location of the center, and other parameters of the outlined area. “Statistika” software was used to analyze modeled and empirical data (Table 1).

As seen from the table, the theoretical assumptions concerning areas with log normality in the selected districts are true.

The model also shows that at a particular moment of time in a randomly selected area the lakes must be distributed according to the Poisson distribution. The analysis was performed in the same regions. In the “Vectorizator” the number of lake centers within the randomly selected area (in this case, it was circle-shaped) of constant size was calculated. Statistical distributions of lake centers were obtained. Several experiments were performed for each region with circles of various diameters. Then in the “Statistika” software we obtained distribution parameters and checked the correspondence with the Poisson distribution. Most of the obtained results correspond to the Poisson distribution at the 0.95 significance level.



Figure 2. Partial image of region No. 5.

To study the dynamics of morphological structures related to thermokarst development, a West Siberian plain region near the Pyakupur River was selected. Materials for various periods were used in the study (1987, 2001, 2007). Satellite images (Landsat, IRS) and maps (Fig. 2) were used as a source of information about the morphological structure of the studied territory.

Using the “Vectorizator,” the lakes in the selected region for each date were digitized.

In order to evaluate the significance of the changes, the image interpretation error was estimated. To estimate the error, multiple independent measurements of lakes within various areas were performed; the root mean square deviation was considered to be the limiting error (Fig.3):

Points on the graph indicate actual errors, while the solid

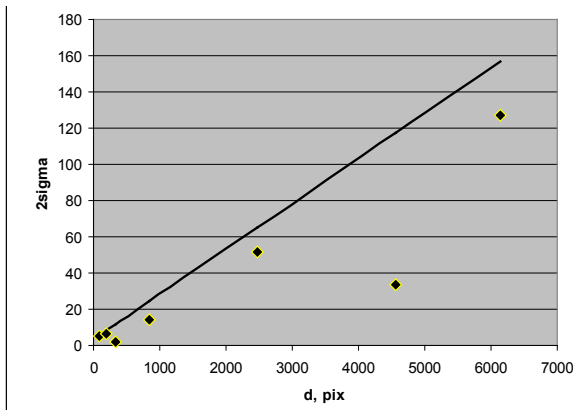


Figure 3. Graph for the 1987 image.

Table 2. Distribution parameters and their correspondence to the log normal distribution for lakes area increment.

Year of imagery	χ^2	Degree of freedom number	χ^2 criterion value at the 0.95 significance level
2001-1987	12.99	2	5.99 (9.21)
2007-2001	11.09	1	3.84 (6.64)
2007-1987	2.51	1	3.84 (6.64)

line shows the relation used to calculate interpretation error values for lakes of various sizes. The analysis showed that changes in lake sizes are larger than the interpretation error even when this highly exaggerated relation is applied.

Size distribution of thermokarst lakes for various periods of time is similar to a log normal distribution. However, as seen in the table, the use of chi-square criterion identifies significant deviations for smaller time periods (14 and 6 years) and correspondence with distribution for a larger period (20 years) (Table 2).

Thus the suggested mathematical model assumptions for lacustrine thermokarst plains were verified with experimental data.

Estimating Risk of Damage to Linear Structures

The developed mathematical models allow solution of the problem of linear structure damage by a particular hazardous process under homogeneous physical and geographical conditions. Since sizes of focus of hazardous processes comply with the Poisson distribution and each focus develops independently, the numbers of damages to a linear structure by the process will also be distributed according to the Poisson distribution (Viktorov 2006):

$$P(k, t) = \frac{[2\gamma(t)L\bar{r}(t)]^k}{k!} e^{-2\gamma(t)L\bar{r}(t)} \quad (3)$$

where $\bar{r}(t)$ is an average focus radius at a certain moment of time t , $\gamma(t)$ is average density of focus location, L is object length.

This distribution parameter is equal to the product of linear structure length, density of focus distributions, and

their average diameter. The average density of damage sections is:

$$\gamma_l(t) = 2\gamma(t)\bar{r}(t) \quad (4)$$

This means (Viktorov 2006) that the probability that a linear object will be damaged by at least one focus is equal to

$$P_{dl}(L) = 1 - e^{-2\gamma(t)\bar{r}(t)L} \quad (5)$$

Correspondingly, the stability of an engineering structure (probability of not being damaged by a hazardous geological process) is described by the following equation:

$$P_{dl}(L) = e^{-2\gamma(t)\bar{r}(t)L} \quad (6)$$

It is also easy to obtain (Viktorov 2006) the average risk (mathematical expectation of damaged district length) to the linear engineering structure:

$$R_l(L) = [1 - e^{-\gamma(t)s(t)}]L \quad (7)$$

The obtained theoretical equations were validated on several test regions.

Equation 5 for the estimation of probability of linear object damage was validated based on the following reasoning. Assume we are in the region before the thermokarst process begins. Due to the fact that the region is homogeneous, we have no reason to select any other location for the linear structure and it may be built in any point within the district with equal probability. The focus of the process developed later and could or could not have damaged the linear structure. The real situation may be modeled as follows: In the software (with the help of a random-number generator) we randomly place the linear object (of various lengths) within the selected region (with already existing focuses) and then count the number of lines not damaged by the process. A specific procedure for validation of the formula (5) was implemented as follows: with the help of a random-number generator a set of random placements of parallel sections of various lengths were made for square-shaped regions containing the digitized lakes. These lines represented location of the linear structure. Then the number of lines crossing thermokarst focuses was calculated. The percentages of sections not damaged by the process focuses from the total number of the placed sections of the given length were obtained and compared to the ones estimated by the formula (stability function, additional to damage).

During calculation, some problems occurred caused by the fact that lakes may merge together in the process of their development, and modeling did not account for such cases. In case of lake merger, the following distribution parameters are changed: average density of focuses, average area, and average focus diameter. An effort was made to consider lake mergers and to recalculate the number of lakes without separation of merged lakes. The separation was based on visual estimation. Though it was possible to take merger into account during calculation of the number of lakes, some problems occurred with average diameter and area recalculation. These problems are to be solved in the future.

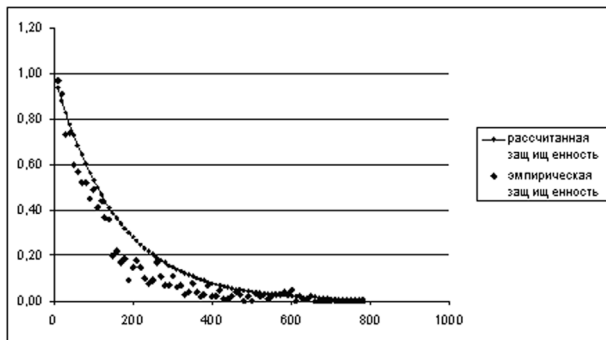


Figure 4a. Comparison of theoretical and empirical values of the stability of linear structure of various lengths to thermokarst processes (length in pixels – X axis, protection – Y axis) before lake merger correction.

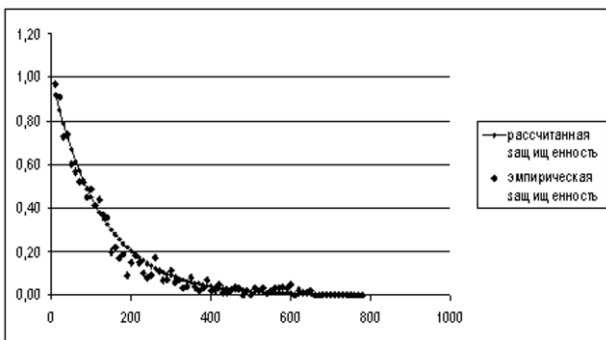


Figure 4b. Comparison of theoretical and empirical values of the stability of linear structure of various lengths to thermokarst processes (length in pixels – X axis, protection – Y axis) after lake merger correction.

Nevertheless, even the limited corrections allow significant improvement in the result (Fig. 4a, before correction; Fig. 4b, after correction).

Conclusions

The results of analysis show a general correspondence between calculated and empirical data.

The results allow us to suggest a method for assessing risk damage for engineering structures due to hazardous exogenic geological processes. The method includes the following basic elements:

- division of a heterogeneous region into homogeneous fragments;
- use of repeated remotely sensed imagery to calculate model parameters;
- estimation of average focus density and average focus diameter for a particular time period,
- calculation of probability of a linear structure to be damaged.

The results of our study are as follows:

- 1) Mathematical risk assessment models based on a mathematical landscape morphology method for damage of linear engineering structures by hazardous exogenic geological processes were developed.
- 2) Models were experimentally validated for the territories where thermokarst processes develop.
- 3) The possibility of assessing risk of damage to the

linear engineering structures by hazardous exogenic geological processes using repeat remote-sensing images was demonstrated.

References

- Elkin, V.A. 2004. Regional estimation of karst hazard and risk (Case of the Republic of Tatarstan). Dissertation abstract for Ph.D. in Geol-Min Science. Moscow: IGE RAN, 24 pp.
- Kapralova, V.N. 2008. Using remote sensing data and mathematical landscape morphology methods in thermokarst processes study. International Year of the Planet Earth: Geo-ecology, Engineering Geology and Hydrogeology Challenges. Moscow: GEOS *Sergeevskie chteniya* No. 10, pp. 430-434.
- Kapralova, V.N. & Viktorov, A.S. 2009. Modeling of lake thermokarst lowlands morphological structure and its geo-ecological value. Modeling for Geo-ecological Tasks Solving. Moscow: Geos *Sergeevskie chteniya* No. 11, pp. 174-178.
- Korolyuk, V.S., Portenko, N.I., Skorokhod, A.V. et al. 1985. *Handbook of Probability Theory and Mathematical Statistics*. Moscow: Nauka, 640 pp.
- Natural risks estimation and management. 2003. All-Russian Conference "Risk-2003" materials, Moscow: Izd. Ros. univer. druzh. narodov, V. 1, 412 pp.
- Perlstein, G.Z., Levashov, A.V., & Sergeev, D.O. 2005. Analysis of thermokarst's early stage with deterministic methods. *Transaction of the Second European Permafrost Conference*. Potsdam, pp. 143-144.
- Ragozin, A.L. (ed.). 2003. Natural risks estimation and management. Thematic Volume. Moscow.: Izd. firma "KRUK", 320 pp.
- Viktorov, A.S. 1998. *Mathematical Morphology of Landscapes*. Moscow: TRATEK, 180 pp.
- Viktorov, A.S. 2006. *Main Problems in Mathematical Morphology of Landscapes*. Moscow: Nauka, 252 pp.

The Transition Layer in Permafrost-Affected Soils, Northeast European Russia

D. Kaverin, G. Mazhitova, A. Pastukhov
Institute of Biology, Syktyvkar, Russia

F. Rivkin
Company "Fundamentproject," Moscow, Russia

Abstract

We studied the transient layer in three mineral and three organic permafrost-affected soils from the Sedyaha River basin located in the northern forest-tundra of the southern discontinuous permafrost zone, Northeast European Russia. The upper permafrost often appears to have some features of a transient layer. It is a gradual transition zone between the active layer and the epigenetic permafrost. Based on ice content, the transient layer is better expressed in organo-genic soils rather than in mineral profiles. A significant increase in the active layer thickness and related subsidence is demonstrated from the three CALM sites.

Keywords: active layer; Northeast European Russia; permafrost-affected soils; transition layer; upper permafrost.

Introduction

Shur et al. (2005) developed the concept of the transient layer (zone), a layer of ground between the active layer and permafrost that cycles through freezing and thawing at frequencies ranging from decades to millennia. It is detected in the upper permafrost according to specific structure and relatively higher ice content at depths of 0.5–2 m. This layer periodically appears as a part of the active soil profile. The transient layer, because of its high ice content, is considered to be the original buffer protecting permafrost from spasmodic thawing. The transient layer was first revealed by Yanovsky (1933) in the Pechora Basin, Northeast European Russia, in 1933. He noted that signs of pedogenic processes are marked not only in the active layer but also in the upper layers of permafrost. In terms of ecological sustainability, cold tundra soils should be studied as a complex “upper-permafrost active layer.”

Regional Background

The study area of the Sedyaha River basin is located in the northern forest-tundra of the southern border of the discontinuous permafrost zone, Northeast European Russia (Oberman & Mazhitova 2003) (Fig. 1). Permafrost is rather warm (0 to -2°C) and very unstable in the region. The watershed terrain is represented by thermokarst depressions. Surface sediments consists of peat layers of different thicknesses (up to several meters) underlain by Pleistocene lacustrine clays. Vegetation is dwarf-shrub (lichen, moss) tundra (Fig. 3). Cryosols and Cryic Histosols are widespread in the area. The mean annual air temperature is -5.3°C; mean annual thaw degree days is 1100°C-days; and mean annual precipitation is 600 mm.

Objectives and Methods

We studied the transient layer in tundra mineral profiles (1–3) and organic profiles (4–6) of permafrost-affected soils (Fig. 2). Organogenic soils were developed in peaty deposits of different thickness (up to 4.5 m). Field work was conducted at the end of August 2007.

Permafrost cores were extracted by drilling. Both power (up to a depth of 10 m) and manual drilling (up to a depth of 1.5 m) were employed.

Results

The upper permafrost layer is often characterized by ataxic or layered cryostructure (Fig. 3). Peaty permafrost-affected soils are differentiated with ice-enriched and ataxic, thick-layered cryogenic structure. Empty cavities observed in the upper peaty permafrost layers can be explained by freeze-thaw cycling in the past. Ice layer thickness, up to



Figure 1. Location of the study area.

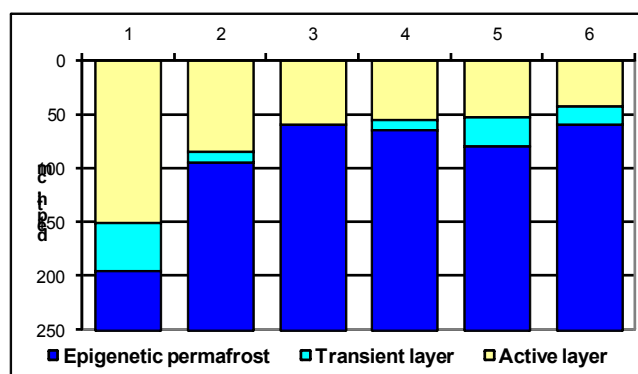


Figure 2. Profile structure according to the concept of three-layered model of permafrost-affected soils.

Table 1a. The pH and carbon contents in permafrost-affected profiles.

Soil horizon	Depth, cm	δf H ₂ O	Ń, %
1. Ednoglevic Cambisol (Geliñ), permafrost 150 cm			
İ i	0-(1-5)	4,68	5,5
B	(1-5)-15	5,19	0,45
B(g)	15-55	5,38	0,2
C(D)	55-100	5,88	0,36
frozen loam	188-190		0,38
frozen loam	225-230	6,35	0,36
frozen loam	245-250		0,48
frozen loam	270-280		0,79
frozen loam	335-345	7,22	0,79
frozen loam	380-400		0,81
frozen loam	475-485	6,99	0,96
frozen loam	565-575		1,01
frozen loam	575-595	7,36	-
frozen loam	620-640		0,84
frozen loam	620-625	7,52	0,87
frozen loam	770-780	7,56	-
frozen loam	850-860	7,48	0,99
frozen loam	950-990		0,8
2. Histit-Turbic Cryosol, permafrost 85 cm			
Oi	0-9	3,85	44,4
Oe	9-20	4,17	19,5
Bg	20-30	4,87	0,6
Bgt	30-40	5	1,35
BgtC	40-75	5,18	1,88
frozen loam	80-85		0,47
frozen loam	115-120		0,64
frozen loam	145-150		0,75
frozen loam	160-170		0,96
frozen loam	185-190		0,76
frozen loam	230-275		-
frozen loam	340-440		-
frozen loam	430-440		2,8
3. Turbic Cryosol, permafrost 174 cm			
Oi	0-(3-7)		33
Bh	(3-7)-15	5,72	3,1
G	15-30	5,17	0,68
B	30-60	5,71	0,21
C	120-140		0,23
C	140-150		0,33
frozen loam	174-180		0,25
frozen loam	200-205		-

Table 1b. The pH and carbon content in organogenic profiles.

Soil horizon	Depth, cm	δf H ₂ O	Ń, %
4. Crvi-Folic Histosol, permafrost 55 cm			
Oi	0-(5-11)	3,82	48,6
Oe1	11-36	4,25	49,3
Oe2	36-45	4,44	46,9
frozen peat	55-65	5,11	40,7
frozen peat	75	5,94	6,2
frozen loam	90-100	5,37	1,15
frozen loam	100-120	5,39	4,1
frozen loam	130-140	5,74	0,4
frozen loam	140-180	6,03	-
frozen loam	180-240	7	0,48
frozen loam	325-330	7,49	0,99
frozen loam	420	7,51	0,96
frozen loam	520-580	7,29	0,99
frozen loam	655-660	7,16	1,17
frozen loam	855-860	7,35	0,83
frozen loam	955-970	7,52	0,99
5. Crvi-Folic Histosol, permafrost 52 cm			
Oi	0-7	3,87	43,3
Oi	7-40	3,79	45,5
Oe	40-52	4,7	48,4
frozen peat	70-80	5,36	46,9
frozen peat	80-100	5,17	45
frozen peat	130-150	5,04	46,2
frozen peat	170-190		46
frozen peat	190-195	5,13	2,1
frozen peat	240-260		1,77
frozen peat	330-335	5,34	27,5
frozen peat	410-420	5,52	39
frozen peat	450	5,63	18,3
frozen loam	480-540	5,75	1,03
frozen loam	540-580	5,97	1,85
frozen loam	660-670	7,46	1,04
frozen loam	820-830	7,52	1,1
frozen loam	980	7,5	1,05
6. Crvi-Folic Histosol, permafrost 42 cm			
İ i	0-21	3,57	45,8
İ e	21-41	3,76	47,9
İ e	41-42		-
frozen peat	40-60	4,18	50,7
frozen peat	60-70	4,25	52,3
frozen peat	75-80		47,8
frozen peat	110-120	3,19	43,1
frozen peat	135-150	3,02	39
frozen peat	160-170		5,8
frozen loam	250-260		0,27

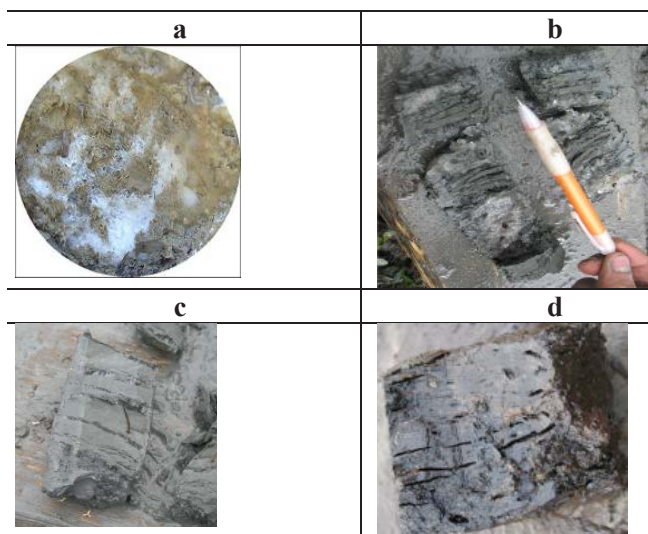


Figure 3. Cryogenic structure: a – ataxic, b, c – layered (mineral horizons), d – layered (peaty horizon).

several centimeters, increases down the profile. Gradation of ice-enriched and non-ice horizons can be considered as evidence of certain ice aggregation under climate fluctuations in the past. Shur (1988) notes that the thickness of the transient layer in the upper permafrost could be up to 20–30% of the active layer thickness. Our detailed study of the upper permafrost (1–2 m deep) revealed a rather homogenic structure of the frozen horizon. If we take into account the deeper permafrost layers (up to 10 m), this ice-enriched horizon may be observed in the very upper permafrost (upper 1–2 m), which underlies the active layer. This increase in

ice content in the upper permafrost was determined in five profiles (Fig. 4 a, b). The gravimetric ice content varies from 40–70% in loamy soils and up to 300–800% in peaty soils.

The upper permafrost layer is characterized by gradual changes in chemical parameters (C, pH, etc.) between the soil active layer and the underlying epigenetic permafrost. The pH increases gradually down the profile from acidic values in the active layer to slightly alkaline in deeper permafrost (below 5–6 m). This may be explained by the specific conditions of organic matter preservation in the permafrost. Organic matter frozen in upper permafrost layers over decades and centuries could affect its structure and degree of decomposition under thawing conditions.

The mineral soils (Cryosols) in the upper 10–20 cm are distinguished by a lower C (%) content in comparison with both the active layer and deeper epigenetic permafrost. Additional decomposition and eluviations occur during sporadic thaw periods.

Soil Cryogenic Dynamics

Data collected within the Circumpolar Active Layer Monitoring (CALM) program provide a significant source of information about the characteristics and dynamics of the transition zone. A significant increase in active layer thickness is demonstrated at the three CALM sites situated in Northeast European Russia (Mazhitova et al. 2004, Mazhitova & Kaverin 2007).

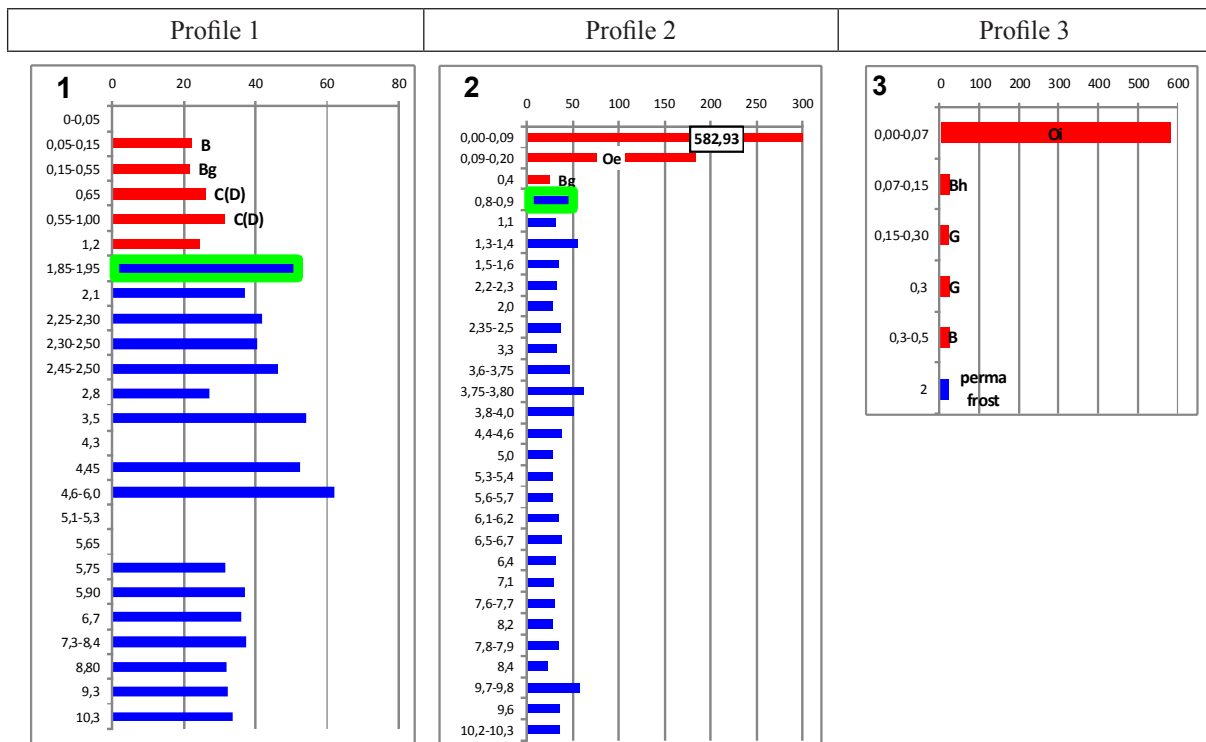


Figure 4a. Gravimetric water (ice) content in the active layer and permafrost in mineral profiles (%). Blue is permafrost; green denotes the transition layer (see Fig. 2).

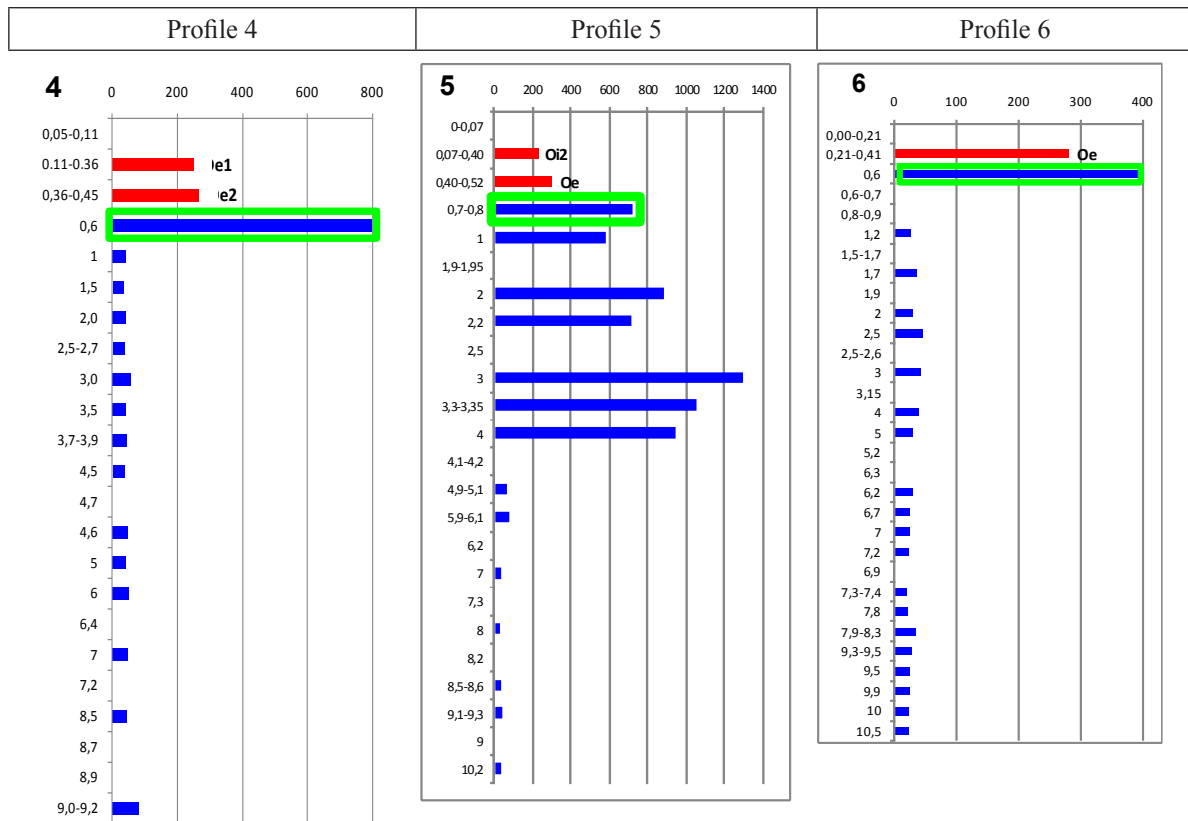


Figure 4b. Gravimetric water (ice) content in active layer and permafrost in organogenic profiles (%).

Besides active layer thickness, subsidence has been measured at the CALM R2 site since 1999. Site-averaged surface subsidence totaled 13 cm with an increase in the active layer depth of 25 cm. Permafrost retreat (as a summary result of both subsidence and active layer increase) was 38 cm during 1999–2010 (Fig. 5).

In upper permafrost horizons, volumetric ice content can be approximated by a “normalized subsidence” index (subsidence, cm to permafrost downward retreat, cm ratio). We calculated the average index for the CALM R2 site for 11 years and received a value of 0.54 (ice content of thawed upper permafrost was about 54%). Such high ice content is

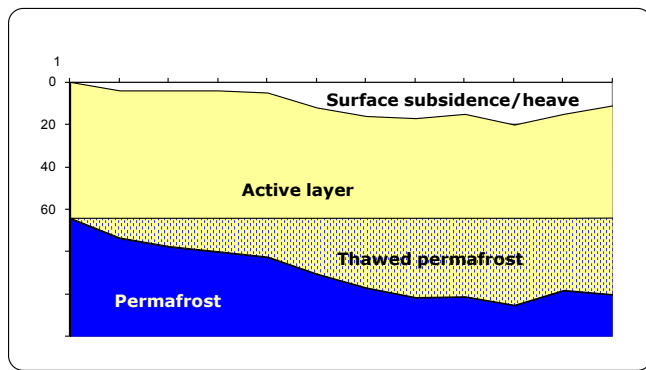


Figure 5. Active-layer thickness, surface subsidence and permafrost retreat at the R2 (Ayach-Yakha) CALM site.

Table 2. Diagnostic features of the transient layer in the upper permafrost.

Profile/Feature	Cryogenic structure	Cryo turbations	Ice content, %	C, %	$\delta^{13}C$
1	+		+	+	+
2			+	+	+
3				+	+
4			+	+	+
5			+	+	+
6	+		+	+	+

Yellow color – could not be considered as a factor in peaty soils

typical for mineral horizons of the transient layer. Surface subsidence is caused by thaw of the ice-saturated layer in upper permafrost.

Diagnostic Features of the Active Layer

The presence and absence of the transient layer in the upper permafrost was determined according to morphological and physical-chemical parameters (Table 2). In the investigated profiles, the most significant features of the transient layer appear to be its high-ice content and relatively lower acidity and carbon content. Considering these factors, this uppermost permafrost layer appears to be a gradual transition zone between the active layer and epigenetic permafrost beneath. However, it is not as clearly expressed as in the permafrost-affected soils of Eastern Siberia.

Summary

- 1) The upper permafrost often appears to have some features of a transient layer in tundra soils of Northeast European Russia. It is a gradual transition zone between the active layer and the epigenetic permafrost.
- 2) According to the ice content, the transient layer is better expressed in organogenic soils rather than in loamy profiles.
- 3) Lower acidity in permafrost horizons is the result of specific conditions of the preservation of organic matter.
- 4) During the last decade, surface subsidence processes

are associated with thaw penetration into the ice-enriched (transient) layer of permafrost.

References

- Lupachev, A.V. & Gubin, S.V. 2007. Role of pedogenesis of pedogenesis in the formation of permafrost transition layer structure. *Earth Cryosphere* 12 (no. 2): 75–83.
- Mazhitova, G.G. & Kaverin, D.A. 2007. Dynamics of seasonal thaw depth and surface subsidence at a Circumpolar Active Layer Monitoring (CALM) site in the European Russia. *Earth Cryosphere* 11 (no.4): 20-30 (in Russian).
- Mazhitova, G., Malkova, G., Chestnykh, O. et al. 2004a. Active layer spatial and temporal variability at European Russian Circumpolar-Active-Layer-Monitoring (CALM) sites. *Permafrost and Periglacial Processes* 15:123-139.
- Oberman, N.G. & Mazhitova, G.G. 2003. Permafrost mapping of Northeast European Russia based on period of the climatic warming of 1970-1995. *Norsk Geografisk Tidsskrift – Norwegian Journal of Geography* 57 (2): 111-120.
- Shur, Y.L. 1988. The upper horizon of permafrost soils. In *Proceedings of the Fifth International Conference on Permafrost*. Tapir Publishers, Trondheim: Norway. Vol. 1, 867-871.
- Shur, Y., Hinkel, K.M., & Nelson, F.E. 2005. The transient layer: implications for geocryology and global-change science. *Permafrost and Periglacial Processes* 16(1): 5-11.
- Yanovsky, V.K. 1933. Expedition to Pechora for determination of southern border of permafrost. *Proceedings of Permafrost Commission, Leningrad*, vol. 2, 65-149 (in Russian).

Ice Volume Estimates in the Bolshezemelskiy Artesian Basin Permafrost

V.Z. Khilimonyuk, E.N. Ospennikov, S.N. Buldovich, E.I. Gorshkov
Lomonosov Moscow State University, Faculty of Geology, Department of Geocryology, Moscow, Russia

Abstract

The methods for quantitatively estimating the ice volume in the permafrost zones of the Bolshezemelskiy Artesian Basin, Russian European North, are described. Quantitative values for total ice volume in selected geocryological regions and in the entire territory are given. The total ice volume in the region of 87,900 km² is approximately 2,300 km³.

Keywords: cryolithozone; ice volume; permafrost; permafrost zonation.

Introduction

The quantitative estimate of ice volume in the studied area is of significant interest due to the fact that permafrost degradation resulting from climate change will result in the release of frozen water. Permafrost degradation will start to supplement the underground water reservoir in the hydrogeological structures and will contribute to the exchange of underground water.

The general estimate of epigenetic hydrogeological conditions is an extremely complicated and multi-faceted problem, not studied in this research. However, quantitative determination of the currently immobilized volume of underground waters in the frozen part of the geological section may be undertaken in detail based on the existing summary data related to geocryological conditions and territorial zoning of permafrost.

Methodology and Results

The given estimation methods were as follows. At the first stage, a schematic map of permafrost zoning was prepared for the studied territory (1:500,000). On its basis, the quantitative estimate of underground ice content was performed.

The main purpose of the permafrost zoning was for the regional estimate of the increment of underground water deposits that would result from the possible thaw of the permafrost. This task defined the permafrost zoning features and its primary focus on the permafrost cryolithological characteristics and the estimate of ice content.

To make a permafrost zoning map, the available literature and geological, geocryological, and cartographical (satellite and aerial photographs, etc.) information and materials for the studied territory were used (Ershov 1997, VNIIOkeangeologiya 2001). We also used the materials containing data on permafrost formation conditions, distribution nature, thickness, ice content, and temperature regime including geophysical surveys.

Changes in permafrost conditions in both latitudinal and longitudinal directions are typical of the territory. Distribution and temperature of permafrost and thawed grounds depend on latitudinal zonality. In addition to general permafrost zonality, there are regional and local deviations from it caused by a number of natural factors.

Permafrost structure and thickness, in general and regarding the studied territory, are related to heat exchange

conditions on the surface during the Pleistocene-Holocene period of geological development. In the southern part of the studied territory, permafrost temperature and thickness clearly comply with the current heat exchange conditions. From here to the north permafrost thickness gradually increases from a dozen meters to 400–500 m. However, in the southern regions of the studied territory there are non-thawed, Pleistocene formations 30–150 m below the surface. They are related to the regions with thick unconsolidated sediments, and together with the Holocene permafrost, they form the “two-layered permafrost” (i.e., permafrost beneath thawed ground, or relict permafrost). In the northern subzone, the Pleistocene dynamics of heat exchange conditions on the studied territory did not result in annual ground thawing from the surface. That is why the uniform (continuous) vertical structure and large thickness are typical of permafrost here (Ershov 1988, VNIIOkeangeologiya, 1997, Oberman 1981).

In general, zonality is clearly shown also in the distribution ground ice content. In the south, the cryolithozone is represented mostly by permafrost that contains ice, because permafrost thickness in the artesian structure is less than the depth of saline waters and salt brine solutions. In low sea terraces of the northern part of this area, the permafrost may not contain crystal ice.

Based on cryogenic structure and ice content, the following ground conditions are clearly distinguished: consolidated and semi-consolidated rock formations, and unconsolidated Quaternary sediments and formations. Typical of rock formations are low fracturing and porosity and low ice content not exceeding a few percent of the total volume. As a rule, underground moisture redistribution during freezing and thawing is unlikely. In addition, some differences in cryolithological properties are typical of the major types of rocks (magmatic, metamorphic, and sedimentary). In unconsolidated sediments, ice saturation is the result of the ground composition, their genesis, and diagenetic modifications.

Cryogenic structure and ice content are also influenced by the possibility of moisture migration during changes in ground temperature and moisture due to annual ground freezing or thawing or even during changes in ground temperature. The result is not only that the cryogenic structure inherits defective zones of grounds (generally, cavities and pores), but also that special types of cryogenic structures emerge due to moisture migration during freezing. In addition, in unconsolidated sediments, the initial moisture distribution changes. In general, significantly higher moisture from

5–10% to 90–95% is typical of unconsolidated formations. Thus the ground composition and structure are among the most important features of the typical permafrost conditions.

There are significant differences in the permafrost structure itself. For instance, in the zone of island distribution, permafrost is usually one-layered and is represented by disperse or rocky epigenetically frozen materials. In zones of massive and island distribution, as well as discontinuous distribution, permafrost often consists of disperse epigenetically frozen formations underlain by rocky formations. This is due to the permafrost's great thickness and low-temperature regime. In most northern regions, syngenetically frozen ground underlain by epigenetically frozen formations start to emerge quite intensively. High-ice content of massive ice inclusions (ice-wedge, injection, segregated ice) is typical of the ground, resulting in significantly greater volume of total ground ice. On the Arctic coast, these grounds are generally underlain by non-ice-bearing permafrost or cryopegs.

The abovementioned characteristics and principles of permafrost structure were used as the main features to define typical cryolithological sections and to estimate their ice content. This is based on the ice content of the section and its separate horizons and thickness. Such estimates, based on understanding the dimensional development of a particular cryolithological section, allowed accurate estimates of total ice deposits in permafrost of the Bolshezemelskiy Artesian Basin.

A cryogenic description of the genetic types of formations was focused on the description and estimation of the ice macro-inclusions, which are determined by the ground moisture and composition as well as on the identification of the freezing type identification (syngenetic or epigenetic).

A cryolithological description was performed for all permafrost layers and considered during the overall calculation of underground ice deposits. The ice, after permafrost thawing, in the form of water may be drained from the rock formations and thus increase underground water deposits.

During the study, it was determined that the ground ice content of the major genetic complexes of sediments does not change significantly laterally or vertically. Ice content changes mostly within a relatively narrow range of 0.05–0.25. That is why the permafrost thickness may be used to calculate the total ice content of unconsolidated sediments.

The important feature of permafrost vertical structure is the relict permafrost horizon mostly confined to island permafrost. This relict permafrost layer 100–200 m from the surface has a vertical thickness of up to 200 m or more.

Another important factor is the principle of permafrost area distribution. Complicated permafrost distribution is caused by the interaction of landscape climatic conditions, relief, ground composition and properties, hydrological and hydrogeological situation, and the history of Neogene-Pleistocene age development. On the other hand, distribution of talik permafrost is related to zonal heat exchange conditions on the Earth's surface. Also the principle of distribution of permafrost area results in the existence of sub-latitudinal belts within which there is a particular ratio between the distribution of thawed and frozen ground. The following zones (belts) occur in the studied territory:

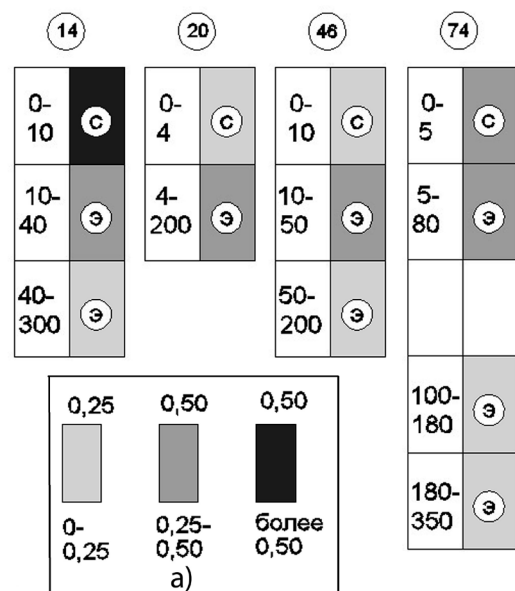


Figure 1. Examples of typical permafrost sections where: a) volumetric ice content of the ground; б) 0-10, 100-180, etc.; depth of permafrost top and base, m; в) S, E – syncryogenic and epicryogenic ground, respectively. Above the columns there is an index number of a typical geocryological section; on the whole, there are 75 of them specified.

- (1) the region of cooled negative temperature grounds;
- (2) the region of mostly uniform permafrost distribution (more than 95% of the total area);
- (3) the region of discontinuous permafrost (75–95% of the area);
- (4) the region of island permafrost (25–50% of the total area);
- (5) the region of rare-island permafrost (less than 25% of the total area); and
- (5) the region of mostly thawed ground with isolated permafrost islands and short-term permafrost (frozen “pereletoks”).

The ice volume estimate was performed based on the geocryological zoning with percentage determination of the ratio between frozen and thawed ground areas (see above). In addition, in the coastal regions with high ground salinity the corresponding ice content reduction was considered (Fig. 2).

The data allow calculation of the total amount of ice content in the entire permafrost section for a given unit of surface area. This value measured in m (m^3/m^2) may be considered as the thickness of a pure ice layer equivalent to total ice content in the permafrost section.

Then each area outline for a particular sediment genetic type was determined. Having multiplied the obtained value by the ice “equivalent thickness” value, we determined the total volume of underground water located within the limits of the studied area. This volume corresponds to the amount of underground water withdrawn from the hydrogeological section as a result of many years of ground freezing.

As expected, the total ice content in the permafrost significantly changes within the limits of the studied territory; the “equivalent” ice layer thickness varies from several meters to 50–60 m or even 70 m.

The ice content characteristics obtained for certain areas of the region containing genetically different sediments were averaged within the limits of the smallest zoning units. The analysis of the area characteristics shows that, in general, the

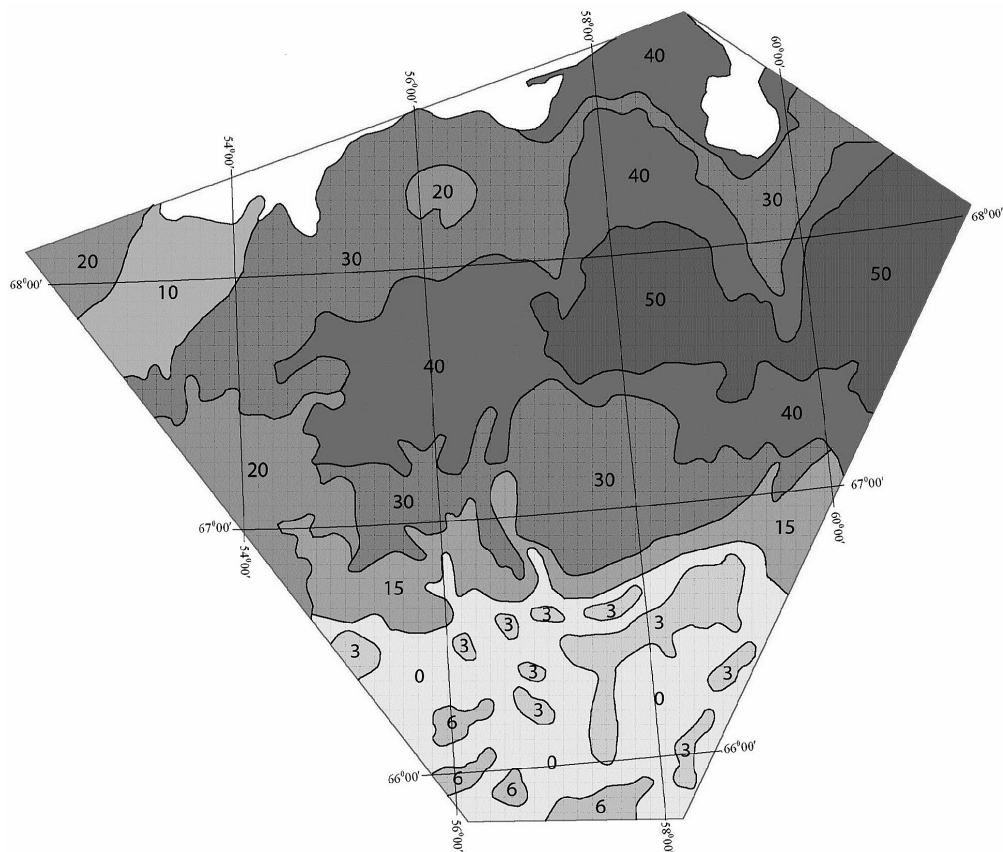


Figure 2. Map of the territorial zonation of Bolshezemelskiy Artesian Basin according to ice content in the frozen ground where 0, 3, 6...50 are the average integral, within the enclosed area, of the specific value of ice content in the overall permafrost section (unit area; m³/m². or equivalent) ice layer thickness (m).

thicker and more uniform the permafrost thickness the larger is the ice layer “equivalent” thickness.

It is worth noting that the general regularity of the changes in permafrost ice content is often inconsistent. The inconsistencies occur primarily due to geological factors, namely the occurrence of rocks close to the surface. In this case, the small thickness of unconsolidated, ice-rich sediments results in relatively low ice content in the permafrost, notwithstanding its high total thickness. Also, the presence and characteristics of the relict permafrost layer influence the areal distribution and regularities of summarized ice content.

Conclusions

The results of the study highlight the following: The total ice volume in permafrost on the entire permafrost territory is extremely large and amounts to approximately 2,300 km³. Considering the territorial area of 87,900 km², the average equivalent ice layer thickness is about 26.2 m. With the average outflow in the Pechora River estuary of 127 km³/year (4000 m³/sec), the melting of the ice deposits in permafrost of the territory is equivalent to 18 years of discharge for this large arctic river.

References

- Ershov, E.D. (ed.). 1997. Geocryological map of the USSR of 1: 2,500,000 scale. *Kartopredpriyatie, Vinnitsa, Ukraine*, 16 sheets (in Russian).
- Ershov, E.D. (ed.). 1988. USSR Geocryology. USSR European territory. *Nedra Moscow*, 358 pp. (in Russian).
- Oberman, N.G. 1981. Permafrost formation history of Polar, Subpolar and Northern Ural. *Eurasia Permafrost Development History (case study of particular regions)*. Moscow, pp. 73-78 (in Russian).
- VNIIOkeangeologiya, 2001. State geological map of the Russian Federation. 2001. Of 1:1,000,000 scale (new edition). Sheets R-38-40, R-40-42, Q-38-39, Q-40-41. Explanatory letter. SPb, Izd-vo VSEGEI, (MPR of Russia, VSEGEI, MAGE, VNIIOkeangeologiya, PMGRE) (in Russian).

Environmental and Geological Problems of Subarctic Territories and Possible Solutions

V.Z. Khilimonyuk, A.V. Broushkov, S.I. Grebenkin

Lomonosov Moscow State University, Faculty of Geology, Department of Geocryology, Moscow, Russia

Abstract

Further development of the Arctic is one of the most important priorities in Russia. Environmental and geological problems of the subarctic territories and possible solutions are discussed.

Keywords: cryolithozone; environmental problems; geological problems; geocryological monitoring; permafrost.

Introduction

The report of Vladimir Putin, Head of the Russian Government, at the International Arctic Forum held at Moscow State University in September 2010 defined the priorities in development of the Arctic and described the problems of subarctic territories (particularly, contamination from various wastes). Putin noted the importance of the search for solutions by means of development and introduction of innovative technologies.

Everyone knows that the Far North districts experience severe climatic conditions: air temperatures of -50 degrees and colder, low amount of solar radiation, winters of 9 months and longer, and short cold summers. But one other fact is frequently dismissed: permafrost occupies about 70% of the Russian Far North.

It is evident that permafrost strata and the processes in them are a natural component of the environment. They define the conditions of humidification, soil formation, presence of biota, landscape stability, and land surface stability, as well as subsistence resources. Most of the Siberian taiga would not exist in the absence of permafrost

Contamination and waste disposal are critical environmental problems in the Arctic. A huge amount of waste has been collected to date as a result of the long history of development of these territories, including mineral resource exploration and mining. Waste materials are frequently stored and buried in unauthorized zones.

Wide areas containing dumps of solid household waste are formed around northern cities, creating environmentally hazardous zones. The volume of disposed waste is continuously growing. The average production level of waste utilization in the Russian Federation is about 30%. Only 2% of the total volume of waste is extracted in the form of secondary raw material. The remaining 98% pollutes the environment, adversely impacting the population and environmental safety (Committee of the Federation Council on Resources and Environmental Protection 2011).

Today there is no documentation concerning waste utilization in the Far North. Specifically, there are no documents for the creation of facilities for solid household waste disposal that reflect the peculiarities of the Far North regions where permafrost exists. Neutralization using a biological method is required at disposal facilities for solid household waste. However, as is known, the negative ambient temperatures not only fail to assist in decomposition of any waste, but delay it. Biological decomposition processes

cease at negative temperatures; the biomass does not decay but is preserved.

New utilization technologies with the use of psychrophilic bacteria, including methanogenic ones, should be used in the polar regions. They will accelerate waste decomposition processes. Then the methane formed can be collected and used.

The problem of treatment of drainage water is also very important. The city of Yakutsk is a good example. As a result of household drainage water, the presence of a cryogenic aquiclude (permafrost) preconditions the formation of highly mineralized groundwater near the surface and flooding of city residential areas. Permafrost barriers predetermine the formation of negative-temperature, highly mineralized, supra- and intrapermafrost groundwater (cryopegs) at the depth of up to 20 m in the ground stratum. The water mineralization reaches up to 200 g/l at individual, long-inhabited areas of the city. The concentration of these elements is increased by 30–60 to 300–500 times and more as compared to the background values in fresh and salty suprapermafrost waters (Anisimova 2005).

In the meantime, the burial of radioactive waste in permafrost is more reliable and the cryolithozone can serve as a reliable reservoir for radioactive waste disposal (Ershov et al. 1995, 1997).

Most of Russia's oil and gas reserves are present in the cryolithozone (70.8% of oil reserves are concentrated in Western Siberia). Utilization of waste formed in the process of oil production and in cases of oil spillage is one of the most complex and multifaceted environmental problems. A wide range of devices and technologies is proposed for neutralization and utilization of oil waste and ground cleanout of oil products. Nonetheless, only a few of them take into account the geocryological and climatic conditions of the Arctic.

The environmental state of the subarctic territories depends to a large extent on the state of the permafrost. Moreover, the change of the ground thermal state in the upper part of the section is usually accompanied by activation of postcryogenic processes and development within the zone where their occurrences previously were insignificant or were not noted at all.

Consequently, estimation of the dynamics of the geocryological conditions as a result of climate change and under the impact of human activity is very important. The problem is that we do not know the current state of permafrost (i.e., whether it is stable or thawing).

Discussion

Environmental problems in the Arctic (and not limited to that region) are associated with global climate change. The discussion of possible scenarios for global and regional climatic changes in the 21st century has developed during the recent decades. Three main approaches are used for possible climate change prediction:

- the use of general atmospheric circulation models based on an increase of CO₂ and other greenhouse gas content in it;
- examination of paleoclimatic analogues;
- empirical analysis of current meteorological characteristic variations (cycle and trend analysis) (Bases... 2008).

The range of forecasted values of CO₂ equivalent content in the atmosphere in the 21st century is extremely wide. Nonetheless, the majority of researchers working with the general circulation models assume doubling of the carbon dioxide concentration by the end of the 21st century. Forecasts of the global mean air temperature variation are based on that.

Assessment of the forthcoming global climate change is ambiguous. The following scenarios are developed: significant warming (Budyko et al. 1992), moderate warming (Borisikov 1990, Pavlov 1992, 1997, 2001), and even cooling (Shpolyanskaya 1981, 2001, Balobaev 1983, 1991). Nonetheless, it is evident that the mean annual air temperature is increasing. The permafrost response to climate changes is locally observed as well.

The trend of increased permafrost temperature during the recent 20–30 years and permafrost degradation are observed in many cryolithozone regions. Permafrost warming in mountain regions is confirmed. This was reflected in many reports of the recent conference of Russia's geocryologists held at Moscow State University. The data on warming by 3°C is present in the Arctic Forum documents. Nonetheless, it is not that unambiguous. There is no substantiated estimate in general.

Greenhouse gas emissions into the atmosphere present a very important problem. Up to 10% of undecomposed organics is present in permafrost. Bulk methane emission will occur in global climate warming and permafrost degradation scenarios. Even without it, intensive methane greenhouse gas emission occurs in the process of hydrocarbon (oil and gas) production and transportation. Up to 560 Mt of methane are annually emitted into the atmosphere. The shared use of the associated and dissolved gas does not yet exceed 50%. Its utilization is still a critical problem. Most gas leakage in the process of gas transportation occurs as a result of the high risk of accidents in pipelines. Most of the built (45,000 km for 2004) and designed oil and gas transportation systems occur in the cryolithozone, and permafrost is one of the reasons for the increased risk of accident.

The change of operational conditions of structures in the cryolithozone, if designed without regard to global climate warming, is one of the most important consequences of environmental permafrost degradation. The fact is that strength and deformation properties of the permafrost serving as the basis for engineering structures depend much on the temperature. The former decreases and the latter grows as tempera-

tures rise. This leads to structural deformations and material damage. The results of calculations conducted at the Geocryology Department of Moscow State University (Khrustalev et al. 2008, 2011) showed that almost all buildings erected before 2001 will be deformed as a result of global climate warming by the end of the forecast period (2100).

Minor changes in the permafrost thermal regime, both as a result of natural evolutionary change in the Earth's thermal field and as a result of technogenic impact, lead to changes not only in the geophysical environmental function, but also in the functions of resource, geodynamic, and geochemical lithosphere. This is like a chain reaction leading to significant transformations of the environmental properties of the cryolithosphere. During the recent decades, starting especially in the 1960s and 1970s, Russia's northern ecosystems suffered significant technogenic impact due to intensive exploration of various mineral deposits. Cryogenic processes are activated and become destructive with the economic development of the territory.

The estimation of the current permafrost dynamics and the probability of thawing, creation of a system of environmental monitoring in the North, and forecast of the permafrost state for the next decades are required for the development of the northern regions.

Fundamental climate, glaciological, and permafrost studies in relation to the general dynamics of the lithosphere and biosphere are required. Also needed is the development of simulation methods for the permafrost thermal regime pursuant to climate changes and under the impact of engineering structures.

It is proposed to:

- 1) Estimate the current state of permafrost and make a forecast for the next decades. Required for that is the creation of a national environmental and geocryological permafrost state monitoring grid; currently there is not even a single, unified methodology for permafrost thermal regime monitoring. Several complex stations (climate, ground, soil, gas exchange, biota monitoring) will be needed in the country.
- 2) Compile geocryological maps for the entire Russian territory and an atlas of the Russian Arctic sea coast and shelf.
- 3) Develop numerical models for ground thermal exchange.
- 4) Create new technologies for ground stabilization on the Arctic coast and shelf.
- 5) Research the biogeochemistry sphere, and study permafrost bioresources, greenhouse gas emissions, recovery of ancient microorganism strains for application in biotechnologies.

References

- Anisimova, N.P., Pavlova, N.A., & Stambovskaya, Ya.V. 2005. Anthropogenic transformation of suprapermafrost water ecological functions on low terraces of the Lena River within the Tuymaada Valley. *Materials of the Third Conference of Russia's Geocryologists*. Vol. 2. Moscow: Izdatelstvo MGU, 212-216 (in Russian).
- Balobaev, V.T. 1991. *Geothermics of Cryolithosphere of the Asian North*. Novosibirsk: Nauka, 193 pp. (in Russian).

- Balobaev, V.T. & Pavlov, A.V. 1983. Cryolithozone dynamics in relation to climate changes and anthropogenic impacts. *Geocryology Problems* Moscow: Nauka, 184-194 (in Russian).
- Budyko, M.I. & Izrael, Yu.A. (eds.) 1987. *Anthropogenic Climate Changes*. Leningrad: Gidrometeoizdat (in Russian).
- Budyko, M.I., Izrael, Yu.A., & Yanshin, A.L. 1992. Global warming and its consequences. *Meteorology and Hydrology* 12: 5-10 (in Russian).
- Borisenkov, E.P. 1990. *Climate Change and a Human*. Moscow: Znanie, 60 pp. (in Russian).
- Ershov, E.D. (ed.). 2008. *Fundamentals of Geocryology*. Part 6. Geocryological forecast and environmental problems in cryolithozone. Moscow: Izdatelstvo MGU, 768 pp. (in Russian).
- Ershov, E.D., Parmuzin, S.Yu. et al. 1997. Permafrost as the medium for environmentally hazardous waste burial. *Geoecology* 1: 23-39 (in Russian).
- Khrustalev, L.N., Klimenko, V.V. et al. 2008. Permafrost thermal field dynamics in the southern cryolithozone districts at different climatic change scenarios. *Cryosphere of the Earth* 1. Vol. 12: 3-11 (in Russian).
- Khrustalev, L.N., Parmuzin, S.Yu., & Emelyanova, L.V. 2011. Northern infrastructure reliability in the changing climate conditions. Moscow: Universitetskaya Kniga (in Russian).
- Pavlov, A.V. 1997. Permafrost-climatic monitoring of Russia: Monitoring methodology, results, forecast. *Cryosphere of the Earth* 1: 47-58 (in Russian).
- Pavlov, A.V. 2001. Cryolithozone response to modern and expected climatic changes in the 21st century. *Subsurface Exploration and Protection* 5: 8-14 (in Russian).
- Shpolyanskaya, N.A. 1981. *West Siberian Permafrost Zone and Trends in Its Evolution*. Moscow, 168 pp. (in Russian).
- Shpolyanskaya, N.A. 2001. Climatic rhythms and cryolithozone dynamics: An analysis of the evolution in the past and change forecast for the future. *Cryolithozone of the Earth* 1. Vol. 5: 3-14 (in Russian).

Assessment of Landslide Geohazards in Typical Tundra of Central Yamal

A.V. Khomutov

Earth Cryosphere Institute, SB RAS, Tyumen, Russia

Abstract

Results of the retrogressive thaw slumping geohazard assessment in various landscapes of Central Yamal are presented. The territory is differentiated according to the probability of retrogressive thaw slumping. Four groups of natural terrain units were identified within the study area depending on the probability of the re-occurrence of retrogressive thaw slumps. The percentage of the thaw slumping occurrence within a natural terrain unit determines its sensitivity to possible re-occurrence, depending on the size of the area modified by recent retrogressive thaw flow. At the same time, the sites of recent thaw slumps are considered non-hazardous because the re-occurrence of thaw slumping within these sites in next centuries is unlikely.

Keywords: landscape map; landslide geohazard map; natural terrain units; retrogressive thaw flow.

Introduction

Retrogressive thaw slumping is the most active geomorphic process in areas with widespread occurrence of massive ice(y) beds (Leibman 2005). Development of thaw slumping in the areas of the shallow occurrence of massive ice beds should be considered the most hazardous type of slope instability. Slumping on such slopes can re-occur even in case of a slight increase in summer air temperatures combined with minimal technogenic impact (Leibman & Kizyakov 2007, Burn & Zhang 2009).

The slopes with seasonal ground ice that is formed at the base of the active layer in a certain combination of climatic factors over a period of several years are less sensitive to the impact (Leibman 1997). Retrogressive thaw flows along such icy surfaces (cryogenic active-layer detachment slides) can re-occur at the same site once in a few hundred years. However, this periodicity is not fixed in time, and the adjacent areas may be affected by these processes during other periods under the conditions of significant increase of summer precipitation and a simultaneous increase of air temperature. Cryogenic active-layer detachment slides are the largest in size and, consequently, in mass. This is why they are so hazardous.

Assessment of the landslide hazard in different terrain types, including the permafrost zone, is one of the most important tasks of science nowadays. To determine the risks of earth flow processes, scientists use qualitative estimates based on identification of sites with different landslide characteristics (Kazakov & Gensiorovsky 2008). To ensure landslide control during construction, assessment of the landslide situation is carried out using qualitative and quantitative methods which include characterization of geomorphological and hydrogeological conditions; engineering geological sections of landslides; mapping of landslide process manifestations based on satellite imagery and air-photo interpretation and ground-truthing; and actual measurement data and geophysical surveys in areas affected by landslides (Postoev et al. 2008). There are examples of the landslide risk assessment using a points system to determine landslide occurrence probability (Chekhina et al 2004).

Because of the active development of the hydrocarbon fields located in the North, especially in the areas of

occurrences of hazardous geomorphic processes, it is necessary to evaluate the landslide threat. This evaluation is done with extensive use of the data provided by remote sensing based on previously identified patterns of the retrogressive thaw flow development and the occurrence of thaw flows in areas characterized by certain terrain conditions.

Study Area

Estimates of the thaw slumping hazard were carried out at the "Vaskiny Dachi" key site in the Central Yamal within the watershed of Seyakha and Mordyyakha rivers (Fig. 1).

The study area is a hilly plain with narrow divides and long gentle slopes. The highest elevations (up to 58 m a.s.l.) are found within flat-topped remnants of the Salekhard Plain. The territory is intensely dissected by narrow river valleys and small streams, gullies, and ravines. The development of gullies is determined by the amount of potential relief energy; therefore, the most extensive gullies are found at high geomorphological levels. The dissection depth of the Salekhard and Kazantsevskaya plains is up to 50 m. Most of the territory (about 60%) is represented by gentle slopes with slope angle up to 7°; slopes with slope angle from 7° to 50° occupy approximately 10% of the area; and the remaining 30% include floodplains, lake basins, and narrow-topped ridges (Leibman et al. 2003).

Active development of slope processes is a characteristic feature of the remnants of marine terraces composed of ice-rich deposits with massive ice beds. On the slopes with the shallow occurrence of massive ice beds, thermal cirques are developed, which transform into a semi-circular steep headwall as the massive ground ice bed melts (Leibman 2005).

As a landscape type, the Vaskiny Dachi key site is located in the subzone of typical (moss and lichen) tundra, gradually changing into the subzone of low-shrub tundra (Trofimov 1975).

Within the watersheds, dense dwarf arctic birch is widespread, regardless of the thickness of snow cover. Better drained slopes of the elevated terrain are occupied by shrub-moss-lichen tundra. On gentle poorly drained slopes, compared to well-drained ones, shrubs and low shrubs are better developed and mosses predominate. On convex tops



Figure 1. Key site location.

and wind-swept hill slopes, shrub-moss-lichen tundras with non-sorted circles are predominant. River valleys, thermocirques, and earth flow bottoms with fairly thick snow cover in wintertime are characterized by willow bush tundra (bush height corresponds to snow cover thickness). Sedge, sphagnum, and flat-hummocky bogs as well as moors are common on flat surfaces of watersheds and terraces, on low lake shores, in the upper parts of river valleys, and in other depressions.

Methods and Results of Study

In order to estimate the landslide geohazard, a map of natural terrain units of the key site area was used. Terrain zoning of the key site developed specifically for the analysis of the landslide geohazard was performed. At the initial stage, geomorphological levels differing by the nature of the geological structure and relief were allocated according to Leibman & Kizyakov (2007). Higher geomorphological levels provide greater amplitude of the relief, longer slopes, and respectively greater earth flow probability (Leibman 2005). Then the relief elements which were likely to see the development of the earth flow process were identified. Horizontal surfaces and bottoms were selected where the formation of cryogenic earth flows was not possible as well as the tops where earth flow formation was unlikely to occur. The next stage was slope examination. Estimates of earth flow hazard on the slopes are based on previously developed conceptual models of cryogenic earth flow (Leibman & Kizyakov 2007). Analysis of the current earth flow process reveals that earth flows mostly descend along concave slopes (Leibman 2005). However, the descent of new earth flows is less likely to occur along concave slopes affected by modern earth flow processes than on concave slopes with ancient earth flows. The conditions for repeated earth flows

have developed on some plots differing in size (from the first few meters to hundreds of meters, depending on the age of the earth flow surface) and are located on the slopes affected by earth flows in the past. These conditions include thick turfness of the surface and a seasonally thawed layer consisting of sandy and silty loam slope deposits.

By earth flow hazard, we mean the probability of surface damage due to the earth flow body displacement ("zone of flow-off [source]"), the formation of the sliding surface ("transit zone"), and unloading of the earth flow body ("accumulation zone"). From the landscape point of view, the process of earth flow changes all of the relief elements. The watershed edges are affected in the zone of the outflow, resulting in detached cracks in the watershed and subsidence due to suffusion. The slope surface in the transit zone is left bare, which gives an impetus to the development of thermal erosion. Saline rocks come to the surface, resulting in specific vegetation succession. The earth flow body is unloaded at the bottom of the slope, onto the valley, or into the ravine in the accumulation zone. This leads to the change of the hydrological regime, blocking of slope, and valley water flow and formation of backwater lakes with thermokarst being developed.

Percentage of recent thaw slumping occurrence within a terrain unit

Based on the map of natural terrain units (NTCs), analysis of the key site area affected by cryogenic active-layer detachment slides in 1989 was accomplished. The distribution of thaw slumps went down in 1989 for each of the 19 selected NTCs that were examined. For this purpose, all landslides were combined into three groups depending on their coverage area: less than 0.002 km², from 0.002 to 0.01 km², and more than 0.01 km². Attribution of cryogenic earth flows to a particular NTC was done as follows: An earth flow is attributed to a particular NTC if the earth flow body has descended directly from the surface of this NTC, starting from the top point of the block displacement edge, even assuming that the contour of this NTC directly borders only with the sliding surface of the earth flow while the earth flow body stopped within the neighboring NTC.

The largest earth flows with an area over 0.01 km² and reaching 0.08 km² are found on concave sliding slopes with sliding surfaces of ancient earth flows (NTC 13 - Table 1, Fig. 2), as well as on relatively graded parts of drained flat watershed surfaces (4). Single large earth flows are attributed to smooth hummocky slopes with predominantly sedge-moss cover (12) as well as to the slopes on gentle rolling surfaces (1) and relatively graded areas of flat watershed surfaces (3) with predominantly shrub-moss-lichen vegetation and patches of shrub.

Earth flow sizing from 0.002 to 0.01 km² are mostly confined to all NTCs listed in the previous paragraph, most commonly to the ancient shrubby earth flow slopes (13) and to the slopes within rolling watersheds (1). Individual earth flows are confined to drainage channels (14), sides of ravines, gullies (18), and valleys of small streams (19).

Small earth flows with area size of less than 0.002 km² are common on steep sides of ravines and valleys of small streams (18, 19) and are often confined to the boundaries of these NTCs with the boundary parts of flat and rolling

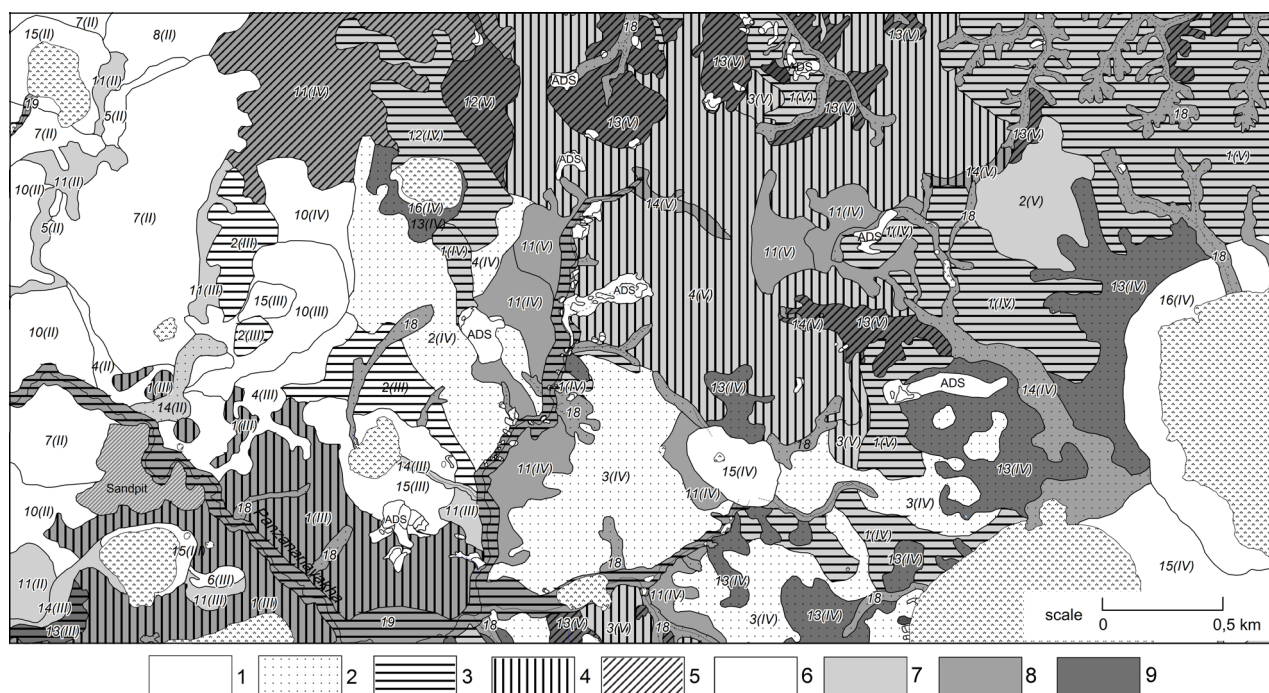


Figure 2. Section of NTC differentiating map according to the extent of impact and possible manifestations of retrogressive thaw slumping. The extent of impact by recent thaw slumping: 1 – not affected (0%), 2 – slight damage (0–1%), 3 – average damage (1–5%), 4 – strong damage (5–10%), 5 – very strong damage (10% and more). The extent of possible thaw slumps: 6 – minimum, 7 – average, 8 – high, 9 – maximum. ADS – active-layer detachment slide, 5(II)–14(V) – NTC index (geomorphological level).

watersheds (1-4) which are embedded with ravines and water stream valleys. Often these earth flows are confined to the marginal parts of relatively well-drained sub-horizontal surfaces adjacent to lake basins.

The impact of modern cryogenic earth flow differs within the same NTC located at different geomorphological levels. NTCs with calculated earth flow damage (earth flow descended in 1989) in percentage terms (Table 1) were combined into five groups according to the degree of affectedness by modern cryogenic earth flow (Table 2, Fig. 2 hatch).

The highest damage is on ancient earth flow slopes (13) and low-angled slopes with hummocky shrub-sedge-sphagnum communities (12) on V marine plain. These NTCs have the largest area size affected by earth flows that occurred in 1989 (16 and 20% respectively).

High damage level by modern earth flows is observed in flat watersheds with shrub-moss tundra (3), with hummocky tundra (4), and in gullies (14) on V marine plain, as well as in rolling watersheds (1) III of alluvial-marine plains. Valleys of water streams (19), despite the fairly large number of small earth flows, are characterized by an average level of damage by modern cryogenic earth flow. Ravine-gully network (18) is characterized by a low degree of affectedness by modern earth flow because the area size of minor earth flow spreading on steep ravine sides is insignificant. Only gully channels (14) on II above-flood-plain terrace are characterized by a low degree of damage by modern earth flow due to a single earth flow that descended into the lake basin as a result of cutting the surface by a track used by vehicles.

Most of the other NTCs at all levels are not affected by modern earth flow, except for rolling watershed surfaces (1) on plains V and IV and flat watershed plains with slightly

hummocky tundras (2) in III alluvial marine plain due to the descent of cryogenic earth flows where these NTCs border on gullies, ravines, valleys of water streams, and deep lake basins. Concave earth flow slopes (13) in III alluvial marine plains and smooth slopes (12) on IV coastal-marine plain are also characterized by an average level of damage.

The NTC damage due to modern earth flow does not exceed 20%. Therefore, the surfaces that are free from modern earth flow and can undergo cryogenic earth flow amount to 80%. The development of cryogenic earth flow in the next 300 years is unlikely to occur (Leibman & Kizyakov 2007) on the surfaces that have been subjected to modern earth flow. This is because of the lack of active layer formed on the sliding surfaces overgrown with pioneer vegetation groups and characterized by unformed organic horizons and often by active thermal erosion.

Thaw slumping geohazard estimates

Natural terrain units affected by recent thaw slumps are considered sensitive to slumping; the more sensitive, the larger the area affected by the earth flow process. The parts of the NTCs with no earth flows are the most dangerous in terms of their possible activation. According to this principle and based on the analysis of cryogenic active-layer detachment slide distribution in 1989 in different NTCs and on the degree of NTC damage due to modern earth flow, the selected NTCs were combined into four groups according to the degree of cryogenic earth flow possibility (earth flow risks, Table 2, Fig. 2 background).

The group of cryogenic earth flow minimal risk included all horizontal surfaces (except for the flat watershed surfaces (2-4) V of marine plain): water-logged surfaces (7, 8, 10) within the II above floodplain terrace; khasyreys (alases)

Table 1. Percentage of active-layer detachment slides occurrence in 1989 within different geomorphological levels.

NTC	NTC title	Damage by landslides in 1989, % of NTC area size at geomorphological levels				
		V*	IV	III	II	II
1	Rolling sub-horizontal watershed surfaces (arched hilltops and their slopes) with polygonal shrub-grass-lichen tundra and with wind erosion forms on sands and sandy silty loams	3.6	2.9	6.2	-	-
2	Flat sub-horizontal watershed surfaces with slightly hummocky grass-shrub-moss-lichen and hummocky shrub-grass-moss tundras on sandy silty loams and clayey silty loams (with occasional wind erosion forms)	0.0	0.2	1.5	-	-
3	Flat sub-horizontal watershed surfaces with grass-shrub-moss tundras on sandy silty loams and clayey silty loams with patches of polygonal grass-shrub-lichen-moss tundras on sands and sandy silty loams	8.0	0.6	0.0	-	-
4	Flat sub-horizontal watershed surfaces with hummocky shrub-grass-moss tundras on sandy silty loams and clayey silty loams	7.4	0.6	0.0	0.0	-
5	Edge parts of flat sub-horizontal surfaces with slightly hummocky and polygonal grass-shrub-moss-lichen tundras on sandy silty loams	-	-	-	0.0	-
6	Flat sub-horizontal surfaces with polygonal flatly-hummocky cloudberry-sedge-lichen-sphagnum peats on peaty sandy silty loams, clayey silty loams and peat	-	0.0	0.0	-	-
7	Flat sub-horizontal surfaces with shrub-sedge-sphagnum and grass-moss bogs on peaty sandy silty loams and clayey silty loams (with fragments of peat)	-	0.0	0.0	0.0	-
8	Flat sub-horizontal surfaces with grass-moss bogs on sandy silty loams and clayey silty loams	-	0.0	-	0.0	-
9	Flat rear parts of floodplain with hummocky sedge-moss and sedge-cowberry-moss communities on clayey silty loams and clays	-	-	-	-	0.0
10	Flat low-angled surfaces with grass-moss-shrub tundras on sandy silty loams and clayey silty loams (occasionally on clays)	-	0.0	0.0	0.0	-
11	Flat smooth slopes of hummocky mixed-herb-gramineous-moss willow bushes with some dwarf arctic birch on clayey silty loams and clays	0.0	0.0	0.0	0.0	-
12	Flat smooth slopes with hummocky shrub-sedge-sphagnum communities on sandy silty loams and clayey silty loams	20.5	1.2	-	-	-
13	Concave smooth landsliding slopes with mixed-herb-gramineous and willow bush on clayey silty loams and saline clays	15.9	0.7	4.1	-	-
14	Gully channels with cotton-grass-sedge-moss communities on clayey silty loams and clays	6.7	0.1	0.0	0.2	-
15	Khasyreds (alases) with predominantly shrub-lichen communities and with peaty sandy silty loams and peat in better-drained areas, cotton-grass-sedge-moss willow bush and shrub-sedge-sphagnum bogs and with peaty clayey silty loams and peat in less drained areas	-	0.0	0.0	0.0	-
16	Low lake terraces with hummocky sedge-moss communities on peaty sandy silty loams and clayey silty loams	-	0.0	0.0	-	-
17	Localized drain lake basin with patches of cottongrass-arctophila communities on sands	-				
18	Narrows, draws and ravines with flat marshy grass-moss bottom and steep hummocky sides with grass-moss willow bush and dwarf arctic birch on clayey silty loams and clays	0.9				
19	Valleys of small rivers and streams with mixed-herb-moss willow bush on clayey silty loams and clays	2.3				

* V – V marine plain, IV – IV coastal-marine plain, III – III alluvial marine plain, II – II above the floodplain terrace, II – floodplain of the Mordyyakha River

(15), low lake terraces and localized drain lake basin (16, 17); a plot belonging to the floodplain of the Mordyyakhi river (9); drained boundary parts of sub-horizontal surfaces (5) on II above floodplain terrace. This group also includes surface areas affected by earth flows in 1989.

The NTCs with average cryogenic earth flow probability cover arching peak plains (1) within the plains IV and V, flat watersheds (2-4) on V marine plain, smooth slopes with

grass-moss communities (12) on IV coastal-marine plain, as well as smooth slopes with willow bushes (11) and gully channels with grass-moss communities (14) on III marine alluvial plain, and II above flood-plain terrace. Such NTCs are characterized by either low gradient on extended slopes that are favorable for large earth flow formation or border on concave bushy slopes with earth flows older than 1989 (13), ravines (18), the valleys of water streams (19), or the sides of

Table 2. Level of NTC damage due to modern cryogenic earth flow (1) and the differentiation of NTCs according to cryogenic earth flows possibility (2) in the “Vaskiny Dachi” key area.

1 \ 2	Minimum	Average	High	Maximum
No damage (0%)	3(III), 4(II, III), 5(II), 6(III, IV), 7(II, III), 8(II, IV), 9I, 10(II, III, IV), 15(II, III, IV), 16(III, IV), 17	2(V), 11 (II, III), 14(III)	11 (IV, V)	-
Low (0-1%)	2-4(IV)	14(II)	14(IV), 18	13(IV)
Average (1-5%)	2-229.	1(IV, V), 12(IV)	19	13(III)
High (5-10%)	-	3-4, 2006.	1114, 2006.	-
Very high (> 10%)	-	-	-	12-13(V)

deep lake basins. The likelihood of active-layer detachment slides increases at the boundaries with such NTCs.

The group with high cryogenic earth flow probability includes slopes of well-drained arched top surfaces (1) on III plain ending with steep ledges on the borders with other NTCs and, as a rule, with ravines and valleys of streams and lake basins with high earth flow probability. Based on the same principle which was used for the previous group, this group includes extended slopes with willow bush (11) on IV and V plains with little gradient which is nonetheless sufficient for large earth flow formation. Higher likelihood of large earth flows is complicated by an increased likelihood of small earth flows due to the high dissection of these NTCs by gully-ravine network. Consequently, this group includes drainage channels (14) on IV and V plains, ravines and stream valleys (18, 19) with steep sides which increase the probability of small earth flows. The maximum likelihood of earth flows is typical of concave bushy slopes having sliding surfaces of ancient earth flows (13), except for the sliding surfaces of earth flow bodies in 1989. The same group covers extended smooth slopes with shrub-moss communities (12) on V marine plain.

Preserved sand pits did not present any danger of cryogenic earth flow at the time of the study. Only mashes and thermokarst were forming on the surface in hollows and wind erosion on the ramparts. The surface is covered with pioneer vegetation groups. Only steep sides of ramparts bordering the Panzananayakha River valley were favorable to small earth flow. Earth flows can also be activated at the places where travel ruts cross slopes, especially if the ruts are in perpendicular position to the slope. The ruts going over the ravine tributaries can intensify the process of gullying, which is conducive to earth flow because gullying increases the area of the slopes.

NTC areas with varying degrees of earth flow possibility are distributed as follows: NTCs with maximum danger occupy 14.4% of the studied area; NTCs with a high degree of risk occupy 19.5%, with an average of 26.0%. NTCs that are relatively resistant to the probable activation of cryogenic earth flow (minimum degree of its possible manifestation) cover less than half of the territory including the lakes (40.1%).

Conclusions

This study proposed an earth flow hazard estimate method based on analysis of the spreading of modern cryogenic earth flows and the damage of natural territorial complexes

due to modern earth flow.

NTC damage due to modern earth flow determines the sensitivity of these NTCs to possible earth flow activation depending on the area occupied by the surface modified by modern earth flow within each NTC.

The surfaces affected by modern earth flow are not dangerous in terms of recurrence of the earth flow process in the future, as the conditions to form a horizon of ice-rich material—the basic precondition for the emergence of cryogenic earth flow—have not yet appeared at the base of a “new” seasonal thawing layer.

The application of this method revealed the following:

At all geomorphological levels, except for the II terrace above the floodplain of the Mordyyakha River and the floodplain itself, there remains a very high risk of cryogenic earth flow activation on concave bushy slopes.

The danger of large earth flows increases when moving from low geomorphological levels to high ones along flat smooth slopes fully or partially covered with bushes. The probability of minor earth flows on supposedly horizontal surfaces increases with the development of gully-ravine network roughness as well as with the development of stream valleys regardless of the geomorphological level.

The studied landscapes are characteristic of the typical tundra throughout Central Yamal. Thus the obtained results can be used in zones of prospective development with widespread ground-ice sheet and shrub-covered tundra (which are indicators of the hazardous slope process development continuing since the late Holocene) to the north of the Yuribey River. The most comprehensive assessment of earth flow hazard using the results of this study may be carried out in the territory of the Bovankovskoe located nearby. However, it is important to consider the impact of presently constructed infrastructure as well as gas production and transportation facilities under construction.

References

- Burn, C.R. & Zhang, Y. 2009. Permafrost and climate change at Herschel Island (Qikiqtaruk), Yukon Territory, Canada, *J. Geophys. Res.* 114, F02001, doi:10.1029/2008JF001087.
- Chekhina, I.V., Rivkin, F.M., Koreysha, M.M., & Popova, A.A. 2004. Development of evaluative maps of cryogenic processes natural risks on the Varandey peninsula coast. Cryosphere of oil and gas provinces: Materials of Int. Conf. – Tyumen, p. 131 (in Russian).
- Kazakov, N.A. & Gensiorovskiy, Yu.V. 2008. Exogenetic geodynamic and channel processes in low-hill terrain

of the Sakhalin Island as risk factor for pipelines "Sakhalin-2." *Geoekologiya. Inzhenernaya Geologiya, Gidrogeologiya, Geokriologiya* 6: 483-496 (in Russian).

Leibman, M.O. 1997. Cryolithological specifics of seasonally thawed layer on slopes in connection with the process of cryogenic earth flow. *Kriosfera Zemli* 1 (2): 50-55 (in Russian).

Leibman, M.O. 2005. Cryogenic slope processes and their geoeological consequences under the conditions of sheet ice spreading: Dissertation abstract ... Dr. of Geology and Mineralogy. *IKZ SO RAN*. Tyumen, 48 pp. (in Russian).

Leibman, M.O., Kizyakov, A.I., Sulerzhitsky, L.D., & Zaretskaya, N.E. 2003. Dynamics of the landslide slopes and mechanism of their development on Yamal peninsula, Russia. *Proc. of the 8th Intern. Conf. on Permafrost*. Lisse, Netherlands, Balkema Publishers. I: 651-656.

Leibman, M.O. & Kizyakov, A.I. 2007. Cryogenic earth flows of the Yamal and the Yugorsky Peninsula. – Moscow. Tyumen, *IKZ SO RAN*, 206 pp. (in Russian).

Postoev, G.P., Lapochkin, B.K., Kazeev, A.I., & Nikulshin, A.S. 2008. Estimation of landslide hazard on construction sites. *Geoekologiya. Inzhenernaya Geologiya, Gidrogeologiya, Geokriologiya* 6: 547-557 (in Russian).

Trofimov, V.T. (ed.). 1975. *The Yamal Peninsula*. Moscow, 278 pp. (in Russian).

Heat and Mass Transfer in Water-Saturated Ceramics with Macro Inclusions of Ice

V.S. Kolunin, A.V. Kolunin, A.D. Pisarev
Earth Cryosphere Institute, SB RAS, Tyumen, Russia

Abstract

The results of experiments on the study of the heat and mass transfer properties of water-saturated ceramics with macro-inclusions of ice are discussed. It is shown that the system possesses thermo-osmotic and thermo-barometric properties. The total set of transfer coefficients is determined and compared with the theoretical values. The calculated results agree with the experimental data within a factor of ten. A way to improve the predictive ability of the theory is identified by the consideration of hydrodynamic properties of the unfrozen water film between ice and the skeleton of the porous medium.

Keywords: freezing; frozen ground; ice; heat and mass transfer; porous medium; water.

Introduction

The freezing of fine-grained saturated soil disturbs its homogeneity and initiates the formation of cryogenic structures. The spatial redistribution of the system components is accompanied by the deformation of the soil skeleton and ice transfer relative to the soil particles. The theory of the role of ice movement in heat and mass transfer processes in the model porous media that possessed a rigid framework was previously studied (Kolunin 2005). In particular, it was revealed that heat and mass flows through porous medium with ice inclusions are expressed in terms of the entire complex of thermodynamic forces—the gradients of temperature and liquid pressure. The present work aims to experimentally determine the transfer coefficients of a rigid porous sample with macro-inclusions of ice and to make a comparison with the theory.

Experimental Method

A model cell of biporous medium was chosen as the object for study. This was a cylinder of porous ceramics with a cavity (Fig. 1b), which was placed in the experimental setup (Fig. 1a) at the temperature below 0°C. The ceramics (11) were saturated with distilled water, while the cavity (10) in the central part of the sample was filled with ice. The porous

medium at the side of the cavity consisted of three ceramic rings separated by a thin layer of sealant (13). Thus it is assumed that the whole mass flow through the middle part of the sample is transferred by ice inclusions by means of regelation. That is, the ice melts when approaching the wall of the cavity, then, moving away from the wall, it recovers its shape at the opposite side as a result of water freezing.

The main characteristics of the sample and the elements of the setup are presented in Table 1.

The preparatory stage of the experiment includes the following operations: evacuation of the sample and supply tubes, filling the system with degassed water, one-sided freezing of the ceramic sample with consequent thawing of tubes (7) and holding capacities (14) (Fig. 2), and further freezing of water in the cavity. The preparatory stage takes from three days to one week. Ceramics serve as a phase barrier against the penetration of ice into the holding capacities (14) up to -0.05°C.

The values of heat and mass flows through the sample due to the temperature difference of brass plates (2) or due to the difference in liquid pressure in the gaps (14) are measured in the experiment.

The temperature is measured at four points (8) (Fig. 1a) by differential copper-constant thermocouples. The cold thermocouple junction is maintained at 0°C by means of its immersion into a thermos with distilled water and crushed

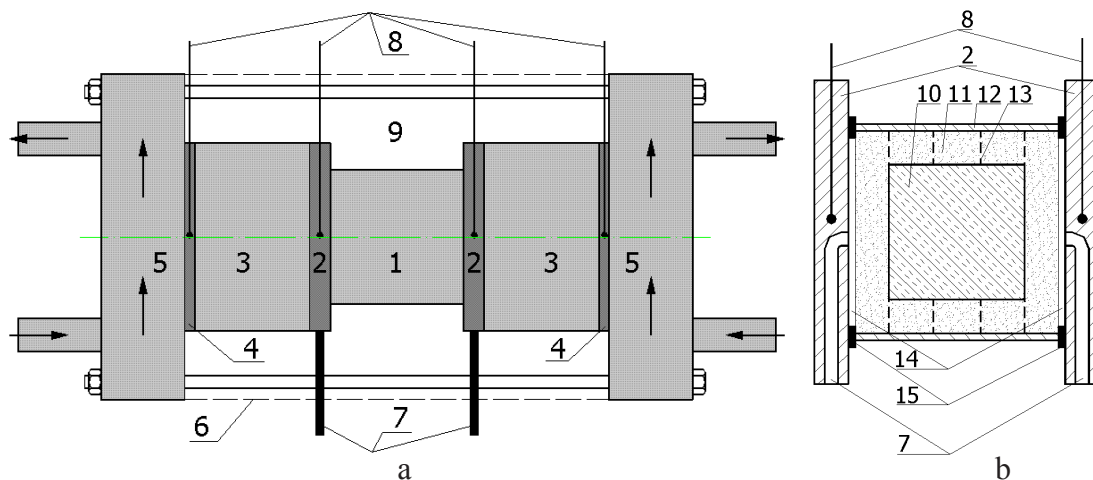


Figure 1. The setup for measuring the heat and mass transfer parameters. a. General view. 1 - sample, 2 - brass plates, 3 - measuring cylinders made of Plexiglas, 4 - copper plates, 5 - brass heat exchangers through which temperature controlled liquid is pumped, 6 - a screen made of copper foil, 7 - water tubes, 8 - measured ends of differential thermocouples, 9 - foam. b. Sample with the plates. 10 - cavity, 11 - porous ceramics, 12 - a plastic frame, 13 - seals of porous ceramic rings (sealant), 14 - gaps filled with water, 15 - rubber seals.

Table 1. Characteristics of the elements of the experimental cell.

Element of setting (Fig. 1)	Diameter (outer), mm	Height, mm	Coefficient of thermal conductivity, W/(m·°C)	Coefficient of hydroconductivity, m ² /(Pa×s)
Cavity (ice) (10)	20.2	16.5	2.2	
Ceramics (11)	29.7	26.9	1.4	1.9×10 ⁻¹³
Frame (12)	32.2	26.9	0.35	
Graduated cylinder (3)	44.5	31.4	0.21	
Foam (9)	79	102.5	0.044	

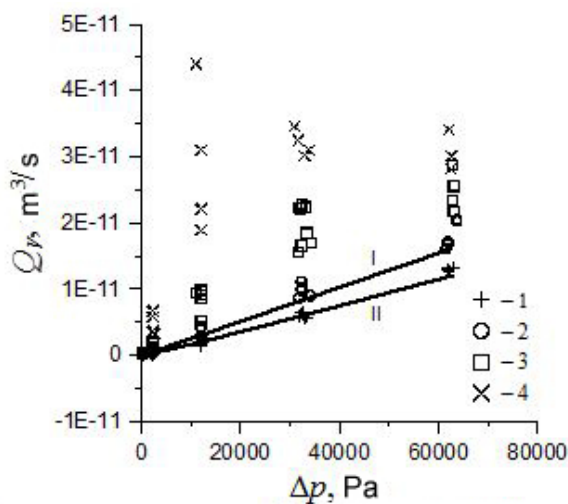


Figure 2. The dependence of the volumetric liquid flow Q_v through the sample depending on the pressure difference Δp at the sample boundaries at different average temperatures t_0 . Symbols – experimental data at different average temperatures: -0.04 (1), -0.03 (2), -0.02 (3), -0.01 (4); lines – calculated results at various temperature drops on brass plates: I - zero, II - maximum of the experimental data (Fig. 3).

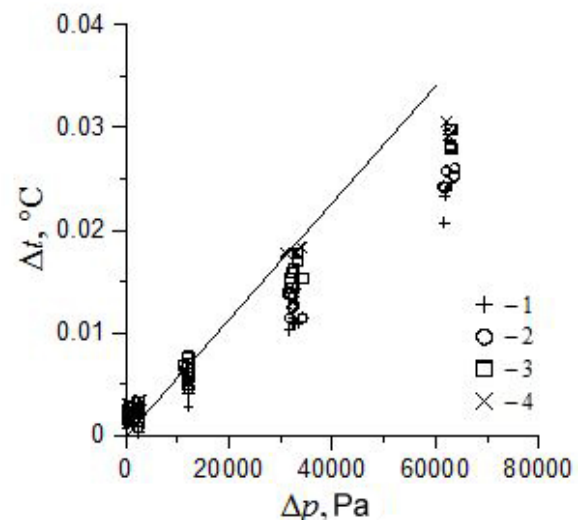


Figure 3. Temperature difference Δt between the base of the sample (brass plates 2, Fig. 1) depending on the liquid pressure drop Δp . Symbols – experimental data at different average temperatures: -0.04 (1), -0.03 (2), -0.02 (3), -0.01 (4); the line – the results of calculation.

ice. The thermos, in its turn, is placed in the refrigerator with the temperature slightly above 0°C .

Standard cylinders (3), through which the heat transfer between the sample and massive thermostatically controlled plates (heat exchangers) is carried out, are tightly pressed to the external bases of the plates (9) in order to determine the heat flow. The value of the axial heat flow in the cell is calculated according to Fourier's law from the measured temperatures at the base of the standard cylinders.

The liquid flow is estimated from the movement of the liquid meniscus in calibrated capillary tubes connected to the channels (7).

A single measurement takes from 12 to 36 hours. During this time, the temperature settings are maintained in the heat exchangers. The volume of liquid passing through the sample is determined during the same period of time.

In order to meet the difference between the voltage and the temperature drop at the thermocouple junctions, a standard calibration characteristic is used (Thermocouples 2002).

Thermo-EMF of the thermocouples is digitized by a 24-bit, six-channel analog-to-digital converter and is registered at intervals of 10 seconds. In order to improve the accuracy of measurement, the chosen frequency of digitizing is a multiple of network interference (50 Hz).

Using a thermostat, the absolute error was measured

at no more than $\pm 0.01^{\circ}\text{C}$. The error in measuring of the temperature difference by means of the differential method is less than $\pm 0.004^{\circ}\text{C}$.

The standard deviation of the average temperature of the heat exchangers for most measurements does not exceed 0.0005°C , and that of the brass plates does not exceed 0.005°C .

In order to compare the results of measurements with the theory, a computer program was developed to solve two related problems: the heat transfer problem in the inside part of the master unit and the filtration problem in ceramics. The input parameters are the temperature of heat exchangers (5) and the pressure in the gaps (14) (Fig. 1a). The program calculates the rate of ice flow in the cell cavity, the temperature of the brass plates (2), and the values of heat and liquid flows through the base of the sample.

Results

Figure 2 shows the results of the measurements of water flow through the sample under the liquid pressure gradient at different average temperatures of the sample. The experiment reveals that the value of mass flow through the sample decreases with the decrease of average temperature. This can be explained by the hydraulic resistance of the

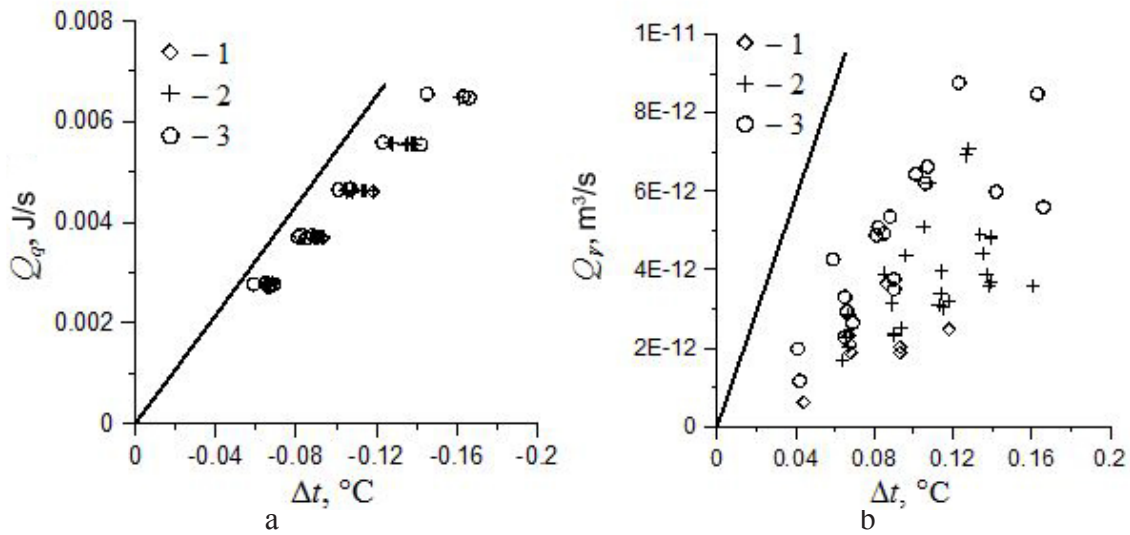


Figure 4. Flows of heat (a) and mass (b) through the sample depending on temperature difference at its base. Symbols – experimental data at different average temperatures t_0 [°C]: –0.04 (1); –0.03 (2); –0.02 (3). Lines – calculation results.

film of unfrozen water separating the ice and the porous medium skeleton (Gorelik & Kolunin 2002). However, the comparison with the theory that does not consider this factor shows that the calculated value of the mass flow is less than that observed in the experiment. Could it be that the true value of the velocity of ice was above the theoretical value?

The temperature difference of the brass plates serves as an indicator of the ice velocity (Fig. 3). When approaching the cavity wall an ice column is melted and heat absorption occurs. A reverse process occurs on the opposite side of the inclusion—water freezing and heat release. Being spatially separated, the heat sources and sinks change the temperature field of the environment and create a temperature difference on the plates, which is proportional to the velocity of ice.

The experimental data in Figure 3 show that with the decrease in the average temperature of the sample the temperature difference on the plates decreases as well, which means that the ice velocity in the cavity also decreases. Such system behavior can be explained by the dependence of hydraulic resistance of the film of unfrozen water on temperature. The fact that the experimental points turn out to be lower than the estimated ones—the hydraulic resistance is not taken into account in theory—is not inconsistent with this explanation.

Based on the results of thermophysical measurements, we can conclude that the true ice velocity in the cavity does not exceed the theoretical velocity. In this case, in order to explain the higher values of liquid flow in the experiment in comparison with the theory (Fig. 2), it is necessary to introduce some additional factors. In our opinion, the most likely cause of the variations between the theory and the experiment data is the presence of unfrozen liquid channels between the cavity walls and the ice column. Thus, according to the calculations, if the waterproofing insulation between the ceramic rings is removed (Fig. 1b, 13), the mass flow in the system increases by almost 50 times.

One cannot exclude the possibility of liquid movement through ice along unfrozen intergranular channels, the properties of which are discussed in several papers (Ketcham & Hobbs 1969, Mader 1992).

Experimental values of heat flows and liquid consumption

as a function of temperature difference on the base of the sample are shown in Figure 4. An approximately linear relationship between the flow values and the temperature drop at the boundaries of the sample is observed. Lowering of the average temperature under otherwise equal conditions leads to a decrease in values of heat and mass flows. A comparison with theory shows that, in contrast to the results of the experiments in which the flows were created by the pressure gradient (Fig. 2) in both diagrams (Fig. 4), the experimental points lie below the calculated values and show a much greater data spread.

Measurement results show that the system has thermo-osmotic and thermo-barometric properties (i.e., the temperature gradient creates mass flow through the sample, while the pressure gradient creates heat flow). Therefore, the equations of heat and mass transfer in a general view form the basis of experimental data processing:

$$j_V = C_{pp} \frac{\Delta p}{\Delta x} + C_{pt} \frac{\Delta T}{T_0 \Delta x} \quad (1)$$

$$j_q = C_{qp} \frac{\Delta p}{\Delta x} + C_{qt} \frac{\Delta T}{T_0 \Delta x}$$

where j_V – volumetric flow density [$\text{m} \cdot \text{s}^{-1}$] and j_q – heat flow density [$\text{J} \cdot \text{m}^{-2} \cdot \text{s}^{-1}$] through the sample base; Δp , ΔT – drops of liquid pressure [Pa] and temperature [K] at the top of the sample Δx [m]; C_{pp} , C_{pt} , C_{qp} , C_{qt} – transfer coefficients; $T_0 = 273.15$ K.

The results of two experiments conducted under various boundary conditions form two sets of data (experimental points). The first set was obtained in the experiment in which the flows were created by the liquid pressure gradient at zero temperature drop in the heat exchangers. The points of the second set are the data of the experiment in which the temperature gradient at zero drop in liquid pressure is the driving thermodynamic force. The transfer coefficients are determined according to two experimental points from the first and second sets on the basis of formula (1).

As one can see in Figures 2–4, the heat and mass flows and, therefore, C -coefficients depend on the average temperature of the sample, which for this reason is included into a set

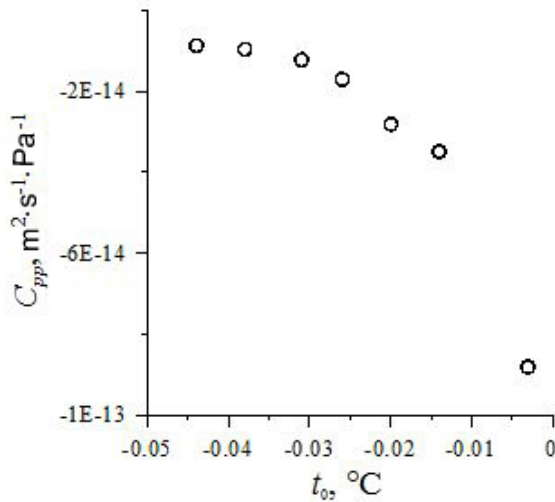


Figure 5. Dependence of C_{pp} coefficient on average temperature of the sample.

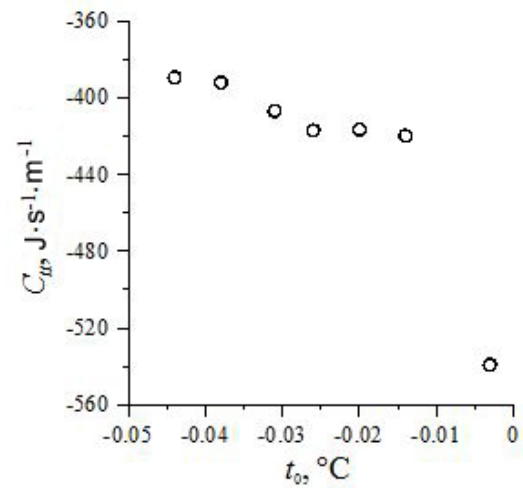


Figure 6. Dependence of C_{ii} coefficient on average temperature of the sample.

of parameters of the resulting measurements. Experimental points are unevenly distributed on the temperature scale, so at first the values of temperatures with maximal concentration of experimental points were found. Then, near these nodal temperatures the groups of experimental points were formed. A system of equations (1) for all combinations of points from the first and second sets was solved in each group of data, and then the average transfer coefficient was calculated.

The coefficients depending on the average temperature of the sample are shown in Figures 5–7. One can see that with temperature decrease the absolute values of the coefficients become smaller.

The entire measurement cycle consisted of seven series. After each series, except for the fourth, the system was rinsed with distilled water for a period from 1 to 7 days. The need for this rinsing was revealed during the experiment. In the first series it was observed that the values of mass flows through the sample are much smaller than the calculated ones. At the end of this series, the temperature of the ice-water phase equilibrium turned out to be equal to -0.017°C , which corresponds to the concentration of non-electrolyte solution of approximately 0.01 mole/liter. The concentration falls within the range of 0.001 to 0.01 mole/liter, within which, according to theoretical estimates (Kolunin & Kolunin 2006), a sharp decrease occurs in ice velocity relative to the skeleton of the porous medium.

Rinsing of the system with distilled water for a week was performed in order to test the assumption of the presence of impurities in the water. Figure 8 shows the values of C_{pt} coefficient found as results of measurements in series 1 and 2.

The results of measurements in series 6 and 7 were used to calculate the experimental values of transfer coefficients.

A theoretical model (Kolunin 2005) provides values of C -coefficients presented in Table 2. Symmetry violation of C -coefficients is the consequence of heat transfer between the sample and the environment through the lateral surface.

Comparison of the coefficients of heat transfer C_{ii} (Fig. 6 and Table 2) shows that the absolute value of the theoretical ratio is higher than the experimental one almost across the

full range of temperatures. The regelation movement of ice makes a significant contribution to the C_{ii} coefficient. Thus if the ice is stationary relative to the ceramics, the theoretical value of the C_{ii} coefficient is equal to $-345 \text{ J} \cdot \text{m}^{-1} \cdot \text{s}^{-1}$.

The theory predicts a higher rate of ice velocity compared to the experimental results. This difference may be caused by two factors: the theory does not consider the hydro-resistance of the film of unfrozen water between the base of the ice column and the cavity walls, and the theory also assumes there are no soluble compounds in the water. Both of these factors reduce the ice velocity relative to the ceramics.

The absolute value of the coefficient of mass transfer C_{pp} obtained from the theory (Table 2) is less than the experimental value (Fig. 5) across almost the entire temperature range. Given the previous conclusion, the most probable reason for this difference is the flow of liquid between the lateral surface of the ice inclusion and the cavity walls. The liquid transfer in the channels increases the magnitude of the total flow of water substance under a pressure gradient practically without changing the speed of the ice movement.

In turn, both factors—a decrease in the rate of regelation ice flow and the presence of unfrozen channels between the areas of ice melting and water freezing—lead to the fact that the values of off-diagonal transfer coefficients C_{pt} and C_{tp} measured in the experiment are considerably smaller than the theoretical values (Table 2 and Fig. 7).

The experimental values of C -coefficients allow us to determine the parameters of the process at which the laws of heat and mass transfer should be applied in general terms.

The components of the mass transfer law (1) have the same order when the following formula is fulfilled:

$$|\Delta T| \approx \left| \frac{C_{pp} T_0}{C_{pt}} \Delta p \right| \quad (2)$$

Taking $C_{pp} = -2 \cdot 10^{-14} \text{ m}^2 \cdot \text{s}^{-1} \cdot \text{Pa}^{-1}$ and $C_{pt} = 5 \cdot 10^{-7} \text{ m}^2 \cdot \text{s}^{-1}$ (Figs. 5–7), it follows from equation (2), for example, that at a pressure drop of 10^5 Pa the temperature change is $|\Delta T| \approx 1 \text{ K}$. Thus the thermo-osmotic contribution into mass transfer through frozen ground becomes visible at a temperature

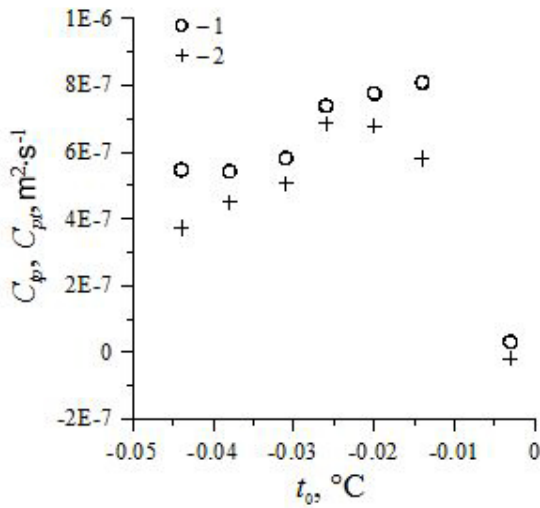


Figure 7. The dependence of off-diagonal transfer coefficients C_{pp} (1) and C_{pp} (2) on the average temperature of the sample.

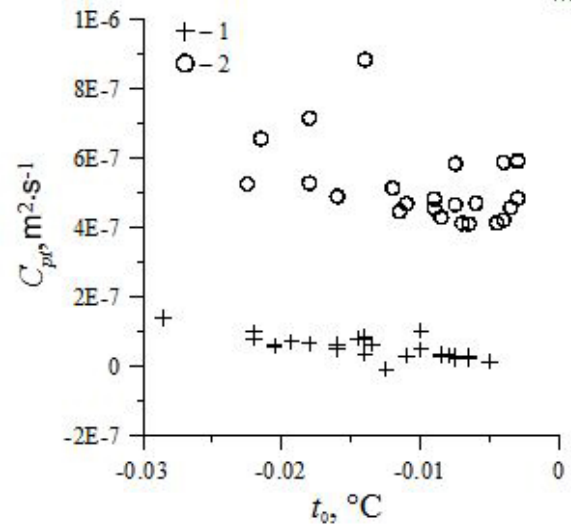


Figure 8. The dependence of the transfer coefficient C_{pt} on the average temperature of the sample for series 1 and 2 of the measurements.

Table 2. Theoretical values of the transfer coefficients of the cell.

C_{pp} , $\text{m}^2\text{S}^{-1}\text{Pa}^{-1}$	C_{pp} , m^2S^{-1}	C_{pp} , m^2S^{-1}	C_{pp} , $\text{J}\cdot\text{m}^{-1}\text{S}^{-1}$
$-9.15 \cdot 10^{-15}$	$1.40 \cdot 10^{-6}$	$1.37 \cdot 10^{-6}$	-555

change of not less than 1 K per 1 atm of pressure drop in liquid. This condition is fairly commonly fulfilled in nature.

Similarly, for a pressure drop of liquid, higher than at which the law of heat transfer should be applied in general terms, we have

$$|\Delta p| \approx \left| \frac{C_{tt}}{C_{tp} T_0} \Delta T \right| \quad (3)$$

Assuming $C_{tt} = -420 \text{ J}\cdot\text{m}^{-1}\text{s}^{-1}$ and $C_{tp} = 5 \cdot 10^{-7} \text{ m}^2\text{s}^{-1}$ (Figs. 5–7), from equation (3) we obtain $|\Delta p/\Delta T| \approx 3 \cdot 10^6 \text{ Pa}\cdot\text{K}^{-1}$.

The estimates above were obtained for a porous medium with macro-inclusions. Coefficients C_{pt} and C_{pp} included in equations (2) and (3) are determined largely by hydraulic properties of the channels between the areas of ice melting and water freezing, hence by the size of the inclusion. With the ice size decrease, the role of channels' conductivity increases and, as a result, the value of off-diagonal coefficients should be smaller. Currently there is no sufficient experimental data, based on which one can determine the importance of micro-inclusions of ice in the heat and mass transfer processes in frozen porous media. An indirect confirmation of the conclusion about the influence of ice size upon the value of C_{pp} coefficient is provided by the results of experimental work (Horiguchi & Miller 1980), that is, the macro-inclusions of ice between the membranes that show thermo-barometric properties, not the frozen ground. Despite the fact that in the experiment with the frozen ground the ice content is about 26 g/g, the thermo-barometric effect is negligibly small. A possible reason for this phenomenon is the lack of large inclusions of ground ice, and the velocity of the micro-inclusions under a drop of pressure of liquid is much less than the velocity of the macro-formations of ice.

Conclusions

Based on the above, the following conclusions can be made.

- In a porous medium containing ice and water, the pressure difference in liquid creates not only the mass flow but also heat flow.
- The theoretical model can be used to predict heat and mass transfer processes in frozen porous media containing macro-formations of ice.
- To improve the predictive power of the original theoretical model, it is necessary to take into account the hydraulic properties of the unfrozen water film separating the ice and porous medium.
- The unfrozen water film between ice and fine-pore medium increases the filtration properties of frozen porous ground but reduces the mass transfer of water in the ice phase.
- The following factors have a significant effect on the rate of regelation ice flow: the presence of soluble compounds in water, hydro-resistance of the film between the ice and porous skeleton, and the presence of hydroconductive channels between the areas of ice melting and water freezing.
- The mass transfer in an open system through frozen porous media under temperature gradient leads to the accumulation of soluble compounds in the area where water is turning into ice, while the mass-transfer processes initiated by liquid pressure gradient are accompanied by natural purification of the system.
- Heat transfer in frozen ground near the temperature of freezing is described by Fourier law with the accuracy sufficient for practical purposes, whereas mass transfer is subjected to the general law. The filtration rate depends on the gradient of liquid pressure and temperature.

References

- Gorelik, Ya.B. & Kolunin, V.S. 2002. *Physics and Modelling of Cryogenic Processes in Lithosphere*. Novosibirsk, Academic Publishers "Geo," 318.
- Horiguchi, K. & Miller, R.D. 1980. Experimental studies with frozen soil in an «ice sandwich» permeameter. *Cold Regions Science and Technology* 3: 177-183.
- Ketcham, W.M. & Hobbs, P.V. 1969. An experimental determination on the surface energies of ice. *Philosophical Magazine* 19: 1161-1173.
- Kolunin, V.S. 2005. Heat and mass transfer in porous media with ice inclusion near freezing-point. *International Journal of Heat and Mass Transfer* 48 (no. 6): 1175-1185.
- Kolunin, V.S. & Kolunin, A.V. 2006. Heat and mass transfer in saturated porous media with ice inclusions. *International Journal of Heat and Mass Transfer* 49 (no. 6): 2514-2522.
- Mader, H.M. 1992. Observation of the water-vein system in polycrystalline ice. *Journal of Glaciology* 38 (no. 130): 333-347.
- Thermocouples. Nominal static characteristics*. GOST R8.585-2001, Moscow, Russian State Standard, 2002, 78.

Method for Estimating Properties of Cryopegs from the Yamal Peninsula

I.A. Komarov, N.V. Kiyashko
Lomonosov Moscow State University, Moscow, Russia

Abstract

Methods for estimating the onset of freezing temperatures, phase composition, density, pH, heat capacity, and thermal conductivity of cryopegs of the Yamal Peninsula are given. They are implemented with the help of a software product that was developed and tested with extensive experimental material. The software uses the following input data: initial value of total mineralization; cryopeg concentration and composition based on chemical analysis of samples; and the analysis of approximate ratios for estimation of the above-mentioned properties in which only the total initial mineralization value is used.

Keywords: cryopegs; density; freezing temperature; heat capacity; phase composition; Yamal Peninsula.

Introduction

The problems of temperature and the water-salt regime of saline waters and cryopeg prediction are relevant because of intense development of the shelf territory and seaside lowlands in large gas- and oil-bearing provinces (the Yamal Peninsula and others). These regions are characterized by a sea salinity type. Disregarding pore fluids mineralization may result in serious inaccuracy in predicting calculations. A review of various numerical schemes is provided in our previous publication (Komarov 2003).

The term “cryopeg” is defined differently in the literature. The most commonly used definition, and the one used in this paper, was introduced by N.I. Tolstikhin: “Cryopegs (cryosalt waters) are natural saline waters with negative temperatures.”

To implement the prediction models, the following information is necessary: freezing temperature of the cryopeg, density, unfrozen water content and ice content, and dependence of thermo-physical properties on temperature. Calculation methods for these properties are usually limited by cases in which a pore fluid may be conventionally considered as binary (two-component solutions $H_2O + NaCl$). They are based on various modifications of the cryoscopic formula from the solutions theory with or without consideration of the isotonic coefficient. However, they operate at relatively low pore fluid mineralization. The normality of readily soluble salts in pore fluids and cryopegs may reach values of 2–3 and more.

The behavior modeling of the chemical aspect of polyionic water-salt systems at negative temperatures eventually depends on the calculation of phase composition for the systems with various bulk chemical compositions within specific grid cells with certain temperature and pressure on each time step. Using K. Pitzer’s model (Pitzer 1987) for the activity coefficients and water activity calculation in the CRREL laboratory for the Na-K-Ca-Mg-Cl-SO₄-H₂O system, software was developed to calculate the chemical equilibrium between water electrolyte solutions, ice and salts (Mironenko et al. 1987). Using this model in the FREZCHEM2 numerical code (Bvolkov et al. 2005, Komarov et al. 2006), a new method to estimate the temperature of sea-water cryopegs formation based on a desulphatization curve (temperature dependence of sulphate-ion concentration) was suggested. Chemical analysis of a

particular cryopeg sample, with the help of modeling, allows us to reconstruct the minimum temperature value at which formation of the cryopeg ion-salt composition occurred. This formation of temperature corresponds to the onset temperature of mirabilite crystallization for each cryopeg sample, and is accurately fixed on the desulphatization curve. In addition, for the correct determination of the formation temperature of a sea-water cryopeg (ion-salt composition) it is not necessary to know the initial composition of the sea water from which the cryopeg was formed. With the help of the suggested method and based on the desulphatization curve, a number of temperature/ ion-salt composition conditions for cryopeg formation of the Yamal Peninsula were estimated.

Software Product

However, further research progress was limited by the model’s abilities and the apparatus developed. For example, to conduct the data analysis of ground water extracts and cryopeg samples, apart from the seven mentioned components that used the FREZCHEM2 model, it is necessary to consider the presence of carbonates, bicarbonates, and corresponding salts of calcite, dolomite, gypsum, and iron compounds. It is also necessary to consider the presence of the gas phase, in particular H_2O , CO_2 , CH_4 . Real physical processes occurring in nature show that the calculation of the following parameters is reasonable: a) overlying ground pressure; b) the presence of water-bearing horizons (i.e., in cases when the ground or the cryopeg exchanges some component with the environment in an open-system regime); and c) the cases when newly formed salt solid phases precipitate from the ground or the cryopeg pore fluid during freezing and do not return into the liquid phase at increased temperatures (fractional crystallization).

There are no limitations mentioned above in the thermodynamic model and the corresponding FREEZBRINE software. This software was tested and used to analyze cryopeg temperature and water-salt regime (Komarov et al. 2008, Komarov & Mironenko 2010). The calculation procedure for the balanced composition of the water-salt systems is provided in the work by Mironenko & Polyakov (2009). Balanced composition of the system at temperature T , pressure P , and the given bulk chemical composition is found through the Gibbs free energy minimization method

on a number of linear limitations as a system of mass balance equations. In the software, equilibrium constants of the chemical reactions (solubility product, dissociation and hydrolysis constants, and solubility of gases) were used. They were approved, partly regained and approximated as a temperature function by J. Marion (Marion 2002). As opposed to the FREEZCHEM2 software, which is calibrated according to data of Nelson & Thompson (1954), the FREEZBRINE software is calibrated according to data of Gitterman (1937). It includes the following chemical components that may be formed in the system:

Solution (23 components):

cations : Na⁺, K⁺, Ca²⁺, Mg²⁺, H⁺, Mg(OH)⁺, Fe²⁺, FeOH⁺;

anions: Cl⁻, SO₄²⁻, OH⁻, HCO₃⁻, CO₃²⁻, HSO₄⁻, NO₃⁻;
.; indifferent: CO₂,aq, FeCO₃,aq, CaCO₃,aq, MgCO₃,aq, H₂,aq, O₂,aq, CH₄,aq, H₂O(l);

Gases (8 components): O₂,g, H₂,g, CH₄,g, CO₂,g, H₂O,g, HCl,g, HNO₃,g, H₂SO₄,g;

Solid phases (56 components), the main ones are: H₂O(cr,l), NaCl*2H₂O, HALITE, SYLVITE, CaCl₂*6H₂O, MgCl₂*6 H₂O, CaCl₂*2 MgCl₂*12 H₂O, Na₂SO₄*10 H₂O, MgSO₄*6 H₂O, K₂SO₄, MgSO₄* K₂SO₄*6 H₂O, Ca SO₄* 2 H₂O, ANHYDRITE, Na₂ SO₄* 3K₂ SO₄, CALCITE, MAGNESITE, Ca CO₃*6 H₂O, NaH CO₃, Na₂ CO₃*10 H₂O, DOLOMITE, ARAGONITE, VATERITE, HNO₃*3 H₂O, KNO₃, Na NO₃, Na₃ H(SO₄)₂, Mg SO₄* H₂O, Fe SO₄* 7 H₂O, FeCl₂*6 H₂O, FeCl₂*4 H₂O, SIDERITE, etc.

The FREEZBRINE software operates in various modes: closed and open systems; equilibrium or fractional crystallization; freezing/thawing; pressure change; ideal/non-ideal gases; and water evaporation/condensation. The closed system is the one that does not exchange the material with the environment. Its balanced composition including activity for all components is completely determined by the given T and P of the bulk chemical composition of the system. Balanced crystallization means that when external conditions (temperature or pressure) are changed, all system phases (for instance, ice, salts, electrolyte solution) formed earlier may interact with each other again. At the same time, it is possible that a mobile phase after partial crystallization moves to another point dimensionally separated from the earlier formed solid phases. Or the solution is separated from the earlier formed salts by the sheet of ice that prevents their interaction. Such crystallization, called fractionation, occurs during the temperature drop when the newly formed solid phases are constantly removed from the system.

In the selected modes, the model allows for simultaneous calculation of one of the following scenarios:

Freezing-thawing. In this case, a number of equilibria are calculated within the given temperature range with the given interval of temperature change under the constant given pressure. If the temperature decreases, the calculation is completed at the eutectic point (total solution crystallization).

Pressure change. A series of equilibria are calculated within the given pressure range with the given pressure change interval under the constant given temperature.

Evaporation. A number of equilibria are calculated at constant temperature and pressure during water removal from the system. The final water content is given in grams. The initial content by default is taken as equal to 1000 grams.

The software input data are the initial value of total mineralization and the concentration of the main components of the cryopeg chemical composition (Na,K,Ca,Mg, Fe,Cl, SO₄,HCO₃ etc.) obtained based on the chemical analyses of the samples.

Output data for the selected range and each given interval, for instance temperature, include the information on water, ions and salt content in the liquid, solid and gaseous phases, solution density and pH, and the main thermodynamic parameters (molarity, molality, chemical potential, etc.).

The FREEZBRINE software does not take into account the possibility of finding organic impurities in the cryopeg, sulphate reduction (waste product of bacteria) and chemical reactions such as sulphate reduction with sulphide and hydrogen sulphide formation. At low temperatures, the rate of the interactions of solutions with minerals of adjacent aluminosilicate ground are incomparably smaller than the rate of water-salt and water-gas equilibria or the rate of solutions freezing or thawing. For this reason, the aluminosilicate ground is considered to be relatively chemically inert.

The operation of the FREEZBRINE software was tested on a large experimental material. The comparison of the results obtained using the FREEZBRINE software and those obtained using the FREEZCHEM2 software with similar initial chemical composition of a cryopeg showed satisfactory convergence in general, though there were some differences related to different calibrations of these models for the temperature of certain mineral precipitation from solution into solid phase.

The data from the Yamal Peninsula cryopegs were processed using the FREEZBRINE software. Data on 48 cryopegs from the Yamal Peninsula that were obtained by L.N. Kritsuk and I.D. Streletskaya at various geomorphological levels (terraces, bottomlands, laidas) were processed. More detailed information is provided in the work of Kritsuk (2011), including information about cryopeg sampling sites, the depth of their locations, total mineralization, and chemical composition in the form of Kurlov's formula and pH. The principles of the formation of the ion-salt composition were addressed by Fotiev (2009). Comparison of field data on the pH value with the data calculated via the FREEZBRINE software is given. In particular for laidas (Table 1), the data showed satisfactory convergence; the inaccuracy did not exceed 10%. Quality correspondence between such factors as alkaline-acid environment was also fulfilled.

Estimates of Approximate Ratios

For engineering practice, it is crucial to have approximate formulae for expressing the estimation of cryopeg characteristics in which only the total mineralization initial value is used.

For this reason, the data obtained by the FREEZBRINE software were correspondingly processed.

Onset freezing temperature

To estimate the temperature at the onset of freezing [T_{br} (°C)] of a cryopeg, a polynomial type equation was used depending on its total mineralization [M (g/l)]. Ratios of such type—for instance, Krummel's formula (Doronin &

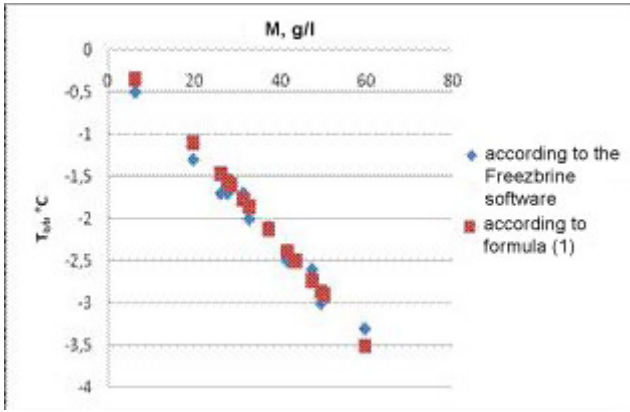


Figure 1. Comparison of data for the onset of the freezing temperature T_{br} for the terraces calculated by the FREEZBRINE software and according to formula 1.

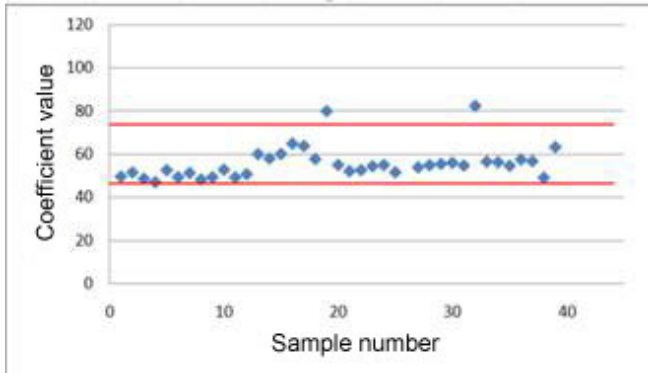


Figure 2. Results of combined statistical processing of data for the laida, bottomland, and terraces showing that, initially approximated, they remain in the confidence range $x \pm s$.

Khasin 1975)—are used to calculate T_{br} of sea water. Data on 17 cryopeg samples were processed from laidas and bottomlands, and 14 samples were processed from terraces. The calculated ratio is as follows:

$$T_{br}(M) = -10^{-3} \cdot (X \cdot M + 0,04 \cdot M^2), \quad 5 \leq M \leq 130 \quad (1)$$

where X is a coefficient depending on cryopeg location: X = 50.0 for laida; X = 55.8 for bottomland; X = 58.9 for terraces (the example in Fig. 1).

Statistics processing showed that the data divided according to the laidas-terraces-bottomlands principle were in the confidence range $x \pm s$: $x_{cp} = 50.0$ and $s = 1.78$ for laidas; $x_{cp} = 58.9$ and $s = 7.34$ for terraces; $x_{cp} = 55.75$ and $s = 2.74$ for bottomlands. For the overall data $x_{cp} = 57.14$ and $s = 11.42$ (Fig. 2).

Cryopeg density

To calculate cryopeg density ρ_{uw} (g/cm³) which increases with the decrease in temperature [T (°C)] and mineralization M(g/l) increase, the following ratio is suggested:

$$\rho_{uw} = 1 + 10^{-3} \times [34,8 - (0,08 \cdot T) + (M - 35)], \quad 5 \leq M \leq 130 \quad (2)$$

The value of the cryopeg density does not depend much on its location and may be calculated according to formula 2 with an inaccuracy of 10%. Due to lower sensitivity of the density value to the temperature factor than to the degree

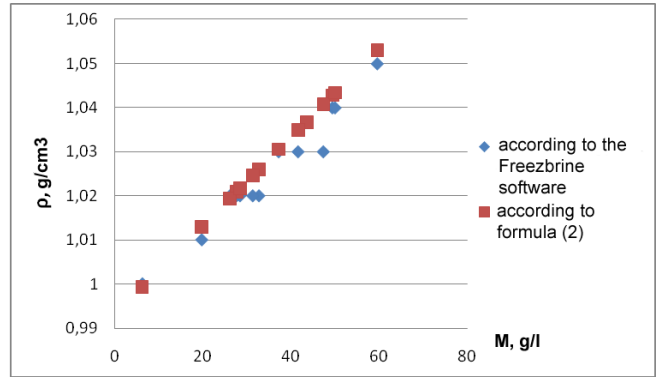


Figure 3. Data comparison for cryopeg density ρ , g/cm³ for terraces calculated by the FREEZBRINE software and formula 2 (averaging in temperature range from 0 to -20°C).

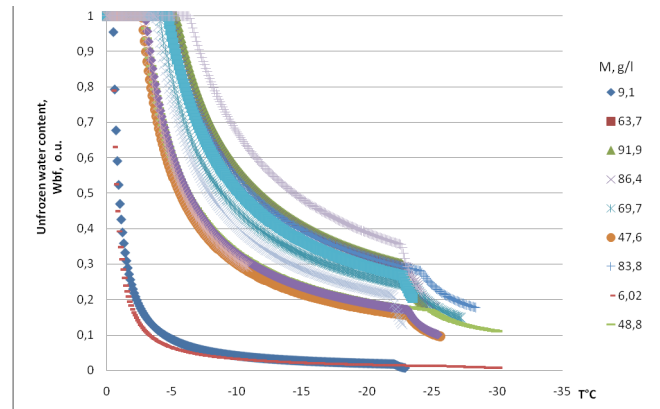


Figure 4. Dependence of unfrozen water composition on temperature and mineralization $W_{uw} = f(T, M)$ calculated by the FREEZBRINE software.

of mineralization, this factor may be disregarded in actual calculations (Fig. 3).

Cryopeg phase composition

Phase composition for the case of the laidas have typical temperature curves as shown in Figure 4. It shows that unfrozen water composition significantly depends on mineralization. When temperature decreases below the onset of the freezing point, the amount of ice increases as well as the mineral formation of mirabilite, calcite, gypsum, and others. However, for practical purposes it is reasonable to take into account only the impact of hydrohalite precipitation from solution (NaCl × 2H₂O) at the temperatures of -22 to -23°C (Fig. 4). Estimation of unfrozen water composition depending on temperature and mineralization $W_{uw}(T, M)$ may be performed according to equations 3, 4, and 5 using Table 2:

$$W_{uw}(T, M) = 1, \quad 0 > T > T_{br}, \quad 5 \leq M \leq 130 \quad (3)$$

$$\frac{W_{uw}(M, T) - W_{uw}(M, -22,5)}{W_{uw}[T_{br}(M)] - W_{uw}(M, -22,5)} = \left(\frac{T + 22,5}{T_{br}(M) + 22,5} \right)^N$$

$$T_{br} \geq T \geq -22,5, \quad 5 \leq M \leq 130 \quad (4)$$

$$\frac{W_{uw}(M, -22,5) - W_{uw}(M, T)}{W_{uw}(M, -22,5)} = \exp\left[\Psi \cdot \left(\frac{-22,5}{-22,5 - T} \right) - 1,8\right]$$

$$T \leq -22,5, \quad 5 \leq M \leq 130 \quad (5)$$

where $W_{uw}(M, T)$, $W_{uw}[T_{br}(M)]$, $W_{uw}(M, -22,5)$

Table 1. Chemical composition and pH of the laidas from the Yamal Peninsula cryopegs (Kritsuk, 2010).

Field data							Calculated data from the FreezBrine software	
#	Sampling point	Cryopegs lenses depth, m	Ground water level, m	Mineralization, g/l	Kurlov's formula	pH	pH	Tbf
1	Bely Island	-	-	111.8	$\frac{Cl_{197}SO_4 2HCO_3 1}{Na_{76}Mg_{21}Ca_3}$	6.8	6.62	-6.6
2	Khassale ness	-	-	83.4	$\frac{Cl_{196}SO_4 3HCO_3 1}{Na_{76}Mg_{20}Ca_4}$	6.9	6.75	-4.8
3	Sharapovy Koshki Islands	-	-	93.2	$\frac{Cl_{191}SO_4 8HCO_3 1}{Na_{76}Mg_{20}Ca_4}$	-	6.71	-5.2
4	Cape Burunny	-	-	103	$\frac{Cl_{190}SO_4 9HCO_3 1}{Na_{78}Mg_{19}Ca_2}$	-	6.79	-5.7
5	Kharasavey Village	3.5	1.2	31.3	$\frac{Cl_{190}SO_4 10}{Na_{96}Mg_4}$	7.7	7.04	-1.7
6	Cape Kharasavey	3.2	1.4	80	$\frac{Cl_{190}SO_4 9HCO_3 1}{Na_{78}Mg_{19}Ca_3}$	-	6.87	-4.4
7	Litke Island	4.6	1.5	72.8	$\frac{Cl_{194}SO_4 4HCO_3 2}{Na_{76}Mg_{21}Ca_3}$	7.2	6.64	-4.1
8	Litke Island	2	1	74.9	$\frac{Cl_{195}SO_4 4CO_3 1}{Na_{73}Mg_{23}Ca_4}$	6.4	6.79	-4.0
9	Litke Island	2	1.5	101	$\frac{Cl_{194}SO_4 5HCO_3 1}{Na_{78}Mg_{19}Ca_3}$	6.2	6.7	-5.8
10	Coast of Sharapov Shar Bay	3.8	0.6	71.1	$\frac{Cl_{197}SO_4 3}{Na_{94}Mg_5Ca_1}$	-	7.27	-4.1
11	Coast of Sharapov Shar Bay	9.8	1.2	98.3	$\frac{Cl_{195}SO_4 5}{Na_{85}Mg_{13}Ca_5}$	-	7.19	-5.6
12	Coast of Sharapov Shar Bay	4.2	-	79.8	$\frac{Cl_{194}SO_4 6}{Na_{78}Mg_{18}Ca_4}$	-	7.2	-4.5
13	Coast of Sharapov Shar Bay	1.6	-	35.3	$\frac{Cl_{196}SO_4 6}{Na_{77}Mg_{19}Ca_4}$	-	7.21	-5.5

Unfrozen water composition is characterized according to equation 1 by current value at the given temperature T ; at freezing onset temperature, and at $T = -22.5$, respectively; and (Table 2) N and Y - coefficients (Table 2), T_{bf} .

Cryopeg heat capacity

Cryopeg freezing solution specific heat capacity value C_{uw} (J/g ×K) is determined as:

$$C_{uw}(M, T) = 10^{-3} \cdot [C_{wt}(T) - 4.55 \cdot M], \quad 5 < M < 130, T > T_{bf} \quad (6)$$

where C_{wt} – according to Table 3, M (g/l), T_{bf} – according to equation 1.

Cryopeg freezing solution volumetric heat capacity value Cr (J/sm³×K) is:

$$Cr(M, T) = C_{uw}(M, T) \cdot \rho, \quad 5 < M < 130, T > T_{bf} \quad (7)$$

where $C_{uw}(M, T)$ – according to formula 6, r_{uw} – according to formula (2), T_{bf} – according to equation 1.

The specific heat capacity value of the cryopeg with ice is:

$$C(M, T) = C_{uw}(M, T) \cdot W_{uw}(M, T) + C_i(T) \cdot [1 - W_{uw}(M, T)], \quad 5 < M < 130, T \leq T_{bf} \quad (8)$$

where $C_{uw}(T, M)$ is according to formula 6, $W_{uw}(T, M)$ is according to equations 4 and 5, $C_i(T)$ is the heat capacity of ice according to formula 9, and T_{bf} is according to equation 1.

$$C_i(T) = 2.12 + 0.0078 \cdot T \quad (9)$$

herein C_i (J/g K), T (°C).

The thermal conductivity coefficient of most electrolyte solutions typically decreases when concentration increases (except NaOH and Na₂SO₄) and increases when temperature

Table 2. Equation coefficients values (4-5) for the Yamal Peninsula cryopegs.

M, g/l	$W_{uw}[T_{bf}(M)]$	$W_{uw}(M, -22,5)$	N	Ψ
$10 \leq M < 35$	0.99	0.4	2.2	0.03
$35 \leq M < 70$	0.98	0.2	1.3	0.02
$70 \leq M \leq 130$	0.96	0.1	1.1	0.004

Table 3. Calculated values of the temperature dependence C_{wt} (T) of the specific heat capacity of water (Tsurikov 1976).

T_s , °C	C_{wt} , J/kg K	T_s , °C	C_{wt} , J/kg K	T_s , °C	C_{wt} , J/kg K
0.0	4210	-2.8	3890	-13	3510
-0.2	4150	-3.2	3860	-14	3490
-0.4	4110	-3.6	3840	-15	3470
-0.6	4060	-4.0	3820	-16	3450
-0.8	4030	-5.2	3800	-17	3440
-1.0	4010	-6.0	3700	-18	3430
-1.2	3990	-6.8	3670	-19	3410
-1.4	3970	-8.0	3630	-20	3400
-1.6	3950	-8.8	3600	-21	3390
-1.8	3930	-10	3570	-22	3380
-2.0	3920	-11			
-2.4	3900	-12			

Table 4. Temperature dependence of coefficient f_t .

T, °C	30	20	10	0	-10	-20	-30
f_t	1.025	1.0	0.973	0.946	0.919	0.892	0.865

increases. For cryopegs of the sea salinity type, the following ratio could be recommended:

$$\lambda_{uw} = (\lambda_o - 0.0009 \cdot M) \cdot f_t, T > T_{bf} \quad (10)$$

where λ_o is 0.58 (W/m · K); thermal conductivity coefficient of water (H₂O) with mineralization M = 0; T = 20 °C and pressure P = 1atm; f_t is the coefficient depending on temperature (Table 4).

For cryopegs of the continental salinity type, a little higher value λ_{uw} should be expected due to the fact that the relative concentration Na₂SO₄ is higher there.

The thermal conductivity of the solid phase can be conditionally taken as the thermal conductivity of fresh ice λ_i :

$$\lambda_i = \lambda_o (1 - 0,0159 T), T_{bf} \geq T \quad (11)$$

where $\lambda_o = 2,22$ W/m; · K = thermal conductivity of fresh ice with T = °C.

The thermal conductivity of the cryopeg λ , when the liquid and solid phase may be present, is calculated by formula 12:

$$\lambda = \lambda_{uw} + (\lambda_i - \lambda_{uw}) \cdot [1 - W_{uw}(M, T)], 0 \geq T > -40 \quad (12)$$

where λ_{uw} calculated by the formula 10, λ_i by formula 11, $W_{uw}(M, T)$ for the case when $0 > T > T_{bf}$ calculated by formula 3, λ_{uw} by formula 10, for the case when $T_{bf} \geq T \geq -40$ by formula 4 or 5, and T_{bf} by formula 1.

Acknowledgments

The authors would like to thank S.M. Fotiev, L.N. Kritsuk, and I.D. Streletskaia for useful advice and discussions, as well as student G.E. Oblogov, who provided assistance in performing the calculations using the FREEZBRINE software.

References

- Doronin, Y.P. & Khasin, D.E. 1975. Sea ice. L.: Gidrometeoizdat, p. 318.
- Fotiev, S.M. 2009. Cryogenic metamorphosis of grounds and underground waters (conditions and results) Novosibirsk, Academicheskoe izdatelstvo. *Geo* p. 279.
- Gitterman, K.E. 1937. Sea water thermal analysis (concentrating salt solutions with natural freezing). Trud. Solyanoy lab. AN SSSR. M., Izd-vo AN SSSR, ed. 15, p.1, 5-24.
- Komarov, I.A. 2003. Thermodynamics and heat-and-mass transfer in dispersed frozen grounds. M.: Nauchny mir, p. 608.
- Komarov, I.A. & Mironenko, M.V. 2010. Modeling water-ion composition of saline frozen grounds and cryopegs with changing thermobaric conditions. Works of the International conference "Relevant directions of applied mathematics in energetics and information-communication technologies" M.: Izd-vo MGTU im. N.E. Bauman, pp. 23-29.
- Komarov, I.A., Mironenko, M.V., & Pustovoyt, G.P. 2008. Software product development for temperature and ion-salt regime prediction for saline grounds and cryopegs. Reports at the International conference "Cryogenic resources of polar and mountain regions, condition and perspectives of engineering permafrost studies" Tyumen, pp. 404-407.
- Komarov, I.A., Volkov, N.G., Mironenko, M.V., Fotiev, S.M., Streletskaia, I.D., & Kovalchuk, A.N. 2006. Prediction methods for temperature and water-ion regimes in saline grounds and cryopegs (problems, solutions). Materials of the International Conference "Theory and practice of estimating the Earth cryosphere condition and its changes prediction" Tyumen, pp. 30-35.
- Kritsuk, L.N. 2010. Ground ice of East Siberia. M.: Nauchny mir, p. 351.
- Marion, G. 2002. A molal-based model for strong acid chemistry at low temperatures (200 to 298 K), *Geochim. Cosmochim. Acta* 66: 2499–2516.
- Mironenko, M.V., Grant, S.A., Marion, G.M., & Farren, R.E. 1997. FREZCHEM2. A Chemical Thermodynamic Model for Electrolyte Solutions at Subzero Temperatures CRREL Report 97-5, October, 40 pp.
- Mironenko, M.V. & Polyakov, V.B. 2009. Procedure of calculation of balanced composition of water-salt systems based on Pitzer's model. *Geokhimiya* No 10. pp. 1103-1107.

- Nelson, K.H. & Thompson, T.G. 1954. Deposition of salts from sea water by frigid concentration. *Journal of Marine Research* 13 (2), pp. 166-182.
- Pitzer, K.S. 1997. A thermodynamic model for aqueous solutions of liquid-like density. *Reviews in Mineralogy* 17, pp. 97-142.
- Tsurikov, V.L. 1976. Liquid phase in sea ice. M.: Nauka, p. 207.
- Volkov, N.G., Komarov, I.A., Mironenko, M.V., & Fotiev, S.M. 2005 Estimation methods for cryopeg ion-salt composition formation temperature. *Kriosfera Zemli* (no 4): 54-61.

Cryogenic Risks and Railroad Resources in Permafrost Regions

V.G. Kondratyev

Zabaikalye State University, TransIGEM, Chita, Russia

Abstract

Railroad construction in permafrost regions of Russia, the United States, Canada, and China has been ongoing for more than 100 years. Nonetheless, no one has ever been able to build a track that is immune from deformations caused by differential settlement of the embankment resulting from the thawing of ice-rich, perennially frozen soils. This paper presents data on the conditions of embankments of the Zabaikalye Railway, the Qinghai-Tibet Railway, and the Baikal-Amur Railway. The paper discusses the possibility of providing railroad embankment stability by using methods based on the lowering of the mean annual ground temperature in order to preserve the ground in its perennially frozen condition. These methods include control of the natural cooling and warming factor ratio to reduce heat generation in the embankment and the adjacent area accompanied by the increase in heat consumption. Results of site investigations along the Qinghai-Tibet Railway and the East-Siberian Railway are presented.

Keywords: BAM; cryogenic resource; embankment deformation; permafrost; stabilizing measures; railways.

Introduction

Operation of railroads in regions underlain by permafrost or characterized by deep seasonal ground freezing (approximately 70% of the Russian territory) involves significant material and labor costs for maintenance and repairs. Numerous deformations of railroad embankments and other facilities occur because of settlement from the thawing of ice-rich ground and frost heaves of the wet, fine-grained soils at the base of embankments.

The Turinskaya-Kadakhta haul (Fig. 1), which is a part of the Zabaikalye Railway (6278 km), is a typical example. It is known as the “gold haul” due to continuous track re-alignment work and repair costs. In 2009 the odd track was re-aligned 12 times and the even track 10 times; in 2010 the odd track was re-aligned 11 and the even track 9 times.

Systematic track deformations have been observed there since 1948, and starting in 1969 a rail speed limit of 40 km per hour and sometimes 15 km per hour was applied.

The railway continually bears losses due to lost train traffic and additional costs for tracks and the overhead contact system, which also requires frequent repairs. In 1995 the total loss for the site with minor transportation volume (75% of the 1999 volume) consisted of RUR 241,302 adjusted to 1991, including losses due to train slowdown

of RUR 195,302 or 81% of the total loss. The expenditures for track alignment and ballasting amounted to RUR 30,000 or 12.4%, and additional expenditures for deformation of the overhead contact system were RUR 16,000 or 6.6% (Kondratyev 1997).

The railroad track has been deformed (for the second decade now) on the East-Siberian Railway, in the area of the Kazankan switching track (1374 km of the BAM, Fig. 2).

Only one of the original four tracks remains in place, and it needs regular re-alignment and frequent repairs.

Approximately RUR 500 million has been spent during the past eight years for site repairs, including the use of seasonal cooling units and rockfill (Fig. 2), but the problem of track stabilization remains unsolved. The train speed is still limited to 15 km per hour, and the threat of a sudden derailment and service disruption on the Baikal-Amur Railway (BAM) remains. This track section is electrified, and the overhead contact system requires constant repairs. As far back as 1926, the founder of permafrost science (geocryology), Mikhail Ivanovich Sumgin, wrote that the maintenance of deformed buildings and structures along the Zabaikalye and the Amur railways alone had cost 50 million gold rubles for the State, excluding losses due to railway traffic schedule violations (Sumgin 1937). Unfortunately, not much has changed since that time regarding this problem.



Figure 1. Zabaikalye Railway track deformation, 6278 km, February 2011.



Figure 2. East-Siberian Railway track deformation, 1374 km of the Baikal-Amur Railway (BAM), July 2011.

Five railways, which belong to the Russian Railways JSC (Northern, Sverdlovsk, East-Siberian, Zabaikalye, and Far East railways) operate in areas underlain by permafrost. The total length of the sections of the railways underlain by permafrost is approximately 5000 km. Track within approximately 15% of this length experiences permafrost-related deformations that result in train speed reductions.

For example, during the first few operational years (by February 1992) there were 188 problem sections that experienced deformation of the railway with a total length of 186.6 km or 19.2% of the 965 km line located in the eastern part of the Baikal-Amur Railway and at the Tynda-Urgal line (Yakovlev, 1992). In 2004, the length of the problem railroad sections increased to 325.4 km, making up 34.2% of the total railroad length. In 2007, 192.4 km of track line (20.6% of its length) continued to deform despite constant repairs. Despite considerable material costs, the Far East Railway has failed to significantly improve the track. The train speed on the BAM is 60 km per hour along most of the route, 70 km per hour at individual sections, and along 49 sections the speed is limited to 25-40 km per hour.

As far as the entire BAM is concerned, 4238 problem sections with a total length of 1101 km (35% of the total length of the railroad) were identified in 1992 between Ust-Kut and Komsomolsk-on-Amur. The embankment settlement caused by permafrost degradation in the subgrade made up approximately 69% (Yakovlev 1992).

Discussion

High deformation of the BAM is due to the fact that the specifications for geotechnical site investigations, design, and construction of railways in permafrost areas did not require preservation of the permafrost condition in the embankment. These specifications, along with a reference manual specially prepared for the BAM construction (Site investigation.... 1977) have been in effect for many decades. It has always been assumed that the so-called “optimal embankment height” and berms would limit the depth of subgrade ground thawing, and that the allowance in the embankment height and width as well as placement of ballast fill during the first operational years would compensate for

possible settlement. These assumptions have not proved to be true on the BAM. Berms mainly had the opposite effect. They contributed to an increase in the ground thaw basin under the embankment and to an increase in the scale of settlement and its duration.

BAM operation showed that the traditional method of railway maintenance by means of embankment settlement compensation with uplifting of assembled rails and sleepers on ballast is not efficient either technically or economically. Berms and sorted hard rock fills on embankment slopes and thermosyphons used on the BAM are too expensive and not always efficient.

The prevention of embankment deformation on ice-rich permafrost has been a problem for many decades not only in Russia (Yelenevsky & Nizovkin 1936, Sumgin 1937, Petrukhin & Potatuyeva 1987, Bushin 1992, Kondratyev 2011) but also in the United States (Fig. 3) (Berg & Aitken 1973), Canada (Hayley 1988), and China (Fig. 4) (Wu Ziwan et al. 1988, Feng Wenjie et al. 2011).

Construction of the Qinghai-Tibet (Qinghai-Hisan) Railway in China in 2001–2006 is the newest railroad construction in permafrost regions. The scale of the construction and the expenditures involved were colossal. An attempt was made to find a technical solution that would ensure the stability of the track built on ice-rich permafrost that is prone to thaw settlement.

The modern railroad was built in extremely complex mountainous terrain and geological conditions: 80% of the 1142-km-long route from Golmud to Lhasa crosses areas with elevations above 4000 m; approximately 50% of the route crosses terrain underlain by permafrost, with ground temperatures ranging from -0.5 to -3.6°C and permafrost thickness ranging from 5–25 m to 60–130 m and more. The passenger train passes the highest point of the route (5,072 m) across the Tanggula Shan Range at the speed of 100 km per hour, and the entire trip from Golmud to Lhasa takes only 13 hours.

According to Chinese specialists, no troublesome sections that could affect the train traffic have been observed during three years of Qinghai-Tibet Railway operation. Nonetheless, according to their own field data collected in 2006–08 (Lin Zhanju et al. 2009), the following permafrost-related



Figure 3. Alaska Railroad track deformation near Fairbanks, July 2008.



Figure 4. Qinghai-Tibet Railway track deformation, August 2006.

geohazards are already developing along the embankment: thermokarst, differential settlement on thawing, retrogressive thaw flows, thermal erosion, and frost heave.

For example, 250 thermokarst lakes with a total area of 6,000 to 1,200 m² were identified in 2007 in the 100-m-wide corridor located on either side of the embankment. About 70% of the lakes have an elliptical shape and 12% have an elongated shape. Eighty percent of the thermokarst lakes do not freeze to the bottom in winter.

Differential settlement of the railway embankment due to permafrost thaw in the subgrade was mainly identified along the sections of wider embankments and at the bridge abutment sites. Analysis of monitoring data between July 2003 and December 2007 for the thaw settlement for the embankments indicated that 3.2 to 6.0 m height at 56 sites showed that the higher the embankment, the greater the settlement. Settlement of 13–15 cm occurred with the embankment height below 5 m, whereas, 17–23 cm occurred with the embankment height above 5 m; the average was 17.8 cm. Thirty-five sites (63%) are characterized by “warm” permafrost with ground temperature above -0.5°C; seven sites have temperatures from -0.5 to -1.0°C; 12 sites are without permafrost; at 26 sites (46%), ice content is 20% to 50%; at 18 sites (32%), ice content is below 20%.

The maximum settlement of the embankment (18.6 cm) was recorded near the 6.0-m-high rock block embankment.

At a bridge abutment site, the minimum settlement was 3 cm. A continuous increase in embankment settlement was observed during the monitoring period. The total length of the troublesome sections of the embankment (those experiencing differential settlement) was 15.76 km in 2005 and 18.56 km in 2007. Moreover, in 2007, berm settlement was observed along the sections with the total length of approximately 1 km, while in 2005 no such settlement was observed.

In April 2009, 43 bridges along the section from Yerdagou to Beluhe were examined at 172 points (4 points per bridge). The study revealed that settlement occurs in 73% of the points, and in 44 points (35.2%) settlement exceeded 10 cm. Judging by this trend, the number may increase.

Therefore, the beginning of the Qinghai-Tibet Railway operation once again confirms the urgency of the embankment stabilization problem on ice-rich permafrost.

The Russian railroad innovation development strategy provides for a potential increase of transportation via the Trans-Siberian Railway and the BAM in order to meet the economic and social demands. Plans also include increases in freight train axial and unit loads, the weight and length of trains, and train speed. But first it is necessary to improve the embankment conditions, especially at the sites underlain by ice-rich permafrost where train speed has for decades been limited to 25–40 km per hour.



Figure 5. Sun and precipitation awnings on the Qinghai-Tibet Railway at the site of ice-rich ground in the subgrade, August 2006.



Figure 6. East-Siberian Railway sun and precipitation awnings at 1841 km on the BAM, May 2011.

New engineering concepts and improvement of scientific and methodological foundations are needed. Geocryological support of maintenance, reconstruction, and upgrading of the Trans-Siberian Railway and the BAM and other roads in the permafrost zone is required. The frost-based approach should penetrate the whole process of railroad embankment and facilities operation. Management of geocryological road conditions should become the cornerstone of the new approach.

In areas underlain by ice-rich permafrost of significant thickness, the natural cold, as the main resource of the permafrost zone, should be used to preserve the foundation soils in a frozen state or to halt permafrost thawing if the process is already underway.

We proposed several methods of supporting the railway embankment subgrade on permafrost (Kondratyev, 2011). These methods are based to decrease the mean annual ground temperature and preserve the foundation soils in a perennially frozen state. This is done through regulation of natural cooling and warming factors, reduction of heat inflow, and the increase of heat consumption in the embankment and the adjacent territory.

Special devices and methods (e.g., sun and precipitation awnings, reflecting painting, snow removal, and impervious barriers) are used to reduce the effect of solar radiation on the roadbed surface and the adjoining territory to improve the albedo and outgoing radiation of the surface. These strategies also prevent summer precipitation seepage into the

embankment and seepage of surface and suprapermafrost waters into the base of the embankment. Technical solutions are suggested to stabilize the embankment, using special cooling pipes at the base of the embankment.

These technical solutions have received approval in papers, reports, and monographs published in Russia and abroad. They were used in pilot projects of the Amur-Yakutia Railway Mainline and the Ulak-Elga Approach Line construction as well as in technical and economic documents on stabilization measures for the Zabaikalye Railway.

Some of them have been applied in China on the Qinghai-Tibet Railway. One of those devices is the sun and precipitation awning (Fig. 5), which, according to the natural monitoring data (Niu Fujin & Shen Yongping 2006), decreases the ground temperatures by 3–5°C and maintains the stability of the embankment on ice-rich permafrost.

The awning was used with positive results on the Qinghai-Tibet and the Cinkan motor roads. According to the data of natural monitoring conducted on the Qinghai-Tibet motor road in 2010, the awning is capable of reducing the radiation balance by 80–90% and reducing the embankment surface temperature by 6–8°C (Feng Wenjie et al. 2011).

The pilot use of sun and precipitation awnings on the BAM was initiated in 2009. The first awning made of defective sleepers was installed at 1841 km of the East-Siberian Railway in December 2009. It was installed above the roadside and drainage ditch (Fig. 6) to raise the permafrost table in the embankment, which, in turn, reduced



Figure 7. Transversal ventilated reinforced concrete pipes in the roadbed of the Qinghai-Tibet Railway (photograph by Niu Fujin).

seepage under the embankment. The awning sizes are 2.75 x 2.75; 41 x 5.25; 2.75 x 2.75 m; the area is 231 m². At the time of installation, the thickness of the active layer was more than 3.5 m, and as of October 5, 2010, it was 1.68 m, for a decrease of 2.1 in less than a year. The practical effect is obvious. Prior to awning installation, the track was annually re-aligned four or more times, up to 250 mm in total. In 2010 the track was aligned only once, up to 100 mm. Track stability is significantly improved with awning installation on the slope that is exposed to the south. It should be noted that the capital repair of the first track in 2008 (RUR 6.354 million per km) and the midlife repair of the second track in 2009 (RUR 6.065 million per 1 km) on the site had no positive effect. The expenditures for awning installation were RUR 11,511.59; the rock fill would cost RUR 263,976.80, which is 24 times higher.

Conclusions

The results of our investigations show that the awning can become the main anti-deformation device for railway and motor road embankments built in areas underlain by ice-rich permafrost. Use of the awning provides for intense winter cooling of the roadbed and its subgrade. It also eliminates direct solar radiation and summer precipitation infiltration. If the permafrost in the subgrade is preserved during the whole period of road operation, the need for additional anti-deformation measures is eliminated, the structure of the embankment is simplified, the road capacity increases, and maintenance-free periods are extended.

We proposed another technical solution: an embankment with transversal cooling pipes (Fig. 7), both reinforced concrete and plastic, with automatic shutters for the warm period. It has been used at the Qinghai-Tibet Railway.

In some conditions, other ground temperature reduction methods in the embankment are effective as well. Subgrade preservation in the permafrost state by means of natural cooling and heating factor ratio regulation may be used (Kondratyev, 2011).

Thus the operational reliability of railways and motor

roads in the permafrost zone is predetermined mainly by the proper selection of the design and construction methods and techniques and by proper maintenance. Sites that are underlain by ice-rich permafrost that cannot be removed beforehand should be protected from degradation through use of the main cryogenic resource (i.e., winter cold) during the entire operation period.

References

- Berg, R.L. & Aitken, G.W. 1973. Some passive methods of controlling geocryological conditions in roadway construction. *Proc. North American Contribution 2nd International Conference on Permafrost*, Yakutsk, USSR, pp. 581-596.
- Bushin, A.V. 1992. On tasks for provision of railway roadbed reliability in modern conditions. *Zh.-d. transport Series Put i putevoye khozyaystvo*: *EI/TsNIITEI MPS*. No. 5-6, pp. 1-14 (in Russian).
- Feng Wenjie et al. 2011. Radiation effect analysis of the awning measure on the embankment slope field test in cold regions. *Proceeding of the IX International Symposium on Permafrost Engineering*. 3-7 September, 2011, Mirny Russia, pp. 319-325.
- Hayley, D.W. 1988. Maintenance of a railway grade over permafrost in Canada: *Proc. 5th Int. Conf. on Permafrost*. Vol. 3. pp. 43-48.
- Kondratyev, V.G. 1997. Technical and economic substantiation of roadbed stabilization on ice-rich permafrost for one of the Zabaikalye Railway sites. *Zh.-d. transport. Series Stroitelstvo. Proyektirovaniye*": *EI/TsNIITEI MPS*. No. 2, 54 pp. (in Russian).
- Kondratyev, V.G. 2011. *Stabilization of the roadbed on permafrost*. Chita: PoligrafResurs, 177 pp. (in Russian).
- Lin Zhanju et al. 2009. Roadbed Diseases and Their Development States along the Qinghai-Tibet Railway. *Proceeding of the Eighth International Symposium on Permafrost Engineering*. 15-17 October, 2009, Xi'an, Cnina, pp. 489-501.

- Niu Fujin & Shen Yongping 2006. *Guide of Field Excursion after Asian Conference on Permafrost (Aug. 10-16, 2006)*. Lanzhou, China, 28 pp.
- Petrukhin, N.A. & Potatuyeva, T.V. 1987. *Roadbed and permafrost interaction*. Tomsk: Tomsk University Publishing House, 160 pp. (in Russian).
- Research and design of the Baikal-Amur Mainline route*. 1977. Reference aid. Edited by D.I. Fedorov. Moscow: Transport. 280 pp. (in Russian).
- Roads and airfields in cold regions. 1996. ASCE, New York, 321 pp.
- Sumgin, M.I. 1937. *Permafrost within the USSR*. Publishing House of the USSR Academy of Sciences. Moscow.-Leningrad (Issue 2), 379 pp. (in Russian).
- Wu, Ziwang et al. 1988. Roadbed engineering in permafrost regions. Lanzhou University, pp. 43-50.
- Yakovlev, V.E. 1992. Current maintenance and capital repair of the roadbed in BAM conditions. *Zh.-d. transport. Series Put i putevoye khozyaystvo: EI/TsNIITEI MPS*. Issue 5-6, pp. 14-28 (in Russian).
- Yelenevskiy, V.V. & Nizovkin, G.A. 1936. Railway construction in permafrost conditions. Moscow: *Transzheldorizdat*, 239 pp. (in Russian).

Experimental Study of Isotope Composition of Bound Water

V.N. Konishchev, V.V. Rogov, V.N. Golubev, S.A. Sokratov
Faculty of Geography, Lomonosov Moscow State University, Moscow, Russia

Abstract

Laboratory tests on isotopic composition of water and ice in structure-forming soils were carried out. The results of the tests have shown that the interactions between water and soils, water migration, and ice formation during the freezing process cause isotope fractionation influenced by soil composition and freezing conditions.

Keywords: ice; isotopes; migration; soil; water.

Introduction

Isotope study of ice formations in the cryosphere—glaciers, ice sheets, massive ground ice—has become the main method of obtaining information about past conditions. At the same time, there is a significant lack of information on the structure-forming ice. No current data exist on the difference between the isotope composition of free and migrated moisture or on the correlation between them. However, we presume that due to the different characteristics of “unfrozen” and free water, the isotope composition of the former may be different from the isotope composition of the latter.

The concentration and distribution of stable isotopes of oxygen and hydrogen in frozen ground ice are defined by the isotope composition of the initial moisture and its mass transfer processes caused by the environment. The environment refers to soil moisture in the soil itself, which impacts the distribution of moisture and isotopes to the extent determined by the mineral composition, size, and parameters of interaction between the current phase of moisture cycle and particles in each particular case. These characteristics of soil particles are the factors that define the specific surface area and surface energy as well as certain amounts of ground water that do not freeze at subfreezing temperature and are often defined as “unfrozen” water. Characteristics of this water are affected by ions, atoms, and molecules, which mold the surface of soil particles; the characteristics of volumetric water are different (Cheverev 2004). For that reason, there may be a discrepancy between the corresponding composition of molecules containing heavy isotopes of hydrogen and oxygen. The predominance of heavy isotope molecules in the main volume of soil moisture or in “bound” water can be associated with Van der Waals interaction between water dipoles, atoms, and molecules found on the mineral particle surfaces as well as with the occurrence of hydrogen and ionic bonds between uncompensated charges on their surface and ions of H^+ , OH^- , H_3O^+ , OD^- , H_2DO^+ , produced as a result of water dissociation.

The energy of Van der Waals interaction between heavy isotopes in water molecules, atoms, and molecules on mineral particle surfaces is 10% higher than that of the lighter isotopes. However, since the interaction of water dipoles with each other is at least one order of magnitude greater than their interaction with atoms and molecules on mineral particle surfaces, the predominant concentration of heavy isotopes in water molecules shall involve the bulk of ground (free) water. This notion is confirmed, to

some extent, by the data presented in the paper by Fedorov (1999). He showed that the system of “constitutional water of clay minerals—water of sedimentation basin” undergoes significant isotope fractionation of hydrogen and oxygen. It was found that the tightly bound water contents in clay minerals (at least, the water found in the monolayer) is isotopically lighter in hydrogen and heavier in oxygen than the water that maintains isotopic equilibrium with clay minerals. The difference in D values may be as large as -160‰ (for sericite) and +28‰ for ^{18}O (for gibbsite) compared with the SMOW standard. Fedorov states that the main reason for hydrogen and oxygen isotope fractionation resulting from the formation of crystallization water in clay minerals and their variations is the bond energy of water and ion H_3O^+ , H^+ , OH^- with the solid state.

However, due to the relatively small net volume of “bound” water, this factor may hardly be considered crucial for reallocation of heavy and light isotope water molecules due to interaction with soil. In addition, it is known that the phase transition intensifies the accumulation of heavy isotopes in free water (Vasilchuk 2011). At the same time, the scale of this effect is not clarified for soil yet, because the amount of “bound” water is insufficient.

Experiments and Results

To draw more substantial conclusions regarding the importance of isotope differentiation resulting from water and dispersed particle surface interaction, a series of experiments was carried out. For the experiments, we have taken samples of fine-grained (“edomny”) clayey silt from Duvanny Yar on the Kolyma River, samples of kaolinite from the Prosyankovskoe Field, and samples of bentonite from the Khakasskoe Field.

The first experiment was on soil wetting. The equal amounts of air-dried samples of bentonite, kaolinite, and clayey silt were sufficiently wetted (in the proportion 3:1) with distilled water of particular isotope composition, and then they were continuously mixed for 72 hours. After that, the water was settled and its isotope composition was analyzed. The results of the isotope analysis of the volumetric water shown in Figure 1 demonstrate relatively small changes in the initial and output values. ^{18}O values for all samples in free water rose insignificantly: by 0.2–0.3‰, D value changing even less. The experiment showed that the wetting of dry soil, when water divides into tightly bound and free, induces differentiation, but that it occurs on a rather small scale.

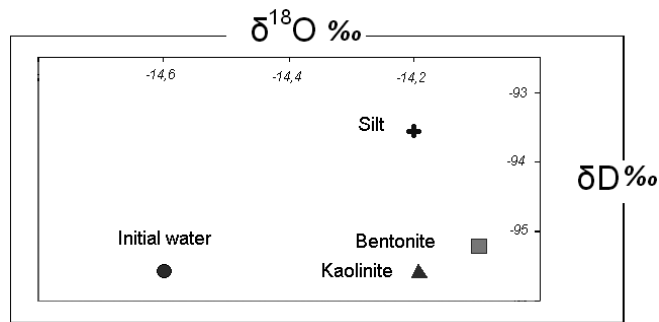


Figure 1. Composition of heavy water isotopes in the samples taken from Experiment 1.

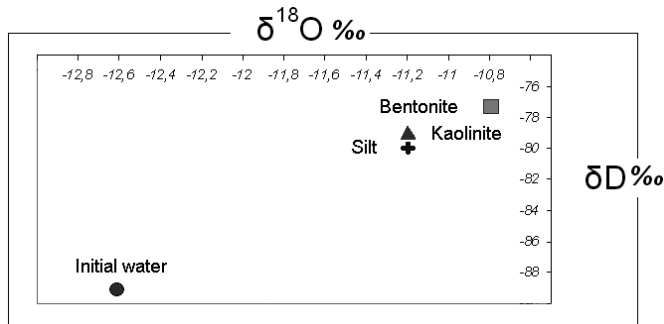


Figure 2. Composition of heavy water isotopes in the samples of soil taken from Experiment 2.

The second experiment was aimed at finding out to what extent the fractionation of hydrogen and oxygen affects loosely bound and capillary types of water that are principally involved in cryogenic migration due to freezing of wet and disperse deposits. The samples were saturated with distilled water so that the maximum moisture content, determined at room temperature, was reached. The samples were kept in this state for 24 hours. Then the water from the samples was squeezed with a lever and analyzed for heavy isotopes of oxygen ($^{18}\text{O}\text{‰}$) and deuterium ($\text{D}\text{‰}$).

The obtained data showed that the fractionation of water isotopes occurs due to interaction between water and soil. Figure 2 demonstrates that this process is more intensive than wetting. Meanwhile, the relative increase in heavy isotopes exceeded 10%. At the same time, this process is quite complex and reveals a correlation between the properties of clay minerals and the nature of fractionation, although the oxygen and hydrogen composition of drained water is “heavier,” which is true for all represented soils.

Apparently, the drained water is composed of a mixture of capillary and interstitial water (i.e., water that is minimally influenced by surface forces of the mineral skeleton). Then we can draw a reasonable conclusion that the water left unsqueezed is also a mixture of different water categories but with a much greater weight of water associated with the soil. Thus we can assume that intensive interaction predominantly occurs between soil and lighter water isotopes. Moreover, bentonite, with the virtue of its higher adsorptive capacity, shows even more intensive interaction than the other isotopes.

The difference between the third and the second experiment is in the fivefold pre-expulsion freezing-thawing (-20°C to $+20^{\circ}\text{C}$) of the samples. Expulsion repeats in the third experiment and the obtained water was then analyzed

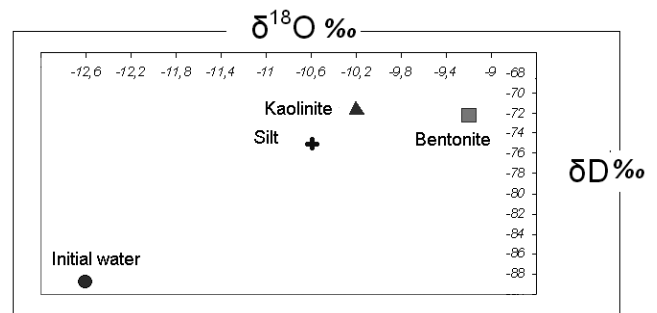


Figure 3. Composition of heavy water isotopes in the samples of soil taken from Experiment 3.

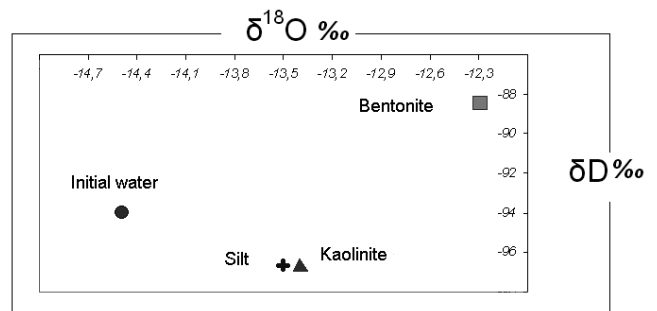


Figure 4. Composition of heavy water isotope in the samples of soil taken from Experiment 4.

for heavy isotopes.

It was revealed that the squeezed water in frost-bound samples was heavier in all cases (Fig. 3), while the relative increase in the heavy isotopes in water was more than threefold, compared to the previous experiment.

The results obtained due to freezing of the samples showed that the fractionation of water isotopes can be amplified differently for different types of water isotopes, depending on the soil properties and freezing conditions, but the ground water always remains “lighter” compared to the original value. However, as shown above, the soil moisture left unsqueezed is a mixture of different water categories, not all of which are involved in migration and segregated ice-formation. It may inevitably incur another fractionation. Therefore, the fourth experiment was carried out to determine isotopic values of ice schlieren formed in the soil samples. For this purpose, the samples were exposed to freezing in a special unit for one-dimensional freezing. Concurrently, layered cryotexture with schlieren 3–4 mm thick developed in the upper part of kaolin. Ice formation was less intensive in clayey silt with schlieren 1–1.5 mm thick. Reticulate cryotexture with schlieren up to 1.5 mm thick developed in bentonite. Inclusions in ice were separated from the sample and its isotope composition was assessed after thawing.

The data presented in Figure 4 show that the water, which creates inclusions in ice, is “heavier” in terms of oxygen. Its amount is smaller than that in the previous experiment.

In addition, as for kaolinite and clayey silt, the ratio of hydrogen in the water is “lighter,” bentonite being the only exception. This falls in line with the acknowledged notion that different categories of water both interstitial (“loosely” bound) and “tightly” bound are involved in migration. Outstanding deuterium values in the samples of bentonite may be attributable either to its nature or to the character

of ice formation. However, research should be continued to clarify this presumption, since the fractionation may be influenced by cryotexture and other cryolithic parameters.

Conclusions

This study approaches the data on isotope composition of segregated ice in frozen rock masses of different regions from a new viewpoint: they are “heavier” in oxygen, if compared to the ice formed by the surface water. Earlier on, this discrepancy was attributed to the water source (Konyakhin et al. 1996). Deuterium values in segregated ice require additional verification and explanation.

Acknowledgments

Funding for the study was provided by the Russian Foundation for Basic Research, Project No. 09-05-00536-a. Isotope analysis of the samples was carried out at the Stable Isotope Laboratory at the Department of Landscape Geochemistry and Soil Geography, Faculty of Geography, Moscow State University, using a Delta V mass spectrometer with a standard “gas-bench” option by Y.K. Vasilchuk, N.A. Budantsova, and Y.N. Chizhova. The results were calibrated in compliance with IAEA international standards (VSMOW, GISP).

References

- Cheverev, V.G. 2004. *Nature of cryogenic characteristics of soils*. Moscow: Nauch. Mir, 234 pp. (in Russian).
- Fedorov, Y.A. 1999. *Stable isotopes and evolution of hydrosphere*. Moscow: Istina Publishing, 369 pp. (in Russian).
- Konyakhin, M. A., Mikhalev, D.V., & Solomatin, V.I. 1996. *Isotope and oxygen composition of ground ice*. Moscow: Moscow State University, 155 pp. (in Russian).
- Vasilchuk, Y.K. 2011. Experimental study of isotope fractionation due to congelation ice formation. *Kriosfera Zemli (Earth Cryosphere)* 15. (no. 3): 51-55 (in Russian).

The Use of Sites with a Dense Network of Thaw Tubes to Monitor the Thickness of the Seasonally Thawed Layer in Central Yakutia

P.Ya. Konstantinov, A.N. Fedorov, I.S. Ugarov, R.N. Argunov
Melnikov Permafrost Institute, SB RAS, Yakutsk, Russia

Y. Iijima

*Research Institute for Global Change, Japan Agency for Marine-Earth Science and Technology,
Yokosuka-city, Japan*

Abstract

The use of thaw tubes is most advantageous in areas where a simple mechanical probing method may yield incorrect results. These areas may include soils with high gravel content, dry sandy soils, and soils with high salinity. Sandy soils with deep thawing generally predominate in Central Yakutia, which considerably limits the application of mechanical probing for mass measurements. The best results in this case can be achieved with the use of thaw tubes. However, a small number of thaw tubes installed within the investigated landscape limits assessment of the multi-year dynamics of seasonal thawing. In order to increase the statistical validity of the obtained data, two sites near Yakutsk were equipped with a dense grid of thaw tubes in 2008. Seventy-seven thaw tubes were installed at Site 1, located at the second terrace above the floodplain of the Lena River within a grass meadow. Thirty-six thaw tubes were installed at Site 2, located in the native larch forest in the denudation-accumulative plain. The research gave preliminary results on the influence of different meteorological factors on interannual variability in the thickness of the seasonally thawed layer (STL). The data on the maximum STL thickness collected at different points of each experimental site have low variability. This indicates that the landscape conditions are homogeneous, and the selected sites are optimal for the study of the multi-year dynamics of seasonal thawing depth. In 2012, the sites have been included in the CALM database as R42 and R43.

Keywords: soil moisture content; seasonal thawing depth; seasonally thawed layer; ground temperature.

Introduction

The application of thaw tubes in permafrost areas relies on the principle of using ice/water phase changes to register the position of the 0° isotherm in the ground. This principle was first implemented in the device proposed by A.I. Danilin in the 1950s. Later, other thaw tube models were developed (Rickard & Brown 1972, Mackay 1973) and came into widespread use in geocryology investigations in Canada and Alaska. The Circumpolar Active Layer Monitoring (CALM) program currently uses thaw tubes as one of the basic methods, along with mechanical and thermometric methods (Nelson et al. 2008, Shiklomanov et al. 2008). The advantages and disadvantages of thaw tubes are described in the geocryological literature (Nixon & Taylor 1998, Nixon 2000, Leibman 2001, Nelson & Hinkel 2003, Nixon et al. 2003, Tarnocai et al. 2004). They are employed primarily at sites where a simple mechanical probing may yield incorrect results. These sites may include soils with high gravel content, dry sandy thawing soils, and high-salinity soils. One considerable advantage of thaw tubes is their strict adherence to the principle of measurements being conducted at the same points. This is especially important in multi-year monitoring. The use of water as a working instrument does not require preliminary calibration and is characterized by almost unlimited time stability. Meanwhile, even if a slight discrepancy occurs between the position of the zero-degree isotherm established by the tube and the actual position of the phase boundary in the ground (or the upper surface of plastic frozen ground for clayey soils) as a result of the difference between the freezing points of ground and water, the obtained statistical parameters of the observation series in time will not be affected because the error will occur on

a systematic basis. Some thaw tube models allow for the monitoring of ground heaving and subsidence. Installation of thaw tubes requires much more effort, as compared to mechanical probing of thaw depth measurement. For this reason, only two or three thaw tubes are usually used at a single monitoring site even in the contemporary studies. This considerably decreases the statistical validity of the collected data. The application of a small number of thaw tubes within an investigated landscape is not enough to objectively assess the multi-year dynamics of seasonal thawing.

Research Methods

Dry soils with deep thawing generally predominate in Central Yakutia, and these conditions considerably impede the application of a probe for multiple measurements and can result in errors. For instance, well-drained sand horizons even in the unfrozen state create inadequate resistance for a probe. Therefore, the surface of frozen ground cannot always be reliably determined. Apart from that, probes and drills when applied multiple times at the same location may cause a significant disruption in the composition of dry soils, leading to changes in soil moisture. Therefore, since 1998, the laboratory of cryogenic landscapes of the Permafrost Institute of SB RAS has employed thaw tubes of a simplified design to study the interannual variability of seasonal thawing depth (Konstantinov et al. 2006, Konstantinov et al. 2008, Konstantinov 2009). The measuring device is a polypropylene tube with an outer diameter of 25 mm (inner diameter of 20 mm), one end of which has a welded polypropylene plug. The plugged end is lowered into the specially drilled small-diameter borehole. The borehole depth is established so that the lower end of the tube should be not

less than 1 m below the level of the maximum thawing depth at the site, while the upper end could be 10–15 cm above the ground surface. The space around the tube in the borehole is filled with the drilled ground and carefully compressed. The tube is further filled with distilled water up to the level of the ground surface. Measurements are performed with a commonly used metal tape measure (or measuring rod) the end of which is lowered into the measuring tube down to the line between water and ice at the time of measurement. The difference between the tape measurement and the length of the end of the tube projected above the surface will mark the depth of the zero-degree isotherm relative to the ground surface. The possible heaving of the measuring tube (to a certain limit) does not influence the accuracy of measurements, as the whole water column in the tube is in a frozen state before the beginning of each summer season. Even if a change in the level of the tube position occurs, the water will thaw in it according to the heat content of the ground after the winter period and according to the summer heat coming from the ground surface without being influenced by thaw tube heaving. Only if the lower end of the measuring tube heaves up above the permafrost table will the device be unsuitable for measurements.

In order to increase the statistical validity of the collected data, two sites near Yakutsk were equipped with a dense grid of thaw tubes in 2008. The sites were recently included into the monitoring network of the CALM program.

Experimental Site 1 is located near the Melnikov Permafrost Institute. This site is located at the second terrace above the floodplain of the Lena River (elevation 100 m) near the top of the upland where the vegetation cover is represented by a grass meadow. The STL and the upper permafrost horizons are composed of sandy silt. The site represents a rectangle with sides of 50 and 30 m. All 77 thaw tubes within the site are installed along 7 lines with 5 m intervals. Thawing depth measurements are made once every 10 days over the duration of the warm season. The TR-52 one-channel temperature loggers by T&D Corporation were also installed within the site in order to measure air temperature, ground surface temperature, and ground temperature at the depth of 3.2 m.

Experimental Site 2 is located 30 km northwest of Yakutsk, within the Lena-Kenkeme interfluvial area. The territory is a denudation-accumulative flat plain with elevations of 200–215 m. The upper layer of sediments is represented by a continuous cover of ice-rich quaternary sediments of small thickness with polygonal ice wedges. The site is in an area of native larch forest with cowberry cover. Clayey silt predominates in the STL composition as well as in the upper part of the permafrost. The size of the site is 50 x 30 m. All 36 thaw tubes within the site are installed along 6 lines in 10 m intervals. Thawing depth measurements are made once a month over the whole warm season. The TR-52 one-channel temperature loggers are installed within the site in order to measure air temperature, ground surface temperature, and ground temperature at the depth of 3.2 m.

Results

The winter season plays a dominant role in the formation of thermal conditions in the upper horizons of permafrost.

Table 1. The statistical indicators of maximum thawing depth, cm (Roman numbers represent the month of the year).

site №	Statistical indicator	2007/08	2008/09	2009/10
Site 1	n	77	77	77
	X_m	2.03	1.99	1.97
	σ	0.09	0.08	0.08
	V	0.05	0.04	0.04
	D_{th}	02.V	24(IV)	22(IV)
Site 2	n	36	36	36
	X_m	1.24	1.22	1.23
	σ	0.11	0.11	0.10
	V	0.09	0.09	0.08
	D_{th}	10.V	03.V	01.V

n – number of measurement points; X_m – mean value of maximum thawing depth, m; σ – standard deviation, m; V – coefficient of variation; D_{th} – the date of the beginning of thawing.

Table 2. The snow cover depth at the end of the month, cm.

site №	Year	X	XI	XII	I	II	III	IV
Site 1	2007/08	11	15	20	25	32	41	16
	2008/09	5	14	15	16	18	22	0
	2009/10	7	17	20	22	23	23	0
Site 2	2007/08	17	24	30	35	39	50	42
	2008/09	16	25	31	32	34	38	0
	2009/10	17	25	29	32	32	33	0

Table 3. The monthly sums of summer precipitation, mm (The Yakutsk weather station).

year	V	VI	VII	VIII	IX	Σ_{v-ix}
2007/08	5	16	50	41	34	146
2008/09	29	3	26	46	26	130
2009/10	41	29	30	9	23	132

A conditional year-period instead of a calendar year is employed in our research. October 1 is considered the beginning of the winter freezing season. This approximately corresponds to the mean multi-year date of the beginning of ground freezing near Yakutsk. The mean annual values of meteorological variables are calculated for the given conditional year. Double signs are used to mark it. For instance, double sign 2007/08 means that the conditional year from October 1, 2007, to September 30, 2008, is considered. The text, tables, and figures herein will consider only conditional years.

Table 1 illustrates the statistical indicators of the maximum thawing depth at the experimental sites for three years of observations. The maximum STL thickness data collected at different points within each experimental site have low variability, indicating the homogeneous landscape conditions.

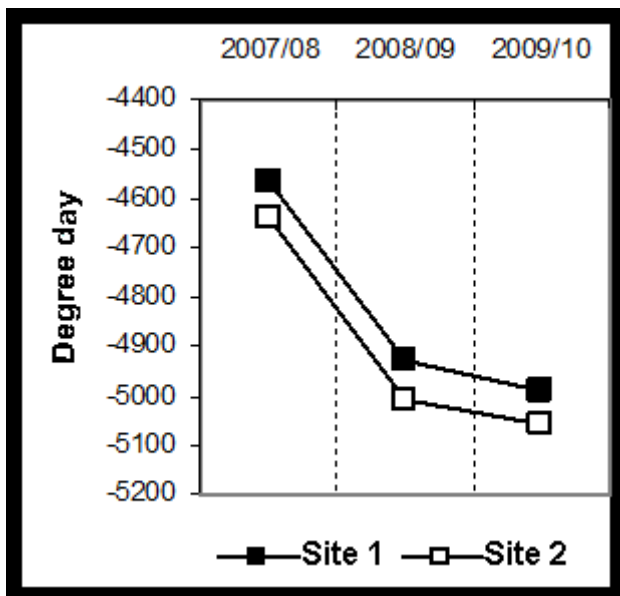


Figure 1. Degree-days of freezing at 2 m height

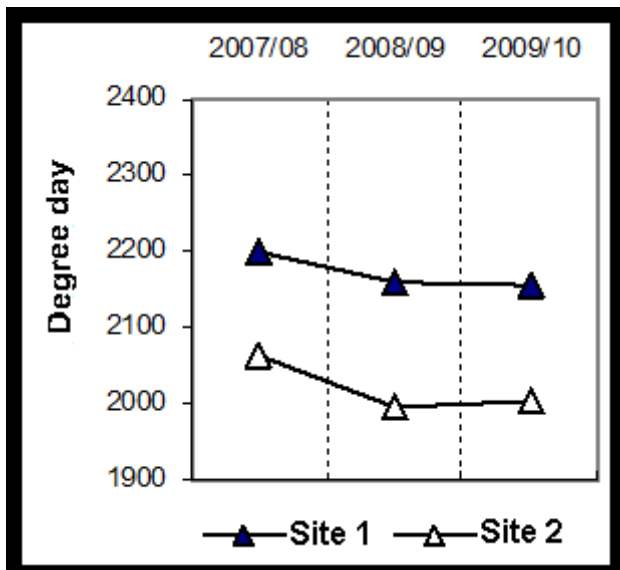


Figure 2. Degree-days of thawing at 2 m height.

Tables 2 and 3 and Figures 1 through 5 illustrate the values of main meteorological variables for the period of observations comprising three year-periods (2007/08, 2008/09, and 2009/10). 2007/08 was marked by the coldest winter, the warmest summer, high thickness of the snow cover, and higher values of ground moisture content before winter. Due to the warming influence of snow, the given year was marked by higher temperature of ground mineral surface. The following two year-periods (2008/09 and 2009/10) were marked by a decrease in degree-days of freezing (DDF) and degree-days of thawing (DDT), a decrease of snow cover depth, an increase in winter temperature sums at a ground surface, a lowering of the temperature of surface, and a slight lowering of ground moisture content before winter. The summer precipitation sums were very similar during the three year-periods. A slight decrease in the maximum thawing depth is observed at the meadow site during the years with smaller sums of summer air temperatures and lower ground temperature. The correlation between the maximum thawing depth of soils and the dates when the season of their thawing starts was not

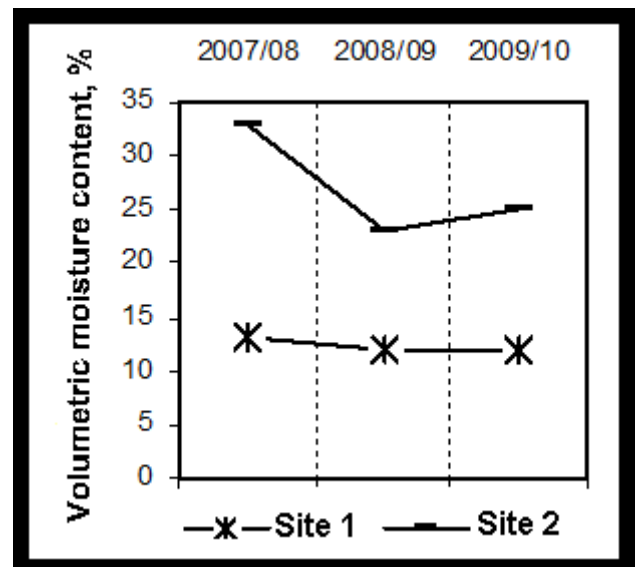


Figure 3. Volumetric soil moisture content before winter (averaged values of the whole profile of the STL).

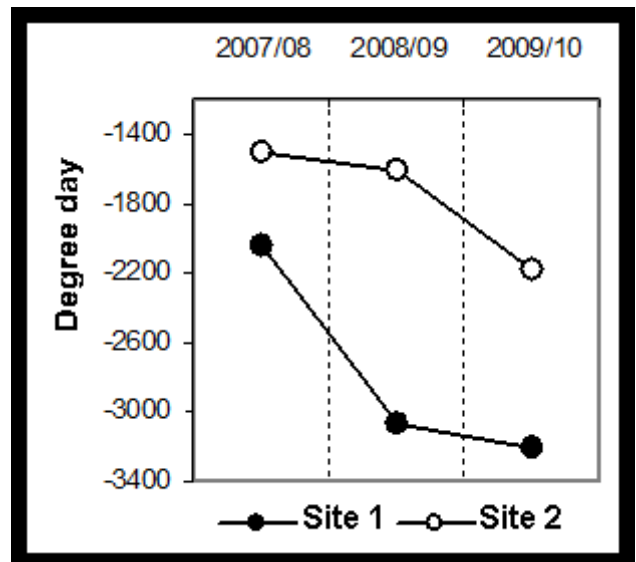


Figure 4. Degree-days of freezing at the ground surface.

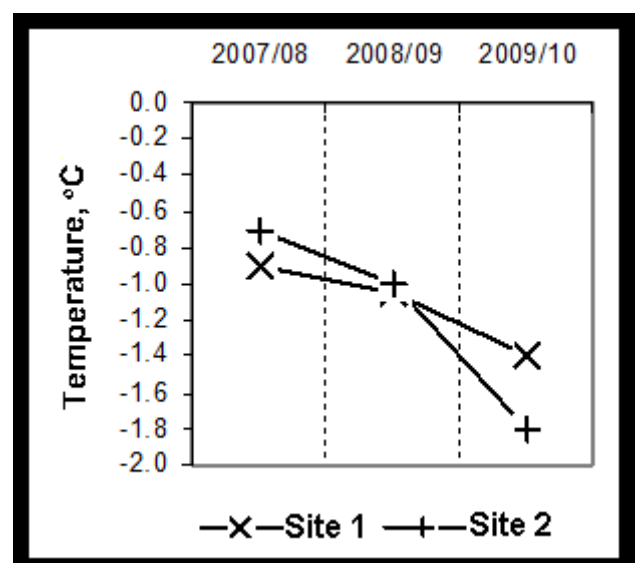


Figure 5. The mean annual ground temperature at the depth of 3.2 m.

found. For instance, in 2007/08, the maximum thawing depth at Site 1 reached its highest value, although the date when thawing started that year occurred 8–10 days later than in the following periods. The maximum thawing depth at the forest site remained nearly stable during 3 years. This makes it impossible to find any correlation with the main meteorological variables for the period considered. It must be noted that the observations extend over a very short period of time. This is why we should not draw definitive conclusions. In some years, meteorological factors and ground conditions may mutually exclude their influence on the process of ground thawing. Soil moisture content has a particular significance in this respect, as phase transitions in the STL absorb most of the ground heat flow. Considering all this, it is rather difficult to establish the influence of interannual variations of soil moisture content on the depth of thawing. Its values are spatially heterogeneous even within short distances in the ground, while soil moisture content at experimental sites is measured only in the point locations.

Conclusions

Due to the predominance of dry sandy soils with deep thawing in central Yakutia, the use of thaw tubes for monitoring of interannual STL thickness yields more valid results, as compared with other research methods. The installation of a dense grid of thaw tubes at monitoring sites makes it possible to considerably improve the statistical validity of collected data. The data on the maximum STL thickness collected at different points of each experimental site have low variability. This indicates that the landscape conditions are homogeneous enough to regard the selected sites as optimal for the study of the multi-year dynamics of seasonal thawing depth. The observations cover a very short period of time, and therefore the obtained results do not allow us to draw definitive conclusions regarding the influence of various meteorological and soil factors on the interannual variability of thawing depth at the study area.

Acknowledgments

The authors would like to thank Suzuki Kazuyoshi from the Japan Agency for Marine-Earth Science and Technology for assistance in organizing the research and P.V. Efremov and M.I. Petrov from the Melnikov Permafrost Institute for assistance in field observations.

References

- Konstantinov, P.Ya. 2009. *Manual on monitoring site establishment for permafrost temperature observations*. Yakutsk, Izd-vo In-ta merzlotovedeniya SO RAN 68 pp. (in Russian).
- Konstantinov, P.Ya., Argunov, R.N., Gerasimov, E.U., & Ugarov, I.S. 2006. On correlation between seasonal thawing depth and interannual variability of mean annual ground temperature. *Kriosfera Zemli* XIII, No. 3, 15-22 (in Russian).
- Konstantinov, P.Ya., Argunov, R.N., Gerasimov, E.Y., & Ugarov, I.S. 2008. The Influence of the Winter Season on Active Layer Depth in Taiga Landscapes, the Yakutsk Vicinity, East Siberia. In *NICOP 2008: Proceedings of the Ninth International Conference on Permafrost*. D.L. Kane, K.M. Hinkel (eds.). Institute of Northern Engineering, University of Alaska Fairbanks, 1: 983-986.
- Leibman, M.O. 2001. The dynamics of the seasonal thawed layer of grounds and methods of its depth measurement in different landscapes of Central Yamal. *Kriosfera Zemli* 1, 3: 17-24 (in Russian).
- Mackay, J.R. 1973. A frost tube for the determination of freezing in the active layer above permafrost. *Canadian Geotechnical Journal* 10: 392-396.
- Nelson, F.E., Shiklomanov, N.I., & Hinkel, K.M. 2003. Methods for measuring active-layer thickness. In *A Handbook on Periglacial Field Methods*. O. Humlum, and N. Matsuoka (eds.). Longyearbyen, Norway: University of the North in Svalbard, (< http://www.unis.no/RESEARCH/GEOLOGY/Geo_research/Ole/PeriglacialHandbook/ActiveLayerThicknessMethods.htm>).
- Nelson, F.E., Shiklomanov, N.I., Hinkel, K.M., & Brown, J. 2008. Decadal Results from the Circumpolar Active Layer Monitoring (CALM) Program. In *NICOP 2008: Proceedings of the Ninth International Conference on Permafrost*. D.L. Kane, K.M. Hinkel (eds.). Institute of Northern Engineering, University of Alaska Fairbanks, 2: 1273-1280.
- Nixon, F.M. 2000. Thaw-depth monitoring. In *The Physical Environment of the Mackenzie Valley, Northwest Territories: a Base Line for the Assessment of Environmental Change*. *Geological Survey of Canada Bulletin* 547: 119-126.
- Nixon, F.M. & Taylor, A. 1998. Regional active layer monitoring across the sporadic, discontinuous and continuous permafrost zones, Mackenzie Valley, northwestern Canada. In *Proceedings 7th International Conference on Permafrost*. Lewkowicz & M. Allard (eds). Collection Nordicana No. 57, Yellowknife, 23–27 June 1998. Laval: Centre d'études nordiques, Université Laval, 815-820.
- Nixon, F.M., Tarnocai, C., & Kutmy, L. 2003. Long-term active layer monitoring: Mackenzie Valley, northwest Canada. In *Proceedings of the Eighth International Symposium on Permafrost Engineering*. Phillips, M., Springman, S.M. & Arenson, L.U. 2. Lisse: A.A. Balkema, 821-826.
- Rickard, W. & Brown, J. 1972. The performance of a frost-tube for the determination of ground freezing and thawing depths. *Ground Science* 113: 149-154.
- Shiklomanov, N.I., Nelson, F.E., & Streletskiy, D.A. 2008. Decadal Results from the Circumpolar Active Layer Monitoring (CALM) Program. Data Collection, Management, and Dissemination Strategies. In *NICOP 2008: Proceedings of the Ninth International Conference on Permafrost*. D.L. Kane, K.M. Hinkel (eds.). Institute of Northern Engineering, University of Alaska Fairbanks, 2:1647-1652.
- Tarnocai, C., Nixon, F., & Kutny, L. 2004. Circumpolar-Active-Layer-Monitoring (CALM) Sites in the Mackenzie Valley, Northwestern Canada. *Permafrost and Periglacial Processes* 15: 141-153.

Evaluation of the Ground Ice Content Based on Data from the NOAA Satellite: The Case of the Western Coast of the Yamal Peninsula, Russia

S.G. Kornienko

Institute of Oil and Gas Problems, RAS, Moscow, Russia

Abstract

Data obtained from the thermal channels of the NOAA satellite during summer monitoring may be used to evaluate the ground ice content in areas of continuous permafrost. The evaluation method is based on detection of the differences in the growth rate of the seasonal radiation temperature of the Earth's surface (SRTS) in areas with different ice and moisture contents of soils. The SRTS is estimated based on the day and night measurements made by the satellite. When estimating, we consider the parameter that characterizes the thermal inertia of the near-surface layer of the daily temperature fluctuations. Based on the territory of the Kharasavey and the Kruzenshtern gas condensate fields of West Yamal, we show that the SRTS's dynamics makes it possible to more reliably reveal the differences in the ground ice content within the natural complexes of the same type (specifically, marine terraces). The division of the territory into regions according to the ground ice content was made by means of the interpretation of the SRTS and of the parameter that characterizes the thermal inertia in the layer of the daily temperature fluctuations.

Keywords: ground ice content; permafrost; radiation temperature; remote sensing; surface temperature; thermal inertia.

Introduction

The development of permafrost areas in the Far North is closely linked with maintaining the reliability of technical facilities and with the minimization of geoecological and geocryological risks. Therefore, it is important to devise new methods and technologies, including ones that use remote sensing data, to make it possible to characterize and control the state of permafrost at construction sites and at the sites of industrial and economic facilities.

A series of recent foreign publications indicates the possibility of mapping permafrost heterogeneity based on annual observations of surface temperature variations, particularly according to the data of the MODIS scanner of the Terra satellite and the data of meteorological observations at key sites (Hachem et al. 2009). The method was developed on the basis of work that describes the connection between the mean annual surface temperature of ground and the permafrost temperature. At the same time, the authors point out that there are errors linked with the impact of the heterogeneous snow and vegetation cover.

Already in the 1970s, researchers examined the possibility of mapping tabular massive ice to characterize the ice content of frozen soils by applying the data of remote thermal infrared sensing during the snow-free summer and fall periods (Leschack et al. 1973, Gorny & Shilin 1978). However, this approach was not developed. One of the reasons for that lies in a significant masking influence of the layer of the daily temperature fluctuations that is, as a rule, heterogeneous in the conditions of heat exchange. The characteristics important in this respect include the surface albedo, soil texture, the type and the thickness of vegetation cover, and their moisture content (Pavlov 1975). At the same time, the differences in the physical and thermophysical characteristics of the layer of daily temperature fluctuations under certain conditions can be established based on remote sensing data in the visible and thermal infrared range (Lyalko 1992). The increased volume of the airborne and satellite information including thermal infrared sensing data

creates prerequisites for the development of new mapping methods of permafrost heterogeneity. For instance, based on the data from NOAA's satellite summer monitoring and on the method devised by the author, we detected differences of soils according to their ice content for the western coast of the Yamal Peninsula.

Method of Evaluation of Ground Ice Content Based on the Radiation Temperature of the Ground Surface

It is known that the temperature field of the ground surface has a clear daily and annual periodicity and, if there is no snow cover and no crystallization processes of soil moisture, it can be approximately described with this equation (Tikhonov & Samarskiy 1972, Pavlov 1975):

$$T_s(0, \tau) = T_0 + \sum_{i=1}^N a_i \cos\left(\frac{2\pi}{t_i} \tau + \varphi_i\right) \quad (1)$$

where T_0 is the mean annual surface temperature; a_i is the amplitude of the temperature fluctuations of a separate harmonic on the surface; t_i is the period of fluctuations, τ is time; φ_i is the initial phase of fluctuations; N is the number of harmonics; i is the number of a harmonic.

The amplitudes of the daily and the annual temperature fluctuations of the ground surface depend on the thermophysical properties of the upper layer down to the penetration depth of the corresponding fluctuations. The differences in amplitudes of the annual temperature fluctuations provide most of the information that enables us to evaluate the ice content of soils and the occurrence of tabular massive ice. The maximum contrasts of the surface temperature linked with the contrast in ice content of soil and with tabular massive ice occur in the period of maximum heating (i.e. at the end of August and at the beginning of September) (Leschack et al. 1973, Kornienko & Razumov 2009). It is obvious that the surface temperature contrasts for the soils of the same type will also depend on

the difference in their moisture content. This fact should be considered when interpreting the anomalies of the surface thermal field.

The differences of thermal properties (and in ice content) of soil in the snow-free period may be characterized on the basis of the difference of the mean daily values of the surface temperature obtained after snow melt and in the period of maximum heating of the ground surface. For the territory of West Yamal, these periods occur at the end of June and at the end of August, respectively. A rapid increase in the surface temperature is observed during this period of summer temperature fluctuations (Vasiliev et al. 2011). Since the penetration depth of the summer temperature fluctuations depends on the effective thermal diffusivity of soils, it makes sense to speak about some minimum depth down to which the ice content of soils can be compared. According to the available data (Leschack et al. 1973), it will consist of approximately 2-3 m. The depth of the active layer in West Yamal does not exceed 1.5 m (Baulin et al. 2003), while the penetration depth of the daily temperature fluctuations (including the vegetation cover) does not exceed 0.3–0.4 m.

The mean daily values of the surface temperature can be determined based on the data from satellite monitoring in different times of the day and on the meteorological data (Hachem et al. 2009). If there are no meteorological data available, researchers may use the distributions of the radiation surface temperature. They are obtained at the points of the daily surface temperature inversion when the differences in thermal properties of the daily temperature fluctuations layer make the minimum contribution to the distribution of the surface temperature (Leschack et al. 1973, Gorny et al. 1993). However, the time of the satellite or aerial thermal monitoring most often does not correspond to the time points of the daily surface temperature inversion. The initial values of the radiation surface temperature may be modified in this case. The modification must consider the heterogeneity of physical and thermal properties of the near-surface layer of the daily temperature fluctuations (Lyalko 1992).

The thermodynamic temperature (T_s), the radiation temperature (T_r), and the coefficient of the surface radiation (ε) at the given wave:

$$T_r = T_s \sqrt[4]{\varepsilon} \quad (2)$$

The thermal inertia P depends on the thermal conductivity (λ), the specific heat capacity (C) and on the density (ρ) of material:

$$P = \sqrt{\lambda C \rho} \quad (3)$$

The difference in the radiation surface temperature of the day and night measurements taken within a day or even a week makes it possible to determine the so-called apparent thermal inertia (E) in the layer of the daily temperature fluctuations. The apparent thermal inertia is connected with the thermal inertia by this equation (Kahle & Alley 1985, Gorny et al. 1993):

$$E = \frac{1 - A}{\Delta T_r} = KP \quad (4)$$

where A is the albedo; ΔT_r is the difference between the day and night measurements T_r ; K is the coefficient dependent on the insolation conditions and on the meteorological conditions. In the northern tundra, the E parameter characterizes the effective thermal inertia in the near-surface layer of the daily temperature fluctuations including the ground, the low shrub vegetative cover, and the moss and lichen cover. The main variations exhibited by the effective thermal inertia in uniform soils of the daily temperature fluctuations layer are linked with the difference of their moisture content.

It is well-known that the thermal conductivity of the porous materials of the same type with different moisture content may be characterized based on the thermal inertia (Vavilov 1991). Therefore, we suggest that the division of the territory into regions according to thermal properties of the daily temperature fluctuations layer is based on the E parameter, as it is linked with the surface albedo and the thermal inertia. When thermal properties of the soil exhibit the contrast lateral heterogeneity (e.g., silty clay and peat), it becomes more efficient to make a preliminary division of the territory according to these types and to determine the distributions of the E parameter separately for each ground type.

In agreement with this approach, there was developed a method that makes it possible to obtain a new information parameter (the so-called seasonal radiation temperature of surface) that corresponds to the radiation surface temperature at the periods of the daily inversion. The main point of this method is the fact that one of the initial T_r distributions is corrected on the basis of the E distribution. The major steps of the correction algorithm include:

- determination of the E parameter;
- quantification of the E distribution in the N number of zones (formation of the E_N distribution);
- determination of the reference zone E_j (j is one of N) from the number E_N . The maximum number of the T_r distribution values agrees with the reference zone E_j ;
- determination of the constant components T_{rM} of the T_r distributions in each zone E_j ;
- addition of the difference of the constant components T_{rM} of the j and the i zones of E_N to the T_r values in each zone E_i (i – from 1 to N) and formation of the SRTS distribution.
- smoothing (low-pass filtering) of the obtained SRTS distribution to exclude the local high gradients at the boundaries of the E_N zones.

The mean or the median values of the initial T_r distributions can be assumed as the constant components T_{rN} of each zone E_N . It is assumed that the range of T_r distribution values is linked only with the SRTS within the territory with a single thermal inertia (or E) in the daily temperature fluctuations layer. This range is also assumed to be capable of giving information on the contrasts of the mean annual surface temperature and on the contrasts of thermal properties of the ground down to the penetration depth of the summer or the annual temperature fluctuations. To gain the overall picture of the SRTS anomalies across the entire territory, we correct T_r distributions (i.e., they are reduced to the thermal properties of the reference zone E_j). As a rule, the final SRTS distribution is represented in the relative temperature values

(contrasts). It should be noted that the data from both the night and day measurements can be used for the correction. The research shows that the final SRTS distributions are almost identical.

At the final research stage, we interpret the difference of the SRTS distributions (based on the data from the monitoring at the beginning and at the end of the summer period) in order to characterize the ice content of soils and the possible occurrence of tabular massive ice deposits.

Evaluation of the Ground Ice Content Based on the NOAA Satellite Data

To test the method, we selected the territory of the central part of the Yamal Peninsula (between 70°N and 72°N), specifically, the site on its western coast near the Kharasavey and Kruzenshtern gas and condensate fields (the land area is about 3100 km²). This territory is located at the border of the northern and central tundras and is characterized by continuous permafrost and by landscapes of different ages with marine terraces, floodplains, and tidal flats (Melnikov & Grechishchev 2002). Its permafrost conditions are characterized by the occurrence of sandy silts in the permafrost sediments with large ice wedge (up to 10 m) and tabular massive ice bodies up to 10–15 m thick.

The territory has widespread landscapes of the first, second, and third marine terraces that are formed by the sandy and clayey sediments with the low shrub, grass, moss, and lichen vegetation. Different vegetation types are dominant depending on the degree of ground drainage (Baulin et al. 2003). Floodplain landscapes are less widespread. They are composed mainly of silty clay and are heavily swamped. Tidal flat landscapes with the sediments of silty sands and silts are covered with lakes and are also heavily swamped. Peat bogs occur locally on the flat surfaces of almost all the landscapes. The permafrost continuity is broken only under riverbeds and lakes depending on the dimensions, depth, and age of the water body.

The heterogeneity of the ice content of the sediments of the upper horizon is determined by the distribution of ground ice (to the depth of 2–3 m) and by wedge ice. Tabular massive ice deposits close to the surface are found mainly in the sediments of the first, second, and third marine terraces (Baulin et al. 2003, Kritsuk 2010).

Three pairs of day and night photographs made from the NOAA satellite (the AVHRR radiometer) in June and July of 2000 and at the end of August of 1998 were used in the research. The AVHRR radiometer has five spectral channels two of which (4th and 5th ones) register the radiation in the remote thermal infrared area. The spatial resolution of the radiometer is 1.1 km, while the sensitivity of T_r is 0.1°K. The satellite photographs were processed and analyzed using the ENVI 4.8 software. The maps were drawn to a scale of 1:1 000 000.

The preliminary stage of data processing included the calibration of photographs, geometric and atmospheric correction, as well as masking of large water bodies. To calculate the E parameter based on the data of the 4th thermal spectral channel, we determined the difference ΔT_r . To calculate it based on the data of the 1st and 2nd channels, we determined the albedo (A). The photographs were divided

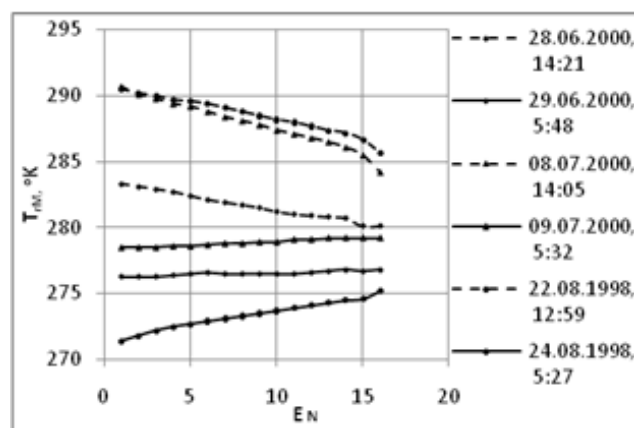


Figure 1. The dependence of the median values of the radiation surface temperature (T_{fm}) on the “apparent thermal inertia” (E_N).

into “day” and “night” ones only for convention, because at the given latitudes there is only the polar day in summer.

Relying on the geothermal investigations carried out for the plain territories, we know that the distribution of the radiation surface temperatures will depend on the variations of the radiation coefficient (ϵ) and also on the insolation conditions, cloud cover, and wind speed (Lyalko 1992). The insolation conditions and the wind speed in this case were assumed as equal across the entire territory of the examined region, considering that this region has a relatively small area. The impact of heterogeneity ϵ on the radiation temperature anomalies was assessed based on the method described Leschack et al. (1973): specifically, based on the correlation between the ratio of the T_r values (measured in different spectral channels of the thermal infrared range) and the T_r distribution of one of the spectral channels. In this case, the T_{r4}/T_{r5} and T_{r4} distributions of the day and night monitoring (obtained according to the data of the 4th and 5th spectral channels of the AVHRR radiometer) did not have any significant correlations. This indicates that the ϵ variations exerted an inconsiderable impact on the T_r distribution. A similar conclusion was drawn in the research work of Leschack et al. (1973) for the regions of Alaska.

Figure 1 shows the graphs of the median values in the initial distributions of the radiation temperature T_{fm} (obtained in the day and night measurements) against the E_N parameter calculated on the basis of the same distributions. In the given case, the entire range of the E_N parameter values with the 95% confidence interval was quantified in $N=16$ zones. Zone E_1 includes the sites with the minimum thermal inertia (dry and drained sites), while zone E_{16} characterizes the sites with the maximum thermal inertia (moist sites).

Figure 1 also shows the dates and the local time of monitoring. The values T_{fm} of the day monitoring decline from left to right (the dashed lines), while those of the night monitoring decline from right to left (the solid lines).

This dependence may serve as a criterion indicating that the monitoring time is close to the point of the daily inversion, since during the daily full inversion the trend T_{fm} must be parallel to the abscissa axis. The night monitoring as of June 29, 2000, is the closest to the point of the morning inversion, because the maximum difference of the values T_{fm} makes up only about 0.5°K. Nevertheless, all the initial

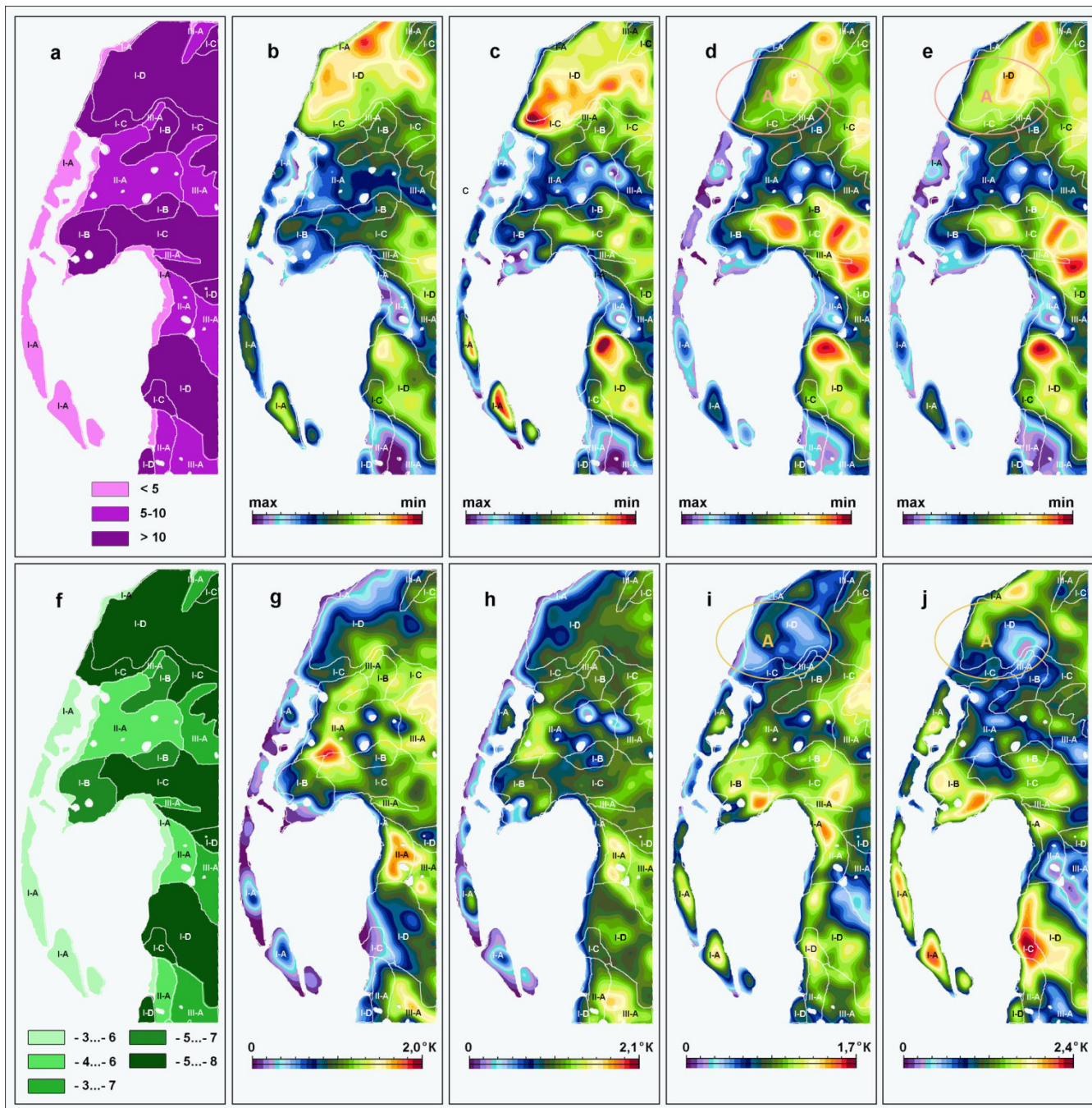


Figure 2. The map sections of the macro ice content of the ground in % (a), the permafrost temperature in °C (f) (Baulin et al. 2003), the distribution of the parameter E (b, c, d, e), the SRTS (g, h, i) and the SRTS difference (j) near the Kharasavey and Kruzenshtern gas and condensate fields obtained according to the data from the NOAA's satellite monitoring: for June 28 and 29, 2000 (b, g); for July 08 and 09, 2000 (c, h); for August 22 and 24, 1998 (d, i). The natural complexes (Baulin et al. 2003) are: (I-A) – layda; (I-B) – 1st marine terrace; (I-C) – 2nd marine terrace; (I-D) – 3rd marine terrace; (II-A) – the lower reaches of large rivers; (III-A) – a floodplain.

T_r distributions were modified according to the algorithm described above.

Figure 2 presents the maps that characterize the obtained distributions of the parameter E (Fig. 2 b, c, d) and the SRTS (Fig. 2 g, h, i) for different dates of satellite monitoring in comparison with the maps of the wedge ice content in frozen soils (Fig. 2a) and of permafrost temperature (Fig. 2f). Figure 2 also presents the distribution of the mean value of the parameter E (Fig. 2e) calculated according to the values E of June and August and the distribution of the SRTS difference (Fig. 2j) of August and June. The value ranges of all the obtained distributions are assumed with

a 95% confidence interval. All the images also show the boundaries and the notation of major natural complexes. On the west, the territory is bounded by the Kara Sea.

The parameter E distributions in different monitoring periods (Fig. 2b,c,d) are rather similar and mainly characterize the natural complexes. The areas with the minimum values E (with high heat insulation of the surface layer) are associated with marine terraces (I-B, I-C, I-D). Marine terraces are characterized by a higher wedge ice content and lower permafrost temperatures by comparison with the lower reaches of rivers (II-A) and floodplains (III-A) within which the parameter E is very high. The temporal

variations of the parameter E are presumably linked with the change in the moisture content of the layer of daily temperature fluctuations or of the state of the vegetative cover.

The SRTS variations in time are more significant (g, h, i). It should be noted that the Kara Sea exerts a significant cooling influence on the SRTS distribution at the examined segment of the shore zone according to the monitoring data obtained at the end of June and at the beginning of July (g, h). This is due to the fact that the sea ice near the shores melts only partly in this period. The pattern of the SRTS anomalies at this time is close to the pattern of the permafrost temperature distributions (Fig. 2f) and the wedge ice content (Fig 2a). The areas with low values of permafrost temperature for marine terraces are mainly characterized by lower SRTS values in comparison with floodplains and the lower reaches of rivers. At the end of August the influence of the sea is less pronounced. The SRTS distribution by this time has considerably changed (i): the floodplains and the lower reaches of rivers already reveal background and abnormally low SRTS values, which is more clearly displayed in the southern part of the region. Such dynamics is probably explained by the fact that the SRTS distribution at the beginning of summer (closer to the period of the inversion of annual temperature fluctuations) reflects more the contrasts of the mean annual surface temperature and less the differences in the thermal inertia in the layer of summer temperature fluctuations. By the end of summer, the differences in the thermal inertia of the dry and moist areas in the layer of the summer temperature fluctuations lead to formation of the surface temperature contrasts opposite in sign. This decreases the contrasts dependency on the mean annual values of the surface temperature.

This thesis is illustrated by the distribution of the SRTS difference in August and June (Fig. 2j). The given distribution excludes the SRTS contrasts dependent on the mean annual surface temperature (and therefore on the permafrost temperature), and reflects the anomalies linked with the thermal inertia of soils in the layers of the summer temperature fluctuations. The areas with a high moisture content of soils (all areas of floodplains and lower reaches of rivers) are characterized by abnormally low values of the SRTS difference.

At the same time, a large anomaly of low values in the SRTS (i) and in the SRTS difference is marked within the 2nd and 3rd marine terraces (zone A) in the north of the region. This anomaly cannot be caused by the moisture content of soils because the indicated zone is characterized by widespread drained areas with low values of parameter E (Fig. 2b,c,d,e). It occurs presumably due to a higher wedge ice content in the layer of the summer temperature fluctuations in comparison with other sites of marine terraces that exhibit the same values of the E parameter. In this scale, there are no data characterizing the ice content range of soils at marine terraces in order to assess the reliability of the obtained results. At the same time, a wide range of values of the SRTS difference within their boundaries (up to 2.4°K) is probably linked with the differences in the ice content of soils in the layer of the summer temperature fluctuations. The low temperature anomaly of the SRTS (Fig. i) and the anomaly of the low values of the SRTS difference (Fig. j)

both identified in the north of the region may be connected with the tabular massive ice bodies detected here close to the surface (Kritsuk 2010). Similar studies using the new data of satellite monitoring in the summer and fall period is required in order to confirm the preliminary conclusions drawn here.

Conclusions

- 1) We developed the calculation method of the seasonal radiation surface temperature that corresponds to the radiation surface temperature at periods of the daily inversion of the surface temperature. The method is based on the analysis of data from day and night satellite monitoring both in the visible and thermal infrared ranges as well as on the determination of the parameter that characterizes the thermal inertia of the near-surface layer of the daily temperature fluctuations.
- 2) Based on the case of the western coast of Yamal Peninsula, it was shown that the SRTS contrasts in the first half of the summer are close in the character of anomalies to those of the permafrost temperature. Using the difference of the SRTS distributions of August and June in the layer of the summer temperature fluctuations within the marine terraces, we identified the differences in the thermal inertia of soils that are presumably linked with differences in their ice contents. The areas with high ice and moisture content of soils can be distinguished from each other on the basis of the complex interpretation of the SRTS distributions and of the parameter that characterizes the thermal inertia in the layer of the daily temperature fluctuations.
- 3) The research results may be used to characterize and monitor the state of frozen soil at the sites where technical facilities are located or are being constructed. They may also be applied to determine the depth of aquifer occurrences in the steppe, desert, and semi-desert regions.

References

- Baulin, V.V., Dubikov, G.I., Aksenov, V.I. et al. 2003. *The geocryological conditions of the Kharasavey and Kruzenshtern gas condensate fields (the Yamal Peninsula)*. Moscow, GEOS, 180 pp. (in Russian).
- Gorny, V.I. & Shilin, B.V. 1978. Application of thermal aerial surveys for geotechnical site investigations in permafrost areas. *The method of geotechnical site investigations and mapping of permafrost regions*. Yakutsk, pp. 85-96 (in Russian).
- Gorny, V.I., Shilin, B.V., & Yasinskiy, G.I. 1993. *The thermal aerial and satellite monitoring*. Moscow, Nedra, 128 pp. (in Russian).
- Hachem, S., Allard, M., & Duguay, C. 2009. Using the MODIS Land Surface Temperature Product for mapping permafrost: An application to Northern Quebec and Labrador, Canada. *Permafrost and Periglacial Processes* 20: 407-416.
- Kahle, A.B. & Alley, R.E. 1985. Calculation of thermal inertia from day-night measurement separated by days or weeks. *Photogramm. Eng. & Remote Sens.* 51 (1): 72-75.

- Kornienko, S.G. & Razumov, S.O. 2009. Modeling of temperature contrasts at the surface of grounds that are heterogeneous in their ice content. *Kriosfera Zemli* 13,(2): 55-61 (in Russian).
- Kritsuk L.N. 2010. *Ground ice in Western Siberia*. Moscow, Nauchny mir, 352 pp. (in Russian).
- Leschack, L.A., Morse, F.H., Brinley, Wm.R., Ryan, N.G., & Ryan, R.B. 1973. Potential use of airborne dual-channel infrared scanning to detect massive ice in permafrost. *North American Contribution Permafrost*. Second International Conference, Washington, D.C. pp. 542-549.
- Lyalko, V.E. (ed.). 1992. *Aerial and satellite methods in geocology*. Kiev, Naukova dumka 205 pp. (in Russian).
- Melnikov, E.S. & Grechishchev, S.E. (eds.). 2002. *Permafrost and development of oil and gas regions*. 2002. Moscow, GEOS, 402 pp. (in Russian).
- Pavlov, A.V. 1975. *The heat exchange between the soil and the atmosphere in the northern and middle latitudes of the USSR territory*. Yakutsk: Yakutskoe knizhnoe izdatelstvo, 304 pp. (in Russian).
- Tikhonov, A.N. & Samarskiy, A.A. 1972. *The equations of mathematical physics. A study guide for universities*. Moscow, Nauka. 735 pp. (in Russian).
- Vasilev, A.A., Streletskaya, I.D., Shirokov, R.S., & Oblogov, G.E. 2011. The evolution of the cryolithozone in the near-shore and marine area of Western Yamal under the changing climate. *Kriosfera Zemli* 15 (2): 56-64 (in Russian).
- Vavilov, V.P. 1991. *Thermal methods of nondestructive testing. Reference book*. Moscow, Mashinostroenie, 240 pp. (in Russian).

Phytomass Reserves and Characteristics within the Active Layer of the Forest-Tundra Bog Ecosystem

N.P. Kosykh

Institute of Soil Science and Agrochemistry, SB RAS, Novosibirsk, Russia

Abstract

This paper discusses phytomass reserves and characteristics of the active layer in permafrost ecosystems of West Siberia. The study area, located in a forest-tundra zone in the vicinity of Pangody, is an example of such ecosystems. The amount of plant matter increases in these ecosystems in the following sequence: mesotrophic pools in alases, palsa hummocks, oligotrophic pools, spaces between palsas. Dead plant material and litter prevail in all the elements of the relief. The amount of living phytomass reflects the ecosystem type and the plant community. The phytomass in bog ecosystems of the forest-tundra varies from 800 to 3100 g/m² and is determined by the temperature regime, microrelief, and species composition of the plant community.

Keywords: active layer; biological productivity; forest-tundra; mortmass; permafrost ecosystems: phytomass.

Introduction

In the forest-tundra zone, the distribution of bogs is determined by permafrost, climatic conditions, and relief. Permafrost contributes to the unique bog topography, expressed as flat-hummocky forms. Forest-tundra occupies 13.7 million hectares in West Siberia. Up to 27% of its area is covered with bogs. The main criteria for distinguishing elementary bog ecosystems in forest-tundra landscapes include vegetation cover, peat layer thickness, and permafrost. Based on these features, alas ecosystems (mesotrophic pools) and flat-hummocky bog ecosystems (hummocks, spaces between palsa hummocks, and oligotrophic pools) can be distinguished. Within palsas in flat-hummocky bogs, the spaces between hummocks are the first indicators of thermokarst subsidence. In our study area, the active layer thickness on palsas is measured at around 40–50 cm and is underlain by permafrost. The thickness of peat horizon in pools is 60–80 cm. Over the summer, soils in the central portion of pools thaw completely to the mineral base. During the five-year period of observations, there was no change in the vegetation cover, despite increases in thawing degree-days and summer precipitation. The preservation and progressive growth of bogs mostly depends on the presence of permafrost and the vegetation cover, which, in turn, determine the productivity of bog ecosystems. According to studies, in high-altitude grass-sedge bogs in the Altai Mountains, the disappearance of permafrost leads to the reduction in biomass reserves by 2.5 times. The reserves of living phytomass also decrease. At the same time, net primary production increases by 33% compared to the year when the permafrost was 40 cm from the surface (Kirpotina et al. 2011).

Study Results

The goal of this study was to determine the modern structure of the active layer in bog ecosystems of the forest-tundra zone and the distributional pattern of plant matter reserves in bog ecosystems related to the composition of vegetation cover and microrelief. The study area comprises the forest-tundra zone (Fig. 1) and is located in the Nyda-Nadym interfluve east of Pangody Town (65°52'N, 74°58'E).

The climatic characteristics of the study area as observed from 1950 to 1965 are shown in Table 1. The lowest temperatures were registered during the winter period, and the most precipitation occurs during the summer.

Cape Bolvanskiy, Urengoy, and Nadym geocryological stations, located in tundra, forest-tundra, and northern taiga, respectively, are considered to be analogous areas. At the Bolvanskiy station, monitoring of the ground thermal regime in boreholes was conducted for 28 years (1983–2011), and seasonal thaw depth has been monitored at the CALM site since 1999 (Malkova 2011). Temperature monitoring in boreholes at the Urengoy Station has been conducted since 1975, and active layer at the CALM site has been measured since 2006 (Drozdoz et al. 2010). In the Nadym area, an integrated monitoring of ecosystems has been conducted since 1970, and the CALM active layer has been monitored since 1997 (Moskalenko 2006). During the 2004–2010 study period, an increase in the Thawing Degree Days (DDT) and

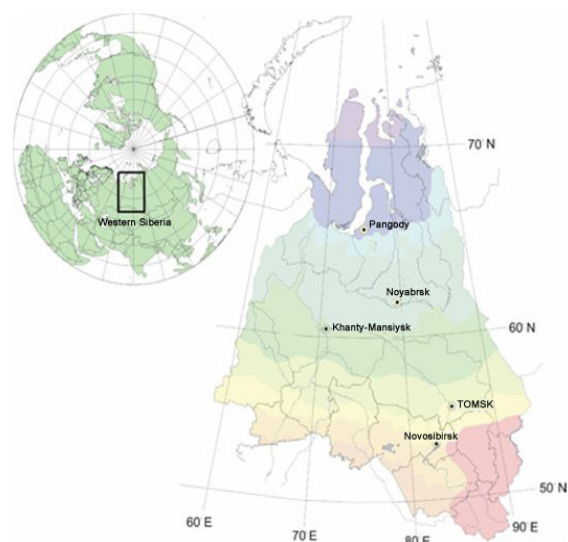


Figure 1. Location of the study area near Pangody Town.

Table 1. Climatic characteristics of the study area.

Weather station location	Precipitation, mm			Average temperature, T°C		
	Year	X-III	IV-IX	Annual	January	July
Nadym	432	142	290	-6.6	-23.6	14.7

Table 2. Characteristics of the key area ecosystems.

Ecosystem	Microrelief	Plant community	Dominants
Palsa	Hummock	Low shrub-lichen	<i>Ledum decumbens</i> (Ait.) Lodd. Ex Steud., <i>Andromeda polifolia</i> L., <i>Oxycoccus microcarpus</i> Turcz. Ex Rupr., <i>Cladonia stellaris</i> (Opiz) Brodo, <i>Cl.rangiferina</i> (L.) Harm., <i>Sphagnum fuscum</i> (Schimp.) Klinggr.
	Spaces between hummocks	Low shrub-sphagnum-lichen	<i>Andromeda polifolia</i> , <i>Oxycoccus microcarpus</i> , <i>Cladonia stellaris</i> , <i>Cl.rangiferina</i> , <i>Sphagnum balticum</i> (Russ.) Russ. Ex C.Jens.
Oligotrophic pool	Hollow	Sedge-sphagnum	<i>Carex rotundata</i> Wahlenb., <i>Sphagnum lindbergii</i> Schimp. Ex Lindb., <i>S.balticum</i> .
Mesotrophic pool (young alas)	Hollow	Sedge-sphagnum	<i>Carex rostrata</i> , <i>Carex lasiocarpa</i> , <i>Eriophorum polystachion</i> , <i>Comarum polustre</i> , <i>Sphagnum riparium</i> , <i>S.squarosum</i>

summer precipitation was observed (Moskalenko 2009, Moskalenko 2010). Comparison of the results from different sites allows the assessment of modern trends in permafrost development within these northern regions, which have similar natural, geological, and geocryological conditions.

Within our study area, we have selected an oligotrophic flat-hummocky bog and a young alas where three sampling plots were established representing palsa, oligotrophic pool, and mesotrophic alas pool. The characteristics of sampling plots are shown in Table 2. The plant communities and relief were described in the most typical bog areas based on a generally accepted method. At selected locations, samples of plant matter were collected at different depths up to 30 cm. Low shrubs and herbs were removed at several 40x40 cm plots. Mosses, along with the root systems of herbs and low shrubs, were collected with a 1 dm³ sampler from the moss surface. In the laboratory the collected samples were divided into the following fractions: photosynthesizing parts of herbs, low shrubs, mosses, annual and perennial low shrub shoots, living and dead belowground parts of herbs and low shrubs, and buried stems.

As a rule, the active layer of hummocky bogs in the forest-tundra zone does not exceed the thickness of 40 cm. Within the active layer, the biological productivity of ecosystems is determined. This includes evaluation of phytomass, dead plant material reserves, and ecosystem production, which depends on the type of ecosystem and microtopography. The total plant matter reserves in forest-tundra bogs vary from 13,000 to 32,000 g/m² in different years. The maximum amount is observed within the spaces between hummocks, where by the end of the summer the active layer thaws faster than on hummocks, and the additional inflow of water from the adjacent hummocks results in soil moisture increase and accumulation. This, in turn, leads to die back of lichens and the emergence of pool-type mosses. As a result, plant matter reserves in such areas may reach 32,000 g/m² during some years, which is 2–3 times more than the reserves in other bog ecosystems. In northern bog ecosystems, due to slow plant decomposition and burial in peat and the proximity of permafrost, the dead plant reserves significantly exceed the phytomass even in the upper portion of the active layer, where the main biological processes take place (Fig. 2).

In all ecosystems, dead plant matter or mortmass (M) dominates, accounting for 70–90% of the total reserves.

Dead plant reserves consist of undecomposed remains of mosses, lichens, and/or buried vascular plant remains that died off at different points in time. The composition of dead plant reserves may vary greatly in different ecosystems of bogs and depends on the species composition of the plant community. The aboveground dead plant reserves that consist of dead grass, dead wood, and vascular plant litter vary from 22 to 123 g/m², depending on the species composition of the plant community. The minimum dead plant reserves are formed in oligotrophic pools due to the small sizes of the vascular plants. Besides, the litter often quickly mineralizes in ecosystems and disappears from the moss surface or transforms into the ground moss layer. It may occur especially quickly in mesotrophic alas pools, where the fraction of the vascular plant litter does not exist.

The fraction of aboveground dead plant reserves on elevated surfaces, such as palsas, is formed by the leaves of evergreen low shrubs accumulating over several seasons and slowly decomposing, which is reflected in its maximum values. During severe and windy winters, the snow is blown off the tops of the hummocks in open flat-hummocky bogs without forest cover. At these sites, the dry dead low shrub branches account for up to 30% of the total aboveground low shrub phytomass.

In forest-tundra conditions, dead plant reserves are large and depend on the topography. Significant fluctuations in the reserves are observed in different years. As we have already noted, the maximum reserves are observed in the spaces between palsa hummocks of the flat-hummocky bog (9000–33,000 g/m²). The dead plant reserves are less on hummocks (9000–17,000). In oligotrophic pools, the dead plant reserves vary from 13,000 to 19,000 g/m², while in mesotrophic pools the dead plant reserves are not large and do not exceed 12,000 g/m². In the contrasting microrelief elements (palsa hummocks and flat low-lying areas), we observe smaller fluctuations in the reserves than in the spaces between hummocks, where permafrost thaw is uneven and accompanied by thermokarst subsidence. Therefore, changes in the dead plant reserves within the same ecosystem, but in different microrelief elements, are greater than those in different ecosystems.

Living plant matter, or phytomass (Ph), of the ecosystems in question is the most important fraction and it may vary significantly from 800 to 3100 g/m², depending on the

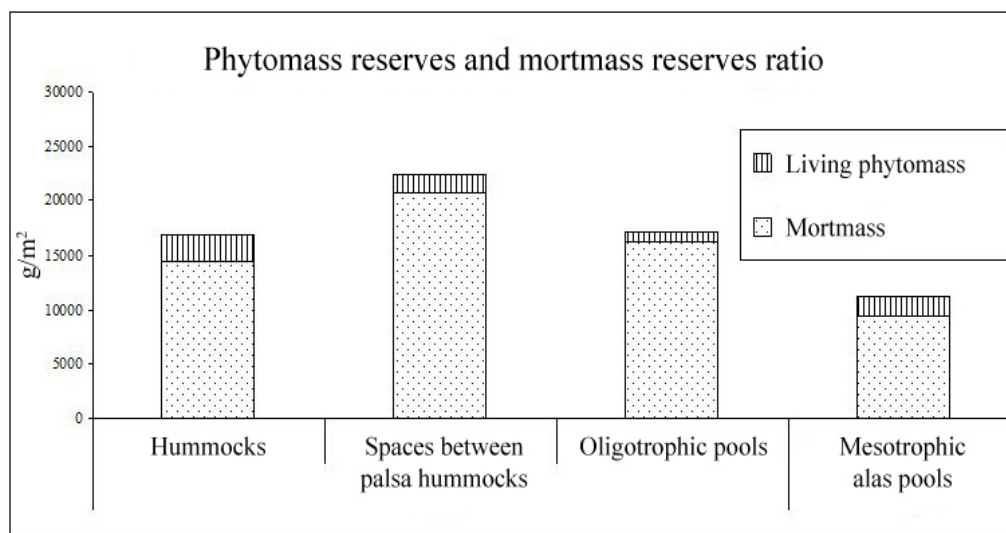


Figure 2. Plant matter reserves for different ecosystem microrelief categories.

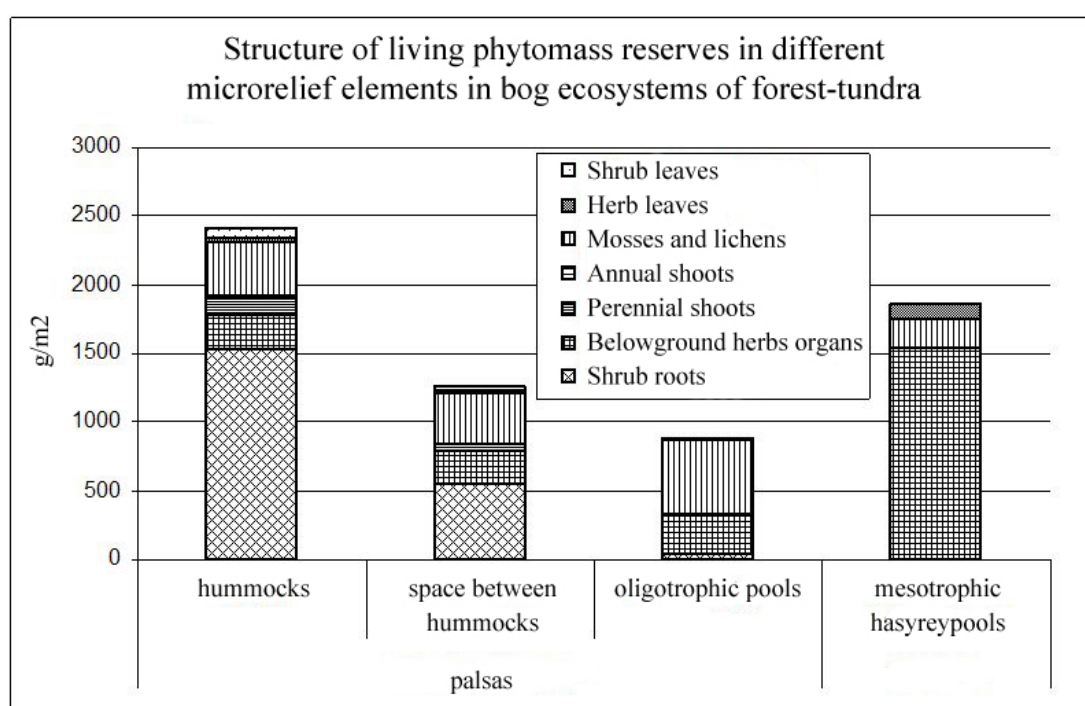


Figure 3. Changes in the living plant matter structure in different relief elements.

vegetation type, ecosystem, and relief (Fig. 3). The minimum reserves are formed in oligotrophic sedge-sphagnum pools. They amount to 800 g/m² and may increase up to 1000 g/m² in some years. The phytomass reserves on palsas reach their maximum values on hummocks. They may vary from 1000 to 3100 g/m² in different relief forms. The phytomass formation on palsas depends on microrelief. The reserves on hummocks are twice as large as in the spaces between hummocks. In severe climatic conditions of the North, low shrubs have a great influence on the formation of lichen hummocks. The largest part of the phytomass (60–80%) on the positive elements of relief is formed by the underground parts of the low shrubs, many of which consist of buried stems and large roots of *Ledum decumbens*. The reserves of mosses and lichens compose a habitat-forming near-surface layer, which determines the conditions of survival of other plant groups. They reach considerable values of 300 to 440 g/

m², which accounts for 25% of the total phytomass reserves. The aboveground phytomass of vascular plants accounts for 10 to 20% of the total reserves. In negative relief elements of oligotrophic pools, the phytomass structure changes. Sphagnum mosses or mosses associated with underground parts of sedges and cottongrass are often dominant here. The aboveground phytomass of vascular plants amounts to only 5%. In mesotrophic alas pools, the phytomass reserves are formed by sedges and cottongrass, the same being true for oligotrophic pools. Due to their larger habitat, reserves are formed that are 2–3 times greater than those in poor oligotrophic pools.

Certain phytomass fractions in different bog ecosystems differ qualitatively and quantitatively. The fraction of photosynthesizing parts that creates organic matter is one of the most important as it determines the growth of all other fractions in the ecosystem. Depending on the species and

its effectiveness, given favorable weather conditions, the reserves of the green phytomass of herbs and low shrubs in the positive relief elements vary from 16 (spaces between hummocks) to 115 g/m² (hummocks) in palsa ecosystems. Equally large reserves of green phytomass (100 g/m²) are formed in mesotrophic pools by sedges and cottongrass. The minimum amount of vascular plant leaves (19 g/m²) is produced by plant communities in oligotrophic pools where *Carex rotundata* and *Eriophorum russeolum* are predominant. The phytomass reserves of perennial low shrubs vary from 7 g/m² (oligotrophic pools) to 160 g/m² (palsas). The annual shoots may account for 5–10% of the phytomass of perennial low shrub shoots. The perennial parts fraction is especially important, due to the fact that it is a structural element of the lichen hummock and reaches 155 g/m². Its role in the spaces between hummocks decreases by seven times.

The reserves of green phytomass of the near-surface layer formed by mosses in pools and by lichens on palsas vary spatially. The reserves of green phytomass of the near-surface layer are formed depending on the ecosystem's eutrophy. Maximum reserves are observed in the negative elements of relief, in oligotrophic pools (540 g/m²), while minimum reserves are observed in mesotrophic alas pools (205 g/m²). On palsas, the reserve amount drops to 370 g/m². The living phytomass reserves are formed by different plant groups in different relief elements. In hollows and pools, they are formed by sedges and cotton grass; in elevations and palsas, they are formed by low shrubs. The habitat-forming role of mosses is preserved in pools, whereas on palsas 90% of mosses are substituted by lichens, whose species diversity surpasses other plant groups. They grow slowly, but the living mass is preserved for many years and accumulates to up to 900 g/m². In addition, in certain years favorable conditions for lichen podetia formation are observed in spaces between hummocks; and the podetia mass may be greater here than on palsas.

The total dead plant reserves within the active layer consist of peat and vegetative remains of mosses and vascular plants that reflect the type of biological turnover. Climatic conditions and the presence of permafrost are the main factors influencing the turnover rate and accumulation of dead plant reserves. The biological turnover parameters that we have discussed can be used for the quantitative assessment of ecosystem functioning. The analysis of empirical data using these criteria demonstrated that in bog ecosystems the functional connection between photosynthesizing and belowground phytomass, as well as between belowground phytomass and vascular plant production, is practically directly proportional. The ratio of dead plant reserves to phytomass reserves increases in the following sequence of microrelief elements: mesotrophic pools, palsa hummocks, oligotrophic pools, spaces between palsa hummocks. The average rate of turnover of dead plant reserves in northern ecosystems is very low and is about 30 years on palsas. In addition, there is a trend toward a slowdown of turnover of dead plant reserves in spaces between hummocks. Rapid thawing in mesotrophic alas pools during summer periods results in an increase of up to five years in the turnover rate.

Conclusions

According to our study, the modern structure of the active layer in bog ecosystems of forest-tundra depends on the plant community as well as on microrelief and the presence of permafrost. The amount of plant matter increases in the following ecosystem sequence depending on microrelief: mesotrophic alas pools, palsa hummocks, oligotrophic pools, and spaces between palsa hummocks. Dead plant reserves dominate in all relief elements. The amount of living phytomass is related to the ecosystem type and to the plant community. The phytomass of bog ecosystems in forest-tundra varies from 800 to 3100 g/m² and is determined by the temperature regime, microrelief, and species composition of the plant community.

References

- Drozdo, D.S., Ukraintseva, N.G., Tsarev, A.M., & Chekrygina, S.N. 2010. Changes of permafrost temperature field and in the state of geosystems on the territory of the Urengoy oil and gas field during the last 35 years (1974-2008). *Kriosfera Zemli* 14 (no. 1): 22-31.
- Kirpotina, L.V., Kosykh, N.P., & Mironycheva-Tokareva, N.P. 2011. Productivity of sedge bogs in Gorny Altai. *Western Siberian peatlands and carbon cycle: past and present* (WSPCC 2011), Third International Field Symposium (27 June–5 July 2011), Khanty-Mansiysk. pp. 111-114.
- Malkova, G.V. 2011. Permafrost temperature and seasonal thawing depth monitoring at Bolvanskiy station in the Pechora delta. *Proceedings of the Fourth Russian Conference on Geocryology*, Lomonosov Moscow State University 7-9 June 2011 Vol. 2, part 5, pp. 111-118.
- Moskalenko, N.G. (ed.). 2006. *Anthropogenic changes of ecosystems in the Western-Siberian gas province*. Moscow: Institut kriofery Zemli SO RAN. 358 pp.
- Moskalenko, N.G. 2009. Changes in ground temperature and vegetation under the influence of the changing climate and technogenesis in Nadym Region of Western Siberia. *Kriosfera Zemli* 13 (no. 4): 18-23.
- Moskalenko, N.G. 2010. Natural and anthropogenic dynamics of swamp ecosystems in northern taiga of Western Siberia. *Osvoenie Severa i problemy prirodovosstanovleniya* Syktyvkar: Institut biologii, Komi NTS UrO RAN. pp. 141-148.

Impact of Thawing on Ground Deformation

P.I. Kotov

Lomonosov Moscow State University, Moscow, Russia

Abstract

Laboratory experimental data are presented on heat flow (one-dimensional from top down, or three-dimensional from all sides) impact on deformation characteristics of thawing soils with massive and layered cryogenic structures. Mathematical modeling using the HEAT software was conducted in order to reveal the relationship between thaw depth and time. Relationships between the thawing and compression coefficients and the heat flow direction were determined.

Keywords: compression coefficient; heat flow; HEAT; soil thawing; thawing coefficient.

Introduction

At present, a significant amount of experimental and theoretical information on mechanisms and principles of settlement in thawing soils of various composition and structure has been developed. Two main approaches for the evaluation of the deformation properties have been determined: quantitative (based on physical characteristics) and experimental (determination of thawing and compression coefficients). Based on the first approach, about 15 relationships between the settlement in thawing fine-grained soils and physical properties have been determined. These relationships were summarized by Roman (2002). It is noted that it is almost impossible to formulate the generalized empirical dependence of thaw settlements on physical properties due to the fact that thaw settlements are determined by many factors that cannot be quantitatively estimated (Roman 2002, Tsytovich 1973). Therefore, the estimate of the soil thaw settlements is focused on experimental determination of the deformation characteristics. Plate-loading field tests (using a steam-heated plate) conducted in test pits and cuts are labor-consuming and expensive and cannot be used widely for geotechnical site investigations. Due to this fact, the most common tests are laboratory compression tests. The method of deformation characteristics determination in odometers providing plane parallel thawing as suggested by Tsytovich (1973) does not allow, due to labor consumption, the performance of laboratory identifications in bulk. The current work was focused on model study of heat flow impact on the sample thawing rate and laboratory compression tests with plane parallel and multi-sided direction of these flows.

One- and Three-Dimensional Heat Flow

Heat interaction in the lithosphere-atmosphere system occurs due to radiative, conductive, and convective heat transfer with soil moisture phase changes. However, no solutions were obtained in this way. All practical methods of calculation including normative ones stated in construction rules and regulations (CRR 2.02.04-88) take into account only the conductive mechanism of heat transfer. It was the mechanism used in the study.

Conductive heat transfer is described by the empirical Fourier's law, which states the proportional dependence between heat flow density "q" and temperature gradient "T":

$$q = -\lambda \text{ grad}T. \quad (1)$$

where λ is the thermal conductivity coefficient.

Fourier's law and energy conservation law are followed by the basic equation describing the thermal conductivity process:

$$C \partial T / \partial t = \text{div} (\lambda \text{ grad}T), \quad (2)$$

where C is volumetric heat capacity and t is time.

During water phase changes into ice and vice versa, soil thermal conductivity and heat capacity change. For this reason, the thermal conductivity equation is written separately for frozen and unfrozen areas, i.e., a two-equations system is obtained with two unknown temperatures $T_1(x, y, z, \tau)$ in the unfrozen area and $T_2(x, y, z, \tau)$ in the frozen one.

The phase-boundary position is also an unknown function of time, which is defined based on the specific condition that evaluates the energy conservation law during the evolution (absorption) of phase change hidden heat, known as the Stefan condition. It belongs to the non-linear tasks class and has neither accurate nor approximate analytic solutions except for the simplest cases.

During the study, the simplest task solution was used based on the HEAT software (Emelyanov 1994), which was developed to solve non-steady non-linear tasks of thermal conductivity with distributed thermal sources and movable phase boundaries in one- or two-dimensional areas, and with the help of a finite difference technique with initial and boundary conditions settings. Initial conditions describe the temperature field in a certain moment of time that is taken as a starting point. Boundary conditions describe heat exchange of the investigated system with the ambient environment.

Boundary Conditions Test Properties

In order to solve the issue of soil thawing in a compression device, the cylinder coordinate system was given and the following data were used. Silty sandy loam was taken as the initial soil. The design characteristics are given in Table 1.

Air temperature value was taken as +20°C, metal with air heat exchange coefficient - 9 W/(m²·°C) (conditions of type 3).

Initial soil temperature in the compression device was -2°C.

Ordinary compression ring sizes with the diameter of 7 cm and height of 3.5 cm were taken as the initial conditions.

Table 1. Soil properties used in the calculations.

Soil Type	Total Moisture content, W_{tot} , %	Moisture Content due to unfrozen water, W_{H_2O} , %	Soil mineral matrix density, ρ_d , g/cm ³	Soil thermal conductivity coefficient, $W/(m \cdot ^\circ C)$		Soil volumetric heat capacity, $W \cdot h/(m^3 \cdot ^\circ C)$		Latent heat of phase changes, Q_ϕ , $W \cdot h/m^3$
				Thawed, λ_T	Frozen, λ_M	Thawed, C_T	Frozen, C_M	
Sandy silt	20	1	1.5	1.86	1.97	435	400	24000

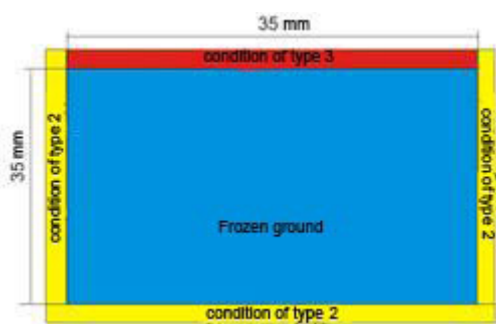


Figure 1. Layout for numerical experiment for one-dimensional thawing.

For one-dimensional thawing, the following layout was given in cylindrical coordinates: radius 35 mm, height 34 mm, and vertical and horizontal layouts by 17 blocks. In the upper part, where the interaction between the metal plate and sample is performed, the conditions of type 3 were given, in all other blocks those were the conditions of type 2 with zero thermal flow (Fig. 1).

For three-dimensional thawing, the following layout was given in cylindrical coordinates: radius 35 mm, height 17 mm (thawing occurs, and half-ring is used), vertical layout from above and from below, so only 17 horizontal parts are observed. In the upper part, where the interaction between the stamp and sample is performed, and from the right, where the ring wall and soil interaction is performed, the conditions of type 3 were given. In all other parts, those were the conditions of type 2 with zero thermal flow (Fig. 2).

According to the calculations, the time needed for soil thawing was identified. Then all data remained the same; only the sample height was changed in order to identify thawing-depth dependence on thawing time. The following dependence was obtained (Fig. 3).

According to the well-known solutions in thermal physics for the one-dimensional conditions, the thaw depth (h) is directly proportional to the square root of the duration of thawing (t):

$$h = \beta_t \sqrt{t}, \quad (3)$$

where βt is the thermal coefficient depending on the thermal conductivity, heat capacity, amount of heat for phase changes, temperature of thawing soil surface, etc.

The aforementioned theoretical ideas and particular test results performed by other researchers as well as field observations result in the fact that the shape of curves showing that frozen soil thaw settlement changes and consolidation in time depends not only on physical properties of thawing

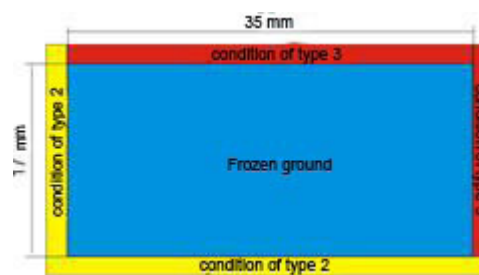


Figure 2. Layout for numerical experiment for three-dimensional thawing.

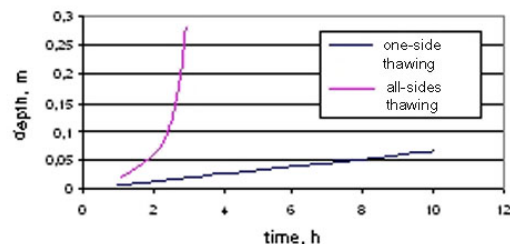


Figure 3. Relationship between thaw depth and duration of thawing.

soil and the value of outer load, but also on temperature regime of the heated soil surface.

Coefficient β was calculated based on the data on soil thaw settlement and thawing time for one-dimensional thawing as well as on the mathematical model for three-dimensional thawing (Table 2).

As it is seen from the table, coefficient β during three-dimensional thawing in all soil types is smaller. This identifies the difference in physical and thermal-physical properties of the soil after thawing.

Thus the thawing rate during three-dimensional and one-dimensional thawing significantly impacts the physical part of the consolidation process. Therefore, increased thawing rate during three-dimensional thawing first leads to larger stabilized settlement, faster filtration of water from the soil (due to the fact that during thawing filtration coefficient increases by several digits), and consequently the soil physical properties change after thawing. This particular difference in soil behavior during thawing shows the difference in deformation characteristics in various thawing conditions.

Experimental Test Procedures

Experimental research on the deformation characteristics was performed on the samples with disturbed structure taken from a 3-m depth in the area of an oil pipeline originating from the deposits of Bolshekhedskaya depression located in

Table 2. β values in various thawing conditions.

Soil Type	Cryogenic structure	Thawing type	Density, g/cm ³	Humidity, %	β
Silty sand	massive	One-Dimensional	1.89	25	2.5
		Three-Dimensional	1.89	25	1.4
Sandy Silt	massive	One-Dimensional	1.77	27	4.7
		Three-Dimensional	1.77	27	2.4
	layered	One-Dimensional	1.61	40	6.5
		Three-Dimensional	1.61	4040	3.6
Clayey silt	massive	One-Dimensional	1.82	28	3.9
		Three-Dimensional	1.82	28	2.1
	layered	One-Dimensional	1.51	45	8.8
		Three-Dimensional	1.51	45	4.6

Table 3. Geological-genetic characteristics and mineral composition of the studied soils.

Soil Type	Origin, age	Overall mineral composition, %	
Silty sand	<i>pm Q_{III} kz</i>	80.7	quartz
		6.2	microcline
		13.1	albite
Sandy Silt	<i>la Q_{III} kz</i>	75.1	quartz
		8.2	albite
		5.2	microcline
		0.5	anthophyllite
		9.5	illite
		1.5	smectite
Clayey silt	<i>a Q_{III} kg</i>	51.1	quartz
		7.1	microcline
		18.3	albite
		6	smectite
		7.5	illite
		10	kaolinite

the territory of Yamal-Nenets Autonomous Region.

Geological and genetic characteristics and mineral composition identified by the X-ray diffractometry are given in Table 3. Granulometric composition was determined by the areometric method for clayey soils and by a sieve method for sandy soils. The analysis results are given in Table 4.

The samples were cylindrically-shaped with the diameter of 70 mm and height of 35 mm. Three samples with equal moisture and density were used with the given massive- and layered-cryogenic structure. The dried model soil was passed through the sieve with the diameter of 1 mm. The initial moisture was given by humidification of the pre-cooled sample in a chamber with distilled water. Sample density was established with the help of a layer-by-layer compaction method. In the initial state, the samples had equally distributed moisture and density. When prepared, the samples were placed in a cooling chamber at the temperature of -17°C to form a massive cryogenic structure, and a layered structure was obtained with the help of the layer-by-layer water addition onto the frozen sample surface. The samples were maintained for two days at the temperature of -2°C and were

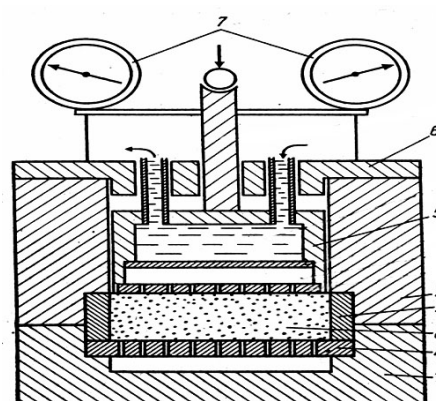


Figure 4. Odometer scheme. 1- base; 2 – leading cylinder; 3 – operational non-thermally conductive ring; 4- perforated disk; 5 – stamp; 6 – lid; 7 – indicators; 8 – sample.

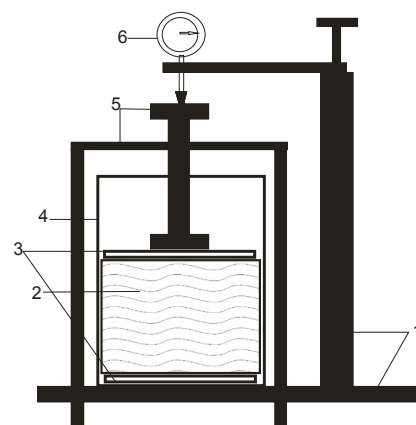


Figure 5. Compression device scheme. 1- support; 2 – metal ring with sample; 3 – perforated stamps; 4 – outer cylinder; 5 – leverage for load supply; 6 – indicator.

placed into the devices. The first set was performed in odometers made of Plexiglas, which provided thermal insulation of the samples on their side surface, thus allowing for plane parallel thawing (Fig. 4). The second set of experiments was performed in a compression device (Fig. 5).

Tests identifying deformation characteristics of thawing samples are performed in three stages:

Table 4. Particle size distribution of the studied soils.

Soil Type	Particle content in each size group, %							
	Particle diameter, mm							
	1 - 0.5	0.5 - 0.25	0.25 - 0.1	0.1 - 0.05	0.05 - 0.01	0.01 - 0.005	0.005 - 0.001	< 0.001
Silty sand	1.2	7.5	45.3	30	6	4	4	2
Sandy Silt	0.3	1.0	2.4	38.1	39.3	4.4	10	4.5
Clayey silt	0.2	0.1	19.4	43.8	6.0	15.4	4.1	11.0

Stage I – consolidation of the frozen sample at freezing temperature with the load of 0.05 MPa.

Stage II – thawing of the sample at the same load. Consolidation of the frozen and thawing sample is performed until relative stabilization is reached. Indicator readings of 0.01 mm per 12 h. are taken as relative stabilization.

Stage III – consolidation of the thawed sample with incrementally increasing load. After the thawed sample deformation stabilized (under natural load) the load was increased by 0.05 Mpa for clayey samples and by 0.075 Mpa for sandy samples. Each load stage was maintained until settlement reached relative stabilization, which was taken as equal to 0.01 mm per 12 hours.

In total, there were five load stages.

According to the data obtained, relative settlement dependence on time at each load stage was identified (Fig. 6a) as well as relatively stabilized settlement dependence on voltage (Fig. 6b). Based on these dependencies, thawing coefficient (A) (equal to relatively stabilized thaw settlement without load) and compression coefficient (m) (calculated as the slope ratio of the right line to the axis of abscissa) were determined (Fig. 6b).

Results

Test results showed that deformation characteristic values differ depending on thawing conditions. In addition, compression coefficient was increasing during one-dimensional thawing in comparison with three-dimensional thawing (with massive cryogenic structure in silty sand; by 1.5 times, in sandy silt; by 2 times in clayey silt; by 3 times with layered cryogenic structure; by 2.5 times both in silty sandy loam and clayey silty loam). At the same time, thawing coefficient was increasing in the samples with three-dimensional thawing with the difference not exceeding 10% (Table 5).

As can be seen, moisture after thawing and consolidation were not the same in identical samples (Table 5). The observed difference is caused not by the same filtration ability of devices in the studied thawing conditions that impacted the deformation characteristics values.

As test results show, the main thaw settlement in the compression conditions occurs during the thawing period. Nevertheless, for all soil types the ratio between thaw settlement at stage one and fully stabilized settlement (the settlement after thawing and consolidation at stage 5)

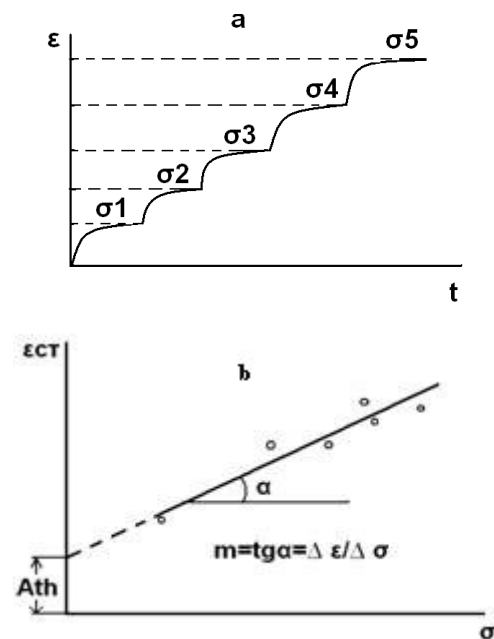


Figure 6. Relationships between relative settlement development and time at each load stage (a), and between relatively stabilized settlement dependence and stress (b).

is different (Table 6). By and large, in the samples with massive cryogenic structure more than 82% of settlement occurs during thawing. Meanwhile, the highest values are typical for the samples during three-dimensional thawing. This is due to fast filtration of water during instant thawing as well as to the fact that during slower thawing bound water may be captured by mineral particles, which prevents further filtration. There is no bound water in sand, so the thawing conditions had almost no impact on the ratio between thaw and consolidation settlement.

Conclusions

Experimental studies of soil thawing and compression coefficients provide the following results that depend on the direction of thaw:

- 1) Thawing conditions and permeability of the devices impact the thawing deformation characteristics of samples with both massive- and layered-cryogenic structures. All the data were obtained based on statistical processing of three similar experiments.

Table 5. Soil deformation characteristics.

Soil type	Cryogenic structure	Thawing type	Density, g/cm ³	Moisture content prior to thawing, %	Moisture content after thawing and consolidation, %	m, MPa ⁻¹	A, u.f.
Silty sand	massive	One-Dimensional	1.89	25	12	0.0403	0.0998
		Three-Dimensional	1.89	25	7	0.024	0.1063
Sandy silt		One-Dimensional	1.77	27	11	0.0702	0.1927
		Three-Dimensional	1.77	27	6	0.0349	0.206
Clayey Silt		One-Dimensional	1.82	25	11	0.0945	0.1569
		Three-Dimensional	1.82	25	7	0.0298	0.1752
Sandy silt	Layered	One-Dimensional	1.61	40	16	0.1336	0.3191
		Three-Dimensional	1.61	40	10	0.0557	0.345
Clayey silt		One-Dimensional	1.51	45	18	0.1668	0.3622
		Three-Dimensional	1.51	45	12	0.0774	0.3797

Table 6. Comparison of thaw and consolidation settlements.

Soil Type	Cryogenic structure	Thawing type	Thaw settlement, St	Fully stabilized settlement, Sp	St/Sp
Silty sand	massive	One-dimensional	0.1016	0.1134	0.91
		Three-Dimensional	0.1052	0.1142	0.92
Sandy silt		One-dimensional	0.1859	0.2101	0.88
		Three-Dimensional	0.1962	0.2148	0.91
Clayey silt		One-dimensional	0.1574	0.1802	0.87
		Three-Dimensional	0.1657	0.1825	0.91
Sandy silt	Layered	One-dimensional	0.2992	0.3517	0.85
		Three-Dimensional	0.3143	0.3573	0.88
Clayey silt		One-dimensional	0.3287	0.3997	0.82
		Three-Dimensional	0.3496	0.3981	0.88

Thawing coefficient in all studied soils is higher during three-dimensional thawing. This difference from various samples did not exceed 10%.

The compression coefficient in the samples with massive- and layered-cryogenic structure was higher during plane parallel thawing in comparison with three-dimensional thawing (in the sand it was 1.5–2 times higher; in sandy silt it was 2–2.5 times higher; in clayey silt it was 2.5–3 times higher).

- 2) Thaw settlement of the samples with massive cryogenic structure for silty sands is 92% of the fully stabilized settlement; for silty sandy loam it is from 88 to 91%; and for clayey silty loam it ranges from 87 to 91%. The highest values are typical for the samples with three-dimensional thawing.
- 3) Thaw settlement of the samples with layered cryogenic structure for sandy silt is 85 to 88% of the fully stabilized set, and for clayey silty loam is 82 to 88%. The highest values are typical for the samples with three-dimensional thawing.

- 4) With the help of experimental data, the difference in physical and thermal-physical properties of the sample after thawing was revealed. Thus it was shown that thawing conditions impact quantitative values of deformation characteristics.
- 5) Identification of deformation characteristics in three-dimensional thawing conditions allows rejecting thermostatic control and reduces the test period. However, in order to ensure reliability of the data obtained it is necessary to improve test methods and processing of experimental data results obtained during three-dimensional thawing.

References

- Emelyanov, N.V., Pustovoyt, G.P., Khurstalev, L.N., & Yakovlev, S.V. 1994. *Calculation program for thermal interaction between engineering constructions and permafrost soil*. Certificate #940281 as of July 12, 1994 Ros APO.

GOST, 12248-96. Methods of laboratory identification of durability and deformability characteristics.

Roman, L.T. 2002. Frozen ground mechanics. MAIK *Nauka Interperiodika*, 221 pp.

Tsytoich, N.A. 1973. *Frozen ground mechanics*. M., Vysshaya shkola, 465 pp.

Ground Ice in the Cryolithozone, Yamal Peninsula

L.N. Kritsuk

*All-Russian Scientific and Research Institute of Hydrogeology and Engineering Geology (VSEGINGEO)
Moscow, Russia*

Abstract

This paper describes results of the author's long-term geocryological studies in the northern part of West Siberia. The complex studies carried out by VSEGINGEO along gas pipeline routes and within oil and gas fields on the Yamal and Gydan peninsulas defined the specific morphological features of the ground ice masses, the landscape indicators of their near-surface occurrence, and genetic criteria of the massive ground ice. A complex methodology of the ground ice study and mapping of the discrete ice bodies was developed. The studies allow the author to reveal the fundamental regularities in the formation and spatial variability of permafrost conditions and permafrost-related features in various parts of the West-Siberian cryolithozone. They also allow the author to propose an original solution of the widely discussed and controversial problem concerning the origin of thick, deposit-forming massive ice beds, and to re-interpret the Pleistocene history of the region.

Keywords: cryohydrotectonics; faults; ground ice; hydrochemistry; indicators; isotopes.

Introduction

It is known that ground ice, abundant in the arctic and subarctic cryolithozone, is a component of the perennially frozen ground. It determines the physical and mechanical properties of the ground and represents a potential geohazard for economic development in permafrost regions. The problem of the origin and spatial distribution of large ground ice bodies has recently grown into a critical geotechnical issue due to the development of oil and gas fields in the northern part of West Siberia. Numerous accidents at exploratory and producing well sites, as well as the failure of some elements of the northern infrastructure, have been linked to the melting of these natural formations. The most challenging part of the problem is to identify and map these thick deposit-forming masses of ground ice not defined in the surface relief. The origin of these massive ground ice bodies is still open to debate. The key to the solution of this fundamental problem is to determine the nature of the in situ water that constitutes ground ice of various types, and to reveal the mechanism of ground ice formation.

Methods and Objectives

In 1978, the All-Union Scientific and Research Institute of Hydrogeology and Engineering Geology (VSEGINGEO) initiated long-term projects on the study of massive ground ice in the northern part of West Siberia.

Massive ground ice bodies were logged in the process of regional engineering-geocryological investigations at study sites along the proposed alternate routes of the Yamal-Center gas pipeline. Massive ground ice bodies were also logged in exposures in river banks and lake shore bluffs and along sea coasts within the gas-condensate fields. They were found in the process of borehole drilling (up to 15 m deep) and during geophysical (VES) surveys to depths of more than 100 m. Concurrent with regional investigations, complex studies of massive ground ice were carried out at selected test sites where ground ice bodies were found exposed. These studies used controlled methods with the direct involvement of the author.

The complex studies were carried out during a period of nine years at six test sites, three of which were earlier and repeatedly visited by Russian and foreign geocryologists. The sites are the Cape Kharasavey area, Yamal Peninsula; the Seyakha River valley (Bovanenkovo gas condensate field), Yamal Peninsula; Sredne-Yamal gas condensate field; Marre-Sale polar station; the Tadibeyakha River valley, Gydan Peninsula; and the Yuribey River valley, Gydan Peninsula. (See Fig. 1 and photographs of some of the test site outcrops under study, Figs. 2–5.)

The following tasks were established for the complex studies of massive ground ice:

- 1) Determine the morphology and size of large massive ground ice bodies exposed in the cliffs of fluvial terraces, lake shores, and along the sea coast.



Figure 1. VSEGINGEO engineering and geocryological operational map for the northern part of West Siberia 1 - VSEGINGEO operational area, 2 - VSEGINGEO permafrost research station, 3 - test sites for massive ground ice studies, 4 - thick ice-wedge ice.



Figure 2. Dome-shaped layered massive ground ice body exposed in the Seyakha (Mutnaya) River valley, West Yamal, 1980.



Figure 3. Horizontally layered ground ice outcrop covered by a layer of silty clay, the right bank of the Seyakha (Mutnaya) River, 1985.

- 2) Identify the genesis of the in situ water of the ice deposits and its freezing mechanisms.
- 3) Reveal regularities in the spatial distribution of the massive ice bodies.

A unique complex of methods was applied to the study of the ground ice deposits at the test sites, including both traditional cryolithological methods of ground ice exposure and remote sensing techniques. This included the complex of geophysical methods, aerial photography, satellite imagery interpretation at various scales, and aircraft-supported reconnaissance and survey. The studies included large-scale topographic-geodetic surveys and extensive borehole drilling to a depth of up to 20 m. Detailed core logging and sampling of ground ice and host sediments were taken for laboratory analyses of lithology, moisture and ice content, chemistry, and isotopic composition of water and ice. The collected data were statistically processed.

Results

1. A complex of the following geophysical survey methods was used at the test sites to solve the first tasks: electrical profiling (EP) and vertical electrical sounding (VES) with subsequent detailed drilling along the survey lines. Seismic, magnetic, and gravimetric survey methods were used at some of the test sites.

The difference in the physical properties of water, ice, and rock (density, resistivity, magnetic properties, velocity



Figure 4. Horizontally layered massive ground ice exposed at the base of a relict thermo-cirque on the left bank of the Yuribey River valley, central Gydan, 1984.



Figure 5. Symbiosis of a thick ice wedge and a horizontal ice bed in the Yuribey (Gydan) River valley, 1984.

of a seismic wave propagation, etc.) is the basis for the application of the geophysical methods of the ground ice study. An example of such symbiosis is shown in Figures 6 and 7. The "fault" zones in Figure 7 are defined by the magnetic and gravimetric methods (Matveyev et al. 1990).

2. The use of complementary isotope and hydro-chemical methods for the study of massive ground ice and host sediments at the test sites contributed to the identification of the origin of the in situ water that comprises the massive ground ice, as well as the mechanism of freezing (Anisimova & Kritsuk 1983, Kritsuk & Polyakov 1989, Kritsuk & Polyakov 1993). The physical regularities in the isotopic composition of water molecules in different natural objects and variations in the chemical composition of ground water freezing under different conditions due to the cryogenic metamorphism and ion concentration is the scientific basis for application of these methods for genetic and paleogeographic reconstructions (Anisimova 1983, Michel 1984, Souchez & Jouzel 1984).

Comparative analysis of the isotope data and the ground ice and in situ water chemistry data provides evidence for their genetic relationship; identifies the origin of the in situ water; defines the ground freezing conditions; determines the mechanism of the formation of various ground ice types and their relative age; and evaluates the present and the relict hydro-geological conditions of the region.

Statistical analysis of the extensive isotope data on ground ice and in situ water in the region identified a genetic

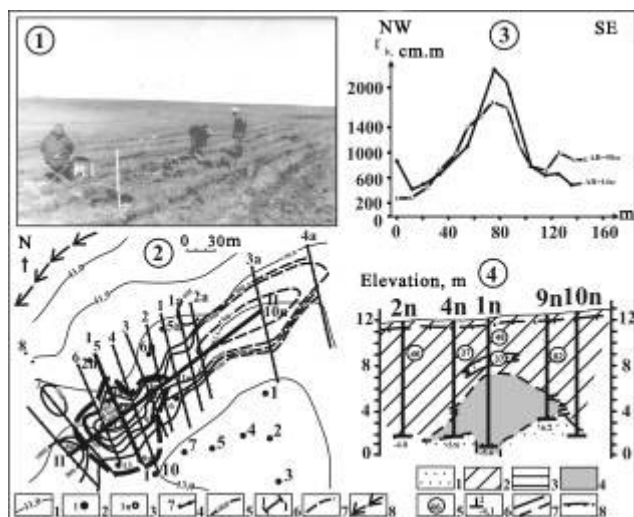


Figure 6. Results of VSEGINGEO's geological and geophysical investigations at the Kharasavey Cape in 1978. 1 - flat surface of the marine terrace underlain by sediments hosting a dome-shaped massive ice body at a significant depth. 2 - detailed electrical profiling isohm chart: 1- topographic contour lines; 2-borehole completed by Communication Institute, which penetrated a massive ground ice body; 3-VSEGINGEO borehole; 4-electrical profiling contour line and points; 5-isolines with a distance between AW=50 m; 6-cryolithological section line; 7- assumed massive ice body limit; 8-water flow direction in the creek channel. 3 - electrical profiling graphs at different distances 4 - geocryological section that exposed the massive ice body: 1-sand; 2-clayey silt; 3-clay; 4-ice; 5-average moisture content; 6-VSEGINGEO borehole; 7-lithological boundary (defined, assumed); 8-permafrost limit.

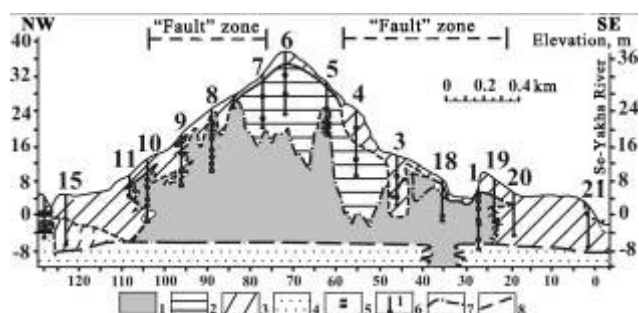


Figure 7. Results of the complex study of the geocryological section with a thick massive ice body in the Seyakha (Mutnaya) River valley. 1-ground ice; 2-clay; 3-clayey silt; 4-sand; 5-ice interlayers; 6-VSEGINGEO borehole; assumed limit of the massive ice body: 7-upper limit; 8- lower limit.

relationship between ground ice of various morphologies and natural water of different origins (Fig. 8).

Figure 8 clearly shows that natural water of different origins (mainly meteoric, both ground water and surface water) produced different types of massive ground ice. Nonetheless, the modal values of the Oxygen-18 isotope distribution curves for different natural objects revealed genetic relationships between the following types of ground ice and natural water: tabular sheets of massive ice (massive ice beds) and icings found along the structural fringe of the West Siberian Plate (the Polar Urals and Putorana Plateau); structure-forming ground ice and present summer precipitation as well as river and lake water; and ice-wedge ice and relict ground water in the southern part of West Siberia. The equally clear relationship between massive

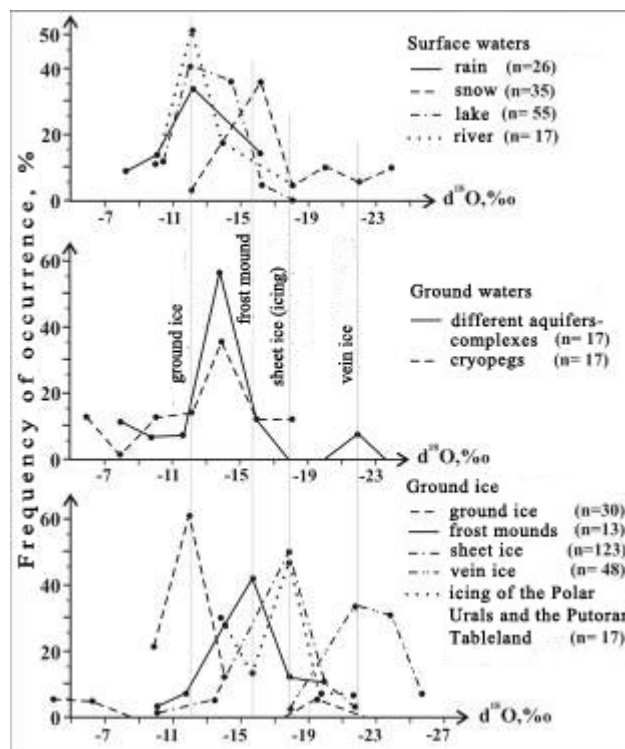


Figure 8. Ground ice oxygen isotope composition in Yamal and Gydan and its relationship with natural water.

ground ice of different morphology and natural water was revealed by comparing their chemical composition (Fig. 9).

Figure 9 shows the fresh and ultra-fresh (mainly hydrocarbonate) sodium-calcium-magnesium chemical composition of tabular sheets of massive ground ice (massive ice beds) typical of intrapermafrost water of the Pur-Nadym watershed and the icings of the Polar Urals and Putorana Plateau (Kritsuk 2010). It also shows increased magnesium ion content, high mineralization, and sulphate-hydrocarbonate calcium or sodium composition of thick ice-wedge ice. This testifies to a different degree of cryogenic metamorphism and its concentration of in situ water ions. This kind of ion distribution in ground ice testifies to the injection mechanism of its in situ water freezing (Anisimova 1981).

3. The regularities in spatial distribution of the large masses of ground ice were determined based on analysis of the results of the ground ice-complex study at the test sites, the regional survey materials, the geomorphological analysis, the study of hydrogeological conditions, and the analysis of geological and structural maps.

It turned out that all the test sites under study, as well as other massive ground ice outcrops within the Yamal and Gydan peninsulas described in the academic literature, are located in the areas of local tectonic structures within the platform cover of the West Siberian Plate. These tectonic structures, in turn, are associated with deep fault zones in the platform base.

Geological and geophysical studies conducted within the West Siberian Plate in the second half of the twentieth century revealed the block structure of the platform base. The studies showed widespread fault tectonics development both in the base and in the platform cover and high tectonic activity in the region at the Cenozoic stage (Shablinskaya

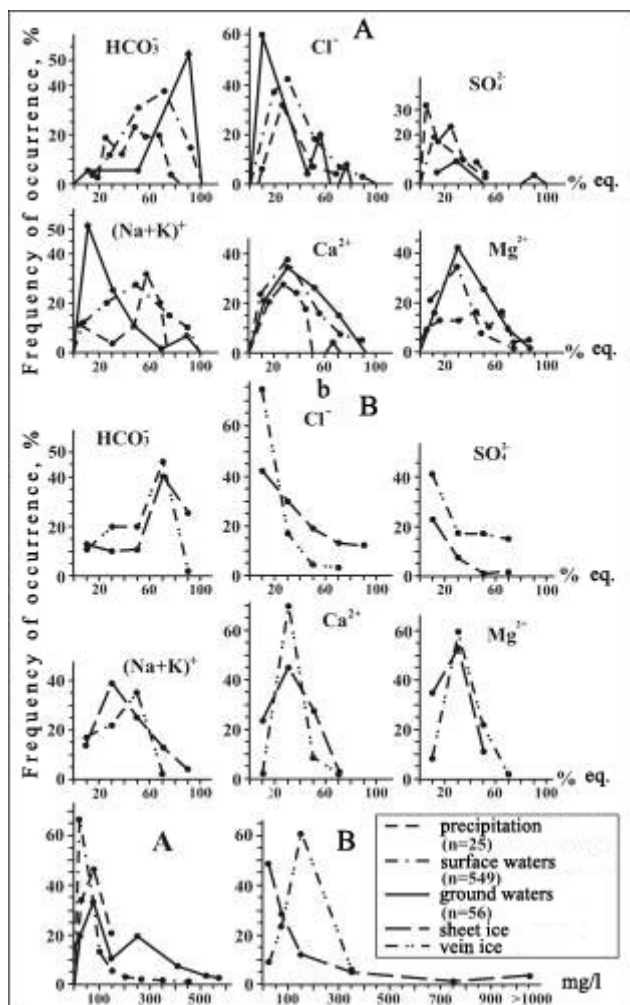


Figure 9. Chemical composition of natural water (A) in the West Siberian cryolithozone and massive ground ice (B) in the Yamal and the Gydan peninsulas

1982). Due to the inherited tectonic development of the region, the main structural elements of the platform base (large ring structures, deep faults) and the platform cover (geological structures of different orders and shallow faults) are well defined in the present-day topography and drainage pattern. Therefore, they are well identified on small-scale aerial photos and satellite images.

The specific features of the local tectonic structure development during the Cenozoic age predetermine significant complexity of the hydrodynamic conditions in the region. The conditions existed prior to the permafrost aggradation, during the periods of partial thawing of permafrost, and at present.

Active growth of the local tectonic structures in the region during the Cenozoic age and the hydrodynamic specifics have been associated with the formation of weakened zones and faults both within the structures and especially along the fringes of the structural blocks. The blocks have been undergoing differential movements of variable amplitudes.

Widespread development of Mesozoic and Cenozoic fault tectonics within the local structures of the platform cover (well-defined in the present relief and the drainage pattern as lineaments and arcuate relief features) transformed the structures into unique artesian basins with the fracture-sheet ground water. The following was determined on

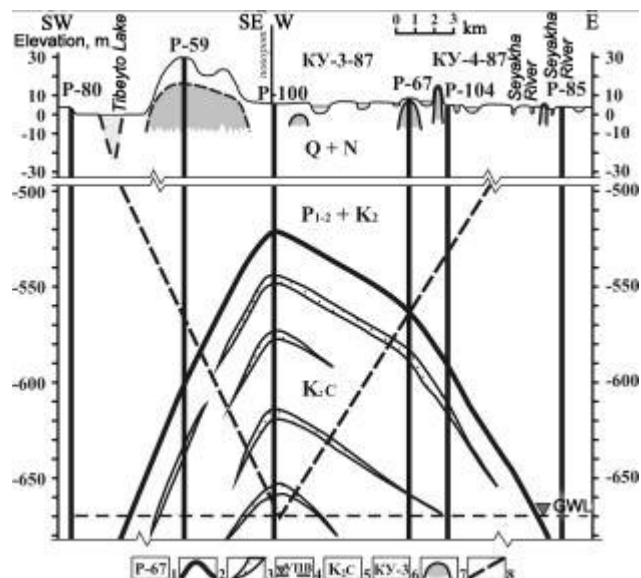


Figure 10. Relationship between drainage pattern and thick tabular sheets of massive ice in the Seyakha (Mutnaya) River valley and geological and structural factors (Bovanenkovo gas and gas condensate field) 1-exploratory well; 2-Cenomanian deposit table; 3-sandy layers; 4-ground water level; 5-geological ground index; 6-VSEGINGEO work site; 7-ground ice; 8-assumed fault zones.

the basis of hydrogeological study of oil and gas fields in the West Siberian cryolithozone: low mineralization (3–5 to 7–10 g/l), lack of vertical hydro-chemical zoning and mainly zero sulphate content in deep ground water; mosaic pattern of pressure heads of sheet waters and their hydrochemical composition; column-like distribution of high and anomalously high strata pressures within local structures in saturated and productive beds of Mesozoic and pre-Mesozoic deposits most clearly observed in the multi-strata section across the oil and gas fields on the Yamal Peninsula and within the Nadym-Pur watershed (Kruglikov et al. 1985). The increase of vertical pressure gradients by 3–6 digits over the lateral ones (together with homogeneous hydro-chemical and anomalously light oxygen isotope composition in deep groundwater) is indicative of the movement of ground waters from various aquifers and their complexes through the tectonic fracture system, and of active manifestation of the recent neotectonic movements.

As the detailed engineering and geocryological investigations by VSEGINGEO have shown, the distribution of ice-rich permafrost and ground ice within the oil and gas field areas on the Yamal and the Gydan peninsulas or the areas of intrapermafrost groundwater feed and discharge within the Pur-Nadym watershed are directly associated with these tectonically weakened zones (Fig. 10).

Ring and linear morphostructures and morphosculptures are widespread at the sites underlain by thick massive ice deposits. The occurrence of massive ground ice bodies of various morphology and geometry at the present or in the past is associated with these structures, which were termed cryohydrogenic or cryohydrotectonic (Kritsuk 2001).

Numerous circular and linear relief features (of various orders) are well-defined on the various scale topographic maps, aerial photos, and satellite imagery of the West Siberian cryolithozone. They form a concentric radial drainage and gully erosion pattern, the analogue of the neotectonic

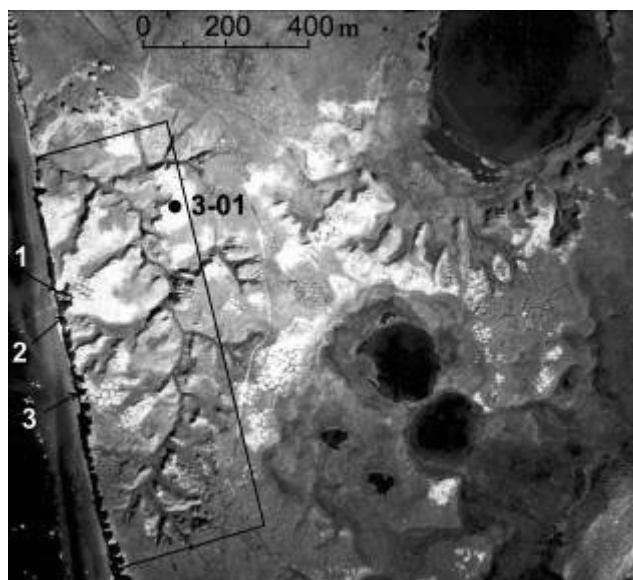


Figure 11. Large-scale aerial photograph of test site No. 6 (Marre-Sale) on the west coast of the Yamal Peninsula (3-01 – deep borehole which penetrated a massive ground ice body within the 5 to 12 m depth interval).

ring structures of the central type. Their appearance is similar to that of the neotectonic morphostructures, which correspond to the second- and third-order local oil and gas-bearing structures of the platform cover. Dome parts of these morphostructures are watersheds of large and medium rivers, while concentric elements are presented by arcuate (whereas radial elements are by linear features) river tributaries and gully networks. Both cryohydrogenic and postcryogenic morphostructures (and morphosculptures) are easily interpreted on medium- and large-scale aerial photos, whereas their distribution areas are well-defined on satellite images. The concentric radial gully network with the radius of 0.5 km studied in detail at the VSEGINGEO test site in the Marre-Sale area is a good example of the classic cryohydrogenic morphostructure (Fig. 11).

Figure 11 shows the area of detailed fieldwork (the vertically oriented rectangle); the studied exposures of large massive ground ice bodies are shown with arrows and numbers.

Conclusions

The completed complex studies of massive ground ice on the Yamal and Gydan peninsulas, combined with the analysis of geological-structural and hydro-geological specific features of the regions, allowed the author of this paper to suggest an original hypothesis on the origin of massive ground ice. According to this hypothesis, thick tabular sheets and wedges of massive ground ice on the Yamal and Gydan peninsulas represent the elements of specific cryohydrogeological systems (associated with local geological structures of the platform cover), including surface and ground waters as well as ground ice of different morphology and size. The initial formation of these systems was caused by freezing of the relict tectonic lake depressions and river valleys, and this resulted in the formation of numerous closed freezing systems. This interpretation was also given for the Canadian North (Mackay 1979). Different periods

of cyclic climate fluctuations during the Pleistocene and the Holocene led to multiple complete or partial thaw of the permafrost and to the melting of the ground ice contained in it. This resulted in the formation of post-cryogenic morphostructures. The repeated freezing of the ground and ground water led to the formation of specific landforms—cryohydrogenic morphostructures and morphosculptures.

Evidence of the relict ice-wedge polygonal systems can be seen in relief features and in the drainage and erosion patterns found in various areas of the cryolithozone.

The appearance of these morphostructure indicators in the relief and the ease with which they can be interpreted from aerial photography and satellite imagery is the methodological basis of their mapping at different scales (Kritsuk 2010).

The determined spatial (and, thus, genetic) relationship between thick massive ice deposits and regional fault zones indicates that similar origin can be attributed to the ground ice found in other parts of the cryolithozone: in Siberia, Alaska, and Canada. Analysis by the author of all available materials on the known localities underlain by thick massive ground ice bodies undoubtedly points to this relationship. This included superimposing these localities over structural, tectonic, and fault maps and interpretation of high-resolution satellite images of the areas underlain by massive ground ice.

Acknowledgments

The author sincerely thanks Professor O.N. Tolstikhin, Doctor of Sciences (Geology and Mineralogy), for his expert opinion about the studies and results.

References

- Anisimova, N.P. & Kritsuk, L.N. 1983. Use of cryo-chemical data in studying ground ice deposit genesis. *Geocryology problems*. Moscow, Nauka: 230-239 (in Russian).
- Anisimova, N.P. 1981. Cryohydrogeochemical peculiarities of the permafrost region. Novosibirsk, Nauka: 153 pp. (in Russian).
- Kritsuk, L.N. 1990. Ground and surface ice of West Siberia during the Pleistocene age. *Materials of glaciological studies*. AN SSSR, Edition 69, Moscow: 93-102 (in Russian).
- Kritsuk, L.N. 2001. Cryo-hydrotectonics and ground ice of West Siberia. *Materials of the second conference of Russia's geocryologists*. Moscow, Izd-vo MGU, Vol. 3: 155-163 (in Russian).
- Kritsuk, L.N. 2005. Yamal and Gydan vein ice. *Materials of the third conference of Russia's geocryologists*. Moscow, Izd-vo MGU, Vol. 3: 145-154 (in Russian).
- Kritsuk, L.N. 2010. *Ground ice of West Siberia*. Izd. Nauchny Mir, Moscow, 350 pp. (in Russian).
- Kritsuk, L.N. & Anisimova, N.P. 1985. Chemical composition of sheet ice and its relation with ground waters. *Cryo-hydrogeological studies*. Yakutsk, SO ANSSSR: 94-108 (in Russian).
- Kritsuk, L.N. & Polyakov, V.A. 1989. Isotope studies of natural waters and ground ice in West Siberia. Moscow, *Inzhenernaya geologiya*. No 4: 76-94 (in Russian).

- Kritsuk, L.N. & Polyakov, V.A. 1993. Isotopic and chemical composition of ground ice in West Siberia. *Permafrost Sixth International Conference. Proceedings*, Beijing, China. South China University of Technology Press., vol.1: 897-903.
- Kruglikov, N.M., Nelyubin, V.V., & Yakovlev, O.N. 1985. Hydrogeology of the West-Siberian oil and gas megabasin and hydrocarbon accumulation formation peculiarities. Leningrad, Nedra: 279 pp. (in Russian).
- Mackay, J.R. 1973. Problems in the origin of massive ice beds. *Western Arctic, Canada Second International Conference on Permafrost*. North American Contribution. National Academy of Science. Washington, D.C: pp. 233-238.
- Mackay, J.R. 1979. Pingos of the Tuktoyaktuk Peninsula area Northwest territories. *Géographie physique et Quaternaire* 33 (no 1): 3-61.
- Matveev, V.S., Kritsuk, L.N., & Baskakova, I.N. 1990. Use of magnetic and gravimetric methods for ground ice study. *Inzhenernaya geologiya* No 3: 85-90 (in Russian).
- Michel, F.A. 1986. Isotope geochemistry of frost-blister ice. North Fork Pass, Yukon, Canada. *Canadian journal of Earth sciences* Vol. 23, No.4: 543-549.
- Shablinskaya, N.V. 1982. *Fault tectonics of the West-Siberian and the Timan-Pechora platforms and Paleozoic oil and gas content problems*. Leningrad, Nedra: 155 pp. (in Russian).
- Souchez, R.A. & Jouzel, J. 1984. On the isotopic composition in δD and $\delta^{18}O$ of water and ice during freezing. *Journal of Glaciology* 30 (no.106): 369-372.

Problematic Aspects of the Study and Exploration of the Arctic Cryolithozone

V.S. Krupoderov, V.A. Dubrovin

All-Russian Research Institute for Hydrogeology and Engineering Geology (VSEGINGEO), Moscow, Russia

Abstract

This paper discusses modern problems in the study and exploration of the arctic regions of the Russian cryolithozone, including the shallow shelf zone of the arctic seas. A series of actions is proposed for the successful development of approaches aimed at studying and developing the subsurface extractive industries of the cryolithozone.

Keywords: cryolithozone; geocological test site; monitoring; permafrost; regulations; subsurface.

Introduction

It is well-known that approximately 11 million sq km of our country's 17 million sq km is characterized as cryolithozone, with a thickness varying from several meters to 1.5 km. This huge area consists of permafrost of different composition and genesis. Ice inclusions can be found ranging from ice-cement to macro-glacial bodies up to tens of meters thick and up to hundreds of meters long, containing fluids of various chemical compositions. Russia's cryolithozone area exceeds the total areas of such countries as Canada, the USA, and China. The cryolithozone contains a large portion of the mineral resources of the country, such as gold, tin, mercury, diamonds, oil, and gas. Whatever methods and technology are used for extraction of these minerals, significant changes in natural conditions of the development areas take place in the subsurface and on the surface.

Despite the importance of the cryolithozone in the ecological setting and in the construction and operation of industrial and civil facilities and recreational areas, there is not a single government program aimed at its comprehensive study.

Technogenesis has spread intensively into previously uninhabited, remote, and poorly studied arctic regions of the cryolithozone over the past 30–40 years. This imposes a special responsibility on the state and society related to environmental impacts in these areas. The main problems that require attention are as follows:

- 1) Development of a conceptual approach, methods, and scale of the geological (hydrogeological, geotechnical, geocryological, and geocological) study of newly developed areas.
- 2) Tightening of requirements for the design of facilities for the mining industry and transport corridors, and for the development of engineering activities that prevent the development of adverse thermodynamic and hazardous cryogenic processes, as well as ways of utilization of industrial and household waste.
- 3) Creation of independent expert panels consisting of representatives of specialized institutions for discussion of the implementation of economic development projects in new arctic regions of the cryolithozone, including the coastal zone and the continental shelf of northern seas.
- 4) Changing the existing narrow departmental approaches to the use and storage of geological investigative materials that do not represent a state secret.

- 5) Urgent need for the development and production of transport equipment for the operation of geological organizations in the country's arctic regions during the summer.
- 6) Study of the experience and environmental impacts in oil and gas regions in the north of West Siberia.

Main Points

Advanced study of territories on the basis of the state of geological and integrated hydrogeological, engineering, and geological survey mapping at the scale of 1:200,000 does not seem possible for the cryolithozone area. This is not only for financial reasons; it is based on the intended purpose and further use of these expensive materials. For primary users of geological information, such as industrial subsurface developers, preparation for field projects or follow-up exploration projects on land or at sea usually begins at the scale of 1:100,000. The 1:200,000 scale is clearly insufficient.

In addition, the current rate of publicly funded hydrogeological mapping of the country at the scale of 1:200,000 (outside the cryolithozone) does not exceed 3–4 pages per year. If we assume that such methods and pace of study are applied to ensure the development of mineral resources in the North or in East Siberia, it will take, according to conservative estimates, a little more than 150 years to complete the mapping. In this respect, the need for the development of an environmental doctrine on subsurface use in arctic regions, including the area of the shelf, seems urgent. This doctrine must be based on a full range of advanced regional and monitoring investigations of a geotechnical, hydrogeological, and geocryological nature. The investigations must be done in the most promising development areas to form a system of state geocryological (geocological) test sites (Dubrovin 2001, 2009). The founders of these test sites should be the state and regional authorities and subsurface developers. Geocryological (geocological) test sites must be created in the areas of prospective economic development of the cryolithozone and in the areas of existing industrial and energy complexes, where activities pose a serious threat to ecological safety.

The goal of work at the test site and the main results of this work should provide:

- Information for subsurface developers about potential geocological hazards during field development at all stages of the process of geological exploration from study to conservation;

- Information for administrative bodies regulating subsurface usage with guidance on the periodic monitoring and compliance for environmentally sound exploration and exploitation of mineral deposit areas in the zone of active and passive tectogenesis.
- Information for regional administrative bodies with materials of the environmental assessment of the areas under development.

The first of the aforementioned problems can be solved with the use of the materials of areal geotechnical and hydrogeological studies as well as of background monitoring at regional test sites. The second can be addressed with monitoring of sites, based on the results of special control surveys. The third can be solved based on the study of exploration experience in cryolithozone regions having conditions of various degrees of complexity. The main outcome of these studies should be the results of monitoring activities, current and predictive assessment of the subsurface state and natural environment, and the development of research studies, including legal documents regulating the environmentally safe exploitation of natural resources in the region.

Problem 1

The test sites should be established for at least 5–6 years prior to the start of the active phase of the development of the territory. At the initial stage it is essential to carry out a comprehensive geocryological, geotechnical, and hydrogeological initial survey at the 1:500,000 scale, as well as hydrogeological and geocryological research for at least 2–3 years. The survey and mapping scale mentioned is, in our opinion, the most optimal for displaying regional features and characteristics of the cryolithozone. It serves as a convenient basis for creating an environmental portrait of the territory under development. There is also the possibility of detailed characterization of subsurface use facilities and transport corridors in a generalized form. This scale of regional studies is unjustly ignored.

Initial or “express” surveying and mapping are carried out on the basis of the interpretation of aerial and satellite images, fund materials and route surveys, geophysical works, and drilling of a limited number of reference boreholes. In the course of further research and the creation of a supervisory monitoring network at the test site that includes drilling of observation boreholes, geophysical works, and monitoring, the resolution of the maps is increased. At the subsequent investigative stages, particularly during the allocation of previously unallocated subsurface key sections (KS), the geocryological/hydrogeological survey at the 1:100,000 scale is marked on the test site area taking into account the principal scheme for development of the mineral deposits. This KS survey, which is mandatory for the test site, has to be conducted by the investor during the preparation of materials for the investment feasibility stage under the license agreement for the geological study or use of the subsurface. Therefore, by the time of the assignment of the deposits or fields for use, an original map (scale 1:500,000–1:100,000) of the geocryological test site area is created for subsequent development of the geoecological model of the area under development. This cartographic model contains

monitoring data using both background and site monitoring.

It is important to note that the scientific and methodological basis of the state monitoring of the subsurface conditions does not currently meet modern standards due to the fact that it does not consider the cryolithozone as an object of research and monitoring. In our opinion, the structure of the state monitoring of the subsurface must include a “cryolithozone module” at the subsystem level.

Development of the Master Plan of the control network of background geocryological test sites, regional observational boreholes, and sites equipped with autonomous, automated means of observation for the cryolithozone area, should become a priority for state monitoring of the state of the subsurface (geological environment). This should include the coastal zone and the shallow marine shelf of the Arctic Basin, for studying and evaluating the impact of periodic fluctuations in climate (global changes). It is important to emphasize that although there is some experience in regional monitoring of the cryolithozone territory, there is practically no experience in geocryological studies within the shallow shelf zone of the arctic seas. As the comprehensive study of the test site progresses, the data on its conditions and structure can be extrapolated to the surrounding area.

It is obvious that only in this case may the newly explored area acquire an “owner,” who will be responsible for the environmental impacts throughout the entire development cycle, from exploration to abandonment of the deposit.

Problem 2

All the regulatory and procedural documents regulating activities at the test site area should be mandatory. This approach will make it possible to concentrate the funds to ensure environmental safety and to determine the degree of responsibility between the state, the federal subject, and developers for the condition and protection of the subsurface in the areas under development. The need to raise the infrastructure design environmental requirements for the mining industry is dictated by a number of facts that became known during the study of the materials of the “Program of complex development of hydrocarbon fields in the Yamal-Nenets Autonomous District and North of Krasnoyarsk Region” (the “Program ...”) and other documents. In these documents, there is no hydrogeological study of the area or assessment of the interaction of sub-permafrost waters with varying degrees of salinity (3 to 5–10 g/l) and pressure (10–25 atm) on the structure of production wells. The underestimation of this interaction can seriously affect the stability of these structures during their operation. The need to study and consider the redistribution of snow cover in the area under development is not mentioned either. The influence of this is so great that no global climate change can be compared with it. Estimates and field data show that in northern latitudes an increase in the thickness of snow cover from 0.3–0.4 to 1.5–2.0 m may lead to an increase in soil temperature at the depth of 10 m by 3°C within 4–5 years. Route surveying of the facilities under construction of the first line of the Bovanenkovo-Ukhta gas pipeline within the Yamal section showed that the snow cover thickness in the open storage areas, field camps, compressor stations, bridges, walls of highway embankments, and other structures varies from 1.2 m to 2.5 m. Of particular importance are the areas

where snow accumulates as a result of road clearing. Here piles of snow, located in close proximity to engineering structures and power lines, often reach a height of over 3 m during the winter. In late April to early May, snow removal is conducted in field camps. In the cold season, snow prevents cooling of the ground, and in spring, the melting of snow occurs 1.0 to 1.5 months earlier because of removal. Thus the “natural and anthropogenic” impacts on the increase of the permafrost temperature reach their maximum. It will not be a surprise if areas with a lowered permafrost table are soon detected in the built-up area of the Bovanenkovo field. Exactly the same or similar methods of “thermal amelioration” were applied in the middle of the last century in the development of dredging ground in the gold mines of Chukotka.

Design decisions reached their climax in the sphere of municipal solid waste disposal. The construction project for the municipal solid waste landfill in the Bovanenkovo field was executed in the shortest possible time. It is extremely hard to imagine who of our descendants this “gift” is meant for. The perfectly preserved baby mammoths “Dima” from Susuman Village, “Masha” and “Lyuba” from the Yamal Peninsula, and the nameless remains of Gydan mammoths are 10 to 40 thousand years old. Everybody thought that nuclear waste disposal carried out near the coast of Novaya Zemlya would never affect future generations. It should be emphasized that the construction of landfills is regulated by the above-mentioned “Program of complex development of hydrocarbon fields in the Yamal-Nenets Autonomous District and North of Krasnoyarsk Region”.

We consider it unacceptable in the 21st century to construct landfills in newly developed regions of the Arctic. In our opinion, this approach should be completely eradicated.

The process of recycling and incineration of waste could be an alternative, but not at the temperature of 600–700°C, which promotes the formation of carcinogenic dioxins and other substances. It should be done at temperatures over 1000°C to eliminate the possibility of the formation of hazardous substances. Taking into account the fact that the abovementioned “Program...” provides for gas flaring in the amount of 3.6 billion m³, it is not difficult to find a source for the fire; one only needs to make a decision.

Problem 3

Creating a system of independent expert panels is important not only for the initial design phase, but also for evaluating the effectiveness of design decisions. These panels will monitor the subsurface state and protect the geological environment. They will implement engineering measures aimed at preventing the development of adverse geological (cryogenic) processes and phenomena.

Unfortunately, such authority does not currently exist in the system of the Ministry of Natural Resources of Russia (“Federal Service for Supervision of Natural Resources Usage,” “Federal Agency on Mineral Resources”). Existing regulatory authorities perform inspections that only investigate the compliance with the design decisions. Needless to say, a designer himself has a right to carry out such an inspection, but whether he wants to do it voluntarily is a rhetorical question.

Improvement of the quality of the design can be achieved

if pilot tests are carried out during pre-project preparations. These tests will evaluate the measures of engineering protection of the territory, with specialized institutions participating in the monitoring. Such regulations for large subsurface developers (RAO GAZPROM, etc.) should be registered at the legislative level.

We believe that a commission of independent experts should be created under the jurisdiction of the Federal Agency on Mineral Resources, which is the main manager of the state subsurface fund.

Problem 4

The exchange of geological information that does not represent a commercial or state secret between the federal agencies and their institutions and the subsurface developers practically does not occur, especially during the process of implementation of the projects related to additional site appraisal for remote regions. This greatly reduces the operational efficiency of the geological institutes and organizations of the Ministry of Natural Resources of Russia and the Federal Agency on Mineral Resources.

The solution to this problem is the creation of regional databases for the system of geocryological test sites. These databases should contain available geological data on the test site and should be free of charge for all those working in the region. The use of this information outside the test site should be strictly regulated.

Problem 5

Transport vehicles are needed during the summer in the forest tundra and tundra and on the Arctic coast. This need became evident as the delivery of cargo and personnel by helicopters is absolutely unprofitable and other types of transport are not available. We believe that if geological research in the areas of hydrogeology, engineering geology, geocryology, and geoecology in the Arctic is not performed during the summer period, the obtained results cannot be considered complete.

Development of transport equipment should be recognized as one of the main governmental tasks aimed at the support of science and applied programs of research and development for the Arctic. This should be carried out by geological organizations of the Ministry of Natural Resources of Russia and expeditions of the RAS institutes.

This applies not only to transport equipment, but also to drilling and geophysical and laboratory equipment. We believe that raising a question about the development of the “Program of technical re-equipment of geological industry, design and academic institutions that conduct works in the arctic regions of the country” is long overdue.

Problem 6

More than 40 years have passed since the commissioning of “Medvezhye,” the first of the largest gas fields in the North of West Siberia. Urengoyskoye, Yamburgskoye, and other gas fields were later developed. These fields occupy a leading position in the country’s gas economy, yet their geological and environmental impact and the experience of their development still have not been summarized.

One of the main subjects of such a study is the question of adequacy of the zone of technogenic influence on gas

industry facilities in relation to the size of license areas that are allocated for subsurface use. It is necessary to evaluate the change in the hydrogeological conditions, resources, structure, and quality of groundwater in industrial and recreational areas. It is necessary to evaluate the loss of land resources due to gully-thermoerosional processes, the area of territories not undergoing recultivation, and the rate of recovery from damage to vegetation cover. It is essential to perform an analysis of the effectiveness of regulatory activity during the development of the territory and to create recommendations for recording the experience of subsoil development and exploration in the region.

Of extreme importance is the development of regulations on the establishment of an environmental fund for abandonment of mineral deposits based on the example of the oil and gas industry.

The obtained materials may serve as a basis for designing new facilities for subsurface use in the Arctic and subarctic.

Conclusions

The following actions should be taken as soon as possible for the development of approaches aimed at studying and developing the extractive industries in the cryolithozone:

- 1) Develop a strategy and create a governmental program for a comprehensive regional geocological (hydrogeological, geotechnical, geocryological) study of the cryolithozone in the near- and mid-term prospect for the development of mineral deposits. This should include a gradual increase in the amounts of advanced work and should include the following tasks:
 - A study of the state of hydrogeological, geotechnical, and geocryological conditions in areas where development is planned and in large oil and gas fields that are in the final stages of production. Geocological impacts of the development should be assessed.
 - Development of a new structure of the state monitoring of the subsoil conditions with consideration for the tasks of studying the cryolithozone as a unique natural object. A general control network of observatory stations and test sites in the cryolithozone should be developed for the evaluation and prediction of the cryolithozone response to periodic global climate change.
 - Development of a scientific basis and recommendations for the organization of geocryological monitoring within the shallow part of the arctic shelf, and creation of a number of test sites within the observational network for the shallow waters that are under priority development.
- 2) For the successful implementation of the projects under state contracts it is essential to ensure a real cost-effective information exchange both within the Ministry of Natural Resources of Russia as a whole, and at the inter-agency level with the most important subsurface developers (RAO GAZPROM, etc.) that are engaged in subsurface license agreements.
- 3) Recommend that the Ministry of Natural Resources of Russia prepare materials for the introduction of a legislative initiative on the inclusion of the following

mandatory sections in the projects of field development in the cryolithozone:

- Pilot experiments in order to test the environmental protection measures.
- Regulations for the establishment of the ecological Fund governing the abandonment of deposits.
- Address the Russian government with a proposal to create programs for technical equipment of the geological industry, design and academic institutions that work in the Arctic; form a commission of independent experts under the Ministry of Natural Resources of Russia for the pre-testing of large-scale, subsurface projects in the cryolithozone of the Arctic, including the coastal zone and continental shelf of the arctic seas.

References

- Dubrovin, V.A. 2001. Conceptual approach to regional and monitoring geocryological research in the Arctic and Subarctic. *Proceedings of the Second Conference of Russian Geocryologists* Vol. 3 Moscow: MGU pp. 90-97.
- Dubrovin, V.A. 2009. Geocryological research in the system of subsoil use: problems, tasks and solutions. *Razvedka i Okhrana Nedr* 9: 36-42.
- Krupoderov, V.S. Tasks and prospects of the hydrogeological, geotechnical and geocryological exploration of the subsoil in the development of mineral resources of the country. *Razvedka i Okhrana Nedr* 9: 6-10.
- Krupoderov, V.S., Kurennoy, V.V. Golitsyn, M.S., & Dubrovin, V.A. 2007. The main directions for the development of regional hydrogeological, geotechnical, geocryological and geocological works. *Razvedka i Okhrana Nedr* 5: 2-6.

Geotechnical Solutions for Slope Stabilization Along the Amur Highway Characterized by Permafrost Degradation of Road Embankments

S.A. Kudryavtsev, T.Yu. Valtseva, R.G. Michailin
Far Eastern State Transport University, Khabarovsk, Russia

Yu.B. Berestyani
DV-Geosynthetika Scientific Research Company, Khabarovsk, Russia

Abstract

This paper gives an overview of the research, geotechnical investigations, design work, and numerical modeling conducted to support the upgrade of the Chita-Khabarovsk section of the Amur Highway. This section of the highway is located in an area of irregular topography and sporadic distribution of warm permafrost below the road embankment, both of which contributed to the complexity of the task. The incorporation of modern geosynthetic materials into the design of the road embankments provides rational design solutions, allows for reliable future maintenance of the upgraded section of the highway, and preserves permafrost at the base of the road embankment.

Keywords: freeze-thaw; geosynthetics; irregular topography; permafrost; stress-strain state.

Introduction

The studies described in this paper are part of the Amur highway section improvement project. The section of the Amur highway described in this study traverses the territory characterized by complex permafrost-related geotechnical conditions. The entire section is located within terrain characterized by uneven topography and sporadically distributed permafrost that is degrading at the base of the road embankment. This combination of features results in the development of irreversible slope deformation.

The main purpose of this study is to develop rational geotechnical solutions that will allow stabilization of the deformed parts of the embankment and the road base in a timely manner. The design solutions should meet regulatory requirements for strength and frost resistance within the territory of the Russian Federation. The design should also provide the bearing capacity of moving loads that may occur within these complex geological conditions. The design presented here is a summary of the results of research, engineering tasks, calculations, and applied solutions. Analysis of a number of possible approaches and means to achieve the target goals showed that the most productive option would be to use several modern geotechnical software products together, such as "FEMmodels" and "Plaxis." The combination of these software products allowed us to simulate the operation of a structure according to its stress-strain state and thermodynamic processes during multi-year cycles of freeze-thaw, and to assess the stability of the ground mass and structures as well.

Based on the analysis of the original data and during implementation of the models, it was established that calculation and theoretical research for current structures of the road and its foundation (as well as for recommended structures) must be done to completely and properly assess and compare the current indices of strength and deformation. Certain design elements were developed to prevent saturation of the structure, which could result in slope failures.

The parameters of operational reliability and bearing capacity of the recommended structures were determined using numerical methods that took into account the

properties of specific geosynthetic materials.

Assessment of the thermodynamic freeze-thaw parameters for the recommended structures led to a determination of the criteria for changes in temperature-moisture fields over a two-year cycle and freeze-thaw boundaries during the main periods of each season. Absolute freeze-thaw values within the embankments and road base over ten-day periods were obtained via numerical modeling. Diagrams of frost heave deformation in the structures over a two-year period were produced using this information.

Analysis of the stress-strain data for various structural elements, the specific character and values of frost heave within the structures, and the structures' stability assessment confirmed the suitability of the selected methods.

Comparison of the stresses and resulting deformations in the elements under load, and the correspondence of the obtained frost heave values to the Russian Federation standards on frost heave, confirmed the quality of the recommended geotechnical measures and their long-term operational reliability.

Baseline Data and Causes of Deformation

Analysis of initial data on the geological structure, hydrogeological conditions, and permafrost extent and characteristics along the highway section under study provide cause-and-effect relations to be determined between natural/anthropogenic factors and slope process activation. The minimum depth of the permafrost table along the highway section is 3.6 m. The base of permafrost along the highway section is unknown. Some perched groundwater levels are found locally within depressions in the permafrost table.

The existing facilities and structures for the regulation of surface water flow (culverts, etc.) are either partially functional or do not work at all.

The absence of impermeable liners within the ditches on the upper part of the embankment slopes causes surface water leakage through underlying layers of sand and silty clays (with interbeds of sand and gravel), which results in water reaching the upper boundary of warm permafrost. This

naturally causes thawing and degradation of the underlying permafrost. A thawed saturated soil layer above the warm permafrost table is a predetermining factor for sliding of this layer along the permafrost table. The distribution of forces and deformations on this surface is not uniform and depends on many factors, including the moisture content.

The physical and mechanical properties of the areas where active sliding was occurring were used in calculations of the stress-strain state and the stability of the ground and structures. We considered the physical and mechanical properties of ground recommended for calculations in the report on geotechnical investigations, only to select actual physical and mechanical properties of the ground in this study. The actual properties of the road base and structures were used to calculate the parameters of the structures and to conduct geotechnical modeling.

The development of design and technological approaches was based on active and passive measures, with decreasing natural and anthropogenic influence on the structures.

A wide range and variety of geosynthetic materials and their composites are available. These differ in type, purpose, technical characteristics, quality of manufacture and of original raw material, and life cycle. However, today the effective use of geosynthetic materials is uncommon in areas with severe climatic conditions, including those with seasonal freezing and permafrost. The Amur study area is similar to areas in the Far East where patches of permafrost can also be found at the base of the road embankments. The authors have analyzed several structures of this type in recent years and have developed certain design measures aimed at stabilization of deformation using modern technologies and promising geosynthetic materials. At present, all these structures are operational and their performances are monitored. The results either completely coincide or are very close to the calculated parameters of the stress-strain state.

It is recommended that the geosynthetic materials used in protective and load-bearing structures be combined with traditional elements to minimize deformations in the structures, duration of the deformations, and operation costs.

Study Methodology

High quality modern programming methods in the fields of geotechnics and foundation engineering were used to assess geological and geocryological conditions at the site. The “FEM models” program was developed by geotechnical engineers at Georeconstruction, a scientific and industrial company in St. Petersburg, under the direction of Professor V.M. Ulitsky.

The program helps solve three-dimensional thermophysical and stress-strain state tasks for roads/embankments with several million variables. The program performs finite element modeling for different problems in the construction field. The basic feature of the program is the ability to solve combined calculation tasks for a road base and its embankments. Such calculations meet the requirements of standard regulation documents (SNIP 2.02.83*, TSN 50-302-2004), which demand the structure calculation take into account the behavior of the road base. The road base is modeled in three dimensions, taking into

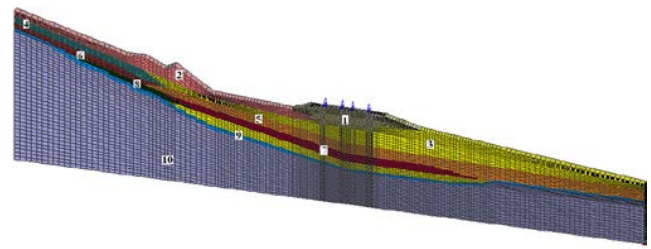


Figure 1. Structure design scheme: 1- fill; 2 – thawed gravelly sand, damp; 3 - light silty clay with fine gravel up to 20%, damp; 4 - heavy silty clay with fine gravel up to 10% and damp sand interlayers; 5 - light stiff clayey silt with fine gravel up to 10% and damp sand interlayers; 6 - light stiff sandy silt with fine gravel up to 20%; 7- stiff gravelly silty clay; 8 - heavy frozen (low ice) silty clay of massive cryostructure with fine gravel up to 10%; 9 – thawed ground layer; 10 – permafrost.

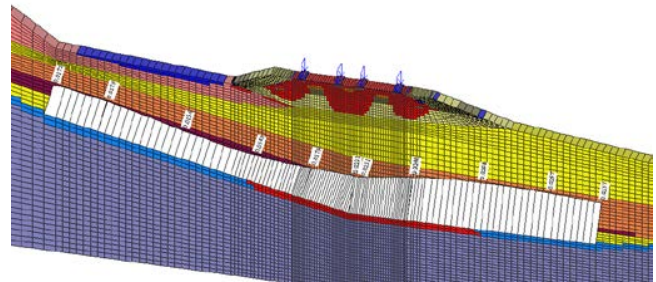


Figure 2. Areas of elastic (blue) and plastic (red) deformations and curves of horizontal displacement of a soil mass within the thawed zone (m).

account its behavior and using modern models of soil mechanics, which enable us to avoid simplified approaches.

Based on analysis of the existing models of freezing and thawing, Professor S.A. Kudryavtsev developed the “Thermoground” mathematical model to numerically model freezing, frost heave, and thaw over an annual cycle using a three-dimensional approach. This model forms a component of the “FEM models” program. An elastoplastic model with finite surface described by the Mohr-Coulomb criterion was used to determine behavior of a structure on weak, thawing foundation soil. The selection of this model was determined by the fact that its parameters can be obtained during standard geotechnical site investigations. This allows the numerical calculations to be in good agreement with traditional engineering methods of displacement calculation. In addition, deformation of structures on weak, thawing foundation soils can also be described with enough precision.

The program used to solve dimensional thermal and deformation problems is called “Thermoground” and has the following characteristics:

- The thermal problem is solved by taking into account phase changes of water into ice within the range of negative temperatures for non-standard thermal conditions in a three-dimensional soil space.
- Relative thaw deformations of the ground are determined by taking into account water migration, which depends on the distance from the freezing front to the groundwater table (where the winter trend is known).
- The stress-strain state of the road base is determined by taking into account anisotropy of the frost heave

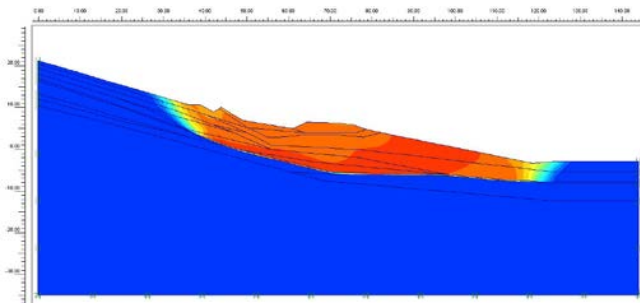


Figure 3. Results of construction stability calculation.

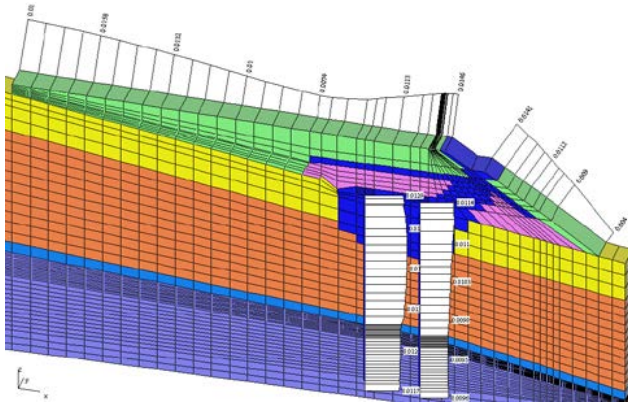


Figure 4. Diagram of horizontal displacement of pile-grid construction elements (m).

deformations; the maximum ground deformation during thawing is determined according to the physical characteristics (moisture, ice content) obtained by solving for freezing stages.

The stability of the original structures on existing natural slopes and the design solutions over the period of their implementation are determined with the help of the Plaxis 2D program. This program can solve complex geotechnical problems associated with the stages of construction, operation, and reconstruction of structures.

The geotechnical parameters shown in Figure 1 were used for the geotechnical modeling of a structure's behavior.

It is evident from Figure 2 that areas of plastic deformation under load are spread across the entire mass of the road fill, which means that the road has insufficient bearing capacity.

Plastic deformation is restricted to the thawed zone. This means that the ground can creep along the thawed layer. The analysis of horizontal deformation shows dynamic progressive displacement of the structure along the thawed layer.

The stability of the structure on the hillside was calculated with the Plaxis 2D program (v8). Analysis shows that the sliding surface is of a pronounced and predetermined nature and is located on top of the permafrost (Fig. 3). Infiltration of surface water seeping from above into the road base is the obvious cause of permafrost thaw. The clayey soil above the permafrost becomes wetter, which leads to a change in physical and mechanical characteristics that affect stability. The stability index of the soil in this case is close to one (1.0017).

To reduce or completely stop this plastic deformation, measures must be taken to increase the bearing capacity of the road base and embankments. To decrease the risk of ground creeping along the thawed layer, it is also

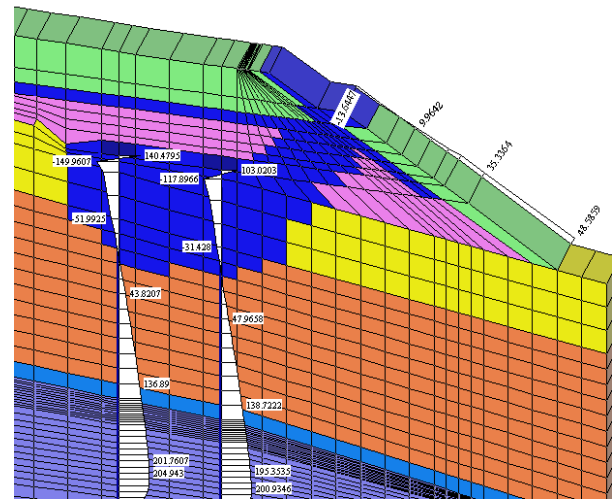


Figure 5. Diagram of horizontal stresses in pile construction (kPa).

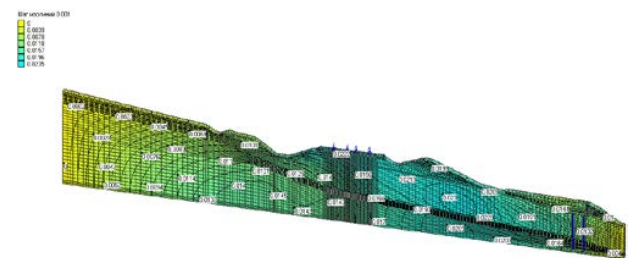


Figure 6. Isolines of horizontal displacement of elements in a structure, in meters

necessary to actively reduce permafrost thaw. This can be achieved through the regulation of surface water flow and the prevention of moisture penetration into the road base/embankment via the use of heat insulators.

Passive restraining structural measures should also be undertaken to ensure operational reliability of the structure during the stabilization of deformations in areas of potential creep.

Numerical Modeling of Structure Behavior under Extreme Conditions

While these measures were being developed, the original data and the results of numerical modeling of the original structure and its road base/embankments were modeled. The behavior of strengthening structures and constructive measures (connected with the stress-strain state and the change in freeze-thaw processes that promote a decrease in influence of natural and anthropogenic factors on effective functioning of the highway) was also considered and modeled.

The pile-grid structure was found to experience the greatest effect from the shearing and sliding of the ground and the embankment on a natural hillside. Numerical modeling of the embankment together with the road base allowed calculation of optimal parameters and confirmed the results of analytical calculations. Figures 4, 5, and 6 show the results of the modeling of strengthened elements within an embankment.

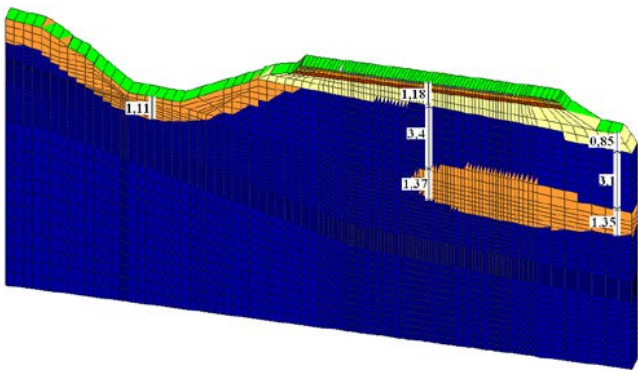


Figure 7. Freeze-thaw magnitudes of ground in September, first year (m).

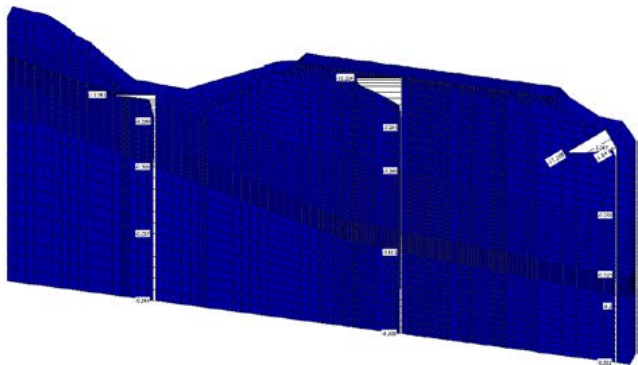


Figure 8. Diagram of ground temperatures and freeze in March, second year (°C).

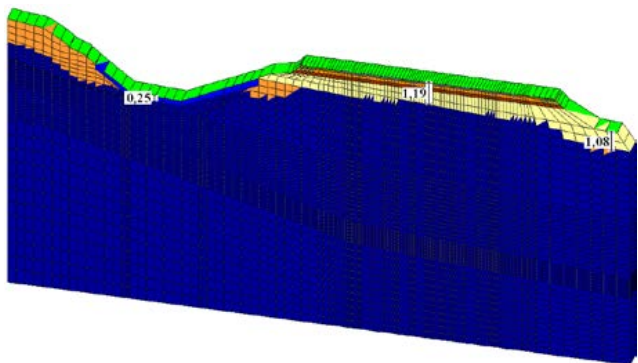


Figure 9. Freeze-thaw magnitudes of ground in September, second year (m).

Numerical modeling of freeze-thaw processes was carried out using the "Thermoground" geotechnical module developed by Professor S.A. Kudryavtsev (FESTU) and geotechnical engineers from St. Petersburg (Georeconstruction-Fundmentproject, Co.).

Numerical modeling of thermodynamic processes is needed in order to obtain a qualitative and quantitative picture of freeze-thaw and frost heave of an embankment over a year-long period or longer. Modeling must also be carried out to determine the depth of freezing and thawing of the embankment in different seasons, the effective use and geometrical parameters of heat isolation elements, and the probability of freezing of taliks which may keep the embankment partly frozen for a period of time. The maximum amount of heaving on the road carriage-way was also defined.

For this study, the most important parameter for operational reliability of the structure is the area of the material sliding

where the highway base and the top edge of the adjacent ditch (with a heat isolation element) are located.

Figures 7, 8, and 9 show the results of numerical modeling of thermodynamic processes during the first and second years of operation.

The following results were achieved after freeze-thaw modeling:

- 1) In January of the first year of the structure's operation, ground freezing along the road centerline was 1.54 m from the surface, while it was 1.38 m on the ditch slope. Beneath the frozen layer, a lens of unfrozen material (talik) with a thickness of 6.42 m formed along the road centerline and another 6.04 m thick formed on the structure's slope. In January of the second year, after a heat insulator was emplaced, the entire structure froze.
- 2) The ground did not completely freeze during the first year. In March, the thickness of the frozen ground along the road centerline was 2.32 m, while on the structure's slope it was up to 1.71 m. Beneath the frozen layer, a lens of unfrozen material (talik) 5.63 m thick formed along the road centerline and another 5.6 m thick formed on the structure's slope. In the second year, complete freezing of the ground was observed between January and March.
- 3) In September of the first year of the structure's operation, the maximum ground thaw in the area of perspective heat insulation was 1.11 m. The structure thawed up to 1.18 m along the road centerline and up to 0.85 m on the slope. Beneath the thawed layer, a lens of frozen ground 3.4 m thick formed along the road centerline and another 1.35 m thick formed on the structure's slope. Under this frozen layer, a lens of unfrozen ground (talik) was preserved. It had a thickness of 1.37 m along the road's centerline and 1.35 m on the slope. In September of the second year of the structure's operation, maximum ground thaw in the area of perspective heat insulation was only 0.25 m. The structure thawed up to 1.19 m along the road centerline and up to 1.08 m on the structure's slope.

Conclusions and Recommendations

To stabilize deformations both in the embankment foundation soils and in the embankment as well as in separate structures and to limit degradation of the uppermost permafrost layer, design solutions that both actively and passively improve the hydrogeological and permafrost conditions of the site are recommended.

Active construction methods

- Hillside ditch construction to provide surface flow, with complete isolation of surface water from the sand layers below.
- Addition of hydro-insulation and thermal insulation layers to protect shallow permafrost from degradation and to completely prevent surface water from percolating into the underlying material and reaching the permafrost table.

Passive construction methods

- Production of the required bearing capacity of the

pavement by laying a pseudo-plate of integral two-axis geogrid EGRID 4040L into the mixture of crushed rock and sand.

- Stabilization of the sliding unit and provision of traffic safety over the period of restoration of geological equilibrium, which can be achieved by means of a gravitational pile structure placed at the calculated point on the lower part of the slope.

The numerical modeling of thermodynamic processes in this study showed that it is possible to freeze the ground under the ditch to the permafrost table and to keep it frozen. This is achieved by placement of a heat isolation layer of the calculated thickness in the ditch. The conditions of initial freezing must be reached before the insulator is placed.

According to the results of geotechnical modeling, the magnitudes of frost heave on the road surface are 40 cm and 38 cm, which is less than required in ODN 218.046-01.

The stability of the structure has sufficient limits due to the constructional design solutions for the calculated cross sections.

The mitigating measures suggested are based on the results of the stability calculation and modeling of thermodynamic processes of the structure and its foundation soils and include the following:

- Active deforming slope areas along the studied road section should be unloaded;
- For several reasons, including safety, excavation should begin after day temperatures go below 0°C. The excavations should be carried out in stages followed by freezing after each;
- Material and structure placement should be performed after maximum freezing of the foundation soils under the structure and before daytime temperatures rise above 0°C.

References

- Kudryavtsev, S.A., Berestyanyy, Y.B., Valtseva, T.U., & Barsukova, N.V. 2006. Practice of use of positive properties of geosynthetic materials on building objects in severe climatic conditions of the Far East of Russia. *1st International Conference on New Developments in Geoenvironmental and Geotechnical Engineering*. November 9-11, 2006. University of Incheon. Korea. pp. 423-427.
- Kudryavtsev, S.A., Berestyanyy, Y.B., Valtseva, T.U., Fedorenko, E.V., & Mikhailin, R.G. 2008. Design study of geosynthetic material system protecting highways from stone fall. *Fourth International Conference on Scour and Erosion*. 5-7 November, 2008 Surugadai Memorial Hall, Chuo University. Tokyo, Japan. pp. 651-654.

Providing the Optimal Temperature for Underground Plant Seed Storage in Permafrost

G.P. Kuzmin, V.N. Panin

Melnikov Permafrost Institute, SB RAS, Yakutsk, Russia

Abstract

Relatively low negative temperatures are required for long-term plant seed storage. When underground storage is created in permafrost in most parts of the cryolithozone, additional chilling is necessary to maintain the temperature of the surrounding permafrost massif. Experimental studies evaluate the possibility of maintaining the required temperature for long-term plant seed storage in an underground cryostorage by means of cold outer air. The effectiveness of cryostorage chilling designs depends on the thermal conductivity of the wall coating material protecting the surrounding permafrost from the desiccation and destruction caused by ice sublimation. To maintain a sufficiently low temperature during the summer months, it is recommended to accumulate the cold from ambient air in the surface layers of permafrost, and to locate a storage room at a depth where the phase lag of temperature fluctuations is equal to the duration of the cooling device operation.

Keywords: cooling device; long-term seed storage; optimal temperature; permafrost; underground storage.

Introduction

Plant seed storage at negative temperatures and low humidity allows seed viability to persist for long periods of time. Currently, many countries maintain seedbanks in facilities where the sub-zero temperatures required for long-term plant seed storage are provided by coolers or natural cold with additional artificial chilling. The Svalbard Global Seed Vault in Norway, where permafrost and artificial chilling are used, belongs to the latter type (Kershengolts et al. 2008). The drawbacks of such storage areas are high energy demands and the possibility of thermal regime violations during power outages. Long-term plant seed storage depending exclusively on natural cold resources, with no additional machines or mechanisms, is an alternative method.

The SB RAS Institute for Biological Cryolithozone Problems was able to store legume and grain legume seed for more than 30 years at temperatures of -4 to -5°C in underground chambers created in the permafrost. The seeds' biological properties—viability and reproduction—were well preserved (Kershengolts et al. 2008).

The optimal temperatures for plant gene pool storage are not finally defined, but preliminary studies and long-term seed storage experiments completed by biologists show that temperatures between -6° and -8°C are favorable. In the cryolithozone, such ground temperatures are typical only at high latitudes, and therefore additional chilling of the surrounding permafrost is needed in most of the cryolithozone area. In the winter, when the surface air temperature falls below the permafrost temperature in the vicinity of an underground cryostorage, outside air is the only source of natural cold.

Today many underground coolers for storage of frozen products are being built in Russia's cryolithozone. Yakutia alone has more than 400 operating underground coolers, the majority of which use natural cold as a resource (Kurilko et al. 2011). Winter cold charging is implemented by means of natural draft or forced ventilation. Nonetheless, the problem of temperature stabilization in the cryolithozone in summer remains, due to the seasonal change of outside air temperature.

During the chilling of underground facilities with cold air, it is important to consider ice sublimation leading to the drying up and degradation of surrounding ground layers. As experimental studies show, permafrost degrades significantly if it interacts with cold air flow for long periods (Kuzmin 2002). In this respect, only a no-contact cold-air chilling method should be used for plant seed cryostorage. Convective air motion in utilities and pipes occurs due to atmospheric pressure differences of the air columns in descending and ascending flow channels and the variations in air pressure above them caused by wind.

In this study, experiments were completed in existing underground facilities to evaluate the feasibility of chilling permafrost around a cryostorage with cold outer air delivered through metal pipes. Temperature and air flow velocity in chilling pipes, as well as the ground temperature dynamics in the cryostorage walls, were monitored. This report gives recommendations on chilling schemes and summer temperature stabilization for cryostorage.

Parameters of a Pilot Underground Facility and Cooler

The pilot facility is located in the area of Yakutsk, where permafrost thickness reaches 250–300 m and the annual mean air temperature according to long-term data is -10.3°C . The length of the period with daily mean temperature below 0°C is 211 days. The natural ground temperature at a 20 m depth is -2.3°C . The seasonal thawing depth at the open site is 2.2 m. Soils up to a depth of 22 m consist mainly of small-grained sand with separate sandy silt layers and inclusions of layers of plant remains. The soil density in the 0–20 m depth range varies from 1.79 to 1.94 g/cm^3 , and the moisture content varies between 19 and 29%.

The pilot facility is a horizontal underground chamber with a round cross-section 3.2 m in diameter and 50 m long, located at a depth of 23 m (Fig. 1).

Its walls are lined with approximately 5 cm of ice. The chamber is vented by means of a 10 m long vertical shaft with a rectangular cross-section (0.5 x 1.3 m). The shaft is encased in a steel pipe 1220 mm in diameter, with a welded

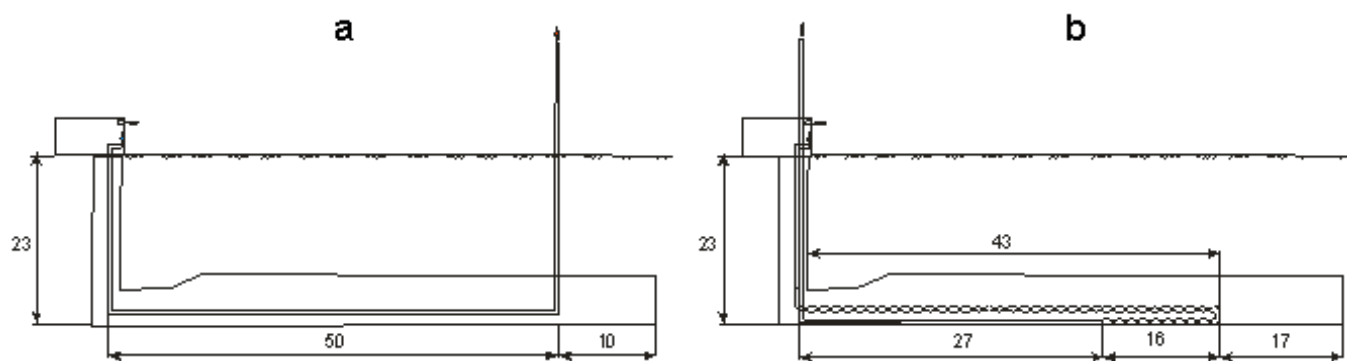


Figure 1. Schematic of air cooling devices in the pilot facility *a* – 2009-2010; *b* – 2010-2011.

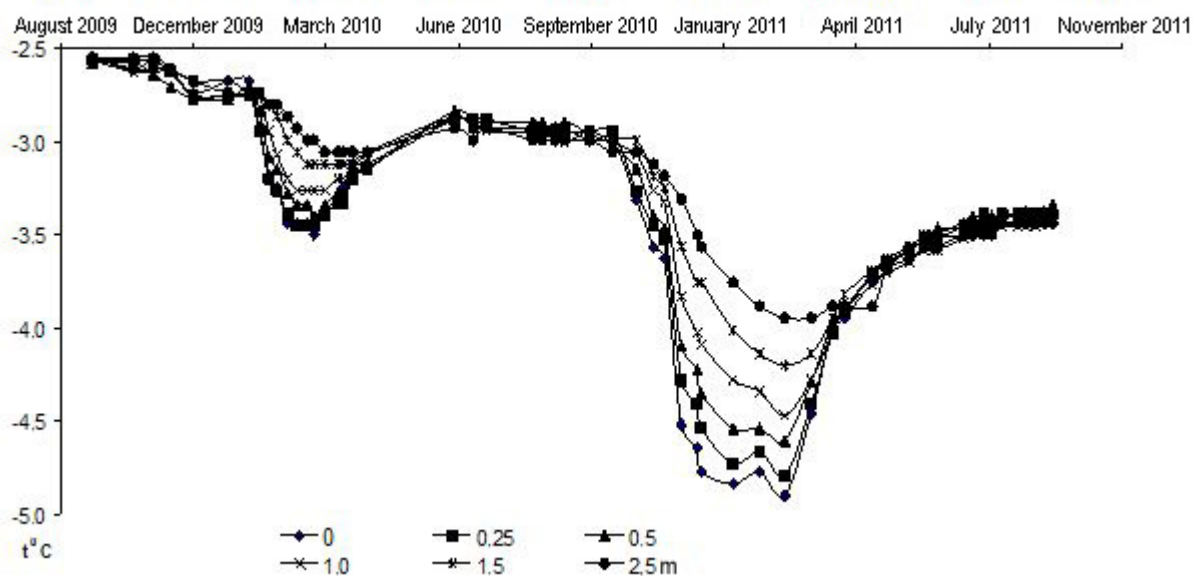


Figure 2. Ground temperature dynamics around the pilot facility at the depth of 0–2.5 m.

bottom and a hatch in its upper part. The casing is equipped with small platforms every 3.5 m and with vertical ladders.

The cooler consists of intake and exhaust vertical ducts and a horizontal heat-exchanger. The upper open end of the intake air duct is located at ground level, and the heat-insulated air duct for exhaust air extends 5 m above ground level.

In 2009, the heat-exchanger was made of aluminum flat pipes 200 mm in diameter and 50 m long. The exhaust pipe extended through the well drilled at the chamber end 50 m from the intake shaft. In 2010, the heat-exchanger length was increased. It was made of 27-m-long flat aluminum pipes and 59-m-long corrugated aluminum pipes that were successively connected with each other and air ducts located in the shaft casing.

The pilot facility was equipped with sensors for air temperature metering in the cooler and the ground around it. The velocity of the airflow circulating in the cooler was also measured.

Results and Discussion

Some results of the monitoring conducted in 2009–2010 in the pilot working are given below.

Figure 2 shows the ground temperature dynamics at different depths from the horizontal chamber wall, when it

was chilled with cold outer air.

Analysis of these data shows that during the employment of the convective cooling system in 2009-2010, the maximum temperature in the chamber fell down from -2.3 to -3.8°C , with a similar decrease during the first and the second winters. The difference between the maximum summer and the minimum winter temperatures in the chamber after the second operational year of the cooling system was insignificant, about 0.5°C . The airflow velocity in the cooler depended on the outside air temperature (Fig. 3).

The scatter of data in Fig. 3 may be explained by changes in ground temperatures around the wall of the shaft. With exactly the same outside air temperatures measured at the different time moments, the airflow velocity at the next moment was always lower than the flow velocity at the previous moment (though this decrease was very small).

Ice formation on the heat-exchanger surface as a result of water vapor condensation is a significant disadvantage of the underground storage cooler design under study. This evidently leads to the development of slow sublimation of ice and the surrounding permafrost and to some reduction of heat transfer from air in the storage to cold air flow in the heat-exchanger. A compact ice layer up to 10 mm thick accumulates on the pipe's surface during one chilling cycle, requiring periodic removal.

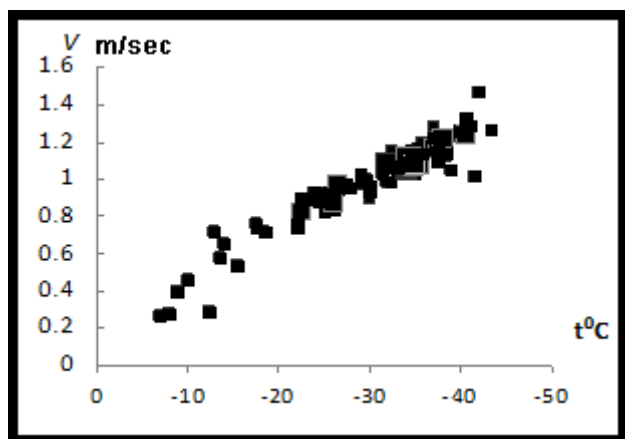


Figure 3. Descending air flow velocity dependence on temperature at the initial section of the pipe 300 mm in diameter.

The increase of the length and area of the heat-exchanger by 1.7 times in 2010 did not cause significant air flow velocity change in the cooler. Consequently, the chilling capacity of the cooler was augmented by increasing the heat exchanger length without a change in the intake and exhaust pipe dimensions.

A convective air cooler with appropriate design and appropriate heat-exchanging surface can ensure temperature decreases in underground facilities required for long-term plant seed storage. Without a waterproof coating, the processes of ice sublimation and drying of the surrounding permafrost will occur during the whole operation period of the storage. The chilling capacity of the cooler should be determined by the desired application to achieve the optimal temperature in the underground storage after initial and subsequent operational cycles. If the optimal temperature is reached after the first cycle, the cooler capacity will not be fully used during subsequent operation. If the optimal temperature is reached after a number of cycles, the storage operation does not begin immediately after construction.

The permafrost chilling around the storage with cold outside air does not provide sufficient temperature stability required in the storage. In summer the temperature in the storage increases slightly.

The following is recommended for the elimination of the discussed drawbacks.

Underground cryostorages are structures with a long operational period and should therefore have waterproof coatings to prevent the surrounding permafrost from drying and degrading. The following chilling schemes for an underground cryostorage are suggested, depending on the ratio between the thermal conductivity of the coating material λ_n and the thermal conductivity of the surrounding permafrost λ :

- at $\lambda_n \geq \lambda$ the air flow descends directly via the facility or the channel laid inside it;
- at $\lambda_n < \lambda$ the air flow descends via channels laid in permafrost behind the waterproof coating.

It is suggested that the cold in winter should be accumulated with the help of air chilling pipes in the surface layers of the permafrost massif to ensure temperature stabilization in the underground cryostorage in summer. It is also suggested that the cryostorage should be positioned at the depth defined with the equation of phase shift of temperature fluctuations

(Kudryavtsev 1978), taking into account the chilling pipe depth h :

$$z = 2\delta\sqrt{\pi\lambda / CT} + h$$

where δ – phase lag is assumed equal to the duration of cooling device operation (6 months for Yakutsk), λ and C – ground thermal conductivity and heat capacity coefficients; T – outer air variation period (8760 hrs). Insulation is provided to reduce heat seepage into the ground above the surface chilling pipes.

Conclusions

The optimal temperature for plant seed keeping in underground storage in cryolithozone conditions with insufficiently low surrounding permafrost temperature can be attained with the help of convective air coolers. In winter, the required temperature is maintained with the help of an air cooler within the storage or in permafrost behind the waterproof coating of its walls. In summer, the chilling is achieved by means of a cold temperature wave from the chilling pipe system located near the surface and the heat insulation from summer heating.

References

- Kershengolts, B.M., Ivanov, B.I., Desyatkin, R.V., Remigaylo, P.A., Fedorov, I.A., & Chzhan, R.V. 2008. *Use of natural permafrost cold for long-term storage of genetic resources*. Moscow: Vestnik VOGiS, 2008, Vol. 12, No 4: 524-533 (in Russian).
- Kudryavtsev, V.A. (ed.). 1978. *General geocryology*. Moscow: Izd-vo MGU, 464 pp. (in Russian).
- Kurilko, A.S., Kiselev, V.V., Khokholov, YU.A., & Romanova, E.K. 2011. *Thermal regime regulation for underground storages and special structures*. Yakutsk: Izd-vo Instituta merzlotovedeniya SO RAN, 245 pp. (in Russian).
- Kuzmin, G.P. 2002. *Underground structures in cryolithozone*. Novosibirsk: Nauka, 176 pp. (in Russian).

Impact of Mineral Composition on Heat-Conducting Properties of Frozen Volcanic Ashes from Kamchatka

E.P. Kuznetsova, R.G. Motenko
Lomonosov Moscow State University, Moscow, Russia

Abstract

This paper describes the results of an experimental study investigating the thermal-conducting properties of thawed and frozen volcanic ashes sampled from Kamchatka. The data were categorized according to their sensitivity to the degree of saturation (S_r). The impact of mineral composition on the studied thermal-conducting characteristics was identified. For example, at a fixed S_r value, the thermal-conducting characteristics (thermal conductivity and thermal diffusivity) are higher for ashes containing acidic glass (this composition was defined as opal) and lower for ashes with mafic glass (allophane).

Keywords: allophane; frozen ashes; heat conductivity; opal; thermal conductivity.

Introduction

Pyroclastic ash is the least stable solid phase of sediments and is predisposed to different mineral transformation in all lithogenetic stages. Volcanic ashes mainly consist of volcanic glass. They also include plagioclase, feldspar, quartz, and pyroxene (Dahlgren et al. 1993). As a result of volcanic activity, volcanic glass is transported great distances and is then weathered, forming secondary minerals. Among the alteration products caused by weathering and diagenesis are smectites, halloysite, kaolinite, allophane, palagonite, and others.

Most of Kamchatka is covered by a stratum consisting of tephra (pyroclastics transported by air from the volcano crater) and buried soil beds. Volcanologists call it a soil-pyroclastic cover (SPC) (Melekestsev et al. 1969). In Kamchatka, this cover is of a Holocene age. Ashes from major eruptions form clear key inter-layers in host deposits, which can be identified within huge areas. The stratum between the key ash inter-layers is of a pyroclastic nature and includes both minor or remote eruption products and secondarily redeposited ashes (Bazanova et al. 2005).

Geocryological prognosis and estimation of main geocryological characteristics (e.g., thickness, active layer depth) in areas with widely spread permafrost are impossible without knowing the thermal characteristics of frozen grounds. The present studies on the thermal properties of pyroclastic volcanic deposits are insufficient. The existing data refer, in general, to the volcanic massive rocks or tuffs or for those in an unfrozen state. Moreover, it is difficult to analyze the available data due to a lack of records regarding age, humidity, and density of these volcanic deposits.

The main goal of this research was to study the thermal conductivity and thermal diffusivity of frozen volcanic ashes in Kamchatka and to identify their sensitivity to mineral composition.

Objective

Volcanic ashes representing the eruption products of different volcanoes were sampled for laboratory research. Some of them belong to marker ash inter-layers of major and catastrophic volcano eruptions in Kamchatka, which

occurred in different years. Others relate to the strata between the key beds. Marker ashes are dated and have their own index accompanied by numbers or letters. For example, the tephra (pyroclastics transported by air from the volcano crater) of the Shiveluch volcano “Sh₂” is 950 years old; “Sh₃” is 1400 years; “Sh₅” is 2550 years; and “Sh₈₃₀₀” is 8300 ¹⁴C years. The Khangar volcano tephra horizon with the index “Khg” is 6850 ¹⁴C years old, and the Ksudach volcano ashes with the index “KS₁” are 1800 ¹⁴C years old (Ponomareva et al. 2007).

The sampling locations are concentrated in the area of the Klyuchevskoy volcano group. The samples were taken at elevations from 290 to 1630 m (see Table 1). The age of the ashes studied is within 35–9000 years. Table 1 gives the data on water-physical properties of the samples obtained in their natural condition. The ash humidity ranged from 13 to 64%, and hygroscopic water W_g – 0 to 4.14%, dry density ρ_d – 0.9 to 1.6 g/cm³, solid density ρ_s – 2.1 to 2.8 g/cm³.

The particle size distributions of the studied ashes are given in Figure 1. All the ashes belong to fine-grained sands according to GOST 25100-95. The predominant fraction in most of the samples is 0.1–0.05 mm, while for Samples 2–4 it is the fraction 0.05–0.01 mm, and for Sample 17 it is 0.25–0.1 mm.

According to silicon dioxide content of the volcanic glass, our samples belong to three types: andesite, basaltic, and rhyolite.

The IR-absorption spectra allowed identifying the composition of ashes with mafic (basaltic and andesitic) glass as allophane, and the composition of ashes with acidic (rhyolitic) glass as opal (Kuznetsova et al. 2009, 2011a, Motenko & Kuznetsova 2010).

Allophanes (from Greek *alophanes*, “turning out to be different”) are amorphous minerals of variable chemical composition. They mainly consist of $Al_2O_3 \cdot SiO_2$ and H_2O (Betekhtin 1950). Wada (1989) gives the approximate chemical formula of allophanes as $Al_2Si_2O_5 \cdot nH_2O$. They belong to sheet silicates because they have similar chemical composition and some common structural peculiarities with them, but they differ from them through the lack of crystalline texture. Allophane is fully amorphous and was found for the first time as a product of volcanic ash transformation. Allophane consists of hollow spheres with an outer diameter

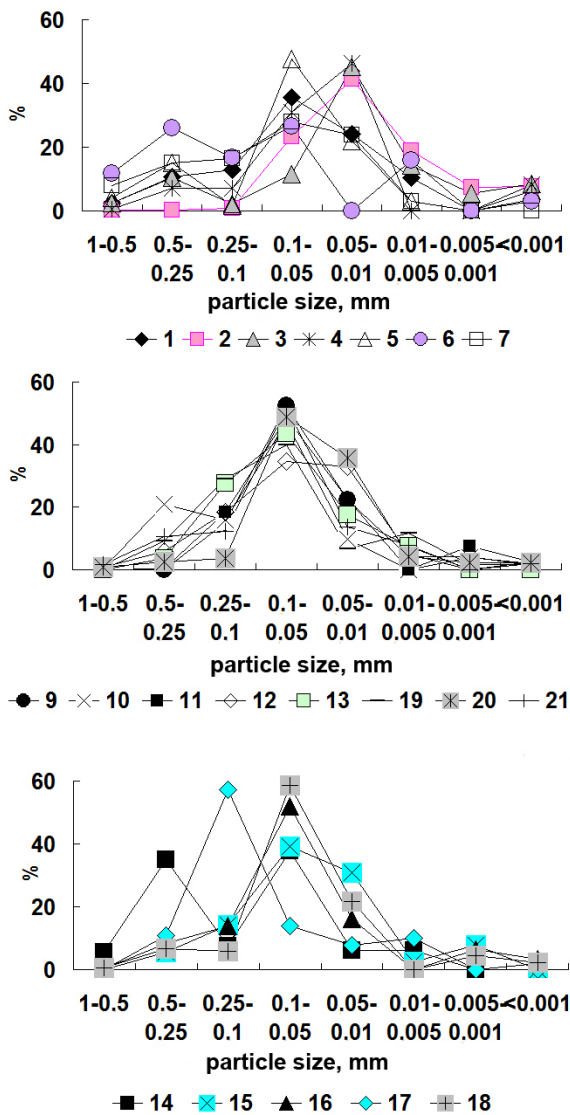


Figure 1. Particle size distribution of the studied ashes.

of about 4–5 nm (Henmi & Wada 1976). Based on one of the construction models, a single allophane particle is a hollow sphere with defects in the wall texture that consequently form micro-pores 0.3–2.0 nm in diameter (Paterson 1977, Wada & Wada 1977). The moisture retention capacity of allophanes is associated with the presence of very small pores. The outer surface area estimated for this model is 800 m²/g (Theng et al. 1982).

Opal (from Sanskrit *upalah*, “stone”) is amorphous silica, silicon dioxide hydrate, the chemical formula of which is SiO₂·nH₂O, where n usually varies from 0.5 to 2.

Two types of opal silicon are the most common for volcanic ashes: pedogenic (more known as laminar opal silicon) and biogenic (diatoms). Laminar opal silicon emerges at the early weathering stages and is characterized by the existence of spheric bunches of reticulate-like spheres of hydrated silicon. Opal silicon is formed in silicon-rich environments, precipitating from over-saturated solutions that appear due to surface evaporation and, probably, water freezing in soils (Shoji et al. 1993, Nanzyo 2002). Its abundance decreases with the increasing volcanic soil age as a result of particles weathering.

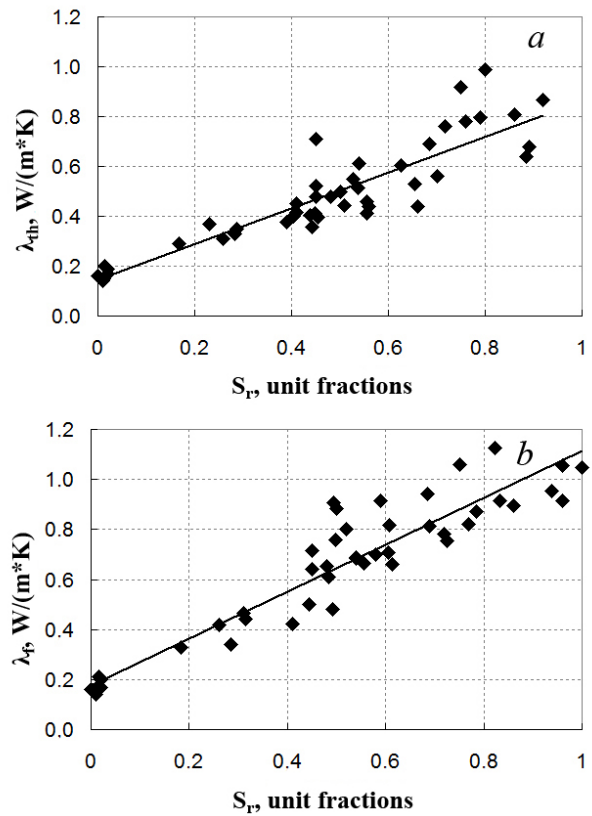


Figure 2. The dependence of heat-conductivity coefficients (λ_{th} and λ_f) on the degree of saturation (S_r) for the studied fine-grained volcanic grounds in the thawed (a) and the frozen (b) states.

The study of the phase composition of moisture revealed the presence of unfrozen water in frozen ashes. The content of this water depends on the peculiarities of mineral composition. The abundance of unfrozen water in ashes with opal at minus 10°C varies from 0 to 2–3% with the age increase from 35 to 8300 years. In ashes with allophane, it varies from 2 to 11% with the age increase from 1500 to 9000 years (Motenko & Kuznetsova 2009a, Kuznetsova et al. 2011b).

The study of heat capacity showed that the heat capacity values of the volcanic materials range from 750 to 1000 J/(kg·K) (at 0°C). The specific heat capacity values for ashes vary from 1000 to 2200 J/(kg·K) in the thawed and from 900 and 1500 J/(kg·K) in the frozen state with the W increase from 13 to 80% (Kuznetsova & Motenko 2011).

Methods

The particle size distribution was defined with the pipette method (GOST 12536–79). The mineral composition of ashes was determined through the IR absorption spectrometry using the IR Fourier FSM-1201 spectrometer (LOMO, Russia) (Plyusnina 1977). The thermal-conducting properties of ashes were determined with the regular regime method of the first type (Ershov 2004).

Results

These results are from experimental studies of thermal-conducting characteristics of volcanic ashes of different

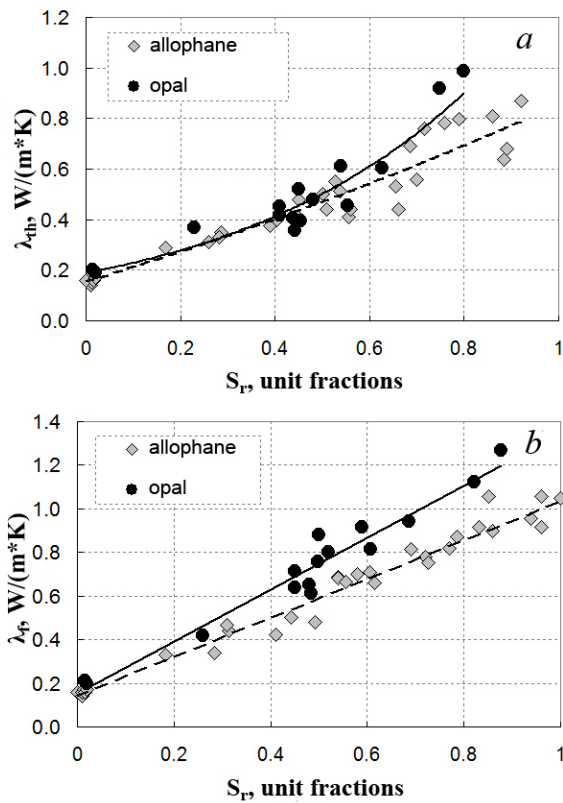


Figure 3. The dependence of heat-conductivity coefficients (λ_{th} and λ_f) on the degree of moisture content (S_r) for volcanic ashes in the thawed (a) and the frozen (b) states depending on the mineral composition.

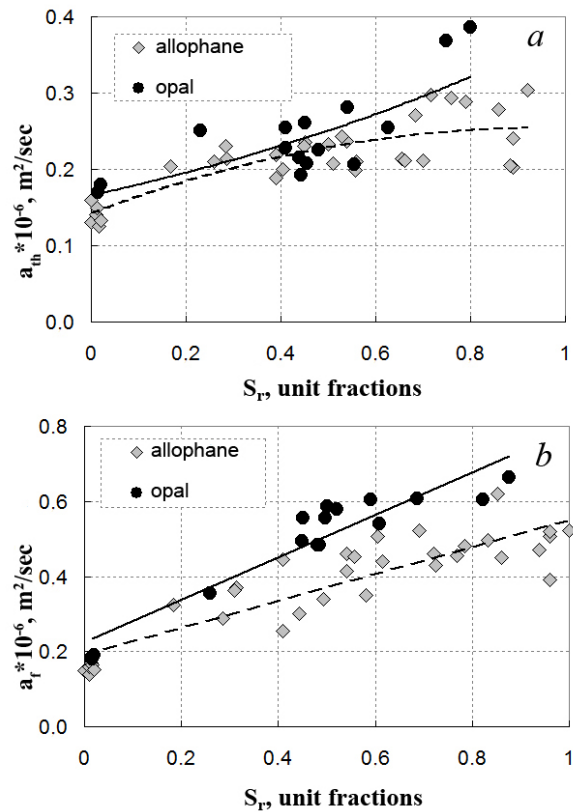


Figure 4. The dependence of thermal-conductivity coefficients (a_{th} and a_f) on the degree of moisture content (S_r) for volcanic ashes in the thawed (a) and the frozen (b) states depending on the mineral composition.

age, mineral composition, humidity, density, and phase composition of water. The thermal conductivity values are 0.13–0.15 W/(m·K) in the absolutely dry state for all ashes studied. The thermal conductivity coefficient for thawed ashes λ_{th} varied from 0.37 to 0.9 W/(m·K), and for frozen ashes λ_f from 0.45 to 1.12 W/(m·K). This refers to a humidity W variation from 10 to 80% and a dry density ρ_d variation from 0.7 to 1.65 g/cm³ (Motenko et al. 2008, Kuznetsova & Motenko 2011).

The degree of saturation S_r is the generalizing parameter in the interpretation of the results for thermal-conducting properties of similarly fine-grained ground (this parameter includes density, porosity, and moisture). The S_r values were calculated (GOST 25100-95) and the dependences of thermal conductivity and thermal diffusivity coefficients on degree of saturation in the thawed and the frozen state were established for the studied samples.

Figure 2 shows all the thermal conductivity values obtained for the studied Kamchatka ashes. The following estimated dependences were calculated as a result of this data treatment:

$$\lambda_{th} = 0.7315 \cdot S_r + 0.133 \quad R^2 = 0.83,$$

$$\lambda_f = 0.9434 \cdot S_r + 0.153 \quad R^2 = 0.87,$$

where S_r – degree of saturation, unit values.

The maximum data amplitude for the thermal conductivity coefficient in the thawed state was 48%, and in the frozen state 40%. This is associated with the differences in the dispersion, the mineral composition, the ground dry density, and, for frozen samples, unfrozen water contents (Motenko & Kuznetsova 2009b, Motenko & Kuznetsova 2011,

Kuznetsova & Motenko 2011).

However, if we consider the differences in the mineral composition, we observe the following. In figures 3 and 4 we present the diagrams of thermal conductivity and thermal diffusivity sensitivity on the degree of saturation for opal and allophane ashes. The values for ashes with acidic glass, the composition of which was identified as opal, occurred in the upper part. The values for ashes with mafic glass, the composition of which was defined as allophane, occurred in the lower part.

In this case, the maximum data amplitude for the thermal-conducting coefficients in the thawed and the frozen states reaches 30%.

For practical purposes, the heat and thermal conductivity coefficients of ashes with different mineral composition can be estimated with the following equations:

For ashes with acidic glass (containing opal):

$$\lambda_{th} = 1.2516 \cdot S_r^2 - 0.065 \cdot S_r + 0.219 \quad R^2 = 0.92,$$

$$\lambda_f = 1.1929 \cdot S_r + 0.153 \quad R^2 = 0.95;$$

For ashes with mafic glass (containing allophane):

$$\lambda_{th} = 0.138 \cdot S_r^2 + 0.562 \cdot S_r + 0.154 \quad R^2 = 0.9,$$

$$\lambda_f = 0.8948 \cdot S_r + 0.142 \quad R^2 = 0.96.$$

The correlation value of the heat conductivity coefficients in the frozen and the thawed (λ_f/λ_{th}) states is very important in addressing practical geocryological problems because heat is transferred by conduction through the frozen and thawed zones in the process of freezing or thawing. Let us look at the dependence of λ_f/λ_{th} on humidity for volcanic ashes (Fig. 5). All values are averaged by three curves. Curve I approximates the data for ashes of marker layers with opal

Table 1. Characteristics of the ashes studied.

Sample No.	Sampling point	Source volcano	Tephra index	Height, m	Depth, m	Mean age, ¹⁴ C years	Moisture content <i>W</i> , %	Hygroscopic moisture <i>W</i> _g , %	Skeleton density ρ_{sp} , g/cm ³	Solid particles density ρ_{sp} , g/cm ³
1	Tolbachinskiy Pass	—*	—*	1630	0.2	1500	38	2.04	1.1	2.69
3					0.55	1500	64	4.3	0.9	2.70
5					0.75	1500	31	1.67	1.3	2.73
7					2.5	1500	30	1.24	1.5	2.80
2	Near Large Fissure Tolbachik Eruption cones (LFTE)	Tolbachik	—*	1330	0.2	30	21	0.3	1.1	2.52
4	Cones in the Kamen Volcano area	—*	—*	1000	0.15	ND	21	0	1.3	2.64
6					0.4	ND	13	0.2	1.5	2.71
9	Moraine complex of the Bilchinok glacier, right slope of the bold mountain	Ksudach	KS-1	695	0.36	1800	42	1.32	0.9	2.47
10					0.56	~2500	37	1.94	1.3	2.79
11	Moraine complex, right slope of the Bilchinok glacier valley	Shiveluch	Sh ₂ Sh ₃ Sh ₅	746	0.45	950	32	0.46	1.1	2.66
12					0.70	1400	36	0.81	1.1	2.61
13					1.2	2550	32	1.0	1.1	2.52
14	Left slope of the Bilchinok glacier valley, at the forest boundary	—*	—*	290	1.15	~6000	34	3.94	0.9	2.79
15					1.32	6850	36	2.52	0.8	—
16					1.5	6850 – 8300	42	4.14	0.9	2.1
17					1.71	8300	11	1.67	1.0	2.71
18	Seismic station on Podkova, Klyucheyskoy volcano slope	Shiveluch	Sh ₈₃₀₀ —*	800	1.8	~9000	69	7.3	0.8	2.46
19					0.65	950	32	0.3	1.0	2.68
20	Klyucheyskoy volcano slope	Klyucheyskoy	—*	800	0.85	950-1400.	31	0.79	1.1	2.75
21					1.17		30	0.87	0.9	2.74

* the specified volcanic ashes do not form key beds because they are the products of minor or remote eruptions. Consequently, they cannot be referred to a particular source volcano or a particular tephra index.

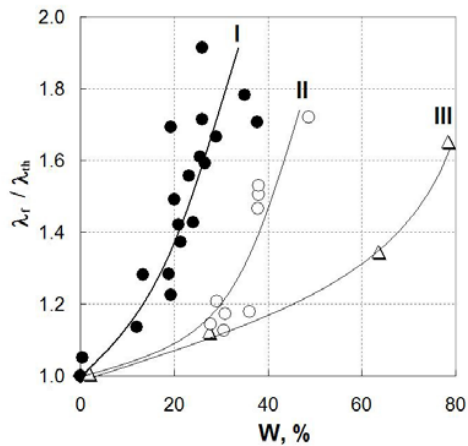


Figure 5. The dependence of the λ_f/λ_{th} correlation on humidity for volcanic ashes with different compositions (I– III– see Text).

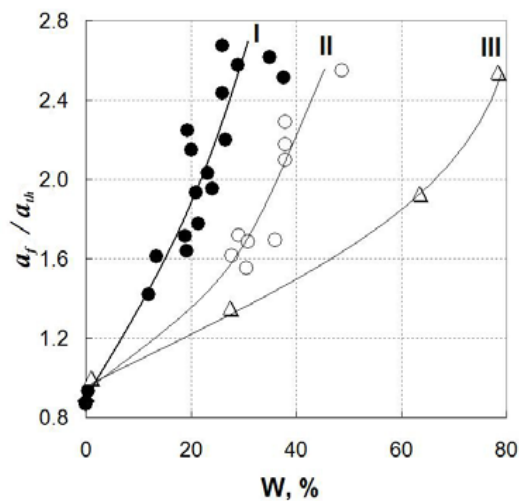


Figure 6. The dependence of the a_f/a_{th} correlation on humidity for volcanic ashes with different compositions (I– III– see Text).

composition. Curves II and III approximate the data for both marker ashes and pyroclastics between them with allophane composition. The curve slope is defined by the correlation between unfrozen water and ice (Kuznetsova & Motenko 2011, Motenko & Kuznetsova 2011). As the diagrams show, the correlations λ_f/λ_{th} and a_{th}/a_f are higher for the ashes with opal as compared to the ashes with allophane.

Similar dependences on moisture were obtained for the a_f/a_{th} correlation (Fig. 6).

Conclusions

The impact of mineral composition on the thermal-conducting properties of Kamchatka volcanic ashes was determined. The generalization of the experimental data on thermal conductivity and thermal diffusivity in the form of sensitivity to the degree of moisture content S_f showed that the thermal-conducting characteristics with the fixed value S_f are higher for ashes with acidic glass, the composition of which was identified as opal. They are lower for ashes with mafic glass, the composition of which was defined as allophane. The correlations λ_f/λ_{th} and a_{th}/a_f are higher for ashes with opal as compared to ashes with allophane.

Acknowledgments

The authors would like to thank the employees of the Mineralogy Department, senior researchers M.F. Vigasina and L.V. Melchakova, for the completion of IR studies. The authors would also like to thank the Volcanology and Seismology Institute of the RAS FEB, namely, Muravev YA.D., Cand.Sc. (Geography), Deputy Director, and V.V. Ponomareva, D.Sc. (Geography), for the opportunity to participate in fieldwork in Kamchatka in 2009–2011 and for valuable consultations.

References

- Bazanova, L.I., Braytseva, O.A., Dirksen, O.V., Sulerzhitskiy, L.D., & Dankhara, T. 2005 Ash falls of major Holocene eruptions at the Ust-Bolsheretsk - Petropavlovsk-Kamchatsky traverse: sources, chronology, frequency. *Volcanology and seismology* 6: 30-46.
- Betekhtin, A.G. 1950. *Mineralogy*. Moscow: Geologicheskaya literatura, 545 pp.
- Dahlgren, R., Shoji, S., & Nanzyo, M. 1993. Mineralogical characteristics of volcanic ash soils. In *Volcanic ash soils - genesis, properties and utilization*. S. Shoji, M. Nanzyo, & R. Dahlgren. Developments in Soil Science 21, Elsevier, Amsterdam: 101–143.
- Ershov, E.D. (ed.). 2004. *Geocryological research methods*. Moscow, izd-vo MGU, 512 pp.
- GOST 12536–79. 1979. *Grounds. Methods of laboratory determination of particle size distribution and micro-aggregate composition*. Moscow: Izd-vo standartov, 18 pp.
- GOST 25100–95. 1996. *Grounds. Classification*. Moscow: Izd-vo standartov, 35 pp.
- Henmi, T. & Wada, K. 1976. Morphology and composition of allophane. *American Mineralogist* 61: 379-390.
- Kuznetsova, E. & Motenko, R. 2011. The influence of allophane appearance on the thermal conductivity of frozen volcanic ashes (Kamchatka). *Euroclay 2011*. Antalya, Turkey, pp. 95-96.
- Kuznetsova, E.P. & Motenko, R.G. 2011. Heat-conducting characteristics of the Kamchatka volcanic ash *Doklady IV konferentsii geokriologov Rossii, 1*. Moscow: Izd-vo MGU: 91–97.
- Kuznetsova, E.P., Motenko, R.G., Vigasina, M.F., & Melchakova, L.V. 2011b. Unfrozen water research in Kamchatka volcanic ash. *Vestnik MGU. Seriya Geologiya* 1: 62-67.
- Kuznetsova, E.P., Motenko, R.G., Vigasina, M.F., & Melchakova, L.V. 2009. IR-spectroscopy and thermal study of different-age volcanic ash. *Ezhegodnyy seminar po eksperimentalnoy mineralogii, petrologii and geokhimii. Vestnik otdeleniya nauk o Zemle RAN* 1 (27): 83.
- Kuznetsova, E.P., Motenko, R.G., Vigasina, M.F., & Melchakova, L.V. 2011a. Relation of mineral composition and volcanic glass transformation velocity. *Doklady pervogo Rossiyskogo soveshchaniya "Gliny 2011"*, Moscow: 75–76.
- Melekestsev, I.V., Kraevaya, T.S., & Braytseva, O.A. 1969. Soil-pyroclastic cover and its value for tephro-

- chronology in Kamchatka. *Kamchatka volcanic facies*. Moscow: Nauka. 61–71.
- Motenko, R.G, Tikhonova (Kuznetsova), E.P., & Abramov, A.A. 2008. Experimental study of thermal properties for frozen pyroclastic volcanic deposits (Kamchatka, Kluchevskaya volcano group). In *NICOP 2008: Proceedings of the Ninth International Conference on Permafrost*. D.L. Kane, K.M. Hinkel (eds.). Institute of Northern Engineering, University of Alaska Fairbanks, 2: 1251-1254.
- Motenko, R.G. & Kuznetsova, E.P. 2009a. Formation of phase composition of water in the frozen volcanic ashes (Kluchevskaya volcano group, Kamchatka). *Proceeding of the eighth international symposium on permafrost engineering*. China: 518-521.
- Motenko, R.G. & Kuznetsova, E.P. 2009b. Estimate of unfrozen water content for frozen volcanic ashes of different ages. *Proceeding of Futuroclays meeting*. Newcastle: 26-27.
- Motenko, R.G. & Kuznetsova, E.P. 2010. Allophane and palagonite as the product of volcanic glass alteration of different ages. *Proceeding of 2010 SEA-CSSJ-CMS Trilateral Meeting on Clays*. Seville, Spain: 142.
- Motenko, R.G. & Kuznetsova, E.P. 2011. The role of ice content and unfrozen water in the heat conductivity assessment of volcanic ash (Kamchatka) *Ice and snow* 2: 99-104.
- Nanzyo, M. 2002. Unique properties of volcanic ash soils. *Global environmental research* 6, 2: 99–112.
- Paterson, E. 1977. Specific surface area and pore structure of allophone soil clays. *Clay minerals* 12: 1–9.
- Plyusina, I.I. 1977. *Infrared mineral spectra*. Moscow: Izdvo MGU, 175 pp.
- Ponomareva, V.V., Churikova, T.G., Melekestsev, I.V., Braitseva, O.A., Pevzner, M.M., & Sulerzhitsky, L.D. 2007. Late Pleistocene- Holocene Volcanism on the Kamchatka Peninsula, Northwest Pacific region. *Volcanism and Subduction: The Kamchatka Region*. American Geophysical Union Geophysical Monograph Series 172: 165-198.
- Shoji, S., Nanzyo, M., & Dahlgren, R. 1993. *Volcanic ash soils: genesis, properties, and utilization*. Elsevier, 288 pp.
- Theng, B.K.G., Russell, M., Churchman, G.J., & Parfitt, R.L. 1982. Surface properties of allophone, halloysite and imogolite. *Clay and Clay minerals* 30, 2: 143–149.
- Wada, K. 1989. Allophane and imogolite. In *Minerals in Soil Environments*. J.B. Dixon and S.B. Weed (eds.), 21: 1051–1087.
- Wada, S-I. & Wada, K. 1977. Density and structure of allophone. *Clay Minerals* 12: 289-298.

Modeling of Active Layer and Runoff: A Case Study from Small Watersheds, Kolyma Water Balance Station

L. Lebedeva

St. Petersburg State University, St. Petersburg, Russia

O. Semenova

State Hydrological Institute, St. Petersburg, Russia

Abstract

Hydrological processes taking place in the Arctic have some distinctive features related to permafrost and the active layer. The goal of this research is to verify the algorithms of the “Hydrograph” hydrological model in permafrost regions. Verification is based on the data derived from the runoff observations and progression of the active layer at the Kolyma Water Balance Station (KWBS). Analysis of the KWBS observation materials indicated that the active layer thickness varies across a wide range within a limited territory and depends on the landscape type. This research identified three major landscape types, which differ considerably in the regime and progression of active layer formation. They are stone taluses (golets), tundra open woodland, and swamp larch forest. The systematization of the properties of their soil and vegetative covers made it possible to assess the values of the “Hydrograph” model parameters without the application of calibration methods. The active layer dynamics and the dynamics of the runoff formation were jointly modeled for the KWBS venues using the same set of values of the model parameters. The estimated maximum thawing depths were in satisfactory accordance with the observed data. However, the estimated start of freezing occurrence is considerably later than the observed one. Analysis of the results of the runoff hydrograph modeling indicated that those model algorithms that describe the process of water filtration into frozen ground during the snow-melting period do not reflect natural processes adequately enough and require further development. This is caused by the fact that the role of the surface runoff during snow-melt is exaggerated, while the amount of water that percolates through the soil and freezes in it is underestimated. The results of runoff modeling in the summer period under the conditions of a thawed active layer are evaluated as satisfactory. This paper shows the importance of observation data for the improvement of the runoff formation models in the permafrost zone. The situation can be considerably improved by reestablishing monitoring at the Kolyma Water Balance Station.

Keywords: active layer; “Hydrograph” model; Kolyma Water Balance Station; permafrost; runoff formation.

Introduction

The arctic hydrologic cycle, which is currently being exposed to the influence of both climate change and anthropogenic disturbances, is the subject of numerous investigations. Permafrost is one of the major factors in runoff formation in the polar regions.

Active layer formation essentially depends on the properties of a particular landscape. The difficulty of studying hydrological processes lies in the need to consider the energy component of the hydrologic cycle. For instance, the heat balance of permafrost determines the following processes: water infiltration into permafrost, formation of permafrost aquiclude, water exchange between surface and subsurface waters, and seasonal runoff redistribution due to freezing of liquid precipitation or the melted water in the ground.

Our knowledge of arctic hydrologic processes remains incomplete, and that is why mathematic formulas presented as models of various processes are developed and tested based on the data produced by field observations.

Many researchers work to develop a physically based distributed hydrological model that describes the energy and moisture dynamics under conditions of a certain watershed at the required level of detail. This is made to estimate river runoff characteristics and evaluate the variable states of a permafrost zone basin.

For instance, Canadian researchers (Pomeroy et al. 2007)

worked on the design and improvement of the physically based Cold Region Hydrological Model (CHRM). The CHRM describes in detail such processes as snow accumulation, wind-blown snow redistribution, snow melting (with the employment of energy balance equations), water infiltration into permafrost, and evaporation. The peculiarity of the approach suggested by the Canadian scientists is that the model parameters are not calibrated in the course of calculations. Presently, the CHRM offers only a limited opportunity for estimating the runoff from the territory of the whole basin, despite the fact that it has an elaborate algorithm for hydrological process modeling at a specific point.

The US investigations of the runoff formation processes in permafrost regions are carried out in Alaska. A deterministic distributed model, ARHYTHM, was developed for the basins of the Kuparuk and Innait rivers based on field research aimed at the description of thermal and hydrological processes in the arctic territories (Zhang et al. 2000). The ARHYTHM authors revealed the hydrological importance of such processes as phase transitions in soil, snow melting, summer evapotranspiration, and formation of the active layer.

Russia has long-term experience in special hydrometeorological observations in the network of water balance stations located in various geographical zones of the country.

The Kolyma Water Balance Station (KWBS) located in the upper reaches of the Kolyma River is unique for mountainous permafrost areas. A wide range of special observations have been conducted there since 1948. The data collected at the station were applied to develop, test, and improve hydrological models multiple times (Gusev et al. 2006, Kuchment et al. 2000, Semenova 2010).

Our country's research experience in the field of runoff modeling in permafrost areas (Gusev et al. 2006, Kuchment et al. 2000, Semenova 2010) indicates that temperature changes and phase transitions in soil exert a significant influence on hydrological processes. They determine the possibilities of water infiltration into soil and the formation of surface, soil, and underground runoffs.

The "Hydrograph" hydrological model used in this research was applied multiple times in estimating runoff in the polar regions (Pomeroy et al. 2010, Semenova & Vinogradova 2009, Vinogradov et al. 2011, Lebedeva & Semenova 2011). The calculations presented in these investigations made it possible to conclude that the "Hydrograph" model, in case its algorithms are further developed, will have a great potential to be applicable in both research and practical tasks in permafrost zones, including watersheds that partially or totally lack observation data.

Goals and Objectives

The need to consider the influence of permafrost on hydrological processes leads to the fact that the algorithms utilized in models must be capable of functioning both under permafrost conditions and outside them. To meet this requirement, they must be based on general physical principles of runoff formation instead of local empirical relationships. The deterministic distributed "Hydrograph" hydrological model employed in this research was constructed on these principles (Vinogradov 1988, Vinogradov & Vinogradova 2010).

According to the physically based approach, active layer formation as well as runoff formation at a watershed should be described by means of one and the same set of values of the model parameters. This becomes possible if the physical properties of landscapes (measured in the field) are used as parameters.

The goal pursued in this research is to verify the algorithms of the "Hydrograph" hydrological model in permafrost areas employing the data of the observations over the runoff and over variable states of the active layer.

The following procedures were carried out to achieve this: analysis of seasonal thawing depths of ground under different conditions at the Kolyma Water Balance Station (KWBS), systematization of landscape properties, determination of model parameters, and estimation of the thawing depth as well as the runoff.

A small watershed of the Kontaktovy Stream (21.6 km²) at KWBS was selected as a research target.

The systematization of the parameters describing the thawing process and runoff formation under the given natural conditions allowed us to use the values of these parameters to model water discharge in four larger basins under similar conditions in northeastern Russia (Semenova & Lebedeva 2012). The modeling process is facilitated by the fact that

the conditions of the Kolyma station are representative of the extensive territory of northeastern Siberia (Boyarintsev 1988).

The "Hydrograph" Model

The "Hydrograph" model is a deterministic hydrological model with distributed parameters. It describes runoff formation processes based on their physical features.

The concepts that form the basis of the modeling scheme and its algorithms are described in detail in the works following Vinogradov (1988), Vinogradov & Vinogradova (2010), and Vinogradov et al. (2011). A description of the "Hydrograph" model in these collected works may be found in the paper by Semenova & Lebedeva (2012).

The major advantages of the "Hydrograph" model are:

- universality (i.e., the opportunity to apply it to basins of any size without changing model structure);
- use of physical properties of landscapes observed in nature as the model parameters;
- use of data of standard meteorological observations (precipitation, air temperature, and air humidity deficit) as input.

The mathematical description of runoff formation processes of the model includes canopy interception; snow cover formation; snow melting and snowmelt release; surface retention; soil heat and moisture dynamics; formation of surface, soil, and underground runoffs; and evaporation and transformation of surface and channel runoffs.

The concept of runoff elements used in the "Hydrograph" model for spatial discretization of basins is one of the key ones. The basin territory is divided into several conditionally homogeneous parts called runoff elements. It is assumed that the characteristics of soil, vegetation, relief, and other components of the landscape are constant within each runoff element, while the runoff formation process is uniform. A considerable part of the model parameters is determined separately for each runoff element and in this way they are being systematized.

Materials

General information on KWBS

The Kolyma Water Balance Station (KWBS) is located in the upper reaches of the Kolyma River in the zone of continuous permafrost. Standard as well as special and experimental hydrometeorological measurements were carried out at the station from 1948 to 1997. Special and experimental measurements included the monitoring of the active layer formation, snow measuring surveys at different landscapes, monitoring of evaporation on various underlying surfaces, and others (Fig. 1) (Observation materials... 1948–1990). Water balance observations were suspended at the KWBS since 1997. Only meteorological observations and runoff observations at seven streams are presently carried out.

The local relief is mountainous. The slope height varies from 800 to 1700 m. The mean annual air temperature in the period from 1950 to 1990 was -11.6°C, and the annual precipitation sums ranged from 250 to 440 mm (Zhuravin 2004).

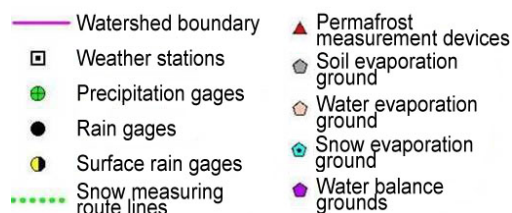
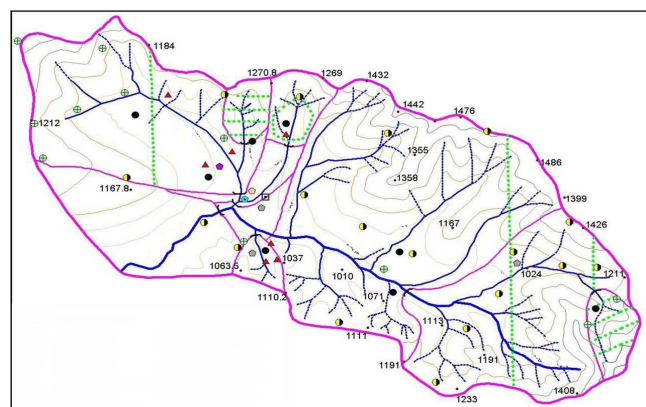


Figure 1. Map of the Kolyma Water Balance Station.

The KWBS landscapes

Six major types of landscape are found at the KWBS according to Korolev (1982): golets (stone taluses), mountain tundras, moss and lichen larch open woodland, thickets of cedar elfin wood, sparse larch forests with bushes, and swamped sparse stands of larch with bushes.

Relying on this classification as well as on the description of soils, vegetation, and geological structure, and on other information that accompanies the data provided by observations, it is reasonable to distinguish three runoff elements: golets (stone taluses), tundra open woodland, and swamp larch forest (Fig. 2).

Golets occupy the upper and steep parts of slopes where only crustose lichens grow. Mountain tundras and open woodlands are spread in saddles as well as in the middle parts of slopes. Sparse larch trees, cedar elfin wood, moss, and lichens grow here. Swamp larch forests occupy flat valleys and terraces.

The active layer observations

Approximately 20 permafrost measurement devices (thaw tubes) were in operation at the KWBS in different periods of time. Their period of observations ranged from 3 to 25 years.

Analysis of the data given by observations over the dynamics of soil thawing and soil freezing indicated that active layer depth exhibits considerable variability across the station's territory and depends mainly on the type of landscape. Figure 3 illustrates soil profile characteristics of two different landscapes and their typical progressions of thawing and freezing.

The maximum depth of the active layer registered during the entire observation period at KWBS was 1.7 m, while according to the expedition data by Bantsekina (2003) it reached 2.3 m. Such depths are typical of golets with undeveloped soil profile and no vegetation (Fig. 3). Water easily seeps through rock debris down to the aquiclude formed by the permafrost table and rapidly flows down into a channel. Thus, dry conditions are created. The minimum

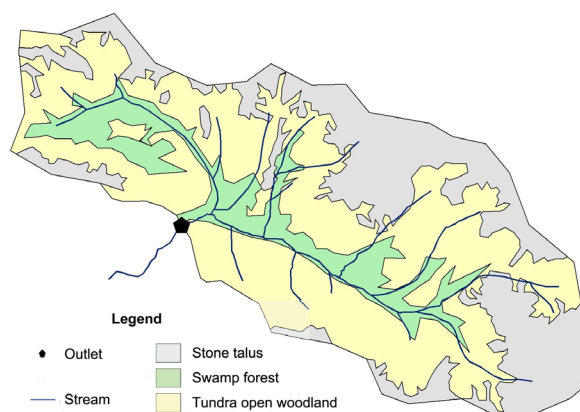


Figure 2. Major landscapes on the territory of the KWBS.

thawing depth (.6 m) is observed in swamp forests with a considerable peat layer in their soil profile (Fig. 3) and soil surface covered with a moss layer, which impedes heat exchange and favors the development of moist conditions.

The runoff observations

Water discharge was measured at nine watersheds of the KWBS with the area ranging from 0.27 km² to 21.6 km² and the mean heights ranging from 985 to 1370 m. Boyarintsev (1988) notes that small watersheds at the KWBS reflect local peculiarities of the runoff formation that are typical of certain landscapes, while larger basins are representative of the entire region's territory.

When the soil begins to thaw directly after snow melting in spring, melt waters form a surface runoff everywhere except for the territories occupied by golets. A considerable part of melt water percolates through the frozen ground and freezes. This ice constitutes an additional source of water in summer; that is why runoff is observed in the warm season even when precipitation does not fall for a long time (Boyarintsev 1988). The described process of seasonal water distribution is most developed in the golets area where almost the whole volume of melt water seeps into the ground.

Results

The active layer modeling

Two permafrost measurement devices (thaw tubes) reflecting the peculiarities of two major types of soil thawing were selected to model the active layer depth. One of them is installed at the slope of the southern aspect in the golets zone at the height slightly above 1000 m, while the other is located within a swamp forest of the stream valley at the height below 900 m. The observation data covering the period of 1977–1978 are available for the permafrost measurement device in the golets zone, and the data of the period from 1980 to 1984 are available for the second device in the swamp forest.

Physical properties of soils and of vegetation are the main parameters of the "Hydrograph" model that determine soil moisture and heat dynamics. Twenty estimated soil layers (ESL) with the thickness of 10 cm were distinguished in each soil profile to perform estimations. Each estimated soil layer is characterized by a set of parameters that reflect both its thermal and hydrological properties. The values of the

Table 1. The values of soil parameters of the “Hydrograph” model.

	P, DQ	D, kg/m ³	HC, J/kg*°C	TC, W/m*°C	MWRC, DQ	IC, mm/min
Moss	0.80	900	1930	0.5	0.60	10
Peat	0.80	1750	1930	0.8	0.50	0.3
Clay with rock fragments	0.50	2650	750	1.7	0.15	1
Stone talus	0.55	2600	750	2.3	0.13	1.8
Parent rock	0.50	2650	750	2.3	0.13	1.8

See the notation in the text

parameters were determined based on literature as well as on the description of soil profiles that accompanied observation materials (Observation materials... 1959–1991, Guide... 1988, Bantsekina 2003).

Table 1 presents the values of such parameters as porosity (P), density (D), maximum water retention capacity (MWRC), infiltration coefficient (IC), thermal conductivity (TC), and heat capacity (HC). These values characterize soil layers in the dry state.

According to the observation materials at the KWBS (1959–1990), the active layer is in the air-dry state by the time it is covered by snow in autumn. Meanwhile, all the ground pores below it are filled with ice. Based on this, the initial values of ice content in 6 upper ESLs of a swamp forest and in 16 ESLs of the golets area were determined as equal to the values of their maximum water retention capacity, while in the lower ESLs they equaled the porosity values.

Estimates of both the moisture content (ice content) and the temperature in an ESL are done simultaneously. Meanwhile, the values of infiltration coefficient, thermal conductivity, and heat capacity of an ESL are specified according to the moisture content (ice content) in the layer.

The maximum water retention capacity varies in a wide range from 0.13 in the golets area to 0.50 in the peat horizon of soil of the swamp open woodland. Thermal conductivity takes values from 2.3 to 0.8 W/m*°C, while heat capacity takes values from 750 to 1930 J/kg*°C in the soils of golets area and those of forest, respectively.

Figure 4 shows a comparison of the estimated and the observed active layer depths for the selected permafrost measurement devices. The maximum thawing depth measured is in good agreement with the maximum thawing depth calculated. However, freezing according to the model estimates occurs considerably later, as compared to the observation data. The assumed reason for this is that the estimated heat-insulating influence of the snow cover in autumn was significantly exaggerated.

The runoff modeling

The runoff of the Kontaktovy Stream (the area is 21.6 km²) was modeled for the period from 1971 to 1984. The values of soil and vegetation parameters used were the same as in the estimates of the active layer depth. Figure 5 shows

a comparison of the observed and the estimated runoff hydrographs for the period of 1981–1982.

The observed mean annual runoff was 287 mm for the modeling period of 14 years, while the estimated mean annual runoff was 220 mm. The mean error is 24%. The maximum difference between the observed and the estimated values of annual runoff reached 49% in 1983, which was one of the driest years (precipitation sum was only 307 mm). This is attributed to the fact that the absolute errors in dry years exerted a more considerable influence, which increases the relative error. The errors less than 20% are observed in wet years (e.g., 1972, 1975, 1977, 1979, 1981, and 1984). Overall, the model slightly underestimated runoff.

As Figure 5 shows, the maximum deviation of the estimated water discharge from the observed water discharge occurs during the snow-melting period of the year. According to the estimates, all the melt water forms a rapid surface runoff above the soil that is still frozen, including the golets territory (40% of the watershed’s area). Therefore, the flood reaches a high peak directly by the end of snow-melting period. The research by Bantsekina (2003) based on the field study at the experimental site of the golets zone at the KWBS shows that all the water produced at the beginning of a snow-melting period freezes in the active layer and forms infiltration ice. Channel runoff starts only when 90% of the seasonally thawed layer heats above 0°C.

The calculated and the observed hydrographs are in good agreement with each other in the second half of summer as well as in autumn.

Soil moisture content plays an important role in the permafrost zone; it both accumulates water at a watershed and regulates such moisture and heat flows as evaporation and phase transitions in the active layer (Hinzman et al. 2003). It is still an important task to integrate the calculation algorithms of soil thawing and water infiltration into frozen ground into hydrological models. Despite the fact that such algorithms were designed to approach specific tasks (Arzhanov et al. 2007, Kudryavtsev 2004, Perlshteyn 2009), only a few efforts were made to directly incorporate the description of these processes into hydrological models (Gray et al., 2001, Kuchment et al. 2000, Zhang et al., 2008), including the “Hydrograph” model (Vinogradov et al. 2011). The major difficulty encountered in the permafrost zone is to implement such hydrological properties of soil layers as the maximum water retention capacity and the infiltration coefficient in the process of water phase transitions. Conceptualization of these processes in modern models relies more on the data from empirical observations. For instance, in the research of Lebedeva & Semenova (2011), the comparison between the algorithms that describe the water infiltration processes into frozen soil and the algorithms that are used in the CRHM model (Pomeroy et al. 2007) and in the “Hydrograph” model was made (Vinogradov et al. 2011). The comparison indicated that similar results in runoff estimates may be obtained when conceptually different approaches are employed. According to the authors of this research, the basis for the accomplishment of the set task may be formed only if the data of the observations over soil moisture content and runoff at small watersheds with uniform landscape parameters are jointly analyzed, while the measured hydrological properties of soil are simultaneously systematized.

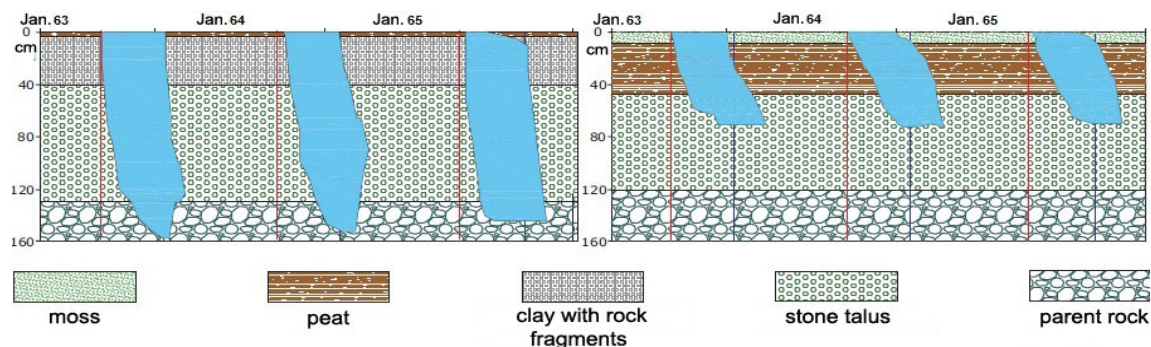


Figure 3. The soil profile and the typical thawing process in the stone talus (on the left) and in the soils of a swamp forest (on the right).

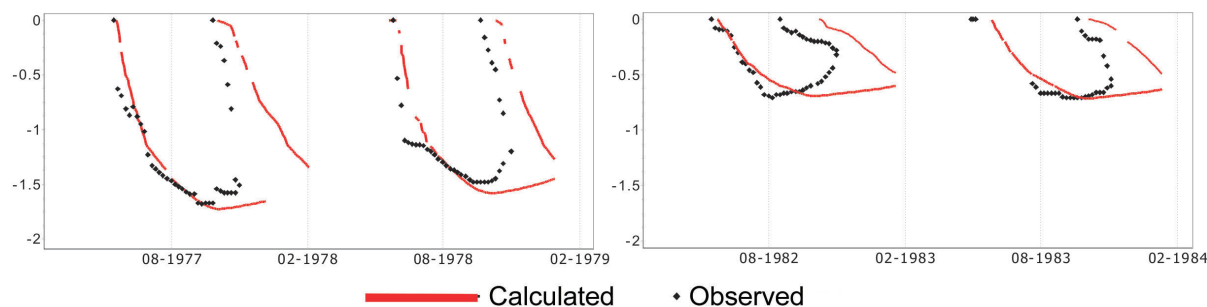


Figure 4. The estimated and observed thawing depth of soil in the stone talus (on the left) and in a swamp forest (on the right).

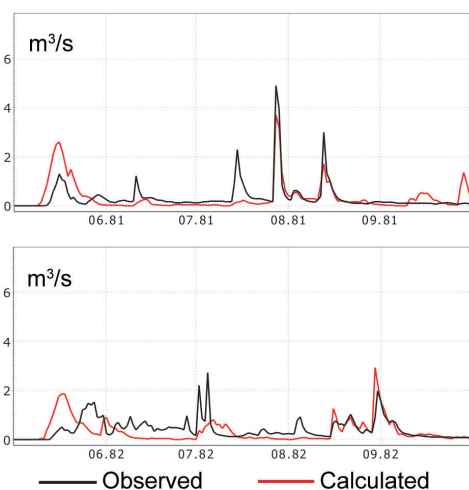


Figure 5. The estimated and the observed runoff hydrographs (m^3/s), the Kontaktovy Stream, 1981–1982.

In conclusion, it may be inferred that the model parameters representing hydrophysical properties of frozen soils considerably determine the results of the runoff estimate. Presently we cannot attain satisfactory results in the runoff modeling, despite the fact that they were attained in the modeling of thawing processes. The research requires further development of algorithms of water infiltration into frozen soil of the golets zone.

Conclusions

The goal of this research was to assess the capacity of the “Hydrograph” model to reflect the runoff formation in the permafrost zone. The data of observations over soil thawing were applied to make the parameters more accurate. The

particularity of the “Hydrograph” model lies in the fact that physical properties of soil and vegetation cover are used as parameters.

Analysis of the data on the dynamics of the active layer revealed that its thickness depends on the type of soil and vegetation, through which the height, inclination, and aspect of a slope indirectly influence the thawing process. The active layer depth exhibits high variability within the territory of the KWBS, varying from 0.6 m in swamp forests and stream valleys to 1.7 m on bare stone taluses and upper slopes.

The results of the active layer depth modeling showed that such model parameters as soil porosity, maximum water retention capacity of soil, its heat capacity, and thermal conductivity play an important role in the estimate of the heat dynamics in soil. They may be determined based on information on the soil profile and maintain steady values.

The estimated thawing depth of soil in summer coincides with the observed values at both landscapes, while the estimated complete freezing of the active-layer in the cold period occur considerably late in comparison with the observed values. Potentially this problem can be solved by the specification of the algorithm estimating the thermal-insulating influence of snow.

Water discharge in the outlet of the Kontaktovy Stream was modeled with the use of the same values of the model parameters as when estimating the depth of the active layer. The modeling results show that the algorithm block of the model describing the process of water filtration into frozen ground during the snow melting period does not reflect the actual processes adequately enough and requires further development. The results of runoff modeling in the summer period under the condition of a thawed active layer are evaluated as satisfactory.

Model estimates based on long-term detailed observations over the processes in the permafrost zone represent a necessary step toward a reliable parameterization of physically based models. The soil and vegetation parameters corrected and systematized in the process of this research may be applied to evaluate the runoff in the basins with similar natural conditions (Semenova & Lebedeva 2012).

This work shows the importance of observation data for the improvement of the runoff formation models in the permafrost zone. The situation can be considerably improved by reestablishing monitoring at the Kolyma Water Balance Station

Acknowledgments

The investigation was carried out with the support of the Russian and German O. Schmidt Laboratory for Polar and Marine Research.

References

- Arzhanov, M.M., Eliseev, A.V., Demchenko, P.F., & Mokhov, I.I. 2007. Modeling of fluctuations in the temperature and hydrologic regime of the near-surface permafrost with the use of climatic data (reanalysis). *Kriosfera Zemli* vol. 11, No 4, 65-69.
- Bantsekina, T.V. 2003. The hydrothermal regime peculiarities of the seasonally thawing layer of coarse clastic slope sediments in the spring and summer period (Case of the upper Kolyma upland): Dissertation abstract of the Candidate of Sciences (geography). Yakutsk, 23 pp.
- Boyarintsev, E.L. 1988. The azonal factors of rainfall runoff formation on the territory of the Kolyma Water Balance Station. *Trudy DVNIGMI*, 135th edition: 63-97 (in Russian).
- Guide for ground temperature regime forecast in Yakutia*. 1988. In-t merzlotovedeniya SO AN SSSR, Yakutsk.
- Gusev, E.M., Nasonova, O.N., & Dzhogan, L.Ya. 2006. Runoff modeling at small watersheds of permafrost zone based on the SWAP model. *Vodnye Resursy* vol. 33, No 2: 133-145. (in Russian).
- Hinzman, L.D., Kane, D.L., & Yoshikawa, K. 2003. Soil Moisture Response to a changing climate in arctic regions. *Tôhoku Geophysical Journal* 36(4):369-373.
- Korolev, Yu.B. 1982. The hydrological role of the Upper Kolyma vegetation. *Izvestiya AN SSSR. Ser. Biol.*, № 4: 516-529 (in Russian).
- Kuchment, L.S., Gelfan, A.N., & Demidov, A.I. 2000. Runoff formation model at watersheds of permafrost zone (Case of the Upper Kolyma). *Vodnye Resursy* vol. 27, No 4: 435-444 (in Russian).
- Kudryavtsev, S.A. 2004 Estimates of freezing and thawing processes based on the "Termoground" program. *Reconstruction of cities and geotechnical construction*. - SPb.-M. - No 8: 83-97.
- Lebedeva, L.S. & Semenova, O.M. 2011. Evaluation of climate change impact on soil and snow processes in small watersheds of European part of Russia using various scenarios of climate. *Technical Documents in Hydrology* (in review).
- Lebedeva, L.S. & Semenova, O.M. 2011. Comparison of two approaches to simulate soil water dynamics in the permafrost landscapes. *EGU General Assembly 2011, Book of abstracts*.
- Observation materials of the Kolyma Water Balance Station*. 1949-1985, edition 1-27. Magadan (in Russian).
- Perlshteyn, G.Z. 2009. Use of simplified models for evaluation of thermal state of cryolithozone. *11th Sergeevskie chteniya*, Moscow, 208-212.
- Pomeroy, J., Semenova, O., Fang, X., Vinogradov, Y., Ellis, C., Vinogradova, T., MacDonald, M., Fisher, E., Dornes, P., Lebedeva, L., & Brown, T. 2010. *Wolf Creek Cold Regions Model Set-up, Parameterisation and Modelling Summary* Centre for Hydrology, Report 8.
- Pomeroy, J.W., Gray, D.M., Brown, T., Hedstrom, N.H., Quinton, W.L., Granger, R.J., & Carey, S.K. 2007. The cold regions hydrological model: a platform for basing process representation and model structure on physical evidence. *Hydrological Processes* 21, 2650-2667.
- Semenova, O.M. & Vinogradova, T.A. 2009. A universal approach to runoff processes modelling: coping with hydrological predictions in data-scarce regions. New Approaches to Hydrological Prediction in Data-sparse Regions. *Proc. of Symposium HS.2 at the Joint IAHS & IAH Convention*, Hyderabad, India, September 2009.
- Semenova, O.M. & Lebedeva, L.S. 2012. Estimate of Runoff Engineering Characteristics with Shortage of Data of Hydrometeorological Observations in North-Eastern Russia. *Collected works of the 10th international conference on Permafrost* (in Russian).
- Vinogradov, Yu.B. & Vinogradova, T.A. 2010. *Mathematical modeling in hydrology*. M.: Akademiya, 366 pp. (in Russian).
- Vinogradov, Yu. B., Semenova, O.M., & Vinogradova, T.A. 2011. An approach to the scaling problem in hydrological modelling: the deterministic modelling hydrological system. *Hydrological Processes*, n/a. doi: 10.1002/hyp.7901.
- Vinogradov, Yu.B. 1988. *Mathematical modeling of runoff formation processes. Experience in critical analysis*. L.: Gidrometeoizdat, 312 pp. (in Russian).
- Zhang, Y., Carey, S.K., Quinton, W.L., Janowicz, J.R., & Flerchinger, G.N. 2010. Comparison of algorithms and parameterizations for infiltration into organic-covered permafrost soils. *Hydrological and Earth System Science*, 14, 729-750.
- Zhang, Y., Carey, S., & Quinton, W., 2008. Evaluation of the algorithms and parameterizations for ground thawing and freezing simulation in permafrost regions. *J. Geophys. Res.*, 113, D17116, doi:10.1029/2007JD009343.
- Zhang, Z., Kane, D.L., & Hinzman, L.D. 2000. Development and Application of a Spatially Distributed Arctic Hydrologic and Thermal Process Model (ARHYTHM). *Journal of Hydrological Processes* 14(6), 1017-1044.
- Zhuravin, S.A. 2004. Features of water balance for small mountainous watersheds in East Siberia: Kolyma Water Balance Station case study. *Northern Research Basins Water Balance IAHS publ.*, 290, 28-40.

Gradient of Seasonal Thaw Depth along the Yamal Transect

M.O. Leibman, A.V. Khomutov, P.T. Orekhov
Earth Cryosphere Institute, SB RAS, Tyumen, Russia

O.V. Khitun
Komarov Botanical Institute, RAS, St. Petersburg, Russia

H. Epstein, G. Frost
University of Virginia, Charlottesville, USA

D.A. Walker
University of Alaska Fairbanks, Fairbanks, USA

Abstract

Seasonal thaw depth was measured in 2007–2010 along a transect spanning the main bioclimatic subzones of arctic tundra on the Yamal Peninsula and Franz Josef Land. Data obtained at the end of the thaw season at Vaskiny Dachi and Bely locations in the central Yamal were used to calculate thaw rates and determine dates of maximum thaw depth. Zonal change of seasonal thaw depth across bioclimatic subzones is observed only when similar terrain types are compared. The range of seasonal thaw depths measured in different lithological and geobotanical conditions within one bioclimatic subzone greatly exceeds the difference when comparing similar terrains in adjacent subzones, and is comparable to variability in thaw depth along the entire 1,500-km transect.

Keywords: bioclimatic subzone; lithology; monitoring; seasonal thaw; vegetative cover.

Introduction

The seasonally thawed layer is one of the most important and most studied characteristics of permafrost (Mackay 1977, Leibman 1998, Yershov 1998, and many others). The north of West Siberia is covered by a large amount of field data demonstrating the spatial variability of this parameter (Melnikov et al. 2004). The results of seasonal thaw depth monitoring conducted at the Earth Cryosphere Institute (ECI SB RAS) research polygons “Nadym,” “Marre-Sale,” and “Vaskiny Dachi” are compared in a number of articles (Leibman et al. 2011, Melnikov et al. 2004, Vasiliev et al. 2008 a, b). These sites are located in the Yamal Peninsula region and are part of the Russian component of the CALM international project.

The seasonally thawed layer study along the Yamal transect (Fig. 1) was carried out within the Greening of the Arctic (GOA) and Circumpolar Active Layer Monitoring (CALM) projects of the International Polar Year (IPY), and the Yamal Land-Cover and Land-Use Change (LCLUC) project of the University of Alaska Fairbanks (Walker et al. 2009, 2011b, 2012). In addition to the original CALM site at Vaskiny Dachi, which was established in 1993, two sites were set up next to the Obskaya-Bovanenkovo railroad at Laborovaya (near the 147 km distance mark). Three additional sites were established at Vaskiny Dachi, three sites near Kharasavey, two sites at Bely Island near the Popov weather station, and two sites on Hayes Island of the Franz Josef Land Archipelago near the Krenkel weather station. Most sites were 50x50 m in size; the main CALM site at Vaskiny Dachi is 100x100 m; and one site at Bely Island is 25x25 m. All sites were subdivided into two groups: a group of “zonal” sites, determined as mesic moderately drained, with relatively fine-grained deposits, including all the silty, loamy, and clayey sites; and a group of sandy sites (Table 1). The Russian transect is unique because both sandy and relatively fine-grained conditions exist at all of the locations

along the climate gradient. This is rarely found in other regions of the Arctic, including Alaska and East Siberia. Two sites at Hayes Island are separated from the transect by the island’s position far from the mainland as well as by the mainly sandy composition of the near-surface deposits. These sites are poorly drained and contain a relatively high amount of clay and silt particles in the sand, and thus they are discussed under a “zonal” group.

The transect crosses the main bioclimatic subzones (Fig. 1) shown in the circumpolar vegetation map (Walker et al. 2005): from south to north, subzones E (Laborovaya), D (Vaskiny Dachi), C (Kharasavey), B (Bely Island) and A

Table 1. Soil texture (%) and volumetric soil moisture (%) at the sites within the transect. Sandy sites are highlighted.

Site code*	Sand	Silt	Clay	VSM
La1	18	59	23	37
La2	94	4	3	20
VD1	28	62	9	30
VD2	38	54	8	30
VD3	93	5	3	24
Kh1	23	54	23	35
Kh2	72	22	6	21
BO1	38	44	18	13
BO2	51	42	7	32
BO3	84	12	4	8
Kr1	60	33	7	38
Kr2	81	16	2	33

* La, Laborovaya; VD, Vaskiny Dachi; Kh, Kharasavey; BO, Bely Island; Kr, Hayes Island.

** Grain size at Bely Island was not obtained at the same sites as those with active layer measurements, yet landscape features and thus general characteristic probably are quite close.

(Hayes Island). The transect length on the mainland Yamal is 635 km, and the Hayes Island site is located 900 km further north of Bely Island.

Climate along the Transect

The climatic parameters controlling the seasonal thaw depth generally follow the latitudinal gradient. The weather station data from south (Salekhard) to north (Marre-Sale,

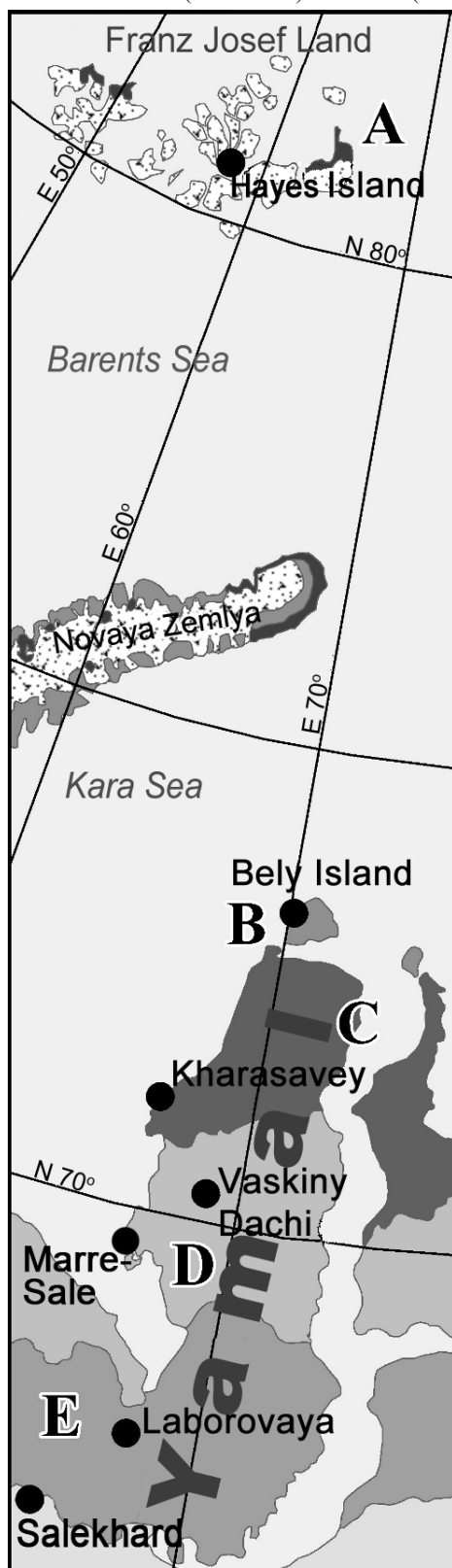


Figure 1. Study locations within the bioclimatic zones of the Yamal transect.

Popov, and Krenkel) are characterized by an almost linear decline in annual and summer mean temperatures. The meridional mean annual air temperature gradient for the Yamal Peninsula is approximately 3–4°C in different years over the 775-km distance between the Salekhard and the Popov weather stations (Pogoda Rossii website).

Table 2 shows climatic controls for the seasonal thaw depth for the first year of measurement during the GOA project and for the years of repeated monitoring at the Popov (Bely Island site) and Marre-Sale (the nearest to the Vaskiny Dachi site) weather stations. We think that the duration of the summer season as well as summer precipitation are important controls in addition to the thaw index (sum of monthly mean temperatures above 0°C in degree months).

Thaw Depth Controls

It is known that the air temperature only partially controls the seasonal thaw depth because thaw is affected by many other environmental factors, namely soil texture, drainage, composition, and thickness of the above-ground vegetative cover (Walker et al. 2003).

The Yamal plain has features that distinguish it from other plains of the Arctic: the thick layer of Quaternary deposits in its central and northern parts, relatively high elevations, and more intensive dissection of the terrain. The southern part of Yamal is in the Ural foothills with low-mountain terrain and bedrock located close to the surface. The range of lithologies is wide and includes coarse-grained deposits, sand, clay, and peat. Active slope processes and abundance of patterned-ground formations create a well-developed drainage structure. Hilltops with vast barren areas of wind-blown sands are widely distributed as well. The wide variety of surface deposits contributes to the unusually wide range of seasonal thaw depths. Additional complications are associated with saline marine sediments in the area north of the Yuribey River, which did not undergo thawing during the Holocene climatic optimum. Moreover, the upper layers are continuously moved down slopes, bringing the saline sediments to the surface as a result of slope processes. Saline soils cause difficulties in measuring thaw depths with standard methods and in the determination of the notion of the thaw depth itself. For example, the difference between the depth of positive ground temperatures and the depth of the first ice lens occurrence can be 50–80% in saline clays

Table 2. Climatic parameters in the initial year of measurements.

Weather station	Start of thaw	End of thaw	Thaw period (days)	Thaw index (degree months)	Summer precipitation, (mm)
Salekhard*	26.05.07	12.10.07	137	46.9	312
Marre-Sale**	15.06.07	17.10.07	124	29.4	126
	01.06.10	18.10.10	140	16.5	186
Popov	20.06.09	14.10.09	117	15.3	246
	05.06.10	28.09.10	115	9.9	146
Krenkel	28.06.10	26.08.10	60	0.85	No data

* Nearest to Laborovaya (about 170 km to the south).

** Nearest to Vaskiny Dachi (about 100 km to the southwest).

(Leibman 1998). For this reason, we excluded points with saline clay in the active layer from this discussion.

These thaw depth controls combined with normal variation in site features that are present at any location in the Arctic, such as the soil texture, surface and slope drainage, terrain dissection, wind erosion, and the intensity of slope processes, create exceptionally high variability of the thaw depth within the framework of bioclimatic zonation.

Brief Description of Study Locations

The two study sites at Laborovaya are located in depressions where the coarse-fragmented materials of the Urals are found quite deep from the surface and cannot hinder the measurement of the seasonal thaw depth. Consequently, this location has high vegetative cover, even on the sandy alluvial site.

At Vaskiny Dachi, significant terrain dissection caused by landslides and thermal erosion processes and large areas of windblown sands are observed. Consequently, the vegetative cover is reduced over much of the area.

The Kharasavey site is located in the coastal zone of the Kara Sea. Marine sands prevail within the site, but the surface here is lower than in Central Yamal, and dissection of the land by drainage networks is not as pronounced. Relatively good drainage conditions are mainly associated with the proximity to the coast. Peatlands are quite common and form a polygonal pattern organizing drainage network. Yet on clayey soils the surface is moist, with water filling polygonal troughs.

The Bely Island location is close to sea level. It is quite wet on internal portions of terrace surfaces and flat slopes composed of silty and clayey deposits with patterned ground features, but relatively well-drained sites are also common along the edges of the low sandy terraces. This is the reason for a significant range of seasonal thaw depths.

Hayes Island is located far from the Yamal Peninsula and should not be considered a continuation of the Yamal transect per se because such conditions are not found in the continental part of Eurasia. The local geology consists mainly of sandstone and intrusive volcanic materials that differ significantly from the marine sediments of the Yamal Peninsula. Most vegetative cover is composed of biological soil crusts. Small vascular plants and mosses are concentrated in shallow depressions associated with patterned-ground features. Active-layer deposits at both sites fall into the range of silty sand to sandy loam. Thus the degree of drainage is the main factor determining the small differences in the seasonal thaw depth. These in their turn are defined by the microtopography of the surface, including patterned forms.

Results of Seasonal Thaw Monitoring

Seasonal thaw depth measurements were completed at different sites in different periods of the warm season. To identify zonal regularities, field measurements were adjusted to the maximum seasonal thaw depth value, with the use of both quantitative methods, and empirical thaw rate curves obtained at Bely Island and Vaskiny Dachi (Table 3).

The diagrams (Figs. 2–4) show the average of maximum seasonal thaw depth values at each site in 2007 and 2010—

Table 3. Average of maximum thaw depths in the year of initial measurement at the sites along the transect.

Sites	Year	Average maximum thaw depth (cm)	
		Sandy	Zonal
Laborovaya	2007	110	84
Vaskiny Dachi	2007	113	82
Kharasavey	2008	92	75
Bely Island	2009-2010	100-90	54-50
Hayes Island	2010	33	

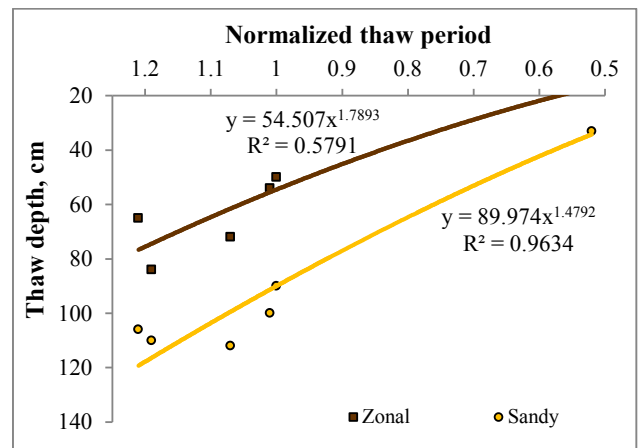


Figure 2. Dependence of the average (for a particular site) thaw depth in zonal and sandy sites on the normalized against the period of observation average duration of the thaw period in 2007 and 2010.

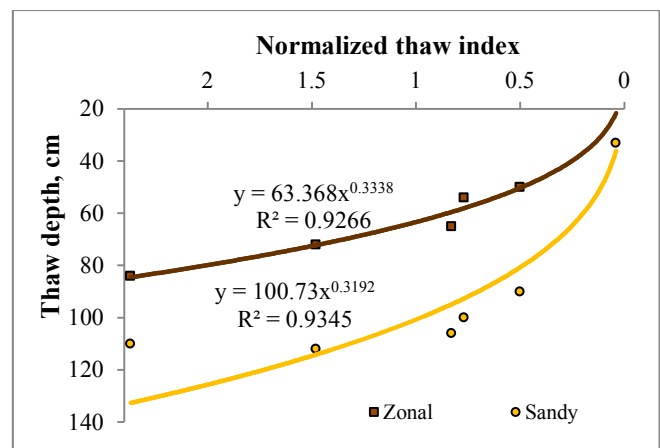


Figure 3. Dependence of the average (for a particular site) thaw depth in sandy and zonal sites on the normalized against the period of observation average thaw index in 2007 and 2010.

the years with different major climatic parameters given in Table 2. To operate with non-dimensional quantities, we divided each parameter into an average value of the data array to obtain “normalized” values ($x_{norm} = x_i/\bar{x}$). As the diagrams show, the thaw period duration is more important than the thaw index. Further north, the reduction of the duration of the warm period is accompanied by the reduction of the thaw depth in similar lithological conditions. The increase of the sum of summer precipitation also slightly increases the seasonal thaw depth, with even higher values for clayey soils as compared to sandy and silty.

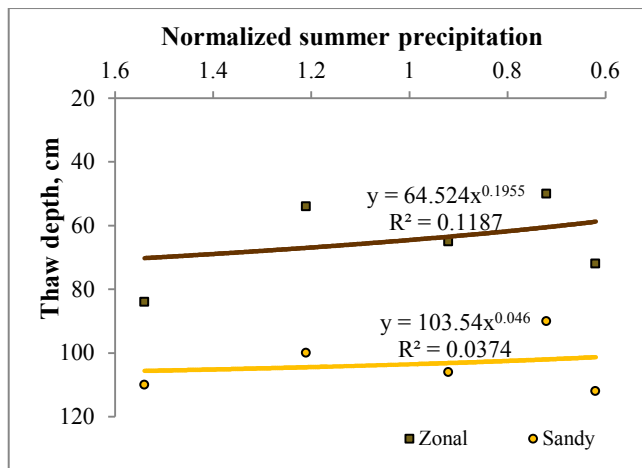


Figure 4. Dependence of the average (for a particular site) thaw depth in sandy, silty and clayey deposits on the normalized against the period of observation average summer precipitation in 2007 and 2010.

Vaskiny Dachi site

The duration of the warm period and thaw index are related to the average thaw depth values at four sites at Vaskiny Dachi (Table 4).

The CALM site has variable soil conditions, the VD1 site is mainly clayey, the VD2 site is sandy and silty yet well vegetated, and the VD3 site is sandy with a sparse vegetative cover. Differences in soil texture and ground cover explain the differences of the seasonal thaw depths. The impact of climatic parameters can be estimated by comparison of the average thaw depth values for relatively homogeneous conditions within each location.

The 17% increase of the duration of the warm period in 2010 compared to 2007 was accompanied by a sharp reduction of the thaw index. The seasonal thaw depth slightly increased at the site with mixed conditions (CALM site) and slightly decreased at the other sites. The main difference is that a significant area of the CALM site is occupied by windblown sands, while the other sites are well vegetated. In addition, 2010 had higher precipitation (Table 2). Consequently, the general increase of thaw depths at the CALM site can be explained by infiltration at the surfaces that lack vegetation.

The thaw rate monitoring at Vaskiny Dachi shows the following results. We provisionally assign August 31, 2011, as having 100% of thaw depth (maximum thaw) measurements. On August 12, 2011, the thaw depth measurements as compared to August 31 (19-day time span) make up on average 96% of the maximum thaw in the range of 75–100%. The daily mean air temperature for this period is around 8°C. After August 17, 2011, the daily mean air temperature decreased to 4°C. The measurements on August 17 (14-day time span) were on average almost 99% of the maximum thaw in the range of 82–100%. Consequently, measurements on August 31 can be adequately assumed to be very close to maximum under a 10-day average air temperature of about 4°C.

Bely Island site

The thaw depth measurements on Bely Island were made three times in 2009 and two times in 2010 (Table 5). In 2009, the measurements at the sandy site as of July 27 showed

Table 4. Climatic parameters (according to data from the Marre-Sale weather station) and average seasonal thaw depths at four sites of Vaskiny Dachi in 2007 and 2010.

Year	Thaw period (days)	Thaw index (degree months)	Thaw depth (cm)			
			CALM	VD1	VD2	VD3
2007	124	29.4	85	72	72	112
2010	140	16.5	87	67	65	106
$\Delta\%$	117	56	102	93	90	95

Table 5. Climatic parameters (according to the data from the Popov weather station) and average seasonal thaw depths (cm) at two sites on Bely Island at different dates in 2009 and 2010.

Date	Thaw period (days)	Thaw index (degree months)	Thaw depth (cm)		
			BO CALM 1	BO CALM 2	
27.07.09	117	15.3	74	32	
15.09.09			100	54	
15.10.09			98	54	
15.09.10	115	9.9	90	50	
15.10.10			88	47	

48 to 83% of the maximum thaw observed on September 15th, with the average values being 74% and the positive air temperature range exceeding +3°C. The measurements on October 15 (mean daily air temperature fell below 0°C on October 14) showed the beginning of upward freezing. In 2010, the mean daily air temperature fell below 0°C on September 28. Consequently, the upward freezing reached 3 cm on average by October 15 (the date of the second measurement), with air the temperature fluctuating between -5 and +2°C. Upward freezing on the clayey site at some points reached 12 cm. Nonetheless, thawing (up to 6 cm) continued at several points at this site as well.

The analysis of vegetation did not identify the reason for the simultaneous occurrence of these two different processes under identical climate conditions. The analysis of species plant composition at the CALM2 site on Bely Island discussed by Khitun et al. (2011) and Leibman et al. (2011) allows a qualitative estimate of the thermophysical vegetation properties, and could explain the different responses of separate sites to the lowering of the air temperature. We suggest that most of the points where upward freezing was active corresponded to the wettest sites with boggy cottongrass tundra, dense grass (70–90% cover, including abundant litter), discontinuous moss mat, with frequent domination of *Amblystegiaceae s.l.* mosses.

With almost identical durations of the warm period in 2009 and 2010, the thaw index varied significantly (Table 5). This caused differences in average thaw depth of about 10%.

Thermal regime and upward freezing

It was established that in the areas with mean annual ground temperature below -3°C, upward freezing begins earlier than downward freezing (Grechishchev 2002, Grech-

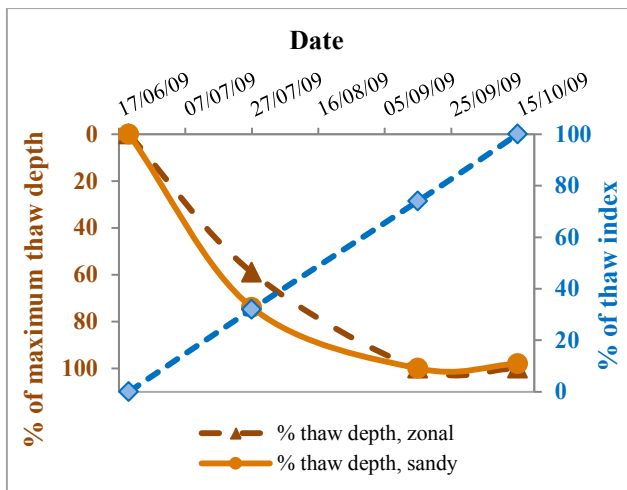


Figure 5. Thaw rates according to the results of the 2009 monitoring at two Bely Island sites.

ishchev & Grechishcheva 1997). According to our data, the ground temperature at the depth of zero annual amplitude at the Bely Island and Vaskiny Dachi sites varies from -4 to -7°C. Upward freezing here starts earlier than from the ground surface.

Figure 5 shows the thaw rates calculated as the percent of average measured thaw depth (\bar{x}_i) relative to the average of the maximum thaw depth observed on September 15 ($\bar{x}_i/\bar{x}_{Sept} \cdot 100$). The curve indicates that upward freezing starts after September 15 (with the average daily temperature down to +3°C). This is shown by the bend of the curve based on the measurement data from October 15 (Fig. 5) and the thaw depth reduction on the same date as compared to the records from September 15 (Table 5).

It can be seen from the thaw index line calculated as thaw index at the specific date (TI_i) related to maximum thaw index, in percent ($TI_i/TI_{max} \cdot 100$) that maximum thaw is achieved after about 75% of the thaw index occurred. In 2010, 75% of the thaw period was achieved after 86 days from the start of the warm period (Table 2) on August 30, which means that active-layer depth measurements on September 15 showed less than maximum because upfreezing already started. On October 15, it reached up to -12 cm for BO CALM2 site (-3 cm on average for both sites).

Maximum thaw in the sandy site is achieved earlier than in the zonal one. This is evidently associated with lower latent heat consumption for phase transition.

Seasonal Thaw Depth Gradient

The results of the seasonal thaw depth measurements quantitatively confirm the zonal regularity in the change of this parameter. Figure 2 shows that while moving southward from bioclimatic subzone A (Hayes Island) to subzone E (Laborovaya), the average thaw depth in sandy deposits with a discontinuous vegetative cover increases from 33 cm (the predicted value of 64 cm if drained sand surfaces are found on Hayes Island) to 110 cm in the Laborovaya area (up to 120 cm according to individual measurements). When examining only the Yamal part of the transect for which the most reliable data are provided (Vaskiny Dachi in the center and Bely Island in the north), it turns out that

the average thaw depth on sands with sparse ground cover increases from 90 cm in subzone B to 120 cm in subzone D, and in clayey deposits from 50 to 70 cm, respectively; while moving from subzone B (73°20'N) to subzone D (70°20'N), separated by approximately 330 km.

Similar research conducted in Alaska (Walker et al. 2003, 2011a) demonstrates a much narrower range of thaw depth variation (25–62 cm) within three bioclimate subzones E, D, and C, with the thaw index changing from 34 to 9 degree-months while moving northward. This air temperature range corresponds to subzones D, C, and B on the Yamal transect (Table 2) with the average thaw depth range of 50–113 cm. Such differences between the Yamal and the Alaska transects are mostly due to the more clayey composition and thicker organic layer of Alaskan deposits. These differences compensate for greater surface vegetation biomass along the Yamal transect as compared to the Alaskan transect (Walker et al. 2012). The higher biomass of Yamal ground cover is enclosed in a thinner organic layer and thus has higher density and less insulation effect.

Therefore, zonal variations of the average thaw depth are up to 10 cm per 100 km for Yamal, and 30–40 cm or 2–2.5 cm per 100 km for the whole transect (approximately 1500 km along the meridian). Such a “longspun” gradient accentuates the ambiguity of the impact of air temperature on the thaw depth.

Due to the extremely low heat supply, the thaw depth in the vicinity of Hayes Island associated with a very sparse vegetative cover, is comparable to the thaw depth in peat or in very mossy sites of Central Yamal. Individual measurements in vegetated polygon troughs show the thaw depth of 28.5 cm on average (approximately 30% lower than adjacent more poorly vegetated centers of polygons), despite the fact that the moss thickness in the troughs does not exceed a few centimeters.

Conclusions

The zonal change of climatic controls influences the seasonal thaw depth directly and indirectly. In similar terrains, the average thaw depth noticeably declines from the south to the north.

Thaw stops and upfreezing starts when the air temperature falls to 3–4°C (about 75% of the duration of the thaw period).

The thaw depth associated with the particularities of local natural conditions within one bioclimatic subzone make up 30–40 cm, the same as when moving 1500 km to the north, at the farthest contours of tundra bioclimatic subzones.

Acknowledgments

This study was possible thanks to the field grant of the SB RAS, the USA National Science Foundation, Grant No. ARC-1002119 to George Washington University and No. OPP-0120736 to the University of Alaska Fairbanks, and the National Aeronautics and Space Administration grant No. NNG6GE00A and No. NNX09AK56G to the University of Alaska Fairbanks. The authors are grateful to N.I. Nikonov, the chief of the Popov hydrometeorologic station, for performing active-layer measurements in September–October.

References

- Grechishchev, S.E. 2002. Peculiarities of mechanical stability of thawing slopes in cryolithozone *Kriosfera Zemli* №4, pp.49-53 (in Russian).
- Grechishchev, S.E. & Grechishcheva, O.V. 1997. Peculiarities of mechanism of the transient layer formation and embankment stability in cryolithozone *Results of fundamental studies of the Earth Cryosphere in Arctic and Subarctic*: Transactions of International conference, Pushchino, April 23-26, 1996. Novosibirsk: Nauka, pp. 214-221 (in Russian).
- Khitun, O.V., Ermokhina, K.A., Leibman, M.O., & Khomutov, A.V. 2011. Plant indicators of the seasonally thawed layer thickness on Bely Island *Materials of the Forth conference of Russian geocryologists*, M.V.Lomonosov Moscow State University, 7-9 June 2011, Moscow, Universitetskaya kniga, 2011, 3: 350-356 (in Russian).
- Leibman, M.O., Moskalenko, N.G., Orekhov, P.T., Khomutov, A.V., Gameev, I.A., Khitun, O.V., Walker, D., & Epstein, H. 2011. Interrelation of cryogenic and biotic components of geosystems in cryolithozone of the West Siberia along the "Yamal" transect. V.M.Kotlyakov (editor-in-chief) *Polar Cryosphere and continental waters*. Paulsen Editions. Moscow-Saint-Petersburg, pp.171-192 (In Russian).
- Leibman, M.O. 1997. Cryolithological peculiarities of the seasonally thawed layer on slopes, associated with the cryogenic landslide process. *Kriosfera Zemli*, 2:50-55 (in Russian).
- Leibman, M.O. 1998. Active layer depth measurements in marine saline clayey deposits of Yamal Peninsula, Russia: procedure and interpretation of results *Permafrost*. Proceedings of the Seventh International Conference on Permafrost, June 23-27, 1998, Yellowknife, Canada: 635-639.
- Mackay, J.R. 1977. Probing for the bottom of the active layer. Report of activities, Part A *Geological Survey of Canada*, Paper 77-1A: 327-328.
- Melnikov, E.S., Leibman, M.O., Moskalenko, N.G., & Vasiliev, A.A. 2004. Active-Layer Monitoring in the Cryolithozone of West Siberia. *Polar Geography*, Vol. 28, No. 4: 267-285.
- Pogoda Rossii website: <http://meteo.infospace.ru/>.
- Vasiliev, A.A, Drozdov, D.S., & Moskalenko, N.G. 2008b. Permafrost temperature dynamics of West Siberia in context of climate changes. *Kriosfera Zemli* № 2, pp.10-18 (in Russian).
- Vasiliev, A.A, Leibman, M.O., & Moskalenko, N.G. 2008a. Active Layer Monitoring in West Siberia under the CALM II Program. *Permafrost*, Proceedings of the Ninth International Conference on Permafrost, Fairbanks, USA, June 29-July 3 2008. 2: 1815-1820.
- Walker, D.A., Jia, G.J., Epstein, H.E. et al. 2003. Vegetation-Soil-Thaw-Depth Relationships along a Low-Arctic Bioclimatic gradient, Alaska: Synthesis of Information from the ATLAS Studies. *Permafrost and Periglacial Processes*, 2003. 14. P.103-123.
- Walker, D.A., Epstein, H.E., Raynolds, M.K. et al. 2012. Environment, vegetation and greenness (NDVI) along the North America and Eurasia Arctic transects. *Environmental Research Letters*. 7:(2012) 015504 (17 p.) doi:10.1088/1748-9326/7/1/015504.
- Walker, D.A., Kuss, H.P., Epstein, H.E., Kade, A.N., Vonlanthen, C., Raynolds, M.K., & Daniëls, F.J.A. 2011a. Vegetation of zonal patterned-ground ecosystems along the North American Arctic Transect. *Applied Vegetation Science* 14:440-463.
- Walker, D.A., Forbes, B.C., Leibman, M.O. et al. 2011b. Cumulative effects of rapid land-cover and land-use changes on the Yamal Peninsula, Russia. *Eurasian Arctic Land Cover and Land Use in a Changing Climate* VI (New York: Springer) 206-236 DOI 10.1007/978-90-481-9118-5_9.
- Walker, D.A., Leibman, M.O., Epstein, H.E. et al. 2009. Spatial and temporal patterns of greenness on the Yamal Peninsula, Russia: Interactions of ecological and social factors affecting the Arctic normalized difference vegetation index. *Environmental Research Letters* 4 16 doi:10.1088/1748-9326/4/4/045004.
- Walker, D.A., Raynolds, M.K., Daniëls, F.J.A. et al. 2005. The Circumpolar Arctic Vegetation Map. *Journal of Vegetation Science* 16 267-282 10.1658/1100-9233(2005)016[0267:TCAVM]2.0.CO;2.
- Yershov, E.D. 1998. *General Geocryology* (Studies in Polar Research). New York: Cambridge University Press, 580 pp.

Deposits of Gas Hydrates as a Potential Source of Mercury on the Continental Slope and Shelf in Northeast Sakhalin

L.N. Luchsheva

InfoGeoProekt, Moscow, Russia

A.I. Obzhairov, A.S. Astakhov

V.I. Il'ichev Pacific Oceanological Institute, FEB RAS, Vladivostok, Russia

Abstract

Increased mercury content in oil and gas is typical for deposits generated in deep faults of the Earth's crust. Mercury is a prime pollutant of the hydrosphere as well as an element indicating geological processes. A lot of plumes and deposits of gas hydrates are to be found in the oil- and gas-rich shelf and slope of East Sakhalin. Therefore, studies of mercury content in water and bottom sediments in the area are of high priority. Flameless atomic absorption spectrophotometry was used to measure mercury content. Abnormally high concentrations of mercury in sea water (up to 1.8 mkg/l) were registered in 1998 and 2000 in containment areas of gas plumes. The amount exceeded the threshold limit value and background concentration limit by 18-fold and 35-fold, respectively. An abnormally high mercury content was recorded for bottom sediments in the area of the cold gas plume Fakel Obzhairova. The mercury content in the upper layer (470 ng/g) exceeded the background concentration limit by 30-fold. The highest mercury content in the sediments was registered in the layer containing gas hydrates (1830 ng/g) and deeper. It was concluded that the mercury anomalies in the upper layer of bottom sediments indicate the containment of inactive gas plumes. Layers containing gas hydrates serve as lithologic screens that detect flows of endogenous mercury. Natural destruction and industrial mining of gas hydrates may lead to intensive emissions of endogenous mercury into the shelf waters and degradation of the environment.

Keywords: gas hydrates; gas plumes; mercury; methane; Sakhalin shelf.

Introduction

Increased mercury concentrations occur in the environment not as the result of human impact, but from mercury degassing processes within the mineral resources of the Earth. Increased content of mercury in oil and gas is typical for deposits generated in deep regional faults of the Earth's crust (Ozerova & Pikovsky 1962). This toxic metal is a prime pollutant of the hydrosphere; its consumption with products containing polluted water may threaten human life.

For this reason, areas of the ocean shelf that have intensive hydrothermal gas activity cause profound concerns due to the risk of mercury contamination of sea water, bottom sediments, and waterborne organisms. Recently, undersea deposits of gas hydrates have been considered as a prospective source of fossil fuel. Fields of gas hydrates can, however, serve as a source of mercury in the ocean environment.

In 1998 and 2000, as part of the KOMEX Russian-German program and the Methane Monitoring in the Sea of Okhotsk sub-program, we studied the mercury content in sea water and bottom sediments in East Sakhalin and the adjacent part of the continental slope (Luchsheva et al. 2002).

The samples were analyzed by means of wet ashing with aqua regia and active oxidizing agents: potassium permanganate and potassium persulphate. In order to separate dissolved and suspended forms of mercury, the samples of sea water were filtered through membrane filters with the pore diameter of 0.45 μm . Concentration of dissolved mercury was determined by formation of complexes with potassium 8-mercaptoquinolate for codeposition of complexes of mercury ion with 8-mercaptoquinoline (Virtsavs et al. 1977).

Flameless atomic absorption spectrophotometry was employed to measure mercury content in the samples of sea water and bottom sediments. The procedure was conducted with the use of the following mercury analyzers: Hiranuma HG-1 (Japan) and Yulia-2 (Russia) with mercury detection limits of 1×10^{-3} - 5×10^{-4} mkg, with relative error of the method of 3-10% and data control of the standard solution (0.050 mg Hg/ml) produced at Kanto Chemical Co. (Japan).

Research conducted on the shelf and the slope of East Sakhalin in the containment areas of cold gas plumes and gas hydrates beds revealed a periodic occurrence of abnormally high concentrations of mercury in sea water. The data showed that for some years the level of total content of mercury in sea water in these areas amounted to 1.8 mkg/l, thus exceeding the threshold limit value for fishery water by 18-fold (0.1 mkg/l) and exceeding the regional background concentration limit by 35-fold (0.05 mkg/l) (Luchsheva et al. 2002). The portion of the most toxic form of dissolved mercury found in abnormally high concentrations amounted to 80-99%.

According to our data, the mercury content in the eastern shelf of Sakhalin mainly comes from widespread cold gas plumes (Luchsheva et al. 2000). Most plumes have specific locations, but their mode of eruption is not regular. Active periods of the plumes of natural gas depend on the seismotectonic regime of the Hokkaido-Sakhalin fold region.

During the periods of active drainage, the plumes emit large amounts of methane in the shelf waters, creating sound-scattering acoustic anomalies and abnormal concentrations of methane in the water (up to 3000-6000 nl/l) in the lower part of water mass (Obzhairov 1993, Obzhairov et al. 2002).

Monitoring of underwater gas plumes on the eastern shelf

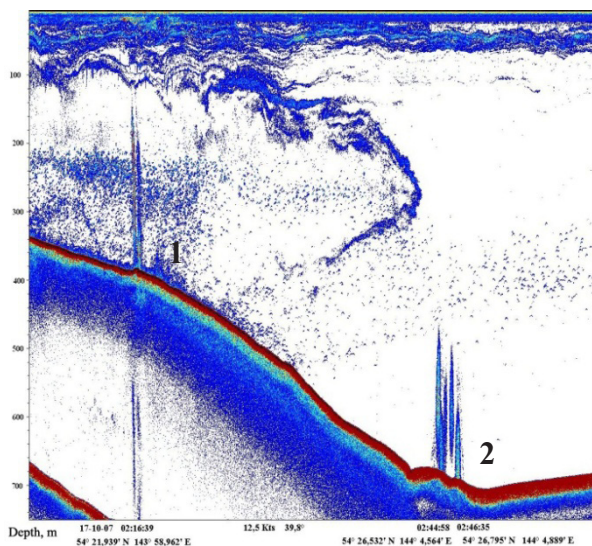


Figure 1. Acoustic fathogram of the methane flow over the gas plumes Gizella (1) and Fakel Obzhirova (2) on the northeast slope of Sakhalin.

of Sakhalin and the adjacent part of the continental slope was conducted in 1998–2000 as part of the Methane Monitoring in the Okhotsk Sea program. It revealed a high occurrence of contrasting acoustic anomalies in the area (Fig. 1).

The intensity of the gas drainage of the plumes changes over time, either growing or diminishing. Figure 2 demonstrates the increase of methane content (3- to 16-fold) in the benthic layer of water in the drainage zones of the three gas plumes on the Sakhalin shelf during the period of increased activity.

Our studies have shown that the active periods of the gas plumes start with emissions of increased amounts of mercury into the benthic water layer. Thus, for the period from 1998 to 2000, the total mercury concentrations near the mouth of the gas plumes grew two- and three-fold (Fig. 3). In 1998, the maximum concentration of mercury content in the benthic water layer (130 ng/l) was recorded near the mouth of the methane plume, when it reached a peak of activity in 2000 (Fig. 2).

Fakel Obzhirova is an active gas plume (see Fig. 1); it was thoroughly studied during marine expeditions as part of the KOMEX Russian-German project. This plume is located at a depth of 700 m on the continental slope of Northeast Sakhalin. The mercury content in sediments of the lithologic column in the area close to the plume proved to be abnormally high in all granulometric types, the distribution of mercury concentrations in sediments being sharply differentiated.

According to our data, the average regional background concentration of mercury in the upper layer of bottom sediments on the East Sakhalin shelf equals 25 ng/g (Luchsheva et al. 2002). Directly in the areas of intensive release of gas jets, the level of mercury concentrations in the upper sediment layer can be relatively low and only exceed the background concentration two- and three-fold (Kot 1996).

However, the mercury content (470 ng/g) in the upper layer of the sediments in the lithologic column, located in the area of Fakel Obzhirova gas plume, was abnormally high and exceeded the regional background concentration value

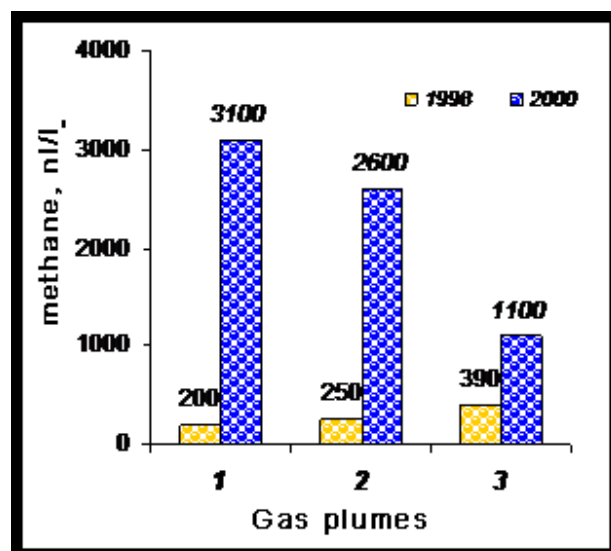


Figure 2. Interannual variations in methane content in the benthic water layer near the mouth of the gas plumes on the eastern shelf of Sakhalin (1998 and 2000).

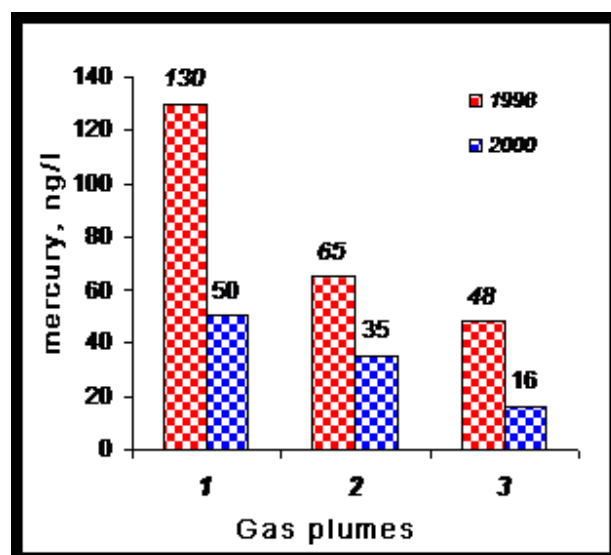


Figure 3. Variations in the levels of total mercury content in the benthic water layer near the mouth of the gas plumes on the eastern shelf of Sakhalin (1998 and 2000).

by 30-fold. A layer of sediments containing gas hydrates was registered at a depth of 2.5 m. The level of mercury content for this layer, and underlying sediments was the highest (up to 1830 ng/g) (Fig. 4).

Gas hydrates are known to be common in oceans and the permafrost zone. They are very sensitive to increasing temperature and decreasing pressure. In addition, the presence of natural hydrates may indicate the deeper lying deposits of oil and gas (Obzhirov 2003).

In the given lithologic column, a considerable irregularity of the vertical portion of mercury concentrations in the layers of the sediments overlying the layer of gas hydrates is associated with different granulometric composition of the sediments. The highest concentrations of mercury were found in the interbedded layers of the most loosely bound, pelito-aleuritic sediments (the average of 970 ng/g). The mercury content in the layer of aleuropelitic sediments filled

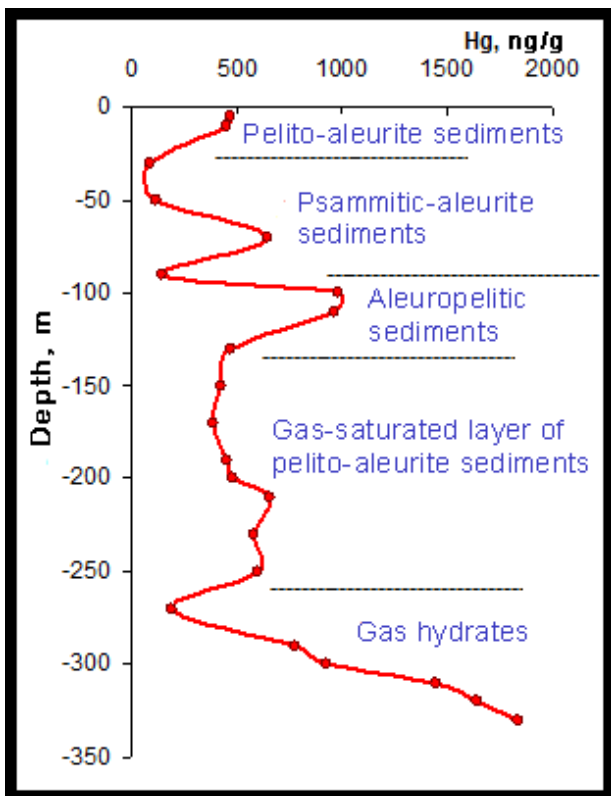


Figure 4. The distribution of mercury (ng/g) in bottom sediments of the lithologic column (Ge 99-29) in the area of the gas plume Fakel Obzhirova. Granulometric types of sediments are cited from Derkachev et al. (2002).

with gas hydrates varied from 780 to 1830 ng/g (the average of 1320 ng/g), and the value sharply increased with depth.

The described principle of distribution of mercury concentrations in the layer of gas hydrates and the underlying sediments is indicative of the constant inflow of mercury-laden endogenous fluids coming from the lower parts of the faults. The layer of sediments containing gas hydrates serves apparently as a shielding horizon (fluid-buffer), which prevents migration of oil and mercury-laden fluids into the upper horizons of the sedimentary rock from the deep fault zone. Periods of degassing of the gas plumes, formed in the given fault are, apparently, closely associated with its geomorphic processes.

The mercury content in the layers of the lithologic column with aleuopelitic sediments (an average of 520 ng/g) was significantly lower than in loosely bound pelito-aleuritic sediments. The lowest mercury content was registered in the coarsest, psammitic-aleurite sediments (an average of 140 ng/g).

The distinctive feature of the given lithologic column is the high degree of saturation of bottom sediments with carbonate concretions and crusts (Derkachev et al. 2002). Authigenic carbonates are known to perform a stabilizing role in the preservation of deposits of gas hydrates (Astakhov et al. 1993), apparently, as well as in the isolation of endogenous mercury-laden fluids.

The layered structure of the sediments in the given lithologic column (see Fig. 4) reflects, apparently, the processes of mixing and fractionation in bottom sediments

determined by an active phase of the Fakel Obzhirova gas plume. Coarse-grained sediments with the insignificant specific absorption surface are the first to develop near the mouth of the plume; therefore the observed mercury content in these sediments is the lowest.

Loosely bound sediments with a larger specific absorption surface absorb more mercury and settle much slower. Therefore, not only the nature of lamination and the thickness of the layers of coarse and loosely bound sediments of the given lithologic column, but also their mercury composition may reliably reflect the duration of the time intervals between the active and dormant states of the Fakel Obzhirova gas plume.

During our study of the lithologic column in the area of the powerful Fakel Obzhirova gas plume, the surface layer of the sediments was composed of aleuopelitic sediments with an abnormally high mercury content. The formation of this contrasting mercury anomaly in the surface layer of the sediments could only happen providing the dormant state of the plume. This mercury anomaly indicated the location of the gas plume as inactive while no contrasting methane anomalies occurred in the water mass during the period.

In this regard, it may be concluded that the detection of contrasting mercury anomalies in the upper layer of the bottom sediments on the East Sakhalin shelf may indicate the drainage areas of inactive gas plumes, as well as deposits of gas hydrates.

When the gas plumes become active, deposits of gas hydrates start to dissociate and endogenous mercury is released. As a result, the mercury enriches the overlying bottom sediments and escapes into the sea water and the atmosphere. The intense emission of mercury into the marine environment may result from industrial mining of gas hydrates. This fact should be taken into account when considering the prospects of development of the deposits on the sea shelf from the sanitary, hygienic, and environmental points of view.

References

- Astakhova, N.V., Obzhirov, A.I., Astakhov, A.S. et al. 1993. Authigenic carbonates in the areas of gas anomalies in the marginal seas of East Asia. *Tikhookeanskaya Geologiya (Pacific Geology)* 4: 34-40 (in Russian).
- Derkachev, A.N., Obzhirov, A.I. Borman, G. et al. 2002. Authigenic mineral formation coupled with cold gas-fluid emanations on the bottom of the Sea of Okhotsk. In *Conditions for formation of bottom sediments and related mineral resources in marginal seas*. Likht, F.R. (ed.). Vladivostok: Dalnauka, 47-60 (in Russian).
- Kot, F.S. 1996. Mercury in the area of Paramushirsky Vent (Kuril Ridge). *Environmental and Biogeochemical Research in the Far East*. Vladivostok: Dalnauka, 140-143 (in Russian).
- Luchsheva, L.N., Obzhirov, A.I., & Biebow, N. 2000. The distribution of mercury and methane in the water column at the East Sakhalin shelf and slope, Sea of Okhotsk. *Abstracts of 3rd Workshop on Russian-German Cooperation in the Sea Okhotsk - Kurile Island Arc System*. Moscow, April 17-20, 2000: 40.

- Luchsheva, L.N., Obzhairov, A.I., & Konovalov, Yu.I. 2002. Distribution of mercury. In *Methane Monitoring in the Sea of Okhotsk*. Obzhairov, A.I. (ed.). Vladivostok: Dalnauka, 95-113 (in Russian).
- Obzhairov, A.I. 1993. *Geochemical gas fields in benthal layers of seas and oceans*. Moscow: Nauka, 139 pp. (in Russian).
- Obzhairov, A.I. 2003. Correlation between gas hydrates and deposits of oil and gas in the Sea of Okhotsk. *Genesis of Oil and Gas*. Moscow: GEOS, 226-228 (in Russian).
- Obzhairov, A.I., Vereshchagina, O.F., & Sosnin, V.A. et al. 2002. Methane monitoring in the waters of the eastern shelf and slope of Sakhalin Island. *Geology and Geophysics* 7: 605-612 (in Russian).
- Ozerova, N.A. & Pikovsky, Yu.I. 1982. Mercury in hydrocarbon gases. In *Geochemistry of ore formation*. Moscow: Izdatelstvo Nauka, 102-136 (in Russian).
- Virtsavs, M.V., Veveris, O.E., & Bankovsky, Yu.A. 1977. Concentration of heavy metals through codeposition by means of thyoxine. *Reports from the 2nd All-Union Conference on the Concentration Methods in Analytical Chemistry*. Moscow, Jan. 13-15, 1976: 202-203 (in Russian).

GIS-based Assessment of Contemporary Climate and Permafrost Changes in Northern Russia

G.V. Malkova, A.V. Pavlov

Earth Cryosphere Institute, Siberian Branch of the Russian Academy of Sciences, Tyumen, Russia

Abstract

The changes of contemporary climate and permafrost extent in Russia from 1965 through 2010 have been mapped and assessed using data from weather and permafrost monitoring stations and observation sites. A series of new small-scale maps has been compiled for estimating local and regional trends, namely: (1) a map of mean annual air temperatures for the past decade and warming relative to the climate norm; (2) maps of thawing and freezing indices that show changes in air temperature in warm and cold seasons for 2000–2010 relative to the climate norm; (3) a map of mean annual air temperature and permafrost trends (warming rates) for 1965–2010. The contemporary ground warming trends lag behind the air warming rates throughout the permafrost extent in Russia. Meteorological risks of the permafrost territory have been rated on the basis of air temperature and maximum snow thickness changes. Currently about 30% of the permafrost territory falls in the zone of high risk because of significant climate change.

Keywords: air and ground temperature trends; climate warming; GIS mapping; permafrost monitoring.

Introduction

The present permafrost extent in Russia occupies 65% of the total surface area. Permafrost formed during the Quaternary cooling and sea-level fall in the Arctic Basin and degraded during long, warm interglacial intervals. Cold and warm events of different durations and intensities alternated during the entire history of permafrost formation (Rozenbaum & Shpolyanskaya 2000, Shpolyanskaya 2008, Fotiev 2010). The responses of permafrost to climate change are commonly delayed due to inertia. The lag is spatially uneven, being controlled by regional and local factors (Melnikov et al. 2006).

The overall mean air temperature increase for the twentieth century over the territory of Russia was 1.29°C, whereas global warming was 0.74°C (Open-file Report 2008). The highest warming rates were recorded in the 1980s in subarctic Russia. Since 2000, the warming trends have decreased notably while the foci of maximum warming shifted to the arctic areas. At the same time, a number of climate parameters have become more variable, especially the mean annual air temperature, precipitation, and snow thickness.

The qualitative and quantitative characteristics of climate (air) and permafrost (ground) warming trends have been the subject of many studies in Russia and abroad (Anisimov & Belolutsкая 2003, Vasiliev et al. 2008, Izrael et al. 2006, Pavlov & Malkova 2005, 2009, Shpolyanskaya 2008, Melnikov & Pavlov 2006, Zhang & Osterkamp 1993, Nelson et al. 1993, among others). As an outcome of these studies, the existing methods of observations at weather and geocryological stations, as well as related predictions, were found to be uncertain (Izrael et al. 2007, Pavlov 2008). Other results include estimating the sensitivity and resistance of permafrost to the current climate change at regional and local levels (Pavlov et al. 2011), and the analysis of natural hazards associated with warming in arctic and subarctic areas. The hazards were attributed to a unidirectional increase in air temperature and snow thickness (Kitaev et al. 2001, Skachkov et al. 2007, Melnikov et al. 2007). The present northward retreat of the southern boundary of

continuous permafrost in Russia (relative to the climate norm period) was estimated to reach tens of kilometers (Pavlov & Malkova 2008).

If the warming continues, the thermal state of permafrost can change dramatically with associated partial degradation, which is fraught with grave consequences for the environment and for operation of nature-controlled technological systems (pipelines, roads, and other industrial and civil structures).

Methods

High-resolution GIS mapping is an efficient and convincing tool for estimating regional trends in climate and the permafrost state. For the first time, climate changes in northern Russian for the second half of the twentieth century were assessed on the basis of mapping (Pavlov 2003). The analytical map of that study showed three grades of air temperature changes: weak, moderate, and strong. This approach to climate change assessment, with GIS technologies, was later used repeatedly (Pavlov & Malkova 2005, 2009, Pavlov & Malkova 2008). The methodology and approaches employed in electronic mapping were reported earlier (Melnikov & Kondratieva 1998, Pavlov & Ananieva 2004, Pavlov & Malkova 2005). The GIS software package allows updates of information-mapping attributives from meteorological and geocryological databases. All weather stations and objects of monitoring have precise geographic locations and are used as references in further mapping. The electronic-based maps can be readily updated as new climate and permafrost data become available.

A database from about 100 reference weather stations was obtained by selecting stations that provide sufficiently long series of observations and reliably continuous data. It was impossible to achieve uniform coverage of different regions and northern Russia as a whole. A great number (about 50%) of reference stations are located in northern West Siberia and Central Yakutia, while the regions of southern Central Siberia, Transbaikalia, Taimyr Peninsula, Kolyma lowland, and Amur catchment remain poorly covered. This makes our models less reliable for those areas.

There are currently four main sources of new data on the thermal state of permafrost collected with advanced measurement methods:

- Soil temperature measurements at depths to 3.2 m at many weather stations within the permafrost zone;
- Geothermal measurements in boreholes of different depths, from a few tens to hundreds of meters, as part of the global network within the international TSP (Thermal State of Permafrost) project;
- Measurements of active layer thickness and temperature within the international CALM project (Circumpolar Active Layer Monitoring);
- Integrated studies and measurements at reference stations of permafrost monitoring.

The highest quality estimates of contemporary permafrost changes can be obtained through synthesis of the mutually complementary data from all four sources. Unfortunately, the sites of permafrost monitoring are as unevenly distributed as the weather stations. They are mostly restricted to the industrial zones of northern Russia and lowland permafrost zones (European north, northern West Siberia, and Central Yakutia). GIS modeling is less reliable for permafrost than for air temperature trends.

Digital map modeling was carried out using different scales, rates, relative indices, and coefficients. The warming rates were analyzed with harmonic, correlation, and regression analyses of time series collected in the course of permafrost and climate monitoring.

In 2003–2005, a set of small-scale digital maps created and compiled in a single format at the Institute of Cryosphere (Tyumen) characterized different aspects of warming in northern Russia (Pavlov & Malkova 2005). The models were based on data acquired at the boundary between the twentieth and twenty-first centuries. Further studies demonstrated the greater efficiency of such detailed digital maps for regional-scale assessments of climate and permafrost trends.

In this study, the dynamics of different parameters of the contemporary climate (including the trends of the past decade) are used as a basis in the assessment of meteorological risks in the Russian permafrost zone.

Map Models of Changes in Contemporary Climate and Permafrost

The frequency of contemporary climate anomalies is commonly estimated by comparing meteorological data over the past decade with the climate norm (a mean of a climate parameter over the period from 1961 through 1990). The climate norm (isolines in Figure 1) within the Russian permafrost zone varies from -2 to -16°C.

In as much as mean annual air temperatures in 2000–2010 have been anomalously high in many areas, there are only two warming grades (moderate and strong) used in the map of Figure 1. Warming is strong over most of the territory (temperature rise more than 1°C, red color) while moderate warming trends (yellow) are restricted to local areas in the European north, in West and Central Siberia, and in the Russian Far East (Primorie).

Regional features of warming patterns since the mid-1960s (the conventional onset of contemporary warming

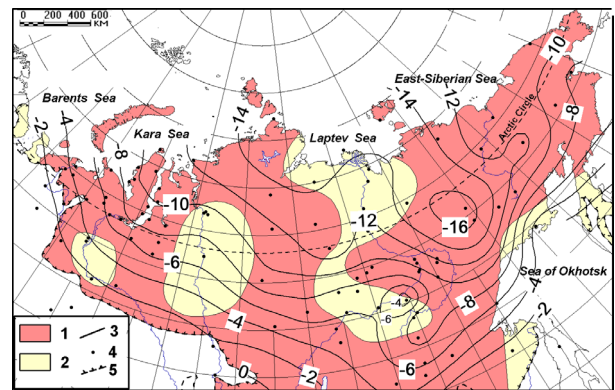


Figure 1. Changes of mean annual air temperatures in northern Russia over the past decade. 1, 2 – temperature rise relative to climate norm: high ($\Delta T_{\text{air}} > 1^\circ\text{C}$) (1) and moderate ($0.7^\circ\text{C} \leq \Delta T_{\text{air}} \leq 1.0^\circ\text{C}$) (2); 3 – mean annual air temperature isolines (climate norm); 4 – weather stations; 5 – southern limits of permafrost extent.

in most of northern areas) are shown in the map of mean annual air temperature trends (Fig. 2). According to the basic map of these trends presented earlier for 1965–2000 (Pavlov & Malkova 2005, 2009, Pavlov 2008), the warming rates were from 0.01 to 0.09°C/yr. The mean annual warming rates (Fig. 2) make up prominent N-S (western arctic and subarctic areas) and ring (eastern sector) zones. The warming rates are the highest (to 0.08–0.09°C/yr) in southern Siberia and the lowest (less than 0.02°C/yr) in the European north, in northern Central Siberia, and in the upper reaches of the Kolyma.

The air temperature patterns for 1966–2010 (see color contours in Figure 2) differ markedly from those of the basic period, namely:

- No N-S features show up in the spatial distribution of the trends.
- The variations of warming rates are generally much lower.
- The lowest rates (0.03–0.04°C/yr) are concentrated in the Lena-Olenek interfluvium, in the middle reaches of the Yenisei, in the northern Yamal Peninsula, and in the Yugor Peninsula.
- The single large maximum trend in the basic period gave way to three smaller ones (0.05°C/yr or more) in the subarctic areas.

Thus the warming rates in specific areas are variable in time while the foci of maximum trends move in space. Each following year may be expected to bring about more correction to the mean linear air temperature trends and thus change the mapped patterns.

In addition to climate change in yearly cycles, there are other controls of current warming, namely, seasonal variations of air temperature that cause significant effects on the permafrost zone. Therefore, it is important to estimate these changes separately for warm and cold seasons. Mapping of this kind was undertaken earlier (Pavlov & Malkova 2005, Pavlov 2008) but without regard to climate change in 2000–2010.

The map in Figure 3 shows six color-coded grades of the air temperature norm in warm seasons: less than 15, 15–30, 30–45, 45–60, 60–75, and more than 75°C/month.

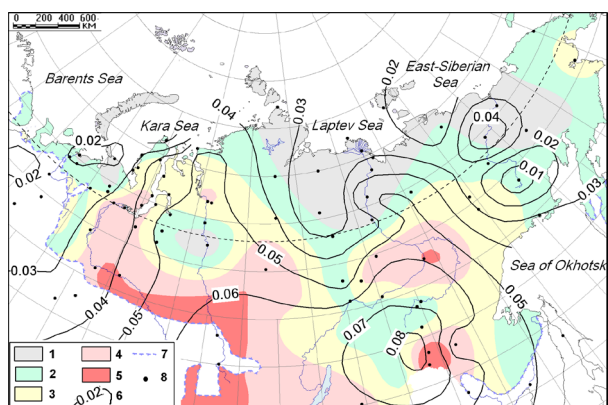


Figure 2. Mean annual air temperature trends. 1–5, trends (warming rate), in °C/yr, for 1966–2010: 1 – less than 0.03; 2 – 0.03–0.04; 3 – 0.04–0.05; 4 – 0.05–0.06; 5 – more than 0.06; 6 – basic trend (warming rate), in °C/yr for 1966–2000; 7 – southern limits of permafrost extent; 8 – reference weather stations.

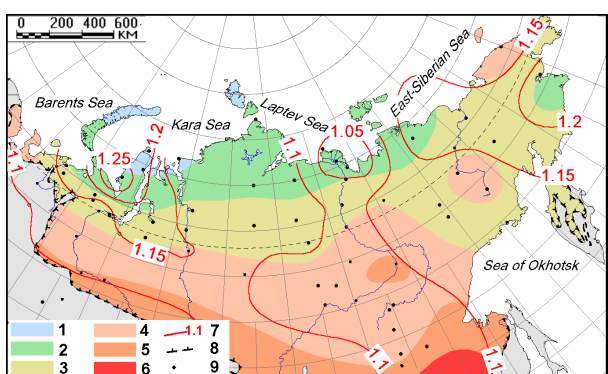


Figure 3. Warm-season increase in air temperature in the permafrost zone of Russia. 1–6 are norms of temperature sums in °C/month: less than 15 (1); 15–30 (2); 30–45 (3); 45–60 (4); 60–75 (5); more than 75 (6); 7 – relative thawing index n_{th} ; 8 – southern limits of permafrost extent; 9 – weather stations.

The mapped air temperature norm shows W-E zoning as the duration of the warm season increases from north to south.

Comparative estimates of air temperature changes in warm seasons were obtained using relative thawing index (n_{th}), as in our previous publications (Pavlov & Malkova 2005, Pavlov 2008), which is the ratio of the summer air temperature sum in 2000–2010 to the norm (n_{th} is shown as isolines in Figure 3).

The n_{th} index exceeds 1.0 over the whole territory of northern Russia, which is evidence of warmer summer seasons relative to the norm. In most northern areas, $n_{th} > 1.1$; therefore, the summer warming is over 10%. Summer warming is the greatest (n_{th} above 1.25 or over 25%) in the western Yamal and is weaker (no more than 10% of the norm) in Central Siberia, including Yakutia. The map generally characterizes the risks of permafrost degradation under changing climate. The climate conditions in areas of significant summer warming (mainly in northern West Siberia and extreme northeast Russia) are favorable for increasing permafrost temperature and thickness of the active layer (seasonal thaw depth).

For the map of contemporary air temperature increase in cold seasons (Fig. 4), the six color-coded grades of the

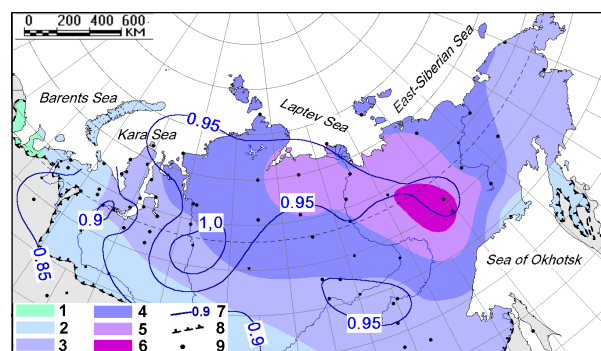


Figure 4. Cold-season increase in air temperature in the permafrost zone of Russia. 1–6 are norm of temperature sums, in °C/month: above -60 (1); -60...-100 (2); -100...-140 (3); -140...-180 (4); -180...-220 (5); below -220 (6); 7 – relative freezing index n_f ; 8 – southern limits of permafrost extent; 9 – weather stations.

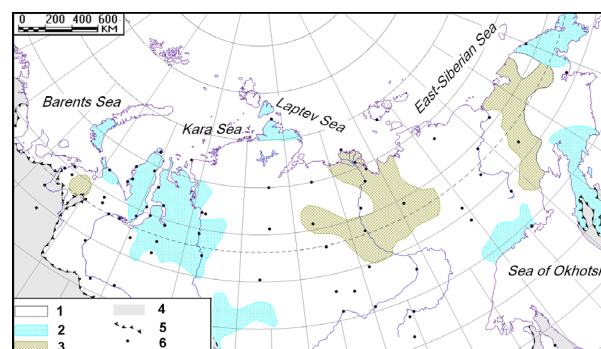


Figure 5. Snow thickness change in the north of Russia for 1976–2010. 1 – minor change (± 10 cm); 2 – 10–20 cm thickening; 3 – 10–20 cm thinning; 4 – territory outside permafrost zone; 5 – southern limits of permafrost extent; 6 – weather stations.

temperature norm sums of negative temperatures are: above -60 (1); -60...-100 (2); -100...-140 (3); -140...-180 (4); -180...-220 (5); below -220 (6) °C/month. The winter air temperatures are the lowest in continental Siberia while relatively warm winters are typical of Kamchatka and European Russia.

Winter air temperature rise was estimated using the relative freezing index (n_f), as in our previous publications, which is the ratio of the winter air temperature sum in 2000–2010 to the norm (Pavlov et al. 2007). The n_f index approaches 1 (corresponding to stable air temperature in the winter season) only near the town of Turukhansk and is 0.9–0.95 (warming of no more than 5–10%) in most northern areas. Generally, air warming in winter is lower than in summer.

Changes in the thermal regime of permafrost are largely influenced by snow cover thickness. According to the report of the Meteorological Services of Russia on climate in the country for 2010 (<http://www.meteor.ru>), the maximum snow thickness changes for the past 35 years were ± 10 cm relative to the norm over the greatest part of the permafrost zone. The snow cover became 10–20 cm thicker in northern West Siberia, in the Yugor Peninsula, and in the Kamchatka and Chukchi Peninsulas, but more than 10 cm thinner in northern Yakutia and in northeastern Russia. These data were used to compile a map of snow thickness change in the north of Russia (Fig. 5).

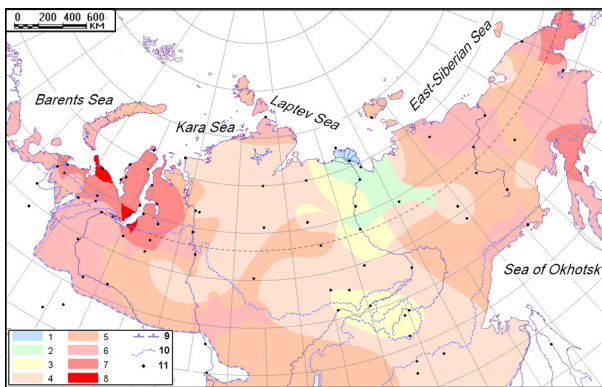


Figure 6. Meteorological risks for permafrost in Russia. 1–8 – risk grades; 9 – southern limits of permafrost extent; 10 – limits of permafrost continuous from the surface; 11 – weather stations.

The total effect of the climate change on permafrost (with regard to contributions from each climate parameter) was estimated using a numerical score. The scale of summer air temperature increase had four grades (1 for n_{th} from 1.0 to 1.05 [n_{th} is relative thawing index]; 2 for n_{th} from 1.05 to 1.1; 3 for n_{th} from 1.1 to 1.15; 4 for $n_{th} > 1.15$). Winter warming was less significant, and only three grades were applied (1 for n_f from 1.0 to 0.95 [n_f is relative freezing index]; 2 for n_f from 0.95 to 0.9; 3 for $n_f < 0.9$). For the snow thickness changes there were three grades: thinning (-1), minor change (0), and thickening (+1).

The respective layers of different climate parameters were superposed one upon another in the GIS mapping package, and the scores were summed up for the whole permafrost territory of Russia to compile a map of meteorological risks for permafrost under current climate change (Fig. 6).

The zones rated from 1 to 3 may be interpreted as areas of low risk. They are especially the Lena delta, northern Yakutia, and partly southern Yakutia, totally occupying 8% of the permafrost zone.

Areas of moderate risk (rated 4–5) cover much larger permafrost territories (63%) including Central and East Siberia and a part of southeastern West Siberia.

The western and eastern flanks of the permafrost zone belong to high-risk areas (rated 6–8). The highest risk is expected for northern West Siberia and the Chukchi Peninsula (rated 7–8) where all analyzed climate parameters cause a warming effect. The areas of high risk occupy slightly less than 30% of the permafrost zone.

The reliability of the meteorological risk model may be judged on comparison with geocryological monitoring data. Permafrost monitoring at reference stations shows increasing warming rates for frozen ground to follow those for climate (Vasiliev et al. 2008, Skachkov et al. 2007, Malkova 2010). Pavlov (2008) concluded that the current mean annual ground temperature trends have been generally lower than the air warming rates throughout the Russian permafrost zone: from 0.02 to 0.07 °C/yr, 0.05°C/yr on average for air (Fig. 2) and from 0.004 to 0.050 °C/yr for frozen ground. The ground warming rate average over all of northern Russia is 0.03°C/yr. The obtained patterns were imaged in a map of linear permafrost temperature trends from 1975 through 2010 (Fig. 7).

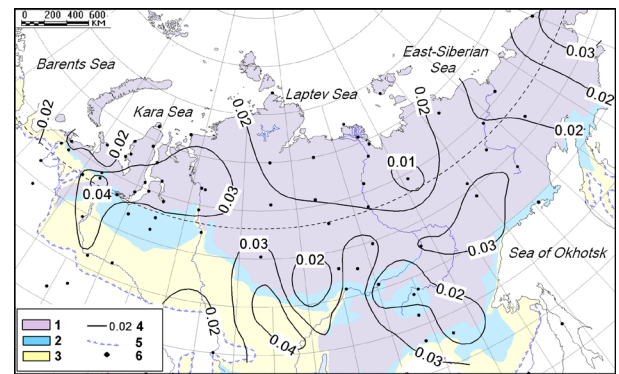


Figure 7. Linear temperature trends of frozen ground in permafrost zone of Russia from 1975 through 2010. 1–3 – extent of permafrost: 1 – continuous, 2 – discontinuous, 3 – sporadic and patched; 4 – warming rates (isolines and values), °C/yr; 5 – southern limits of permafrost extent; 6 – weather stations and permafrost observation sites.

The first thing that becomes evident when comparing the maps of Figure 6 and Figure 7 is the perfect match of the low-risk zones in northern Yakutia and in the Lena delta (Fig. 6) with the zone of lowest permafrost warming rates (0.01–0.02°C/yr) (Fig. 7). The zones of highest ground warming rates (more than 0.03°C/yr) commonly coincide with zones of high meteorological risk.

Other climate factors that influence considerably the temperature regime of frozen ground include vegetation, surface topography, thermophysical properties of the ground, and moisture patterns. These and other factors may account for some discrepancy between the mapping-based assessment of the risks and field observations at stations of permafrost monitoring.

Conclusions

The reported study continues years-long research by the authors on the effects of climate on the state of permafrost. Changes in principal climate parameters for the past decade relative to the norm have been assessed using digital map models and turn out to cause a warming effect throughout the permafrost zone.

The compiled map of meteorological risks for permafrost shows clearly a spatial mismatch of increasing air warming rates in cold and warm seasons, as well as snow thickness changes. It is their total effect calculated using a numerical score system that controls the mean annual temperature trends of frozen ground. The zones of highest ground warming rates coincide with zones of high meteorological risks.

Acknowledgments

The study was supported by grants 08-05-00421a, 09-05-10030k, and 10-05-10027k from the Russian Foundation for Basic Research. It was carried out as part of an Integration Program of the SB RAS Presidium, as well as the CALM and TSP international projects.

References

- Anisimov, O.A. & Belolutskaia, M.A. 2003. Effect of climate change on permafrost: predictions and estimates of uncertainty, in: *Problems of Environment Monitoring and Modeling of Ecosystems*. Гидрометеоиздат, St. Petersburg, pp. 21–38 (in Russian).
- Fotiev, C.M. 2010. *Cryogenic Metamorphism of Rocks and Groundwater: Conditions and Results*. GEO, Novosibirsk, 279 pp. (in Russian).
- Izrael, Yu.A., Pavlov, A.V., Anokhin, Yu.A., Myach, L.T., & Sherstyukov, B.G. 2006. Statistics of changes in climate parameters in the permafrost zone of Russia. *Meteorologiya i Gidrologiya* 5, 27–38.
- Izrael, Yu.A., Anokhin, Yu.A., Myach, L.T., & Sherstyukov, A.B. 2007. Possible changes in the elements of climate and permafrost in the 21st century in the territory of Russia: Assessment and predictions. In *Cryogenic Resources of Arctic Regions*. Proc. Intern. Conf. TyumNGU, Salekhard, Book 1, pp. 127–129.
- Kitaev, L.M., Razuvaev, V.I., & Martuganov, R.A. 2001. Spatial patterns of annual variations in interacting fields of climate and snow cover in northern Eurasia. *Kriosfera Zemli* V (4), 84–97.
- Malkova, G.V. 2010. Mean annual ground temperature monitoring on the steady-state station “Bolvansky.” *Kriosfera Zemli* XIV (3), 3–14.
- Melnikov, V.P. & Pavlov, A.V. 2006. Contemporary climate change in the North and its geocryological consequences. In *Assessment of the State of Permafrost and prediction of its Changes: Theory and Practice*. Proc. Workshop, Book 1, pp., 37 – 41 (in Russian).
- Melnikov, V.P., Pavlov, A.V., & Malkova, G.V. 2007. Consequences of contemporary global change in permafrost. *Geografiya i Prirodnye Resursy* No. 3, 19–26.
- Melnikov, E.C. & Kondratieva, K.A. 1998. Circumpolar map of permafrost and ground ice. Scale 1: 10 000 000. *Kriosfera Zemli* II (4), 59–61.
- Nelson, F.E., Lachenbruch, A.H., Woo M.-K. et al. 1993. Permafrost and Changing Climate. In *Permafrost, Proc. Sixth Int. Conf.*, Book 2. SCU of Technology Press, Beijing, pp. 987–1005.
- Open-file Report on Climate Change and its Consequences in the Territory of Russian Federation, 2008. http://climate2008.igce.ru/v2008/pdf/resume_ob.pdf
- Pavlov, A.V. 2008a. Permafrost Monitoring. GEO, Novosibirsk, 229 pp. (in Russian).
- Pavlov, A.V. & Malkova, G.V. 2005. Contemporary Climate Change in the Russian North. GEO, Novosibirsk, 54 pp. (in Russian).
- Pavlov, A.V. & Malkova, G.V. 2009. Small-scale mapping of trends of the contemporary ground temperature changes in Russian North. *Kriosfera Zemli* XIII (4), 32–39.
- Pavlov, A.V., Malkova, G.V., Скачков Ю.Б., Коростелев Ю.Б. 2011. Evolution of permafrost associated with dynamics of contemporary climate in northern Russia. In *Proc. 4th Conf. Geocryologists of Russia*, Lomonosov Moscow University, June 7–9 2011, Book 2, Part 6, Университетская Книга, Moscow, pp. 274–281.
- Pavlov, A.V. & Malkova, G.V. 2008. Regional geocryological dangers associated with contemporary climate. In *Proceedings of the Ninth International Conference on Permafrost*, University of Alaska Fairbanks, 2: 1375–1381.
- Romanovsky, V.E., Kholodov, A.L., Marchenko, S.S. et al. 2010. Thermal state of permafrost in Russia. *Permafrost and Periglacial Processes*. Special Issue: The International Polar Year. Vol. 21 (2), 136–155.
- Rozenbaum, G.E. & Shpolyanskaya, N.A. 2000. Late Cenozoic History of Arctic Permafrost and its Future Evolution Trends. Nauchnyi Mir, Moscow, 104 pp. (in Russian).
- Shpolyanskaya, N.A. 2008. *Global Climate Change and Evolution of Permafrost*. Moscow University Press, Moscow, Department of Geography, Moscow, 131 pp. (in Russian).
- Skachkov, Yu.B., Skryabin, P.N., & Varlamov, S.P. 2007. Results of 25-year long summer permafrost monitoring at the Chabyda site (Central Yakutia). In *Cryogenic Resources of Arctic Regions*. Proc. Intern. Conf. TyumNGU, Salekhard, Book 1, pp. 167–170.
- Vasiliev, A.A., Drozdov, D.S., & Moskalenko, N.G. 2008. Permafrost temperature dynamics of West Siberia in context of climate changes. *Kriosfera Zemli* XII (2), 10–18.
- Zhang, T. & Osterkamp, T. 1993. Changing Climate and Permafrost Temperatures in the Alaskan Arctic. In *Proc. Sixth Int. Conf.*, Book 1. SCU of Technology Press., Beijing, pp. 783–788.

The Dynamics of Seasonal Soil Freezing in Central Russia

A. Maslakov, V. Grebenets, D. Ablyazina, D. Shmelev, A. Radosteva, V. Pastukhov,
V. Antonov, A. Bykovskiy, G. Gavrilov, A. Gorbatyuk, D. Mandzhiev, P. Melnik, A. Saveleva,
A. Smirnov, G. Khmelniyskiy, A. Shpuntova
Lomonosov Moscow State University, Department of Geography, Moscow, Russia

G. Kraev

Center for Forest Ecology and Productivity, RAS

D.A. Streletskiy

George Washington University, Washington DC, USA

Abstract

The spatial regularities of seasonal freezing depend on climatic conditions, lithological properties, conditions of heat exchange at the ground surface, landscape structure, and other factors. Observations showed that the seasonally frozen layer in Central Russia was mainly influenced by the microclimatic and ground conditions. The research allowed us to establish the correlation of the freezing depth and cryogenic structures with snow cover structure and with meteorological characteristics. Evaluation of the ground freezing dynamics enables us to predict the development of deformations associated with cryogenic heaving, to improve the parameterization of the spring flood assessments, and to incorporate the influence of seasonal freezing on agriculture and soil processes.

Keywords: cryogenic heaving; landscape; Central Russia; lithology; seasonal freezing; snow cover.

Introduction

Seasonal freezing takes place almost everywhere in Central Russia. It is characterized by variable intensity, spatial non-uniformity, and considerable temporal variability. The spatial and temporal regularities of seasonal freezing are affected by several factors, including meteorological, climatic, geological, and landscape conditions, as well as anthropogenic transformations. The depth of seasonal freezing is directly monitored only at a few zonal meteorological observatories. However, the observatories do not reveal the impact of different geographical complexes typical of the region and the differences in the snow cover and lithology.

One of the basic tasks of modern cryolithology and hydrometeorology is to determine the response of the cryosphere to climate changes. As one element of the cryosphere, the seasonally frozen layer also reflects such responses. It often determines the development of geographical complexes, influences the change of the gas exchange between soil, vegetation, and atmosphere, and affects the formation of microrelief as well as the conditions of runoff from the territory. The phenophases of vegetation cover are different under different freezing depths. The seasonal freezing of soil exerts quite a significant impact on the operation of economic facilities. Thus the monitoring of the development of the seasonally frozen layer has practical importance in management of the natural environment.

Research Methods

The primary tasks of the 13-year-long monitoring of the dynamics of the seasonally frozen layer in Central Russia were to establish the main factors determining the depth of seasonal freezing and to assess the contribution of each factor to the variability of the seasonally frozen layer in various landscape and ground conditions under different meteorological conditions.

Field research was carried out in the zone of mixed forests of Central Russia: in the Kaluga Region, the Vladimir Region, and the Moscow Region. The meteorological data necessary for analysis of the results were obtained at the nearest weather stations.

The dynamics of seasonal freezing was monitored in the following areas (Fig. 1):

- The middle reaches of the Protva River in the territory of the Satino Educational Research Field Base of Moscow State University (MSU) in the winters of 1999–2003;
- The middle reaches of the Klyazma River in the vicinity of the educational and scientific base of MSU near the town of Petushki in the winter of 2003–2004;
- The right bank of the Moscow River near the Zvenigorod Biological Station of MSU in the winters of 2004–2006, 2007–2009, and 2011–2012;
- The right bank of the Oka River near the town of Pushchino of the Moscow Region in the winter of 2006–2007;
- The bank of the Mozhaysk Reservoir near the village of Krasnovidovo in the winter of 2009–2010.

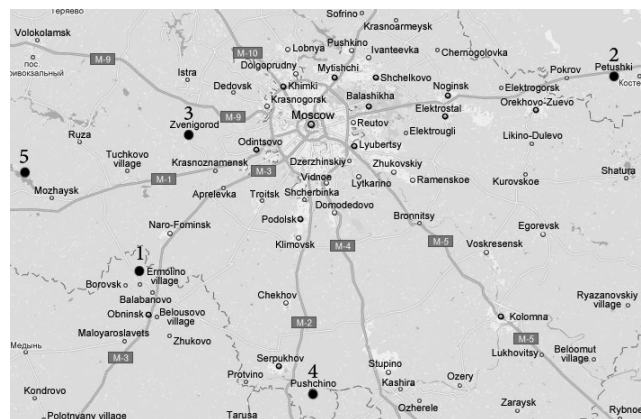


Figure 1. The map of the field research area: 1 – Satino; 2 – Petushki; 3 – Zvenigorod; 4 – Pushchino; 5 – Krasnovidovo.

The dynamics of seasonal freezing was monitored at 10–25 key sites (along 5-km-long transects) representative of the landscape diversity of the territory. The measurements were made twice during each cold season: at the beginning of formation of the seasonally frozen layer (usually the last ten days of November and the first ten days of December) and in the period of maximum freezing (the second and third ten days of February). The thickness of the seasonally frozen layer in test pits and the thickness of the snow cover were measured with a steel tape. The cryogenic structures and the thickness of the snow cover were described. The air temperature, the surface temperature, and the temperature in the soil layer and in the snow cover were measured with thermometers. At the first stage of research, we directed special attention to the detailed description of the landscape conditions including soil and ground conditions.

Results and Discussion

Monitoring revealed that the variability of the seasonally frozen layer within one geographical complex is low in comparison with the differences of the seasonally frozen layer between geographical complexes.

The dominant factor that determines the thickness of the seasonally frozen layer

Microclimatic and ground conditions exerted the main influence on the development of the seasonally frozen layer within one physical and geographical region (the central part of the East European Plain).

As Table 1 shows, the average depth of the seasonally frozen layer varies within a broad range from 0–1 cm (silty clays covered with a thick layer of leaf litter that produces heat in the chemical reactions of decomposition, oxidation, etc.) to 30–40 cm in sandy grounds and in sandy and silt clay soils in spruce forests located on the slopes of the watershed. The analysis indicates that the determining factors are winter weather conditions, including mean daily air temperature, precipitation, and snow redistribution due to wind speed.

The maximum thickness of the seasonally frozen layer for all the years of monitoring reached 0.98 m at the dirt road in 2006 and 0.66 m at the natural levee composed of fine silty sand in 2003. Freezing was favored by the following factors: lack of snow cover at this place during the winter; movement of the freezing front from two directions (from the top and from one side); the anthropogenic compaction of ground; the low pre-winter soil moisture content and the considerable decrease of air temperature in the second half of February.

Snow usually covers the Central Region by the end of November. However, at the beginning of the winter of 2004, an intensive freezing of ground developed in conditions of snow-free surface. The air temperature reached -20°C already at the first stage of observations. The average depth of the seasonally frozen layer within different terrain types reached 12–16 cm. The pre-winter soil moisture content represents a significant factor that determines the development of seasonal freezing. For instance, seasonal freezing was not observed in the saturated silty grounds at the bottom of a small watercourse under the ice crust in the cold winter of 2009–2010 (Krasnovidovo, the sum of the

Table 1. Seasonal freezing layer in Central Region (the average values within geographical complexes).

Ground systems	Geographical complexes	Average value of the seasonal freezing layer (cm) depending on DHF	
		15400-20500	> 20500
Sands	mixed forest on watershed surface	0	no data
	coniferous forest on slope	2	33
	plowed field on the watershed surface	6	no data
	meadow on floodplain	3	no data
Sandy silts	mixed forest on the watershed surface	1	22
	coniferous forest on slope	6	38
	plowed field on the watershed surface	1	25
	meadow on the floodplain	8	no data
Silty clays	mixed forest on the watershed surface	0	30
	coniferous forest on the slope	no data	31
	plowed field on the watershed surface	14	24
	meadow on the floodplain	8	25

degree-hours of freezing is 22766). There was no seasonally frozen layer in the sandy silts (with the snow height of 40 cm) at the floodplain of the Mozhaysk Reservoir. This is related directly to the fluctuations of the reservoir level, which altered the groundwater regime.

Dependence of the seasonally frozen layer on snow cover

Abnormally high air temperatures were registered in the winter of 2003-2004. Its mean values reached -6.4°C . Thick snow cover (up to 0.5 m) with ice sun-crust layers indicated numerous winter thaws. The freezing of ground under natural conditions within different geographical complexes (the swamp at the high floodplain, the meadow at the terrace, the spruce forest at the terrace, etc.) of the Klyazma River valley did not take place even by the end of the cold period. Meanwhile, seasonal freezing of the sand reached 0.4–0.5 m by this time at the experimental site protected from the snow during the entire winter. Minimum values of cryogenic heaving of the ground were registered in this region.

Snow cover was the factor that determined the development of the seasonally frozen layer in the winter of 2004–2005. The peculiarity of this winter lies in the large

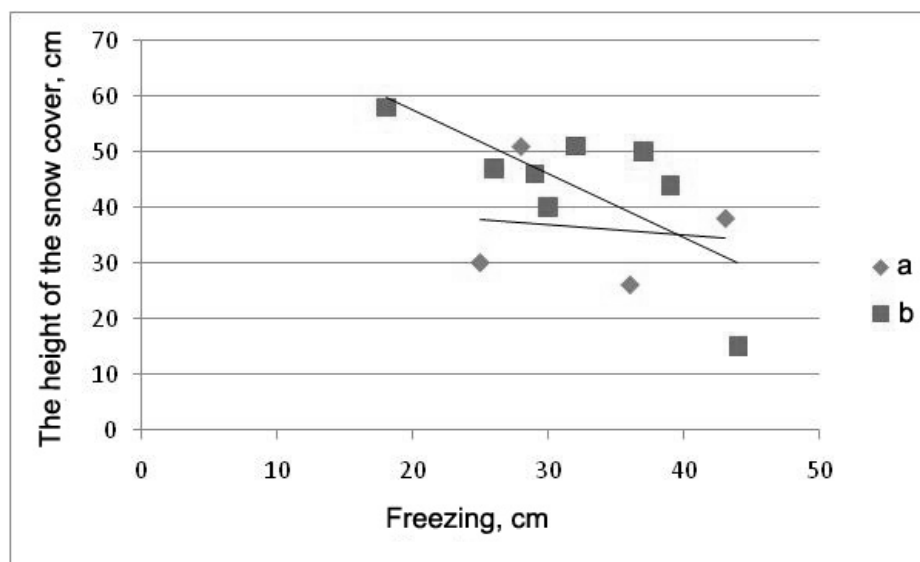


Figure 2. The dependence of seasonal freezing on the thickness of the snow cover (a - coniferous forest on the slope; b - meadow on the floodplain).

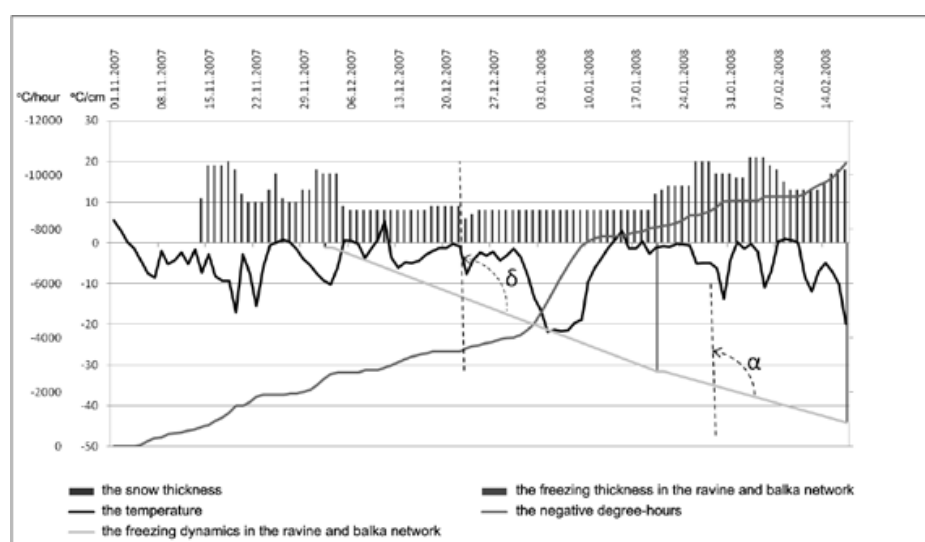


Figure 3. The dynamics of seasonal freezing depending on the snow cover depth and the temperatures at the snow surface in the ravine and balka network (based on data in the winter of 2007-2008).

amount of snow and in the anomalies of the spatial and temporal distribution of the snow cover on the territory of Russia. Disruption of the snow accumulation process played an important role in formation of the seasonally frozen layer. It corresponded with intensive snow melting in December and January (in some days the snow melted completely) and in the subsequent rapid increase of snow cover in February and March (due to abundant snowfalls) that remained up to the second ten days of April. Observations in the Zvenigorod area revealed that practically there was no seasonally frozen layer by the end of the cold period when the snow thickness was more than 0.5 m. With snow thickness below 0.4 m, the seasonally frozen layer was 0.08–0.1 m and up to 0.20 m when the snow thickness was 0.15–0.20 m (Fig. 3). Similar data were collected near the village of Krasnovidovo, where seasonal freezing was not observed even in the cold winter with snow thickness exceeding 60 cm.

In the winter of 2007–2008, we observed a similar trend

when the temporal heterogeneity of the snow cover provided considerable seasonal freezing. In the coldest period of the winter (the middle of January), the thickness of the snow cover was minimal (less than 20 cm) for all the time that it existed. During this period, the depth of the seasonally frozen layer increased by approximately 30 cm, while during the rest of the winter it increased by less than 15 cm (Fig. 3)

Dependence of the seasonally frozen layer on landscape conditions

Seasonal freezing at the Zvenigorod was studied in various landscape conditions and at different geomorphological levels (the watershed, the 1st, 2nd and 3rd terraces above the floodplain, the high and low floodplains of the Moscow River, the ravine and balka network) (Table 2). The research sites have different characteristics of vegetation litter, remoteness of the water bodies, and degree of anthropogenic disturbance. Vegetation and leaf litter play an important role in the

Table 2. The snow cover thickness and the depth of seasonal freezing depending on the climatic and geomorphological conditions based on the research data at the Zvenigorod training ground.

Winter, years	Sum of negative degree-hours	Watershed					
		High and the low floodplains and the 1st terrace above the floodplain		Forest at the terrace		Road at the terrace	
		The snow thickness, cm	Seasonal freezing, cm	Snow thickness, cm	Seasonal freezing, cm	Snow thickness (cm)	Seasonal freezing, cm
2004/05	14600	27	20	32	35	14	40
2005/06	21325	47	28	39	60	4.5	98
2007/08	10500	20	22	17	35	9	88
2008/09	11287	31	15	30	25	12	73

development of freezing when it occurs practically without snow. They serve as an insulator and, at the same time, emit heat while decomposing. The ground freezes most of all at the sites with almost no vegetation. High values of seasonal freezing were also observed in the spruce and birch forest at the 3rd terrace above the floodplain. However, within the valley of the Moscow River the depth of seasonal freezing is, as a rule, less than at a watershed due to the extra snow accumulation and the warming effect of the river.

The freezing depth is also influenced by anthropogenic disturbance. Heavily trampled sites with compacted ground or dirt roads freeze faster and have a thicker seasonally frozen layer than undisturbed sites covered with vegetation.

Ravines represent one of the main examples of territories with various landscape conditions. A well-developed complex ravine and balka network is typical of the west of the Moscow Region. This is explained by a number of factors: erosion, the presence of many large and small watercourses, land plowing, and disturbance of the natural vegetation cover.

The first peculiarity of the cryogenic processes ongoing in the ravine and balka network is their heterogeneity, as reflected in the values of snow cover thickness and thickness of the seasonally frozen layer.

The relief contributes to the differentiation of the snow cover thickness as well as of the seasonal freezing thickness on rather small territory. This is related to considerable variation of the lithology, vegetation, relief and of the regime of groundwater within one terrain type (ravine). The research reveals heterogeneity of freezing all over the ravine and the different intensity of cryogenic processes.

The thickness of the seasonally frozen layer may attain high values at the sides of ravines due to a thin snow cover and sparse vegetation (e.g., in the winter of 2007–2008 freezing reached 70 cm at the ravine sides near the Biological Station of MSU, Fig. 4).

In spring, long-term thawing of the seasonally frozen ground may initiate a viscous and plastic soil flow on the underlying permafrost (solifluction). The deep seasonal freezing can also cause displacement of ground blocks that

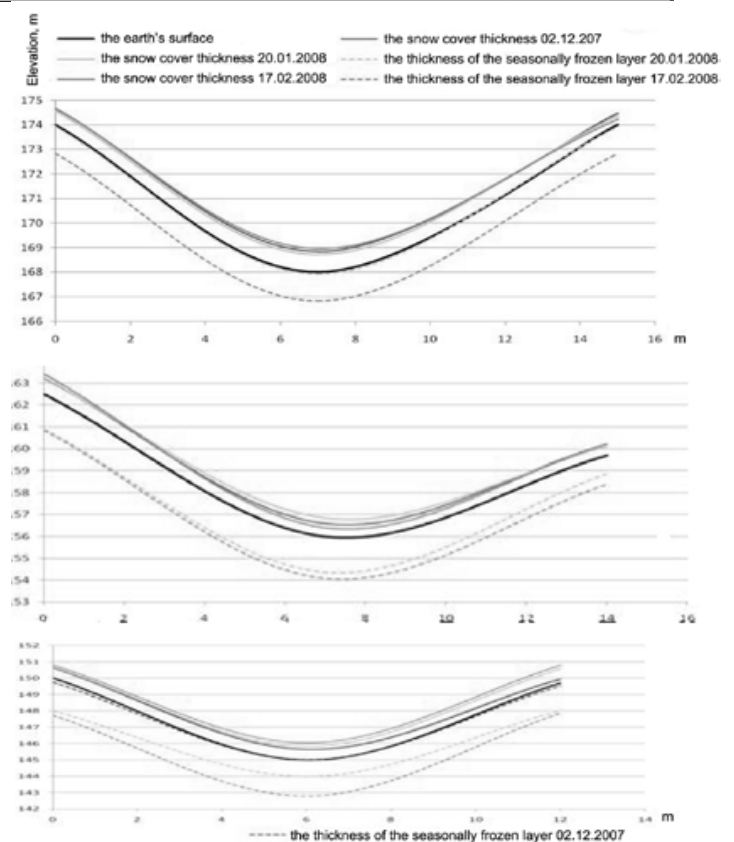


Figure 4. The cross profiles of the Andreevskiy Ravine (the upper part, the middle part and the mouth of the ravine, respectively) in the vicinity of the Zvenigorod Biological Station of MSU on the basis of observations made in the winter of 2007-2008.

may occur due to the irregular thawing of frozen blocks. The indicated displacement occurs most actively in the upper parts of ravines. This is related to their considerable instability and intensity of other geomorphological processes. Besides, landslides can take place due to the high moisture content of the layers that have just thawed.

Impact of the seasonally frozen layer on geotechnical systems

Seasonal freezing of ground favors the development of many natural and technogenic processes. The standard foundation depth for low-load buildings should be more than the

estimated freezing depth of the ground, which is around 1.5 m in Central Russia (Building Code SNiP 2.02.01-83). Frost weathering of the ground increases the number of dispersed particles, which activates differential ground heaving in the course of freezing and causes subsidence in the course of thawing. This, in turn, results in the destruction of highway beds and in deformations of low-rise and low-load buildings. It is necessary to direct particular attention to cryogenic heaving that is well-developed in Central Russia and that depends on the phase transitions of water in the active layer. Depending on the ground type, the pre-winter moisture content, and the nature of freezing, heaving can attain considerable values. In general, in the seasonally frozen grounds, a massive cryogenic structure is formed. The reticulate cryogenic structure forms under conditions of freezing from the top and from one side; it is observed at anthropogenically modified areas such as plowed fields with furrows and soil heaps. Despite the fast freezing, separate parts of profiles contain layered cryostructures corresponding to the fine silty grounds (sandy silts and clayey silts) that possess the most favorable conditions for ice formation (heaving). During observations, we discovered an interesting form of seasonal freezing (“ice-moss”) representing a moss cover cemented with ice that fills the voids. Nevertheless, cryogenic heaving develops rather actively on this territory, which is favored by the ground and temperature conditions. Observations revealed that low-load structures erected on clayey silt grounds are much more deformed under the influence of cryogenic heaving than those on sandy grounds. For instance, in the area of the Protva River, approximately 20% of fences, posts, and wooden buildings were deformed.

Conclusions

Seasonal freezing is a common process in Central Russia, but it exhibits various intensity, spatial non-uniformity, and considerable variability from year to year. The spatial and temporal regularities of seasonal freezing are influenced by many factors. The determining factor among them is meteorological. Lithological and landscape conditions as well as the degree of anthropogenic disturbance may provide variations of the active layer depth on rather limited territories.

Development of the seasonally frozen layer is accompanied by changes in the regime of the subsurface and surface runoff and by a rapid reduction in the activity of biological, chemical, and soil processes. The formation of layered cryogenic structures alters the structure and composition of the ground, which affects their physical and mechanical properties, their moisture capacity and other properties studied in geotechnical site investigations.

This research showed that the actual depth of the seasonally frozen layer ranged from 0 cm to 1.2 m and depends on the complex of climatological and lithological factors even in the abnormally cold winter period of 2005–2006. Placement of foundations of low-load (lightweight) buildings and structures at the indicated depth does not ensure their stability in frost-susceptible soils. Differential deformations of the buildings may occur due not only to direct but also tangent forces of cryogenic heaving.

Evaluation of the dynamics of the seasonally frozen layer makes it possible to predict spring flooding. The snow cover exhibits high density and thickness and does not penetrate into the frozen ground during melting.

Acknowledgments

This research was performed with the financial support of “The Leading Science Schools of Russia” program (NSH-32.71.2010.5), the CALM program of the U.S. National Science Foundation (grant OPP-0352957), and ConocoPhillips Russia Inc.

References

- Ablyazina, D.I. et al. 2004. The research on the processes of seasonal freezing of ground in the northeast of the Kaluga Region. *Proceedings of the XI International Conference of Students, Doctoral Students and Young Scientists “Lomonosov 2004”*, Ivanov, A.N. (chief editor): Izd-vo MGU, 7 pp.
- Alisov, B.P. 1969. *The climate of the USSR*. M.: Vysshaya Shkola, 104 pp.
- Building Code 1995. *Foundations on permafrost*. SNiP 2.02.01-83. TSITP Gosstroya Rossii, M. 71 pp.
- Kudryavtsev, V.A. (ed.). 1978. *General Geocryology*. M.: Izd-vo MGU, 464 pp.

The Salinity of Cryogenic Quaternary Deposits in the Yenisey North

A.G. Matyukhin, I.D. Streletskaya

Lomonosov Moscow State University, Faculty of Geography, Moscow, Russia

Abstract

New data on the degree of salinity of the main geological-genetic complexes of Quaternary deposits of the Yenisey North are presented. The thickness of Quaternary deposits varies from a few meters in the mountains and foothills of the Taymyr Peninsula to over 100 m to the south of Cape Sopochnaya Karga (the right bank of the Yenisey River). To the north of Ust-Port Village (68°N), Quaternary deposits of marine genesis are saline. The salinization is associated with the conservation of sodium chloride salts in frozen marine deposits of Pleistocene and Holocene age. Pleistocene marine deposits, thawed and then refrozen, are mainly sodium sulfate in composition. Saline marine deposits are overlain by non-saline ones: slope, aeolian, fluvial, lacustrine, biogenic, and ice-complex deposits. A map of the distribution of cryogenic saline Quaternary deposits of the Yenisey North (scale 1:1,000,000) to the depth of 15–20 m was created.

Keywords: frozen ground; Quaternary deposits; saline permafrost; water-soluble salts.

Introduction

Degree of salinity (D_{sal} , %) is a property that determines the amount of water-soluble salts in deposits (GOST 25100-95). Saline cryogenic deposits include ground in which the content of readily soluble salts in grams per 100 g of dry ground is higher than 0.05% for silty sands, 0.1% for sands, 0.15% for silts, 0.20 % for silty clays, and 0.25% for clays (SNIP 2.02.04-88). The presence of water-soluble salts in the ground reduces their freezing temperature and the bearing capacity of frozen ground. Salts have a corrosive effect on concrete foundations, metal, and reinforced concrete structures.

The particularity of the Yenisey region is the widespread distribution of saline cryogenic fine-grained deposits in the upper part of the geological section. The salinization of the ground is connected with sedimentation during marine transgressions of Pleistocene and Holocene age (Danilov 1978, Svitoch 2002, and others). The accumulation of deposits with salt solutions occurred during the periods of sea transgression. The freezing of deposits right after the sea level became lower provided for the preservation of sedimentary marine salts in them ($\text{Na} \gg \text{Mg, Ca; Cl} \gg \text{SO}_4, \text{HCO}_3$).

To the north of Ust-Port Village (68°N), saline Pleistocene marine deposits form terrace levels of different elevations varying in the range of 80–100 m. Marine deposits are desalinated to the depth of seasonal thawing or overlain by a member of non-saline continental deposits of various genesis. The thickness of saline Quaternary marine deposits may reach 200 m, and in the Yenisey River valley saline deposits below sea level occur up to depths of 100 m.

To the south of 68°N, marine Pleistocene deposits thawed during the warm Holocene periods and are desalinated to depths of 30–50 m (Dubikov & Ivanova 1990).

To date, the factual information on the salinity degree of Quaternary deposits in the north of West Siberia has been partly generalized. A 1:3,500,000 scale map of frozen ground salinity in the Yamalo-Nenets Autonomous Okrug (Dubikov et al. 2004) was created. The degree of salinity and the composition of water-soluble salts of Quaternary deposits of the eastern Gydan, the coasts of Yenisey Gulf,

and the Kara Sea islands are virtually unexplored and are not shown on the map.

A comprehensive expedition was conducted by the Earth Cryosphere Institute, SB RAS, Russian National Research Institute of Ocean Geology, and the Faculty of Geography of Moscow State University within the framework of the International Polar Year project. The new data obtained during the fieldwork allowed us to establish the features of salt distribution in the frozen ground of the major geological-genetic complexes of the Yenisey North. For the first time, a 1:1,000,000 scale map of the salinity of the cryogenic Quaternary deposits of the Yenisey North to depths of 15–20 m was created and can be used for geotechnical site investigations.

Study Area

The Yenisey North includes the lower Yenisey River regions, Yenisey Gulf, Eastern Gydan, and Western Taymyr (Fig. 1). These territories are characterized by a severe marine arctic and subarctic climate. According to the local weather stations, the mean annual air temperature ranges from -9.6°C to -11.1°C. The area is characterized by continuous permafrost with thickness of up to 500–700 m and the mean annual temperature of -9° to -11°C. Closed taliks occur only under the beds of rivers flowing into the Yenisey Gulf.

The geological structure of the region is composed of outcrops of both Upper Cretaceous and Paleozoic bedrocks, unconsolidated Quaternary fine-grained marine and coastal marine deposits, and continental deposits that host ground ice (Danilov 1969, 1978, Soloviev 1974). At the base of coastal cliffs of the Yenisey River and the Yenisey Gulf, there are outcrops of marine clayey deposits of the Sanchugov suite. For this region, they are relief-forming deposits. The age estimates of this suite vary from the Middle Pleistocene (Saks 1951) to Late Pliocene-Eopleistocene (State... 2000). Sanchugov clays underlie sand deposits of the Kasantsev horizon, which contain numerous mollusk shells. Boreal fauna, rich foraminifera complexes, and the radiocarbon dating of organic remains contained in the Kazantsev horizon deposits (Saks 1951, Troitskiy 1966, Kind 1974, Gusev

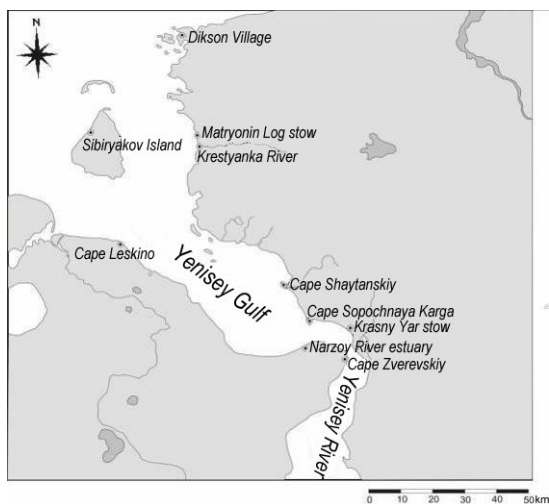


Figure 1. Study area. Black points represent the sampling locations for the determination of degree of salinity (D_{sal} , %) of the Quaternary deposits.

2011) allow us to relate it to the sediments of the Eemian transgression. Continental conditions of sedimentation in the Yenisey Gulf are typical of the coldest stage of the last glaciation, which took place 18–20 thousand years ago. The formation of the second fluvial terrace of the Yenisey River can be dated back to the same period, as well as the ice-complex deposits with syngenetic polygonal wedge ice with thickness of up to 10 m in the area of Dikson Village. Holocene deposits are represented by a complex of sediments of slope, lacustrine, fluvial, and biogenic genesis, and on the coasts by sediments of marine genesis.

Research Methods

The degree of salinity and salt composition of Quaternary deposits were analyzed based on 10 key sections located along the coasts of the Yenisey Gulf (Fig. 1) and Sibiryakov Island. Major geological-genetic complexes of Quaternary deposits that form the main geomorphological levels are presented. A collection of 100 samples of sandy-clayey deposits was assembled. Based on these deposits, the degree of salinity (D_{sal} , %) and the composition of water-soluble salts were determined. Samples weighing 250 g were selected from frozen fine-grained deposits of different genesis, and they were then transported to the geochemical laboratory in waterproof bags to avoid the loss of water-soluble salts during thawing. Analysis of the samples was carried out in St. Petersburg and Moscow laboratories (Russian National Research Institute of Ocean Geology and Ecological and Geochemical Research and Education Centre of the Faculty of Geography of M.V. Lomonosov Moscow State University, respectively).

Results

Strata of Middle Pleistocene saline sandy-clayey deposits (Sanchugov suite) that form the highest surfaces (80–100 m) outcrop in coastal cliffs near Cape Leskino (North Gydan) and Cape Shaytanskiy (Western Taymyr).

The cryostructure of the deposits is porous (structureless),

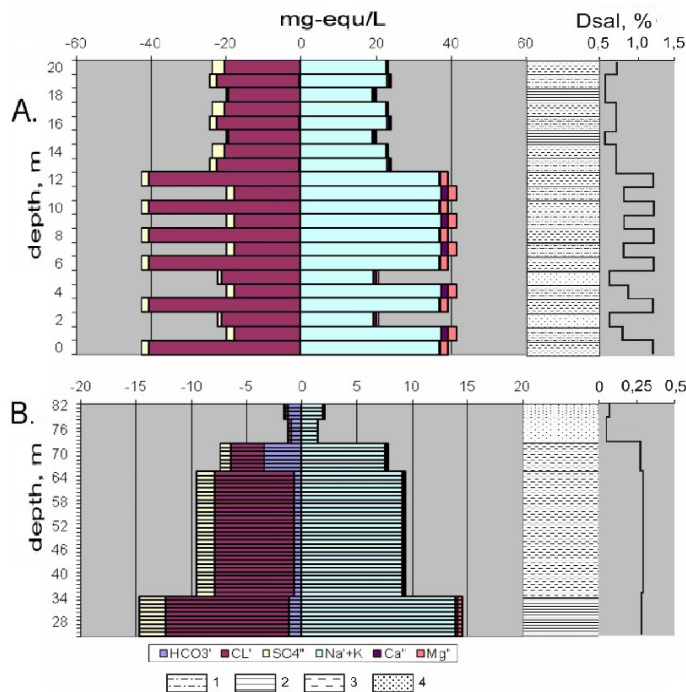


Figure 2. The distribution of ions of water-soluble salts in the Middle Pleistocene sandy-clayey deposits in the northern Gydan and western Taymyr regions: A. Cape Leskino; B. Cape Shaytanskiy; 1 – silt; 2 – clay; 3 – silty clay; 4 – sand. The content of anions is shown in the graph with a minus sign.

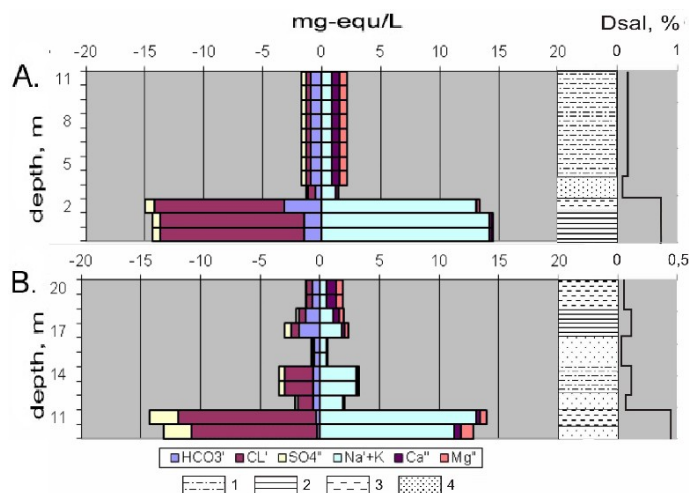


Figure 3. The distribution of ions of water-soluble salts in Late Pleistocene sandy-clayey deposits of the Western Taymyr: A. Cape Sopochnaya Karga; B. the Krestyanka River estuary. The content of anions is shown in the graph with a minus sign. For 1, 2, 3, and 4 – see Figure 2.

with no visible ice. Degree of salinity reaches 0.06% in silty sands at the depth of 6.0 m, and 1.2% in silty clays and clays; the salt composition is marine, sodium chloride (Fig. 2, A, B). To the depth of 6 m, marine deposits might have been desalinated as a result of slope processes and thawing during the warm periods of the Holocene.

In the area of Cape Sopochnaya Karga and the Krestyanka River estuary, non-saline, Late Pleistocene fluvial deposits with the thickness of 15–20 m are underlain by saline Late Pleistocene (Kazantsev) clayey and sandy marine deposits (salinity degree is 0.5% in clays, and 0.1% in sands) (Fig. 3, A, B).

Coastal outcrops in the Dikson Village area are composed of the Late Pleistocene and Holocene non-saline, silty con-

Table 1. Degree of salinity of Quaternary deposits of the major geological-genetic complexes.

Section location	Deposits age and genesis	Mean values of degree of salinity of deposits (D_{sal} , %)		Salts composition
		Sandy	Clayey	
Narzoy River estuary	m, gm II	-	0.6	Sodium chloride
Cape Leskino	m, gm II	-	0.8	Sodium chloride
Cape Shaytanskiy	m, gm II	0.06	0.4	Sodium chloride
Krasny Yar	m I	-	0.6	Sodium chloride, sodium sulfate
Krestyanka River estuary	m, pm III ¹	0.1	0.3	Sodium chloride
Cape Zverevskiy	m, gm II	0.1	0.2	Sodium sulfate
Cape Sopochnaya Karga	m, pm III ¹	-	0.5	Sodium chloride
Matrenin Log	m, pm III ¹	0.1	0.3	Sodium chloride
Sibiryakov Island	mIV	1.3	0.7	Sodium chloride

tinental deposits of ice complex, that dip below the modern sea level. It is assumed that fine-grained deposits are underlain by bedrocks that outcrop in coastal cliffs and tidal flats.

Holocene saline marine sands and silts with numerous peat inclusions form the 3-m-high coastal cliff of Western Sibiryakov Island (Opokina et al. 2010). The degree of salinity of silts below the active layer is 0.19%, and it increases to 0.9% at the depth of 2.3–2.5 m. The degree of salinity of sands at the depth of 2.8 m reaches 1.3%; the salt composition is consistently sodium chloride. Such distribution along the section of water-soluble salts is typical of young accumulative marine surfaces: laidas, beaches, and shoals, where salts are expelled downward within the section during freezing (Vasilchuk et al. 1984).

The degree of salinity of sandy-clayey Quaternary deposits of the major geological-genetic complexes is shown in Table 1.

Salinity Map of Cryogenic Quaternary Deposits of the Yenisey North

A 1:1,000,000 scale map of salinity of cryogenic Quaternary deposits of the Yenisey North to the depth of 15–20 m was created (Fig. 4). The 1:1,000,000 State Geological Map of Pliocene-Quaternary Deposits of the Russian Federation (National... 2000) and the extended 1:1,000,000 scale geomorphological scheme of the region prepared by the authors were used as references.

The map was based on the following:

- 1) The principle of geological-genetic complexes determining the units that include ground of the same formation and that emerged in the same facial conditions (i.e., in the same physical and geographical conditions);
- 2) Geomorphological features of the area: Late Pleistocene deposits form terrace levels of different age that are well-defined in the relief with absolute elevations in the range 0 to 120 m;
- 3) The established distribution patterns and changes in the composition of ions of water-soluble salts within the section.

According to the degree of salinity of cryogenic Quaternary deposits, the study area was divided into the

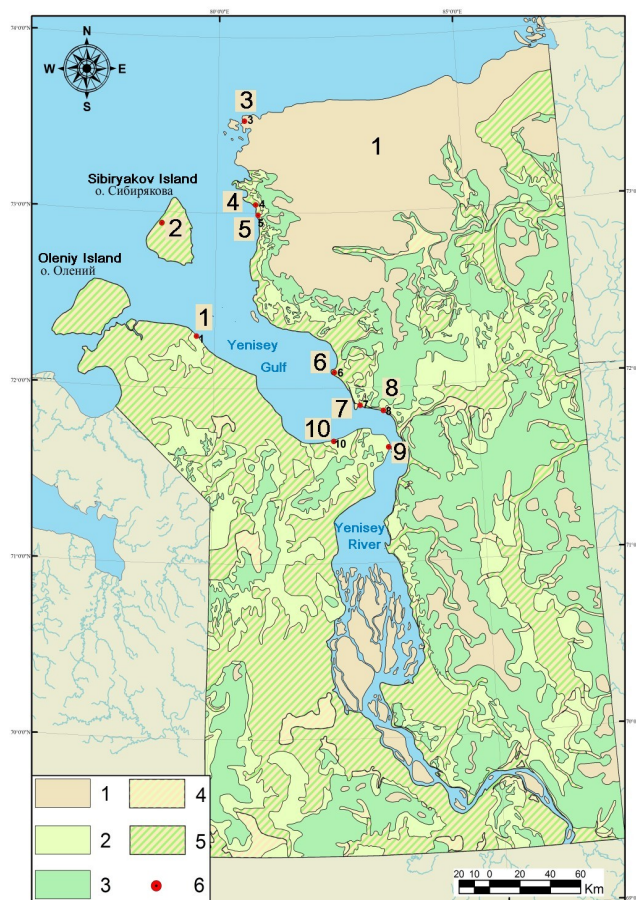


Figure 4. The 1:1,000,000 scale map of the salinity of cryogenic Quaternary deposits of the Yenisey North to the depth of 10–15 m. The degree of salinity of fine-grained deposits: 1. Non-saline (0–0.05%); 2. Slightly saline (0.05–0.2%); 3. Saline (more than 0.2%); 4. Non-saline deposits are underlain by slightly saline deposits; 5. Non-saline deposits are underlain by saline deposits; 6. Key sections: 1. Cape Leskino; 2. Sibiryakov Island; 3. Dikson Village; 4. Matrenin Log; 5. Krestyanka River estuary; 6. Cape Shaytanskiy; 7. Cape Sopochnaya Karga; 8. Krasny Yar; 9. Cape Zverevskiy; 10. Narzoy River estuary.

following regions:

- regions of non-saline deposits forming the surfaces with elevations of over 120 m; they mainly include coarse ground and hard rocks.

- regions where salinity occurs below the seasonally thawed layer of Middle Pleistocene sandy-clayey marine deposits (Sanchugov deposits) and that form surfaces with elevations of 60-120 m.
- regions of the marine sandy-clayey deposits that are slightly saline below the seasonally thawed layer of the Late Pleistocene (Kazantsev) and that form surfaces with the elevations of 30-60 m.
- regions that have a two-layer section structure and form surfaces of less than 30 m in elevation. Non-saline Late Pleistocene and Holocene continental deposits are underlain by saline Late Pleistocene marine clayey and sandy deposits.

Conclusions

The coasts of the Yenisey Gulf and watershed surfaces below the elevations of 80–100 m are composed predominantly of Pleistocene sandy-clayey marine deposits. The degree of salinity of these deposits does not exceed 0.1% in sands and reaches 1.2% in silty clays and clays. The amount of salts increases downward in the section. This can be explained by slope processes and the desalination of the upper horizons due to the thaw depth fluctuations. The fluctuation of the degree of salinity of deposits within the section is also connected with the change in lithology (salt content in sands is several times lower than in clays). Thawing and re-freezing of marine sediments alters the composition of the ions of water-soluble salts from sodium chloride to sodium sulfate.

A widespread distribution of saline cryogenic ground allows the reconstruction of marine conditions of sedimentation in the Yenisey North during most of the Pleistocene.

The deposits froze immediately after the regression of the sea, and that allowed the preservation of sedimentary salts within them. Such conditions can be observed in modern marine accumulative surfaces.

The upper part of the section is composed of non-saline continental deposits of the Late Pleistocene-Holocene age.

A 1:1,000,000 scale map of the degree of salinity of cryogenic Quaternary deposits in the Yenisey North to the depth of 10–15 m was created.

References

- Aksenov, V.I. 2008. *Saline permafrost of the Arctic coast as the base of buildings and facilities*. Moscow: Izd-vo "Vse o mire stroitelstva", 340 pp. (in Russian).
- Danilov, I.D. 1969. Permafrost-facial structure of watershed Pleistocene deposits of the lower reaches of Yenisey *Problemy kriolitologii*, Issue 1, Izd-vo MGU, pp. 93-105. (in Russian).
- Danilov, I.D. 1978. *The Subarctic Marine Plain Pleistocene*. Moscow, Izd-vo MGU, 198 pp. (in Russian).
- Dubikov, G.I. & Ivanova, N.V. 1990. Saline frozen grounds and their distribution on the territory of the USSR. *Saline frozen grounds as the base of buildings and facilities*. Edited by S.S. Vyalov, Moscow: Nauka, pp. 3-9 (in Russian).
- Dubikov, G.I., Ivanova, N.V., & Sokolskaya, V.B. 2004. Salinity of frozen grounds. In *Yamalo Nenets Autonomous Okrug Atlas*, Edit. Larnik, S.I. – Omsk Cartographic Factory FSUE, pp. 162-163 (in Russian).
- Gusev, E.A., Arslanov, H.A., Maksimov, F.E., Molodkov, A.N., Kuznetsov, V.Yu., Smirnov, S.B., Chernov, S.B., & Zharebtsov, I.E. 2011. New geochronological data on Neopleistocene-Holocene deposits of the Yenisey lower reaches. *Problemy Arktiki i Antarktiki* 2 (88), pp. 36-44 (in Russian).
- Kind, N.V. 1974. Late Quaternary geochronology according to isotope data. Moscow. *Trudy GIN AN SSSR*, Issue 257, Nauka, 255 pp. (in Russian).
- Opokina, O.L., Slagoda, E.A., Streletskaya, I.D., Suslova, M.Yu., Tomberg, I.V., & Hodzher, T.V. 2010. Cryolithology, hydrochemistry and microbiology of Holocene lacustrine and repeatedly wedge ice of Sibiriyakov Island in the Kara Sea. *Priroda shelfov i arhipelagov Evropeiskoi Arktiki*. Issue 10. Moscow: GEOS, pp. 241-247 (in Russian).
- Saks, V.N. 1951. Quaternary deposits of the northern part of the West Siberian Plain and the Taimyr depression *Tr. NIIGA*. Moscow, Vol. 14, pp. 167-282.
- Soloviev, V.A. 1974. Experience of the study of ground ice of the Yenisey North for the purpose of paleogeographic and neotectonic reconstructions. *Prirodnye usloviya Zapadnoi Sibiri*, Issue 4, Moscow, Izd-vo MGU, pp. 34-48 (in Russian).
- State Geological Map of Pliocene-Quaternary deposits of the Russian Federation, scale 1:1,000,000. 2000. St. Petersburg Cartographic Factory VSEGEI (in Russian).
- Stein, R., Niessen, F., Dittmers, K., Levitan, M., Schoster, F., Simstich, J., Steinke, T., & Stepanets, O. 2002. Siberian river run-off and late Quaternary glaciation in the southern Kara Sea, Arctic ocean: preliminary results. *Polar Research* 21(2): 315-322.
- Streletskaya, I.D., Gusev, E.A., Vasilev, A.A., Kanevskiy, M.Z., Anikina, N.Yu., & Derevyanko, L.G. 2007. New results of comprehensive studies of Quaternary deposits of the Western Taimyr. *Kriosfera Zemli*, 11 (3): 14-28 (in Russian).
- Streletskaya, I.D. & Vasilev, A.A. 2009. The isotopic composition of polygonal wedge ice of the Western Taimyr. *Kriosfera Zemli* 13 (3): 59-69 (in Russian).
- Svitoch, A.A. 2003. *The marine Pleistocene of Russia's coasts*. Moscow: GEOS, 362 pp. (in Russian).
- Troitskiy, S.L. 1966. *Quaternary deposits and the relief of flat coastal areas of Yenisey Bay and the neighboring part of Byrranga Mountains*. Moscow, Nauka, 207 pp. (in Russian).
- Vasilchuk, Yu.K. & Trofimov, V.T. 1984. On findings of highly mineralized repeatedly wedge ice. *Izv. AN SSSR, seriya geologicheskaya*, 8, Moscow, pp. 129-134 (in Russian).

Stability and Growth of Gas Hydrates at Pressures below Ice-Hydrate-Gas Equilibrium

V.P. Melnikov, A.N. Nesterov, A.M. Reshetnikov
Earth Cryosphere Institute, SB RAS, Tyumen, Russia

V.A. Istomin
VNIIGAS, Razvilka, Moscow Region, Russia

Abstract

This paper presents the results of a study of gas hydrate behavior in the thermodynamic zone enclosed on the phase diagram between the ice-hydrate-gas equilibrium line and the line of the supercooled water-hydrate-gas metastable equilibrium. We demonstrate experimentally that within the indicated area in the absence of ice in samples hydrates may exist for a long time in a metastable phase. Also, growth of metastable hydrates on supercooled water droplets is possible. The growth rates of metastable hydrates were measured, depending on the type of gas and system supercooling.

Keywords: gas hydrates; metastable states; phase equilibrium.

Introduction

It is commonly assumed that the self-preservation of gas hydrates is achieved through the formation of impermeable ice coatings on the surface of hydrate particles in the initial stage of hydrate dissociation (Davidson et al. 1986, Yakushev 1988, Yakushev & Istomin 1990). The formation of ice in the process of hydrate dissociation has been determined experimentally. However, the very mechanism of the ice-coating formation is under-studied and remains poorly understood. One of the proposed and theoretically based mechanisms of self-preservation suggests that the dissociation of hydrates at temperatures below 273 K can proceed through the formation of interstitial supercooled water (Istomin et al. 2006). Subsequently, the formation of supercooled water in the process of hydrates dissociation was confirmed experimentally (Melnikov et al. 2007, Istomin et al. 2008, Melnikov et al. 2009, Ohno et al. 2011). The dissociation of hydrate samples in the case of pressure drop (Fig. 1) began not upon crossing the ice-hydrate-gas equilibrium line (Curve 1), but upon crossing the metastable supercooled water-hydrate-gas equilibrium line (Curve 2).

Of particular interest is the behavior of hydrates in the area enclosed by the lines of ice-hydrate-gas equilibrium (Curve 1) and metastable supercooled water-hydrate-gas equilibrium (Curve 2, Fig. 1).

In the present work, the behavior of hydrates in the indicated area is examined.

Experimental Method

A detailed description of the apparatus and methods of obtaining hydrates is provided in Reshetnikov (2010). Methane, propane, and carbon dioxide hydrates were used as objects of research. The method that was chosen for studying the behavior of gas hydrates was the visual observation using light microscopy, supplemented by the measurements of pressure and temperature in the studied system.

The main element of the apparatus is a reactor designed for an operating pressure of 15 MPa. On the side surface of the reactor there are viewing windows for visual observation of processes occurring within the reactor. The reactor is placed inside the Teledor thermostated chamber. Observation of the

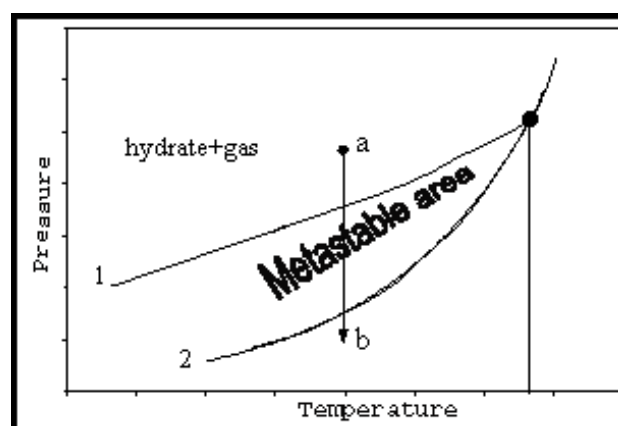


Figure 1. Regions of the water-gas system state diagram.
a – initial system state; b – after the pressure drop.

processes of hydrate formation/dissociation is carried out using a B-630 cathetometer. The ocular of the cathetometer telescope is connected to a digital camera. The image from the camera is displayed on a monitoring screen and simultaneously recorded by a DVD recorder.

The procedure of the hydrate sample preparation was as follows. Distilled water in the amount of 1.5–2.5 g was sprayed in the form of small droplets onto the surface of a transparent Plexiglas plate. The reactor and the plate had been previously cooled to 253–258 K, so when the water was sprayed, ice particles formed on the plate surface. The shape of the particles was close to that of a spherical segment with a base diameter of 0.15–2.5 mm and a height of 0.3 mm. Thus ice was used in order to obtain hydrates. After the reactor had been filled with gas, it was slowly heated above the ice-melting point. The melting of the ice facilitated the hydrate forming reaction. It should be noted that our numerous attempts to obtain hydrates from the water droplets that had not been previously frozen were not successful.

In order to study the behavior of the obtained hydrate samples outside their thermodynamic stability zone, the specified temperature was set inside the reactor. Afterwards, the pressure was slowly reduced. The pressure drop rate was regulated so that it did not cause the temperature drop inside the reactor. The dissociation of the hydrates was determined

from the visually observed collapse of their surface, the appearance of liquid phase islands, and evolution of gas bubbles from the liquid.

Results and Discussion

Our study of the hydrate behavior in the area enclosed by the lines of ice-hydrate-gas equilibrium and metastable supercooled water-hydrate-gas equilibrium, as well as isotherms of $T=253$ K for methane hydrates, $T=263$ K for propane hydrates, and $T=249$ K for carbon dioxide hydrates, has shown that in this region hydrates may exist for a long time as a metastable phase without visible dissociation. For example, in one of our experiments, continuous observation of methane hydrates lasted 14 days at 1.9 MPa and 268 K (Fig. 2). There were no visual changes recorded in the hydrates (Fig. 2b), although the equilibrium pressure of methane hydrate dissociation (P_{eq}) into ice and gas at the given temperature was 2.17 MPa. However, when the pressure was then lowered in the reactor at the rate of 0.02 MPa/min, the formation of water was observed immediately upon crossing the line of supercooled water-hydrate-gas metastable equilibrium (Fig. 2b). The formation of supercooled water indicates that the hydrate samples did not contain unreacted ice. It also means that the ice was not formed during the time of observation of the hydrates outside their thermodynamic stability zone.

Further studies showed that the dissociation of metastable hydrates into supercooled water and gas is reversible. If upon the completion of the hydrate dissociation (when hydrates could no longer be visually detected in the supercooled water droplets), the pressure in the reactor is increased above the pressure of supercooled water-hydrate-gas metastable equilibrium (above Curve 2, Fig. 1) but below ice-hydrate-gas equilibrium pressure (below Curve 1, Fig. 1), we observed the growth of the solid phase film (Fig. 3). This film was not ice, which is the stable phase at the given P, T conditions.

We verified that the solid phase film melted when the pressure was again decreased below the pressure of supercooled water-hydrate-gas metastable equilibrium. Moreover, the appearance of ice nuclei in the supercooled water was supposed to cause its instantaneous bulk crystallization, whereas in our case the solid film propagated across the surface of the supercooled water droplets at terminal velocity. Based on these observations, we came to the conclusion that it is metastable hydrates (methane hydrates in the actual example) that are the solid phase that grows across the surface of the supercooled water droplets.

This growth does not contradict classical thermodynamics. Two phases (hydrates and supercooled water) that are metastable in relation to the third phase (ice) can co-exist. In this case, the normal conditions of the phase equilibrium are satisfied on Curve 2 (Fig. 1): $T_w = T_h$, $P_w = P_h$, $\mu_w = \mu_h$ (Skripov & Koverda 1984), where μ is the chemical potential of water, and indexes represent co-existing phases of supercooled water (w) and hydrate (h). In the area above Curve 2 the chemical potential of water in hydrates μ_h is lower than the chemical potential of supercooled water μ_w , which causes the growth of hydrates on the surface of supercooled water droplets (Fig. 3).

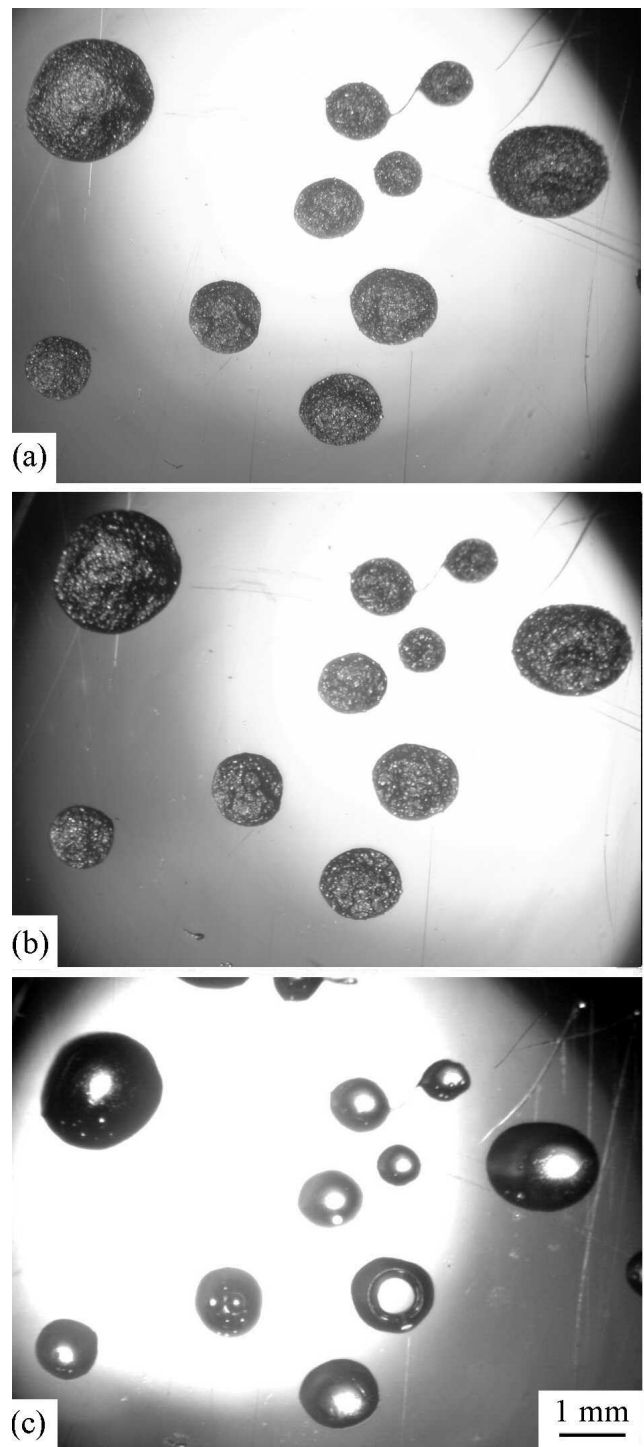


Figure 2. (a) Stable and (b) metastable methane hydrates at 268 K. (a) $P=8.5$ MPa; (b) 336 hours after the pressure in the reactor was decreased to $P=1.9$ MPa; (c) dissociation of metastable methane hydrates upon crossing the supercooled water-hydrate-gas metastable equilibrium line once the pressure in the reactor was decreased from 1.9 MPa to 1.6 MPa. $P_{eq}=2.17$ MPa at $T=268$ K.

The characteristics of the metastable hydrate growth are connected with the stochastic nature of nucleation and the influence of the supercooled water droplet size on the induction period of hydrate formation. We can see that in Figure 3 hydrates are not formed simultaneously in all of the water droplets, and four minutes after the nucleation of the first droplets, at least two water droplets still persist (Fig. 3, the droplets are marked by arrows).

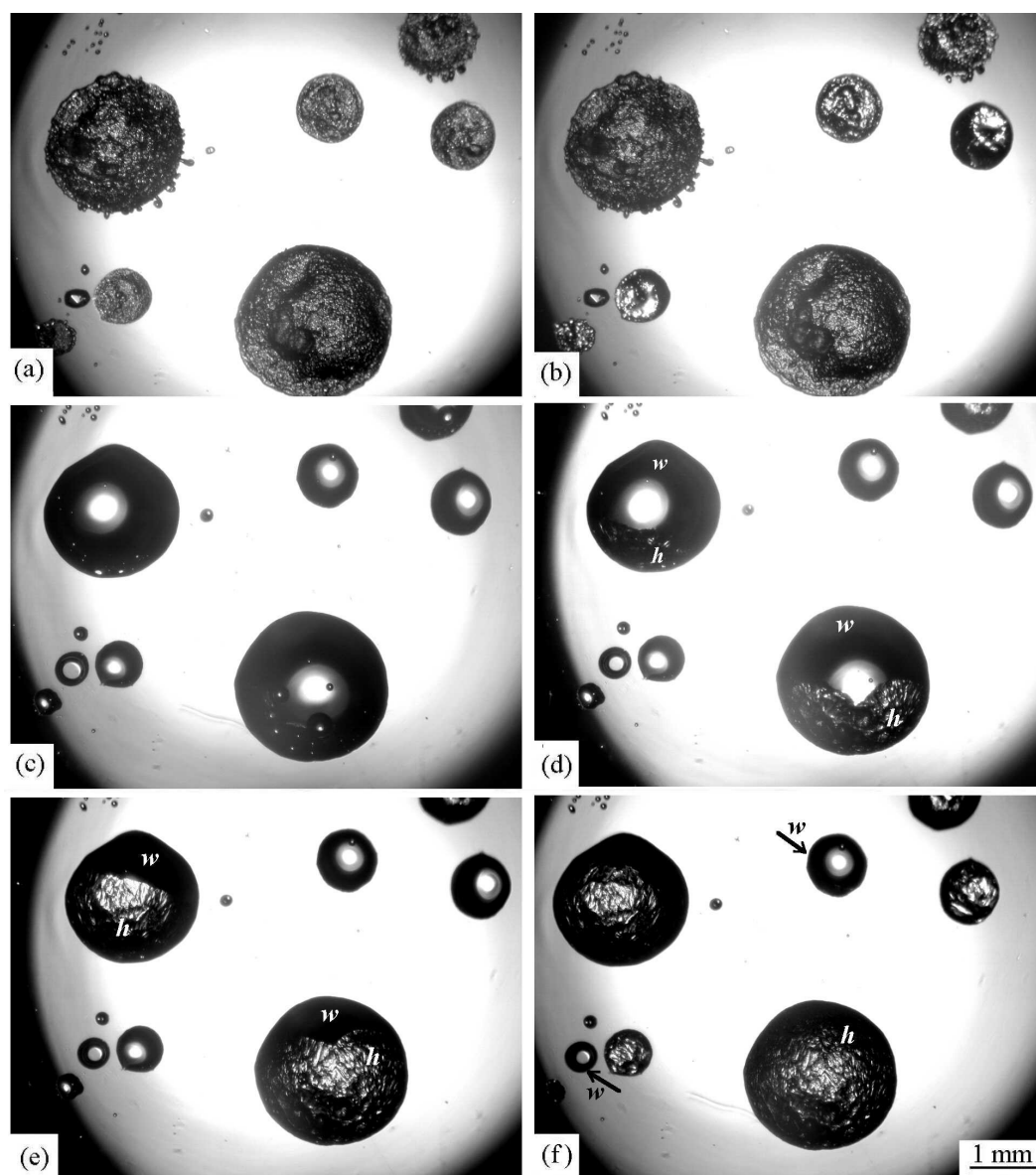


Figure 3. (a) Metastable methane hydrates; (b and c) their dissociation into supercooled water and gas; (d through f) growth of a metastable methane hydrate film at the surface of supercooled water droplets at 268 K. (a) 2 hours after the pressure in the reactor was isothermally decreased to 1.8 MPa. No changes in the samples were observed during this time (time = 0 min); (b) the first evidence of hydrate dissociation upon pressure drop appeared at 1.61 MPa (11 = min); (c) at 1.28 MPa (time = 45 min); (d) when the pressure in the reactor was increased to 1.8 MPa, hydrate film appeared on the surface of the largest droplet (time = 48 min); (e) at $P=1.8$ MPa the growth of the hydrate film is observed on the surface of two largest droplets of supercooled water (time = 49 min); (f) at $P=1.8$ MPa no hydrates are observed in at least two water droplets (time = 52 minutes).

Figures 4, 5, and 6 show the results of the measurement of the surface growth rate of the metastable hydrate film on the surface of water droplets as a function of system supercooling ΔT . In these experiments, water with previous hydrate history was used to obtain melting hydrates at pressure slightly below the supercooled water-hydrate-gas metastable equilibrium pressure. The hydrates were melted for 30 minutes until the hydrate phase visually disappeared. Then the pressure in the reactor was increased to the value that provides the required system supercooling $\Delta T = T_{eq} - T$, where T_{eq} is the equilibrium temperature of hydrate formation at the given pressure in the reactor and T is the temperature in the reactor. For supercooled water, T_{eq} is the temperature of the supercooled water-hydrate-gas metastable equilibrium.

Figures 4, 5, and 6 show that the rate of hydrate growth

depends not only on the system supercooling ΔT , but also on the system temperature. When the temperature decreases, the growth rate decreases at a constant degree of supercooling. In this case, the growth rate of metastable hydrates decreases in the sequence carbon dioxide \rightarrow methane \rightarrow propane. The growth rate is influenced by the solubility of gases in water and the hydrate structure type. Based on the studied gases, carbon dioxide dissolves in water much better than methane or propane. Also, propane has type II cubic structure, while methane and carbon dioxide have type I cubic structure.

Conclusions

It was established that hydrates may exist for a long time as a metastable phase without visible dissociation where

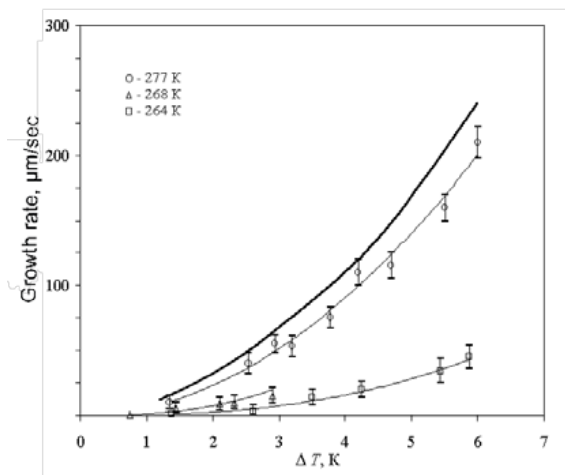


Figure 4. The growth rate of methane hydrates on the surface of water droplets as a function of supercooling and temperature. The heavy line represents an exponential trend for the growth rate of stable hydrates on the surface of volumetric water according to the published data.

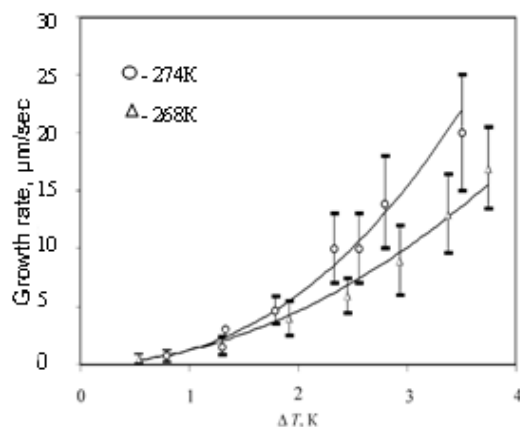


Figure 5. The growth rate of the film of metastable propane hydrates on the surface of water droplets as a function of supercooling and temperature.

hexagonal ice is the stable water phase. This occurs in the case where the thermobaric area is enclosed on the phase diagram by the ice-hydrate-gas equilibrium line, the line of the supercooled water-hydrate-gas metastable equilibrium, and the isotherm 253 K for methane hydrates, 263 K for propane hydrates, and 249 K for carbon dioxide hydrates. The stability of such hydrates is not connected with the known effect of hydrate self-preservation. It is caused by the difficulties in the solid-phase transition hydrate→ice.

Experimental evidence of metastable gas hydrate growth on the surface of supercooled water at pressure below the ice-hydrate-gas equilibrium pressure was obtained. The surface growth rates of the metastable methane, propane, and carbon dioxide hydrates were measured at different temperatures and system supercooling degrees. We demonstrated that the surface growth rate of metastable hydrates decreases in the sequence carbon dioxide→methane→propane.

Acknowledgments

This work was supported by RFBR (Grant 10-05-00270-a), the integration project of SB RAS (09-62), and the Program of Fundamental Research of ESD RAS (project 11-b).

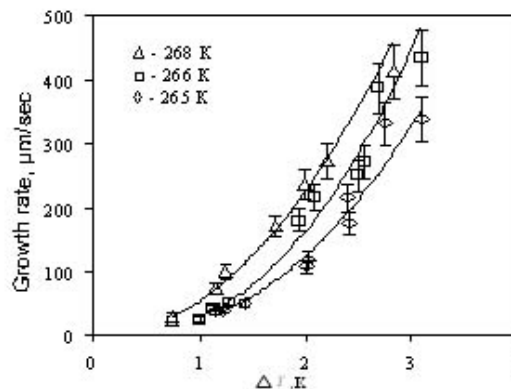


Figure 6. The growth rate of the film of metastable carbon dioxide hydrates on the surface of water droplets as a function of supercooling and temperature.

References

- Davidson, D.W., Garg, S.K., Gough S.R., Handa, Y.P., Ratcliffe, C.I., Ripmeester, J.A., Tse, J.S., & Lawson, W.F. 1986. Laboratory analysis of naturally occurring gas hydrate from sediment of the Gulf Mexico. *Geochimica et Cosmochimica Acta* 50: 619–623.
- Istomin, V.A., Kvon, V.G., & Durov, V.A. 2006. Metastable states of gas hydrates. *Gazovaya promyshlennost. Gas hydrates* (Special issue): 32–35.
- Istomin, V.A., Nesterov, A.N., Chuvilin, E.M., Kvon, V.M., & Reshetnikov, A.M. 2008. Different gases hydrates dissociation at temperatures below 273 K. *Gazokhimiya* (No. 3), 2: 30-44.
- Melnikov, V.P., Nesterov, A.N., & Reshetnikov, A.M. 2007. Formation of supercooled water in the process of propane hydrate dissociation at $T < 270$ K. *Doklady Akademii Nauk*. (No. 2) 417: 217-220.
- Melnikov, V.P., Nesterov, A.N., Reshetnikov, A.M., & Zavadovsky, A.G. 2009. Evidence of liquid water formation during methane hydrates dissociation below the ice point. *Chemical Engineering Science*. 64: 1160-1166.
- Ohno, H., Oyabu, I., Iizuka, Y., Hondoh, T., Narita, H., & Nagao, J. 2011. Dissociation behavior of C_2H_6 hydrate at temperatures below the ice point: Melting to liquid water followed by ice nucleation. *Journal of Physical Chemistry A*, 115. 8889-8894.
- Reshetnikov, A.M. 2010. Experimental study of metastable states in the process of gas hydrate dissociation at temperatures below 273 K: *Doctor of sciences dissertation*. Tyumen, IKZ SO RAN, 123 pp.
- Skripov, V.P. & Koverda, V.P. 1984. Spontaneous crystallization of supercooled liquids. Moscow. *Nauka*, 232 pp.
- Yakushev, V.S. 1988. Experimental study of methane hydrate dissociation kinetics at negative temperatures. EI VNIIGazproma, ser. *Development and exploitation of gas and gas condensate fields* 4: 11-14.
- Yakushev, V.S. & Istomin, V.A. 1990. Peculiarities of gas hydrate existence in rocks at negative temperatures. *Geokhimiya* 6: 899–903.

A Technological Approach to Minimize Problems of Thermal Erosion During Development of Yamal Gas-Condensate Deposits

S.P. Mesyats, N.N. Melnikov

Mining Institute of the Kola Science Center (RAS), Apatity, Murmansk Region, Russia

Abstract

We explore the technological possibility of developing a sustainable sod grass cover without topsoil application following concepts of natural soil development. Rapid accumulation of the organic layer is achieved by applying a polymer cover after grass sowing, which encourages establishment of a highly productive plant community. Formation of sod grass cover is the most ecologically appropriate solution to prevent wind, water, and thermal erosion.

Keywords: gas-condensate field; development; cryogenic processes; thermal erosion; damaged land; sod grass cover formation.

The West Siberian oil-and-gas-bearing province is a major source of hydrocarbon production in Russia. The territory under consideration (the region of the Urengoi, Bovanenkovskoe, Kharasaveiskoe and Tambey fields) lies in the northern part of the West Siberian Plain from the Kara Sea coast to 66°N latitude.

Development of large-scale gas-condensate and gas- and oil-condensate fields in the northern regions of West Siberia began in the mid-1970s and is proceeding at an increasing pace. This results in destruction of tundra cover, disturbing natural permafrost conditions. The scale of destruction directly depends on the degree of technogenic disturbance and the landscape environment (Fig. 1).

The territory of the Yamal gas-condensate fields has extensive areas of perennially frozen ground. It is characterized by severe climatic conditions with low solar insolation, low negative temperatures, excessive humidity, and strong wind activity. The high vulnerability of these tundra ecosystems is due to difficult permafrost conditions, thermal instability of the permafrost, rugged terrain, and limited development of the low-stature plant community under extreme conditions. A thin soil layer, nutrient-poor conditions, and near-surface permafrost decrease the soil's resistance to technogenic loadings, causing low potential for recovery of the soil-vegetative cover.

During the exploration, production, collection, and transportation of oil and gas, soil is disrupted by numerous

oilfield activities and facilities—wells, technological reservoirs, transmission facilities, pipelines, oil-gathering points, facilities for oil and gas treating, group pumping stations, compressors, oil processing stations, transportation services, and others. Development of oil and gas fields in the permafrost region leads to disruption of the soil cover, which acts as a heat insulator. In turn, this results in rapid thermal erosion.

Partial or total disruption of soil-vegetative cover increases the depth of the active layer (the layer of seasonally thawed soil) and triggers cryogenic processes such as thermokarst, solifluction, frost-heaving, shattering, and cracking with greater intensity than under natural undisturbed conditions. If under undisturbed conditions the rate of soil flow due to solifluction is several centimeters per year, with disturbance these rates may reach up to 5–7 m per day, especially on very saturated, wet slopes. This rapid solifluction can transport, within a 24-hour period, thousands of square meters of the upper meter of surface soil from hillslopes to the foot of the slope (Research ... 1989).

Thermokarst failures lead to subsidence as a result of local thawing of permafrost. “Technogenic” thermokarst is caused by the formation of micro-impoundments of water which lead to liquefaction on the flat and low areas where damage to the soil-vegetative cover has occurred. The process of soil heaving occurs as soils accommodate the volume increase as water freezes into ice. This results in elevated microtopography, which can deform overlying building construction. The most vulnerable soils are lowlands and flat areas consisting of sandy-loam and silty soils. In winter, abrupt temperature fluctuations due to snow accumulation can cause frost cracking and changes in soil temperature regime.

The highest rate of formation of cryogenic processes occurs at industrial sites, drilling and operational wells, and along pipelines. These processes result in substantial damage to oil-field facilities (deformation, soil settlement, and subsidence in exploratory well heads, foundation pile buckling, etc.). This impacts the reliability and overall condition of facilities.

In this regard, restoration of disturbed ground in Yamal is relevant not only for solving ecological problems and restoring grasslands, but also for addressing the stability of operational facilities in the permafrost region. Examples around the world show that the best way to stop erosion is



Figure 1. General view of territory with completion of an exploratory well.

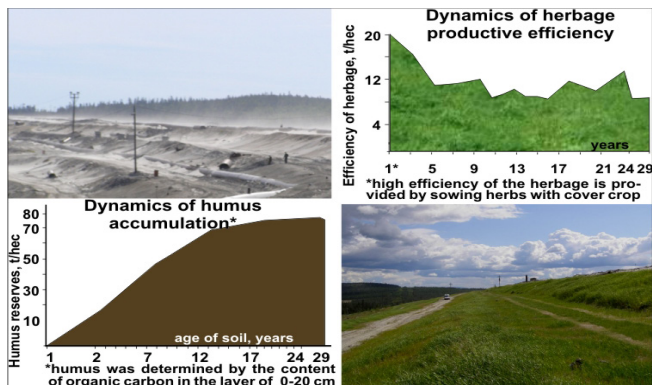


Figure 2. Results of long-term monitoring of biological recovery of vegetation on a mineral substratum without applying a topsoil layer in waste dumps in the Arctic.

by establishing a grass sod cover. A traditional approach to biological reclamation is to apply a topsoil layer and sow grass seed. However, removing topsoil from another area by definition involves disturbance, so this practice simply shifts the area of disturbance. In the tundra, peat removal inevitably leads to increases in thermal erosion processes. Additionally, the cost of reclamation in the mining industry is 4.5% of the world mineral market or 14.1% of the initial investment (Counting the Cost 1994). Therefore, it is important to develop effective methods for establishing sod cover on disturbed mineral substrate at a lower cost.

Specialists at the Mining Institute of the Kola Science Center RAS have developed techniques for remediation of degraded lands using grass sod on the original parent material without applying a topsoil layer (Mesyats 2004).

The biological productivity of the selected plant community is the determining factor in developing the grass sod. An evolutionarily fixed property of some plants is to absorb a certain quantity of specific chemical elements from the bulk pool in the mineral substrate, which increases productivity, vegetation cover, and the retention of organic matter, resulting in rapid soil development. During this development, accumulation of organic matter leads to formation of humus, which is a specific organic substance allowing long-term accumulation of elements as organo-mineral complexes.

Successful establishment of sod is accomplished by applying a polymer cover after grass sowing on top of starter mineral fertilizers. The polymer cover solves a set of problems by improving the environment in the rooting zone and providing stable substrate for high-productivity grass establishment. Under northern conditions, it results in fast humus accumulation in the substrate, about 80 tons per hectare (Fig. 2).

According to current conceptual understanding, the “humus-vegetation” system is characterized by feedback loops that determine the natural system’s capacity for self-regulation. The system is regulated by a positive feedback, where each of the partners stimulates development of the other and, through this, its own development (Fig. 2).

Investigation of the impacts on the polymer of solar radiation, photochemical, and thermal effects, as well as the study of the polymer’s diffusion, adsorption, and mass transport characteristics, have shown that the polymer cover displays high erosion resistance, good gas and

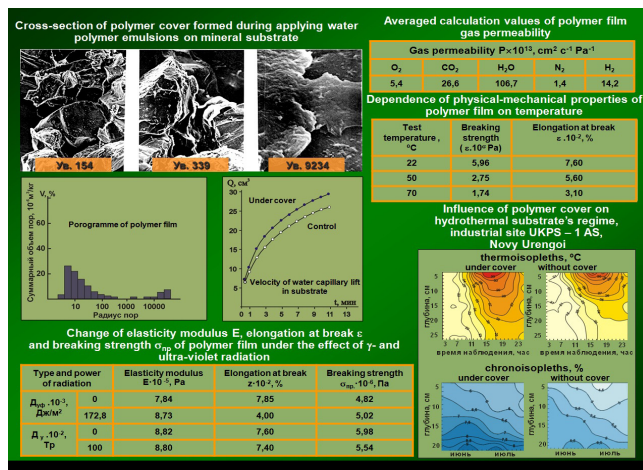


Figure 3. Physical, chemical, and operating properties of polymer cover.

water permeability, resistance to atmospheric precipitates, tolerance of temperature fluctuations, resistance to radiation, and low ecological impact, and it is biodegradable over time (Fig. 3) (Mesyats & Melnikov 2005).

Creation of the polymer cover minimizes wind and water erosion, optimizes the hydrothermal regime, increases biochemical root zone activity, and localizes technogenic disturbance, preventing its propagation into adjacent environments and trophic chains.

The technology has been proven over 30 years of implementation on diverse surfaces under different climatic zones, including the Arctic.

In the aftermath of the Chernobyl nuclear power plant disaster, this technology served as the basis of a comprehensive program of dust suppression to limit the distribution of radioactive dust. Soil-vegetation cover has been reestablished on thousands of hectares of disturbed areas thanks to this technology.

Well-developed technological solutions have been applied for many years by various mining enterprises to mitigate impact from activity of the Kola mining and industrial complex. The bio-geo-barrier created in the concentrated ore tailings that cover thousands of hectares, stops wind and water erosion, conserves technogenic raw materials, and protects the environment (Melnikov 2010).

Monitoring of the grass sod cover suggests that the overall pattern of development is the same at different sites despite differences in climatic conditions and the mineralogical and chemical makeup of the technogenic raw material.

The polymer cover forms and maintains grass stands with fast growth and sustained high productivity, through various phenological stages of plant growth and development, including reproduction and annual self-regeneration without care.

For the first three years, the organic layer develops and is slightly more pronounced than later in recovery.

The basic features of the organic humus-accumulative layer are formed by the end of the first decade; over the second decade monitoring reveals that qualitative and quantitative traits increase in abundance.

Sustained high bioproductivity of the seeded plant community ensures rapid humus accumulation and buildup of organic reserves (Fig 2).



Figure 4. Creation of vegetation cover in Yamal test areas the third year after sowing without applying a topsoil layer.

The formation of the organic-rich topsoil layer soon after seeding causes more rapid transition during succession to a plant community with a structure similar to the surrounding landscape. The development of a layered canopy and increased biodiversity increases turf resilience and ensures long-term persistence (Research 1991).

The Yamal testing area was founded during geological

prospecting operations at the Bovanenkovskoe field (open-pit No. 4), the Khrasaveiskoe field (an old open-pit), the Tambej oil-bearing province (drilling site No. 30 TEGRB), and an industrial site UKPG–IAS (New Urengoi) (Fig. 4). Observations were carried out systematically from 1987 to 1991.

During the observation period, a selection of grass mixtures composed of several grass species and agrotechnical conditions for their cultivation were identified. Techniques for the application of the polymer cover were also developed. The phenological stages of growth and development of the seeded plant community were measured, including density of grass, sod cover, and winter resistance of separate species.

In determining the composition of the seed mixtures, except for the analysis of agro-climatic characteristics, the characteristics of new tundra soil and the biological traits of each species were taken into consideration. The natural vegetation cover of Yamal is composed of such local Graminoids as *Festuca pratensis* and *Festuca ovina*, *Poa pratensis*, ecotypes of *Festuca rubra* and *Calamagrostis*. Perennial herbs were among the first plants to populate disturbed lands during recovery. This property is complementary since it accelerates the structural organization of species diversity that provides resilience of the vegetation cover over time. Selection of species with various life histories and phenology provides for more consistent biomass accumulation and incorporation into the disturbed substrate over time. Therefore, grass mixtures should preferably be composed of species that differ by their requirements and ecological niches.

The recommended plant community includes Graminoids with high productivity, the ability to persist in the stand over long periods of time and, in turn, facilitate more complete use of environmental resources.

After observing the condition of seeded plant communities after several growing seasons, it was noted that the inclusion of hardy grass species that were resistant to deer grazing was necessary for sustained sod establishment.

In the short term, the time of sowing during the growing season played a large role. Observations indicate that sowing in mid-June gives multi-year grasses going into winter the maximum number of short (wintering) shoots and adequate supplies of nutrients in the tillering node.

Development of agrotechnical methods, including selection of grass mixture composition was carried out under the oversight of the Polar Experimental Plant-growing Station of the Russian Academy of Agricultural Sciences.

During monitoring of seeded plant communities, the rapid accumulation of soil nutrients was observed. After three years, treated plots exceeded reference soils in virtually all agrochemical indices. Polymer cover creates the optimum conditions for soil microflora and improves plant root nutrition. It also provides for plant biomass growth, organic matter accumulation, and fast formation of a biogenous-humus accumulative layer (Research 1990).

Pilot testing was carried out in the Bovanenkovskoye deposit (open-pit mine No. 4) and the drilling site of Tambej oil and gas province. Technical solutions concerning the application of aqueous polymer emulsion in order to create polymer cover after grass sowing were tested (Fig. 5). On

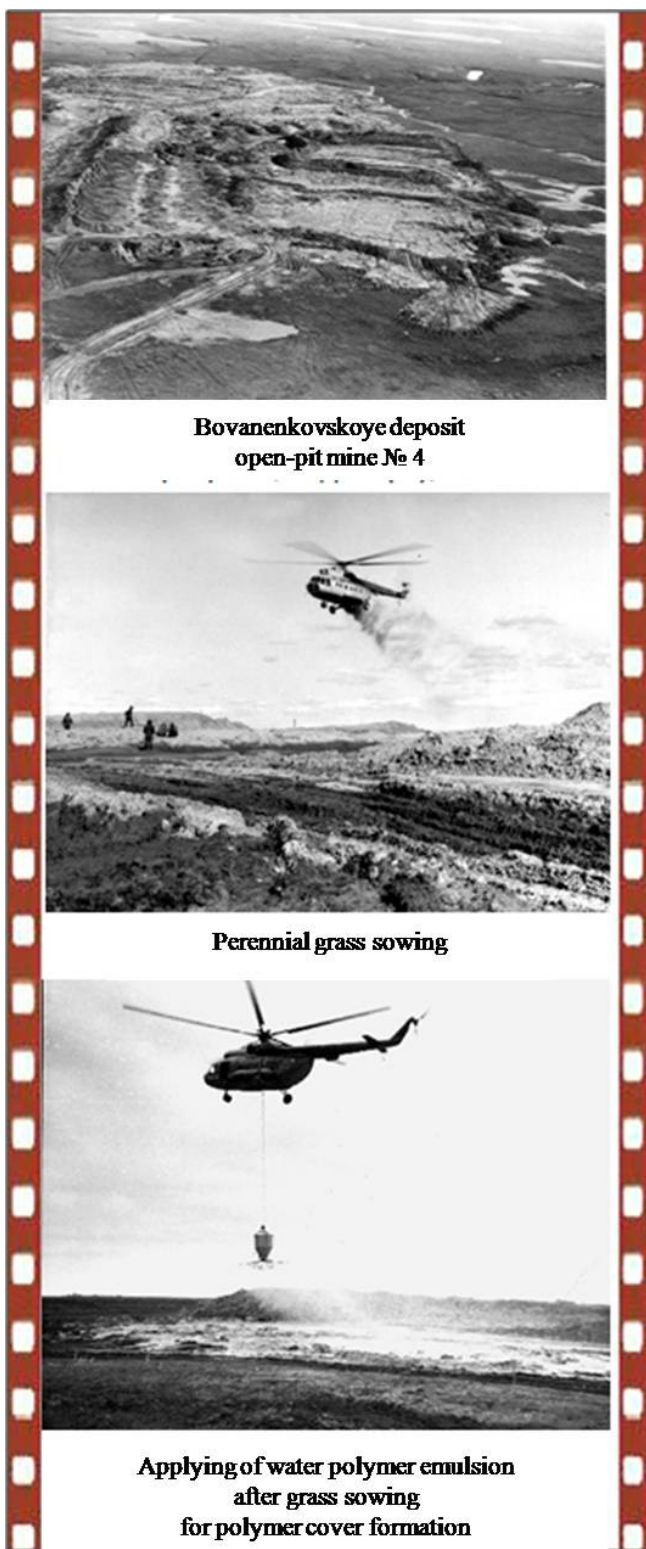


Figure 5. Pilot testing of the aqueous polymer application in Bovanenkovskoye deposit (open-pit mine No. 4).

the basis of those studies and pilot tests, protocols have been developed on remediation (regeneration) of soil-vegetative cover for the degraded lands of Yamal.

In 1991, an international conference “Environmental measures during oil and gas fields development in the Arctic regions” was organized by “Gazprom” state gas jointly with Amoco Co., USA. Consensus was reached at the conference that this was the most economically, technologically, and ecologically effective technology, and it was recommended

for a feasibility study for projects on the Yamal gas-condensate fields during development of infrastructure.

The technology proposed is:

- universal: it is effective in different substrate types, in different climatic zones, and applicable on any relief;
- technological: its use of mass-produced, multipurpose technique allows for fast technological realization on projects of various scales;
- highly productive: it allows remediation of large areas in a short time;
- environmentally friendly and cost effective: materials used are relatively cheap, nontoxic, and biodegradable.

The formation of resistant sod grass cover during remediation of degraded lands in the permafrost region, in addition to solving environmental problems, increases stability of operational facilities by minimizing thermal erosion. Expenses are of a one-time nature since restored lands do not need re-treatment.

References

- Counting the cost of environmental management. 1994. *Mining Journal* 322 (no. 8272): 287.
- Melnikov, N.N. (ed.). 2010. *Innovative technologies and advanced methods for engineering support of mining and processing operation*. Collected Book of Innovation Projects, Apatity, St. Petersburg.
- Mesyats, S.P. 2004. Restoration of soil-ecological functions of the territory as a conceptual model of adaptive technologies of damaged lands remediation. *Ecology of Anthropogene and Modern Age: Nature and Man*. Scientific Papers Collection of the International Conference, Volgograd-Astrakhan, 24-27 September 2004, St. Petersburg, Humanistika, pp. 398-408.
- Mesyats, S.P. & Melnikov, N.N. 2005. Concept and technological solutions of damaged lands remediation of mining and industrial complexes. *Formation of Fundamentals of Nature Management Modern Strategy in Euro-Arctic Region*, Apatity, KSC RAS, pp. 357-364.
- Research memorandum (final). 1987. In order to study the technogenic changes of environment and to develop measures of landscape protection of Urengoi and Medvezhy deposits and sites of the main gas pipelines. TYUMENNIIGIPROGAS, Tyumen, pp. 54-62.
- Research memorandum (final). 1990. Development of methods of damaged lands remediation in the area of Urengoi gas and chemical complex. MI KSC RAS, Apatity, p. 115.
- Research memorandum. 1991. Adjustment of agrotechnical techniques of vegetative cover restoration in landscapes of Bovanenkovskoye deposit. MI KSC RAS, Apatity, p. 47.

Impact of Oil Pollution on the Depth and Cryogenic Structure of the Seasonally Frozen Layer at Samotlor Field, West Siberia

E.S. Miklyaeva, V.A. Soldatov

Lomonosov Moscow State University, Department of Geography, Moscow, Russia

Abstract

This paper presents the results of the field study of oil pollution at Samotlor Field in West Siberia in summer and winter periods. It shows that light hydrocarbons of oil may remain in the seasonally frozen layer for a long period of time. The impact of oil pollution on the depth and the cryogenic structure of the seasonally frozen layer was established.

Keywords: alkanes; cryogenic structure; cryolithozone; ecology; hydrocarbon pollution; seasonal freezing.

Introduction

The modern oil production industry tends to relocate toward the northern regions of discontinuous and continuous permafrost. This includes the Vankor oil and gas field in Middle Siberia, the Varandeyk oil field in the European North, the exploitation prospects of the Yamal oil and gas condensate fields, and resources of the arctic shelf. Considering the fact that ecological requirements are being increased and new technologies are being incorporated, ecological conditions will be much more favorable at the new fields in comparison with the sites of long-term management of mineral resources. However, a potential hazard still remains as the territories may be polluted by oil and oil products due to emergencies. In this regard, the problem of hydrocarbon pollutants on seasonally and perennially frozen ground is of increasingly great interest.

Currently, data are collected on the distribution and transformation of oil and oil products in the seasonally frozen and the seasonally thawed layers. Researchers are studying the impact on the parameters of the seasonally frozen and the seasonally thawed layers. Special field research in the distribution of pollutants in freezing and thawing ground is playing an important role.

Our research was carried out in the “oldest” area of oil production in West Siberia, at the Samotlor Field, which has been technogenically disturbed for more than 40 years. The area is being intensively restored, but hydrocarbon pollution still remains the major geochemical factor that alters the natural environment (Solntseva 1998).

The geocryological zone of the field is characterized by an island type of permafrost distribution (less than 10% of area occupied by permafrost), but recently permafrost islands were not observed, which is probably related to intensive technogenic activity. The long-term seasonal freezing of ground occurs in the entire territory.

Methods

In order to investigate the impact of oil pollution on the seasonally frozen soil layer, an oil-polluted site within the second terrace above the floodplain of the Ob River was selected in the southwestern part of Samotlor Field. The site has an area of 1 ha and is characterized by the degrees of oil pollution that are average and high (15000-100000 mg/kg and more for the mineral soils). The oil was spilled here

five years ago. Natural landscapes are occupied by cedar and spruce green moss forests on the sod-podzolic soils. The upper part of the ground is composed of the upper Pleistocene interstratified silts and silty clays.

The investigated site is located on a slope of eastern aspect with an elevation difference of 11 m (57–46 m a.s.l.). The vegetation cover at the polluted area is in a suppressed state. The grass (mostly Gramineae) is characterized by spotted distribution. Stunted undergrowth of birch and aspen also occurs in this area. Hypsometrically a low shrub bog is located below the oil-polluted area.

Field research was conducted in summer (August 2009) and winter (January 2010). During the summer fieldwork, three test pits were dug out on the slope of the selected site. Test pit #1 is located at the upper part of the landscape catena. Test pit #2 is located at the middle slope, and test pit #3 is found at the foot of the slope. The depth of the test pits was up to 60 cm, while the distance between them is 50–55 m.

Each soil horizon of the test pits was described and the samples were selected to define the hydrophysical properties of ground and to analyze the oil pollution. Samples for the definition of the content and composition of hydrocarbon pollution were put in special containers where they were hermetically sealed in order to prevent the evaporation of hydrocarbon compounds.

In winter 2010, test pit #4 was dug at the upper part of the catena not far from test pit #1 under the same landscape and ground conditions. Each horizon of the new test pit was also sampled for laboratory analysis. While describing the ground horizons, special attention was paid to the depth of seasonal freezing as well as to the cryogenic structure of the ground. The temperature was measured within the ground profile. Temperature measurements were made with lag thermometers lowered into the ground at different depths from the surface and kept there for 3 hours.

Outside the oil-polluted area, “background” test pit 0 was established in which the same procedures were carried out: lithology and cryogenic structure were described, while temperature and depth of seasonal freezing were measured.

The general hydrocarbon content in the samples was determined by Dr. M.S. Rosanova, Department of Soil Science, Lomonosov Moscow State University. The content and composition of n-alkanes of medium and light (volatile) oil fractions were defined by the Dr. Yu.A. Zavgorodnyaya at the same department.

Research Results

The soils at the investigated site are mainly represented by silty clay and less often by silt. The upper part down to the depth of 6 cm is composed of the black, structureless litter with some peat. The litter in test pit #1 at the upper catena has a clear indication of pollution of high-molecular hydrocarbons. Silty clay contains more clay particles with depth. Silt with some clay is found in test pit #2 at the slope and in test pit #3 at the foot of the slope within the intervals of 6–14 cm and 6–18 cm, respectively. The color of the clayey and silty sediments in the upper part is dark brown and dark red, while their composition is dense or of average density. In general, the profile composition is rather homogeneous, which is important for the research on oil pollution.

Analysis of the samples indicated that most of the oil products (the general hydrocarbon content) are concentrated in the upper 6 cm layer of test pit #1. The oil product content in it consists of 363,000 mg/kg (of dry ground). Thus one-third of the dry mass of this layer is attributed to the oil components (the resin and asphaltene fraction is not considered). This is the so-called “bitumen” crust. It developed due to the proximity of the pollution source and due to the considerable sorption capacity of the litter with low moisture content.

In general, the investigated test pits are characterized by the decrease of the pollutant content down the profile, whereas the distribution of oil products is quite variable. The rapid decrease of oil product concentration is observed toward the bottom of test pit #1 at the upper part of the catena from 363,000 mg/kg in the upper 6 cm to 300 mg/kg at the depth of 50 cm. The decrease of oil product concentration in test pit #2 at the slope is indicated less clearly (from 30000 mg/kg close to the surface to 4000 mg/kg at the depth of 50 cm). Test pit #3, located at the foot of the slope, was marked with two peaks of oil product content: 18000 mg/kg in the near-surface horizon and 15000 mg/kg in the lowest horizon.

A decrease in oil product content may be noted in the litter down slope (363000 mg/kg, 30000 mg/kg and 18000 mg/kg at the foot of the slope), which is explained by the fact that the pollution source becomes more remote. At the same time, the increase of oil product content is marked down slope in the lower part of the profile at the depth of 50 cm (300 mg/kg, 4000 mg/kg, 15000 mg/kg), which occurs due to subsurface oil redistribution.

The general content of oil products is not an indicator of contemporary oil pollution, of the degradation rate of oil, or of the peculiarities of the pollutant distribution in the ground after a long period of time. The total concentration of normal (saturated) alkanes may be used as such an indicator.

Saturated alkanes were selected as the major indicator of the state of oil pollution because of the persistence of their migration capacity over time (explained by their “saturation”). Another factor in their selection was the possibility of their considerable degradation due to microbiological activity and photochemical reactions. (Cycloalkanes and arenes are much less exposed to degradation.)

Figure 1 shows the diagram of n-alkanes distribution in the upper 40 cm of ground on the slope within the investigated site. The diagram was drawn based on the data about the content of n-alkanes in the soil horizons of each test pit.

The drawn diagram of n-alkanes distribution shows that the subsurface lateral runoff was one of the main directions of oil migration. The radial migration of oil in test pit #1 was probably observed down to the depth of 14–17 cm. Then the main flow of the pollutant went down the slope toward test pit #2. The highest concentration of n-alkanes was measured from the lower horizon of test pit #3, which corresponds well with the assumption that the filtration of most methane hydrocarbons occurs in the ground at a depth of 20–40 cm from the surface (Pikovskiy 1993). Thus rather high, medium hydrocarbon concentrations (diesel) and even a volatile fraction may remain below the turfed upper horizons for a long time, accumulating high molecular hydrocarbons as well as resin and asphaltene substances.

The contemporary state of oil pollution at the investigated site may be characterized through the use of the ratio of the sum of “light” n-alkanes (C15–C24) to the sum of “heavy” ones (C-25–C34). The content of “light” n-alkanes exceeds that of “heavy” ones in almost all the horizons of test pits 1–3. The exception is the horizon within the interval of 0–6 cm of test pit #1 where the ratio is 49/51 and by the lower horizon of test pit #3 where it is 47/53. In the middle parts of the profiles, this ratio ranges from 60/40 to 89/11. The ratio of the light alkanes to the heavy ones is 85/15 in the lower part of the profile of test pit #1, which indicates that the light hydrocarbon fraction remains in the lower part of the profile.

Thus, five years after the oil spill, the portion of “light” n-alkanes (making up 80–90% of the oil) remained almost unchanged in some horizons of the test pits, while in the rest of the horizons it decreased slightly. These facts indicate the preservation of oil pollution at the site investigated and, therefore, the extremely low degradation rate of the hydrocarbons in the grounds of the seasonally frozen layer. Only the upper horizon of test pit #1 (the “bitumen” crust) and the lower horizon of test pit #3 make an exception. The considerable degradation rate of n-alkanes in the former case (the “bitumen” crust) is linked to the fact that the soil horizon is close to the surface and is well aerated. Besides, it is linked to the possibility of photochemical decomposition of methane hydrocarbons. In the latter case (test pit #3), it is most probably caused by the fact that during the spring flooding they are carried into the bog mass located hypsometrically lower.

Field research conducted in the winter period revealed that the depth of the zero degree isotherm in test pit #4 located within the oil-polluted site was only 15 cm during the fieldwork (Fig. 2), which does not represent the typical value of the depth of seasonal freezing for the site investigated. Meanwhile, the depth of the zero degree isotherm in “background” borehole #0 was not reached, which means that it was more than 30 cm (Fig. 3). As the figures show, the temperature distribution is also different. Although the temperature values are similar at the ground surface (the snow thickness at both sites is 50 cm), we see that the temperature gradient of the polluted ground is twice as high as that of the unpolluted ground. According to the temperature measurements, the temperature gradient in the upper 4 cm of test pit #1 reached 1.45°C/cm, while in the upper 3 cm of the “background” test pit it was 0.87°C/cm. This horizon represents a “bitumen” crust, one-third

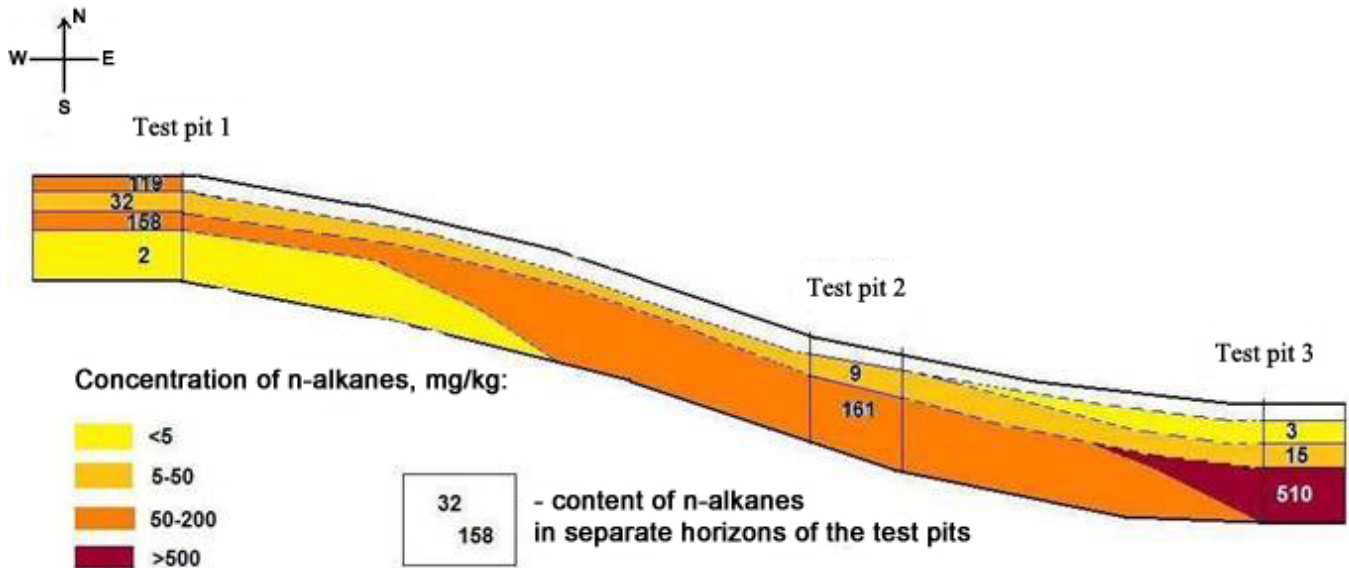


Figure 1. Distribution of n-alkanes in the upper ground horizons of the oil-polluted site.

of which consists of high molecular oil hydrocarbons that significantly affect the thermal conductivity of ground (Motenko et al. 2000).

Three types of cryogenic structures were described for the profile of test pit #4: the massive cryogenic structure developed at the depth of 0–7 cm followed by the reticulate cryogenic structure (7–11 cm). At the depth of 11–15 cm there occur well-marked ice lenses reaching 10 mm in length and 2–3 mm in width. The distance between the ice lenses is 5–6 mm (Fig. 2). The entire profile of the “background” test pit is characterized by a massive cryogenic structure (Fig. 3).

It should be also noted that the layer with maximum segregation ice formation in test pit #4 is associated with the horizon characterized by the highest content of n-alkanes (158 mg/kg). Such a ratio is not accidental. Field research conducted in Khimkinskiy District near Moscow in winter 2005/2006 (monitoring of the seasonal freezing of the ground polluted by diesel) revealed that the maximum values of segregated ice formation were obtained in the horizons that were the most polluted by the diesel fuel (Miklyaeva & Zepalov 2008). As the portion of n-alkanes in diesel exceeds 90%, it is absolutely relevant to draw an analogy between the results of this field research and the results obtained within the oil-polluted site on the territory of Samotlor Field in winter 2010.

The increase of ice formation under the freezing of ground polluted by diesel was also shown in laboratory work by S.E. Grechishchev.

It should be noted that in the freezing ground polluted with the diesel fuel, the values of the temperature regime and of the depth of seasonal freezing were close to the values at the unpolluted site. It is evidently high-molecular hydrocarbons as well as resin and asphaltine substances that exert influence on the temperature regime of the ground and, therefore, on the depth of seasonal freezing. The pollution by hydrocarbons of medium and light fraction (diesel and petrol) does not affect these parameters. However, it increases the intensity of segregated ice formation, alters

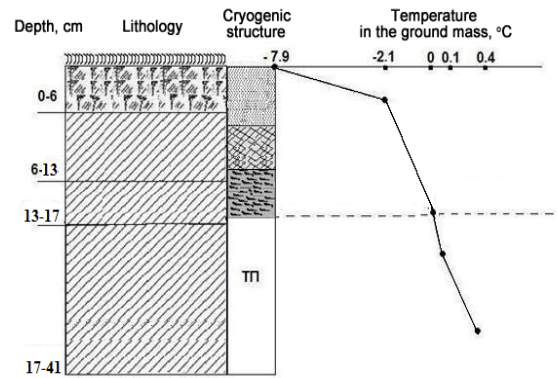


Figure 2. The lithology, cryogenic structure, and the temperature of ground within the profile of test pit #4.

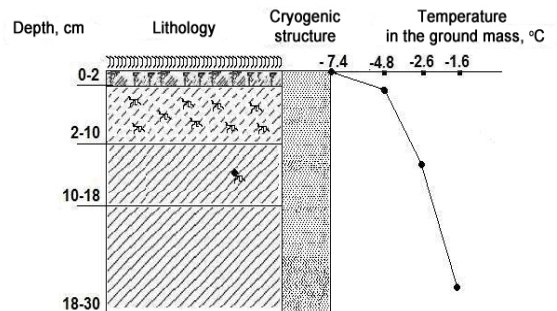


Figure 3. The lithology, cryogenic structure, and the temperature of ground within the profile of “background” test pit #0.

the cryogenic structure, and, according to our previous investigations, increases the ground heaving.

Thus the oil pollution of the seasonally frozen layer within the investigated area exerts a significant impact on the parameters of the seasonally frozen layer. First of all, it causes a general decrease of the freezing depth and, secondly, it increases segregated ice formation in the horizons with the high content of methane hydrocarbons

Acknowledgments

We would like to express our gratitude for the assistance in research to the Dr. M.S. Rozanov, Dr. Yu.A. Zavgorodnyaya, and the staff of the Soil Station of Lomonosov Moscow State University, who determined the hydrocarbon content of the samples in the laboratory.

References

- Miklyaeva, E.S. & Zepalov, F.N. 2008. The peculiarities of seasonal freezing of ground polluted by the diesel fuel: The natural experiment in the Khimkinskiy region near Moscow). *Kriosfera Zemli* 12, No. 2 (in Russian).
- Motenko, R.G., Cheverev, V.G., & Zhuravlev, I.I. 2000. The impact of oil pollution on the thermophysical properties of frozen dispersed ground. *The collection of works: Geophysical investigations of cryolithozone*. 3rd edition, Moscow, 2000, pp. 13-138 (in Russian).
- Pikovskiy, Yu.I. 1993. *The natural and technogenic flows of hydrocarbons in the environment*. Moscow: Izd-vo MGU (in Russian).
- Solntseva, N.P. 1998. *Oil production and geochemistry of natural landscapes*. Moscow: Izd-vo MGU, 256 pp. (in Russian).

Design of Reliable Bases and Foundations in Permafrost Regions

M.A. Minkin, O.A. Potapova
Fundamentproekt, Moscow, Russia

Abstract

The methodology for reliable assessment of bases and foundations on permafrost is developed. It is based on the models of the control of natural-technical geosystems. Examples are provided for assessments of site selection for structures and technical solutions for bases and foundations.

Keywords: bases; foundations; natural-technical geosystems; natural-territorial complexes; project models; reliability value; technical concepts.

Introduction

Implementation of reliable bases and foundations in the cryolithozone is associated with the solution of a number of scientific and practical problems, including:

- design and construction provisions with the necessary and reliable engineering-geocryological information;
- development of a standardized methodology for structures on permafrost;
- development of the most efficient foundations and methods of foundation construction under specific engineering-geocryological conditions;
- establishment and improvement of process-based methods for estimating thermal and mechanical interaction of structures with permafrost;
- design and implementation of measures for the engineering preparation of the ground for the bases, for the protection of the construction area and facilities, and for environment preservation;
- maintenance of the projected thermal and water regimes of the ground and foundation loads;
- geotechnical monitoring and control of the structure's bases and foundations in the process of construction and operation.

Long-term experience in northern regions development has shown that solutions to such problems are possible only with the help of a systematic approach to the construction and operation of engineering structures. First, this means that bases and foundations should be considered as components

of natural-technical geosystems, including both engineering structures and natural environment zones.

Second, the individual approach to engineering structures should take into account the peculiarities of the structures and the engineering-geocryological conditions. This approach must match the design methodology used for all structures. The methodological sequence chart is given in Figure 1.

Taking into account the diversity of engineering structures and their technogenic impacts as well as the complex natural conditions of the northern regions, the management and control of natural-technogenic geosystems is required at all stages of their construction and operation. During design and research operations, this control is provided by project models and during construction, operation, and demolition of real structures. The principle chart (Fig. 2) shows target functions, quality criteria, and control methods for the geotechnical and natural subsystems of natural-technogenic geosystems.

Control of the project model consists of the selection of the best option for structure layout and the most efficient process and design parameters as well as methods of the preservation or improvement of the parameters of natural-technogenic geosystems.

Control of real structures includes the following provisions: the design values for the parameters of a natural-technogenic geosystem; operational evaluation and forecast of this system's state; the development of stabilizing emergency or liquidation activities; and bringing the

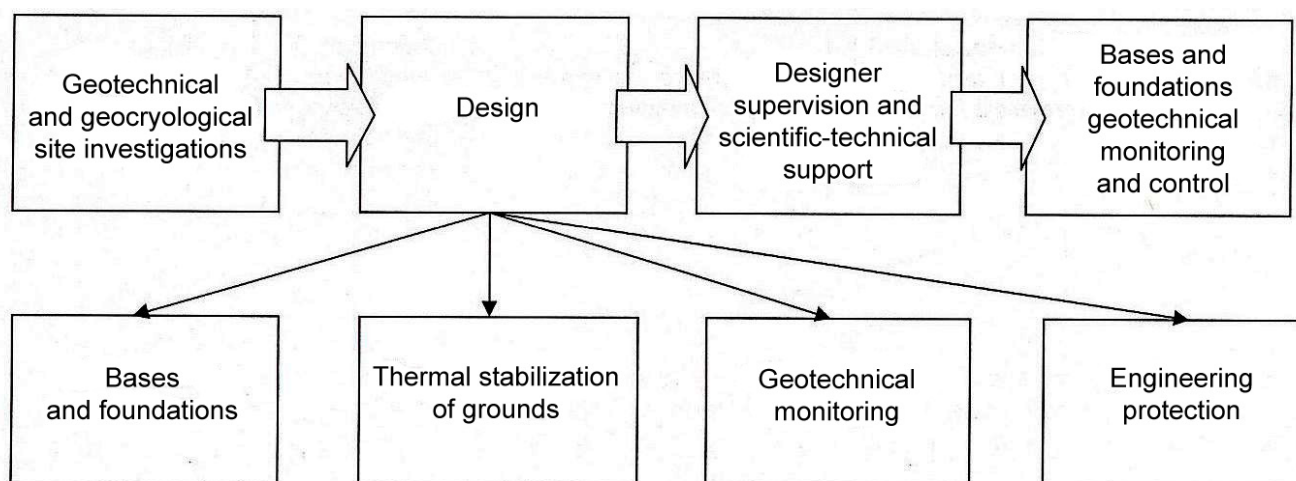


Figure 1. Flow chart of bases and foundations design.

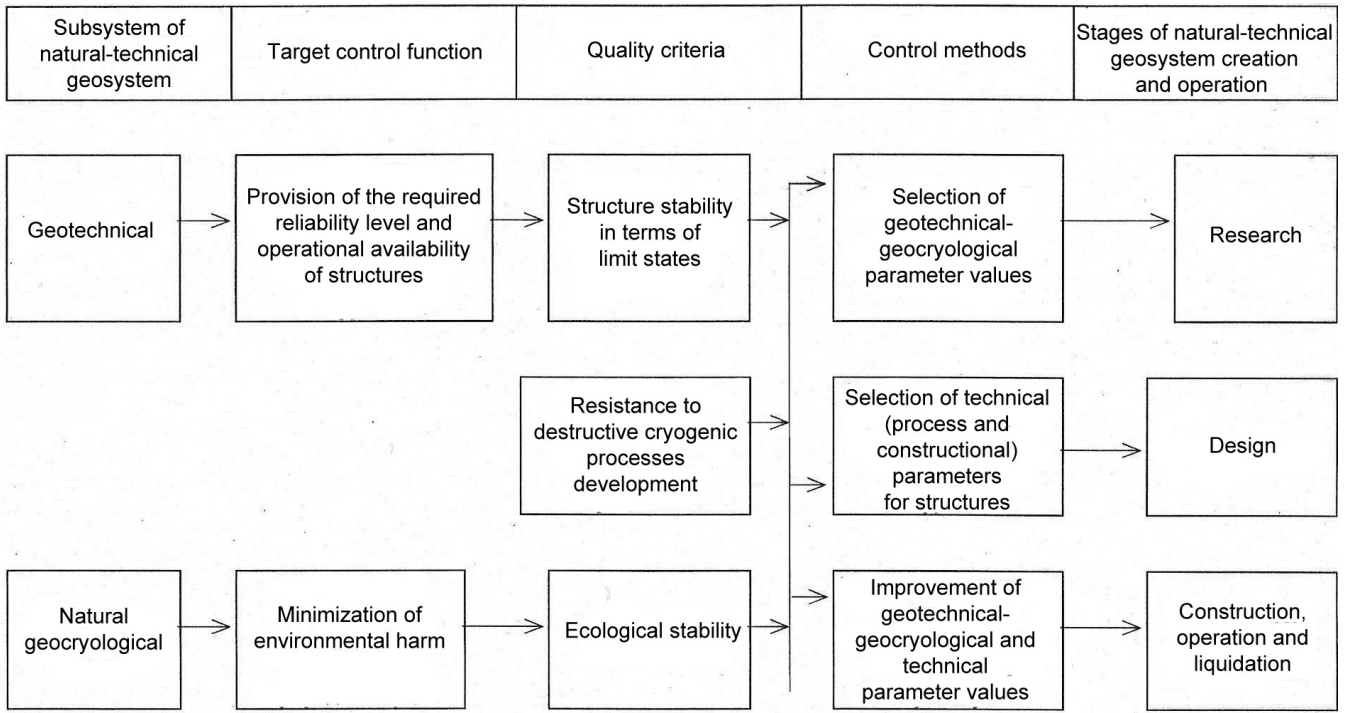


Figure 2. Principle control chart for natural-technical geosystems.

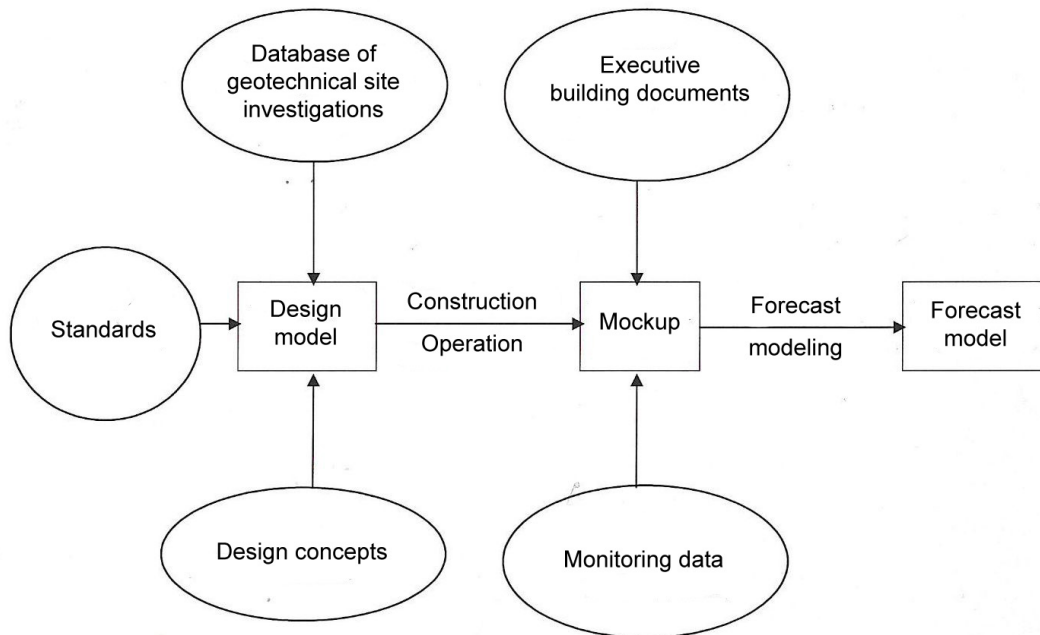


Figure 3. Chart of the development of informational models for a natural-technogenic geosystem.

natural-technogenic geosystem into the regime that ensures the operational availability of structures and the safety of the natural environment. The chart of the development of informational models for a natural-technogenic geosystem is given in Figure 3.

The quality of a natural-technical geosystem is evaluated based on the reliability value (i.e. the probability of meeting the quality criteria given in Table 1). The reliability value is defined by the method of multi-variant computer modeling, with the local databases serving as the method's informational basis (Minkin 2005).

Let us describe several examples of reliability studies for the design models of natural-technical geosystems. The first example is related to the selection of the site for a gas

processing facility at one of the gas fields in the north of West Siberia. Three options (Table 2) of positioning the gas processing facility within different natural-territorial complexes were examined.

The first option is to locate the gas processing facility within two types of natural-territorial complexes: 1a (80% of the area) and 3v,g (20%). If the ground is used according to Principle I, the reliability value P is 0.21; if it is used according to Principle II, P=0.60. The second option is for positioning the gas processing facility (natural-territorial complex 3v,g – 75%, natural-territorial complex 4g,d – 25%). The use of ground according to Principle I gives P=0.69, while Principle II gives P=0.

For the third positioning, reliability values are (natural-

Table 1. Quality criteria of natural-technogenic geosystems.

System	Subsystem	Condition of quality loss	Logical correlation	Legend
Geotechnical	Building – ground base	By foundation bearing capacity	$F_u(\tau) \geq F(\tau)$	$F_u(\tau)$ – foundation bearing capacity at the moment τ ; $F(\tau)$ – foundation load at the moment τ .
		By foundation settlement	$S(\tau) \leq S_u$	$S(\tau)$ – combined foundation and building deformation at the moment τ ; S_u - maximum allowable deformation.
		By frost heave resistance	$F_y(\tau) \geq F_n(\tau)$	$F_y(\tau)$ – forces keeping the foundation from heaving, including foundation load at the moment τ ; $F_n(\tau)$ – frost heave forces influencing the foundation at the moment τ .
	Underground pipeline – ground base	By the strength of pipe material	$G_n(\tau) \leq G_{lim}$	$G_n(\tau)$ – longitudinal stress in the pipeline at the moment τ ; G_{lim} - critical strength of metal.
		By the pipe stability in the longitudinal direction	$F_{gr}(\tau) \leq F_{lim}$	$F_{gr}(\tau)$ – longitudinal compression strength at the moment τ ; F_{lim} - critical pipe resistance in the longitudinal direction.
		By the pipe resistance to floating	$F_{act}(\tau) \leq F_{pas}(\tau)$	$F_{act}(\tau), F_{pas}(\tau)$ – expulsive and restraining forces at the moment τ .
Geotechnical	Road – ground base	Base bearing capacity	$F_{ur}(\tau) \geq F_r(\tau)$	$F_{ur}(\tau), F_r(\tau)$ – bearing capacity of the road pavement and the load transferred to the pavement at the moment τ .
		Base deformations	$S_r(\tau) \leq S_{ur}$	$S_r(\tau)$ – joint base and pavement deformation at the moment τ ; S_{ur} - maximum deformation value.
Natural geocryological	Thermokarst-hazardous	By the resistance to thermokarst development	$S_{th,t} \leq S_{th,0.5t}$ or $S_{th,t} > S_{th,0.5t}$ and $V_{th} < 2$	$S_{th,t}, S_{th,0.5t}$ - surface settlement for the period $t, 0.5t$ years; $V_{th} < 2$ – mean surface settlement velocity, cm/yr
	Frost-heave-hazardous	By the resistance to frost heave formation	$d_{th,t} \leq d_{th,0.5t}$ or $d_{th,t} > d_{th,0.5t}$ and $V_{th} < 1$	$d_{th,t}, d_{th,0.5t}$ - frost heave deformation for the period $t, 0.5t$ years; $V_{th} < 1$ - mean deformation velocity, cm/yr
	Crack-hazardous	By the resistance to cryogenic cracking	$[(1-\nu) \times \sigma_{th}] / (\psi \times E_{th}) \geq \alpha_{\infty} \times T_{01} $	ν – Poisson coefficient for permafrost σ_{th} - long-term tensile permafrost strength limit; E_{th} – long-term permafrost deformation module; α_{∞} – coefficient of linear temperature extension of permafrost; T_{01} – mean surface temperature during the coldest month; ψ – dimensionless coefficient.
	Thermal erosion-hazardous	By the resistance to thermal erosion	$E/K_1 < 0.01$ and $T/K_2 < 0.01$	E – kinetic energy of the stream; T – stream temperature; K_1, K_2 – parameters of mechanical and thermophysical washaway of permafrost.
	Solifluction-hazardous	By the resistance to solifluction movement	$\tau \leq \tau_{sh}$	τ – ground shear stress value; τ_{sh} – ground resistance to shear strength.
	Icing-hazardous	By the resistance to icing formation	$H_i \leq H_{cr}$	H_i - value of cryogenic pressure in permafrost; H_{cr} - critical value of cryogenic pressure.

territorial complex 1a – 100%): $P=0.11$ (Principle I) and $P=0.75$ (Principle II). In terms of resistance to the development of unfavorable cryogenic processes, the first option results in $P=0.87$, the second option in $P=0.37$, and the third option in $P=1.0$.

Therefore, the third option when the ground base is used according to Principle II (i.e., in the thawed and thawing state) is the most favorable for the positioning of the gas processing facility.

Since the value of the reliability of the natural-technical geosystem $P=0.75$ for this option is below the regulatory value ($P_r=0.95$), additional activities are required to increase

the reliability. These activities can include a more detailed study of engineering-geocryological conditions and changes of the foundation design.

The second example is dedicated to the assessment of the impact of technical solutions on base reliability.

The reliability values of bases for the following different options of technical solutions are given for typical structures in Table 3: without special activities for ground cooling, with a ventilated cellar, with a seasonally operating cooling device. Moreover, the table shows the obtained estimates of the territory resistance to the development of cryogenic processes (thermokarst, frost

Table 2. Values of base reliability for different options of positioning the gas processing facility.

Positioning option number	Natural-territorial complex		Engineering-geocryological conditions				Reliability value							
	Index*	Area occupied, %	Permafrost area, %	Ground conditions and ice (i) content	Permafrost table depth, m	Mean annual temperature, °C	Geotechnical subsystem				Natural geocryological subsystem			
							Principle I		Principle II		Resistance to cryogenic processes			
							Mean value		Mean value		Mean value	Mean value		
1	m,laLT ² , 1a	80	50	Fine and medium sands without visible ice	2.0 to >15.0	+0.5 to -1.4	0.11	0.21	0.75	0.60	1.0	0.87		
	m,laLT ² , 3v, g	20	100	Silty clay, silt and sand alternation i _i up to 0.3-0.5	2.0 to 2.9	-0.3 to -2.5	0.62						0.0	0.37
	m,laLT ² , 3 v, g	75	100	Silty clay, silt and sand alternation i _i up to 0.3-0.5	2.0 to 2.9	-0.3 to -2.5	0.62						0.0	0.37
2	m,laLT ² , 4 g, d	25	100	Peats, organic-rich silty clay underlain by sand and silty clay i _i up to 0.3-0.5	0.4 to 1.0	-2.8 to -5.2	0.93	0.69	0.0	0.0	0.36	0.37		
3	m,laLT ² , 1a	100	50	Fine and medium sands without visible ice	2.0 to >15.0	+0.5 to -1.4	0.11		0.75		1.0			

*- The natural-territorial complex indexes in all tables are given on the basis of the work (E.S. Melnikov, 1983).

Table 3. Reliability assessment of natural-technical geosystems.

	Within boundaries of structures					Within the impact zone of structures			In natural conditions			
	Industrial and residential buildings of a framed type			Utilities corridors		Resistance to the formation of						
Natural-territorial complex index	Without additional activities	With a ventilated cellar, without a seasonally operating cooling devise	With preliminary cooling with a seasonally operating cooling devise and a ventilated cellar	Without a seasonally operating cooling devise	With a seasonally operating cooling devise	thermo-karst, frost heave	cryogenic cracking	Total	thermo-karst, frost heave	cryogenic cracking	Total	
1zh	0.0	0.30	1.0	0.0	1.0	0.10	1.0	0.10	0.20	1.0	0.20	
1d	0.0	0.40	1.0	0.0	1.0	0.20	1.0	0.20	0.40	1.0	0.40	
6b	0.0	0.92	1.0	0.0	1.0	0.0	1.0	0.0	0.60	0.95	0.57	

heave, cryogenic cracking) under natural conditions and in the structure's impact zone. Assessment of the reliability of natural-technical geosystems was completed based on the structure's operational availability criteria and the criteria of resistance to the development of destructive cryogenic processes given in Table 1. The reliability value was defined based on the relation $P=1-n/N$, where N is the number of

calculation options, n is the number of failures. The failure was registered if at least one criterion was not met for any calculation option.

The characteristics of engineering-geocryological conditions of the natural-technical geosystems under study are given in Table 4.

The Stephen-type calculation method for the solution of

Table 4. Engineering-geocryological conditions of the natural-territorial complexes under study.

Natural territorial complex index	Ground dominating in the section of structures' bases	Permafrost area, %	Depth of seasonally thawed layer / seasonally frozen layer m	Permafrost table depth, m	Mean annual ground temperature °C
1d	Fine and medium sands with silty clay interlayers up to 0.5-1.5 m thick	60	2.4 – 4.0	2.4 – 15.0	+0.2 ... -2.0
1a	Fine and medium sands	50	2.0 – 3.3	2.0 – 15.0	+0.5 ... -1.4
6b	Fine and medium sands alternation with silty clay and silt, ice content 0.05-0.5	100	0.7 – 2.2	0.7 – 2.2	-1.3 ... -2.8

multi-front problems on the basis of an implicit difference scheme was used as the mathematical apparatus for computer modeling. Statistical parameters for calculations were selected with the Monte Carlo method. The obtained estimates (Table 3) show that the described types of natural-territorial complexes are not resistant to technogenic loads without additional activities, and natural-technical geosystems formed within them are characterized by low reliability. In this regard, while the reliability of permafrost in the bases of industrial and residential buildings for the 6b natural-territorial complex can be provided by means of a ventilated cellar, for the 1d and 1zh natural-territorial complexes, the pre-construction cooling of permafrost and the freezing of non-frozen ground is required. The required value of base reliability for utilities at all three natural-territorial complexes can be achieved only by means of cooling during the entire operational period.

All the described types of natural-territorial complexes are characterized by low resistance to the development of thermokarst and heave processes in natural conditions ($P=0.20-0.60$), particularly in the impact zone of structures ($P=0.0-0.20$).

In natural conditions, the studied types of natural-territorial complexes are mainly resistant to cryogenic cracking, solifluction, and thermal erosion ($P=0.80-1.0$). And in the case of technogenic destructions, they are resistant to cryogenic impact and non-resistant to solifluction and thermal erosion.

The completed studies allow the selection of technical solutions for design that ensure the required reliability of structure bases.

References

- Minkin, M.A. 2005. *Methodology and methods of engineering-geocryological research*. Institut upravleniya, informatsii i biznesa. Ukhta, 252 pp. (in Russian).
- Cryolithozone landscapes in the West-Siberian gas province*. Edited by E.S. Melnikov. Izdatelstvo Nauka, 1983, 165 pp. (in Russian).

Impact of Permafrost Degradation on Northern Taiga Ecosystems in Western Siberia

N.G. Moskalenko

Earth Cryosphere Institute, SB RAS, Tyumen, Russia

Abstract

The goal of this ongoing study is to examine the interaction of permafrost and vegetation on ecosystems of the Western Siberia permafrost zone. Results of long-term monitoring of northern taiga ecosystem changes under the impact of permafrost degradation, caused by climatic changes and human-induced disturbances, are presented. Changes of various ecosystem components—microrelief, vegetation and soil covers, active layer thickness, soil and permafrost temperature, cryogenic processes—are investigated. The impact of an increase in the amount of atmospheric precipitation on the development of bog formation on flat, poorly drained sites is monitored. Long-term observations of the permanent plots have shown that vegetation removal lowered the permafrost table up to 2–3 m.

Keywords: climate change; ecosystem; fire disturbance; human-induced disturbances; landscape; permafrost; vegetation.

Introduction

Warming of the climate from the end of twentieth century and active industrial development in areas of the northern permafrost zone were accompanied by permafrost degradation, especially in the zone of sporadic permafrost. This important geocryological problem is examined in the works of many researchers (Ershov et al. 1994, Pavlov 1997, Parmuzin & Chepurnov 2001, Izrael et al. 2002, Kakunov & Sulimova 2005, Perlstein et al. 2006, Oberman 2007, Nelson et al. 1993, Osterkamp et al. 1999). However, in these works not enough attention was given to the estimated impact of permafrost degradation on ecosystems. In the present report, the author tries to fill this deficiency based on long-term monitoring of changes in the northern taiga ecosystem of Western Siberia.

Location and Observations

Research on ecosystems was carried out since 1970 on the Nadym stationary site (Fig. 1), located 30 km southeast of the town of Nadym (Moskalenko, 2006) in the zone of sporadic permafrost distribution (Melnikov, 1983). Patches of permafrost, occupying up to 50% of some areas, are closely associated with peatlands, peat bogs, and frost mounds of the III fluvial-lacustrine plain, having elevations ranging from 25 to 30 m. The plain comprises sandy deposits interbedded with clays, with an occasional covering of peat (Andrianov et al., 1973).

Ecosystem changes are observed as a result of 40 years of monitoring on permanent plots and transects in natural conditions and along the route of the Nadym-Punga gas pipeline. Observations include microrelief, species composition, vegetation cover, height, frequency, dominant plant species, soil and permafrost temperatures, and thickness and moisture of the active layer.

Results

During the last decades in the north of Western Siberia, air temperatures rose and the amount of atmospheric precipitation increased (Fig. 2 A, B.). In this connection, the

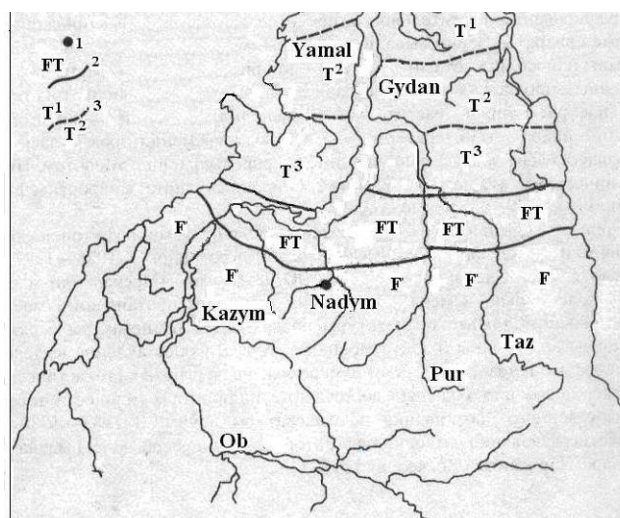


Figure 1. Location of the Nadym site. 1 – site, 2 – boundaries of zones (T – tundra, FT – forest tundra, F – taiga) 3 – boundaries of subzones (T¹ – northern, T² – typical, T³ – southern).

process of bog formation on flat, poorly drained surfaces of plains becomes more active. As a result, open woodlands (tussocky and hummocky, pine-larch, cloudberry, wild rosemary, lichen, peat moss) were replaced by andromeda-cotton grass-sedge-peat moss bogs. Hummocky ground settled, and the lenses of permafrost thawed.

The frequency of wild rosemary (*Ledum palustre*), which dominated the cover of the open woodland on the natural undisturbed plot, fell sharply after 1996 (Fig. 3).

On the disturbed plot, the frequency of wild rosemary remained low. After repeated disturbance in 2004 when the gas pipeline was replaced and the new, high embankment with broken drainage condition was built, the plot was flooded, and the wild rosemary dropped out of community composition. The frequency of cotton grass (*Eriophorum polystachium*) under natural conditions for the past decade increased, and it began to dominate the cover. In the disturbed conditions, the frequency of cotton grass is sometimes higher than in the natural conditions, but after repeated disturbance and flooding of the plot it has sharply decreased.

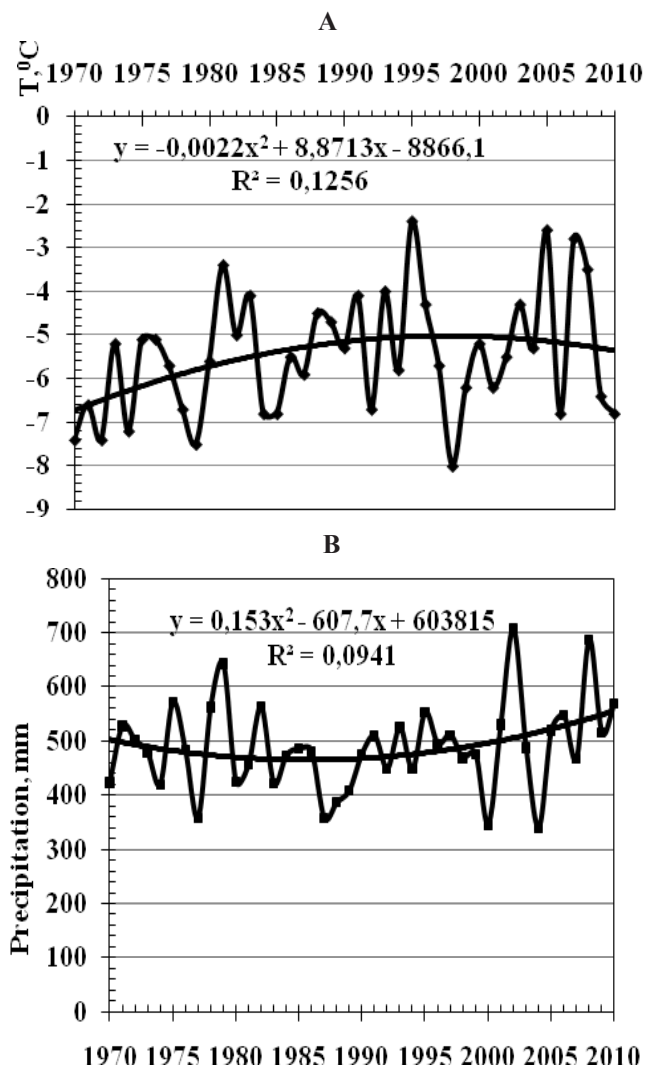


Figure 2. Mean annual air temperature (T°C, A) and precipitation changes (B).

On flat peatlands, previously covered by cloudberry-wild rosemary-peat moss-lichen plant communities, the rarified cloudberry-sedge-cotton grass-*Polytrichum* communities covering only 55% of the ground surface developed. This occurred five years after removal of the vegetation cover, disturbance of microrelief, and removal of the top 20 cm of peaty horizon. In these communities, *Rubus chamaemorus*, *Carex globularis*, *Eriophorum vaginatum*, and *Polytrichum commune* dominate. In seven years, the continuous grass-moss cover has already developed. After 10 years, a moss cover, along with the *Polytrichum* mosses and peat mosses (*Sphagnum fuscum*, *S. angustifolium*) start to play an appreciable role.

On the flat peatland, the number and the areas of pools increased after the laying of the gas pipeline that disturbed drainage conditions of surface waters. Activation of thermokarst on disturbed flat peatland with warm permafrost (-0.2 ... -0.5°C) and surface settlement of peat led to the further increase in the pool area. Bog formation increased starting in 1983 with gas pipeline construction. This resulted in increased drainage disturbance of surface waters and has caused flooding of the western part of the disturbed plot and dying off in this part of the plot of dwarf shrubs, cloudberry, cotton grass, and lichens.

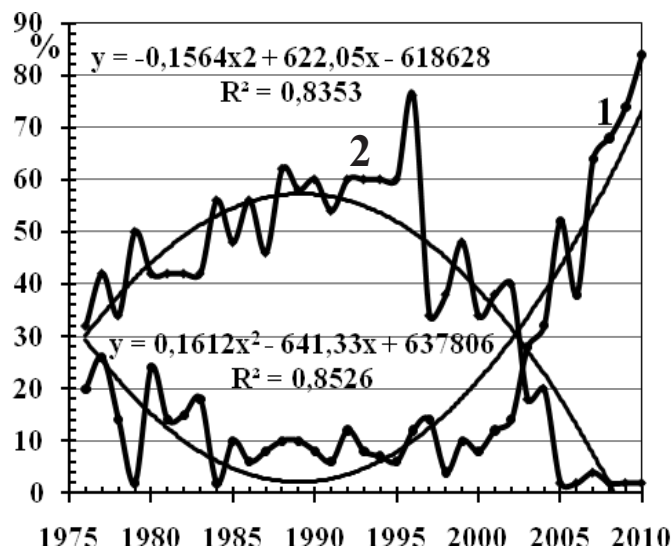


Figure 3. Frequency changes of *Ledum palustre* (I) and *Eriophorum polystachium* (II) on flat boggy site.

The number of species on the disturbed flat peatland in the first years has decreased with the disappearance of some species of dwarf shrubs, mosses, and lichens. This was reflected in a biological spectrum of the new community distinguished from a spectrum of initial community by reduction of a chamaephyte role and increase of a cryptophyte role. Furthermore, all these species again have appeared, and distinctions in the biological spectrum are not significant. However, the introduction in the new community of some cryptophyte species (*Carex limosa*, *Eriophorum scheuchzeri*), previously not observed, and the appearance of shoots of tree species (*Betula tortuosa*, *Pinus sibirica*, *Larix sibirica*), also absent in natural conditions on flat peatland, have increased the number of common species. This was reflected in a biological spectrum in which the role of phanerophytes and cryptophytes has increased.

The plant community formed on disturbed flat peatland, having increased moisture, appreciably differs from the initial plant community having fewer wild rosemary, cowberry, cloudberry and lichens, conceded the place to cotton grass and *Polytrichum* mosses.

In 2004, after the repeated disturbances associated with the replacement of a gas pipeline, the vegetation cover and peat was cut off on 75% of a plot on flat peatland, with only fragments of peat horizon remaining. The coverage of surface grasses and dwarf shrubs decreased up to 12%, and mosses up to 25%. The common number of species decreased to 30%. Woody plants dropped out of the cover (larch, pine sibirica, birch), some species of dwarf shrubs (*Chamaedaphne calyculata*, *Empetrum nigrum*) and lichens (*Cladina rangiferina*, *Cladonia amaurocraea*, *Cetraria islandica*, *Flavocetraria cucullata*) are absent also.

In 2005, because of drainage disturbance by a high embankment of the gas pipeline, 50% of the plot was flooded to a depth of 10–30 cm. By 2010, because of partial washout of the embankment, the area of flooding was reduced up to 35%. On the disturbed plot cotton grass-sedge-*Polytrichum* cover was formed and is dominated by *Carex vesicaria* and *Polytrichum commune*. The coverage of surface grasses increased up to 46%, and mosses up to 35%. Individual

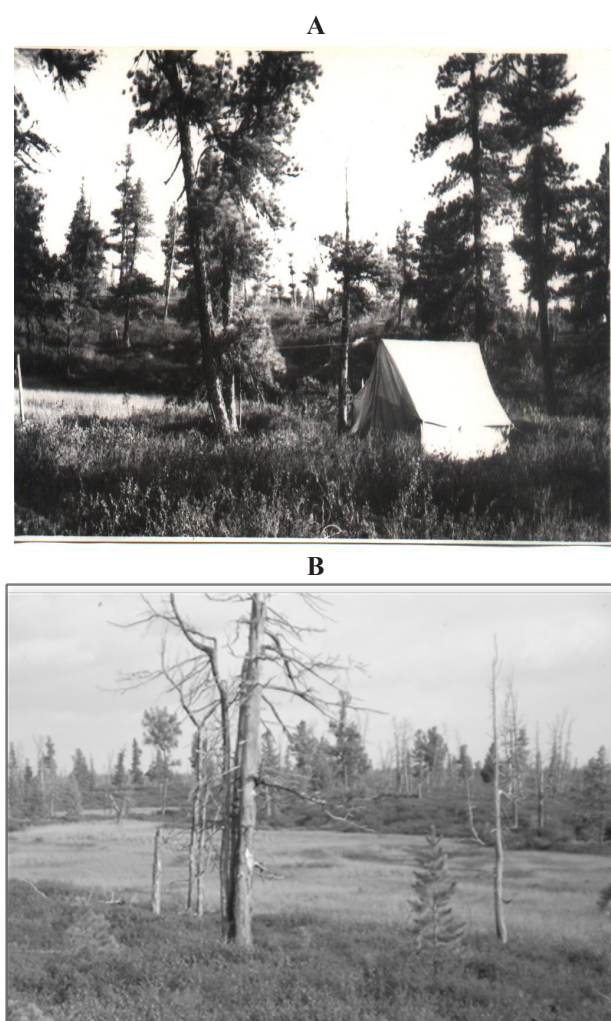


Figure 4. Frost mound before fire (A) and 35 years after it (B).

shoots of birch (*Betula tortuosa*) and pine (*Pinus sibirica*) appeared, but *Empetrum nigrum* and lichens continued to be absent.

On the disturbed peatland plot 10 m from the gas pipeline, the permafrost table has lowered to a depth of 10 m based the data of geophysical studies (Ponomareva & Skvortzov 2006).

On sites affected by fire, recovery of a vegetation cover proceeds faster than in areas with the vegetation removed, and recovery of the vegetation cover close to initial plant communities is more often observed.

For example, on frost mounds with *Pinus sibirica*-wild rosemary-peat moss-lichen open woodland, after 35 years following a fire *Betula nana*-wild rosemary-peat moss-lichen with *Pinus sibirica* 2 m in height had developed (Fig. 4).

On the permanent plot located on a flat southern slope, the frost mound height is 3 m. In a well-defined microrelief of tussocks and hummocks, heights up to 0.8 m are characteristic. Pools are usual, sometimes filled with water. Soil is sandy peat-gley, and frozen at 0.5 m depth. Average peat horizon thickness is 30 cm. A crown density of *Pinus sibirica* is 0.1, its height 7–8 m. The coverage of grasses and dwarf shrubs makes up 40–50%. The grass-dwarf shrub cover had a two-layer structure: the upper layer in height is 0.3–0.35 m composed of wild rosemary and *Betula nana*, and the lower layer in height is 0.05–0.15 m with

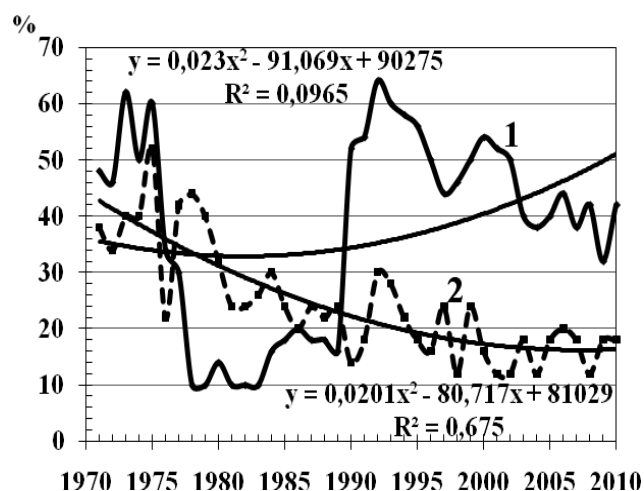


Figure 5. Frequency changes of *Cladina stellaris* (1) and *Sphagnum fuscum* (2) on the frost mound.

abundant cowberry (*Vaccinium vitis-idaea*), *Chamaedaphne calyculata*, cloudberry and sedge (*Carex globularis*). Peat mosses and lichens make up the continuous ground cover.

In June 1976 the plot of grass-dwarf shrub cover, and a forest stand was completely burned. Within two months following the fire, the surface cover of 25% consisted of shoots of *Carex globularis*, *Betula nana*, wild rosemary, and cloudberry. In pools the moss coverage of up to 30% was maintained.

One year after the fire the sedge-cloudberry-peat moss group was formed, and the next year it was replaced by the cloudberry-sedge-wild rosemary-peat moss community. This was the result of the fast recovery of the former role of wild rosemary. In this community, the coverage of grasses and dwarf shrubs increased up to 35% and mosses up to 40%. In the next years, the coverage of grasses and dwarf shrubs reached its initial value (40–50%), but mosses still covered less than half of plot surface. The occurrence of lichens sharply decreased after the fire, and within 16 years had considerably increased. The frequency of *Cladina stellaris* had recovered (Fig. 5), and its reduction for the last decade is connected to the increased amount of atmospheric precipitation that is observed in undisturbed conditions. The frequency of *Sphagnum fuscum* remains two times less than in the initial community. The frequency of *Betula nana* has increased by two times, probably in connection with the rise in air temperature.

On the cloudberry-wild rosemary-lichen palsa peatlands, 40 years after the fire three cloudberry-*Betula nana*-wild rosemary-lichen-*Polytrichum* communities are found. These communities differ from the initial communities by ground vegetation composition (smaller percentage of lichens) and an increase in the presence of *Betula nana*. The last, apparently, is in connection with the increase of the air thawing index and snow thickness over the last decades.

In 1971, when the route of a gas pipeline was cleared away, all sites with palsa peatland adjacent to the route were burned, including our 1970 plot on which we carried out the detailed description of a vegetation cover, measurements of active layer thickness, and permafrost temperature.

This plot is located at the top of a peaty hillock with heights of 2 m and with a cloudberry-wild rosemary-

lichen plant community. In the microrelief off the plot are characteristically small *Dicranum* hummocks with heights of 0.1–0.3 m and pools with bog dwarf shrubs (*Andromeda polifolia*, *Chamaedaphne calyculata*) and mosses. The soil of the plot is peaty, and maximum thickness of the active layer is 0.6 m. The coverage of grasses and dwarf shrubs equaled 45%, and mosses and lichens 90%. In a grass-shrub cover, two layers are found: an upper layer in height 0.2–0.4 m made up of wild rosemary and *Betula nana*, and a lower layer in height up to 0.15 m formed of cloudberry and cowberry. In ground vegetation, lichens predominated over a *Cladina* genus and frequent *Dicranum* mosses but with low coverage.

In 1975, four years after the fire at the top of the peaty hillock where the vegetation had been described in 1970, a permanent 10 x 10 m plot on the soil surface was established. On this plot, from 1975 to the present time, annual geobotanical descriptions are performed.

A 10-m borehole was drilled at the hillocky top near the geobotanical plot. According to the drilling record, the peat thickness is 1 m; below that lies sand with layers of clay 3.75 m thick. From 1975 to 1983, year-round temperature measurements of soil and permafrost were observed, and they were carried out annually until September 2000. Since 2001, year-round measurements of temperature by loggers were obtained. Starting in 1983, thickness and moisture of the active layer during the entire season were measured, and more recently the summer maximal values were recorded.

In four years since the fire on the peaty hillock, the cotton grass-cloudberry-*Polytrichum* community is found in which the coverage of grasses made 15%, and mosses 50%. After the fire, the species on the plot were 42% of their common number in 1970. Change of species number could still be large, but the appearance of new grass species (*Eriophorum russeolum*, *Carex limosa*, *Chamaenerium angustifolium*) and shoots of birch (*Betula tortuosa*) compensated for the significant decrease of species number. It has been related to the disappearance of five dwarf shrubs (*Vaccinium uliginosum*, *V. vitis-idaea*, *Empetrum nigrum*, *Andromeda polifolia* and *Chamaedaphne calyculata*), *Eriophorum vaginatum*, one species of lichens (*Alectoria ochroleuca*), and three species of mosses (*Sphagnum fuscum*, *Pleurozium schreberi*, *Hylocomium splendens*). In the first years of vegetation recovery, the frequency and coverage of *Polytrichum* mosses strongly increased. Occurrence of dwarf shrubs has decreased, bog grasses that were absent earlier have appeared, and the occurrence of shrubs increased.

In five years after the fire on the hillocky landscape with cotton grass-cloudberry-*Polytrichum* community, the coverage of grasses was 20% and mosses 50%. The next year there was an appreciable increase in the occurrence of *Betula nana*, which led to changes of the grass-moss community with the *Betula nana*-cloudberry-cotton grass-*Polytrichum* community. The coverage of grasses and dwarf shrubs in this community gradually grew and reached its initial value in 14 years after the fire. At this time, an appreciable role of wild rosemary began to occur. The ground vegetation covered up to 85% of a plot surface, but it still has consisted of *Polytrichum* mosses. The thickness of the active layer in this plant community has increased to 65–70 cm.

The frequency of lichens has increased, but the coverage

Table 1. Stages of vegetation recovery after fire in different ecosystems.

Stages and their duration (years)	Ecosystems	
	I	II
Grass-moss (1-5)	1a	1б
Shrub-grass-moss (6-15)	2a	2б
Shrub-grass-lichen-moss (16-35)	3a	3б
Grass-shrub-moss-lichen (36-50)	4a	4б

Ecosystems I – cloudberry-wild rosemary-lichen palsa peatland, II – frost mound with *Pinus sibirica* wild rosemary-peat moss-*Cladina* open wood. Plant communities: 1a – cottongrass-cloudberry-*Polytrichum*, 1б – sedge-cloudberry-peat moss, 2a – *Betula nana*-cloudberry-cottongrass-*Polytrichum*, 2б – cloudberry-sedge-wild rosemary-peat moss, 3a – cloudberry-*Betula nana*ερηνικοβο-wild rosemary-*Cladina*-*Polytrichum*, 3б – *Betula nana*-wild rosemary-peat moss-*Cladina*, 4a – cloudberry-*Betula nana*-wild rosemary-*Cladina*-*Polytrichum*, 4б – *Pinus sibirica* *Betula nana*-wild rosemary-peat moss-*Cladina*.

on the surface did not exceed 1–3%. However, the coverage of lichens gradually continued to increase, and in 23 years after the fire it has reached 8.5%. The coverage of lichens has increased for 40th year, to 18.5%, and includes the *Betula nana*-wild rosemary-cloudberry-*Cladina*-*Polytrichum* community in which the occurrence of cotton grass has decreased. The number of dwarf shrubs and mosses by this time has appreciably increased, but remained less than in undisturbed cover due to the absence of bog dwarf shrubs (*Andromeda polifolia*, *Chamaedaphne calyculata*) and one species of mosses (*Hylocomium splendens*). The bog grasses that appeared at the early stages of plant community recovery in 2005 have disappeared from the plant community.

Stages of vegetation recovery after the fire on the frost mound and the palsa peatland are presented in Table 1. Comparison of rates of vegetation recovery in these ecosystems demonstrates that on flat weakly drained tops of frost mounds the vegetation recovery is faster than on better drained, palsa peatlands. The domination in ground vegetation of *Polytrichum* mosses and the lower occurrence of lichens persists longer.

Analysis of the measurements of active layer thickness on palsa peatland has shown an increasing trend (Fig. 6A) as a result of the increase of the air thawing index (temperature trend for 1970–2010 of 0.2°C in a year). The thickness of the active layer increased by 30% in the period of observation. Formation on the peatland of continuous *Betula nana*-wild rosemary-cloudberry-*Cladina*-*Polytrichum* vegetation cover has not led to a reduction of the active layer thickness.

The analysis of permafrost temperature measurements in boreholes has shown that on palsa peatlands there was a marked maximal of 1.4°C rise. The temperature of permafrost at the depth of 10 m (layer with minimum annual fluctuations of temperatures) for the period of observation on the palsa peatland (Fig. 6B) increased from -1.8°C to -0.4°C.

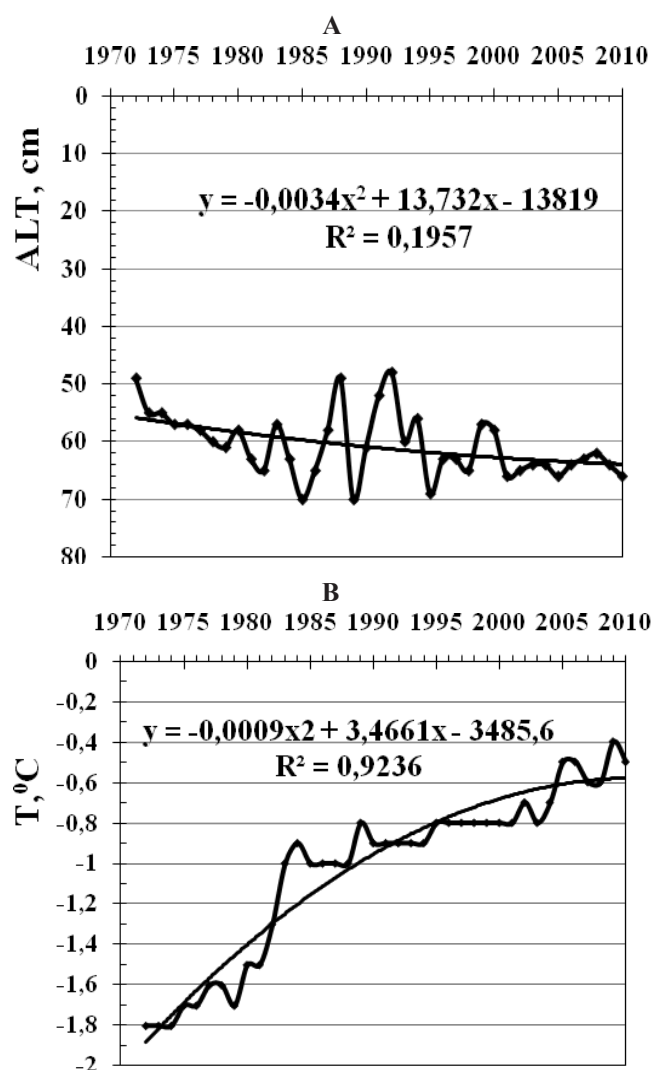


Figure 6. Active layer thickness (ALT, cm) and permafrost temperature at the depth of 10m (T°C) on palsa peatland.

Conclusions

Long-term monitoring of northern taiga ecosystem changes provides information on permafrost degradation caused by climatic changes and human-induced disturbances on a vegetation cover.

During the last decades in the north of Western Siberia, a rise in air temperature and an increase in the amount of atmospheric precipitation are observed. In this connection, the process of bog development on flat poorly drained surfaces of plains became more active. As a result, tussocky and hummocky pine-larch cloudberry-wild rosemary-lichen-peat moss open woodlands with lenses of permafrost on the hummocks are replaced by andromeda-cotton grass-sedge-peat moss on thawed bogs.

After removal of the vegetation cover of cloudberry-wild rosemary peat moss-lichen peatland, surface settlement, development of thermokarst and bogginess and an increase of the permafrost table up to 2–3 m occur. The formation of cotton grass-peat moss bog is maintained here 39 years after disturbance. On the disturbed peatland plot located 10 m from a gas pipeline, the permafrost table has lowered up to a depth of 10 m based the geophysical data.

On cloudberry-wild rosemary-lichen palsa peatlands 40 years after a fire, cloudberry-*Betula nana*-wild rosemary-lichen-*Polytrichum* plant communities are formed. These plant communities differ from the initial communities by composition of the ground cover (smaller participation of lichens) and an increase in occurrence of *Betula nana* connected with an increase of the air thawing index.

The measurements of active layer thickness on the palsa peatland have shown an increasing trend caused by the increase in the air thawing index, with a trend for 1970–2010 of 0.2°C/year. The permafrost temperature at the depth of 10 m has increased 1.4°C.

Acknowledgments

This research was supported by the Circumpolar Active Layer Monitoring (CALM) project (National Science Foundation, Grant NSF OPP-9732051, OPP-0225603); Thermal State of Permafrost (TSP) project (NSF RC-0632400, ARC-0520578), and RFBR (Grant No. 09-05-01068-a).

References

- Andrianov, V.N., Kozlov, A.N., & Krizuk, L.N. 1973. Engineering-geocryological conditions of pool of middle current Nadym River. *Trudy of VSEGINGEO* 62: 79-89 (in Russian).
- Ershov, E.D., Maksimova, L.N., & Medvedev, A.V. 1994. Reaction of permafrost to global changes of a climate. *Geoecology*, No. 5: 11-24 (in Russian).
- Izrael, J.A., Pavlov, A.V., & Anokhin, J.A. 2002. Evolution of permafrost zone at modern changes of a global climate. *Meteorology and a hydrology*, No. 1: 10-18 (in Russian).
- Kakunov, N.B. & Sulimova, E.I. 2005. Dynamics of geocryological conditions on territory of northern part Timan-Pechora oil-gas province for last 220 years and the forecast of their changes. *Materials of research-and-production conference Problems of engineering - geological maintenance of construction of oil-and-gas complex objects in permafrost zone. M.: FGUP PNIIS*: 107-110 (in Russian).
- Melnikov, E.S. (ed.). 1983. *Landscapes of Permafrost Zone of the West Siberian Gas Province*. Novosibirsk, Nauka: 166 pp. (in Russian).
- Moskalenko, N.G. (ed.). 2006. *Anthropogenic Changes of Ecosystems in West Siberian Gas Province*. Moscow, Earth Cryosphere Institute, 358 pp. (in Russian).
- Nelson, F.E., Lachenbruch, A.H., Woo., M.-K. et al. 1993. Permafrost and changing climate. *Permafrost: Proc. of the Sixth Intern. Conf. Beijing, China*, South China Univ. of Technol. Press, Vol. 2: 987-1005.
- Oberman, N.G. 2007. Some features of modern degradation of permafrost zone in the Pechora-Ural region. *Materials of International Conference Cryogenic resources of polar regions*. Salekhard, vol.1: 96-99.
- Osterkamp, T. & Romanovsky, V. 1999. Evidence for warming and thawing of discontinuous permafrost in Alaska. *Permafrost and Periglacial Processes* 10: 17-37.

- Parmuzin, S.J. & Chepurnov, M.B. 2001. Existential dynamics of permafrost in the European North and Western Siberia in XXI century in connection with possible changes of a climate, *Materials of the Second Conference of Geocryologists in Russia*. M.: the Moscow State University, vol. 2:231-235 (in Russian).
- Pavlov, A.V. 1997. The forecast of permafrost zone evolution in the north of Western Siberia (according to monitoring). *Results of basic researches of the Earth permafrost zone in Arctic and Subarctic regions*. Novosibirsk, Nauka: 94-102 (in Russian).
- Perlshtein, G.Z., Pavlov, A.V., & Buisikh, A.A. 2006. Changes of permafrost zone in conditions of modern climate warming. *Geoecology (engineering geology, hydrogeology, geocryology)*, No. 4: 305-312 (in Russian).
- Ponomareva, O.E. & Skvortsov, A.G. 2006. Methods and results of studying of exogeneous geological processes in Nadym area of Western Siberia. *The theory and practice of an estimation of the Earth Cryosphere State and the forecast of its change: Materials of International Conference, Tyumen, TGNGU vol.1: 272-274*.

Long-Term Temperature Regime of the Northeast European Permafrost Region During Contemporary Climate Warming

N.G. Oberman

MIREKO Mining Geological Company, Syktyvkar, Russia

Abstract

This paper discusses the data of 30- and 40-year-long permafrost monitoring on the pediment plain and the glacial-marine plain, respectively. The sites are located in the Vorkuta hydrogeological permafrost area within the zone of discontinuous warm permafrost. The variability of mean decadal changes in permafrost and talik temperatures at depths of 10–15 m depends on meteorological, permafrost, hydrogeological, and other factors. The variability of amplitudes of these changes over the entire monitoring period is examined. Mean annual values of ground warming for permafrost and taliks under various natural conditions are estimated for the entire monitoring period.

Keywords: climate; cryolithozone; decadal; Northeastern Europe; permafrost temperature; warming.

Introduction

Contemporary global warming has affected Northeastern Europe (Fig.1). A large number of publications have been dedicated to the potential and actual impacts of climate warming on permafrost in this region (Oberman 1996, 2001, Pavlov 1997, Kakunov & Pavlov 1997, Oberman & Mazhitova 2003, Kakunov & Sulimova 2005, Pavlov & Malkova 2005, Malkova 2007, Oberman 2007, 2008, Oberman & Shesler 2009, Romanovsky et al. 2010, Pavlov et al. 2011).

It is now generally accepted that the temperature of permafrost in the study area has increased under the influence of climate change over the past decades. Trends in mean annual ground temperature for Northeastern Europe at depths of 10 to 15 m varied from 0.010 to 0.078°C/year between the 1970s (1980s) and 2006 (2007). These trends depended on environmental factors and on duration and timeframes of the 20- to 37-year-long observations (Oberman 2008). Similar trends in the same area at depths of 3 to 10 m over the period of 1965–2005 were 0.024°C/year (Pavlov et al. 2011). We believe that in order to predict future changes in permafrost temperature, it is essential to determine the features of the long-term regime in typical permafrost and geological conditions. It is also important to define more precisely the role of climatic and landscape factors in permafrost formation. This paper is devoted to resolving these problems.

Study Area and Methods

It is obvious that the longest observational series are preferable for analysis of the monitoring results. In the region, such observational series can be found only at the Vorkuta permafrost-hydrogeological test site, and therefore that site was chosen for this report. The area comprises the southern tundra landscapes of the pediment and glacial-marine plains. Quaternary strata with thicknesses of 60 to 100 m are widespread. The pediment plain is composed of terrigenous (mainly) and carbonate rocks, overlain by discontinuous Quaternary sediments 2 to 10 m thick. Climatic conditions make the territory (see the next section) a part of the waterlogged permafrost region. Sporadic permafrost distribution on the pediment plain recorded

in 1970 (immediately prior to the climate warming) has now been replaced by isolated patches of permafrost. The discontinuous permafrost on the glacial-marine plain has been partly replaced by sporadic permafrost and even by isolated patches of permafrost in some areas. Over the same period of time, the permafrost temperature has changed from -1.0...-2.5°C to -0.3...-1.1°C. The thickness of permafrost varies from 20 to more than 200 m.

In order to solve the problems mentioned above, permafrost monitoring data were used. Monitoring was performed by the MIREKO Mining Geological Company, which includes the former Vorkuta complex geological expedition and “Severuralgeologiya” and “Polyarnouralgeologiya” institutions. The ground temperature was measured using mercury thermometers with the scale division of 0.05÷0.10°C, which were placed in insulated cases. Starting in 2007, measurements were made with Hobo dataloggers. Ground temperatures were measured by both types of devices by a representative of Geophysical Institute, University of Alaska Fairbanks. The average was ±0.05°C (Oberman 2008). Observation frequency varied from a few times a month to once every three months. Measurements using dataloggers had a frequency of two times a day. If the observation frequency over the year was irregular, the obtained results were averaged, and the calculated mean annual value may be incorrect to some extent. To avoid this, data averaging was performed stepwise: at first, we calculated mean monthly values, then mean quarterly values, and only after that the mean annual value was calculated.

Solution of the existing problems is possible by comparing changes in the basic meteorological parameters and changes in ground temperatures on the typical relief and microrelief elements of main terrain units over synchronous long-term periods of equal duration. For further analysis, we will assume that the duration of these periods is 10 years, taking into account the climatic rhythms with periods of 10 to 11 years (Parmuzin & Shatalova 2001).

Results

Over the entire 40-year period, the average air temperature steadily increased from one decade to another (Table 1). Therefore, for all decades, the changes in ground temperature at the depth of 10 to 15 m are positive for permafrost areas

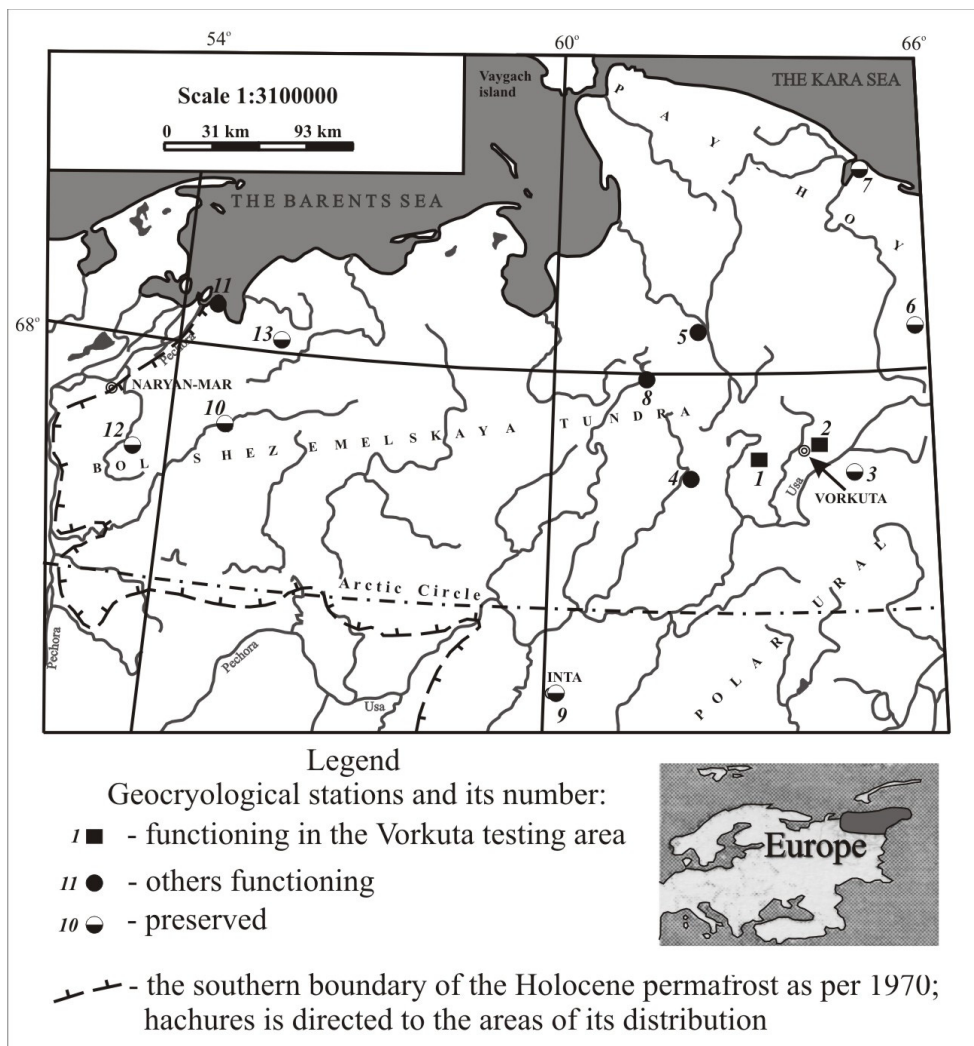


Figure 1. Regional map.

that are composed of Quaternary sediments of the glacial-marine plain, and also in open and closed taliks in the bedrocks of the pediment plain (Table 2, boreholes: VK-1615, ZS-25, ZS-124, and K-887, UP-34, YA-1).

However, at some sites, positive changes were recorded in only one to three of four analyzed decades. In other words, in these cases even the mean decadal changes in air temperature do not determine whether the changes in ground temperature will be positive or negative.

One such case is caused by a well-known factor: recent removal of water covers that provided insulation for the ground, which occurred approximately 70 and 38 years ago. As a result, cooling of the thawed and newly formed frozen soils occurred on the bottom of the drained thermokarst lakes (ZS-34 and ZS-16, respectively). In the course of the recent long-term “optimum,” the long-term cooling of these sediments has been replaced by their warming in the past 10–20 years.

Another reason for the ground cooling that was recorded over the period of 1991–2000 is typical of closed taliks of the glacial-marine plain (ZS-12 and 8S). This decade was characterized by minimum precipitation for the 40-year period (Table 1). This resulted in a minimum flow of atmospheric heat into the taliks. We assume that in 1991–2000 the decrease in precipitation infiltration had a greater

Table 1. Dynamics of changes in meteorological conditions at the Vorkuta weather station.

Meteorological parameters	Mean values for the periods, years:			
	1971-1980	1981-1990	1991-2000	2001-2010
Mean annual air temperature, °C	-6.3	-5.6	-5.6	-5.1
Total precipitation, mm/year	530	560	506	526
Maximum annual snow thickness*, cm	47	37	76	79

Note: * - based on the snow survey data.

influence than air temperature had on the temperature of taliks and their interstitial underground waters. This is because of the almost dominant role of the convective heat flow in the process of formation of the thermal regime of taliks and because of the stability of air temperature in comparison with the previous decade. At the same time, the warming of taliks on the pediment plain is strongly affected by water in fissures and karst-fissures due to increased (in comparison with interstitial waters) infiltration rates. In the open taliks and in the closed taliks over 60 m deep, ascending heat flow

Table 2. Dynamics of permafrost temperatures for the Vorkuta test area.

Boreholes	Initial temperature, °C	Temperature change, °C/year, for the period of:			
		1971-1980	1981-1990	1991-2000	2001-2010
glacial-marine plain					
ZS-25, permafrost	-2.30	+0.013	+0.039	+0.018	+0.054
VK-1615, as above	-1.15	+0.039	+0.01	+0.019	+0.016
ZS-124, as above	-2.96	–	+0.077	+0.057	+0.055
ZS-12, closed talik	+0.13	+0.023	+0.036	-0.018	+0.013
8S, as above	±0.0	+0.033	+0.036	-0.01	+0.033
ZS-16, permafrost	-0.18	-0.019	-0.004	-0.008	+0.014
ZS-34, open talik	+1.25	-0.037	-0.057	+0.002	+0.017
Pediment plain					
YA-3, permafrost	-0.95	–	+0.016	+0.017	+0.019
YA-1, permafrost with lowered table	-0.35	–	+0.013	+0.015	+0.015
UP-34, closed talik	+0.14	–	+0.058	+0.026	+0.032
K-887, open talik	+0.70	+0.029	+0.024	+0.008	+0.025

Table 3. Mean rates of long-term and amplitudes of permafrost temperature changes.

Boreholes	Permafrost conditions	Lithology for the depths of 0 to 15 m.	Period, years	Temperature changes:	
				mean for the period, °C/year	The amplitude of the mean decadal values, °C/year for the last 40 years*
Glacial-marine plain					
VK-1615	permafrost	silty clay	1971-2010	+0.020	0.029
ZS-25	as above	as above	1971-2010	+0.032	0.041
ZS-16	as above	peat, silty clay	1971-2010	-0.004	0.033
ZS-12	closed talik	silty clay, clay	1971-2010	+0.013	0.054
8S	as above	silty clay, silt	1971-2010	+0.02	0.046
VK-1618	open talik* ²	silty clay	1972-2010	+0.024	–
ZS-34	as above	peat, silty clay	1975-2010	-0.028	0.074
Pediment plain					
YA-3	permafrost	silty clay	1981-2010	+0.017	0.003
YA-1	permafrost with lowered table	as above	1981-2010	+0.014	0.002
UP-34	closed talik	limestone	1981-2010	+0.039	0.032
K-887	open talik	sandstones, argillites	1981-2010	+0.019	0.017

Note: * – on the pediment plain – for last 30 years;
 *² – initial temperature: +0.4 °C.

from the pressure aquifer also contributes to such impact. As a result, in spite of the stable air temperature (in comparison with the previous decade), the temperature of taliks on this plain increased in 1991–2000 (in boreholes K-887 and UP-34 located near the absorbing water karst sinkhole). However, the temperature of permafrost also increased in 1991–2000. Therefore, it is obvious that in these cases the dominant role belongs to the snow cover, the mean decadal thickness of which increased in 1991–2000 from 37 to 76 cm, in comparison with the previous decade (Table 1).

The values of changes in mean decadal ground temperature are very variable in space and time (Table 2). The maximum warming intensity up to +0.08 °C/year is recorded in highly

thermo-conductive peatlands with high-ice content (ZS-124), as well as in taliks with karst waters (UP-34). The maximum cooling intensity, up to -0.06 °C/year, is typical of the freezing talik under the lake drained in 1973 (ZS-34). It can be presumed that the most significant permafrost and talik warming should be recorded during the warmest period: 2001–2010. This actually took place in some interfluvial areas with permafrost (ZS-25) and in peaty beds of recently drained lakes (ZS-16 and ZS-34). However, in most cases such a trend is not recorded; this confirms a conclusion by Pavlov et al. (2011) about the lack of synchrony between climate warming and ground warming. For example, the maximum warming of permafrost in the interfluvial areas,

composed of peat and in some cases mineral soils, was recorded in the coldest decades (ZS-124 and VK-1615). Such an apparent paradox can be explained not only by the decrease in heat amount required for the partial melting of ground ice, but also by the simultaneous increase in the thermal conductivity of sediments due to the decrease in their temperature. The maximum warming of taliks in most cases happened during the period of 1981–1990, which was characterized by the average air temperature for the 40-year period and the maximum annual amount of precipitation. The heating effect of the precipitation infiltration into the ground was probably the reason for the increase in ground temperature (ZS-12, 8S, and UP-34).

We suggest measuring the average for the regional ground warming rates for the period that represents the climatic norm (i.e., for the period not less than 30 years long) and also for the most typical permafrost conditions. Such conditions within each terrain unit are the conditions characteristic of the permafrost and talik areas. Initial data for calculation of such mean values for these areas are shown in Table 3.

For the 40-year period, the rate of increase in mean permafrost temperature for the glacial-marine plain is from 0.02 to 0.032°C/year, which is generally higher than that of taliks: from 0.013 to 0.024°C/year (Table 3). Possible reasons for this difference include increased thermal conductivity of permafrost and the additional amount of heat required for the phase transitions in the thawing base of closed taliks. The warming of open taliks is more intensive than that of closed taliks. That is probably due to the additional ascending heat flow from deeper horizons and to the lack of heat flow required for permafrost thawing. On average, the temperature increase rate for the sediments of this landscape is 0.026°C/year for permafrost areas and 0.019°C/year for taliks.

Unlike the rest of the glacial-marine plain, peaty beds on the drained thermokarst lakes underwent cooling over the 40-year period. The maximum cooling intensity was recorded over a short period of time following the drainage (i.e., in case of the minimum degree of thermal equilibrium between cooling sediments of the lake bed and surrounding frozen ground).

The increased permafrost temperature trends recorded at the glacial-marine plain are not characteristic of the pediment plain. We believe that the strong influence of the hydrogeological factor is the main reason for this anomaly. This conclusion is based on the following facts. First, with the decrease in the infiltration rates of ground waters in the fissure-karst – fissure interstitial ground water sequence, atmospheric heat flow into taliks should also decrease. We assume that this fact determines the gradual decline in the rate of their temperature increase from 0.039 to 0.019, and to 0.014°C/year (Table 3, UP-34, K-887, and YA-1 respectively). Second, the increased rate of permafrost temperature is lower than that of taliks with fissure waters and especially with fissure-karst waters. The average intensity for the 30-year period of warming of permafrost and taliks composed mainly of terrigenous rocks and clayey sediments is 0.017°C/year. This is lower in comparison with the glacial-marine plain; warming rates are probably caused by the lower value of the Earth's heat flow in this area.

Another indicator of the long-term thermal regime is

the amplitude of the mean decadal changes in the ground temperature. On both plains, depending on the values of this amplitude, areas and sites with permafrost and taliks may be distinguished. Thus the values of amplitude of the ground temperature increase at the glacial-marine plain vary in the range 0.029–0.041°C/year with average 0.035°C/year for the permafrost areas and between 0.046 and 0.054°C/year with average 0.05°C/year for talik sites. Corresponding values of the amplitudes on the pediment plain are 0.03°C/year for the permafrost areas and between 0.002 and 0.032°C/year with average 0.017°C/year for talik sites (Table 3). We explain these differences in the amplitude values by the specifics of the thermal condition of permafrost and taliks. While for the permafrost areas the main factor of ground temperature formation is the conductive heat flow from the Earth's surface, for taliks it is normally added to the convective heat flow. We assume that such overlay of heat flows should provide a greater variety of forming ground temperatures and, thus, it should increase their long-term amplitudes, which has in fact been observed.

It is significant that in the local areas of recent cooling we can see the same trend which is observed on the remainder of the plains. The amplitudes of mean decadal negative temperature changes in permafrost (0.033°C/year) are lower than those in taliks (0.074°C/year) (Table 3, ZS-16 и ZS-34).

Ground temperatures in the eastern, western, and northern parts of the Northeastern Europe are characterized by a very similar reaction to global climate warming. It is mostly synchronous with the chronological changes in the basic meteorological parameters (Oberman 2008). This gives us reason to assume that the main features of the long-term ground temperature regime examined earlier on the basis of the data provided by the Vorkuta test stations are typical of the whole region.

Conclusions

- 1) We have determined the mean decadal values of changes and amplitudes of ground temperature in the discontinuous permafrost zone for 30-year and 40-year periods for the pediment plain and the glacial-marine plain, respectively. These values depend on meteorological, permafrost, hydrogeological, and other factors. Changes in air temperature are not always the factor that determines the value and direction (positive/negative) of mean decadal changes in ground temperature. When the mean decadal air temperature is stable, the value of the mean decadal sum of total annual precipitation becomes significant for some areas of the glacial-marine plain and particularly for closed taliks. During such periods, the changes in permafrost temperature at the pediment plain are determined by the anomalous increased thickness of snow cover. Warming of taliks at this plain is caused by the combined effects of the hydrogeological factor and snow cover. The maximum intensity of the mean decadal warming, up to 0.08°C/year, has been recorded in frozen peatlands and water-bearing taliks in karst-affected rocks. The highest cooling rate of up to -0.06°C/year was recorded on the bottom of a thermokarst lake that was drained 38 years ago.

- 2) For the glacial-marine plain, the mean values of ground temperature increase for the whole period of observations are 0.026°C/year for permafrost and 0.019°C/year for taliks. Warming rates at the pediment plain for the same permafrost conditions are generally equal and reach 0.017°C/year. For the glacial-marine plain, the average amplitudes of mean decennial changes in the ground temperature for the whole observation period are, 0.035°C/year for permafrost and 0.05°C/year for taliks. For the pediment plain, these values are 0.003°C/year for permafrost and 0.017°C/year for taliks. The difference in the amplitudes in permafrost areas and talik sites is caused by almost total water saturation of soils and rocks in taliks. Similar differences can also be seen in the amplitudes of ground temperature changes in cooling permafrost and open taliks at the drained lake beds.
- 3) The main features of the long-term ground temperature regime which were identified and examined based on the permafrost monitoring data from the Vorkuta test stations are generally typical of the entire permafrost region of Northeastern Europe.

Acknowledgments

The author is grateful to all his coworkers and especially to N.B. Kakunov, who worked side by side with the author to perform permafrost observations that formed the basis of this paper. Financial support was provided by the Russian Federal Agency for Mineral Resources Use and, starting in 2007, by the Geophysical Institute, University of Alaska Fairbanks, USA.

References

- Kakunov, N.B. & Pavlov, A.V. 1997. Evaluation and prediction of the cryogenic soil thermal regime in the Russian North in connection with the anticipated climate change. *Cryopedology-97: Abstracts of the International conference, Syktyvkar, Russia*, August 5-8 1997: 121 (in Russian).
- Kakunov, N.B. & Sulimova, E.I. 2005. Results of ground temperatures observation on the European part of the North-East of Russia in the 1970-2003 period of climate warming. *Proceedings of the Third Conference of the Russian Geocryologists, Moscow*, June 1-3 2005: Vol. 2, 84-90 (in Russian).
- Malkova, G.V. 2007. Summary of the results of temperature measurements at the Bolvansky geocryological station. *Proceedings of the International conference "Cryogenic resources of polar regions," Salekhard, Russia*, June 17-21 2007: Vol. 1, 140-143 (in Russian).
- Oberman, N.G. 1996. Geocological specifics and recent trends of the natural and man-induced dynamics of the permafrost region of the East-European Subarctic. *Proceedings of the 1st Conference of Geocryologists of Russia, Moscow*, June 3-5, 1996: Book 2, 408-417 (in Russian).
- Oberman, N.G. 2001. Intra-secular dynamics of the permafrost of the European North-East of Russia. *Proceedings of the 2nd Conference of Geocryologists of Russia, Moscow*, June 6-8, 2001: Vol. 2, 212-217 (in Russian).
- Oberman, N.G. & Mazhitova, G.G. 2003. Permafrost mapping of Northeast European Russia based on the period of climatic warming 1970-1995. *Norwegian Journal of Geography* 57, No.2: 111-120.
- Oberman, N.G. 2007. Global warming and changes in the permafrost conditions of the Pechora-Ural region. *Razvedka i ohrana nedr* 4: 63-68 (in Russian).
- Oberman, N. 2008. Contemporary Permafrost Degradation of Northern European Russia. *Ninth International Conference on Permafrost*. Fairbanks, Alaska, USA. June 29 – July 3, 2008: Vol.2, 1305-1310.
- Oberman, N.G. & Shesler, I.G. 2009. Observed and predicted changes in permafrost conditions within the European North-East of the Russian Federation. *Problemy Severa i Arktiki Rossiyskoy Federatsii* 9: 96-106 (in Russian).
- Parmuzin, S.Y. & Shatalova, T.Y. 2001. Dynamics of seasonally thawed and seasonally frozen soil layers in connection with short-period climate fluctuations. *Osnovy geocryology. Part 4. Dinamicheskaya geocryology*. Moscow University, 284-302 (in Russian).
- Pavlov, A.V. 1997. Permafrost-climatic monitoring of Russia: methodology, results of observation and forecast. *Kriosfera Zemli* 1, 1: 47-58 (in Russian).
- Pavlov, A.V. & Malova, G.V. 2005. Contemporary changes of climate in northern Russia: *Album of small-scale maps*. Novosibirsk: Academic publishing "GEO," 54 (in Russian).
- Pavlov, A.V., Perlshtein, G.Z., & Tipenko, G.S. 2011. Quantitative prognosis methods of permafrost response to contemporary climate changes. *Proceedings of the 4th Conference of the Geocryologists of Russia, Moscow*, June 7-9, 2011: Vol. 2, 281-288 (in Russian).
- Romanovsky, V.E., Drozdov, D.S., Oberman, N.G., Malkova, G.V., Kholodov, A.L., Marchenko, S.S., Moskalenko, N.G., Sergeev, D.O., Ukraintseva, N.G., Abramov, A.A., & Vasiliev, A.A. 2010. Thermal state of permafrost in Russia. *Permafrost and Periglacial Processes* Vol.21, 2: 136-155.

Quaternary Deposits and Geocryological Conditions of Gydan Bay Coast of the Kara Sea

G.E. Oblogov, I.D. Streletskaya
Lomonosov Moscow State University, Moscow, Russia

A.A. Vasiliev
Earth Cryosphere Institute, SB RAS, Moscow, Russia

E.A. Gusev
Gramberg All-Russia Research Institute for Geology and Mineral Resources of the World Ocean, St. Petersburg Russia

H.A. Arslanov
St. Petersburg State University, St. Petersburg, Russia

Abstract

A description of the geological and geocryological structure of coastal exposures of Gydan Bay is presented. The data on isotopic and chemical composition of ground ice, texture, and age of deposits are presented. Two generations of polygonal wedge ice are distinguished: the Late Pleistocene and the Holocene. The conditions of sedimentation, freezing, and denudation of deposits during the last glaciation and the Holocene optimum are determined.

Keywords: Gydan Bay; permafrost formation; Quaternary deposits.

Introduction

Gydan Bay of the Kara Sea is one of the least accessible areas of the northern parts of Western Siberia. The data on geomorphology, Quaternary sediments, and modern processes in the north of Western Siberia were discussed by Saks (1951). The Quaternary deposits of the area were studied and mapped during geological mapping by the Arctic Geology Research Institute (Sokolov & Znachko-Yavorskiy 1957).

The permafrost conditions and Quaternary deposits of the Gydan Peninsula were thoroughly studied in 1973–1985 by the Tyumen expedition of the Department of Soil Science and Engineering Geology, Geology Department of Moscow State University (Trofimov et al. 1986). As a result of these investigations, the regional stratigraphic scheme of Quaternary deposits was developed; tabular massive

ice, wedge ice, and modern processes of thermokarst and thermal erosion were studied.

Based on the section of the organo-mineral complex in the Mongatalyanyakha River estuary, which is located near the section in the Era-Maretayakha River estuary studied by the authors, Vasilchuk (1992) obtained a series of radiocarbon Late Pleistocene datings at different elevations above sea level: at 3.5 m, $30,200 \pm 800$ years BP (GIN-2470); at 4.5 m, $28,600 \pm 800$ years BP (GIN-2638); at 5 m, $25,100 \pm 220$ years BP (GIN-2471); and at 5.9 m, $21,900 \pm 900$ years BP (GIN-2469). Peatland at the elevation of 9.3 m had a radiocarbon age of $3,900 \pm 100$ years BP (GIN-2468).

The fieldwork conducted in 2010 by MSU, the Earth Cryosphere Institute, and the All-Russia Research Institute for Geology and Mineral Resources of the World Ocean covered the western and eastern coasts of Gydan Bay (Fig. 1). The description of the geological and geocryological structure of the Quaternary deposits and the data on isotopic and chemical composition of ground ice, texture, and age of deposits are presented in this paper.

Results and Discussion

Era-Maretayakha River estuary

The studies were conducted near the Era-Maretayakha River estuary located on the eastern coast of the Gydan Peninsula. The structure of the coastal bluff consists of inclined eroded surfaces with elevations of 10–25 m and a steep thermal erosion bluff descending to the modern beach (Fig. 2.1).

To the depth of 4.7 m (Fig. 2.1, section 1006), the upper part of the section is represented by frozen lacustrine and peat deposits with a significant ice content. Thick layers of almost pure ice are interbedded with poorly decomposed peat. Radiocarbon dating of a peat sample from the depth of 3.8 m provided an age of $8,500 \pm 90$ yr BP (LU-6535).

Lower silty sediments are exposed (the silt particle content is more than 54%; Fig. 2.1, section 1007). The



Figure 1. The research areas location: 1 - Era-Maretayakha River estuary; 2 - Cape Pakha-Sale.

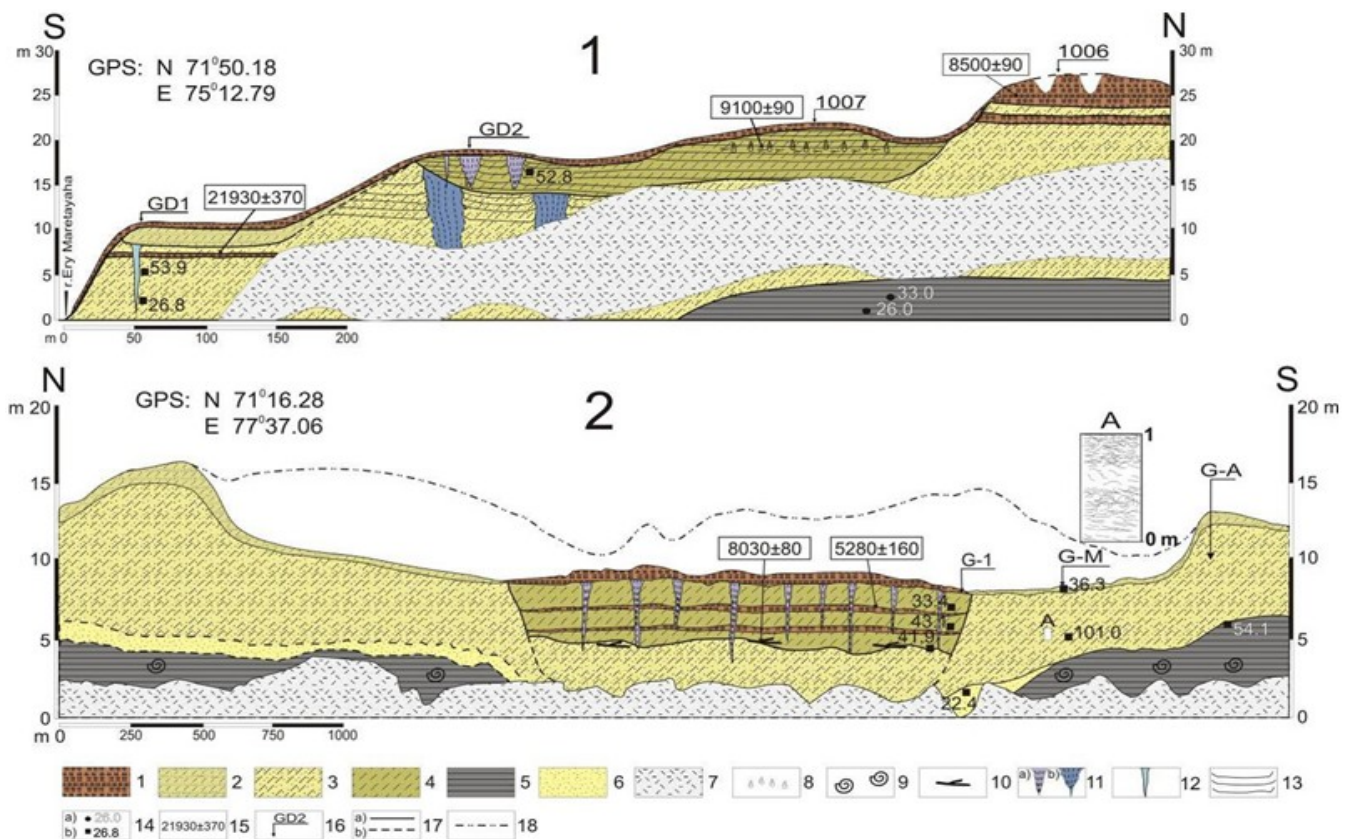


Figure 2. The scheme of the structure of the coastal exposures of Gydan Bay: 1 – Era-Maretayakha River estuary; 2 – Cape Pakha-Sale. Legend: 1 – peat; 2 – interbedded sandy silts and sands; 3 – silts; 4 – peaty silts; 5 – clays; 6 – sands; 7 – slump; 8 – fresh-water lacustrine shells; 9 – sea mollusks; 10 – wood debris; 11 – wedge ice: a) Holocene, b) Late Pleistocene; 12 – ice in fractures; 13 – belt-like cryostructure; 14 – gravimetric moisture content (in %): a) total, b) of mineral interlayers; 15 – radiocarbon age of organic inclusions, years BP; 16 – number of section; 17 – lithologic boundaries: a) identified, b) assumed; 18 – position of the surface that did not undergo thermal erosion.

sandy silts contain peat, plant roots (the organic carbon content reaches 0.9%), and freshwater mollusk fragments. The deposits are ice-rich. The total gravimetric moisture content is about 53%. The cryostructure is belt-like. The cryostructure between the belts is reticulate. Radiocarbon dating of plant roots obtained from the depth of 4 m showed the age of $9,100 \pm 90$ yr BP (LU-6534). The amount of sand particles in soil increases with depth, while the organic content decreases (organic carbon content reaches 0.2%). Closer to the Era-Maretayakha River estuary, in the section of a surface about 10 m high, silts are interbedded with fine sands and peat interlayers. The cryostructure of deposits is porous (structureless). The total gravimetric moisture content decreases with depth from 54 to 27%. High ice content of the deposits allows us to assume their syngenetic nature. The peat interlayer in sandy deposits at the depth of 2.2 m has the radiocarbon age of $21,930 \pm 370$ yr BP (LU-6542). In the northern part of the exposure, the silts from the depth of 20 m are underlain by ice-rich clays with a reticulate cryostructure. The upper contact of clays and silts is sharp and goes under the sea level at the southern part of the exposure. In clays, the mineral blocks with the dominating size of 10×10 cm are divided by ice lenses up to 1 cm thick. The moisture content of mineral blocks is 26.0–33.0%. The isotope analysis of segregated ice (-8.48‰ for $\delta^{18}\text{O}$ and -63.4‰ for δD) and the cryogenic structure point

to the epigenetic nature of frozen deposits. The clays have a high content of organic carbon (0.89%). Most likely, the clays were accumulating in a shallow, relatively warm sea.

Two generations of polygonal wedge ice (PWI) (Fig. 2.1, section GD2) are exposed in the section: the upper PWI with the width of 1.2 m on top and the height of 3.6 m and the large lower PWI with the width of 2.5 m on top and the height of more than 10 m. The silts containing PWI have a high ice content. The gravimetric moisture content at the depth of 1.3 m is 52.7% (Fig. 3).

The isotope composition of the upper PWI varies from -23.6 to -18.3‰ for oxygen ($\delta^{18}\text{O}$) and from -179.9 to -134.3‰ for hydrogen (δD); the deuterium excess (d excess) varies from 9 to 12‰. Unfortunately, we were unable to sample the PWI of the lower generation. These wedges are observed in deposits with the age of more than 10,000 years, and the isotopic composition of most wedge ice is rather low. This suggests that the ice wedges were formed mostly during the Late Pleistocene.

Large syngenetic ice wedges were not observed in the southern part of the exposure. It is possible that they were eroded by slope processes or partly thawed. Here, thin (width of up to 0.4 m) ice wedges with the average vertical extent of 4.5 m (section GD1) penetrate into sands and silts. The content of oxygen and hydrogen stable isotopes in the ice does not change with depth and varies from -24.6 to -22.6‰



Figure 3. Silts containing two generations of polygonal wedge ice.

for $\delta^{18}\text{O}$ and -193.1 to -176.5‰ for δD ; the deuterium excess does not exceed $6\text{--}7\text{‰}$. The noticeably high content of chlorine ions (8.8 mg/l) was detected in the ice wedges. The isotope composition of wedge ice most likely indicates the Late Pleistocene age of the ice.

Based on the simple linear relation between the average January temperature (t_j) and the isotope composition of oxygen ($\delta^{18}\text{O}$) in the PWI that was suggested by Vasilchuk (1992), the average January temperature during the PWI formation was determined: $t_j = -1.5\delta^{18}\text{O} (\pm 3^\circ\text{C})$, which equates to $-36.0 \pm 3^\circ\text{C}$.

Cape Pakha-Sale

The northern coast of Gydan Bay near Cape Pakha-Sale was another area of our research (Fig. 2.2). Here, marine and coastal-marine sand and silt deposits were exposed in coastal bluffs with the height of $15\text{--}20\text{ m}$. More ancient marine deposits are overlain by the Late Pleistocene-Holocene continental sediments with plant detritus. Numerous bone fragments that were washed out of coastal bluffs are scattered along the beach.

A lens of lacustrine deposits with the thickness of 4 to 6 m and the visible length of 1200 m contains laminated silts with organic matter (organic carbon content reaches 1%). Sandy silts transform into silts with some clay at the depth of 2 to 4 m . The amount of organic debris decreases. The content of silt particles increases from 35% at the depth of 1.4 m to 56% at the depth of 3.7 m . Ice content increases with depth. The total moisture content of silts increases from 33% at the depth of 1.4 m to 64.7% at the depth of 3.2 m . The cryostructure of sandy silts is layered. The age of wood inclusions at the depth of 2.6 m at the contact of sandy silts and silts with some clay is $5,280 \pm 160\text{ yr BP LU 6540}$. At the depth of 6 m , sandy silts with high organic content are

replaced by dusty sandy silts. In particle size distribution and in the content of organic carbon they are similar to sandy silts that contain the lens of lacustrine sediments. The total moisture content at the layers contact was 41.9% . The radiocarbon age of wooden inclusions at the contact was $8,030 \pm 80\text{ yr BP LU 6541}$. The cryostructure of the lower silts is reticulate. Most likely, these are lacustrine talik deposits.

The lens of lacustrine deposits is embedded into a layer of silts that form the slopes of thermokarst depression and 15 m high surface. Sediments include 83% silt. Up to the depth of 4.0 m , the 15 to 20 cm thick layers with a higher ice content alternate with 80 to 90 cm thick layers containing less ice. The cryostructure is belt-like, and between the belts it is micro-lenticular (Fig. 2.2, inset A). The gravimetric moisture content of silts reaches 101% . Silts are underlain by grey, fine-grained sands. The sand layer thickness reaches 3 m (Fig. 2.2, section G-1). The sand cryostructure is porous (structureless). The gravimetric moisture content is 22.4% . The sand interlayer wedges out in the southern part of exposure. Sands in the northern part and silts in the southern part of the exposure are underlain by clays containing abundant fauna of marine mollusks. Moisture content at the contact of clays and silts is 64.1% .

Lacustrine deposits include a PWI complex. The ice wedges form a polygonal network on the surface with the polygons of 18 to 55 m across. Ice wedges have a width of $20\text{--}50\text{ cm}$ on top and a vertical extent of $2\text{--}5\text{ m}$. The polygonal wedge ice is brownish white, vertically foliated, and oxidized at the contact with hosting soils. The PWI isotope composition is -19.1‰ for oxygen ($\delta^{18}\text{O}$) and -146.2‰ for hydrogen (δD), the deuterium excess ($d\text{ excess}$) is 7.2‰ . A relatively low chlorine ion content (5.0 mg/l) is typical of ice wedges that were formed without the influence

of sea water. According to the data by Vasilchuk (1992), PWI from the north of the Gydan Peninsula is characterized by average values of $\delta^{18}\text{O}$ about -18‰.

The filling of thermokarst depression occurred in two stages. During the first stage in the beginning of the Holocene, deposits accumulated in the lake during the destruction of coasts that consisted of ice-rich silts. Coarser sand sediments accumulated at the end of the filling of the lake basin. A horizon with relatively low ice content and post-cryogenic cryostructure indicates the existence of a talik under the lake.

Conclusions

The deposits studied in coastal cliffs of Gydan Bay are of the Holocene and Late Pleistocene age. The two generations of PWI that we distinguished are also of different ages: the lower one is the Late Pleistocene, and the upper one is the Holocene. The formation of the lower generation of syngenetic PWI (polygonal wedge ice) occurred during the last glaciation, when the sedimentation in a shallow and relatively warm sea was replaced by continental sedimentation. Similar conditions existed in the Sopochnaya Karga area in the Enisey River estuary, where the sediments of the second fluvial terrace were accumulating at that time (Streletskaia et al. 2007). A drastic landscape change occurred during the climatic optimum of the Holocene. At this time, shrubs and even trees existed here. A large number of freshwater mollusks lived in the lakes, and these are not present in the modern lakes of the Gydan tundra. After the optimum, sediments, including peaty strata, froze. During the climatic optimum, the Late Pleistocene PWI of the lower generation partly or completely degraded. Thermokarst depressions were formed, and an active formation of gullies along degrading ice wedges occurred. The Holocene cooling that occurred 5,000 to 4,000 years ago (according to the estimates, January temperatures at that time dropped to $-27\pm 3^\circ\text{C}$) caused frost cracking and the formation of the upper generation of ice wedges. They show higher isotope content compared to the Holocene PWI in the areas of Dikson, Sopochnaya Karga (Streletskaia & Vasiliev 2009, Streletskaia et al. 2011, Siegert et al. 1999), Sibiryakov Island, and in other arctic regions (Pavlova et al. 2010). Syngenetic Holocene ice-rich deposits containing PWI blanket a high surface and adjacent slopes. They fill thaw lake basins and old thermokarst cirques, which formed due to thawing of tabular massive ice bodies.

References

- Gusev, E.A., Arslanov, H.A., Maksimov, F.E., Molodkov, A.N., Kuznetsov, V.Yu., Smirnov, S.B., Chernov, S.B., & Zherebtsov, I.E. 2011. New geochronological data on Neopleistocene-Holocene deposits of the lower reaches of Enisey. *Problemy Arktiki i Antarktiki*, No 2 (88), pp. 36-44 (in Russian).
- Pavlova, E.Yu., Anisimova, M.A., Dorozhkina, M.V., & Pitulko, V.V. 2010. Traces of ancient glaciation on Novaya Sibir Island (the Novosibirsk Islands) and the region's natural conditions during the Late Neopleistocene. *Led i sneg*, 2 (110), pp. 85-92 (in Russian).
- Saks, V.N. 1951. Quaternary deposits of the northern part of West Siberian Lowland and the Taymyr Depression. *Trudy NIIGA*. Volume XIV, pp. 3-114 (in Russian).
- Sokolov, V.N. & Znachko-Yavorskiy, G.A. 1957. New data on the Gydan Peninsula geology. *Informatsionny byulleten Instituta Geologii Arktiki*, Issue 6, pp. 4-10 (in Russian).
- Streletskaia, I., Vasiliev, A., & Meyer, H. 2011. Isotopic Composition of Syngenetic Ice Wedges and Palaeoclimatic Reconstruction, Western Taymyr, Russian Arctic. *Permafrost and Periglac. Process.*, 22: 101-106. Published online in Wiley Online Library (wileyonlinelibrary.com) DOI: 10.1002/ppp.707.
- Streletskaia, I.D., Gusev, E.A., Vasiliev, A.A., Kanevskiy, M.Z., Anikina, N.Yu., & Derevyanko, L.G. 2007. New results of comprehensive research of Western Taymyr Quaternary deposits. *Kriosfera Zemli* 11, (no. 3): 14-28 (in Russian).
- Trofimov, V.T., Badu, Yu.B., & Vasilchuk, Yu.K. 1986. *The Gydan Peninsula engineering-geological conditions*. Moscow: Izd-vo MGU. 212 pp. (in Russian).
- Vasilchuk, Y.K. 1992. *Ground ice oxygen isotopic composition (paleogeocryological reconstructions experience)*. Izd. Otdel. Teoreticheskikh problem RAN. MGU, PNIIS. 2 Vols. V.1. 420 pp., V.2. 264 pp. (in Russian).

Thermal Monitoring of Ground Temperature Stabilization Systems

S.N. Okunev, G.M. Dolgikh, S.N. Strizhkov, N.A. Skorbilin
Fundamentstroyarkos LLC Scientific Production Association, Tyumen, Russia

Abstract

The results of long-term monitoring of ground temperatures for the foundations of buildings and engineering structures having systems and devices of ground temperature stabilization are analyzed. The statistical data on the installed systems, thermal wells and their distribution by different cryolithozone districts is given. The peculiarities of the organization and completion of geotechnical monitoring of Fundamentstroyarkos LLC Scientific Production Association are described.

Keywords: cryolithozone; temperature stabilization systems; thermometric monitoring.

The heat exchange between the ground and buildings, structures, and the ambient medium should be taken into account and regulated in the process of design, construction, and operation of buildings and engineering structures in the cryolithozone. In the process of economic development, changes in thermal and moisture regimes of the ground, especially when the temperature crosses 0°C, cause changes in the ground composition, structure, and properties. These changes affect the strength, bearing capacity, and compressibility of permafrost, as well as the intensity of thermal erosion, icings, thermokarst, solifluction, and other cryogenic processes and phenomena. This can lead to significant destruction and deformation of buildings and engineering structures and irreversible adverse consequences for the environment.

About 30% of the entire housing stock in the Russian arctic coastal region is deformed. Most of these buildings are in an emergency state or in a condition not provided for in their design. Repair and reconstruction of damaged buildings amount to about 10% of their cost. Permafrost settlement due to its thawing or heaving is the main reason for the deformations. Railroads, highways, underground communication lines, and other engineering structures suffer great economic losses due to similar causes (Ershov 2002).

The protection of territories from hazardous cryogenic processes, the reliability of engineering structures and primarily their foundations, and environmental safety should be ensured at all stages of the construction and operation of geotechnical systems and engineering structures. In the functioning of technical facilities, much depends on natural means (Ecological encyclopedia 2000).

The most effective methods of emergency prevention during building, construction, and operation of engineering structures include temperature stabilization, the freezing of thawed grounds, and the chilling of near-0°C frozen grounds. To this effect, Fundamentstroyarkos has developed, produced, and widely used systems of ground temperature stabilization (GTS). These systems include the HNP systems (horizontal, naturally operating pipe systems); the VNP systems (vertical, naturally operating, pipe); HSs (individual seasonal cooling units, heat stabilizers); seasonal cooling units (seasonal deep cooling units); and others (Dolgikh et al. 2002). Mounting of GTS systems and devices for ground freezing in the foundation of engineering structures is accompanied by the installation of thermometric wells (pipes, heat pipes). They are primarily designed for the

control of the dynamics of the ground temperature field and the efficient operation of these systems.

The activities of Fundamentstroyarkos include the development, production, installation, monitoring, and scientific-methodological support of GTS systems. The company covers most of the regions of Russia and the eastern regions of the Ukraine (Fig. 1).

In total, 104,428 GTS systems and devices produced by Fundamentstroyarkos were installed between 1993 and 2010. These include 1,029 HNP systems, 337 VNP systems, and 103,071 HSs and seasonal cooling units (Volkova 2011). They were distributed by territories as listed in Table 1:

A significant number of HNP systems are installed at different structures in the Yamal-Nenets Autonomous District and the Vankor Oil and Gas Field located in the Krasnoyarsk District. A similar situation is observed for VNP systems. The Republic of Sakha (Yakutia) is a leader in using these systems in dams in the vicinity of Mirny City. Most HSs and seasonal cooling units are located in the structures of the Yamal-Nenets Autonomous District. However, taking into account 60,000 units of this class installed along the Vankor-Purpe oil pipeline, even more of them are located in the Krasnoyarsk District area.

The installation of GTS systems is completed according to the designs of ground temperature stabilization. The designs are developed and applied by Fundamentstroyarkos based on special engineering (geotechnical, engineering-geocryological, engineering-hydrological and hydro-geological) investigations. Construction and technological peculiarities of the designed structures, their heat and mechanical interaction with permafrost, foundations, and possible changes in geocryological conditions, also due to the predicted global climate warming, are taken into account. In this regard, the local construction conditions, the environmental protection requirements, and the available experience of design, construction, and operation of buildings and structures in similar conditions are considered.

Geotechnical monitoring to a considerable extent ensures control over the operational reliability and longevity of buildings and structures. GTS systems installed in their foundations monitor the working capacity and efficiency of these systems and the state of the ground temperature field in the foundations. Geotechnical monitoring is a system of complex control, forecast, and control of the state of geotechnical systems used to ensure reliability at all stages of the life cycle of geotechnical systems.



Figure 1. Locations of Fundamentstroyarkos activities.

In Fundamentstroyarkos geotechnical monitoring includes the following activities (Volkova 2011):

- Visiting the proposed geotechnical monitoring site by Fundamentstroyarkos specialists;
- Examination of the adjoining territory to identify the indicators of flooding, ground undermining and settling, and the deformations of basis and foundations;
- Examination of the state of the blind area, columns, grillages for any deformation indicators;
- Examination of heat and water supply and sewage networks for leakage indicators;
- Outer examination of the GTS systems superstructure for any mechanical damages and the integrity of the lacquer coating, photo logging;
- Examination of the GTS systems superstructure for leakage indicators in welded joints and valves;
- Measurement of the coolant pressure in systems with the help of a manometer;
- Measurement of the coolant level in systems with a heat method at the heating boundary of the condenser block collector (in winter at temperature below 15°C);
- Determination of the coolant circulation frequency in GTS systems;
- Measurement of the superstructure temperature of GTS systems. The temperature of the superstructure part should be 5–15°C higher than the ambient air temperature when the systems are operating;
- Validation of the GTS systems working capacity;
- Air temperature measurements inside and outside the structure;
- Wind speed measurements to assess heat exchange processes between the devices and the ambient air;
- Ground temperature measurements in heat pipes and compilation of the map of temperature measurements;
- Processing of the received data;
- Operational analysis of GTS systems. Formulation of conclusions and recommendations;
- Preparation of the technical report.

The following additional activities are carried out if any non-correspondence between the GTS systems working capacity characteristics and the parameters indicated in the construction documents are revealed.

- Determination of the defect;
- Control of special mounting operations, coolant recharging;
- Repeated instrumental measurement of coolant leakages and pressure measurement in the GTS system; decision-making on the GTS system working capacity with the preparation of the act of concealed works.
- GTS system commissioning control.

The obligatory temperature measurements of ground both in the process of structure construction and operation play a significant role in the program of the geotechnical monitoring of GTS systems. This is stipulated by SNiP 2.02.04-88 (1988) for all basis and foundation designs for buildings and engineering structures erected on permafrost. The number, the depth, and the position of devices required for ground temperature monitoring in heat pipes (i.e., thermometric monitoring and its program) are defined by the GTS system designs developed by Fundamentstroyarkos. These designs take into account the purpose, the degree of reliability, and the linear dimensions of buildings and structures built. The results of the analysis of geotechnical investigations, the plot plan of territories development, and the peculiarities of

Table 1 - Territorial distribution of facilities with GTS systems and thermometric wells

No	Region, District	Number					Beginning of Thermal Measurements
		of Facilities	HNP systems	VNP systems	HSs	Heat Pipes	
1	Yamalo-Nenets Autonomous District, including	444	606	110	37533	2471	
	Urengoy Field	72	3	22	12387	711	X.1989
	Bovanenkovo Field	136	145	-	5433	343	VII.2004
	Zapolyarnoe Field	73	47	23	3987	284	IV.1998
	Kharasavey Field	20	175	-	190	209	XI.1997
	Yamburg Field	30	83	14	2340	197	III.2002
	Samburg Field	45	88	5	1368	192	VI.2003
	Yuzhno-Russkoe Field	17	-	-	6929	148	V.2006
	Yubileynoe Field	13	6	12	1155	73	XI.2000
	Medvezhe Field	5	5	5	221	25	IX.2002
	Sandibinskoe Field	1	12	2	-	20	V.2002
	Salekhard	10	18	3	1449	115	VI.1996
	Labytnangi	14	4	24	1256	96	V.1996
	Samburg Village	7	20	-	289	40	VI.2003
	Nadym	1	-	-	529	18	I.1995
2	Krasnoyarsk District, including:	58	282	-	63001	362	
	Vankor Field	58	282	-	63001	362	IV.2006
3	Republic of Sakha – Yakutia, including:	26	-	191	1218	269	
	Mirny area	26	-	191	1218	269	I.2004
4	Yamalo-Nenets Autonomous District, including	8	76	36	1015	82	
	Varandey Village area	8	76	36	1015	82	III.2006
5	Khabarovsk District, including:	5	46	-	75	49	
	Khakandzhin Field	5	46	-	75	49	XI.2002
6	Irkutsk District, including	1	10	-	157	8	
	Verkhnechonskoe Field	1	10	-	157	8	XII.2008
7	Chukotka Autonomous District, including:	2	-	-	72	7	
	Zapadno-Ozernoe Field	2	-	-	72	7	V.2006
	Total:	544	1020	337	103071	3248	

the heat interaction of buildings, structures, pipelines, and grounds in their bases are also used to the full extent for these purposes.

According to GOST 25358-82 (1982), the ground temperature measurements should be conducted in wells prepared and settled in advance, with portable or fixed metering sets (electrical temperature sensor garlands) with the corresponding metering devices or inertia mercury thermometer garlands. The temperature of frozen, freezing, and thawing grounds should be expressed in Celsius degrees with rounding up to 0.1°C. In Fundamentstroyarkos, the measurements of ground temperature in the network of heat pipes drilled at the territory of the structure are usually carried out with the help of a complex consisting of the MTsDT 0922 multi-zonal digital temperature sensor and the PKTsD-1/16 multi-channel portable digital sensor controller.

The following particularities should be noted concerning heat pipe design, their optimal layout at the site, and the

completion of monitoring studies:

- In the process of structure and buildings construction with installed GTS systems, the objects of thermometric monitoring include basis, foundations and GTS systems themselves. All the elements are evaluated in their close interaction with each other. This makes it necessary to measure ground temperatures as close to the foundations as possible, without going outside the impact zone of these systems. The wells serving for the determination of background ground temperatures are the only exception.
- Two main conditions should be followed for optimal heat pipe positioning within the designed site: firstly, they should be placed quite regularly within the site with the space between two neighboring wells not exceeding 15-20 m according to STO Gazprom 2-2.1-435-2010 (2010); secondly, additional wells should be drilled in critical points that include drainage trays as well as

inlets and outlets of sanitary engineering utilities and those of the additional heat source.

- The possibility of a more rational and efficient heat pipe layout with regard to the whole designed area should be used during the simultaneous design at several neighboring sites.

The thermometric studies of Fundamentstroyarkos at the structures with installed GTS systems have a long record (Table 1).

Approximately 25% of all heat pipes under study are installed at the structures with GTS systems located at the Urengoy Field area and the adjoining areas of Novy Urengoy City, the Farafontevskaya station, the Eastern Urengoy, and the Severo-Esetinskoe Fields, and gas pipeline routes. Such structures include gas processing facilities, booster compression stations, other engineering structures, and different production and auxiliary buildings. CFS-2 and BCS-2 in the Novy Urengoy area were the very first structures in the specified area where regular thermometric monitoring was initiated by Fundamentstroyarkos in October 1989.

In November 1997, thermometric monitoring was commenced at the Kharasavey Field area. It was conducted at a number of structures – the transient fuel and lubricants storage, the production building of Yamalavtoservis JSC, and the heated parking for construction machinery of the Yamalstroygazdobycha Trust.

Thermometric monitoring at the Zapolyarnoe Field began in April–May 1998. Heated parkings, PAES-2500 aggregates and indoor switchgears, and the Weisman boiler station were the subjects of monitoring.

Thermometric ground monitoring is conducted at 11 structures with GTS systems located at the Yubileynoe Field. The fire station in November 2000 was the first facility to be included in the monitoring.

The repair-production division in Yamburg Village was the first structure with GTS systems at the Yamburg Field where thermometric measurements were conducted in March 2002.

In September 2002 the monitoring of the ground temperature in the base of the structure with GTS systems was initiated in the Medvezhye Field area. This was the building of the shift camp canteen at GP-7.

Some time later, the first thermometric monitoring was conducted in June 2003 at the Samburg Field and the Samburg Village area in the ground under the facility for gas and condensate preparation, under the methanol tank farm, and under a service-operational block with a communication center.

The highest number of structures with installed GTS systems (136 structures) is located at the Bovanenkovo Field area, where 343 heat pipes were constructed for thermometric monitoring. The first monitoring started in July 2004 in the grounds under the buildings of a heated parking and of the fire station of the GP-1 industrial base.

The HNP and VNP systems are not used at the venues of Yuzno-Russkoe Field, which is the specific feature of the area. This was compensated by the installation of a significant number of HSs (about seven thousand devices). The thermometric monitoring there began in May 2006 at the structures of a gas processing facility.

Thermometric studies at the structures with GTS systems produced by Fundamentstroyarkos were located immediately within settlements started even earlier than at hydrocarbon fields.

Nadym City was the first of such settlements. Dwelling house No. 10 in Nadym has a long record of thermometric monitoring (from January 1995). In its base there are more than 500 HSs and 18 heat pipes controlling them.

First thermometric monitoring was conducted in May–June 1996 in Labytnangi Town on the structures with GTS systems: the buildings of the Municipal Department of Internal Affairs and the 84-apartment house at Dzerzhinskogo Street.

Ground temperature measurements started almost at the same time in Salekhard, in the bases of the Salekhard Fish Canning Plant and the Air Terminal buildings. These buildings have a long record of thermometric monitoring which began in June 1996 and October 1999, respectively.

Outside the Yamal-Nenets Autonomous District, the Vankor Field in the north of Krasnoyarsk District is a spectacular example of a large-scale use of GTS systems for the freezing of ground in the basis of engineering structures. About 300 HNP systems and more than 63 thousand HSs, including the main Vankor-Purpe crude oil pipeline, are installed there. Regular ground temperature monitoring is carried out in 362 heat pipes for the control of their operation. This monitoring started in April 2006 at the 5000 m³ tanks for the storage of diesel fuel located at the Preliminary Water Discharge Unit (South) and for fire water storage at the site of central field facilities.

The ground basis temperature measurements with GTS systems were conducted in November 2002 for the first time outside the Yamal-Nenets Autonomous District area. They were carried out within the gold-silver Khakandzha deposit (the building of the gold processing plant) located in the north of the Khabarovsk District. The locations of the GTS systems installation is supplemented with three more areas that are quite remote.

In the City of Mirny (Eastern Yakutia) a unique experience of successful ground freezing and stabilization was obtained in the dam on the Liendokit River and the waterworks facility at the Irelyakh River with the use of Fundamentstroyarkos GTS systems. GTS systems are also installed at other structures in this district: ground basis of production and auxiliary buildings and structures of the Mirny mining-and-processing integrated works, the control and monitoring station for production effluents, and the biological treatment facility for household effluents. The thermometric monitoring started in January 2004 from the Stage 1 tailings pond of the Mirny mining-and-processing integrated works.

Various and significantly large-scale activities of GTS systems installation and application are carried out near Varandey Village in Yamal-Nenets Autonomous District. These systems are used for ground freezing and stabilization in ground basis of buildings and engineering structures of the Varandey oil export terminal, the Dresvyanka machine and tractor station, and the Yuzhno-Khylchuyuskoe Oil and Gas Field. The thermometric monitoring in this area was initiated at the Oil Storage and the Closed Garage structures in March and May 2006 respectively.

In 2006 ground temperature monitoring was conducted at the structures with GTS systems belonging to the main gas pipeline “Gas Processing Facility of the Zapadno-Ozernoe Field – Automated Gas Distribution Station of Anadyr” (Chukotka Autonomous District).

Thermometric ground studies were conducted in December 2008 under the tank farm of start-up complex No. 1 of the Verkhnechonskoe Oil and Gas Field located at the Eastern Siberia-Pacific Ocean pipeline route in the northern part of the Irkutsk District.

Therefore, the large-scale introduction of Fundamentstroyarkos technologies of ground freezing and thermal regime stabilization in ground basis of buildings and structures in permafrost areas was followed by active thermometric studies within the program of geotechnical monitoring. Consequently, unique data on ground temperature in basis of building and other engineering structures were received from more than three thousand thermometric wells with the monitoring record of up to 10–15 years. The obtained data are of significant practical importance for the reliable and timely assessment of the ground thermal field state. The data are useful for the efficient work of GTS systems and devices of ground freezing, structure heat insulation, and the search for and neutralization of technogenic sources with increased heat emission. In addition to the aforementioned practical benefits, the data received are of great scientific value for the study of ground heat exchange processes and dynamics and for the study of technogenic structures built on these grounds. This is especially topical in light of the growing popularity of modern scientific hypotheses on global climate warming.

References

- Dolgikh, G.M. et al. 2002. *Practical experience of buildings and facilities bases construction in permafrost conditions*. Tyumen, OOO NPO Fundamentstroyarkos (in Russian).
- Ecological encyclopedia*. 2000. Moscow, Izdatelskiy dom Noosfera, 930 pp. (in Russian).
- Ershov, E.D. 2002. *Principles of geocryology*. Moscow, Izvo MGU, 685 pp. (in Russian).
- GOST 25358-82. 1982. Grounds. Method of field temperature determination (in Russian).
- SNiP 2.02.04-88. 1988. Bases and foundations on permafrost. Moscow, GUP TsPP, 52 pp. (in Russian).
- STO Gazprom 2-2.1-435-2010. 2010. Design of bases, foundations, engineering protection and monitoring of Gazprom OJSC facilities in the Ultima North conditions (in Russian).
- Volkova, E.V. 2011. Analysis of geocryological monitoring of temperature ground stabilization systems in the bases in the Ultima North areas: “Strategy of Innovation Development, Construction and Development of the Ultima North Districts” all-Russia’s scientific and practical conference of young scientists and specialists, April 19-20, 2011. Tyumen, 12 pp. (in Russian).

Permafrost Structures and Deformations in Quaternary Sediments of West Yamal Peninsula

O.L. Opokina, E.A. Slagoda, A.I. Bazhenov
Earth Cryosphere Institute, SB RAS, Tyumen, Russia

Abstract

The structure of Late Pleistocene-Holocene permafrost was studied in West Yamal. Complex deformations were observed in the cliff exposures in the Marre-Sale Cape area, including folds and combinations of faults and folds. They are associated with Holocene syngenetic ice wedges and intrusive massive ice bodies including laccoliths and wedges. Deformations caused by thawing and subsidence of deposits in taliks and by heave processes associated with the freezing of taliks and of the active layer were distinguished. We came to the conclusion that folds and faults in the Marre-Sale Cape deposits are mainly cryogenic in genesis.

Keywords: active layer; deformed sediments; intrusive massive ice; taliks; wedge ice.

Introduction

Folding and fault deformations at different scales are widely developed in the Late Pleistocene-Holocene sediments in West Yamal. Dislocations of the same type can be caused by various geological processes, including post-sedimentary or synchronous processes with cryogenic sedimentation. To determine the genesis of deformation in the permafrost regions, it is required not only to study the spatial variability of the deformations, but also to detect their relationship with ground ice.

For the permafrost features of West Yamal, various authors have identified the different ground ice types: wedge ice and fissure ice, thick heterogeneous tabular massive ice bodies, and complicated ice bodies forming stocks and laccoliths. Deformations of strata that host massive ground ice were explained by sedimentary and diagenetic (post-sedimentary) processes, tectonic block movements, fault activation, glacier movement, and the action of cryogenic processes (Danilov 1983, Kritsuk 2010, Kuzin & Astafev 1975, Melnikov & Spesivtsev 2000, Streletskaya et al. 2006, Forman et al. 2002).

In 2008–2010, numerous studies of natural exposures were performed along the coastal bluff in the area of the Marre-Sale polar station (Fig. 1). The research area belongs to marine terraces formed by sea transgressions, regressions, and neotectonic movements (Trofimov et al. 1987). Erosional, thermokarst, eolian, and polygonal terrain forms are widespread within second and third marine terraces. Dislocated shallow-marine clays with sand lenses of Kazantsev and Ermakov age, Kargin and Sartan continental sands and silts that enclose Holocene lacustrine-bog and eolian deposits have been observed in the 4-km-long coastal exposure to the south of the Marre-Yakha River. They are characterized by discontinuous lateral bedding, a variety of deformations, cryogenic structures, and massive ice types (Vasilchuk et al. 2006, Forman et al. 2002, Kanevskiy et al. 2005, Streletskaya et al. 2006, Vasilev et al. 2007).

Considerable data exists on the geological structure of the Late Pleistocene deposits in West Yamal. Therefore, our research was mainly devoted to the study of the relationships of different permafrost structures with surrounding sediments and with each other. Fold and fault deformations are identified in the exposures. They are associated with

frost boil systems, ice-wedge polygons, intrusive, repeatedly intrusive, and segregated massive ice bodies, with thawed-out frost mounds, and thermokarst features.

Minor deformations of sediments are widespread on top of the Marre-Sale section. They are typical for the structures that formed as a result of frost heave and soil convection, including frost boils, thawed-out frost mounds, and cryoturbation features in the active layer deposits. Cryoturbation features are most frequently observed within watershed divides, drained lake basins, and river valleys. They form in the layer whose thickness in the study area ranges from 0.3 to 1.5 m (Vasilev et al. 2006) and is not present in homogeneous sands.

Frost boils are widespread within the third marine terrace. They are presented by rounded or irregularly shaped non-vegetated spots, surrounded by a mineral rim (Fig. 2). The diagonal size of frost boils reaches 1 m; they are located at a distance of more than 0.1 m from each other. Fine sands with lenses of peaty silt and silty clay with peat layers are observed in frost-boil sections. The deposits are discontinuous and bent upwards by intrusions of underlain silty sand. Silts and sands in the intrusion channel are folded and mixed. In the center of the channel they have vertical bedding. The width of the deformed structure reaches 1.4 m. The vertical size is limited by the thickness of the active layer of 1.2 m. The formation of frost boils is associated

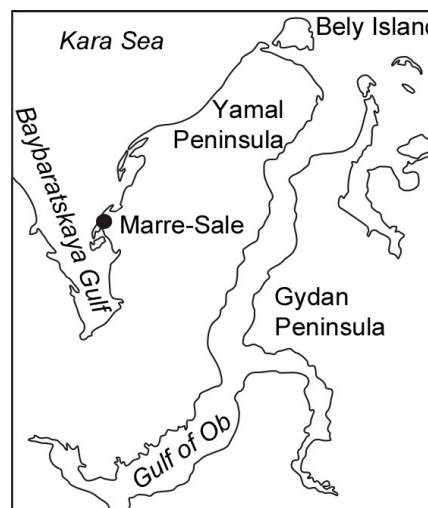


Figure 1. Marre-Sale key site location.

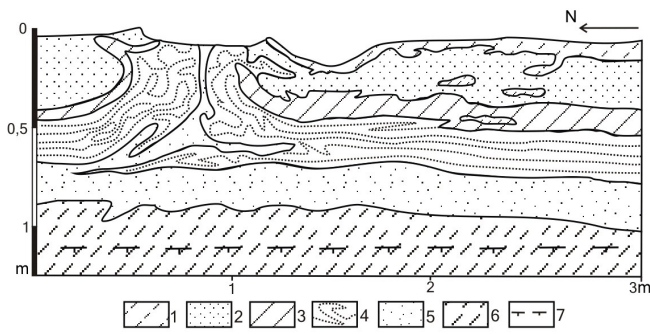


Figure 2. Frost-boil section. 1 – dark-brown peaty silt; 2 – brown fine sand; 3 – gray clayey silt with peat layers; 4 – gray very fine sand; 5 – yellow-brown silty sand; 6 – gray silt; 7 – permafrost table.

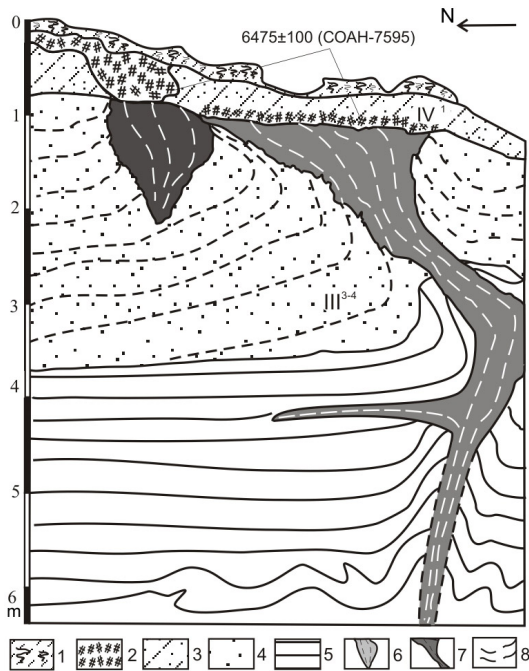


Figure 3. Fold deformations at the contact with intrusive and wedge ice. 1 – subsurface silt cover; 2 – allochthonous peat lenses and inter-layers; 3 – light-brown silt; 4 – gray sand with silt lenses; 5 – dark-gray marine clays; 6 – wedge ice; 7 – intrusive ice; 8 – lamination.

with the freezing of the saturated active layer (Romanovskiy 1993).

Three varieties of the Holocene ice wedges are identified in the top unit of the section. Their syngenetic or epigenetic origin was defined based on their structure, chemical and isotopic composition, their correlation with cryostructures, and deformations of the surrounding sediments (Opokina 2010).

The first variety includes syngenetic ice wedges forming in deposits of khasyreys (thaw lake basins). They are wedge-shaped and small in size, reaching 1.5 to 2 m vertically and 0.2 to 1 m in width on top. Minor folds are registered near their contacts in the surrounding sediments; horizontal layering and layered (belt-like) cryostructures are slightly bent upwards (Fig. 3). This indicates the fast growth of the wedge relative to the sedimentation rate (Vtyurin 1975).

The second variety includes syngenetic ice wedges in lacustrine-fluvial clayey sands (5200±110 years SOAN-

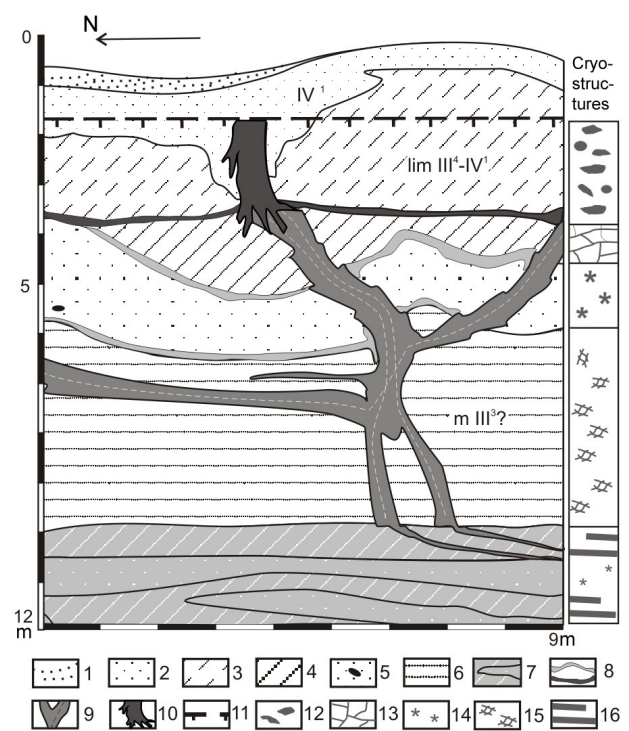


Figure 4. Dikes of intrusive massive ice. 1 – eolian sand; 2 – light-gray fine sand formed in shallow lakes; 3 – lacustrine light-brown silt; 4 – lacustrine dark-gray silty clay; 5 – proluvial gray sand with silt lenses; 6 – marine dark-gray clay; 7 – shallow-marine brown-gray silty clay with sand and silt lenses; 8 – inclined, horizontal ice lenses and layers; 9 – dikes of intrusive ice; 10 – Holocene ice wedge; 11 – permafrost table. Cryostructures: 12 – ataxitic; 13 – lenticular-reticulate; 14 – porous; 15 – reticulate; 16 – lenticular-layered.

7942; 7910±140 years SOAN-7941). The ice wedges are formed by atmospheric precipitation and have fringes of remelt ice along their margins. The wedges are characterized by larger sizes (3 m vertically, 2 m wide on top); they deform the surrounding sediments with the formation of steep syncline folds up to 1–1.5 m amplitude. The deformations are caused by the slow growth of wedge ice relative to more intensive sedimentation.

The third type includes epigenetic ice wedges that penetrate into subvertical intrusive massive ice bodies from the top (Fig. 4). They have a columnar shape and small size. Their ends, split into multiple vertical ice veins, penetrate into the intrusive massive ice body. The surrounding sediments near ice wedges are bent steeply downwards and form narrow syncline folds, which we detect as pseudomorphs formed on the melted-out part of the intrusive ice. Sand layers located between pseudomorphs form flat anticline folds with the amplitude up to 0.5 m.

Curved tilted dikes of intrusive ice were observed in ice-rich shallow-marine clays of probably Kargin age (see Fig. 4), 0.3 km to the south of the polar station Marre-Sale. They break through and flatten out the sequence of sediments including silt, silty clay with sand layers and with lenses of transparent segregated ice, and dark-gray clays with reticulate cryostructure. Sand layers are folded near the margins of massive ice bodies. Air bubble trains are pressed out from sand into the ground ice. Clays are oxidized near the contacts with ground ice bodies. Deeper in the section

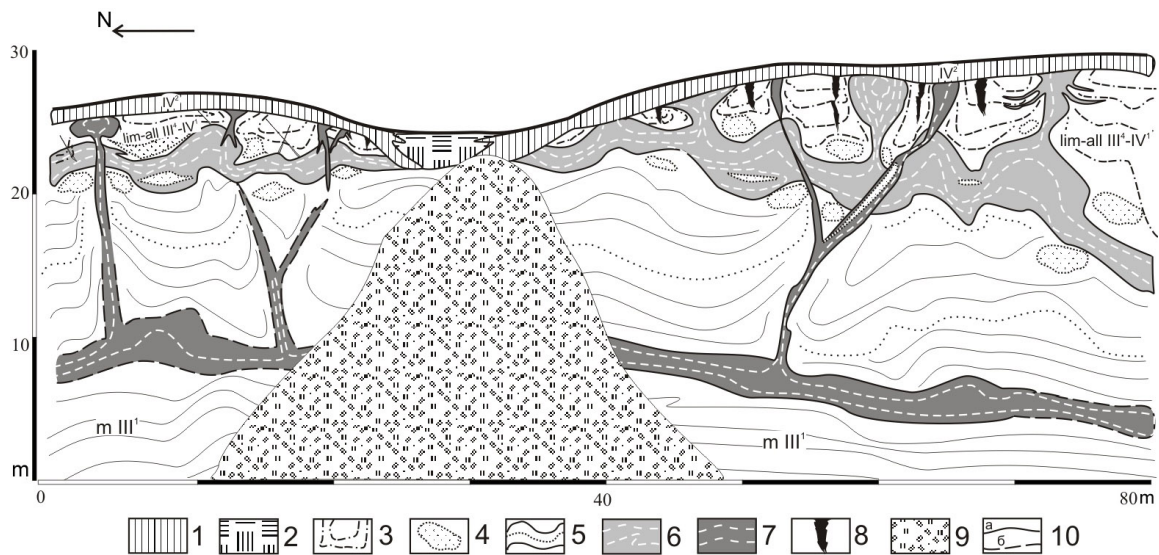


Figure 5. Heterogeneous massive ice.. 1 – subsurface soil horizon; 2 – allochthonous peat lenses and layers; 3 – lacustrine silts and sands with autochthonous peat; 4 – variegated sands; 5 – marine dark-gray clays; 6 – upper tabular massive ice body; 7 – middle tabular massive ice body; 8 – wedge ice; 9 – slump; 10 – boundaries: reliable (a), assumed (b).

the wedges split into large layers. They intrude into the upper part of the massive ice at the depth of 9–10 m, abruptly reduce in width and bend steeply. All this indicates a break in the frozen strata and in the tabular massive ice body as well as a lateral pressure on hosting frozen ground that occurred during the formation of the epigenetic intrusive ice body.

Major fold deformations in the Late-Pleistocene-Holocene lacustrine-fluvial deposits are associated with repeatedly intrusive ice in the form of stocks and laccoliths that complicate the upper tabular massive ice body (Fig. 5) (Slagoda et al. 2010). They are exposed 0.7 km to the south of the Marre-Sale station on the third terrace in 0.3-km-wide thermocirques. The horizontal part of the massive ice body is confined to the contact between marine clay with sand lenses and lenticular-layered cryostructure, and variegated sand with ochreous and black iron compound spots and porous and lenticular cryostructures. Ice laccoliths are located in lacustrine silt and sand with autochthonous organic inclusions ($10,930 \pm 105$ years, SOAN-7597). The age of these deposits is Late Pleistocene-Early Holocene (Forman et al. 2002).

The vertical protrusions of the upper massive ice body vary in shape and size depending on the volume of the melted out ice from the top and the shear plane position. These ice bodies may be shaped as whole laccoliths or stocks (remains of laccoliths with a thawed-out dome), and anticline folds of the upper ice body where the ice layers were truncated in the bent zones (Slagoda et al. 2012, in press).

The thickness of tabular ice bodies reaches 7 to 10 m. The top part is 10 to 15 m. Horizontal lamination and layered (belt-like) cryostructures of lacustrine deposits are broken, bent upwards, and overtilted near the widened part of laccoliths, forming the recumbent folds (folds with a horizontal axial plane). The fold amplitude reaches 3 to 4 m, and the width reaches 4 to 5 m. At the top these permafrost structures and surrounding sediments are eroded and covered by eolian and lacustrine sand with peat lenses (3410 ± 60 years, SOAN 7595).

Low-amplitude folds in marine clay are associated

with the middle body of intrusive ice. Horizontal, slightly deformed and inclined massive ice fragments 2 to 4 m thick are locally exposed in the middle part of the section at the height of 5 to 9 m above sea level (Fig. 5). This ice body is locally complicated by vertical ice protrusions in the form of wedges and laccoliths 1.5 to 3 m wide and up to 15 m high. These protrusions of the middle massive ice unit dislocate the surrounding clays, variegated sands, and silts, forming folds, and they penetrate through the upper massive ice body.

Intrusive ice bodies of different morphology are exposed to the north of the Marre-Sale station. Their lower tips can be observed from sea level to the upper boundary of marine clay. They form wedge-shaped cracks, either narrow, filled with ice, or closed, with oxidized walls. In the upper part of the section, these ice-filled cracks and fissures break through sand blocks surrounded by ice wedges, expand, and split into inclined veins and wedge-shaped ice bodies. These foliated laccoliths are isometric in plan, reach up to 10 m in diameter, and have concentric structure. Their vertical size reaches 6 m in the top part of the section. Near such laccoliths, clays and silts with porous and ataxitic cryostructures are steeply bent upwards at 1.5 to 2 m. The overlain layered sands and silts with lenticular cryostructure form recumbent folds with amplitude up to 2 m and width of 2.5 to 3 m (Fig. 3).

In the lower part of the section, marine clays of Kazantsev age overlain by foliated ice laccoliths are crossed by multiple cracks and characterized by vertical stratification, which is emphasized by lenses of light-colored silt and sand. The deposits are folded, and three morphological types of folds are identified. The first are large flat asymmetric syncline folds up to 100 m and more in size with the amplitudes of several meters. Second are middle-size folds: symmetric anticline crest folds with vertical and inclined layers and smooth syncline level folds. The vertical size of anticline folds is 8 to 10 m and the width is 1 to 3 m. The width of syncline folds reaches 15 to 30 m. Third are the minor folds (up to 1–2 m), turn-ups, and flexure-forming bends, which complicate the folds of larger scale.

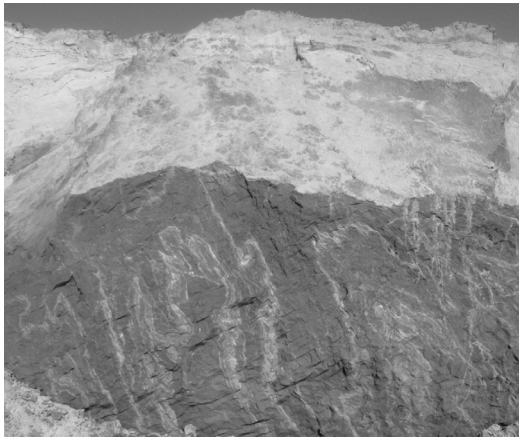


Figure 6. Fold deformations and post-cryogenic platy structure in thawed and refrozen clays.



Figure 7. Syncline fold in thawed and refrozen Late Pleistocene-Holocene sands underlain by clays.

The folds associated with melting of complex intrusive ice bodies and ice wedges were detected in the complex of tabular (thawed and refrozen) sediments in the bottom of khasyrey (drained lake basin) near the creek estuary in the vicinity of the polar station. Kanevskiy et al. (2005) were the first to report the occurrence of tabular sediments in the Marre-Sale Cape section. Thawing of sediments was accompanied by gradual subsidence of the Late Pleistocene-Holocene silts and underlying sands and clays. In clays, there are corrugated folds emphasized by sand layers. There are also post-cryogenic sedimentary deformations (cracks) corresponding to the primary reticulated cryostructure (Fig. 6). Porous cryostructure and angularly shaped ice lenses near the former talik bottom are associated with the subsequent epigenetic freezing of clay. The overlying sands and silts fill up pockets on top of the clay layer with the formation of syncline folds. They have vertical lamination above clay protrusions (Fig. 7).

The tabular massive ice body of segregated origin up to 300 m long with a maximum height of 6 m is exposed 33.5 km to the south of the Marre-Sale station in the lower part of a 12–17-m-high bluff. The ice body forms a large anticline fold. Ice lamination is generally parallel to the overlying frozen silty clays and clays with sand and silt layers, with reticulate cryostructure. The top part of clay layer was eroded and overlain by a sand layer with cryoturbation structures. The shape of ice body complicated by large folds was determined by the freezing front position, low freezing rate, and water saturation of saline marine sediments.

The structures of thawed frost mounds with pseudomorphs formed along ice wedges were observed in the coastal exposure of the low lacustrine-marine terrace, 12 km south of the Marre-Sale station. This section of frost mound consists of three units: (1) a subsurface layer with pseudomorphs, (2) brown sands with humus streaks of silty clay, and (3) light-gray sands in the bottom. Pseudomorphs are wedge-shaped, 0.3 m wide in the top and 0.7 m in height. In the bottom they were bent by the frost heave during the frost mound formation, and the surrounding sands are oxidized and broken by cracks parallel to the frost mound surface. Brown sands with streaks of silty clay have signs of high-ice content (i.e., dense reticulate post-cryogenic structure). They are also folded and protruded upwards. Frequent vertical oxidized cracks and traces of melted-out ice lenses are noted in light-gray sands. All this indicates that the frost mound had an ice or an ice-rich core formed in the process of freezing of the water-saturated sands underlain by an impermeable layer. The frost mound is 2.5 m high and more than 4 m wide, and its top part was eroded by wind action.

Conclusions

Data on the structure of Late Pleistocene-Holocene permafrost in West Yamal provide evidence that minor deformations in the form of folds or combinations of folds and faults are associated with frost heave processes. Medium-size fold deformations are associated with syngenetic wedge ice. Large fold deformations in lacustrine-fluvial and marine deposits are related to the formation of repeatedly intrusive and segregated massive ice. Fold deformations are associated with fault deformations caused by frost cracking, frost heave, and cracking of frozen strata under the impact of cryogenic pressure during talik freezing. The formation of folds in frozen Late Pleistocene-Holocene deposits in West Yamal is mainly caused by the formation of secondary repeatedly intrusive massive ice bodies.

Acknowledgments

This work is completed with the support of the fundamental programs of IPY 2007/2008, RAS Presidium 20.6 and 20.7, ESB RAS-11.4.

References

- Danilov, I.D. 1983. *Methods of cryolithological research*. Moscow: Nedra, 200 pp. (in Russian).
- Forman, S.L., Ingolfsson, O., Gataullin, V., Manley, W.F., & Lokrantz, H. 2002. Late Quaternary stratigraphy, glacial limits, and paleoenvironments of the Marresale area, western Yamal Peninsula, Russia. *Quaternary Res* V.57: 355-370.
- Kanevskiy, M.Z., Streletskaya, I.D., & Vasilev, A.A. 2005. Regularities in formation of Western Yamal Quaternary deposits cryogenic structure (case of Marre-Sale). *Kriosfera Zemli* Vol. IX. No 3: 16-27 (in Russian).
- Kritsuk, L.N. 2010. *Ground ice of Western Siberia*. Moscow: Nauchny mir, 352 pp. (in Russian).

- Kuzin, I.L. & Astafev, N.F. 1975. Cryogenic dislocations at the Yamal Peninsula western coast. *Izvestiya VGO*. Vol. 107. No 6: 510-515 (in Russian).
- Melnikov, V.P. & Spesivtsev, V.I. 2000. *Cryogenic formations in the Earth lithosphere*. Novosibirsk: Izd-vo SO RAN, 343 pp.
- Opokina, O.L. 2010. Genesis of Quaternary deposits cryolithogenic deformations in the Kara region. Author's abstract. Ph.D. Thesis. (Geology and Mineralogy) Tyumen, 20 pp. (in Russian).
- Romanovskiy, N.N. 1993. *Lithosphere cryogenesis bases*. Moscow: MGU, 335 pp. (in Russian).
- Sladoga, E.A., Melnikov, V.P., & Opokina, O.L. 2010. *Repeatedly-intrusive ice stocks in Western Yamal deposits* DAN. Vol. 432, No 2: 264-266 (in Russian).
- Sladoga, E.A., Opokina, O.L., Rogov, V.V., & Kurchatova, A.N. 2012 (in press). Ground ice structure and varieties in Upper Neopleistocene – Holocene Deposits of Western Yamal (Cape Marre-Sale). *Kriosfera Zemli* No 1. (in Russian).
- Streletskaya, I.D., Kanevskiy, M.Z., & Vasilev, A.A. 2006. Massive ice in dislocated Quaternary deposits of Western Yamal. *Kriosfera Zemli* Vol. X. No 2: 68-78 (in Russian).
- Trofimov, V.T., Badu, YU.B., Vasilchuk, YU.K. et al. 1987. *Geocryological zoning of the West-Siberian Platform*. Moscow: Nauka, 224 pp. (in Russian).
- Vasilchuk, Yu.K., Krylov, G.V., & Podborny, E.E. (eds.). 2006. Cryosphere of oil and gas condensate fields of the Yamal Peninsula. In Vol. 1 of *Cryosphere of the Kharasavey gas-condensate field*. 3 Vols. Tyumen: TyumenNIIgiprogaz LLC, St. Petersburg: Nedra, 347 pp. (in Russian).
- Vasilev, A.A., Simonov, S.A., & Streletskiy, D.A. 2006. Assessment of cryolithozone response to climatic changes (case of Western Yamal). *Conference reports: Theory and practice of assessment of the Earth's cryosphere state and its change forecast* Vol. 1. Tyumen, TGNGU: 62-65 (in Russian).
- Vasilev, A.A., Yakimov, A.S., Shirokov, R.S. & Nagornov, D.I. 2007. Peculiarities of Western Yamal coastal outcrops. Conference abstracts: Cryogenic resources of polar regions. Vol. 1. Pushchino: 111-112.
- Vtyurin, B.I. 1975. *Ground ice in the USSR*. Moscow: Nauka, 215 pp. (in Russian).

Territorial Biospheric Resources of the Bolshezemelskaya Tundra Cryolithozone under Intensive Exploration of Hydrocarbon Deposits

G.G. Osadchaya

Institute of Management, Information and Business, Department of Ecology and Natural Resources Management, Ukhta, Russia

T.Yu. Zengina

Lomonosov Moscow State University, Faculty of Geography, Moscow, Russia

Abstract

The Bolshezemelskaya Tundra cryolithozone forms part of the Northern Eurasian Centre of Environment Stabilization. Preservation of the cryolithozone is the basis of sustainable development of the region. According to estimates conducted for a number of deposits that have been explored for a considerable amount of time, the increase of the damaged soil area may lead to the loss of biospheric functions and restrictions on development within the framework of conventional types of natural resource management. This may occur within 20 to 30 years in the case of active exploitation of all explored hydrocarbon resources.

Keywords: biospheric balance; cryolithozone; hydrocarbon deposits; natural resource management.

Introduction

The Russian North is a part of the Northern Eurasian Centre of Environment Stabilization and in a special way ensures not only regional but also global equilibrium. Large and so far only slightly damaged regions of the Russian North may be considered to be a part of the so-called territorial biospheric resources which, according to N.F. Reymers' definition (1994), are territories with stable remaining ecosystems that can be naturally reproduced and have preserved their biospheric functions. According to the modern definition, territorial biospheric resources are areas of the Earth's surface that have global biospheric functions and are not subject to considerable human impact. Therefore, the Bolshezemelskaya Tundra, as a part of this territory, is of great interest from the point of view of preserving the biospheric balance in the northeastern part of the European territory of Russia.

The Bolshezemelskaya Tundra is a part of the rich Timano-Pechorskaya Oil and Gas Province (TPOGP). Possible future development of hydrocarbon deposits may cause serious environmental problems in this region, especially since permafrost provides ecosystem functions that are fragile and vulnerable to external factors. During recent decades, the lands of TPOGP have become the platform for an active oil and gas extraction industry and for transportation infrastructure development, especially pipeline infrastructure. The areas of land that are involved in industrial expansion are increasing every year. The main part of the deposit has not been developed yet; its development is only being planned. Therefore, evaluation of the current ecological state of the TPOGP cryolithozone, the prospects of its further development, and subsequent environmental deterioration arouse great interest from the point of view of preserving this territory as a part of the Northern Eurasian Centre of Environment Stabilization and as the basis of traditional natural resource management in the region.

The cryolithozone zonal landscapes of the Bolshezemelskaya Tundra are represented by tundra subzones: mainly the southern meadow-tundra and

also southern and northern forest-tundra as well as the northernmost taiga. According to zonal analysis, there are two cryolithozones: the northern cryolithozone with predominant development of permafrost and the lowest possible potential of self-recovery, and the southern cryolithozone with mostly thawed soils and with higher self-recovery potential (Tumel & Koroleva 2008).

According to conventional thought, geocryologic zonality within the Bolshezemelskaya Tundra corresponds to zonal landscapes (Table 1, Fig. 1). At the same time, tundra and northern forest-tundra subzones are located in the northern cryolithozone, which is characterized by the development of continuous and discontinuous permafrost. The zone of southern forest-tundra and the northern part of the extreme northern taiga almost coincide with the southern cryolithozone, which is characterized by massive and isolated patches of permafrost.

According to V.G. Gorshkov's (1990) theory of biospheric energetic regulation and N.F. Reymers' (1994) calculations of different zonal combinations of environmental conditions, the ideal (providing ecological equilibrium) area of intensively and extensively developed territories for the entire Bolshezemelskaya Tundra cryolithozone is 10%. Annual phytomass production was the main parameter in deriving this figure. It is obvious that the size of the area permissible for intensive exploitation in the northern cryolithozone is considerably lower than 10%, as annual phytomass volume in this region is two times less than in the southern cryolithozone. This value can be conventionally set at 5% or less.

Methods

The analysis of the territorial deterioration level is based on field measurement data, statistical and cartographic data, cadastral measurements of real estate, and interpretation of aerial photography and satellite imagery in order to estimate the current condition of the Bolshezemelskaya Tundra. Remotely sensed information was processed with ArcView-3.2, ArcGIS-9.2, GlobalMapper-11, and a

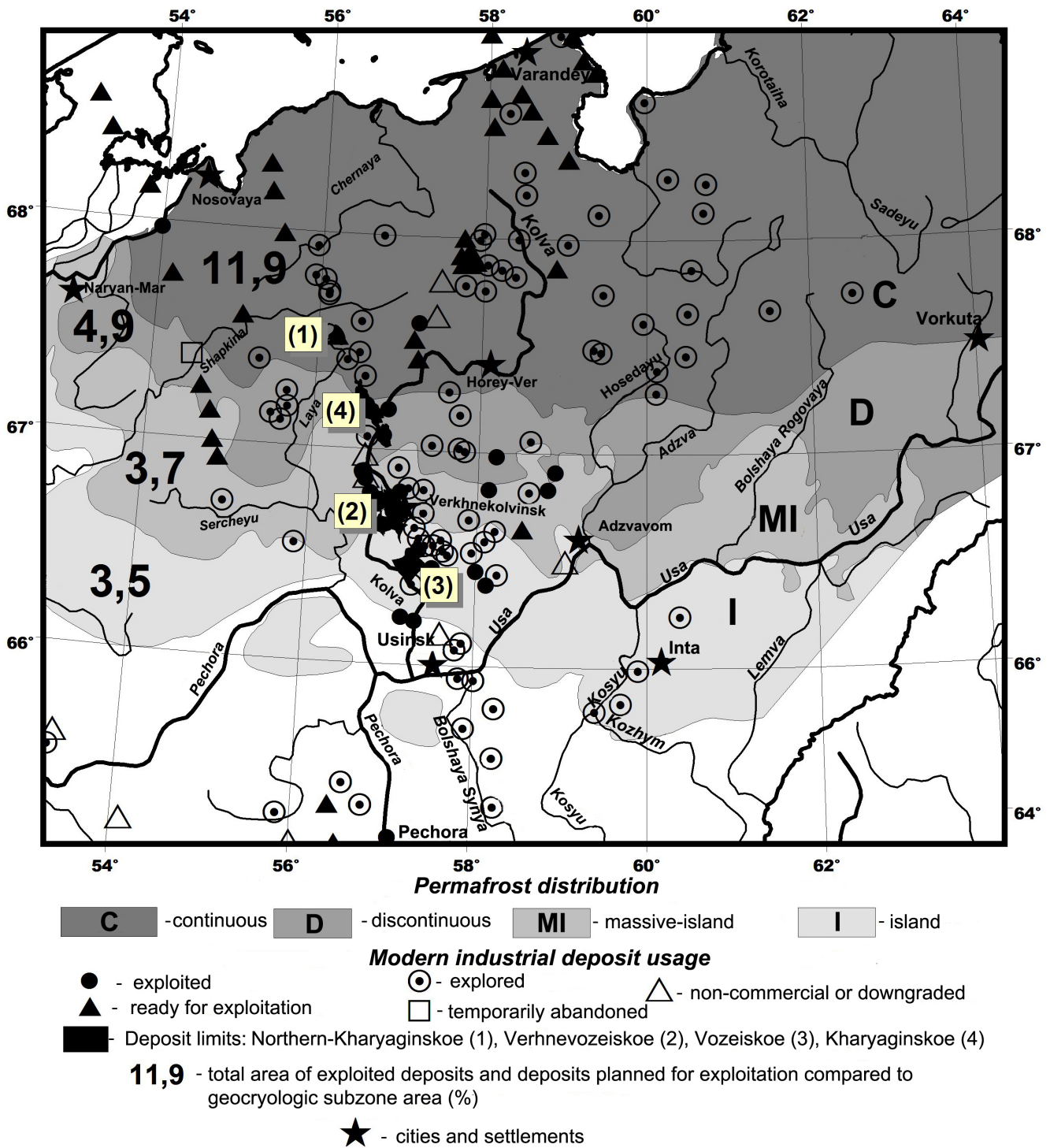


Figure 1. Cryolithozones of the oil and gas fields, current state and development prospects of the Timano-Pechorskaya Oil and Gas Province.

specialized IDRISI package intended for the editing and interpreting of multi-zonal images. The remote sensing materials included LANDSAT-7/ETM+ zonal images with spatial resolution of 30 m for the thematically oriented RGB-synthesis and receiving colored images in false colors as well as ASTER/Terra color synthesized images with the resolution of 15 m. Also, satellite images displayed on the Google-map web site were widely used. For the most exploited regions, the web site offers highly detailed images with spatial resolution considerably less than 10 m. This created the opportunity to both reveal the smallest details and to carry out a large-scale mapping of the damaged territories.

Results and Discussion

During the first stage, the estimate was performed on the lands damaged in the Bolshezemelskaya Tundra cryolithozone development area and adjoining territories. Analyses show that the highest damages can be found in such regions as Vorkuta, Inta (including areas with infrastructure), along the railway Moscow-Vorkuta, along the concrete highway Usinsk-Haryaga, in the regions of underground oil and gas pipelines, and on unpaved and winter roads. According to estimates, 0.1% of lands are damaged in the northern cryolithozone and 0.6% are damaged in the southern cryolithozone due to development and large infrastructure facilities.

Table 1. Natural and geocryological zonation of Bolshezemelskaya Tundra.

Natural zones and subzones	Geocryologic subzone (of cryolithozone total area %)	Permafrost area (%)	Geocryological zone (of cryolithozone total area %)	Acceptable area for intensive exploitation
tundra zone	<i>Continuous</i> permafrost (43%)	> 90	northern cryolithozone (58 %)	< 5%
northern forest-tundra subzone	<i>Discontinuous</i> permafrost (15%)	50 -90		
southern forest-tundra subzone	<i>Massive patches</i> (17%)	10 -50	southern cryolithozone (42 %)	< 10%
northern part of extreme northern taiga subzone	<i>Patches</i> (25%)	> 10		

Table 2. Damaged lands in certain hydrocarbon deposits within Timano-Pechorskaya Oil and Gas Province cryolithozone.

Deposit	Exploitation period (years)	Permafrost Distribution	Large infrastructure facilities	Total damage area (%)	Territory potential for reindeer breeding
Northern Haryaginskoe	10	<i>Continuous</i>	Concrete highway, main oil pipeline	1	Preserved
Haryaginskoe	20–25	<i>Continuous</i> (32 % of the area)	Not present	2	Partially preserved
		<i>Discontinuous</i> (68 % of the area)	Concrete highway, main oil pipeline	8	Lost to considerable extent
Verhnevozeyskoe	25–30	<i>Massive patches</i>	Concrete highway, main oil pipeline	5	Lost
Vozeyskoe	30	<i>Massive patches</i> (10 % of the area)	Concrete highway, main oil pipeline	8	Lost
		<i>Patches</i> (90 % of the area)	Concrete highway, main oil pipeline	13	Lost

During the second stage, the damage in the areas of hydrocarbon extraction was estimated. The most considerable damage was detected in areas of developed and temporarily abandoned deposits. Approximately 20 such deposits exist within the Bolshezemelskaya Tundra cryolithozone. For detailed analysis, four oil reserves of the Kolvinsky megalithic bank that had a considerable exploration period were selected. Both the analysis of the situation and estimates of damaged lands were based on recent aerial and satellite images. The results are presented in Table 2.

Analysis of the obtained information shows that the biospheric capacity of a territory having well-developed transport infrastructure is considerably exceeded after 20 to 30 years of development due to the increase of the damaged land area in the region. As a rule, social functions of the territory are lost as well. These include the conditions for reindeer herding, which is the traditional type of regional natural resource usage. Other traditional types of natural resource usage such as fishing and hunting can suffer as well. The most acute situation is in the regions with interconnecting hardtop roads and large diameter oil pipelines.

The total deposit area was measured to estimate possible

consequences in case development of all explored deposits was initiated. According to available data, the area of deposits in proportion to the total area of geocryologic subzones increases from south to north. This is predictable, considering the fact that the “funnel-shaped” TPOGP widens to the north. For example, from the island of the patchy permafrost subzone to the continuous permafrost subzone, the total deposit area accounts for 3.5%, 3.7%, 4.9%, and 11.9% of the total subzone area, respectively (Fig. 1). At the same time, the acceptable area of intensively developed territories decreases from south to north. Therefore, it is obvious that development of all explored reserves combined with the existing infrastructure and development areas will lead to exceeding the natural limits based on physical parameters of the region. This will account for the loss of biospheric cryolithozone functions, at least in the most vulnerable northern part.

Conclusions

The current approach to exploitation of European Northeastern cryolithozone hydrocarbon resources must be reconsidered in order to preserve the Bolshezemelskaya Tundra as a part of the Russian ecological region. Protection

of regional biospheric resources must be the main priority. Where licenses are issued for subsurface resource management, the amount of land resources used for industrial infrastructure must be clearly defined and tightly controlled. Simultaneously, when performing territorial planning at the pre-investment stage, it is necessary to clearly define the limits of natural resource management and to focus not on the economic but rather on the ecological and social functions of the territory (Osadchaya 2009). To gain more effective control over the process of cryolithozone regional exploration, an ecological examination should again be given independent status. The examination should be implemented not only for the separate venues of the deposit, but also for the entire deposit. In the case of mechanical deterioration or chemical pollution of the surface, re-cultivation and scientifically based natural resource restoration are to be urgently implemented. These measures will help to reduce the recovery period of the corresponding ecosystems (Archegova 2009).

References

- Archegova, I.B. (chief ed.). 2009. Ecological principles of natural resources management in the Russian North. multiple authors. Syktyvkar: *KNTS, UrO RAN*, 176 pp.
- Gorshkov, V.G. 1990. Biospheric energetics and environmental stability: Scientific and technical results. *VINITI. Ser. Teoreticheskie i obshchie voprosy geografii. T.7.* Moscow, 238 pp.
- Osadchaya, G.G. 2009. Territorial resource preservation as one of factors of cryolithozone sustainable development (case study of Bolshezemelskaya Tundra) *Kriosfera Zemli* v.XIII, No. 4, pp. 24-31.
- Reymers, N.F. 1994. Ecology (theories, laws, rules, principles and hypotheses), Moscow. *Rossiia Molodaya*, 367 pp.
- Tumel, N.V. & Koroleva, N.A. 2008. Permafrost and landscape differentiation of Russian cryolithozone as the basis of ecologo-geological studies No. 2, pp.11-14.

Thermophysical Properties of Moss Cover and its Influence on the Thermal Regime of the Ground, Spitsbergen Archipelago

N.I. Osokin, A.V. Sosnovskiy
Institute of Geography, RAS, Moscow, Russia

Abstract

The effects of moss cover on the thermal regime of the ground were examined in the vicinity of Barentsburg Village (West Spitsbergen). Measurements showed that the ground temperature under an 8-cm-thick moss cover is 4°C lower than in sites where the cover is not present, while the temperature gradient in the moss is an order of magnitude greater than in ground. Experimental studies of thermophysical properties of some moss species were carried out. The values of thermal conductivity coefficients of the moss skeleton were estimated, which allowed the calculation of the thermal conductivity coefficients of moss at various moisture contents, and at positive and negative temperatures. It was shown that the thermal resistance of moss cover in winter is 4–6 times lower than in summer, which corresponds to the thermal resistance of a snow cover 1–3 cm thick. Thus, in the cold season, moss cover is not a significant obstacle to the cooling of underlying grounds. In the period of positive air temperatures, the presence of moss cover lowers the temperature of ground and reduces the depth of thawing by more than 50%.

Keywords: moss cover; permafrost; temperature; thawing; thermal conductivity; thermal insulation.

Introduction

Climate warming causes the degradation of permafrost, which in turn is accompanied by a number of negative phenomena, including a decrease in the bearing capacity of pile foundations. Permafrost occupies up to 65% of Russia. According to predictions, up to a quarter of houses in a number of northern cities may face the threat of destruction by 2030 (Tsalikov 2008). In Western Siberia, about 7000 oil and gas pipeline accidents annually are associated with permafrost deformation and the loss of stability of foundations.

The change of heat flow in the system, which includes the atmosphere, surface covers, and underlying ground, can lead to the formation and growth of taliks and degradation of permafrost. To estimate the influence of climate warming and snow cover on permafrost, one must take into account the presence of the moss cover and its thermal insulating properties. The moss cover is a transfer medium between the lower layers of the atmosphere and the underlying ground, and it affects the thermal regime and the dynamics of the thawing of permafrost.

The moss cover is characterized by a great variety of

species. Moreover, different kinds of moss have different thicknesses and thermophysical properties. An important parameter that to a large extent determines the variability of the thermal resistance of the moss cover is its moisture content (the ratio of water weight to the weight of dry moss). During the cold season, the water in moss freezes, which can significantly increase the thermal conductivity coefficient of the moss cover and reduce its thermal insulating properties.

Experiments were carried out to determine the thermophysical properties of moss cover. The goal was to study the effect of moss cover on the ground temperature regime and to estimate the thermophysical properties of some moss species prevailing in West Spitsbergen.

Impact of Moss Cover on Ground Thermal Regime

Mean daily positive air temperature in Spitsbergen Archipelago is about 4–6°C. Therefore, moss cover, which reduces the temperature of the ground surface by a few degrees, has a significant impact on the thermal regime of the underlying ground. Measurements taken in the vicinity of Barentsburg Village (West Spitsbergen) showed that the temperature of the ground under an 8-cm-thick moss cover is 4°C lower than in sites where the cover is not present.

The depth of thawing of permafrost under the 8-cm-thick moss cover was 0.98 cm. At a neighboring site that did not have moss cover, the ground temperature at the same depth was 4°C and the depth of thawing was 1.9 m (Fig. 1).

The depth of penetration of diurnal variations of air temperature into the ground under the moss cover was 0.1 m, whereas without the moss cover it was 0.3 m. The rate of ground thawing in late July to early August, given the thickness of the thawed layer of 0.71.0 m, was about 1 cm per day. If the moss cover is 7–8 cm thick, the rate is 3 times lower.

Measurements showed that the temperature gradient in moss was an order of magnitude greater than in the ground (Fig. 2).

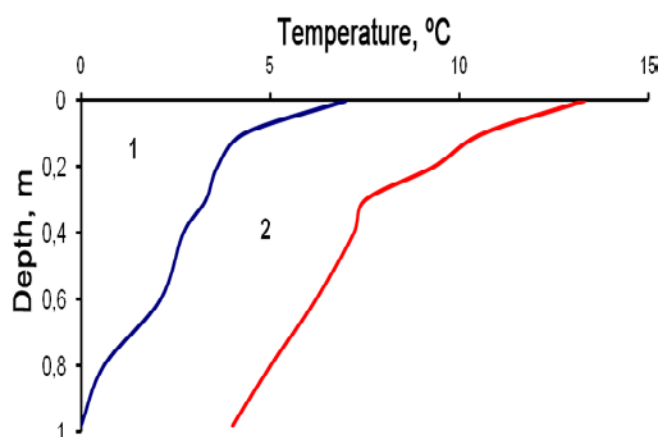


Figure 1. Ground temperature: 1 – under the moss cover 8 cm thick; 2 – without moss cover.

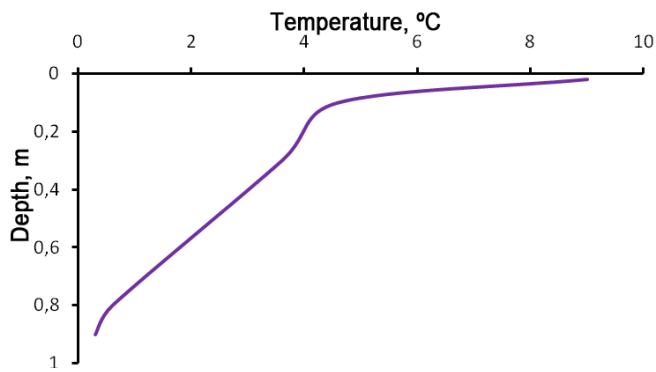


Figure 2. The temperature distribution in the 8-cm thick moss and in the ground.

The results presented above were obtained at different sites for various species of moss and are characterized by different thermophysical properties. In order to evaluate the effect of the moss cover on the thermal state of the ground, one must know the thermophysical properties of the main species of moss prevailing in the area. At present there are only some separate averaged data concerning thermophysical properties of several species of moss.

Thermophysical Properties of Some Moss Species

According to P.N. Skryabin (Pavlov 1980), in the summer of 1978 at the Syrdakh Station, values of thermal conductivity of 0.08–0.30 W/(m*deg) were obtained for green moss (characterized by high species diversity) with a moisture content of 74–350%. At the average moisture of 200%, the thermal conductivity of moss was 0.14 W/(m*deg).

In order to determine the thermophysical properties of different species of moss, we conducted experiments in the vicinity of Barentsburg Village in Spitsbergen. Thickness, density, and moisture content of different species of moss were measured. Moss sampling was carried out on a cloudy day, 24 hours after a slight drizzle. Different types of moss located not far from each other (at a distance of a few hundred meters) showed different values of moisture content. The scatter of values was from 100 to 200% and based on 5–6 samples for each of five moss species that were selected (Table 1).

One of the most common species of moss in the vicinity of Barentsburg Village (West Spitsbergen) is *Hylocomium splendens var alascanum* (*H. splendens var alascanum*) (Fig. 3).

The highest values of density, both in vivo and after drying, were obtained for the moss *Gymnomitrium sp.* (liverwort). Three samples were obtained from three sites with the following density: 400 to 414 kg/m³; 550 to 600 kg/m³, and 600 to 700 kg/m³. Moisture content of moss (total moisture) was calculated as the ratio of water weight to the weight of dry residue.

In order to determine the thermal conductivity coefficient of the most common species of moss in West Spitsbergen, the temperature of moss and ground was measured. Temperature measurements in *H. splendens var alascanum* at depths of 4 and 7 cm were 8.5 and 6.6°C, respectively. The temperature



Figure 3. *Hylocomium splendens var alascanum*.

in the ground under this moss at the depths of 21 and 31 cm was 4.7 and 4.1°C, respectively. Therefore, the temperature gradient in the moss and ground is 6.3 and 6.0 deg/m, respectively. During the experiments, the temperature of air and moss surface on a cloudy day remained practically unchanged. In sunny conditions, at any time during the day, the moss surface can become significantly warmer.

For moss *Sanionia uncinata* (*S. uncinata*), the temperatures at the depths of 4 and 8 cm were 8.5 and 6.3°C, respectively (the temperature gradient in the moss was 5.5 deg/m). The ground temperature at the depths of 21 and 28 cm was 4.8 and 4.3°C, and the temperature gradient in the ground was 7 deg/m. From the equality of heat flow at the ground-moss border, we find that the thermal conductivity coefficient is inversely proportional to the temperature gradient. Therefore, considering the temperature gradients in the moss and in the ground, we find that the thermal conductivity coefficient of moss *H. splendens var alascanum* is 10.5 less than that of the ground. The thermal conductivity coefficient for moss *S. uncinata* is 7.9 less than that of the ground. This is possibly due to a larger value of the density of moss *S. uncinata* than that of moss *H. splendens var alascanum*, at 231 vs. 176 kg/m³.

The results of field experimental studies (measurement of the temperature profile in the ground when heated and cooled) and of the calculations according to a mathematical model, showed close agreement based on a density of ground 600 kg/m³, with moisture content of 18%, and the coefficient of ground thermal conductivity of 1.33 W/(m*deg). This coefficient value of thermal conductivity corresponds to the data of Construction Norms and Regulations (SNiP 2.02.04-88, 1997) for clayey silt.

Therefore, the values of the thermal conductivity coefficient for mosses *S. uncinata* and *H. splendens var alascanum* can be assumed to be 0.17 and 0.13 W/(m*deg), respectively. A larger coefficient value for thermal conductivity for *S. uncinata* is possibly connected with a larger value of its density than that of *H. splendens var alascanum* at 231 vs. 176 kg/m³.

Laboratory measurements of the density of the moss skeleton and the heat capacity of some species of moss were required to assess the contribution of different moss components to its thermal resistance. Measurements of the

Table 1. Average thickness of moss, its density and moisture content.

Moss	Thickness, cm	Average density, kg/m ³		Moisture content, %
		initial	after drying	
<i>Sanionia uncinata</i>	2...5	231	96	141
<i>Rhacomitrium canescens</i>	4...11	160	62	158
<i>Gymnomitrium sp.-</i>	0.5...1.7	405/602*	211/224	92/169
<i>Dicranun sp.</i>	4...6	205	96	114
Moss <i>Hylocomium splendens var alascanum</i>	5...8	176	59	198

* Average value for six moss samples with increased moisture content.

Table 2. Moss parameters in summer and winter at the same density.

Moss	ρ_{moist}	ρ_{dry}	ρ_{skel}	v_{skel}	v_{water}	v_{air}	λ_{moist}
	<i>summer</i>						
<i>Sanionia uncinata</i>	231	96	190	0.51	0.14	0.36	0.17
<i>Hylocomium splendens var alascanum</i>	176	59	230	0.26	0.12	0.63	0.13
	<i>winter</i>						
<i>Sanionia uncinata</i>	231	96	190	0.51	0.15	0.34	0.42
<i>Hylocomium splendens var alascanum</i>	176	59	230	0.26	0.13	0.61	0.36

skeleton volume of some moss species were carried out by means of water displacement when slowly immersing the sample into water. Based on a series of experiments, the density of moss skeleton was determined.

To describe the process of thermal conductivity of multi-component media with a predominantly longitudinal or transverse (the direction of heat transfer) arrangement of components, we applied the model of Voigt and Reiss, respectively (Dulnev & Novikov 1991). The Voigt model demonstrates maximum values of the thermal conductivity coefficient, whereas the Reiss model gives minimum values. The actual structure of the medium is a combination of these models.

The two moss species examined possess a vertically oriented structure, so it is advisable to apply Voigt model of thermal conductivity

Thermal conductivity coefficient of moist moss λ_{moist} depends on the share of the volumes of air n_{air} , water n_{water} and moss skeleton n_{skel} according to the formula

$$\lambda_{\text{MB}} = \lambda_{\text{B3}} v_{\text{B3}} + \lambda_{\text{B0}} v_{\text{B0}} + \lambda_{\text{MCK}} v_{\text{MCK}} \quad (1)$$

where λ_{air} , λ_{water} and λ_{skel} are the coefficients of thermal conductivity for air, water, and moss skeleton: $v_{\text{skel}} = \rho_{\text{dry}} / \rho_{\text{skel}}$; $v_{\text{water}} = (\rho_{\text{moist}} - \rho_{\text{dry}}) / \rho_{\text{water}}$, and $v_{\text{air}} = 1 - v_{\text{dry}} - v_{\text{water}}$. In winter, instead of λ_{water} the coefficient of thermal conductivity of ice is applied λ_{ice} , and v_{water} is replaced by $v_{\text{ice}} = (\rho_{\text{moist}} - \rho_{\text{dry}}) / \rho_{\text{ice}}$. Here ρ_{moist} , ρ_{dry} , and ρ_{skel} are the densities of moist moss, dry moss, and moss skeleton; ρ_{water} and ρ_{ice} are the density of water and ice. The thermal conductivity coefficient of moss skeleton was determined through the comparison of calculated values according to Formula (1) and the measured values of thermal conductivity in view of the moss parameters (Table 2).

As a result, the thermal conductivity coefficient was obtained for the skeleton of moss *S. uncinata* equaling $\lambda_{\text{skel}} = 0.16 \text{ W/(m}\cdot\text{deg)}$ and a slightly larger value for moss *H. splendens var alascanum* at $0.18 \text{ W/(m}\cdot\text{deg)}$. It must be noted that the skeleton density of moss *H. splendens var alascanum* is higher than that of moss *S. uncinata* by 1.21 times. The obtained values of λ_{skel} were used to calculate the thermal conductivity coefficient of moss in the winter period (Table 2). We note that the density of moss skeleton is about two times lower than that in pine and four times lower than in oak. The thermal conductivity coefficient of oak along the fibers is $0.35\text{--}0.42 \text{ W/(m}\cdot\text{deg)}$ if the gravimetric moisture is 6–8%, whereas it is $0.20\text{--}0.21 \text{ W/(m}\cdot\text{deg)}$ across the fibers. In pine it is $0.35\text{--}0.41 \text{ W/(m}\cdot\text{deg)}$ along the fibers if the gravimetric moisture is 8%, whereas it is $0.12\text{--}0.14 \text{ W/(m}\cdot\text{deg)}$ across the fibers (Koshkin & Shirkevich 1962).

Knowing the value of thermal conductivity coefficient of the moss skeleton, one can calculate the thermal conductivity coefficient of moss at various moisture contents in cold and warm periods of the year by means of Formula (1). Calculated values of thermal conductivity coefficient can be approximated using the following linear relations: for *S. uncinata* in the warm period of the year $\lambda_{\text{summer}} = 0,0005w + 0,0946$ and in the cold period $\lambda_{\text{winter}} = 0,0023w + 0,0946$; for *H. splendens var alascanum* during the warm period $\lambda_{\text{summer}} = 0,0003w + 0,0645$ and during the cold period $\lambda_{\text{winter}} = 0,0014w + 0,0645$. These relations show that if the moss moisture content is 150% and 300%, the thermal conductivity coefficients of *S. uncinata* and *H. splendens var alascanum* in winter are 2.4 and 3.0 times larger than in summer. These results are consistent with the data concerning moss-peat covers that increase their thermal conductivity 2.5–3.0 times upon freezing (Balobaev 1991).

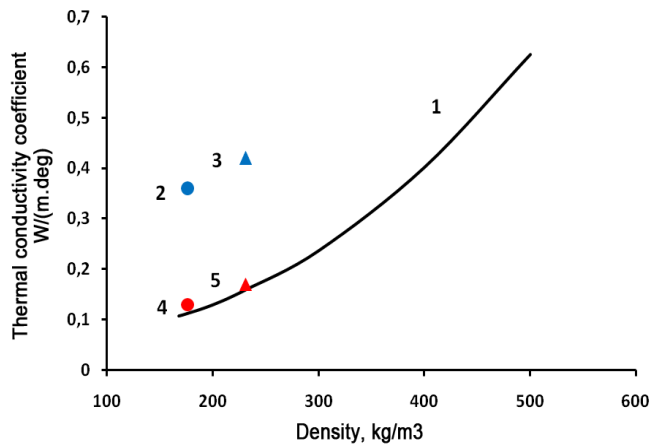


Figure 4. Thermal conductivity coefficients: 1 is snow; 2 and 4 are *H. splendens var alaskanum*; 3 and 5 are *S. uncinata*; 2 and 3 are in winter; 4 and 5 are in summer.

Comparison of Thermal Conductivity Coefficients of Snow and Moss Covers

In winter, the moss cover serves as a heat insulator in addition to the snow cover. Let us compare the values of their thermal conductivity coefficients.

The coefficient of effective thermal conductivity of snow λ_{snow} depending on its density ρ_{snow} was calculated by Formula (2) obtained through the processing and analysis of more than 20 well-known empirical dependences taken from the literature (Osokin et al. 2001):

$$\lambda_{\text{snow}} = 9.165 \cdot 10^{-2} - 3.814 \cdot 10^{-4} \rho_{\text{snow}} + 2.905 \cdot 10^{-6} \rho_{\text{snow}}^2, \text{ W/(m}\cdot\text{K)}. \quad (2)$$

The results of the calculations of the coefficients of thermal conductivity of snow and moss are presented in Figure 4.

From Table 1 and Figure 4 it is evident that in winter the moss cover with the moisture content of 150–200% has a thermal conductivity coefficient that is 2.5–3.0 times larger than in summer and corresponds to the snow density of about 400 kg/m³. The density of moss under the snow cover during the period of negative air temperature reaches 450–750 kg/m³. The moisture content of moss in this case may exceed 400%. Therefore, the value of the coefficient of thermal conductivity of moss in winter will be 4–6 times larger than in summer. The insulating properties of surface covers are defined by the values of their thermal resistance. In winter, the thermal resistance of the moss cover, the ratio of its thickness to the coefficient of thermal conductivity, corresponds to the thermal resistance of the snow layer 1–3 cm thick. Thus during the cold season the moss cover is not a significant obstacle to the cooling of underlying ground. During the warm season its impact on the thermal regime and thawing of ground is significant.

The obtained thermophysical characteristics of some species of moss cover allow for the calculation of their thermal resistance at different moisture contents of moss in the cold and the warm periods of the year. The application of the obtained dependencies makes it possible to give more accurate predictions concerning the effects of climate change on the thermal state of permafrost and its degradation.

References

- Balobaev, V.T. 1991. *Geothermics of permafrost zone of the lithosphere of Northern Asia*. Novosibirsk, Izd-vo Nauka, Sib. otd., 193 pp.
- Dulnev, G.N. & Novikov, V.V. 1991. *Transfer processes in inhomogeneous media*. Leningrad, Energoatomizdat, 179 pp.
- Koshkin, N.I. & Shirkevich, M.G. 1962. *Handbook of elementary physics*. Moscow, Fizmatgiz, 68-69.
- Osokin, N.I., Samoylov, R.S., Sosnovskiy, A.V., Zhidkov, V.A., & Chernov, R.A. 2001. Role of snow cover in ground freezing. *Izvestiya AN Seriya geograficheskaya* No 4, pp. 52-57.
- Pavlov, A.V. 1980. *Calculation and regulation of ground permafrost regime*. Novosibirsk, 240 pp.
- SNiP 2.02.04-88. 1997. *Basements and foundations on permafrost grounds*. Ministry of Construction of Russia. Moscow: State Unitary Enterprise (GUP) Center of Project Products in Construction, 52 pp.
- Tsalikov, R.Kh. 2008. Risks and threats for the northern territories of the Russian Federation due to the global climate change. *Materials of the Scientific and Practical Conference «Comprehensive Provision of Safety in the Northern Regions of the Russian Federation»*, Moscow, pp. 122-130.

Separation of Mobile Forms of Chemical Elements during the Formation of Segregated Ice

V.E. Ostroumov

Institute of Physical-Chemical and Biological Problems of Soil Science, Russian Academy of Sciences, Pushchino, Moscow Region, Russia

Abstract

This paper discusses the data of multi-component spectral analysis of acetate-ammoniacal extracts that characterize the elemental distribution inside mineral interlayers in frozen clayey silt with laminated cryogenic structure. The curve shapes of distribution of mobile forms for 27 elements are compared. The non-coincidence of the accumulation zones of elements that have different mobility in a fine-grained system is described. The non-coincidence of concentration zones observed is explained by the separation of the components of a complex pore solution during mass transport and ice segregation in freezing ground.

Keywords: chemical elements; concentration zones; freezing ground; mobile forms; pore solution; segregated ice formation.

Introduction

Permafrost, being a heterogeneous structured mixture of ice, unfrozen water, and the mineral dispersed phase, is a low-permeable system. While freezing, mass transport occurs almost exclusively in the zone of phase transfer and leads to ice segregation and to the formation of cryogenic structures. Segregated ice formation is accompanied by the formation of concentrated zones of dissolved substances due to pore solution transport from the thawed zone to the growing ice inclusions. Thanks to this mechanism, concentration zones in mineral interlayers are always positioned at that side of the inclusion of segregated ice from which the pore solution was delivered to the growing ice during the freezing period (i.e., at the side of the heat flow). Earlier it was indicated that in the zones of maximum concentration the contents of cations and anions do not always coincide. The observed disagreements allowed the assumption that the transport of the pore solution in the process of ice segregation is accompanied by the separation of components having different mobility. This work is aimed at the experimental validation of this assumption based on the multi-component chemical analysis of soil samples.

Materials and Methodology

Tests were carried out on medium clayey silt sampled in the vicinity of Moscow, for which the chemical composition, structure, physical-chemical, and physical properties, including thermo-physical and mass-exchange parameters, are known.

The samples in the air-dried state were ground with a rubber pestle in a porcelain mortar to destroy the aggregates. Then they were screened through a sieve with a cell diameter of 1 mm. The mass was moistened until it obtained plastic consistency. Then it was treated in a mechanical homogenizer and loaded homogeneously into cylindrical cells with pressure-tight closed end walls made of heat-conductive material. The size of the cells (diameter 60 mm, length 120 mm) was chosen so that several samples with the dry substance weight of about 0.2 g could be received within a single mineral interlayer in the process of layer-by-layer

sampling. A sample of such weight is sufficient for further chemical analysis.

Cells filled with the soil paste were held in the isothermal chamber at +0.1...+0.3°C for two days until equilibrium was achieved. Then the cells were opened from one side, and a part of the soil in the column was replaced with distilled water at the same temperature to the height of approximately 30 mm. The water was separated from the soil with a paper filter; the cell was closed pressure-tight and installed upright (with the water on top) in the same thermostatically controlled chamber between rigid blocks with the controlled temperature in a heat-insulated shell. As soon as the temperature field in the specimen was stabilized, the temperature in the lower block was changed step-wise to the constant value of -12°C. Such freezing mode leads to the formation of two or three well-formed segregated ice interlayers inside the specimen, each more than 5 mm thick. Starting from the moment when the specimen in the cell became completely frozen, the upper block temperature was reduced gradually during 12–16 hours until it reached -12°C. Then the cells with the frozen ground were kept isothermally at -12°C for 2–3 days to achieve equilibrium. Afterwards, the specimens were extracted from the cells in a cold room; the cryogenic structure was described, and samples were taken for further analysis.

The samples of soil from the cells were taken from mineral interlayers between layer-by-layer ice lenses with a 1 mm step near ice lenses and up to a 20 mm step in remote parts. This sampling method provides the detailed information on distribution of mobile substances in the mineral interlayers, including concentration zones. The weight of the samples taken (about 0.2 g of dry substance each) was defined so that the concentration of elements in the extracts could be reliably measured with the help of spectral analysis. After the samples were obtained, they were weighed on analytical scales before drying and then after drying until they reached an air-dried state at room temperature. This allowed for the approximate estimate of the moisture content in the material and to avoid tight binding of mobile forms of elements that occurs at higher temperatures. Air-dried samples were ground with a rubber pestle in a porcelain mortar, and weighed portions were obtained for extraction.

The extraction was conducted with an acetate-ammoniacal buffer at pH=4.8 that is recommended for the study of mobile forms of chemical elements (Agrochemical Methods 1975, van Reeuwijk 2002) and was successfully used in the previous studies of fine-grained frozen soils. The produced extracts were centrifuged for complete sediment separation and were analyzed with the ICP spectrometry method using the Perkin Elmer Optima 5400 DV spectrometer.

The concentrations of 27 elements (Ag, Al, B, Ba, Bi, Ca, Cd, Cl, Co, Cr, Cu, Fe, Hg, In, K, Li, Mg, Mn, Na, Ni, P, Pb, S, Si, Sr, Tl, Zn) were measured in the extracts. The list of the analyzed elements includes all the elements contained in the main ions of the pore solution that generate mobile forms, except for oxygen and nitrogen, as well as the most common micro-components. The most widespread micro-components were also studied. The elements included in this list differ significantly in properties and form a part of various compounds and generate both anion and cation forms in the pore solution. As a result, they have different migration capacity in the system of fine-grained soil. Following extraction, the concentration of elements in dry substance was estimated based on their content in the extracts. The total content of mobile forms of elements in each sample was calculated as the total of the content of all the components.

The elements under study were present in the samples in significantly varying quantities. That is why all the values were rated within the amplitude of real deviations individually for each element to compare their content distribution within the profile of mineral layers. As a result, the plots of distribution for mobile forms of elements (relative units) along the height of the mineral layers between segregated ice lenses were obtained.

Independent tests were completed on four similar specimens in order to check the data reproducibility. Similar results were obtained in all four cases. Additional control measurements were conducted in order to check the regularity of element distribution in specimens that did not undergo cryogenic treatment. The control confirmed the homogeneity of the research material. The number of samples taken and extracts analyzed in each specimen was 14 to 22, and the total number of element tests was about 2300. Therefore, the scope of measurements is sufficient to make reliable conclusions.

Results and Discussion

Figure 1 shows the distribution of the total content of mobile forms of elements along the specimen axis in the cell within a pair of neighboring mineral layers separated by a lens of segregated ice.

Here and hereinafter the zero point of the specimen length (horizontal axis) corresponds to the ice lens surface. Positive length values correspond to the part of the mineral layer that is located at the side of the front surface of the ice lens. In the process of ice segregation, the front surface of the growing lens was oriented toward the heat source. The flow of liquid pore solution from the rear zone was directed toward the front surface. The negative length values correspond to the part of the mineral layer that is located at the side of the rear surface of the segregated ice lens. The rear surface during

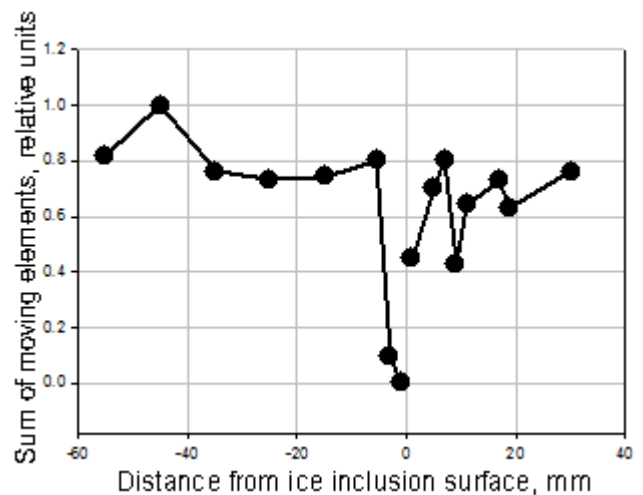


Figure 1. The distribution of the sum of mobile forms of elements in the interlayer of frozen clayey silt in the front (positive length values along the specimen axis) and the rear (negative length values along the specimen) zones of the segregated ice inclusion.

the ice segregation period was oriented toward the low-temperature side.

The maximum value is observed to the right of the ice lens on the distribution curve of the total content of mobile substances (Fig. 1). It corresponds to the concentration zone of soluble substances that were delivered to the ice surface during the ice segregation period. The minimum value to the left of the ice lens corresponds to the rear zone of the mineral layer. This curve almost accurately reproduces the data obtained earlier on the distribution of ordinary salts in concentration zones in the process of soil freezing. The shape of the distribution curve of the sum of mobile forms of chemical elements confirms that ice segregation is accompanied by the formation of the concentration zone of the pore solution near the front surface of the growing ice lens.

The data of the multi-component analysis allows the study of groups of elements, identifying them in accordance with A.I. Perelman's geochemical classification of elements. We will describe potassium as an example in the class of cation-forming elements, iron in the class of elements with high redox activity, and copper in the class of conservative microelements forming mainly low-mobile forms (Fig. 2).

Potassium distribution (Fig. 2) reflects the existence of the concentration zone (the local maximum in the front zone to the right of the lens) and is similar in shape to the distribution of the sum of mobile substances (Fig. 1). Potassium, like other main components of the chemical composition of the pore solution and the absorbing complex, makes a significant contribution to the distribution of the sum of mobile substances. Of the three elements described, the highest difference in the content at the rear and the front zones of the ice lens is observed in the case of potassium. The relative accumulation of iron is observed in the rear zone (not in the front zone as for potassium). Due to comparatively low absolute content of mobile iron as compared to the main ions in the pore solution, its contribution to the distribution of the total quantity of mobile substances is low. However, iron is qualitatively different from potassium in terms of the relative accumulation zone. The intermediate shape of

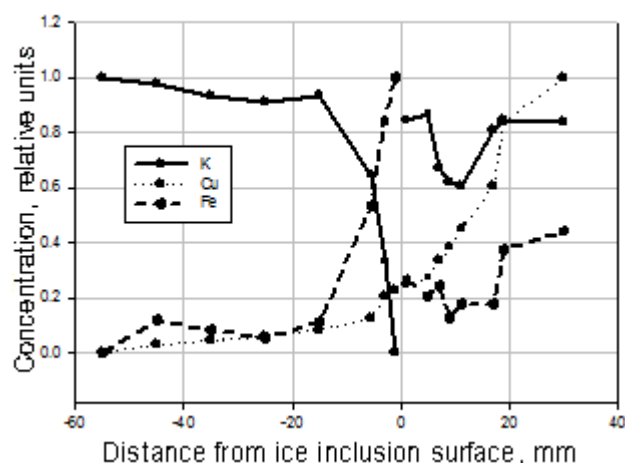


Figure 2. Potassium, copper and iron in the rear and the front zones of the segregated ice lens.

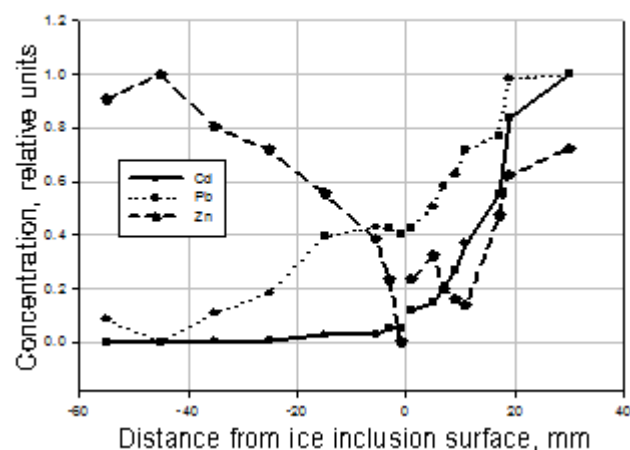


Figure 4. Distribution of micro-elements with least mobility in fine-grained systems.

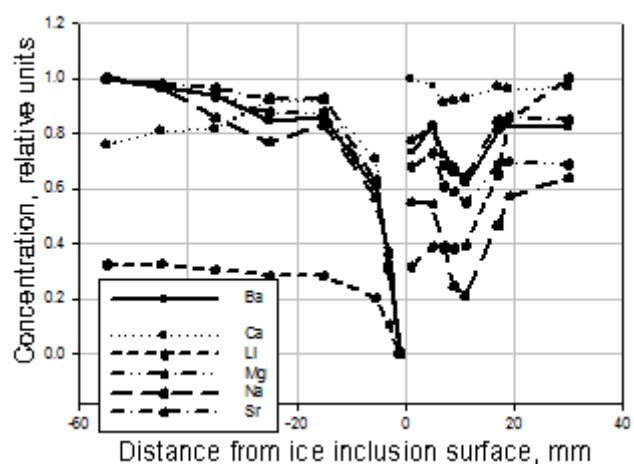


Figure 3. Elements forming mostly cation forms in the system of fine-grained soil.

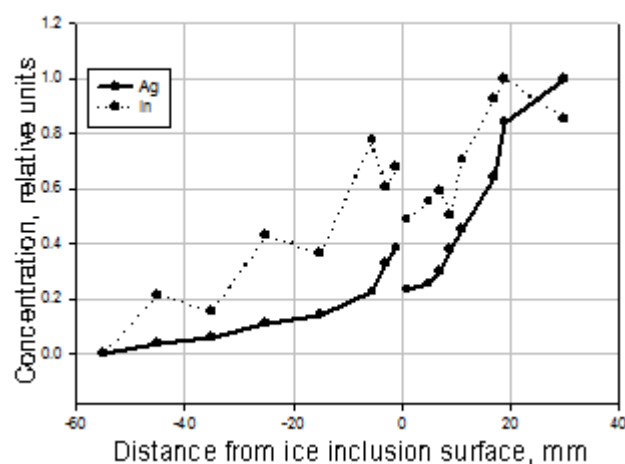


Figure 5. Silver and indium in the zones of segregated ice lens.

the distribution curve is observed in the case of copper. The copper content gradually grows from the internal part of the lens reaching the maximum value at a comparatively large distance from the concentration zone of most soluble substances.

Therefore, the distributions of potassium, copper, and iron in the mineral layer are different. A different shape of the distribution curve for components with different mobility is explained by their separation in the process of mass transport during ice segregation.

Let us describe other elements belonging to the same groups of the geochemical classification as potassium, copper, and iron. The group of cation-forming elements, in addition to potassium, includes the elements of the first and second groups of the periodical system. Of those, barium, calcium, potassium, lithium, magnesium, sodium, and strontium were analyzed. Their distributions have a similar pattern despite the high variety of cation properties and their possible adsorbed, complex, and molecular forms (Fig. 3). Non-coincidence of the local maximum values of calcium and sodium from one side and other elements from the other side is the only difference observed between the curves in Figure 3.

The greatest calcium and sodium accumulations are observed in proximate vicinity to the lens, and other accumulations of elements in the second layer of the front zone of the lens. The increase in the resolution of the distributions obtained would probably allow tracing the element separation beginning here. The data of Figure 3 generally show that the behavior of all the elements of the first and second groups in the system under study is similar.

As for the analyzed elements, the group of micro-elements with low mobility includes copper, zinc, lead, cadmium, silver, indium, mercury, thallium, and bismuth. The shapes of cadmium and lead distribution curves are similar, even with the concentration increase with their transfer from the rear zone to the front zone. Unlike lead and cadmium, zinc is forced out from the zone of ice inclusion to the internal part of the mineral layer (Fig. 4).

In the case of silver and indium, local maxima are observed in the rear zone with the highest concentration in the middle part of the mineral layer (Fig. 5).

A visible reduction of mercury and thallium contents in the rear zone is observed, while lead and bismuth show more even distribution there (Fig. 6).

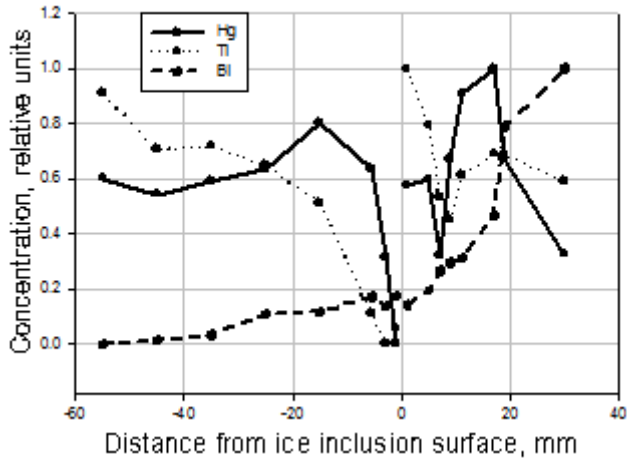


Figure 6. Mercury, thallium, and bismuth in the zones of segregated ice lens.

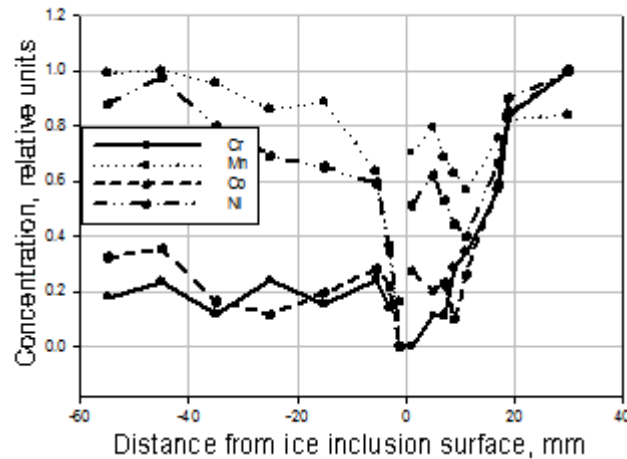


Figure 7. Elements most actively participating in redox transformations.

The variety of chemical compounds in which these elements can be present in the system of fine-grained soil defines the peculiarities of their migration properties and is evidently a reason for the formation of various differences in the distribution shapes.

In the group of elements actively participating in redox transformations (sixth to eighth groups of the fourth period), iron is the only element with an expressed maximum content value in the rear zone of the ice lens (Fig. 2). Chrome accumulation in the rear zone is less pronounced. Manganese, cobalt, and nickel are accumulated in the front zone of segregated ice (Fig. 7).

The difference in the shapes of element distribution curves for Ni, Mn, Cr, Co, and Fe shows that segregated ice formation is accompanied by the separation of these elements.

In the group of elements contained in anions in pore solutions, phosphorus and chlorine are accumulated in the front zone. Boron and sulphur accumulation is observed in the rear zone, with the maxima of these elements not coinciding. These data show that the re-distribution of anion-forming elements (P, Cl, S, B) in the process of ice segregation in the soils occurs differently (Fig. 8).

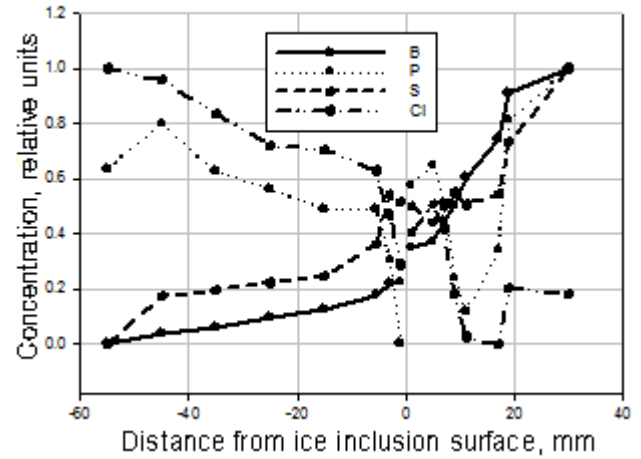


Figure 8. Elements mainly formed as part of anions.

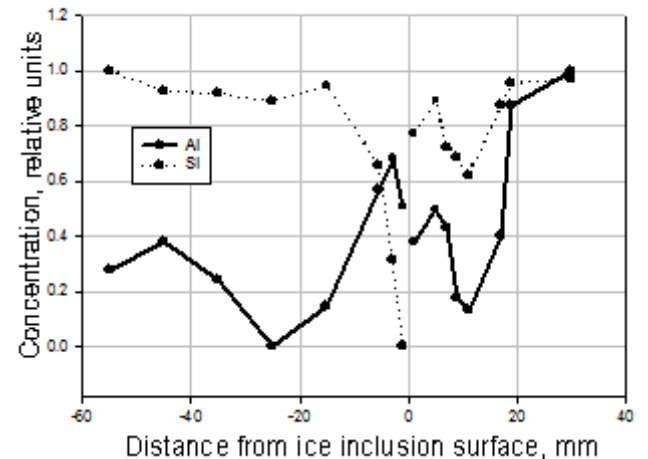


Figure 9. Distribution of elements for which the mobility is controlled by the reaction of the medium.

Aluminum and silicon mobility in soil systems is to a large extent determined by the reaction of the medium. In acid medium, both these elements form stable mineral sediments, and their mobility significantly grows in alkaline medium. Only an insignificant part of the total silicon and aluminum content can transfer to the acid acetate-ammonia extract. These elements in the acid-soluble fraction are probably associated with organic substance.

Like that of most macro-components, the relative accumulation of mobile silicon and aluminum is observed in the front zone of the ice lens (Fig. 9). However, the behavior of aluminum and silicon in the rear zone is different. The maximum of the relative aluminum content is located closer to the ice lens than the zone with the highest silicon content. Evidently, this difference is also associated with different mobility of elements in the clayey silt material of the mineral layer.

Conclusions

The data of the multi-component spectral analysis show that the distributions of elements in the mineral layer of freezing soil between ice lenses have different forms. Most

of the cationic elements formed during the dissociation of compounds are accumulated in the zone of the pore solution concentration near the front surface of the segregated ice. On the contrary, the accumulation of anions occurs mainly in the rear zone and probably inside segregated ice lenses. Uniform distribution is observed for a part of the elements under study. Different shapes of distribution plots for elements in the mineral layer confirm that segregated ice formation is accompanied by the separation of the pore solution components having various mobility.

Acknowledgments

This work is supported by the Russian Foundation for Basic Research, Project 11-05-00789.

References

- Agrochemical methods of grounds research*. 1975. Moscow: Nauka, 656 pp. (in Russian).
- van Reeuwijk, L.P. (ed.). 2002. *Procedures for Soil Analysis*. Technical Paper 9, 6th Edition. International Soil Reference and Information Centre, FAO, United Nations. Wageningen, Netherlands, 120 pp.

Influence of “Landscape Position Marginality Degree” on the Intensity of Dangerous Processes

E. Panchenko

Lomonosov Moscow State University, Department for Cryolithology and Glaciology, Moscow, Russia

Abstract

Data were collected on unfavorable processes due to development along the Obskaya-Bovanenkovo Railway embankment on the Yamal Peninsula. A permafrost landscape map at the landscape subtype level was created for this site based on field monitoring and drilling data. Sites of hazardous process development were indicated on the map, and the spatial analysis of their distribution was conducted. The intensity of process development along the road embankment depended exponentially on the embankment's proximity to the nearest landscape boundary (landscape position marginality degree or LPMD). It was also found that the nature of hydromorphic process development on the roadside area (water-logging, swamping, and thermokarst) depends on the LPMD as well, and that the contribution of waterlogging is the most significant.

Keywords: construction; cryolithozone; landscapes; embankments; exogenous processes; roads.

Introduction

Landscape conditions within the cryolithozone are characterized by a number of important distinctions that should be taken into account when constructing infrastructure. First, the presence of permafrost significantly complicates the geotechnical conditions of construction. This is because there is a high risk of destabilizing the lithocryogenic layer underlying natural landscapes due to exogenous disturbance of the natural thermodynamic balance and the subsequent development of hazardous cryogenic processes. Second, significant complexity in surficial geology, even within the same landscape contour, is typical of cryolithozone natural territorial complexes. This complexity increases the variety of geotechnical conditions (Panchenko 2009). Third, the relations between the components of permafrost landscapes are frequently paragenetic and syngenetic due to the presence of the lithocryogenic layer, which ensures the complexity of their response to any external impact. Fourth, the intercomponent landscape relations in the cryolithozone are quite unstable in their response to external loads, which can trigger various unfavorable cryogenic processes as well, including the hazard of the alteration of natural permafrost-landscape conditions.

Line facilities, roads in particular, are subject to the impact of various processes because they stretch across multiple landforms. Each of these landforms has its own landscape components and geotechnical conditions, which differ in arrangement of material and energy flows and in the ways in which thickness and mode are positioned (Grechishchev 2002).

The structure of permafrost landscapes, both natural and altered by technogenesis, systematically varies along the area adjacent to the line facility. It can then be expected that the impacts of exogenous processes will also show regular behavior and spatial arrangement. This potential correlation makes it relevant to study the interaction between occurrences of exogenous disturbance and the landscape position of unfavorable permafrost responses. In the investigation below, this question is considered, using the example of a section of the Obskaya-Bovanenkovo Railway. This study will examine how the dependence

mentioned above determines the interaction of technogenic linear facilities and permafrost landscape conditions.

Study Area

Analysis of the landscape differentiation of the intensity of various technogenic and natural exogenous processes and phenomena was performed at a selected site, 320–371 km along the southern part of the new railway line on the Yamal Peninsula (Fig. 1).

The site was selected based on the location of this section of road within a relatively short interval. It includes representative geological-geomorphological complexes that are present along the whole route, and it includes most of the peninsula's typical landforms. The road corridor crosses the following landscape types: quaternary marine terraces of different ages, large river valleys, small drainage networks (including valleys of small streams, ravines, and draws), and thermokarst lakebeds. The fact that an important geobotanical boundary—the boundary between typical (suffruticous) and southern (shrub) tundra—passes approximately along the Yuribey River valley was also an important reason for the selection (Chernov & Matveeva 1997).

The underlying substrate in the study area varies with surficial geology and includes fine-grained soils (from silty clay to silts) and organic deposits. Permafrost temperature characteristics also vary significantly, depending on the position in the landscape. The warmest soil temperatures are observed at the highest geomorphological levels (5th Salekhard marine terrace) and reach 5.5 to 6.5°C, while temperatures in modern erosion complexes and river valleys reach only 0°C (Trofimov et al. 1989).

Research Materials and Methodology

A complex landscape map was created for the study area. It has a width of 800 m and is drawn at a scale of 1:10,000 (Fig.2). The map consists of two informational blocks.

The first block includes information on the structure of natural territorial complexes in this area. Landscape contours were arranged hierarchically into groups, types, and subtypes. The classification of landscape contour



Figure 1. Location of the research area.

groups was based on geographic zone. The following landscape types were identified: typical tundra lowland marine accumulative plains; south tundra marine lowland accumulative plains; and intrazonal thermodenudation complexes. The contours of landscape type were identified based on specific stratigraphic formation complex of surface deposits (macro- or mesorelief formation type). According to this principle, seven landscape types were identified within the mapped area. One type corresponds to one geomorphological level within marine valley landscapes. Landscape contour subtype served as the lower mapping level. Landscape subtype identification within landscape contours was based on the differentiation of lithological surficial complexes and drainage conditions (Melnikov 1983). Twenty types of landscape subtypes were defined in total within the chosen site. Information on the basis of the contours of various levels of natural territorial complexes that were identified included:

- project data, including the 1:10,000 topographic map along the road route with a 1-km cross-section and longitudinal engineering geocryological sections along the route;
- content of field landscape descriptions conducted within this site between June and August 2008.
- High-resolution satellite images (SPOT 5).

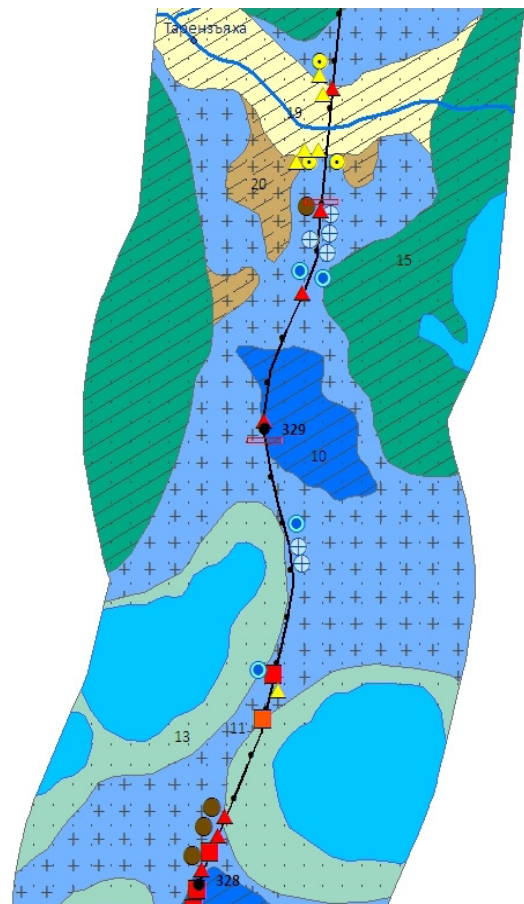


Figure 2. Section of the key site landscape map.

The second informational block of the map is represented by the unfavorable exogenous processes and phenomena in the embankment, and on the adjoining natural territory. The information for this block is based on the findings of the expedition's research along the route completed by PNIIS OJSC in the course of monitoring. The visual identification of processes and phenomena associated with the disturbance of the natural surface and road embankment, as well as with the representation of them in the topographic map along the embankment (scale 1:1,000), were carried out within this area during traverses in 2008 and 2009. In 2008 the mapping was conducted during the construction stage of the railway embankment, and in 2009 during the embankment operational stage. For the monitoring mapping, a specific list of processes was selected. The selection was based on these criteria:

- processes selected are the most frequent and specific to the research area;
- processes selected are the most unfavorable for road rigidity and landscape cryogenic sustainability.

The mapping list includes the following exogenous processes:

- deflation intensification;
- thermal erosion intensification on the natural surface;
- hydromorphization processes including waterlogging, thermokarst, and bogging. They were combined due to the difficulty of discrimination between types during visual on-ground mapping);

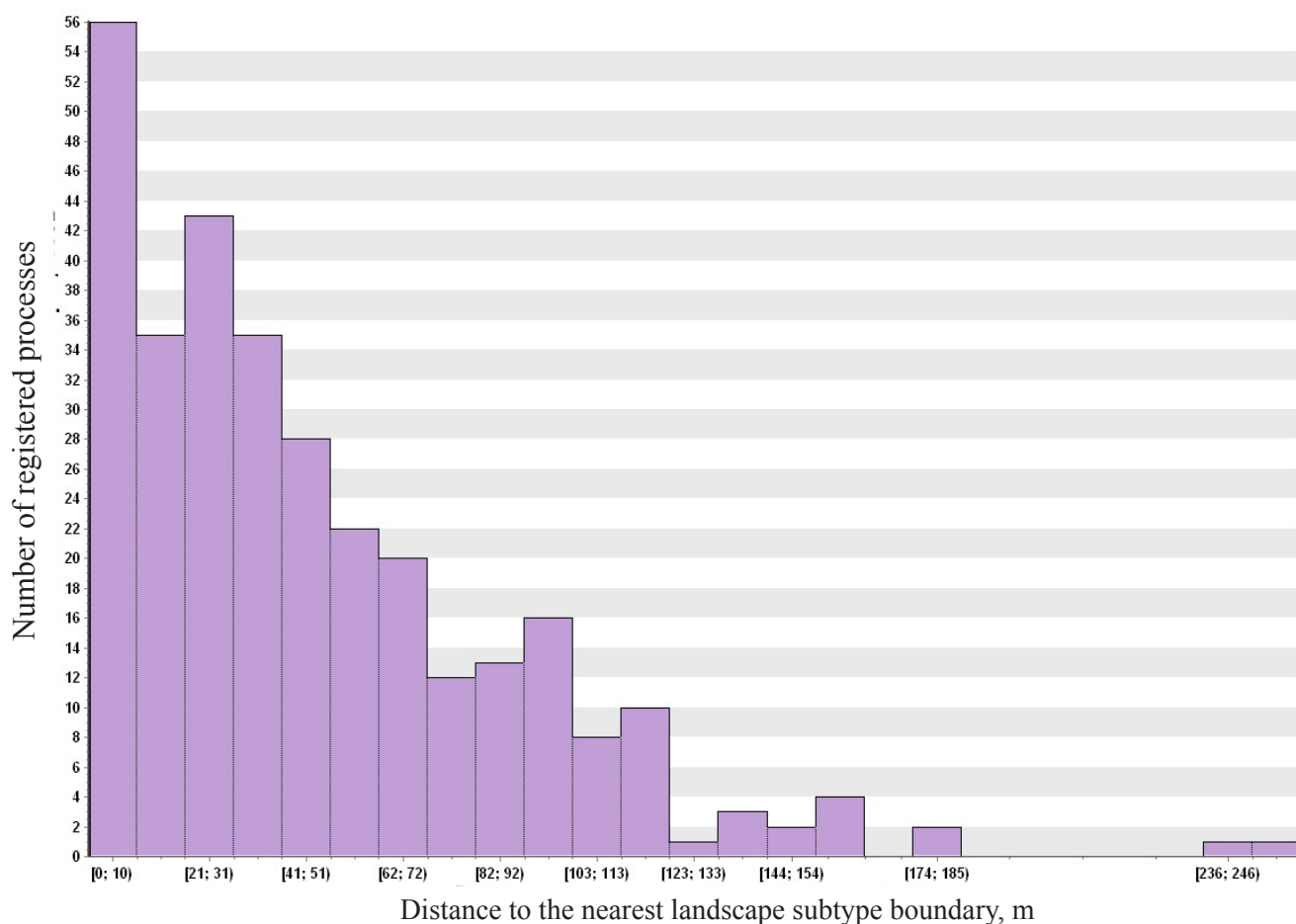


Figure 3. Dependence of the occurrence of natural technogenic processes and phenomena on the LPMD.

- formation of deluvial-proluvial deposits made of embankment material on the natural surface;
- thermal erosion development on the embankment;
- landslides on embankment slopes;
- subsidence of the roadbed.

Each process is depicted on the map in point form. In cases of extended swamping or water-logging zones along the embankment, one point for each 50 m of its identified length was marked. The location of symbols designating the development of a process or phenomenon corresponds to the proximity relative to the road survey. The selection of the depicted processes clearly shows the primary purpose of the map: namely the analysis of the engineering geocryological state of the road.

The analysis of landscape related to development of hazardous processes within the key site was carried out using the produced map.

The decision was made to carry out the graphic analysis of hazardous processes and phenomena based on the mapped material (Berlyant et al. 2003). Analysis of the distribution of various process and phenomenon types was conducted depending on their relationship to a specific natural territorial complex type using a process distribution density histogram based on landscape position.

Results

In total, 312 points of various exogenous processes and phenomena occurred within the key site. It was noted during analysis of the visual map that many identified processes are localized within the marginal zones of a natural territorial complex (i.e., where the boundaries of various landscape subtypes types meet). Analysis of the dependence of the occurrence of natural process on the distance to the closest landscape subtype border was accomplished (Fig.3). Findings for the whole sampling of plotted process points display a strong exponential relationship between process intensity and landscape position marginality degree (LPMD); that is, the closer the road embankment is located to landscape margins, the more likely exogenous processes are to occur. In general, this can be explained by the fact that each landscape subtype has its own typical dynamic structures, and the transition between them occurs in contact zones. This creates an increased dynamic intensity and variety at marginal zones. A road intrudes into a natural dynamic equilibrium as an outside force and therefore causes an increased dynamic imbalance, which is especially noticeable in the landscape marginal zones. The qualitative analysis of this dependence can be carried out based on the division of the general histogram of dependence of each process on the degree of area marginality.

The most interesting dependence histogram in this case appears to be the one for hydromorphization processes:

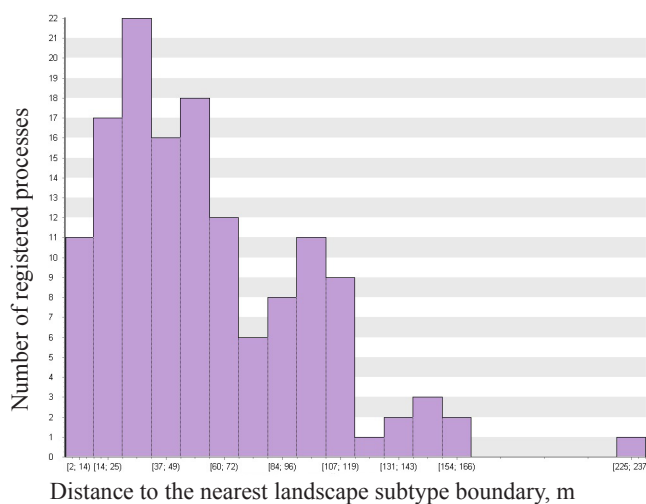


Figure 4. Hydromorphic processes (swamping, water-logging, thermokarst) intensity dependence on the LPMD.

waterlogging, bogging, and thermokarst (Fig.4). It shows three distinct maxima of different sizes: the largest at 30–45 m from the closest landscape margin, midsized at 95–110 m, and the smallest at 140–160 m. The presence of several maxima can be explained as a result of the mapping method. During field monitoring along the road embankment, three different processes (water-logging, bogging, and thermokarst) were plotted because they are almost always indistinguishable from one another in visual on-ground mapping. It should be pointed that these processes are heterogeneous and should be divided for engineering investigations. Water-logging implies the hydromorphization of roadside areas owing to the barrier effect of the road embankment usually in the permafrost zone. This area has a frozen core or is simply constructed of denser material compared to the natural grounds (Grandpre et al. 2010). The process of bogging appears when the permafrost table is subsiding because of the disturbance or succession of vegetation cover (Azimov 1990, Forbes 1988). The process of thermokarst could also be mapped during fieldwork because thermokarst water bodies in the first stages of their development are quite small and have irregular boundaries, so they can be easily confused with the two previously mentioned processes. However, the display of three clear-cut maxima on the histogram helps to discriminate between these three processes and allows us to infer that they contribute unequally to the whole process of roadside hydromorphization.

It should be noted that the absolute values of the remoteness from the nearest landscape boundary is characterized only within the key site. The relative position and the identified dependence extremes give significantly more valuable information. It is logical to expect the positioning of the maximum waterlogging development to occur most closely to marginal zones where surface turns are most evident. Following this reasoning, the second maximum correlates with the swamping process that is most typical of near-horizontal, flat, or slightly inclined, poorly drained sites of a natural-territorial complex that are located at some distance from the margin in more drained areas. The third maximum corresponds to the occurrences of natural thermokarst processes found at the farthest distance from the natural

territorial complex marginal zones: that is, in conditions of autonomous eluvial landscapes at the minimum degree of drainage. Also, the histogram helps to conclude that waterlogging contributes most significantly to the general process of hydromorphization of the roadside area, because of the impact of the static barrier of the road embankment on natural dynamic patterns. The contribution of bogging, which mostly relates to the dynamic impact of transport pressure on the stage of road construction, is almost half as large.

Conclusions

During two field seasons (2008, 2009), a comprehensive field survey of the development of unfavorable exogenous processes was collected along the 50-km section of the Obskaya-Bovanenkovo Railway. A landscape map at the level of landscape subtypes depicting points of unfavorable process development was prepared for the area based on field descriptions and engineering geocryological drilling. A total of 312 points occurred within the study area. Spatial analysis using a graphic analytical method revealed a clear dependence between the intensity of process development and the position of the road embankment in the landscape.

First, the intensity of the development of hazardous processes exponentially and positively depends on the landscape position marginality degree (LPMD); the shorter the distance from the embankment to the nearest landscape subtype boundary, the more frequent are such processes. This can be explained by the increased dynamic intensity and variety at the marginal zones of a natural territorial complex that is disturbed by construction and where the development of various processes can have synergetic and paragenetic effects.

Secondly, the contribution of waterlogging to the general hydromorphic process and to the warming of roadside areas turned out to be more significant than that of swamping or thermokarst. At the same time, in agreement with the first conclusion, waterlogging develops in the most marginal parts of a natural territorial complex, whereas thermokarst, with the least contribution to the general hydromorphic process, develops at the maximum distance from the landscape boundaries. It should also be noted that waterlogging, which is associated with the barrier effect of the embankment and is the most prevalent process, is typical of the road operational stage, which speaks to the durability and longevity of this process.

Acknowledgments

The author would like to thank Associate Professor N.V. Tumel, Candidate of Sciences (Geography), Associate Professor V.I. Grebenets, Candidate of Sciences (Geology and Mineralogy), and I.I. Shamanova, Candidate of Sciences (Geology and Mineralogy) for their help in the preparation of material.

References

- Chernov, Y.I. & Matveyeva, N.V. 1997. Arctic Ecosystems in Russia. Wiegolowski F.E. (ed.). Amsterdam: Elsevier *Polar and Alpine Tundra*, pp. 361-507.

- Azimov, S.A. 1990. Man and nature of the North: Harmony of contrasts. *Vestnik AN SSSR* 2: 118-132.
- Berlyant, A.M., Vostokova, A.V., Kravtsova, V.I., Lurye, I.K., Svatkova, T.G., & Serapinas, B.B. 2003. *Map science*. Moscow: Aspekt Press, 477 pp.
- Forbes, B.C. 1988. Cumulative impacts of vehicle traffic on high arctic tundra: soil temperature, plant biomass, species richness and mineral nutrition. *Proceedings of Seventh International Conference, Yellowknife (Canada)*, Collection Nordicana N55, pp. 269-274.
- Grandpre, I., Fortier, D., & Stephani, E. 2010. Impact of groundwater flow on permafrost degradation: implications for transportation infrastructures. *Proceedings of GEO2010. International Conference, Calgary (Canada)*, pp. 534-540.
- Grechishchev, S.E. 2002. Roads and aerodromes. Geocryotechnogenic processes. In *Oil and gas field permafrost and development*. Melnikov E.S., Grechishchev, S.E. (eds.) Moscow: Geos, pp.313-318.
- Melnikov, E.S. 1983. *Cryolithozone landscapes in the West-Siberian gas province*. Novosibirsk: Nauka, 164 pp.
- Panchenko, E.G. 2009. Railway and exogenous processes interaction in the cryolithozone: Case of the Ob-Bovanenkovo route at the Yamal Peninsula. *Magazine Promyshlennoye i grazhdanskoye stroitelstvo* 11: 21-23.
- Pavlov, A.V. 2008. *Cryolithozone monitoring*. Novosibirsk: Geo, 292 pp.
- Trofimov, V.T., Baulin, V.V., & Vasilchuk, U.K. 1989. Geocryological zoning of the West Siberian plate. In *USSR Geocryology*, Ershov, E.D. (ed.). Western Siberia. Moscow: Nedra, pp. 159-162.

Preventive Localization of Adverse Exogenous Geological Processes in the Cryolithozone

V.V. Pendin, T.P. Dubina, O.S. Ovsyannikova
Russian State Geological Prospecting University (RSGPU), Moscow, Russia

S.D. Ganova
MSMU, Government of Moscow, Russia

Abstract

The cryolithozone territory in northern West Siberia, even in its natural state, is subjected to intense thermal erosion, solifluction, and cryogenic cracking. There is, therefore, an urgent need for the immediate development and implementation of protective measures. These include construction of frost drainage belts with the leveling of embankment slopes; route flattening with filling of trenches, thermokarst depressions, and thermo-erosional furrows with clay-rich soil; filling of bare areas of the route with peat and covering the peat with a 0.15–0.20 m layer of coarse drainage in order to protect it from desiccation and deflation; and diversion of surface water by construction of diversion embankments of compacted clay-rich silt.

Keywords: cryogenic cracking; engineering-geocryological conditions; gas pipelines; protective measures; solifluction; thermal erosion.

Introduction

The northern territories of West Siberia are characterized by complex engineering-geocryological conditions. Intensive development of those areas requires the predictive assessment of adverse exogenous geological processes associated with the construction and operation of gas pipelines. The cryolithozone territory in northern West Siberia, even in its natural state, is subjected to intense thermal erosion, solifluction, channel processes, and cryogenic cracking.

The pressures of technogenic development connected with the exploration of the Medvezhe, Urengoy, and Zapolyarnoye gas condensate fields (GCF), as well as with the operation of collecting pipes and the pipelines running from the fields, cause the activation of erosion and thermal erosion. As a result, the area of tundra is increasingly becoming devoid of erosion-preventing vegetation. Therefore, rill and gully erosion becomes prevalent and can soon lead to negative consequences such as changes in soil cover in the entire environment, accidents, and damage to engineering structures. Rill erosion on slopes, linear gully erosion, and stream channel erosion are closely interconnected and form a common erosional-accumulation process (Golovenko et al. 1995).

Measures for Processes Localization

The intensity of thermal erosion depends on an entire group of causes and conditions (Table 1). As a result of site observations along the routes of the existing gas pipelines in the cryolithozone, it was established that when modern construction technology is used, the pipelines' operational mode starts to malfunction beginning in the first several years. As a rule, in the third to fourth year of operation up to 30% of the pipeline embankment is damaged in some way (Sharapova 1991). In this connection, there is an urgent need for rapid development and implementation of protective measures.

Besides thermal erosion, cryogenic cracking and solifluction processes associated with gas pipeline routes are developed within the cryolithozone. Therefore, preventive measures should be integrated and should allow for localization of the three mentioned negative processes.

A set of measures should be carried out upon completion of construction work to ensure the reliable operation of a pipeline. These are conducted in the following sequence:

- 1) Technical restoration: flattening of the embankment and the route, the filling of construction depressions, ditches, thermokarst, and thermoerosional furrows, the filling of embankments and bare areas with peat or clay-rich soil, and the strengthening of the solifluction and thermal erosion slopes;
- 2) Determination of the nature of soil moisture in route areas in support of biological recultivation;
- 3) Biological recultivation of the embankment and the route: restoration or creation of topsoil cover, sowing of grass seeds, placement of moss-vegetative covers (mats), fertilization, creation of a maintenance service for the vegetation along the route.

Measures in horizontal route sections

In almost all horizontal route sections where the surface slope does not exceed 1.5°, the measures of technical recultivation should be aimed at creating conditions for the self-regeneration of the vegetation cover along the route and development on the mounded embankment of the pipeline. In this case, preference should be given to the measures that promote the formation and growth of moss cover, as mosses with a thickness of 0.3 m result in a decrease in the depth of thawing of 0.3–0.5 m. For such sections, the following measures should be carried out:

- Flattening and leveling of the embankment so that the steepness of the cross slopes does not exceed 1:5 if the embankment is created with the use of fill, preferably clay-rich soil.
- Flattening of the route with filling of ditches,

Table 1. Causes and conditions that define the thermal erosion process.

Causes		Conditions	
Climatic	Solid and liquid precipitation	Relief	Surface steepness
	Wind		Slopes length
	Relative humidity		Slope aspect
	Air temperature		Slopes surface shape
Hydrological	Runoff regime of thaw water and rainwater	Vegetation	Low shrubs
	Pattern of flow		Herbs
Exogeo-dynamic	Frost cracking		
	Permafrost degradation	Neotectonic	Neotectonic movements direction
	Thermokarst	Geological	Mode of occurrence
	Solifluction		Composition, condition and properties of soils
	Lateral erosion of rivers and rills, etc..	Geocryological	Cryogenic structure of soils
Industrial	Natural vegetation cover disturbance		Soil temperature
	Tracks		
	Roadside ditches		
	Open trenches		
	Filling embankments with icy unconsolidated soil		
	Additional runoff of industrial and sewage waters, etc.		

thermokarst depressions, and thermoerosional furrows with clay-rich soil.

- Covering the embankment with a moss and peat mat of 0.2–0.3 m in order to reduce the depth of seasonal thawing and create favorable conditions for the formation and establishment of a vegetation cover. The mat width must exceed the embankment width by 2 m on either side.
- Filling bare areas with 0.15–0.2 m of peat.
- Removal of excess water accumulated at the base of the embankment by constructing water diversion berms or dams of compacted clay-rich silt. The berms are constructed at an angle to the embankment and are covered with 0.2–0.3 m of peat in order to reduce the depth of seasonal thawing within and under the berms.

Peat possesses the “structural cohesion” that results from the combined effect of capillary, molecular, and colloidal forces as well as of undecomposed plant remains (Trofimov 2005). That is why peat is not destroyed by flowing water. Sometimes erosion of peatlands occurs as a result of the erosion along a polygonal wedge ice, and not from the destruction of peat itself. In mineral tundra areas, where the conditions for revegetation and overgrowth of the embankment are not very favorable, it is advisable to carry out active measures developed by soil scientists and geobotanists to protect the peat mounding from deflation during the periods of winter and summer desiccation. These include summer watering with sowing of grass and winter snow retention by way of installing shields and snow fences (Tvorogov 1990).

Canadian experts recommend covering the slopes with specially prepared wood chips in order to reduce the depth of

seasonal thawing and, consequently, reduce the solifluction and thermal erosion processes (Pick 1987).

Measures in sub-horizontal sections

In the sections of the route where surface slope exceeds 1.5°, the following measures are recommended to improve pipeline stability after the completion of construction:

- Flattening and leveling of the embankment slopes so that the cross slope does not exceed 1:5.
- Creating a moss and peat mat 0.2–0.3 m thick and the width exceeding the width of the embankment by 2 m on either side.
- Covering the mat with a layer of coarse or rubbly drainage materials 0.15–0.20 m thick. With such thickness of the fill, the crushed stones form 1.5–2 layers. This does not prevent the overgrowth of the embankment but contributes to the protection of peat from desiccation and deflation. Each linear meter of the embankment requires 2–2.5 m³ of drainage material.

In order to prevent solifluction and the development of thermal erosion on the embankment and along the route, it is recommended that drainage frost belts be constructed across the slope. In contrast to the frost belt, the drainage frost belt is constructed in the following manner. A trench 0.3–0.5 m deep and 1.5 m wide is dug across the slope. The trench is filled with peat flush with the surface. A berm 0.2–0.3 m thick is made of drainage material containing crushed stone that is placed on top of the peat, which then ensures the preservation of the natural surface discharge on the slope. The sharp decrease in the depth of seasonal thawing under the frost belt results in the occurrence of supporting walls in the layer of sliding soil during solifluction. The distance

between the walls (i.e., between drainage frost belts) decreases with the increasing intensity of the solifluction and thermal erosion processes. In areas with intense thermal erosion and solifluction, the distance between drainage frost belts shall not exceed 15 m. The stone dike of the belt ensures also the protection of the peat from ablation and deflation in summer.

A drainage frost belt constructed above the pipeline helps to solve two problems. First, it protects the embankment soils from gradual sliding down the slope along the trench. Second, the belt disturbs the continuity of the pipe's backfilled soil mass when it refreezes. Therefore, the distance between the cracks created by frost cracking sharply increases, and this has a positive effect on the stress-strain state of the pipe and its insulation. A quantity of 6–8 m³ of peat and 2.5–3 m³ of drainage material is required when creating a drainage frost belt that crosses the main and most disturbed part of the route having the width of 5–7 m on either side of the pipeline embankment. On slopes composed of sand, the formation of both surface and groundwater flow is normally observed in backfilled soils of the pipeline trench. This flow results in the destruction, deconsolidation, and washing-out of the embankment.

To greatly decrease the thermal erosion process, the construction of drainage belts is recommended. A drainage belt is a layer of drainage material containing crushed stones that crosses the pipeline trench and, more precisely, the pipe embankment. On both sides, this layer is adjoined with berms of material containing crushed stones dumped in the form of mounds that are 1.5 m wide at the bottom with the length of 5–7 m each. The mound height varies from 0.3 m at the embankment to 1.5 m at the far end.

Measures on sloping areas

On the slopes composed of sandy soil with steepness of 6° and more, the following measures are recommended. First, for the complete cessation of erosion, a drainage belt should be constructed on the surface of or below the aquiclude (impermeable ground) in three layers: the outside layer is 0.5 m and contains debris or gravel, the next layer is the main layer of crushed stone 1.5 m thick; it is followed by another layer of debris or gravel 0.5 m thick. Second, the embankment should be covered between the drainage belts with drainage materials containing crushed stone 0.15–0.2 m thick in order to prevent sand erosion the entire length of the slope.

The distance between the drainage belts depends on the steepness and the type of sandy soil. It should not exceed the length of the path on which streams of water acquire a velocity sufficient for washing out this soil type.

When covering the embankment with drainage material that armors the embankment, the distance between the drainage belts sharply increases. However, there should be at least two belts on a slope, including one belt at the slope base.

A volume of 6.5 m³ of crushed stone and up to 4 m³ of debris (or gravel) is required to construct such a drainage belt on the surface of the aquiclude or below it. As mentioned above, 2.5–3 m³ of drainage material is required for one linear meter.

Conclusions

It should be noted that when the embankment is made with the continuous placement of non-woven fabric, the fabric can be damaged by cryogenic cracking during the operation. Therefore, non-woven fabric should be laid in separate sections. The length of these sections should be equal to the distance between the cryogenic cracks obtained as a result of predictive calculations considering the ground type and ground cooling conditions above the pipeline. It is also advisable to use geofabrics, which ensure the preservation of top soil in the most difficult and erosion prone sections of the embankment.

As noted above, a drastic decrease in the number of cryogenic cracks in the embankment soils should be expected when constructing frost and drainage frost belts that disturb the continuity of the soil mass above the pipe.

Acknowledgments

This work was carried out in the framework of the project 11-05-00122 funded by RFBR.

References

- Golovenko, S.S., Grigoriev, V.Ya., Krylenko, I.V., Matveev, B.V., & Sidorchuk, A.Yu. 1995. Erosion-accumulation processes on the Yamal Peninsula and their evaluation in connection with industrial development in the region: Case of Bovanenkovo gas condensate field. *Eroziya pochv i ruslovye protsessy* Moscow: Izd-vo Mosk. un-ta, pp. 104-120.
- Trofimov, V.T. (ed.). 2005. *Gruntovedenie*. Moscow: Izd-vo MGU, Izd-vo Nauka, 1024 pp.
- Pick, A. 1987. Use of wood chips for permafrost slope stabilization. *CSEER Centen. Conf. Montreal, May 19-22. 1987. Proc* Vol. 2 sec. 1. Montreal, pp. 345-365.
- Sharapova, T.A. 1991. Underground laying of gas pipelines in grounds with high ice content. *Nadezhnost gazoprovodnykh konstruksii*. Moscow: VNIIGaz, pp. 102-107.
- Tvorogov, V.A. 1990. On restoration of vegetation cover (recultivation) in extreme conditions of the Far North. *Geokriologicheskie issledovaniya na severe Zapadnoi Sibiri*. Novosibirsk: Nauka, pp. 47-54.

Gas Shows in the Permafrost of the Bovanenkovo Gas-Bearing Structure

E.E. Podborny

Tyumen NIIGiprogez OJSC, Tyumen, Russia

Abstract

The geological and cryolithological structure of permafrost containing accumulations of free methane and gas hydrates was studied. As a result, the following parameters were determined: the geocryological and cryolithological characteristics of the layers containing large gas hydrate accumulations; the conditions and regularities that link the gas content of frozen and cooled ground to their composition, structure, and properties; the occurrence rate and intervals as well as the average thickness of gas-containing interbeds and lenses and gas- and water-containing interbeds in geologic and genetic sediment complexes of the Bovanenkovo field; the way that gas shows itself during drilling and testing of wells; and the fact that gas shows are associated with sandy or clayey soils within permafrost. This paper shows that cryolithogenesis performs a decisive role in the composition of permafrost above the gas-bearing structure.

Keywords: Bovanenkovo field; gas hydrates; methane; permafrost.

Introduction

The ground of the Post-Cenomanian sediments within the Bovanenkovo field contains a certain quantity of gas in the depth interval of 10–750 m. It also contains gas hydrates in the zone characterized by thermodynamic conditions favorable for the formation of hydrates and, particularly, in the permafrost part of the profile. The gas content is registered based on the data yielded by mud logging and on the gas shows occurring in the course of drilling, including sudden expulsions of drilling fluid. The tests conducted in parametric wells revealed considerable rates of gas flow in permafrost layers (hundreds and thousands m³/d).

The materials provided by drilling of parametric and production wells constituted the source of information on the gas shows in the frozen part of permafrost of the Bovanenkovo gas-bearing structure (Baulin et al. 1996, Budantseva 2006, Kleymenov et al. 1998, Kondakov et al. 2006, Badu 2011a, b, Podborny 2011, Cherepanov et al. 2011). The diagram reflecting the location of gas shows is continually extended as new production wells are drilled (Fig. 1).

The data on the principles for the physical and chemical formation of different states of natural gas in the cryolithosphere as well as the basic regularities of the genesis, migration, accumulation, and phase transitions of natural gas in the permafrost zone are summarized in the works of Yakushev (2010), Chuvilin et al. (1999), Istomin et al. (2006) and Yakushev et al. (2003).

The small dimensions of deposits are observed in the profile where the gas-bearing sand facies are replaced with frozen silty clays. Gas shows in sands were registered at different depths at the same cluster of wells when the distance between wells was up to 200 m. Small dimensions of deposits are also indicated by rapid drops of the layer pressure occurring in the course of well flaring. According to estimates, the area of gas deposits can make up from several tens of thousands to 80,000 m², while their thickness reaches 4–5 m, and their length reaches 50–60 m.

The degree of cryogenic lithification of sediments determines the existence of collector layers in the permafrost profile. The visible ice content is registered down to the depth of 35–45 m (while the absolute thickness ranges from

3 to 6 m) within the floodplains and drained basins of alases where gas shows are registered. At watershed areas (with absolute elevations up to 30–40 m), the visible ice content is registered down to the depth of 90–100 m and deeper. Besides, in the upper part of the profile there was registered sheet ice with varying thickness and high ice content of syncryogenic sediments, which do not stimulate the formation and preservation of gas-bearing deposits under relatively low temperatures.

Gas Shows in Permafrost in the Course of Parametric Well Drilling

Gas shows in permafrost in the course of parametric well drilling were registered based on sparging or expulsion of the drilling fluid, on the data of geophysical investigations

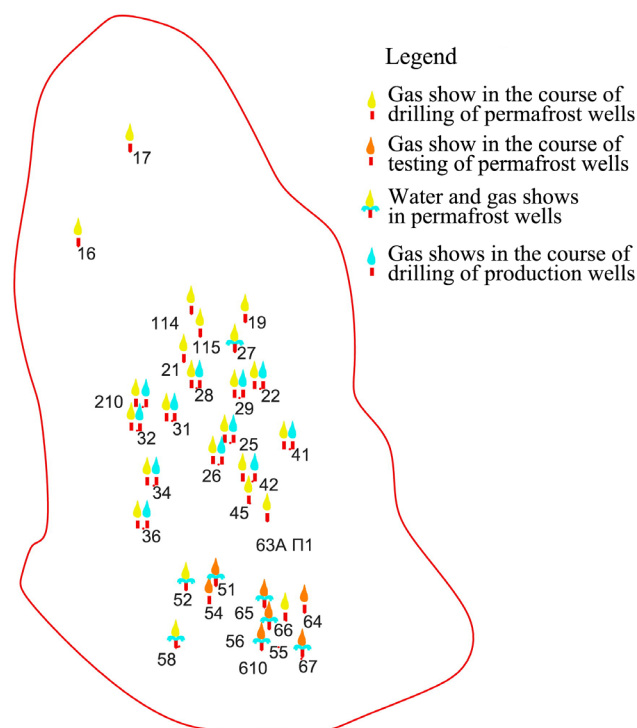


Figure 1. Location of the gas shows observed in the course of drilling of parametric and production wells in the permafrost of the Bovanenkovo field.

Table 1. The rate and mean intervals of occurrence and the thickness of the layers of gas-containing and gas- and water-containing sediments in the geologic and genetic sediment complexes of permafrost.

Geologic and genetic complex	Occurrence rate among all gas and water containing layers, %	Occurrence interval, m		Layer thickness, m
m, pm III ₁	6.5	25.9	29.3	3.5
mg II _{2,4}	80.6	81.6	89.8	8.3
m I ₂ -II ₁	8.1	124.7	130.4	5.7
mg I ₁	4.8	181.8	189.3	7.5

Table 2. The nature of saturation, the occurrence rate among all layers containing gas and water, the average intervals of occurrence, and the thickness of the layers of gas containing as well as gas- and water- containing sediments in the geologic and genetic sediment complexes of permafrost.

Geologic and genetic complex	Nature of the layer saturation	Occurrence rate, %	Occurrence interval, m		Layer thickness, m
			from	to	
m, pm III ₁	gas shows in the course of drilling	3.2	30.2	32.7	2.5
	gas in the course of testing	3.2	21.5	26.0	4.5
mg II _{2,4}	gas shows in the course of drilling	29.0	76.2	80.8	4.6
	gas in the course of testing	42.0	74.5	81.8	7.3
	gas and water shows in the course of drilling	6.5	84.5	102.3	17.8
	gas and water in the course of testing	3.2	91.0	94.5	3.5
m I ₂ -II ₁	gas shows in the course of drilling	6.5	149.4	153.7	4.4
	gas and water in the course of testing	1.6	100.0	107.0	7.0
mg I ₁	gas shows in the course of drilling	1.6	166.0	174.0	8.0
	gas in the course of testing	3.2	197.5	204.5	7.0

into wells, and on the testing of collector layers (Tables 1, 2 and 3).

It is established that the intervals of gas shows in permafrost of the Bovanenkovo gas-bearing structure are found in the sediments of the Late, Middle, and Early Neopleistocene in the range of 15 to 220 m from the surface. More than 80% of gas manifestation intervals were encountered in the sediments of the Salekhard Suite of the Middle Neopleistocene and most often in the silty clays with the inclusions of lenses and layers of sand. Most often, gas shows occur in the areas with reducing thickness of permafrost under the beds of the lower Mordy-Yakha and the lower Se-Yakha rivers as well as in areas having the largest alases and lakes.

Weak gas flows (50–100 m³/d) were obtained in the sediments of the Kazantsevskaya Suite of the Upper Neopleistocene within the depth interval of 28–33 m (the hard frozen part of the profile), from the sediments of the Kazymyskaya Suite of the Middle Neopleistocene within the depth interval of 100–150 m (the plastic frozen part of the profile), and from the sediments of the Poluyskaya Suite of the Lower Neopleistocene within the depth interval of 166–210 m (the cooled part of the profile).

Thirty percent of the tested gas facilities have initial flow rates up to 200 m³/d, 38% up to 1000 m³/d, 22% up to

3000 m³/d, and 10% of intra-permafrost gas deposits up to 3000 m³/d.

The production layers (the flow rate is 1000 m³/d and higher) usually bed within the depth interval of 60–115 m (the plastic frozen part of the profile). The layers with the maximum flow rates ranging from 5 to 14000 m³/d were identified in the lower part (the plastic frozen and the cooled parts of the profile). The flow rates reaching 800 m³/d were registered in the hard frozen part of the profile with the absolute elevations of minus 35 to 85 m. The low values of the initial flow rates (up to 50 m³/d) are characteristic of the layers bedding in the absolute height interval of minus 179 to 187 m, which constitutes the plastic frozen and the cooled parts of the profile. It should be noted that gas-saturated layers were not discovered in the Paleogene sediments that usually occupy the cooled part of the profile.

Gas Shows Occurring in Permafrost in the Course of Drilling of Production Wells

The ground containing gas is registered in permafrost of each production well in the course of drilling based on the data of mud logging (Table 4).

The collector layers saturated with hydrates most often

Table 3. The occurrence rate and average intervals of the gas content in the ground of different composition.

Geologic and genetic complex	Nature of the layer saturation	Type of ground	Occurrence rate, %	Occurrence interval, m		Layer thickness, m
				from	to	
m, pm III ₁	gas	sand	1.6	32	33.3	0.9
		silty clay	1.7	28	32.0	4.0
	gas in the course of testing	silty clay	1.6	28	33.0	
mg II _{2,4}	gas	sand	1.6	74	78.5	4.5
		silt	1.6	76	84.0	8.0
		silty clay	25.8	76	80.7	4.4
	gas in the course of testing	sand	4.9	67	73.0	6.3
		silt	4.8	76	85.5	9.8
		silty clay	32.2	76	82.6	7.2
	gas, water	silt	3.3	76	88.6	13.1
		silty clay	3.2	94	116.0	22.5
	gas and water in the course of testing	silty clay	3.2	91	94.5	3.5
m I ₂ -II ₁	gas	silty clay	6.4	149	153.7	4.4
	gas and water in the course of testing	silt	1.7	100	107.0	7.0
		silty clay	1.6	138	144.0	6.0
mg I ₁	gas	silty clay	1.6	166	174.0	8.0
	gas in the course of testing	silty clay	1.6	209	215.0	6.0
		clay	1.6	186	194.0	8.0

Table 4. The depth intervals (m) of the gas show occurring in permafrost in the course of drilling of production wells.

Well	from	to	Well	from	to	Well	from	to
2502	33.0	594.7	2803	29.5	501.0	3203	25.6	120.0
2503	11.1	599.4	2804	96.0	562.6	3300	0.0	544.1
2504	15.1	603.1	2805	89.0	539.2	3301	14.6	537.6
2505	11.3	660.1	2806	49.0	648.0	3302	24.0	601.4
2506	88.4	624.3	2903	10.0	528.3	3303	13.9	750.0
2507	10.0	654.1	2904	10.0	606.5	3304	32.2	535.3
2601	44.5	553.0	2905	10.0	626.5	3305	120.0	502.6
2602	450.6	683.4	2906	10.0	564.0	3306	22.2	572.2
2603	10.0	775.0	2907	10.0	530.5	3307	120.1	450.0
2604	10.0	500.0	3101	47.0	750.0	3308	120.0	571.0
2605	10.0	572.6	3104	450.0	568.0	3309	120.0	367.2
2606	10.0	450.1	3106	10.0	595.5	3310	120.0	596.0
2800	28.0	450.0	3107	120.0	615.2	3311	120.0	750.0
2801	90.2	530.5	3108	10.0	683.2	3401	25.1	633.2
2802	70.0	540.0	3201	42.0	716.0	3402	10.3	576.1

are represented by hydrophilic ground. The sediments of gas hydrates also exhibit unusual electrical resistivity values in the profile, since a gas hydrate, as well as ice, is an insulator. Their electrical resistivity ranges within 4 to 160 ohm-m. High resistivity is a rather reliable indication of a gas hydrate.

The walls of the well are almost undamaged in the interval containing gas hydrates in contrast to the underlying water-saturated collector layers in which the walls deteriorate.

The accumulations of gas hydrates are often underlain by the water-bearing part of the same collector layer that contains free or dissolved gas. The presence of gas in the

water-bearing part of the collector layer is explained by the fact that the formation of a gas hydrate in the gas-bearing interval is impossible below the stability boundary, which means that the stability boundary of gas hydrates coincides with the bottom of their accumulation.

Data Interpretation

We compared the data from the parametric drilling performed by Krios Scientific and Technical Firm and the data from the geophysical investigations of wells carried out by Gazprom Geofizika LLC. As a result, we obtained a comprehensive geotechnical description of the profile of one well cluster belonging to the Bovanenkovo field.

According to data from the parametric permafrost well, the interval of 7–32.8 m is composed of near-shore and marine gray silty sands of the Kazantsevskaya Suite (the Late Neopleistocene), which contain organic-rich interbeds and lenses. The cryogenic structure of the sands is structureless (no visible ice). In silty clay interbeds, it is layered with micro- and fine ice lenses. According to data from the geophysical investigations of wells, this interval contains a zone of icy sandy soils with high electrical resistivity (100–160 ohm-m) in which the wellbore washout exceeds the zone investigated with a caliper.

The interval of 30–120 m is composed of marine and glacial marine sediments of the Salekhard Suite (the Middle Neopleistocene), which are represented by dark gray silty clays containing leather coats, inclusions, and interbeds of black organic matter and sometimes containing the interlayers of gray and dark gray fine sands. However, down to the depth of 50 m, the profile of this interval is composed of the interstratification of clays, silty clay, and silts (1–1.5 m thick) with the high electrical resistivity (1530 ohm-m) similar to that of the layers containing ice or a gas hydrate.

The interval of 50–120 m is also composed of thin-bedded alternating clays, silty clay, and silts, but their electrical resistivity decreases from the roof to the bottom (from 25 to 2.5 ohm-m). The ice films with thickness reaching 1 mm can be observed on the cleavage planes. The cryogenic structure is mostly massive but contains single horizontal schlieren (0.5–1 mm thick) in the upper part of the interval.

The upper part of the profile (120–200 m) in the interval of 120–280 m is represented by silty clays containing interbeds of clays and silts. The interbeds of silts and silty clays with low collecting properties (judging by the increase of the electrical resistivity up to 7.7–28 ohm-m) are saturated with gas hydrates.

The lower part of the interval (200–280 m) is marked with thick layers of silts and sands (distinctively icy) with high gas indications in the stratum fluids.

According to the geophysical characteristics, the interval of 280–500 m is thawed. The ground in this interval belongs to the low temperature, thawed grounds. No ice-bearing soils were detected, and the gas indications are background. The lower part of this interval is marked with a water-saturated collector layer with high gas indications that prove the presence of the dissolved gas in the layer.

Thus the cryolithological characteristics of the profile are confirmed by the data from the geophysical investigations conducted by Gazprom Geofizika LLC. The icy grounds in

the upper part of the profile (from 0 to 20–30 m) constitute the hard frozen part of permafrost. The frozen grounds in the plastic frozen part of the profile contain separate interbeds of the collector layers (cooled grounds) that are saturated with gas hydrates and water down to the depth of 260–270 m. Below, down to the depth of about 400 m, lie low-temperature thawed grounds containing interbeds of the water-saturated collector layers.

It is assumed (Kondakov et al. 2006) that the free gases of intrapermafrost deposits are of biogenic origin. The gases sorbed in permafrost contain an admixture of gases migrated from the underlying gas deposits. The gases sorbed below the permafrost bottom belong to the mixed gases.

According to the geologists of the All-Russian Petroleum Scientific Research Institute of Geological Exploration (Kleymenov et al. 1998), the gas generation accompanied by the formation of a separate gas-producing profile in the Post-Cenomanian stratum was ongoing for many millions of years up to the time when the climate began to grow colder and permafrost started forming in the Early Neopleistocene. Freezing cemented the ground mass, and its cooling created optimal conditions for the transition of the gas into the hydrate state and for the formation of the zone of hydrate development and stability within a broad range of the Post-Cenomanian profile. The hydrates of this profile are disclosed only by the wells. The disclosure occurs when thin collector layers dispersed in the clayey profile are put out of the cryologically bound and stable state by thawing and decompression in the course of drilling. They are associated with lenses and interbeds of organic-rich silty sands and silts with low salinity and moisture content but with a high freezing point.

The primary source of gas shows occurring in the wells is the gas accumulation having excessive pressure that is dispersed in the profile of the Post-Cenomanian stratum. Sand interbeds occurring in the zone of gas hydrate stability are the most hazardous in terms of gas shows.

Conclusions

Regarding gas hydrates as a cryolithological component of permafrost, we would like to add the following statements to the well-known concepts of gas hydrate genesis and distribution in the cryolithosphere:

- 1) The epigenetic freezing preserved the degree of gas saturation of permafrost ground that had developed by the beginning of the cryogenic lithification of the profile.
- 2) The migration of gases in the fluid system of grounds has been ongoing for several million years. The freezing of ground within the gas-bearing structure registered in its cryogenic texture began at the end of the Middle and at the beginning of the Late Neopleistocene. The gas-hydrate shows in the sediments accumulated during this period were registered only in the lower parts of the Kazantsevskaya Suite of the Late Pleistocene, while the upper (syncryogenic) layer of ice-rich sands forms a thick barrier, a cover preventing migration of the deep gas. The Late Neopleistocene freezing in older sediments suspended the migration of gas-bearing fluids. Gas hydrates were registered in the frozen part of the permafrost section. The

migration of gases or their new formation continued only in the largest taliks located below the river beds and lakes and only in the Holocene after the polygonal wedge ice and sheet ice deposits had undergone a powerful thermokarst process.

- 3) As gas shows (long-term and maximum in volume) are associated with massifs of sand layers and horizons, they should be supposed to have gotten into them with pressure waters of a complex hydrogeologic system of the Middle and Early Neopleistocene.
- 4) The accumulations of gas hydrates in the frozen silty clay part of permafrost develop from local organic matter that is digested by microbacteria.
- 5) Gas hydrates in the thawed part of the profile develop according to the thermobaric conditions of the hydrate formation zone.
- 6) Russian as well as foreign scientists showed that the cryolithosphere is generally permeable to gas; that is why gas hydrates can form in it from the deep gas that migrates from below through lithological heterogeneities and faults. The zones with high gas saturation developed above the dome of the gas-bearing structure due to the fact that an impermeable cover of ice-rich ground (a few tens of meters thick) formed in the ground massif during the Late Neopleistocene.

The Bolvansky and the Urengoy stations have similar geological, geomorphological, and landscape conditions. Similar mean summer air temperatures and snow accumulation conditions are climatic factors that influence the thermal regime formation and the seasonal thawing depth of permafrost at both stations. The mean annual air temperature in the north of West Siberia turned out to be 5°C colder than in the European North, which is explained by more severe conditions in the winter period.

The thawing depth of ground is controlled primarily by the mean summer air temperatures and is similar at both stations. Monitoring results testify to the increase of thawing depth at the drained areas of the southern tundra during the recent 10–12 years. However, this trend is not confirmed, as compared to the 1980s.

Low mean annual and mean winter air temperatures in West Siberia determine rather severe geocryological conditions in tundra landscapes with permafrost temperature equaling -4 to -5°C, while in the European North they fall within the interval of -1 to -2°C.

A large climatic warming trend (equaling 0.06 –0.07°C/yr) is typical of the examined regions in the recent 30 years. Meanwhile, in West Siberia, a warm maximum is related to the end of the 1990s. It was marked with the occurrence and further disappearance of tree vegetation in the southern tundra landscapes.

The general reaction of the cryolithozone to climate warming lies in the fact that the highest increase rates of mean annual temperature of permafrost in both regions are typical of low temperature landscapes, while the lowest increase rates are typical of high temperature landscapes.

In the European North, the ground temperature trends in natural landscape conditions are 2 to 7 times lower than the air temperature trends, while in West Siberia they are only 1.5 to 2.5 times lower.

Acknowledgments

This research was carried out based on the high quality materials provided by the investigations of Krios Scientific and Technical Firm and Gazprom Geofizika LLC.

References

- Badu, Yu.B. 2011a. Permafrost of the gas-bearing structures in the north of Western Siberia. *Materials of the Fourth Conference of Geocryologists of Russia*. Lomonosov Moscow State University Vol. 2 Part 5. Moscow, The University Book, 9-15 pp. (in Russian).
- Badu, Yu.B. 2011b. The geological structure of permafrost in the north of Western Siberia. *Engineering Geology* No. 1, pp. 40-56 (in Russian).
- Baulin, V.V., Aksenov, V.I., & Dubikov, G.I. 1996. *The geocryological conditions of the Bovanenkovo field. Vol. 2. The geotechnical monitoring of the Yamal facilities*. Tyumen, IPOS SO RAN. 240 pp. (in Russian).
- Budantseva, N.A. 2006. Gas shows in frozen ground. *The cryosphere of oil, gas and condensate fields on the Yamal Peninsula. Vol. 1. The cryosphere of the Kharasavey gas condensate field*. St. Petersburg: Nedra, pp. 235-247 (in Russian).
- Cherepanov, V.V., Menshikov, S.N., Varyagov, S.A., Bondarev, V.L., & Mirotvorskiy, M.Yu. 2011. The nature of gas shows occurring between columns at the Bovanenkovo oil and gas condensate field. *Geology, geophysics and development of oil and gas fields*. No. 9, pp. 48-54 (in Russian).
- Chuvilin, E.M., Yakushev, V.S., Perlova, E.V., & Kondakov, V.V. 1999. The gas component of permafrost within the Bovanenkovo oil and gas condensate field (the Yamal Peninsula). *Reports of RAS*, Vol. 369, No. 4, pp. 522-524 (in Russian).
- Istomin, V.A., Yakushev, V.S., Makhonina, N.A., Kvon, V.G., & Chuvilin, E.M. 2006. The effect of self-preservation of gas hydrates. *Gas industry, special issue Gas Hydrates* pp. 36-46 (in Russian).
- Kleymenov, V.F., Razmyshlyayev, A.A., & Plyushchev, D.V. 1998. Prediction of emergency gas shows in the wells penetrating the permafrost profile. *Geology, geochemistry, geophysics and development of oil and gas*. Moscow: VNIGNI 149-162 (in Russian).
- Kondakov, V.V., Yazynin, O.M., Lendengolts, V.A., & Galyavich, A.Sh. 2006. The nature of intrapermafrost gas shows in the cryolithozone of Yamal. *The theory and practice of evaluation of the Earth cryosphere state and prediction of its changes*, Tyumen. Vol.2, pp.106-108 (in Russian).
- Podborny, E.E. & Badu, Yu.B. 2011. The correlation between the profiles of the Cenozoic sediments in northern Yamal. *Materials of the Fourth Conference of Geocryologists of Russia*. Lomonosov Moscow State University Vol. 2. Part 5. Moscow, The University Book, pp. 143-148 (in Russian).
- Yakushev, V.S. 2010. *Natural gas and gas hydrates in the cryolithozone*. Moscow, Izd-vo VNIIGAZ, 200 pp. (in Russian).

Yakushev, V.S., Perlova, E.V., & Makhonina, N.A. 2003.
Intrapermafrost gas and gas hydrate accumulations in
Western Siberia. Collection of Works: *Gas resources of
Russia in the 21st century*. Moscow. VNIIGAZ, pp.171-
184 (in Russian).

Effects of Solid Microparticles on Grinding of Ice

L.S. Podenko, N.S. Molokitina
Institute of Earth Cryosphere, SB RAS, Tyumen, Russia

Abstract

This study is concerned with the effects of solid hydrophobic and hydrophilic particles on grinding of ice. Experiments revealed a previously unknown effect that the efficiency of ice dispersion increases in the presence of hydrophobic silica nanoparticles, but it remains almost the same in the presence of hydrophilic particles.

Keywords: agglomeration; dispersion; hydrophobic particles; ice.

Introduction

Processes of ice dispersion are widespread in nature and have important implications for respective technologies. Ice dispersion may be subject to effects from hydrophobic particles that are released in abundance into the air and frozen ground as a result of natural activity. Knowledge of these effects is useful in the search for agents increasing the efficiency of dispersion, but they remain poorly explored.

When being dispersed, solid particles undergo stages of shearing, fracture (disintegration), and formation of additional surfaces (Frolov 1988). Inasmuch as the dispersed system tends to reduce its surface area, the particles tend to agglomerate. This is the principal obstacle in the process of mechanical grinding.

Hydrophobic particles can stabilize dispersion systems consisting of micrometer water droplets by preventing the latter from coalescing (Brinks & Murakami 2006). Intense mixing of water, air, and hydrophobic silica particles produces the so-called dry water dispersions with up to 98% by weight (wt.) of liquid water. Thus one may expect hydrophobic particles to impede agglomeration of ice particles and thus increase the dispersion efficiency.

In order to check the hypothesis, we set up experiments in which pure and PVA-reinforced ice was dispersed in the presence of hydrophobic particles. Ice reinforced by water-soluble PVA polymer (polyvinyl alcohol) was chosen for its strength, which is much greater than in ordinary pure ice (Smorygin 1988). The microstructure and behavior of ice dispersion systems were analyzed by means of optical microscopy and proton magnetic resonance spectroscopy (NMR), the latter being especially workable when applied to water dispersions encapsulated by hydrophobic silica nanoparticles (Podenko et al. 2011).

Experimental Procedure

Pure ice was obtained by freezing distilled water at -10°C , and PVA-reinforced ice was prepared from a PVA aqueous solution frozen at the same temperature. The PVA solution had a concentration of 5% wt. corresponding to gel formation, the gelation being additionally catalyzed with 1% wt. boric acid.

Ice was dispersed in a cooler using a TU 16-579.005-75 device with a volume of 0.3 l. at -10°C .

The dispersed ice was stabilized with self-assembling hydrophobic silica (Aerosil R 202), which proved to be

an efficient stabilizer of water dispersions (Melnikov et al. 2011). The powdered silica particles, 10-14 nm, made ~ 0.1 μm aggregates. The contact angle of wetting for the Aerosil powder was 98° . The hydrophilic component consisted of hydrophilic silica (diatom earth D 3877 Sigma-Aldrich) particles less than 1 μm .

The structure of the obtained dispersed systems was analyzed using *Motic DM III* Digital Microscopy and proton magnetic resonance spectroscopy on a Niumag *MicroMR* NMR pulsed relaxometer, operated at the resonance frequency 20 MHz, according to the procedure reported in (Podenko et al. 2011).

Results and Discussion

The dispersion efficiency of solids depends on their mechanical properties and the agglomeration capacity of newly formed particles (Frolov 1988). Ice particles are known to easily and rapidly agglomerate (Smorygin 1988), which makes it difficult to obtain highly dispersed ice by means of mechanical grinding.

Therefore, one may expect that the dispersion efficiency would increase in conditions that preclude immediate contacts between newly formed particles.

Moderately hydrophobic dispersed materials (with wetting contact angles 90° to 120°) stabilize dispersions of water drops as they make a coating adhesively held on drop surfaces and a self-assembling network of hydrophobic aggregates that fill the space between the droplets (Fornly et al. 2009).

The same mechanism may prevent ice particles from agglomeration and thus reduce their sizes by impeding direct contacts between the surfaces of new particles.

The hypothesis was checked through special experiments on ice dispersion in the presence of hydrophobic and hydrophilic silica particles. For this ~ 5 mm pure ice or ice together with 5% wt. of silica powder was dispersed in a blender for 30 seconds.

Thus obtained fine-grained ice was sieved through a calibrated mesh at -10°C to obtain two powder fractions of the particle sizes $d < 140$ μm and < 70 μm . The ice content in the fraction was inferred from weight loss of the powder on its drying at 105°C . Thus the percentages of ice in the fraction relative to the original ice weight (Table 1) were found by weighing.

One can see from Table 1 that $d < 70$ μm particles are very few in the absence of hydrophobic silica but more abundant when ice is mixed with Aerosil.

Table 1. Results of ice dispersion experiments.

Original system	Starting ice weight, g	Ice in fraction $d < 140 \mu\text{m}$, %	Ice in fraction $d < 70 \mu\text{m}$, %
Pure ice	70	7.1	0.1
Pure ice/aerosil mixture	73	25.6	16.6
PVA-reinforced ice	70	< 0.1	-
PVA-reinforced ice/Aerosil mixture	73	1.8	-
Pure ice/diatom earth mixture	73	6.2	-

According to Forny et al. (2009), sieving gives notably larger particle sizes in the dispersion encapsulated by hydrophobic aerosil, possibly because self-assembling Aerosil particles may bind mechanically the stabilized particles.

The size distribution of the polydispersed ice particles being hard to analyze with optical microscopy, we applied NMR to estimate the minimum particle sizes of ice in the disperse system.

This application of NMR spectroscopy relies upon the following facts: As Aerosil-stabilized ice particles are thawing, water forms micrometer droplets (Fig. 1) (Melnikov et al. 2011) with their sizes expected to be commensurate with or larger than ice particles, proceeding from water density change on ice-to-liquid transition and from possible coalescence of the droplets. Therefore, the possible limit of particle sizes of dispersed ice in a fraction can be inferred from the sizes of water droplets produced by ice thawing. The sizes of water droplets were measured using NMR relaxation spectroscopy applying the method from (Podenko et al. 2011).

The minimum ice particle size in the $d < 70 \mu\text{m}$ fraction estimated in this way was $\sim 4.5 \mu\text{m}$. Thus the smallest sizes of ice particles dispersed in the presence of hydrophobic silica were reduced at least ten times from 70 to $4.5 \mu\text{m}$.

This particle size reduction may result either from additional mechanical fracture caused by hard silica particles or from hydrophobic coating that prevents agglomeration.

Ice dispersion experiments in the presence of hydrophilic silica (diatom earth) are aimed at identifying the factor responsible for the activation effect. The resulting percentages of $d < 140 \mu\text{m}$ ice remained almost the same as in the experiments without diatom earth. Therefore, it is the hydrophobic coating rather than fracture that obviously is the activation agent. The protective coating consists of self-assembling particles of hydrophobic silica.

The influence of mechanical properties of ice on its dispersion was explored in PVA-reinforced ice, which is much stronger than pure ice. As Table 1 shows, reinforced by a soluble polymer notably reduces the dispersion efficiency (ice percentages less than 0.1% in the sieved $d < 140 \mu\text{m}$ fraction). The reason may be either greater mechanical strength of ice or more efficient agglomeration of PVA-reinforced ice particles relative to pure ice.

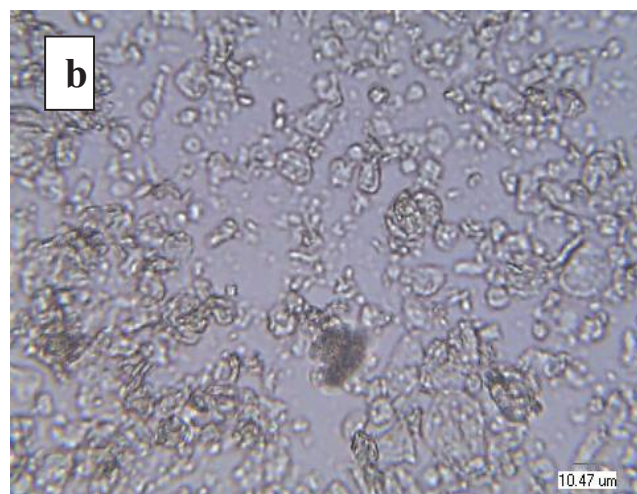
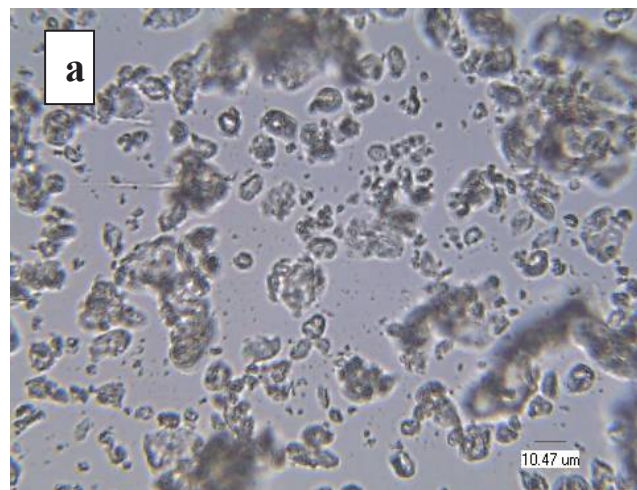


Figure 1. Ice/Aerosil dispersed system thawing at room temperature. a: thawing time 10 s; b: thawing time 300 s.

We compared the agglomeration rates of pure and ice reinforced particles to study the proneness of the latter to agglomeration. For this $d \geq 140 \mu\text{m}$ fractions of pure and reinforced ice particles obtained in the presence of Aerosil R 202 were divided into several equal parts and placed in a cooler at -15°C . Then samples taken after two, six, and forty days of cooling were thawed and their NMR relaxation spectra were measured in order to estimate the sizes of water droplets derived from PVA-reinforced ice, following the earlier reported procedure (Podenko et al. 2011). The NMR data were used to assess how the dispersed ice particles changed in size by agglomeration in the course of storage.

The patterns of spin-spin relaxation times (T_2) of dispersions obtained by thawing of pure and stabilized ice (pure ice/Aerosil and reinforced ice/Aerosil fractions) consisted of three relaxation components, which indicates polydispersed size distribution of water drops and, hence, also of ice particles (Figs. 2, 3).

In this respect, the weighted mean relaxation time (T_{2c}) was found as

$$T_{2c} = \frac{1}{\sum_{i=1}^3 A_i} \sum_{i=1}^3 A_i T_{2i}$$

where A_i is the integral intensity i of the T_2 component, T_{2i} is the most probable time T_2 for the i -th component.

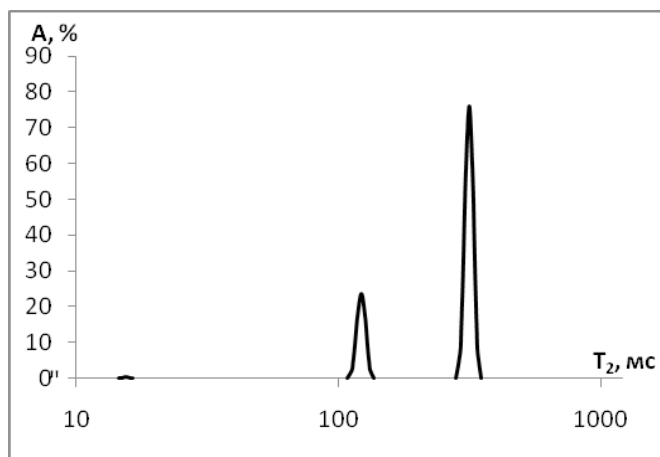


Figure 2. T_2 pattern of thawed disperse system pure ice/Aerosil, at 30°C.

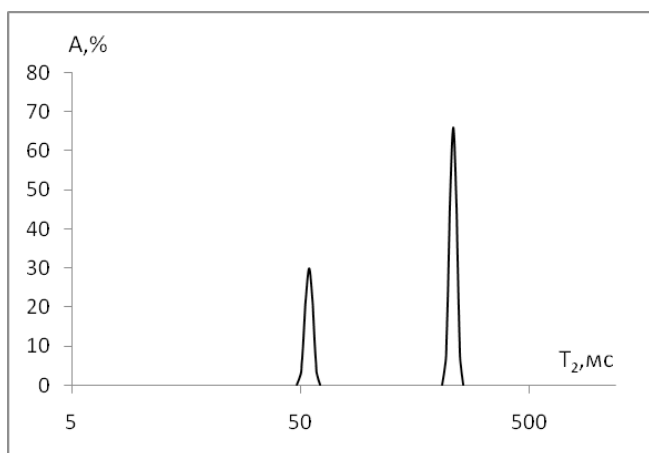


Fig. 3. T_2 pattern of thawed disperse system PVA-reinforced ice/Aerosil, at 30°C.

Table 2. NMR relaxation parameters for thawed ice/Aerosil dispersions.

Storage time, day	pure ice/Aerosil		PVA-reinforced ice/Aerosil	
	T_{2c} , ms	ΔT_{2c} , %	T_{2c} , ms	ΔT_{2c} , %
2	262	0	150	0
6	266	2	171	14
40	416	43	211	41

The calculated relaxation times T_{2c} for thawed ice dispersions stored at -15°C and relative increments T_{2c} (ΔT_{2c}) are found as $(T_{2c} - T_{2c0})/T_{2c}$, where T_{2c0} is the time T_{2c} for thawed fresh ice dispersions as listed in Table 2.

The maximum relative change of T_{2c} and, hence, the change of ice particle sizes in the course of storage have turned out to be similar for both disperse systems of pure and PVA-reinforced ice (Table 2). It means that the agglomeration rates are similar as well, and the presence of PVA does not cause significant influence on the process.

Therefore, the low dispersion efficiency of PVA-encapsulated ice is due uniquely to its higher mechanical strength.

Conclusions

In the course of the reported study, we have discovered that the presence of hydrophobic silica nanoparticles can increase the efficiency of ice dispersion. The reason is that self-assembling hydrophobic silica particles coat the newly forming ice particles and thus prevent them from agglomeration.

PVA-reinforced ice has lower dispersion efficiency than pure ice due to its higher mechanical strength.

The presence of hydrophilic silica particles causes almost no change on the ice dispersion degree.

The obtained data indicate that hydrophobic particles released into the Earth’s cryosphere can accelerate ice dispersion processes.

Acknowledgements

This study was supported by Grant 10-05-00270-a from the Russian Foundation for Basic Research and was carried out as part of Project 13.7.4 of the RAS Presidium Program and Interdisciplinary Project 62 of SB RAS.

References

- Brinks, B. & Murakami, R. 2006. Phase inversion of particle-stabilized materials from foams to dry water. *Nature Materials* 11: 865-869.
- Forny, L., Khashayar, S., Pezron, I., Komungier, L., & Guigon, P. 2009. Influence of mixing characteristics for water encapsulation by self-assembling hydrophobic silica nanoparticles. *Powder Technology* 189: 263-269.
- Frolov, Yu.G. 1988. A Course of Colloid Chemistry. Surface Phenomena and Disperse Systems. *Khimiya*, Moscow, 464 pp. (in Russian).
- Melnikov, V.P., Podenko, L.S., Nesterov, A.N., Komissarova, N.S., Shalamov, V.V., Reshetnikov, A.M., & Larionov, E.G. 2011. Freezing of water drops in “dry water” dispersion. *Kriosfera Zemli* 2: 21-28 (in Russian).
- Podenko, L.S., Nesterov, A.N., Komissarova, N.S., Shalamov, V.V., Reshetnikov, A.M., & Larionov, E.G. 2011. Proton magnetic relaxation in “dry water” disperse nano-system. *Zhurnal Prikladnoi Spektroskopii* 2: 282-287.
- Smorygin, G.I. 1988. Making Manmade Ice: Theory and Methods. *Nauka*, Novosibirsk, 282 pp. (in Russian).

Climate Change, Frost Action, and Permafrost-Related Processes in the Northern Taiga Region of West Siberia

O.E. Ponomareva, A.G. Gravis, N.M. Berdnikov
Earth Cryosphere Institute, SB RAS, Tyumen, Russia

T.A. Blyakharchuk
IMCES, SB RAS

Abstract

Old and recently forming frost mounds, heaving areas, and flat-topped peat plateaus occupy almost 70% of the Nadym Permafrost Station. Repetitive surveys from 1971 to 2000 show that during this period uplift of these landforms prevailed over their occasional subsidence. After 2000, frost heave was less intensive than in the preceding period while thaw settlement increased and old thermokarst forms were reactivated. These processes together with an increasing depth of the active layer and increasing permafrost temperature compromised the stability of peatland geosystems. This paper provides data on and discusses thaw settlement of soils, forms of permafrost degradation, perennial frost heave, and new permafrost formation and its impact on hydrophilic vegetation.

Keywords: climate change; frost mounds; perennial heaving; surface uplift; thermal subsidence; thermokarst.

Introduction

About 70% of the Nadym Monitoring Site (NMS) area is occupied by flat-topped peat plateaus and numerous isolated frost heave mounds and heave plateau areas (Melnikov et al. 1983). There are confined areas of contemporary warm temperature permafrost. The study of frost heave mounds at the NMS was initiated by Nevecherua (1980) in 1971 in relation to construction of the Nadym-Punga gas pipeline. Segregated ice was found and some had ice-rich cores near the surface (Nevecherya 1980). It was also found that mounds can be divided by age as relic and young or contemporary and young mounds continue to grow while relic mounds degrade in the contemporary environment (Evseev 1976). The occurrence of recently growing frost mounds next to the gas pipeline could compromise the pipeline's integrity. Monitoring of the dynamics of frost mounds was initiated to address this concern, and the monitoring still continues. It was found that frost mounds and flat-top heave plateaus were in the actively heaving stage until the end of the twentieth century. Thermokarst during that time was not an active process.

An increase in air temperature was observed in the 1970s and an increase in precipitation has been documented since the 1990s. Both lead to a slow but persistent increase in permafrost temperature and in active layer thickness. This was accompanied by extensive development of shrubs and positive feedback of snow retention. It was expected that all these factors should have a disturbing impact on the stability of frost heave mounds and intensification of thermokarst. Our instrumental measurements only partially confirmed these assumptions.

Vasilchuk et al. (2008) also found that climate warming can have an ambiguous effect on frost heaving.

Research Area

The NMS is located in the Nadym River basin southeast of the city of Nadym in the northern taiga (Fig. 1).

The geomorphology of the NMS includes the 3rd fluvial-lacustrine plain, the 2nd above-floodplain terrace of the Nadym River, and the floodplain of the Kheigiyakha River, which is the left tributary of the Nadym River. Most of the monitoring focused on the 3rd fluvial-lacustrine plain and some of it takes place on the Kheigiyakha River floodplain. The surface sediments vary in thickness from several centimeters to 2 m, reaching 6 m at isolated points of the floodplain. The upper mineral part of the soil section within these levels is presented by silty sands layered with numerous thin layers of silt and silty clay, which include some organic. Underlying silty clay and clay beds occur from 4 to 8 m. High ice content is typical for the silty clay and clay, in which water content on a dry weight basis reaches 100% and greater. The table of relict permafrost is located at approximately 100 m. Contemporary permafrost is confined to hillocky and flat-topped peat plateaus as well as to frost mounds. Permafrost temperature at 10 m depth under hillocky peatland has increased from -1.8° to -0.4°C during the last 40 years (Moskalenko 2011). Permafrost temperature on flat peatlands has increased from -0.9° to -0.12°C (Moskalenko et al. 2006). Frost actions and permafrost-related processes include seasonal frost heave, perennial frost heave, and slow developing thermokarst,

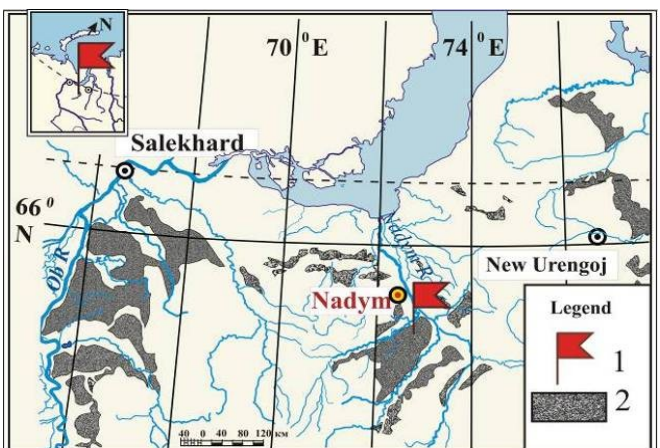


Figure 1. Nadym Station location. 1– station, 2 – 3rd fluvial-lacustrine plain.



Figure 2. Old (A) and young (B) frost mounds.

which increases the swamping or flooded areas. We distinguish between old hillocky peatlands and frost mounds (which can be more than 300 years old) and young (formed during the monitoring period) (Fig. 2b). The ages of old mounds were determined by tree rings (Moskalenko et al. 2006) and C14 methods (Matyshak 2009).

Permafrost table lowered under swamped depressions (Fig. 3).

Objectives and Methods

Perennial frost heave is monitored by repeated differential leveling tied to the deeply embedded stable benchmarks. The positions of the benchmarks are controlled on the basis of two geodetic beacons located at the surface of the 2nd above-floodplain terrace of the Nadym River. Perennial frost heave at this terrace is inactive. Leveling is conducted at the end of August when seasonal frost heave is almost completely compensated by seasonal thaw settlement. Such monitoring began in 1971, and the number of studied sites has been growing since then. Today's monitoring includes 500 monitoring points located at the CALM site and along seven reference lines on most landforms in the vicinity of the NMS. Permanent stakes are located along four reference lines from 200 to 250 m long, spaced 2 m apart. Stakes along three profiles with the total length of 2 km are located at irregular spacing. The CALM site 100x100 m in size has the grid spacing of 10 m.

Results of differential leveling are analyzed together with data on the thaw depth and permafrost temperature. Thaw depth is measured by a permafrost probe in the beginning of September. Permafrost temperature is measured with 2- and 4-channel loggers in boreholes 10 m deep and in



Figure 3. Flooded subsidence with depressed permafrost table.

a borehole 30 m deep. Measurements are conducted year round at 6-hour intervals. Continuous meteorological data are provided by the Nadym weather station located 30 km north of the NMS.

Climatic Change

We have analyzed data for monthly and mean annual characteristics of climatic parameters for the Nadym Station for the entire weather monitoring period available since July 1959 for air temperatures and since January 1961 for precipitation. The data show a positive trend since the beginning of the 1970s. To date, the climate in general has become milder, and the amount of precipitation has increased.

Climate change appears as an increase of air temperatures, mainly in spring (May) and summer. The trend of positive degree-months during 1970-2010 was 0.2 °C*month per year, which has led to an increase in active layer depth by 25% and an increase in permafrost temperature on hillocky peatlands by 1.4°C (Moskalenko 2011). The increase in air temperature in May can be seen in Figure 4 and in October in Figure 5. The period with air temperature below 0°C has decreased by 15–20 days on average.

Precipitation also increased with an increase in snowfall in October when soil freezing begins (Fig. 6).

Although the trend of climate change is unfavorable for perennial frost heave, deviations of climatic parameters in some years still make this process possible.

For example, a combination of low snow thickness and low air temperatures was observed in 1968, 1974, 1984, and in 1998 (Fig. 7). For instance, the monthly mean air temperature in November 1998 was the only one below -30°C for the entire observation period, and it was 15°C lower than the mean monthly November temperature. At the same time, the amount of precipitation was 33% less than the mean value.

Despite an unfavorable trend, perennial frost heave can persist due to the occurrence of favorable conditions.

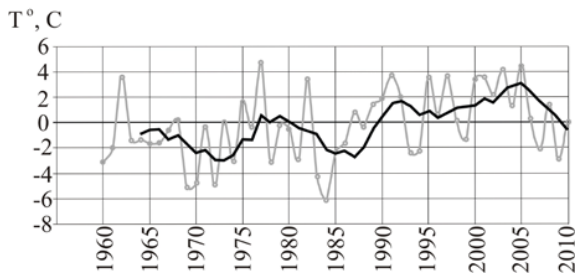


Figure 4. Changes in monthly mean air temperature for May (°C) with the trend line (five-years running average).

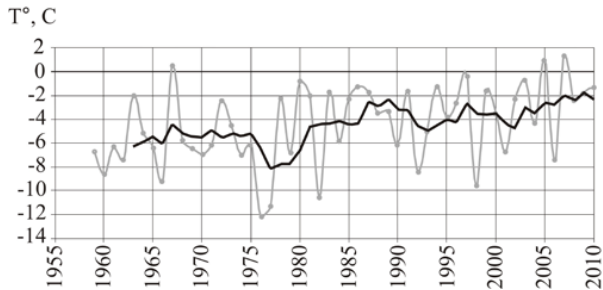


Figure 5. Changes in monthly mean air temperature for October (°C) with the trend line (five-years running average).

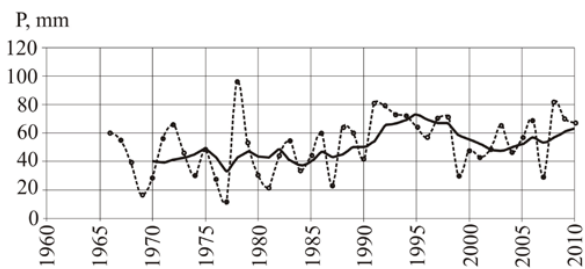


Figure 6. Change in precipitation in October (T°C) and the trend line (five-years running average).

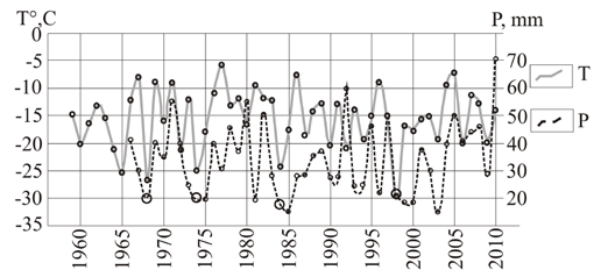


Figure 7. Change of precipitation amount in November (mm) and air temperatures (°C).

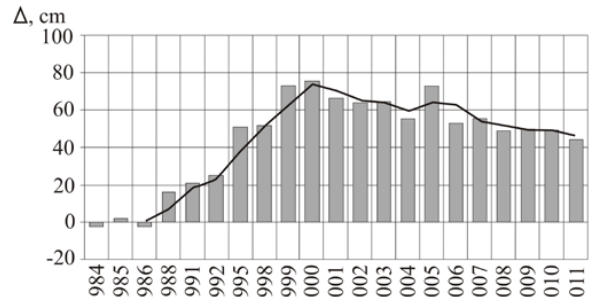


Figure 8. Change in peat-mineral frost mound elevation (Δ , cm) from its position in 1980 with the trend line (five-years running average).

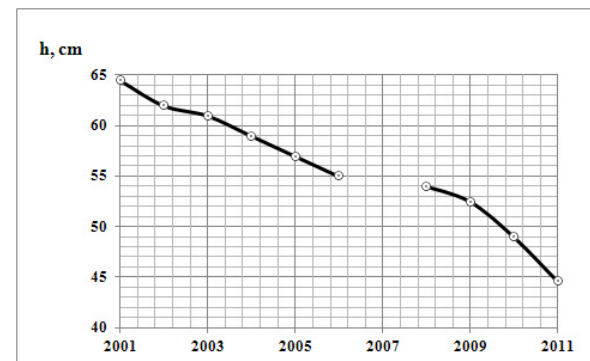


Figure 9. Change elevation (cm) for a young frost mound.

Perennial Frost Heave

Deviation of surface elevation from its position at the beginning of monitoring has been analyzed for individual points and has been averaged for 2 to 4 points.

The data analysis showed that pulsation of all monitoring points on old mounds and flat-topped peat plateaus occurs every year with a change in amplitude and final result.

In general, surface uplifting prevailed before 2005. The maximum registered uplift amplitude reached 15–20 cm per year. Significant surface uplift was observed in 1988, 1995, 1999, and 2005 after severe winters with low snow covers at part of the mounds and in the center of flat-topped peat plateaus. For example, after the exceptionally severe and low snow winter of 1998–1999, surface elevation measured in August 1999 was 21 cm higher than in 1998 (Fig. 8).

Following such uplift, surface elevations of frost mounds and peatland stabilized or experienced a decrease due to thaw subsidence. Surface stabilization (or subsidence) is predetermined according to the Nadym weather station data by the fact that milder winters always follow a severe winter. The thaw settlement is 5 to 15 cm per year. After 2005, frost heave uplift became insignificant and thaw subsidence prevailed. The surface is now 25 to 35 cm lower than it was in 2005.

A young frost heave mound that was first observed in

1973 settled as well (Fig. 9). Its settlement was triggered by construction work in 2000, which partly destroyed the vegetative cover. This frost heave mound has been monitored since 2001, when its height was at 65 cm (Fig. 9). It has settled 20 cm during 10 years without uplifting. The intensity rate of settlement varied from year to year; reaching a maximum of 5 cm per annum.

Reactivation of the old 1-m-deep thermokarst depression (Fig. 10A), located at the top of the old peat-mineral frost mound, is another example of the predominance of subsidence over heaving. The depression was formed in the area affected by fire in summer 1971. During 2005–2009 observations in this area, the depression size has remained the same but the vegetative cover in it has changed primarily due to an increase in shrubs in the depression. In August 2009, N.G. Moskalenko and P.T. Orekhov (pers. comm.) noted an increase in the depression size (Fig. 10D), and a monitoring grid was arranged at this site. Leveling data for 2009 and 2010 showed that the depression is growing laterally, while its depth has not changed. Edge recession occurred slowly and reached 15 cm per annum in only some points. The depression size did not change significantly in 2011 (Fig. 10C) as compared to 2010 (Fig. 10B).

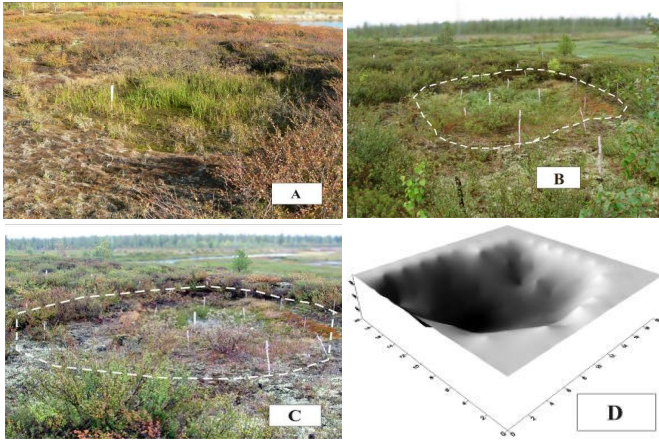


Figure 10. (A) Old thermokarst depression in 2005; (B) 2010; (C) 2011; and (D) 3D image of depression in 2009 produced with Surfer software.

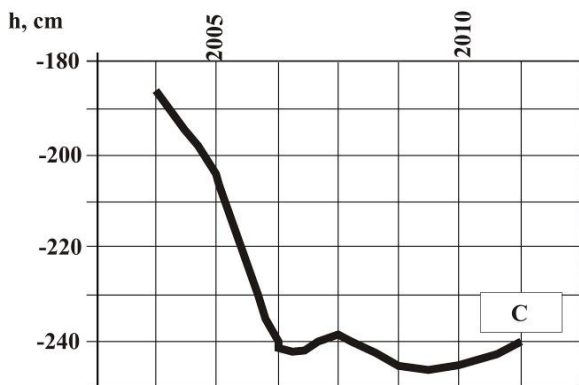
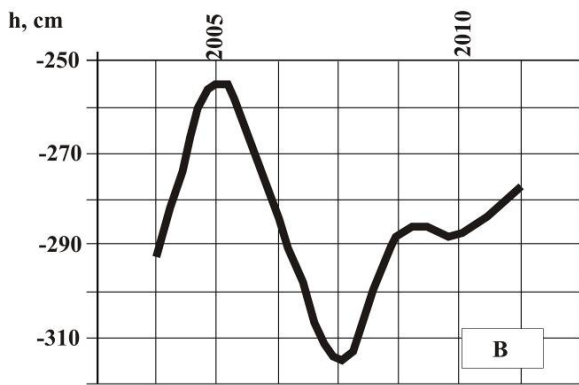
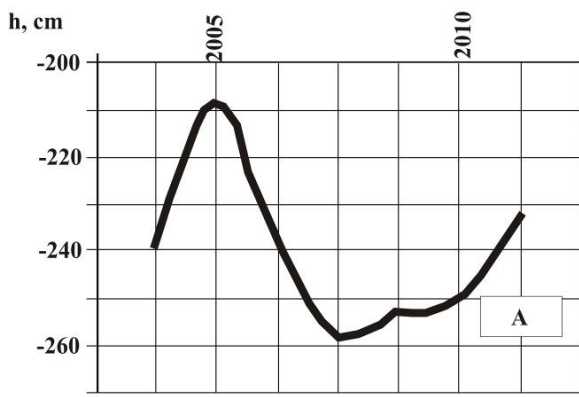


Figure 11. Change in elevation (cm) within the CALM site for the bog (A); the tundra (B); and the flat-topped peat plateau (C).

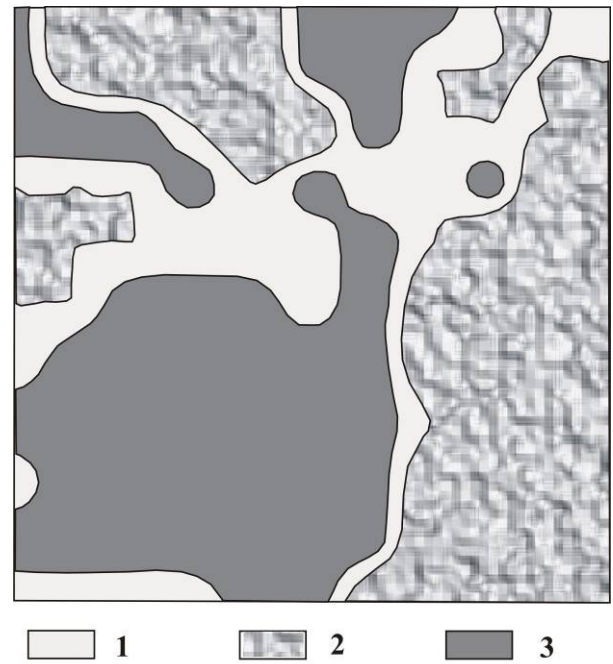


Figure 12. CALM site. 1 – tundra, 2 – bog, 3 –flat-topped polygonal peatland.



Figure 13. New permafrost formation in drained swamp hollows. Sites revealed in 2011 (A) and older ones with dead hydrophilous vegetation (B).

Depression expansion is slow because of the low water content of the surface soil. The frost mound from the surface is composed of peat underlain by sand and sandy silty loams with sand interbeds. Peat thickness on the bottom of the thermokarst depression is only 0.23 m.

It can be expected that the thermokarst depression will grow in the future due to a continued increase of shrub height, an increase of ground surface coverage, an increase of summer precipitation, climate warming, and an increase in thickness of the active layer.

The flat-topped peat plateau within the CALM site after 2004 also experienced subsidence (Fig. 11C).

There are two more landforms—bog and tundra—within the site in addition to the flat-topped peat plateau (Fig. 12). The surface of the sites occupied by tundra and bogs in particular increased as a result of heaving after 2007. New permafrost formation with vegetation succession was identified at these sites.

New permafrost formation was also noted in drained swamp hallows outside the CALM site. There permafrost formation is accompanied by formation of frost heave mounds and ridges (Figs. 13A and 13B).

Most young frost heave mounds and ridges in drained swamp hallows appeared in 2010 and 2011 (Fig. 13 A). Permafrost formation with ridge uplifting leads to the death of hydrophilic vegetation. Possibly both of these processes developed earlier, but only a single ridge with dead hydrophilic vegetation was found in bogs by 2011 (Fig. 13B). It should be noted that degradation of hydrophilic vegetation ridges occurs with a general increase in summer precipitation and growth areas of bog (by 1.5%) and lake (by 2.7%), as evaluated from the 1989 and 2004 summer satellite images.

Conclusion

This study shows that climate warming and an intensification of precipitation led to a change in frost action and permafrost-related processes in the north taiga of Western Siberia. Uplifting of frost heave mounds and flat-topped peat plateaus caused by perennial heaving almost ceased. This was replaced by thermal subsidence at some undisturbed sites and active thermokarst at disturbed sites. At the same time, new permafrost formation driven by vegetation succession took place on bogs and was accompanied by frost heaving.

Acknowledgments

N.G. Moskalenko and Yu.L. Shur shared data from their 1971–1999 studies in the area and provided valuable advice. This study was supported by the TSP project of the U.S. National Science Foundation (NSF grants ARC-0632400, ARC-0520578), by the CALM project (NSF grants OPP-9732051 and OPP-0225603), and by the RFFI grant No. 09-05-01068-a.

References

- Evseev, V.P. 1976. Frost mounds formed by ice segregation in the northeast of the European part of the USSR and Western Siberia. *Izd-vo MGU. Problemy kriolitologii* Issue V, pp. 95-159 (in Russian).
- Matyshak, G.V. 2009. Soil formation peculiarities in the north of Western Siberia in cryogenesis conditions. Author's abstract of Ph.D. thesis. Moscow, MGU. 25 pp. (in Russian).
- Melnikov, E.S., Veysman, L.I., Moskalenko, N.G. et al. 1983. *Landscapes of cryolitozone (permafrost region) in the West-Siberian natural gas province*. Novosibirsk, Nauka, 166 pp. (in Russian).
- Moskalenko, N.G. 2011. Fire impact on vegetation and permafrost in north-taiga hilly peatlands of Western Siberia. *Proceedings of the Fourth Conference of Russia's Geocryologists*. MGU. June 7-9, 2011, vol. 3, parts 7-12, pp. 239-245 (in Russian).
- Moskalenko, N.G., Vasilev, A.A., Gashev, S.N. et al. 2006. *Anthropogenic changes in ecosystems of the West-Siberian gas province*. Earth Cryosphere Institute, SO RAN, 358 pp. (in Russian).
- Vasilchuk, Yu.K., Vasilchuk, A.K., Budantseva, N.A., & Chizhova, Yu.N. 2008. *Palsa of frozen peat mires*. Moscow University Press. 257 pp. (in Russian).

Ice Energy as a Model of Activity of Exogenic Geological Processes

V.L. Poznanin

Institute of Mineralogy, Geochemistry and Crystal Chemistry of Rare Elements (IMGRE), RAS, Russia, Moscow

Abstract

This paper discusses the justification and use of the internal energy of ice as a model of activity of exogenic processes. The ice is shaped like a cube with a side length of 11 m. It is kept at the temperature of 0°C and at normal atmospheric pressure. The internal energy of the model is equal to the fusion heat of the ice cube, which is 4.09×10^{11} J. The model height reflects the main property of exogenic processes—mobility that is implemented in ice in the form of material strength with the plastic limit of 0.1 MPa (10^5 J/m³). Ice energy logically fits into the modern system of spatiotemporal and energy levels of the organization of exogenic geological processes. Based on the correlation between the energy of the processes and that of the ice model, quantitative criteria and parameters of the activity of exogenic geological processes up to catastrophes were obtained.

Keywords: exogenic processes; geological processes; ice energy.

Introduction

The starting point of this study is the assumption that life's beginnings are in the ice of cosmic bodies. The assumption is explained from the perspective of the evolution of the universe and the Earth. The assumption made is fully implemented on our planet in the form of interaction between the cryosphere and the biosphere as parts of the geographic envelope.

The modern state of the cryosphere is characterized by the presence of atmospheric, hydrospheric, above-ground, and underground ice. Ice boundaries in polar regions migrate seasonally at the temperature of 0°C and in conditions of normal atmospheric pressure. Ice contains microorganisms, and, along with the biological substance, possesses internal energy that is a measure of mechanical, thermal, and biochemical processes.

The idea of using the internal energy of ice as a model of activity of geological processes emerged as a result of summarizing the field data obtained through the monitoring of gully thermoerosion processes in Transbaikalia, Yakutia, and West Siberia (1978–1992). At that time, the concept of hydrothermal flow capacity (10 and 419 kW) was formulated as a measure of a process's activity established by the statistical data of the parameters in the “temperature – discharge” and “turbidity – heat loss” domains.

Criteria of Activity of Exogenic Processes

Ice was chosen as a model activity of exogenic processes due to the following considerations:

- Ice inside crystals is an “absolutely” pure chemical substance.
- Ice has a “vapor-liquid-solid” triple point.
- Ice exists simultaneously in three states in all natural spheres.
- Ice is characterized by energy (thermal) parameters—heat of fusion, heat of vaporization (sublimation), specific heat, and thermal conductivity.
- Ice possesses the main property of exogenic processes—mobility (i.e. it can flow or disintegrate under the pressure of more than 0.1 MPa and 1 MPa, which corresponds to the volumetric energy of ice equal to 10^5 and 10^6 J/m³).

The model of activity of exogenic processes is a cube with

a side length of 1 or 11 m and density of 917 kg/m³ that is kept at the temperature of 0°C under normal atmospheric pressure of 760 mmHg (approximately 0.1 MPa) and is characterized by internal energy; heat of fusion of ice, $E_1 = 3.07 \times 10^8$ J and 4.09×10^{11} J, respectively. The internal energy of the model can be used as a measure of any natural process; mechanical, thermal, geochemical, electromagnetic, or biological, since the progress of any process is accompanied by the absorption and release of energy. Energy is a universal indicator of the state of objects, processes, and phenomena; it directly or indirectly reflects all the basic physical characteristics: mass, dimension, time, temperature, electric charge, number of structural units (mole), and luminous intensity.

The essence of the exogenic processes lies in the directional movement of rocks, water, ice, and gas masses in any proportion from purely “dry” (rockfall, sandstorms) to purely aqueous or glacial (abrasion, exaration) (Table 1). All of them are characterized by the presence of potential, kinetic or thermal energy that is a measure of their internal state at different levels of the organization of exogenic geological processes. These levels are a system of interconnected objects: geological, landscape, geodynamic. These objects are differentiated, respectively, by the gravitational criterion (potential energy), radiation thermal criterion (thermal energy), and dynamic criterion (kinetic energy).

Ten levels of organization of the exogenic geological processes with different energy of photosynthesis were identified at eight operating levels (J) (Table 2). The levels were defined within the spatial boundaries (10^{-8} to 10^7 m) and temporal intervals (10^{-7} to 10^{12} sec) as following: point – 10^{-23} to 10^{-11} ; elementary – 10^{-8} to 10^{-1} ; model – 10^{-1} to 10^4 ; detailed – 10^5 to 10^{10} ; topical – 10^{11} to 10^{13} ; local – 10^{13} to 10^{16} ; territorial – 10^{16} to 10^{20} ; regional – 10^{21} to 10^{25} . The levels of organization of the exogenic processes represent a universal system of hierarchically superordinated geodynamic objects: processes of any genetic type (class) that do not depend on genesis. The simplest process of particle shift at the point level, as the levels progress, gradually becomes more complex, up to denudation of regions, continents, and the planet as a whole. All levels together reflect the spatiotemporal and energetic unity of exogenesis and the actual trend of the development processes for natural geodynamic background of the planet's surface.

Table 1. Genetic classification of exogenic geological processes

Types	non-aqueous			aqueous			
Subtypes	physical fields-related (ethereal)		aerial	aqueous as such		glacial	
Classes	gravitational	thermal	eolian	fluvial	infiltrational	glacial	cryogenic
Subclasses	Rockfalls (rock slides)	desquamation crack- formation	erosion deflation transportation	mud flows erosion abrasion	landslides suffusion karst	avalanches exaration nivation	cracking heaving thermokarst solifluction thermoerosion
Physical factors of the processes	gravitational						
	thermal						
	eolian						
	fluvial						
	infiltrational						
	glacial						
	cryogenic						

Table 2. Levels of the exogenic geological processes organization

№	Level name	Geosystematic content of the levels				
		geological	landscape	spatiotemporal		geodynamic
10	global	lithosphere surface	-	up to 40,000 km	-	planetary denudation
9	continental (segmental)	upper layers of the planet plates	continent landscapes	up to 10,000 km	-	continental denudation
8	regional	surface layers of geostructures	landscape countries	160 to 4000 km	up to 10,000 years	denudation complexes
7	territorial	rocks formations (genetic complexes)	landscapes of different ranks	30 to 160 km	1 to 100 years	genetic flow complexes
6	local	lithologic-and-facies types of rocks	sub-landscapes	3 to 30 km	1 mon to 1 yr	genetic types of asynchronous flows
5	topical	geological bodies consisting of one type of rock	facies	0.25 to 3 km	4 to 40 days	main type of flows* of rocks, water, ice**
4	detailed	ground masses of unconsolidated and hard rocks		4 to 250 m	1 to 100 hours	flows structuring
3	model	blocky soils with or without filling		0.3 to 3 m	1 to 100 min	mass movement, transport
2	elementary	gravelly-sandy sediments		0.1 to 14 cm	0.01 to 10 sec	break-off and rupture
1	point	particles of silt-clayey and bedrock sediments		10 ⁻⁶ to 10 ⁻² cm	10 ⁻⁷ to 10 ⁻³ sec	shift

* the concept of flows includes shifting of rocks due to heaving and cracking of all types

** the proportion of solid, liquid and gas components of the flows may vary

The energy of real exogenic processes can be logically compared to the established energy of the levels of their organization. Thus the energy of the wind transporting a ground particle—a sand grain with the diameter of 10⁻⁴ m at the velocity of 0.1 m/sec—is 10⁻¹¹ J at the point level. The energy of pushing a particle sized 10⁻² m during solifluction, creep, or nivation is in the range of 10⁻³ to 10⁻⁵ J at the elementary level. The energy of the fall of a boulder with

the diameter of 0.3 to 0.5 m or fall of the equivalent mass of sandy-gravelly ground on the edge of a river terrace from the height of 2 to 4 m is 10² to 10³ J (model level). The energy of gully thermoerosion during water stream incision at the depth of 2 m for the period of three hours with the potential activity of the process equal to 419 kW is already 4x10⁹ J at the detailed level. The energy of cryogenic creep at the topical level with the maximum value of the potential of the

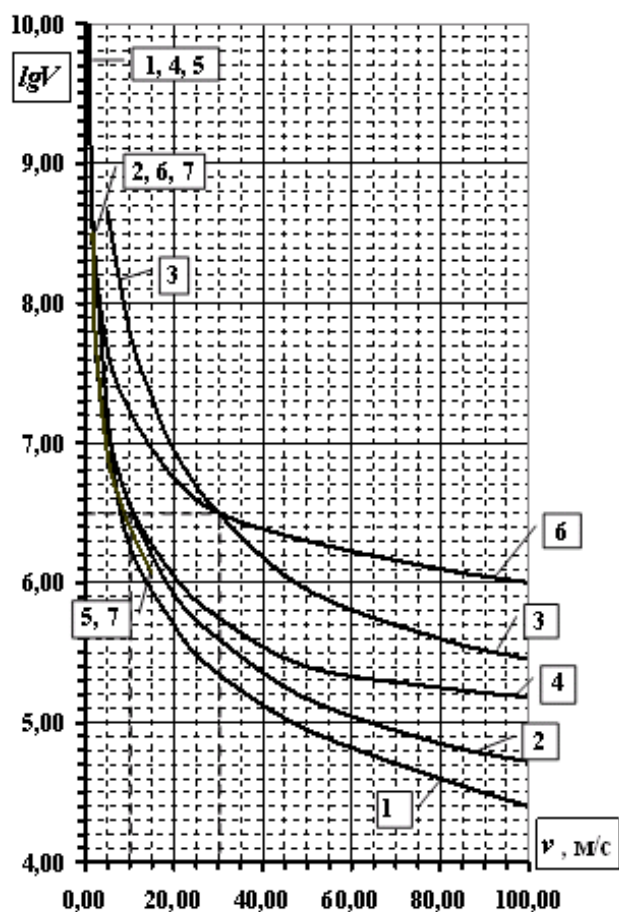


Figure 1. The calculation criteria of catastrophic development of exogenic geological processes. Vertical axis is the logarithm of the volume of the material transported, m^3 ; average velocity of the material movement, m/sec : 1 – rockfalls; 2 – cracking; 3 – deflation; 4 – mud flows; 5 – landslides; 6 – snow avalanches; 7 – cryogenic creeps.

engineering-geological contour equal to 400 kJ/m^2 reaches 10^{11} to 10^{12} J. And the energy of the well-known Kolka Glacier catastrophe of 2002 equal to 10^{15} J corresponds to the energy value of the local level of the exogenous processes organization. At the territorial and regional levels of the exogenic geological processes, we should consider the manifestation of not just one process, but of several most significant ones, their complexes (Table 2). Internal energy of the ice models, $E_1 = 3 \times 10^8$ and $E_2 = 4 \times 10^{11}$ J, perfectly fits into the designed system; any of the exogenous processes of any level of organization is characterized by a strictly determined share (number) of the model's energy. This fact allowed the development of the criteria and parameters of activity of exogenic processes.

Criteria of Catastrophic Development of Exogenic Processes

The criteria of activity of exogenic processes are based on the relation between the energy of the processes and their models. The energy of the processes (potential, kinetic, thermal) is implemented in a way of a directional movement of volumes (masses) of rocks at different velocities over different distances. The amount of transported material

determines the damage area of various parts, territories of different levels, causing the energy to stop being accumulated by the landscapes (photosynthesis) and people (manufacturing). The movement velocity is a dynamic characteristic of pressure upon a natural or industrial obstacle that is damaged or destroyed in case its durability is lower than the density multiplied by the velocity squared. The processes activity is generally divided by qualitative gradation into low, medium, high, and catastrophic. If we apply the relation between the process energy E_i and the model energy E_1 and E_2 to this scale, we will obtain the quantitative criteria of activity: low $E_i/E_1 < 1.0$; medium $E_i/E_1 > 1.0$; high $E_i/E_2 < 1.0$; and catastrophic $E_i/E_2 > 1.0$. Therefore, the activity of an exogenic process of any level of organization can be assessed quantitatively, where the first gradation is "safe" and the fourth one is "catastrophic."

The catastrophe of exogenic geological processes is a sudden quick movement of large masses of rocks, which causes irreparable damage to landscapes and industrial objects. Based on the quantitative value of the second model, the relation between the volumes of rock masses and their velocity rates was calculated for every genetic type (class) of process in the form of the aggregate of the catastrophe curves (Fig. 1).

Use of the energy model of activity made it possible to determine the criteria of the catastrophic development of all the exogenic processes at any energy level that possess the following parameters:

- 1) The area with irreparable damage or dying landscapes with complete cessation of photosynthesis is 0.74 to 1.1 km^2 .
- 2) The volume of the rock masses that were unexpectedly transported by the processes is around $1,000,000 \text{ m}^3$.
- 3) The velocity of the catastrophic movement of the masses is 8 to 30 m/sec and higher.
- 4) The number of the simultaneously manifested processes with an energy value lower than that of the model is 20 to 8000 .
- 5) The length of the section with the development of the processes of different energy level or the area of a square with the side is from 120 m to 50 km .

It is possible to predict the catastrophes of exogenic processes in a hazardous area (basin) several months to 1 minute in advance based on the change in the character of the current events curve in time (key features, increase in energy, area, number of cases etc.), but only in case it is done by a specialist with a high level of professional training who possesses perfect knowledge of the process formation mechanism.

Conclusions

Potential possibilities for the practical use of ice model energy for the model of activity of exogenic processes are the following:

- creation of special ecological, geotechnical, and other thematic maps of any scale for any territory based on the total energy (power) of exogenic processes in the domain of the "energy-activity" legend;
- design of protective engineering structures, the cost of which may not exceed the total cost of the energy of the

exogenic geological processes;

- direct cost analysis of the catastrophe consequences due to the universality of energy; one J has a fixed price (10-6 rubles) through one kW-hour of electricity;
- real-time prediction of natural catastrophes of different nature based on the changes in any of the parameters in time (volume, area, level, number of cases, etc.).

Evaluation of Landscape Conditions for Environmental Management in the Discontinuous Permafrost Subzone (Bolshezemelskaya Tundra)

A.M. Rocheva

Management, Information and Business Institute, Ecology and Environmental Management Department, Ukhta, Komi Republic, Russia

Abstract

The evaluation of permafrost landscape conditions, the identification of landscape regional and local-level geosystems, and the assessment of their stability and developmental dynamics are required in permafrost zones. A combination of these evaluation results and environmental management constraints within these geosystems allows the optimization of the environmental management process in northern territories. It also allows for the preservation of valuable biospheric functions and the consideration of the social and economic demands of the indigenous population.

Keywords: cryolithozone; environmental management limitations; landscape; northern forest tundra; stability.

Introduction

The study of the natural conditions of potential industrial development areas is the basis for natural and economic zoning, for the evaluation of the resistance of natural complexes to various types of anthropogenic impact, and for optimal territorial organization which considers the environmental, social, and economic functions of the territory. The landscape is the core of the study of complex natural physical and geographic conditions.

The landscape is treated as a natural formation. The term “landscape” is used for the designation of a natural territorial complex of any rank, in which “...all basic components—terrain, climate, water, ground, vegetation and animals—are in complex inter-relation and interaction forming a single continuous homogeneous system under developmental conditions” (Reymers 1990, GOST... 1987).

The natural system hierarchy is quite complicated and in large geological structures can contain five to ten levels. However, no more than three levels are used for practical evaluation of the area: zonal, regional, local (in the landmark ranking). The site relationship to a specific vegetation zone serves as the basis for zonal landscape identification. The relationship to a specific genetic surface is used for regional landscape identification. A landmark is a complicated natural geosystem occupying a terrain mesoform or its part with typical microrelief determined by a combination of ecosystem and soils variables (Annenskaya, Vidina & Zhuchkova 1962). A landscape structure is a combination, correlation, and interaction of landscape components including lower-rank complexes (GOST... 1987).

The purpose of this study was to evaluate permafrost-landscape conditions at a regional scale for the northern tundra region of the discontinuous permafrost subzone and to assess its environmental management limitations.

The northern forest tundra subzone of the European Northeast is administratively located mainly within the Nenets Autonomous Area, the Vorkuta District, and the northern parts of the Intinsky and the Usinskiy Districts of the Komi Republic. This area is a part of the Bolshezemelskaya Tundra and is characterized by discontinuous permafrost. It occupies 15% of the cryolithozone in the European Northeast.

The northern forest tundra landscape is characterized by less extensive distribution of forest and bog vegetation assemblages and by the domination of peatlands and zones with tundra-type vegetation. About 20 types of local landmarks are formed (Osadchaya et al. 1997). A specific combination of ground, vegetation, micro- and mesorelief, moisture content, permafrost characteristics, and modern exogenous processes is typical of each landmark. The identified natural-territorial complexes in the landmark rank form a specific pattern (or structure) of the regional landscapes. The following types of regional landscapes can be considered indicative in the subzone, depending on the age and the genetic type of the surface:

- A. Early Pliocene abrasion-accumulative alluvial-marine watershed surface with the elevation of 220–330 m;
- B. Middle Pliocene abrasion-accumulative marine watershed surface with the elevation of 180–220 m;
- C. Late Pliocene abrasion-accumulative marine watershed surface with the elevation of 160–180 m;
- D. Early Pleistocene abrasion-accumulative marine (glacial marine) watershed surface with the elevation of 120 (115)–160 m;
- E. Early Pleistocene abrasion-accumulative marine watershed surface with the elevation of 90(100)–115(120) m;
- F. Abrasion-accumulative lacustrine-alluvial Early Pleistocene watershed surface with the elevation of 70–90(100) m;
- G. Middle Pleistocene erosional-accumulative lacustrine-alluvial watershed surface with the elevation of 60–70 m.

Moreover, Late Pleistocene river terrace landscapes are sporadically developed (H). The intrazonal erosional-accumulative alluvial Holocene landscape is formed in river and creek valleys (Ivanov 2011).

Landscapes A, B, and C are found in the eastern part of the subzone adjoining the Urals. Landscape D is confined to the eastern part of the area as well, but is also sporadically developed in the center and the west of the subzone. As for the tectonic structure of the Bolshezemelskaya Tundra, they are confined to synclinal structures. Landscapes E and F are most widely developed. They are typical of both synclinal and anticlinal structures. Landscapes G and H are confined to major river valleys.

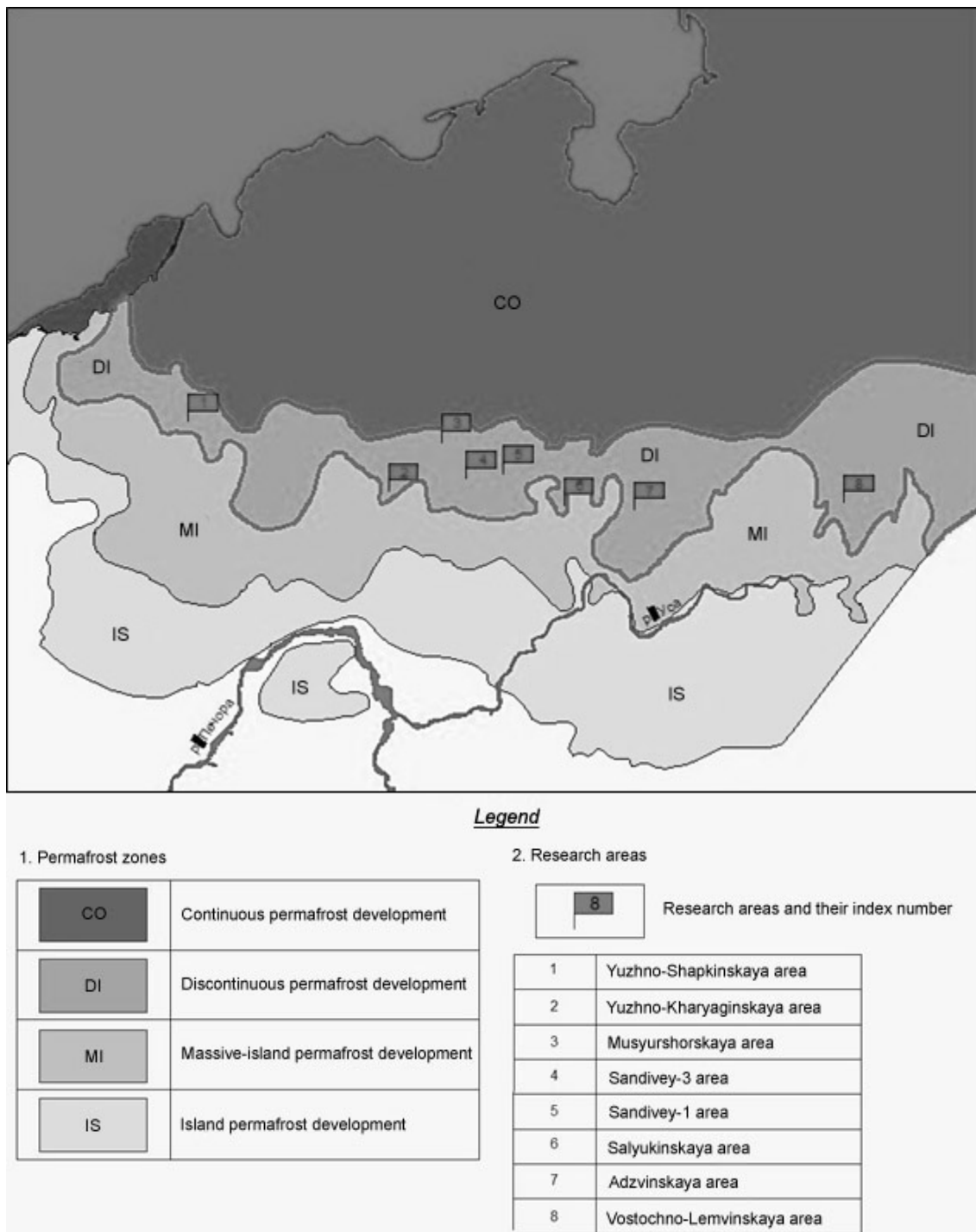


Figure 1. Location of research sites within the permafrost zones.

The data for the nine key sites with the average area of approximately 100 sq. km, the minimum area of about 50 and the maximum area of about 300 sq. km (Fig. 1) was used for the landscape structural analysis. Similarly, landscape maps of 25,000 or 1:50,000 scales are available for each key site. The use of these maps during industrial development of the area at the stage of pre-investment territorial planning allows definition of areal project elements at the sites with minimum potential environmental and social impact parameters, as well as with regard to their permafrost and geotechnical peculiarities.

At the first stage, regional landscapes were identified within the key sites. After that, the structure of landmarks forming the landscapes was studied for each landscape.

All landscapes were divided into groups on the basis of the nature of vegetation: forest, peatland, bog, tundra, meadow, or water meadow. Only the first four groups were analyzed, since meadows in this subzone are extremely rare and are usually confined to intrazonal landscapes, and water meadow landmarks belong to the intrazonal ones by definition.

Forest landmarks in the subzone belong to the category of near-tundra forests and play an important biospheric role. In some cases they serve as food resources for reindeer breeding (winter pastures). Fir is a generally dominating species, with birch subdominating, although the ratio can be opposite in different forest landmarks. The forests in the subzone are located in valley areas, watershed slopes, and peaks. Permafrost is quite rare in forests.

Tundra zones are mainly developed on high watersheds where they dominate. In lower geomorphological levels they are found in a close combination with peatlands and bogs. Tundra landmarks are usually defined on the basis of the mesorelief features. Landmarks with middle-size blocky and inexplicitly blocky mesorelief, flat-undulating and, rarely, small-size blocky mesorelief are typical. Tundra is the main food resource for reindeer (pastures, mainly in late autumn and early spring); sites with shrubs and lichens are most valuable.

Peatlands are present at all geomorphological levels in different proportions. Alases and flat peatlands prevail; raised peatlands are rarer. Dominating permafrost is typical of peatland landmarks. These sites are almost never used as food resources for reindeer breeding.

Bogs are not very typical of the subzone. They can be observed in the landscape structure of the territory in certain cases only. Several main types of bogs are identified. Shrub-covered sedge, moss, and sedgemoss bogs are developed most widely. There is almost no permafrost within bogs; only individual new formations can be observed. Bog margins are restrictedly used as food resources.

Viewing the cryolithozone primarily as a biospheric resource and the basis for the preservation of traditional environmental management, one should be guided by specific natural criteria, including the stability of the landscape which is closely associated with the stability of geocryological conditions. Development in the cryolithozone should first comply with environmental legislation and consider the fact that a part of the environment is not protected by legislation to the full extent or not protected at all. The interests of the indigenous population should also be taken into account. Any time-limited use of the area should be managed in a way that provides for the minimum possible harm to the natural ecosystems. Industrial infrastructure should be placed at sites that have the maximum potential for self-recovery.

Conclusions are based on evaluation of environmental conditions in discontinuous permafrost areas and analysis of the limitations of environmental management.

Environmental management limitations provide for the maximum possible preservation of the natural ecosystems while conducting non-traditional economic development of the area. Environmental management limitations, according to Osadchaya (2009), are divided into environmental, social, and engineering categories. The first two ensure the stable development of the area, and the third provides for stability of technogenic systems. The environmental group of limitations is divided into legislative and geo-ecological. Social limitations associated with preservation of the traditional economy are called "nature resource" limitations. Geotechnical limitations are associated with industrial development.

Legislative limitations within the sites surveyed are those defined by the federal legislation for protected natural territories (PNT), including water protection zones and coastal protection belts. Water protection zones are usually wider than coastal protection belts, which is why we are guided by their parameters hereinafter.

Geo-ecological limitations include limitations referred to as the areas with environmental-forming functions having biospheric status that is either defined in legislation and lacks the implementation mechanism or is not defined at all. Such

areas include near-tundra forest zones, alases, and arbuscle (dwarf tree) development zones, as well as flowing bogs. The lakes, typical of the area, are thermokarst in genesis. By definition, they are positioned in polygonal grid clusters with repeated wedge ice (i.e., they are hydrologically connected with each other, communicate, and are connected to the hydraulic network). Therefore, these are flowing formations and their contamination is prohibited. Moreover, these are dynamic systems where lake transition to alases and vice versa are possible (according to V.V. Elsakov and F.A. Romanenkov). Therefore, although alases sites are not defined by the legislation as a specific type of area for environmental management, there should be geo-ecological limitations applied to them. As for the arbuscle sites, they have the same status as tundra forests according to the regional legislation of the Nenets Autonomous Area, because they are of great nature-stabilizing value. It is evident that operational forest cutting (defined as an aspect which is limiting environmental management) will not be conducted. However, these sites can be disturbed in case of the development of hydrocarbon deposit. That is why they are defined in this work as sites with geo-ecological limitations.

Nature-resource limitations apply to territories where traditional environmental management is conducted. Winter, late spring, and early autumn reindeer herding is carried out in the research areas. In the first case, sites with forest vegetation type are most valuable; in the second case it is the valley sites; and in the latter case all sites with the tundra vegetation type are most valuable. Therefore, the group of these limitations includes all forest and tundra landmarks except for the arbuscle sites because most of green material in them is already missing during the herding period. While organizing non-traditional environmental management, the sites least valuable for traditional economic types should be used where possible. This will allow for one of the conditions for the stable development of the region.

Geotechnical limitations at the pre-investment stage are defined with a high degree of conventionality and should be specified in the process of preparation of the front-end engineering design. Alases are unambiguously referred to as the areas with limitations due to their instability, high water content, particularities of the geotechnical properties, and of ground composition. Such limitations are also applied to repeated wedge ice zones that occur in peatlands and adjoining lake shores and alases. Therefore, the repeated wedge ice zones are mainly found in the water protection zone of lakes and are considered earlier in the legislative limitations. Construction at such sites is associated with an increased technogenic risk. Moreover, it is not recommended to carry out construction in thermokarst development zones and intensively flooded thermokarst depressions with extremely low carrying capacity. Construction of facilities is not recommended on raised peatlands. The current permafrost settings at these sites are not stable; frost mounds are actively growing and the permafrost area is expanding. For building linear facilities, it is not recommended to place them underground at adjoining sites without significant expenditures. Some bog types can be referred to as sites with complicated geotechnical conditions. This is primarily a group of swamp and grass-sedge bogs and thermokarst depressions.

Therefore, construction in some organogenic ground zones is optimal in terms of traditional use of the area and its environmental stability preservation. Nonetheless, such construction is quite expensive in terms of geological engineering and economics

Conclusions

A combination of results based on the landscape structural analysis for the research areas and the identification of limitations of environmental management lead us conclude that the sites most suitable for non-traditional economic development in terms of preservation of biospheric and social functions are located within the landscape of the Lower Pleistocene abrasion-accumulative marine watershed surface (elevations 90(100)–115(120) m) and the landscape of the Lower Pleistocene abrasion-accumulative lacustrine-alluvial watershed surface (elevations 70–90(100) m).

References

- Annenskaya, G.N., Vidina, A.A., Zhuchkova, V.K. et al. 1962. *Geographical Landscape Morphological Structure*. Moscow: Izd-vo MGU, 184 pp.
- GOST 17.8.1.01-86 (ST SEV 5303-85) 1987. *Nature Protection. Landscapes Terms and Definitions*. Izd.ofits. Moscow: Gos.kom. SSSR po standartam.. 10 pp.
- Ivanov, N.F. 2011. Geological and geomorphological structure of the Timan-Pechora province *21st century management problem: Proceedings of the All-Russia Scientific-Practical Conference*. Ukhta: Institut upravleniya, informatsii i biznesa, 264 pp.
- Osadchaya, G.G., Kirikova, N.S., & Dolgova, N.N. 1997. Unified regional differentiation of natural complexes in the Timan-Pechora province cryolithozone for the purpose of geo-ecological evaluation of the territory/. *Geotechnical subsurface use and environmental protection provision: Proceedings of the International Scientific and Practical Conference*. Perm: PGU, p.129.
- Osadchaya, G.G. 2009. Preservation of the territorial resource as one of the conditions of stable cryolithozone development (the case of the Bolshezemelskaya tundra). *Kriosfera Zemli*. 13, (no. 1): 24-31.
- Reymers, N.F. 1990. *Environmental Management: glossary-reference book*. Moscow: Izd-vo Mysl. 453 pp.

Observations of Microorganisms in Segregated Ice Using Methods of Electron Microscopy

V.V. Rogov

Lomonosov Moscow State University, Faculty of Geography, Moscow, Russia

A.N. Kurchatova

Tyumen State Oil and Gas University, Tyumen, Russia

Abstract

Methods of optical and electron microscopy were used to find microorganisms in situ in the inclusions of segregated ice. The conditions of their viable preservation and the connection with the processes of ice formation are discussed. An experiment on the migration of microorganisms in the process of freezing of fine-grained soils was conducted. It is suggested that ice inclusions in frozen ground are the most suitable environment for the preservation and, perhaps, for the life of various forms of microorganisms.

Keywords: ice; microorganisms; microscopy; permafrost.

Introduction

A significant portion of the earth's crust, or lithosphere, especially in the sub-polar latitudes and high mountains, consists of permafrost—a unique heterogeneous physical-chemical system. A special role in the structural organization of permafrost is played by microorganisms, the lowest in mass though a very important biotic component. Their content can reach 10^2 – 10^{10} cells per 1 g of soil.

The first knowledge about microorganisms in permafrost was obtained in Russia at the end of the nineteenth century as a result of the examination of mammoths discovered in Siberia. Currently viable microorganisms in continental ice and different genetic types of frozen deposits are reliably identified. Bacteria, fungi, diatoms, and other microorganisms were discovered in the ice core of the Antarctic Vostok Station in 1979 (Abyzov et al. 1979). A bacterial community was found in the Antarctic permafrost (Kochkina et al. 2001). Many studies of microorganisms in frozen ground were carried out from syncryogenic deposits of the Kolyma Lowland, where viable microorganisms were for the first time identified in frozen fine-grained sediments (Zvyagintsev 1992, Gilichinskiy et al. 1996, Vishnevetskaya et al. 1997, Vorobeve et al. 2002). At the same time it was found that their distribution does not depend on temperature or depth, but rather on water and ice content in the frozen ground and on the presence of organic remains.

The data obtained suggest that the earth's biosphere expands over the cryolithosphere as well. According to Gilichinskiy (2002), negative temperatures of the cryolithosphere do not limit viable preservation. On the contrary, a stable regime is a factor contributing to the preservation of biological systems and the production of adaptive mechanisms for the renewal of viability in the cells. As a result, life there is maintained longer than in other habitats.

The possibility of the active existence of microorganisms in frozen ground is increasingly discussed in recently published works. It is noted that the largest number of microorganisms is typical of frozen deposits, whereas they are rare or completely non-present in ground ice (Vorobeve et al. 1997). However, one must admit that, firstly, there is a great variety of types of ground ice,

and, secondly, they were insufficiently studied in regard to microorganisms. In addition, it should be pointed out that the research technique applied to microbiology of frozen deposits and ground ice uses, as a rule, traditional methods and methods of analysis accepted for objects outside the cryosphere. In this connection, approaches and methods should be developed to allow for the analysis of the existence of microorganisms directly in their environment—in frozen ground.

Research Methods

In order to estimate the distribution of microorganisms in segregated ice, which is the most important component of frozen fine-grained deposits, samples from a key geocryological section of the Mamontova Gora on the banks of the Aldan River (Yakutiya) were examined. The riverbank here is intensively washed away (more than one meter per year), and the deposits from which the samples were taken obviously remained in a frozen condition for a long time. They date probably from the Middle Pleistocene.

The detection of microorganisms in ice samples was carried out by means of visual and photographic identification. Optical and electron microscopy were used for specimens that have been prepared in different ways.

Fresh spalls were examined in frozen condition after vacuum cryogenic drying, but the most detailed information was obtained from the examination of the replicas of frozen samples. This technique was developed by one of the authors (Rogov 2009). It was used earlier in the study of frozen ground micro-structure. Initial analysis of the replicas was carried out by means of an optical microscope, and microorganisms were found in the ice layers of the examined samples at that stage of the research. More detailed information was obtained by use of the LEO 1450 VP scanning electron microscope. A built-in spectrometer was used in order to confirm the presence of the detected microorganisms.

Results and Discussion

The examined samples included stratified finely dispersed deposits with the alternation of lighter layers of aleurite (0.5–

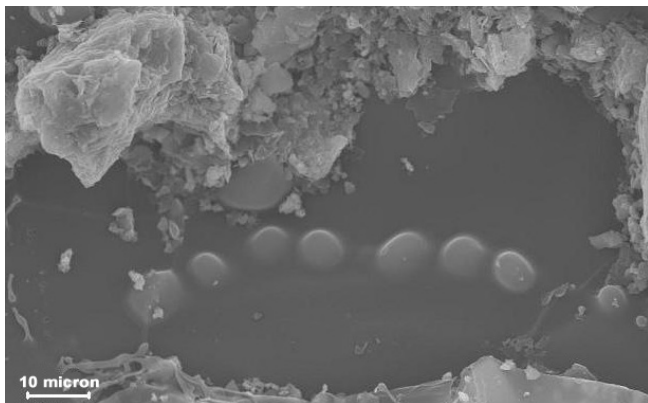


Figure 1. The arrangement of microorganism cells in the schlieren of segregated ice of clayey silts of the Mamontova Gora exposure.

1 mm thick) with darker and thicker (3–5 mm) layers having similar particle size distribution. The cryogenic structure of the samples was a combination of thin (0.05–0.1 mm) broken interlayers that generally inherited the stratification of deposits with vertical, sometimes interrupted, veins less than 0.1 mm thick. The ice layers themselves are composed of isometric and slightly elongated crystals of polygonal shapes ranging from 10 x 15 to 30 x 80 microns.

A detailed analysis of biodiversity is not yet completed, but initial studies show the presence of numerous and diverse viable microorganisms in the deposits under examination. The domination of bacteria is observed, and among them representatives of the genera *Arthrobacter*, *Bacillus*, *Micrococcus*, and *Pseudomonas* prevail. The species composition does not show any major differences from other findings in the frozen deposits of Northeast Russia (Karasev et al. 1998).

In the ice samples, there were microorganisms identified with large cells from 5 to 10 microns, round and egg-shaped. They were located in the middle of an ice layer (schlieren) along its extent in groups up to 5–8 cells, although some cells were located singly at the contact of ice and soil skeleton (Fig. 1).

In addition to the aforementioned microorganisms, rod-shaped microorganisms with rounded ends and were found in ice interlayers (Fig. 2). These microorganisms are very similar in size and shape to those previously detected during the seeding of *Bacillus*. They were also located both in the mass of the ice interlayer and at the contact with mineral particles.

The comparison of both cell shapes with the crystal structure of ice interlayers indicates that they are located within the crystals, and not on their borders, as was shown for the microorganisms in the Antarctic ice (Doyle et al. 2008). Spectrometric studies more accurately defined the morphological indicators of the presence of cells by confirming their organic origin. They revealed the presence of salts (in particular, calcium chloride) around the cells. The distribution of salts and colloids in the form of a netted film (“coat”) around the cells was observed in the process of examination of the samples in the specimens obtained by cryogenic vacuum drying.

The arrangement of the detected cells in the segregated ice interlayers prompts discussion of the connection between the processes of ice formation and redistribution

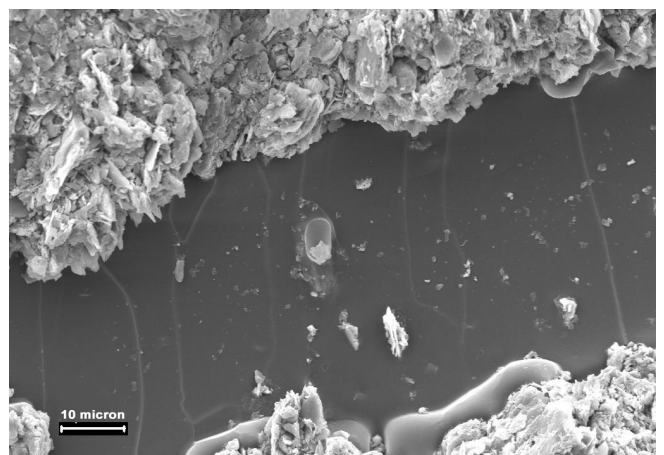


Figure 2. The arrangement of rod-shaped cells among the crystals of segregated ice of clayey silts of the Mamontova Gora exposure.

of microorganisms during freezing. It can be assumed that microorganisms existed long before freezing and were an integral part of the ecological system of the lacustrine sediments, and their arrangement observed today was formed later in the course of the freezing of the sediments. However, according to the laws of ice formation in fine-grained soil, moisture migration toward the freezing front first led to the formation of ice-cement inclusions and then to the formation of interlayers of segregated ice. Probably it was at this point when the cells of microorganisms could have been captured by the growing crystals and enclosed in ice schlieren. Further viability of cells could be maintained due to the adsorption of salt ions out of the pore solution even before freezing, which prevented ice formation in the cell itself as well as around it. It should be noted that some cells do not lose connection with mineral substrate, which is perhaps also necessary for their survival.

In order to test this hypothesis, a special experiment was conducted. In a plastic cylinder 50 mm in diameter and 250 mm high, a soil system was developed consisting of sterile kaolin saturated by distilled water up to 40% and underlain by a layer of coarse-grained (0.5–1.0 mm) sand. The sand was saturated with a solution containing *Bacillus cereus* with complete filling of pores. This system was frozen in a special unit under the condition of one-dimensional freezing at the surface temperature of -4°C . A stratified cryogenic structure with ice interlayers 3–4 mm thick was formed after the upper three centimeters of the kaolin sample were frozen. The next layer of the sample (7.5 cm) had massive structure, whereas the bottom layer (2.5 cm) remained thawed. Samples with the volume of 250 mL were taken from both the upper and lower layers of the sample in order to identify the assumed migration of bacteria into the frozen zone. The estimate of bacteria redistribution by means of seeding without cultivation indicated the presence of 71 colonies in a Petri dish for the upper part of the sample (frozen ground with segregated ice), and 25 colonies for the lower part (frozen ground with massive structure). Microscopic observations revealed the presence of a few cells located singly in the layers of segregated ice.

Thus the experiment confirmed the possibility of the movement of microorganisms in the process of moisture

migration toward the freezing front and their location in the interlayers of segregated ice. The mechanism of such movement is not yet entirely clear. Probably it is caused by the cryogenic drying of soil accompanied by the formation of shrinkage fractures along which the moisture and cells migrate to the growing ice crystals.

Conclusions

Based on the study of natural samples and on the data of laboratory experiments, one can conclude that it is the ice inclusions in frozen deposits that provide the most comfortable environment for the preservation and, perhaps, the active existence of various forms of microorganisms. The connection discovered between the distribution of microorganisms and the processes of freezing and ice formation in sediments and soils confirms the possibility of their viable preservation.

The method of microorganism study in permafrost suggested by the authors does not claim to solve all the existing problems. However, it allows us to more comprehensively understand the conditions of the existence of microorganisms in the cryolithosphere, and it can supplement the range of traditional methods and approaches. Further studies will evaluate the strengths and weaknesses of this method.

Acknowledgments

This work was supported by RFBR, project No 09-05-00538-a.

References

- Abyzov, S.S., Bobin, N.E., & Kudryashov, B.B. 1979. Microbiological analysis of glacier in the Central Antarctica. *Izvestiya AN SSSR, seriya biologiy* No 6, pp. 828-836.
- Brushkov, A.V., Griva, G.I., Melnikov, V.P., Sukhovey, Yu.G., Repin, V.E., Kalenova, L.F., Brenner, E.V., Subbotin, A.M., Trofimova, Yu.M., Tanaka, M., Katayama, T., & Utsumi, M. 2009. Relic microorganisms of cryolithozone as possible objects of gerontology. *Uspekhi gerontologii* 22(2):253-258.
- Doyle, S., Amato, P., & Christner, B. 2008. Life in and under the Antarctic ice sheets. *Microscopy today* 16 (3): 6-10.
- Gilichinskiy, D.A. 2002. *Cryobiosphere of the Late Pleistocene: permafrost as an environment for the preservation of viable microorganisms*. Doctor of Sciences (Geology and Minearology) thesis abstract Tyumen. 58 pp.
- Karasev, S.A., Gurina, L.V., Gavrish, E.Yu., Adanin, V.M., Gilichinskiy, D.A., & Evtushenko, L.I. 1998. Viable actinobacteria in ancient Siberian permafrost. *Kriosfera Zemli* 2 (no 2): 69-75.
- Kochkina, G.A., Ivanushkina, N.E., Karasev, S.G., Gavrish, E.Yu., Gurina, L.V., Evtushenko, L.I., Spirina, E.V., Vorobeva, E.A., Gilichinskiy, D.A., & Ozerskaya, S.M. 2001. Arctic and Antarctic microorganisms under conditions of long-term natural cryopreservation. *Mikrobiologiya* 70 (4): 412-420.

- Vishnevetskaya, T.A., Erokhina, L.G., Gilichinskiy, D.A., & Vorobeva, E.A. 1997. Blue-green and green algae in the Arctic permafrost deposits. *Kriosfera Zemli* 1 (no 2): 71-76.
- Vorobeva, E.A., Gilichinskiy, D.A., & Soin, V.S. 1997. Life in cryosphere: A look into the problem. *Kriosfera Zemli* 1 (no 2): 41-51.
- Vorobeva, E.A., Soina, V.S., Zvyagintsev, D.G., & Gilichinskiy, D.A. 2002. Viable Ecosystems of cryolithosphere. *Bakterialnaya paleontologiya*. Moscow. Izd-vo PIN RAS, pp. 155-169.
- Zvyagintsev, D.G. 1992. Microorganisms in permafrost. *Uspekhi mikrobiologii* 2: 3-26.

Solution to a Series of Problems of Frozen Ground Mechanics Using Time-Analogy Methods

L.T. Roman

Lomonosov Moscow State University, Moscow, Russia

Abstract

Based on theoretical and experimental research, the possibility of using time-analogy methods to forecast long-term creep and strength of frozen ground for the period of time comparable to the life cycle of buildings is shown. Various test types were considered as well as the scale effect under the conditions of model determination of adfreeze forces.

Keywords: analogy; forecast; creep; frozen ground; strength; stress, temperature.

Introduction

Time-analogy methods are widely used in mechanics of deformable solids (Ferry 1953, Urzhumtsev 1982). They are based on experimental detection of the relation between deformation, stress, and time on the basis of its showing acceleration by the affecting factors. For frozen ground, these factors are: rise of temperature, increase of stress, and modification of parameters of physical properties such as salinity, ice content, and peat content. The main task of using time-analogy methods is to determine the correlation between periods t_1 and t_2 , during which the same deformation value is reached or destruction occurs with various predetermined values of the accelerating factors. The correlation between these periods is determined by the reduction ratio (a):

$$a = t_1 / t_2 \quad (1)$$

We have shown the applicability of time-analogy methods in the mechanics of frozen ground with consideration of their specific rheological properties, and we have substantiated the reduction ratio from the mechanical and physical positions regarding the creep and destruction processes. We have also specified the effectiveness of using temperature-, stress-, and salinity-time analogies (Roman 2002). Experimental data obtained under various stress conditions were analyzed as follows: uniaxial and triaxial compression; shear; shear on adfreezing surfaces; and spherical punch indentation (Roman 1987, Roman & Kuleshov 1990, Roman & Volokhov 1994, Tsyrendorzhieva & Roman 1994, Roman 2002). Figure 1 shows a generalized example revealing the essence of time-analogy methods in the study of frozen ground creep.

Experimental Techniques

Six or seven frozen ground samples are examined under isothermal conditions. Depending on the analogy type, the experimental conditions are as follows: the temperature-time analogy requires examining each sample under the given temperature (θ). The load on a sample must make up the same share of quasi-instantaneous strength at the temperature of (θ). Thus the influence of stress on deformation is brought to the same level along the entire range of the experimental temperature. The requirement should be observed for the conditions of *creep* estimates on

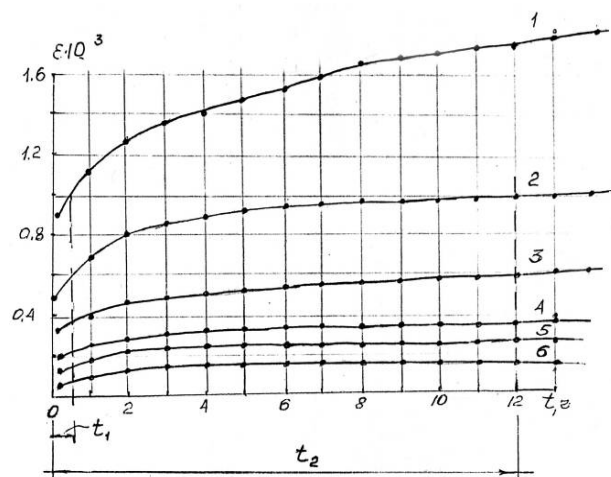


Figure 1. Creep curves ε of frozen clayey silt (uniaxial compression, temperature $\theta = -4^\circ\text{C}$) under various stress values σ , MPa: 1-1.2; 2-1.0; 3-0.8; 4-0.5; 5-0.36; 6-0.2.

the first and second stages. Using the experimental data, a family of curves is plotted for the dependence of yield (I) on time (t) in the semilogarithmic scale ($I - \lg t$). Yield is the ratio of differential settlement (ε) to stress (σ):

$$I = \varepsilon / \sigma \quad (2)$$

Assuming a linear relation between deformation increment and stress, yield is a reciprocal value of the deformation module.

Relations ($I - \ln t$) for other types of analogies are made in a similar way. Yield curves must be similar. The requirement is observed for frozen ground when experimental stress in samples is related to the area occupied with soil particles and ice rather than to geometric cross-section area. Approximately, it may be calculated through division of experimental stress by the parameter K , depending on physical properties: density of soil particles (ρ_s), dry ground (ρ_d), ice (ρ_i), total moisture content (W_{tot}), and at the expense of unfrozen water (W_w):

$$K = \rho_d [1/\rho_s + (W_{tot} - W_w)/\rho_i] \quad (3)$$

The similarity of yield curves allows defining the increment of the reduction ratio $A = \ln a$ within each pair of neighboring

curves. The new reduced time for each experimental point will make up:

$$\ln(ta) = \ln t + \ln a \quad (4)$$

By moving the yield curve by the reduced time value, we get a generalized curve for accelerating yield for a time period ten times longer than the duration of the experiment.

Deformation Forecast

Figures 2, 3, and 4 show the examples of plotting generalized yield curves using the method of temperature-, stress-, and salinity-time analogy.

The yield forecast under any temperature within the experimental range may be performed based on the definition of the reduction ratio through its dependence on the parameters of the creep accelerating factor (Figs. 3b, 4b), including for any intermediate values of temperature or stress. Then, after expressing the generalized curve via an analytical equation, we calculate yield for the forecast period for any values of its accelerating factors.

Approbation of long-term deformation forecast using the stress-time analogy method is performed through comparison of long-term (over four years) data on frozen ground creep obtained by A.V. Brushkov in the Amderma underground laboratory. The following samples were tested:

sand, sandy silt, and clayey silt for uniaxial compression under temperature -3°C . Sandy silt and sand samples were selected from the Zyryan-age third marine terrace deposits on the left bank outcrop of the Erkuta-Yakha valley, 20 km from its mouth. Clayey silt was selected at the depth of 1 to 3 m in the central part of the Yamal Peninsula at the latitude of Cape Kharasavey in the marine Kazantsev deposits located to the east of Lake Tyurin-To. Physical properties of the soils tested are shown in Table 1.

The tests were held in two stages. In the first stage, five to seven duplicate samples were tested under permanent stress, yet different for each sample. The first stage duration was nine to ten days. In the second stage, sample testing continued at one of the stresses accepted in the first stage that caused either damping creep or creep at a constant rate. The testing of these samples lasted for more than four years. The

Table 1. Average values of soil physical properties.

Soil type	ρ g/cm^3	W_{tot}	$D_{\text{sal}}\%$	K_{np}	$\theta_{bf}^{\circ}\text{C}$	W_w
Clayey silt	1.85	0.46	1.0	0.021	-1.45	0.31
Sandy silt	1.85	0.36	0.2	0.0055	-0.49	0.18
Sand	1.90	0.26	0.1	0.0038	-0.22	0.1

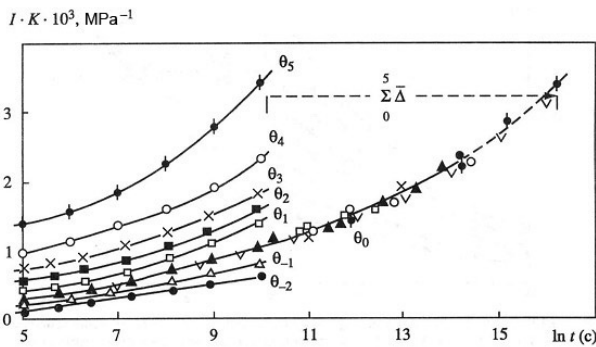


Figure 2. Experimental yield curves and a generalized forecast curve for cottongrass-sphagnum peat (spherical punch indentation) under different temperatures:

$\theta_1 = -9,5^{\circ}\text{C}$; $\theta_2 = -8,5$; $\theta_3 = -6$; $\theta_4 = -4$; $\theta_5 = -2,5$; $\theta_0 = -13$; $\theta_{-1} = -25,5$; $\theta_{-2} = -28^{\circ}\text{C}$

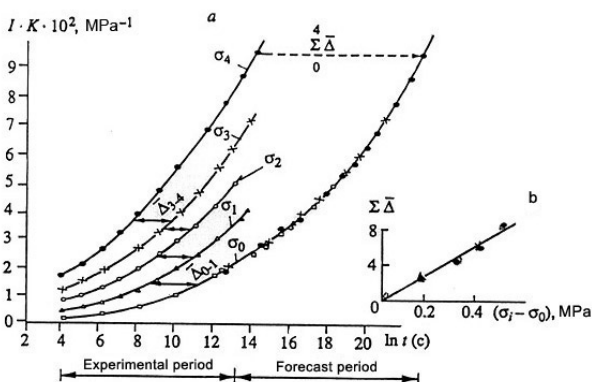


Figure 3. The family of yield curves for frozen upland cotton grass-sphagnum peat under uniaxial compression, temperature $-4,5^{\circ}\text{C}$ and various

stress (a) $\sigma_0 = 0,2 \text{ MPa}$; $\sigma_1 = 0,36$; $\sigma_2 = 0,5$; $\sigma_3 = 0,6$; $\sigma_4 = 0,7$ and correlation $\sum \Delta \ln a_{\sigma} - (\sigma_i - \sigma_0)$ (b)

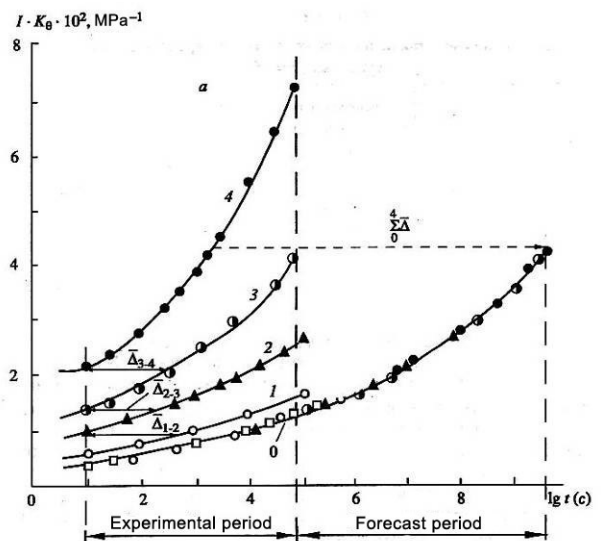


Figure 4. The family of yield curves for frozen clayey silt, NaCl saline under uniaxial compression ($\sigma=1,26 \text{ MPa}$), temperature -5°C and the correlation

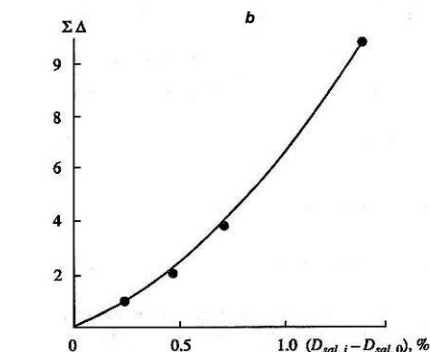


Figure 4. The family of yield curves for frozen clayey silt, NaCl saline under uniaxial compression ($\sigma=1,26 \text{ MPa}$), temperature -5°C and the correlation

$\sum \lg a_{D_{\text{sal}}} - (D_{\text{sal},i} - D_{\text{sal},0})$ (b) under various salinity D_{sal} : 0-0%; 1-0,2; 2-0,4; 3-0,7; 4-1,5%

experimental results were processed using the least squares method. By the average values of deformation developing in time, families of creep curves were built in the semi-logarithmic scale. As we can see, the best compliance of the forecast and experimental curves was obtained for sandy silt. Forecast values for clayey silt and sand were overvalued by 1.5% and 6%, respectively. Yet the cause of the decrease of sand deformation experimental values is unclear. Perhaps it was caused by temperature decrease in the experimental section of the underground laboratory.

Some examples of general deformation long-term module definition obtained using the time-analogy method are shown in Tables 2, 3, and 4.

Strength Forecast

As we know, frozen ground strength is closely connected with creep, and destruction is defined by the third stage of creep (Vyalov 1978, 2000). Long-term strength is affected by the same factors as long-term creep. The intensity of the process of strength decrease in time, as well as that of deformation, depends on soil physical properties, temperature, and stress. That is why the time-analogy methods may also be applied to forecasting long-term strength. The prerequisites for experimental data processing remain the same as those for forecasting long-term deformation. Yet the stress-time analogy method is excluded since the long-term strength curve under constant temperature is a single generalized curve revealing the influence of stress on strength. All other factors affecting strength in a similar way to time

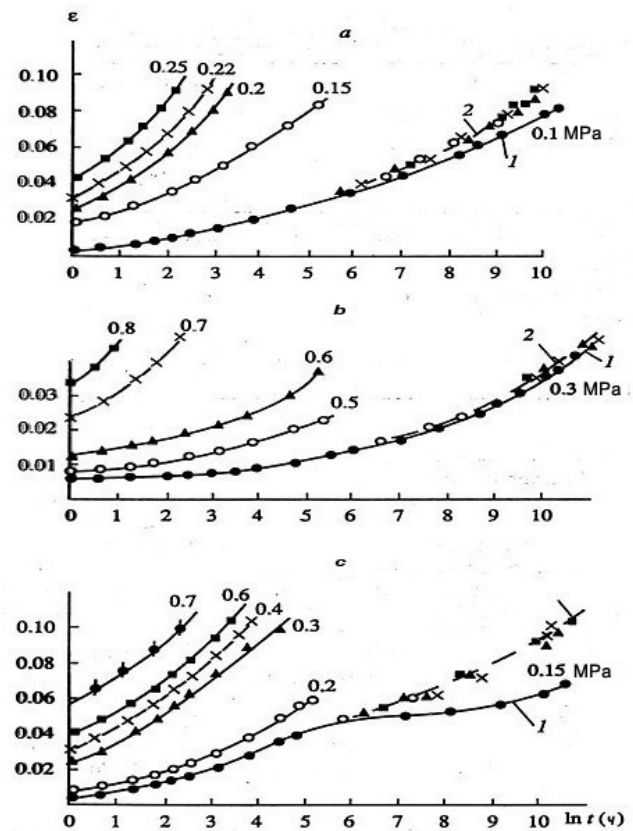


Figure 5. Frozen ground creep curves (uniaxial compression) 1 - experimental data of A.V. Brushkov, 2 - forecast data using the stress-time analogy method; a - clayey silt; b - sandy silt, c - sand.

Table 2. General deformation module, the temperature-time analogy (acc. to Tsyrendorzhiyeva 1994).

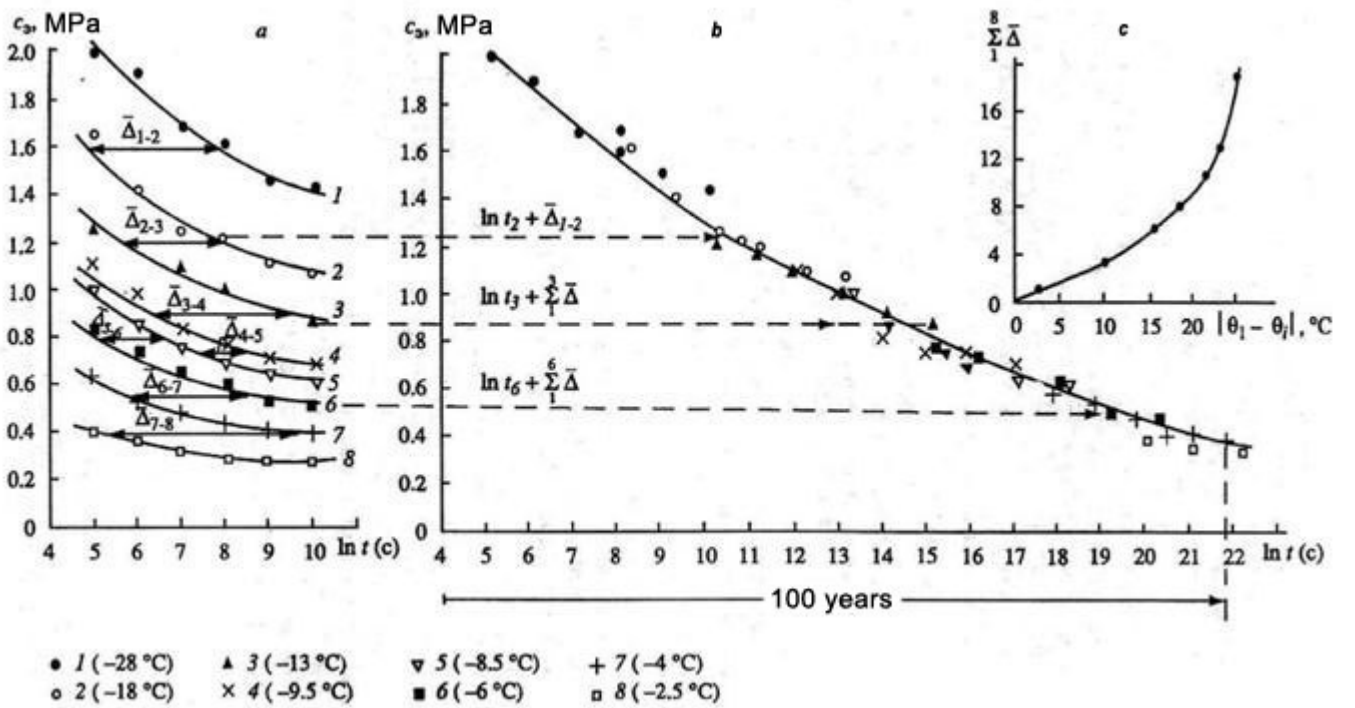
Test	Soil type	General deformation module E_{σ} , MPa for the period of 50 years under temperature, °C					
		-3	-4	-5	-7	-8	-12
Flat punch indentation with a single load $\sigma = 0,3\sigma_0$	Poly-mineral clay	21	30	48	65	80	95
	Kaolinite clay	12	15	21	27	38	41
	Sandy silt	24	34	54	74	92	108

Table 3. General deformation module, saline-time analogy (acc. to Roman & Kuleshov 1990).

Soil type	Test	General deformation module E_{σ} , MPa for the period of seven years under salinity D_{sal} , %				
		0.0	0.2	0.4	0.7	1.0
Clayey silt, $\rho = 1.86$; $W_{tot} = 0.28$	Uniaxial compression, $\theta = -5.7^{\circ}\text{C}$	40	21	14.5	10	5

Table 4. General deformation module, stress-time analogy (acc. to L.T. Roman, 1987).

Soil type	Test	General deformation module E_{σ} , MPa for the period of 50 years under stress σ , MPa				
		0.15	0.4	0.6	0.75	0.90
Cotton grass-sphagnum peat: $\rho = 1.07 \text{ g/cm}^3$; $\rho_s = 1.97 \text{ g/cm}^3$; $W = 230\%$; $WH = 130\%$; $\theta_{п.з.} = -0.010\text{C}$	Uniaxial compression, $\theta = -4.50\text{C}$	90	50	40	22	15



a – experimental correlations $c_3 - \ln t$; b – generalized curve $c_3 - \ln t$ (for $\theta = -28^\circ\text{C}$); c – correlation $\frac{8}{1} \bar{\Delta} - |\theta_1 - \theta_7|$

Figure 6. An example of plotting a generalized curve of long-term equivalent cohesion for frozen peat using the temperature-time analogy method.

Table 5. Long-term equivalent cohesion C_3 , MPa of upland peat ($\rho = 1.07 \text{ g/cm}^3$, $W_{\text{tot}} = 2.3$) for the time period of 100 years.

Equivalent cohesion C_3 , MPa under temperature $\theta^\circ\text{C}$							
-2.5	-4.0	-6.0	-8.5	-9.5	-13.0	-18.0	-28.0
0.08	0.15	0.18	0.20	0.23	0.27	0.32	0.45

allow us to obtain a family of long-term strength curves, find a generalized curve, and make a forecast for a period exceeding the experimental one. The temperature- and salinity-time analogy methods are the most applicable ones. A principal possibility of using these methods is proved by the examples of various types of tests including complex stress conditions (Roman 2002). The methodical sequence of experimental data processing is illustrated by the results of the forecast of frozen peat equivalent cohesion (Fig. 6). A family of $\sigma - \ln t$ graphs is plotted with an indication of confidence intervals. A “reference” temperature θ_0 is chosen; its value corresponds to the experimental one and is close to the lowest temperature interval. The average value $\Delta = \ln t$ is determined subsequently, starting with the “reference” curve. A generalized curve is plotted for the lowest experimental temperature by shifting the experimental points along the time axis by the value of $\Sigma \Delta = \Sigma \ln t_i$. To obtain generalized curves under the conditions of higher temperatures, it is necessary to:

- 1) Plot $\Sigma \Delta = \Sigma \ln t_i$ against $\theta_i - \theta_0$ (Fig. 6c).
- 2) Obtain an analytical equation of the generalized curve.
- 3) Calculate strength for any temperature θ_i within the experimental range using this equation.

The calculation should be made for the time period corresponding to: $\ln t_0 + \Sigma \Delta \ln a_i$ where t_0 corresponds to the maximum time of the forecast period of the generalized

curve. The obtained strength values for the conditions θ_i will also correspond to the maximum time period for the generalized curve.

Research has shown that generalized curves are well approximated by power equations in the form of:

$$\sigma_i = b(\ln t)^a \tag{5}$$

where a and b are parameters depending on the soil type, temperature, and the load mode. Their values are defined according to the solution of the equation of the generalized curve obtained using a graphic method.

The obtained values of long-term equivalent cohesion based on the above data and their processing using the temperature-time analogy method are shown in Table 5.

Consideration of the Scale Factor

As many researchers have shown, the quantitative values of frozen ground and ice mechanical properties depend on the size of the samples being tested. The largest influence of the scale effect is detected in testing frozen-in model piles (Tsytoovich & Vologdina 1936, Vyalov 1959, Grechishchev 1966, Velli et al. 1966, Kardymon, 1967, Roman 1987 et al.) The data clearly detect the decrease of long-term shear resistance on the adfreeze surfaces with the increase of model pile size both in the case of full geometric similarity (when the model length is increased in proportion to the diameter increase) and in the case of affine scaling (when only one dimension is changed, either diameter or length).

To take the scale effect into consideration, attempts to find empirical ratios were made (Kardymon 1967, Velli et al. 1966) to apply physical and mathematical modeling for this purpose (Vyalov 1959, Grechishchev 1966). We (Roman

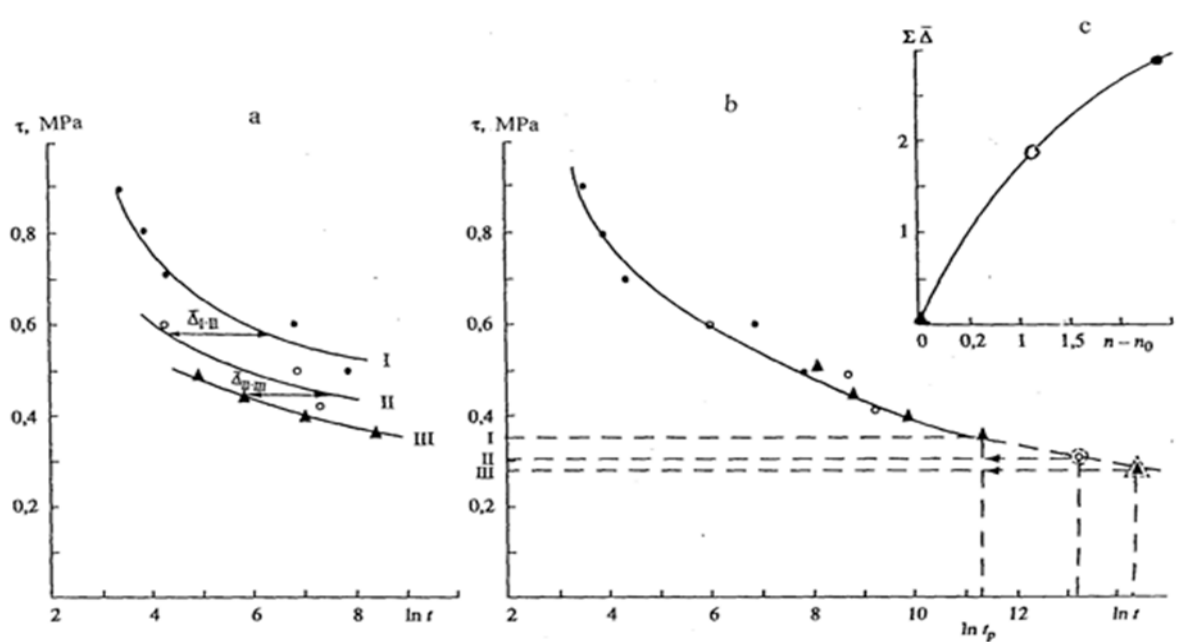


Figure 7. Forecast of long-term shear resistance on adfreeze surfaces of similar model piles using the scale-time analogy method. a - shear dependence on time; b - generalized curve of long-term strength for model I; c - reduction ratio dependence on similarity factor.

2002) obtained a solution allowing consideration of the scale effect in detection of specific shear resistance of model piles frozen into soil and spherical punch indentation based on the assumption of even distribution of defects within the area of the lateral surface of the models. To express the relation between the number of defects and similarity factors, we used the theory of long-term soil destruction developed by Vyalov, Pekarskaya & Maksimyak (1970) based on the data of microscopic research of developmental patterns of soil damage in the course of its deformation and destruction. These solutions allow the calculation of a conventional, undamaged surface area and the extent of each model damage. Such an approach provides the possibility to calculate the strength of models with any factor of geometric similarity including natural size piles, using an experimentally defined long-term value of shear resistance for one and the same time period for two similar models.

Experimental data processing showed a possibility of using the scale-time analogy method in detection of long-term shear resistance through testing model piles under laboratory conditions. Similarity factor increase is a strength-decreasing force. Figure 7 shows an example of experimental data processing.

References

- Ferry, J. 1953. *Viscoelastic Properties of Polymers*. Moscow: Inostrannaya Literatura. 535 pp.
- Grechishchev, S.E. 1966. Mechanical processes similarity criteria in permafrost. *Materials of the 8th All-Union inter-institutional meeting on geocryology 5*: 192-209. Yakutsk (in Russian).
- Kardymon, A.P. 1967. *Research of ground shear resistance on lateral surface of frozen-in piles of different shapes*. Autoabstract of the dissertation for candidate of technical sciences degree. Vladivostok. 21 pp. (in Russian).
- Roman, L.T. 1987. *Frozen Peat Soils as Construction Foundations*. Moscow: Nauka. 220 pp. (in Russian).
- Roman, L.T. 2002. *Mechanics of Frozen Ground*. Moscow: MAIK Nauka/Interperiodika. 426 pp. (in Russian).
- Roman, L.T. & Kuleshov, Yu.V. 1990. *Forecast of long-term frozen saline ground deformations using time analogy methods*. Moscow: Nauka. 73-83 (in Russian).
- Roman, L.T. & Tsyrendorzhieva, M.D. 1994. Forecast of frozen ground deformation using the temperature-time analogy method in punch tests. *Vestnik (Bulletin) of Moscow State University. Geological Series 1*: 19-23 (in Russian).
- Roman, L.T. & Volokhov, S.S. 1994. Applicability of the stress-time analogy method for forecasting frozen ground deformation in various test types. *Geology Part II*: 134-139. Moscow: Moscow State University (in Russian).
- Tsyrendorzhieva, M.D. & Roman, L.T. 1994. Forecast of frozen ground deformation using the temperature-time analogy method in punch tests. *Vestnik (Bulletin) of Moscow State University, Geological Series 18-25* (in Russian).
- Tsytovich, N.A. & Vologdina, I.S. 1936. *Laboratory Research of Frozen Ground Mechanic Properties*. Moscow: USSR Academy of Sciences. 83 pp. (in Russian).
- Urzhumtsev, Yu.S. 1982. *Forecast of Long-Term Resistance of Polymer Materials*. Moscow: Nauka. 222 pp. (in Russian).
- Velli, Yu.Ya., Karpov, V.M., & Ivanov, B.N. 1966. The results of field and laboratory research of adfreeze forces of frozen ground. *Works of a meeting-seminar for exchange of experience of construction under severe climatic conditions*. Vorkuta: Izd. Krasnoyarskogopromstroy NIIproekta (in Russian).
- Vyalov, S.S. 2000. *Frozen Ground Rheology*. Moscow: Stroyizdat. 464 pp. (in Russian).

- Vyalov, S.S. 1978. *Rheological Basics of Ground Mechanics*. Moscow: Vysshaya Shkola. 447 pp. (in Russian).
- Vyalov, S.S. 1959. *Rheological Properties and Bearing Capacity of Frozen Ground*. USSR Academy of Sciences. 190 pp. (in Russian).
- Vyalov, S.S., Pekarskaya, N.K., & Maksimyak, R.V. 1970. On physical essence of deformation and destruction processes of clayey ground. *Beddings, Foundations and Ground Mechanics* 1: 7-10 (in Russian).

Changes in the Areas of Thermokarst Lakes in the Territory of the Bovanenkovo Field (Yamal) over the Last 20 Years

G.S. Sannikov

Promneftegazekologiya Geoecological Company, LLC, Tyumen, Russia

Abstract

Using cartometry, changes in the dimensions of thermokarst lakes located in the territory of the Bovanenkovo oil and gas condensate field (Central Yamal) were conducted for the last 20 years. The resulting measurements revealed a small but stable decrease in the areas of thermokarst lakes as well as a small increase in their number at low elevations.

Keywords: cartometry; exogenic processes; morphological analysis; thermokarst lakes.

Introduction

There is a great interest in the reaction of permafrost to contemporary global climate changes. This issue is examined in a wide range of works (Pavlov & Malkov 2005, Vasilev et al. 2008, Pavlov 2008). Geocryologists still do not have one common point of view on the nature of changes in the properties of permafrost. One of the indicators of the changes is the dynamics of contemporary exogenic relief-forming processes in the cryolithozone. At the same time, the most indicative process is that of thermokarst (i.e., thawing of ground ice with the formation of concave landforms at the surface). Changes in the areas of thermokarst lakes were assessed earlier (Bryksina et al. 2006, Kravtsova & Bystrova 2009, Smith et al. 2005). However, such investigations were not conducted on a large scale in the zone of continuous permafrost.

To evaluate the dynamics of thermokarst on the territory of the Bovanenkovo field, the author employed the method of morphological analysis of the relief. This paper describes the main points of the method and presents verification of its validity for the territory of the Bovanenkovo oil and gas condensate field located on the Yamal Peninsula.

Geology and Geomorphology

The key research site, located at the western Karskiy megaslope in the central part of the Yamal Peninsula, stretches from the Seyakha River in the south to the middle reaches of the Yunetayakha River in the north. Geomorphologically, we can single out the surfaces of a floodplain (the lower altitude level with the absolute height of 0.5–8.7 m) and the surfaces of the 3rd marine terrace (the upper altitude level, the absolute height is 23–32 m). The floodplain and the 3rd marine terrace are interconnected with a broad stretch of slopes, the steepest gradient of which does not generally exceed 5–6°.

The upper part of the section is represented by the marine sediments of the Middle and Upper Pleistocene: the Salekhardskaya suite and the Kazantsevskaya suite (Lazukov 1970). It is also represented by alluvial sediments as well as alluvial and marine sediments, all of which relate to the Upper Pleistocene and the Holocene. Lithologically, these layers are interbedded with clays, silty clays, silts, and silty sands. The characteristic peculiarity of the Upper Pleistocene marine sediments lies in the fact that they contain thick ground ice deposits at depth intervals from 2–5 to 8 m from the surface.

The permafrost in the territory is characterized by temperatures ranging from -6 to -9°C, typical depth of seasonal thawing equal to 0.3–0.8 m, and various cryogenic structures of the seasonally thawed layer and the underlying permafrost.

The most characteristic exogenic processes taking place on the territory of the Bovanenkovo field are thermokarst, frost cracking, solifluction (slow and rapid), thermal erosion, thermal denudation, cryoplanation, and cryogenic heaving. Thermokarst and cryogenic heaving more often occur at the lower altitude levels, while cryoplanation, thermal erosion, and thermal denudation more often take place at the upper altitude levels. Frost cracking and solifluction occur at both levels of relief, although their characteristic manifestations on various surfaces may differ considerably.

Morphological Analysis of the Intensity of Exogenic Relief-Forming Processes

To determine the intensity of exogenic relief-forming processes at the key research site, we employed the method of morphological analysis. As there is still no clear concept of the term “morphological analysis” in earth sciences, the author considers it necessary to define what is meant by this term in the given paper.

The term suggests that the morphological analysis makes it possible to determine the inner content of an object and the processes ongoing within it, based on the study of the form of the object (a rock fragment, a living organism, etc.). In geomorphology the morphological analysis makes it possible to establish the origin, the age, and the developmental history of a certain landform, based on research into its outlines as well as its length and cross profiles.

One of the ways to use the morphological analysis is to evaluate the dynamic component of the relief. At the same time, it should be considered that the contemporary relief serves as an “instant photograph” that reflects what was ongoing in the past, what processes were forming the relief, and how they will develop in the future. The present work is devoted to the analysis of such “photographs” belonging to different times.

Thus the term “intensity of morphological analysis” will mean the evaluation of the intensity of contemporary exogenic processes, based on the study of the morphological and morphometric characteristics of the landforms existing on the research territory, and on the study of their spatial distribution.

At the first stage of the research on the key site, we made a morphological analysis of the stability of the Bovanenkovo field's relief, based on a topographic map with a scale of 1:100,000. The method of this research was described earlier (Sannikov 2010). In this paper, we will outline the main principles of the given research.

To characterize the intensity of contemporary exogenic processes ongoing on the territory of the Bovanenkovo field, we selected the following major characteristics: hypsometric level, area covered with lakes, and the density of morphological elements (lake basins). These parameters were selected for the following reasons:

- 1) The lakes are distributed all over the research territory.
- 2) The irregular distribution of lake basins across the area makes it possible to determine the reasons for this irregularity.
- 3) The diversity of lake forms and dimensions represents the result of the different impacts of exogenic processes and their nature and intensity.

The data of the parameters were calculated on a regular 2x2 km grid (4 km²). The choice of such an area was preconditioned by the size of the largest lakes belonging to the research site (if the area of the square were smaller, the largest lakes would occupy its entire area). Thus the size of the square is the smallest among the possible ones.

The coefficient reflecting the share of the area covered with lakes was estimated according to the formula:

$$K_l = S_l / S,$$

where S_l – the area of lake basins within a square, S – the area of the square.

The density of morphological elements (the horizontal dissection and the relative density of contours) (Simonov 1999, 2005) was estimated according to the formula:

$$K_{hor.dis.} = N / S,$$

where N – the number of lake basins within a square. The dimension of this coefficient is 1/km².

After these coefficients were calculated and the squares were colored according to their values, we drew morphometric maps of the research site (Fig. 1).

As a result, the research territory was divided into areas with different stability. The method of this division and the parameters according to which we assessed the degree of the relief stability at various areas were also described by the author in the previous work devoted to this topic (Sannikov 2010). We should only note here that the following statement serves as one of the conclusions of this research: uplands represent relatively stable areas and the changes in surface topography occur only around large lake basins. More significant changes are typical within low floodplains that are characterized by high degree of horizontal dissection of the relief.

At the second stage of the research, we made the same measurements based on the air photographs from 2003 and on the photographs made from the Quickbird and GeoEye satellites in 2009 (with a spatial resolution is 0.6 m). For some areas we evaluated the actual change in the forms

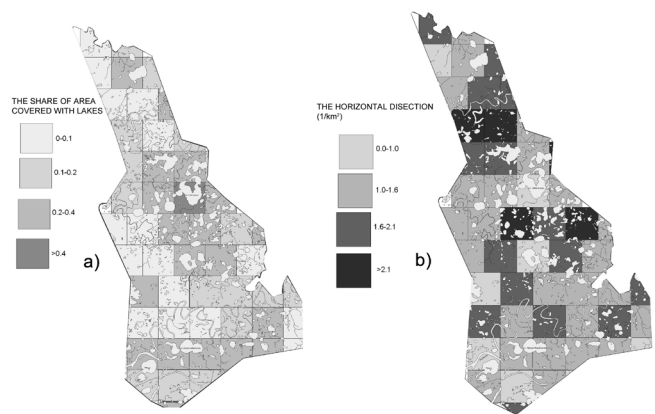


Figure 1. Maps of the research site showing the amount of area covered with lakes (a) and the length dissection (b).

and dimensions of thermokarst lakes that took place in the periods of 14 and 6 years. The periods cover, respectively, the time between the last measurements using the topographic maps at a scale of 1:100,000 and the dates when the air and satellite photographs were made. As a result, we accomplished 3 tasks: 1) we verified the methodology suitable for the morphological analysis with the use of satellite photographs; 2) we assessed the accuracy of the prediction based on the results from the study of topographic maps through the specification of the outlines of indicative landforms; and 3) we estimated the change in the area of thermokarst lakes that took place for periods of 14 and 6 years.

The next step of the research was to estimate the changes in the area of lakes at the key site for the period of 20 years (1989–2009). The digitized shorelines of lakes from the maps and from the photographs were superimposed on each other and differences between them were measured by means of the MapInfo GIS environment.

Analysis of the maps revealed some regularities in the dynamics of the development of the lake shorelines within the research site. The regularities are described in the following section.

Results

When comparing cartogram pairs (the maps showing the amount of area covered with lakes and the density of morphological elements) made on the basis of each data source, we observe that the values of the coefficients in the squares do not coincide. In other words, the squares with a high K_l (share of the area covered with lakes) have a low coefficient of horizontal dissection ($K_{hor.dis.}$), and vice versa. The reasons for this phenomenon are rather obvious. A great number of small lakes can be located within a square, but this does not result in a high coefficient of the area covered with lakes. At the same time, large water bodies may have an area comparable to that of a square. The correlation coefficient equaling -0.2 indicates a weak inverse relationship (according to the Chaddock scale), and most probably it indicates an almost absolute absence of any relationship between these two parameters (Simonov 1999).

The next stage of the research, after we superimposed two sequential maps on each other, was to superimpose

Table 1. The K_1 and $K_{hor.dis.}$ values at different geomorphological surfaces

Geomorphological surface	Predominant values of K_1		Predominant values of $K_{hor.dis.}$	
	Source	Value	Source	Value
Fragments of the 2 nd and 3 rd marine and lagoon-marine terraces	Topo 1989	0.0-0.1.	Topo 1989	1.0-1.6.
	AFS 2003	0.0-0.1.	AFS 2003	1.0-1.6.
	Kosmo 2009	0.0-0.1.	Kosmo 2009	1.0-1.6.
Surfaces of the hasyrey model	Topo 1989	0.0-0.1.	Topo 1989	>2.1
	AFS 2003	0.0-0.1.	AFS 2003	1.8-2.1.
	Kosmo 2009	0.0-0.1.	Kosmo 2009	1.8-2.1.
Slopes	Topo 1989	0.0-0.1.	Topo 1989	1.6-2.1.
	AFS 2003	0.0-0.1.	AFS 2003	1.6-2.1.
	Kosmo 2009	0.0-0.1.	Kosmo 2009	1.6-2.1.
Low and the middle floodplain	Topo 1989	0.1-0.2.	Topo 1989	1.6-2.1.
	AFS 2003	0.2-0.3.	AFS 2003	1.6-2.1.
	Kosmo 2009	0.2-0.3.	Kosmo 2009	1.7-2.2.
High floodplain	Topo 1989	0.2-0.4.	Topo 1989	1.0-1.6.
	AFS 2003	0.3-0.4.	AFS 2003	1.0-1.6.
	Kosmo 2009	0.3-0.4.	Kosmo 2009	1.0-1.6.

the boundaries of geomorphological areas from the morphometric maps. The results from the analysis of the superimposed maps are presented in Table 1.

As shown in Table 1, the surfaces that are most covered with lakes belong to the floodplain areas. The data presented in Table 1 are similar to those of Romanenko (1999). Meanwhile, we can see that the horizontal dissection of the floodplain is small in comparison with the surfaces of alases and its value is close to the same parameter as for the interfluvial surfaces.

If we consider Table 1 from the perspective of the change in the examined morphometric coefficients that occur over time, we will see that it is very small. The increase in the coefficient of the area covered with lakes and in the coefficient of horizontal dissection at the floodplain levels should be regarded as the only significant trends. This indicates that these geomorphological levels are the most active. We did not observe any considerable trends for the change in coefficients of the other parameters.

Changes in Area of Thermokarst Lakes

To verify the accuracy of the morphological analysis of the intensity of cryogenic morphogenesis, we studied the change in the form and dimensions of the shorelines of thermokarst lakes located within the key research site. For this purpose, these shorelines were digitized in the MapInfo environment and, further, they were superimposed on each other. It should be mentioned that we considered only significant displacements of the shorelines when quantitatively processing the changes that took place. The displacement by 10 m was considered significant in a given observation, which corresponds to 0.1 mm on the analyzed material having the smallest scale of a topographic map (1:100,000).

The measurements showed that:

- 1) The decrease in areas of large lakes of watersheds was statistically significant. On average, the general decrease made up 7% or approximately 7 km². Similar data on the evolution of large thermokarst lakes in Southern Yamal were reported by Kravtsova & Bystrova (2009).
- 2) At the same time, the area of small and average lakes increased on the surface of the floodplain level. The general increase made up about 5% or about 1 km².
- 3) A slight increase is observed in the number of lakes. Besides, new lakes develop mainly on low geomorphological levels as well as in linear depressions covered by earth flows.
- 4) The formation of new lakes of the technogenic genesis was observed irrespective of the geomorphological surface. The lakes were formed due to the development of flooding processes and due to thawing at the places of technogenic disturbances (the repeated use of vehicular transport or drilling operations). The area and dimensions of such lakes are small, while the period of their existence covers a few years.

The results of cartometric investigations presented above show that the processes of thermokarst and of thermal abrasion that determine the lake growth are currently active only at low hypsometric levels. At the same time, these processes are inactive on watersheds, while the landforms developed from them earlier are in the state of degradation. The rate at which thermokarst forms increase or decrease is relatively low in most cases.

The process of the gradual decrease in the area of a thermokarst lake may be observed as an example for a nameless lake located on the rear surface of the 3rd marine terrace. Figure 2 shows that there is no significant difference between the positions of the shoreline in 1989 and 2003. However, the shoreline retreated by more than 30–35 m within the period from 2003 to 2009. The extent of the retreating area is about 350 m. A group of gas wells is presently located at the shore of this lake. Nevertheless, the reason for the decrease in the lake's area is not the anthropogenic factor, as neither the site with the well cluster nor the road blocked the flows of the runoff into the lake.

In Figure 2, we can see the position of the lake's shorelines drawn on the basis of the data collected for different years. The changes can be caused by thaw slumps at the areas indicated by the arrows (Leybman & Kizyakov 2007). It is at these areas that the exposed shore is relatively elevated above the water boundary, and therefore thaw slumps may

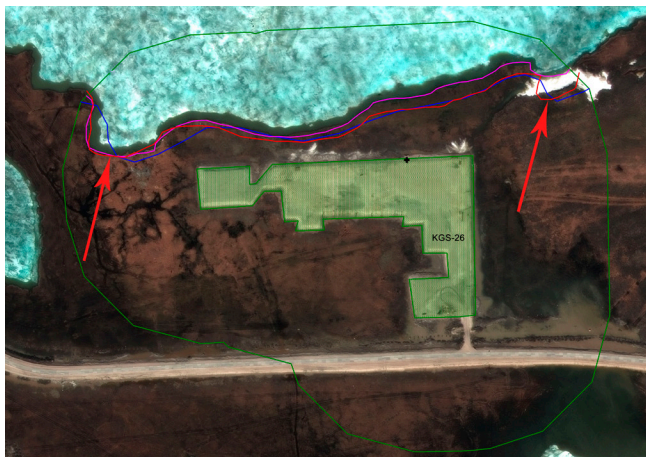


Figure 2. The position of the shoreline for different years. for the nameless lake located in the vicinity of site KGS-26 Blue – 1989, red – 2003, purple – 2009. The arrows indicate the areas of the development of thermal destruction processes.

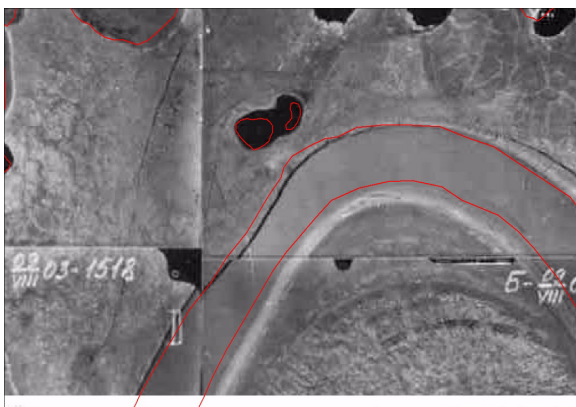


Figure 3. The merging of two small lakes into one lake. The red lines mark the lakes' boundaries in 1989. Image from AFS 2003.

occur there. As a result, the masses of thaw slumps that went into the lake may slightly alter the contours of the shoreline

The reverse process (the merging of two or more small lakes into one larger lake) is also ongoing locally on the low floodplain characterized by a small increase in the number of small lakes (Fig. 3). Such a process becomes possible when shores are actively migrating by thermal abrasion and thermokarst. However, this process occurs extremely rarely and is observed only on the low floodplain of the Seyakha River.

Conclusions

The following statements may be regarded as the main results of the cartometric research performed:

- 1) The method of morphological analysis for the intensity of contemporary relief formation is partly confirmed by its validity in relation to the identification of the areas where modern exogenic processes develop most actively.
- 2) The surfaces of the low floodplain represent the most unstable areas that are the most active in respect to thermokarst development in the territory of the Bovanenkovo oil and gas condensate field.
- 3) Most of the large and average lakes located at the watershed surfaces are characterized by relatively slow

retreat of their shorelines.

- 4) The floodplain levels are characterized by formation of new thermokarst lakes and with a small increase in the areas of old ones.

Further research is required in order to study the reasons for the changes occurring in the shapes of the thermokarst lakes of the Bovanenkovo field. In our view, the processes of change in lake areas indicate the reduction of thermokarst potential on the watershed surfaces. At the same time, the lakes indicate that the remaining deposits of ice-rich sediments in the floodplains are relatively susceptible to thermokarst. Also, we think that these sediments are involved in the thawing process due to changes in the river network in the valleys of the Seyakha and Yunetayakha Rivers.

References

- Bryksina, N.A., Evtyushkin, A.V., & Polishchuk, Yu.M. 2006. Research into the dynamics of the changes in thermokarst landforms with the use of satellite photographs. Abstracts, All-Russia Open Conference. *The Contemporary Problems of Remote Sensing of the Earth from Satellites*, Moscow, IKI RAN, November 13-17, 2006 (http://d33.infospace.ru/d33_conf/vol2/123-128.pdf).
- Kravtsova, V.I. & Bystrova, A.G. 2009. The changes in the dimensions of thermokarst lakes in different regions of Russia over the last 30 years. *Kriosfera Zemli* 13, (no. 2): 16-26.
- Lazukov, G.I. 1972. *The Anthropogene of the Northern Half of Western Siberia* (stratigraphy), M, izd-vo MGU, 322 pp.
- Leibman, M.O. & Kizyakov, A.I. 2007. *Cryogenic thaw slumps on the Yamal and the Yugorsky Peninsulas*. Moscow: Institut kriosfery Zemli SO RAN, 206 pp., 12 color illustrations
- Pavlov, A.V. 2008. *Monitoring of the cryolithozone*. Novosibirsk, Akadem. izd-vo "Geo", 229 pp.
- Pavlov, A.V. & Malkova, G.V. 2005. *Contemporary changes of climate in northern Russia*. Novosibirsk, Akadem. izd-vo "Geo", 54 pp.
- Romanenko, F.A. 1999. *The dynamics of lake basins in Central Yamal*. Erosion Processes of Central Yamal. Edited by A.Yu. Sidorchuk and A.V. Baranova, St. Petersburg, izd-vo Gomelskogo TSNTDI, 350 pp.
- Sannikov, G.S. 2010. The plan form and dimensions of thermokarst lakes as an indicator of the stability of the Yamal relief. The geomorphology theory and its application to regional and global studies. *Chiteniya pamyati N.A. Florensova*. Irkutsk, isd-vo IZK SO RAN, 238 pp.
- Simonov, Yu.G. 2005. *Geomorphology. The methodology for basic research*, St. Petersburg, Piter, 397 pp.
- Simonov, Yu.G. 1999. *The explanatory morphometry of the relief*. Moscow, GEOS.
- Smith, I.C., Sheng, Y., MacDonald, G.M., & Hinzman, L.D. 2005. Disappearing Arctic lakes. *Science* 2005, 308, (no. 5727): 1429.
- Vasilev, A.A., Drozdov, D.S., & Moskalenko, N.G. 2008. Permafrost temperature dynamics of Western Siberia in context of climate changes. *Kriosfera Zemli*, 12, (no. 2): 10-18.

Estimate of Engineering Characteristics of Runoff under Conditions of Limited Data on Hydrometeorological Observations, Northeastern Russia

O.M. Semenova

State Hydrology Institute, St. Petersburg, Russia

L.S. Lebedeva

St. Petersburg State University, St. Petersburg, Russia

I.N. Beldiman

Khotugu Oruster (the North Rivers), Yakutsk, Russia

Abstract

In cases where a shortage of observational data is combined with considerable environment change, the methods for estimating runoff characteristics using the statistical approach of extrapolating observational data may yield incorrect results. The deterministic-stochastic (DS) modeling approach is suggested as an alternative that combines a joint application of two models: the “Hydrograph” deterministic hydrological model and the Stochastic Weather Model (SWM). This paper presents the results of DS-modeling applied at small watersheds on the upper reaches of the Kolyma River. The observation data of the Kolyma Water Balance Station were employed in the research.

Keywords: runoff characteristics; deterministic-stochastic modeling; “Hydrograph” deterministic model; Kolyma Water Balance Station; permafrost; Stochastic Weather Model.

Introduction

The Russian Northeast might soon become one Russia’s most dynamic regions in terms of economic development. In order to develop rich natural resources, it is necessary to tackle the tasks of geotechnical site investigations and construction. At the same time, the remote and difficult-to-reach Northeast represents the region of Russia that is least represented in the network of hydrometeorological observations.

Many researchers have noted signs of significant environmental changes during the past 20 years. With the shortage or even absence of observational data, the application of methods to estimate runoff characteristics based on the statistical approach of extrapolation of observational data (the Code of Rules...) may become groundless and even hazardous.

The Northeast region is in the permafrost zone, and that location represents the primary factor determining the processes of runoff formation. The change in the state of permafrost ground (for instance, periods and the depth of seasonal thawing) under the influence of climate change may significantly transform the hydrologic regime.

When historical observation data ceased to be representative, the method of deterministic-stochastic (DS) modeling seemed to be the only solution to the problem of obtaining the distribution curves of runoff characteristics for engineering purposes.

It is almost impossible to research the most complicated physical processes determined by the occurrence of permafrost without special observational data. This fact was clearly understood in the USSR, and it was the reason why the remote Kolyma Water Balance Station (KWBS) was constructed in 1948 during the difficult postwar era. All special observations were stopped at the KWBS in 1997 due to the unpopular resolution passed by officials of the Federal Service of Russia for Hydrometeorology and Environmental Monitoring. But despite this, the data of continuous observations at the KWBS collected for more than forty

years still represent a unique source of material for the development and testing of hydrological models (Kuchment et al. 2000, Gusev & Nasonova 2006, Semenova 2010, Lebedeva & Semenova *in review*, Lebedeva & Semenova 2012). These data were also utilized in this research.

Deterministic-Stochastic Modeling in Hydrology

The joint application of two models form the basis of DS-modeling: the deterministic hydrological model and the stochastic weather model (SWM).

The deterministic hydrological model describes runoff formation processes at a watershed based on physical principles. The algorithms of the deterministic model represent a mathematical description of the processes of the hydrologic cycle with different degrees of detail and conceptualization.

The stochastic weather model provides meteorological input for the deterministic hydrological model. The stochastic weather model helps to generate the spatio-temporal images of the weather within a river basin.

The DS-modeling has the following operational algorithm:

- 1) Implementation of the deterministic model in the given basin. It includes assessment of the hydrological model parameters, modeling of runoff hydrographs, and assessment of the effectiveness of the estimates by comparing the estimate and observed runoff values.
- 2) Evaluation of the parameters of the stochastic weather model based either on daily meteorological observations of precipitation, temperature, and air humidity at the weather stations located in the given basin or on their estimated values.
- 3) Stochastic modeling of the daily meteorological data for any period of time (e.g., 100–1000 years) with the help of the SWM.
- 4) Modeling of runoff hydrographs for the given period of time (100–1000 years).

5) Construction of curves showing the distribution of maximum, minimum, and other runoff characteristics for the given period of time (100–1000 years).

Thus the DS modeling output may have an unlimited series of hydrological data that allow the determination of all the necessary characteristics of the annual, maximum, and minimum runoffs.

The Deterministic “Hydrograph” Model

The deterministic “Hydrograph” hydrological model represents a mathematical system with distributed parameters. It describes runoff formation processes in basins with various physical and geographical characteristics. It was developed under the guidance of Professor Yu.B. Vinogradov. The structure and contents of the “Hydrograph” model are thoroughly described in a monograph by Vinogradov (1988) and in a textbook by Vinogradov & Vinogradova (2010).

The “Hydrograph” model describes all the processes of runoff formation that form the above-ground hydrologic cycle. A diagram of the model is presented in Figure 1.

The network meteorological information, which is composed of the daily values of air temperature, air humidity deficit, and precipitation layer, is used as meteorological input to the model.

The main parameters of the model are the physical properties of the landscapes that may be observed in nature and are classified according to the types of soil, vegetation, and other characteristics. They also may be modified in case of changes in the properties of the basin’s landscape. This means that the same sets of model parameters may be applied to estimate the runoff for different basins located within the same landscape and climatic zone. Without hydrological observation data, the parameters are evaluated based on information about the physical and geographical conditions of the basin.

To evaluate the parameters within an investigated basin, researchers single out homogeneous geographical zones called runoff elements (runoff formation complexes) according to which model parameters are systematized. Besides, the entire area of the basin is covered with a hexagonal grid the points of which are the representative points of the established unit area. Such characteristics as height, inclination, slope aspect, and the type of the dominant runoff element are determined for each representative point.

In the process of deterministic modeling, the observed meteorological information is interpolated into a representative point, while during the DS-modeling it is generated by the SWM.

Runoff formation processes are modeled for each representative point. The obtained runoff values are further translated into the basin outlet according to the time lag established for each representative point.

The “Hydrograph” model solves the problem of the heat and moisture dynamics in a soil column, which is absolutely necessary when utilizing it in permafrost areas. The soil is divided by depth into a certain number (3–20) of estimated layers (ESLs) that are normally, but not necessarily, identical and equal to 0.1 m. The model parameters are distributed both vertically (soil column) and horizontally (system of representative points).

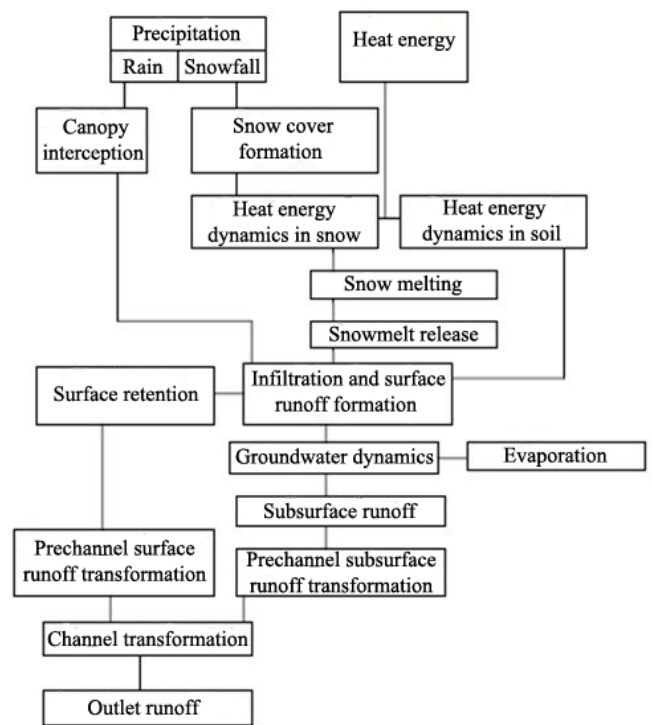


Figure 1. Diagram of the “Hydrograph” model.

The energy and moisture balance is calculated for each ESL within the estimated time interval (i.e., the temperature and moisture of the ESL as well as its thawing and freezing depths). The example estimates of active layer dynamics for the various KWBS landscapes and the comparison of their results with the observed data may be found in the publication by Lebedeva & Semenova (2012).

The “Hydrograph” model considers the heterogeneous distribution of the snow cover on the basin’s territory as well as the inclination influence on many hydrometeorological processes.

The model output is the continuous runoff hydrograph in the outlet for a necessary number of years. At the same time, the variable states of soil and of snow cover are estimated.

The results of the “Hydrograph” model application both to runoff hydrograph estimates and to estimates of the variable states of snow cover and soil in the permafrost area of Russia (Semenova & Vinogradova 2009, Semenova 2010, Vinogradov et al. 2011, Lebedeva & Semenova *in review*) and of Canada (Pomeroy et al. 2009) indicate that, on the one hand, this model describes runoff formation processes thoroughly enough, while, on the other hand, it has the robust algorithm and the possibility to assess its parameters based on data about the physical and geographical conditions of a basin.

The Stochastic Weather Model

The stochastic weather model was developed by a group of researchers under the guidance of Professor Yu.B. Vinogradov (Vinogradov 1988, Vinogradov & Vinogradova 2010).

The model makes it possible to generate daily meteorological values at the given regular points of a basin both as reproduction of data that do not differ from the

Table 1. Characteristics of the small watersheds.

No	River - discharge site	Basin area, km ²	Mean multi-year water discharge, m ³ /s	Number of representative points	Distance between representative points, km	Mean elevation, m	Number of weather stations (including those within the basin)
1	Ayan-Yuryakh - Emtegey	9560	62	15	29	1140	2(0)
2	Debin - Beliche	3460	30	9	23	880	4(0)
3	Detrin - the mouyh of the Vakkhanka River	5630	47	15	22	920	6(2)
4	Tenke - at 2.2 km above the mouth of the Nilkoba River	1820	21	10	16	930	3(0)

historically observed ones and with artificially determined parameters (e.g., when estimating the runoff under the conditions of a predicted climate change).

The temporal and spatial correlations of the meteorological values as well as their intra-year flow are taken into account in the course of the estimates.

The parameters of the stochastic weather model are evaluated based on the observed series of daily meteorological information of weather stations and, further, they are interpolated into representative points. It is assumed that reliable assessment of the model's parameters requires not less than 25–30 years of observational data.

The system of the model's parameters is conditionally divided into three large groups: annual and daily parameters as well as the parameters of spatial correlation.

The stochastic weather model makes it possible to estimate the extreme values of the meteorological variables that were not monitored during the observational period.

Research Area

Four small basins were selected in the upper reaches of the Kolyma River for the research objectives. Their geographical locations and major characteristics are presented in Figure 1 and Table 1.

The investigated territory is found within the region of the Kolyma Water Balance Station. A brief description of the physical and geographical conditions of the investigated area may be found in Lebedeva & Semenova (2012).

Results of Deterministic Runoff Modeling

The “Hydrograph” model parameters were assessed and corrected based on the KWBS observational data in three stages (Lebedeva & Semenova 2012).

During the first stage, three major types of landscapes were singled out at the KWBS (stone talus [golets], tundra open woodland, and swamp larch open woodland). These are located with certain dependency on the elevation and the slope aspect. The values of the model parameters for each runoff element determined on the basis of the properties of the dominant soil and vegetation types were made more accurate in the course of the modeling of active layer formation.

The runoff hydrographs for the small watersheds of the

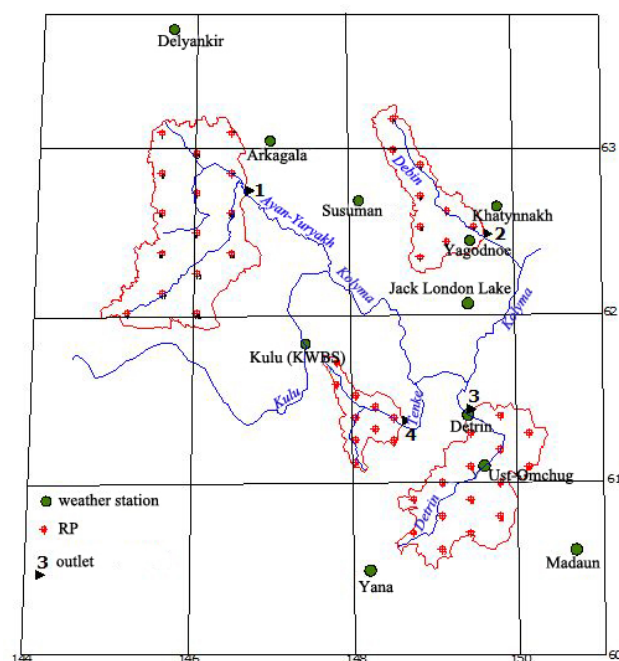


Figure 2. Map of small watersheds in the area of the upper Kolyma with the representative points and weather stations.

KWBS were modeled based on more accurate parameters.

The results produced by modeling of both the soil variable states and runoff hydrographs at the KWBS were acknowledged as satisfactory. For this reason, the listed runoff elements were singled out in the larger investigated basins with the same dependency on the elevation and aspect of the locality. The values of the model parameters corresponding to them were accepted.

The runoff hydrographs with the daily estimated interval were modeled for the period of 1977–1984 for four mountain watersheds located within the continuous permafrost zone of the Kolyma River basin. The statistical analysis of the modeling results is presented in Table 2, while the example of the visual comparison of the estimated and observed runoff hydrographs is shown in Figure 3.

The investigated region has a complex orographical structure that exerts a considerable impact on the precipitation distribution. For this reason, the data given by the weather stations located outside the examined basins (Table 1) often turn out to be unrepresentative, despite the

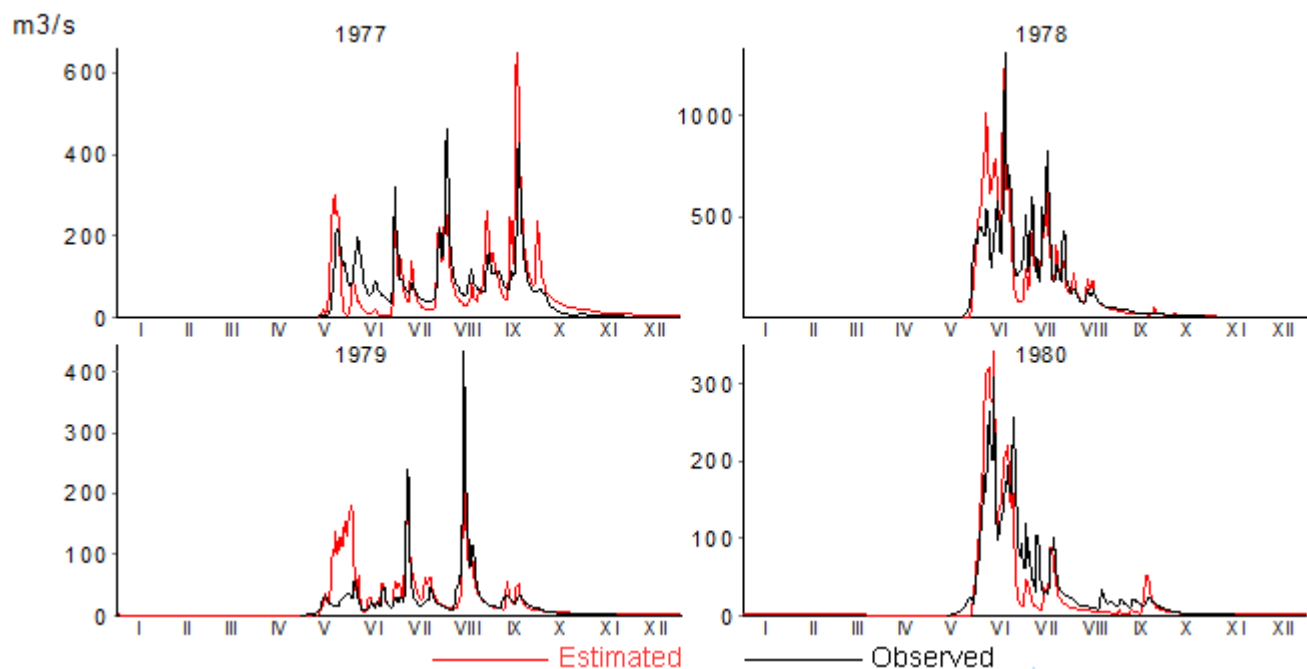


Figure 3. The estimated and observed runoff hydrographs in the upper reaches of the Kolyma basin (1977–1978: the Detrin River, the mouth of the Vakhanka River; 1979–1980: the Tenke River, 2.2 km from the mouth of the Nilkoba River).

seeming proximity. For instance, there is not a single weather station in the Ayan-Yuryakh River basin (the basin with an area of 9560 km²). All the estimates were made based on the Kulu and Arkagala weather stations. In addition to the fact that both weather stations are considerably remote from the watershed, they are also separated by ridges and located at leeward slopes. The authors assume that the deviations of the estimated runoff values from the observed ones are mostly explained by the problem of precipitation interpolation in mountain conditions.

As Table 2 shows, after the modeling the estimated maxima of water discharge are slightly higher than the observed ones. This is presumably explained by the overestimated contribution of the surface component to runoff hydrograph formation linked with the underestimated volume of water infiltration into the ground. The estimated and the observed mean runoff layers are in good agreement with each other. In general, the results produced by the deterministic runoff modeling may be regarded as satisfactory, especially where there is a shortage of meteorological data and where only general information on the physical and geographical conditions of the examined areas is present.

Assessment of Runoff Characteristics with Limited Data or Unrepresentativeness

The main task of hydrology in engineering and construction design is to estimate such runoff characteristics as maximum and minimum discharge and volumes of floods with the given probability. The Code of Rules (CR) SP-33-101-2003 (2004) is currently the only instrument officially accepted in Russia that is designed to make such estimates. The Code's methodology employs various extrapolation techniques of the observed series of data to the specified values of runoff probability. It is proposed to use basin-

Table 2. Statistical criteria of runoff modeling results at the watersheds of the upper reaches of the Kolyma River, 1977–1984.

Basin (river - discharge site)	Q1	Q2	V1	V2
Ayan-Yuryakh - Emtegey	878	1054	234	232
Debin - Beliche	386	412	301	309
Detrin - the mouth of the Vakhanka River	688	740	296	318
Tenke - at 2.2 km above the mouth of the Nilkoba River	248	291	267	311

Q1 and Q2 - the mean observed (1) and the mean estimated (2) maximum water discharge (m³/s); V1 and V2 - the mean observed (1) and the mean estimated (2) runoff layers (mm).

analogues when no observational data are available or when their number is insufficient.

The quality of the hydrometeorological data provided for the country decreased rapidly over the last 20 years. The historical observational series does not reflect the ongoing changes in the hydrologic regime, which relates more to permafrost areas. Besides, there is no tested method of incorporating environmental change (climate and landscape) predictions into hydrological estimates.

The estimated data series formed the basis for the creation of the distribution curves of maximum water discharge in the investigated basins.

As an illustration, three curves characterizing the distribution of maximum water discharge in the Tenke River basin are shown in Figure 4. This basin has the longest data series (53 years) among all the investigated basins.

Thus Curve 1 reflects the observed values, Curve 2 reflects the estimated values of maximum water discharge for the period of 1977–1984 according to the available

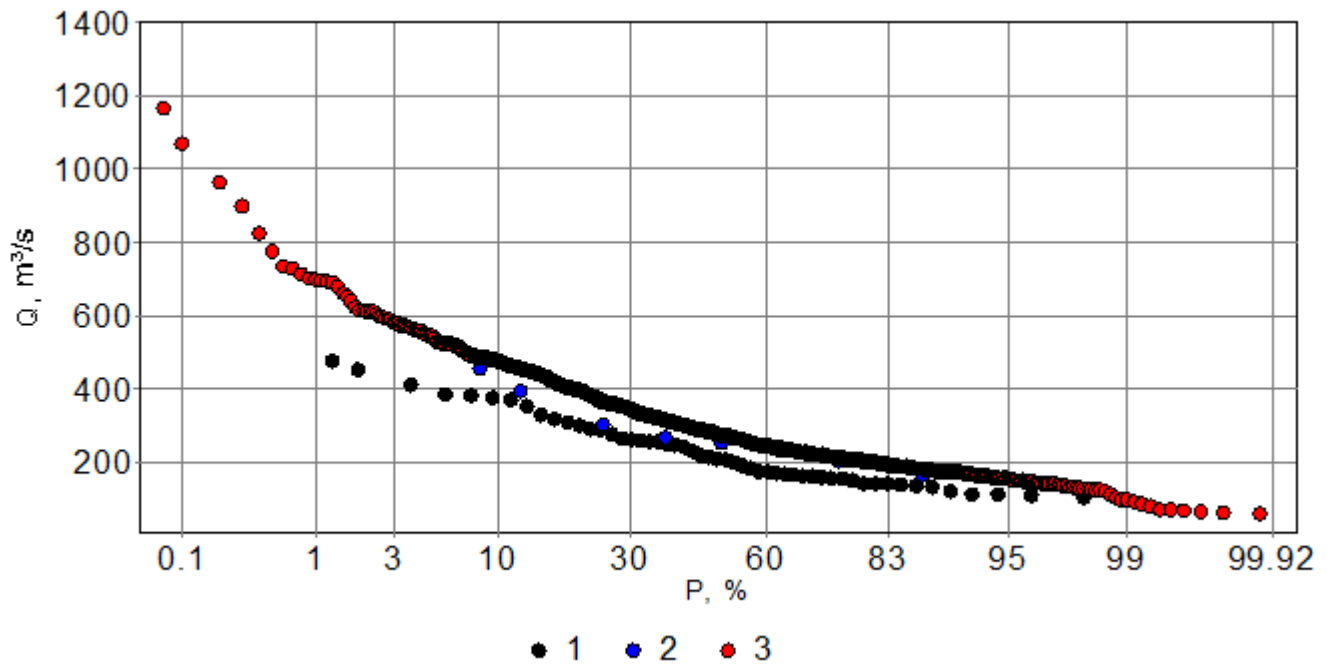


Figure 4. The curves of distribution of the estimated and the observed maximum water discharge (m^3/s) in the Tenke River basin, 2.2 km from the mouth of the Nilkoba River (1, 2, 3 - see text).

historical data of meteorological observations, and Curve 3 characterizes the 1000-year-long series obtained on the basis of DS-modeling. As Figure 4 shows, there is a slight overestimation of the calculated water discharge in comparison with the observed values. However, in general, all three curves correspond to each other.

It should be noted that Figure 4 shows the results of the estimates made on the basis of historical data (i.e., the generated series of meteorological data have the same parameters as the historical observation series). However, a researcher may be faced with a task of evaluation of runoff characteristics under the predicted climate or landscape changes. In the first case, the parameters of the stochastic weather model may be modified according to the predicted climate changes. If landscape changes that may entail a considerable transformation of the hydrologic regime (e.g., forest fires) are expected or probable, the specification of the deterministic “Hydrograph” model parameters makes it possible to consider such cases.

Conclusions

It is necessary to note that Semenova (2009) demonstrated the effectiveness of the application of the DS-modeling method in runoff estimates for small watersheds located in various physical and geographical zones of Russia. The present report demonstrates the DS-modeling results for the basins located in the permafrost zone.

It is shown that the application of the DS-modeling method is possible if there are two models available. The deterministic runoff formation model (such as “Hydrograph”) must possess an adequate description of hydrological processes, while its parameters must have a physical meaning. A stochastic weather model (such as the SWM) must, on the one hand, consider the entire complexity

of meteorological processes (e.g., the temporal and spatial correlation of meteorological variables) and, on the other hand, be universal in application.

In modern conditions, when the historical series of observation data ceases to be representative due to ongoing environmental changes, DS-modeling becomes the only possible solution to the problem of obtaining curves of runoff characteristics distribution for engineering purposes.

Acknowledgments

The authors would like to express their gratitude to the Russian and German Otto Schmidt Laboratory for Polar and Marine Research for assistance in the research within the framework of the grant program in 2009-2011.

References

- Gusev, E.M., Nasonova, O.N., & Dzhogan, L.Ya. 2006. Runoff modeling at small watersheds of permafrost zone based on the SWAP model. *Vodnye Resursy* 33 (no. 2): 133-145 (in Russian).
- Kuchment, L.S., Gelfan, A.N., & Demidov, A.I. 2000. The runoff formation model at watersheds of permafrost zone (the case of the upper reaches of Kolyma). *Vodnye resursy* 27 (no. 4): 435-444 (in Russian).
- Lebedeva, L.S. & Semenova, O.M. (submitted). Permafrost active layer depth as the main factor controlling runoff generation within the upper Kolyma river basin: process analysis and modelling. *Polar Science* (in review).
- Lebedeva, L.S. & Semenova, O.M. 2012. Modeling of active layer and runoff: A case Study from small watersheds, Kolyma Water Balance Station (*this volume*).
- Pomeroy, J., Semenova, O.M. et al. 2010. *Wolf-Creek Cold Regions Model Set-up, Parameterization and Modelling*

Summary. University of Saskatchewan Centre for Hydrology. Report No. 8.

- Semenova, O.M. 2009. Deterministic-stochastic modelling of hydrological extremes in small basins. *Technical Documents in Hydrology* 84: 167–172. Unesco, Paris, SC-2009/WS/11.
- Semenova, O.M. 2010. Experience with modelling of runoff formation processes at basins of different scales using data of water-balance stations. *IAHS publ.* 336: 167–172.
- Semenova, O.M. & Vinogradova, T.A. 2009. A universal approach to runoff processes modelling: coping with hydrological predictions in data-scarce regions. *IAHS publ.* 333: 11 – 19.
- The code of rules on design and construction. The determination of the main hydrological characteristics.* 2004. SP-33-101-2003 (in Russian).
- Vinogradov, Y.B., Semenova, O.M., & Vinogradova, T.A. 2011. An approach to the scaling problem in hydrological modelling: the deterministic modelling hydrological system. *Hydrological Processes* 25: 1055–1073. doi:10.1002/hyp.7901.
- Vinogradov, Yu.B. 1998. *The mathematical modeling of runoff formation processes. The experience in critical analysis.* L.: Gidrometeoizdat, 312 pp. (in Russian).
- Vinogradov, Yu.B. & Vinogradova, T.A. 2010. *Mathematical modeling in hydrology.* M. Akademiya, 366 pp. (in Russian).

Stressed-Deformed State of Trenchless Polyethylene Pipelines Installed at Negative Temperatures

A.A. Serebrennikov, I.G. Lavrov, D.A. Serebrennikov
Tyumen State Oil and Gas University, Tyumen, Russia

Abstract

This paper examines the issues of the trenchless installation of polyethylene pipelines with their bending under negative temperatures. Recommendations are given on the combination of pipe dimensions and their bend radii under different temperatures of the surrounding air. This allows the pipe material to function in the zone of elastic-plastic deformation and to remain below the yield point.

Keywords: negative temperatures; polyethylene pipeline; trenchless technologies.

Introduction

Many countries have extensive experience in the use of polyethylene pipelines in gas transmission and distribution systems. The production of small-diameter tubes in coils enhanced the scientific and engineering investigations aimed at the development of a pipe-laying technology that can reduce the cost of pipeline construction. The advantages of such technology are the reduction of excavation work and an increase in the speed of pipeline installation. This technology is primarily applied to install pipelines based on the principle of cable and drain laying machines. These machines, termed trenchless, eliminate the stages in which a trench is excavated and backfilled. Specifically, the machines with a cutting device are utilized to install pipelines between villages (see Fig. 1).

Coils (Fig. 1, 1) with polyethylene pipes with tubing diameters from 63 to 110 mm are installed on the wheeled cart attached to a tractor. As the cart advances, pipe (Fig. 1, 4) is constantly delivered from the coil to a directing duct (Fig. 1, 3) installed in front of the cutter (Fig. 1, 2) and is laid at the necessary depth. In the course of the laying procedure, the pipes are welded and the coils are replaced with new ones. While moving along the directing duct, a pipe is considerably bent. Therefore, it is necessary to research its stressed-deformed state in order to determine the conditions under which it will preserve its strength properties.

Regulatory documents concerning the conditions of pipe laying specify that this technology cannot be used during

times of negative surrounding air temperature. The current regulatory document, titled “Design and construction of gas pipelines of polyethylene tubes and reconstruction of worn-out gas pipelines,” allows the use of polyethylene with the minimum required strength (MRS) of 8.0 MPa (PE80) and higher. However, its restrictions concerning temperature conditions are copied from the previous regulatory document developed for the pipes of polyethylene PE63. According to this, pipes cannot be laid when the temperature of the surrounding air is below -15°C and they cannot be unwound from the coils under the temperature below $+5^{\circ}\text{C}$. In terms of new materials employed in pipeline installation, the indicated restrictions are unreasonably tough and require verification.

The Institute of Nonmetallic Materials of SB RAS carried out experimental investigations in order to study the behavior of the PE63 and the PE80 polyethylene under low temperatures. The investigations proved that the PE80 polyethylene (unlike PE63) preserves the necessary elastic properties when the temperature decreases down to -60°C . The investigations also proved that it is safe to rigidly fix the ends of the PE80 polyethylene pipes, as the tension in the axial direction arising from the temperature deformations (down to -25°C) will not exceed the ultimate strength. However, there were few investigations on the change of the strength and deformation properties of the PE80 polyethylene bent under negative temperatures.

Thus it is necessary to study the stressed-deformed state of polyethylene pipes when they are bent in order to understand the possibility of the use of trenchless pipe under negative temperatures.

The stressed state of a bend was analyzed based on the method that takes into account the deformation of the tube material in the elastic-plastic zone.

To determine the tension, we used the following dependence:

$$\sigma = E_c (\varepsilon_r + \varepsilon_s + \varepsilon_{\eta}) \quad (1)$$

where E_c is the secant modulus, MPa; ε_r is the relative deformation resulting from pipe bending; ε_s is the relative deformation resulting from the action of a bending moment and the stretching force; ε_{η} is the relative deformation of the change of the cross section shape.

The secant (variable) modulus is the parameter that

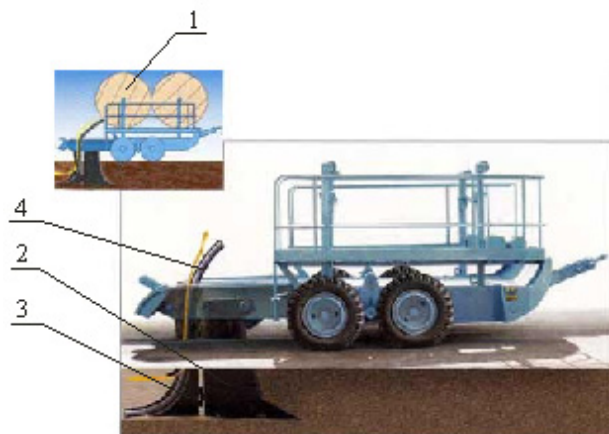


Figure 1. General view of a pipe-laying machine.

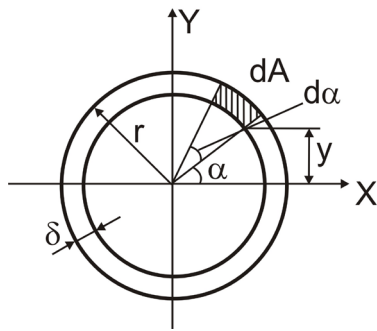


Figure 2. Diagram of the cross section of a pipe. (dA – an elementary area of the cross-section, r – the radius of the pipe, delta – the thickness of the pipe wall).

characterizes the nonlinear properties of the pipe material in the zone of elastic-plastic deformations.

The relative deformations resulting from pipe bending and from the change of the cross section shape are determined in the following way:

$$\epsilon_r = \frac{r}{R}, \quad \epsilon_\eta = \frac{\eta}{R+r}, \quad (2)$$

where r is the outer radius of the pipe (m); R is the bend radius of the pipe (m), eta is the change of the cross section radius (m).

To define the relative deformation (epsilon S), it is necessary to find the internal forces arising in the cross section of the pipe. The internal forces can be determined through the tension at any point by intergration over the cross section area of the pipe wall (Fig. 2) in accordance with the formulas of the stressed state:

$$N_s = \int_A \sigma_s dA, \quad M_s = \int_A \sigma_s y dA \quad (3)$$

After we examined the element of the pipe (with the length dS) the side of which was exposed to the force components (Fig. 3) and made the equilibrium equations, we obtained:

$$\frac{1}{R} \frac{dN_s}{d\phi} + \frac{1}{R^2} \frac{dM_s}{d\phi} = 0, \quad (4)$$

$$\frac{1}{R^2} \frac{d^2 M_s}{d\phi^2} - \frac{N_s}{R} = q,$$

where N_s is the longitudinal force arising when the pipe is bent (H); Q_s is the transverse force (H); M_s is the bending moment along the axis S (H×m); q is the distributed external load (H/m).

After the initial and boundary conditions were determined, we solved the system of the differential equations (4).

To consider the temperature factor, it was suggested to determine the secant modulus based on the following ratio:

$$E_c = \frac{E_t}{1 + b_t \sigma^2}, \quad (5)$$

where b_t is the coefficient that defines the change of the secant modulus depending on the value of deformation, MPa⁻².

We analytically obtained the necessary generalizing dependences of the change in the elasticity modulus (E) and in the yield point (sigma_t) on the temperature factor for the PE80

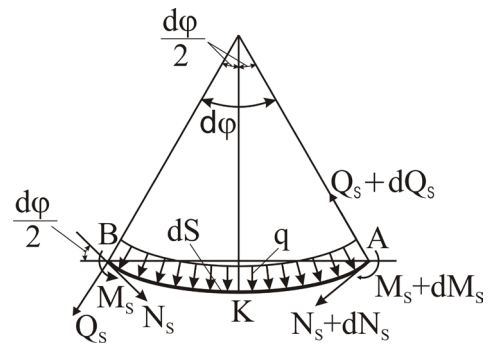


Figure 3. The element of the rod. N_s – the longitudinal force arising when the pipe is bent and dN_s – its increase (H); Q_s – the transverse force and dQ_s – its increase (H); M_s – the bending moment and dM_s – its increase (H×m); q – the distributed load (H/m).

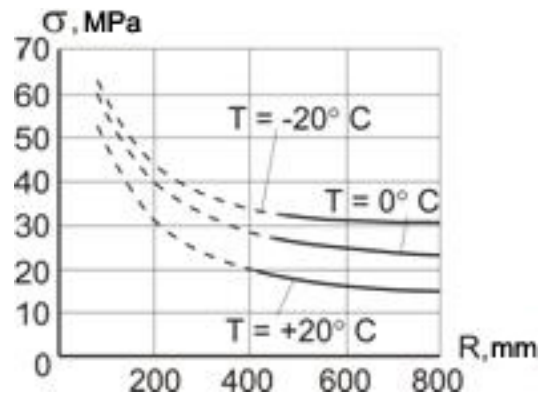


Figure 4. The change of tension under bending of a PE80 polyethylene pipe with the diameter of 63 mm (--- – unacceptable tension; — – acceptable tension).

polyethylene. This was based on the results of investigations carried out in the Institute of Nonmetallic Materials of SB RAS (the validity of the approximation for the range from +20°C to - 60°C makes up 0.97):

$$E_t = E_{20} \cdot \left(-0,6 \cdot \frac{T_t}{T_{20}} + 1,6 \right), \quad \sigma_t = \sigma_{20} \cdot \left(-0,3 \cdot \frac{T_t}{T_{20}} + 1,3 \right) \quad (6)$$

where E_t is the elasticity modulus of the pipe material at the current value of temperature, MPa; E₂₀ is the elasticity modulus of the pipe material at 20°C, MPa; sigma_t is the yield point of the pipe material at the temperature T_t, MPa; sigma₂₀ is the yield point of the pipe material at 20°C, MPa; T_t is the temperature of the surrounding air, °C; T₂₀ is the temperature of the surrounding air equaling 20°C.

The obtained dependences (6) were utilized in ratio (5) to determine the secant modulus and evaluate the found tensions (1).

The solution of the system of differential equations (4) based on the finite difference method for a particular case revealed its precision by comparison with the results of the calculation in the form of Navier-Stokes.

The stressed-deformed state of the pipe wall was calculated depending on the bend radius and on the temperature of the surrounding air for all the standard dimensions of pipes produced in coils by the corresponding factories (diameters are 20, 25, 32, 40, 63, 110 mm).

The example of the calculation results for the pipes with the diameter of 63 mm is presented in Figure 4.

Analysis of the calculation results shows that the tension arising in the wall of a pipe being bent considerably increase when the temperature goes down. This regularity is linked with the elasticity modulus of the material that increases when the temperature goes down.

The calculation results make it possible to recommend the combination of pipe dimensions and its bend radius under different temperatures of the surrounding air that allow the pipe material to function in the zone of elastic-plastic deformations and to remain below the yield point.

In order to verify the key points of the theoretical investigations, we performed the experiments on the determination of the polyethylene pipe deformations under negative temperatures (Serebrennikov & Lavrov 2007).

The indirect evaluation system was applied to research the tension arising in the wall of the pipe under bending. Meanwhile, we assumed that the pipe material will not change its physical and mechanical characteristics when exposed to the bending pressure, if the following conditions are satisfied:

- 1) the ratio of the pipe's bending radius to its diameter after the pipe was exposed to the bending pressure is not less than 20 (SP 42-103-2003); and
- 2) the pipe ovality after removal of the bending pressure does not exceed the maximum acceptable value regulated by State Standard R 50838-95.

The complex of theoretical and experimental investigations proved that it is possible to lay trenchless polyethylene pipes (polyethylene PE80, SDR 11) that are bent under negative temperatures (down to -20°C) with certain restrictions in the bend diameters.

Thus we proved that it is reasonable to correct some points in the regulatory documents, which will increase both the working season and the utilization coefficient of the facilities.

References

- Serebrennikov, A.A. & Lavrov, I.G. 2007. Determination of the acceptable bend radii of the PE80 polyethylene pipes depending on the temperature factor. *Izvestiya vuzov. Oil and Gas* No. 2, pp. 42–45.

Identification, Diagnostics, and Ranking of Geocryological Hazards for Long-Distance Pipelines and Other Linear Structures

D.O. Sergeev, J.V. Khalilova, G.Z. Perlshtein, A.N. Khimenkov, E.M. Makaricheva
Sergeev Institute of Environmental Geoscience Russian Academy of Sciences (IEG RAS), Moscow, Russia

A.N. Ugarov
Extreme Situations Research Center (ESRC), Moscow, Russia

Abstract

Long-distance transport systems are vulnerable to various negative effects from permafrost in variable climate-landscape zones. Some of these effects are caused by the impact of structures themselves on the environment, while others are linked with natural permafrost dynamics. Here the authors develop a flexible classification of geocryological hazards, taking into account static geological and geomorphological conditions, variable climatic and hydrologic impulses, and impacts from engineering activity in areas underlain by permafrost.

Keywords: impact zone; geocryological hazard; highway; monitoring; pipeline; railroad.

Introduction

Geocryological hazard is the risk of negative consequences due to geologic or permafrost-related activity on engineering structures or elements of the landscape. The same geocryological process can entail different magnitudes of risk and various negative effects in variable climate-landscape zones along long-distance transport systems (pipelines, railroads, etc.).

In most areas, geological surveying takes into account this natural variability with special engineering-geological zonation. However, this approach is not effective in permafrost regions because the geocryological conditions change with regional climate trends and with intensive local building activity. Changing conditions are sometimes caused by the engineering structure itself (Sergeev & Khimenkov 2006). Another problem is the different rates of geocryological processes; there is a need to distinguish the slow change of the ground temperature regime from rapid and stochastic thermal erosion and other thermal denudation movements.

The goal is to predict costs for engineering protection during the desired lifetime of transport systems by taking into account natural and human-induced geocryological dynamics.

Identification of Geocryological Hazards

The first step of investigation depends on collecting information about ice-rich ground distribution and identifying geocryological activity in areas where dangerous processes have been evident in the past. Aerial or space photographic surveys allow the identification of sites with actual or potential geotechnical problems. Aerial visual surveys can be most efficient in cases with very rapidly shifting geocryological conditions.

The list of dangerous geocryological processes includes, but is not limited to, thermokarst, thermal erosion, icing, frost heave, ice mounds, and ground movements. The list of dangerous conditions includes ice-rich ground, drainage disturbances, and likelihood of fire.

It is very important to distinguish natural permafrost

dangers from human-induced activity. For example, if gradual change in climate leads to a change of geocryological conditions, this could be apparent after 5–10 years of structure use. On the other hand, inappropriate preventative measures against erosion and improper construction practices could lead to intensive thermokarst after just 1–2 months of the summer (Fig. 1).

Special investigation, monitoring, and modeling allows for identification of sites with active or possible permafrost activity that can affect the engineering structure or landscape properties.

Diagnostics of Geocryological Hazards

Diagnostics are based on the interpretation of landscape structure change during construction and use of the transport system.

At this stage of the investigation, geocryological hazards are linked with the vulnerability of particular elements of the transport system. The vulnerability depends on the rate and intensity of permafrost processes (Koff et al. 2009). Rapid processes complicate the situation because the safety of the transport system requires an immediate management response to the danger. Without modeling and consideration of different circumstances, this response is not always effective (Fig. 1).

Continuous monitoring of hazard data shows the spatial heterogeneity and tendencies of the processes. The distribution of geocryological phenomena along the transport system is heterogeneous due to the tectonic, climatic, hydrologic, and hydrogeologic conditions and tendencies.

The possible influence of geocryological processes on linear infrastructure can be divided into four categories:

- Type
- Intensity
- Extent
- Duration

The type of influence is a consequence of the contact between ground and technical elements (mechanical, thermal, chemical, etc.).

The intensity (level) of influence is characteristic of the



Figure 1. Thermokarst development at the anti-erosion gravel pad. The photo in the bottom right corner shows the same place eight months earlier.

energetics of the process (rate and dimension of phenomena). The estimation of the process activity also takes into account the one-way or cyclical character of the influence.

The extent of the process is defined by the spatial area affected by the dangerous phenomena. This characteristic is not very useful for linear engineering because it is sensitive to the buffer zone dimension selection.

The duration of the geocryological process determines many of the negative consequences for the engineering structure. An intensive short-term process leads to damage similar to a long-term and low-intensity one. The duration of short-term processes may be from seconds to days (e.g., rock falls, landslides, debris flow). Long-term processes may persist up to decades (e.g., permafrost temperature trends due to climate change).

The areas of geocryological phenomena interact with elements of the engineering structure to determine the cause and nature of the negative impact (Sergeev et al. 2010). Figure 2 shows an analysis of the position of the borders of the impact zone.

For parameterization of the numerical models, it is important to consider the technical elements that affect the geocryological conditions. Depending on the physics of the geocryological process, different combinations of models can be used (ground temperature regime, water migration, ground mechanics, etc.). If the sequence of human actions

is known (building operations or temperature impulses in the pipeline), such information can be used with combined modeling to predict the state of the nature-engineering system after a fixed interval of time. Combined models can be developed for typical cross-sections, chosen after expert analysis of a longitudinal cross-section of the transport system (Fig.3).

The goal of this analysis is to detect “weak links” which are sensitive to external disturbance (thermal exchange conditions, climate events, etc.).

Figure 2 and Figure 3 show that each highlighted element in the engineering system influences the environment and changes the geocryological conditions in different seasons. The models take into account these changes. For example, the highway embankment affects the water drainage conditions and leads to pond formation. In summer, the bottom of the pond may have a mean temperature much higher than the soil surface temperature (Perlshtein et al. 2005). In winter, the temperature evolution depends on pond depth and snow drift conditions. There are principal effects that must be taken into account in the ground temperature model.

Different elements of the engineering system can accelerate or decelerate the permafrost change. The most important circumstance is the mobility of the impact zone border during the year. It depends on three fundamental causes:

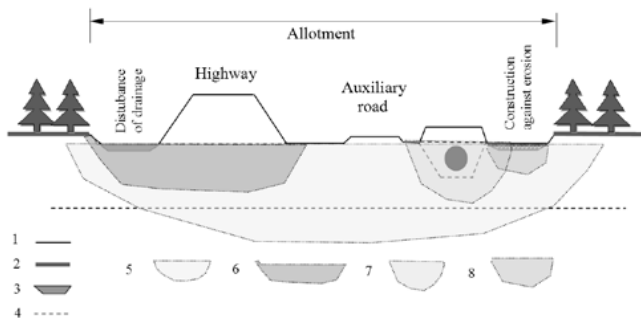


Figure 2. Generalized scheme of cross-section of the nature-engineering system of the pipeline corridor: 1 – Disturbed surface, 2 – Undisturbed surface, 3 – Pond, 4 – Border of rock deposits. Impact zones of: 5 – Corridor in whole, 6 – Highway, 7 – Pipeline, 8 – Engineering protective structure.

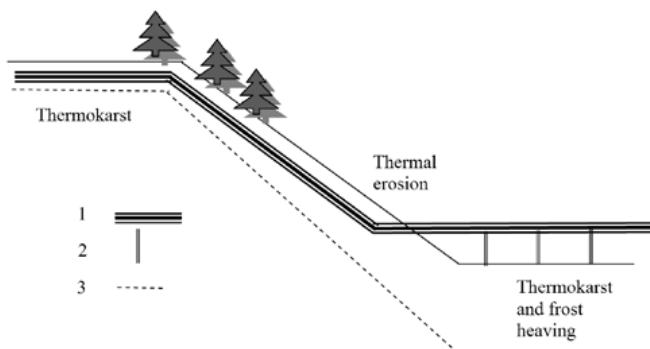


Figure 3. Generalized scheme of longitudinal cross-section of nature-engineering system of the pipeline corridor: 1 – Pipe, 2 – Pile, 3 – Border of rock deposits.

- Human activity (surface disturbance, reclamation, engineering protection operations),
- Climate events,
- Evolution of the geocryological processes that change the common situation.

Analysis of the longitudinal cross-section shows the extent of the activity and the interaction of processes along the structure. For example, a thermokarst in the valley will progress less than in the watershed divide surface, though the total settlement here will be greater (Fig. 3). The settlement amount under the slope will control the erosional activity (Fig. 3).

Detecting the extent of impact zones helps to determine the amount of additional investigation and monitoring work needed. It also helps to conceptualize the modeling areas.

In mathematical models, the static and dynamic factors must be separated. The static factors are geothermal heat flux, relief, and geological conditions. The variable factors are climate conditions, water balance, and surface properties.

The goal of modeling is to provide the necessary information to estimate the probability and intensity of the direct impact of geocryological processes (thermal settlement, frost heaving, etc.) on engineering structures. When impact prediction is impractical (due to a combination of processes), an expert estimate of linear object vulnerability is recommended. Such estimates must be prepared for each stage of the desired lifetime of the plant (prospecting, building, exploitation, reconstruction, liquidation).

The result of the diagnostics is a description of possible interaction between the elements of the nature-engineering system.

Ranking of Geocryological Hazards

Ranking of hazards helps in mitigation efforts and in additional investigations (observing, modeling, sampling, etc.). It also aids in planning of additional protective engineering structures.

In practice, the universal risk criteria are impractical. The ranking can be prepared with different priorities: safe engineering, resource optimization, and environmental preservation (Leshinsky et al. 2006, Sergeev et al. 2009). For each priority, the set of criteria is variable. These criteria include the proximity of the geocryological phenomena of the engineering structure (“danger category”), the impact intensity (“areas, dimensions, and frequency of phenomena”), the complexity of the impact (superposition of geocryological processes), the situation stability (positive or negative trend in process characteristics values), the impact duration, and the effectiveness of previous engineering protection procedures.

Each geocryological phenomenon should be ranked in a way that reflects the actual likelihood of risk, realizing that this could be different from year to year. It is possible to calculate a comparable ranking of different areas by taking into account a common set of ranking criteria. However, this ranking would be specific to individual tectonic-geomorphological provinces.

A ranking of the basic practical recommendations should be developed. This provides the possibility to predict the economic loss due the geocryological process activity.

Conclusion

The presented system approach provides a sequence of investigations for testing the probability of dangerous impacts along a long-distance system with highly variable environmental conditions.

A potential approach for developing and implementing this method is the identification of the processes and circumstances more or less likely to exhibit stochastic behavior. This will help in selecting the site and areas of focus for detailed modeling or direct monitoring.

Acknowledgments

This investigation was completed following Program 4p of the Russian Academy of Science Presidium. Special thanks to investigators of the Institute of Physical and Technical Problems of the North SB RAS.

References

- Koff, G.L., Chesnokova, I.V., Bogomolova, T.V., & Zaigrin, I.V. 2009. Experience in engineering geological typification and mapping of geoenvironmental risk factors (by the example of “East Siberia-Pacific Ocean” oil pipeline route). *Geoecology. Engineering geology, Gidrogeology, Geocryology* №2: 172-179 (in Russian).

- Leshinsky, V.B., Mikheev, A.A., Sergueev, D.O., Sergeev, O.N., Startzev, Y.P., & Yavelov, A.V. 2006. Working-up and approbation of the method of environmental managing of gas-main pipelines construction. *Geoecology. Engineering geology. Hydrogeology. Geocryology*, #3: 264-273 (in Russian).
- Perlshtein, G.Z., Pavlov, A.V., Levashov, A.V., & Sergeev, D.O. 2005. Non-temperature factors of the heat exchange between active layer and atmosphere. *Proceedings of the III Conference of geocryologists of Russia*, Moscow, Russia, 1-3 June 2005, MSU: 86-91 (in Russian).
- Sergeev, D.O. & Khimenkov, A.V. 2006. Recommendations towards evaluation for harmful consequences caused by geocryological processes induced by changing climate. *Proceedings of the Arctic Regional Center, Volume IV, FEB RAS Marine Investigations in the Arctic*, Vladivostok, Dalnauka: 69-75 (in Russian).
- Sergeev, D.O., Khimenkov, A.V., Stanilovskaya, Y.V., & Antonov-Druginin, V.P. 2010. Some Aspects of Permafrost Hazards Evaluation. *Extended Abstracts to the Proceedings of the 11th Congress of the IAEG. Geologically Active*. 5-10 September 2010 Active, Auckland, Aotearoa, New Zealand: 193.
- Sergeev, D.O., Perlshtein, G.Z., Khimenkov, A.V., Tipenko, G.S., & Pystina, N.B. 2009. Identification and quantitative assessment of permafrost hazards to land resources in the central Part of Yamal Peninsula. *Geological Engineering Problems in Major Construction Projects. Proceedings of the International Symposium and the 7th Asian Regional Conference of IAEG*: 526-527.

Water in the Form of Spatially Ordered Droplets Near the Vapor-Water Boundary

A.V. Shavlov, V.A. Dzhumandzhi, S.N. Romanyuk
Earth Cryosphere Institute, SB RAS, Tyumen, Russia

Abstract

This paper describes the results obtained during laboratory measurements of the geometric and electric parameters of spatially ordered droplet structures near the surface of heated water. The possibility of the formation of similar structures in atmospheric clouds and fogs was examined. The influence of droplet ordering on the shear viscosity of clouds was estimated.

Keywords: charge; cloud; droplet; shear viscosity; water.

Introduction

Recent research (Shavlov & Dzhumandzhi 2010) discussed a supposition that charged water droplets and ice crystals contained in clouds and fogs may form spatially ordered structures and influence the physical and mechanical properties of the atmosphere. Specifically, they may influence the velocity of its heat and mass transfer and, as a consequence, the dynamics of the cold accumulation (or discharge) in the Earth's cryosphere. This assumption was based on the laboratory observation over the formation of a droplet cluster that has a single-layer, spatially ordered structure near the surface of the heated water (Fedorets 2004). To define the actual role of such formations in the atmosphere, it is necessary to comprehensively examine them in the laboratory. The research goal was to carry out a laboratory investigation of the physical properties of a droplet cluster (geometric characteristics, electric charge of droplets, viscosity of a cluster) and to estimate the distribution of the ordered droplet structures in the atmosphere.

Results

In order to obtain a droplet cluster, we subjected a thin water layer to pointed heating (Fedorets 2004). The droplet cluster was registered with a digital camera. The geometric characteristics of the droplets were determined based on the number of pixels in the video. The error made up $\pm 0.5\text{px} = \pm 2\mu\text{m}$. The temperature of the water surface was determined with an error of $\pm 1/-10^\circ\text{C}$.

Figure 1 shows the typical view of a cluster. The droplets are spatially arranged in the form of a flat hexagonal grid. The rounded shape of the cluster indicates that it has a surface tension. Figure 2 shows the dependencies of the distance between the droplets L of the diameter D and of the levitation height of the droplets above the water surface H under various temperatures T . The height H was defined as half the visible distance between the centers of a droplet and its mirror view in the water at the view angle close to the tangent to the water surface. Figure 2 suggests that the sizes of all the droplets increase with the rise in temperature. Meanwhile, the following empirical regularities were established among L , D , H : $D \approx 1,26H$; $L \approx 4,8H$.

The calculation of a theoretical gap value h_0 between the droplets and the water surface as well as the comparison of this value with the experimental gap value h (Fig. 3) rendered it possible to establish that the levitation of droplets above

the heated water surface is underlain by Stokes' mechanism. According to this mechanism, the gravitational force of a droplet is entirely balanced by the force that acts on it from the side of vapor flow rising from the water surface:

$$M \cdot g = 3 \cdot \pi \cdot \eta \cdot v \cdot D \cdot \left(1 + \frac{D}{2 \cdot h_0} \right)$$

where M is mass of a droplet, g is gravitational acceleration, η is vapor viscosity, v is vapor velocity.

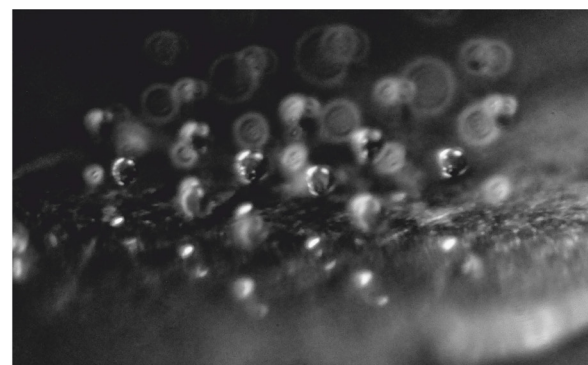
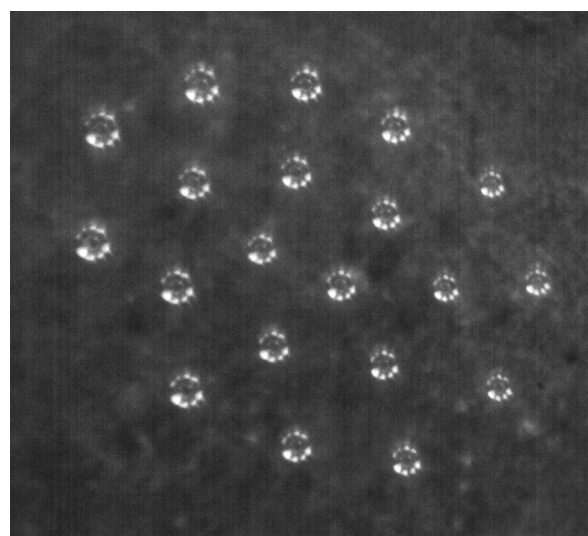


Figure 1. Photograph of a droplet cluster at the view angles of 90° and 30° and under the temperature of 90°C .

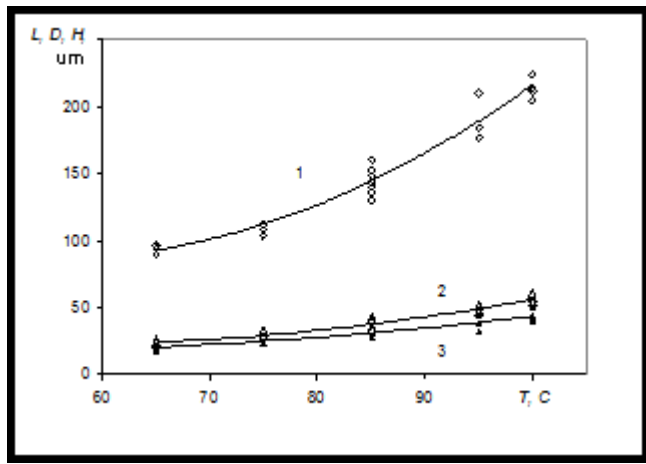


Figure 2. The temperature dependencies of the distance between the droplets L (1), of the diameter D (2), and of the levitation height of droplets H (3)

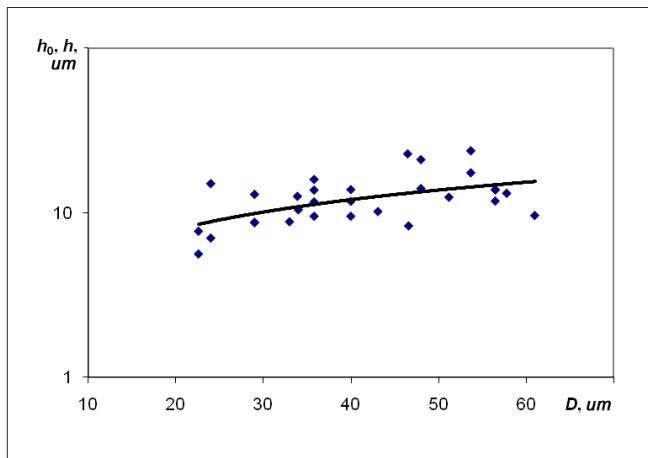


Figure 3. The gap size between the droplet and the water surface depending on the droplet diameter. Solid curve (h_0) - estimate based on the Stokes gravitational equilibrium; marks (h) - results of the experiment.

The droplets of the cluster in the external electric field behaved like positively charged particles; the levitation height of the droplets decreased under the positive potential at the electrode located above the cluster (water surface served as another electrode), while under the negative potential at the upper electrode it increased. In agreement with the formula

$$z = \frac{\Delta h}{h} \frac{Mg}{(1 + 2h/D)eE}$$

the electric charge of the droplets z was estimated in units of elementary charge e based on the relative change of the gap value $\Delta h/h$ between the droplets and the water surface with the external electric field E turned on. Under the water temperature of 95°C , the charge made up $z=1,7 \cdot 10^3$. When the temperature decreased, the charge decreased in proportion to the square of the droplet diameter or in proportion to its surface area. Meanwhile, the charge of the droplets turned out to be independent from the change in the evaporation intensity (condensation) under the changing temperature.

Among the possible mechanisms of the droplets interaction responsible for the spatial ordering of droplets,

the mechanism based on the high-frequency correlation of a volumetric charge in the plasma between the droplets turned out to be the most appropriate (Shavlov & Dzhumandzhi 2010). According to this mechanism, droplets must position themselves at the distance of two Debye radii from each other. This rule applies well to a droplet cluster. Indeed, the theoretical value of the distance between the droplets is determined by the formula

$$L = 2 \cdot \left(\frac{D}{2} + H \right) + 2 \cdot L_D$$

It includes the droplet radius $D/2$ and the thickness of the plasma shell of a droplet that equals H ; L_D – the Debye radius in the vapor.

$$L_D = \sqrt{\frac{\epsilon_0 \cdot k \cdot T}{e^2 \cdot n}}$$

After we substitute the theoretical value of the concentration n and the empirical correlation $D \approx 1,26 \cdot H$ in the formula

$$n = \frac{2kT\epsilon_0}{e^2 H^2}$$

we obtain $L=4,7 \cdot H$. Meanwhile, the experiment suggested the dependency (see above) $L=4,8 \cdot H$ in which the numerical coefficient differed from the coefficient in the theoretical dependency by only a few percent.

To measure the viscosity coefficient in the droplet cluster, a viscous flow was activated in it. For this purpose, the symmetry axis of the cuvette with the heated water was slightly declined from the vertical position. The flow with the maximum relative velocity in the outer droplet layer developed in the cluster (Fig. 4). The flow velocity rapidly decreased down to zero, as the number of the droplet layer increased toward the center of the cluster. The viscosity coefficient η (Fig. 5) was estimated based on the Navier–Stokes equation for a flat one-dimensional stationary flow of incompressible fluid under the shear stress applied to the outer layer:

$$\frac{d}{dx} \left(\eta \frac{dV}{dx} \right) = -\sigma_0 \delta(x - x_1)$$

Its integration yields a formula

$$\eta \frac{dV}{dx} = \sigma_0$$

indicating that the viscosity is in inverse proportion to the gradient of the shear velocity, where σ_0 is shear stress, V is shear velocity, and $\delta(x-x_1)$ is the Dirac delta function. Figure 5 suggests that the shear viscosity of the droplet cluster layers rises as the layer number increases. The viscosity coefficient value in the fourth layer is already approximately ten times higher than the viscosity of the air η_0 surrounding the cluster. The viscosity coefficient η depends on the relative movement velocity of the layers, which is typical of non-Newtonian fluid.

The results achieved in the investigation of the droplet clusters were applied to assess the distribution of similar structures (not only two-dimensional but also three-dimensional) in atmospheric clouds and fogs. For this purpose, the value of the droplet concentration in a cloud

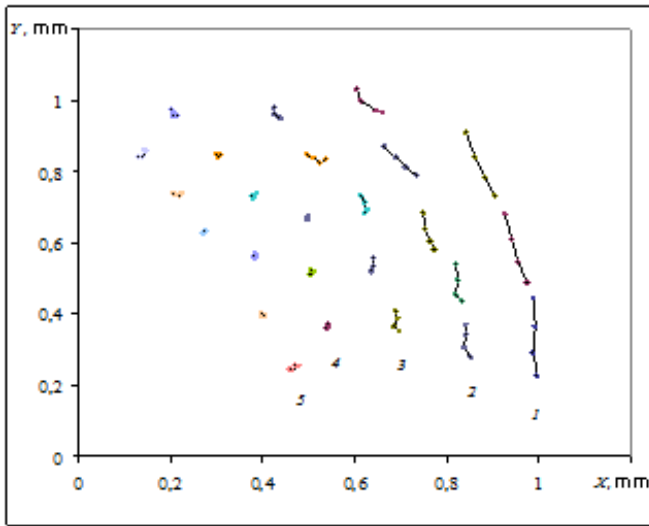


Figure 4. The coordinates X , Y of the droplets at the time points of 0, 0.5, 0.8, 1.3 are joined by the solid lines and form the flow trajectories. The layers are numbered from 1 to 5.

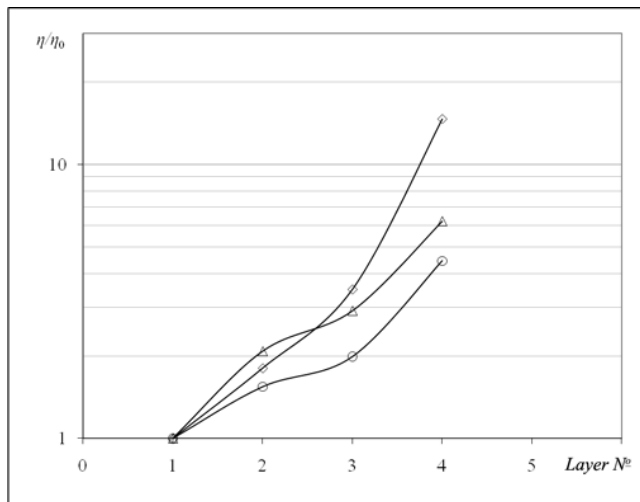


Figure 5. The shear viscosity coefficient η in the different layers of the cluster under the temperature of 90°C . η_0 - the air viscosity.

taken from the reference literature was compared with the estimated concentration value for an ideal ordered droplet structure in which the droplets position themselves at the distance of two Debye radii from each other. With the electrical conductivity characteristic of a cloud $\lambda_0=10^{-11}$ Ohm $^{-1}$ m $^{-1}$ and with the mobility of light carriers $\mu=10^{-4}$ m 2 V $^{-1}$ s $^{-1}$ the Debye radius makes up $LD\approx 10^{-3}$ m. Then the concentration must equal $N=(2LD)^{-3}\approx 10^8$ m $^{-3}$. The mean droplet concentration in real clouds equals a close value $N=3\cdot 10^8$ m $^{-3}$, while in fogs it equals $N=(1\div 6)\cdot 10^8$ m $^{-3}$. Thus the droplets in clouds and fogs may be actually ordered spatially.

The viscosity was estimated in the cloud with the hypothetical presence of droplets ordering in it. For this purpose, we applied Frenkel's formula adapted to describe the viscosity of a droplet cluster:

$$\eta = \hbar \cdot N \cdot \exp\left(\frac{\Delta}{kT}\right) \approx \hbar \cdot N \cdot \exp(0,04 \cdot z)$$

where \hbar is the Planck constant, N is the droplet concentration, Δ is the activation energy of viscosity. With the charge

of droplets $z>10^3$, the viscosity becomes equal to the air viscosity and may exceed it.

The increase in the viscosity of a cloud, in its turn, may result in the decrease of the convective heat conductivity and the convective mass transfer. For instance, for a variety of problems connected with convection the Rayleigh number

$$\mathfrak{R} = \frac{g \cdot \beta \cdot A \cdot d^3}{\chi \cdot \mu}$$

may characterize the condition of gas stability in the gravitational field with the presence of the temperature gradient A directed downward where β is the coefficient of thermal expansion, χ is thermal diffusivity of the gas, μ is kinematic viscosity, d is characteristic linear size of the structure. A change in the viscosity may exert an influence on the presence or non-presence of natural convection as well as on the velocity of the heat and mass transfer in a cloud.

According to the results yielded by the investigation of a droplet cluster, a high viscosity value may be obtained when the gradients of the shear velocity are low. When the shear velocity gradients are high, which is typical of an aircraft flight, the viscosity goes down with the increase of the shear velocity, and the deviation of the cloud viscosity from the air viscosity may be small.

The mechanical and thermophysical characteristics of a cloud as a droplet structure obviously depend on the charge of droplets z . Based on the experiments, it was shown above that the charge of droplets is determined by the surface area of a droplet and does not depend on the intensity of the evaporation (condensation) processes on its surface. The size and the charge of droplets may be considerable in storm clouds, and the thermophysical properties of clouds may significantly differ from the properties of the air. This effect may become even more considerable in the clouds containing ice crystals, as the size and the charge of ice crystals greatly exceed those of water droplets.

Research into the spatially ordered droplet structures forming in the supersaturated water vapor represents a new important subject of the Earth's cryology focusing on the objects in which the water is close to the freezing point or is in the solid state.

References

- Fedorets, A.A. 2004. The droplet cluster. *Pisma v ZHETF*, 8th edition, 79: 457-459.
- Shavlov, A.V. & Dzhumandzhi, V.A. 2010. Spatially ordered structures in storm clouds and fogs. *Phys. Lett. A.*, 374: 2561-2565.

Glaciation of Siberia as Viewed from the Position of Earth Cryology: Glaciers as a Component of the Cryolithozone

V.S. Sheynkman

Earth Cryosphere Institute, SB RAS, Tyumen, Russia

Abstract

The glaciation of Siberia was associated with the permafrost zone and was superimposed on the development of permafrost during the entire Pleistocene. In this case, glaciers fall under the influence of cryogenesis. By means of energy and mass exchange, the glaciers become closely connected with the ice of cryogenic origin that may form both around and on top of glaciers. This is due to the fact that the ice that forms glaciers freezes in the same way as the ground around them. As a result, there develops a single permafrost and glacial complex that becomes a specific component of the cryolithozone. The ice composing it interacts, and from the point of view of Earth cryology, it is reasonable to regard their combination as a special cryoglacial system.

Keywords: cryoglacial systems; cryolithozone; glaciers; permafrost-glacier interactions; Siberia.

Introduction

Data collected on the contemporary and ancient glaciers of Siberia indicate that glaciers are usually deeply cold and located in the permafrost zone. Along the mountains of Siberia from the south and from the east, the glaciers display zonality. However, they are all uniform in the fact that they are cold at present, and therefore they were so in the past when they were spreading during climate cooling (Sheynkman 2007, 2011). The development of glaciers becomes specific in this case (i.e., it is closely associated with the formation of the surrounding permafrost). The glaciers of Siberia formerly covered a considerable part of the territory and are being actively developed today. Their impact on the development of permafrost can occur also at present. It is necessary, therefore, to devise approaches that take into account both the peculiarities of permafrost formation under the influence of glaciation and the specificity of their interaction as components of the Earth's cryosphere. The main points of this issue are discussed in this paper.

The State and the Core of the Problem

All ice, being frozen moisture, depends in some manner on the cold. It is customary to think that we deal with a glacial phenomenon if an ice substance formed in the atmosphere fell onto the Earth's surface as solid precipitation and, having accumulated in a large quantity, thus provides a source for glaciers. However, if glaciers appear to be in the permafrost zone, they must freeze and actually become a component of the cryolithozone like everything on the Earth's surface. This is due to the fact that freezing of the rocks in terms of glaciers behaves in the same way as in terms of any other formations that are composed of a mineral substance other than ice (Sheynkman 2008, Sheynkman 2007, 2011).

If the freezing of rocks implies that they are cooled below 0°C, then the freezing of a glacial mass will mean the formation of cold ice with a temperature that is constantly below 0°C. This gives glaciers special characteristics that sharply differ from those of glaciers with warm ice (i.e., in the isothermal state at 0°C), a case usually regarded from the standpoint of the alpine school of thought. The long-term preservation of warm glaciers is sustained by an abundant

source of snow, snow metamorphization, and with the resulting high specific melting heat of the ice formation. Cold glaciers are also sustained by the freezing of ground in their body; the solid ice cooled below 0° actually becomes cryotic ground, while the saturated meltwater or water layers that are frozen from above become frozen ground.

If glaciers become a component of the cryolithozone, it is obvious that the approaches and concepts regarding their composition and their impact on permafrost must differ from the approaches and concepts that have been used in alpine science for more than two centuries. These traditional approaches do not take into account the concept that glaciers formed within the permafrost zone are different from those formed outside the permafrost zone. The customary alpine stereotypes are often canonized and assume central importance in Siberia. For this reason, the state of permafrost linked with the development of glaciation is explained through a number of versions that seriously differ from each other.

One such stereotype, sometimes used even by geocryologists (Balobaev 2005), suggests that glaciers exhibit heat-insulating properties. The main point here is that the basis of the alpine model is formed with abundant snow that saturates glaciers and has good heat-insulating properties, while in Siberia, with its continental climate, snow precipitation is inconsiderable and, therefore, its influence is insignificant. The thermal conductivity of the monolithic ice that composes the main body of glaciers equals approximately 2.2 W/(m•K); these values and the values later in the paper are given according to Bogorodskiy & Gavrilov (1980). This is comparable with the thermal conductivity of rocks that range on average from 2 to 4 W/(m•K). For this reason, the glaciers located in the permafrost zone will be exposed to freezing (as well as the ground around them) and will further the freezing of the ground under them by conducting the cold in winter and reducing the heat flow from above in summer. This is due to the fact that the heat of melting ice is high and equals $3.3 \cdot 10^5$ J/kg (only some types of metals exhibit higher values). The upper ice layer takes the summer heat input, while the heat used to melt it is carried away from the glaciers with meltwater.

Thus glaciers represent a specific regulator of the freezing of the ground beneath them. Becoming the permafrost table,

the surface of glaciers will raise or lower this table in the course of their growth and reduction, while the freezing of rocks lying under them will decrease or increase, respectively. The freezing is also influenced by the fact that the thermal field of glaciers is unsteady due to their movement and their developmental history. Although the heat capacity of ice is twice as low as that of water, it is sufficiently high, about 2.1 kJ/(kg·K), which is three times as high as the heat capacity of hard rocks. Therefore, the cold reserve accumulated by the ice can reach high values. Further, the glaciers can transfer it from their upper zone (with lower temperatures) into their lower zones (with higher temperatures). The cold reserve accumulated in the previous colder epochs may also be conveyed to the surrounding ground. In other words, the specificity of the ice forming the glaciers in Siberia can accumulate a great cold reserve and, at the same time, convey it to the surrounding ground.

Presently, all the ice centers of Siberia are located in the mountains. Their temperatures are being measured. Although the present time is an interglacial period, the collected data definitely indicate that these glaciers are deeply frozen and lie mostly on the frozen bed (The catalogue of glaciers... 1966–1981, Mikhaleiko 2007, Sheynkman 2008, Aizen et al. 2006). In the Urals (where the glaciers formed as a result of snowdrifts that lie much lower than the snowline) they have a zero temperature only in the firn zone, while in the area of glacier tongue they are heavily frozen (approximately down to the depth of 50 m). Further to the east, all glaciers of Siberia are completely frozen.

The available thermometric data on the glaciers allow us to conclude that their thermal field is unsteady. The variation of temperature is standard in small glaciers, with its minimum value at the depth of zero-point fluctuations at 12–16 m. However, the variation of temperature is different in large glaciers. The decrease of the temperature down to -16°C is observed at the depth of 60 m in the alimentation zone of glaciers located on the slopes of the highest peak of Siberia (Mt. Belukha) in western Altai. Only then the temperature slowly rises with the gradient of $0.15^{\circ}/10$ m. Meanwhile, the temperature in the Inylchek glacier of the adjacent Tian Shan drops to -16°C at the depth of 30 m, but then it rises with the gradient of only $0.06^{\circ}/10$ m. The temperature at the bed does not exceed -10°C in both cases (Aizen et al. 2006). That is, the glaciers are somewhat heat-insulated at the surface, but their deep layers (like those in the Arctic) distinctly hold an earlier cold reserve.

All the glaciers in the Siberian mountains are deeply frozen. The glaciers appear to be closely connected with the other ice forms of permafrost origin (forming both at the glaciers and in their proximity). These facts give special features to the geologic work done by the glaciers since icings connected with them also perform a dynamic geologic activity. Acting on the relief alternately with the glaciers, they considerably change the form of valleys (Sheynkman 1986, 1991). Thus the connection between the ice forms is realized by means of the energy and mass exchange and the geologic work that they collectively carry out. The developing permafrost and glacial complex becomes a specific component of the cryolithozone. If the ice forms are perceived in their interaction, then this complex may be regarded as a peculiar cryoglacial system from the standpoint of Earth cryology (Sheynkman 2011).

Although the information on the specificity of the Siberian glaciation model seems to speak for itself, it appeared only at the end of the 20th century. For a long time, this model was complicated in the record of the development of glaciers under permafrost conditions. A number of authors still use the alpine canons. For this reason, we would like to emphasize the points that make the two approaches conceptually different.

The alpine glaciation model

The traditional alpine model suggests that the moisture carried over from the ocean to the continent passes for a relatively short distance over land. The part of moisture that falls in the solid phase is preserved for some time by the glaciers resting mostly on a frozen bed. In this case, the active metamorphism of the snow in its abundance under the relatively mild climate comes into the foreground, while the contribution of the cryogenic component retreats into the background. For instance, the air temperature in the highest part of the Alps is negative all year round and the upper layers of the glaciers in the accumulation zone are considerably cooled. However, the air temperature rapidly rises with the decrease in elevation, and the main body of the glaciers in this case consists of the warm ice at 0°C . The Caucasus is similar in this respect (Pogorelov 2002, Mikhaleiko 2007).

We would like to emphasize that the cold in this case assumes a subordinate role in the development of glaciers and its reserve is restricted in them. The cold that the glaciers receive at their location comes only from the atmosphere with their initial substance (snow precipitation) and through cooling the surface layers of the ice in the cold season of the year. The heat coming to the glaciers is mainly used to overcome the melting threshold characterized by high heat of melting ice. The consumed heat is compensated by new portions of the ice mass actively coming into the zone of ablation.

The mechanism of glacier formation described above characterizes the geosystems identified by the author as cryoglacial systems of the warm type (Sheynkman 2007, 2011) (Fig. 1). It is subdivided into the cryoglacial systems of warm and moderately warm subtypes. The first subtype is distinguishable when the warm ice entirely prevails in the body of the glacier (Fig. 1-I). The cryoglacial systems of the second subtype are distinguished when the cold (mainly cryogenic) component takes a certain part in the development of glaciers. This is reflected in the appearance of the constantly cooled layers in the upper part of the glaciers, as noted above. A certain amount of cold can be transferred from this point downward by the substance of the glaciers as this cold transfer is realized dynamically (i.e., while glaciers move across the valley) (Fig. 1-II). In this case, however, the influence of this cold on the glacial process as a whole will be small.

It is important to realize that the glaciers will react to the climate cooling and interact with the permafrost forming around them conceptually differently under the organization of matter and energy than those in Siberia located in the interior of the continent. This occurs due to the fact that with the decrease in the ablation, the firn line will rapidly descend first on the warm glaciers causing their active growth because

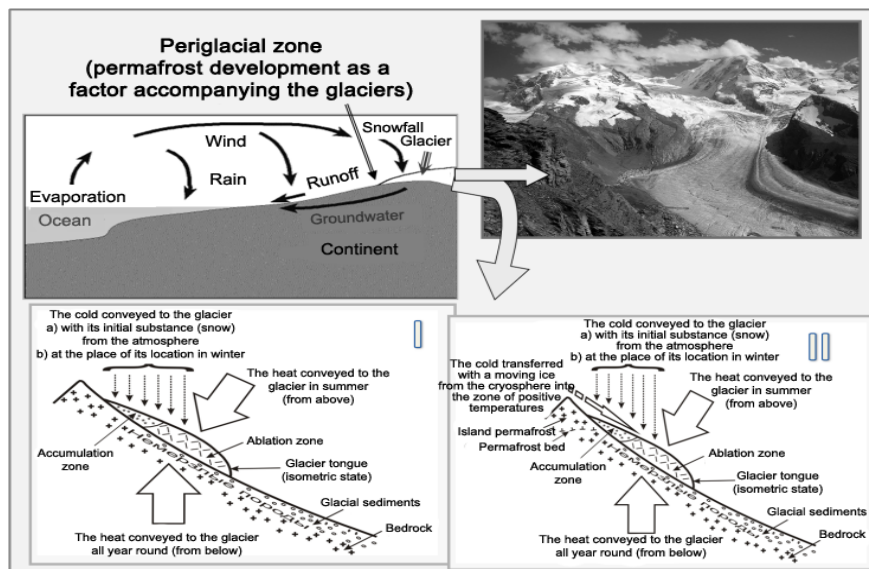


Figure 1. The structure of the cryoglacial systems of the warm type.

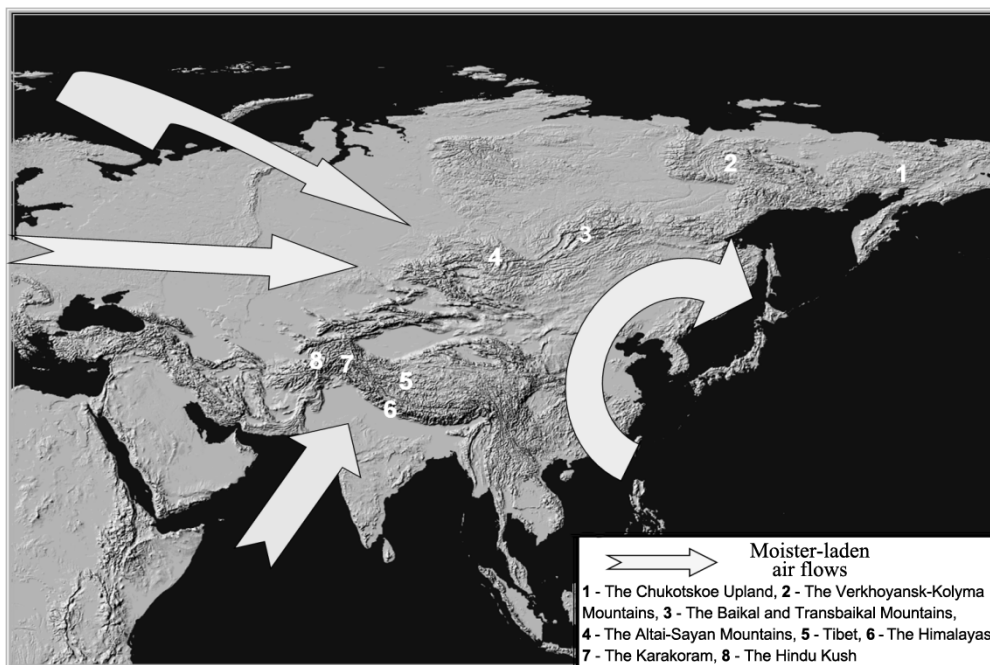


Figure 2. The mountain structures of north Siberia and the impact exerted on them by the main moisture-laden air flows.

of the abundant snow accumulation preserved during the first periods of time. This glaciation phase (cryohygrotic, cold and moist) will further be replaced with the cold and dry cryoxerotic phase (Velichko 1981). This means that the environment will undergo cryoaridization (i.e., the territory will be cooled as the climate continentality will increase) (Sheynkman 2007, 2011). This may occur spatially (e.g., as it occurs today, from the southwest to the northeast along the mountains of Siberia) and in time during the transition from the interglacial period to the glacial one.

In the warm type of cryoglacial system, the glaciers and the ground around them will be the first to be affected by freezing under climate cooling, while the bed under them will be unfrozen for a long time, causing the permafrost to concentrate in the zone near the glaciers that is the most cooled. When cryoaridization comes into its full force, the freezing will be able to affect the glaciers as a whole and

the ground under them. At the well-pronounced (initially hygrotic) glaciation phase, glaciers can reach the final stage of their development even under the geologically rapid replacement of the Quaternary cryochrons with thermochrons.

The Siberian glaciation model

Research experience shows that application of the alpine model is unacceptable in Siberia (Sheynkman 2008, Sheynkman 2011). Permafrost operates as a background factor (not the periglacial one) in this case and the moisture is distributed and preserved differently.

Overcoming great distances and losing much of its quantity on its way, the moisture comes to Siberia mainly with the western transfer of air masses from the Atlantic and the Western Arctic (Fig. 2). Permafrost also retains much of its moisture, while during the Quaternary cryochrons a

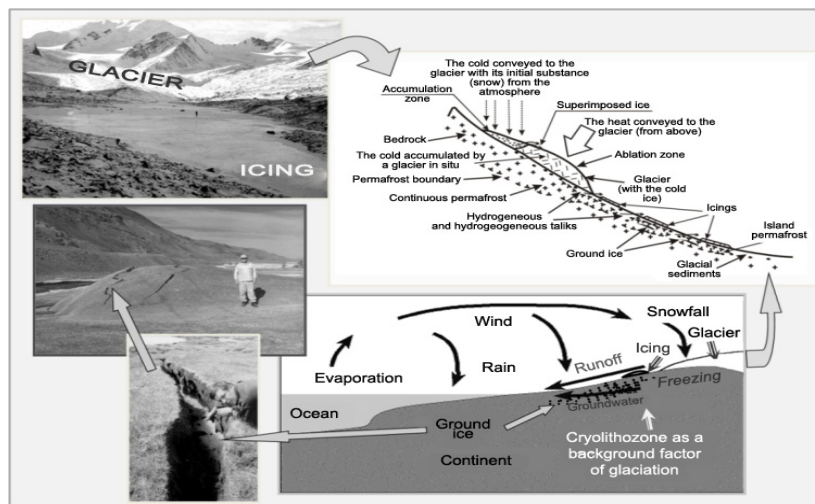


Figure 3. The structure of the cryoglacial systems of the moderately cold type.

considerable part of the moisture was intercepted by the ice sheet lying in the northwest of Eurasia. For this reason, the general moisture volume transported from the ocean into the center of Siberia cannot be large at present and could not be so in the past. As a result, there remains relatively little quantity of moisture to form the glaciation; it is enough only to sustain the mountain glaciers.

It is important that the glaciers of Siberia initially appear under the developed cryoaridization with the active summer thawing and little humidification typical of the continental climate. As these glaciers are found in the permafrost zone, the major role in their formation is performed by the cold conveyed to glaciers both from the atmosphere (with solid precipitation) and in situ at the Earth's surface all year round.

It is the cold (i.e., the cryogenic component) and not the abundant snow accumulation that determines the development of Siberian glaciers. This is not explained by the long winter. It is due to the fact that the cold accumulated by the glaciers in winter and conveyed to them by the surrounding permafrost is used to restore the ice mass in the ablation period. The meltwater does not always run off such glaciers in the warm period of the year; a part of this meltwater and the firn moistened by it freeze directly on the cold ice. As a result, there forms a superimposed ice that is by essence the product of cryogenesis on the glacier itself. In addition to nourishment by means of the sedimentary and metamorphic transformation of the snow mass, glaciers are also considerably sustained by the congelation component.

Cryogenesis affecting the glaciers makes them active even if most of them lie below the firn line, as the nourishment zone in this case is that of the superimposed ice. Besides, cryogenesis in the periglacial zone determines the interception of a large part of the ice runoff by icings, which also contributes to the preservation of glaciers. This occurs because the icings of Siberia are sometimes comparable with glaciers in their area; much heat is spent to thaw a large quantity of the ice at their surface, which reduces the thermal impact on the glaciers at higher elevations (Koreysha 1991, Sheynkman 2008, 2010). In such cases, we single out the cryoglacial systems of the cold type that are observed everywhere in the mountains of Siberia and subdivided into moderately cold and cold cryoglacial

systems (Sheynkman 2007, 2011).

Moderately cold cryoglacial systems are zonally distinguished in the southwestern part of the mountains in Siberia (Altai). This region is generally characterized by rather hard conditions with distinct cryogenic processes including those connected with the formation of continuous permafrost (Fig. 3).

Nevertheless, conditions in the south of West Siberia will be slightly milder in comparison with those in the east and the northeast of Siberia, which serves as the reason to single out the corresponding type of the cryoglacial system. The cold cryoglacial systems are distinguished in East Siberia and most often occur in its northeastern part where the low-temperature, continuous permafrost is developed (Fig. 4).

It should be noted that the conditions are generally rather severe all over the mountains of Siberia. Few data have been collected on the temperature of the glaciers and the permafrost around them in Siberia. However, the available data are supplemented by the fact that a number of cryogenic indicators characteristically reflect the state of the cryoglacial systems (e.g., the appearance and disappearance of certain cryogenic formations on the glaciers and in the periglacial zone).

The cryoglacial systems of the cold type are generally characterized by ice with the congelation component (superimposed ice) on their glaciers and by the development of ground ice and icings in their periglacial zone. The criterion of the transition from moderately cold cryoglacial systems to cold ones is the appearance of the low temperature permafrost in this zone and the development of such indicators of deep freezing as large perennial icing and ice wedges within this zone both in the proximity of glaciers and at some distance from them (Fig. 4).

In other words, the moderately cold cryoglacial system has in general the same basic characteristics as the cold one. It differs from the latter only by the fact that it is located in slightly milder conditions and the freezing of rocks at its location is less distinct. The continuous permafrost in the periglacial zone is usually replaced here with the island permafrost, while the criterion of the transition of one cryoglacial system type to another is the disappearance of ice wedges and the transition of icings from the perennial

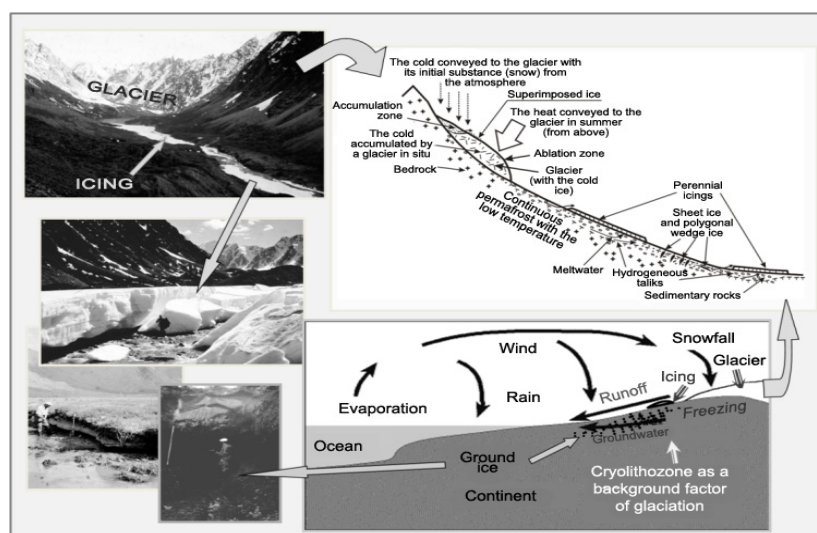


Figure 4. The structure of the cryoglacial systems of the cold type.

state to a mainly seasonal state. Although such icings may have large dimensions, they remain frozen here only during the years with the coldest winter (Fig. 3).

Ice nourishment with the dominance of the congelation component often becomes the major source for the glaciers of the cold cryoglacial systems. In the warm season, glaciers can remain snowless almost across their entire area and fully active at the same time, as they are still sustained in this period.

Cryogenesis helps them to remain active both when they are located considerably lower than the climatic snowline and when most of the glaciers are found considerably lower even than the firn line. This is due to the fact that their nourishment line is then determined in a different way: by the distribution limit of the superimposed ice. Apart from that, because of the cryogenesis, a considerable part of the ice runoff is intercepted in the periglacial zone by icing and by ground ice. These are closely connected with the glaciers and contribute to a higher degree of preservation of the glaciers lying above.

First of all, this relates to large perennial icings. As noted above, icings absorb an essential part of the heat brought with air flows in the valley where they are found, which provides for their extensive area (that is sometimes comparable with the area of glaciers). As icings have an extensive area, this heat is spent to melt a large quantity of ice at once, which decreases the thermal impact exerted on the glaciers located above them (Grave et al. 1964, Sheynkman 1986, 1991, Koreysha 1991).

The glaciation in Siberia inland of the continent, reacts differently also to climate cooling. Glaciers will grow slowly due to the fact that the glaciation is characterized by developed cryoaridization. The latter means that snow nourishment is low (and it lowers with the increase of cryoaridization), while the summer ablation is high under the continental climate. As the cryohygroic phase does not actually take place in the course of development of these glaciers, they will not react to the climate cooling as rapidly as will the glaciers of the warm cryoglacial systems.

A greater amount of moisture will be preserved by icings and ground ice in the periglacial zone of such glaciers. And the glaciers of the cold cryoglacial systems in Siberia may

manage to attain only the stage of large valley forms for the geologically short cryochrons. Glaciers could reach the final stage of their development (as ice sheet) only in the Western Arctic that is still under the influence of the Atlantic.

It is also necessary to mention the cryoglacial systems with some heat-insulated and azonal elements occur in the area where rocks are deeply frozen. Such cryoglacial systems are linked with the formation of snow drift glaciers. For instance, they occur in the Polar Urals and in the Kuznetsk Alatau. These ridges are stretched in the meridional direction and the wind drift on their slopes can provide an abnormally large quantity of snow mass. This snow mass nourishes small glaciers located considerably below the general climatic snowline (sometimes by 1 km). Such glaciers covered with a thick layer of snow will be heat-insulated to a higher degree despite the fact that they are located in the permafrost zone. These azonal phenomena and formations have a local significance and do not conceptually affect the general picture of the development of cryoglacial systems.

Conclusions

This paper suggests that Siberian glaciation that occurred in the permafrost zone is characterized by specific features. The cold-type Siberian glaciers are singled out by the author as a cryoglacial system. Their development is not restricted by chionosphere (tropospheric influence), as the cryogenic component alters the glaciation mechanism not only in the genetic aspect (in terms of ice formation), but also in the structure. The freezing of rocks in this case closely connects with ice formation of permafrost and that of glacial origin forming one permafrost and glacial complex. In this case, it is necessary to consider glaciation from the standpoint of Earth cryology.

Such complexes become a specific component of the cryolithozone. When examining their elements and interaction, it is reasonable to study and evaluate all of these ice complexes as a specific cryoglacial geosystem, according to the views of the Earth cryology. This is especially important when analyzing the conditions of former glaciation. If conditions of glacier advances and retreats are underestimated when their development is

superimposed on permafrost formation, then the general picture of environmental changes will be considerably distorted, including the specificity of permafrost dynamics under the influence of changing glaciation.

References

- Aizen, V.B., Aizen, E.M., Joswiak, D.R., Fujita, K., Takeuchi, N., & Nikitin, S.A. 2006. Climatic and atmospheric circulation pattern variability from ice-core isotope/geochemistry records (Altai, Tien Shan and Tibet). *Annals of Glaciology* 43: 49-60.
- Balobaev, V.T. The new aspects in the theory of ice complex formation in the arctic lowlands. 2005. *Materials of the Third Conference of the Geocryologists of Russia*. V. 1. Moscow, MGU: pp.138-145.
- Bogorodskiy, V.V. & Gavrilov, V.P. 1980. *Ice. The Physical Properties, the Modern Methods of Glaciology*. L. Gidrometeoizdat, 384 pp.
- Grave, N.A., Gavrilova, M.K., Gravis, G.F. et al. 1964. *Freezing of the earth's surface and glaciation of the Suntar-Khayat Ridge*. Moscow, Nauka, 144 pp.
- Koreysha, M.M. 1991. *Glaciation of the Verkhoyan-Kolyma area*. Moscow, RAN, 144 pp.
- Mikhalevko, V.N. 2007. *The internal structure of the glaciers at the tropical and temperate latitudes*. Moscow, URSS, 315 pp.
- Pogorelov, A.V. 2002. *The snow cover of the Greater Caucasus*. Moscow. Akademkniga, 288 pp.
- Sheinkman, V.S. 2011. Glaciation in the High Mountains of Siberia. Quaternary Glaciations: Extent and Chronology – a closer look. Eds.: J. Ehlers, P.L. Gibbard & P.D. Elsevier, Amsterdam. *Development in Quaternary Science* 15: 883-907.
- Sheinkman, V.S. 2007. Peculiarity of glaciation in the high mountains of Siberia. *Data of glaciological studies* No. 102: 54-64.
- Sheynkman, V.S. 1986. *The icings in the glacier valleys. Glaciology of Siberia*, edition 3. Tomsk, izd-vo Tomskogo un-ta. pp. 105-117.
- Sheynkman, V.S. 1991. The icings in the Altai mountains. *The Problems of Icing Science*. Novosibirsk, Nauka 166-176.
- Sheynkman, V.S. 2008. Quaternary glaciation in the mountains of Siberia: general regularities and data analysis. Moscow, RAN. *Materials of glaciological studies* No. 105: 51-72.
- Sheynkman, V.S. 2010. Glaciation of the mountains of Siberia: The interaction between glaciers and cryogenic ice.). Moscow, Nauka. *Led i sneg*, No. 4 112:101-110.
- Shpolyanskaya, N.A. 2011. The spatial relationship between ice sheets and permafrost (between surface and underground glaciation). Moscow, RAN, *Led i sneg*, No. 1: 75-80.
- Velichko, A.A. 1981. On the question of the consistency and the conceptual structure of Pleistocene climatic rhythms. *The Issues of the Pleistocene Paleogeography of Glacial and Periglacial Zones*. Moscow, Nauka. pp. 220-246.
- Vinogradov, O.N. (ed.). *The catalogue of the USSR glaciers*. 1966-1981. Leningrad, Gidrometeoizdat.

Composition of Water-Soluble Salts in Late Cenozoic Deposits, Northeast Yakutia

D.G. Shmelev

Lomonosov Moscow State University, School of Geography, Department of Cryolithology and Glaciology, Moscow, Russia

Abstract

A description of the chemical composition of water extracts from the Late Cenozoic permafrost in the Primorskiy Lowlands in Yakutia is given. The distribution of chemical parameters for the glacial complex deposits is analyzed. Its regional types and development features are identified with the help of statistical analysis.

Keywords: composition; Late Cenozoic; Primorskiy Lowlands, Yakutia; water extract; water soluble salts.

Introduction

The chemical characteristics of deposits are one of the most important aspects of paleogeographical reconstructions. Consideration of chemical features is required for the genetic identification of stratigraphic varieties.

In the scientific literature, the problem of the development of the Yakutian Primorskiy Lowlands during the Late Cenozoic age is one of considerable debate. There is a series of studies in which different particularities of the material composition of deposits (including chemical properties), hosted vein ice, and flora and fauna residuals are interpreted in ways that produce absolutely different hypotheses and theories (Shumskiy 1960, Popov 1965, Sher 1971, Rozenbaum 1973, Arkhangelov et al. 1979, Tomirdiario 1980, Konishchev 1981, Schirrmeister et al. 2003, Sher et al. 2004). The purpose of this study is to compare the chemical and physical-chemical parameters of deposits with different genesis and age in order to allow for their further genetic interpretation.

Research Area and Methodology

The research area is located in the Yakutian Northeast, in the territory of the Primorskiy Lowlands, between the Lena River estuary and the Kolyma River estuary (Fig. 1). The elevation of the highest watersheds does not exceed 80 m. Alas basins formed during the Holocene age are widely developed. The area is distinguished by severe climatic conditions. The permafrost thickness reaches 500 to 600 m. The temperature at the zero annual amplitude level is -7 to -11°C (Arkhangelov et al. 1989).

The upper stratum of the Late Cenozoic deposits was sampled with the help of UKB-12/25 core drilling. The following characteristics were determined from the specimens:

- composition of water-soluble salts;
- mineralization (dry residual of water extract);
- medium reaction (pH).

The Ca/Cl coefficient is an indicator of the continental or marine genesis of deposits: high values are typical of continental conditions and low values are typical of marine conditions (Konishchev & Plakht 1991).

A total of 460 specimens were analyzed. These included 155 belonging to the Late and Middle Pleistocene ice complex (a yedoma horizon and the Maastakh suite), 40 samples of the alas complex, 50 samples of the Khallerchinskaya suite,

15 samples of the Kuchuguyskaya suite, 50 samples of the Konkovskaya suite, 120 samples of the Olerskiy horizon, and 30 samples of the Tumus-Yarskaya suite. The data on particle size distribution and total carbon according to F.N. Tyurin were based on the same sample for comparison with chemical characteristics.

A great number of research studies of the Late Cenozoic unconsolidated deposits of the Yakutia Primorskiy Lowlands were undertaken. Many methods were used: lithological-facial, paleobotanic, paleontologic, and isotopic. All of them provided good results for the development of accumulation diagrams for individual districts. However, the problems of comparison of results obtained with different methods, as well as the problems of the correlation between regions with a different history of terrain development, occur when comparing local stratigraphic diagrams with each other and with the general scale of the Pleistocene dissection.

The following summarized section (Table 1) was used in the process of dissection of the deposits.

Results

The typical stratigraphic section of the *Tumus-Yarskaya* suite, referred to as Neogene age, was intersected in the

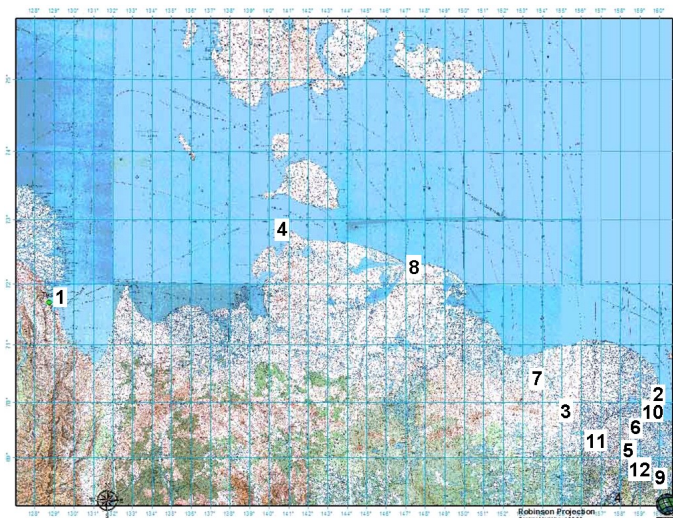


Figure 1. Research area: 1 – Bykovskiy Peninsula, 2 – Cape Chukochoy, 3 – middle reaches of the Alazeya River, 4 – Cape Svyatoy, 5 – western edge of the Khallerchinskaya tundra, 6 – Malaya Kon'kovaya River, 7 – upper reaches of the Bolshoy Khomus-Yuryakh River, 8 – Khaptashninskiy Yar, 9 – Anyuy River, 10 – Yakutskoye Lake, 11 – middle reaches of the Bolshaya Chukochoya River, 12 – southern edge of the Khallerchinskaya tundra, 13 – Duvanny Yar.

Table 1. Summarized section of the Late Cenozoic unconsolidated deposits in the Yakutia Primorskiy lowlands (Sher 1971, Guide book... 1979, Kraev 2010).

System	Series	Stage	Horizon, suite	Description, comments
Quaternary	Holocene		Alas	peated aleurites
		Pleistocene	Upper	Edoma
	Khallerchinskaya			syncryogenic fluvial-marine sands
	Kuchuguyskaya			syngenetic fluvial aleurites
	Middle		Kon'kovskaya	epicryogenic fluvial-marine sands
			Maastakh	ice complex
Lower	Olerskiy	epicryogenic lacustrine-fluvial and fluvial aleurites and sands		
Neogene	Pliocene		Tumus-Yarskaya	epicryogenic fluvial sands

middle reaches of the Alazeya River. Identical continental sands of Neogene age were sampled at the Malaya Konkovaya River, the Bykovskiy Peninsula, Cape Chukochy, and Yakutskoye Lake. The top of this suite is positioned 15 to 16 m below sea level in the area of the East Siberian Sea coast, and 10 m below sea level in the area of the Alazeya and the Malaya Konkovaya rivers and on the Bykovskiy Peninsula. The bottom suite was not intersected. The intersected sands from the Alazeya River are characterized by a complex composition of water-soluble salts; Ca, Na, Cl, and SO_4^- cations are present. The Ca/Cl ratio was 0.39, the water extract dry residual was 0.15 mg/l, and medium reaction was neutral (pH=6.5). Chloride-sodium salting, the Ca/Cl correlation equal to 0.31 (higher mineralization of 0.39 mg/l), and neutral to low-alkaline medium reaction (pH varies from 7.0 to 8.2) are characteristic of the deposits in the area of Cape Chukochiy and Yakutskoye Lake.

The Olerskiy horizon was observed and sampled in the middle reaches of the Alazeya and the Bolshaya Chukochya rivers. The deposition occurred at the boundary of the Neogene and the Early Neo-Pleistocene ages. The deposits are represented by lacustrine-fluvial sands and aleurites (Sher 1971, Kaplina et al. 1981, Sher et al. 1981). The composition of the water extract is complex. It is chloride-sodium at the Alazeya River; Cl and HCO_3^- anions and Na and Ca cations are equally present in the middle reaches of the Bolshaya Chukochya River; the Ca/Cl ratio of 1.1 indicates the continental genesis; the medium reaction is neutral

(7.3); the mineralization is low. The differences between the two sites are significant: for the Alazeya River the Ca/Cl ratio was 0.76 with mineralization of 0.12%, and for the Bolshaya Chukochya River it was 1.18 with mineralization of 0.06 mg/l.

The Kon'kovskaya suite, which formed during the Middle Neo-Pleistocene age was intersected at Cape Chukochiy and in the Yakutskoye Lake area where it was drilled with a series of boreholes. According to the drilling data, the suite's top is positioned at sea level. Its thickness is approximately 10–15 m. The deposits are represented by salted sandy aleurites with the inclusions of cryopeg lenses (Rivkina et al. 2006). The composition of the water extract (chloride-sodium) testifies to the marine nature of salting. The content of C and Na was higher than that of other ions by 10 times. The Ca/Cl ratio was very low at 0.12; the pH value was close to neutral (7.3). Very high mineralization of deposits, 0.38 mg/l, was observed.

The Kuchuguyskaya suite was sampled with the help of boreholes at Cape Svyatoy Nos. The intersected thickness of the band is approximately 10 m. The deposits are referred to as the Middle Neo-Pleistocene age based on the data of stratum dating with unstable chlorine isotopes (age of 220,000 to 330,000 years) (Blinov et al. 2009). They are characterized by ultra-fresh composition (dry residual of 0.11 mg/l), and alkaline medium reaction (pH 7.6 m). The equal amounts of Cl, SO_4^- , and HCO_3^- anions and Ca, Na, and Mg cations were present in the composition of water-soluble salts. The Ca/Cl ratio was 1.05, which is characteristic of continental deposits and confirms their fluvial genesis (Blinov et al. 2009).

The Late and Middle Neo-Pleistocene ice complex deposits are represented by the yedoma horizon and the Maastakh suite. These are thick (up to 30–50 m) silts and silty clays strata with syngenetic polygonal wedge ice (Popov 1965). These deposits are widespread within the research area and were studied at the Bykovskiy Peninsula, Cape Svyatoy Nos, Cape Chukochiy, in the upper reaches of the Bol. Khomus-Yuryakh River, in the middle reaches of the Alazeya, the Kolyma (Duvanny Yar), and the Bolshaya Chukochya rivers, in the Khromskaya Gulf (Khaptashninskiy Yar).

The composition of the water extract of the ice complex deposit can be characterized as hydrocarbonate-calcium. The content of Na (Duvanny Yar, Cape Chukochiy, Yakutskoye Lake) and Mg cations and Cl anions (Duvanny Yar, Khaptashninskiy Yar, Cape Chukochiy, Yakutskoye Lake) can be higher depending on the location. The Ca/Cl correlation for the ice complex deposits was 2.18; in particular, for the Alazeya River it was 4.76, the Bykovskiy Peninsula was 1.51, the Duvanny Yar was 2.07, Cape Svyatoy Nos was 0.93, the middle reaches of the Bolshaya Chukochya River was 0.9, the Khaptashninskiy Yar was 0.89, the Bol. Khomus-Yuryakh River was 0.82, Cape Chukochiy was 0.4, and Yakutskoye Lake was 0.2. The medium reaction is neutral (mean pH 7.29; pH varies from 5.5 to 8.5). The mineralization of sediments is low and they are considered to be the fresh type at 0.11 mg/l (variation from 0.02 to 0.34 mg/l).

The Khallerchinskaya suite composes the upper 15–20 m surface located on the Kolyma and the Malaya Kon'kovaya interfluvium. It is composed of the Late-Pleistocene sand

deposits with a thickness of up to 50 m (Plakht et al. 1986). The sampling was conducted at two districts: at the western district, in the area of the Ekhameskeveey Creek, and at the southern district, on the Kolyma River left bank. The composition of the water extract can be characterized as chloride-calcium-sodium. The average pH value for sands of the Khallerchinskaya suite was 6.8, and it varied from 5.5 to 8.3. The pH values of boreholes in the western and the southern districts differ significantly: 6.4 and 7.4, respectively. The mineralization of sand does not differ from the ice complex deposits of the same age and was 0.09 mg/l. The Ca/Cl ratio, although lower than that of the ice complex (0.96), corresponds to the Khallerchinskaya suite deposits of the continental type.

The *alas* deposits were formed as a result of the thermokarst destruction of the ice complex during the Holocene (Kaplina 2009). The thickness of the *alas* band varies significantly (from several meters to 15–20 m). It frequently replaces the ice complex completely and overlies directly more ancient deposits (Sher 1971, Sher 1997, Kaplina 2009). *Alas*es were sampled at Bykovskiy Peninsula, Cape Chukochiy, Malaya Kon'kovaya River, Bol. Khomus-Yuryakh River, and Kolyma sites. Two types of horizons can be identified in the structure of the *alas* stratum: specifically *alas* (Holocene lacustrine-bog) and *taberal* (thawed and re-deposited ice complex deposits) (Kholodov et al. 2003). The composition of water extract for both horizons is similar: chloride-sodium. It is hydrocarbonate-magnesium only in the upper reaches of the Bol. Khomus-Yuryakh River, and hydrocarbonate-calcium at the Bykovskiy Peninsula. The Ca/Cl ratio was 0.94, decreasing in individual cases (Cape Chukochiy) to 0.13. The maximum values are characteristic of the Bykovskiy Peninsula (almost 5.5). The *alas* complex mineralization, as in the case of the ice complex, was low at 0.09 mg/l. The average pH value for the *alas* complex was 7.26. Differentiation into more acidic deposits (*alas* deposits as such) with pH 6.67 and *taberal* deposits with a neutral medium reaction (pH 7.59) is observed.

The deposits discussed are characterized by quite homogeneous particle size distribution. These are mainly silty sand/silt strata. The deposits of ice complex, *alases*, and the Olerskiy horizon are the most silty, and the Khallerchinskaya and the Tumus-Yarskaya sands are the least silty.

The carbon content varies quite significantly in different stratigraphic units. The maximum values are typical of the *alas* complex and the Olerskaya suite (1.89% and 1.84%, respectively), while the organic content in the *alas* complex in lacustrine-bog deposits is higher than in the *taberal* ones (Kholodov 2003). The carbon content in the ice complex was lower (1.64%), but local extreme values (up to 11%) can be observed due to buried organics. The lowest values were observed in the Kuchuguyskaya, the Khallerchinskaya, the Kon'kovskaya, and the Tumus-Yarskaya suites (1.13%, 1.06%, 0.92%, and 0.62%, respectively).

Discussion

A large database on the chemical composition of the ice complex deposits allowed us to compare them in their dependence on regional particularities (Fig. 2).

The analysis showed that most ice complex specimens

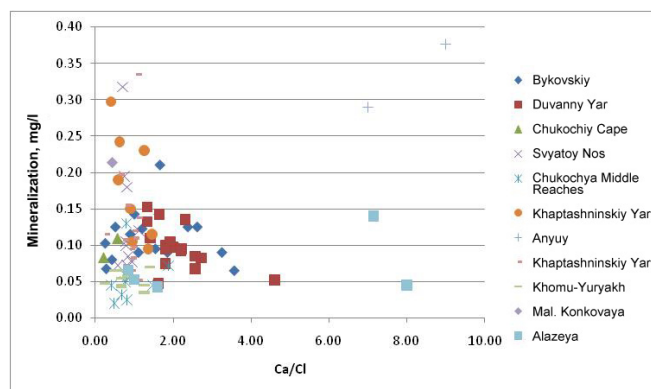


Figure 2. Mineralization and Ca/Cl coefficient ratio for ice complex deposits.

fall in the zone with mineralization of 0.05–0.15 mg/l and Ca/Cl values of 0.7 to 2.0. It can be assumed that the accumulation of deposits occurred in continental conditions. No evident “marine features” were detected for the ice complex specimens obtained on the Laptev Sea and the East Siberian Sea coasts (Khaptashninskiy Yar, Cape Svyatoy Nos, the Bykovskiy Peninsula). They can have both marine (dry residual of 0.2–0.3 mg/l, Ca/Cl of less than 1) and continental (dry residual of below 0.1 mg/l, Ca/Cl of above 2) characteristics.

Extreme values are also identified in Figure 2, such as in the area of the middle reaches of the Alazeya River (Ca/Cl 8.0), Cape Chukochiy (Ca/Cl 0.39), and the Khaptashninskiy Yar (sediment mineralization 0.34 mg/l).

Specimens with maximum mineralization in the stratum are located in the lower part of the ice complex band, and at the boundary with underlying deposits characterized by elevated salt content (Kraev 2010). A similar situation is observed at the Bykovskiy Peninsula and Cape Svyatoy Nos. Therefore, one can speak of elevated ice complex mineralization at the boundary with underlying deposits.

The trends of reduced Ca/Cl and increased pH when moving from southeast to northwest toward the Kolyma River estuary can be noted for the Kolyma lowland area. For example, the extremely high Ca/Cl values were noted in the middle reaches of the Alazeya River. At the same time, the sediment mineralization is low (0.05–0.15 mg/l), the medium reaction is neutral (pH 6.5–7.0), and the ice complex as such beds on the Olerskiy deposits with the chloride-sodium composition of the water extract. In the middle reaches of the Chukochya River, where the ice complex is also underlain by the Olerskiy suprahorizon, the Ca/Cl values vary between 0.5 and 2.0, pH 7.2–7.7, and mineralization of 0.05–0.13 mg/l. In the area of the Malaya Kon'kovaya River, these parameters are 0.45, 0.75, and 0.214 mg/l, respectively. Extremely low values are characteristic of the ice complex in the area of Cape Chukochiy and Yakutskoye Lake (Ca/Cl of 0.2–0.4 with dry residual 0.6–0.18 mg/l and pH 7.5–8.0). Therefore, one can speak of the intensification of marine conditions when moving toward the sea in this area.

Despite quite high variation of the chemical characteristics of the ice complex deposits, three groups of the distribution of ice complexes were identified in the process of the statistical

analysis (i.e., during the check for normal distribution of the values of chemical parameters Ca/Cl, mineralization, pH):

- 1) Cape Chukochiy, the middle reaches of the Chukochya and the Malaya Kon'kovaya Rivers, Yakutskoye Lake (Ca/Cl 1.3, pH 7.39, mineralization 0.13 mg/l);
- 2) Khaptashninskiy Yar, the upper reaches of the Bolshaya Khomus-Yuryakh River and Cape Svyatoy Nos (Ca/Cl 2.47, pH 7.02, mineralization 0.12 mg/l);
- 3) Duvanny Yar and the Anyuy River (Ca/Cl 1.68, pH 7.35, mineralization 0.12 mg/l).

These groups correspond to the ice complex types specified earlier in the literature: Chukochiy, Oygosko-Shirokostanskiy, Omolono-Anyuyskiy (Konishchev & Plakht 1991).

Deposits in the alas complex (both specifically alas and taberal) are clearly differentiated based on the medium reaction. More acidic Holocene lacustrine-bog deposits were formed in the water-logged, anaerobic conditions at the beginning of thermokarst thawing. The underlain taberal deposits preserved their properties identical to those of ice complexes. For example, the Kon'kovskaya deposits and continental sands (supposedly of the Tumus-Yarskaya suite) intersected in the Cape Chukochiy area are very similar to each other in their chemical properties; they differ from all others through the chloride-sodium nature of salting, high mineralization, a low Ca/Cl ratio, and identical pH values. Meanwhile, the total carbon content differs by almost two times: 0.92% in the Konkovskaya deposits versus 0.62% in the Tumus-Yarskaya deposits.

The sands of the Tumus-Yarskaya suite were formed in the Middle Neogene age as fluvial (Plakht et al. 1986, Rivkina et al. 2006). In the research area (Cape Chukochiy and Yakutskoye Lake) they occur under the Kon'kovskaya suite. According to the data from the spores and pollen analysis, the accumulation conditions were represented by the northern larch taiga subzone (Plakht et al. 1986). The chemical characteristics, like those of the fluvial-marine Kon'kovskaya Middle-Pleistocene suite (Arkhangelov et al. 1979), can be explained only by the epicryogenic nature of the Tumus-Yarskaya suite. Long-term exposure to a thawed state under the sea (during the Middle Pleistocene transgressions) caused diffusion of the Cl and Na ions down in the stratum.

Conclusions

The following conclusions were revealed in the process of examining chemical characteristics of the Late Cenozoic deposits in the northeast of Yakutia:

- 1) Low mineralization (up to 0.1–0.15 mg/l), neutral medium reaction (pH in most cases varies from 6.5 to 7.5), and the continental composition of the water extract (hydrocarbonate-calcium) are characteristic of almost all the deposits in the area under study.
- 2) The statistical analysis of chemical characteristics allowed us to identify the regional types of ice complexes: Chukochiy, Oygoysko-Shirokostanskiy, Omolono-Anyuyskiy.
- 3) The trends of increasing pH and declining Ca/Cl when moving toward the Chukochya River Estuary from southeast to northwest (i.e. the intensification

of “marine” conditions) were identified for the ice complex specimens from the Kolyma lowland.

- 4) Two horizons are identified in the structure of the alas complex; specifically these are alas and taberal, differing from each other through pH values. The most acidic values of alas deposits as such were caused by water saturated, anaerobic conditions of thermokarst lakes. Taberal deposits are similar to ice complexes in their properties.
- 5) The Kon'kovskaya suite and continental sands (supposedly of the Tumus-Yarskaya suite), which intersected at Cape Chukochiy and the Yakutskoye Lake area, are characterized by high mineralization (above 0.3 mg/l) and chloride-sodium salinization. Meanwhile, the sands most probably have a continental (fluvial) genesis. Their marine salinization can be explained only by the epicryogenic nature and long-term bedding under the fluvial-marine deposits of the Konkovskaya suite.

Acknowledgments

This work was completed on the basis of the analytical material provided by the Soil Cryology Laboratory of the RAS Institute for Physical-Chemical and Biological Soil Science Problems, Pushchino.

References

- Arkhangelov, A.A., Konishchev, V.N., & Rozenbaum, G.E. 1989. Primorsk-Novosibirsk Region. In *Regional geocryology*. A.I. Popov (ed.). Moscow, Izdatelstvo MGU, pp. 128-151 (in Russian).
- Arkhangelov, A.A., Kuznetsova, T.P., Kartashova, G.G., & Konyakhin, M.A. 1979. Genesis and conditions of Upper Pleistocene ice-rich siltstone formation in the Kolyma lowland (Case of the Chukochy Yar). In the collected works *Problemy kriolitologii*. Issue VIII. Ed. A.I. Popov. Moscow, Izdatelstvo MGU, pp. 110-136 (in Russian).
- Blinov, A.V., Beer, Y., Tikhomirov, D.A., Shirmeister, L., Meyer, H., Abramov, A.A., Basilyan, A.R., Nikolskiy, P.A., Tumskoy, V.E., Kholodov, A.L., & Gilichinskiy, D.A. 2009. Permafrost dating with the help of cosmogenic radionuclides (Report 1). *Kriosfera Zemli*. 13, (no. 2): 3–15 (in Russian).
- Guide book for the scientific tour with the subject “Late Cenozoic deposits of the Kolyma lowland”*. 1979. Tour XI. XIV Pacific Ocean Scientific Congress Ed. Sher, A.V. & Kaplina, T.N. Moscow: AN SSSR, 116 pp. (in Russian).
- Kaplina, T.N. 2009. Alas complexes of Northern Yakutia. *Kriosfera Zemli*. 12, (no.) 4: 3-17 (in Russian).
- Kaplina, T.N., Lakhtina, O.V., & Rybakova, N.O. 1981. *Cenozoic deposits in the middle reaches of the Alazeya River (Kolyma lowland)*. Izv. AN SSSR. Ser. geol., No 8, pp. 51–63 (in Russian).
- Kholodov, A.L., Rivkina, E.M., Gilichinskiy, D.A., Fedorov-Davydov, D.G., Gubin, S.V., Sorokovikov, V.A., Ostroumov, V.E., & Maksimovich, S.V. Evaluation of the quantity of organic substance supplied to the Arctic basin in the process of the thermal abrasion of the Laptev Sea and the East Siberian Sea coasts. *Kriosfera Zemli* (in Russian).

- Konishchev, V.N. 1981 *Fine-grained ground composition formation in cryolithosphere*. Novosibirsk, Nauka, 197 pp. (in Russian).
- Konishchev, V.N. & Plakht, I.R. 1991. Mechanism and sources of salting of the ice complex deposits in Yakutia. In the collected works *Denudatsiya v kriolitozone*. Moscow, Izdatelstvo Nauka, pp. 29-37 (in Russian).
- Krayev, G.N. 2010. Methane distribution regularities in permafrost in Russia's Northeast and its air emission forecast. Author's abstract of the Candidate of Sciences (geography) thesis. Moscow, TsEPL RAN, 20 pp. (in Russian).
- Kunitskiy, V.V. 1989. *Lena lower reaches cryolithology*. Yakutsk, In-t merzlotovedeniya So AN SSSR, 164 pp. (in Russian).
- Plakht, I.R., Kudryavtseva, N.N., Kartashova, G.G., Gilichinskiy, D.A., Arkhangelov, A.A., Konyakhin, M.A., Kolesnikov, S.F., & Enina, O.A. 1986. *Specialized permafrost-geological research at the East Siberian Sea shelf and the Kolyma lowland paleoshelf*. Funds of PGO Yakutskgeologiya, 216 pp. (in Russian).
- Popov, A.I. (ed). 1965. Northern Eurasia permafrost. In the collective works *Podzemny led*. Issue II. Moscow, Izdatelstvo MGU, pp. 27-40 (in Russian).
- Rivkina, E.M., Kraev, G.N., Krivushin, K.V., Laurinavichus, K.S., Fedorov-Davydov, D.G., Kholodov, A.L., Shcherbakova, V.A., & Gilichinskiy, D.A. 2006. Methane in the permafrost of the Arctic eastern sector. *Kriosfera Zemli*. 10 (no. 4): 23–38 (in Russian).
- Rozenbaum, G.E. 1973. Modern alluvium of the rivers of the Eastern Subarctic plain (Case of the Yana and the Omoloy Rivers). In the collective works *Problemy kriolitologii*. Issue III. Ed. A.I. Popov. Moscow, Izdatelstvo MGU, pp. 7-63 (in Russian).
- Schirrmester, L., Christine, S., Kuznetsova, T., Kuzmina, S., Andreev, A., Kienast, F., Meyer, H., Bobrov, A. 2002. Paleoenvironmental and paleoclimatic records from permafrost deposits in the Arctic region of Northern Siberia. *Quaternary International* 89: 97-118.
- Sher, A.V. 1981. On the substantiation of the age of unconsolidated deposits in the Alazeya River middle reaches (Kolyma lowland) *Dokl. AN SSSR*, 258 (no. 1): 179–182 (in Russian).
- Sher, A.V. 1971. *Pleistocene mammals and stratigraphy in Northern America and the USSR Far Northeast*. Moscow, Nauka, 310 pp. (in Russian).
- Sher, A.V., Kuzmina, S.A., Kuznetsova, T.V., & Sulerzhitsky, L.D. 2005. New insights into the eichselian environment and climate of the East Siberian Arctic, derived from fossil insects, plants, and mammals. *Quaternary Science Reviews* 24:533–569.
- Shumskiy, P.A. 1960. On the problem of vein ground ice genesis. In the collective works *Sbornik statey po obshchemu merzlotovedeniyu*. Akademiya Nauk SSSR. Trudy instituta Merzlotovedeniya im. V.A. Obrucheva. Vol. XVI. Moscow. Publishing House of the USSR Academy of Sciences, pp. 81–98 (in Russian).
- Slagoda, E.A. 2004. *Cryolithogenic deposits in the Primorskiy plain of the Laptev Sea: Lithology and morphology*. Tyumen, Izdatelstvo Express, 120 pp. (in Russian).
- Tomirdiario, S.V. 1980. *Eastern Siberia Later Pleistocene and Holocene loess-ice assemblage*. Moscow, Nauka, 184 pp. (in Russian).

Features of Pleistocene-Holocene Permafrost History of the Western and Eastern Sectors of the Russian Arctic and Subarctic

N.A. Shpolyanskaya

Lomonosov Moscow State University, Moscow, Russia

Abstract

On the basis of analysis of massive genetic ground ice, different geological history and different transgressive and regressive regimes of the western and eastern sectors of the Russian Arctic were revealed. The possibility of the formation of permafrost with tabular massive ice bodies directly under marine conditions was revealed. A mechanism of bottom sediment freezing is proposed. A new genetic classification of tabular massive ice bodies was developed. Spatial patterns of the occurrence of tabular massive ice bodies are also related to a problem of the Arctic Basin level fluctuations. More likely, the latter are related not to glacioeustatic processes, but mostly to regional tectonic movements. We believe that the Pleistocene glacial cover had a limited distribution in the Russian North and that the plains of the Russian Arctic and Subarctic to the east of the Kanin Peninsula were mostly unglaciated.

Keywords: massive ground ice; Quaternary history; Russian Arctic; subsea permafrost zone; tabular massive ice; wedge ice.

Introduction

Thick beds of tabular massive ice are widespread in the plains of the Russian Arctic and Subarctic (Fig. 1). They differ in morphology, nature of deposits, macro- and micro-structure, chemical composition, and therefore in their genesis. This fact makes it possible to divide massive ice into several genetic types. Different ice types typically belong to certain areas or stratigraphic units and almost never mix spatially. Once formed, ground ice remains intact until it melts. Since the lifetime of such ice is comparable to geological time, massive ice bodies can reveal very important paleogeographic information.

The main feature of the massive ice distribution is a stark distinction between the western and eastern sectors of the Russian Arctic and Subarctic. In the eastern sector, wedge ice is widespread almost everywhere, while in the western sector tabular massive ice dominates. Genetically, these types of massive ice belong to essentially different formations, and this fact suggests a significant difference in geological history of two sectors of the Russian Arctic.

Western Sector of the Russian Arctic

West Arctic land

Tabular massive ice is widespread in the plains of Western Siberia and the northeast of European Russia. The ice beds occur in the form of large bodies of an indefinite shape which occur as genetically heterogeneous formations. The bodies are dozens of meters long and up to ten meters high. Our long-term studies allow us to distinguish four genetic types of tabular massive ice: subsea, coastal-marine, intrusive, and buried surface ice (Shpolyanskaya 1991a, Shpolyanskaya & Streletskaya 2004).

Subsea ground ice

Subsea ground ice is the type of massive ice that is most widespread and, as a rule, is confined to dislocated marine deposits. In most cases, it exists in the form of ice-ground formations with thin lamination of soil and ice layers, which often have a very complicated configuration. Its structural

features indicate that originally it was formed in relatively deep-water subsea conditions along with simultaneous (syngenetic) accumulation and freezing of bottom sediments. The microstructure of the ice itself proves this. Earlier, we proposed and considered the possibility of subaqueous ice formation in the arctic seas (Shpolyanskaya 1991b, 2005). When the sea depth varies from 40–50 to 200–250 m, the bottom water temperatures are almost constant and reach the lowest negative values of -1.6 to -1.8°C. Such conditions are favorable for the freezing of bottom sediments. According to numerous reports, the salinity of pore waters of bottom sediments, which prevents freezing, usually decreases with depth.

At a certain depth from the sea bottom surface, the balance of temperature and salinity becomes favorable for soil freezing. At this depth interval, crystallization of pore solution occurs. Basic facets of ice crystals grow along the surface of mineral particles and sedimentary layers. As a result, ice lenses always inherit the soil layer shape, even if the layers are heavily deformed. The process is accompanied by segregation of soil and ice layers and formation of a layered ice-soil stratum. Earlier, we proposed a process of thermal diffusion of salts as a main cause of desalination that increases with depth (Shpolyanskaya 1991, 1999, 2005).

With sediment accumulation, the interval where freezing conditions were created moves up and ice-soil stratum grows upward. Salt redistribution occurs during freezing. While crystal facets grow, they force salt ions to move into layers adjacent to ice crystals. Coalescence of crystals leads to squeezing out the solution from inter-crystalline layers, and the ice remains fresh. This mechanism works in different ways in different types of soils. During the freezing of silty sediments with high surface energy for freezing, salts are completely adsorbed by the particle surface. Free pore water concentration corresponds to the freezing temperature all the time, and ice crystals grow without interruption. During the freezing of sandy sediments with low surface energy, salts are not adsorbed by mineral particles but remain in the solution. In this case, areas with very high concentration, which cannot be frozen, form along with the growth of crystals. In the newly accumulated sediments, ice formation

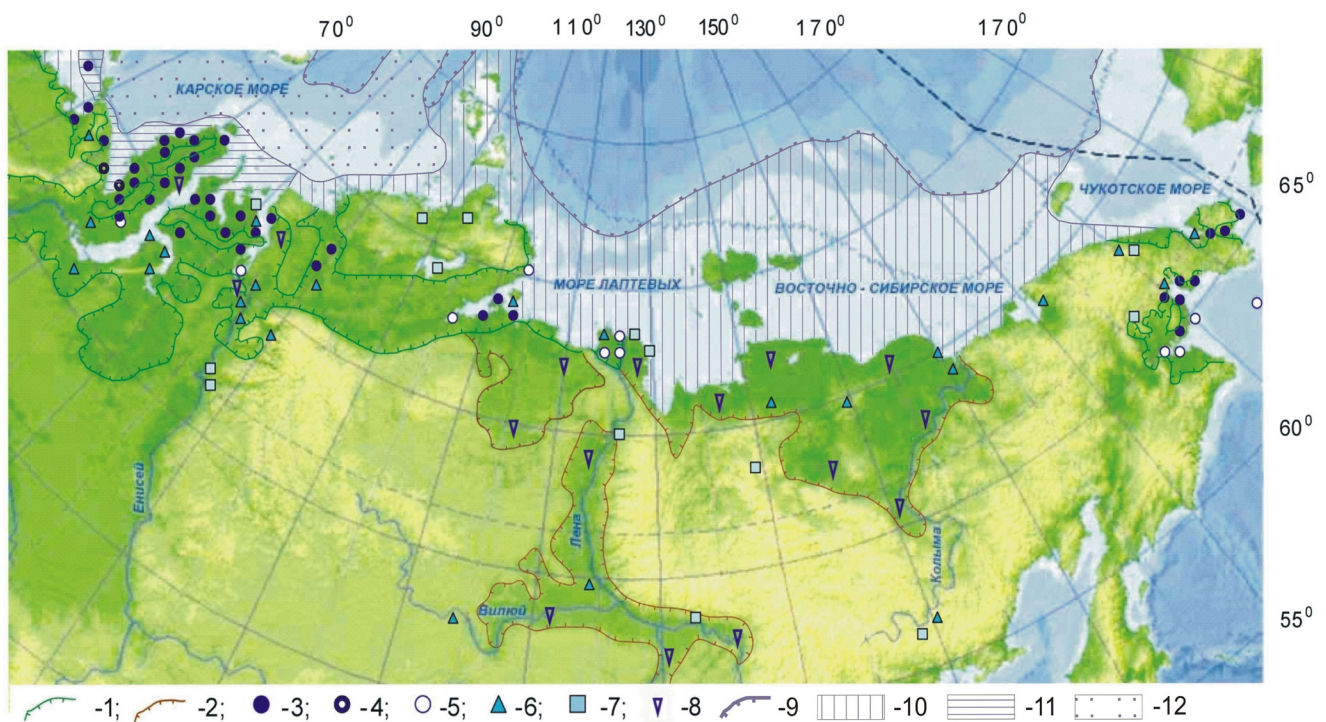


Figure 1. Map of massive ground ice occurrence. Prepared by I.D. Streletskaia and N.A. Shpolyanskaya. The shelf boundaries are shown according to V.A. Solov'ev and S.I. Rokos with additions by N.A. Shpolyanskaya. 1 - Late Pleistocene marine plain boundaries; 2 - Pleistocene lacustrine-alluvial plains boundaries; 3-8 – thick tabular massive ice beds; 3 - subsea genesis; 4 - mixed genesis; 5 - coastal-marine genesis; 6 - intrusive genesis; 7 - buried surface ice; 8 - wedge ice; 9 - shelf outer boundary; 10-12 - shelf permafrost: 10 - relict permafrost with a temperature of 0...-2°C, up to 200 m thick or more; 11 - modern permafrost with a temperature of 0...-1.5°C, up to 100 m thick; 12 - cryotic unfrozen soils with newly formed permafrost islands with a temperature of 0...-1.5°C, up to 100 m thick.

does not occur until the salinity decreases to the necessary value as a result of the thermal diffusion process. Crystal growth resumes and continues until the concentration of the expelled solution reaches a critical value. As a result, a nonfreezing zone appears again. This is the manner in which cryopeg lenses are formed in the freezing of bottom sediments. Such a mechanism is confirmed by the existing data. For example, in the Baydaratskaya Bay area up to 12 cryopeg layers were detected in 42 boreholes (Melnikov & Spesivtsev 1995). Such cryopeg distribution can be explained by interruptions in the ice formation during the freezing of sandy and silty sediments. In Central Yamal in the section of saline marine sediments of Kazantsev age that contained tabular massive ice (Streletskaia & Leibman 2002), cryopegs were found in the sandy section part only. They are not present in the clayey part.

Coastal-marine ground ice

Coastal-marine ground ice is found in the same areas as subsea massive ice bodies. It is formed in the marginal parts of sea basins (Shpolyanskaya 1991). Ice layers are formed by freezing of suprapermafrost water horizon at the base of the active layer during the periods of regular flooding in coastal areas. Along with sedimentation in these areas, the active layer and the suprapermafrost water horizon move upward. As a result, rhythmically layered, ice-soil stratum grows upward, forming syngenetic permafrost. The structure of this stratum is represented by thick sub-horizontal soil and ice layers without significant dislocations.

Ground ice of subsea and coastal-marine genesis occurs

only in marine and coastal-marine deposits within the arctic lowland plains, described as marine plains by Popov (1959), Lazukov (1989), Danilov (1978), and now by Velichko et al. (2011). The occurrence of the described ground ice confirms their opinion. It should be noted that in Chukotka such ice occurs within the territory where Velichko et al. (1992) show marine transgression of Kazantsev age. The fact that this ice has been commonly observed in the Kazantsev deposits means that it was formed in the absence of glaciation and, therefore, it cannot be buried glacier ice and, contrary to existing opinions, does not indicate the existence of a past ice sheet. In our opinion, this ice was formed in a sea basin at least 50 m deep, and its occurrence confirms a sea basin existence at that time. This ice is also prevalent in the Zyryan deposits often overlain with the Kargin deposits, mainly in Western Yamal, the Yamal and Priuralsky coasts of Baydaratskaya Bay, in Taymyr within the North Siberian lowland, and in Chukotka. Its presence points to the marine conditions remaining in these areas during Zyryan and Kazantsev times, although the sea depth during these periods was changing.

Intrusive ground ice

In addition to the described types of ice, the tabular massive ice of intrusive genesis also occurs on the plains. Such ice always has marks of water pressure injection. It usually occurs in the intrusive groundwater discharge areas and in closed lake basins during freezing of the lake taliks. It forms epigenetically in subaerial conditions and occurs mostly in the Sartan deposits. Intrusive ice is also a

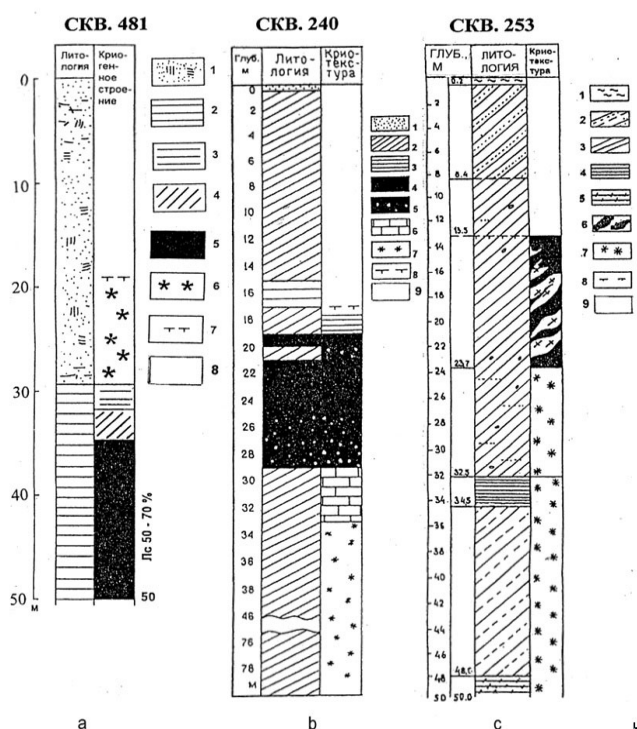


Figure 2. Sections of subsea permafrost of the Barents-Kara Shelf (Melnikov & Spesivtsev 1995).

a - borehole 481 in the Kara Strait area (sea depth is 65 m). 1 – sand with inclusions of organic material; 2 – clay; 3 - 6 cryogenic structure; 3 – horizontally layered; 4 – dislocated subvertical with large ice lenses; 5 – ataxitic (tabular massive ice); 6 – porous; 7 – permafrost table; 8 – cryotic unfrozen sediments.

b – borehole 240 in the Baydaratskaya Bay (sea depth is 13-14 m). 1 – sand; 2 – silty clay; 3 – clay; 4 - 7 cryogenic structure; 4 – tabular massive ice; 5 – ataxitic; 6 – reticulate; 7 – porous; 8 – permafrost table; 9 – cryotic unfrozen sediments.

c – borehole 253 in the Kara Sea on the Rusanovskaya Field (sea depth is 130 m). 1 – silt; 2 – rhythmical interbedding of sand, sandy silt and silty clay; 3 – silty clay; 4 – clay; 5 – argillite-like firm clay; 6 – tabular massive ice; 7 – porous cryostructure; 8 – permafrost table; 9 – cryotic unfrozen sediments.

glaciation antagonist. Its distribution (Fig. 1) indicates the absence of glaciation in the Sartan Epoch.

Buried surface ice

Buried surface ice also occurs in the region. It is very different from the above-described types of ice in its macro- and micro-structure. It has a distinctive large-block bedding represented by the alternation of thick layers of clear ice and compacted soil layers. The ice micro-structure is different from that of subsea ice; the bedding in crystal structure is either absent or reflects the annual thickness of firm layers. Their chemical composition is stable hydrocarbonate. Such ice occurs mainly in mountain areas and foothills. Its limited distribution (Fig. 1) is evidence of a small area of ancient glaciations in the Russian North.

Wedge ice

Ice wedges are wedge-shaped or column-shaped in section and form a polygonal net in plan. They form only in continental conditions on periodically flooded surfaces.



Figure 3. Ground ice in the dislocated subsea sediments of the Barents-Kara Shelf (Melnikov & Spesivtsev 1995, Bondarev et al. 2001).

Basic conditions for ice-wedge formation include the formation of a polygonal fracture system as a result of repeated thermal-contraction cracking of soil surface and subsequent water penetration into the cracks. Wedges can grow epigenetically or syngenetically. Syngenetic wedges grow upward along with accumulation of sediments, mainly in the conditions of coastal-marine, lacustrine-alluvial, and slope sedimentation. Occurrence of wedge ice indicates the absence of glacial ice sheet during its formation. In the north of Western Siberia, wedge ice is common in the eastern parts of the Yamal and Gydan Peninsulas, in the Sartan, and the underlying Karginsky sediments. It indicates the lack of the glaciation in those periods. Occurrence of wedge ice in the eastern parts of Yamal and Gydan in the same deposits which have subsea and coastal-marine ice in the western parts of Yamal and Gydan indicates differential tectonic movements in this region.

West Arctic Shelf

Permafrost with tabular massive ice is widespread in the western sector of the arctic shelf (Fig. 1). Subsea permafrost was found at water depths from 0 to 230 m (Bondarev et al. 2001). The permafrost table can lie at the approximate depth of 20 to 40 m under the sea floor or rise to the bottom surface. The base of permafrost sinks to 100 m and lower. In the sections of subsea permafrost sediments there is often a large amount of ice, sometimes up to 100% (Fig. 2).

Many authors consider permafrost to be relict in the west Arctic Shelf. However, the fact of permafrost occurrence at depths from 0 to 230 m indicates its heterogeneous nature. Even if we accept the idea of the Sartan Sea regression to the isobath of 100 to 120 m which led to the freezing of shelf soils under subaerial conditions, there are still vast areas with the sea depth from 100 to 230 m where permafrost must have formed directly under subsea conditions. The scale of sea regression in the Late Pleistocene is also questionable; according to Danilov (2000), the lowering of the sea level was only -30 to -50 m.

The analysis of shelf permafrost shows that the structural features of the ice-rich subsea sediments, for example in the Kara Strait or in the Rusanovskaya Field (Bondarev et



Figure 4. Dislocated tabular massive ice of subsea genesis in the "Tadibeyakha" section (Western Gydan Peninsula). Photograph by N.A. Shpolyanskaya.

al. 2001, Rokos et al. 2009), are very similar to the above-described dislocated strata with tabular massive ice which we called subsea ice (Figs. 3 and 4). The structure of these frozen sediments formed in deep-sea conditions of the Barents-Kara Shelf corresponds to the proposed mechanism of initial subsea freezing (Shpolyanskaya 2010). Therefore, the plains of the western sector of the Russian Subarctic should be considered the Pleistocene transgressive marine plains. They are the former shelves analogous to the modern Arctic Shelf and the north of Western Siberia and the northeast of European Russia that experienced a transgressive regime during most of the Pleistocene. It also indicates the absence of glacial sheets in these periods.

Eastern Sector of the Russian Arctic

East Arctic land

In the eastern Siberia plains, in contrast to the western sector, massive ice is almost entirely represented by wedge ice, which forms the so-called ice complex.

Wedge ice

Wedge ice is most common in the Yana-Indigirka and Kolyma lowlands, the Central Yakut lowland, and the New Siberian Islands. Here, unlike the western Arctic sector, the sediments containing ground ice are continental, including alluvial, alas, slope, coastal-marine, and lagoon deposits. Starting with the Pliocene, the deposits of Prymorskaya Lowland are represented by lacustrine-alluvial, alluvial and lacustrine-bog deposits. The Olerskaya Suite deposits (Eopleistocene and early Neopleistocene) contain pseudomorphs formed as a result of thawing of wedge ice (Arkhangelov et al. 1989, Nikolskiy & Basilyan 2002). On the Dmitri Laptev Strait coast and on Great Lyakhovsky Island, the stratum with wedge ice formed in the middle Neopleistocene 200,000–180,000 years ago, according to $^{230}\text{Th}/\text{U}$ analysis (Schirmeister et al. 2002). The late Neopleistocene, starting from the Kazantsev time, is also represented exclusively by continental deposits (Alekseev et al. 1992). Only in the Middle Pleistocene was there a limited sea transgression which flooded a narrow coastal

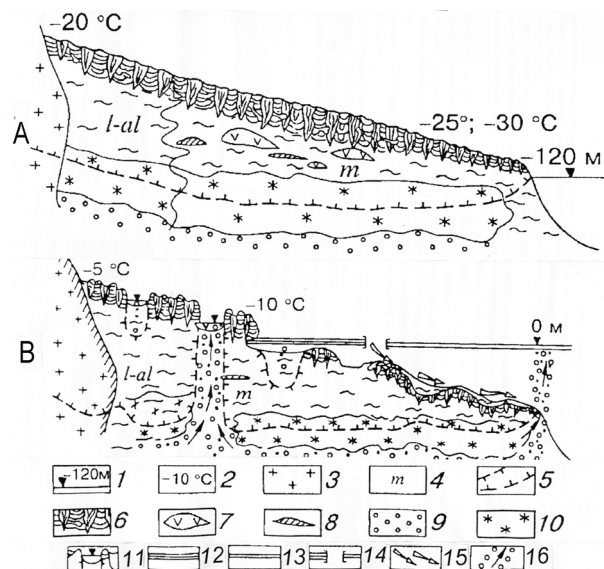


Figure 5. The Laptev Sea shelf structure (Romanovskiy et al. 1997). A – 20,000-18,000 years ago, B – present time. 1 - sea level; 2 - average mean annual temperature of soil; 3 - bedrock; 4 - the genesis index of Quaternary deposits; 5 - permafrost boundary; 6 - ice complex; 7 - tabular massive ice; 8 - lens of cryopeg; 9 - deposits containing free gas; 10 - deposits with gas hydrates; 11 - thermokarst lake; 12 - fast ice; 13 - young sea ice; 14 - open lead; 15 - cold salt brine; 16 - greenhouse gases flow.

strip approximately from the Lena River mouth to Chaun Bay (Alekseev et al. 1992) and formed a marine terrace with an age of 138,000 years (Bolshiyarov et al. 2009).

East Arctic Shelf

In contrast to the western sector, permafrost of the eastern sector of the Arctic Shelf is entirely relict (Figs. 1 and 5). An ancient ice complex of the Zyryan and Sartan age flooded by a postglacial transgression was detected in this area (Romanovskiy et al. 1997). Occurrence of the subsea ice complex is evidence of the continental environment in this area (as opposed to the western sector) during the whole Pleistocene under conditions of constant severe climate and the absence of a glacial ice sheet.

Concluding Observations

First, the spatial patterns of the ground ice occurrence in relation to their genesis indicate the absence of glacial ice sheets in the Pleistocene and Holocene in the Russian North plains, most likely, to the east of the Kanin Peninsula. Mountain-valley glaciation sometimes changing into reticulate glaciation occurred only in mountain areas.

Second, the eastern and western sectors of the Russian Arctic and Subarctic evolved differently in the Pleistocene, and the transgressive-regressive regime affected them in different ways. During almost the entire Pleistocene (excluding the Sartan time), the western sector plains formed under conditions of predominantly marine sedimentation, and the eastern sector plains formed under conditions of continental, predominantly lacustrine-alluvial and lagoon, sedimentation. Only the regression of the last part of the late Neopleistocene (the Sartan time) and the Holocene

transgression proceeded simultaneously in both sectors.

Third, the currently accepted synchronism was not detected. Our conclusions contradict the common opinion about the leading role of global glacioeustatic processes in sea level variations. It should be noted that such doubts are reflected in some other recent works. For example, after his study of the Antarctica glaciers and their paleodynamics, Verkulich (2009) concluded that the growth of ice masses in Antarctica was not the main reason for the sea level fall in the last glacial maximum (22,000–17,000 years ago), and the subsequent deglaciation of Antarctica was not the primary reason for the start of the process of global deglaciation. Both processes followed global climate and sea level change. He presents data on the reefs, according to which the start of the rapid sea level fall was 32,000 years ago, well ahead of the start of the active growth of glacier ice in Antarctica. The synchronism of the major climatic events of the southern and northern hemispheres is well known, and it was supported by a large number of dates in the work of Verkulich as well. That is why certain conclusions for Antarctica can be correlated with the Arctic areas. The period of 32,000 years ago was a relatively warm (close to modern climate) Kargin time, and if the sea level began to fall, it was not related to glaciation dynamics in any region. Moreover, in Northern Siberia there are many evidences of a small sea transgression at that time. All these facts strengthen doubts about the leading role of glacioeustatic processes in sea level variations and bring tectonic movements to the forefront. The new data on a complex heterogeneous tectonic organization of the Arctic Basin add credibility to this version. The mid-oceanic ridge (the Gakkel Ridge) within the Arctic Basin and the junction of the Eurasian and Amerasian tectonic plates have a significant influence on the irregular fluctuations in the level of the Arctic Basin, and their influence appears to be considerably higher than the effect of glacioeustatic processes.

References

- Alekseev, M.N., Arkhangelov, A.A., Grinenko, O.V., Kim, B.I., Patyk-Kara, N.G., Plakht, I.G., & Reynin, I.V. 1992. The Laptev and the East Siberian Seas shelf in the Mesozoic and the Cenozoic. *Atlas of Palogeographic Maps*, Vol. 2 (edit. M.N. Alekseev). Robertson GRUP-GIN ANSSR.
- Arkhangelov, A.A., Konishchev, V.N., & Rozenbaum, G.E. 1989. Primorsk-Novosibirsk Region. *Regional cryolithology*. Moscow: Izd-vo MGU, 128-151 (in Russian).
- Bolshiyarov, D. Yu., Grigorev, M.N., Shnayder, V., Makarov, A.S., & Gusev, E.A. 2009. Sea level variations and ice complex formation on the Laptev Sea coast. System of the Laptev Sea and the adjacent Arctic seas. Moscow: *Izd-vo Mosk. Un-ta.*, 349-356 (in Russian).
- Bondarev, V.N., Loktev, A.S., Drugach, A.G., & Potapkin, Yu.V. 2001. Methods of research and determination of subaqueous permafrost. *Sedimentological Processes and Marine Ecosystems Evolution in Marine Periglacial. Sb. nauchn. tr.*, Volume 1. Apatity, Kolskiy nauchnyy tsentr: pp. 15-19 (in Russian).
- Danilov, I.D. 1978. The Pleistocene of Subarctic marine plains. Moscow, *Izd-vo Mosk. un-ta*, 198 p.p. (in Russian).
- Danilov, I.D. 2000. Subsea permafrost of the Arctic Shelf and associated lithomorphogenesis Cryogenic Processes. *Okeanologiya*, 40 (no. 5):756-764 (in Russian).
- Lazukov, G.I. 1989. The Pleistocene of the USSR Territory. Moscow, *Vysshaya shkola*, 320 pp. (in Russian).
- Melnikov, V.P. & Spesivtsev, V.I. 1995. Geotechnical and geocryological conditions of the Barents and the Kara Seas shelves. Novosibirsk, Nauka, 195 pp. (in Russian).
- Nikolskiy, P.A. & Basilyan, A.E. 2002. Cape Svyatoy Nos - reference section of Quaternary sediments of the north of Yano-Indigirka Lowland. *Mat-ly III Vseros. Soveshch. Po Izucheniyu Chetvert. Perioda*. Smolensk, pp. 186–188 (in Russian).
- Popov, A.I. 1959. The Quaternary period in Western Siberia. Ice Age on the USSR European part and Siberia Territories. Moscow. *Izd-vo Mosk. un-ta* (in Russian).
- Rokov, S.I., Dlugach, A.G., Kostin, D.A., Kulikov, S.N., & Loktev, A.S. 2009. Permafrost of the Pechora and the Kara Sea shelves: Genesis, composition, distribution and occurrence. Geotechnical investigation. *Vserossiyskiy inzhenerno-analiticheskiy zhurnal*. No. 10, 38-41 (in Russian).
- Romanovskiy, N.N., Gavrilov, A.V., Kholodov, A.L., Khubberten, H.-V., & Kassens, H. 1997. Reconstruction of paleogeographic conditions of Laptev Sea Shelf for Late Pleistocene-Holocene glacioeustatic cycle. *Kriosfera Zemli*. 1. (no. 2): 42-49 (in Russian).
- Schirmmeister, L., Sigert, C., Kuznetsova, T., Kuzmina S., Andreev, A., Kienast, F., Meyer, H., & Bobrov, A. 2002. Paleoenvironmental and paleoclimatic records from permafrost deposits in the Arctic region of Northern Siberia. *Quaternary International* 89: 97-118.
- Shpolyanskaya, N.A. 1991a. Structure and genesis of Western Siberia tabular massive ice. *Vestnik Mosk. un-ta, geografiya* No. 5: 73-83 (in Russian).
- Shpolyanskaya, N.A. 1991b. Subsea Permafrost formation in the Arctic. *Mater. glyatsiol. issled. Khronika, obsuzhdeniya* issue 71: 65-70 (in Russian).
- Shpolyanskaya, N.A. 1999. Cryogenic structure of dislocated strata with tabular massive Ice as indicator of their genesis (North of Western Siberia). *Kriosfera Zemli* Vol. VI, No. 4: 61-70 (in Russian).
- Shpolyanskaya, N.A. 2005. Modern problems of the Arctic Shelf permafrost region. *Izvestiya RAN, Seriya Geograficheskaya* No. 1: 102-111 (in Russian).
- Shpolyanskaya, N.A. 2010. Features of permafrost of the Arctic western Sector in the Shelf-Land System. *Vestn. Mosk. un-ta. Ser. 5. Geografiya*. No. 6: 58-66 (in Russian).
- Shpolyanskaya, N.A. & Streletskaya, I.D. 2004. Genetic types of massive ice and its distribution pattern in the Russian Subarctic. *Kriosfera Zemli*, 8 (no. 4): 56-71 (in Russian).
- Streletskaya, I.D. & Leibman, M.O. 2002. Cryogeochemical interrelationship of tabular massive ice, cryopegs and their host sediments of Central Yamal. *Kriosfera Zemli* 6, (no. 3): 15-24 (in Russian).
- Velichko, A.A., Peci, M., & Frenzel, B. (eds.) 1992. *Atlas of Paleoclimates and Paleoenvironments of the Northern Hemisphere. Late Pleistocene-Holocene*. Budapest, Stuttgart, 153 pp.

- Velichko, A.A., Timireva, S.N., Kremenetski, K.V., MacDonald, G.M., & Smith, L.C. 2011. West Siberian Plain as a Late Glacial desert. *Quaternary International* doi: 10.1016/j.quaint.01.01.
- Verkulich, S.R. 2009. Deglaciation conditions and behaviour in Antarctica marginal zone. *Kriosfera Zemli* 8 (no. 2): 73-82 (in Russian).

Forecast of Air Temperature Change in Yakutia to the Middle of the Twenty-First Century

Yu.B. Skachkov, L.G. Neradovskiy
Melnikov Geocryology Institute, SB RAS, Yakutsk, Russia

Abstract

A forecast of the annual mean surface air temperature T_a through 2050 was completed using the classical harmonic analysis method on the basis of the data from six weather stations located in different parts of Yakutia. The Stadia software of A.P. Kulaichev was used for this purpose. The forecast methodology provided for the creation of Fourier models in their original form and with the removal of inter-annual T_a variation harmonics for a period of 3-6 years. Consequently, not only general trends, but also common specific peculiarities of Fourier model behavior for the whole Yakutia were defined. They are most clearly observed in the long T_a series of Yakutia (180 years) and Verkhoyansk (122 years). These results indicate that climate warming observed in Yakutia will occur according to a moderate scenario. The T_a growth rates will slow down in the nearest future and will enter a long stabilization stage. The latter is considered a fragment of the century background connected with the sphere of maximum phase equilibrium. The temperature increase will most evidently exceed the climatic level achieved to date, with no more than 0.7–1.0°C by 2050.

Keywords: forecast; Fourier models; annual mean air temperature; Yakutia.

Introduction

The issue of forecast investigations is made acute by the following factors: the irreversibility of the global and regional climate changes occurring today and their negative consequences; the lack of knowledge obtained about the causes of current climate changes and their spatial and time regularities; and the uncertainty of the reaction of the cryolithozone associated with this. At the current stage of human societal development, this issue is in much demand. Long-term strategic planning is needed for the economy and industrial development in the northern territories of Russia, and in particular in a region as large as the Republic of Sakha (Yakutia).

Purpose of Investigations

The purpose of investigations is to analyze the data of the weather stations located in different parts of Yakutia and to prepare a digital long-term forecast of the annual mean surface air temperature by 2050. Modern computer technologies of mathematical modeling by means of the classical method of harmonic analysis were used to achieve the purpose defined.

Climate Characteristics

Yakutia is characterized by extreme continental climate and high inter-annual variability of the annual mean air temperature T_a . The variation between 1966 and 2009 is on average 4–5°C at all weather stations. The variation minimum (-3.4°C) was noted in Batamay Village, and the maximum (-5.6°C) in Tiksi Village and Chulmane Village.

Global climate warming that started in the second half of the 1960s affected the Northern Hemisphere and covered the area of Yakutia as well. The warming in this region between 1966 and 1988 was relatively smooth and was characterized

by almost zonal distribution of increased air temperature.

The climate warming process occurred in a more sharp way at the beginning of the 1990s. An increase in air temperature is noted within the entire Yakutia area. Moreover, it is spatially inhomogeneous: the increase of T_a to the south from 64°N was 1.5–2°C and above, and in the northwest and the northeast of Yakutia was 0.5–1°C. It should be noted that winters make the most significant contribution to the increase of the annual mean air temperature. They became warmer, particularly in Central and Southern Yakutia. Summer warming is not as noticeable yet (Skachkov 2005).

Temperature trends within Yakutia tend to be warming. This process is also inhomogeneous in space. The contribution of winter temperatures to annual mean values still remains significant. However, the number of weather stations that had a statistically significant rise of summer mean air temperatures grew as well. All these stations are located south of the latitude of Verkhoyansk (69°N).

Temperature variations occurred quite synchronously but with varying amplitude (Fig. 1) in a significant part of Yakutia during the monitoring period (1966–2009). The

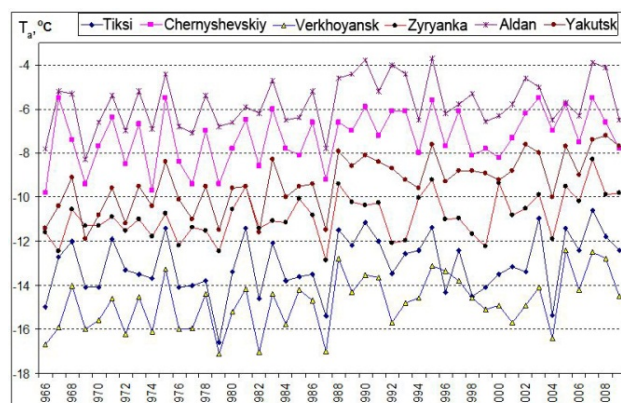


Figure 1. Space-time variability of the annual mean air temperature in Yakutia between 1966 and 2009.

Table 1. List of weather stations.

Monitoring station	Period of monitoring	Forecast beginning	Length of T_a series
Aldan	1926-2009	1930	80
Yakutsk	1830-2009	1830	180
Chernyshevskiy	1966-2009	1966	44
Zyryanka	1965-2009	1965	45
Verkhoyansk	1888-2009	1888	122
Tiksi	1933-2009	1936	74

paired correlation ratios between the six points located at a significant distance from each other also indicate the high degree of conformity of inter-annual mean air temperature changes.

The noted regional behavioral peculiarities of the temperature series in time and space served as the basis for the numerical air temperature forecast in Yakutia.

Forecast Methodology

The actual material used is sufficient in volume and content for the identification of change regularities of the annual mean air temperature in Yakutia that could occur in the coming decades with different degrees of probability.

The problem of forecasting the long-term T_a temperature series as well as other such problems does not have any specific solution. This is because we cannot predict the future condition of human society. Forecast methods, while being mathematically sophisticated, allow only the visualization of some features or indicators of the future in general, and stable regularities of the present.

This is precisely why the main attention during the forecast was paid not to the accurate adherence to the formal procedures of numerical analysis, but to the search for the representative actual data (T_a temperature series). This material contains basic periodical regularities to the maximum possible completeness indicators.

From the abundant available material, six weather stations were chosen from the southern, northern, western, eastern, and central parts of Yakutia (Table 1) for exploratory statistical analysis.

The algorithm of the Fourier model creation method was used as a tool for the mathematical forecast. It was developed by A.P. Kulaichev and used in one of the processing modules of the Stadia software (Kulaichev 2006). Its main advantage as compared to other programs is the adjustment of the reverse Fourier transformation to the peculiarities of the T_a basic series structure, including its frequency filtration, noise clearance, and other details of digital processing.

The adjustment of the forecast model is conducted by means of successive approximations of the time series based on the criterion of the least squares for three parameters: amplitude, phase, and frequency, for each non-zero spectral component of the model.

Each of the three parameters is changed iteratively by the Stadia software in such a way that the maximum

model approximation to the time series becomes possible. Consequently, the adjustment on the basis of frequency leads to non-repetition of the beginning of the time-temperature series model in the forecast.

The forecast methodology provided for the examination of several generation options of the Fourier models for each weather station, and was based on two principles: with no transformations in the basic form, and with the removal of short-period components (3 to 6 years) of inter-annual T_a variations.

When short-period variations are accumulated, they are so strong (about 60% of the whole spectrum energy) that they shield long-term and more regular temperature changes, prohibiting, or more specifically, complicating their detection. This in turn reduces the quality and the reliability of the long-term forecast. This is precisely why the tails (ends) of spectra were cut, and thus the noise (short-period variations) was removed from the basic T_a series.

Such selective filtration procedures to some extent allowed us to receive the plausible evaluation of the forecast on the basis of short time series (Chernyshevskiy & Zyryanka).

As for the problem of forecast evaluation reliability, we note that the method of artificial increase of the length of the time series in their initial part suggested and used by some researchers is principally unsuitable for the solution of such problems. It only deliberately increases the share of randomness and uncertainty in the results.

That is why the T_a series were used for the forecast in the form in which they were received for the monitoring period. The preference in this connection was given to the forecast evaluations for the longest series. These are Yakutsk and Verkhoyansk. Nonetheless, these series also turned out insufficient in length. These did not allow us to obtain the spectral evaluation of the century-long period (above 100 years) or elements of the annual mean temperature variability with the required accuracy and resolution.

Consequently, only the element with the period of 60 years could be used for long-term forecast. It is observed in the long T_a series that the energy peak value occurs in the initial part of the spectra. The 60-year harmonics is stable not only in Yakutia but in the arctic region as well (Frolov et al. 2007).

Therefore, it was decided to use it as a reference element for the forecast of the trend change of annual mean air temperature in Yakutia until 2050.

The Fourier models were calculated with the use of the procedure of inter-annual variability smoothing by means of the averaging interval of 10 years with successive interval shift along the set T_a series with the step of one year. The MezoZawr software was used for that simulation. As compared to other programs (e.g. Statistica-6), this software correctly fulfills the smoothing operation for complex multi-component series.

Forecast Results

The large volume of the results of graphical forecast cannot all be presented. Consequently, this work presents the description of forecast results on the basis of the longest T_a series diagram of Yakutsk only (Fig. 2).

The preservation of the short-period element in the

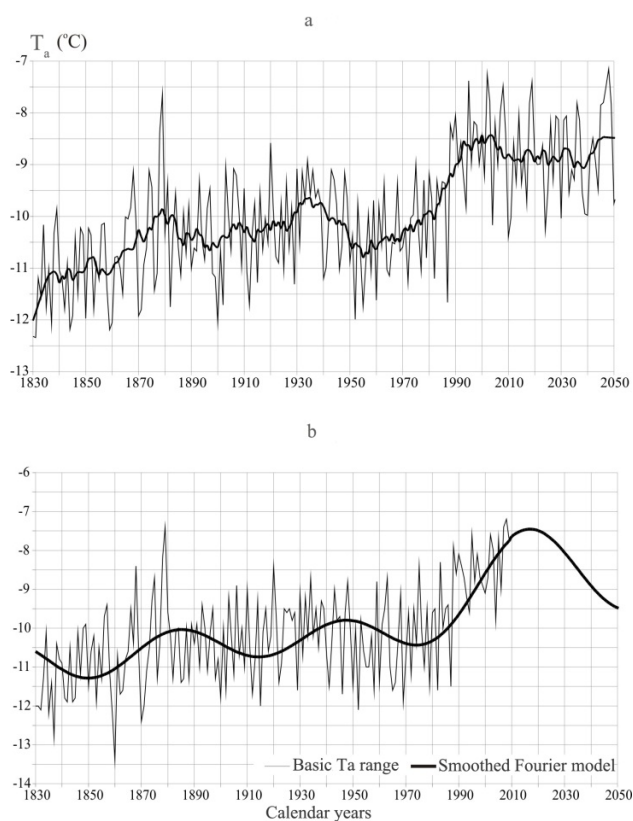


Figure 2. Diagram of basic T_a temperature series and its Fourier models with forecast until 2050: a – smoothed model in the 10-year averaging interval; b – with filtration of periodic elements more than 60 years long.

spectrum and the noise clearance at the 35% energy level provides for good convergence of the general shape and details of the T_a series and its Fourier model on the basis of the morphological parameter (the average distance between them is 0.24°C).

The forecast part of the T_a series model preserves the features of the basic process: strong oscillations of the inter-annual variability of air temperature. At this background, it is hard to detect and make a decision on the existence of the trend of temperature rise or fall. Only temperature regime stabilization within the interval minus 8.5 to 9.0°C can be stated. The situation becomes clear after the smoothing of the model with a sliding interval of 10 years (Fig. 2a). It becomes clear that in the 10-year cycle, the air cooling process that started in 2002 is slow and will continue until 2040. After that, a warming period with the air temperature returning to -8.5°C is expected.

A more simplified forecast pattern is observed in the process of the T_{av} series model creation with the omission of the harmonics of the spectrum more than 60 years long (Fig. 2b). In this forecast version, the warming in Yakutsk will continue reaching the maximum level (-7.5°C) in 2015. Then, starting from 2020, a monotonous fall of air temperature will begin. It will reach the level of -9.5°C by the end of the forecast period. The difference in comparison with the achieved climatic level is high and is equal to two degrees.

The forecast for Yakutsk agrees with the results of hydrometeorological and ice conditions investigations in the arctic region (Frolov et al. 2007). Using the natural 60-year

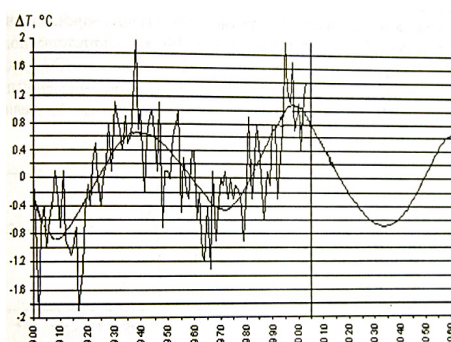


Figure 3. Changes of the anomaly of the annual mean air temperature in the 70 – 85°N latitudinal zone in the 20th century and at the beginning of the 21st century and its background forecast (Frolov et al. 2007).

cycle of air temperature change as the basis for long-term forecast, the researchers came to the following conclusion: “It is most probable that the warm period will be over in approximately 2015–2020. Further temperature reduction, as per the forecast, will approximately continue until the middle of the 2030s. Then the transition to the successive warming can be expected again. This one, like the previous one, will be limited in time.”

We would like to explain that the forecast evaluation in the arctic region was received for only one harmonics 60 years long with the amplitude of 0.6°C , and with no regard to the linear air temperature trend.

It is remarkable that the forecast evaluations of the temperature range obtained for different climatic conditions almost coincide with the maximum warming and cooling phases. As was already mentioned above, it consists of 2°C in Yakutsk and 1.8°C in the arctic eegion (Fig. 3). The difference is 0.2°C .

We will describe one more result of the investigations conducted recently by P.I. Melnikov of the Geocryology Institute, SB RAS. This is required to substantiate the objectivity and, to some extent, the reliability of the forecast obtained for the conditions of the Central Yakutia lowlands where Yakutsk is located (Balobaev et al. 2009). They were conducted on the basis of the classical harmonic analysis chart with the calculation of the air temperature for a very long time period, until the end of the next century.

According to the forecast, the beginning of stable cooling in Yakutsk will occur in 2018 and will continue until 2048. Then warming will occur again with stable and lower temperatures than for the previous climatic period at the level of minus 9 to 10°C .

Outputs

The comparison of the specific peculiarities and the general trends of Fourier diagrams behavior that models the temperature series of varying length and spectral composition allows us to make the following conclusions:

- 1) Based on the combination of the amplitude-phase attributes, it is expected that the climate warming observed in Yakutia will occur according to a moderate scenario, like in West Siberia.

- 2) The linear rate of annual mean air temperature increase will slow down in the next several years and will reach a long-term stage of fading or stabilization. It will most evidently exceed the achieved climatic level by no more than 0.7–1.0°C by the end of the forecast period.
- 3) The asymptotic (stabilization) site found on the basis of the combination of forecast temperature diagrams for six weather stations is considered a fragment of the century background joining the area of the maximum phase equilibrium.

Here, cooling periods 5 to 30 years long that are local in time, place, and amplitude (0.5–0.7°C) are expected.

Conclusion

It is premature to speak of a long-term change of the climatic situation toward abrupt cooling beginning in the nearest years. The actual data do not present convincing arguments for this scenario.

The turning point toward long-term and severe climate cooling will most probably occur in Yakutia starting in 2050–2060. It will reach a temperature minimum at the beginning of the following century.

References

- Balobaev, V.T., Skachkov, Yu.B. & Shender, N.I. 2009. Climate and permafrost thickness change forecast for Central Yakutia till 2200. *Geography and Natural Resources* 2: 50-55 (in Russian).
- Frolov, E.I. et al. 2007. *Scientific investigations in the Arctic Region. Volume 2. Climatic changes in the ice cover of the Eurasian shelf seas*. St. Petersburg: Nauka, 158 pp. (in Russian).
- Kulaichev, A.P. 2006. *Complex data analysis methods and means*. 4th edition, amended and added. Moscow: FORUM: INFRA-M, 512 pp. (in Russian).
- Skachkov, Yu.B. 2005. Trends of modern air temperature changes in the Republic of Sakha (Yakutia). Investigations of the cryogenic regions landscapes. Yakutsk: Izd-vo IMZ SO RAN, *Problems of Yakutia's Geography* 9: 27-31 (in Russian).

The Impact of Development and Fire on the Thermal State of Permafrost, Central Yakutia

P.N. Skryabin, S.P. Varlamov
Melnikov Permafrost Institute, SO RAN, Yakutsk, Russia

Abstract

The spatial and temporal changes of the ground thermal state were assessed based on the results of research carried out on the left and right banks of the Lena River in the vicinity of Yakutsk. The thermal impact on the upper permafrost horizons from forest cutting, forest fires, soil cover removal, and some other factors was monitored and evaluated. The research includes long-term field studies with the help of the method of geographical analogy. The thermal state monitoring network includes terrains with natural conditions as well as those affected by human impacts. The thermal state of permafrost was studied to the depth of mean annual amplitudes. The field studies include a repeated survey of the disturbed terrain. They also include the monitoring of snow depth and density as well as soil properties, seasonal soil thawing, and ground temperature. The studies revealed a considerable increase in the mean annual temperature of soil as well as an increase in the active layer depth after forest cutting, soil cover removal, and cutting of burned-out forest in the inter-*alas* type of terrain. The development of permafrost-related processes was also revealed. The dynamics of mean annual temperature of soil was quantitatively assessed in areas with different patterns of forest cutting as well as in burned-out areas in relation to stages of the succession of the recovering vegetation.

Keywords: active layer; forest fire; human impact; soil temperature; thermal state monitoring.

Introduction

Assessment of the thermal state of the upper permafrost horizons in association with climate warming and development plays a specific role in contemporary permafrost studies.

The most successful investigations on this issue are ongoing in the northern regions of Russia, Canada, Alaska, and Europe (Varlamov et al. 1990, Osterkamp et al. 1994, Pavlov 1994, Burgess & Lawrence 1997, Harris et al. 2000, Romanovsky et al. 2003, 2010, Christiansen et al. 2010, Lin Zhao et al. 2010, Smith et al. 2010). The soil temperature regime represents one of the key factors that determine the stability of engineering structures. Pipelines, railways, roads, and transmission lines are increasingly constructed in Central Yakutia and are accompanied by significant impacts on the environment. Changes are also observed near villages and cities that are continually affected by human activity. Human disturbances of various types and magnitudes (forest clearing, forest fires, soil cover removal, etc.) alter permafrost conditions, including the soil temperature regime. These changes trigger adverse permafrost-related processes and cause the deterioration of the environment as a whole.

For many years, the Permafrost Institute studied the temperature regime of permafrost to the depth of the zero temperature amplitude in areas affected by development (Shimanovskiy 1942, Melnikov 1950, Pavlov 1975, and others). An analysis of previous works showed the need for more detailed studies of human impacts on spatial and temporal changes in the thermal state of permafrost.

Monitoring of the ground temperature regime by the authors in Central Yakutia since 1987 reveals its spatial and temporal patterns related to human impacts. The results of these studies were published earlier (Skryabin et al. 1992, Varlamov 2006, Skryabin 2007 et al.). The present report summarizes the results of the long-term studies in the northern area of the Tommot-Yakutsk Railroad, along the Taas Tumus-Yakutsk Pipeline right of way, and the Yakutsk-Mundulakh Water Pipeline.

Research Sites and Methods

The investigations were carried out on the right and left banks of the Lena River in the vicinity of Yakutsk (Fig. 1). The research area is characterized by continuous permafrost with active ice wedges and the occurrence of supra- and intra-permafrost water-bearing taliks.

Long-term thermal monitoring is required in areas that previously were affected by human impacts and recently have undergone recovery. The studies were carried out in terrains characterized by low terraces, sand-ridges, inter-ridge depressions, inter-*alas*, and flat interfluvial plain. These terrains differ in genesis and soil characteristics. The monitoring network includes 70 sites with different effects of human activities. Among them, 8 sites had soil cover removed, 27 sites were in forest cutting areas, 15 sites were in burned-out areas, and 21 sites were in the burned-out and deforested areas. The research includes complex terrain studies and monitoring of the thermal state of soil in natural and disturbed conditions.

Results and Discussion

Monitoring data allowed us to quantitatively assess the dynamics of the thermal state of permafrost-affected terrain and under natural conditions (Fig. 2). Considerable inter-annual changes in the mean annual soil temperature were observed in the inter-ridge-depressions and small valleys. The thermal state of soil there was mainly affected by winter factors such as snow and the magnitude of the air freezing index. For instance, the lowest temperature of soil was registered in the small-valley type of terrain during the season of 1986–1987, with its abnormally late formation of snow cover, and during the seasons of 1994–1995, 2002–2003, and 2003–2004, with abnormally small amounts of snow precipitation. The maximum increase in the soil temperature was registered in the seasons of 1999–2000 and 2007–2008 with warm winters and abundant snow. Over

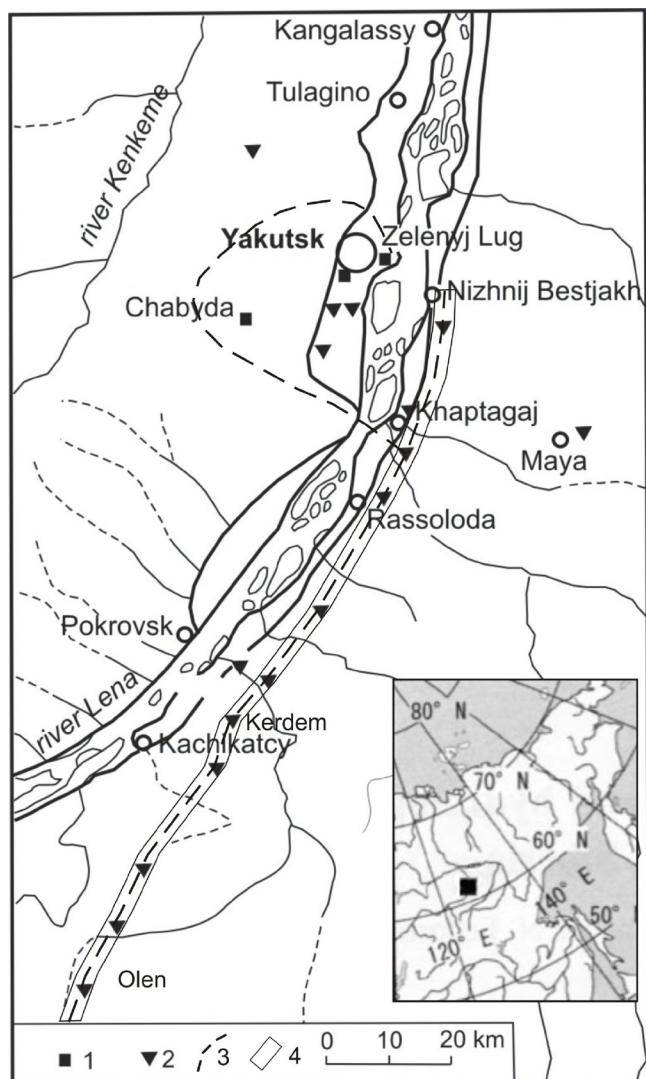


Figure 1. Research area map 1 – permafrost stations, 2 – monitoring sites, 3 – railway, 4 – areas of terrain mapping.

the 24-year period of thermal monitoring (1987–2010), the trends of the mean annual soil temperature in various terrain types range from slightly negative ($-0,003 \dots -0,009^{\circ}\text{C}/\text{year}$) to positive ($0,005 \dots 0,073^{\circ}\text{C}/\text{year}$).

For the present increase in the mean annual air temperature, the natural thermal state of the upper permafrost horizons is evaluated as rather stable. This can be explained by the dynamics of snow accumulation.

The changes in the main parameters of the soil thermal state under anthropogenic disturbance were analyzed on the basis of monitoring data.

Sites with removed soil organic cover

Moss and peat layers with a thickness of 0.15 to 0.25 m were removed in 1990 along the northern site of the Tommot-Yakutsk Railroad in the sand-ridge type of terrain. As compared to natural conditions, the mean annual soil temperature at the depth of 6 m after organic layer removal increased by 4°C in the third year. After 18 years and intensive growth of young dwarf birch on the disturbed land, the difference in the mean annual soil temperature decreased to 1.8°C . The thickness of the active layer in the disturbed area at that time was 2.3 m, which is 2.4 times greater than in natural conditions.

In 1992, a larch forest in the inter-alas type of terrain was clear-cut along the Yakutsk-Mundulakh Water Pipeline right of way. The soil cover was heavily affected by traffic. After 18 years, the temperature of soil at the depth of 10 m increased by 2°C and the depth of the active layer increased by 1.4 m. This triggered surface subsidence of 0.6 m with the development of patterned relief. In the larch forest of an inter-alas terrain, soil temperature increased from 0.2 up to 1.0°C at the depth of zero annual amplitude after the moss cover was removed. The increase in thickness of the active layer did not exceed 0.5 m but was accompanied by subsidence.

In 1989, a larch forest was clear-cut at the slope of inter-alas terrain, and the soil surface cover and the upper layer of soil were removed. Abundant precipitation in June triggered the development of thermal erosion along the road with formation of a ravine. After five years, the length of the ravine reached 340 m, its width was 10–16 m, and its depth was 6 m. Formation of an alluvial fan 0.5 m thick during two years killed the forest, and the soil temperature at a depth of 10 m increased by 1.5°C after four years. In March 1989, in the alas type of terrain, snow was removed along with a sedge hummock and dwarf thicket. A year later, the thickness of the active layer in the disturbed area increased by 0.4 m, and the temperature of soil at a depth of 10 m increased by 0.4°C . Seven years later, the thickness of the active layer was 0.5 m greater, and the soil temperature was 0.7°C greater than in the undisturbed area.

Forest cutting

Different patterns of forest cutting (e.g., shelterwood cutting, selective cutting, and clear-cutting) were accompanied by different effects on permafrost conditions. The impact of forest cutting on the soil temperature regime in the sand-ridge type of terrain was studied at seven sites. Clear-cutting of a pine forest led to a rapid increase of 0.8 m in the active layer depth and a rise in the soil temperature of 0.4°C . In old forest cut areas with recovering larch and pine forest, a decrease in soil temperature of 0.9°C and decrease in the active layer depth of 0.3 m were recorded. Selective forest cutting at four sites of the sparse pine forests in the winter time without disturbing the soil cover did not essentially disrupt the thermal state of soil.

Selective cutting of a larch forest in the inter-alas type of terrain resulted in an increase in the soil temperature from 0.2 to 0.4°C . Tree cutting there was conducted in winter with a stable snow cover, and the moss cover with its insulating effect was preserved. Natural vegetation recovery is very active at these sites.

Selective forest cutting accompanied by disturbance of the soil surface cover in the inter-ridge-depression type of terrain caused an increase of 0.3 to 0.7°C in the soil temperature at the depth of 10 m during three years. An even greater increase in the soil temperature of 1.5 to 2.0°C was observed after 5 to 7 years at the site where moss and ledum cover was destroyed by a fire and the burned-out stand partly fell.

Monitoring of the soil thermal regime in the flat interfluvial plain type of terrain was conducted in two previously cut forest areas that had recovering soil surface cover and new larch and birch undergrowth forest. The active layer there is still 0.5 to 0.6 m deeper and soil temperature 0.4 to 0.7°C greater than in undisturbed conditions.

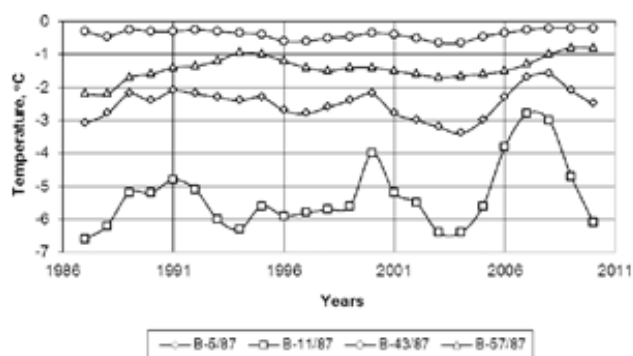


Figure 2. Change of the mean annual soil temperature at the depth of 10 m in different types of terrain: inter-ridge-depression (V-5/87), small valley (V-11/87), low terrace (V-43/87) and inter-alias (V-57/87).

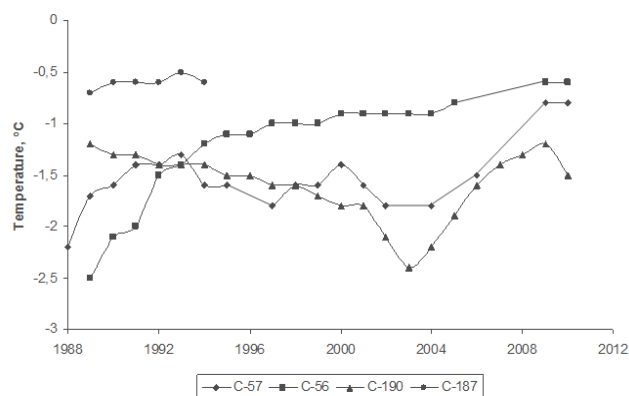


Figure 3. Change in mean annual temperature of ground in the larch forest (S-57) under shelterwood cutting (S-187), selective cutting (S-56) and clear-cutting (S-190) in the inter-alias type of terrain.

Our study also revealed the effect of different patterns of forest cutting on mean annual soil temperature. At the stage of young growth (10–30 years) in areas of clear-cutting of sparse pine forest, the thermal state of soil was close to that in a recently clear-cut area. Forest recovery after clear-cutting of a larch and pine forest at the stage of birch and shrubbery development (10–20 years) causes a decrease in soil temperature of 0.3 to 0.6°C. At the sites recovering after cutting of the shelterwood of a larch forest at the stage of grass (3–8 years) as well as birch and shrubbery development (10–20 years), there occurred an increase in soil temperature of 0.5 to 1.2°C, compared to natural conditions. At a site of old forest clear-cutting that has experienced natural recovery of birch and larch growth (thicket), soil temperature decreases by an average of 1°C after 10 to 30 years. In this area, the warm 2005–2008 winters with thick snow cover favored a rise in soil temperature of 2.1°C. The winters of 2009–2010 with low snow cover resulted in a decrease of soil temperature (Fig. 3).

Forest fire

The effect of fire on soil temperature regime was studied at 10 sites in the sand-ridge type of terrain. The fire of July 1987 destroyed a thin grass and bearberry soil cover and fall of a young pine stand in the following year. It led to a rapid temperature increase of approximately 1.5°C during the first two years after the fire. After three years, one could

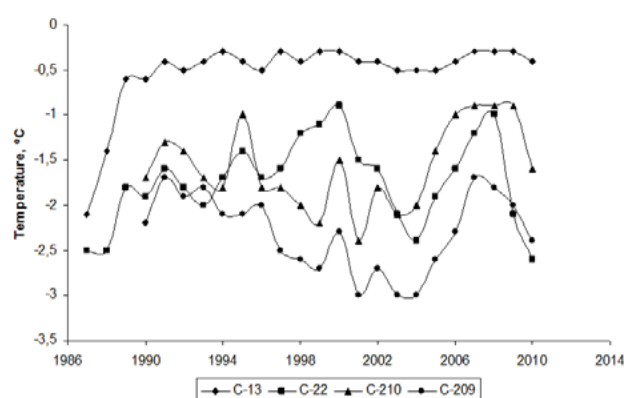


Figure 4. Mean annual soil temperature of in the pine forest (S-22), in the burned-out and felled area (S-13), in the sand-ridge terrain type and in the larch forest (S-210), at the burned-out and felled area in the inter-alias terrain type (S-209).

observe the natural recovery of birch trees and shrubbery and a decrease in soil temperature. The difference from natural conditions did not exceed 0.3 to 0.4°C.

Forest fire and forest cutting are typical human activities. Their impact on soil thermal regime in the low terrace type terrain was studied at monitoring sites in the larch forest (natural conditions) and at the site where the burned-out larch forest was clear-cut after the fire of 1986. A year after the fire and removal of trees, soil temperature increased 0.5°C and the active layer thickness increased by 0.15 m. After three years, soil temperature increased 0.8°C and the thickness of the active layer increased by 0.43 m. Twenty years after the fire, soil temperature was 0.5°C lower than it was eight years after the fire, as a result of the natural recovery of the birch and larch thicket.

Temporal change in the thermal state of permafrost soil after the fire of 1986 and forest cutting was studied in the inter-alias type of terrain. Selective cutting with disturbance of the soil cover after the fire caused a rise of 0.3–0.5°C in the temperature of soil during the first five years. Natural recovery of the grass and moss cover as well as a birch and larch thicket at stages 2-3 of succession reduced the solar radiation to the soil surface and resulted in a gradual decrease in soil temperature of 0.5–0.8°C (Fig. 4).

The influence of forest fires and forest cutting on the soil thermal state was studied along the Taas Tumus-Yakutsk Gas Pipeline in the inter-alias type of terrain. In 2002, a fire in the birch and larch forest caused most of the stand to fall. In the winter period, the burned-out forest was logged. Equipment working in the winter led to compression of snow and a decrease in its heat-insulating properties. This caused a lowering in the mean annual temperature of 0.3°C at a depth of 15 m. The depth of the active layer of clayey silt with high moisture content in the burned-out area increased by 0.5 m, as compared to the control site in natural conditions. At the end of the snowy winter in 2008, the active layer did not freeze completely, and the seasonally frozen layer was 2.2 m thick. A pereletok (residual thaw layer) 0.8 m in thickness formed under this layer. This pereletok was completely frozen the next winter with a thin snow cover. Eight years after disturbance, the active layer depth in the burned area had increased by 1.8 times as compared to

natural conditions, and soil temperature at a depth of 15 m increased by 1.8°C.

The impact of forest fires on the thermal state of soil in the flat interfluvial plain type of terrain was studied in two previously burned areas. At the sites where natural recovery of the larch and birch forests is ongoing, we observed an increase of 0.3–0.4 m in the active layer thickness and an increase within the range of 0.4–0.7°C in the temperature of the ground, in comparison with natural conditions.

Conclusions

We arrived at the following conclusions:

- 1) The removal of a soil cover in the sand-ridge, alas, and inter-alas types of terrain causes a rise in the mean annual soil temperature and an increase in the active layer depth and triggers the development of hazardous processes.
- 2) At the forest cutting sites, the maximum increase in soil temperature and in the active layer depth are observed in the inter-ridge-depression and inter-alas types of terrain, while the minimum increase occurred in the sand-ridge type of terrain.
- 3) Thawing of soil and an increase in the thickness of the active layer at the burned-out sites are especially hazardous in the inter-alas type of terrain with ice-rich permafrost close to the surface. Such terrain is characterized by the development of adverse cryogenic processes.

References

- Burgess, M.M. & Lawrence, D.E. 1997. Thaw settlement in permafrost soils: 12 years of observations on the Norman Wells pipeline right-of-way. In *Proceedings of the Canadian Geotechnical Society Conference*, Ottawa: 77-84.
- Christiansen, H., Eitzelmueller, B., Isaksen, K., Juliussen, H., Farbrot, H., Humlum, O., Johansson, M., Ingeman-Nielsen, T., Kristensen, L., Hjort, J., Holmlund, P., Sannel, A.B.K., Sigsgaard, C., Akerman, H.J., Foged, N., Blikra, L.H., Pernosky, M.A., & Odegard, R.S. 2010. The thermal state of permafrost in the Nordic area during the international polar year 2007-2009, *Permafrost and Periglacial Processes* 21: 156-181.
- Harris, C., VonderMohl, D., & Isaksen, K. 2000. The European pace project transect of instrumented permafrost boreholes: preliminary results of permafrost monitoring. *Abstracts Rhythms of natural processes in the earth's cryosphere*, Pushcnino: 256.
- Melnikov, P.I. 1950. Permafrost in the Yakutsk area. In *Permafrost Investigations in YaSSR*, vol. 2. Moscow-Leningrad: USSR Acad. Sci. Press, 52-70 (in Russian).
- Osterkamp, T.E., Zhang, T., & Romanovsky, V.E. 1994. Evidence for a cyclic variation of permafrost temperatures in Northern Alaska. *Permafrost and Periglacial Processes* vol. 5: 137-144.
- Pavlov, A.V. 1975. *Heat Exchange between Soil and Atmosphere in Northern and Temperate Latitudes of the USSR*. Yakutsk: Yakut Publishing House, 302 pp. (in Russian).
- Romanovsky, V.E., Sergueev, D.O., & Osterkamp, T.E. 2003. Temporal variations in the active layer and near-surface permafrost temperatures at the long-term observatories in Northern Alaska. In *Proceedings of the Eighth International Conference on Permafrost*, Zurich: 989-994.
- Romanovsky, V.E., Drozdov, D.S., Oberman, N.G., Malkova, G.V., Kholodov, A.L., Marchenko, S.S., Moskalenko, N.G., Sergueev, D.O., Ukraintseva, N.G., Abramov, A.A., Gilichinsky, D.A., & Vasiliev, A.A. 2010. Current Changes of Climate and Permafrost in the Arctic and Sub-Arctic of Russia. *Permafrost and Periglacial Processes* vol. 21: 136-155.
- Shimanovskii, S.V. 1942. Effect of pavements on the ground thermal regime. In *Permafrost Investigations in the Yakut Republic*, vol. 1. Yakutsk, 44-55 (in Russian).
- Skryabin, P.N. 2007. The effect of road embankments on ground thermal regime in Central Yakutia. *Permafrost Engineering, Proceedings of the Seventh International Symposium*, 21-23 November 2007, Chita, Russia: 61-64. Yakutsk: Permafrost Institute SB RAS Press (in Russian).
- Skryabin, P.N., Varlamov, S.P., & Skachkov, Yu.B. 1992. Evaluation of changes in the ground thermal regime caused by environmental disturbance. In *Natural Resource Management in Permafrost Regions*. Moscow: Nauka, 165 pp. (in Russian).
- Smith, S., Romanovsky, V.E., Lewkowicz, A.G., Burn, C.R., Allard V., Clow, G.D., Yoshikawa, K., & Throop, J. 2010. The thermal state of permafrost in the Nordic area during the international polar year 2007-2009. *Permafrost and Periglacial Processes* vol. 21: 117-135.
- Varlamov, S.P., Skachkov, Yu.B., & Skryabin, P. 1990. Interannual variability of ground thermal parameters at Chabyda station. Central Yakutia. In *Permafrost Changes and Economic Development*. Yakutsk: Permafrost Institute Press, 68-75.
- Varlamov, S.P. & Skachkov, Yu.B. 2006. Ground ice contents in the northern section of the Tommot-Kerdem railway project (Olen station to Kerdem station). In *Earth Cryosphere Assessment: Theory, Applications and Prognosis of Alterations, Proceedings of International Conference*, 29-31 May 2006, Tyumen, Russia, vol. 2: 212-214 (in Russian).
- Zhao, Lin, Wu, Qingbai, Marchenko, S.S., & Oberman, N. 2010. Thermal state of permafrost and active layer in Central Asia during the international polar year. *Permafrost and Periglacial Processes* 21: 198-207.

Structure and Composition of Complex Massive Ice Bodies in Late Pleistocene-Holocene Sediments of the Marre-Sale Cape, West Yamal

E.A. Slagoda, O.L. Opokina, A.N. Kurchatova
Earth Cryosphere Institute, SB RAS, Tyumen, Russia
Tyumen State Oil and Gas University, Tyumen, Russia

V.V. Rogov
Lomonosov Moscow State University, Moscow, Russia
Tyumen Scientific Center SB RAS, Tyumen, Russia

Abstract

Ground ice studies were performed at the Marre-Sale Cape coastal bluff exposure in 2008–2010. They have provided new data not only on the lithology and deformation patterns of sediments, but also on morphology, chemistry, isotope composition, and crystallography of the ice in ice wedges and complex massive ice bodies. The new data provide valuable evidence for the origin of the complex sequence of sediments containing massive ground ice.

Keywords: Holocene; isotope composition; Late Pleistocene; massive ice; intrusive ice; wedge ice.

Introduction

Permafrost of the Marre-Sale Cape area in the Western Yamal Peninsula has a long history of research. The same sediments have been assigned either to marine, glacial, or lacustrine-fluvial facies (Kuzin & Astafiev 1975, Trofimov et al. 1987, Ershov 1989, Forman et al. 2002). The ice has been interpreted either as buried shelf glaciers (Kaplyanskaya & Tamogradsky 1982, Gataullin 1990, Astakhov 2006) or as intrusive and wedge ice (Kuzin & Astafiev 1975, Melnikov & Spesivtsev 2000, Dubikov 2002). Kritsuk (2010) showed a relation between complex intrusive tabular and intrusive wedge ice with cryohydrotectonics (joint action of permafrost, groundwater, and tectonic processes). Kanevskiy et al. (2005) and Streletskaya et al. (2006) distinguished epigenetic and syngenetic wedge ice, upper and lower bodies of massive ice, and so-called tabular (thawed and refrozen) sediments.

Judging by the continuing discussion on the genesis of the massive ground ice, the existing criteria used for determining the ice origin are insufficient. To reveal diagnostic features of the complex massive ice bodies, field work was performed in 2008–2010 on a remarkable coastal exposure along the Marre-Sale Cape.

Permafrost Structure of the Marre-Sale Cape Section

The Marre-Sale permafrost sequence includes the Salekhard and Kazantsevo suites as well as Zyryan, Karga, Sartan, and Holocene deposits represented by clay, silty clay, silt, and sand with uneven bedding and fold deformations. Massive ice bodies are exposed in the eroding cliffs along the second and third marine plains over a distance of 4 km south of the Marre-Yakha River mouth (Fig. 1).

The lower section consists of the Kazantsevo (mIII¹) gray marine clay and silty clay with thin layers of light-color sand. The clay shows horizontal or slightly inclined lamination and has minor corrugated folds or large folds in some places.

It has porous, layered-reticulate ice with large lenses, or

lenticular cryostructures, and the gravimetric water content varies from 67 to 86%. The clay upper boundary is uneven, eroded, and uplifted along its contacts with the massive ice bodies. It lies at a depth of 4 to 6 m in the northern part and as deep as 20 m below the surface in the southern part of the cliff section, where it is locally submerged below the sea level. The visible thickness of clay is up to 20 m (Fig. 2).

The clay is overlain by variegated silty sand with ochre or grayish-black iron stains associated with the remains of plants. The sand unit correlates with the Karga deposits (all, m III²⁻³) (Forman et al. 2002). Sand has porous, lenticular, or layered cryostructures, and gravimetric water content is from 24 to 95%. The thickness of sand reaches 4 to 6 m in the northern part of the study area. In the southern part, this unit is detached by the massive ice bodies, and the layers of sand are folded and uplifted next to the ice bodies.

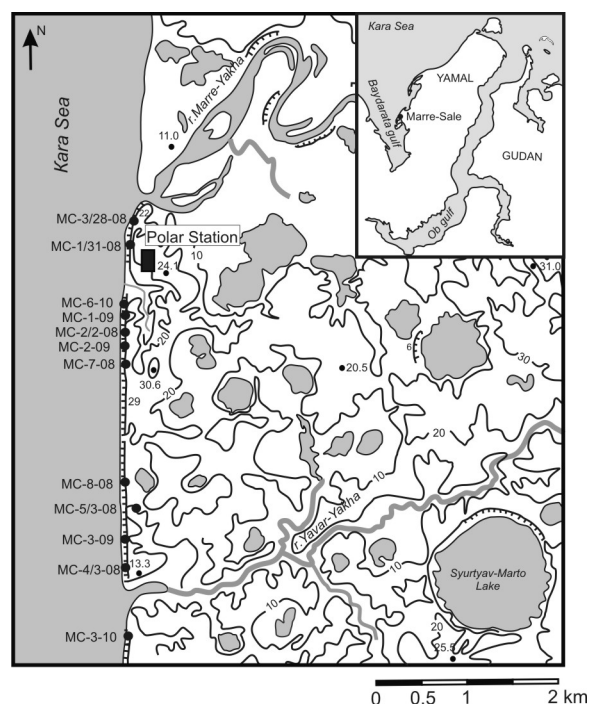


Figure 1. Location of studied sections along the Marre-Sale coastal exposure.

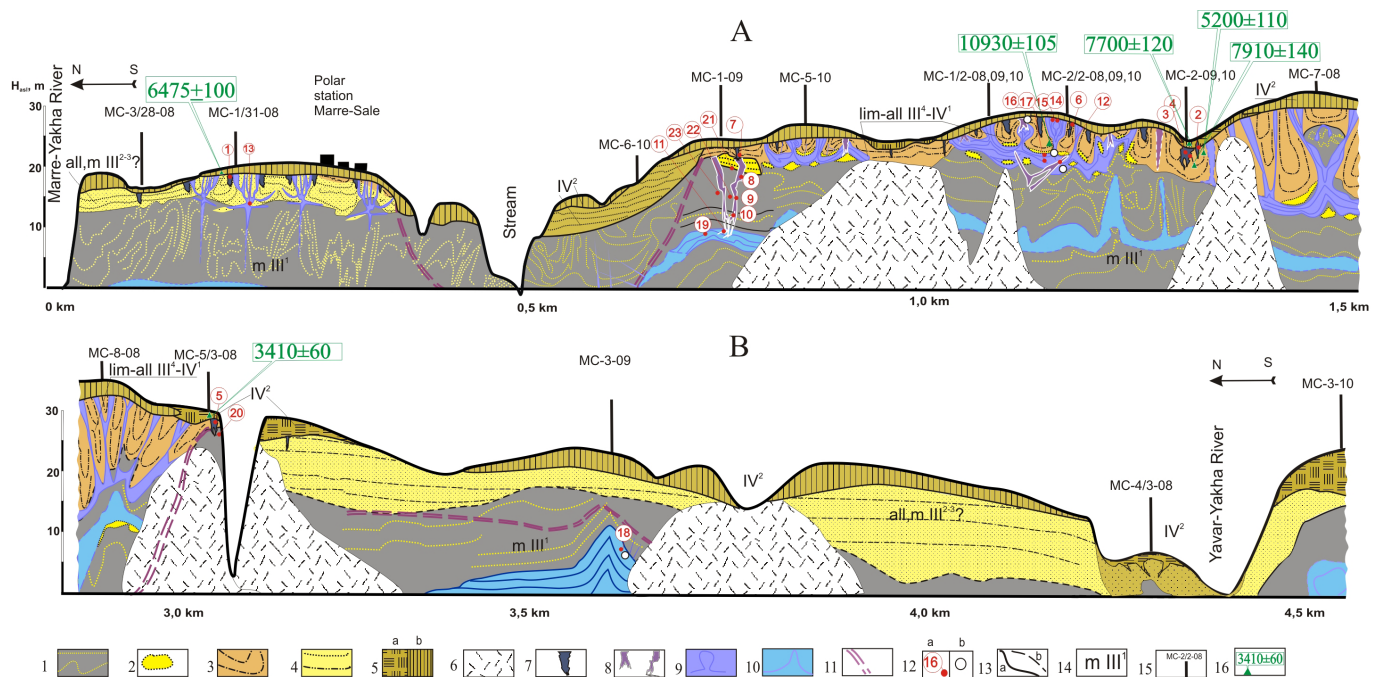


Figure 2. Cryostratigraphic units of Marre-Sale Cape exposure: 1 – clay with sand layers and deformed bedding, Kazantsevo interstadial; 2 – variegated sand, Karga interstadial; 3 – layered silt with plant remnants, Sartan glacial-Holocene; 4 – layered sand, presumably Sartan-Holocene; 5 – Late Holocene deposits: sand (a) and peat (b); 6 – slump; 7–10 – ground ice: polygon wedge ice (7), wedge-shaped ice bodies (8), tabular massive ice: upper ice body (9), lower ice body (10); 11 – boundaries of refrozen taliks; 12 – ice samples: chemistry and isotope analyses (a) and crystallography (b); 13 – observed (a) and presumed (b) boundaries; 14 – indices of stratigraphic units; 15 – studied sections and their numbers; 16 – radiocarbon ages of deposits, ^{14}C yr BP.

The next unit consists of brown silt with sand lenses and laminated yellowish fine sand. Sand layers 1 to 3 cm thick contain remnants of moss, in situ plant roots, and peat pockets up to 10 cm across. The cryostructure of silt is poorly developed layered (belt-like); gravimetric water content varies from 11 to 44%. The cryostructures of sand are porous or lenticular (gravimetric water content 33%). The sand is more ice-rich near the massive ice bodies. The top part of this unit is eroded, and its thickness varies from 0 to 3 m in the north to 5 to 10 m in the south. The in situ plant remnants have radiocarbon ages of $10,930 \pm 105$ ^{14}C yr BP (SOAN-7597), 7910 ± 140 ^{14}C yr BP (SOAN-7941), and 5200 ± 110 ^{14}C yr BP (SOAN-7942) at depths 5, 1.5, and 1 m, respectively. The sediments of this unit were deposited continuously since 15 to 5 ^{14}C kyr BP (lim-all III¹-IV¹) within a lacustrine-alluvial plain (Forman et al. 2002).

The overlying discontinuous subsurface soil horizon (up to 1.5 m thick) consists of brown silt, sand with plant roots, and oxidized sand with cryoturbation and peat lenses. A thickness of peat reaches over 1 m in depressions. The sand below 0.8–1.3 m is frozen, with porous cryostructure and gravimetric water content of 22%. In the northern part of the exposure, the radiocarbon age of redeposited peat from the depth 1.3 m is 6475 ± 100 ^{14}C yr BP (SOAN-7596). In the southern part, the ages of autochthonous and allochthonous mosses sampled at a depth of 0.6 m are 3410 ± 60 (SOAN-7596) and 7700 ± 120 (SOAN-7940) ^{14}C yr BP, respectively. The subsurface soil horizon (IV²) contains redeposited plant remnants from the underlying units, which is the evidence for denudation and erosion of Sartan-Holocene silt. This sedimentation is still taking place.

Morphology of Massive Ice Bodies

In 2008–2010, from 14 to 22 retrogressive thaw slumps 12 to 18 m wide were observed over a distance of 150 m in the northern part of the Marre-Sale Cape area (MS-31-08). The section contained vertically foliated, regularly shaped polygonal wedge ice and deformed wedge-shaped ice bodies with wavy lamination.

The ice wedges are up to 1 m wide and 2–4 m high, depending on the depth of erosion, and they have truncated upper parts. The surface above them has a polygonal net with polygons 14–18 m across. The sand with lenticular-layered cryostructures gradually rises at 5–10 cm along the contacts with ice wedges, and lenses of segregated ice are attached to wedge ice, which indicates the syngenetic nature of ice wedges. The bands of glassy ice along the lateral contacts of some ice wedges near the deformed ice bodies may be produced by local thawing and recrystallization of wedge ice.

The deformed ice bodies are fragments of circular structures 10–16 m in diameter. They consist of broad (0.7–1 m) and narrow (0.1–0.3 m) arched ice bodies, which are exposed as the slumps retreat. The deformed ice bodies are up to 0.8 m wide above the clay and then continue downward as oxidized vertical cracks filled with ice (up 0.2 m wide and 3–5 m high), which can be considered water supply channels. Before thawing from the top, they apparently formed small frost mounds (hydrolaccoliths) with alternating parallel ice and sand layers. Because of this, we called them foliated laccoliths.

The upper body of massive ice with horizontal segments and vertical protrusions was studied for three years in the

central part of the Marre-Sale Cape area in an exposure 24–30 m high (sections MS-2/2-08,09,10). A horizontal ice body 1.2–2.0 m thick with foliated structure was exposed along the boundary between gray clay and variegated sand. Parallel ice layers gradually bent upward to form a 6-m-high vertical protrusion in the frontal wall of a thaw slump at the center of a polygon. Clay with thin sand layers beneath the ice protrusion is deformed and drawn into the ice. At the top, the protrusion intrudes into variegated sand and silt. It is narrower (4 m) at 4.5 m depth and broader (10 m) on the top. The ice margins have bands of glassy ice. The ice consists of alternating wavy layers 2–10 cm thick and lenses of pure transparent ice and dark ice containing clay, sand, and ochre films. The central part of the protrusion and the overlying sediment contain lenses of glassy ice and ice with large air bubbles, as well as intersecting thin layers delineated by mineral inclusions. South of the MS-5-10 section, the upper massive ice body gradually descends from 16–18 m to 8–10 m above the sea level over a distance of 300 m and generally parallels the clay-sand boundary. There vertical ice protrusions are located every 10 to 25 m. Most of them have truncated tops, but undisturbed dome-shaped ice bodies also can be observed (section MS-1/2-08). These vertical sediment-poor ice protrusions complicate the structure of the upper ice body and can be considered the fragments of hydrolaccoliths.

At the central part of the exposure (sections MS-1/2-10; MS-1-09), there are also vertical and inclined wedge-shaped bodies 1.5–7 m high and 0.3–2.8 m wide on tops. Morphologically, they are similar to ice wedges. They intersect the folded upper massive ice body, deform the overlying sand and silt layers, or sometimes penetrate through the clay into the massive ice body. The ice in these “wedges” is yellowish and vertically foliated, with inclusions of sand and iron hydroxide. The lateral contacts of the “wedges” are oxidized and have bands of glassy ice.

In 2003–2004, a fragment of the lower massive ice body with an inclined dike was studied near the section MS-2/2-08 at the depth of 20–25 m in marine clay with sand layers (Streletskaia et al. 2006). In 2009, a similar 4-m-thick massive ice fragment with low-angle anticline fold consisting of wavy sub-horizontal layers (0.1–0.3 m thick) of clear glassy ice and ice with air bubbles and mineral inclusions was observed in clay with reticulate cryostructure at section MS-1-09.

In the southern part of the Marre-Sale Cape area (section MS-3-09), the lower massive ice body, which formed a large anticline fold, was exposed over a distance of 300 m with a visible ice thickness of 2–5 m. The ice layers are generally parallel to the bedding of the host clay with reticulate cryostructure. Ice contains angular clay inclusions and air bubbles. Sharp boundaries between ice and clay are locally delineated by thin silt streaks. The lower massive ice body, 1.5–2.0 m thick, is exposed in section MS-8-08 in marine clay. The ice body is folded, with rare anticline folds 12–15 m high locally deforming both the clay and the overlying sand and silt units. The overlying sediments include thawed and refrozen oxidized clayey deposits (“tabular complex”) with reticulate post-cryogenic structures.

Thus several morphologic types of ground ice have been distinguished in the Marre-Sale area, namely (1) polygon

wedge ice, partly thawed and refrozen near laccoliths, (2) an upper tabular massive ice body overlying marine clay, with horizontal segments and intrusive parts (foliated laccoliths), (3) epigenetic wedge-shaped ice bodies that dissect tabular massive ice, and (4) a lower massive ice body in clay with large anticline folds.

Ice Chemistry

The ice chemistry of the lower massive ice body is markedly different from the other ice types. Content of total dissolved solids (TDS) in the ice is rather high (up to 350 mg/l), with more than 50% sodium chloride and less than 10% calcium and magnesium bicarbonates, which may be evidence of a large contribution from marine pore water to the ice formation. Ice from the section MS-1-09 has typical seawater ratios of the main ions: 0.9 for $(rNa^+ + rK^+)/rCl^-$ and 0.2 for rMg^{2+}/rCl^- . TDS is lower and Na bicarbonate content is higher in samples from the section MS-3-09, possibly due to additions of fresh water as the overlying sediments were thawing. This is consistent with the occurrence of thawed and refrozen sediments on top of the section.

The ice chemistry of the upper massive ice body is Na-Ca bicarbonate, which is typical of fresh groundwater of the desalination zone (Fotiev 2009). Different fragments of the upper ice bodies have similar chemistry. The hydrolaccoliths in sand deposits are generally less saline in their upper parts than the lower massive ice body in ice-rich silty clay.

As TDS increases in the horizontal parts of the upper massive ice body, Na bicarbonate content becomes higher than the total content of Ca and Mg bicarbonates, which is typical of freezing taliks (Anisimova 1981). TDS is the highest in the lenses of transparent ice with large air bubbles, where NaCl reaches up to 70% of TDS (with averages of 20 to 40%).

The epigenetic wedge-shaped ice bodies have their TDS and ion compositions similar to those of the upper massive ice body. Relatively high contents of Ca and Mg bicarbonates may be explained by the partial cryogenic metamorphism of groundwater.

Unlike the ice of the lower massive ice body, the polygonal wedge ice produced by snowmelt water has an ultrafresh Na bicarbonate chemistry. Relatively high content of chlorides in syngenetic wedges is related to their proximity to the sea. All samples contain sulfates, which is common to the wedges formed in the peat of thaw lake basins of the different regions. Rather high content of Mg^{2+} bicarbonate in the refrozen lateral wedge boundary may be related to the partial ice metamorphism.

The chemical compositions of different types of ground ice indicate the source of water responsible for ice formation: meteoric water for polygon wedge ice; groundwater of silt-sand sediments for the upper massive ice body and wedge-shaped ice bodies; and pore water of marine clay for the lower massive ice body and for some horizontal parts of the upper massive ice body.

Isotope Composition

The distinguished ice types in the Marre-Sale section also differ in their isotope composition of oxygen-18 ($\delta^{18}O$),

Table 1. Structure and composition of massive ground ice at Marre-Sale Cape.

Type	Morphology	Contact with surrounding sediments	Relationship with other massive ice types	Ice structure	Chemistry (TDS, g/l)	Isotopes, ‰
Syngenetic polygonal wedge ice	Wedges (1.5-2.0 × 4.5-5.0 m); 14 × 18 m polygonal net	Silt layers and cryostructures are slightly bended upward along ice wedge contacts	Usually are not connected with tabular massive ice bodies	White transparent ice with vertical air bubbles; refrozen lateral contacts with hydrolaccoliths and wedge-shaped ice bodies	$TDS_{0,04} = \frac{HCO_3 49Cl44SO_4 7}{(Na+K)63Ca22Mg15}$ High contents of chlorides due to winter aerosols $rCa^{2+}/rCl = 1$	$\delta^{18}O = -16.2$ $\delta D = -122.2$
Epigenetic wedge-shaped massive ice	Upright, deformed, or inclined wedge-shaped ice bodies (0.5-1.0 × 6.5-7 m)	Layered sand and silt are deformed together with cryostructures	Dissect the horizontal parts of the upper massive ice body	Yellowish vertically foliated ice with inclusions of sand and iron hydroxide	$TDS_{0,085} = \frac{HCO_3 56Cl35SO_4 9}{(Na+K)54Ca30Mg16}$ Increase in Na ⁺ and Mg ²⁺ content may evidence for cryogenic concentration of groundwater; $rCa^{2+}/rCl = 0.9$	$\delta^{18}O = -23.7$ $dD = -183.1$
Vertical parts of the upper massive ice bodies: massive (a) and foliated hydro-laccoliths (b)	Protrusions of gently deformed layers (a); deformed wedge-shaped bodies – fragments of circular structures, 10 to 16 m in diameter that continue in clay as oxidized cracks filled with ice (water supply channels) (b)	Ice bodies dissect and deform the surrounding sediments	Connected with horizontal parts of upper massive ice bodies,	Vertically foliated ice with soil fragments; bands of glassy ice along lateral contacts; lenses of glassy and bubbly ice at central parts of vertical protrusions	$TDS_{0,070} = \frac{HCO_3 57Cl33SO_4 10}{(Na+K)53Ca27Mg20}$ Increase in Na ⁺ and Mg ²⁺ may indicate a cryogenic metamorphism of groundwater; $rCa^{2+}/rCl = 0.8$	$\delta^{18}O = -22.9$ $\delta D = -177.1$
Horizontal parts of the upper massive ice bodies	Continuous horizontal wavy layers (0.1 to 0.2 m) of ice and ice-rich soil, total thickness about 2 m	Ice layers are parallel to clay/silt contact; generally conformable with host sediments	Connected with vertical protrusions; are dissected by wedge-shaped ice bodies	Pure glassy ice (a); dark ice with clay, sand, ochre films and air bubbles (b); ice lenses with large randomly oriented air bubbles (c)	$TDS_{0,260} = \frac{HCO_3 53Cl45SO_4 2}{(Na+K)85Ca8Mg7}$ Highest TDS in lenses of bubbly ice; $rCa^{2+}/rCl = 0.2$	$\delta^{18}O = -14.8$ $\delta D = -110.5$
Lower massive ice bodies with large anticline folds	Continuous wavy 0.1 to 0.3 m layers; visible thickness up to 5 m, anticline folds up to 12 m	Generally concordant with clay containing layers of silt and sand	Not observed	Pure glassy ice (a); ice with angular clay aggregates and air bubbles	$TDS_{0,280} = \frac{Cl66HCO_3 27SO_4 7}{(Na+K)86Ca6Mg8}$ $rCa^{2+}/rCl = 0.1$	$\delta^{18}O = -15.7$ $\delta D = -120.4$

deuterium (δD), and calculated values of deuterium excess (d_{ex}) found as $d_{ex} = \delta D - 8\delta^{18}O$ (Dansgaard 1964). In global-scale precipitations, $d_{ex} = 10\%$, while values of $d_{ex} < 10\%$ correspond to isotope fractionation by evaporation, sublimation, and freezing-thawing.

The lower massive ice body has higher contents of heavy isotopes due to the contribution of marine pore water. Generally, the isotope composition is similar to that of modern saline lakes on the upper surface of the Marre-Sale area (Kritsuk 2010).

Ice in the upper massive ice body and in epigenetic wedge-like bodies is richer in light isotopes (Table 1). Its $\delta^{18}O$ and δD values are similar to those in modern winter precipitation

in West Yamal, but differ from those in summer precipitation and in modern lakes, possibly because the former taliks in thaw lake basins are recharged from snowmelt water.

The isotope composition of polygonal wedge ice is heavier than that in the upper massive ice body but lighter than that in the lower massive ice body. Polygonal wedge ice has isotope values corresponding to the d_{ex} global line of meteoric water which, along with its chemistry, indicates its origin from meteoric water, unlike tabular massive ice. Growing ice wedges in peatland have 3 to 4‰ heavier isotope composition, similar to other regions (Derevyagin et al. 2003).

Crystallography

The crystallographic analysis shows features of similarity and difference among the massive ice types distinguished in the Marre-Sale area. The glassy coarse-crystalline ice in the lower massive ice body may have formed by migration of water during the epigenetic freezing of marine clay (Rogov 2009). A similar structure appears in lenses of glassy ice at the central parts of vertical protrusions in the upper massive ice body.

Hydrolaccoliths and epigenetic wedge-shaped ice bodies have a vertically foliated structure formed by soil inclusions, which results from repeated injections of water and suspensions during the freezing of closed taliks. In thin ice layers between soil inclusions, ice crystals are elongated, $3\text{--}5 \times 7\text{--}10$ mm. In thick ice layers, they are isometric or irregularly shaped and indistinctly oriented. Air bubbles are randomly distributed. Unlike polygon wedge ice, the hydrolaccoliths and wedge-shaped ice bodies often have discontinuous crossings of mineral bands.

The vertical foliation in polygon wedge ice is formed by long crystals with vertically oriented trains of air bubbles trapped between them.

Conclusions

The analysis of permafrost structure of the Marre-Sale section has implications for the chronological sequence of massive ice formation.

- 1) Syngenetic ice wedges occur in 5–15 ¹⁴C kyr lacustrine-fluvial sediments (i.e., the wedge-ice system genetically related with hydrolaccoliths of the upper massive ice bodies formed in the end of the Sartan glacial and in the early Holocene).
- 2) The upper massive ice bodies with foliated and massive hydrolaccoliths and epigenetic wedge-shaped bodies were formed synchronously with the early Holocene polygon wedge ice. In the late Holocene, the hydrolaccoliths were eroded and partly thawed (Slagoda et al. 2010).

Ice in the upper massive ice bodies and wedge-shaped ice bodies have common features indicating their intrusive origin: entrainment of mineral components from the underlying or enclosing sediments; occurrence of crossing ice layers; and thawing and refreezing of frozen soil with formation of glassy ice bands along lateral contacts with massive ice. The ice structure indicates repeated injections of pressurized water and slurry, which produced parallel wavy ice and soil alternating layers. Thus the upper massive ice bodies consist of segregated (in the horizontal parts) and intrusive-segregated ice (in the hydrolaccoliths and epigenetic wedge-shaped bodies). For this reason, the complex upper massive ice bodies have been interpreted as secondary repeatedly intrusive ice.

The horizontal and vertical parts of the upper massive ice bodies differ in the nature of water sources and their position in the section. Massive hydrolaccoliths and horizontal ice segments are the first generation of ice produced by injections of water associated with freezing of disconnected taliks in sand above the impermeable

clay bed, which was infiltrated during the first stage of freezing. Wedge-shaped ice bodies and foliated hydrolaccoliths are the second generation of massive ice formed later by intrusion of water from quicksand lenses located at different depths in clay. During the freezing of these lenses, the water was injected upward through the radial and circular cracks into polygonal blocks of frozen ground.

- 3) The time of formation of the lower massive ice bodies cannot be detected because of the lack of data on their relationship with other types of ground ice. Judging by relatively high TDS, seawater-type salt compositions, coarse ice structure, parallel foliation, and location in marine clay, the lower massive ice bodies have been interpreted as primary tabular massive ice of probably segregated origin, which have formed during the epigenetic freezing in an open system. The morphology of the ice bodies and occurrence of large folds are probably related to the configuration of the freezing front and low ice segregation rates in marine sediments.

The obtained data support the hypothesis of intrusive ice formation associated with freezing of taliks, which was genetically related with ice-wedge polygonal systems. Since the different ground ice types are morphologically similar, the total assemblage of cryological characteristics is required to identify their genesis more precisely.

Acknowledgements

The study was supported by the basic research programs of the International Polar Year (IPY) 2007/2008, Project 20.7 of the RAS Presidium, and Project 11.4 of the RAS Geoscience Department. Additional support was from grant 09-05-00538 of the Russian Foundation for Basic Research.

References

- Anisimova, N.P. 1981. *Water Chemistry Features in the Permafrost Zone*. Nauka, Novosibirsk, 152 pp. (in Russian).
- Astakhov, V.I. 2006. Chronostratigraphic subdivisions of the Siberian Upper Pleistocene. *Russian Geology and Geophysics (Geologiya i Geofizika)* 47 (11): 1186–1199 (1207–1220) (in Russian).
- Baulin, V.V., Belopukhova, E.B., Dubikov, G.I. et al. 1967. *Permafrost conditions of the West Siberian Plain*. Nauka, Moscow, 214 pp. (in Russian).
- Dansgaard, W. 1964. Stable isotopes in precipitation. *Tellus*, 16: 436–468.
- Derevyagin, A.Yu., Chizhov, A.B., & Mayer, H. 2003. The isotope composition of natural waters and modern ground ice in the Laptev Sea area. *Kriosfera Zemli* 7 (3): 41–48 (in Russian).
- Dubikov, G.I. 2002. *Composition and Structure of Permafrost in West Siberia*. GEOS, Moscow, 246 pp. (in Russian).
- Ershov, E.D. (ed.). 1989. *Geocryology of the USSR. West Siberia*. Nedra, Moscow, 454 pp. (in Russian).
- Forman, S.L., Ingolfsson, O., Gataullin, V., et al. 2002. Late Quaternary stratigraphy, glacial limits, and paleoenvironments of the Marresale area, western Yamal Peninsula, Russia. *Quaternary Res.* 57: 355–370.

- Fotiev, S.M. 2009. *Cryogenic Metamorphism of Soils and Groundwater*. GEO Publishers, Novosibirsk, 279 pp. (in Russian).
- Gataullin, V.N. 1990. Massive ice in the western coast of the Yamal Peninsula: structure, composition, and genesis. In *Permafrost Studies in Arctic Regions*. IPOS SO AN SSSR Tyumen, Issue 1, 3–11 (in Russian).
- Kanevskiy, M.Z., Streletskaya, I.D., & Vasiliev, A.A. 2005. Formation of cryogenic structure of Quaternary sediments in Western Yamal (by the example of Marre-Sale area). *Kriosfera Zemli* 9 (3): 16–27 (in Russian).
- Kaplyanskaya, F.A. & Tarnogradsky, V.D. 1982. Glacial deposits in the area of the Marre-Sale polar station, an example from the Yamal Peninsula. *VSEGEI Transactions* 319: 77–85 (in Russian).
- Kritsuk, L.N. 2010. *Ground Ice of West Siberia*. Nauchnyi Mir, Moscow, 352 pp. (in Russian).
- Kuzin, I.L. & Astafiev, N.F. 1975. Cryogenic dislocations in the western coast of the Yamal Peninsula. *Izvestiya VGO* 107 (6): 510–515 (in Russian).
- Melnikov, V.P. & Spesivtsev, V.I. 2000. *Cryogenic Formations in the Earth Lithosphere*. Izd. SO RAN, Novosibirsk, 343 pp.
- Rogov, V.V. 2009. *Fundamentals of Cryogenesis*. GEO Publishers, Novosibirsk, 203 pp. (in Russian).
- Slagoda, E.A., Melnikov, V.P., & Opokina, O.L. 2010. Repeatedly-injected ice stocks in sediments of the Western Yamal Peninsula. *Dokl. Earth Sci.* 432 (1): 663–666 (in Russian).
- Streletskaya, I.D., Kanevskiy, M.Z., & Vasiliev, A.A. 2006. Massive ground ice in dislocated Quaternary sediments of Western Yamal. *Kriosfera Zemli* 10 (2): 68–78 (in Russian).
- Trofimov, V.T., Badu, Yu.B., Vasilchuk, Yu.K., et al. 1987. *Permafrost regions of the West Siberian Plate*. Nauka, Moscow, 224 pp. (in Russian).
- Vtyurin, B.I. 1975. *Ground Ice of the USSR*. Nauka, Moscow, 215 pp. (in Russian).

Some Astronomical Problems of the Cryosphere Evolution

I.I. Smulskiy

Earth Cryosphere Institute, SB RAS, Tyumen, Russia

Abstract

We examined the issues of the astronomical theory of glacial periods from the perspective of celestial mechanics. Previous research showed unstable motions when integrating simplified equations of motion for long periods of time. For this reason, it was concluded that it is impossible to estimate the Earth's insolation for periods covering more than 20 million years. In this research, we solve an unsimplified problem of the orbital motion employing a numerical method. At the same time, the equations were integrated for the period of 100 million years. We obtained all oscillation periods and oscillation amplitudes of the planets' orbits as well as of the moon's orbit and established their stability. Differential equations of rotational motion are also solved with the help of an unsimplified numerical method. We determined the results of the impact exerted separately by planets and by the sun on the Earth's axis. The evolution of the Earth's axis was also examined on the basis of the model of the Earth's rotation. We obtained the periods of its oscillations that coincide with the observed ones. The research revealed that only the solution for unsimplified equations of the Earth's rotation will make it possible to reliably calculate the evolution of the insolation and to determine all the periods of its change.

Keywords: Eccentricity; equations; inclination; insolation; numerical methods; orbital motion; perihelion.

Introduction

When studying the issue of climate warming that occurred in the second half of the twentieth century and developing its models (Climate Change 2007), researchers consider the astronomical theory of glacial periods that was produced by Milankovich (1939). The uncertainties of the climate warming models depend to some

degree on the uncertainties of this theory. A number of researchers (e.g., Bolshakov & Kapitsa 2001) suggested that, since the time of Milankovich, the collection of paleoclimatic data indicate the necessity for further development of the theory. The given research examines the results of the specification of the astronomical theory of paleoclimate from the perspective of celestial mechanics or astronomy.

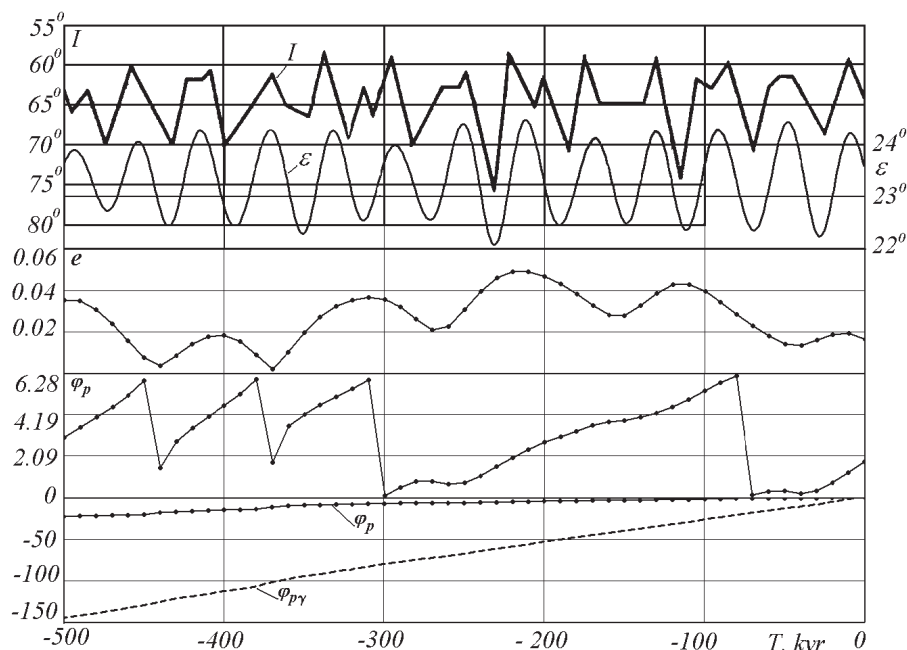


Figure 1. The comparison between the insolation and the parameters of the Earth's orbit: I – insolation at equivalent latitudes at the latitude of 65° of the Northern Hemisphere according to the data of Sharaf and Budnikova (1969) and the angle of inclination of the Earth's orbit to the moving plane of the Equator (ε) according to Berger and Loutre (1991); eccentricity e and the angles (in radians) of the perihelion's position from the fixed φ_p and from the moving $\varphi_{p\gamma}$ ascending node γ – according to our estimates (Melnikov & Smulskiy 2009). T – the time in kyr (one thousand years) that is counted in thousands of years into the past from the modern epoch (12.30.1949).

The Dependence of Insolation on the Orbital and Rotational Motions of the Earth

According to the astronomical theory (Milankovich 1939), the insolation of the Earth's surface is determined by the eccentricity of the Earth's orbit e and by two parameters of the orbit: by the angle of the perihelion position φ_p from the moving ascending angle γ and by the angle of the orbit's inclination ε to the moving Equator. The typical change in the insolation I for the past 500 thousand years is presented in Figure 1. The figure also shows the evolution of the following parameters: the angle of the inclination ε of the moving Earth's equator to the moving plane of the Earth's orbit, the eccentricity e and the perihelion angle φ_p . The perihelion angle φ_p is shown in the form of cycles from 0 to π and in the continuous form. Figure 1 shows that the insolation I changed in the Northern Hemisphere for the past 500 thousand years in an oscillating way: the maximums indicate possible warmings, while the deep minimums indicate possible glaciations when $T = -120$ kyr and $T = -230$ kyr. For example, the maximum of the last warming occurred 10 thousand years ago (when $T = -10$ kyr). It coincides with the time when the ice sheets disappeared in Eurasia and in North America.

As Figure 1 shows, the period of the change in the inclination angle ε (equal $T_\varepsilon = 41.1$ thousand years) represents the main oscillation period of the insolation I . The period of the change in the eccentricity e (equal $T_{e1} = 95$ thousand years) represents the second significant period of the insolation change. The perihelion angle φ_p changes irregularly. The perihelion of the Earth's orbit rotates in the direction of the Earth's orbital motion with the average period $T_p = 147$ thousand years relative to the motionless space. The plane of the Earth's equator precesses in the direction opposite to the orbital motion of the Earth with the period $T_{pr} = 25.7$ thousand years. Therefore, the circulation period of the perihelion (the angle $\varphi_p \gamma$) relative to the moving plane of the equator is on average $T_p \gamma = 21.9$ thousand years. This is the smallest oscillation period of the insolation I that is presented in Figure 1.

The Disadvantages of the Previous Theories and the Research Program

The evolution of the Earth's insolation is determined by the changes of the Earth's orbit and by the changes of the Earth's rotation axis. Since the time of I. Newton, the orbital problem was simplified and reduced to the interaction of two bodies: the sun and a planet or a planet and a satellite. The rest of the bodies were regarded as the factors of minor disturbances and their impact was divided into series. Thus the problem was solved with approximate analytical methods. This approach was also used in the twentieth century, but the accuracy in the representation of solutions with series was constantly improved. For instance, these series presently contain a few hundred members.

The differential equations of rotational motion were simplified more radically: the second derivatives and the products of the first derivatives were disregarded. Researchers considered only the impact of the moon and the sun on the rotational motion of the Earth, while their

motion was described approximately. Thus the analytical expressions were obtained for the precession of the Earth's equator. They did not contain short-period fluctuations of parameters of the Earth's rotational motion. The precession speed of the Earth's axis was basically determined by the observed speed of the precession (i.e., its evolution remained unknown). At the same time, the only obtained oscillation period of the Earth's axis covering 41.1 thousand years could not be confirmed in any other way.

The approximate nature of the solution to the orbital and rotational problems led to the fact that the results began to diverge when these problems were solved for longer periods of time. For this reason, a number of authors (e.g., Laskar et al. 2004) concluded that the Solar System is unstable and that it is impossible to determine the Earth's insolation for the period of time covering more than 20 million years.

In this regard, a need arises to solve these two problems with minimum simplifications, which can be done with the help of modern numerical methods and supercomputers. At first, we must solve the first problem related to the evolution of the orbital motion, the results of which will help to solve the second problem of the evolution of the Earth's axis. The solution for the two problems will allow us to estimate the evolution of the Earth's insolation. Further, when comparing the insolation changes with the evolution of natural processes, we will be able to establish the dependences making it possible to predict the development of cryosphere processes on the Earth.

The Solution for the Orbital Problem

The orbital motion equations represent the system $3n$ of non-linear differential equations (Smulskiy 1999)

$$\frac{d^2 \vec{r}_i}{dt^2} = -G \sum_{k \neq i}^n \frac{m_k \vec{r}_{ik}}{r_{ik}^3}, \quad i = 1, 2, \dots, n, \quad (1)$$

where \vec{r}_i is the radius vector relative to the center of masses of the Solar System; G is the gravitational constant; \vec{r}_{ik} is the radius vector from the body with the mass m_k to the body with the mass m_i ; $n = 11$ (nine planets, the Sun and the Moon).

To solve equation 1, we developed a new method of numerical integration (Smulskiy 1999), which allowed us to solve them for the period covering 100 million years (Melnikov & Smulskiy 2009). Figure 2 shows the evolution of the Earth's orbit parameters for the period of 3 million years into the past.

The eccentricity e undergoes short-period changes with the main period $T_{e1} = 95$ kyr (thousand years) around the average value $e_m = 0.028$. Besides, one observes longer oscillations with the periods $T_{e2} = 413$ kyr and $T_{e3} = 2.31$ Myr that lead to the extreme values of the eccentricity $e = 0.0003$ and $e = 0.065$. Figure 3 illustrates the change of the moving average values of the eccentricity e_s within the interval $2 \cdot T_{e1}$. Besides, we can see the eccentricity oscillations with the longest period T_{e3} .

When solving the orbital problem, we consider the angles of the orbit position relative to the motionless equatorial plane. The longitude of the ascending node φ_Ω of the orbit and the angle of its inclination i undergo the oscillations with the period $T_s = 68.7$ thousand years around the average

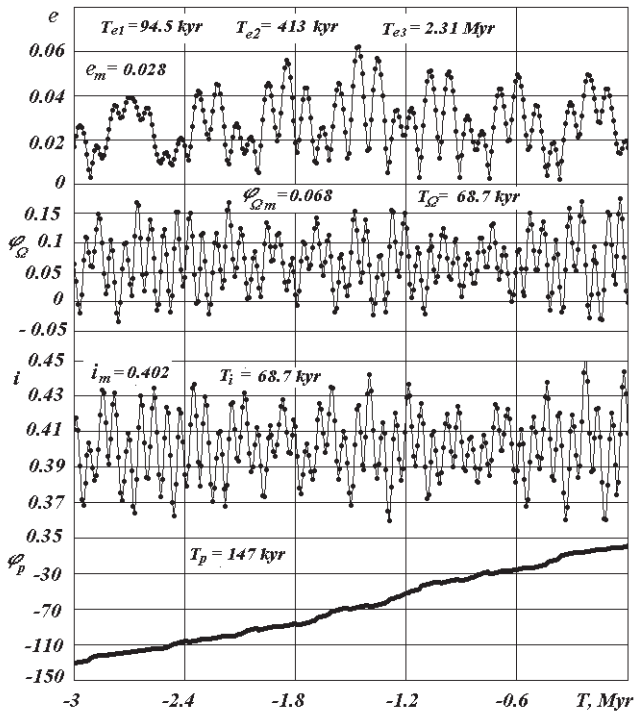


Figure 2. The evolution of the Earth's orbit for the period of three million years into the past: e - the eccentricity; φ_Q - the angular position of the ascending node of the orbital plane; i - the angle of the orbital plane's inclination to the motionless equatorial plane; φ_p - the angular position of the perihelion; T - the time in million years from 1950. The angles are in radians.

value $i_m = 0.402$ radian. The range of oscillations is 5.64° . We established that the changes depend on the rotation of the orbit axis \vec{S} with the period $T_s = 68.7$ kyr around the motionless moment vector \vec{M} of the entire Solar System in the direction opposite to that of the planet rotation around the sun. This rotation or precession of the orbit axis \vec{S} is shown in Figure 3 as the change of the precession angle ψ_s . Apart from the precession motion, the orbit axis \vec{S} undergoes the nutational oscillations of the angle of inclination θ_s to vector \vec{M} . The maximum deviation of axis \vec{S} from moment \vec{M} makes up $\theta_{s\max} = 2.94^\circ$. The main period of nutational oscillations $T\theta_1 = 97.35$ thousand years. The graph shows the moving average values of nutation angle θ_{ss} that were averaged out within the interval $2 \cdot T\theta_1$. In Figure 3 we can see the second period of nutational oscillations $T\theta_2 = 1.164$ million years.

The orbit perihelion (see φ_p in Fig. 2) moves in the direction of the Earth's rotation around the sun, making on average one rotation for $T_p = 147$ kyr. Meanwhile, the perihelion angle φ_p nonmonotonically increases with time and, along with the perihelion rotation in a counter-clockwise direction, we observe the reverse motion in a clockwise direction. As noted above, the periods of a full rotation of the perihelion change by several times.

It was established that the evolution of the planets' orbits as well as of the moon's orbit takes place as a result of four motions: 1) the rotation or, in other words, the precession of the orbit axis; 2) the nutational oscillations of the orbit axis; 3) the oscillations of the orbit eccentricity; 4) rotations of the orbit within its own plane (the perihelion rotation). The research revealed that the axes of the Earth's orbit,

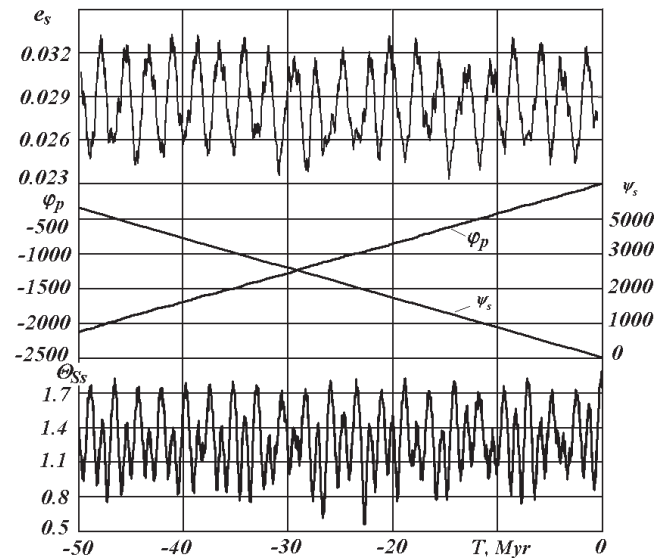


Figure 3. The evolution of the Earth's orbit parameters for the period of 50 million years into the past: e_s - the moving average values of the eccentricity; φ_p - the perihelion angle; ψ_s - the precession angle; θ_{ss} - the moving average values of the nutation angle of the orbit axis. The angles φ_p and ψ_s are in radians, θ_{ss} - in degrees. Myr - one million years.

the planets' orbits and of the moon's orbit as well as the rotation axis of the Earth behave in an identical way. At the same time, unlike the axes of planetary orbits that rotate around the fixed vector of the angular momentum of the Solar System \vec{M} , the axis of the moon's orbit as well as the rotation axis of the Earth precess around the moving axis of the Earth's orbit.

The pericenters of the planets and of the moon rotate in the direction of orbital motion except for Pluto the perihelion of which rotates in the reverse direction.

In Figure 3 the change of the Earth's orbit parameters has a similar view within the interval of $-50 Myr \geq T \geq -100 Myr$ (i.e., the orbit parameters oscillate under the invariable regime). We carried out the same investigations on all planets and obtained the invariable regimes of the oscillations of their orbit parameters. Thus the evolution of the planets' orbits within the investigated interval of 100 million years is invariable and stable. In the works of the authors (Laskar et al. 2004), the chaotic solutions to the simplified equations of motion are explained by the presence of resonances and instabilities that do not occur during the integration of the unsimplified equations of the planets' orbital motion.

Research into the Rotational Motion

We investigate the rotational motion simultaneously by two methods. Utilizing the first method, we integrate differential equations of the rotational motion; in the second method, we model the rotational motion of the Earth with a set of material points.

We developed the differential equations of rotational motion (Smulskiy 2011) based on the theorem of change of angular momentum. Having analyzed the consequences of this theorem, we established that the rotation axis of the Earth will undergo precessional and nutational oscillations with the following periods: 1) with periods equal to half-

$$\ddot{\psi} = -2\dot{\psi}\dot{\theta} \frac{\cos\theta}{\sin\theta} + \dot{\theta} \frac{J_z \omega_E}{J_x \sin\theta} - \sum_{i=1}^n 2G_m \left\{ 0.5 \sin(2\psi) (x_{li}^2 - y_{li}^2) - x_{li} y_{li} \cdot \cos(2\psi) + z_{li} \frac{\cos\theta}{\sin\theta} (x_{li} \cos\psi + y_{li} \sin\psi) \right\}; \quad (2)$$

$$\ddot{\theta} = 0.5\dot{\psi}^2 \sin(2\theta) - \frac{J_z \omega_E \dot{\psi} \sin\theta}{J_x} - \sum_{i=1}^n G_m \left\{ \sin(2\theta) [x_{li}^2 \sin^2\psi + y_{li}^2 \cos^2\psi - z_{li}^2 - x_{li} y_{li} \sin(2\psi)] + 2z_{li} (x_{li} \sin\psi - y_{li} \cos\psi) \cos(2\theta) \right\}; \quad (3)$$

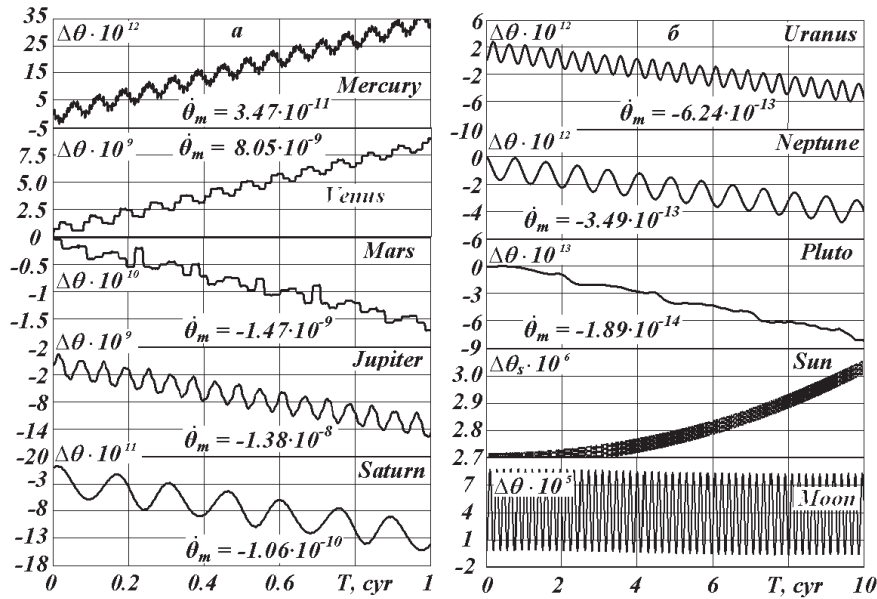


Figure 4. The nutational oscillations and the trends of the Earth’s axis under the separate impact of each planet: a – within the interval of 100 years = 1 *cyr*, b – within the interval of 1000 years; $\Delta\theta = \theta - \theta_0$ – the difference of the nutation angles where θ_0 – the nutation angle in the initial epoch; $\dot{\theta}_m$ – the average speed of nutation in radians per century; the graphs show the periods of main oscillations of the Earth’s axis that equal (from Mercury to the Moon, respectively): 6.6, 8.1, 15.8, 5.9, 14.7, 42, 82.4, 248, 0.5, 18.6 years. The angles are in radians.

periods of the planets, of the sun and of the moon relative to the moving rotation axis of the Earth; 2) with periods equal to the intervals of the nearest planets’ convergence with the Earth in the most remote points from the Earth’s equator; 3) with periods equal to the periods of the passage of impacting bodies at these points at the moments of greatest inclination of the body’s orbital plane to the equatorial plane. These periods will have lengths from several tens of thousands of years to several hundreds of thousands of years.

When solving the problem of the Earth’s rotation, we consider the angle of inclination q to the orbit axis (the nutation angle) and the angle of precession γ relative to the motionless plane of the Earth’s orbit. The differential equations of the Earth’s rotation were obtained in the form seen in equations 2 and 3 above.

$$\dot{\phi} = \omega_E - \dot{\psi} \cdot \cos\theta \quad (4)$$

where J_x, J_y and J_z – the moments of the Earth’s inertia at the axis of the rotating coordinate system xyz ;

$E_d = (J_z - J_x) / J_z$ – dynamic ellipticity of the Earth;

$$G_{mi} = \frac{3Gm_i \cdot E_d J_z}{2r_i^5 J_x} \text{ – the set of parameters;}$$

$\omega_E = \text{const}$ – the projection of the absolute speed of the Earth’s rotation on its axis z ;

$\dot{\phi}$ – the relative speed of the Earth’s rotation;

n – the number of bodies affecting the Earth;

m_i and x_{li}, y_{li}, z_{li} – the mass and the coordinates of affecting body i .

The aforementioned conclusions, drawn from the theorem of oscillation periods, were confirmed during the integration of equations of the rotational motion (2)-(4) under the impact exerted by the planets, by the moon, and by the sun on the Earth separately (see Fig. 4). As the graphs show, the nutation angle θ increases under the influence exerted by the sun, by Mercury, and by Venus, while the influence of other planets decreases it. The graphs show the average speeds $\dot{\theta}_m$ of the change of the nutation angle θ . The speeds depend on the motion of the orbits’ planes of the affecting bodies.

Different types of nutational oscillations can be observed. Most of the bodies create oscillations θ with the half-period of their orbital motion. The maximum oscillations of the nearest planets depend on the period of their convergence with the Earth at the most remote point from the equator. For instance, the periods (see Fig. 4) of 5.9, 14.7, 42, 82.4, and 0.5 years are equal to the half-periods of rotation of the planets and of the sun; the periods of 6.6, 8.1, and 15.8 years are equal to the periods of the planets’ convergence with the Earth at the most remote points from the equator; the period of 18.6 years is equal to the oscillation period of the moon’s orbit plane relative to the equatorial plane.

The rotational motion of the Earth is mostly influenced, firstly, by the moon, then by the sun and by Venus. The main oscillations’ periods of the Earth’s axis presented in Figure 4 are not considered in the astronomical theory of the cryosphere evolution. Our further research is linked with the completion of our approach aimed at the integration of

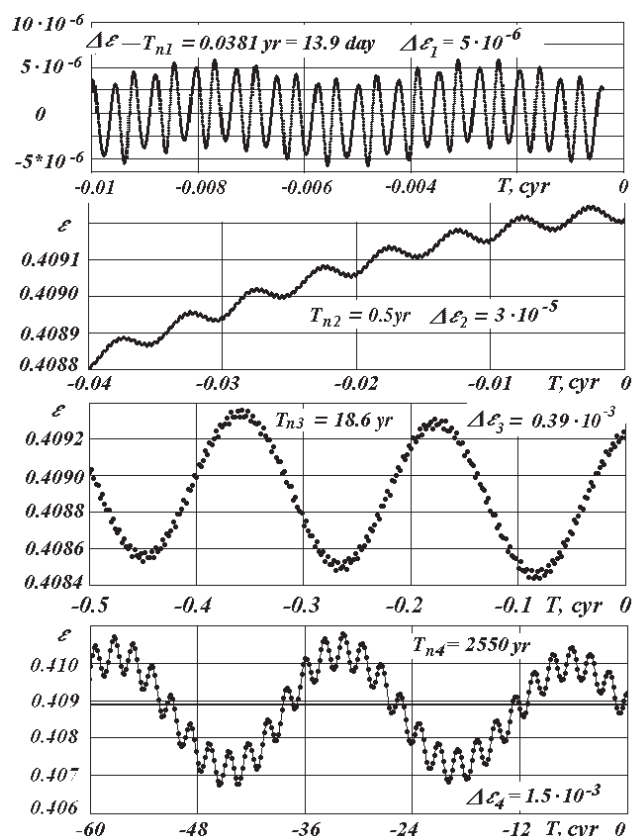


Figure 5. The nutational oscillations of the rotation axis of the compound Earth model No. 3 within different time intervals: $\Delta\varepsilon$ – the deviation of the nutation angle from the moving average angle; $\Delta\varepsilon_1, \Delta\varepsilon_2, \Delta\varepsilon_3,$ and $\Delta\varepsilon_4$ – oscillations' amplitudes, 1 cyr = 100 years. The angles are in radians.

the equations of rotational motion under the joint impact exerted by all planets on the Earth for long periods of time.

The Composite Model of the Rotational Motion of the Earth

The rotational motion is modeled with a set of bodies that are axisymmetrically located in the equatorial plane around the central body. This system evolves under the influence of gravitational attraction of the moon, planets, and of the sun. Meanwhile, the orbit axis of a peripheral body imitates the evolution of the Earth's rotation axis. Several models with different parameters were investigated. Figure 5 shows the nutational oscillations of the rotation axis obtained for Model 3. We examine the angle ε of the Earth's axis position relative to the moving axis of its orbit. The orbit axis of the peripheral body precesses relative to the moving axis of the Earth's orbit in all the models. This result is conceptually important. It makes it possible to control the accuracy of integration of the differential equations of rotational motion within long time intervals.

We obtained the following oscillation periods of the Earth's axis (see Fig. 5): half-monthly periods (13.9 days), semiannual periods (0.5 years), 18.6 years (dependent on the precession of the moon's orbit), and 2580 years. The first three years follow from the theorem of angular momentum and are confirmed with the observation data. The compound models do not have the oscillation period of 41.1 thousand years. Further solutions for the problem of rotational motion

will allow us to clarify the issue of this period and to determine other long periods.

Conclusions

We focused our attention on the issues of the astronomical theory of the cryosphere evolution that are connected with the accuracy of the solution for the orbital and rotational problems. These are the most challenging problems that still have a number of unsolved questions. In contrast with previous research, we solve equations numerically instead of simplifying them. That is why it is possible to shed light on part of the unsolved problems. For example, now we can conclude with certainty that the Solar System is stable. Many peculiarities of orbital motion were established. Solving the problem of the Earth's rotation by two methods, we obtained concepts of its evolution that supplement each other. We hope that this approach will allow us to make the astronomical theory of the cryosphere evolution more accurate.

Acknowledgments

At different stages, the following researchers took part in the research: L.I. Smulskiy, Ya.I. Smulskiy, O.I. Krotov, K.E. Sechenov, A.A. Pavlova, I.A. Shabolina, M.L. Panova, E.F. Safina, and others. The main calculations were made with the help of supercomputers of the Siberian Supercomputer Center of SB RAS (Novosibirsk) and of M.V. Keldysh Institute for Applied Mathematics. The present research was carried out with the support of the grants of the Governor of Tyumen Region and the integration program of the Presidium of RAS No. 13.

References

- Berger, A. & Loutre, M.F. 1991. Insolation values for the climate of the last 10 million years. *Quaternary Science Reviews* 10: 297–317.
- Bolshakov, V.A. & Kapitsa, A.P. 2011. Lessons of the development of the orbital theory of paleoclimate. *Vestnik Rossiyskoy Akademii Nauk* 81 (no. 7): 603-612 (in Russian).
- Laskar, J., Robutel, P., Joutel, F., Gastineau, M., Correia, A.C., & Levrard, B. 2004. A long-term numerical solution for the Earth. *Icarus* 170, 108, Iss. 2: 343-364.
- Melnikov, V.P. & Smulskiy, I.I. 2009. *Astronomical theory of ice ages: New appendixes. The solved and unsolved problems*. Novosibirsk: Akademicheskoe izd-v GEO, 192 pp. <http://www.ikz.ru/~smulski/Papers/AsThAnR.pdf>.
- Milankovich, M. 1939. *Mathematical Climatology and the Astronomical Theory of Climate Change*. M.-L. GONTI, 207 pp. (in Russian).
- Sharaf, Sh.G. & Budnikova, N.A. 1969. Secular changes in the orbital elements of Earth and the astronomical theory of climate change. *Tr. Inst. teoretich. Astronomii*. Issue XIV. L: Nauka. 48, 109 (in Russian).
- Smulskiy, I.I. 1999. *The theory of interaction*. Novosibirsk: Iz-vo Novosibirskogo un-ta, NNTS OIGGM SO RAN. 294 pp. (in Russian). http://www.ikz.ru/~smulski/TVfulA5_2.pdf.

Smulsky, J.J. 2011. The Influence of the planets, sun and moon on the evolution of the Earth's axis. *International Journal of Astronomy and Astrophysics* 1: 117-134.

The climate change, 2007: The Physical Science Basis. Contribution of Working Group I to the Fourth Assessment Report of MGEIK. Iz-vo kembridzhskogo un-ta, 163 pp.

Proof of the Glacier Origin of Tabular Massive Ice

V.I. Solomatin, N.G. Belova

Lomonosov Moscow State University, Department of Geography, Moscow, Russia

Abstract

This paper examines the problem of the genesis of tabular massive ice and suggests a new definition of tabular massive ice. According to this definition, tabular massive ice includes large deposits of ground ice that have the following properties: multi-meter thickness and the length of tens and hundreds of meters; discordant upper contact; inclusions of detritus including large boulders; a wide range of structural and textural characteristics of different scales including dynamic metamorphic structures; and ultra-fresh chemical composition. The discordant upper contact with overlying sediments is irrefutable proof of the buried genesis of massive ice. The paper gives a number of other genetic characteristics of the tabular massive ice structure that prove its buried glacial nature.

Keywords: buried glacial ice; discordant contact; glacial deformations; tabular massive ice.

Introduction

Almost all experts recognize the existence of remnants of ancient glacial ice buried in permafrost. Therefore, it is important to be able to reasonably distinguish the aforementioned formations from other genetic types of ground ice, primarily from the ice of various intrasedimental genesis. At the same time, as even a superficial analysis of the literature shows, the nature of tabular massive ice remains acutely discussed because the solution to this problem determines the understanding of many theoretic and applied issues of cryolithology and paleogeography. Traditionally, the adherents of the marine concepts dominate in geocryology and cryolithology, and naturally they continue to seek the evidence of the intrasedimental genesis of the thick massive ground ice bodies (Vtyurin 1975, Dubikov 2002, Badu 2010, Vasilchuk et al. 2009, Slagoda, Melnikov & Opokina 2010, and others). It was earlier shown (Ershov 1982, Parmuzina 1978, Solomatin 1986, 1993, and others) that the segregated ice formation develops not at the surface (front) of crystallization but in a layer of ground of a certain thickness with the limit temperature values $0^{\circ}\text{C} - \Delta T_{\text{cr}}$ (where ΔT_{cr} is the temperature of ground supercooling that is required to initiate the crystallization of the bound moisture of ground). Hence the physical nature of the process allows us to state that the segregation mechanism can lead to the formation of numerous thin ice lenses, but not to the growth of a single ice interbed with a certain thickness. We also showed (1986, 2008, and other works) that there are no convincing arguments in favor of the possibility of the confined ground water intrusion into monolithic frozen ground, especially if we take into account that the massive ice thickness exceeds tens of meters and its length often exceeds many hundreds of meters. For this reason, we think that the adherents of the intrasedimental growth of massive ice need to seek the physical, cryolithological, structural, petrographical, and other arguments for the segregated or intrusive mechanism of ground ice formation. The latest developments of the spore and pollen method of proving the “non-glacial” nature of tabular massive ice suggested by A.K. Vasilchuk and Yu.K. Vasilchuk (2010) will apparently require some time for this method’s analysis and testing as well as for the collection of factual evidence. It is necessary to explain how pollen and spores get into a layer. The

segregated mechanism is absolutely incompatible with the presence of any particles in the ice that are foreign to the given ground. On the contrary, injected ice can contain absolutely any foreign (chemical and biogenic) elements characteristic of the water and ground environment of ice formation. Furthermore, quite a wide range of landscape conditions is possible for the periphery of the contemporary areas of surface glaciation: from the arctic tundras to tropical forests and savanna vegetation that serve as a source of spores and pollen source for glacial mass. Therefore, it is necessary to find serious proof of the possibility of the spore and pollen method for the genetic identification of massive ice.

First of all, it should be emphasized that the term “tabular massive ice” has for a long time been regarded as the one having the genetic content. Initially it had a strictly morphologic meaning due to the fact that G.I. Dubikov and M.M. Koreysha (who in 1964 were the first to describe tabular massive ice as a separate type of ground ice) did not manage initially to determine the mechanism of its formation. The confusion in the understanding of formation mechanisms of tabular massive ice bodies can be to a certain extent connected with the lack of clear terminological definitions. As a result, many different genetic types may indeed be attributed to tabular massive ice and on this basis the tabular massive ice bodies may be regarded as polygenetic. But what sense does it make to unite the ice types having different genesis under one name? Meanwhile, it is also obvious that morphologically identical ice types cannot have different genesis.

When we speak about typical profiles of tabular massive ice having all its structural characteristics, we should admit that it is a single morphogenetic type occupying its position in the classification system of ground ice, while the notions of the polygenetic nature of massive ice have no basis and would indicate misunderstanding of the nature of the examined formations. Or in each case when we attribute different genesis to separate ice types, we require the corresponding proof of one or the other specific mechanism of ice formation based on appropriate arguments as well as on structural, genetic, and other characteristics.

The ability to distinguish the initial surface types (intrasedimental and buried) of ground ice could be a considerable step on the way to the solution of the examined

problem. Of course, the buried initial surface types can also include buried sea, river, and lake ice, as well as snow patches. It should be noted that the buried state can be reached by the remnants of the peripheral parts of glaciers where terminal, ablation and other types of moraines as well as actively developed fluvioglacial formations. This periglacial zone is characterized by a high degree of flooding of the surface as well as sediment accumulation. Their freezing leads not only to the preservation of glacier remnants but also to the formation of different kinds of intrasedimental ice simultaneously with them. Therefore, the mere presence of the intrasedimental ice does not contradict the buried glacial nature of tabular massive ice. But it should not be united in one genetic type. In each case, we must have criteria for the genetic type of each of the observed kinds of ice. For instance, sea ice can be easily distinguished through its high salinity, while river ice can be easily determined by its typical structures of the orthotropic growth (Solomatin 1986), and so on.



Figure 1. The discordant contact of massive ice with overlying sediments on the Gydan Peninsula. Strong indications of forceful deformations are visible in the massive ice, while the overlying sediments have the bedding that was not disturbed since the time of sedimentation.

Structure and Bedding of Tabular Massive Ice

The definition of tabular massive ice

By tabular massive ice, we propose to understand large bodies of ground ice that are characterized by multi-meter thickness and the length of tens and hundreds of meters; the discordant upper contact; often abundant inclusions of detritus including large boulders; a wide range of structural and textural characteristics of different scales including dynamic metamorphic structures; ultra-fresh chemical composition and low content of heavy oxygen isotopes.

All the ground ice formations that do not have this set of features, distinct characteristics of structure and of the bedding conditions (including those being the consequence of a poor exposure and a profile covered with slumped sediments) should not be attributed to the massive type of ground ice.

The discordant contact of tabular massive ice with overlying sediments

The discordant contact of the layers (Figs. 1, 2, 5) with overlying sediments is emphasized by the profile of the ice structures (folds, stratification, structural and textural heterogeneities), with the presence of deformations in the ice and with the undisturbed bedding of overlying loose stratifications with the initial structures of sedimentation.

Such is the nature of the discordant contact (the contact with erosion) as well as the bedding and structure of the overlying sediments undisturbed since deposited (considering that the ice directly underlying them has the indications of dynamic metamorphism and the structure of macro- and micro-deformations). This may develop under the following conditions: firstly there formed massive ice that underwent deformations and gained its characteristic structural features; and then the ice body was covered (probably with partial thawing) with the sediments of various genesis and preserved in permafrost.

Thus the discordant contact represents irrefutable evidence of the buried genesis of tabular massive ice.



Figure 2. The mass of the dislocated glacial ice that is not reflected in the relief and is covered with a thin layer of undeformed sediments. Location on the northwestern coast of New Siberia Island. Photograph by V.E. Tumskey.



Figure 3. The fold complicated by the shear-fault in the massive ice on the western shore of Baydaratskaya Bay.

Discussion

Other genetic features of the tabular massive ice structure and other arguments of their buried glacial genesis are:

- 1) The deformations (Figs. 1, 2, 4, 5) of many different types and scale are observed in massive ice (fold, shear, fault, microfold deformations, etc.). They vary within the profile and along the length of the ice body. These consequences of the dynamic metamorphism of the ice are absolutely incomparable with any cryogenic processes and completely identical with the glacial tectonics of glacial ice. These arguments make us inevitably conclude that the ice has glacial origin.
- 2) All types of detritus and boulders with the diameter of more than 1 m were encountered in the massive ice (Fig. 4). The presence of coarse detritus in the ice is incomparable with any type of the intrasedimental ice formation and is rather natural for glacial ice.
- 3) Massive ice has (in practically 100% of cases) the ultra-fresh chemical composition (Solomatin 1976, 1986, Belova et al. 2008) that absolutely differs from that of segregated ice and of the water extract of the enclosing sediments. This fact contradicts the intrasedimental genesis of tabular massive ice bodies and is natural for glacial ice.
- 4) The chemical and isotope content of the ice has no directed alterations in the profile but exhibit certain variations with depth that probably reflect a change in the conditions of ice formation and in the conditions of the isotope and oxygen content formation (Solomatin 1976, 1986, 2005, Belova et al. 2008). This is in contradiction with the crystallization of the volume of groundwater in and with the segregated ice formation of bound water, since the fractionation of the composition and the direct enrichment of the chemical and heavy isotope contents with depth are inevitable in both cases.
- 5) In many cases the layers having all the typical peculiarities of the structure of this ice lie in the sandy mass, which does not correspond to the conditions for the development of the segregated process even at a minimum scale or on the scale of massive ice bodies (Solomatin 1986).

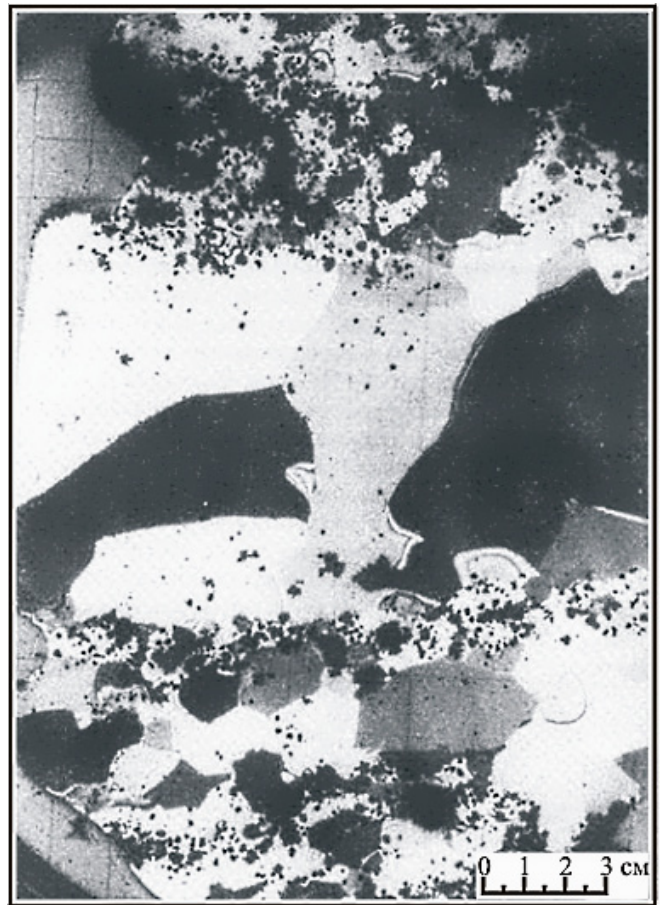


Figure 4. The schistosity emphasized with the ground inclusions; the consequence of layer-by-layer plastic deformations.

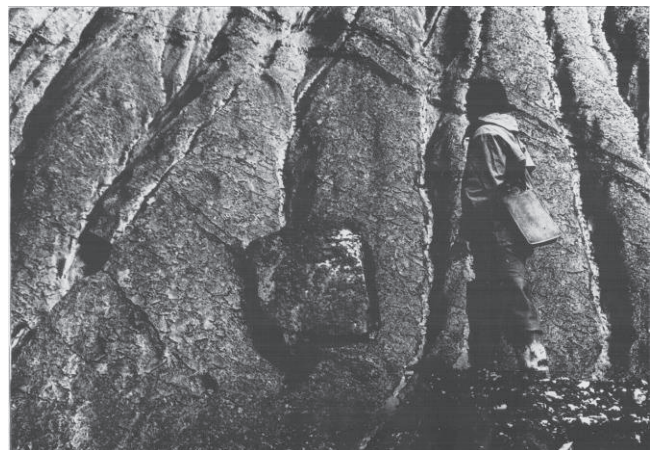


Figure 5. A boulder in massive (glacial) ice at the Ledyanaya Gora exposure on the Yenisey River at the latitude of the Polar Circle. Photograph by E.G. Karpov.

- 6) Most of the layers bed statistically at the contact between the covering fine-dispersed sediments and the underlying coarse-dispersed sediments. This contrasts with the mechanism of the intrusive processes of ice formation, as the generation of hydrostatic and dynamic tension in the water-bearing sand horizon at least requires its partial freezing and, thus, the narrowing of the sectional area of the ground flow. This means that the injected ice must be located not at the contact of a water-bearing layer but at some distance below it (Solomatin 1986).



Figure 6. The massive ice with forceful dislocations that is exposed directly under the active layer and is not reflected in the relief. Location is the western coast of Baydaratskaya Bay. Photograph by F.A. Romanenko.

- 7) In many cases, thick ice layers are covered only with a very thin layer of frozen ground (Fig. 2, 5). In case of intrusive origin of massive ice, an injection of the pressurized ground water and a deformation of the overlying ground with the formation of the frost mound with the intrusive ice core there should have occurred. Therefore, it is absolutely inexplicable why, instead, there occurred a rupture in the stratification of the frozen ground to a considerable distance (up to 1 km?) with the uplift of the ground layer to the height of a few tens of meters without any disturbances. Such a version contradicts all the concepts of physics and mechanics of frozen ground. The very possibility of splitting the low temperature frozen ground by the confined ground water sounds unconvincing.
- 8) Finally, the absence of the corresponding forms of ground heaving in the relief contradicts the intrasedimental genesis of tabular massive ice (Figs. 2, 5). Geomorphologically the areas with tabular massive ice are, as a rule, indistinguishable from the adjacent territories. The observed mound and ridge relief in some areas with tabular massive ice does not correspond to the formation of thick intrasedimental ice bodies. However, it bears a resemblance to the relief of the areas of the dead ice belonging to retreating glaciers (Solomatin 1986).

Conclusions

It should be emphasized once again that tabular massive ice belongs to a single morphogenetic type, despite the entire

variety of conditions of its bedding and its structure. It is characterized by a considerable length that exceeds by many times the vertical dimensions, by the discordant contact with the overlying sediments, by the complex structure varying within the profile and along the length, and by various bedding conditions. There are no reasons to regard a single (in terms of morphology and structure of ice bodies) type of ground ice as polygenetic and to divide it into different formations by genesis.

The materials, experimental data, and theoretical concepts collected at the present time lead to the clear conclusion that tabular massive ice represents a single and separate genetic type of ground ice: the buried remnants of glaciers that formed during deglaciation of the ancient glaciation areas.

Acknowledgments

This paper was prepared within the framework of State Contract P516 of the “Scientific and Pedagogical Staff in Innovative Russia” federal targeted program.

References

- Astakhov, V.I., Kaplyanskaya, F.A., & Tarnogradsky, V.D. 1996. Pleistocene permafrost of West Siberia as a deformable glacier bed. *Permafrost and Periglacial Processes* Vol. 7: 165-191.
- Badu, Yu.B. 2010. *Cryolithology: Textbook*. Moscow: KDU, 528 pp. (in Russian).

- Belova, N.G., Solomatin, V.I., & Romanenko, F.A. 2008. Massive ground ice on the Ural Coast of the Baydaratskaya Bay, Kara Sea, Russia. *Proceedings of the Ninth International Conference on Permafrost*, Fairbanks, Alaska, 1: 107-112.
- Belova, N.G., Solomatin, V.I., Romanenko, F.A., Olyunina, O.S., & Ogorodov, S.A. 2007. The new data on the massive ice of the eastern coast of the Yugorsky Peninsula. *The materials of International Conference "Cryogenic resources of polar regions"*, Vol. 1, pp. 198-200 (in Russian).
- Dubikov, G.I. 2002. *Composition and cryogenic structure of permafrost in Western Siberia*. Moscow: GEOS, 246 pp. (in Russian).
- Ershov, E.D. 1982. *Cryolithogenesis*. Moscow, Nedra, 210 pp. (in Russian).
- Fotiev, S.M. 2011. The formation mechanism of injected ice veins and hydrolaccoliths. *Kriosfera Zemli* 15 (no. 2): 44-55 (in Russian).
- Fritz, M., Wetterich, S., Meyer, H., Schirrmeister, L., Lantuit, H., & Pollard, W.H. 2011. Origin and characteristics of massive ground ice on Herschel Island (Western Canadian Arctic) as revealed by stable water isotope and hydrochemical signatures. *Permafrost and Periglacial Process* 22: 26-38.
- Murton, J.B., Whiteman, C.A., Waller, R.I., Pollard, W.H., Clark, I.D., & Dallimore, S.R. 2005. Basal ice facies and supraglacial melt-out till of the Laurentide Ice Sheet, Tuktoyaktuk Coastlands, western Arctic Canada. *Quaternary Science Reviews* 24: 681-708.
- Parmuzina, O.Yu. 1978. Cryogenic structure and some peculiarities of ice formation in the seasonally thawed layer. *The Problems of Cryolithology* 7: 141-164 (in Russian).
- Slagoda, E.A., Melnikov, V.P., & Opokina, O.L. 2010. Repeatedly injected stocks of ice in sediments of Western Yamal. *Reports of Russian Academy of Sciences* 432 (no. 2): 264-266 (in Russian).
- Solomatin, V.I. 1976. The massive ice in the lower reaches of the Yenisey River (by illustration of the Selyakino section). *The Problems of Cryolithology* 5: 87-94 (in Russian).
- Solomatin, V.I. 1977. Fossil relicts of glacier ice in the north of Western Siberia *MGI* 29: 233-240 (in Russian).
- Solomatin, V.I. 1986. *Petrogenesis of ground ice*. Moscow: Nauka, 215 pp. (in Russian).
- Solomatin, V.I. 2005. Glacier ice in the cryolithozone. *Kriosfera Zemli* 9 (no.2): 78-84 (in Russian).
- Solomatin, V.I., Konyakhin, M.A., Nikolaev, V.I. & Mikhalev, D.V. 1993. The occurrence conditions and the composition of massive ice on the Yamal Peninsula. *MGI* 77: 139-147 (in Russian).
- Vasilchuk, A.K. & Vasilchuk, Yu.K. 2010. Comparison of pollen spectra of massive and glacial ices for cryogenetic indication. *Kriosfera Zemli* 14 (no. 3): 15-28 (in Russian).
- Vasilchuk, Yu.K., Vasilchuk, A.K., Budantseva, N.A., Chizhova, Yu.N., Papesh, V., Podborny, E.E. & Sulerzhitskiy, L.D. 2009. Oxygen isotope and deuterium indication of the origin and ^{14}C age of the massive ice (Bovanenkovo, Central Yamal peninsula). *Reports of Russian Academy of Sciences*, 428 (no. 5): 675-681 (in Russian).
- Vtyurin, B.I. 1975. *Ground ice of the USSR*. Moscow: Nauka, 215 pp. (in Russian).
- Waller, R.I., Murton, J.B., & Knight, P.G. 2009. Basal glacier ice and massive ground ice: Different scientists, same science? In *Periglacial and Paraglacial Processes and Environments*. Knight, J. & Harrison, S. (eds). The Geological Society, London, Special Publications 320: 57-69.

The Ice Complex of Western Taymyr

I.D. Streletskaya

Lomonosov Moscow State University, Faculty of Geography, Moscow, Russia

A.A. Vasilev

Earth Cryosphere Institute, SB RAS, Tyumen, Russia

Abstract

The results of the study of the Western Taymyr ice complex are discussed. Western Taymyr represents a natural boundary of ice complex distribution. In contrast to Yakutia and Alaska, the Western Taymyr ice complex is less thick, includes smaller syngenetic ice wedges, and is younger. The Western Taymyr ice complex formed in two stages. The lower sedimentary layer formed in the Late Pleistocene; the ice wedges have a calcium hydrocarbonate composition and a light composition of oxygen isotopes. The upper sedimentary layer formed during the cold periods of the Holocene, and it is characterized by a sodium chloride composition and a heavier composition of oxygen isotopes. The organic carbon content in the upper sedimentary layer is higher than in the lower one. A conclusion concerning environmental changes at the turn of Pleistocene/Holocene was made.

Keywords: ice complex; isotopic composition; Pleistocene/Holocene; ice wedges.

Introduction

An ice complex (IC) is a unique natural phenomenon. It consists of an ice-rich deposit, mainly of silty composition, with thick syngenetic ice wedges (SIW). It is characterized by heterogeneity of its origin and age. ICs were studied in Chukotka (Kotov 2002), Alaska (Williams & Yeend 1979, Lawson 1983, Carter 1988, Hamilton et al. 1988, Hopkins & Kidd 1988, Kanevskiy et al. 2008, Kanevskiy et al. 2011), and in the north of Canada (Fraser & Burn 1997, Kotler & Burn 2000, Froese et al. 2009). In Yakutia, IC deposits were investigated on the coast of the Laptev Sea and the East Siberian Sea as well as on the mainland (Meyer et al. 2002, Romanovskii et al. 2004, Grosse et al. 2007, Siegert et al. 2009, Romanenko et al. 2011). Previously it was assumed (Tomirdiario & Chernen'kiy 1987) that the IC geographic distribution stretches to the Taymyr Peninsula. The western border of the IC distribution has not been determined until now.

Despite a long record of IC studies, a common view on the deposit formation conditions, genesis, and age is not established. An IC is often called "edoma" or "edoma deposit." An IC on the coasts and the arctic islands of Eastern Siberia is called "a shelf-type edoma." Most Russian researchers consider IC to be an Upper Pleistocene polygenetic formation where eolian, alluvial, deluvial, and solifluction deposits predominate. The compositional homogeneity and the cryogenic structure similarity of the deposits are attributed to cryogenic changes in soils (Konishchev 1981).

In Taymyr, IC deposits were investigated in the Taymyr Lake and the Labaz Lake areas (Chizhov et al. 1997, Derevyagin et al. 1999, Siegert et al. 1999). According to Bolikhovskiy (1987), IC deposits occur in Yamal and Gydan.

The Upper Pleistocene deposits (which can in many respects be attributed to ICs though they have some regional peculiarities) were studied on the western coast of Taymyr, 200 km from the Dikson settlement (73°31'N, 80°34'E) to the Sopochnaya Karga polar station (71°88'N, 82°68'E).

Field works were organized by the Lomonosov Moscow State University Faculty of Geography, VNIIOkeangeologia

(the All-Russian Research Institute for Geology and Mineral Resources of the Ocean) and the Earth Cryosphere Institute of the Siberian Branch of RAS as part of the International Polar Year scientific program.

Study Area

The Western Taymyr region is influenced by mid-latitude circulation patterns and is characterized by the arctic marine climate in the Dikson area and subarctic climate in the Sopochnaya Karga area. The area is characterized by severe climatic conditions; the long-term average January temperature during the period of weather observations is -28.1°C in Dikson, and -30.7°C in Sopochnaya Karga (www.meteo.infospace.ru).

The area lies in the zone of continuous permafrost up to 500–700 m thick with low annual average temperatures of -9°...-11°C. In the Dikson area, thin Quaternary sediments lie on solid rock between low capes and skerries, composed of diabase. To the south of Dikson, the Quaternary strata section is composed of two layers. The base of the section is formed by saline sands, sandy silts, and clays of marine genesis. Their thickness in the Sopochnaya Karga area is more than 100 m. The upper part of the section is represented by alluvial, slope, lacustrine, and biogenic sediments as well as IC sediments 10–12 m thick.

Methodology

The structure, properties, and characteristics of the Western Taymyr IC were studied in the field at the following key areas: Sopochnaya Karga, the Krestyanka River mouth, and Dikson (Streletskaya & Vasilev 2009, Streletskaya et al. 2011). Ice content, granulometric and mineralogical composition, salinization, water-soluble salts composition, and organic carbon content were determined in IC deposits and lower stratum. The analyses were made in the Laboratory of Lithology and Geochemistry of VNIIOkeangeologia, St. Petersburg. Mineralogical analysis was performed by A.V. Surkov. The analysis of radiometric age of the organic impurities in the IC sediments was made in the Laboratory

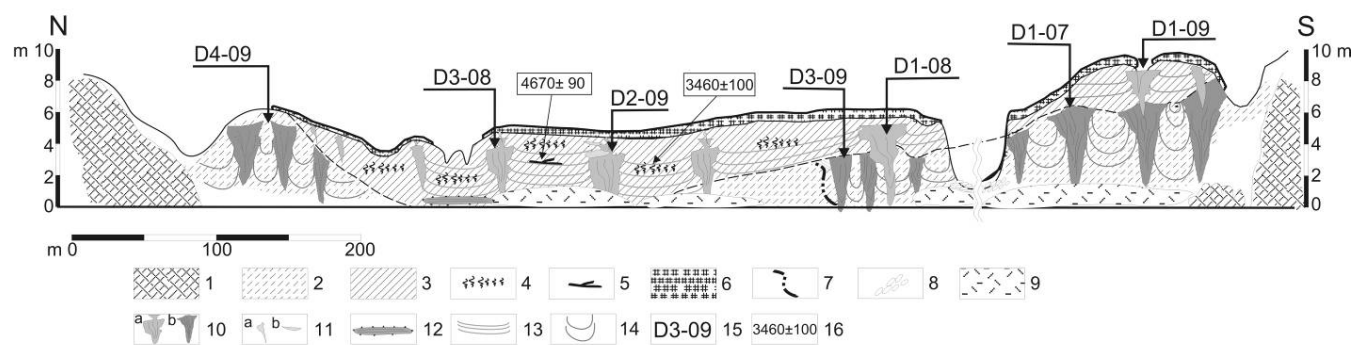


Figure 1. Structural scheme of coastal exposure near Dikson settlement (according to Streletskaia et al. 2011): 1- parental rocks; 2- sandy silt; 3- peaty sandy silt; 4- autochthonous peat, fibrous roots of plants; 5- wood debris; 6- sod; 7- ground wedge boundary; 8- pebbles; 9- beach; 10- ice wedges: a- in upper layer, b- in lower layer; 11- growing ice wedges (a), ice lenses (b); 12- firm; 13- horizontal cryostructures; 14- concave cryostructures; 15- profile number; 16- radiocarbon age of organic inclusions.

of Geology and Cenozoic Paleoclimatology of the Sobolev Institute of Geology and Mineralogy of the Siberian Branch of RAS, Novosibirsk.

In water samples taken from melted wedge ice, oxygen ($\delta^{18}\text{O}$) and deuterium (δD) content and the chemical composition of ice were determined. The content of oxygen and hydrogen stable isotopes was determined in the Isotope Laboratory of the Alfred Wegener Institute for Polar and Marine Research, Research Unit Potsdam, Germany. $\delta^{18}\text{O}$ and δD values are given in permil relative to the international standard Vienna Standard Mean Ocean Water with the accuracy of 0.1‰ and 0.8‰, respectively. The hydrochemical analysis was carried out using standard procedures in the Laboratory of Lithology and Geochemistry, VNIIOkeangeologia, St. Petersburg.

Results

The most complete section of IC deposits was studied in the Dikson area where two layers of syngenetic SIW are exposed in a coastal outcrop (Fig. 1). The IC deposits are ice-rich (total moisture content is more than 86%) and have a rhythmically-belt structure typical for syngenetic deposits. The ice lenses of up to 0.5–1.0 cm thickness with 3 to 12 cm spacing characterize the cryostructure. The cryostructure between the ice lenses is reticulate, ataxitic, and massive, while near the ice lenses it is micro-lenticular. At the contacts of ice lenses and ice wedges, the ice lenses are concave or vertical. The visible thickness of the IC deposits is about 10 meters, but the SIW continues below the sea level, which suggests that the deposits are thicker.

The surrounding syngenetic ice wedge deposits are homogeneous and consist of silt-sized strata, the number of which increases from 82 to 96% with the depth. Coarse silt fraction (0.05–0.01 mm) predominates among the strata. The analysis of heavy fraction in the IC deposits has shown that the source of the material was in situ bedrock of basic composition. Fine grain sediments, forming as a result of bedrock weathering, are represented by aggregated olivine-plagioclase-ilmenite, angular grains of olivine and ilmenite, quartz, and debris of black coal. Minerals in the ilmenite-garnet-tourmaline range are differentiated by density in all the samples from the IC deposits. In the deposits, flattened derrises of basalt in silt fraction are ubiquitous. It is known

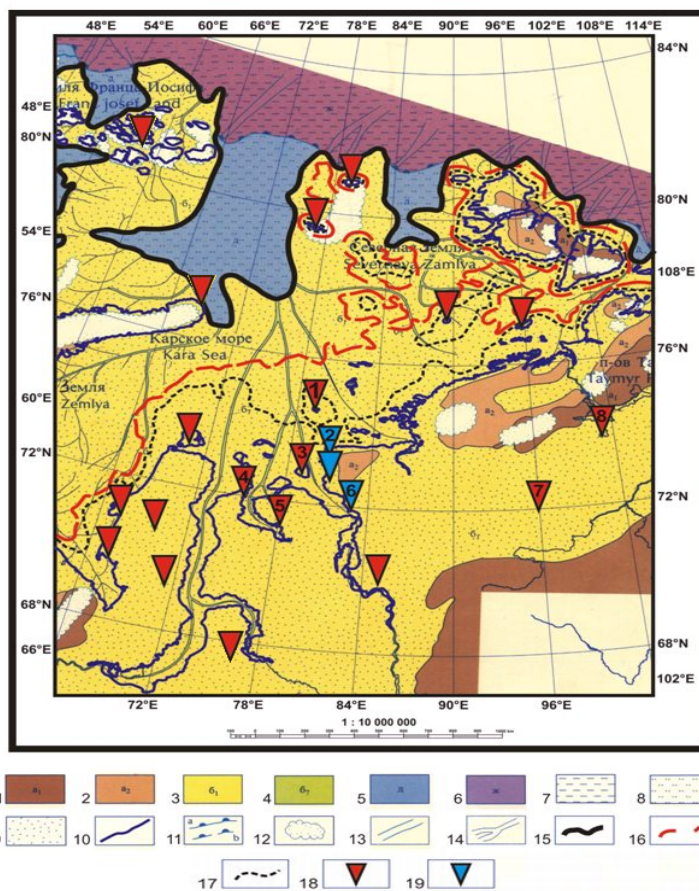


Figure 2. Relict ice wedges in Late Pleistocene – Holocene, Kara Sea (using the Atlas of paleographic maps (1991) and R. Stein et al (2002) with additions by authors and D. Drozdov. 1 – highlands; 2 – hills and lowlands; 3 – alluvial and lacustreme plans; 4 – river valleys and temporary lakes; 5 – continental shelf; 6 – oceanic areas; 7 – mud, clay/ mudstone, shale; 8 – silt, siltstone; 9 – sand, sandstone; 10 – present day coastline; 11 – shelf edge at time of map: a) determined, b) inferred); 12 – ice sheets; 13 – submarine trench, canyon or channel; 14 – river paleovalley, submerged during transgressive phase; 15 – coastline at 18 000 y; 16 – coastline at 11 000 y; 17 – coastline at 9 000 y; 18 – relict ice wedges; 19 – key relict ice wedges sites. Sites with SIW where isotopic composition was studied (see Table): 1 - the Sverdrup Island, 2 - the Dikson settlement, 3 - the Sibiryakov Island, 4 - the Gydan Bay (west coast), 5 - the Gydan Bay (east coast), 6 - Sopochnaya Karga, 7 - the Labaz Lake, 8 - the Taymyr Lake.

that basalt is quickly weathered, and that is why unweathered angular particles in fine grain fraction are indicative of a nearby source of parent material.

Table. Average isotopic composition of ice wedges in the Quaternary deposits.

Areas with ice wedges (see Fig. 2)	Age of the deposits, thousands of years ago							
	>25		12-25		< 10		<1	
	$\delta^{18}\text{O}$, ‰	δD , ‰	$\delta^{18}\text{O}$, ‰	δD , ‰	$\delta^{18}\text{O}$, ‰	δD , ‰	$\delta^{18}\text{O}$, ‰	δD , ‰
the Sverdrup ¹ Island			-24.9	-188.8	-19.9	-143.1		
the Dikson			-26.0	-198.4	-20.7	-154.4	-20.7	-154.1
the Sibiryakov Island					-19.9	-149.9		
the Gydan Bay (west coast)			-24.4	-186.3	-20.8	-156.5		
the Gydan Bay (east coast)					-18.7	-140.7		
Sopochnaya Karga			-26.0	-199.5	-20.3	-149.7	-16.6	-120.6
the Labaz ² Lake	-30.2	-230.6			-23.0	-172.2		
the Taymyr ³ Lake	-29.5	-228.2	-25.3	-196.5	-23.1	-171.4	-20.4	-155.4

¹ Romanenko et al. 2001, 2011, ² Chizhov et al. 1997, ³ Derevyagin et al. 1999.

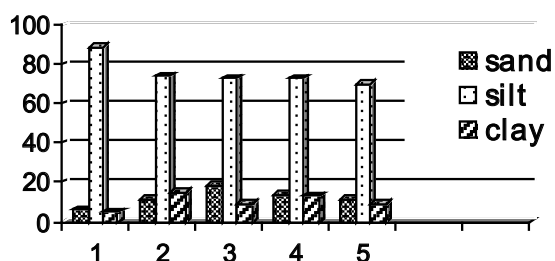


Figure 3. The ratio (percentage of particles) of sand (0.05-2.0 mm), silt (0.05-0.005 mm) and clay (<0,005 mm) fractions in the IC deposits of Western Taymyr (according to the authors' materials), the East Siberian Sea coast (Tomirdiaro & Chernen'kiy 1987) and Alaska, Itkillik River exposure (Kanevskiy et al. 2011). 1 – Dikson; 2 - Shelomskiy Yar; 3 - Ostantsovyy Yar; 4 - Oyagosskiy Yar; 5 - Alaska, Itkillik River exposure.

The organic carbon content in the sediments including the upper layer of ice wedges is 0.6–1.2% and reaches 2.1% due to inclusions of peat and wood fragments. According to the results of radiocarbon dating, the upper layer of the deposits accumulated from 9000 to 3500 y.a. (Gusev et al. 2011).

In the IC deposits including SIW of the lower layer, the organic carbon content is up to 0.6%. Organic matter is regularly spread in the section. There are no large inclusions of plant debris.

The results of the analysis of oxygen ($\delta^{18}\text{O}$) and hydrogen (δD) isotopic composition of SIW show values from -26.8‰ to -20.1‰ ($\delta^{18}\text{O}$) and from -205.0‰ to -150.4‰ (δD). The isotopic composition of the upper layer SIW is from -21.7‰ to -19.5‰ ($\delta^{18}\text{O}$) and from -161‰ to -147‰ (δD). The isotopic composition of the lower layer SIW is 6‰ lighter; it changes from -24.3‰ to -26.8‰ for $\delta^{18}\text{O}$ and from -205‰ to -184‰ for δD . Contemporary growing ice veins of wedges have a heavier isotopic composition from -17.1‰ to -16.2‰ for $\delta^{18}\text{O}$ and from -124‰ to -118‰ for δD in the Dikson area (Streletskaia et al. 2011).

Ice mineralization increases from 63.5 mg/l (SIW of the upper layer) to 360.5 mg/l (SIW of the lower layer). In the

SIW of the upper layer, Cl^- predominates among the anions and Na^+ predominates among the cations. HCO_3^- and Ca^{2+} predominate in the composition of ice wedges of the lower layer.

Discussion

In the Dikson area, SIW in the lower layer of IC are characterized by the average stable isotope content of -26.0‰ for $\delta^{18}\text{O}$ and -198.4‰ for δD and by high concentrations of HCO_3^- and Ca^{2+} in ice. Similar values of isotopic and chemical composition characterize SIW (up to 10 m thick) in the deposits of alluvial terrace (10–15 m high) of the Yenisei River in the area of Sopochnaya Karga (Streletskaia & Vasilev 2009). The formation of the terrace finished 10,000 y.a. (Gusev et al. 2011). In the Dikson area, SIW of the lower layer formed during the MIS2. A calcium hydrocarbonate composition of SIW indicates that winter precipitation formed over the land which occupied the modern shelf after the sea regression during the last stage up to the isobath of 120 m (Fig. 2).

Syngenetic SIW also developed on the Sverdrup Island and other arctic islands (Tarasov et al. 1995, Romanenko et al. 2001). Severe winters of the time of the lower layer SIW formation can be reconstructed according to ice isotopic composition. Temperature estimates (Vasilchuk 1992) show that January temperatures in the Dikson area fell to $-40 \pm 3^\circ\text{C}$, which is approximately $10\text{--}12^\circ$ lower than modern winter temperatures.

The isotopic and chemical composition of SIW of the upper layer of the Dikson area reflect environmental changes in the Early Holocene. In the Dikson area, the average stable isotope content in the SIW of the IC upper layer is -20.7‰ for $\delta^{18}\text{O}$ and -154.4‰ for δD . The predominance of Cl^- among the anions and Na^+ among the cations in SIW chemical composition indicates an increasing role of the ocean in precipitation composition in the Holocene. January temperatures at the time of accumulation of the upper layer of the Holocene SIW were similar to or a little lower

than the modern ones. Intensive cracking and growth of syngenetic SIW were caused by dry winters with little snow accumulation in the Holocene.

The cryogenic structure of the IC of Western Taymyr, Yakutia, Chukotka, Alaska, and Canada is similar. IC sediments accumulate and freeze under conditions of intensive ice accumulation at the base of the active layer.

In the area, the isotopic composition of SIW in the Upper Pleistocene deposits which formed 12–25 thousand years ago has been changing within a narrow range. In the Holocene SIW, the isotopic composition reflects higher winter temperature and substantial sea influence. Stable oxygen isotope content in SIW decreases from the coasts to the inland of the peninsula (see Table).

The isotopic composition of the Western Taymyr ice wedges of the Upper Pleistocene/Holocene age is similar to the isotopic composition of SIW on the coasts of the Laptev and East Siberian seas (Magens 2005, Romanenko et al. 2011). The similarity of ice formation conditions from Taymyr to Alaska makes it possible to use isotopic data as correlation markers (Romanenko et al. 2011).

The ratio of sand, silt, and clay fraction in the IC deposits in the Dikson area are almost identical to the IC deposits of known sections of shores of Yakutia Coastal Lowlands (Shelomskiy Yar, Ostantsovyi Yar, Oyagosskiy Yar) and Alaska (Fig. 3).

Products of cryogenic weathering drifted from the surfaces of watersheds. Aeolian processes played a significant role in the redistribution. The lithologic features of the IC deposits and their occurrence on the slopes and in topographic depressions can be explained by nivation processes, which were widespread during the cool periods (Kunitskiy 2007). Modern snow patches are widespread on the slopes in the Dikson area.

Our data and the results obtained by Siegert et al. (2009) do not confirm the statement (Tomirdiari & Chernen'kiy 1987) about the increasing role of fine grained deposits in IC. The statement, "while moving further away from surrounding mountains," was explained by mechanical differentiation of the material and aeolian redeposition.

During the transition of the last cryochron (MIS2) to the Holocene, the organic carbon content in the IC deposits of Western Taymyr has been increasing. Other areas of IC distribution are also characterized by high organic carbon content in the Holocene sediments (Siegert et al. 1999, Derevyagin et al. 1999, Siegert et al., 2009).

Conclusions

The Western Taymyr coast is the westernmost area of distribution of the last cryochron IC deposits. In contrast to the Yakutia IC, the Western Taymyr IC is less thick (up to 12 m), includes smaller syngenetic SIW, and has formed in the Late Pleistocene/Holocene.

The ratio of sand, silt, and clay fractions and cryogenic structure of the IC deposits of Western Taymyr are similar to IC sections in Siberia, Chukotka, Alaska, and Canada. The mineralogical composition of sediments indicates a close source of parental material.

The Western Taymyr ice complex formed in two stages: in the Late Pleistocene (MIS2) and in the Holocene cold

periods. This is inferred from the profile structure and the difference in SIW chemical and isotopic composition. Lighter composition of oxygen isotopes (-26–25‰) and the predominance of calcium and hydrocarbonate ions are typical for the Late Pleistocene SIW, while a heavier isotopic composition (-19–21 ‰) and the predominance of sodium and chloride ions are typical for the Holocene SIW.

During the Holocene, syngenetic wedges grew in thermokarst depressions, which formed during the Holocene climatic optimum and were subsequently filled with silty sediments. The reworked material of the pre-Holocene IC deposits predominates in the profile sections. Compared to the Late Pleistocene sediments, the Upper Holocene sediments of the IC contain more organic matter.

Acknowledgments

This research was supported by the "World Ocean" program provided by the Russian Academy of Science; the "Leading Scientific Schools of Russia" project NSH-3271.2010.5, the Arctic Coastal Dynamics (ACD) project, and by ConocoPhillips Russia Inc.

References

- Atlas of paleographic maps. Eurasian Shelves in Mesozoic and Cainozoic. 1991. The Robinson Group plc UK GIN AS USSR, Vol. 2 (maps) (in Russian).
- Bolikhovskiy, V.F. 1987. Yedoma deposits of Western Siberia. New data on the geochronology of the Quaternary period. *Proceedings of the 12th INQUA Congress*, Canada, 1987. Moscow: Nauka, 128-135 (in Russian).
- Carter, L.D. 1988. Loess and deep thermokarst basins in Arctic Alaska. *Proceedings of the Fifth International Conference on Permafrost*. Tapir publishers, Trondheim, Norway, 706-711.
- Chizhov, A.B., Derevyagin, A.Yu., Simonov, E.F., Hubberten, H.W., & Siegert, C. 1997. Isotopic composition of ground ice of the Labaz Lake area, Taymyr. *Kriosfera Zemli (Earth Cryosphere)* Vol. 1, No. 3: 79-84 (in Russian).
- Derevyagin, A.Yu., Chizhov, A.B., Brezgunov, V.S., Hubberten, H.W., & Siegert, C. 1999. Isotopic composition of wedge ice of the Sablera Cape, the Taymyr Lake. *Earth Cryosphere (Kriosfera Zemli)* Vol.3. No. 3: 41-49 (in Russian).
- Fraser, T.A. & Burn, C.R. 1997. On the nature and origin of "muck" deposits in the Klondike area, Yukon Territory. *Canadian Journal of Earth Sciences* 34, 1333–1344.
- Froese, D.G., Zazula, G.D., Westgate, J.A., Preece, S.J., Sanborn, P.T., Reyes, A.V., & Pearce, N.J.G. 2009. The Klondike goldfields and Pleistocene environments of Beringia. *GSAToday* 19(8): 4–10. doi:10.1130/GSATG54A.1.
- Grosse, G., Schirrmeister, L., Siegert, C., Kunitskiy, V., Slagoda, E.A., Andreev, A.A., & Derevyagin, A.Y. 2007. Geological and geomorphological evolution

- of a sedimentary periglacial landscape in northeast Siberia during the Late Quaternary. *Geomorphology* 86: 25–51.
- Gusev, E.A., Arslanov, Kh.A., Maksimov, F.E., Molodkov, A.N., Kuznetsov, V.Yu., Smirnov, S.B., Chernov, S.B., & Zherebtsov, I.E. 2011. New geochronological data on Neopleistocene/Holocene deposits in the Yenisei River downstream. *Problems of the Arctic and the Antarctic (Problemy Arktiki i Antarktiki)* No. 2 (88): 36-44 (in Russian).
- Hamilton, T.D., Craig, J.L., & Sellmann, P.V. 1988. The Fox permafrost tunnel: a late Quaternary geologic record in central Alaska. *Geological Society of America Bulletin* 100: 948–969.
- Hopkins, D.M. & Kidd, J.G. 1988. Thaw lake sediments and sedimentary environments. *Proceedings of the Fifth International Conference on Permafrost*. Tapir publishers, Trondheim, Norway: 790-795.
- Kanevskiy, M., Shur, Y., Fortier, D., Jorgenson, M.T., & Stephani, E. 2011. Cryostratigraphy of late Pleistocene syngenetic permafrost (yedoma) in northern Alaska, Itkillik River exposure, *Quat. Res.* doi:10.1016/j.yqres.2010.12.003.
- Kanevskiy, M., Fortier, D., Shur, Y., Bray, M., & Jorgenson, T. 2008. Detailed cryostratigraphic studies of syngenetic permafrost in the winze of the CRREL permafrost tunnel, Fox, Alaska. In *Proceedings of the Ninth International Conference on Permafrost*, June 29–July 3, 2008, Fairbanks, Alaska: Institute of Northern Engineering, University of Alaska Fairbanks, 1: 889–894.
- Konishchev, V.N. 1981. *Formation of the composition of dispersed ground in cryolithosphere*. Novosibirsk, Nauka, 197 pp. (in Russian).
- Kotler, E. & Burn, C.R. 2000. Cryostratigraphy of the Klondike “muck” deposits, west-central Yukon Territory. *Canadian Journal of Earth Sciences* 37: 849-861.
- Kotov, A.N. 2002. Environment of cryolithogenesis of Ice Complex of Chukotka in the late Pleistocene. *Earth Cryosphere* VI (3): 11–14 (in Russian).
- Kunitskiy, V.V. Nival lithogenesis and ice complex on the Yakutia territory: Abstract of a thesis for Ph.D. in Geography, Yakutsk, 2007, 46 pp. (in Russian).
- Lawson, D.E. 1983. Ground ice in perennially frozen sediments, northern Alaska. *Proceedings of the Fourth International Conference on Permafrost*. National Academy Press, Washington, DC, 695-700.
- Magens, D. 2005. Late Quaternary climate and environmental history of Siberian Arctic – Permafrost Records from Cape Mamontovy Klyk, Laptev Sea. Diploma Thesis. University Kiel.
- Meyer, H., Dereviagin, A., Siegert, C., Schirrmeister, L., & Hubberten, H.-W. 2002. Palaeoclimate reconstruction on Big Lyakhovsky Island, North Siberia—hydrogen and oxygen isotopes in ice wedges. *Permafrost and Periglacial Processes* 13: 91–106.
- Paleogeographic Atlas. Shelf Regions of Eurasia for the Mesozoic and Cenozoic. Chief editor M.N. Alekseev 2004., vol.2., Moscow, Nauchnyy Mir, 13-12 (in Russian).
- Romanenko, F.A., Mikhalev, D.V., & Nikolaev, V.I. 2001. Ground ice on the islands next to the Taymyr coastline. *MGI*, 91, 129-137 (in Russian).
- Romanenko, F.A., Nikolaev, V.I., & Arkhipov, V.V. 2011. Change in the isotopic composition of natural ice of the East Siberian Sea coast: Geographical aspect. *Led i Sneg (Ice and Snow)* 1(113): 93-104 (in Russian).
- Romanovskii, N.N., Hubberten, H.-W., Gavrillov, A.V., Tumskoy, V.E., & Kholodov, A.L. 2004. Permafrost of the east Siberian Arctic shelf and coastal lowlands. *Quaternary Science Reviews* 23: 1359–1369.
- Siegert, C., Derevyagin, A.Y., Shilova, G.N., Hermichen, W.-D., & Hiller, A. 1999. Paleoclimate indicators from permafrost sequences in the Eastern Taymyr Lowland. In *Land-Ocean Systems in the Siberian Arctic. Dynamic and History*. H. Kassens, H.A. Bauch, I.A. Dmitrenko, H. Eicken, H.W. Hubberten, M. Melles, J. Thiede, and L.A. Timokhov (eds.). Berlin: Springer-Verlag, Heidelberg, 477-499.
- Siegert, C., Kunitskiy, V.V., & Schirrmeister, L. 2009. Ice complex deposits: Data archive for the reconstruction of climate and ecology on the coast of the Laptev Sea in the Late Pleistocene. The system of the Laptev Sea and the adjacent Arctic seas: Current state and history of development. H. Kassens, A.P. Lisitsyn, J. Thiede, E.I. Polyakova, L.A. Timokhov, and I.E. Frolov (eds.). Moscow: Moscow State University, 317-332 (in Russian).
- Stein, R., Niessen, F., Dittmers, K., Levitan, M., Schoster, F., Simstich, J., Steinke, T., & Stepanets, O. 2002. Siberian river run-off and late Quaternary glaciation in the southern Kara Sea, Arctic ocean: preliminary results. *Polar Research* 21(2): 315-322.
- Streletskaia, I.D. & Vasilev, A.A. 2009. Isotopic composition of polygonal wedge ice of Western Taymyr. *Kriosfera Zemli (Earth Cryosphere)* Vol. 13, No. 3:59 (in Russian).
- Streletskaia, I., Vasilev, A., & Meyer, H. 2011. Isotopic Composition of Syngenetic Ice Wedges and Palaeoclimatic Reconstruction, Western Taymyr, Russian Arctic. *Permafrost and Periglac. Process.* 22: 101-106 Published online in Wiley Online Library (wileyonlinelibrary.com) doi: 10.1002/ppp.707.
- Streletskaia, I.D., Vasilev, A.A., Slagoda, E.A., Gusev, E.A., & Opokina, O.L. 2011. Ground ice of the north of Yenisei area. International Polar Year Results. *Proceedings of the 4th Conference of Russian Geocologists Lomonosov MSU*, June 7-9, 2011. Vol.2. Part 5. Moscow: Universitetskaya kniga, 161-166 (in Russian).
- Tarasov, P.E., Andreev, A.A., Romanenko, F.A., & Sulerzhitskiy, L.D. 1995. Palinostratigraphy of the Upper Quaternary deposits of the Sverdrup Island, the Kara Sea. *Stratigraphy. Geological Correlation* Vol. 3. No. 2: 98-104 (in Russian).
- Tomirdiaro, S.V. & Chernen'kiy, B.I. 1987. *Cryogenic-eolian deposits of east Arctic and Sub-Arctic*. Moscow: Nauka, 196 pp. (in Russian).
- Vasilchuk, Yu.K. 1992. Oxygen isotopic composition of ground ice: An experience in paleogeocryological reconstructions. Moscow: RIO Mosobluprpoligrafizdat, Vol. 1, 420 pp., Vol. 2, 264 pp. (in Russian).

Williams, J.R. & Yeend, W.E. 1979. Deep thaw lake basins in the inner Arctic Coastal Plain, Alaska. In *U.S. Geological Survey in Alaska: Accomplishments during 1978*. K.M. Johnson and J.R. Williams (eds.). USGS Circular, 804-B: B35–B37.

Changes in Surface Area of Thermokarst Lakes on the Basis of Satellite Images

T.V. Tarasenko, V.I. Kravtsova
Lomonosov Moscow State University, Moscow, Russia

Abstract

A number of authors consider thermokarst lakes to be indicators of changes in permafrost conditions under modern climate changes. Such studies pay attention to changes in surface area of thermokarst lakes caused by an increase in air temperature. As a result, an increase in lake area in the continuous permafrost zone is associated with thermokarst activity (permafrost thawing causes the formation of lakes), and a decrease in lake area in the discontinuous permafrost zone is associated with water seepage into the thawed ground and with water evaporation from the lake. However, such studies pay almost no attention to other factors (e.g., atmospheric precipitation) that influence changes in lake area. The influence of precipitation was evaluated for the Central Yakutia territory, where a significant increase in lake area was observed. As a result, a direct relationship between lake area variation and precipitation variation was determined. This raises a question about the possibility of using thermokarst lakes as an indicator of the state of permafrost; various other factors influence the changes in lake area, and these should be taken into consideration.

Keywords: climate warming; lakes area; precipitation variations; satellite images; thermokarst lakes.

Review of Dynamics of Thermokarst Lakes

Increased interest in the dynamics of thermokarst lakes has been noted since the 2000s, when Russian and foreign scientists carried out a number of studies based on the analysis of satellite images over different time periods.

The studies cover continuous and discontinuous permafrost areas of Alaska (Fitzgerald & Riordan 2003, Yoshikawa & Hinzman 2003, Riordan et al. 2006) and Eurasia (Elsakov & Marushchak 2011), including Western Siberia (Smith et al. 2005, Kirpotin et al. 2008, Bryksina et al. 2009) and Russia in general (Kravtsova & Bystrova 2009).

Thermokarst changes in lake areas are mainly studied from the viewpoint of the permafrost reaction to global climate warming. Thermokarst lakes are considered to be possible indicators of the state of permafrost.

All the studies are based on the analysis of satellite images made for at least two different years. The studies examined delineation of water bodies, comparisons of lake distribution in different years, and calculations of quantitative characteristics (the lake areas at different moments of time). In some regions, this research has been accompanied by field studies.

Almost all the studies have used images from the Landsat satellite as the major source of information. The comparison of images has allowed monitoring changes in thermokarst lake areas from the 1970s to the 2000s. These studies have been focused on the analysis of changes within the reference zones of certain regions. The work of Smith et al. (2005) is an exception. It performed an analysis for the vast territory of Western Siberia. The spatial resolution of the Resurs-01/MSU-SK images used was 150 m. The lowest area among other imagery and the areas of the analyzed lakes exceeded 40 hectares.

All the studies performed in Alaska considered the time interval substantiated with aerial photographs from the 1950s to the 2000s. The studies performed in Eurasia considered the period from the 1970s to the 2000s.

Most researchers note a relative stability of thermokarst lakes in the continuous permafrost zone (Fitzgerald & Riordan 2003, Yoshikawa & Hinzman 2003, Riordan et al.

2006, Hinkel et al. 2007, Morgenstern et al. 2008, Grosse et al. 2008). Minor multi-directional changes in the lake areas influenced by local factors (human impact, erosional activity of rivers, their meandering, etc.) were also observed. However, the works by Smith et al. (2005), Kirpotin et al. (2008), and Bryksina et al. (2009) note a 12% increase in lake area in the continuous permafrost zone within Western Siberia. Smith et al. (2005) associate this increase with thermokarst activation under the influence of climate warming (permafrost thawing causes lake formation). A significant increase in the lake area is also observed in the continuous permafrost zone in Central Yakutia (Kravtsova & Bystrova 2009), in the area where a large increase in the air temperature has been observed (Pavlov & Ananyeva 2004). A possible reason for the observed changes was supposed to be the "rejuvenation" of thermokarst relief (i.e., the expansion of the pre-existing lakes and the formation of new ones under the influence of climate warming).

Most researchers note the decrease in lake area in the discontinuous permafrost zone under the influence of climate warming. This is associated with water seepage into the thawed ground and water evaporation from the lake surface. On the contrary, however, the work by Kravtsova and Bystrova (2009) notes an increase in lake area in some reference territories within this zone, in the Transbaikalia basins and in the Far East, for example.

The most contradictory results have been observed in the continuous permafrost zone of Western Siberia. Smith et al. (2005), Kirpotin et al. (2008), and Bryksina et al. (2009) note an increase of 12% in the lake area, while Kravtsova & Bystrova (2009) note a decrease in the lake area. This is the contradiction that encouraged our additional research on the Western Siberian territory in order to identify the real nature of changes in the area of thermokarst lakes.

Dynamics of Thermokarst Lake Areas: Western Siberia

Materials and methods

As mentioned, satellite image analysis was performed to study thermokarst state and dynamics. Thermokarst lakes

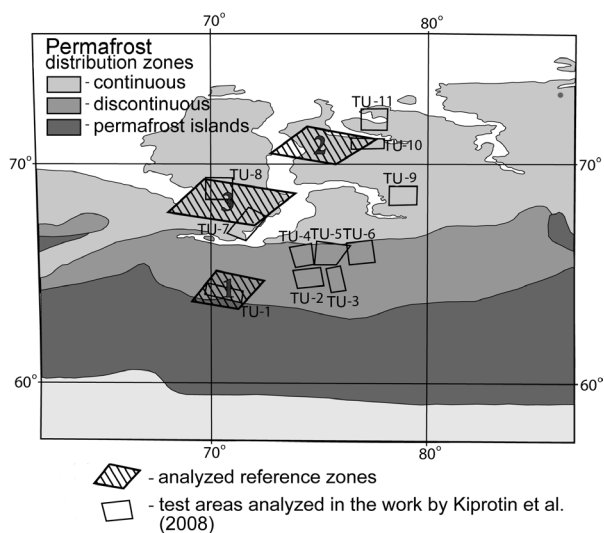


Figure 1. Schematic map of reference zone locations in Western Siberia (boundaries of permafrost zones are shown according to Kirpotin et al. 2008).

are quite reliably interpreted on satellite images, and it is thus possible to measure the changes between a pair of images made at different times.

The study of changes in thermokarst lakes requires a significant amount of work, and therefore it was performed in reference areas. Three reference areas were selected for additional analysis: two are located in the continuous permafrost zone (in the southern part of the Yamal Peninsula and in the Gydan Peninsula), and one is located in the discontinuous permafrost zone (in the upper reaches of the Nadym River) (Fig. 1). The selected reference zones partly overlap with the test areas analyzed by Kirpotin et al. (2008). This makes it possible to compare the results of studies and assess the reasons for contradictions.

Images from the Landsat satellite were used as the basic source. They were chosen because of the availability of such images from the early 1970s to the 2000s, covering a time interval of 20–25 years, and because it was possible to obtain them through the Internet. An important feature of these satellite images is the use of channel in the near-infrared region providing a reliable delineation of water surfaces by the intensity.

The season of acquisition is very significant for the selection of images. It is important to use the images made at the same season of different years, preferably at very close dates. In the study of thermokarst lakes, it is preferable to use images from late summer. This is because ice remains on lakes for a long time even after snow cover melts on the land surface, and this can cause errors in the identification of lake dynamics (Fig. 2a).

Another difficulty in lake delineation involves cloud shadows that are represented in the image in the same tone as the lake (Fig. 2b). Therefore, it is advisable to use images without clouds.

To avoid the influence of aquatic vegetation that can occur in the shallow areas of lakes, it is appropriate to analyze several images made during the vegetation season of different years. Figure 3 shows a range of images that display the development of aquatic vegetation on shallow lakes during the vegetative period of different years. In early

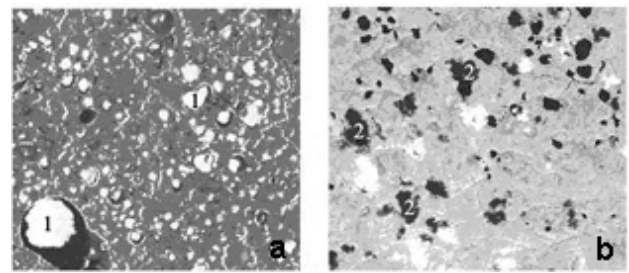


Figure 2. Difficulties in thermokarst lake interpretation in images: a – ice on lakes (1), b – shadows of clouds (2).

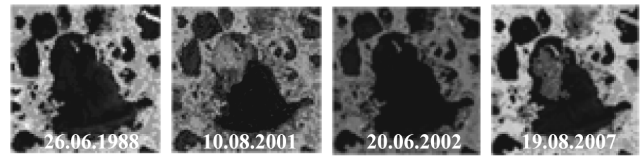


Figure 3. A range of images taken in different years showing aquatic vegetation changes during the vegetation season.

summer (June), lakes are free from vegetation, whereas in August they are partly overgrown with sedges that die off in autumn and are not visible again at the beginning of the next summer. The comparison of such images made in different years can lead to wrong conclusions about changes in the lake area.

During our study, an automated interpretation of thermokarst lakes was performed using the ERDAS Imagine software package on the basis of classification with the training mode. In the ArcGIS software package, the materials of different years interpreted for each area were combined and the changes in thermokarst lakes were identified.

Results

The results of our studies (MSU) for the three reference areas were almost identical. In reference area 1 (in the upper reaches of the Nadym River) located in the discontinuous permafrost zone, almost no changes were detected. Isolated dried thermokarst depressions were observed. Lake drainage was not widespread, and in our area the decrease in the lake area was 4%.

Researchers from Western Siberia (TSU) recorded a decrease of 22% in thermokarst lake area in the corresponding reference area (Kirpotin et al. 2008). However, these authors considered only the largest thermokarst lakes (over 20 hectares), and this can explain the differences in the decrease of lake area. In our opinion, the vegetative growth in shallow-water lake basins or lake drainage triggered by erosion can be the main cause of the drying of such isolated lakes. But it is not the water seepage into thawed ground triggered by the climate warming, because in this case the lake drainage should have occurred not at a local but at a regional scale.

In reference area 2 (the Gydan Peninsula) located in the continuous permafrost zone, an insignificant decrease in thermokarst lake area was detected. For the entire area, it reached about 3%. The greatest changes in thermokarst lakes occur in the areas adjacent to river valleys (Fig. 4), with no changes on flat watersheds. The erosional activity of watercourses is obvious here as well.

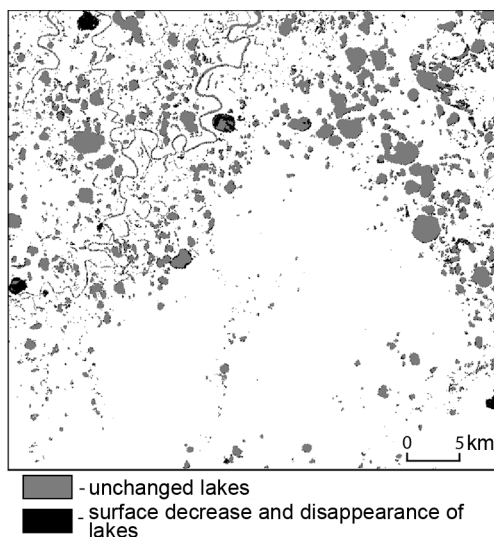


Figure 4. Scheme of thermokarst lake changes in a part of reference area 2 (1985–2001).

In comparison with our results, the researchers from Western Siberia recorded an increase of 10% in thermokarst lake areas in test area TU-10 (Kirpotin et al. 2008), which overlaps with our reference area 2. The reasons for the observed disagreements are not clear. We did not observe the increase in the lake area in the continuous permafrost zone. Perhaps the location of the TU-10 area was marked incorrectly. However, even taking this into consideration, in the continuous permafrost zone we observed a decrease in the area of some lakes, not an increase.

In reference area 3 (in the southern part of the Yamal Peninsula, south of 70°N) located in the continuous permafrost zone, a decrease in thermokarst lake area was observed (Fig. 5), similar to the two previous reference areas. This area overlaps with one of the reference areas analyzed previously by Kravtsova & Bystrova (2009), who could also detect a decrease in lake area.

The researchers from Western Siberia observed an increase in thermokarst lake area of 7% and 10% in test areas TU-8 and TU-7, respectively (Kirpotin et al. 2008). These test areas overlap with our reference area 3. However, one of the latest works by this team (Bryksina et al. 2009) notes that in the continuous permafrost zone to the south of 70°N the areas of lakes have decreased, which coincides with our results. Thus the increase previously observed in this area is considered by these authors to be incorrect.

The source of the discrepancy most probably lies in the differences between the methods of image analysis. In the MSU works, continuous mapping of changes in selected reference areas makes it possible to analyze every case of changes, and in the works of TSU, there is a selective statistical analysis of changes in lakes of particular sizes.

Dynamics of Thermokarst Lake Area: Central Yakutia

Another issue is related to identification of the causes of the increase in lake area for the period of 1976–2000 in the continuous permafrost zone of Central Yakutia (Kravtsova & Bystrova 2009). Could global warming really cause an

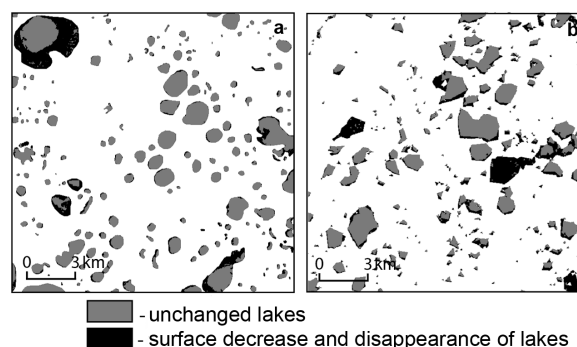


Figure 5. Scheme of thermokarst lake changes in a part of reference area 3: a - 1985–2001, b - 1973–2001.

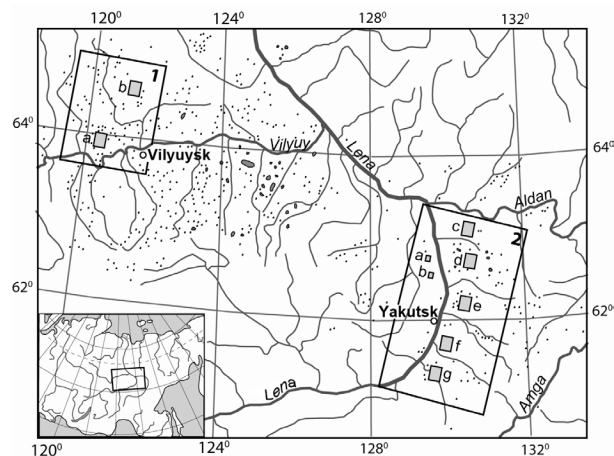


Figure 6. Reference areas location (1 - Vilyuy, 2 - Lena) and key fragments (a-g).

increase in the area of pre-existing thermokarst lakes and formation of new ones? This question is very important because this is the area where an intense air temperature increase has been observed (Pavlov & Ananyeva 2004). In this regard, it was decided to perform a study analyzing the causes of the changes observed, in particular, the influence of precipitation. Interannual and long-term changes in lake areas were analyzed.

Materials and Methods

Research methods are similar to those mentioned when describing the dynamics of thermokarst lake areas in Western Siberia. The study within Central Yakutia is based on the analysis of two reference areas: No. 1 “Vilyuy” and No. 2 “Lena” (Fig. 6). The images from the Landsat satellite taken in the 1970s and the 2000s were used as the basic material. We also used the aerial photographs taken in the 1950s kindly provided by the Production and Research Institute for Survey and Construction JSC. These photographs made it possible to trace the changes in the lake areas from 1950 to 1973.

During the study, an automated interpretation of thermokarst lakes was performed in the ERDAS Imagine software package on the basis of classification with the training mode. The interpreted materials of different time for every area were combined in the ArcGIS software package, and the changes in thermokarst lakes were identified.

Results

During the study of interannual changes in thermokarst

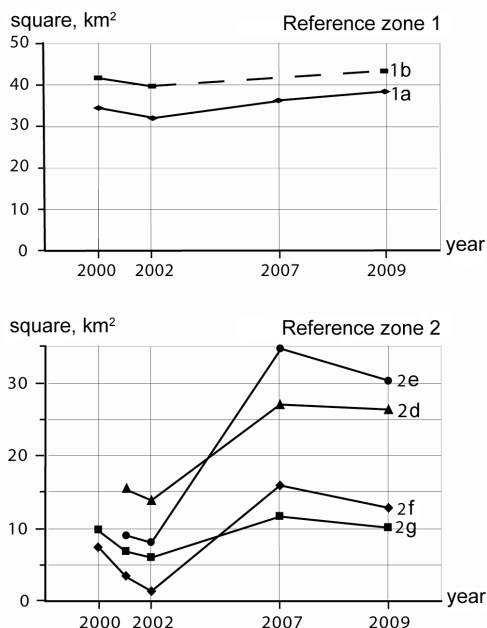


Figure 7. Diagrams of annual changes in the lake areas in reference areas.

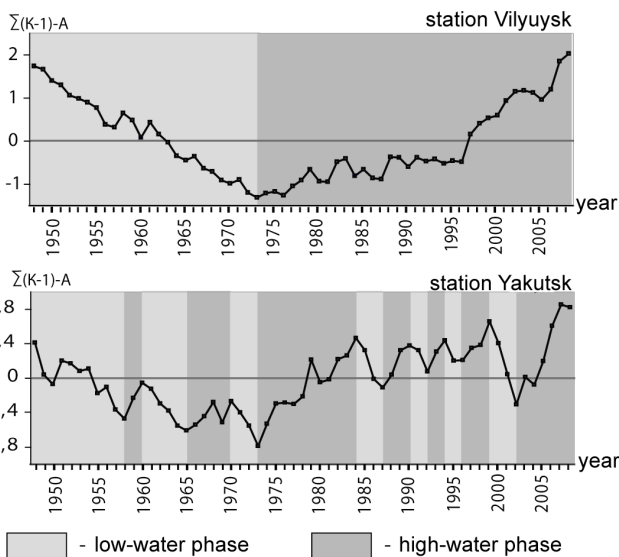


Figure 8. Annual precipitation.

lakes, we analyzed the time period from 2000 to 2009, for which repeated images were available (2000, 2002, 2007, 2009). In the Vilyuy reference area, two fragments were analyzed, and in the Lena reference area four fragments were analyzed (Fig. 7). Diagrams showing changes in the lake areas were made for every fragment (Fig. 7).

According to the diagrams, lake changes for 2000–2002 were minimal in reference zone 1. A small decrease in their area was observed in isolated alases (thaw-lake basins). On the contrary, from 2002 to 2009 the increase in the thermokarst lake area was observed. In reference area 2, an insignificant decrease in the lake area was observed from 2000 to 2002 and also a significant increase from 2002 to 2007. After 2007, a small decrease in the lake area was detected.

To identify the causes of the observed changes, diagrams of annual precipitation were made for stations Vilyuysk and Yakutsk (Fig. 8). According to Battalov (1968), such diagrams provide a more vivid illustration of the cyclical

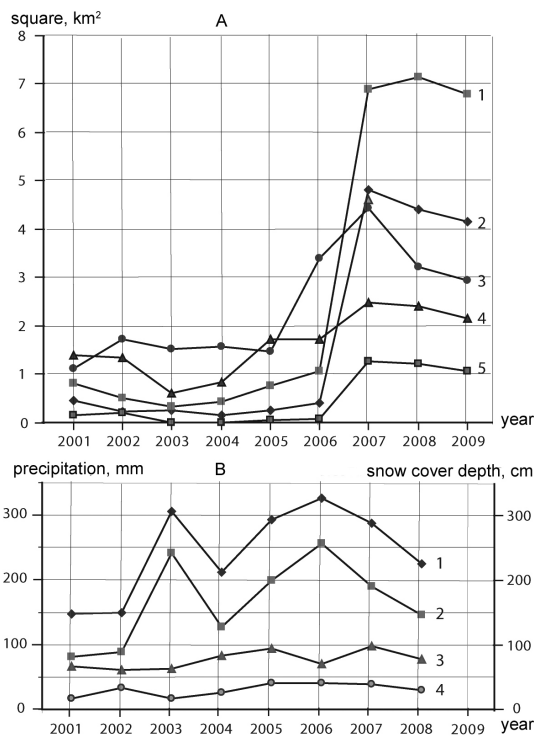


Figure 9. Diagrams of annual area changes of certain large lakes (A): 1 – Tyungyulyu, 2 – Segeley, 3 – Nal-Tyungyulyu, 4 – Abalakh, 5 – Maya. Meteorological characteristics (B): 1 – average annual precipitation, 2 – summer precipitation, 3 – winter precipitation, 4 – snow cover depth.

fluctuations of precipitation. The diagrams represent a long time range from 1948 to 2008, which makes it possible to consider long-term fluctuations of precipitation while conducting an analysis of long-term lake changes.

A significant similarity can be traced when comparing the diagrams of annual changes in the lake areas with standardized differential integral curves. A lake area decrease from 2000 to 2002 corresponds to a low-water phase; an increase from 2002 to 2007 corresponds to a high-water phase. The only exception is the decrease in reference area 1 from 2000 to 2002 during a high-water phase, which is explained by a partial drainage of lakes by water courses.

Due to the lack of satellite images performing lake interpretation throughout the whole area for each year, in reference area 2 the changes of certain large lakes that can be annually observed in gaps between the clouds were considered in a more detailed way. Based on these images, a continuous range of annual measurements from 2001 to 2009 was implemented for these lakes. In the changes of their area, as shown in Figure 9, there is a direct relation to precipitation. However, the precipitation decrease for just one year does not influence the lake area if the precipitation level was high in the previous year. The change in precipitation during at least two years causes the changes in the lake area.

In all the cases considered, variations in the lake area followed the precipitation fluctuation. A direct correlation can be observed: an increase in the sum of precipitation causes an increase in the lake area, and a decrease in the sum of precipitation causes a decrease in the lake area.

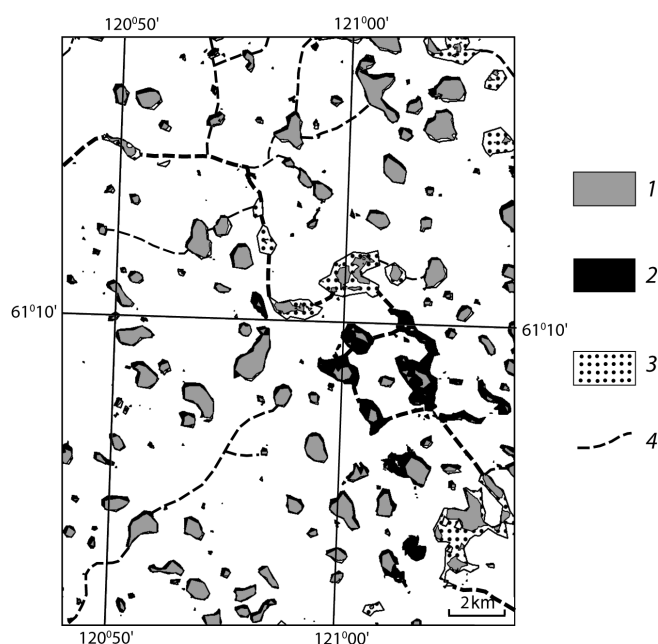


Figure 10. Long-term changes of thermokarst lake areas in reference area Vilyuy (fragment 1b) for 1973–2009: 1 – lakes without changes, 2 – area increase and lakes formation, 3 – area decrease and lakes disappearance, 4 – temporary watercourses.

Long-term changes (changes for 20–30 years) were observed only in reference area Vilyuy, which is characterized by long low-water and high-water periods. In reference area Lena, frequent alternation of short low-water and high-water periods (2–3 years) has been observed. This determines the differently directed changes in the lake areas.

In reference area Vilyuy, long-term changes were detected based on an aerial photograph of 1950, the MSS/Landsat satellite images of 1973, and the TM/Landsat images of 2009. From 1950 to 1973, the decrease in area and the disappearance of large thermokarst lakes on the one hand and the formation of small lakes on the other hand was observed in fragment 1-a. Thermokarst lakes formed in alases were detected using the aerial photograph of 1950. The formation of new thermokarst lakes outside alases was not observed. Perhaps a certain air temperature increase in this period (in 1972–1973 it reached its long-term average annual value after a certain decrease) determined the thawing of ground ice in small alas depressions, while in the large ones ground ice had thawed before and the lake area was decreasing. This decrease is natural for the low-water phase, and it was intensified by the evaporation under conditions of the air temperature increase.

From 1973 to 2009, a general increase in lake area was observed in fragment 1-a. The same increase was observed in the previous research (Kravtsova & Bystrova 2009). The record of annual precipitation at station Vilyuysk (Fig. 8) indicates the low-water phase from 1950 to 1973 and the high-water phase from 1973 to 2008. It is this phase change that could influence the decrease in the area of large lakes from 1950 to 1973 and the increase in lake area from 1973 to 2009.

In fragment 1-b, both an increase and a decrease in some large lakes areas from 1973 to 2009 were observed (Fig. 10).

These were apparently caused by the erosional activity of water courses because all thermokarst lakes that underwent strong changes are located along the main water course and form a continuous system. Here the lake area decrease corresponds to their drainage by water courses, and the increase corresponds to the inflow.

Thus it was detected that in Central Yakutia changes in the area of thermokarst lakes depend on precipitation fluctuation.

Conclusions

This study showed that it is necessary to use extreme caution when considering changes in thermokarst lakes as an indicator of the state of permafrost. Other factors causing changes in the area of thermokarst lakes must be taken into account. These factors include precipitation regime and the erosional activity of watercourses.

Acknowledgments

This work was funded by the Russian Foundation for Basic Research grant 10-05-00267, the Scientific Schools Support grant 3405.2010.5, and the Education and Research Center grant 14.740.11.0200.

References

- Bryksina, N.A., Polishchuk, V.Yu., & Polishchuk, Yu.M. 2009. The study of the interrelation of climate and thermokarst processes changes in continuous and discontinuous permafrost zones in Western Siberia. *Vest. Yugorsk. Gosud. Un-ta* 3: 3-12 (in Russian).
- Elsakov, V.V. & Marushchak, I.O. 2011. Interannual changes of thermokarst lakes in the north-east of European Russia. *Issledovanie Zemli iz Kosmosa* 4: 1-13 (in Russian).
- Fitzgerald, D. & Riordan, B.A. 2003. Remote sensing and GIS used to monitor Alaska wetlands at the landscape level. *Agroborealis* 35, No. 1: 30-35.
- Grosse, G., Romanovsky, V., Walter, K., Morgenstern, A., Lantuit, H., & Zimov, S. 2008. Distribution of Thermokarst Lakes and Ponds at Three Yedoma Sites in Siberia. In *NICOP 2008: Proceedings of the Ninth International Conference on Permafrost*. D.L. Kane, K.M. Hinkel (eds.). Institute of Northern Engineering, University of Alaska Fairbanks, 1: 551-556.
- Hinkel, K., Jones, B., Eisner, W., Cuomo, C., Beck, R., & Frohn, R. 2007. Methods to assess natural and anthropogenic thaw lake drainage on the western Arctic coastal plain of northern Alaska. *Journal of Geophysical Research* 112, F02S16, doi:10.1029/2006JF000584.
- Kirpotin, S.N., Polishchuk, Yu.M., & Bryksina, N.A. 2008. Thermokarst lakes dynamics in continuous and discontinuous permafrost zones of Western Siberia in global warming conditions. *Vest. Tomsk. Gosud. Un-ta* 311: 185-189 (in Russian).
- Kravtsova, V.I. & Bystrova, A.G. 2009. Change of the size of thermokarst lakes in different regions of Russia over the last 30 years. *Kriosfera Zemli* 13 (no. 2): 16–26 (in Russian).

- Morgenstern, A., Grosse, G., & Schirmer, L. 2008. Genetic, morphological and statistical characterization of lakes in the permafrost-dominated Lena Delta. In *NICOP 2008: Proceedings of the Ninth International Conference on Permafrost*. D.L. Kane, K.M. Hinkel (eds.). Institute of Northern Engineering, University of Alaska Fairbanks, 2: 1239-1244.
- Pavlov, A.V. & Ananyeva, G.V. 2004. Assessment of current changes in air temperature in the permafrost zone of Russia. *Kriosfera Zemli* 8 (no. 2): 3-9 (in Russian).
- Riordan, B., Verbyla, D., & McGuire, D.A. 2006. Shrinking ponds in subarctic Alaska based on 1950-2002 remotely sensed images. *Journal of Geophysical Research* 111, G04002, doi:10.1029/2005JG000150.
- Smith, L.C., Sheng, Y., Macdonald, G.M., & Hinzman, L.D. 2005. Disappearing Arctic Lakes. *Science* 308, No. 5727: 1429.
- Yoshikawa, K. & Hinzman, L. 2003. Shrinking thermokarst pond and groundwater dynamics in discontinuous permafrost near Council, Alaska. *Permafrost and Periglacial Processes* 14: 151-160.

Calculation of Frost Heave Tangential Stress with Regard to the Deformability of a Pile Shaft

Z.G. Ter-Martirosyan, P.A. Gorbachev

Moscow State Construction University (State Higher Professional Educational Institution), Moscow, Russia

Abstract

This work describes the problem of a single deformable pile interaction with frost susceptible ground. It is shown that significant reduction of tangential stress influencing the lateral face is possible in the case of the low rigidity of the pile shaft.

Keywords: foundation stability loss; frost heave; ground freezing; pile; pulling force; tangential forces.

Introduction

During the phase change into ice, pore water forms a complex stress and strain state around the foundation. This state varies both along the embedded depth of the pile, and in time. As a result, frost heave forces occur. They cause the foundation to lose stability in the case of under-loading, and insufficient anchoring into thawed permafrost.

The thermal regime at the surface, the freezing intensity, the thermophysical, and the mechanical and rheological ground properties can significantly influence frost heave forces. According to the standards, it is customary to divide them into normal, influencing perpendicularly to the foundation lateral face (p_n), and tangential (τ_n) (SNIP 2.02.04-88).

The study of the stability of pile foundations under the conditions of a complex stress and strain state at the foundation-ground contact, and in the case of frost heave of ground, is a very important scientific problem. It is connected with the safety and reliable operation of buildings and facilities. The determination of tangential stresses occurring in the process of frost heave is the key parameter that is necessary for the solution of this problem.

It is evident that only full-scale testing of piles in conditions of a construction site can give a more accurate

idea about their force interaction with frost susceptible ground. However, such tests are not always possible. Consequently, the forecasting of force pile interaction with freezing ground remains a challenging problem.

General Provisions

This work describes the impact of pile rigidity on the heave tangential stress τ_a distribution along its length. We will use a cylindrical pile-ground mass model with the outer radius $2b$ (pile impact radius) and the inner radius $2a$ (pile radius) to make this description (Fig. 1).

Negative temperature is established at the model surface, as a result of which the ground freezes to the depth $l_1=d_f$. Tangential frost heave forces τ_a occurring as a result of freezing tend to pull the pile to the surface. Consequently, the pile can lose its stability. For this problem we will assume that a pile is anchored to a sufficient depth l_2 into the thawed permafrost. Therefore, the total pulling force N_{pull} is fully balanced by the restraining force N_{res} :

$$2\pi a \cdot l_1 \cdot \tau_a = 2\pi a \cdot l_2 \cdot \tau_{y0} \quad (1)$$

Let us examine the force pile-ground interaction at the moment when the freezing front reaches the seasonal freezing depth d_f . We will also assume that the temperature

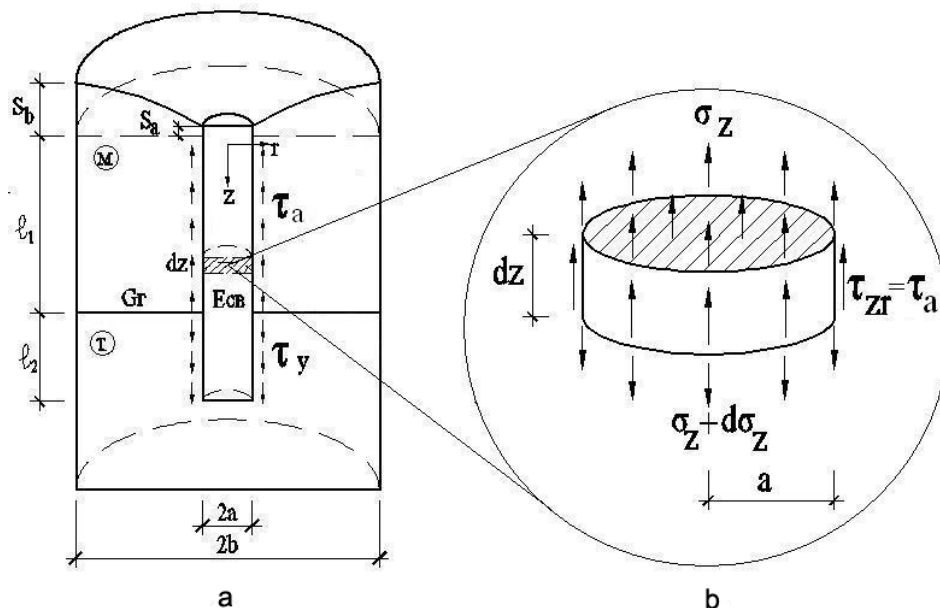


Figure 1. Analytical model of pile interaction with frost susceptible ground.

at this moment is distributed according to the following commonly known dependence:

$$\theta(z) = \theta_\epsilon \cdot \left(1 - \frac{z}{d_f}\right), \quad (2)$$

where θ_1 – permanent temperature at the ground surface, z – current coordinate within the active layer, d_f – freezing depth.

Vertical deformation at the outer radius b of the model can be found in the same way as for the freely heaving ground in compression conditions:

$$\varepsilon_z(\theta) = \frac{1 + \nu}{1 - \nu} \cdot \alpha \cdot \theta, \quad (3)$$

where ν – Poisson’s ratio; α – expansion coefficient; θ – temperature.

Ground uplift S is defined with the equation:

$$S = \int \varepsilon_z dz \quad (4)$$

We will substitute (2) into (3) and integrate. The integration constant C will be found from the boundary condition $S|_{z=d_f}=0$. Consequently, we have:

$$S(z) = -\alpha \frac{1 + \nu}{1 - \nu} \theta_\epsilon \frac{(d_f - z)^2}{2d_f} \quad (5)$$

This dependence will be used in further calculations as the boundary condition.

Main Equations

Let us compile the equilibrium equation for the elementary layer in the ground-pile massif with the thickness dz (Fig. 1b) as follows:

$$\pi a^2 (\sigma_z + d\sigma_z) - \pi a^2 \sigma_z - 2\pi a \cdot \tau_a \cdot dz = 0 \quad (6)$$

The expression (6) can be transformed into:

$$\frac{d\sigma_z}{dz} = \frac{2\tau_a}{a} \quad (7)$$

We will use the known equation linking angular deformation $\gamma(r)$ and tangential stress $\tau(r)$ to find the function τ_a (Ter-Martirosyan 2009):

$$\gamma = \frac{dS}{dr} = -\frac{\tau(r)}{G} \quad (8)$$

where γ – angular deformation; S – ground uplift; r – radius; τ – tangential stress; G – ground shear modulus.

Let us assume the function of tangential stress $\tau(r)$ distribution along the radius r in the form of the following dependence:

$$\tau(r) = \tau_a \cdot \frac{(b-r)^2}{(b-a)^2} \quad (9)$$

where τ_a – tangential stress value at the ground-pile contact (Fig. 2); a, b – pile radius and outer radius of the cylindrical model respectively; r – current radius value, while $r \in [a, b]$.

We will obtain the following, substituting (9) into (8) and integrating:

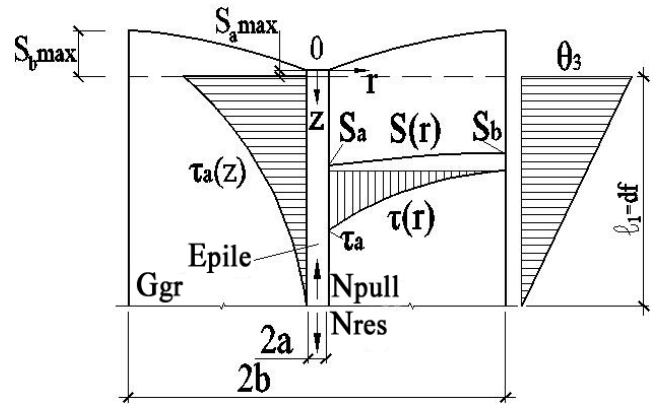


Figure 2. Cylindrical geomechanical model of pile interaction with frost susceptible ground.

$$S(r) = \frac{\tau_a}{3G} \cdot \frac{(b-r)^3}{(b-a)^2} + C' \quad (10)$$

We will find the integration constant C' from the boundary condition $S|_{r=b}=S(z)$, where $S(z)$ – function of uplift change in depth for freely heaving ground which was found earlier (see equation (5)):

$$C' = -\alpha \frac{1 + \nu}{1 - \nu} \theta_\epsilon \frac{(d_f - z)^2}{2d_f} \quad (11)$$

The tangential stress dependence at $r=a$ can be found by substituting C' into the solution (10):

$$\tau_a = \frac{3G}{b-a} \cdot \left(S_a + \alpha \frac{1 + \nu}{1 - \nu} \theta_\epsilon \frac{(d_f - z)^2}{2d_f} \right), \quad (12)$$

where S_a – vertical pile movement defined with the equation:

$$S_a = \int_0^{d_f} \frac{\sigma_z}{E_c} dz \quad (13)$$

where E_{pile} – pile elastic modulus.

We find the following differential equation substituting (13) into (12), and then to the equilibrium equation (7) and differentiating both parts, after some minor transformations:

$$\frac{d^2 \sigma_z}{dz^2} - \lambda \sigma_z = \mu \left(\frac{z}{d_f} - 1 \right), \quad (14)$$

where λ and μ are defined:

$$\begin{cases} \lambda = \frac{2}{a} \cdot \frac{3G}{(b-a)} \cdot \frac{1}{E_c} \\ \mu = \frac{2}{a} \cdot \frac{3G}{(b-a)} \cdot \alpha \cdot \frac{1 + \nu}{1 - \nu} \theta_\epsilon \end{cases} \quad (15)$$

This is a linear differential second-order equation with constant coefficients to include the right part. The general solution of the equation looks as follows:

$$\sigma_z = C_1 e^{\sqrt{\lambda} \cdot z} + C_2 e^{-\sqrt{\lambda} \cdot z} + \frac{\mu}{\lambda} \left(1 - \frac{z}{d_f} \right) \quad (16)$$

We will find integration constants from the boundary conditions:

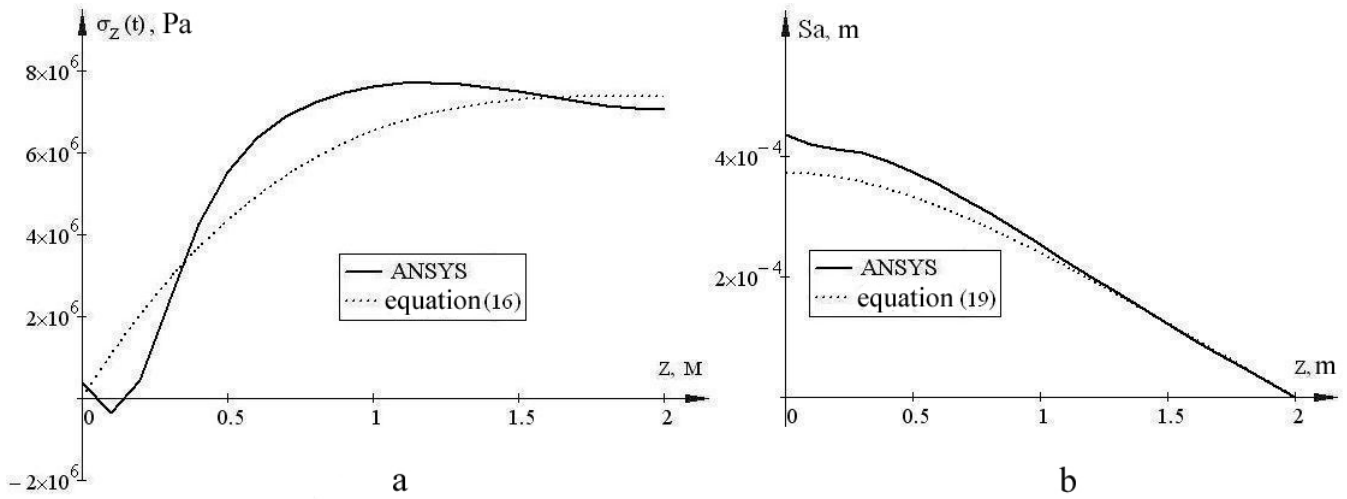


Figure 3. Diagram of vertical stress change σ_z (a) and vertical movement S_a (b) along the pile length.

$$\begin{cases} \sigma_z|_{z=0} = 0 \\ \dot{\sigma}_z|_{z=d_f} = 0 \end{cases} \quad (17)$$

As a result, the following expressions will be obtained for C_1 and C_2 :

$$\begin{cases} C_1 = -\frac{\mu}{\lambda} \left(1 - \frac{\sqrt{\lambda} \cdot e^{\sqrt{\lambda} \cdot d_f} + \frac{1}{d_f}}{\sqrt{\lambda} \cdot (e^{\sqrt{\lambda} \cdot d_f} + e^{-\sqrt{\lambda} \cdot d_f})} \right) \\ C_2 = -\frac{\mu}{\lambda} \cdot \left(\frac{\sqrt{\lambda} \cdot e^{\sqrt{\lambda} \cdot d_f} + \frac{1}{d_f}}{\sqrt{\lambda} \cdot (e^{\sqrt{\lambda} \cdot d_f} + e^{-\sqrt{\lambda} \cdot d_f})} \right) \end{cases} \quad (18)$$

The partial solution of this equation is found by substituting C_1 and C_2 into (16). Then we will substitute it into Expression (13) and integrate. We will find the solution in the form of a function. For this, we will take the indefinite integral and find the integration constant C_3 from the boundary condition $S_a|_{z=0} = 0$. Consequently, the expression for vertical pile movement will look as follows:

$$S_a(z) = \frac{1}{E_c} \left(C_1 \cdot \frac{1}{\sqrt{\lambda}} \cdot (e^{\sqrt{\lambda} \cdot z} - e^{\sqrt{\lambda} \cdot d_f}) - C_2 \cdot \frac{1}{\sqrt{\lambda}} \cdot (e^{-\sqrt{\lambda} \cdot z} - e^{-\sqrt{\lambda} \cdot d_f}) - \frac{\mu}{\lambda} \cdot \left(1 - \frac{z}{d_f} \right) \cdot \frac{d_f}{2} \right) \quad (19)$$

The expression for tangential stress change $\tau_a(z)$ depending on the coordinate z can be received by substituting (19) into (12). By integrating it with the following equation:

$$N_o = 2\pi a \int_0^{d_f} \tau_a(z) dz \quad (20)$$

one can find the expression for the pulling force N_{pull} . The equations for $\tau_a(z)$ and N_{gr} are not given here due to their bulkiness.

Table 1. Basic data.

Ground and pile characteristics	Value
Mechanical ground properties	
Ground deformation modulus E_{gr} , Pa.	$0.22 \cdot 10^9$
Ground Poisson's ratio ν_{gr}	0.3
Ground shear module, G_{gr} , Pa	$8.46 \cdot 10^7$
Ground expansion coefficient, α	$2 \cdot 10^{-3}$
Mechanical pile properties	
Pile 1 (concrete) elastic modulus, E_{pile1} , Pa.	$3 \cdot 10^{10}$
Poisson's ratio for Pile 1, ν_{pile1}	0.3
Pile 2 (ground-concrete) elastic modulus, E_{pile2} , Pa.	$0.22 \cdot 10^9$
Poisson's ratio for Pile 2, ν_{pile2}	0.3
Temperature characteristics	
Temperature at the ground surface $ \theta_L $, °C	3
Heaving start temperature θ_{HS} , °C.	0
Heaving end temperature $ \theta_{HE} $, °C.	3
Geometrical characteristics	
Pile radius a , m	0.3
Outer radius of the cylindrical model, b , m.	2
Seasonal freezing depth d_p , m	2

Examples

As an illustration, let us describe the example with the following basic data:

The result of the basic data substitution into Equations (16), (19), and (12) is shown in the diagrams (Figs. 3, 4). The same problem was solved with the method of finite

elements with the help of the ANSYS software to validate the analytical solution. The results can be seen in the same diagrams.

According to the diagrams (Fig. 3), equations (16) and (19) give satisfactory coincidence with the results of numerical calculation.

Now let us examine the diagrams of basic tangential stress distribution τ_a along the pile length, found both numerically and with the help of equation (12) (Fig. 4).

It follows from the diagram (Fig. 4) that the analytical and the numerical solutions for $\tau_a(z)$ give satisfactory coincidence. Let us independently examine the numerical solution of the problem without regard to the pile flexibility, i.e. $E_{pile} = \infty$ (Fig. 4, Diagram 1): the tangential stress value τ_a in the point with the coordinate $z=0$ (due to its singularity) is significantly higher than the analytical value when taking into account the pile flexibility (Fig. 4, Diagram 2), assuming that the value difference in other points is much lower. That is why Diagram 1 (Fig. 4) should be considered without this point.

In general, the consideration of the flexibility in the case of a high value of the pile elastic modulus gives an insignificant

reduction of tangential stress τ_a (Fig. 4, Diagrams 2 and 4). If the pile elastic modulus is comparable to the ground deformation modulus, the impact of pile rigidity on τ_a becomes even more significant.

The variant with a flexible pile shaft ($E_{pile2} \approx E_{gr}$) was examined within the frames of this problem. This can occur while using ground-concrete piles. In this case vertical movements of the pile shaft are significantly higher than in the previous case due to shaft deformability (Fig. 5).

Tangential stress τ_a along the pile length falls noticeably as well. The maximum tangential stress value τ_a decreased by more than two times in the conditions of the subject example (Fig. 4, Diagram 5).

Conclusions

This work studied the problem of pile interaction with frost susceptible ground when its shaft flexibility is taken into account.

It was shown that vertical movements of the shaft will be low and its deformability can be neglected in case of high pile rigidity. This occurs if the pile elasticity modulus E_{pile} is much higher than the ground deformation modulus E_{gr} .

Also, the case of a flexible pile made of ground-concrete was described. In this regard, the pile elasticity modulus was comparable with the ground deformation modulus ($E_{pile} \approx E_{gr}$). In this case, pile deformability should be taken into account because this significantly reduces the tangential stress at the lateral face and, consequently, the total pulling force influencing the pile.

References

SNiP 2.02.04-88. 2005. Construction norms and rules. Bases and foundations on permafrost. Moscow: GUP TsPP, 21 pp.
 Ter-Martirosyan, Z.G. 2000. *Ground mechanics*. Moscow: ASV, 461 pp.
 Tsytovich, N.A. 1973. *Permafrost mechanics*. Moscow: Vysshaya shkola, 445 pp.

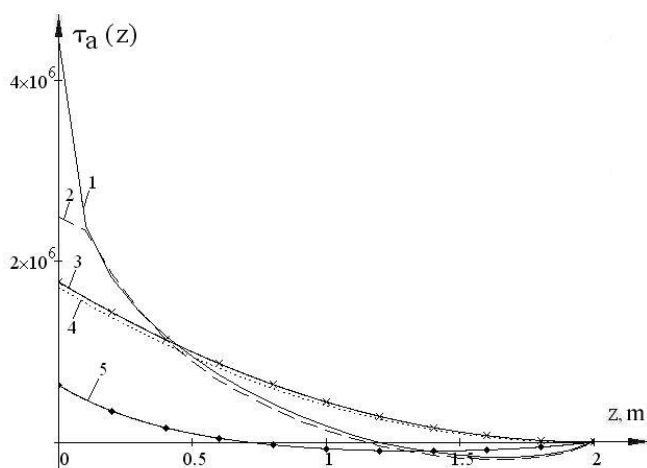


Figure 4. Diagrams of tangential stress change $\tau(z)$ along the pile length: 1) ANSYS solution $E_{pile} = \infty$; 2) ANSYS $E_{pile} \neq \infty$; 3) equation (12) $E_{pile} = \infty$; 4) equation (12) $E_{pile} \neq \infty$; 5) equation (12) $E_{pile} 2 < E_{pile} 1$.

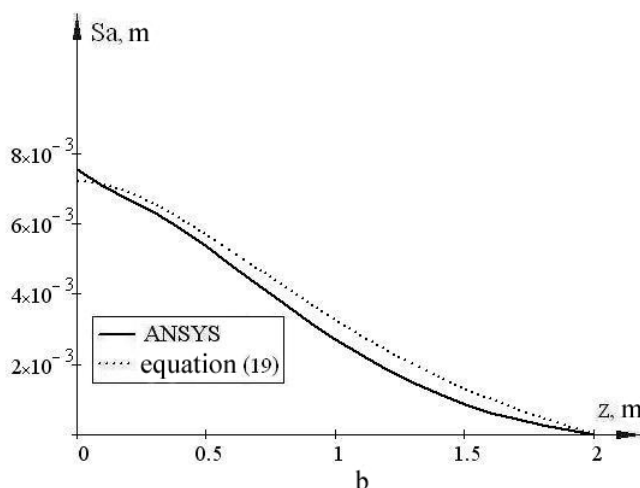
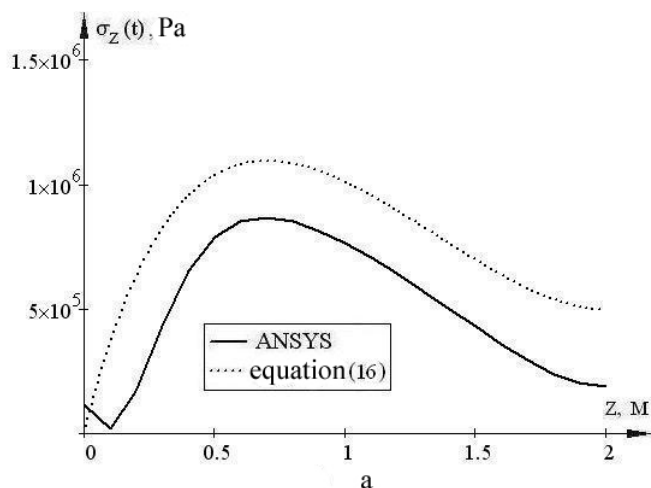


Figure 5. Diagram of vertical stress change σ_z (a) and vertical movement Sa (b) along the flexible pile length.

Permafrost Conditions Associated with the Railroad Bridge Crossing of the Shchuchya River, Southern Yamal Peninsula

S.N. Titkov

Geological Research Institute for Construction, JSC (OAO PNIIS), Moscow, Russia

Abstract

The railroad bridge over the Shchuchya (Pike) River is located in the southern part of the Yamal Peninsula within the Laborovskaya depression. The construction pad, 1.5 to 4 m thick, overlies Late-Pleistocene and Holocene lacustrine and alluvial sediments. The area is located in the zone of continuous permafrost with a thickness of 120 to 150 m. Under the Shchuchya River riverbed there is a closed talik 20 m deep. It transitions, on the right bank, into an inter-permafrost talik 11 m thick at the depths of 14–20 m. The right bank is composed of modern alluvium of the active floodplain with permafrost temperature of -0.2 to -0.3°C . The left bank is composed of the Late-Pleistocene lacustrine and alluvial sediments with soil temperature ranging from -1.1°C at 6 m from the water's edge to -3.0°C at 78 m distance from the river. Over the past 20 years, the temperature of the left-bank permafrost has increased by an average of 0.8°C as a result of the air temperature increase of 1.2°C over the past 50 years. The right-bank soil temperature has not changed over 20 years due to the insulating effect of the construction pad.

Keywords: alluvium; ground temperature; railroad bridge; talik; Yamal.

Introduction

Bridges are the most difficult component of road and railroad construction in the permafrost area because of the extremely unstable boundary zone between the taliks under rivers and frozen banks. Construction pads used in fender pier construction inevitably lead to a change of the natural quasi-stationary conditions of heat exchange through the surface of the permafrost-active layer-atmosphere system. As a rule, active layer depth increases and there is a high risk of activation of thermokarst, solifluction, and thaw slumping. An increase in the temperature of the frozen bank leads to a decrease in the bearing capacity of frozen soils.

During the geotechnical investigations performed in recent years by the Geological Research Institute for Construction (PNIIS), particular attention was paid to the research of the territory's complicated permafrost conditions. Investigations included assessment of slope activity and other cryogenic processes, study of ground ice (including massive ice), cryopegs, and thermal regime of soils. Detailed field studies performed at the site of the bridge crossing over the Shchuchya River in the southern part of Yamal Peninsula made it possible to reveal a number of geotechnical problems that can complicate construction and future maintenance of the bridge.

Study Area

The Shchuchya River flows near the southeastern edge of the Laborovskaya depression, which is clearly expressed in the topography and is located within the three Late-Pleistocene lake terraces formed of lacustrine and alluvial deposits (Trofimov 1983). Horizontal and vertical roughness of the terrain is low. The left bank of the river at the railroad crossing site is formed by the Late-Pleistocene lacustrine-alluvial terrace of Sartan age, 5 to 7 m high. The terrace surface is flat with absolute elevations of 40 to 45 m and is occasionally dissected with shallow gullies and thaw lake basins, mostly ancient. The right bank is a high floodplain

with elevations of 2 to 2.5 m lower than those of the left bank. Directly at the bridge crossing at the surface of both banks is a construction pad 1.5 to 4 m thick. The Shchuchya River width at the construction site is approximately 70 m. During the construction of pads, the channel narrowed by 10 to 15 m, and the river flow accelerated significantly. Beneath the future bridge, the river maximum depth is 5 to 6 m, the river-bed profile is trough-shaped, and the river bottom is almost flat.

Permafrost Conditions

The deposits composing the second lake terrace are sands and silty clays. The upper part of the section is composed mostly of silty sand, sometimes of fine sand with interlayers and lenses of silts and silty clays. Soils contain inclusions of organic detritus, and occasionally there are gravel inclusions. The lower part of the section is composed mostly of silty clays. At some places, the lake terrace sediment is overlain with peat up to 1 m thick. The cryogenic structure of sediments is heterogeneous. The upper layers composed of silty and sandy soils are characterized by the predominance of porous cryogenic structures, which in silty layers are sometimes replaced with dense-layered cryostructures with thin ice lenses and sub-vertical ice veins (layered-reticulate cryostructures). Such character of cryostructures suggests a syngenetic freezing of the upper layer of alluvial deposits. The ice content of the soils due to ice inclusions (i_i) is low. However, due to the high content of pore ice, the total ice content (i_{tot}) reaches 0.52. Lacustrine clay composing the base layers of the section is characterized by mostly porous cryostructures with rare ice lenses divided by 1.5- to 3-m-thick layers without visible ice. The value of i_{tot} in clays and silty clays remains high, reaching 0.42.

Within the Laborovskaya depression and its rims, permafrost occurs everywhere except beneath water bodies (rivers and lakes). Permafrost mean annual ground temperature (MAGT) varies in a wide range, from -0.3 to 0.5°C to -5°C , rarely -6°C . The floodplains of the Shchuchya

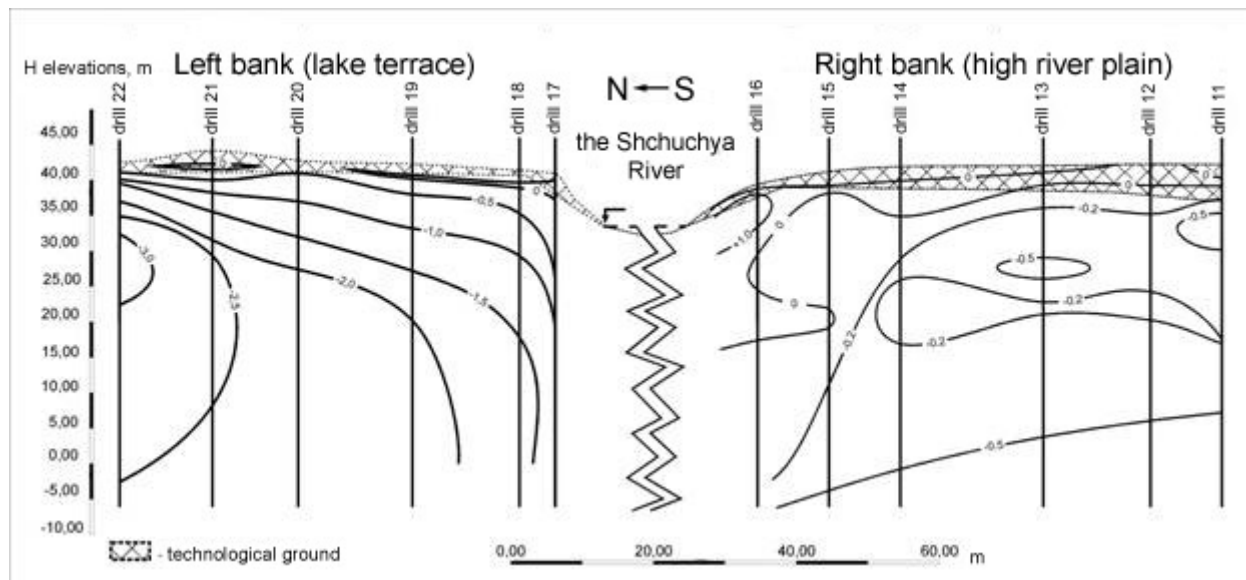


Figure 1. Ground temperature distribution ($^{\circ}\text{C}$) in the Shchuchya River valley. November 2007.

River and its tributaries, as well as floodplains of lake basins, are characterized by MAGT from -0.3 to -1.0°C to -2.5 to -3.5°C . Permafrost thickness in the floodplain does not exceed 120–150 m due to the warming influence of the water flow.

Natural moisture content of frozen lacustrine sediments depends on their particle size and cryogenic structure and varies from 20 to 80–90%. Density of frozen clayey soils varies from 1.89 to 2.3 g/cm^3 , and dry density varies from 1.59 to 1.95 g/cm^3 . Porosity of clayey lacustrine soils is higher than that of alluvial deposits and ranges from 45–50 to 75–80%. A significant thaw settlement can occur in the case of thawing of the upper 10 m of the lacustrine sediments section. Modulus of thaw settlement of silty clay and clay soils of the lake terraces varies from 150 to 300 mm/m ; the modulus of thaw settlement of sandy soil with porous cryostructure reaches up to 30–50 mm/m .

Results

Particular attention was paid to the study of the temperature regime of the bridge foundation. This was performed in boreholes drilled by the Lengiprotrans Institute during the 1986–1988 geotechnical investigations and by PNIIS in 2007. The results of recent measurements are presented in Figure 1.

Measurements of 1986–1988 revealed significant differences in the ground temperature distribution in the right and left riverbanks. On the right bank, MAGT at the depth of 18–20 m was -1.45°C in the borehole located 250 m away from the river. In other boreholes located within 80 m of the river, MAGT always exceeded -0.3°C . A comparison of the results of temperature measurements obtained by the Lengiprotrans Institute about 25 years ago and by PNIIS in 2007 shows that during this time period there were no significant changes in the geothermal conditions of the right bank (Fig. 2).

Under the Shchuchya River riverbed, there is a closed talik 20 m deep, which turns into inter-permafrost talik up to 11 m thick in the sediments of the right bank. The talik tapers out

22–25 m away from the bank. A permafrost overhang 14 to 20 m thick forms near the riverbank (Fig. 1). This overhang provides evidence for a gradual river migration toward the left bank and simultaneous talik freezing at the right bank.

The soils of the left bank are much colder. Permafrost temperatures of the left bank in 1986–1988 were -1.1°C at 6 m distance from the river and -3.0°C at 78 m distance from the river. Permafrost temperatures in boreholes obtained by PNIIS in 2007 show an increase in MAGT over the past 20 years everywhere on the left bank. For example, in 1988 in borehole 371(86) (Lengiprotrans) located at the left bank right near the river, ground temperature was -2.7°C , and in 2007 in borehole No.19 (PNIIS) located 5 m away, the temperature was -1.9°C (Fig. 3). According to the measurements in boreholes more distant from the bank, MAGT also increased.

The results of the temperature logging and study of the frozen core confirmed the previously established pattern: the foundation soil of the right bank piers is represented by high-temperature, plastic frozen silty clay, and the soil at the left bank is represented by solidly frozen silty clay.

Discussion

The causes leading to the distribution and changes of the permafrost temperatures of the Shchuchya River right and left banks are related to the cumulative impact of natural and human-induced factors on the thermal regime of the piers foundation soils. Among the natural factors, there are the geological history of the Shchuchya River valley in the Holocene and the climatic changes at the end of the 20th century to the beginning of the 21st century. Among the human-induced factors, the leading role belongs to disturbances in the natural heat transfer conditions at the bridge crossing site as a result of placement of the construction pad.

The surface structure and geological structure of the upper horizons of the Late Pleistocene-Holocene deposits show that the Shchuchya River left bank in the area of the bridge was not subject to flooding in the Holocene. This is

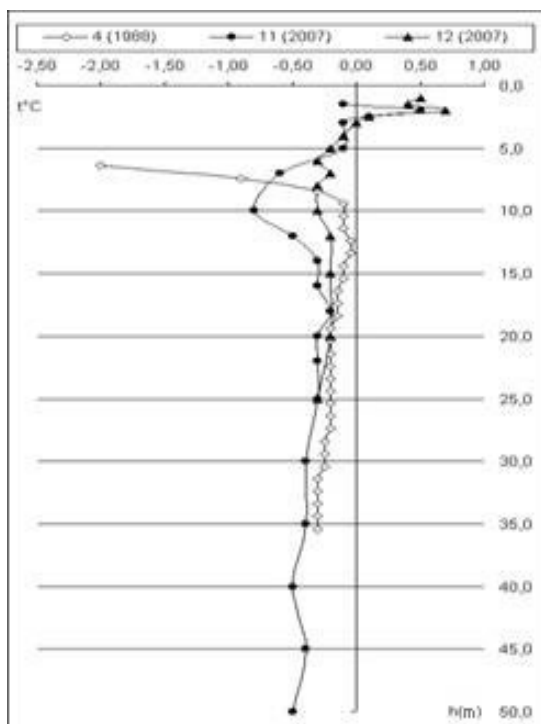


Figure 2. Permafrost temperatures on the right bank of the Shchuchya River, 1988–2007.

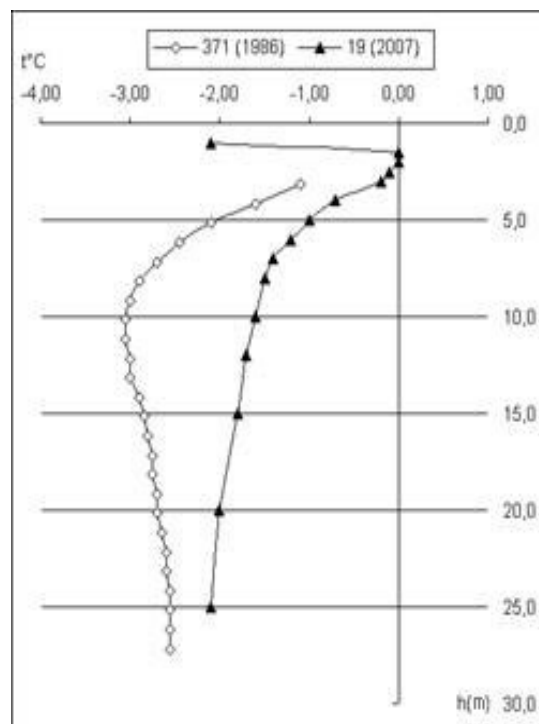


Figure 3. Permafrost temperatures on the left bank of the Shchuchya River, 1986–2007.

probably the reason why the temperatures of soils of the left bank are significantly lower than those of the right bank. The increase in MAGT at the left bank can be associated with climate warming in the recent decades. For example, according to the Salekhard meteorological station over 100 years, the change in mean annual air temperature change in 1965–2005 was 0.05°C per year, and the average annual temperature increase in 2005 was 1.2°C relative to the norm (1951–1988) (Pavlov et al. 2007). Another reason for the soil warming can be the influence of water flow washing out the left bank. At the same time, the soil temperature of the right bank has not increased during the last 20 years, apparently due to the protective effect of the construction pad, which is 2 to 2.5 m thicker on the right bank than on the left one.

Conclusions

Irregularities in the temperature change in permafrost soils at the base of bridge piers on the Yamal Peninsula should be considered when selecting the depth of piers for the bridge foundation and during calculations, design, and construction of seasonal cooling devices around the piers.

References

- Pavlov, A.V., Malkova, G.V., & Skachkov Yu.B. 2007. Current trends in the evolution of permafrost thermal state in climate change. In: *Mat-ly Mezhdunar. konf. "Cryogenic Resources of Polar Regions."* Pushchino 1: 34-38 (in Russian).
- Trofimov, V.T. 1983. About post-glacial terraced lake basins of Polar and Transpolar Trans-Ural Region. In: *Natural Conditions of Western Siberia.*, Izd-vo MGU, Moscow. pp. 11-21 (in Russian).

Permafrost and Landscapes of the Russian European North in the Twenty-First Century

N.V. Tumel

Lomonosov Moscow State University, Faculty of Geography, Department of Cryolithology and Glaciology, Moscow, Russia

Abstract

In the last third of the twenty-first century, the cryolithozone in the Russian European North will decrease at the expense of its contemporary western margin. It is obvious that frozen peatlands to the west of the valley of the Pechora River will thaw completely. The type of contemporary permafrost with the permafrost table directly below the active layer will be preserved almost everywhere. The residual thaw layer between the active layer and the permafrost table will possibly develop in the Bolshezemelskaya tundra at longitudes 54–58°E in typical tundra landscapes of elevated hilly watersheds (elevations of 70–230 m) that are composed of sands with strongly reduced ground covers. Seasonal frost will extend to the permafrost table in silty clays. The depth of seasonal thaw in silty clay soil will increase by 13–19%, the vegetation will be preserved in its present state, and moss thickness will increase by 1–5%.

Keywords: climate prediction; cryolithozone; ground temperature; Russian European North; residual thaw layer; seasonal thawing.

Introduction

The cryolithozone is a region of Russia where the response to climate warming may cause not only changes in permafrost conditions, but also landscape reconstruction, as well as a significant change in the natural geosystems. The study area of possible permafrost and climate reconstruction of natural complexes covers the Russian European North.

The main permafrost characteristics in the geocryological study of the territories are permafrost distribution in the area, its temperature, thickness and cryogenic structure, seasonal thawing and freezing, and permafrost-related processes and phenomena. The first reactions to climate changes are usually the depth of thaw and mean annual permafrost temperature, which affect the area of a particular spatial type of permafrost. Activation of permafrost-related processes and reduction of permafrost thickness should be delayed in time due to permafrost inertia preconditioned by the “ice-water” phase transitions.

It should be noted that there is a particular permafrost property that is most significantly influenced by different combinations of climatic parameters. The depth of seasonal thawing depends primarily on heat exchange in the summer period. Therefore, the trend in thaw depth change is determined by the sum of positive degree-hours of this period (thawing index). The mean annual permafrost temperature is influenced by annual variations in meteorological conditions, where the winter proportion prevails. Therefore, the change in mean annual temperature is primarily related to the trend in winter conditions, including snow cover. Accordingly, changes in the depth of thawing may be different from the changes in ground temperature (Pavlov 2008). In most general terms, a steady increase in ground temperature is observed in the cryolithozone. As for the depth of thawing, there are three possible options for the response to climate warming: increase, steady state, and decrease.

Methods

Permafrost formation and development is a complex process that depends on three main natural components:

climate, landscape, and geological structure. Each of these factors has a different impact on permafrost system components. The mean annual permafrost temperature $t(\text{gr})$ and the depth of seasonal thaw (ξ) result from the interaction of air temperature and landscape features. The most important landscape features are ground cover, composition, and properties of the permafrost soils to the depth of 12–15 m.

The interrelationship between permafrost and landscape conditions is a widely studied problem, both in its natural situation and in terms of environmental disturbance. In this regard, information on the southern region of the cryolithozone may be very valuable. Tyrtikov (1975) demonstrated that a one-directional vegetation change can determine the formation or degradation of permafrost, regardless of short-term climate changes. For example, peat accumulation within the shrub-sphagnum bogs at a rate of 0.5–1 cm/year is the primary cause of the formation of short-term permafrost and further formation of shallow permafrost islands. According to Tyrtikov, the rate of increase for frozen ground thickness after their formation is equal to that of peat formation. According to Osadchaya (2003), in the Bolshezemelskaya tundra there are vast spaces with permafrost that are stable in time but also extremely shallow (2–3 m). These are landscapes where the overgrowth of bogs, peatland formation, shoaling alases, and drained thermokarst degradations are observed.

Thus climate, vegetation, and permafrost form geosystems in which the order of intensity and developmental direction are determined by specific geographical conditions. When predicting climate warming, we must assume that the primary cause of changes in permafrost is, of course, the climate. The first response to its changes is in vegetation, followed by changes in permafrost conditions. The time gap between vegetation changes and permafrost changes is not huge: less than 10 years. This allows us to estimate the permafrost parameters (thaw depth, mean annual temperature) according to the proposed calculation method, as it is based on mean multiannual values of all its characteristics for a given period of time.

The following tasks should be accomplished for the analysis of $t(\text{gr})$ and ξ (Ecological and geographical ... 2011).

- We need to calculate the present thaw depth value (mean for the period of 1961–89) and compare it with the actual data obtained from the field research expeditions. These data were summarized and published in numerous monographs, articles, dissertations, and reports. The convergence of the estimated data and the actual data should confirm the accuracy of the chosen calculation method. The use of a calculation method required the collection of qualitative and quantitative information on the types and properties of ground covers and soils. This information was obtained from publications, including references and regulatory documents.
- We need to calculate the expected thaw depth mean for the periods of 2011–2030 and 2046–2065 in the context of climate warming, using the same procedure.
- We need to give a spatial description of the changes in permafrost conditions of the Russian European North.

In order to calculate the depth of thaw, we used the well-known Stefan's formula modified by Feldman (1977). The classical Stefan's formula has been used by many researchers, who modified it by introducing additional parameters in order to obtain more reliable results. Our choice of Feldman's modification stems from the fact that it was tested on a number of regions in the Russian European North, West Siberia, and Far East. This modification is quite simple due to the fact that its input characteristics can be obtained from publications and during fieldwork. The formula is as follows:

$$\xi = \mu \left[\sqrt{\frac{2\lambda\Omega}{Q_{ph}} + S^2} - S \right] \quad (1)$$

λ – thermal conductivity of unfrozen ground, J/ m.degrees.hr;

Ω – degree-hour sum for the summer period;

Q_{ph} – phase transitions in soil, J/m³;

S – equivalent layer of ground cover, m

μ – dimensionless coefficient, which takes into account the influence that the mean soil temperature has on the active layer.

According to this formula, the depth of thawing is calculated from the soil surface (ξ). During fieldwork, it is usually measured from the surface of the soil and moss covers. It is these measurements that appear in publications and maps. Therefore, two values are given for the depth of thawing: from the soil surface (ξ) and from the moss surface (ξ_{moss}). Formation conditions of ξ are defined by three main groups of factors: upper boundary conditions (on the surface), lower boundary conditions (temperature of permafrost at the base – ξ), active layer soils composition and properties. The upper boundary conditions are determined by two characteristics in the formula. First, it is the sum of degree-hours in the summer when thawing actually occurs (thawing index). In both present and expected versions, it is given as a mean multiannual value for a certain period of time. Therefore, the response of the depth of thaw to changes in the thawing index corresponds to the climate change trend. An integral assessment of heat-insulating properties of the soil vegetation covers that impede thawing is the so-called equivalent layer (S). Its significance is determined in the following manner. Depending on the soil cover

thickness (mostly moss cover) and its thermal conductivity, the thermal resistance of moss (R) is calculated; it is the quotient of power $h(m)$ and thermal conductivity λm . Then R is replaced by an equivalent moss layer (S), where thermal insulation of moss in accordance with the characteristics of the soil, on which this cover is located, is taken into account. The adjustment of thermal insulation of the vegetation cover, with the base soil taken into account, is implemented through the thermal conductivity of soil (λ):

$$S = R_{mx} \times \lambda = h_{mx} / \lambda_{mx} \times \lambda \quad (2)$$

The introduction of the equivalent layer into Stefan's formula in cases where there is a heat-insulating layer (not only moss, but also snow and artificial covers) on the soil surface began in the 1940–50s (Porkhaev 1959).

It is obvious that with the exception of the climatic thawing index, all other characteristics require further study of the landscape situation. Climatic parameters (mean annual air temperatures and the sum of summer degree-hours) in both present and expected versions are set for the discrete cells of the model with the dimensions of 2° of latitude and longitude. Typical and prevailing characteristics of $h(m)$ and its thermal conductivity according to species composition were set within each cell to determine $t(gr)$ and ξ . Afterwards, $R(m)$ and S were calculated. The information on moss cover was obtained from Feldman (1983), Permafrost and reclamation... (2002), Geocryological conditions... (1964), Tumel (1977), and Osadchaya (1994, 2003). The main soils, for which the depth of thawing was calculated, are peat, silty clay, and sand. Their physical and thermal characteristics (water content, density, thermal conductivity) were specified and calculated (phase transitions) using regional monographs, construction norms, and regulations (1990), and works of Pavlov (1975). Heat transfer between the active layer and the underlying permafrost was estimated using the empirical dependence $\mu = 1 - 0.033 |t(s)|$ (Feldman 1977). The mean annual ground temperature $t(gr)$ was given in accordance with the generalizations in the monographs and maps of various scales. The expected version $t(gr)$ was interpolated in accordance with the changes in air temperature and the monitoring data (Pavlov 2008). The calculation results are represented by latitudes. The calculation procedure for ξ and $\xi(m)$ was based on the average climatic characteristics (air temperature and Ω) for 1961–89, 2011–30, and 2046–65. This approach does not take the climate change trend into account, so the estimated ξ by 2030 and 2065 may be somewhat understated. Regional estimates of trend changes in ξ in the Bolshezemelskaya tundra (Vorkuta site) give the value of 0.0007 m/year (the period of 1978–2002) which indicates quite an insignificant increase in the depth of thawing or about 0.02 m for this period. "In case, this trend persists ... we can expect no pronounced changes of seasonal thawing depth in the next 15–20 years" (Pavlov 2008: 172–173).

Another calculation condition is where the landscape-soil characteristics remain unchanged from 1961 to 2030–2065. The description of these conditions in various works from the 1920–30s and until today (i.e., for almost a century) does not indicate any changes in the natural landscape structure of the regions in the study area. Zonal-regional

features of geosystems remain unchanged, although there are local changes in permafrost, particularly at the southern permafrost boundary. Both disappearance and formation of permafrost are observed.

In the Russian European North, the cryolithozone covers a small area from the Kola Peninsula to the Polar Urals. Its maximum width at 56°E is about 300 km. The southern boundary is located at approximately 66°N. There is a significant increase in permafrost severity from west to east. Up to 48°N (the eastern part of the Kanin Peninsula), permafrost is of an island type with temperatures of about -0.5 to -1°C. In the Malozemelskaya tundra, and especially in the Bolshezemelskaya tundra, permafrost conditions are becoming more diverse. In the Bolshezemelskaya tundra, island permafrost is successively replaced by discontinuous and continuous permafrost from the southwest to the northeast. There is large spatial variability in landscapes and permafrost within the territory located at 2° of latitude and longitude. So, during the large-scale studies, 2–3 types of data on soil temperatures, soil composition, moisture content, and thermal resistance of the soil cover were determined and estimated under the same climatic conditions (air temperature, Ω).

There is another preliminary remark that should be made. Mean annual air temperatures and the sum of summer degree-hours consistently increase from west to east in accordance with the climate continentality.

Forecast for 2011–2030

The increase in mean annual air temperature ($t_{\text{air}}^{\text{th}}$) changes very evenly over the period of 2011–2030: less at 66°N (by 1.4–1.6°C) and slightly more at 68°N (by 1.6–1.7°C).

Along 66°N, permafrost–landscape conditions are very diverse. The western part of the cryolithozone (up to 50°E) is characterized by island permafrost. This is mainly peatlands, but it is possible that they also remain in silty clay of boggy landscapes. Ground temperature in both cases is -1°C and higher. The depth of thawing in peat is 0.60–0.62 m; in moist silty clays the value is larger, from 0.77–0.79 m. According to the forecast, a significant increase in air temperature will lead to peat thawing to the temperatures of -0.1 to 0.5°C. The thaw depth will increase up to 0.63–0.65 m. In silty clays the temperature may rise to 0°C; the increase in the depth of thawing by 4 cm will only slightly alter the final value to equal 0.81–0.83 m.

East of 50°E, each longitude is characterized by rapid change in both landscape and permafrost conditions. At 52°E in the Malozemelskaya tundra, forest tundra predominates in the south, and northern taiga predominates further southward. Further eastward, between 56 and 60°E, thawing conditions in the southern tundra, forest tundra, and northern taiga should be examined independently. In the utmost northeast of the Bolshezemelskaya tundra (62° and 64°E) it is tundra, and in some areas it is forest–tundra. The conditions in peatlands can be assumed to be close to those that were set for the western part of cryolithozone, but they vary considerably for silty clay soils. Moisture content, bulk density, and thermal physical properties of glacial-marine and glacial silty clays in the far east can be assumed to be unchanged, but the soil covers should be significantly

differentiated. Moss has the smallest thickness (0.07 m) in tundra; its thickness is 0.1 m in forest-tundra, and 0.17 m in the northern taiga. Therefore, their thermal physical properties also change.

In tundra, the estimated peat depth is 0.53–0.61 m. It increases eastward. The expected depth of thaw is 0.57–0.65 m. Peatlands in tundra thaw to the depth of 0.51–0.6 m, and to 0.59–0.77 m during warming. In the southern area of the cryolithozone and in the northern taiga, the natural depth of thaw is 0.52–0.68 m (i.e., virtually the same as in the forest-tundra). The reason for this is the significant increase in the thickness of moss, which reduces the depth of thawing. During warming, the depth of thawing will increase to 0.59–0.71 m. Silty clays are characterized by the present depth of thawing of 1.05–1.33 m. During warming it will increase to 1.12–1.43 m.

Sands do not remain in their frozen state in all of the tundra landscapes. Quite often it is sands that contain open and closed taliks. Frozen sands are mostly of glacial-marine and glacial types in the east of the Bolshezemelskaya tundra. Their depth of thawing is 1.51–1.86 m. During warming it will increase to 1.62–1.96 m. If the warming trend continues, undoubtedly deep thawing of sands will lead to even more widespread distribution of taliks with a lower permafrost table.

It should be emphasized that the difficulty of assessing changes in the mean annual ground temperature and depth of thawing is that a significant change in landscape conditions takes place within relatively small areas. Therefore, these circumstances determine the extrapolation of the ground temperature. For the same climatic background, it is lower in peatlands than in mineral soils. In tundra it is -2.5°C, and during warming it will increase to -1.5°C. Its value in silty clay tundra soils is -1.3 to -1.5°C, and the expected value is -0.8 to -1.0°C. In forest-tundra and taiga peat, temperatures increase from -0.1 to -1°C, and in silty clays they should not become lower than -0.5°C. Such change in temperatures will lead to a change in thawing from 5 to 13%. The conditions when seasonal frost extends to the permafrost table will persist almost everywhere. Development of a residual thaw layer between the active layer and permafrost is possible in the Bolshezemelskaya tundra at longitudes 54–58°E. This is in the typical tundra landscapes of the elevated hilly watersheds (elevations of 70–230 m) composed of sands, where the soil covers are heavily reduced. The expected thawing here is 1.90–1.96 m.

Forecast for 2046–2065

The modern cryolithozone of the Russian European North has warmer permafrost temperatures. Therefore, the predicted warming leads to more radical changes in the area of permafrost distribution, its temperature, its depth of thawing, and the position of the permafrost table.

We can assume that at 66°N the northern taiga landscapes will replace the forest-tundra and fragments of southern tundra. Mean annual air temperature will increase by 3.3–3.5°C in comparison with the present temperature. This means that in the western sector of the present cryolithozone it will be above 0°C, which rules out the existence of permafrost. Under present conditions, permafrost thickness

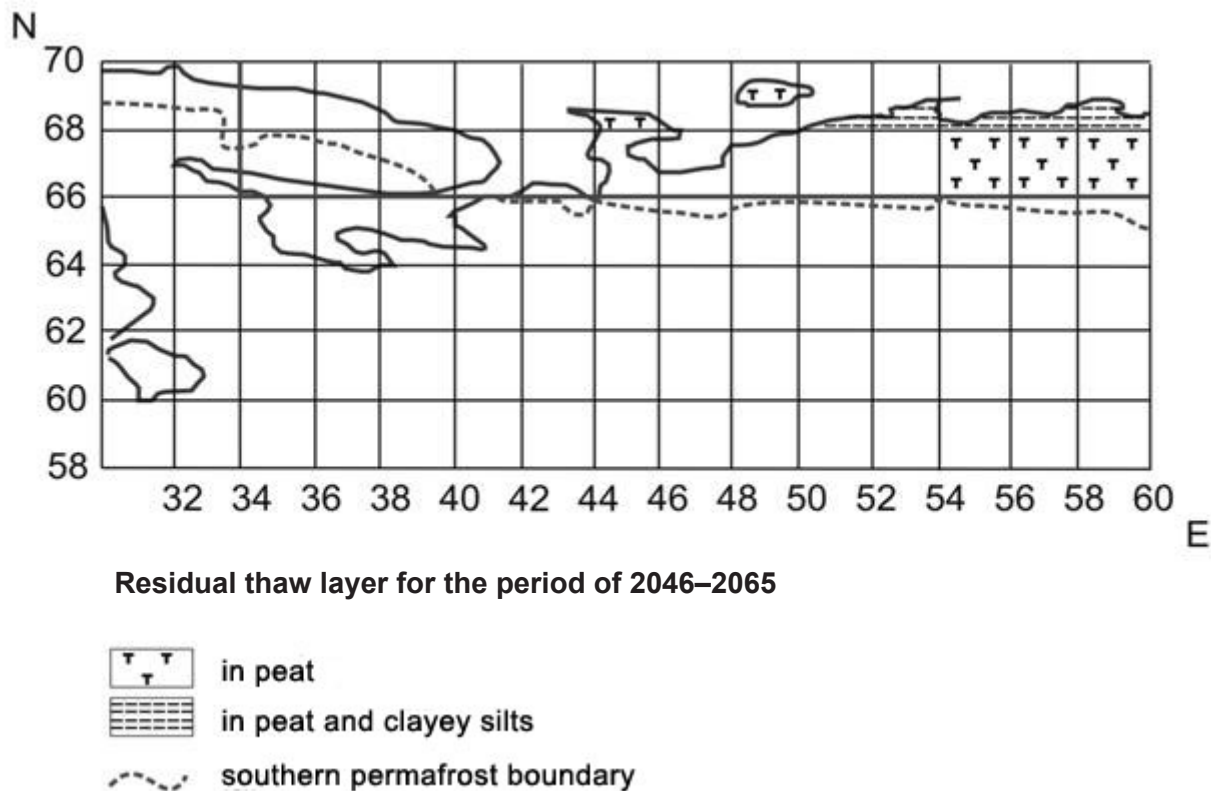


Figure. 1 Expected change in the distribution of cryolithozone in the Russian European North.

here is small, and therefore we can expect it to thaw completely. Rare permafrost islands may persist at the longitudes of 52–60°E (i.e., in the Malozemelskaya tundra and in the west of the Bolshezemelskaya tundra). We can assume a more widespread island permafrost distribution to the east.

Increased summer heat reserve (Ω_{th}) by 14–17%, compared to the modern values, will lead to deeper thawing. In peat it will be 0.58–0.63 m. However, if moss thickness and its insulating properties increase, the depth of thawing will be reduced by 0.1–0.18 m, compared to the present values. According to the field study of Osadchaya (2008), the growth of permafrost that is at least ten years old has been recorded in the modern northern taiga, although its thickness may not exceed 2 m.

Thus at 66°N, the permafrost boundary will retreat to the east. If permafrost is now observed on the Kola Peninsula, its western boundary in the expected version will be located at 52°E along the Pechora River valley. To the east, the southern permafrost boundary will retain its position, but the permafrost temperature along this boundary will be warmer. Permafrost will remain in rare islands in the landscapes of the bogged spruce forest. In a number of modern permafrost massifs composed of peat and glacial lacustrine silty clays, there will be rather deep perennial thawing (more than 1.5–2.0 m) and a residual thaw layer will be formed.

Modern continuous and discontinuous distribution of permafrost at 68°N will be replaced by discontinuous distribution. In landscapes composed of sands, permafrost will thaw deeply from the surface. Taliks in the west along the arctic coast might be open, and closer to Pai-Khoi they might be closed with the formation of the residual thaw layer above permafrost.

An increase in the mean annual air temperature is expected to be within the range of 1.5–3.8°C. Under these circumstances, the depth of thawing in peat will increase and will be equal to 0.55–0.66 m while the present characteristics of soil covers will persist. With the increase in moss thickness and its thermal insulating properties on the Kanin Peninsula, the depth of thawing will be the largest at 0.61–0.64 m. Along the northern border of the Bolshezemelskaya tundra, the increase of ξ is expected to be up to 0.53–0.60 m, with a moss thickness increase up to 0.15 m.

Permafrost of silty clay texture will be preserved only in the Bolshezemelskaya tundra. The depth of seasonal thawing will be 1.25–1.49 m if the soil cover type does not change, and it will be 1.1–1.33 m if it does. In some landscapes, with the increase of heat-insulating properties of the soil cover, a slight decrease in the depth of thawing is possible. The trend of change in the depth of seasonal thawing (ξ_{th}) for the whole study period is shown in Table 1.

Thus, in the last third of the 21st century, permafrost in the Russian European North will decrease by approximately 40% at the expense of its present western margin (Fig.1). It is obvious that frozen peatlands to the west of the Pechora River valley will thaw completely. Rare peatland islands will remain only in the far north of the Kanin Peninsula. In the preserved cryolithozone of the European North, permafrost distribution type will change. In the northern taiga (66°N), rare islands with a permafrost table directly underneath the active layer will be preserved in peat in areas east of Timan Ridge (50°E and further to the east). To the north of 68°N, peatlands will remain frozen throughout the territory, but their mean annual temperature will increase from -0.5 to -2°C. The coldest permafrost in peat will be in the far northeast, closer to Pai-Khoi.

Table 1. Depth of seasonal thawing (68°N) in silty clay tundra soils (in case of unchanged soil covers) for locations in the Russian European North.

E	1961–1989				2011–2030				2046–2065			
	t _{air} , °C	t _{gr} , °C	Ω, degrees/hour	ξ, m	t _{air th} , °C	t _{soil th} , °C	Ωth, degrees/hour	ξth	t _{air th} , °C	t _{soil th} , °C	Ωth, degrees/hour	ξth, m
1	2	3	4	5	6	7	8	9	10	11	12	13
50	-5.6	-0.8	28714	1.26	-3.9	-0.5	31118	1.36	-2.0	-0.0	33528	1.42
52	-5.8	-0.8	31406	1.33	-4.1	-0.5	33885	1.43	-2.2	-0.0	36494	1.49
54	-6.1	-1.5	31673	1.31	-4.5	-0.5	34257	1.39	-2.5	-0.3	36945	1.48
56	-6.5	-1.5	32328	1.32	-4.8	-1.0	34988	1.41	-2.8	-0.3	37711	1.49
58	-6.9	-1.5	30365	1.27	-5.2	-1.0	33043	1.36	-3.2	-0.3	35760	1.46
60	-7.2	-1.5	24727	1.14	-5.5	-1.0	27448	1.23	-3.5	-0.3	30165	1.32
62	-7.6	-2.0	24288	1.10	-5.9	-1.0	27072	1.19	-3.8	-0.5	29789	1.30
64	-7.9	-2.0	22416	1.05	-6.1	-1.5	25238	1.12	-4.1	-0.5	27991	1.25

The depth of thawing in peat will generally increase by 5–15%. However, due to the increase in moss thickness and thermal resistance in some landscapes, it may be reduced by 15–20%. This phenomenon is most expected in northern taiga (at 66°N), where it is already observed under present conditions. As a result of perennial thawing, permafrost composed of sands will be a residual thaw layer. Seasonal frost may extend to the permafrost table in silty clay soils. If vegetation is preserved in its present form, the depth of seasonal thawing of silty clay soils will increase by 13–19%. If moss thickness increases, the depth will increase by 1–5%.

Conclusions

- 1) Out of all the changes in permafrost landscape conditions due to climate warming, the relation between the depth of thawing, the mean annual ground temperature and the area of permafrost distribution with mean annual air temperature, the sum of summer degree-hours, the composition and water content of soils according to their genesis, and landscape zoning was revealed in the adopted spatial climate model through assessment of the properties of the soil cover.
- 2) By 2030, radical changes in permafrost conditions are hardly possible in the natural landscapes on the plains of the cryolithozone's western sector. In the Russian European North the depth of thawing will increase by 5–13%. A residual thaw layer may develop on the hilly watersheds of the Bolshezemelskaya tundra, which are composed of sands.
- 3) By 2065, a significantly different situation is expected to follow the continued warming. In the European North, the present permafrost islands may disappear in the west to the longitude of the lower reaches of the Pechora River, and the total area of the European cryolithozone will decrease by approximately 40%. The predominant

types of permafrost distribution in the Malozemelskaya tundra and the Bolshezemelskaya tundra will be the island and the discontinuous types. The residual thaw layer will develop in section. However, in case of permafrost retreat, the depth of thawing may decrease by 15–20% in organogenic soils.

References

- Feldman, G.M. 1977. *Forecast of permafrost temperature regime and development of permafrost-related processes*. Moscow, Nauka, 254 pp. (in Russian).
- Feldman, G.M. 1983. *Textbook on the forecast of permafrost temperature regime* (the case of Western Siberia). Yakutsk, 39 pp. (in Russian).
- Geocryological conditions of the Pechora coal basin*. 1964. Izd-vo Nauka, 222 pp. (in Russian).
- Kasimov, N.S. & Kislova, A.V. (eds). 2011. *Ecological and geographical consequences of the XXI century global warming on the East-European Plain and in Western Siberia*. 2011. Monograph. Moscow: MAKS Press. 496 pp. (in Russian).
- Osadchaya, G.G. 1994. Methods of determining the influence of moss covers on the ground temperature regime. *Izvestiya RGO*. V. 126. No. 6, pp. 71–77 (in Russian).
- Osadchaya, G.G. 2003. Stabilizing response of permafrost landscapes to the changes in climate conditions. *Kriosfera Zemli*, 7 (no. 4): 21–27 (in Russian).
- Pavlov, A.V. 1975. *Heat exchange between soil and atmosphere in northern and temperate latitudes of the USSR*. Yakutsk. knizhnoe izd-vo. Yakutsk, 301 pp. (in Russian).
- Pavlov, A.V. 2008. *Cryolithozone monitoring*. Novosibirsk. Academ. izd-vo Geo, 225 pp. (in Russian).
- Permafrost and development of oil and gas regions*. 2002. Moscow, GEOS, 400 pp. (in Russian).

- Porkhaev, G.V. 1959. Thermophysical principles of managing interaction between structures and permafrost. *Osnovy geokriologii (merzlotovedeniya), p. II, inzhenernaya geokriologiya*. Izd-vo AN SSSR, pp. 80–118 (in Russian).
- SNiP (Construction Norms and Specifications) II–18–76. 1977. Part II. Chapter 18. Bases and foundations on permafrost. Moscow – Stroyizdat, 45 pp. (in Russian).
- Tumel, N.V. 1977. Temperature regime and cryogenic structure of permafrost in the eastern part of Bolshezemelskaya tundra. *Problemy kriolitologii*. Issue VI, Moscow, Izd-vo MGU, pp. 58–106 (in Russian).

The Possibilities of Industrial Development of Natural Resources on Permafrost-Affected Bog Landscapes and Peatlands of the Bolshezemelskaya Tundra

N.V. Tumel

Lomonosov Moscow State University, Faculty of Geography, Department of Cryolithology and Glaciology, Moscow, Russia

G.G. Osadchaya

Institute of Management, Information and Business, Department of Ecology and Natural Resources Management, Moscow, Russia

Abstract

When organizing industrial development of natural resources in the cryolithozone, it is important to remember that this development is temporary and, therefore, it should be organized with minimum disturbance of the natural ecosystems. We consider areas composed of thick biogenic soils. Specifically, we analyzed permafrost-affected bogs and peatland landscapes. Depending on the geoecological characteristics, the intensity of ongoing cryogenic processes, and on hydrologic conditions, certain types of landscapes are recommended for industrial development in various geocryological sub-zones. The landscapes not recommended for industrial development were also identified. The influence of the modern climatic trend on the stability of organic-rich landscapes was examined.

Keywords: bogs; geocryological zonation; industrial development; lake basin; natural resources; peatlands.

Introduction

The cryolithozone of the Bolshezemelskaya tundra occupies tundra landscape and includes the southern shrub tundra (continuous permafrost), the southern and northern forest tundra (massive-island and discontinuous permafrost, respectively), and the northern part of extreme northern taiga (island permafrost) (Maslov et al. 2005). Practically any nontraditional type of economic activity in the cryolithozone is aimed at the extraction of natural resources, and therefore it is limited to a specific period of development. Spatially, such activity involves the development of areal and linear oil and gas infrastructure, its maintenance and operation.

When organizing industrial development of natural resources in the cryolithozone, it is important to consider its temporary nature. Therefore, development should impose minimum damage to the natural ecosystems, and the production infrastructure should be built in areas that have maximum ability for self-regeneration. This will allow for the preservation of the ecological functions of a landscape and ensure the social component of sustainable development (i.e., the possibility of traditional management of natural resources based on preserved biological resources).

Traditionally, in the North, the areas composed of biogenic soils (peats) are the least favorable for development. Usually, engineers try to avoid the use of such areas and construction of facilities on mineral ground or areas that might have ecological or social significance such as for the protection of forests and reindeer pastures. However, if we prioritize the interests of sustainable development, we will need to abandon this practice; and when creating a production infrastructure, we should also consider the areas composed of peaty or biogenic soils.

Biogenic soils of the region are associated with groups of bogs and peatlands. With rare exceptions (polygonal peatlands), these areas and especially bogs are characterized with high capacity for self-regeneration. According to studies conducted by the Institute of Biology of the Komi Science Center, UB RAS, the self-restoration of ecosystems takes

5–30 years after mechanical disturbances. This period can be reduced if various techniques of environmental remediation are applied. Our studies, including fieldwork, showed that the bog and peatland landscapes are characterized by a certain range of cryogenic processes of varying intensity. These processes can limit the possibilities of industrial development on such landscapes. Cryogenic processes are conceptually different in the southern cryolithozone than in the northern cryolithozone; the southern cryolithozone is underlain by island and massive-island permafrost, while the northern cryolithozone is characterized by discontinuous and continuous permafrost. This allows us to evaluate zonal differentiation in the process of determining the possibilities of industrial use for these landscapes.

The extreme northern taiga is characterized by island (sporadic) permafrost distribution where permafrost occupies less than 10% of the area. Biogenic soils are manifested at the surface by peat mounds and by various types of bogs (ridge-pool and pool bogs, herb-moss and sedge-moss bogs, swampy bogs, shrub-low shrub-moss bogs, etc.).

Permafrost in this geocryological sub-zone is, with rare exceptions, limited only to areas composed of lacustrine-boggy deposits overlain by peat. These are raised peatlands with separate sections of ridge-pool bogs where permafrost occurs on the positive forms of mesorelief (mounds and ridges). In some cases, new permafrost formations develop within bogs. The permafrost is considered very unstable and may degrade even in the absence of anthropogenic climate warming. Our research is aimed at evaluating the degree of activity of cryogenic processes in such sub-zones of island permafrost.

Discussion

First of all, the geomorphological association of permafrost is significantly larger than was previously thought: large massifs of raised peatlands were found not only below elevations of 110–120 m, but also in higher drainage divides in the eastern part of the region with

elevations reaching 180 m. Frost mounds in this landscape occupy 40–75% of the area. Secondly, the extreme southern permafrost is not unstable under the current climate warming but, on the contrary, it is a zone of active modern formation of permafrost islands. The statement that the permafrost will begin to degrade from its southern margins is only partially true. The southern permafrost of the region almost always consists of peatlands with high ice content, which makes them relatively stable landscapes even in terms of serious mechanical anthropogenic disturbances, not to mention the gradual warming. Field studies allowed us to observe numerous cases of growth of peat mounds not only within peatlands but also within bogs (Osadchiy & Osadchaya 2008). Within the latter they grow in areas covered with tree vegetation, although tree vegetation was traditionally thought to indicate the absence of permafrost in the southern cryolithozone.

In general, when determining areas suitable for industrial development within the sub-zone, the areas of raised peatlands are not well suited for development. Here active and rather widespread distribution of heave processes cannot guarantee the stability of natural and technogenic systems. The areas of active cryogenic processes are not significant in bog landscapes. Therefore, limitations on their use can be related to the peat thickness, moisture regime, and other factors. The following areas are generally not suitable for development: swampy bogs, ridge-pool (pool) bogs, herb-moss bogs, shrub-low shrub-moss bogs with peat thickness over 5m, and all drainage bogs (high geocological significance).

Massive-island permafrost, which occupies 10–50% of the area, is typical of southern forest-tundra. Biogenic soils there also form areas of bogs and peatlands, both flat and raised ones. In peatlands, the development of open taliks is typical in depressions between the mounds.

As far as cryogenic processes are concerned, our studies demonstrated that they actively develop in the raised peatlands and have the same characteristics as in the sub-zone of island permafrost. Permafrost is stable in flat peatlands. The development of significant heaving or thermokarst processes is not observed. New permafrost develops in bogs as in the sub-zone of island permafrost, but this development is not as active. However, we did not encounter any new formations of permafrost in the areas covered by trees.

In general, industrial development on raised peatlands is not recommended. However, it is possible to utilize flat peatlands.

New permafrost formation was noted in bogs, but it is rather limited in area. In general, bogs (except for swampy, herb-moss bogs, etc.) are also suitable for development. However, drained bogs should be excluded from economic development due to their high geocological significance.

Thus the active development of cryogenic processes in the southern cryolithozone (perennial heaving with new formation of permafrost of various morphological forms) restricts the use of raised peatlands. General climate warming does not mean that these processes will cease and thus cause permafrost degradation (Tumel & Osadchaya 2006).

In the northern cryolithozone as well as in the southern cryolithozone, bog and peatland landscapes are associated with areas of biogenic soil development.

Our studies revealed that bogs (permafrost hardly exists except for new formations) occur only in the sub-zone of discontinuous permafrost and are marginally developed. Heaving processes are not active and in some areas they are not developed at all. On the whole, low-shrub and shrub-moss bogs (except for drained bogs) are suitable for the construction of facilities. Establishment of facilities on herb-moss bogs is not recommended due to extremely unfavorable engineering and geological characteristics of the soils.

Bog vegetation is also typical of thermokarst depressions. Within thermokarst depressions, warm temperature permafrost occupies 70 to 100% of the area in the discontinuous permafrost zone, while in the continuous permafrost zone it is widespread (rare areas with a residual thaw layer were observed). The active development of perennial heaving processes is not typical of these landscapes either. If certain requirements are met, construction on frozen ground is possible but limited.

The following major types of peatlands are widespread in the northern cryolithozone: flat (including those covered with lakes), raised, polygonal peatlands, and drained lake basins (hasyreys). The inclusion of hasyreys in the peatland group is conventional due to the similarity in vegetation. Raised peatlands occur only in the sub-zone of discontinuous permafrost and are predominantly stable. Activation of cryogenic processes at raised peatlands was not observed; locally, peat mounds disintegrate on their sides at contact with thawed depressions between the mounds. This landscape is suitable for industrial development.

Flat peatlands covered with lakes are developed only in the sub-zone of continuous permafrost. Permafrost occurs everywhere in these peatlands and its temperature varies from 0 to -3.5°C . This landscape should be excluded from development, not so much due to difficult engineering and geological conditions, but rather due to the significance of ponds within its boundaries. In accordance with the Water Code of the Russian Federation, the water protection zone is established around lakes (except for shallow ones). As a rule, the width of the zone does not exceed 50 m. This rule applies to thermokarst lakes that are mostly round in shape if their diameter exceeds 40 m. Therefore, when a large number of shallow ponds exist, their water protection zones overlap, occupying almost the entire peatland area.

Polygonal peatlands as an independent landscape are identified in the sub-zone of continuous permafrost, and as fragments they exist within flat peatlands in the sub-zone of discontinuous permafrost. These landscapes are characterized by ice wedge polygons that are still growing (Osadchaya & Tumel 2007) and with the development of thermal abrasion. They should definitely be excluded from the zone of industrial development. Localized cracking occasionally occurs even under warming climatic conditions, especially in the sub-zone of discontinuous permafrost.

Considering flat peatlands from the perspective of industrial activity, we may recommend their inclusion in the zone of development (except for the localized areas with ice wedge polygons), as they represent rather stable formations (Osadchaya & Kirikova 1998). They are less significant geocologically since they do not represent reindeer pastures and they regenerate successfully if properly developed.

However, it is important to consider the diversity of the geocryological environment within their boundaries. For example, although surfaces are in the sub-zone of continuous permafrost, its temperature varies greatly. In the sub-zone of discontinuous permafrost, permafrost may not occur in the depressions between the mounds. In flat peatlands, the local development of thermal abrasion and thermokarst processes are observed. Observations on peatlands show that under climate warming, permafrost degradation, and hence the radical alteration of the landscape structure of the territory, is not necessarily the consequence of this warming.

Landscapes containing lake basins (hasyreys) are typical of the entire northern cryolithozone, but their permafrost characteristics are somewhat different. Hasyreys represent drainage lake basins that actively freeze and have ledum-lichen vegetation associations on peat mounds and sedge-sphagnum as well as sedge-grass vegetation associations on flat areas. Field studies revealed the following characteristics of hasyreys. In the sub-zone of discontinuous permafrost, permafrost is developed in approximately 10–70% of the area of the hasyreys area and is associated with peat mounds and new formations. As a rule, the permafrost thickness is a few meters. Perennial heaving processes develop actively. In the sub-zone of continuous permafrost, permafrost can occupy 10–100% of the area; permafrost is layered in some areas and its upper layer is 2–6 m thick. Perennial heaving processes as well as the growth of peat mounds are also active (Maslov et al. 2005).

Hasyreys should be excluded from areas of industrial development due to an unstable permafrost environment, complicated engineering and geological conditions, and the fact that they represent valuable forage grounds for reindeer breeding. From an ecological perspective, a hasyre is a drainage system (i.e., it can become a source for chemical pollution). Moreover, there were cases when hasyreys were flooded and became lakes. It would be logical to specify a water protection zone around lakes for hasyreys, but the legislation does not cover this thus far.

As a result, at the zonal level, biogenic soils are subject to restrictions on their use for industrial development. In the southern cryolithozone, raised peatland areas should not be developed, and in the northern cryolithozone, polygonal peatlands and local areas with ice wedge polygons within flat peatlands and hasyreys should not be developed.

At the more localized level, certain types of bogs (definitely all drainage bogs) and flat peatlands covered with lakes should not be developed. However, under certain conditions (peat thickness that does not exceed 5 m), non-drainage bogs with low water content, as well as flat and raised (in the sub-zone of discontinuous permafrost) peatlands can be involved in industrial development. This will make it possible to preserve ecologically and socially valuable areas (protection forests, tundra reindeer pastures, etc.) that are currently most actively used for industrial development.

General patterns of modern cryogenic processes that can potentially affect natural resource development have the following characteristics. In raised peatlands we observe a gradual disappearance of active cryogenic processes from south to north (i.e., from the sub-zone of island permafrost to the sub-zone of discontinuous permafrost). In localized areas of polygonal peatlands, the frost cracking process is

more active in the sub-zone of discontinuous permafrost and less active in the sub-zone of continuous permafrost. For the group of bog landscapes, the maximum activity of heaving processes is observed in the sub-zone of island permafrost in the south and it decreases to the north. Despite climatic warming, flat peatlands represent stable natural formations where thermokarst processes occur locally.

Conclusion

The limited use of bog and peatland landscapes in industrial development of natural resources in the North contributes to the preservation of biospheric and social functions of the territories. Natural characteristics of these landscapes and their suitability for specific development can be reflected on geocryological and landscape maps and in tables of landscape indicators. However, when planning for a specific project in the cryolithozone, it is advisable to compile maps outlining areas restricted for natural resource development (Osadchaya 2009). These maps should include an evaluation of the possibility of using various types of bogs and peatlands along with other types of local landscapes.

References

- Maslov, A.D., Osadchaya, N.V., Tumel, N.V., & Shpolyanskaya, N.A. 2005. *Fundamentals of geocryology*. Textbook. Ukhta: Izd-vo Instituta upravleniya, informatsii i biznesa, 176 pp.
- Osadchaya, G.G. 2009. Territorial resource preservation as one of the conditions for the sustainable development of the cryolithozone: The case of the Bolshezemelskaya Tundra. *Kriosfera Zemli* 13 (no. 4): 24-31.
- Osadchaya, G.G. & Kirikova, N.S. 1998. On the issue of the probability of thermokarst development in the Timano-Pechorskaya Province. *Inzhenerno-geologicheskoe izuchenie termokarstovyykh protsessov i metody upravleniya imi pri stroitelstve i ekspluatatsii sooruzheniy* (IGK-98). St. Petersburg: VNIIG im. B.E. Vedeneeva, pp. 32-35.
- Osadchaya, G.G. & Tumel, N.V. 2007. Cryogenic processes as an indicator of the stable condition of geosystems. *The development of the North and issues of nature recovery: Reports of the VI International Scientific Conference*, October 10-14, 2006, Syktyvkar, pp. 136-139.
- Osadchiy, V.V. & Osadchaya, G.G. 2008. Contemporary permafrost in the southern cryolithozone of the Timano-Pechorskaya oil and gas province. *Proceedings of the International Conference "Cryogenic Resources of the Polar and Mountain Regions. The State and the Prospects of Engineering Geocryology"*. Tyumen April 21-24, 2008, Tyumen: Izd-vo TyumGNGU, pp. 258-261.
- Tumel, N.V. & Osadchaya, G.G. 2006. The meaning of cryogenic processes when evaluating climatic changes in the Bolshezemelskaya tundra. *Theory and Practice of Estimating the State of the Earth's Cryosphere and the Prediction of its Change*. Proceedings of the International Conference. Tyumen: TyumGNGU, Vol. 1, pp. 298-30.

Terrain Indicator Approach and Results for Permafrost Studies

N.G. Ukraintseva, D.S. Drozdov, Y.V. Korostelev, T.A. Korobova
Earth Cryosphere Institute, SB RAS, Tyumen, Russia

Abstract

This paper demonstrates advantages of the landscape indicator (geosystem) approach for permafrost studies. As GIS technologies progress, landscape maps become ever more important as a basis for extrapolating point data and map modeling of the composition, state, and properties of geological systems. Several case examples are described to illustrate the use of landscape maps and cartographic analysis in assessment of permafrost-related landslide areas, in temperature monitoring of permafrost and active layer, and in environmental optimization for petroleum development.

Keywords: active layer; cartography; landscape indicator approach; permafrost monitoring; permafrost-related landslides; permafrost.

Introduction

The state and dynamics of natural and anthropogenic landscape systems in the zone of permafrost are largely influenced by the Earth's external factors (atmosphere, hydrosphere, biosphere, cryosphere) and by technological systems. These links can be detected and the state of the interacting media can be assessed through map and information modeling. Models of this kind include integrated and specific maps with respective databases. There is a separate group of subject maps, especially those related to geological topics such as permafrost engineering and groundwater, in which the mapped object is not visible and cannot always be reliably detected by remote sensing. Field evidence of such objects is restricted to data points from boreholes, trenches, natural (bluffs along lake and river shores) or manmade (walls of quarries and mines) outcrops, which are all reduced to a point on the map. Thus there arises a problem of how to place the point-like information on the map or how to extrapolate the input data.

The problem can be solved using a landscape indicator approach developed by Sergey V. Viktorov (1966), among others. The method consists of correlating hidden components of the environment with exterior physiognomic components, attributes, or properties (indicators). Vegetation, which is closely linked with its substrate, is the most broadly used indicator (e.g., pine forests [*Pinus sylvestris*] commonly grow on sand while spruce [*Picea*] grows on silty clay). However, as the theory of landscapes and the practice of integrative landscape studies have shown, it is the whole system of natural properties of an area, with its landscape pattern being the best expressed physiognomic feature, that is the most reliable indicator of different landscape components (Viktorov 1986, 1998).

In the landscape indicator method, landscape maps are used as a basis for grouping, statistical processing, and extrapolating the parameters of the mapped object. Landscape mapping is based, in its turn, on classification of geographical landscape systems with the use of remote sensing data (Nikolaev 1979, Melnikov et al. 1983, Drozdov 2004).

Landscape Maps as Synthetic Models of Nature

Landscape maps as synthetic models of nature, prepared with regard to correlations among processes and events, become ever more appreciated among researchers. This is due to advances in geoinformation technologies and methods for visual and computer-aided processing of remote sensing data, as well as to the improved quality and resolution of satellite imagery. Digital landscape maps, along with the derived analytical maps, make up an integrated system and are easily comparable with one another. These sets of digital maps resemble regional atlases that were published in the 1960s and 1970s, but are much more informative and technologically efficient (Bozhilina and Ukraintseva 2010). The landscape indicator method has been largely applied to permafrost and engineering geology problems having been advantageous in mapping the composition, state, and properties of the ground (Melnikov, 1983, Melnikov & Grechishev 2002, Drozdov 2004, Rivkin 2005, Trofimov et al. 2007).

Codes for generalization and extrapolation of geological data are designed proceeding from correlations among elements of geological bodies and landscape systems of different hierarchy levels (global, regional, local, and elementary scales). To properly image these elements in map models, one has to be aware that measurements or observations are representative in different ways in terms of statistics, spatial distribution, and content of data (i.e., statistical samples are non-uniform).

The structure of map models depends on the goal and spatial coverage of the mapping. The four basic levels of landscape systems can be further divided according to local geology and landscape patterns (Drozdov 2004) or they can give way to matrix classification of landscape species (Rivkin 2005).

Digital landscape map modeling with this approach has been applied to several areas of Russia (Kansk-Achinsk Coal Basin [KATEK], Bovanenko and Urengoy gas-condensate deposits in West Siberia, etc.), and it yielded a set of analytical maps of geological and cryological properties of the landscape systems.

Digital landscape maps were made for the 1:7,500,000 Circumpolar Arctic Vegetation Map (CAVM 2003), as well

as for a set of small-scale subject maps of Arctic Russia (geological, permafrost, geochemical, biological-climatic, etc.) (Gravis et al. 2003). The ensemble of landscape maps constituting the National Atlas of Russia now includes the first map of potential activity of processes on permafrost landscapes. This activity is graded according to the percentage of landscape area that the processes can involve, with regard to the rates of the processes and their possible changes under natural effects (Tumel and Koroleva 2008).

Modern Facilities of Cartographic Analysis

The advance in computer-aided processing tools for spatial data has brought mapping up to a new level and made it possible to analyze landscape patterns comprehensively, using diverse indices of complexity, heterogeneity, and contrasts (Nikolaev 1979, Ivashutina & Nikolaev 1971, Gerenchuk & Topchiev 1970, Melnikov et al. 1983, Viktorov 1986). GIS technologies allow solving most complicated problems of cartography and give new life to old techniques of mathematical-statistical analysis of maps. A quantitative estimate of landscape heterogeneity and the degree of human-caused disturbance of landscapes is highly demanded information in many fields of economics that deal with nature management.

Thus the mathematical-statistical analysis of maps improves their scientific and practical values. A map becomes a synthetic 2D model of a natural object and, at the same time, a basis for further multipurpose studies.

Patterns of Permafrost-Related Landslides in Typical West Siberian Tundra

Through long-term (since 1978) engineering-permafrost studies in the Yamal and West Gydan peninsulas, we have found that the salinity of frozen ground and permafrost-related landslides collectively maintain the growth of willows (*Salix*) in typical tundra. *Salix* tundra spatially coincides with coastal facies of saline sediments from the surface while willow thickets are indicators of past landslide activity (Ukrainitseva 1997, 2008). These facts were used for reference in mapping landslides in typical tundra.

The territory of the Bovanenko gas and condensate field has been studied most exhaustively while mapping the landslide process in typical tundra of the West Yamal, using the landslide systems mapped at scales of 1:25,000 and 1:100,000. Tall willows serve as landscape indicators of landslides older than 300 years (Leibman & Kizuakov 2007). Pioneer meadow communities with patches of grass-free surfaces indicate present landslides (Ukrainitseva 2008). Salinization of coastal sediments in young landslides involves both frozen ground and active layer (seasonally thawing); salinity is rather high in above-permafrost waters and vegetation (Ukrainitseva 1997). Saline permafrost in old landslides lies 2–5 m below the ground surface; the sections are mostly desalinating (or desalinated according to Brushkov 2007).

As we found out by calculating the parameters of the landslide structure (Fig. 1), the extent of landslide slopes and permafrost with the saline surface layer is largest in the Upper Pleistocene hilly coastal plains affected by thermal

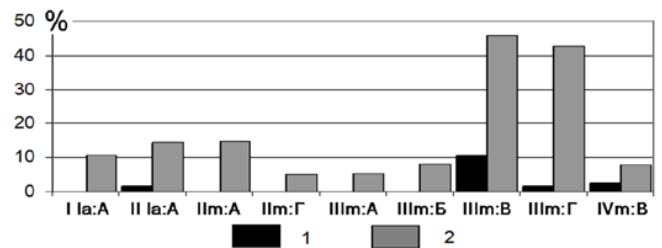


Figure 1. Percentages of young and old landslides in the structure of landscape zones and subzones (Bovanenko gas-condensate field). 1 – young landslides; 2 – old and prehistoric landslides. Landscapes of coastal (marine) terraces (IVm, III m, II m are, respectively, fourth, third, and second terraces). Landscapes of limnic-alluvial terraces (IIIa and IIa are second and first terraces, respectively). Landscape subzones: A – swampy (lakes and bogs); B – dry lakes (khasyrei); C, D – hilly: high (C) and low (D) hills.

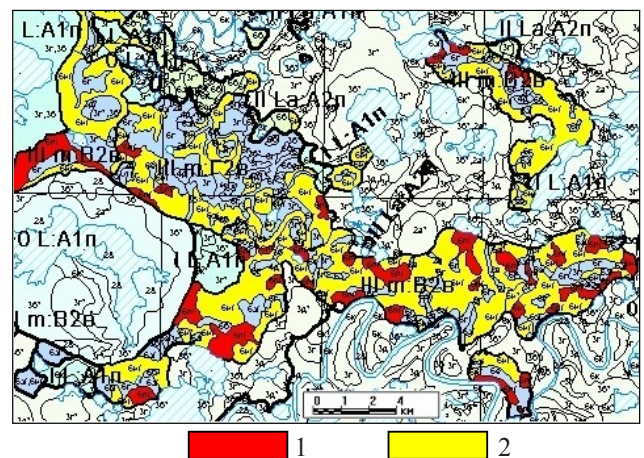


Figure 2. A section of the map of landslide slopes and depths of saline frozen sediments in Bovanenko field. Depth of saline frozen ground: 1 – saline from the surface, slopes with young landslides; 2 – saline from depths of 2–5 m, old landslide slopes overgrown with tall willows.

erosion (III m:V 47%). Young landslides are of much lower percentages than the old and prehistoric unstable slopes at each locality, and are absent from terrace levels I–II.

The results were used to map landslides of different ages and depths of saline permafrost in the Bovanenko field (Fig. 2).

The obtained data were extrapolated onto the entire typical tundra using the 1:1,000,000 Map of Geographical Landscapes of Northern West Siberia published in 1991. The mapped typical tundra includes eight landscape zones, each characterized by a morphological histogram showing the percentages of different subzones. The legend for the large-scale landscape map of the Bovanenko field was generalized and brought up to that of the published map, thus allowing the extrapolation of the data by landscape analogy.

Areas of landsliding cover more than 16% of the West Siberian typical tundra (Fig. 3). This is quite a high percentage given that landslides occur in most rugged elevated terrains. The sliding activity is the maximum (over 30% of the area) in the Central Yamal (12) and Western Gydan (14) areas of hilly topography consisting of permafrost silty clay and clay affected by thermal erosion and having salinity over 0.5% (Dubikov 2002). About 15–20% of the area belongs to landslide slopes within the West Yamal (11), Gydan Ridge

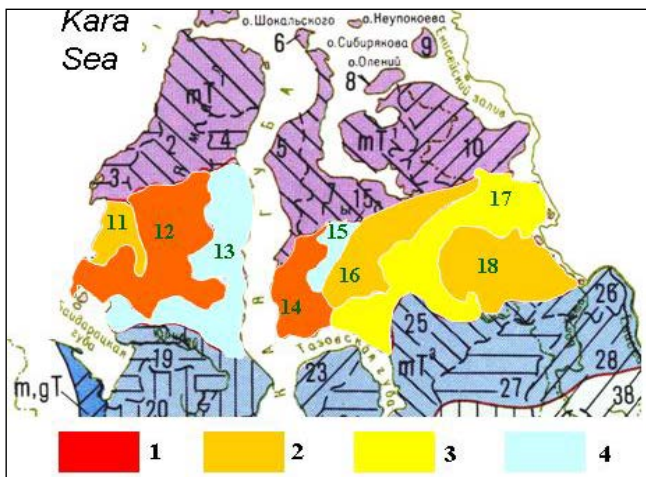


Figure 3. Landslide slopes in typical (subarctic) tundras. 1 – more than 30%; 2 – 15-30%; 3 – 5-15%; 4 – less than 5% Landslide areas: 11 – West Yamal; 12 – Central Yamal; 13 – East Yamal; 14 – West Gydan; 15 – North Gydan; 16 – Central Gydan; 17 – Antipayuta-Tanam; 18 – Tanam.

(16), and Tanam-Yenisei interfluvium (18) areas. These areas are as rugged as 12 and 14, where the activity is maximum, but ground there consists mostly of sand overlying saline marine sediments. The lowest percentages of landslide slopes are in swampy sandy lowlands with a developed river network (areas 13, 15, 17).

Landslide Maps and Permafrost Monitoring

Current subject mapping differs in availability of abundant precise numerical indices for objects and for monitoring work (Bozhilina & Ukraintseva 2010, Melnikov et al. 2009, Pavlov 2008, Malkova 2010).

Engineering-permafrost surveys have come into broad use for development of petroleum provinces in northern Russia. The respective maps are to image qualitative and quantitative parameters of soils, lithology, and hazardous surface processes (activity, surface area involved), and state (frozen or thawed). For frozen ground, these parameters are ice content, temperature, and active layer thickness (thaw depth). Many properties of soils change notably with time, especially because of climate trends. Their reliable imaging requires extensive databases and analysis of spatial and time series.

The question of setting up special monitoring sites to study the dynamics of near-surface permafrost arose in Russia as early as the 1920s and 1930s (Sumgin 1928). Continuous monitoring of ground temperature, dynamics of permafrost-related processes and slope stability has been ongoing for a few decades at several sites in the European Russian North and in West Siberia by the Earth Cryosphere Institute (Tyumen) (Moskalenko 2006, Drozdov et al. 2010, Malkova 2010, Vasiliev et al. 2008). The work has been internationally acknowledged and supported, technologically and financially, by several joint projects. Specifically, the project “Thermal State of Permafrost” (TSP) allowed resuming year-round temperature logging with the use of data loggers for recording and storage of data (Melnikov et al. 2009).

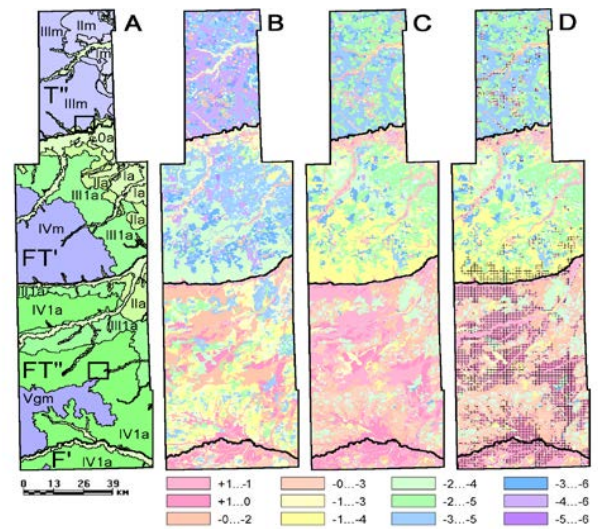


Figure 4. Natural permafrost temperature dynamics at Urengoy field (West Siberia). A: types of landscape systems; B, C, D: maps of ground temperatures for 1977 (B), 1997 (C), and 2005-2009 (D); hashed zone is area of deepening permafrost table; gray line contours northward advance of forest-tundra sparsely growing forests and potential areas of deepening permafrost table.

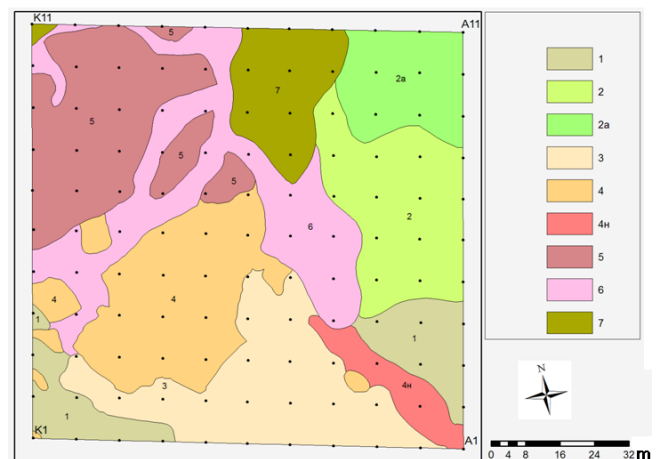


Figure 5. Landscape map of a CALM site in southern forest-tundra (UKPG -5). Landscape subzones (facies): 1 – hummocky moss tundra; 2 – sparse larch-lichen forests; 2a – same, with sag-and-swell topography; 3 – 5 – peatbogs: cloudberry-sphagnum (3), polygonal ledum-sphagnum-lichen (4), same, but disturbed areas (4d), polygonal dwarf-birch (yernik)-ledum-lichen (5); 6 – swampy gullies; 7 – gullies with dwarf birch thickets (yernik) (to 1.0–1.5 m high).

At the regional level, long-term permafrost monitoring data from the Urengoy gas and condensate field were used to compile a set of temperature maps for different time periods (Fig. 4) (Drozdov et al. 2010).

The permafrost temperature increased about 1°C over 20 years (1977 through 1997) and has stabilized in the past decade, while the permafrost table has been deepening over large areas. Therefore, the frozen ground has transcended its stability limit and an unfrozen layer (talik) is developing between the depths of 2 and 5–8 m. A 30–40 km northward advance of pre-tundra, sparse forests may create conditions for permafrost table deepening on watersheds of the northern forest-tundra (Fig. 4, D).

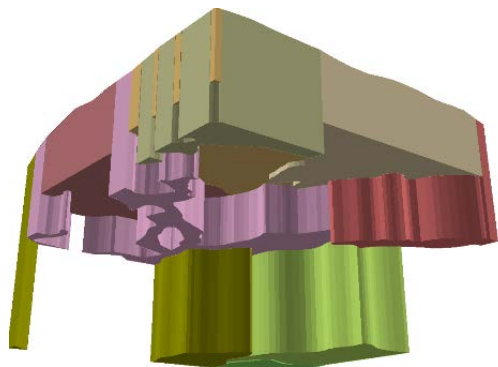


Figure 6. Thaw depths, averaged over landscape subzones, at a CALM site in southern forest-tundra (UKPG -5).

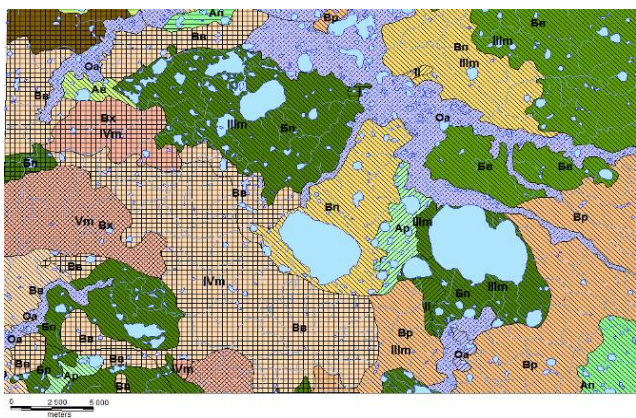


Figure 7. A section of the landscape map of typical tundra in West Yamal.

Since the mid-1990s, monitoring at special sites has been accomplished as part of the CALM (Circumpolar Active Layer Monitoring) international project. As an outcome of the project, landscapes have been classified (at the level of landscape subzones, Fig. 5) and mapped to scale 1:5000.

Maps of this kind can be used as a basis for estimating local variations in the active layer thickness (thaw depth). Spatial map models compiled with GIS tools demonstrate obvious linkage between landscape facies and active layer thicknesses (Fig. 6).

The Landscape Structure of West Yamal

The landscape patterns of the West Yamal territory have been studied in typical tundra using data of 1:100,000 landscape surveys for a proposed pipeline (by VSEGINGEO, St. Petersburg, 1978-1979). For this, the surface area percentages occupied by landscapes of different types and the structure of landscape areas were calculated using a GIS-derived map with vector layers according to landscape ranks (Fig. 7).

The study territory includes two landscape areas of wetland plains; one is less swampy with low hills and the other is more swampy with flat low hills (areas 12 and 13 in Fig. 3). Area 12 has a contrasting landscape pattern dominated by high coastal terraces (III m and IV m) with erosional (flat, gently sloping, and hilly) topography and a

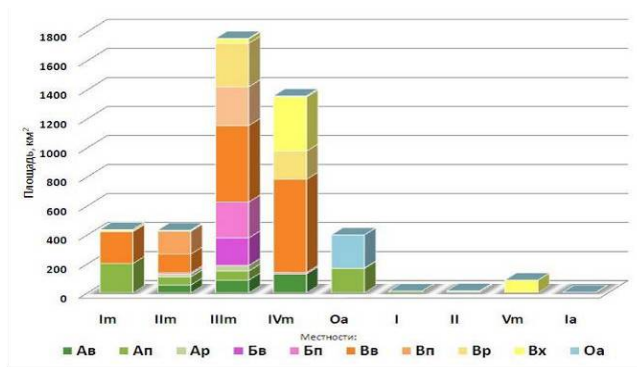


Figure 8. Landscape structure of area 12.

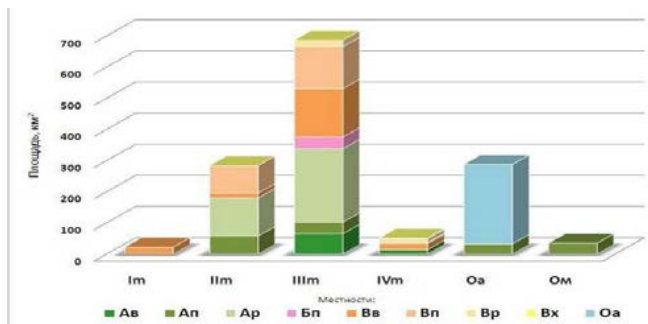


Figure 9. Landscape structure of area 12.

tree-like network of large and small gullies (Cf, Cp, Cu) that occupy up to 55% of the surface area (Fig. 8). Hilly terrains (Ch) cover 11%, and from 10% to 20% belong to areas of flat and undulated topography with lakes and bogs (Au, Af, Ap) and dry lakes (khasyrei) (Bf, Bu) in different landscapes. Large river valleys occupy about 5% of the territory.

Area 13 has a more uniform landscape pattern (Fig. 9) consisting mostly of coastal terraces III and II and large floodplains. The topography is flat or slightly undulated peatlands of lakes and bogs or lakes and kettles (Au, Af, Ap) which make up 44% of the area. Notably less widespread (35%) are eroded terrains with branching gully networks (Cf, Cp, Cu) and river valleys (19%).

Quantitative estimates of the landscape structure in West Yamal demonstrate a correlation between landscapes and terrain types and the diversity of landscape conditions. The coefficients of complexity of the landscape structure may be useful for planning the drilling programs and estimating total exploration costs in projected pipelines and other petroleum development structures.

Conclusions

Landscape maps as synthetic models of nature have been ever more broadly used as a contour and content basis for various GIS-derived maps, for both one-time and monitoring (continuously updated) uses. The landscape indicator approach turns out to be very efficient in map modeling of the state and properties of geological-ecological systems at the regional, local, and elementary levels of generalization.

Data of permafrost monitoring superimposed upon the landscape base maps highlights spatial-time permafrost temperature patterns at both regional and local scales.

The mathematical and statistical analysis of the maps further increases their scientific and practical value. Thus a map becomes a synthetic 2D model of a natural object and, at the same time, a basis for further multipurpose studies and multi-variant predictions.

Solving a regional-scale scientific problem with landscape map modeling can be illustrated by an example of permafrost-related landslides in the typical tundra of West Siberia mapped using local-scale landscape analysis in the Bovanenko gas and condensate field. The basic model we obtained allows predicting redistribution of unstable slopes prone to landsliding in the case of climate-induced changes of landscape boundaries.

Acknowledgements

This study was supported by grants 11-05-00544-a, 11-05-10084-k, 09-05-10030-k, 10-05-10027-k from the Russian Foundation for Basic Research; grant SS 5582.2012.5 from the Grant Council of the President of the Russian Federation; and NSF grants OPP-9732051 and OPP-0225603. It was carried out as part of integration programs of the Presidium of the RAS Siberian Branch, as well as international projects TSP and CALM, (USA). Additional logistic support was provided by *Gasprom Dobycha Urengoy* Ltd.

References

- Bozhilina, E.A. & Ukraintseva, N.G. 2010. Specialized field surveys for nature mapping. *Geodeziya i Kartografiya* 6: 36–41.
- Brushkov, A.V. 2007. Saline permafrost in the Arctic coast: origin and properties. In *Problems of Construction upon Saline Permafrost Soils*, Melnikov V.P. (ed.), Epokha, Moscow, pp. 4-33 (in Russian).
- CAVM Team 2003. Circumpolar Arctic Vegetation Map. Scale 1:7,500,000. *Conservation of Arctic Flora and Fauna (CAFF) Map No. 1*, U.S. Fish and Wildlife Service, Anchorage, Alaska. CAVM.
- Drozdov, D.S. 2004. *Information-Map Modeling of Natural and Technogenic Systems in Geocryology*. Author's Abstract, Ph.D. Thesis, Tyumen, 49 pp. (in Russian).
- Drozdov, D.S., Ukraintseva, N.G., Tsarev, A.M., & Chekrygina, S.N. 2010. Changes of permafrost temperature field and geosystem state on Urengoy oil-gas-field territory during the last 35 years (1974–2008) *Kriosfera Zemli* 14 (1): 22–31.
- Dubikov, G.I. 2002. *Composition and Structure of Permafrost in West Siberia*. GEOS Moscow, 246 pp. (in Russian).
- Gerenchuk, K.I. & Topchiev, A.G. 1970. Structure of natural systems: Information analysis. *Izv. AN SSSR, Ser. Geogr.* No. 6, 132-140.
- Gravis, G.F., Drozdov, D.S., Konchenko, L.A. et al. 2003. The use of the landscape base for subject maps of Arctic Russia. *Biogeografiya* 11: 48-52. Russian Geogr. Society, Moscow.
- Ivashutina, L.I. & Nikolaev, V.A. 1971. Contrasts in the landscape pattern and some aspects of their investigation. *Vestnik, Moscow University, Ser. 5, Geografiya* 5:70-77.
- Leibman, M.O. & Kizyakov, A.I. 2007. *Permafrost-Related Landslides in the Yamal and Yugor Peninsulas*. Institute of Earth Cryosphere, Moscow, 206 pp. (in Russian).
- Malkova, G.V. 2010. Mean annual ground temperature monitoring on the steady-state station “Bolvansky”. *Kriosfera Zemli* 14(3): 3–14.
- Melnikov E.S. & Grechischev S.E. (eds.). 2002. *Permafrost and Development of Petroleum Provinces*. GEOS, Moscow, 400 pp. (in Russian).
- Melnikov, E.S., Veisman, L.I., Moskalenko, N.G. et al. 1983. *Landscapes of the Permafrost Zone in the West Siberian Petroleum Province*. Nauka, Novosibirsk, 165 pp. (in Russian).
- Melnikov, V.P., Vasiliev, A.A., Drozdov, D.S. et al. 2009. Permafrost monitoring: the present-day state of the observation network in Russia; objectives and prospects for future. In *Book of Abstracts, Intern. Workshop on IPY Results*, 28 September 2009, Sochi. Sochi Science Center of the Russian Academy of Sciences, 85 pp.
- Moskalenko, N.G. 2006. *Anthropogenic Changes in Ecosystems of the West Siberian Petroleum Province*. Institute of Earth Cryosphere, Tyumen, 357 pp. (in Russian).
- Nikolaev, V.A. 1979. *Problems of Regional Landscape Studies*. Moscow University, Moscow, 160 pp. (in Russian).
- Pavlov, A.V. 2008. *Permafrost Monitoring*. GEO, Novosibirsk, 229 pp. (in Russian).
- Rivkin, F.M. 2005. GIS Modeling of Conditions for Pipelines in Permafrost. Author's Abstract, Ph.D. Thesis, Tyumen, 51 pp. (in Russian).
- Sungin, M.I. 1928. *Cryotic Soils in the USSR*. N.K.Z. Far East Geophysical Observatory, Vladivostok, 372 pp. (in Russian).
- Trofimov, V.T., Ziling, D.G., & Kharkina, M.A. 2007. Ecological-Geological Maps. Theoretical Background and Compiling Methods. Student's Manual. Vysshaya Shkola, Moscow, 407 pp. (in Russian).
- Tumel, N.V. & Koroleva, N.A. 2008. Permafrost-landscape differentiation of the Russian Permafrost Zone as a basis for geo-environment research. *Inzhinernaya Geologiya* 2: 11-14.
- Ukraintseva, N.G. 1997. Salix tundras of Yamal as an indicator of salination of near-surface sediments. In *Results of Basic Research of the Earth's Cryosphere in Arctic and Subarctic Areas*. Nauka, Novosibirsk, pp. 182-187 (in Russian).
- Ukraintseva, N.G. 2008. Vegetation response to landslide spreading and climate change in the West Siberian tundra. In *Proc., Ninth International Conference on Permafrost*, University of Alaska Fairbanks, June 29–July 3, 2: 1793-1798.
- Vasiliev, A.A., Drozdov, D.S., & Moskalenko, N.G. 2008. Permafrost temperature dynamics of West Siberia in context of climate changes. *Kriosfera Zemli* 12 (2): 10-18.
- Viktorov, A.S. 1998. *Landscape Mathematical Morphology*. Tratek, Moscow, 220 pp. (in Russian).

- Viktorov, S.V. 1966. *Indication of Geographic Studies for Engineering Geology*. Nedra, Moscow, 120 pp. (in Russian).
- Viktorov, A.S. 1986. *Landscape Pattern*. Mysl, Moscow, 179 pp. (in Russian).

The Role of Cryogenic Head in the Formation of Repetitive Wedge Ice and Long-Term Frost Heave

A.A. Urban

Melnikov Permafrost Institute, SB RAS, Yakutsk, Russia

Abstract

Development of cryogenic head assists in ice formation and leads to the occurrence of specific deformations of sedimentary layers in frozen ground. Processes and forms of cryogenic head have been studied insufficiently, with little experimental experience. Individual statements about the impact of cryogenic head on engineering structures do not provide substantial information on the development of conditions for horizontal pressure in frozen ground. In this paper, the traces of cryogenic head in the fluvial deposit stratum with repetitive wedge ice are described, and similar evidence is identified in the long-term frost heave section.

Keywords: cryogenic head; frost heave; hydrolaccolith; repetitive wedge ice.

Introduction

American researcher H.M. Eakin was the first to introduce the term “cryogenic head” into the literature (Eakin 1916). According to his definition, frost heave (mainly upward movement of mineral ground during freezing) should be differentiated from cryogenic head phenomena consisting mainly in the horizontal movement of the same ground. Although Eakin’s statement is arguable to some extent, it is important to take his distinction between cryogenic heave and cryogenic head into account while describing the composition and structure of frozen ground (Hopkins & Sigafos 1951).

Laba (1970) later used the word “head” to designate the expansion of thermal ice during temperature increase. He noted that such expansion also leads to the development of lateral strains. Nonetheless, according to Eakin’s definition, cryogenic head is an independent process associated with the pressure of freezing water in cooling ground.

Patterned ground systems have specific and regular correlations with wedge ice. According to the opinion of most researchers, the disturbance of the horizontal bedding of ground near the contacts with ice wedges is the result of deformation occurring in the frozen state due to the pressure of ice wedges as they expand in width (Dostovalov 1952, Popov 1952, Shumsky 1952). And many factors testify that deformations of organic-mineral ice deposits in the frozen state do occur.

It is known that the pressure created in the process of the growth of ice crystals is directed mostly at a right angle to the cooling ground isotherm (Taber 1929, 1930a, 1930b). Since Taber considered ground cooling as the process developing downward from the land surface, he emphasized the leading role of frost heave, not that of cryogenic head, in the formation of ice in the ground. However, Hamberg (1918) earlier noted the complex nature of the freezing of ground as heterogeneous material and to the probability of pressure development in different planes of the ground during ice formation.

In 1954–1955, V.O. Orlov studied the frost heave and cryogenic head processes at test sites of the Igarka Scientific and Research Permafrost Station. Orlov noted that the pressure created in the process of ground water freezing

“is capable of bending a significantly thick layer of frozen ground” (Orlov 1962). At the same time, Orlov concluded that vertical ground movement in such a bending zone is accompanied by “certain horizontal displacement of the frozen bed, with such displacement amplitude growing towards the ground surface.” The horizontal movement of freezing ground evidently occurs within frost heaves.

According to the data of the present author, deformation of layers by cryogenic head in freezing ground occurs in natural conditions. Such folding accompanied the accumulation of fluvial strata containing repetitive wedge ice and was associated with the formation of frost heaves in the Lena River delta.

Site Description

The study location of the freezing ground territory is in the north of Yakutia, in the area of the Lena River delta (Fig. 1). The area of the Lena River delta is about 29,000 km². This wide territory is subdivided into a relatively low eastern part where Holocene deposits are located, and a higher western part where a significant area is composed of Pleistocene ground (Korotaev 1965). The southwestern zone is represented by ancient island mountains with elevations exceeding 30 m.

The island structures are characterized by the presence of icy silt and clayey silt strata with multiple wedge ice bodies (ice veins) that have significant vertical height. By some researchers, such strata are called “edoma-type” deposits. Other researchers define them as “ice complexes.”

The ice-complex grounds are developed less widely in the northwestern zone of the Lena River delta. In this zone, sand

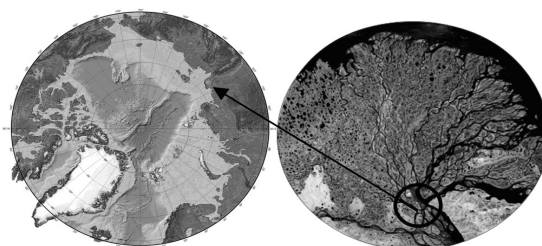


Figure 1. Location of research site.

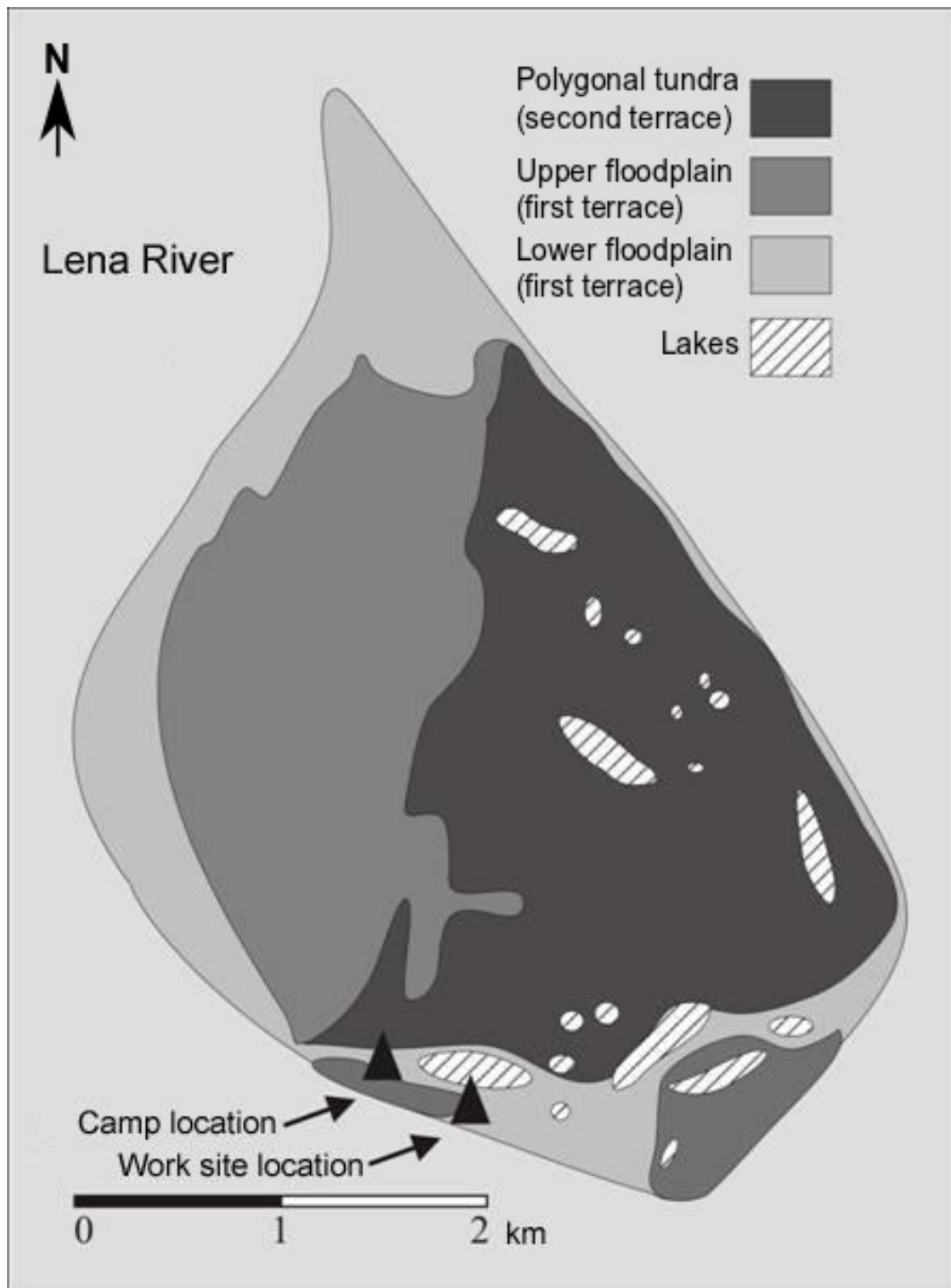


Figure 2. Samoylovskiy Island location.

islands with elevations below 30 m are frequently found (Grigorev 1993).

In the southwest of the Lena River delta where this terrace joins the Chekanovskiy Ridge slopes, the ice-complex deposits compose wide areas of the terrain of the third raised-floodplain terrace. Similar sites are found to the east on Sardakh, Sobo-Sise, and some other islands, and on the Bykovskiy Peninsula. The elevations of the edoma areas in the estuary part of the Lena River vary from 20 to 60 m, but most frequently are 35 to 45 m.

According to the data available, the annual mean air temperature in the Lena River delta is -12.7°C . The mean temperature of January is -30.5 and of July is 7.7°C . The

absolute temperature maximum reaches 32.7 and the absolute minimum -53°C . The daily mean air temperature remains negative up to 9 months per annum.

Annual precipitation in this region is 200 to 250 mm. More than half of the precipitation falls in the summer months (above 100 mm in July and August). A stable snow cover is formed in the second half of September and remains until the middle of June. Snow patches in valleys and on large ravine bottoms disappear only in July-August, and some of them do not melt during the entire summer (Samoylov 1952, Karotaev 1965, Grigorev 1966, Zalogin & Rodionov 1969).

Permafrost thickness ranges from 50 m in the area of Olenekskaya channel to 650 m in the Tiksi Village (Grigorev

Table 1. Lithological description of the outcrop.

Depth range, m	Brief description of ground
0.0-0.25.	Moss-grass cover
0.25-3.0.	Dark-brown, mossy, young, compact, and autochthonous peat with some sand. Woody remains are generally found in the cliff. Gray, medium-grained and silty sand inter-layers in the depth range of 0.5–0.75; 1.2–1.35; 2.0–2.1 m.
3.0-3.3.	Gray, medium-grained and silty sand with a dark-brown peat interlayer.
3.3-3.5.	Light-brown, medium-grained, peat-like sand with inclusions of almost undecomposed woody remains.
3.5-3.8.	Light-gray, medium-grained, peat-like sand with inclusions of woody remains.
3.8-4.0.	Yellow sand with organic admixture and inclusions of woody remains.
Below 4.0 m	Screes. Coast height 9 m.

1966). Permafrost thickness decreases significantly closer to the sea coastline. Both closed and continuous taliks are formed under large lakes and channels.

The permafrost temperature in the estuary part of the Lena River is one of the lowest, as compared to other estuary systems of the Arctic Basin. The permafrost temperature varies from -8 to -13°C at the depth of zero amplitude. The thickness of this zone under different landscape conditions is 10–20 m.

The ice complex is a stratified Late Pleistocene deposit with a complex structure that distinguishes the sections of the third raised-floodplain terrace. The thickness of these icy silts and clayey silts saturated with repetitive wedge ice reaches several tens of meters. Their structure is complicated with lenses of peat-like material and sands with different sized grains. Isolated pebble and gravel inclusions are locally present. The lower part of the thick ice wedges penetrates into the underlying deposits to depths up to 10 m. The ice complex is underlain by sandy, layered, and often thick (up to 7 m) peat-like horizons. The ice complex is sometimes overlapped by lenses of modern lacustrine, bog and eolian sediments, and floodplain deposits (Grigorev 1993).

The parameters of seasonal thawing at the third raised-floodplain terrace significantly vary depending on the degree of moisture content, the characteristics of vegetative cover, and the geomorphological location of the ground. For example, the thickness of the active layer observed in the beginning of September within boggy and peat-like sites ranges from 0.2 to 0.4 m. The thickness of the active layer within the drained surface not covered with vegetation is 0.5–0.7 m. Sometimes the lower boundary of the sandy seasonally thawed layer is traced to the depth of 1 m near the terrace edge and slopes. The depth of seasonal ground thawing in these terraces varies on average from 0.4 to 0.6 m.

Multiple frost-heaved areas are formed on the places of drained lakes and freezing taliks. Such heaves or hydrolaccoliths can be found, for instance, in the area of the Samoylovskiy Island.

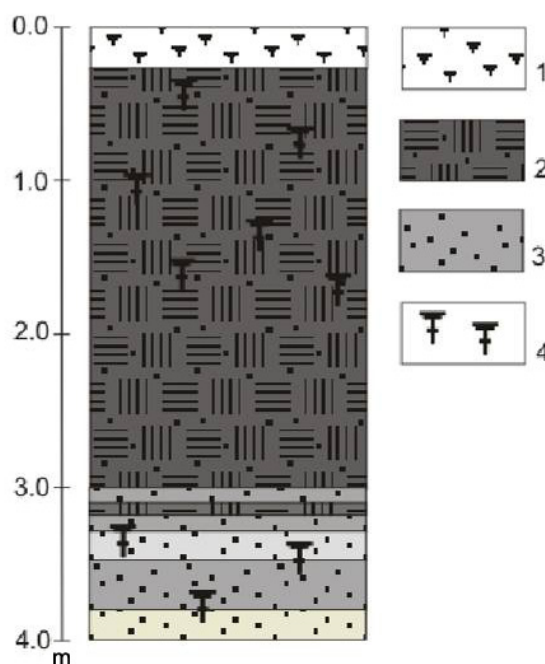


Figure 3. Lithological section of the outcrop 1 – top soil; 2 – peat; 3 – sand; 4 – woody remains.

Research Results

The Samoylovskiy Island area, where the studies were carried out, is located 120 km south of the Laptev Sea ($72^{\circ}22'\text{N}$, $126^{\circ}30'\text{E}$). The area of the island is 5.5–6 km², and low and high floodplain terraces are identified in its terrain. Quaternary freezing strata are present in the composition of both terraces. There are annually and periodically flooded zones within the first terrace (Fig. 2). The surface of the second terrace is composed of patterns varying in shape, size, and degree of moisture content.

According to the 1998 drilling data, the deposits of the second raised-floodplain terrace have peat-like composition in the upper part and silt-sand composition in the lower part of the exposed section. These deposits are characterized by significant ice content. The volumetric ice content of peat is above 80% and of silt about 60%. Moreover, silt and peat layers are characterized by the presence of repetitive wedge ice up to 10 m thick.

The temperature of these deposits at the depth of zero amplitude is -8.5°C . The depth of the active layer, depending on its moisture content, reaches 0.8 m in some places.

The composition and the structure of the ground were studied in the south of the island, along the Olenekskaya channel, observed in a steep coastal cliff along this channel. A description of the outcrop is given in Table 1. The lithological profile of this section is given in Figure 3.

The presence of finely plicated layers which host the repetitive wedge ice is a characteristic feature of this section. Figure 4 shows the whole upper part of the frozen section, bounded by quite wide ice wedges, as a zone of more or less plicated silt and sand peat-like deposits and of autochthonous peat layers.

The intersected block of frozen ground is bounded by formations of repetitive wedge ice. Their exposed vertical dimensions are 2.5 m to more than 5 m with a width of 1–2 m near the lower boundary of the active layer.



Figure 4. General view of the section showing deformation of layers of frozen deposits.

The layers of the host deposit are intensively bent upward along their contact with repetitive wedge ice. This is reflected in the tundra terrain with the formation of ridges above ice wedges. The height of ridges reaches 0.5 m.

In its central part, the section of frozen ground between the ice wedges is represented by less plicated peat and peat-like sandy inter-layers. Minor plication of these layers can be associated with the gradual reduction of cryogenic head outward from the ice wedge.

Layers of peat and peat-like deposits that host the repetitive wedge ice in the given section are mostly folded at the depth of 1–1.5 m. At the depth of approximately 3 m, such organic-mineral layers are bent upward at the edges of the sections of their massif. This shows how strong the strain was in the ground at contact with the growing ice wedges.

Discussion

It is known that repetitive wedge ice is formed by water filling frost cracks and then freezing. Frost cracks, in which this kind of ice is formed, develop as a result of strains caused by intensive cooling of the upper horizons of ground when these strains exceed the tensile strength of the ground. Water fills cracks in spring and summer. Later, new cracking occurs due to cooling the next winter, with ruptures formed in the ice since the ice is less strong than the frozen ground. A series of thin vertical, so-called elementary, ice veinlets joined to each other is formed due to the recurrence of ice cracking cycles and new water filling the cracks and then freezing. Therefore, each ice wedge grows as well as the whole wedge system, and an almost continuous ice network is formed. Cryogenic head develops with the growth of ice wedges. Volumetric strains emerge in the sedimentary stratum. Independent layers contacting the growing repetitive wedge ice are folded, and irregular plication of organic-mineral layers occurs together with the formation of ridges on the surface. Traces of these processes are observed in the observed frozen section.

Such folding of layers occurs also in the process of long-term formation of a frost heave with an ice core. The increase of ice core volume provides for the strained state in the host deposits. The impact of vertical strain shows itself

in the formation of frost heaves through the bending upward of overlying deposits. Horizontal strains lead to the folding of the layered deposits surrounding the heave.

The process of cryogenic head in a freezing mass of fine-grained deposits that contain a sufficiently high degree of moisture content presumably does not depend on the lithological composition of the deposit. Nonetheless, the finer the composition and the higher the ice content of the host deposit, the easier they are deformed. At the same time, it can be assumed that the morphological manifestation of this process is controlled by the strength of the freezing ground.

Researchers L.T. Roman and others found out that the compression strength of frozen young peat is higher than the strength of frozen clayey silt, clay, and pure ice. This is explained by the fact that frozen peat with significant ice content is similar to ice within plant remains (i.e., material with stronger cementing bonds than frozen clay, sand, and pure ice). The impact of ice and moisture content on the strength of frozen ground is very significant. Ground strength gradually increases with the increase of its ice content and the reduction of temperature.

Conclusions

- 1) Plication of layers is noted in the structure of frozen Holocene deposits that contain repetitive wedge ice in the area of Samoylovskiy Island in the Lena River delta.
- 2) The folding of layers is a phenomenon that accompanies the formation of ground ice. In the process of sedimentation with repetitive wedge ice, folding occurs mainly in the horizontal direction. While frost heave features with an ice core are formed, the plicated layers are localized in the top and slope sections of such heaves (hydrolaccoliths).
- 3) The deformation of layering during the formation of ground ice does not depend on the composition of the deposits. It is a result of the process of cryogenic head, which develops in these deposits.

References

- Cook, F.A. 1956. Additional notes on mud circles at resolute Bay, Northwest Territories: *Canadian Geographers* 8: 9–17.
- Corte, A.E. 1962a. The frost behavior of soils: laboratory and field data for a new concept II, Horizontal sorting: *US Army Corps of Engineers, Cold Regions Research and engineering Laboratory Research Rept.* 85 (20). 20 pp.
- Corte, A.E. 1962b. The frost behavior of soils II, Horizontal sorting pp. 44–46 in *Soil behavior associated with freezing Natl. Acad. Sci. Natl. Research Council Highway Research Board Bull.* 331, 115 pp.
- Dostovalov, B.N. 1952. On physical conditions of frost cracking and crack-like ice development in unconsolidated grounds. In *Permafrost research in the Republic of Yakutia*. Issue 3.M., Izd-vo AN SSS, pp. 162–194 (in Russian).
- Eakin, H.M. 1916. The Yukon Koyukuk region, Alaska: *US Geol. Survey Bull.*, 88 pp.

- Grigorev, M.N. 1993. *Cryomorphogenesis of the estuary part of the Lena River*. Yakutsk: In-t merzlotovedeniya SO RAN, 176 pp. (in Russian).
- Grigorev, N.F. 1966. *Permafrost in the Yakutia seacoast zone*. Moscow: Nauka, 180 pp. (in Russian).
- Hamberg, A. 1918. Zur Kenntniser der Vorgänge im erdboden beim gefrieren und Auftauen sowie bemerkungen über die erste Kristallisation des Eises in Wasser: *Geol. Fören. Stockholm, Förh.* 37: 583 – 619.
- Hopkins, D.M. & Sigafos, R.S. 1951. Frost action and vegetation patterns on Seward Peninsula, Alaska: *US Geol. Survey Bull.* 974-C. 51–100 pp.
- Korotayev, V.N. 1965. *Yakutia. Natural conditions and resources of the USSR*. Moscow: Nauka. - 468 pp. (in Russian).
- Laba, J.T. 1970. Lateral thrust in frozen granular soils caused by temperature change: pp. 27–37 in Highway Research Board, *Frost action: Bearing, thrust, stabilization, and compaction: Natl. Acad. Sci. Natl. Acad. Eng., Highway Research Record* 304, 51 pp.
- Orlov, V.O. 1962. *Cryogenic heave of very fine-grained grounds*. Izd-vo AN SSSR (in Russian).
- Popov, A.I. 1952. *Frost cracks and fossil ice problems*. “Trudy In-ta merzlotovedeniya AN SSSR”. Moscow, Izd-vo AN SSSR, 1952, Vol. IX, pp. 8–24 (in Russian).
- Samoylov, I.V. 1952. *River estuaries*. Moscow: Geografizdat. 527 pp. (in Russian).
- Schmid, Josef. 1955. *Der Bodenfrost als morphologischer Factor*; Heilderberg, DR Alfred Hüthig Verlag., 114 pp.
- Shumskiy, P.A. 1952. Fossil ice study in Central Yakutia. In *Permafrost research in the Republic of Yakutia*. Issue 3. Moscow, Izd-vo AN SSSR, pp. 142-161 (in Russian).
- Taber, S. 1929. Frost heaving. *J. Geol.* 37: 428-461.
- Taber, S. 1930a. The mechanism of frost heaving: *J. Geol.* 38:303-317.
- Taber, S. 1930b. Freezing and thawing of soils as factor in the destruction of road pavements: *Public Roads* 11: 113-132.
- Zalagin, B.S. & Rodionov, N.A. 1969. *Estuary zones of the USSR rivers*. Moscow: Mysl., 312 pp. (in Russian).

Large-Scale Mapping of Cryogenic Landscapes in the West Siberian Northern Taiga

E.V. Ustinova

Earth Cryosphere Institute, SB RAS, Tyumen, Russia,

Abstract

Cartographic monitoring is carried out in northern taiga within the Nadym site in natural conditions and along the gas pipeline. Thermokarst activation, frost heave, and water-logging occurred under the influence of anthropogenic disturbances. Deflation has started on drained areas composed of sand. Waterlogging zones emerged in bog areas adjacent to the pipeline. Assessment of the disturbed areas has shown that the initially disturbed natural system area increased by 22% due to the emergence of new lakelets. Using aerial photography images taken prior to the disturbance and at regular intervals thereafter, together with ground surveys conducted at the same time intervals, we created a series of geosystems maps of the investigated area. The series also includes the original geosystems map created in 1970, prior to construction of the gas pipeline. The series of maps shows undisturbed geosystems as well as geosystems exposed to disturbances after construction of the gas pipeline.

Keywords: climate; cryogenic processes; landscape; mapping; monitoring; permafrost.

Introduction

The problem of restoration and preservation of cryogenic landscapes modified under the influence of anthropogenic factors is becoming increasingly important due to progressing commercial development of the West Siberian North. Assessment and mapping of anthropogenic disturbances in permafrost regions is becoming of particular importance for land restoration. A number of researchers have studied this issue (Shamanova & Chekhovskiy 1975, Grigorev 1979, Melnikov et al. 1983, Grave et al. 1983, Sukhodolsky 1980, Nevecherya et al. 1985). Long-term cartographic monitoring of anthropogenic disturbances has, however, not been carried out. In this paper, the author has summarized the results of such monitoring, using the VSEGINGEO Institute and the Earth Cryosphere Institute SB RAS library materials, as well as personal field surveys. The results may be of interest to researchers and surveyors of the cryolithozone.

Study Area and Methodology

The research was carried out within the Nadym site situated 30 km south of Nadym (65°18'N, 72°51'E). The north-taiga landscapes of the Nadym Region of Tyumen Oblast are located in the Poluy-Nadym interfluvium in the northern taiga subzone, in the marginal part III of the lacustrine-alluvial plain.

The object of the research is geosystems of the Nadym site, located along the Nadym-Punga pipeline, where landscape and engineering-geocryological surveying of undisturbed geosystems was carried out in 1970. Later, the following actions were performed in order to assess anthropogenic disturbances: mapping of disturbed geosystems, stationary monitoring of vegetation cover, active layer thickness, soil moisture content, and ground temperature under the influence of climatic changes and anthropogenic disturbances.

Research Results

In order to examine the relationship and interaction of the geosystem components, three profiles were created near

the station. Along these profiles, facies and sub-landscape (tracts) were determined. Profile I-I at the 8th km of the pipeline passed through the peat-mineral frost mound and the mineral frost mound. The observations on the profile began in 1977, five years after the pipeline was put in the embankment. Profile II-II at the ninth km of the pipeline was set up on flat peatland. Profile III-III passes through a boggy hummocky area and through a pit. Observations that give insight into the development of natural processes that occur in the landscape were made while working on the profiles. The 1970 landscape map (Fig. 1) was based on the analysis of library materials. It distinguishes forest geosystems in unfrozen areas, boggy geosystems in newly formed permafrost areas, and peatland geosystems that contain permafrost with high ice content.

Fourteen types of facies were distinguished in the research area in 1970, before pipeline construction began. Dominating facies were represented by hummocky tundra areas with sedge-ledum-moss-lichen cover (tract 46, facie 100), hilly peatlands (tract 4a, facies 60, 61) and bogs (tracts 3a, 3b, 3c; facies 45, 46, 50) relating to a flat waterlogged plain surface (Fig. 1).

Hummocky tundra with a dwarf birch-ledum-moss-lichen cover (facie 100, 20.2%) and cloudberry-ledum-sphagnum lichen peatland (facie 61, 12.3%) occupied the largest area. Ridge-hollow bogs (tract 3b, facie 50, 8.9%) with an andromeda-sedge-sphagnum cover on the ridges and a cotton grass-sedge-hypnum cover on the hollows and a fen grass-moss bog (tract 3a, facie 45, 11.2%) occupied the largest area of the bog geosystems within the site.

The frost mound area was 13.4%; the mineral frost mounds, composed of sands from the surface, occupied only 1.4%. The lakes' total area did not exceed 1.5% in 1970.

The pipeline was placed in operation in 1972. The vegetation cover, thickness and moisture content of the active layer, and ground temperature have been continuously monitored since that year.

The creation of the Nadym-Punga pipeline system corridor had direct and indirect impacts on the adjacent areas. The highest levels of disturbances occurred during the pipe construction in 1971 and 1972 and pipe replacement

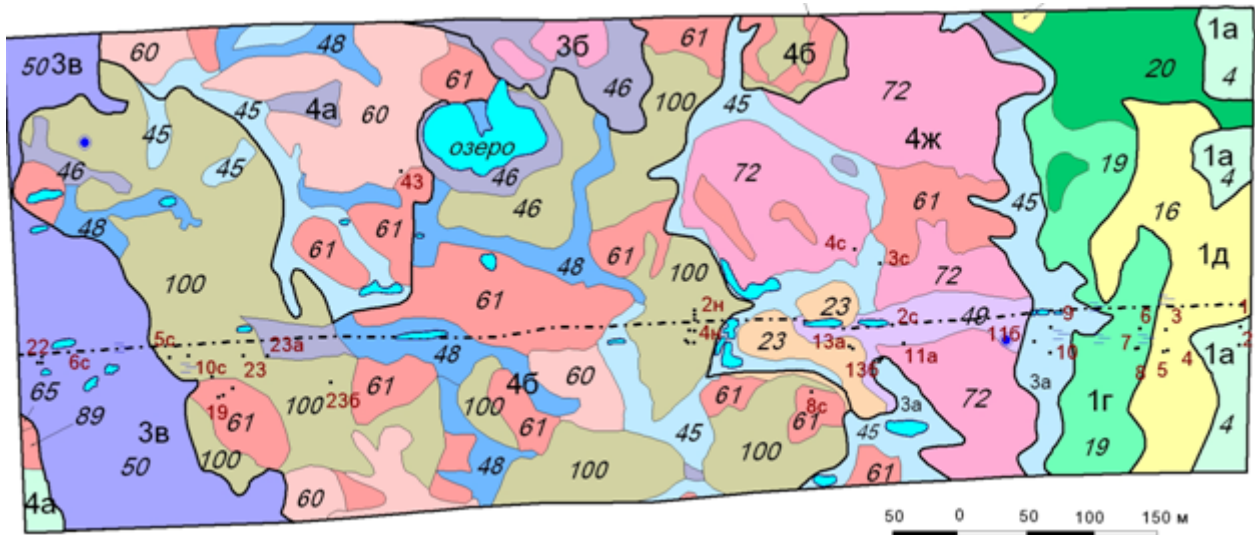


Figure 1. The 1970 landscape map (1, 2c – borehole numbers) 4-birch-pine-lingonberry-green moss-lichen light forest; 16-birch-pine-ledum-green moss-lichen light forest; 19-larch-ledum-sphagnum open forest; 20-larch ledum-lichen-sphagnum open forest; 23-frost mound with a ledum-moss-lichen cover; 45-fen grass-moss bog; 46-cotton-grass-sedge-sphagnum bog; 48- cotton-grass-sedge-sphagnum bog with with peatland elements; 49-shrub-sedge-sphagnum bog; 50- andromeda-sedge-moss bog; 60-cloudberry-ledum-sphagnum peatland; 61-cloudberry-ledum-sphagnum-lichen peatland; 72-cloudberry-dwarf birch-ledum-lichen-moss peat mound; 100-hummocky area with a dwarf birch-ledum-moss-lichen cover; l. – lakes.

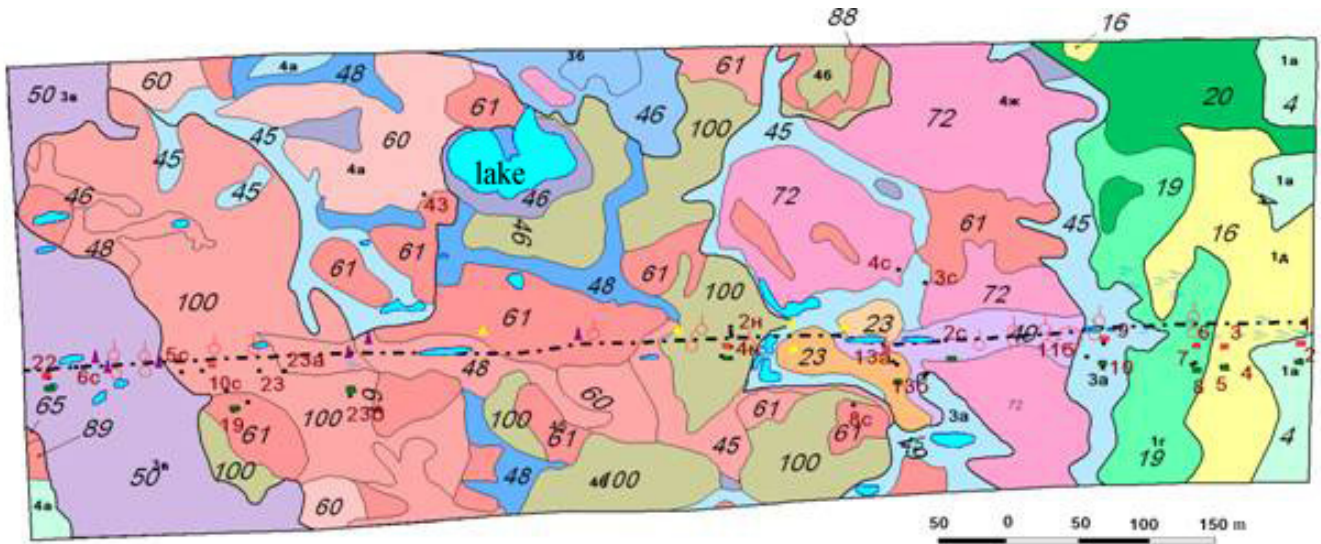


Figure 2. The 1979 landscape map. (1 – bogging, 2 - thermokarst, 3 – sheet erosion, 4 – erosion, 5 – observation sites: green - natural, red – disturbed, 6 – pipeline). For other notes see Figure 1.

in 2004. Lower levels of disturbances occurred during the power line construction in 1974 and embankment filling in 1983. The dirt road along the highway is filled annually.

Images from repeated aerial photography, performed prior to the disturbance and at regular intervals thereafter, as well as ground surveys conducted at the same time, allowed us to compose a series of landscape and engineering-geological maps of the pipeline route for several periods of time.

The areas occupied by sub-landscape (tract) rank ecosystems were calculated and tract distribution (in % of the total region area) histograms were created using the maps. The maps were used to distinguish dominant and subdominant tract types. The inventory of anthropogenic disturbances using aerial photography and field transect results for each facie were used for quantitative assessment of the landscape disturbances in the present geosystems condition. This was accomplished by calculating the area

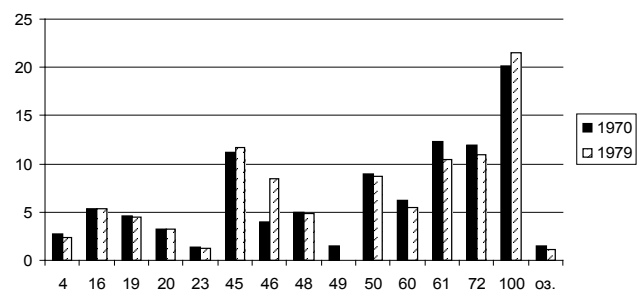


Figure 3. Facies proportion in 1970 and 1979.

disturbance coefficient (K_n), which is defined by the ratio of the disturbed area (S_n) to the total area for each landscape type (S): $K_n = S_n / S$ [2].

By comparing the 1970 and 1979 facies (using Figs. 1 and 2, histograms of Fig. 3), we can see that the area of cotton



Figure 4. The 1988 landscape map. Anthropogenic disturbances (*the numbers to the right of indexes*): 1 - partial vegetation destruction as a result of a single transport passage; 2 - the severe vegetation destruction, microrelief and top soil disturbance as a result of multiple transport passages; 3 - vegetation removal, microrelief disturbance, 4 - vegetation burial and destruction, drain disturbance as a result of removed vegetation gully formation; 7 - vegetation and soil destruction, relief disturbance as a result of constructing quarries; 8 - removal of vegetation and peat layer with the thickness of 0.3-1m.; 9 - vegetation burial and destruction, microrelief drainage disturbance as a result of causeway construction.

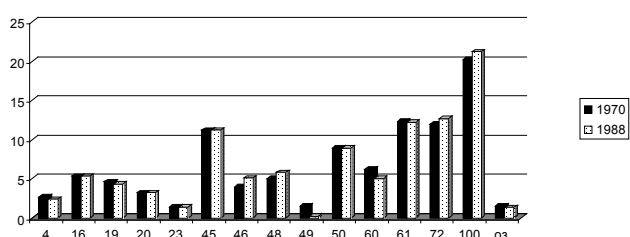


Figure 5. Facies proportion in 1970 and 1988. For legend see Figure 1.

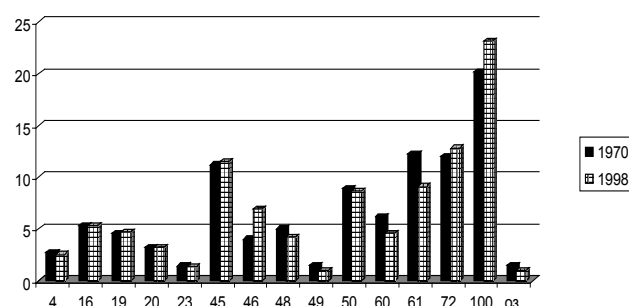


Figure 6. Facies proportion in 1970 and 1988.

grass-sedge-sphagnum bogs increased from 4% to 8.5% due to anthropogenic disturbances (facie 46). On the contrary, the peatland area decreased from 12.3% to 10.4%. The frost peat mound area decreased from 12% to 10.9% because a road was laid through profile I-I and a part of the mound was destroyed.

By comparing the 1988 map (18 years after pipeline construction) (Fig. 4) with the original 1970 map (Fig. 1) and the histogram (Fig. 5), we can see the bog geosystems area grew at the expense of forest geosystems as a result of progressive bogging. The construction of a dirt road in place of the former winter road led to the growth of disturbed areas due to the emergence of new pits, part of which were filled with water. It also led to waterlogging in bog geosystems as a result of drainage disturbance caused by the road. This led to the emergence of new lakelets. The lake by the pipeline was bogged and its area decreased. Small mounds and frost heave areas, up to 1 m in height, emerged at some places of undisturbed bog geosystems.

The embankment earthworks were conducted in 1983. From 1984 to 2004, the restoration of landscapes was observed. By comparing the 1970 and 1998 landscape maps

(Figs. 1, 7) and the histogram (Fig. 6), we can observe the pipeline's influence. Road construction, transport passing through, and power line construction have negative impacts on the permafrost landscapes because linear structures prevent the movement of surface and seepage waters.

Pipeline maintenance and pipe replacement were performed in 2004. According to the data of the repeated large-scale survey (2004–2006), the width of the disturbance area of the natural environment along the I line track of the Nadym-Punga pipeline in the north taiga of West Siberia changed from 40 to 100 m. Analyzing the histogram (Fig. 8) and the map (Fig. 9), we can see the sphagnum bog area increased and the peatland area decreased. This means that the bogging process was in progress.

Analyzing the histogram for all years, starting with 1970 (Fig. 10), it can be concluded that the original spatial geosystems structure did not restore. According to the author's data and the research by O.E. Ponomareva (Anthropogenic Changes 2006), the removal of vegetation cover on flat undrained or partially drained areas led to increased bogging. Peat-moss bogs appeared in these regions. They stay in place under the changed conditions for an infinitely long period of time.

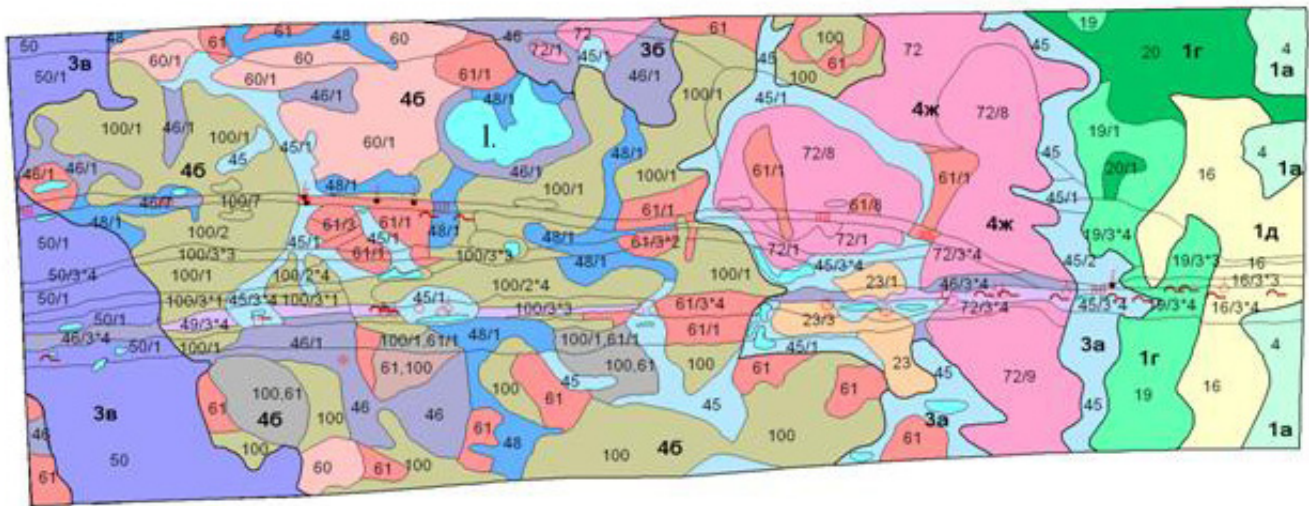


Figure 7. The 1998 landscape map.

The studied geosystems represent specific natural bodies called permafrost landscapes, which are formed, developed, and function under the influence of cryogenic factors. The heat exchange changes due to disturbance of surface moss-peat cover lead to changes in the thermal condition of permafrost landscapes (evaporation changes by 1.5–2.5 times, radiation balance by 5–15%, average annual soil temperatures by 0.7–2°C, seasonal thawing depth by 2–4 times), which leads to the development of cryogenic processes (Anthropogenic Ecosystems Changes... 2006).

The intensity of anthropogenic disturbances on ground thermal conditions is much greater than disturbances caused by climatic changes.

Permafrost landscapes are less resistant to anthropogenic exposures. Irreversible changes including complete deterioration of the original landscape may occur. In that case, a new ecosystem with a different set of components is then formed in its place. For example, a bog is formed in place of a forest or a thermokarst lake appears in an area that was occupied by a tundra ecosystem before the disturbance.

Mapping assessment allowed us to compare the disturbance areas for different years and trace the increase in semi-sustainable geosystem disturbance area width (e.g., in hummocky bogs from 30 to 65 m). Widening of the disturbance area is also associated with the influence of waterlogging as well as the development of thermokarst and bogging in initially undisturbed ecosystems adjacent to the highway. This is due to a change in the surface and ground water drainage conditions. Counting of the disturbed areas has shown that the highest level of disturbances occurred in 2004–2006 during the replacement of pipeline pipes. The area of initially disturbed ecosystems increased by 22% due to the emergence of new lakelets.

Areas where vegetation was completely removed, where the microrelief was disturbed and the upper peat horizon with thickness up to 0.2 m was removed as well, predominate. These regions occupy up to 30–50% of the investigated area. Regions disturbed by track transportation occupy smaller areas (20–30%). The vegetation, soil cover, and microrelief were only partly disturbed there. Areas with other kinds of disturbance (vegetation cover burial and destruction as a result of removed vegetation bulk formation) did not exceed 15%.

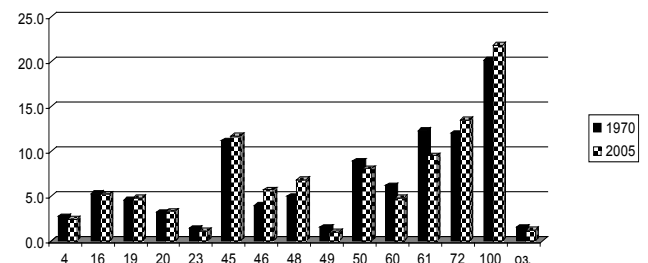


Figure 8. Facies proportion in 1970 and 2005.

By comparing the facies and disturbed area histograms of different years, it can be concluded that bogs are disturbed to the greatest extent. Peat bogs occupy 14% of the total area, and 12% of their area is disturbed. Moreover, regions of indirect anthropogenic influence on adjacent landscapes were found. Embankment filling along the pipeline led to an increase in disturbed areas and waterlogging of bog geosystems. This results in drainage disturbance and, consequently, it all leads to the emergence of new lakes.

The analysis of different time slice maps allowed us to trace the changes in anthropogenic disturbance areas and the tendencies of development of ecosystems under the influence of climatic changes and disturbance. The width of the disturbed area increased in semi-sustainable ecosystems (e.g., twice in hummocky regions).

Conclusions

The long-term landscape and engineering geological surveys (1970–2011) performed along the Nadym-Punga pipeline allowed us to trace land cover changes due to linear construction. Severe technogenic pressure in a sensitive permafrost environment leads to irreversible changes of geosystems. Anthropogenic disturbances, depending on the timing, intensity and environmental conditions, cause a variable degree of geosystem deterioration.

A classification and inventory of anthropogenic disturbances related to pipeline construction and maintenance have been developed. The created landscape map reflects the current condition of geosystems.

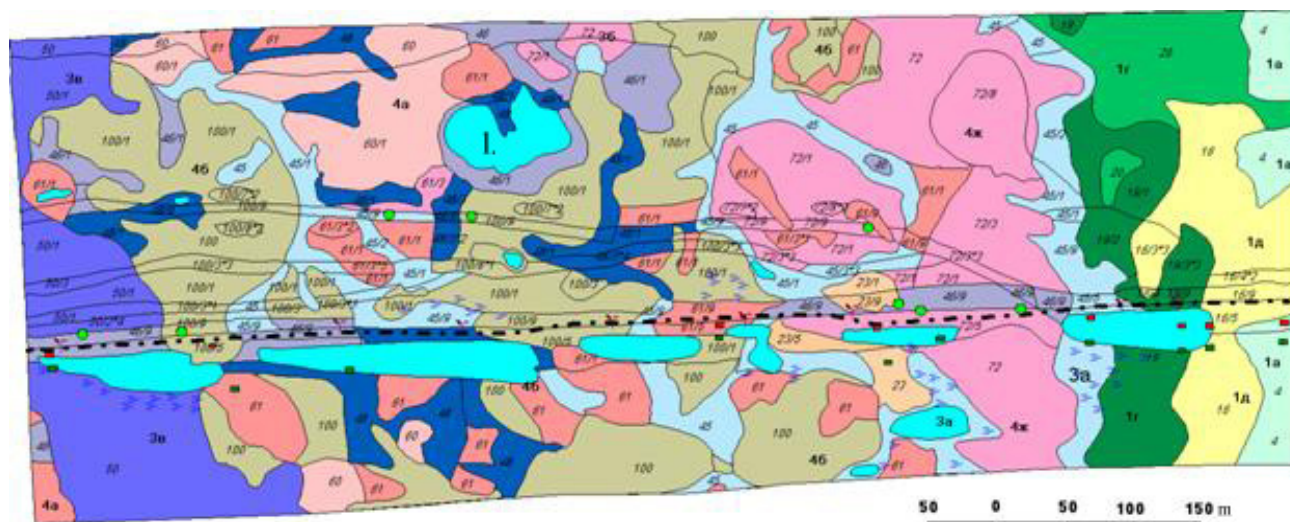


Figure 9. The 2005 landscape map.

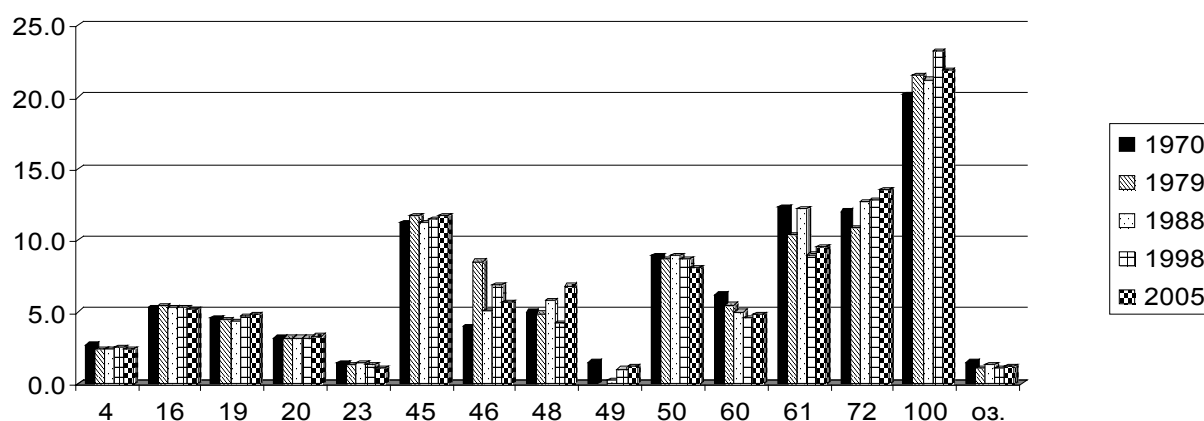


Figure 10. Facies proportion by years.

Surveys show that the landscapes along the Nadym–Punga pipeline suffered multiple anthropogenic exposures, and the geosystems have not been restored to their initial conditions in the last 40 years.

References

- Anthropogenic Changes in Ecosystems of the West Siberian Gas Province*. 2006. Ed. by N.G. Moskalenko. Moscow: RASHN, IKZ SO RAN, 358 pp. (in Russian).
- Grave, N.A., Melnikov, E.S., & Moskalenko, N.G. 1983. Geocryological issues of landscape protection in cryolithozone oil and gas bearing regions exploration. *Vestnik MGU: Geography Series 4*: 36-41 (in Russian).
- Grigorev, N.F. 1979. *Anthropogenic Permafrost Landscapes Formation in Northern Parts of Tyumen Oblast*. Novosibirsk: Nauka: 35-44 (in Russian).
- Melnikov, E.S., Veysman, L.I., Moskalenko, N.G. et al. 1983. *Cryolithozone Landscapes in the West Siberian Gas Province*. Novosibirsk: Nauka, 163 pp. (in Russian).
- Nevecherya, V.L., Ivlev, A.Yu., Ryzhova, V.M., & Kotlova, E.V. 1985. Repeated engineering-geological survey as an engineering-geocryological condition sustainability evaluation methodology in natural gas deposits exploration in the West Siberian North. *Issues in Environmental Protection in Oil and Gas Industry*. Moscow: 69-71 (in Russian).
- Shamanova, I.I. & Chekhovsky, A.L. 1975. The engineering-geological demarcation scheme of the West Siberiantundra zone during the surveys for linear construction. *Geocryological Research in Engineering Survey*. Moscow: Stroyizdat: 31-39 (in Russian).
- Sukhodolsky, S.E. 1980. Natural environment disturbances and their consequences during the linear structures construction in the West Siberian North. *Issues in Environmental Protection in Permafrost Exploration*. Moscow: Nauka: 67-71 (in Russian).

Thermal State of the Upper Horizons of the Permafrost in Central Yakutia

S.P. Varlamov, Yu.B. Skachkov, P.N. Skryabin, N.I. Shender
Melnikov Permafrost Institute, SB RAS, Yakutsk, Russia

Abstract

Studies of the ground thermal state were conducted to evaluate the impact of modern climate warming on the permafrost of Central Yakutia. The long-term analysis of data from weather stations in the region clearly shows a trend of increasing annual mean air temperature, the highest of which is in the north of Russia. The forecast of surface air temperature change was made using the harmonic analysis method. Monitoring of the ground thermal regime under natural conditions has been conducted by the authors since the 1980s in seven physiographic districts on the left and right banks of the Lena River at the Yakutsk latitude. This provides for the identification of long-term dynamics within a wide range of natural conditions. Test studies allowed us to identify the long-term dynamics of the ground thermal state evolution indicators: ground temperature at the base of the active layer and at the depth of zero annual amplitude as well as the active layer depth. The snow accumulation regime is the main determining factor in the formation of the ground thermal state. The long-term variability trends for the active layer depth in the shallow-valley locality type vary from close to zero to low positive values. Low negative trends prevail at the slope locality. During the previous two years, anomalously low-snow winters with late snow cover formation led to intensive ground cooling despite anomalously warm winter and summer seasons. The thermal state of the upper permafrost horizons remains quite stable considering the background of significant climate warming.

Keywords: active layer; climate; monitoring; permafrost; temperature; trends.

Introduction

In recent decades, interest in the problems of permafrost response to predicted climate warming has grown due to the development of modern climate change studies in many countries. The studies cover a wide range of tasks including the evolution of the thermal state of the upper horizons of permafrost. This has become one of the priority subjects in geocryological studies with important scientific and practical value.

The data of weather stations, geocryological stations, and monitoring test facilities, as well as regional and engineering-geocryological investigations, serve as the basis of information for research on the thermal state of the upper horizons of permafrost and for predicting and evaluating changes in permafrost under the expected climate warming.

Problem and Methodology

In Central Yakutia, systematic temperature monitoring in boreholes up to 10–15 m deep has been carried out since 1935 at the permafrost station of the General Branch of the Northern Sea Route. The studies have revealed peculiarities in ground temperature and changes in the active layer under the impact of vegetative and snow covers, the “cultural layer,” and the geological and geomorphological conditions (Melnikov 1950, Solov'ev 1959). In the 1940s, year-round experimental monitoring of the change of the ground thermal regime by removal of the insulation of snow and grass covers and under natural conditions was organized at pilot sites of the Yakutia Scientific and Research Permafrost Station (Shimanovskii 1942, Gerasimov 1950, Efimov 1952). In the 1950s and 1960s, more detailed and comprehensive thermophysical monitoring of the formation of the ground thermal regime was organized according to the improved method at the pilot site of the Permafrost Institute under the guidance of N.S. Ivanov (1963).

In Central Yakutia, local and regional regularities in the formation of the ground thermal regime are defined in most detail with the extensive use of research station methods (Are 1973, Gavrilova 1978). In the 1960s to 1980s, year-round research of the thermal balance was carried out at the Yakutsk, the Syrdakh, the Zeleny Lug, and the Chabyda stations according to a significantly extended program (Pavlov 1975, Pavlov 1979, Skryabin et al. 1998, Varlamov et al. 2002). The studies covered both natural and technogenic landscapes. Daily, seasonal, and annual processes of surface thermal exchange with the atmosphere were thoroughly studied. A series of new mathematical ground freezing and thawing models was developed. The studies of the hydrothermal permafrost regime in conditions of agricultural development and amelioration were carried out in the 1960s to 1980s at the Khatassy, Khorobot, and Amga seasonal stations (Gavriliev et al. 1984, Ugarov & Mandarov 2000).

Today the monitoring studies of the ground thermal regime are conducted at the Chabyda and the Yakutsk stations as well as at test facilities at the northern part of the Tommot-Yakutsk railway route, and at the Yukechi, the Umaybyt, the Kerdyugen, and other facilities. The depth interval of the seasonal ground temperature variations is the research target (depth 10–20 m). The main thermal parameters include active layer depth (ζ), the mean annual temperature at the base of the active layer (T_{ζ}), and the mean annual temperature at 10 m depth (T_{10}).

The 1990s experimental regime studies at the Spasskaya Pad and the Neleger stations were initiated within the international GEMX-GAME, CREST, and JST programs of the joint Russian-Japanese and Russian-Dutch scientific projects. The purpose of the research was to study the long-term temperature dynamics of the ground and upper permafrost horizons, the ground moisture regime, the active layer depth, the water-heat balance, and carbon in stream flows (Fedorov et al. 2006).

Pavlov (2008) summarized the results of the research on the thermal state evolution of the upper permafrost on the territory of Russia for the period between the 3rd International Geophysical Year (1957/59) and the 4th International Polar Year (2007/08). Romanovsky et al. (2010) evaluated the thermal state of the Russian cryolithozone for the recent 20–30 years, but Central Yakutia was not included in the review. This work will fill this gap to some extent.

Modern Climate Change

Forecasts of air temperature change in the twenty-first century are varied. The climate change forecast prepared by the Voeykov Main Geophysical Observatory (MGO) based on extrapolation of climatic characteristics shows that the observed warming trend in Russia will continue in 2010–2015. MGO predicts that mean annual surface air temperature will increase by 0.4–0.8°C compared to 2000, and by 1.5°C in 2030. A further increase of the mean precipitation amount, mainly due to its increase during the cold period, is predicted as well. An increase of winter precipitation of 7 to 9% and an increase of snow accumulations of 2 to 4% are expected in the north of Eastern Siberia (Federal Service... 2005). At the end of the twenty-first century, a surface annual mean air temperature increase of 4–8°C is expected as compared to the mean values of the last two decades of the twentieth century (Meleshko et al. 2008). The forecast of the surface mean annual air temperature changes in Yakutsk prepared in the RAS SB Permafrost Institute with the help of the harmonic analysis method nearly coincides with the forecast of the Main Geophysical Observatory until 2015 and then deviates from it (Shender et al. 1999, Romanovsky et al. 2007). The authors predict a cooling trend of 2–3°C by the middle of the twenty-first century. The researchers are specifically concerned about the predicted increase of winter precipitation quantity and the increase of snow accumulations, which together play a significant role in ground temperature increase.

Results and Discussion

Monitoring of the ground thermal regime under natural conditions conducted by the authors starting in the 1980s in seven physiographical districts on the left and the right banks of the Lena River at the latitude of Yakutsk allows the identification of its long-term dynamics within a wide range of natural conditions (Fig. 1). The value of the long-term monitoring also consists in the formation of a data bank required for model forecasts of possible state changes of permafrost in the case of climate warming. Monitoring points (boreholes and sites) were organized at more than 100 elementary landscape complexes covering nine types of localities with 42 lithogenic variations (Table 1).

The most detailed and long-term monitoring of the ground thermal regime was conducted at the Chabyda station located 20 km south of Yakutsk, near Malaya Chabyda Lake. Here the terrain is characterized by a combination of depressed and uplifted zones of the hilly-knappy plain. The experimental studies were organized in two locality types: shallow-valley, bottom of a creek valley (Sites S-3a, S-8a, Borehole B-1) and at a flow hollow (Site S-8); slope, at a flat slope (Sites

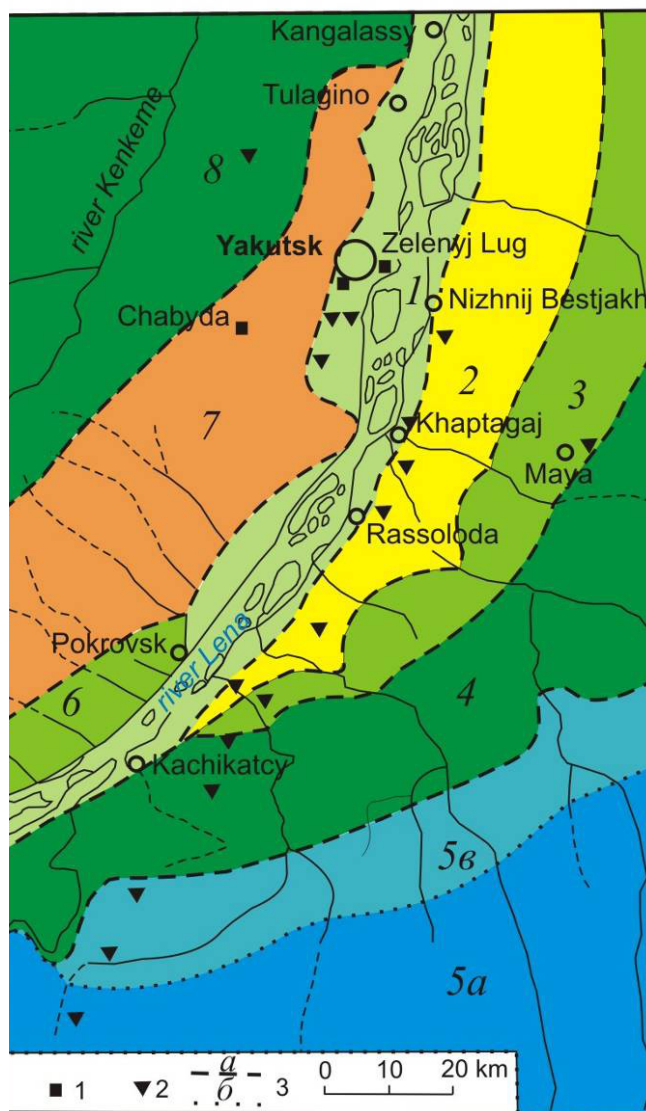


Figure 1. Research area map. 1 – stations; 2 – test facilities (“polygons”); 3 – boundary of physiographic districts (a) and subdistricts (b); 4 – Prilenskiy valley-forest steppe; 5 – Bestyakh sand-ridge; 6 – Tyungyulyun alas; 7 – Lena-Amga alas-valley; 8 – Lena-Amga sandstone (subdistricts: a – sandstone, b – transient of the polygenetic plain); 9 – Prilenskiy left-bank shallow valley-alas; 10 – Prilenskiy left-bank sandstone; 11 – Kenkeme-Lena shallow valley-alas.

S-5, S-6b), at a near-watershed slope (Sites S-7b and S-9) at moderately steep slopes of the northern (Site S-10) and the southern (Site S-11) exposures. The active layer depth in the research area varies from 0.37 to 4.11 m depending on the landscape conditions. The annual mean temperature at the bottom of the active layer varies from 0 to -7.4°C and at the bottom of the annual heat-turn layer from -0.2 to -4.9°C.

Table 2 illustrates the active layer depth and annual mean ground temperature variability.

The 29-year cycle of monitoring the ground thermal state showed that the active layer thickness remains quite stable (Fig. 3) even under the background of a significant increase of the annual mean air temperature (Fig. 2). Significant inter-seasonal changes of the active layer depth are typical of the ground of the shallow-valley locality type. The trend of its increase is noted here, and some reduction is observed in the slope locality type. In the shallow-valley locality type, the

Table 1. Monitoring at test sites in different landscape complexes.

Site	Type of locality	Physiographic District	Beginning of monitoring		
Chabyda	Shallow-valley	Prilenskiy sandstone	1980		
	Slope				
Zeleny Lug	Floodplain	Prilenskiy valley-forest steppe	1986		
Khaptagay, Kerdem			1988		
Yakutsk	Low-terrace		1995		
13th km, Shestakovka			1986		
Khaptagay, Kerdem			1988		
Tamma-Mendin, Lower Bestyakh	Sand-ridge	Bestyakh sand-ridge	1987		
	Inter-ridge-lowland		1993		
Tamma	Shallow-valley		1987		
Mundulakh	Inter-alas	Tyungyulyun alas	1993		
	Alas				
Buluus	Sand-ridge			1987	
	Inter-ridge-lowland				
Taryng	Inter-alas		Lena-Amga alas-valley	1987	
	Alas				
Byldyaana	Inter-alas				
	Alas				
Kirim	Inter-alas				1995
	Shallow-valley				
Verkhnyaya Lyutenga	Upland	Lena-Amga sandstone			1995
	Slope				
	Shallow-valley				
Magan	Inter-alas	Lena-Kemkeme alas	2002		

Table 2. Long-term mean and extreme values of the main thermal parameters for ground of the layer with seasonal temperature variations (Chabyda).

No Sites	Years of Monitoring	ξ , m			T_{ξ} , °C			T_{10} , °C		
		Min	Mean	Max	Min	Mean	Max	Min	Mean	Max
Shallow-valley type of locality										
B-1	1981-2010	0.81	1.07	1.30	-5.1	-2.7	-0.6	-3.4	-2.7	-1.8
S-3a	1986-2010	0.37	0.44	0.53	-7.4	-4.9	-1.3	-4.9	-3.9	-2.8
S-8	1982-2010	0.86	1.16	1.37	-5.5	-3.5	-1.3	-3.3	-2.7	-1.9
S-8a	1986-2010	0.65	1.05	1.45	-6.5	-3.6	-0.1	-4.5	-3.5	-1.8
Slope type of locality										
S-5	1981-2010	3.37	3.55	3.86	-1.0	-0.4	-0.1	-0.6	-0.4	-0.3
S-6b	1986-2010	3.54	3.85	4.11	-0.9	-0.4	0.0	-0.6	-0.4	-0.2
S-7b	1986-2010	1.70	1.86	2.00	-2.2	-1.2	-0.4	-1.5	-1.0	-0.3
S-9	1985-2010	1.31	1.52	1.72	-3.6	-2.4	-1.0	-2.5	-2.2	-1.8
S-10	1986-2010	1.63	1.91	2.11	-2.8	-1.8	-0.7	-2.4	-2.0	-1.6
S-11	1986-2010	1.73	1.92	2.27	-2.2	-0.9	-0.2	-1.5	-1.2	-0.9

particularly pronounced increase of the active layer depth is observed between 2002 and 2008. This is associated with soil moisture increase in the active layer. Subsequently, the raising of the upper boundary of permafrost was noted here.

In the shallow-valley locality type, the long-term active

layer depth variability trends vary from close to 0 to positive (0.4 cm/yr) values. Negative trends are observed, on the contrary, in the slope locality type (-0.1 to -1.9 cm/yr). The slopes of the northern exposition (Site 10), where the positive trend (0.6 cm/yr) is observed, are the only exceptions.

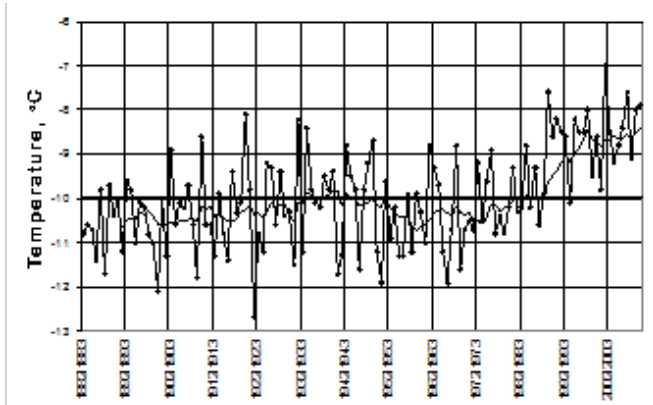


Figure 2. Change of the mean annual air temperature in Yakutsk. Bold line –10-year moving mean, straight bold line - long-term mean.

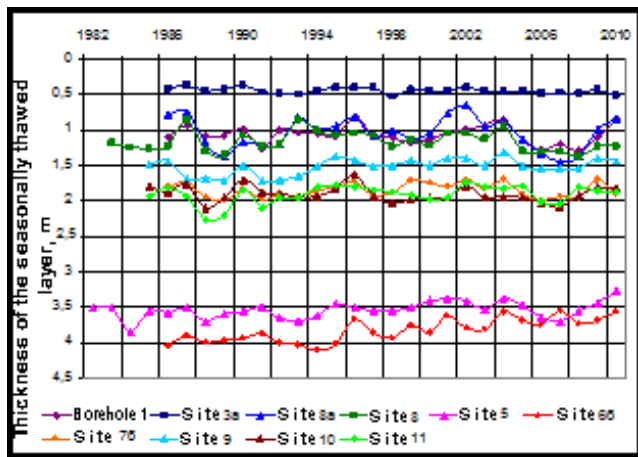


Figure 3. Long-term change of the active layer thickness in various landscape conditions.

The lowest ground temperatures are typically formed during low-snow years with formation of the anomalously late stable snow cover (Fig. 4). Higher temperatures are formed during snow-rich years with anomalously early stable snow cover formation (Fig. 5). The time of stable snow cover formation is the main factor determining the formation of the ground thermal regime. Therefore, in Central Yakutia, atmospheric circulation processes during the cold period of the year are the determining factor of the ground thermal state in the upper 10 meters. It should be noted here that variations in the amplitude of mean winter snow cover depth have significantly grown during the recent decade (Fig. 4). This testifies to unstable circulation processes during the cold period.

The lowest and the highest ground temperatures during the entire monitoring period were noted in 2003 and 2007, respectively (Fig. 5). The winter of 2002-03 was anomalously low-snow with anomalously late stable snow cover formation. The subsequent years were characterized by low-snow winters (Fig. 4) and abundant autumn precipitation.

The ground temperature in different landscapes in general at the Chabyda station area between 2003 and 2007 grew by 0.5 to 6.0°C at the base of the active layer and by 0.3 to 2.7°C at the depth of zero annual amplitude.

Winter 2007-08 was snow-rich in general, but the first half was low-snow followed by late formation of stable snow cover. These meteorological factors led to some ground

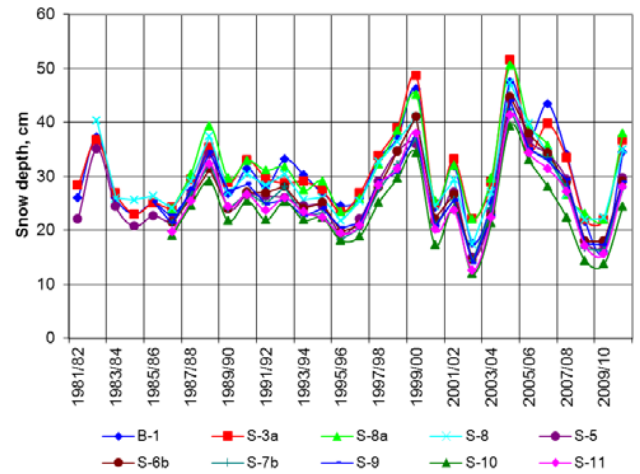


Figure 4. Long-term variation of the mean depth of winter snow cover in different landscape conditions at the Chabyda station.

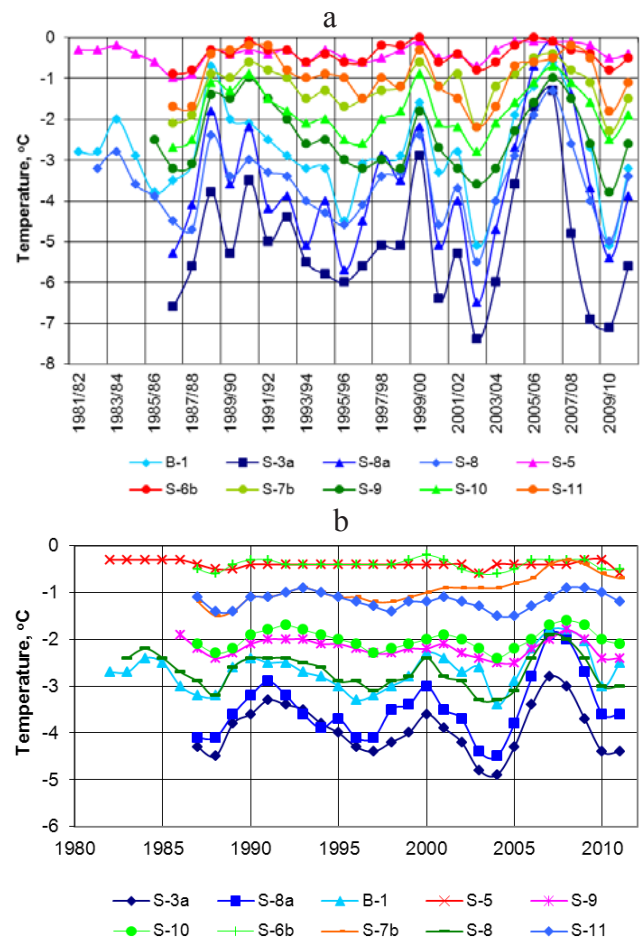


Figure 5. Long-term variation of the annual ground temperature at the active layer base (a) and at depth of zero annual amplitude (b) in different landscape conditions.

cooling at the bottom of the active layer. Two recent winters (2008-09 and 2009-10) were anomalously low-snow with late stable snow cover formation. This led to strong ground cooling despite anomalously warm years.

According to long-term monitoring, the mean annual temperature trends at the depth of zero annual amplitude vary in different physiographic districts from low-negative to positive values, and their dependence is clearly observed by the thermal seasonally of thawed ground types (Table 3).

Table 3. Change of mean annual ground temperature trends near the depth of zero annual amplitude (depth 10 m).

District	Monitoring period	Thermal ground types (°C)	Trends, °C/yr
Prilenskiy valley-forest steppe	1987-2009	0 to-1	-0.003
	1987-2009	-1 to-3	0.011 to 0.029
	1996-2009	-3 to -5	0.039
Prilenskiy left-bank sandstone	1982-2009	0 to-1	-0.003 to 0.038
	1982-2009	-1 to-3	-0.003 to 0.018
	1987-2009	-3 to-5	0.013 to 0.042
Bestyakh sand-ridge	1987-2009	1 to 0	-0.004
	1987-2009	0 to-1	0.005 to 0.035
	1987-2009	-1 to-3	0.009 to 0.066
	1987-2009	-3 to-5	0.056
Tyungyulyun alas-dish	1987-2009	0 to-1	0.010
	1988-2009	-1 to-3	0.006
	1993-2009	-3 to-5	0.045
Lena-Amga alas-valley	1989-2009	0 to-1	-0.009 to 0.008
	1987-2009	-1 to-3	0.005 to 0.031
Lena-Amga sandstone	1995-2009	0 to-1	0.017
	1995-2009	-1 to-3	0.052 to 0.073

Negative trends are noted in the transient-type landmarks of seasonally thawed grounds where the annual mean temperature varies from 0 to -1°C. This is associated with the reduction of the thickness of the active layer (Fig. 3) and the moisture content increase of ground of this layer. The positive trend of the ground temperature at the depth of zero annual amplitude is generally noted in all other thermal ground types. In this case, the lowest trends are typical of landscape complexes with high-temperature permafrost ground and with the greatest active layer depths. The highest trends are found in landscape complexes with low-temperature ground and usually with the lowest active layer depths.

Conclusions

- 1) One of the largest increases of annual mean air temperature was observed during the recent 30 years in Central Yakutia.
- 2) In these conditions, the active layer depth remains quite stable.
- 3) The long-term dynamics of the ground thermal state in the upper 10 meters testifies to its relative stability.
- 4) The snow accumulation regime is the main regulating factor of the stable ground thermal state.

References

- Are, F.E. 1973. Ground temperature regime beneath a draining thaw lake in Central Yakutia. In: *Issues of the Geography of Yakutia*. Leningrad: Gidrometeoizdat, 70-75 (in Russian).
- Efimov, A.I. 1952. Selected results of 3-year ground temperature observations in the Yakutsk area. In: *Permafrost Investigations in the Yakut Republic*, vol. 3. Moscow: USSR Acad. Sci. Press, 8-19 (in Russian).
- Federal Service for Hydrometeorology and Environmental Monitoring (Roshydromet). 2005. *Strategic Prediction for the Period of 2010-2015 of Climate Change Expected in Russia and Its Impact on Sectors of the Russian National Economy*. Moscow, 28 pp.
- Fedorov, A.N., Maximov, T.Kh., Gavriliev, P.P. et al. 2006. *Spasskaya Pad: Integrated Investigations of the Permafrost Landscapes*. Yakutsk: Permafrost Institute Press, 210 pp. (in Russian).
- Gavriliev, P.P., Mandarov, A.A., & Ugarov, I.S. 1984. *Hydrothermal Reclamation of Agricultural Lands in Yakutia*. Novosibirsk: Nauka, 201 pp. (in Russian).
- Gavrilova, M.K. 1978. *Climate and Perennial Freezing of Soils and Rocks*. Novosibirsk: Nauka, 212 pp. (in Russian).
- Gerasimov, N.N. 1950. Annual ground temperature variations in the Yakutsk area. In: *Permafrost Investigations in the Yakut Republic*. Yakutsk, 179-191 (in Russian).
- Ivanov, N.S. 1963. On the thermal regime of the upper earth crust in the Yakutsk area. In: *Heat and Mass Exchange in Frozen Layers of the Earth Crust*. Moscow: USSR Acad. Sci. Press, 9-55 (in Russian).
- Meleshko, V.P., Kattsov, V.M., Govorkova, V.A., Sporyshev, P.V., Shkol'nik, I.M., & Shneerov, B.E. 2008. Climate of Russia in the 21st century. Part 3. Future climate changes calculated with an ensemble of coupled atmosphere-ocean general circulation CMIP3 models. *Russian Meteorology and Hydrology* 33(9): 541-552.
- Melnikov, P.I. 1950. Permafrost in the Yakutsk area. In: *Permafrost Investigations in YaSSR*, vol. 2. Moscow-Leningrad: USSR Acad. Sci. Press, 52-70 (in Russian).
- Pavlov, A.V. 1975. *Heat Exchange between Soil and Atmosphere in Northern and Temperate Latitudes of the USSR*. Yakutsk, 302 pp. (in Russian).
- Pavlov, A.V. 1979. *Thermal Physics of Landscapes*. Novosibirsk: Nauka, 284 pp. (in Russian).
- Pavlov, A.V. 2008. *Permafrost Monitoring*. Novosibirsk: Academic Publishing House "Geo", 230 pp. (in Russian).
- Romanovsky, V.E., Drozdov, D.S., Oberman, N.G., Malkova, G.V., Kholodov, A.L., Marchenko, S.S., Moskalenko, N.G., Sergeev, D.O., Ukraintseva, N.G., Abramov, A.A., Gilichinsky, D.A., & Vasiliev, A.A. 2010. Thermal state of permafrost in Russia. *Permafrost and Periglacial Processes* 21: 136-155.
- Romanovsky, V.E., Sazonova, T.S., Balobaev, V.T., Shender, N.I., & Sergueev, D.O. 2007. Past and recent changes in air and permafrost temperatures in eastern Siberia. *Global and Planetary Change* 56(3-4): 399-413.
- Shender, N.I., Romanovsky, V.E., & Tetelbaum, A.S. 1999. A forecast of the natural variability of climate in Yakutsk and Fairbanks. *Nauka i Obrazovanie* 2: 24-29 (in Russian).

- Shimanovskii, S.V. 1942. Effect of pavements on the ground thermal regime. In: *Permafrost Investigations in the Yakut Republic*, vol. 1. Yakutsk, 44-55 (in Russian).
- Skryabin, P.N., Varlamov, S.P., & Skachkov, Yu.B. 1998. *Interannual Variability of the Ground Thermal Regime in the Yakutsk area*. Novosibirsk: SB RAS Press, 143 pp. (in Russian).
- Solov'ev, P.A. 1959. *Permafrost in the Northern Part of the Lena-Amga Watershed*. Moscow: USSR Acad. Sci. Press, 144 pp. (in Russian).
- Ugarov, I.S. & Mandarov, A.A. 2000. *Overhead Irrigation of Fodder Crops in Central Yakutia*. Yakutsk: Permafrost Institute Press, 128 pp. (in Russian).
- Varlamov, S.P., Skachkov, Yu.B., & Skryabin, P.N. 2002. *Ground Temperature Regime in Permafrost Landscapes of Central Yakutia*. Yakutsk: Permafrost Institute Press, 217 pp. (in Russian).

Pollen and Spores as Indicators of the Origin of Massive Ice

A.C. Vasil'chuk, Yu.K. Vasil'chuk
Lomonosov Moscow State University, Moscow, Russia

Abstract

The comparative study of the remains of spores and pollens in ground ice in the Subarctic and surface ice on Arctic islands was carried out with the purpose of identifying cryogenetic indicators. It is shown that the components typical of tundra pollen spectra and ground-forming ice deposits rarely occur in polar glaciers or their snow cover. These components include cloudberry and aquatic plant pollen poorly adapted for wind transfer, and horsetail and green moss spores. The diagnostic indicators of polar glacier pollen spectra are defined.

Keywords: massive ice; ice caps; pollen spectra.

Introduction

Massive ice deposits are one of the most hazardous of all cryogenic phenomena that influence economic activity within the permafrost zone. Development of areas of the Far North requires study of large-scale massive ice and its genetic origin. Numerous high-level studies, detailed descriptions of ice stratigraphy, and relatively complete analytical reviews exist. However, an unambiguous interpretation has not been possible because the same indicators of structure and composition of ice can be interpreted in totally different ways. The conclusions generally are that the genetic origin of massive ice is either ground ice or buried glacial ice.

The purpose of our work is to demonstrate that palynological analysis and study of the primarily local components of pollen spectra can serve as indicators of the genesis of massive ice.

Results

Ground Ice Palynological Studies

Palynological analysis of several massive ice deposits of different types that are exposed in sections on the Yamal and the Gydan peninsulas (Vasil'chuk & Vasil'chuk 2010a, 2010b) allowed us to verify indicators and evaluate the genesis of the deposits. We carried out studies of Pleistocene massive ice deposits in natural exposures of the western Siberian North; in the lower and upper reaches of the Yuribey River (Yamal); in the area of the Bovanenkovo gas-condensate field; in the valley of the Tanama River (Vasilchuk et al. 1997); and in the Gyda River estuary. Massive ice in the area of the Bovanenkovo deposit is widely developed in the form of beds, laccolites, ice pillars, and lenses. The ice lens section under review is referred to as Late Neopleistocene deposits on the third terrace of the residual outcrop. According to radiocarbon dating received by us, this massive ice was formed within the interval of 25–20 kyr BP (Vasil'chuk et al. 2009). The massive ice structure is horizontally stratified with interlayer thickness of 5–50 cm and more. Ice stratification in the upper part frequently includes silt, clayey silt, and clay in the form of thin layers no more than 1–10 mm thick. The ice is clean and transparent, with rare roundish gas bubbles (2–5 mm in diameter). Sometimes bubbled ice layers up to 5 cm thick are found. The ice in some beds is exceptionally clean “crystal.” Stratified ice with horizontal sediment interlayers between ice layers

is also observed. The ice bed under review is characterized by significant variations in isotopic composition. Here, within the depth interval between 0.2–0.8 m from the top of the bed, $\delta^{18}\text{O}$ varies by more than 10‰: from -12.49 to -22.75‰, and δD varies from -91.7 to -171.9‰ (Vasilchuk et al. 2009, Vasilchuk 2010). The massive ice contains pollen spectra which are similar to those of typical tundra. Ice pollen spectra are characterized by the dominant dwarf birch and sedge pollen and green moss spores with visible content of aquatic plant pollen, mainly *Sparganium* (3–4%). The cloudberry pollen is found in single cases. The ericales pollen is also found (2–3%). The green moss spore content makes up 7–36%. Penecontemporaneous pre-Quaternary pollen and spores were detected in the ice (2–9%). Exotic tree pollen is completely missing, and even pine pollen particularly typical of Arctic glacial snow cover and ice was found in only a single case. Pollen and spore concentration in individual massive ice interlayers is up to 300–1300 un/l. Diatom remains of the *Pinnularia* genus and green algae remains of the *Pediastrum* genus are found in the ice.

The massive ice deposit in the lower reaches of the Yuribey River on Yamal (Vasilchuk 1992, Vasilchuk & Vasilchuk 2010a) occurs at the depth of 15 m in the dark-grey clayey silt stratum of the residual mountain section of the Kazantsevskaya Plain. According to the stratigraphic position, this massive ice was formed more than 50 kyr BP.

In the axial part of the bed there is a trapezoidal ice core 3 m wide in the upper part and 2.5 m wide in the lower part. Ground ice is observed at the contact with this core. It consists of interlayers of ice up to 0.5 m thick and clayey silt interlayers up to 0.2–0.3 m thick. The ground ice layers are inclined with the orientation of the side of the core surface.

The pollen and spore set in the ice forming deposit in the lower reaches of the Yuribey River is characterized by a lack of exotic tree species without signs of re-deposition. The content of pre-Quaternary re-deposited pollen and spores is 10–17%. Cloudberry pollen is found in rare cases, 1–2%. Aquatic plant pollen is noted in a single specimen, 2.5% in a horizontal ice bed. The ericales pollen content varies from 2 to 5%; the content of green moss spores varies from 2 to 12%; the content of horsetail spores is 1–2%. Diatoms and green algae remains are found.

Massive ice was discovered in the upper reaches of the Yuribey River (Vasil'chuk 2010) exposed in clayey silts of the fifth terrace at the depth of 21–22 m. In the central part

of the outcrop, a pear-shaped ice and ground-ice body (up to 3–3.5 m wide and about 3 m high) follows the contour of the deformed host rock layers. A bed of horizontally stratified ice up to 2.5 m wide and about 3 m high lies in the left part of the exposure. This layer is almost in conformity with the near-vertically oriented surrounding ground layers. The typical feature identified by Danilov (1990) has a significantly poorer assemblage of shallow-water foraminifers in clayey silt as compared to the sand stratum. This evidently reflects the process of shoaling in a marine basin during the accumulation period of the sand band.

No exotic pollen of thermophilic tree species without indicators of re-deposition was found in the horizontally stratified ice deposits that are exposed in the upper reaches of the Yuribey River. The coniferous pollen is noted in significant quantities. Meanwhile, the fir pollen content (11–17%) and the Siberian pine pollen content (8–31%) are quite high. Pre-Quaternary, re-deposited pollen and spores are found with a 2–4% ratio. The cloudberry pollen is found in single cases. The aquatic plant pollen is noted in two lower specimens (1–3%). The ericales pollen content made 5–32%. Green moss spores are noted in two upper specimens; their content does not exceed 2%. Horsetail spores are found in a single case. The pollen spectra of the ice deposit under study have indicators of non-glacial origin. Nonetheless, their composition does not contradict the possible burial of local fast-ice floes.

Four layers of lens-shaped ice beds lie in the stratified layer of sandy dark-grey silt and allochthonous brown peat within the interval of 1.40–7.0 m in a section of the Gyda River estuary and its lower terrace. Ice lenses and beds are 0.3–0.4 m thick and 6–8 m long (Vasil'chuk 1992, A. Vasil'chuk 2005). Ice beds are confined to peaty deposits. Syngenetic wedge ice is noted together with the ice beds. Narrow wedge ice up to 1 m wide and 7 m high crosscuts massive ice lenses. Ice beds and peaty silts to the right of the ice vein lie horizontally, and to the left lie at an angle of approximately 20 degrees.

These sediments are very difficult to date with ^{14}C . This is associated with the presence of allochthonous organics and a complex history of terrace deposit formation. According to palynological verification of the ^{14}C dates obtained, the ice beds were formed between 10 and 13 kyr BP. Pollen spectra in the ice lenses (Vasil'chuk 2007) are characterized by the ratio similar to the characteristics of the Arctic and Hypoarctic tundra pollen spectra.

Green moss spores (22–27%) mainly prevail in the pollen spectra in the lowest ice bed that are characterized by extremely negative $\delta^{18}\text{O}$ values (-30.1‰, -34.3‰). The polar willow pollen is 4–14%, and the herbs pollen is 1–16%. The ice itself is undoubtedly inter-ground, which is contradicted neither by its isotopic composition (Vasilchuk 1992) nor pollen and spore composition.

For several years, Japanese researchers studied the massive deposit in the Mackenzie River delta, 4.5 km southwest of Tuktoyaktuk in northwestern Canada (Fujino & Sato 1986, Fujino et al. 1988). The palynological characteristics of the ice-forming deposits received by them differ from the pollen spectra obtained by us for the Yamal ice. Penecontemporaneous pre-Quaternary pollen and spores are contained in a very high concentration in the massive ice

deposit in the Mackenzie River delta. They have a typical yellow-brown tint and are easily identified. The highest pollen and spore concentrations are noted in the visually identified ice interlayers containing grey silt admixture. These are almost exclusively re-deposited pre-Quaternary forms (95–99%). Hosting deposits, on the contrary, are characterized by Quaternary pollen spectra with low coniferous pollen content: *Betula* sp. – 48%, *Alnus* sp. – 38%, *Picea* sp. – 4%, *Pinus* sp. – 1%, *Carpinus* sp. – 1%, *Ericaceae* – 16%. There are no re-deposited forms. Fujino & Sato (1986) reached the conclusion that Quaternary pollen fell into ice, not from the deposits hosting the bed. They made an assumption that the ice bed was of an intrusive type. There are only two clearly expressed indicators that testify to the ice bed of non-glacial origin: re-deposited pre-Quaternary pollen in high concentration and the lack of exotic tree species pollen. We note that the isotopic composition variations are similar to the variations determined by us for ice beds in the section of the third terrace in the Bovanenkov area.

Palynological Data on Surface Ice and Palyno-indicators

For the purpose of reliable comparison with ground ice genesis, we think it rational to discuss the pollen spectra of Arctic glaciers as possible analogues of the ice which certainly has glacial characteristics. It is particularly important to identify the elements of ice and snow pollen spectra in glacial Arctic domes and compare them with those found in buried glacier-type ice or present in ground ice of non-glacial origin.

We studied the pollen spectra of the tundra and Arctic glacier snow cover to identify non-glacial palynological indicators for ice deposits, and we identified the pollen spectra peculiarities that can indicate ice glacial origin.

Bourgeois (1990, 2000) analyzed the pollen and spore composition in the snow cover and ice caps of the Canadian and the Russian Arctic, and came to the conclusion that the structure of Arctic glacier pollen is primarily defined by the peculiarities of air circulation above the glaciers. Groups of far-transported (exotic) and regional components are usually identified in the pollen spectra composition of the glacier ice and snow cover ice. The division of pollen spectra into groups is slightly conditional because Arctic glaciers are primarily located thousands kilometers from the forest boundary. More than 95% of pollen and spores were transported very large distances (Vasilchuk 2007). A group of far-transported exotic pollen of thermophilic tree species and a group of regional north tundra and tundra plant pollen are identified among them. Mainly far-transported exotic pollen and spores are discovered in the snow cover and the ice of the Devon ice cap on Devon Island and the Agassiz ice cap on Ellesmere Island. This is explained by the fact that they are exposed to the impact of air masses moving from south to north. The content of far-transported exotic *Acer*, *Fraxinus*, *Quercus*, and *Ulmus*, *Populus* and *Abies* pollen in the snow of these polar glaciers varies from 3 to 23% (Bourgeois 1990, 2000, Bourgeois et al. 2000). The *Acer*, *Fraxinus*, *Quercus*, and *Ulmus* pollen was found in the ice of the Greenland ice sheet. The exotic pollen content in the Greenland ice is 10–12% (Fredskild & Wagner 1974). Therefore, the presence of exotic thermophilic pollen in ice pollen spectra, without signs of water-deposited or re-

Table 1. Comparison of some pollen and spores in the polar ice caps and massive ice of the Canadian and Russian Arctic.

Pollen and spores	Massive ground ice					Polar ice caps and glaciers					
	Gyda River estuary	Bovanenkovo	Upper reaches of the Yuribey River (Yamal)	Lower reaches of the Yuribey River (Yamal)	Mackenzie River estuary	Akademi Nauk Dome, Komsomol'skiy island	IGAN glacier, Polar Urals	Devon Ice Cap, Devon island	Agassiz Ice Cap, Ellesmere island	Quviavva Glacier, Ellesmere island	Penny Dome, Baffin Island
Exotic (far-transported) pollen	Not detected	Not detected	Not detected	Not detected	Not detected	+	+	++	++	Not detected	+
<i>Rubus chamaemorus</i>	+	+	+	+	No data	Not detected	Not detected	Not detected	Not detected	Not detected	Not detected
Aquiherbosa pollen	+	+	+	+	No data	Not detected	Not detected	Not detected	Not detected	Not detected	Not detected
<i>Ericales</i>	+	+	+	+	No data	Not detected	Not detected	Not detected	+	Not detected	+
<i>Bryales</i>	+++	++	++	++	No data	Not detected	Not detected	Not detected	Not detected	Not detected	Not detected
<i>Equisetum sp.</i>	+	++	++	+	No data	Not detected	Not detected	Not detected	Not detected	Not detected	Not detected
Penecontemporaneous pollen and spores	+	++	++	++	+++	Not detected	Not detected	Not detected	Not detected	Not detected	Not detected
Diatoms	+	+	+	+	No data	No data	No data	No data	No data	No data	No data

Note: + – found in the amount of 0.1-10%; ++ – found in the amount of 10-20%; +++ – found in the amount above 20% from the total sum of estimated grains.

deposition in the aquatic medium, can testify to the glacial genesis of the ice deposit (Table 1). It was found that the content of modern exotic pollen for sub-fossil tundra pollen spectra contains less than 1 pollen grain per thousand estimated grains (Vasil'chuk 2005).

The ericales pollen in ice and snow pollen spectra in polar glaciers is extremely rare. It averages 2 pollen grains per 1000 estimated grains; its maximum content does not exceed 1–2%. For tundra pollen spectra it is a regular component dominating in many cases (Vasil'chuk 2005). That is why the visible presence of the ericales pollen in pollen spectra can testify to the non-glacial ice origin.

Green moss spores are another important indicator. They are not found in the Arctic ice caps (Bourgeois 1990, 2000, Bourgeois et al. 2000) and they have never been found in the glaciers of the Polar Urals. Green moss spores and larch pollen are not present in the ice and the snow cover of the IGAN and the Olen glaciers in the Polar Urals (Surova 1982), despite the fact that these plants are present in the plant communities surrounding the glaciers. We found a low quantity (1–3%) of *Poaceae*, *Cyperaceae* pollen and *Polypodiaceae* spores in the pollen spectra from the snow patch in the area of the Polyarny Village (Polar Urals). These have never been found in the pollen spectra of a small cirque glacier located nearby (Vasil'chuk 2010).

Higher content of *Pinus sylvestris* (26–36%), *P. sibirica* (9–16%), *Betula sect. Nana* (8–11%), and sphagnum moss (18–26%), as compared to pollen spectra from the snow patch, is noted in its pollen spectra. The ericales pollen content in the ice does not exceed 1%. Green moss and horsetail spores are not found in the pollen spectra of snow

and ice (A. Vasil'chuk 2005, Yu. Vasil'chuk et al. 2009). Aquiherbosa pollen is an important indicator. Bourgeois (1990, 2000, Bourgeois et al. 1985, 2000) found that *Potamogeton*, *Sparganium*, and *Typha* aquatic plant pollen is very rare and, according to our estimate, its content is less than 1 pollen grain per 1000 estimated grains. Therefore, the presence of aquiherbosa plant pollen, which is mainly transported by water, can be considered as a sign indicating non-glacial ice genesis.

This list can be supplemented with horsetail spores which are not found in the glacial pollen spectra; their amount in tundra zone pollen spectra is 1-4% on average. The low content of aquatic plant pollen in glacier ice and snow cover is associated with the fact that aquiherbosa plant pollen and spores have almost no ability for air transport, but they are quite adapted for transport in the aquatic medium.

Summing up, we note that the series of components typical of tundra pollen spectra can hardly be found in the ice and the snow cover (see Table 1). These are cloudberry and aquiherbosa plant pollen poorly adapted for wind transport and horsetail and green moss spores. The ericales pollen content in snow on glaciers is much lower than in tundra pollen spectra.

Of glacier pollen spectra, the domination of far-transported *Pinus*, *Picea*, *Abies*, *Acer*, *Fraxinus*, *Quercus*, *Ulmus*, *Populus*, *Abies* and *Juniperus*, *Artemisia*, *Ambrosia* pollen is typical.

Exotic pollen of thermophilic tree species is noted very rarely among far-transported pollen in tundra pollen spectra, including pollen spectra of snow patch and river as well as sea ice floe (no more than one pollen grain per 1000 estimated

grains). In the Yamal Quaternary deposits, exotic pollen can be found much more frequently in the re-deposited state. The typical example of that is the composition of pollen spectra in a snow patch on the Kara Sea beach in the zone of Hypoarctic tundra. Here ericales pollen (25–30%), regional gramineous plant and sedge pollen (19–30%), and herb pollen (9–15%) dominate despite quite high content of far-transported coniferous pollen (11%). Green moss spores dominate amidst the spores in snow patches on the beach and the sea ice floe surface (10–27%). The content of re-deposited forms is low and amounts to 1–3%.

Analysis of the pollen spectra composition of the Gulf of Ob sea ice and ice identified from the surface showed similarity in the composition of the snow patch and the fast ice floe pollen spectra. It is evident that pollen spectra from sea ice floes and snow patch surfaces are much more similar in composition to sub-fossil pollen spectra from the ground surface than the Arctic glacier pollen spectra.

All listed indicators are not always found in pollen spectra. That is why massive ice division on the basis of pollen spectra composition requires further detailing because the listed spectra peculiarities can be influenced by low pollen and spore concentration. Here we would like to demonstrate the fundamental possibility of such division and the usefulness of a detailed palynological analysis for cryogenic massive ice studies.

The differences in ice formation processes, according to Khimenkov & Brushkov (2006), are 1) water burial in a solid phase; 2) free water freezing; and 3) bound water freezing. These also precondition differences in the pollen spectra composition. The following conclusions were made based on pollen and spore analysis in these three ice types:

- 1) Far-transported pollen and spores dominate in buried ice because the formation of surface ice of seas, lakes, and rivers or ice and snow cover usually occurs in winter when the probability of local plant pollen falling on a floe or snow surface is low. Local plant pollen and spore falling within the Arctic glacial domes is selective and is defined by local circulation peculiarities. In this case, a boundary between local and regional components is difficult to draw.
- 2) Re-deposited pollen and spores from underlying strata are frequently present in intrusive ice. Penecontemporaneous Mesozoic and Paleozoic pollen and spores are more frequently found in it as compared to other ice types.
- 3) Much similarity of ice spectra with ice-hosting deposit spectra is noted in segregated ice. The presence of pollen of different species but of the same size can frequently be observed as a result of infiltration sieving of pollen grains and spores in the process of moisture migration through the ground.

In conclusion, we note two important issues that should be taken into account when studying organic remains in ground ice: 1) the possible organic supply to outlet glacier basal ice through cracks, and 2) organic micro-particle accumulation in cryoconite holes.

Knight (1997), studying basal layers of glacial ice, noted that micro-cracks can be formed in the bottom of glacier parts through which fine-ground particles can penetrate from underlying deposits into ice. It is probable that these

can contain pollen and spores, but in this case the ice will be evidently much contaminated and intensively dislocated. Thus its pollen spectra will be derived from the pollen spectra of the underlying deposit.

Conclusions

Long-term palynological studies of ground deposit-forming ice allowed us to identify a number of characteristics typical of their pollen spectra:

- 1) Pollen and spores are contained in almost all varieties of ground ice deposits. Their concentration varies from 50 to 1500 units per 1 kg of ice or 1 liter of melted ice.
- 2) Pollen spectra with characteristics similar to the characteristics of sub-fossil tundra pollen spectra, with dwarf birch, ericales pollen, and green moss spores prevailing, are identified in most of the massive ice deposits.
- 3) In massive ice deposits of pre-Quaternary palynomorphs of the Cenozoic, the Mesozoic, and the Paleozoic ages, re-deposited pollen spectra from more ancient deposits can be frequently found.
- 4) The pollen of hydrophilous plants such as pondweed, bur reed, and reed mace as well as horsetail spores and limnetic diatoms and green algae remains are found in most of the massive deposits studied. This testifies to the non-glacial genesis of the ice.

The results reported generally testify to the following characteristics typical of non-glacial, ice deposit-forming pollen spectra:

- lack of exotic pollen of thermophilic species such as *Acer*, *Fraxinus*, *Quercus*, *Ulmus*, *Populus*, *Tilia*, and *Abies* present in the initial occurrence;
- presence of cloudberry, aquiferbosa species, as well as green moss and horsetail spores; and
- presence of re-deposited pollen and spores.

These characteristics allow the reliable identification of ground ice of non-glacial origin.

References

- Bourgeois, J.C. 1990. Seasonal and annual variation of pollen content in the snow of a Canadian High Arctic ice cap. *Boreas* Vol. 19, N4, 313–322.
- Bourgeois, J.C. 2000. Seasonal and interannual pollen variability in snow layers of arctic ice caps. *Review of Palaeobotany and Palynology* Vol. 108, Iss. 1-2, 17–36.
- Bourgeois, J.C., Koerner, R.M., & Alt, B.T. 1985. Airborne pollen: a unique air mass tracer, its influx to the Canadian High Arctic. *Annals of Glaciology* Vol. 7, 109–116.
- Bourgeois, J.C., Koerner, R.M., Gajevski, K., & Fisher, D.A. 2000. A Holocene ice-core pollen record from Ellesmere Island, Nunavut, Canada. *Quaternary Research* Vol. 54, N2, 275–283.
- Danilov, I.D. 1990. *Ground ice*. Moscow: Nauka, 140 pp. (in Russian).
- Fredskild, B. & Wagner, P. 1974. Pollen and fragments of plant tissue in the core samples from the Greenland Ice Cap. *Boreas* Vol. 3, N3, 105–108.
- Fujino, K., Sato S., Matsuda, K., Sasa, G., Shimisu, O., & Kato, K. 1988. Characteristics of ground ice body

- in the Western Canadian Arctic (II). *Permafrost Fifth International Conference Proceedings*. Vol. 1. Trondheim. Norway Trondheim: Tapir Publishers. 1988, 143-147.
- Fujino, K. & Sato, S. 1986. Stratigraphic analyses of the massive ground ice body in Tuktoyaktuk, Mackenzie Delta, N.W.T., Canada. Characteristics of the Massive Ground Ice Body in the Western Canadian Arctic related to climatology 1984–1985. Ed. K.Fujino. The Institute of Low Temperature Science. Hokkaido University, 9–36.
- Khimenkov, A.N. & Brushkov, A.V. 2006. *Introduction to structural geocryology*. Moscow. Nauka Publ. House, 279 pp. (in Russian).
- Knight, P.G. 1997. The basal ice layer of glaciers and ice sheets. *Quaternary Science Reviews* Vol. 16, Iss. 9, 975–993.
- Surova, T.G. 1982. Subrecent spore and pollen spectra of minor and major snow accumulation zones in the Polar Urals. *Glaciological research materials* Issue 45, 1982, 130–136.
- Vasil'chuk, A.C. 2005. *Pollen spectra formation features in permafrost areas of Russia*. Moscow. Moscow State University Press, 245 pp. (in Russian).
- Vasil'chuk, A.C. 2007. *Palynology and chronology of polygonal ice wedge complexes in Russian permafrost area* Moscow. Moscow State University Press, 488 pp. (in Russian).
- Vasil'chuk, A.C. & Vasil'chuk, Yu.K. 2010a. Local pollen spectra as a new criterion for nonglacial origin of massive ice. Transactions (Doclady) of Russian Academy of Sciences. *Earth Sciences* Vol. 433. Part 1, 985–990.
- Vasil'chuk, A.C. & Vasil'chuk, Yu.K. 2010b. Comparison of pollen spectra of massive and glacial ice for cryogenetic indication. *Earth's Cryosphere* Vol. 14. N3, 15–28 (in Russian).
- Vasil'chuk, Yu.K. 1992. Oxygen Isotope composition of ground Ice (Application to paleogeocryological reconstruction). Department of theoretical problems the Russian Academy of Sciences. Moscow State University, PNIIS. In 2 volumes. Vol. 1, 420 pp. Vol. 2, 264 pp. (in Russian).
- Vasil'chuk, Yu.K. 2010. Massive ice of Bovanenkovo gas-condensate field (The Central Yamal Peninsula). *Engineering Geology* N3, 50–67 (in Russian).
- Vasil'chuk, Yu.K., Vasil'chuk, A.C., Budantseva, N.A., Chizhova, Ju.N., Papesch, W., Podborny, Ye.Ye., & Sulerzhitsky, L.D. 2009. Oxygen Isotope and Deuterium Indication of the Origin and ^{14}C Age of the Massive Ice, Bovanenkovo, Central Yamal Peninsula. Transactions (Doclady) of Russian Academy of Sciences, *Earth Sciences*, 429, 1326–1332.
- Vasil'chuk, Yu.K. & Vasil'chuk, A.C. 1997. Radiocarbon dating and oxygen isotope variations in Late Pleistocene syngenetic ice-wedges, northern Siberia. *Permafrost and Periglacial Processes* Vol. 8, N3, 335–345.

Classification of Tabular Massive Ice Bodies

Yu.K. Vasilchuk

Lomonosov Moscow State University, Department of Geography and Geology, Moscow, Russia

Abstract

A new classification of tabular massive ice bodies is suggested. It includes two new categories: homogeneous and heterogeneous tabular massive ice bodies. Homogeneous tabular massive ice bodies are those whose genesis, composition, and properties are uniform in all the studied parts. Heterogeneous massive ice bodies are those whose genesis, composition, and properties vary in the section. They consist of two or more homogeneous ice bodies or their combinations.

Keywords: allochthonous; autochthonous; heterogeneous; homogeneous; tabular massive ice.

Introduction

When studying tabular massive ice bodies, researchers normally determine the primary factor of their formation. According to this factor, massive ice is usually defined as segregated, intrusive, repeatedly intrusive, buried glacier ice, and so on (Gasánov 1969, Vtyurin 1975, Mackay 1972, 1973, Pollard & Dallimore 1988, Rampton 1988, Zhestkova & Shur 1978).

Vtyurin (1975) gives preference to the segregated type of ice formation:

The segregated type of massive ice bodies is formed as a result of the local and more intensive development of segregated ice formation.... The thickness of ice bodies is determined by the moisture content of ground and by the correlation between the freezing intensity and the rate of moisture inflow. If the former component of the correlation exceeds the latter, there develops a series of thin layers (the thickness of which increases with the increase in the depth of occurrence due to the leveling of the conditions). If the possible speed of moisture inflow exceeds the intensity of freezing, the thickness of massive ice is defined with the moisture content of ground and with the time of ice formation. The most favorable conditions for the formation of large massive bodies of segregated ice are found near the contact between clayey soils and water-bearing coarse-grained sediments at the bottom. The latter contain large reserves of free water that can develop into weakly bound water.

Holmsen (1914) proposed the hypothesis of the infiltrated-segregated genesis of tabular massive ice bodies. He supposed that the formation of thick (up to 15 m) massive ground ice bodies is linked to the infiltration of surface water through the seasonally thawed ground and to the freezing of this water on the top.

Gasánov (1969: 137) thought that the main factor of ice formation is water intrusion. For this reason, he introduced the following into the classification of intrusive ice: seasonal intrusive ice, multi-seasonal intrusive ice (in pereletoks), intrusive ice, repeatedly intrusive ice, and hydrolaccoliths.

Mackay (1972, 1973) proposed that the mechanism of water injection and ice segregation in a closed system to explain the growth of pingo can also be applicable to the mechanism of tabular massive ice formation.

Dubikov (2002) subdivided ice layers into three main

genetic types: intrusive, segregated, and intrusive-segregated. According to the nature of occurrence, he singled out (Dubikov 2002: 220) the ice bodies bedding parallel to the soils containing them (the second type and rarely the first type) and the deposits that are not parallel to the soils containing them (the first and third types). According to the composition, he distinguishes the ice bodies formed by bubbly or glassy massive ice (the first type and rarely the second type); the ice bodies of homogeneous ice-ground (the second type and rarely the first type); the ice bodies consisting of massive ice and of the ice containing an admixture of soil (the second and third type); and the ice bodies consisting of massive ice and of the ice with an admixture of soil and ice-ground (the second and third type). According to the structure, tabular massive ice bodies were divided by Dubikov into simple (the first type and rarely the second type) and complex (the second and third types) ones.

The new classification of tabular massive ice bodies

The heterogeneity of the genetic origin of both parts of different ice layers and of a combination of ice layers in profiles is connected to the conditions of freezing and formation of massive ice. For example, it is difficult to imagine the burial of fast ice at the shore of a lake or the sea that is not accompanied by the formation of lenses of segregated ice in the host sediments (and sometimes by the formation of the layers of massive segregated ice already at the first stage of freezing of sediments containing the buried ice body). If water-saturated soils bed under the deposit, there forms a closed talik after they begin to freeze from above and from below. Further freezing of the talik will lead to intrusion of water or suspension upward or sideward with the formation of intrusive ice.

We suggest introducing two new categories into the classification of tabular massive ice bodies: homogeneous and heterogeneous massive ice bodies (Fig. 1).

Homogeneous tabular massive ice bodies are the ones whose genesis, composition, and properties are uniform in all the studied parts.

Heterogeneous massive ice bodies are the ones whose genesis, composition, and properties vary in the section. They consist of two or more homogeneous massive ice bodies or their combination (Vasilchuk 2011).

Homogeneous tabular massive ice deposits

Homogeneous tabular massive ice bodies are usually

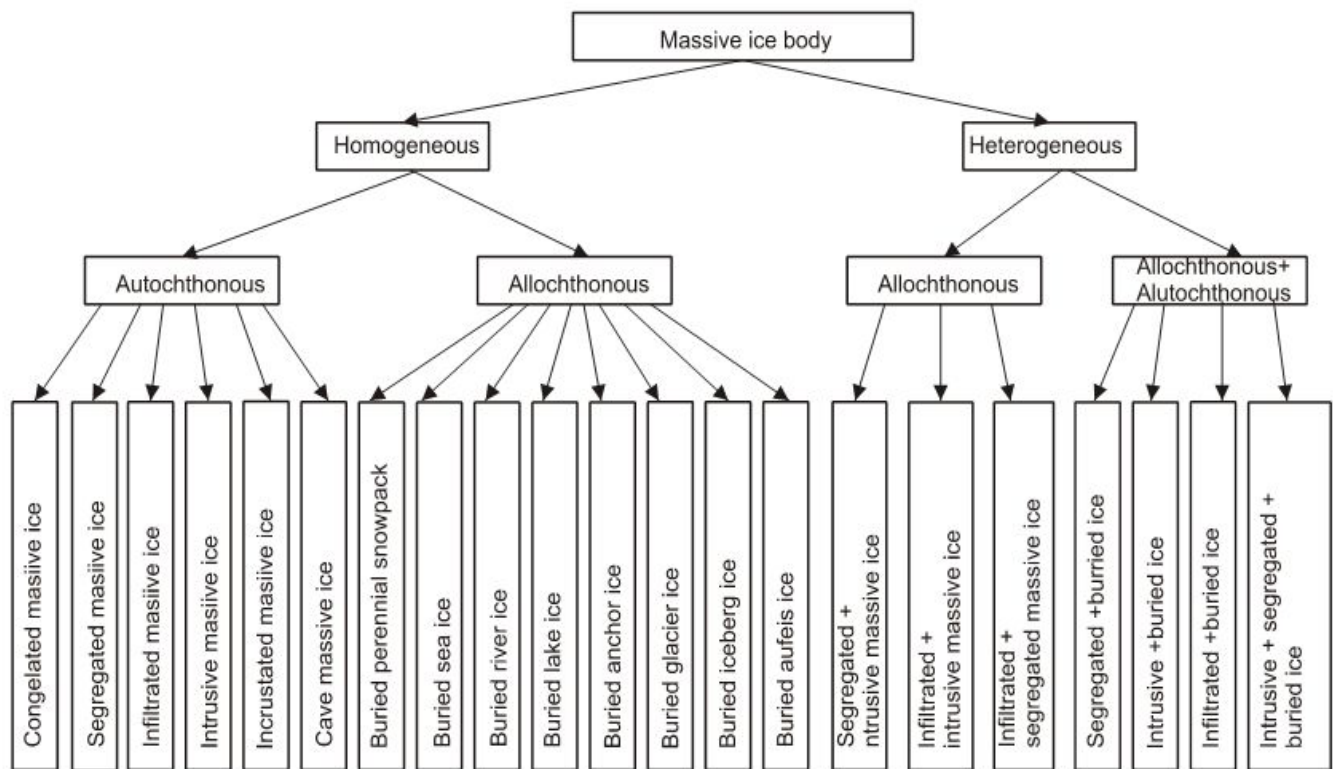


Figure 1. The classification of massive ice bodies considering their homogeneous and heterogeneous nature.

characterized by relatively small dimensions (not more than a few meters thick and not more than 20–30 m wide). Most often they occur as single layers and less often as a combination of layers of the same genesis.

Four lenses of intrasedimental ground ice of the segregated (or infiltrated and segregated) genesis were revealed in the exposure of homogeneous autochthonous complex of tabular massive ice bodies in the section of the first terrace of the Gyda River (Vasilchuk 2011).

Four layers of lens-shaped massive ice (with vertical thickness of up to 0.3–0.4 m and 6–8 m long) were observed in the exposure. The ice layers are very similar in appearance. They are composed of clear ice and, as a rule, associated with the peat series. The features of the structure of the ice layers and their bedding that is parallel to the sedimentation stratification allow us to regard them as intrasedimental formations that formed synchronously with the accumulation and freezing of the ground mass. The ice layers most probably have infiltrated or segregated genesis. The wide range of the $\delta^{18}\text{O}$ fluctuations in these layers (from -33.8 to -16.2‰) indicates freezing under conditions of the closed system with a small water inflow from the outside. Such a wide range of heavy oxygen content is indicative of a very significant cryogenic fractionation in the course of freezing of water whose average $\delta^{18}\text{O}$ value was close to -20‰. This could occur only under conditions of freezing in the closed system when isotopically heavier ice was the first to form (its $\delta^{18}\text{O}$ values are about -16 and -18‰), while the $\delta^{18}\text{O}$ values of the remaining water were about -22‰. The partial freezing of the water led to the formation of ice with the $\delta^{18}\text{O}$ values equaling about -20‰, while the rest of the water had the $\delta^{18}\text{O}$ values of about -24 to -25‰. It was the repeated freezing-out of this water that provided such

extremely low $\delta^{18}\text{O}$ values (about -34‰) in the last portions of the frozen-out water. The low average values of $\delta^{18}\text{O}$ in these tabular massive ice bodies (about -20‰) indicate severe conditions (more severe than the present conditions) of the layers' formation. Along with the tabular massive ice bodies, the syngenetic ice wedges were observed in this exposure. Their total length exceeds 4.5 m. Judging by the radiocarbon dates, the accumulation of the ground mass and the formation of tabular massive ice and syngenetic ice wedges occurred not earlier than 11,000 to 14,000 years ago (Vasilchuk 1992).

It is natural that not only autochthonous but also allochthonous tabular massive ice in permafrost can be homogeneous. We encountered a relatively small homogeneous ice body of buried (allochthonous) type in the sediments of the Kazantsevskaya Suite located in the Oleni Roga 'Deer's antlers' natural landmark of the middle Tanama River. A massive ice body is exposed at the depth of 16.5 m from the surface. Its visible thickness is more than 2 m, and its width is more than 3 m at the base. The structure of the layer is complex: two vertical dykes of light gray silt (up to 3 cm wide) can be observed. They cut across the entire ice layer down to the underlying soil that is compositionally similar to them. A pebble inclusion with the diameter of 3 cm was revealed in the upper part of the right dyke. We also observed that the ice contains horizontal dykes composed of sand. The presence of the differently directed ground layers in the ice may be indicative of the fact that the ice formation was followed by the formation of fissures through which the ice body could be intruded by the water-saturated plastic underlying soils. The fissures could possibly develop as a result of the ice layer movement on the water-saturated ground or in the near-shore zone of the sea.

The marine genesis of the clays containing the ice layer is indicated by the large shells of small forms of gastropods and pelecypods found in them in situ. The chemical composition of the layer is similar to that of the contemporary fast ice of the Kara Sea: its mineralization value reaches 194–390 mg/l with the predominance of sulfates (45–178 mg/l) and chlorides (36–51 mg/l) that are typical of the sea ice (Vasilchuk et al. 1986).

The relatively small exposure of the homogeneous deposit of autochthonous tabular massive ice was studied by the author in the sediments of the second marine terrace near the village of Kharasavey in Western Yamal in 1981 (Vasilchuk 2006). A massive ice body whose vertical thickness was more than 1.5 m and horizontal extent was 10 to 15 m was exposed at this site. The composition of the ice and of the sediments as well as the nature of the relationship between the ice and the host sediments led us to the conclusion that this ice body formed within the ground mass and mainly as a result of water intrusion. The ice bodies at this site have relatively small dimensions both vertically and horizontally. This is generally typical of the homogeneous ice bodies, while the heterogeneous ones are normally much larger.

Heterogeneous tabular massive ice bodies

As a rule, heterogeneous massive ice bodies are larger, although sometimes they can also be small (exposures more often reveal only their small portions).

The relatively small part of the heterogeneous tabular massive ice body in the upper reaches of the Yuribey River was studied by the author in the exposure of the Kazantsevskaya Plain of Yamal in 1977. Two ice layers were exposed there. One of them is buried and the other is intrusive (Vasilchuk 2011).

In the upper part of this exposure, there were found dislocated layered sands (brown as well as ochreous and yellow) with a total thickness up to 10 m. They are underlain by dark gray silty clays (10–11 m thick) with steep contact (close to subvertical). In the upper part, the sediments are slightly sandy and have no visible ice; in the lower part their cryostructure is layered. Two ice “layers” bed within these silty clays. The first one has the visible dimensions of 2.5x4 m. It beds subvertically and its lower end is covered with a slump. The interbed of fine laminated sand of dark gray color 0.1 m thick is observed at the contact of this ice layer with the upper layer of silty clay. The stratification of the silty clay contacting directly with this layer is horizontal. It has no signs of deformations and folding and is oriented along the long axis of the ice layer. The silty clays at some distance from it are heavily dislocated and folded into an anticline fold. The ice layer is stratified and two types of ice structure can be distinguished in it. The upper part of the layer with the thickness of 2 m consists of white ice with a great number of air bubbles, while its lower part is formed of clear ice. The second ice layer was exposed 5 m upstream (to the right from the first one) and was 0.6 to 0.8 m lower than the first one. Its shape in the exposure resembles an inverted pear (or a mushroom). The layers of the host sediment above it are heavily deformed, particularly in the apical part where ruptures are observed. This layer has an intrusive genesis and formed later than the first layer.

The composition of foraminifers as well as of spores and pollen remnants were analyzed in the samples obtained from the host sediments and from the first of the described ice layers. Foraminifers were identified in the upper part of the silty clays and in the overlying sandy sediments. The maximum content of foraminifers was observed in the sands. This means that the dark gray silty clays were deposited in water conditions that were extremely unfavorable for foraminifers (a small, cold, and desalinated basin). The desalination could occur due to the melting of large masses of calved sea ice brought from the north with the constant northern winds and currents. A part of this ice could be buried in the shallow water zone. Later, the conditions changed and the water body apparently became slightly deeper, while its salinity increased. A part of the buried ice could melt away entirely under these conditions and an insignificant part of it could still be preserved, though having melted to a large extent (it is represented with the first of the described ice layers).

The spore and pollen spectra of the host sediments (Vasilchuk & Vasilchuk 2010) are characterized by the overall predominance of the tree species pollen in the general composition (from 58 to 82%) among which the pollen of the Siberian cedar, birch, and fir is predominant. The predominance of the tree species pollen in this case indicates not a warm climate, but the formation of the pollen spectra in the sediments accumulated in the upper littoral due to which the spectra reveal “over-pollination” with the resedimented pollen of the tree species.

But if it is a layer of the buried sedimentary ice, then why does it presently bed subvertically and not horizontally? What forces positioned it in a way that is unnatural for a sedimentary layer?

The development of such a specific structure is linked with the intrusion of masses of water and suspension from the underlying soils in the course of their epigenetic freezing in the Upper Quaternary time. Their injection, the center of which was located near the tabular massive buried ice body, caused a considerable dislocation of the ice layer as well as of the host sediments and the formation of a complex fold.

The exposure of the heterogeneous tabular massive ice body in the upper Yuribey River formed by the joint occurrence of the buried and intrusive ice in permafrost may be regarded as the typical example of the paragenetic combination of allochthonous buried layer of fast ice and autochthonous intrusive massive ice.

The heterogeneous tabular massive ice body with the paragenetic combination of autochthonous segregated ice layer and autochthonous intrusive tabular massive ice body was investigated by the author on the left bank of the Erkutayakha River of Southern Yamal in July 2010.

Two types of massive ground ice are revealed in the 18 to 20 m high exposure composed mainly of layered sands. Its central part contains a stock of deformed ice of a vertical orientation. On both sides at the contact with the stock there was exposed a dislocated tabular massive ice body (Vasil'chuk et al. 2011) the stratification of which is parallel to the inclination of the ice body surface. The layered ice with a general length exceeding 100 m falls steeply from east to west and already at the distance of 15 m. The top of this ice body is found at a depth of more than 8 m.

The variations in stable isotopes of oxygen and deuterium are significant in the ice body: the $\delta^{18}\text{O}$ values vary from -20.2‰ to -24.4‰, while the δD values range from -142.6‰ to -170.1‰. As a rule, the ice is isotopically heavier in the central ice stock, while at the periphery (in the layered ice) it is isotopically much lighter ($\delta^{18}\text{O}$ can be lighter by 3 to 4‰ and δD can be lighter by 25 to 30‰). This is well explained by cryogenic fractionation during the freezing of the talik that was initially open and then became closed.

The investigation of the spore and pollen remnants in the ice made it possible to more exactly distinguish the genetic type of the studied ice body.

The palynospectra studied in the ice of the Erkutayakha River ice body are indicative of the intrasedimental autochthonous genesis of the ice. This is indicated by the typical tundra nature of the palynospectra.

The structure of the tabular massive ice complex at the Erkutayakha River, the isotope composition of the ice, and its spore and pollen spectra indicate that the apical part of the ice body contains intrusive ice, while its distal parts on both sides from the central intrusion contain segregated ice. This means that the tabular massive ice body is heterogeneous and autochthonous and was formed by the combination of the segregated and intrusive massive ice.

The Bovanenkovo field in Yamal containing heterogeneous tabular massive ice is one of the richest areas in the permafrost region in the variety of tabular massive ice bodies. Only the delta of the Mackenzie River is comparable to it (Fujino et al. 1988, Murton 2005). The tabular massive ice of the Bovanenkovo gas condensate field is morphologically rather diverse (Vasilchuk et al. 2009, Vasilchuk 2010). The field contains layered and heavily deformed massive ice bodies as well as ice heavily incorporated with soil and ice layers composed of clear crystal ice. Its genesis is also variable, and the tabular massive ice bodies are heterogeneous. We distinguished combinations both of the autochthonous ice of different nature and of autochthonous ice with allochthonous ice in the profiles of more than 260 boreholes that encountered massive ice at the Bovanenkovo gas condensate field.

In the massive ice bodies of the Bovanenkovo field, the $\delta^{18}\text{O}$ values vary from -12.49 to -23.13‰, and the δD values range from -91.7 to -177.1‰ (i.e., the $\delta^{18}\text{O}$ variations exceed 10‰, while the δD variations exceed 85‰) (Vasilchuk et al. 2009). These variations reflect the diversity of tabular massive ice bodies in this area.

Making a palynological analysis of the ice bodies of the Bovanenkovo field, A.C. Vasilchuk discovered numerous remnants of unicellular green algae and diatoms (Vasilchuk & Vasilchuk 2010). This suggests the existence of a fresh or desalinated water body that alimented the ice body; it was either a large lake or a desalinated bay.

It should be particularly noted that presently not a single massive ice body in the plains areas of the permafrost regions of Russia can be definitely identified as buried glacier ice. The exceptions are mountain and piedmont areas with active glaciation, where burial of the stagnant ice in terminal moraines is a rather common phenomenon. (They also include the piedmonts of the Karyakskiy Ridge, where Kotov [1988] studied a tabular massive ice body in the Tanurer River valley that is possibly of a buried type. Also,

Gasarov [1969] described a buried ice body near the cape of Nygligan, and Korolev [1993] classified the massive ice bodies in the Amguema Valley as buried.)

As a rule, the autochthonous and allochthonous heterogeneous tabular massive ice bodies have very large dimensions both vertically and horizontally. Their ice can be of many different types, from absolutely clear and transparent to opaque ice that is saturated with gas inclusions, and ice heavily incorporated with soil inclusions.

References

- Dubikov, G.I. 2002. *Composition and cryogenic structure of the permafrost strata of Western Siberia*. Moscow, Geos Publ. House, 246 pp (in Russian).
- Fujino, K., Sato, S., Matsuda, K., Sasa, G., Shimizu, O., & Kato, K. 1988. Characteristics of the massive ground ice body in the western Canadian Arctic. In *Proceedings of the Fifth International Conference on Permafrost*. Trondheim, Norway. Tapir Publishers: 143-146.
- Gasarov, Sh.Sh. 1969. *The structure and the formation history of the frozen grounds in Eastern Chukotka*. Moscow, Nauka, 168 pp. (in Russian).
- Holmsen, G. 1914. Spitsbergens jordbunds og de bidrag dens undersøkelse har kunnet gi til forstaaelsen av de i arktiske land optrædende varige isleier i jorden. (Ground ice in Spitsbergen and contributions toward the understanding of perennial ground ice found in Arctic environments). *Det Norske Geografiske Selskabs Årbok B XXIV*, 1912-1913, Kristiania: 1-150.
- Korolev, S.Yu. 1993. The discovery of the Late Pleistocene glacier ice in the valley of the Amguema River (Northern Chukotka). *Reports of the Russian Academy of Sciences* 329 (no. 2): 195-198 (in Russian).
- Kotov, A.N. 1998. The cryolithogenic ridges in the valley of the Tanurer River (Chukotka). *Kriosfera Zemli* 2, (no. 4): 62-71 (in Russian).
- Mackay, J.R. 1972. Offshore permafrost and ground ice, southern Beaufort Sea, Canada. *Canadian Journal of Earth Sciences* 9: 1550-1561.
- Mackay, J.R. 1973. Problems in the origin of massive ice beds, western Arctic Canada. Permafrost. *The North American Contribution to the Second International Conference*, Washington D.C.: National Academy of Sciences. Vol. 1: 223-238.
- Murton, J.B. 2005. Ground-ice stratigraphy and formation at North Head, Tuktoyaktuk Coastlands, Western Arctic Canada: a product of glacier-permafrost interactions. *Permafrost and Periglacial Processes* 16 (1): 31-50.
- Pollard, W.H. & Dallimore, S.R. 1988. Petrographic characteristics of massive ground ice, Yukon Coastal Plain, Canada. In *Proceedings of the Fifth International Conference on Permafrost*. Trondheim, Norway. Tapir Publishers, pp. 224-228.
- Rampton, V.N. 1988. Origin of massive ground ice on Tuktoyaktuk Peninsula, Northwest Territories, Canada. In *Proceedings of the Fifth International Conference on Permafrost*. Trondheim, Norway. Tapir Publishers, pp. 850-855.
- Vasil'chuk, A.C. & Vasil'chuk, Yu.K. 2010. Local pollen spectra as a new criterion for nonglacial origin of

- massive ice. *Transactions (Doclady) of Russian Academy of Sciences, Earth Sciences* 433 (Part 1): 985-990.
- Vasil'chuk, Yu.K. 1992. *Oxygen Isotope Composition of Ground Ice (Application to Paleogeocryological Reconstruction)*. Department of theoretical problems the Russian Academy of Sciences. Moscow State University, PNIIS. In 2 volumes. Vol. 1, 420 pp., Vol. 2, 264 pp. (in Russian).
- Vasil'chuk, Yu.K. 2006. Massive ice bodies. The cryosphere of the Kharasavey gas condensate field. Edited by Yu.K. Vasilchuk, G.V. Krylova & E.E. Podborny. Tyumen-St. Petersburg. *Nedra*: 160-193 (in Russian).
- Vasil'chuk, Yu.K. 2010. Massive ice of Bovanenkovo gas-condensate field (The Central Yamal Peninsula). *Engineering Geology*. No 3: 50-67. (in Russian)
- Vasil'chuk, Yu.K. 2011. Homogeneous and Heterogeneous Massive Ice in Permafrost. *Kriosfera Zemli* 15 (1): 40-51 (in Russian).
- Vasil'chuk, Yu.K., Petrov, O.M. & Vasil'chuk, A.K. 1986. Some remarks on the meaning of stratigraphic arrangement of the massive ice deposit in the Kazantsevsky sediments of Central Gydan. Moscow, Nauka: *The Bulletin of the Commission for the Study of the Quaternary* 55:111-117 (in Russian).
- Vasil'chuk, Yu.K. & Trofimov, V.T. 1988. Oxygen isotope variations in ice-wedge and massive ice. In *Proceedings of the Fifth International Conference on Permafrost*. Trondheim. Norway. Tapir Publishers, pp. 489-492.
- Vasil'chuk, Yu.K., Vasil'chuk, A.C., Budantseva, N.A., Chizhova, Ju.N., Papesch, W., Podborny, Ye.Ye., & Sulerzhitsky, L.D. 2009. Oxygen isotope and deuterium indication of the origin and ^{14}C age of the massive ice, Bovanenkovo, Central Yamal Peninsula. *Transactions (Doclady) of Russian Academy of Sciences, Earth Sciences* 429: 1326-1332.
- Vasil'chuk, Yu.K., Budantseva, N.A., & Vasil'chuk, A.C. 2011. Variations in $\delta^{18}\text{O}$, δD , and the concentration of pollen and spores in an autochthonic heterogeneous massive ice on the Erkutayaha River in the southern part of the Yamal Peninsula. *Doklady Earth Sciences* 438 (Part 1): 721-726.
- Vtyurin, B.I. 1975. *Ground Ice of the USSR*. Moscow, Nauka, 214 pp. (in Russian).
- Zhestkova, T.N. & Shur, Yu.L. 1978. On genesis of tabular massive ice. *The Bulletin of the Moscow State University. Geology Series* 3: 35-42 (in Russian).

Onshore and Offshore Permafrost in the Kara Sea

A.A. Vasiliev

Earth Cryosphere Institute, SB RAS, Tyumen, Russia

P.V. Rekant

All Russian Institute of Ocean Geology and Mineral Resources, St. Petersburg, Russia

Abstract

This study concerns identification of submarine permafrost in the Kara Sea shelf using high-resolution seismic-acoustic profiling. Permafrost in the Kara Sea has been revealed offshore at sea depths to 120 m from acoustic permafrost (APF) markers from high-resolution seismic (HRS) data. The existence of permafrost at greater depths is most likely an exception and may be due to neotectonic subsidence. The permafrost extent in the Kara Sea has been mapped with GIS tools and a respective database on its setting has been developed. The upper surface or table of submarine permafrost lies at 5–60 m below the sea floor. According to statistical processing of the collected seismic-acoustic data, the sub-bottom depth to permafrost is most often (47% of cases) in the range of 10 to 20 m. Gas seeps are hypothesized to have a genetic relationship with submarine permafrost. The study results were used to model the structure of coastal (onshore) and shelf (offshore) permafrost in the Kara Sea.

Keywords: gas seeps; Kara Sea; permafrost table position; submarine permafrost.

Introduction

Studying the extent, settings, and properties of onshore and offshore (submarine or subsea) permafrost in the Arctic is important as it can provide clues to the interaction between the Arctic Ocean and adjacent land and to the history and evolution of the coastal and shelf zones.

According to the present-day views, submarine permafrost (SMP) is remnant terrestrial permafrost (Osterkamp 2001) that formed during times of low sea level in the Last Glacial period (20–18 kyr BP), when the sea retreated to the present isobath of 120 m. This onshore permafrost was flooded during the last transgression (16–5 kyr BP) and thawed from above and from below. Thus submarine permafrost has acquired its present state.

The consideration below is confined to acoustically defined ice-bonded permafrost. The ice-bonded permafrost may form offshore as a result of additional cooling of unfrozen ground by gas seeping at isolated localities (Melnikov & Spesivtsev 1995). It is suggested in the cited study that this newly formed ice-bonded permafrost is the cause of large pingos in the Kara Sea bottom.

The existing knowledge of SMP extent on the Kara shelf, its settings and properties, comes mainly from engineering and geological drilling. Altogether there are about twenty boreholes, some of which have detected submarine permafrost. Thus the available explicit geological evidence is obviously insufficient to reliably characterize SMP. The most detailed review of the state-of-the-art can be found in (Melnikov & Spesivtsev 1995).

The permafrost extent has been shown on small-scale maps based on expert appraisal, but it has no support from field data. There are a few estimates of SMP thickness varying from 2 to 100 m. The available SMP temperature data are controversial. The ground temperature approaches equilibrium in some boreholes and is -1.2°C ; in other holes it reaches -4.5°C .

In recent decades, geophysical methods have been increasingly applied to explore the shelf geology. Data of more than 100,000 km of resolution seismic (HRS) profiles

collected in the Kara Sea are stored at several research institutions. New processing techniques allow identifying submarine permafrost in seismic cross sections. Thus HRS profiling can be used to search for submarine permafrost at sea depths to 120 m.

Methods

The HRS methods are especially useful when explicit geological evidence is insufficient. Today's advanced data acquisition and processing techniques allow using seismic records as an independent source of geological information. With the seismic facies analysis, the seismic wavefield can image the ground structure to depths of 60–70 m, including permafrost (Shlezinger 1998). A seismic-acoustic section is the first approximation equivalent to a geological cross section. The resolvable seismic sequences and subsequences are correlated with geological (stratigraphic) units, such as groups, formations, beds, etc. Undisturbed patterns of stratified sediments in a seismic section indicate the absence of submarine permafrost.

Among the factors that can disturb seismic images in a given region are cryogenic and postcryogenic effects in sediments, as well as features associated with free gas. Together they can produce intricate patterns difficult for interpretation.

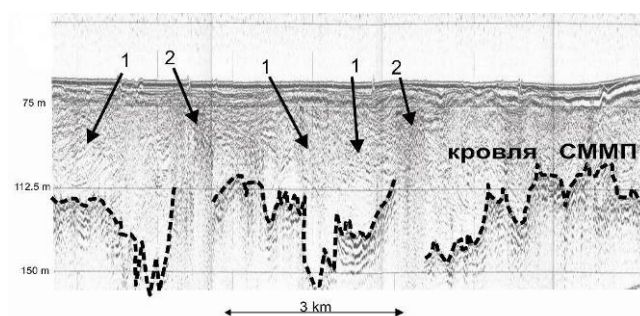


Figure 1. A typical seismic-acoustic cross section from SMP areas. 1 – sites of cryogenic sediment deformation above permafrost; 2 – gas seeps that show up as vertical blanking zones.

As shown for the shelves of the Pechora and Laptev Seas (Rekant et al. 2009), submarine permafrost based on HRS data is detectable from high-amplitude reflections that are seismic-acoustic markers of distinct post-depositional characteristics. The acoustically defined permafrost table commonly corresponds to a prominent reflector of normal polarity produced by abrupt acceleration of acoustic velocity in frozen ground.

Figure 1 shows a typical reflection cross section with seismic-acoustic markers corresponding to the SMP table.

The presence in the sediments of just a little free gas causes seismic interference evident as bright spots or vertical blanking zones (Fig. 1). These gas features, called gas seeps (GS), are hypothesized to have a genetic relationship with submarine permafrost and to be controlled by taliks (Rekant et al. 2009).

The high-resolution seismic-acoustic data agree well with drilling evidence. Most coastal and inner shelf logs from the western Yamal (e.g., near Cape Kharasavey) show a rapidly dipping permafrost table (40 m or more) in shoals between the shoreline and ~5–7-m sea depth. A similar pattern appears from seismic-acoustic data.

Results

Interpretation of more than 100,000 km of HRS profiles in total has revealed several zones of prominent markers of acoustically defined permafrost (APF), as well as zones where such markers are poorly pronounced but are inferred (Fig. 2).

The APF markers are most reliably detectable within shoals in the southern Kara Sea and on the western Yamal shelf. There are also several inferred markers within local rises in the central and northeastern parts of the shelf. The extent of submarine permafrost is controlled mainly by the present sea depth. The greatest number of permafrost markers falls within the sea depth range from 10 to 100 m.

A database consisting of 26,000 records has been created. It provides information on geographical coordinates, sea depths, and depths of the permafrost tables.

The permafrost table position (PTP) in most sites occurs at 5 to 60 m below the sea floor. According to statistical processing of the data, the sub-bottom depths of permafrost show a nearly log-normal distribution, at least in the southwestern part of the Kara Sea and on the Yamal shelf. In most cases (47%) depths range from 10 to 20 m (Fig. 3).

According to statistical relationships between PTP frequency and sea depths, they are directly proportional only at water depth from 100 to 40 m: the deeper the sea, the deeper the permafrost table. On the shoals the relationships are more complex. The reason may be in the slow rise of sea level depth from 100 to 40 m and the rapid rise from 40 m to the present level.

This evidence of sea depths and the acoustically defined permafrost table position have provided the basis for a PTP model for the Kara Sea (Fig. 4). Terrestrial permafrost pinches out rapidly near the shoreline, and further SMP is recorded at sea depths below 10 m. Note that at depths down to 40 m PTP is roughly parallel to the bottom surface but dips steadily below this depth. Only very rarely does SMP appear at depths greater than 120 m.

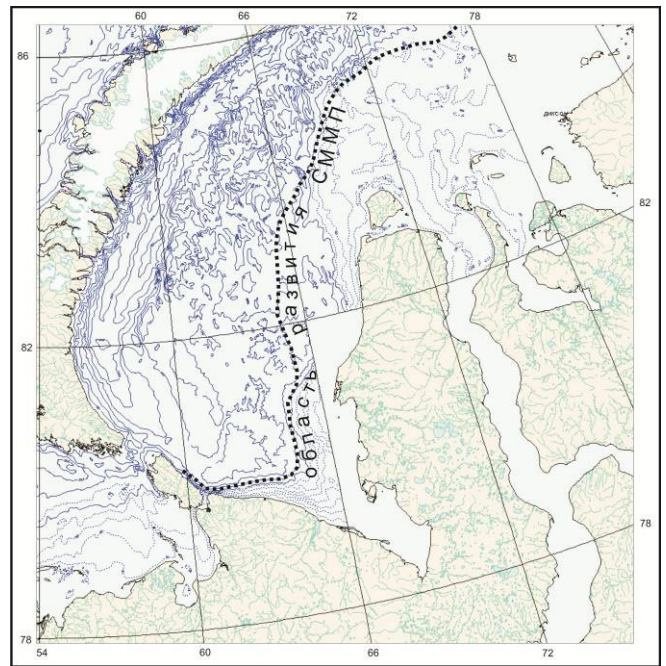


Figure 2. Map of submarine permafrost in the Kara Sea based on seismic-acoustic data.

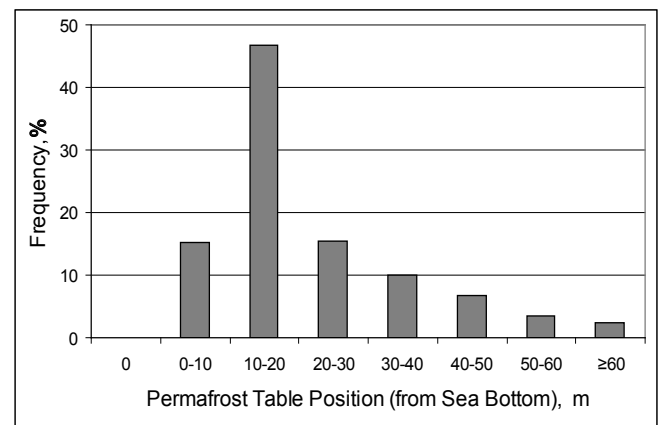


Figure 3. Statistics of SMP frequency in the Kara Sea.

Of special interest are zones of gas seeps. As our data show, they occur most often within reliably detected or inferred permafrost zones. This is implicit evidence of their genetic linkage with subsea permafrost. Gas seeps may originate from zones of deeply buried permafrost tables as free gas is released during permafrost degradation from below.

Conclusions

Acoustic markers of submarine permafrost are reliably detectable in the southeastern Kara Sea and on the Yamal shelf to a sub-bottom depth of 120 m. There are also inferred APF markers near Severnaya Zemlya within local seafloor rises nested in areas of 100–120-m isobaths. The existence of permafrost at greater sea depths is most likely an exception and may be due to neotectonic subsidence.

The permafrost table occurs from 5 to 60 m below the sea floor. The sub-bottom depths to permafrost show a log-normal distribution and are most often within 10–20 m.

Statistical relationships between the permafrost table position and sea depths show direct correlation only when

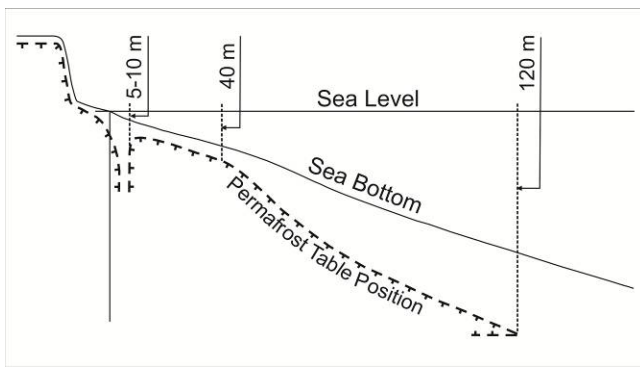


Figure 4. Model of remnant SMP in the Kara Sea.

the water is no shallower than 40 m. The reason may be related to slow sea level rise before and rapid rise from that depth to the present level.

The SMP extent in the Kara Sea has been mapped with GIS tools and the respective database with its conditions has been developed.

There is apparently a genetic relationship between gas seeps and submarine permafrost, and the acoustic markers of gas seeps may additionally indicate deeply buried subsea permafrost.

Acknowledgments

This study was carried out as part of Program 20 of the Russian Academy of Sciences (Basic Problems of Oceanography: Physics, Geology, Biology, Environment) and was additionally supported by grants ARC-0632400 and ARC-0520578 from the U.S. National Science Foundation.

References

- Melnikov, V.P. & Spesivtsev, V.I. 1995. *Engineering-Geological and Geocryological Conditions of the Barents and Kara Shelves*. Nauka, Novosibirsk, 198 pp. (in Russian).
- Osterkamp, T.E. 2001. Subsea Permafrost. Chapter in *Encyclopedia of Ocean Sciences*. Steele, J.H., Thorpe, S.A. and Turekian, K.K. (eds.). Academic Press. pp. 2902-2912.
- Rekant, P., Tumskoi V., Gusev E., et al. 2009. Distribution and features of submarine permafrost near Semenovskoe and Vasilievskoe shoals (Laptev Sea) revealed by high-resolution seismic profiling, in: Kassens H., Lisitzin A.P. (eds.), *System of the Laptev Sea and the Adjacent Arctic Seas: Present and Past Environments*. Moscow University Press, Moscow, pp. 332–348 (in Russian).
- Shlezinger, A.E. 1998. *Regional Seismic Stratigraphy*. Nauchnyi Mir, 379 pp. (in Russian).

Interannual Dynamics of Seasonal Thaw Depths of the Kenkeme-Lena Landscapes

I.S. Vasiliev

Melnikov Permafrost Institute, SB RAS, Yakutsk, Russia

Abstract

The annual dynamics of seasonal ground thaw in 10 natural territorial complexes of the Kenkeme-Lena interfluvium are described based on 15 to 16 years of measurements. The combined effects of biological characteristics and hydrological and temperature conditions of the landscape and climatic forcing on thaw depth dynamics are analyzed. The response of the permafrost system to interannual climatic variability is not consistent from year to year. Different landscapes respond differently to climatic forcing resulting in different, sometimes opposite, temporal trends in thaw depth. Significant deviations in thaw depth correspond to anomalously high summer precipitation, cold winters with low snow accumulations, and dry hot summers.

Keywords: active layer; interannual dynamics; natural landscape complexes; permafrost observations; seasonal thaw depth.

Introduction

The importance of the interannual dynamics of thaw depth in permafrost regions was well understood even at the initial development of geocryology as a science. For example, periodic active layer monitoring in Central Yakutia, particularly in the vicinity of Yakutsk, was established in 1938. However, observations were conducted by different researchers over short periods and in non-systematic fashion (Yefimov 1952, Solovyev 1959, Are & Demchenko 1972, Pavlov 1975).

In 1981, more systematic continuous thaw depth measurements were initiated by the Permafrost Institute of the Siberian Branch of the USSR Academy of Sciences (later the Siberian Branch of the Russian Academy of Sciences) in the area of the Malaya Chabyda and the Umaybyt research stations. Later, active-layer monitoring was extended to the northern part of the Tommot-Yakutsk railway route at the Kerdyugen irrigation system site (1987), to the Dyrgyabay-Ataga site (1991), and to the Yukechi site (1992) (Turbina 1985, Fedorov 1985, Skryabin et al. 1992, 1998, Fedorov et al. 1992, Gavriliev & Ugarov 1996, Gavriliev et al. 1996).

On the Kenkeme-Lena interfluvium, located 20–30 km northeast of Yakutsk, complex systematic permafrost/landscape observational studies were initiated in 1996 within the framework of the joint Russian-Japanese projects. Observations include annual seasonal ground thaw-depth measurements in different, contrasting landscapes of the Kenkeme-Lena interfluvium territorial complex.

Methods

Detailed, large-scale landscape characterization was conducted over the study area to assess the spatial landscape variability. We identified 45 landscape types (Fedorov et al. 2006). At the early stages of research, monitoring of the thaw depth was established on some landscapes (Vasiliev & Gerasimov 2001, Vasiliev & Argunov 2005, Konstantinov et al. 2006). Over the years, new monitoring sites were added on technogenic landscapes developed as a result of subsequent forest logging. The total number of observational sites increased to 46.

At all sites, thaw depth measurements were conducted after September 15 at fixed point locations. The methods of observations varied depending on landscape characteristics. In forested inter-*alas* natural landscapes, thaw depth was determined by mechanical probing with a steel rod at fixed point locations. In meadow inter-*alas*, *alas*, sand-ridge, inter-ridge-lowland, and slope deposited landscapes, measurements were made by drilling and at manually dug test pits.

It is well known that climatic variability is predominantly responsible for interannual variations in the depth of seasonal thaw. Interannual variability of climatic characteristics (snow depth, air thaw index, and summer precipitation) observed at the Yakutsk weather station over the 1996–2010 period is shown in Figure 1.

Results

This paper reports on interannual thaw depth over the 1996–2010 period as observed on 10 contrasting landscape types characteristic of the study area (Table 1 and Fig. 2).

1. *Cowberry larch forest on clayey silty loam soils of the inter-*alas* locality type (southern side of the Neleger *alas*)*. The Tabaga level of the Neogene terrace on the left bank of the Lena River is covered by a thin (up to 3–5 m) Upper Quaternary ice-complex deposit. This is the primary landscape of the inter-*alas* area. The deepest values of thaw depth of 1.15–1.25 m are characteristic of the first half of the 1996–2002 observational period. At that time, the soils had optimal moisture content in response to high average summer precipitation (146–200 mm). The increase in thaw rates corresponds to periods characterized by early summer precipitation and thick snow cover in the previous winter. The dry summer seasons of 2000 and 2001 caused the drying of the active layer resulting in the most shallow observed thaw (1.05–1.07 m). The second half of the observational period (2003–2010) was characterized by an increase in soil moisture/ice content, responding to the anomalously high amount of summer precipitation (191–256 mm) during 2003, 2006, and 2007. High precipitation led to water/ice saturation at the bottom of the active layer in the following years and decreasing thaw propagation due to latent heat

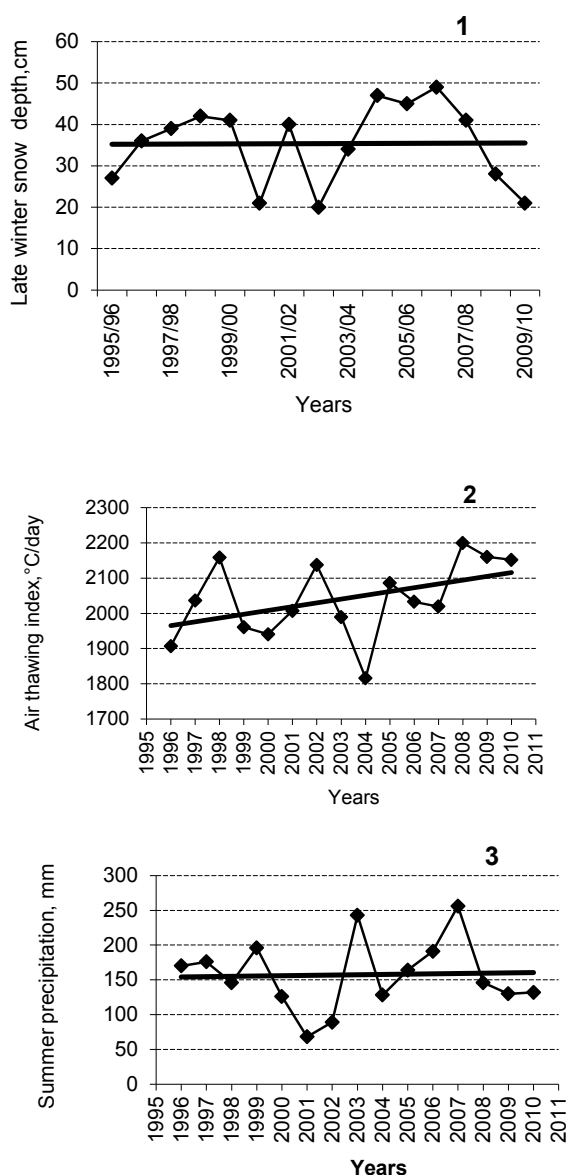


Figure 1. Snow depth (1), thaw index (2), and summer precipitation (3). 1996–2010 trends as observed at the Yakutsk weather station.

effect. As a result, during these years the seasonal thaw depth varied from 0.95 to 1.1 m. Overall, this landscape is characterized by a negative 15-year trend of the seasonal thaw depth (Fig. 2-a.1). The standard deviation is equal to ± 0.08 m, or 7.41% of the 15-year mean value of 1.08 m (Table 1).

2. *Graminaceous herb meadow on sandy silty loam and clayey silty loam soils of the inter-alas locality type (southwestern side of the Neleger alas)*. This is a narrow 30–50-m-wide forest border/inter-alas belt of eastern orientation once occupied by farmland. The landscape is characterized by barely visible subsidence-polygonal microrelief. Grass stand productivity is directly related to the amount of summer precipitation. At this site, the interannual seasonal thaw depth dynamics is similar to the first landscape. The highest seasonal thaw depth values of 2 m and above were recorded, prior to 2002, and the lowest values of 1.6–1.8 m were in 2001, 2003, 2009, and 2010. In addition to the

natural factors mentioned above, the high grass productivity during the 2003, 2006, and 2007 rainy summers contributed to the reduction in seasonal thaw depth on this landscape. Smaller summer thaw depths observed during the dry, warm seasons of 2001 and 2009 are attributable to the very dry soil horizon within the active layer. The negative seasonal thaw depth trend is evident in Figure 2-a.2. The standard deviation of interannual thaw depth at this landscape is ± 0.13 m or 6.84% of the 15-year mean (Table 1).

3. *Mesophytic graminaceous herb meadow on sandy silty loam and clayey silty loam soils of the alas locality type (to the south of the Neleger alas)*. This landscape represents the next topographic level after the meadow inter-alas and is composed of alas-type deposits. The highest seasonal thaw depth values of 2 m or slightly above or below were observed in the summers of 2002, 2006, and 2008. The preceding mild and snowy winter and hot summer influenced the increase of the thaw depth during the summer of 2002, although the amount of summer precipitation was at its 15-year minimum. The anomalously rainy summer of 2006, despite high productivity of the grass, had a favorable impact on the thaw intensity at the open alas meadow surface. In the winter of 2006/2007, freezing of the saturated active layer resulted in shallow thaw propagation in summer 2007. By the end of the thaw season of 2008, the highest value of the active-layer thickness of 2.2 m was recorded. Deep thaw was accompanied by the formation of a saturated layer at the bottom of the active layer. The lowest values of thaw depth were observed during the abnormally dry and abnormally wet warm periods of 2001 and 2003. The overall positive trend in seasonal thaw depth was observed in the open alas meadow (Fig. 2-a.3). This demonstrates a prevailing warming effect of a thick snow cover, mild winters, and high summer precipitation on the ground thermal regime and depth of the seasonal thaw propagation. The standard deviation of the thaw depth on this landscape is ± 0.18 m with the variability coefficient of 10.1% (Table 1).

4. *Arctous-cowberry larch forest on sandy silty loam and sand soils of the sand-ridge locality type (southwestern side of the Tosogolokh lake)*. Pliocene Salban sands underlie this landscape. The highest values of seasonal thaw depths of >1.5 m were observed during the warm periods of 2004, 2006, and 2008. The lowest values are characteristic of the summers of 2001, 2003, 2005, and 2009. The optimal moisture content of the active layer from the previous rainy summer season evidently promoted intensive sand thawing in the dry summer of 2004. The warming effect of summer precipitation led to the increase in thaw depth in 2006 and 2008. In general, summer precipitation has an overall warming influence on sandy soils, resulting in a thaw depth increase. The smallest values of thaw depths in sandy soils are associated with cold winter and dry summer seasons. Hardly visible reduction in thaw depth is evident from the 15-year record (Fig. 2-b.4). Over the period of observations, the standard deviation was 0.10 m and the variability coefficient was 7.04% (Table 1).

5. *Limnas-cowberry thin-trunk larch forest on sandy silty loam and sand soils of the sand-ridge locality type (area in the upper reaches of the Tibigine valley)*. The lithology of this landscape is composed of Neogene Salban sands, similar to the previous landscape. The vegetation cover is dominated

Table 1. Seasonal thaw depth variability at experimental points.

Point no.	Natural-territorial complexes	Seasonal thaw depth, m			Mean square deviation, m	Variation coeff., %	Mean value error, m
		Avg.	Max	Min			
1.	Cowberry larch forest on clayey silty loam soils of the inter-alas locality type	1.08	1.25	0.95	0.08	7.41	0.02
2.	Graminaceous herb meadow on sandy silty loam and clayey silty loam soils of the inter-alas locality type	1.9	2.07	1.63	0.13	6.84	0.03
3.	Mesophytic graminaceous herb meadow on sandy silty loam and clayey silty loam soils of the alas locality type	1.78	2.2	1.4	0.18	10.1	0.05
4.	Cowberry arctous larch forest on sandy silty loam and sand soils of the sand-ridge locality type	1.42	1.57	1.3	0.1	7.04	0.03
5.	Limnas-cowberry thin-trunk larch forest on sandy silty loam and sand soils of the sand-ridge locality type	1.25	1.39	1.12	0.09	7.2	0.02
6.	Lichen-bearberry pine forest on sand soils of the sand-ridge locality type	2.16	2.3	2.03	0.08	3.9	0.02
7.	Limnas-cowberry thin-trunk larch forest on sandy silty loam and sand soils of the southwestern exposed slope 10°	1.24	1.4	1.01	0.12	9.67	0.03
8.	Limnas-cowberry thin-trunk larch forest with some birch on sandy silty loam and sand soils of the northeastern exposed slope 5°	1.36	1.8	1.08	0.19	14.81	0.05
9.	Forest border microzone with larch herb-rich undergrowth on clayey silty loams of the inter-ridge lowland locality type	1.23	1.57	0.85	0.21	17.07	0.05
10.	Birch-larch bluejoint-true moss undergrowth on clayey silty loams on valley bottoms (minor-valley locality type)	1.36	1.62	1	0.17	12.5	0.04

by the dense larch shrub growth that developed after the area was clear-cut in the 1950s. The dense canopy effectively isolates soils from short-term climatic fluctuations. The greatest thaw depth of 1.39 m was recorded during the warm season of 2004. Here, as in our fourth landscape, the optimal moisture content in sands during the dry warm summer probably contributed to the intensive thawing. The smallest values of seasonal thaw depths (1.0–1.1 m) were registered during the summers of 1998 and 2009. The thaw propagation was adversely affected by the cold winter and dry summer seasons. No detectable trend in seasonal thaw depth is evident here (Fig. 2-b.5). The standard deviation of temporal thaw depth variability is ± 0.09 m while the coefficient of variation is 7.2% (Table 1).

6. *Lichen-bearberry pine forest on sand soils of the sand-ridge locality type (bedrock bank edge at the Molotovskaya Pad right bank)*. The continental Jurassic-age sands form the lithologic base of this landscape. The upper surface is complicated by eolian deposits. No abrupt changes in the seasonal thaw depth are observed on this landscape, but the trend toward reduction in seasonal thaw depth is observed (Fig. 2-b.5). The greatest seasonal thaw depths of 2.23–2.3 m were observed in 1999, 2002, and 2008. They are associated with the most rainy and most dry summer seasons following warm snowy winters.

The smallest depths of 2.1–2.03 m correspond to the summers of 2000, 2007, and 2009, characterized by high ice content. The standard deviation of the seasonal thaw depth is equal to ± 0.08 m or 3.9% of the long-term mean value (2.03 m) (Table 1).

7. *Limnas-cowberry thin-trunk larch forest on sandy silty loam and sand soils of the slope (10° steep) forming the left bank of the Tibigine valley*. The Neogene silty-clay loam and sand deposits underline this landscape. Clear-cutting of vegetation in the 1950s was followed by repeated forest fires. Prior to the latest fire, in 2002, the landscape was covered by larch shrubs. The vegetation cover was almost completely destroyed by the fire, and the forest stand died and dried up. The greatest seasonal thaw depth values of 1.3–1.4 m were observed during the rainy thawing seasons of 1999, 2006, and 2008 and during the first two (2003–2004) seasons after the 2002 forest fire. The lowest depth of thaw (1.0–1.15 m) occurred in 1997, 2000, 2001, and 2009 in response to dry summer seasons and warm winters. No trend in thaw depth is evident from the long-term record (Fig. 2-c.7). The standard deviation of thaw depth is ± 0.12 m, and the coefficient of variation is 9.67% (Table 1).

8. *Limnas-cowberry thin-trunk larch forest with some birch on sandy silty loam and sand soils in the bottom of the slope (5° steep) forming the right Tibigine valley side*.

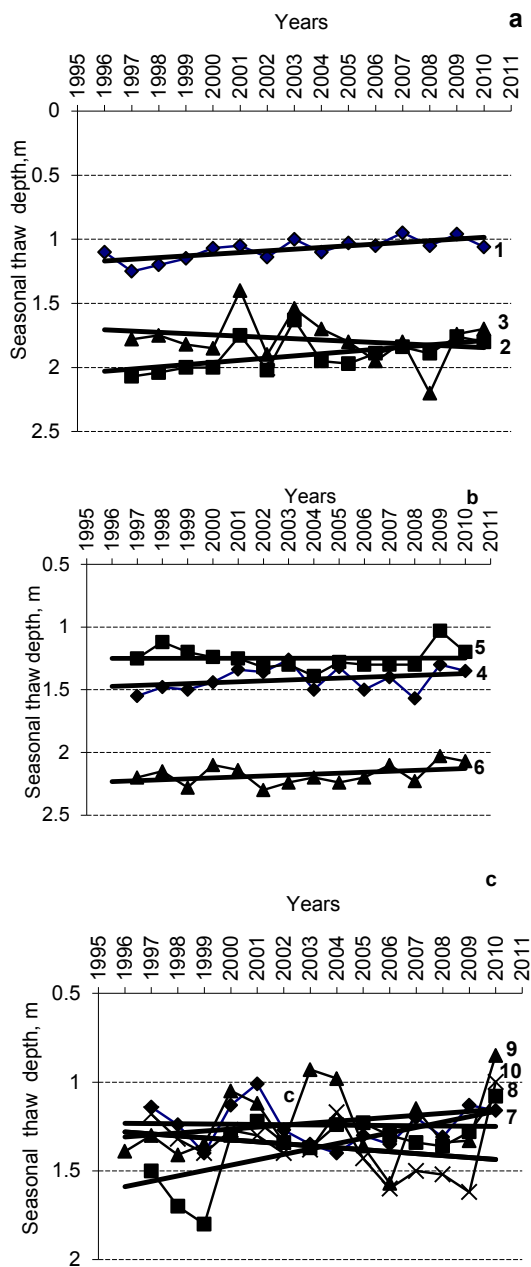


Figure 2. Seasonal thaw depth at the inter-alias (a,1; a,2); alias (a,3); sand-ridge (b,4; b,5; b,6); slope (c, 7; c, 8); inter-ridge lowland (c, 9) and minor-valley (c, 10) locality types.

The vegetative cover suffered almost no 2002 fire damage in this landscape. The trend toward reduction of thaw depth is evident (Fig. 2-c.8). The greatest thaw depths (1.5–1.8 m) were observed in 1997–1999. High values of 1.35–1.4 m were also recorded in 2003 and 2008. The lowest thaw depth value of 1.08 m was observed in 2010. A high amount of summer precipitation during 1999 led to saturation of the active layer and subsequent high ground-ice content, which prevented deep thaw penetration during following summer seasons. Apparently, continuous soil moisture drainage from elevated surfaces contributed to high winter ice content and low thaw propagation (1.2–1.3 m) even during snowy and rainy years. The negative thaw depth trend is evident (Fig. 2-c.9). The standard deviation of the thaw depth on this landscape type is ± 0.19 m, and the coefficient of variation is

14.81% (Table 1).

9. *Forest border microzone with larch herb-rich undergrowth on clayey silty loams of the inter-ridge lowland locality type.* The research area is found within the inter-ridge lowlands at the junction of the Neogene, Paleogene, and Jurassic formations. It is divided into the following landscapes: sedge-peat swampy sparse larch forests, dwarf birch swampy sparse larch forests, sedge-bluejoint hummock swampy sparse larch forests, and peripheral willow-birch margins alternated with forest clearings. The southern parts of forest clearings are occupied by shrubs wood species. The greatest seasonal thaw depths here (1.4 m and above) were observed in 1998 and 2006. The winter seasons of 1997/1998 and 2005/2006 had high snow thicknesses of 0.39–0.40 m, followed by rainy summer seasons, resulting in deep thaw propagation. Similar to other landscapes, the rainy summer and fall of 2003, 2006, and 2008 led to ice accumulation at the bottom of the active layer that prevented deep thaw in the following summers. The negative trend in seasonal thaw depth is evident in Figure 2-c.9. The standard deviation of thaw depth is ± 0.21 m, and the coefficient of variation is 17.07% (Table 1).

10. *Birch-larch bluejoint-true moss undergrowth on silted clayey silty loams in the Tibigine valley bottom (minor-valley locality type).* The Tibigine valley bottom at the study site is cut into the Neogene Salban sands with a thickness of 3–5 m. The vegetation cover sustained significant damage during the 2002 fire. In the following years, the birch-larch undergrowth dried out, and willow shrubs and herbs appeared in the surface cover. In 1999 and 2003, the seasonal thaw depth increased to 1.4 m due to an increase in moisture content, and in 2006–2009 the greatest depth of 1.6 m was associated with anomalously intensive summer precipitation and corresponding flooding of the entire valley bottom. It should be noted that depressions were flooded twice during the research period (in 2003 and in 2006–2009). After refreezing of the saturated soils, smaller seasonal thaw depths (1.0–1.2 m) were usual. But in general, rainy warm seasons during the recent nine years resulted in an increasing trend in thaw depths (Fig. 2-c.10), which is evidently associated with incomplete re-freezing of the saturated active layer. The standard deviation of the seasonal thaw depth at this landscape is ± 0.17 m, and the coefficient of variation is 12.5% (Table 1).

Conclusion

The seasonal thaw depth in contrasting landscapes of Central Yakutia responded differently to the climatic forcing over the past 15 to 16 years (1996–2010). For example, in six out of ten landscapes (sites 1, 3, 4, 6, 8, and 9) negative trends in the seasonal thaw depth are observed. At two landscapes (sites 2 and 10) the seasonal thaw depth increased, and at two landscapes (sites 5 and 7) no long-term trend was evident. Similar results were obtained earlier by other researchers (Skryabin et al. 1998, Pavlov et al. 2004, Pavlov 2008).

Summer precipitation plays a significant role in the increase of the seasonal thaw depth by providing optimal soil moisture content. Mild and snowy winters and early summer rains are also favorable for deep thaw penetration.

On the contrary, dry and ice-saturated conditions within the active layer prohibit deep thaw. Cold and low-snow winters adversely influence the seasonal thaw depth as well, especially in landscapes underlain by sandy soils. High vegetation (grass) productivity on open meadow landscapes during the 2003, 2006, and 2007 rainy summers contributed to reduced seasonal thaw depth.

The highest interannual variability in thaw depth was observed on the valley bottom landscape (sites 7 and 8), the forest border landscape of the transient inter-ridge lowland belt (site 9), the valley bottom (site 10), in open alas meadows (site 3), and inter-alas meadows (site 2). On those landscapes, the standard deviation is 0.12 to 0.21 m and the coefficient of variation is 6.84 to 17.1% of the 15-year mean values. The seasonal thaw depths under the inter-alas cowberry larch forest (site 1), the flat sand ridge thin-trunk larch shrub (site 5), and the sand ridge lichen-bearberry pine forest (site 6) are less dynamic; their standard deviation is 0.08 to 0.09 m, and the coefficient of variation is 3.9 to 7.41%, in relation to climate forcing.

References

- Are, A.L. & Demchenko, R.Y. 1972. Some results of long-term ground thawing monitoring in the Yakutsk surrounding: Experimental heat exchange studies in permafrost. Moscow: Nauka, 91-97 (in Russian).
- Efimov, A.I. 1952. Some results of three-year ground temperature monitoring in the area of Yakutsk: *Permafrost study in the Republic of Yakutia*. Moscow: Izd-vo AN SSSR, 8-19 (in Russian).
- Fedorov, A.N. 1985. Forest felling role in permafrost landscape development in Central Yakutia: *Regional and engineering geocryological studies*. Yakutsk: IMZ SO AN SSSR, 111-117 (in Russian).
- Fedorov, A.N., Bosikov, N.P., Vasiliev, I.S., Varlamov, S.P., & Samsonova, V.V. 1992. Permafrost landscape dynamics in Central Yakutia after technogenic impact. *Rational environmental management in cryolithozone*. Moscow: Nauka, 146-152 (in Russian).
- Fedorov, A.N., Maksimov, T.H., Gavriliev, P.P. et al. 2006. Editors: M.K. Gavrilova, P.Y. Konstantinov, M.M. Shats, *Spasskaya Pad: kompleksnye issledovaniya merzlotnykh landshaftov*. Yakutsk: Izd-vo Instituta merzlotovedeniya SO RAN, 210 pp. (in Russian).
- Fedorov, A.N., Vasiliev, I.S., & Vasiliev, A.I. Landscape Characteristics: *Spasskaya Pad: kompleksnye issledovaniya merzlotnykh landshaftov*. Yakutsk: Izd-vo Instituta merzlotovedeniya SO RAN, 45-54 (in Russian).
- Gavriliev, P.P. & Ugarov, I.S. 1996. Permafrost agrarian landscape functioning peculiarities. Editors: V.T. Balobayev, M.K. Gavrilova, and A.N. Fedorov, *Vliyaniye klimata na merzlotnye landshafty Tsentralnoy Yakutii*. Yakutsk: Assotsirovanny chlen izd-va SO RAN, 122-136 (in Russian).
- Gavriliev, P.P., Ugarov, I.S., & Efremov, P.V. 1996. Cryoecological studies and monitoring of Yakutia land resources: *Znaniye - na sluzhbu nuzhdam Severa (Report abstracts of the Northern Forum First International Conference)*. Yakutsk: Severoved, 186 (in Russian).
- Konstantinov, P.Y., Argunov, R.N., Gerasimov, E.U., & Ugarov, I.S. On seasonal thawing depth relation to inter-annual mean annual ground temperature variability. *Kriosfera Zemli. 3(X):15-22* (in Russian).
- Pavlov, A.V. 1975. *Ground and air heat exchange in northern and middle latitudes of the USSR territory*. Yakutsk: Kn. izd-vo, 302 pp. (in Russian).
- Pavlov, A.V., Skachkov, U.B., & Kakunov, N.B. 2004. Perennial seasonal ground thawing depth variations and meteorological factors interrelation: *Kriosfera Zemli 4 (VIII). 3-11* (in Russian).
- Pavlov, A.V. 2008. *Cryolithozone monitoring*. Novosibirsk: Akademicheskoye izdatelstvo GEO, 229 pp. (in Russian).
- Skryabin, P.N., Varlamov, S.P., & Skachkov, U.B. 1992. Evaluation of ground temperature mode changes due to natural conditions disturbance: *Rational environmental management in cryolithozone*. Moscow: Nauka, 165-173 (in Russian).
- Skryabin, P.N., Skachkov, U.B., & Varlamov, S.P. 1998a. Climate warming and thermal ground state monitoring in Central Yakutia: *Geocryology problems*. Yakutsk: Izd-vo Instituta merzlotovedeniya SO RAN, 31-39 (in Russian).
- Skryabin, P.N., Varlamov, S.P., & Skachkov, U.B. 1998b. Ground temperature mode monitoring studies in Central Yakutia: *Geography and natural resources*. Novosibirsk, 2: 49-55 (in Russian).
- Solovyev, P.A. 1959. *Cryolithozone in the northern part of the Leno-Amga interfluve*. Moscow: Izd-vo AN SSSR, 144 pp. (in Russian).
- Turbina, M.I. 1985. Agricultural development of landscapes with ground ice in Central Yakutia: *Central Yakutia nature protection*. Yakutsk, 31-42 (in Russian).
- Vasiliev, I.S. & Argunov, R.N. 2005. Seasonally thawed layer thickness dependence on ground moisture content in the Lena-Kenkeme interfluve. *Kriosfera Zemli. 3 (IX):10-15* (in Russian).
- Vasiliev, I.S. & Gerasimov, E.Yu. 2001. Variability of active layer thickness, GAME study area. Central Yakutia. *Proceedings. The Fifth International Study Conference on GEWEX in ASIA and GAME*, Nagoya. Japan. October 3-5. Vol. 2, 440-444.

Assessment of the Corrosiveness of Permafrost Landscapes

M.A. Velikotskiy, V.P. Marakhtanov
Lomonosov Moscow State University, Moscow, Russia

Abstract

It is shown that existing concepts of the influence of various natural factors on the corrosion of steel pipelines in the permafrost zone must be corrected. When correcting the concepts, it is necessary to consider the possibility of active corrosion as well as the specificity of pipelines themselves representing macrosystems in relation to the elementary components of the corrosion process. A close relationship between the spatial development of pit corrosion along a pipeline and the heterogeneity of aeration conditions in the surrounding landscapes was established. In accordance with this, it is proposed to use the standard deviation of redox potential values (ΔEh) as the main indicator of landscape corrosiveness.

Keywords: acidity; differential aeration; electrochemical model; permafrost landscapes; pipeline corrosion; redox potential.

Introduction

The degree of the corrosion danger posed by permafrost to steel pipelines is still a debatable issue. Previously, it was believed that the absence of water in the liquid phase of frozen ground and its low temperatures contribute to reduced chemical activity. For example, A.A. Saukov noted that according to the theory of van't Hoff-Ostwald an infinite decrease of natural chemical reactions must occur at about 0°C (Saukov 1951). N.M. Strakhov expressed a similar opinion: according to the van't Hoff-Ostwald law, the rate of chemical reactions is reduced by half with a 10°C temperature decrease. Therefore, it can be stated that low environmental temperatures in the polar regions cause a drastic suppression of chemical processes (Strakhov 1960).

The fallacy of such a notion consisted in the underestimation of the presence of unfrozen water in cohesive frozen ground—clays, silty clays, and silts (Ershov 1986). Unfrozen water with the dissolved carbon dioxide contributes to electrochemical corrosion in frozen ground. Seasonally thawed ground of the cryolithozone is also corrosion-active due to the high content of H^+ ions and of dissolved organic matter. It should be particularly noted that buried pipelines often transport warm gas (with temperatures up to 20°C and higher). Thus, even in winter, there may be thaw areas around the pipe. Moisture conditions and chemical composition in the thaw areas are similar to the active layer in the permafrost zone.

To assess the corrosiveness of ground, we use a large number of indicators: the granulometric composition of ground, the moisture content, the ionic composition of the water extract, the electric resistance of the ground (ρ), the acidity (pH), the concentration of molecular hydrogen (rH_2), and the redox potential (Eh). However, not all the indicators in the cryolithozone have equal importance for the assessment of corrosion activity.

Seasonally thawed ground in the permafrost zone is characterized by high moisture content. The high moisture content predetermines the ground's low electric resistance ρ , which, according to the State Standard of 1989, is an indicator of high corrosiveness. However, this criterion is often ineffective in the evaluation of the corrosiveness of ground within the cryolithozone.

Permafrost is characterized by slightly acidic and acidic conditions of the medium (pH is below 6). This indicator is very important. However, it is also insufficient to draw an unambiguous conclusion on the corrosiveness of the ground.

The index of concentration of molecular hydrogen (rH_2) is commonly used by biologists to assess the living conditions of sulfate-reducing or sulfur bacteria. Sulfur bacteria are not very active in tundra at low temperatures, but they are rather active in the ground around pipelines with warm gas. Therefore, in a number of cases this indicator can be used to assess the corrosiveness of the ground.

The most important indicator of the corrosive activity of the permafrost is the redox potential Eh , the role of which has been underestimated up to the present time. It is generally accepted that the value of Eh depends only on the degree of the aeration of the ground and on pH . However, it is also influenced by the moisture content of the ground, its ionic composition, electrical conductivity, and the activity of sulfur bacteria. Therefore, Eh can be considered as an integral indicator of the corrosion activity of the ground in the permafrost zone.

In Australia, the first researcher who used the redox potential to assess the corrosiveness of the ground was Lorking (Evans 1962). He determined the corrosiveness of soil, depending on Eh and pH , and under the condition when there were no sulfur bacteria. Meanwhile, he utilized the Purbe diagrams (Pourbaix 1963). Much attention to the influence of the redox potential on corrosion was paid by I.A. Denison (1963). According to Denison, the main factor determining the change of corrosion rate in time is the degree of soil aeration. The rate of deep corrosion decreases rapidly with time in soils with oxidizing properties, while in a reducing environment it is proportional to the time of the experiments. According to Denison (1963), severe corrosion of iron must occur in soils with limited aeration (in clays or bogs) while in well-aerated soil all metals are rather corrosion-resistant. The absolute value of the redox potential is used as a criterion for evaluation of the ground's corrosiveness (Strizhevskiy 1986). In this case, high values of Eh indicate low corrosive activity of the ground, while negative values and ones close to zero indicate a high corrosive environment (Strizhevskiy 1986).

All of these authors drew their conclusions based on

research into such electrochemical models as microelements, while a pipeline including the surrounding ground represents a macrosystem where slightly different regularities are possible, compared with those described above. For this reason, it was of scientific and practical interest to perform the corresponding research under real natural conditions of the cryolithozone in the northern part of West Siberia with its developed network of gas pipelines.

Methods

From 2000 to 2009, the authors surveyed gas pipeline systems at the Medvezhe gas field. These systems were built within permafrost landscapes (of tundra, forest tundra, and northern taiga). Particular attention was paid to the corrosive wear of pipes (external corrosion) in different types of landscapes. The territory was preliminarily divided into geographical zones. Based on the interpretation of aerial and satellite photographs, there were observed 24 different units that formed four groups (landscape types): forest, tundra, bog, and peatland landscape type (Marakhtanov et al. 2011). These landscape types significantly differ in a complex of ground properties that affect the corrosion of pipeline metal: in lithological composition, moisture content, chemical composition, and in temperature. The depth of steel pipe corrosion was established in field conditions and the ground was sampled to evaluate its corrosiveness. The samples were

studied in the analytical laboratory of the soil-ecological station of the Institute of Physical-Chemical and Biological Problems of Soil Science, RAS, Pushchino. Some results of these studies are presented in Table 1.

Based on the data presented in Table 1, we made an effort to establish the correlation between the Eh , pH , and ρ values and the depth of corrosion pits in the metal of the pipeline. The results revealed that there is actually no correlation among them. As an illustration, we will use the diagram in Figure 1. The relationship between the depth of corrosion (H) and the value of Eh (Fig. 1) can be approximated with the formula $H \approx -0.0014Eh + 1.49$. The correlation coefficient $r = -0.22$ indicates a lack of a significant connection. Other parameters (pH and ρ) have an even lower correlation with corrosion.

These data allow us to draw conclusions on the electrochemical models that microelements should be applied to pipelines with extreme caution because electrochemically pipelines with the surrounding soils represent macrosystems consisting of separate microelements. Electric currents arise in macrosystems due to the differential aeration that occurs, that is, between ground differing in air permeability (sands-clays) or in relief and between the surfaces with different moisture conditions (depressions-elevations, hummocks-inter-hummock areas). These currents suppress the ones of small systems and represent the main corrosion currents that predetermine the existence of landscape corrosion zones.

Table 1. The main characteristics of ground (Eh , pH , ρ) for different landscape types and the depths of corrosion pits in the metal of the pipeline.

№№ ser. no.	Landscape type	Eh , mV	pH	ρ , $ohm\cdot m$	Depth of corrosion, mm	№ ser. no.	Landscape type	Eh , mV	pH	ρ , $ohm\cdot m$	Depth of corrosion, mm
1	forest	319	5.3	4	2	31	peatland	309	3.9	-	1
2		239	6.4	12	0.5	32		255	5.8	1	0
3		185	5.9	7	0	33		44	5	61	2
4		246	6.2	11	1	34		64	6.4	6	0
5		103	6.3	3	3	35		56	6.1	5	0.1
6		152	5.8	14	0	36		64	5.7	2	0.5
7		222	5.9	64	0	37		64	5.8	3	2
8		209	5.8	49	0.1	38		65	6.7	4	0
9		215	5.2	12	0	39		250	6.4	11	0
10		216	5.2	55	0	40		371	3.8	-	1
11	tundra	282	5.4	6	1.5	41	330	4.6	2	1	
12		72	5.4	9	0	42	325	4.6	17	0	
13		259	6	4	0	43	236	6.4	12	0.5	
14		287	5.4	3	0	44	179	5.3	14	0	
15		285	5.6	10	0	45	168	5.4	-	0.5	
16		287	5.2	12	0	46	48	4	-	1	
17		311	5.1	54	0	47	88	6	-	2	
18		173	6.2	15	0	48	38	4.5	58	2.5	
19		161	5.2	4	0	49	210	5.7	13	0	
20		230	5.8	16	1.5	50	37	3.5	9	0	
21		213	5.5	39	0	51	136	5.3	75	0.1	
22		166	5.7	27	0	52	88	5	-	2	
23		215	6.2	-	0	53	69	4	9	3	
24		209	5.5	19	0	54	46	4.4	6	0	
25		202	6	-	3	55	72	5.8	2	0	
26		97	5.2	-	1	56	75	5.5	-	1	
27		90	5.5	5	0	57	81	5.3	14	0	
28		104	5.4	14	0	58	37	4.6	-	0.1	
29		98	5.5	6	1.5	59	50	3.3	-	2	
30		116	5.3	3	0.5	-					

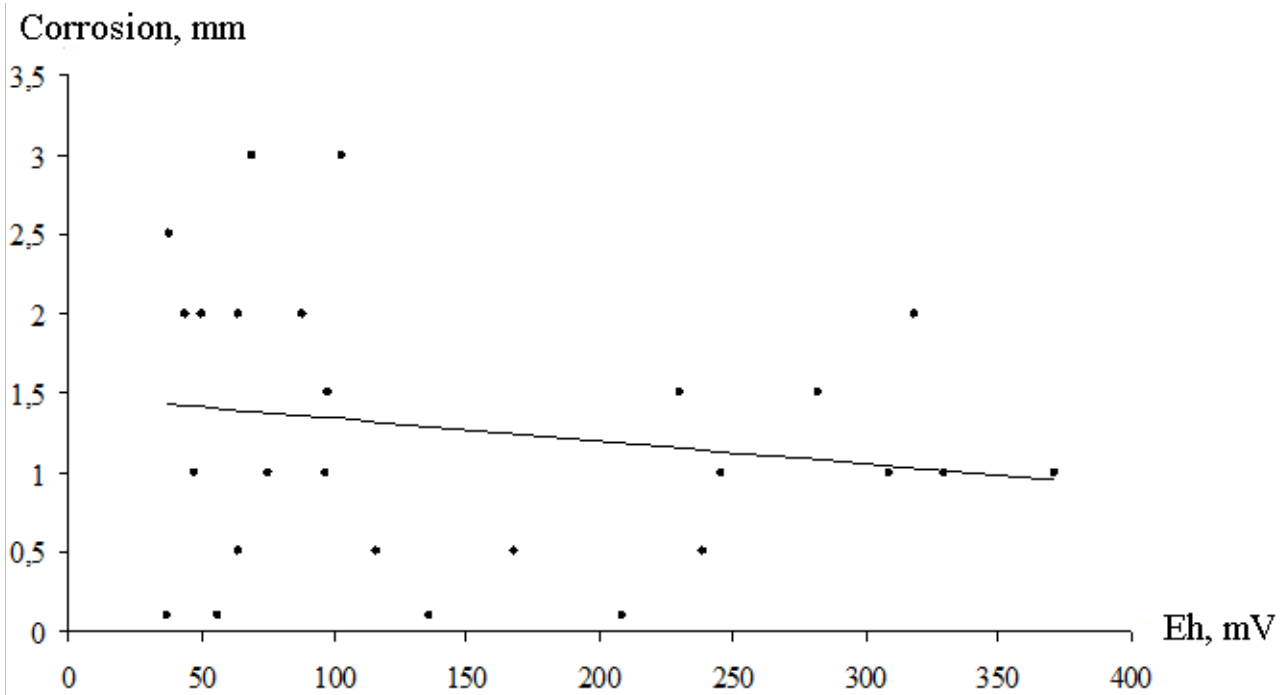


Figure 1. The dependence of the depth of metal corrosion of a gas pipeline on the redox potential *Eh*.

Table 2. Metal corrosion of a gas pipeline in different landscape types.

Landscape type	Length of a pipeline in the given landscape type, m	Length of the sections of the gas pipeline with metal pit corrosion, m	Percentage of the gas pipeline sections affected by corrosion <i>N</i> , %
Forest	31230	349	1.12
Tundra	79555	4458	5.60
Peatland	5932	971	16.37
Bog	23577	5438	23.06

Table 3. Standard deviation (ΔEh) of the redox potential in different landscape types.

Landscape type	ΔEh , mV	<i>N</i> , %
Forest	57	1.12
Tundra	78	5.60
Peatland	104	16.37
Bog	108	23.06

The idea of the role of differential aeration in metal corrosion was first expressed by Evans in 1923. Accordingly, different oxygen access to a pipe may cause differences in electric potentials of up to 0.9 V between different ground conditions and become a major cause of corrosion processes (Evans 1962).

In Russia, Mikhaylovskiy & Tomashov (1958) developed this idea and considered it correct to speak not about corrosive activity of a separate ground or ground of a certain part of a pipeline, but about the corrosive activity of a pipeline as a whole. Nikitenko (1965) noted that relief and vegetation predetermine different moisture content of the ground along the pipeline, which affects the access of oxygen to the pipeline and the value of the difference between the “pipe

and soil” potentials along the gas pipeline. Mingalev (1976) established that the development of local corrosion areas in the oil pipelines in the peatlands of West Siberia is connected with local aeration and that the deepest corrosion cavities are associated with the sites with maximum difference of the oil pipeline and soil potentials from -0.48 to -0.68 V.

Thus the greater the heterogeneity of factors within a certain type of landscape that determines the aeration degree, the more corrosively dangerous is this type of landscape. As there is a close relationship between the degree of aeration and the value of redox potential, the degree of irregularity of the *Eh* value along a pipeline can play a decisive role in the corrosion of the metal.

To confirm this idea, we used the data of the *Eh* value in different landscape types (Table 1) as well as the results obtained by the survey of the technical condition of the gas trunk pipeline of the Medvezhye gas field with its total length of 140 km (Table 2).

Based on the data in Table 1, we calculated the values of the standard deviation of *Eh* showing how widely data points are scattered relative to their mean value. The value of standard deviation (ΔEh) was calculated for each landscape type according to the formula

$$\Delta Eh = \sqrt{\frac{\sum (Eh - \overline{Eh})^2}{(n - 1)}} \tag{1}$$

where \overline{Eh} – the average value for the given landscape type, *n* – the number of data. The results are presented in Table 3, which also includes the *N* values from Table 2.

The data from Table 3 are graphically presented in Figure 2. As one can see in the figure, there is a close relationship between ΔU and *N* (correlation coefficient is 0.96). This relationship is approximated by the parabolic dependence:

$$N \approx 0,00733\Delta U^2 - 0,815\Delta U + 24 \tag{2}$$

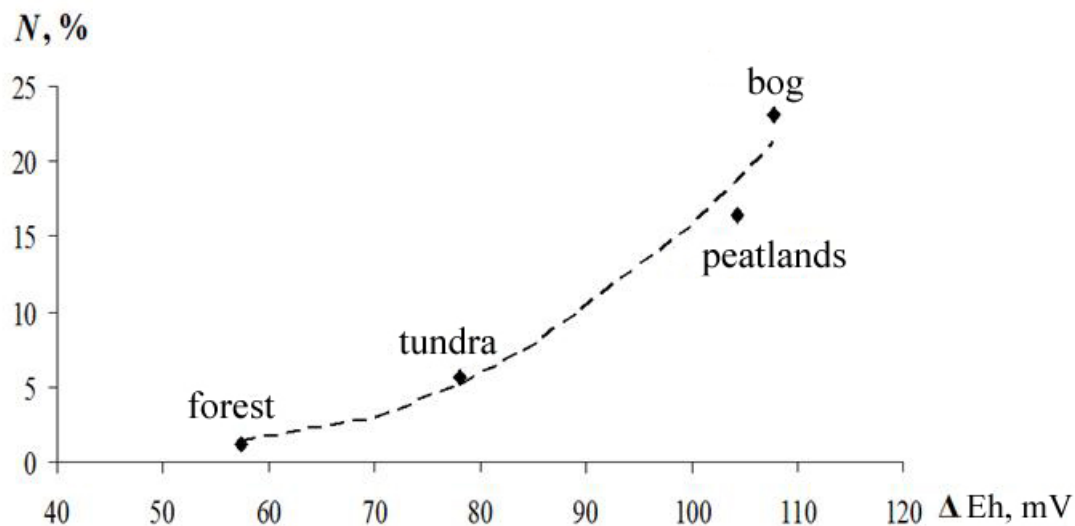


Figure 2. The dependence of the proportion of the gas pipeline's sections with pit corrosion N on the value of the standard deviation of the redox potential (ΔEh).

In addition to ΔEh , the N value was compared with the standard deviations of other parameters from Table 1: ΔpH , and $\Delta \rho$. However, in these cases no significant correlation was noted.

Thus, according to our data, the corrosion of metal pipelines in the permafrost zone most actively occurs in the landscape type with frequent alternation of drained areas (with high Eh) and watered areas (with low Eh), in bogs and peatlands. Besides, the heterogeneity of permafrost conditions, revealed in the alternation of frozen and thawed ground, may have some impact. In tgw forest landscape, the minimum fluctuation of Eh was observed. Therefore, corrosion processes are least active. The observed regularity shows that the factors of ground aeration have a close relationship with the landscape conditions of territories in which a pipeline was buried.

The obtained results allow the following conclusions:

- 1) There is no direct dependence between the absolute value of the redox potential or other traditional indicators of the corrosive properties of ground (pH , ρ) and the depth of corrosion pits. In the permafrost zone, the low values of the redox potential in acidic environments and in the absence of sulfur bacteria indicate high moisture content and the development of gley processes, but not the high corrosiveness of the ground. Similarly, high values of the redox potential in the area of acidic environment under the conditions of high moisture content and in the absence of oxygen are not indicative of the high corrosiveness of the ground.
- 2) The amplitude of the Eh fluctuations is a very effective indicator of the corrosiveness of the ground in the permafrost zone. Sharp fluctuations of this indicator cause the currents of the differential aeration pairs to develop and activate electrochemical processes. In this case the heterogeneity of Eh in the permafrost zone may further increase (as compared to more southern territories) due to the alternation of thawed and frozen zones along the gas pipeline, and, perhaps, also due to the heterogeneity of the cryogenic structure of the ground.
- 3) The amplitude of the fluctuation of the redox potential must be included in the State Standard as the main

criterion for evaluating the corrosiveness of permafrost together with pH , ionic composition of water extract, and the indicator of electrical resistance.

References

- Denison, I.A. 1953. Corrosion of construction materials in underground conditions. In *Corrosion of Metals*. Moscow, pp. 9-28 (in Russian).
- Ershov, E.D. 1986. *Physical Chemistry and Mechanics of Frozen Ground*. Moscow, Izd-vo Mosk. un-ta, 332 pp. (in Russian).
- Evans, Yu.R. 1962. *The Corrosion and Oxidation of Metals*. Moscow, Mashgiz, 856 pp. (in Russian).
- GOST 9.602-89. 1989. *ESZKS. Underground constructions*. Moscow, Izd-vo standartov, 56 pp. (in Russian).
- Marakhtanov, V.P., Velikotskiy, M.A., Chigir, V.G. et al. 2011. Technological, geological and ecological analysis of gas transportation systems of the Medvezhye gas field. *Proceedings of the Fourth Conference of Russian Geocryologists*. Moscow, Iz-vo Mosk. un-ta, Vol. 3, 49-55 (in Russian).
- Mikhaylovskiy, Yu.N. & Tomashov, N.D. 1958. The method of determination of the corrosion properties of grounds. In *Theory and Practice of Corrosion Protection of Underground Constructions*. Moscow, pp. 209-223 (in Russian).
- Mingalev, E.P. 1976. *Corrosion of the Buried Pipelines in the Peatlands of Western Siberia*. Moscow, VNIIOENG, 28 pp. (in Russian).
- Nikitenko, E.A. 1965. The dependence of the corrosion of a steel pipeline on the change in ground conditions along the pipeline route. *Protection of Metals* 1 (no. 1): 91 – 98. (in Russian).
- Pourbaix, M. 1963. *Atlas d'equilibres electrochimiques a 25°C*, Paris.
- Saukov, A.A. 1951. *Geochemistry*. Moscow, Gosgeoltekhizdat, 192 pp. (in Russian).
- Strakhov, N.M. 1960. *Principles of the theory of lithogenesis*. Moscow, Izd-vo AN SSSR, Vol. 1, 212 pp. (in Russian).
- Strizhevskiy, I.V. 1986. *Underground Corrosion and Protection Methods*. Moscow, Metallurgiya, 112 pp. (in Russian).

Geocryological Programs for Specialist Training at Zabaikalsky State University

A.G. Verkhoturov
Zabaikalsky State University, Chita, Russia

Abstract

Considerable attention is paid to geocryologic disciplines in the curriculum for hydrogeological and geological engineering training at Transbaikal State University (TbSU). The majority of graduates tend to find jobs in the southern cryolithozone areas where major challenges in construction and groundwater exploration and management are associated with permafrost. Although the Russian Third-Generation of Educational Standards (RFES-3) does not include geocryology as a required discipline for the Practical Geology (specialization in Groundwater Exploration and Geotechnical Investigation) program, the TbSU Department of Hydrogeology and Engineering Geology provides a significant number of elective courses in geocryology in its curriculum. These include General Geocryology, Geocryological Research Methods, Geocryological Forecast, Physics, Chemistry and Mechanics of Frozen Ground, Engineering Geocryology, and Groundwater in the Cryolithozone. These courses, along with active student involvement in the HGEG Department's permafrost research activities, provide students with the knowledge and practical skills necessary for working in permafrost-affected areas.

Keywords: Geocryology; discipline; department; credit; specialist; standard.

Introduction

Transbaikal State University (TbSU) has been training mining engineers (hydrogeologists and geological engineers) for more than 30 years through its Department of Hydrogeology and Engineering Geology (HGEG). The department was established in response to intense development of the Transbaikalia region and the construction of the Baikal-Amur Railroad. Since the 1980s, the department has been training students in the areas of Groundwater Exploration and Geotechnical Investigation.

Traditionally, HGEG has had close ties with the Department of Geocryology at Lomonosov Moscow State University (MSU). Professor V.A. Kudryavtsev, head of the MSU Department of Geocryology, has actively contributed to the establishment of a team of faculty and researchers in the HGEG Department. For example, Professor Kudryavtsev sent one of his best students, V.G. Kondratev, to Chita. Later, the HGEG Department was further strengthened by the addition of MSU Department of Geocryology graduates D.M. Shesternev (1980), V.S. Petrov (1981), and A.I. Kalinin (1981), all of whom have a Ph.D. in Geology and Mineralogy. Such considerable attention to geocryology at Transbaikal State University is attributable to the complex set of permafrost-related problems faced by hydrogeologists and geological engineers in the southern cryolithozone.

HGEG Department graduates are in high demand due to a revival of the mining industry and new exploration and development in the Transbaikalia region. A large number of jobs are also available in the Amur Region and the Khabarovsk and Primorsky Territories.

The department admits 25–50 tuition-free students annually. Since its formation, the HGEG Department has trained approximately 900 specialists in all areas of geological engineering studies. From 1996 to 2011, the department has provided comprehensive student training at three Russian educational levels (Bachelor of Science, diploma-specialist, and Master of Science) in the Geology and Mineral Exploration program. The department continues to train engineering specialists in Practical Geology,

Groundwater Exploration, and Geotechnical Investigation. The department has 10 faculty members, 73% of whom have doctoral (Ph.D.) degrees and 23% of whom have advanced doctoral degrees. This meets the Russian state requirements for higher education.

The HGEG Department occupies 377 m² of office, training, and laboratory space (Verkhoturov 2010). Lectures are conducted in the TbSU lecture halls. The department's computer lab has six workstations with Internet access. Students also have full access to the two computer labs with 25 workstations in the Geology Department.

Field geologic training is conducted at the TbSU Sretenskiy Research and Educational Station. More specialized field classes (e.g., geophysical, mining and drilling, geotechnical, hydrogeological, and geocryological investigations) are conducted at the Arakhley Field Training Station.

Internship opportunities for students are provided in geological and hydrogeological expeditions and field parties and geotechnical engineering. Civil engineering and mining companies and state and federal agencies offering internships include ZabaykalTISIZ JSC, Vostokgeologiya LLC, Zapadnoe JSC, Zabaykalgeomonitoring FSUE, Priargunskoe Mining and Chemical Enterprise JSC, the INREC SB RAS laboratories of general cryology, and others.

The Department's Research Areas

The HGEG Department conducts research in two areas: 1) engineering geology, geocryology and soil science, and 2) geomechanical provision of open pit mining, construction and operation of engineering structures.

The first research area has both fundamental and practical aspects. Professor V.G. Kondratev leads the program for permafrost and geocryological monitoring of the southern cryolithozone for economic development. In recent years, research under this program has resulted in five patents, four monographs, two Ph.D. dissertations, and three dissertations in preparation. Professor D.M. Shesternev leads an applied research course on Transbaikalia engineering and

geocryological issues. Over the past five years, he has published five monographs and two textbooks on permafrost physics, chemistry and mechanics, and a statistical analysis of geotechnical data. His textbook *Physics, Chemistry and Mechanics of Frozen Soils* has been prepared for publication.

The second research area, led by Dr. V.A. Babello, was established in 2011 and is related to geocryologic problems for the mining industry.

Students at different levels actively participate in the department's research, which provides them with the necessary skills in scientific methods. Student researchers are generally responsible for carrying out tests and experiments and for the development of individual or group research projects under the guidance of an experienced adviser. This work usually leads to the development of master's theses and/or Ph.D. dissertations.

From 2003 to 2008, the department's average annual research expenditures were approximately 2.5 million rubles. In 2009, the research expenditure was 0.8 million rubles, which increased to over 1 million rubles in 2010.

Significance of Initiative Research Programs in Specialist Training

To attract students to scientific research and to increase the HGEG Department's scientific potential, several unfunded initiative programs were developed. In 2007–2010, two programs were established: Ecological State and Management of Transbaikalia Groundwater; and Dynamics of Exogenous Geological Processes in Response to Development and Global Climate Change.

In 2011–2014, two additional research programs will be developed: Artificial Drainage of Potential Mining Areas and its Effect on Groundwater; and Geotechnical Characteristics of the Transbaikalia Region and Their Relation to Climate Dynamics and Development.

The University-wide Student Research Days are held annually in March and April. During these events, students present results of their research and participate in panel discussions. The best students participate in the national and international conferences and student research competitions. Over the last five years, students have published 72 papers and reports based on their unfunded and funded research. Eleven papers were prepared in collaboration with faculty (Fig. 1).

Student research is also summarized in their term papers and theses. In many cases it provides a foundation for Ph.D. studies in Engineering Geology, Geocryology, and Soil Science.

Teams of students from our department took second place in 2005 and the third place in 2007 at the Russian National Hydrogeology and Engineering Geology Student Competition in Tomsk. Our student Roman Korostovskiy was awarded third place in 2006 and first place in 2007 at the Students and Progress in Science and Technology International Conference in Novosibirsk. In 2009, our student Vitaliy Danzanov was awarded third place at the same student competition.

In the past two years, the department's students have regularly participated in scientific conferences, including Problems of Mineral Resources Exploration in the 21st

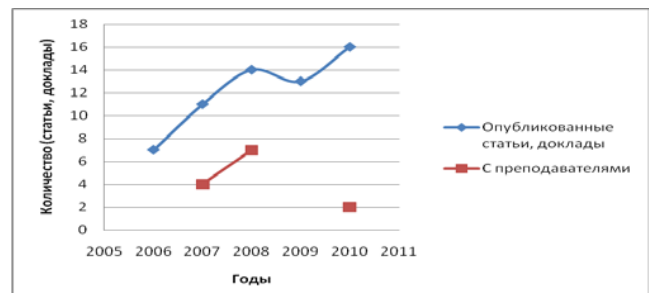


Figure 1. Number of student publications.

Century as Viewed by the Youth in Moscow; Problems of Geology and Exploration of Mineral Resources in Tomsk; and others. The students are repeatedly rewarded with diplomas and honorary certificates.

The students' interest in research has increased after the conferences held at the HGEG Department. In 2008, we hosted the National Research and Practice Conference on Hydrogeology, Engineering Geology, Geocryology, and Geoecology of the Transbaikalia and Adjacent Areas. Students begin to identify themselves as part of the future profession when they participate in conference organization, get to know senior colleagues, study the conference materials, and listen to reports.

The analysis of term papers showed that, other things being equal, the quality of work is higher if it is based on materials obtained by the students during their research at the department, and their grades are better as a result. Research-based student papers are more reasoned and show personal involvement (e.g., field studies, water and soil samples tests, etc.).

Most specialist-degree students use research results to solve specific questions in their graduate research, while the master's students present the thesis as a result of a two-year research project. The defense grades are high when the thesis topic coincides with a research area of the department (either funded or unfunded). If a master's student's thesis is not related to the department's research, the work is usually questionable.

Geocryological Disciplines in the Curriculum

After the shift to the third-generation RFES in 2011, the TbSU HGEG Department developed new curricula which fully comply with the federal state education standard for program 130101.65 Practical Geology, Specialization, Exploration of Groundwater and Geological Engineering.

Transbaikalia, like most Siberian and Far East regions, is located in the area underlain by permafrost. Permafrost plays an important role in groundwater formation and flow regime and affects engineering structures. Often, permafrost degradation causes deformation and sometimes collapse of structures. That is why geocryological disciplines play an important role in our curriculum. The main subjects and the total number of credits for each subject are shown in Figure 2.

One credit corresponds to 36 hours of class time. The average credit value for a discipline in European countries is between 25 and 30 hours. One credit in the American system can be equated to 2 credits in the European system. In accordance with the RFES-3, the total number of credits required for Russian specialist training is 300.

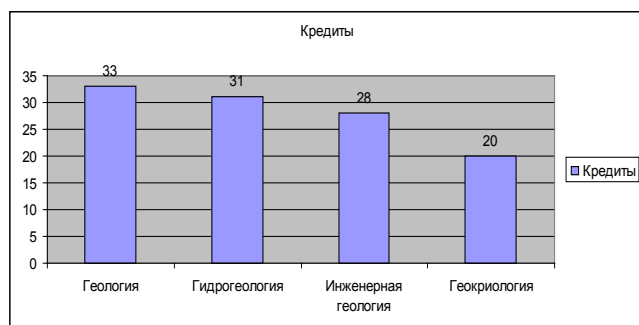


Figure 2. Basic disciplines and the total number of credits.

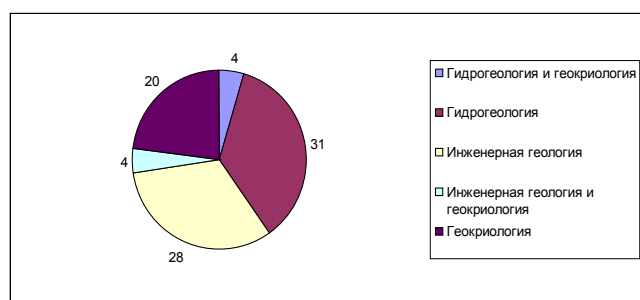


Figure 3. Correlation of basic professional disciplines in the education program in credit hours.

The geocryological classes at the HGEG Department include General Geocryology; Geocryological Research Methods; Geocryological Forecast; Permafrost Physics, Chemistry and Mechanics; Engineering Geocryology; and Cryolithozone Groundwater. Although each course contributes only a small amount of credits (mostly 2 credits) to the overall curriculum, they supplement other required courses and are closely associated with them (Fig. 3).

In Geocryology classes, the department's students are acquainted with geocryological processes and their effect on groundwater and geotechnical conditions. They also develop skills in geocryological research. At the workplace, this knowledge enables them to solve problems more professionally, as evident from positive feedback from employers.

The geocryological classes have been developed over a long period of time since the department's formation. Professors Kondratev, Shesternev, and Petrov have contributed substantially to the development of syllabi and course materials tailored specifically to the specialization of the exploration of groundwater and geological engineering.

At the first stage in the 1970s and 1980s, the students were attending lecturers in General Geocryology and Geocryological Prediction. New issues of the cryolithozone development and the requirements of employers made it necessary to increase the share of geocryological disciplines to 20% of the total professional disciplines.

Students gain necessary skills for work in permafrost areas and for participating in the HGEG Department's research.

Conclusions

The HGEG Department constantly makes efforts to improve the quality of student training. The department's

efforts are praised in positive feedback from the employers of our graduates. Most graduates are employed in the Transbaikalia region, but 2 or 3 people annually go to the Amur region and the Khabarovsk and Primorsky territories. As a rule, the students actively participating in geocryology research develop their own independent research projects. More than 16 people have defended their Ph.D. dissertations, and one person has defended a post-doctoral thesis since the department was founded in 1978 (Kondratev 2008).

References

- Kondratev, V.G. 2008. For the 30th anniversary of the ChitSU Department of Hydrogeology and Engineering Geology. "Hydrogeology, engineering geology, geocryology, and geoecology of the Transbaikalia and adjacent areas." Research and practice conference materials (September, 24-25, 2008). Chita: ChitGU, pp.7-13 (in Russian).
- Verkhoturov, A.G. 2010. The Department of Hydrogeology and Engineering Geology. *Mining Journal* No. 5: 19-22 (in Russian).

Models of Mathematical Landscape Morphology in Cryolithozone Research

A.S. Viktorov, V.N. Kapralova, T.V. Orlov
Sergeyev Geocology Institute, RAS, Moscow, Russia

Abstract

Possibilities for the application of a new approach called mathematical landscape morphology for the solution of the specified problem are shown. Mathematical landscape morphology deals with mathematical analysis of quantitative regularities in the structure of landscape patterns. Mathematical landscape morphology models can be used for different problems of cryolithozone research: analysis of landscape dynamics and forecasting; identification of new regularities indicative of geological conditions; and risk assessment for engineering structures in the cryolithozone. The applicability of the new approach is illustrated through an example of lacustrine-thermokarst and erosional-thermokarst plain landscapes.

Keywords: erosional-thermokarst plains; mathematical landscape morphology; mathematical models; risk assessment; thermokarst plains.

Introduction

Significant research has been devoted to the study of the spatial regularities and temporal dynamics of the permafrost-affected landscapes and to the cryogenic processes responsible for landscape formation (E.S. Melnikov, G.Z. Perlshtein, S.E. Grechishchev, U.L. Shur and others). At the same time, the demand for new approaches to the problem remains. The main objective of this report is to demonstrate the possibilities of the application of a new approach to addressing the problems of quantitative assessment of permafrost landscape morphology. The approach, called mathematical landscape morphology, was developed during the recent decade at the junction of geology, geography, and mathematics (Viktorov 1998, 2006, Viktorov & Trapeznikova 2000, Kapralova 2008, and others).

Mathematical landscape morphology provides a quantitative assessment of regularities in spatial landscape patterns by utilizing comprehensive mathematical analysis. The method focuses on the landscape pattern (morphological structure) of the area, reflected on the land surface as the spatial mosaic of characteristic landscape units developed within the area. It is derived from air photos and/or satellite imagery.

Methods

Development of mathematical models of landscape patterns, which describe the most significant spatial properties of a landscape, is the cornerstone of the mathematical landscape morphology approach. The theory of random processes is the basis of the existing landscape pattern models. The so-called “canonic” mathematical models of landscape patterns are mathematical models of morphological structures formed by a single process in homogeneous physical-geographical conditions. As such, they describe simple landscape patterns. The homogeneity assumption requires an absence of tectonic landforms (faults, folds), abrupt changes in composition and structure of sediments, and other disturbances within the area. At the same time, the requirement does not impose limitations on the sediment composition and structure, the climatic and moisture and ground thermal regimes, or other factors as

long as they are uniform throughout the area. Thus canonic mathematical models of morphological structures serve as the basic elements for developing mathematical models for the landscape pattern of any territory. For example, canonic mathematical models have been developed for morphological structures of fluvial plains, karst and subsidence-suffusion plains, erosion plains, and others (Viktorov 2006).

Amazingly, mathematical equations are able to describe landscapes of a certain genetic type correctly within a very wide range of physical and geographical conditions (composition of deposits, climate, age, etc.). This fact provides a basis for the methods of mathematical landscape morphology. This stability is explained by the similarity in the landscape development processes (erosion, karst processes, etc.) in different natural conditions. It was qualitatively described by Nikolaev (1975) as an “isomorphism of landscape pattern.” Due to this property, the mathematical models of landscape patterns can be developed for the area with particular genetic landscape types without the specification of sedimentary composition structure, climate etc. The local specific conditions are reflected only by different values of the model parameters. The mathematical models of complex morphological structures can be developed theoretically by combining several characteristic canonic models.

Mathematical landscape morphology models can be applied to such areas of permafrost research as analysis of landscape dynamics and forecasting, analysis of landscape regularities, assessment of geological conditions, risk assessment for engineering structures, and others. In this paper we provide several examples to illustrate applications of the mathematical landscape morphology model to analyze thermokarst plains.

First we examined a lacustrine-thermokarst with homogeneous edaphic and geomorphologic characteristics.

The following assumptions were used in the model:

1. The process of initial formation of depressions is probabilistic and progresses independently in non-overlapping areas.
2. All thermokarst depressions within the area have formed simultaneously. The probability of the formation of any single depression in the area depends only on its size (Δs), and is much higher than the probability of

formation of several depressions. Mathematically this assumption can be expressed as:

$$p_1 = \mu\Delta s + o(\Delta s) \tag{1}$$

$$p_k = o(\Delta s) \quad k = 2,3,\dots \tag{2}$$

where μ – average number of depressions per area unit.

3. The thermal-abrasional lake growth occurs independently for different lakes and is directly proportional to heat reserves in the lake and inversely proportional to the surface area of the lake’s bed sides.

4. A lake’s depth is proportional to its radius.

The first two assumptions seem natural because they result from the homogeneity of the area under study and reflect the relatively rare occurrence of thermokarst depressions. The third assumption is based on the fact that the thermal effect of water is proportional to the amount of heat flow through the unit area of the lake surface. Finally, the fourth assumption reflects the fact that the lake’s areal expansion is accompanied by the slow increase in its depth. (This assumption can be replaced with the one of depth constancy).

These assumptions allow us to provide a mathematical analysis of the structural regularities of a thermokarst plain. For example, the statistical distribution of a number of thermokarst depressions (centers) at a randomly chosen site corresponds to Poisson’s law:

$$P(k) = \frac{(\mu s)^k}{k!} e^{-\mu s} \tag{3}$$

where s – area of the test site, μ – average number of depressions per area unit.

If, for the purpose of model simplification, we assume that the initial thermokarst depressions have a unity radius at the moment of occurrence, then the distribution of the lake radius (diameter, area) will be log normal and will have the distribution density described as the following:

$$f_r(x,t) = \frac{1}{\sqrt{2\pi\sigma x}\sqrt{t}} e^{-\frac{(\ln x-at)^2}{2\sigma^2 t}} \tag{4}$$

where a, σ – model parameters.

Both mathematical parameterizations (3 and 4) were confirmed empirically by analysis of remote sensing imagery for sites located in Western Siberia, Alaska, and other regions (Viktorov 1995, 2006, Kapralova 2008). The sample results of such validation are provided below (Fig. 1, Table 1).

A regular expansion of the thermokarst lake was observed at a series of monitoring stations (Burn & Smith 1990). However, the log-normal distribution of lake sizes is observed in the overwhelming majority of cases. This can lead to the assumption that either the distribution of lake age is always log-normal, or the distribution of growth rates is log-normal, or, most probably, that the changes in the growth rate are not detectable within an observation period shorter than 8 years.

Assumptions 3 and 4 can be modified. According to many observations, the growth of lake beds occurs by means of permafrost degradation of the portion of the bank located below the water level, resulting in bank undercutting.

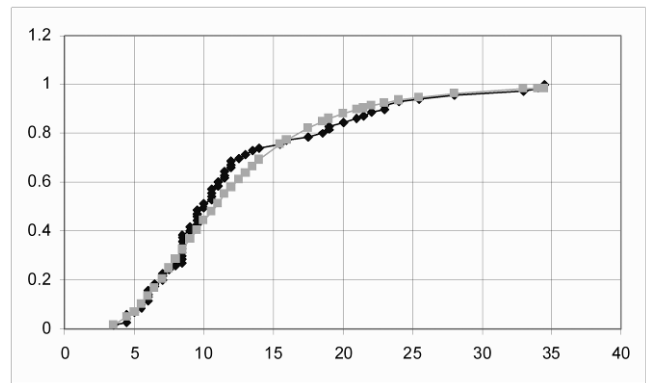


Figure 1 Comparison of the predicted logarithmically normal and the empirical distribution of radii of thermokarst lakes (test site).

Table 1. Comparison of empirical and predicted (Poisson’s law) distributions of the centers of thermokarst lakes (Yamburg site).

Site	N	Nature of value	Mean logarithm	Logarithm standard		
1a	64	diameter	3.16	0.57	9.03	11.07
		area	5.70	1.05	5.79	7.81
		perimeter	4.26	0.61	3.51	9.48
2a	64	diameter	2.88	0.53	2.27	7.81
		area	5.14	0.97	0.43	3.84
		perimeter	3.95	0.57	2.19	7.81
For	70	diameter	3.07	0.52	4.64	7.81
		area	5.55	1.01	9.01	5.99
		perimeter	4.14	0.55	0.89	7.81
4a	34	diameter	3.09	1.53	0.22	3.84
		area	5.54	1.03	5.95	3.84
		perimeter	4.18	0.58	0.41	3.84
5a	105	diameter	2.95	0.50	4.76	11.07
		area	5.39	0.87	8.37	7.81
		perimeter	4.10	0.52	9.77	9.48
6a	100	diameter	4.43	0.30	4.72	11.07

The upper portion of the bank is eroded by mass wasting processes. That is why Assumption 3 can be modified as follows:

3a. Expansion of the lake by thermal-abrasion occurs independently in different lakes and is directly proportional to lake heat storage and inversely proportional to the area of the lake banks below the water level.

The mathematical analysis shows that in this case the same basic equations can be applied.

Results and Discussion

Mathematical landscape morphology models can be used to predict landscape dynamics and landscape-forming processes.

A model of the morphological structure of lacustrine-thermokarst lakes with an asynchronous initiation of the thermokarst processes can be developed using the mathematical landscape morphology approach. Here we examine the lacustrine-thermokarst plain that meets the homogeneity requirements. The model is based on the following assumptions:

The occurrence of thermokarst depressions is probable on non-overlapping areas and occurs independently and continuously within non-overlapping time periods.

1. The probability of occurrence of one depression in the area depends only on the size of the area (Δs) and the length of the time period (Δt) of study, and is much higher than the probability of the occurrence of multiple depressions. In other words:

$$p_1 = \lambda \Delta s \Delta t + o(\Delta s \Delta t) \tag{5}$$

$$p_k = o(\Delta s \Delta t) \quad k = 2, 3, \dots$$

2. The expansion of lakes by thermal-abrasion occurs independently in different lakes and is directly proportional to heat storage in the lake and inversely proportional to the surface area of the lake's banks.
3. The depth of each lake is proportional to its size.

These assumptions differ from the first case of synchronous initiations.

Using these assumptions, we can evaluate the regularities in the structure of a thermokarst plain by analytical methods. It can be shown (Viktorov 1995) that based on the assumptions described above the distribution of the number of thermokarst depressions (centers) at randomly selected areas is described by Poisson's law:

$$P(k, t) = \frac{(\lambda t s)^k}{k!} e^{-\lambda t s} \tag{6}$$

where λ – average number of depressions within a unit area and during a unit time, s – test site area, t – duration of the process.

However, the distribution of lake diameters for the whole population will differ from the log-normal due to the asynchronism of the process initiation. If we assume that initial thermokarst depressions have a unity radius at formation, then the distribution of diameters can be obtained by time averaging (Viktorov 2006).

$$f_d(x) = \frac{1}{t_0} \int_0^{t_0} \frac{1}{\sqrt{2\pi t} \sigma x} e^{-\frac{(\ln x - at)^2}{2\sigma^2 t}} dt \tag{7}$$

An interesting approximation can be obtained in the case of a long period of development. Using the Laplace transformation, we can obtain the following:

$$f_d(x) \approx \frac{1}{at_0 x} \quad \text{at } x \geq 1 \tag{8}$$

Thus the following can apparently be a good approximation of the distribution for normalized lake radiuses:

$$F_d(x) \approx \frac{\ln x}{\ln b}, \quad 1 \leq x \leq b \tag{9}$$

where b – parameter.

These expressions allow evaluating the probability of a particular landscape state after a set period of time. The required values of the model's parameter can be obtained from the repeated remote sensing surveys.

$$\bar{\lambda} = \frac{n_2 - n_1}{t_2 - t_1} \tag{10}$$

$$\bar{a} = M_2 + \frac{M_2 - M_1}{t_2 - t_1} (t_3 - t_2) \tag{11}$$

$$\bar{\sigma} = \sqrt{D_2 + \frac{D_2 - D_1}{t_2 - t_1} (t_3 - t_2)} \tag{12}$$

where t_1, t_2 – period of survey, t_3 – period of forecast, M_1, M_2 – mathematical expectation of the logarithm of lake radius for the corresponding survey period, D_1, D_2 – lake dispersion of the logarithms of lake radius for the corresponding survey period, n_1, n_2 – the density of lakes for the corresponding survey period.

The use of the model allows analysis of more complex problems. Let us consider an erosional-thermokarst plain. The landscape is a slightly undulating near-horizontal surface with prevailing tundra vegetation (cottongrass tundras, sedge-cottongrass tundras, etc.). It includes lakes, drained lake basins, and localized sparse erosional networks. The lakes are isometric, frequently round in shape, and randomly distributed within the plain. Drained lake basins are flat isometric depressions, covered by meadow or bog vegetation and, like lakes, randomly distributed within the plain (Fig. 2).

The first two assumptions of the morphological structure model for erosional-thermokarst plains are similar to the assumptions used to develop the model of lacustrine-thermokarst plains. But they are supplemented by two additional assumptions describing the interactions between the thermokarst and erosional processes:

4. While growing, a lake can drain through an erosional network. The probability of drainage does not depend on other lakes. If the lake is drained, its growth ceases.
5. The development of the erosional forms within a randomly selected area is a random event, and its probability is proportional only to the size of the area.

The difficulty in analysis of the dynamics of such an area relates to the fact that two opposite processes occur: 1) lake growth and the formation of new lakes and 2) lake disappearance due to the drainage initiated by erosional processes. What are the landscape dynamics after a significant time period?

Mathematical analysis (Viktorov 2005) shows that after a significant period of time and regardless of specific conditions, a dynamic equilibrium can be established

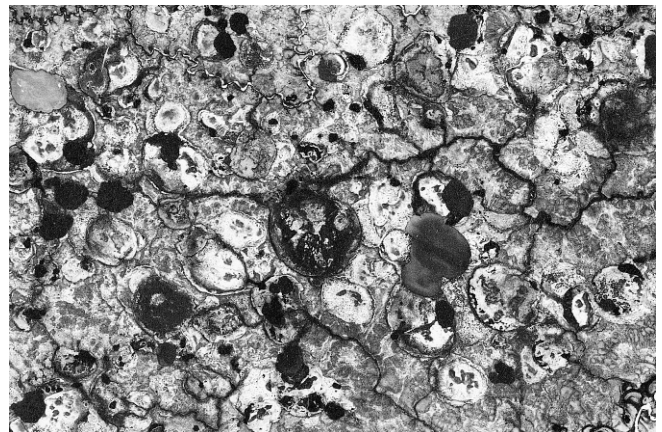


Figure 2. Typical image of the landscape pattern of erosional-thermokarst plains in the materials of a satellite survey.

between the processes of thermokarst lake formation and drainage. This dynamic equilibrium is characterized by relations in the morphological structure of erosional-thermokarst plains. Distributional density of radiuses of thermokarst lakes can be described by the following:

$$f(x, \infty) = -\frac{2}{xEi(-\pi\gamma)} e^{-\pi x^2}, \quad x > 1, \quad (13)$$

Average density of lakes radiuses is

$$\eta(\infty) = -\frac{\lambda}{2a} Ei(-\pi\gamma) \quad (14)$$

Average area of lakes is

$$\bar{s}(\infty) = -\frac{1}{\gamma Ei(-\pi\gamma)} e^{-\pi\gamma} \quad (15)$$

Active area with respect to formation of thermokarst depressions, lake expansion and lake drainage is

$$P_l(\infty) = 1 - \exp\left(-\frac{\lambda}{2a\gamma} e^{-\pi\gamma}\right) \quad (16)$$

Distribution of radiuses of drained lakes is

$$F_h(x, \infty) = 1 - e^{-\pi x^2} \quad (17)$$

where γ – mean density of the sources of erosional forms, a, σ – model parameters, $Ei(x)$ – integral-exponential function.

The relations described above were empirically validated (Fig. 3).

The use of mathematical landscape morphology models allows for the identification of new regularities in the structure of cryolithozone landscapes. For example, it is possible to evaluate the interaction between characteristics of the drained lake basin and the area's erosional network. Such interactions are quite possible because lake drainage is directly related to thermokarst and erosional processes. We will use a morphological model of the erosional-thermokarst plain structure to address this problem. Let us consider the erosional-thermokarst plain that meets the homogeneity requirement, after a significant period since the initiation of thermokarst and erosional processes. In this case, under the assumptions specified above, distributions of the lake's sizes and lake area and distributions of drain lake basins radiuses will correspond to Rayleigh's distribution.

Utilizing Rayleigh's distribution and the mathematical expectation (i.e., mean value) of the radiuses of drained lakes, we can obtain the following:

$$r_h = \frac{1}{2\sqrt{\gamma}} \quad (18)$$

where γ – density of erosional forms. Further, we can derive the following:

$$\gamma = \frac{1}{d_h^2} \quad (19)$$

where d_h – mean drained lake diameter.

Thus the following simple correlation is obtained using mathematical model analysis: the erosional form's location density is inversely proportional to the square of the drained

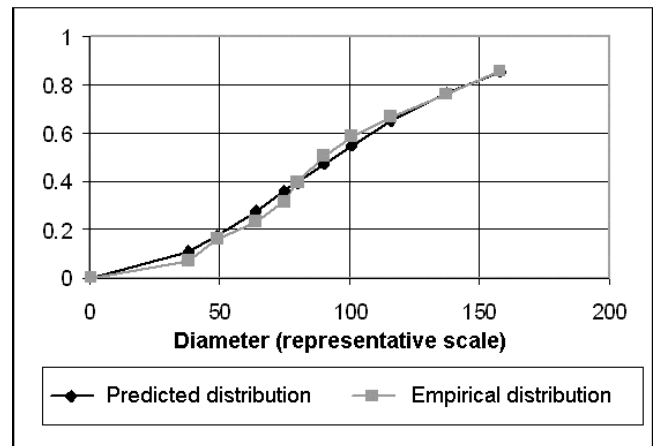


Figure 3. Correspondence of the predicted and the empirical distribution of alas size (site of the Yamburg gas and condensate field).

lake diameter (and, consequently, its area). This result, obtained for homogeneous conditions and a long period of process development, should be validated empirically. Nonetheless, it looks very realistic.

As another example, we evaluate interactions between the area affected by the thermokarst process, the density of the thermokarst lakes, and their area. This problem was solved for a wide class of hazardous geological processes related to circular depressions (suffusion, karst, etc.) including thermokarst (Viktorov 2005, Viktorov 2006). The solution to the problem is based on the following assumption: the damaged area, which is a fraction of the total area occupied by the thermokarst depressions, is equal to the probability of a dart being randomly thrown into the area to hit the thermokarst depression. This problem in turn represents a probability of a minor structure to be damaged by thermokarst processes. This problem has the following solution:

$$P_d(t) = 1 - e^{-\mu(t)s(t)} \quad (20)$$

where $\mu(t)$ – mean density of thermokarst lakes, $s(t)$ – mean lake area, t – time. This solution has passed an initial empirical validation.

Use of the mathematical landscape morphology represents a new approach to the interpretation of remote sensing imagery by providing a quantitative analysis of the image pattern.

Mathematical landscape morphology models allow for the development of new methods and software tools for the textural analysis of remotely sensed images. They allow us to address the following questions of textural analysis:

- Which parameters should be chosen for the analysis?
- Which criteria are significant in comparative analysis of images and validation and/or training sites?

The use of mathematical landscape morphology models allows us to choose a combination of parameters that would be independent and informative, and it provides thorough information on the pattern of the particular research area. Furthermore, the analysis of models allows for the evaluation of significant differences between images and training/validation sites.

The textural analysis software tool is different from many existing types of automated image interpretation routines

by allowing for the possibility of selection of the genetic type of the analyzed area in the menu. By selecting the menu item, the user automatically selects a mathematical model that determines the parameters and criteria necessary for differentiating between different genetic landscape types. Therefore, the analytical method automatically adjusts to the specific area. Then the moving window of specified size runs across the whole image, and textural parameters of the image fragments within the window are compared with model textural parameters.

The first version of the textural analysis software tool that utilizes the principles of mathematical landscape morphology was developed at the RAS Geocology Institute. The textural analysis tool includes the following procedures:

- selection of the training site,
- assignment of the genetic landscape type through the menu,
- automatic analysis of the image texture.

The results are displayed by highlighting the area of the image that has texture, most closely corresponding to the training site.

The software has passed an initial testing for the case of a lacustrine-thermokarst plain in the Russian European North. The area of local uplift was chosen as a training site. An automatic identification of the landscape similar to that of the training site was for two values of the training site area. The overlapping area between two cases was assumed to be an identified area. The comparisons of the identified area with the structural map of Devonian sediments, drawn from geophysical methods, showed that the area identified by the software tool corresponds well to the local geologic structures. In the study area, the landscape pattern is closely associated with the presence of structurally weak zones, due to the stress forming at the prolong edges of structures. Therefore, the validation of the software can be considered successful.

The use of the approaches of the mathematical landscape morphology allows us to address more practical problems, such as the assessment of potential damage to linear structures associated with thermokarst processes. The solution is based on the fact that damage occurs when linear structures cross areas of active thermokarst processes.

For example, it is possible to evaluate the probability of the damage to an engineering structure by active thermokarst processes. The results of analysis (Viktorov 2006) indicate that since sources of active thermokarst are distributed according to Poisson's law and each source area develops independently, the number of potential linear infrastructure damages will also follow Poisson's distribution:

$$P(v) = \frac{[2\gamma(t)Lr(t)]^v}{v!} e^{-2\gamma(t)Lr(t)} \quad (21)$$

where $\gamma(t)$ – mean density of thermokarst lakes, $r(t)$ – mean radius, L – length of a linear structure, and t – duration of process. This distribution parameter is equal to the product of linear structure length, distribution density of the thermokarst sources, and their mean diameter. So the mean density of damage sections can be evaluated by:

$$\gamma_l(t) = 2\gamma(t)r(t) \quad (22)$$

This means (Viktorov 2006) that the probability of linear structure to be damaged by at least one thermokarst source area is:

$$P_{dl}(L) = 1 - e^{-2\gamma(t)r(t)L} \quad (23)$$

To simplify the problem, it was assumed that the linear structure is erected before the initiation of thermokarst processes, that it does not influence the thermokarst processes, and that thermokarst lakes do not drain.

Taking into account the probability of a linear structure's damage by active thermokarst sources that occurs by the time t , we obtain the probability of linear structure damage for the specified time period

$$P_{dl}(L) = 1 - e^{-2[\gamma(t)\bar{r}(t) + \gamma_{dg}(t)\bar{r}_{dg}(t)]L} \quad (24)$$

where $\gamma(t)$, $\gamma_{dg}(t)$ – density of thermokarst lakes and drained lake basins respectively, $\sigma(t)$, $\sigma_{dg}(t)$ – standard deviations of their radiuses, t – duration of process.

We have also obtained a solution for the problem that accounts for the initiation of a thermokarst process caused by linear structures and the situation when active thermokarst processes precede the construction of linear infrastructure.

Conclusions

Mathematical landscape morphology models can be used to solve various problems in permafrost research: analysis of landscape dynamics and forecasting; identification of new regularities; assessment of geological conditions; and risk assessment for engineering structures in the cryolithozone.

Regularities that govern the size and distribution of thermokarst lakes and the distribution of the size of drained lake basins were obtained. Prognostic regularities that define the correlation between the size of drained lake basins and the density of the erosional forms were also obtained. These prognostic regularities also define the correlation between the affected area, the average area, and the density of thermokarst sources.

References

- Burn, C.R. & Smith, M.W. 1990. Development of Thermokarst Lakes during the Holocene at Sites Near Mayo, Yukon Territory. *Permafrost and Periglacial Processes* 1: 161-176.
- Kapralova, V.N. 2008. The use of remote sensing data and landscape mathematical morphology methods in thermokarst processes study // International year of Planet Earth: geo-ecology, engineering geology and hydrogeology challenges. *Sergeevskie chteniya*. Moscow: GEOS. 10: 430-434.
- Nikolayeva, V.A. 1975. On the analysis of steppe and semidesert landscapes on the basis of aerial photography materials. *Vestnik MGU. Ser.geogr.* No 3: 15-21.
- Viktorov, A.S. & Trapeznikova, O.N. 2000. The erosion plain mathematical model as a base for space image

interpretation methods in geoenvironmental research. *Proceedings of the 4th international symposium on environmental geotechnology and global sustainable development*, Boston, USA. 603-612.

Victorov, A.S. 2005. Mathematical Models of Thermokarst and Fluvial Erosion Plains. GIS and Spatial Analysis. *Proceedings of IAMG 2005*, Toronto, Canada 1: 62-67.

Viktorov, A.S. 1995. Mathematical model of thermokarst lacustrine plains as one of the bases for the interpretation of satellite images. *Issledovaniye Zemli iz kosmosa* 5: 42-51.

Viktorov, A.S. 2006. *Main problems in mathematical morphology of landscapes*. Moscow: Nauka, 252 pp.

Composite Cast-in-Drilled Hole Piles in Frozen Soils, Magadan

V.P. Vlasov

Melnikov Permafrost Institute, Northeastern Research Permafrost Station, Magadan, Russia

Abstract

The city of Magadan is located in the warm, discontinuous permafrost zone where the permafrost thickness reaches 12–20 m or more. Composite cast-in-drilled piles are widely used. They are set in boreholes drilled to design depths in strong sub-permafrost unfrozen soil. To provide support for foundations, the piles penetrate the entire permafrost thickness, and the bottom of the hole is filled with compacted debris. The composite piles consist of a supporting debris-soil pillow below, a monolith concrete pole in the middle, and a ferro-concrete pole above. The free space between the hole and the pile walls is filled with mud. This paper considers the basis for the pile method in terms of permafrost engineering, technological procedures, testing, and the load-bearing capacity of composite piles.

Keywords: composite cast-in-drilled piles; discontinuous permafrost; load-bearing capacity; negative friction; stability of engineering structures; thawed soils.

Introduction

The city of Magadan is located in the southern part of the permafrost zone in the extreme northeast of Russia (Ershov 1989). The urban territory occupies a part of Tau Bay on the Okhotsk Sea coast where the Staritsky Peninsula joins the continent. This is a hilly area within a large granitic batholith overlain by Neogene rocks that lie, in turn, under a Quaternary sedimentary cover up to 15 m thick. The pile foundations commonly rely on gravel-pebble debris, coarse and fine sand, loamy sand, and sandy loam soils with high percentages of coarse material. Bedrock sites are very rare. The soils may change markedly in lithology, extent, and thickness even within small building sites (Chapovsky 1977).

The area has undergone repeated tectonic events in different geological periods and is an active zone of seismicity (Malinovsky et al. 2005) with a potential earthquake intensity of magnitude 8 (Strakhov and Ulomov 2000).

The climate is maritime-monsoon type, with mean annual temperature of -3.6°C , mean annual precipitation of 548 mm, and mean annual wind speed of 5.6 m/s (Velli et al. 1977). Shallow aquifers exist under a great many construction sites in the city. Groundwater circulation is maintained by the rugged topography, large seasonal thaw depths (2.5–3.5 m), and abundant precipitation (Malakhaev et al. 1974).

Permafrost Conditions

Magadan, like anywhere in the southern part of the permafrost zone, has very diverse conditions of frozen ground (Ershov 1999), especially its spatial patterns. Permafrost occurs as isolated lenses or patches varying from 100 to 10000 m² in area and from 2 to 30 m in thickness. The permafrost table is most often 3–5 m below the surface or deeper. At some sites, permafrost is layered with alternating frozen and unfrozen zones.

Permafrost in the Magadan region has temperatures that approach 0°C at the depth of zero annual amplitude and commonly stay within 0.1 to 0.2°C below zero. The temperature decreases to -0.5 to -1°C in a few patches in

peaty lowlands or highly elevated urban areas. Generally, urban development and long-term maintenance of built structures notably changed the thermal regime of the territory. Therefore, any estimates of the size and thickness of permafrost patches found during geotechnical investigations cannot be extrapolated in the future. This is because almost any human-caused change in heat transfer on the surface immediately affects the temperature pattern of frozen ground and leads to contemporary degradation of permafrost. Global climate change is a factor in the degradation process.

Nevertheless, the frozen ground within the city, and especially in its outskirts where new construction sites are being developed, still involves all local lithological units that should be taken into account in construction. Neglect of permafrost conditions caused failures and deformation of structures built in the early 1990s (Vlasov 2004a).

In areas of new development, gravely and sandy frozen soils are intermixed with unfrozen layers. They usually have massive (porous) cryostructures, while silty clay and silty sand have layered or reticulate cryostructures. Ice contents are the highest in shallow permafrost. The total water (ice) content at depths to 8–10 m (or sometimes deeper) is 8–12% in gravel, 18–22% in sand and loamy sand, and 30–35% in loam. Occasionally, soils with water content from 40 to 60% occur. Soils are often thaw-susceptible with thaw strain varying from 0.03 to 0.18.

Thawed soils of the same lithology have high water content and are highly compressible at contact with frozen soil. The strength of thawed soil beneath permafrost increases notably and approaches, or may even exceed, that of normal unfrozen soil at some short distances below permafrost (Vlasov 1992).

This natural phenomenon can be explained as follows (Bratsev & Zhukov 1965, Ershov 1999, Eroshenko 1972): The currently thawed soil within the permafrost zone, including the area of Magadan (Kalabin 1960), was perennially frozen in the past but thawed gradually under climate and human-caused effects. Subsequently, the post-cryogenic structure typical of thawed soil was completely destroyed. Solid particles became rearranged under their own gravity with decomposition of soil aggregates under a water-

bearing environment. The excess of water was squeezed from soil pores and substituted by fine soil particles. As a result, the soil became consolidated and gained its present mechanical strength typical for most varieties of thawed soils in the Magadan area.

This is the reason for the wide use of pile foundations on strong thawed soil wherever it occurs.

Geotechnical Considerations

The choice of geotechnical solutions at a construction site is determined by the permafrost setting, with perennially frozen and thawed soils often coexisting, and by the surface area and depth of these soils beneath the foundation. Several considerations are taken into account: (1) warm temperature of the frozen soil; (2) discontinuous patterns of permafrost with different depths to the permafrost table from site to site, often found rather deep below the active layer and with alternating frozen and unfrozen layers; (3) high spatial variability of permafrost patches and its dependence on short-term climate variations and impact of development; (4) high-ice content in frozen soil and, as a consequence, its thaw-susceptibility; (5) wide range of active layer thickness from 1 to 3.5 m, or from 4 to 5 m in especially cold winters when the snow depth is shallow, leading to the formation of "pereletok"; and (6) uneven depths to bearing soils (8 to 20 m or deeper) that are strong enough to provide the required foundation stability.

The Russian Building Code (1990) recommends using the active method in these conditions, i.e., the use of thawing or thawed permafrost soils. The preferable sites are those of bedrock or low-compressible sediments, including naturally thawed or frozen soils that maintain their strength on thawing. These soils, however, are often buried under thick layers of ice-rich permafrost. That is why this method entails special measures for reducing deformation of foundations. Examples of these measures include permafrost pre-thawing, replacing permafrost by unfrozen coarse-grained soil prior to construction, or reinforcing the soil that can subside on thawing. Other ways are to adapt the above-foundation parts of structures to stresses from uneven soil subsidence. For instance, builders may employ elements in which additional stress either never appears or becomes cancelled by hard and strong elements. All these measures, along with procedures for reducing strain heterogeneity, make up part of the anti-seismic construction strategy in active areas of the southern permafrost zone where Magadan is located.

Thus the durability of structures, as well as their service performance in permafrost conditions, should be aided by appropriate design of their above-surface elements and foundations. Special geotechnical pretreatment of soils and control of their mechanical interaction with the foundation should also be considered. Taken jointly, these permafrost engineering approaches aim to provide stability of structures (Ershov 1999).

The main objective of designing work in this respect is to choose the piling options that will be the most efficient in terms of technology and economy. These choices must be made with regard to specific permafrost and geological settings at construction sites and based on the available building experience.

Technological Characteristics of Composite Cast-in-Drilled Piles

Many years of construction experience have confirmed that pile foundations are the optimal solution for stability of structures for the permafrost conditions of the Magadan area (Konash 1977, Vlasov 1992). Piles penetrate weak (prone to subsidence on thawing) soil to reach the reliable strong thawed soil, which reduces the magnitude and heterogeneity of strain at the foundation. Among special piling technologies that may be needed, the method of composite cast-in-drilled hole (CIDH) piles is the most workable in Magadan (Vlasov 1992). This method is authorized by local branch construction norms (BCN 1988), which have been developed into the code of "Standards for Design and Installation of Pile Foundations on Thawing and Thawed Soils in the Magadan Region" following the Law of the Russian Federation No. 384-FZ of 30.12.2009 "Technological Regulations for the Safety of Engineering Structures." The local code contains recommended values of pile driving resistances of soils (beneath the pile base and at the sides) and negative friction specific to the area, as well as correction coefficients to these parameters that depend on the chosen way of pile driving. All input data used for calculations were obtained empirically in the field (Vlasov & Konash 1974, Konash 1977, Vlasov 1992, 1994).

In the calculations, the model load-bearing layer for piles is assumed to consist of sub-permafrost thawed soil whose total subsidence within the compressible thickness does not exceed the allowable limit for the designed structures. The type of piles and pile foundations (e.g., pile clusters, fields, or lines) are chosen proceeding from conditions at a given construction site according to prospecting data and predicted loads on the foundations.

Composite CIDH piles are placed in sub-permafrost thawed soil mainly at sites where the permafrost base lies 12 m or deeper below the surface or below the foundation. In the case of a shallower permafrost base, re-driving of piles is applied if drilled piles are available; otherwise pier, wall, or raft foundations may be used.

The composite CIDH piles that have substituted for camouflet ones (Vlasov 1992) are monolithic systems set in deep boreholes, with their lower part consisting of a drilled-in pole supported by the debris-armored hole bottom and the upper part of a cast ferro-concrete pole embedded into the lower pile to a depth of at least three hole diameters. The diameter of the ferro-concrete element must be at least 15 cm less than the respective hole diameter.

Pile placement in the extremely complex permafrost conditions of the Magadan area, with alternating frozen and unfrozen soil layers of different thicknesses and strengths, often requires impact driving with cable-drilling tools. This method has become widespread in high-latitude territories due to its universal applicability to almost any soil with any large amount of coarse material (coarse debris, cobbles, boulders, etc.) and of any thermal state (Rastegaev 1992). The hole diameter and drilling depth may reach 800 mm and 50 m, respectively. In our case, these parameters are 450–530 mm and 12–20 m, respectively (Vlasov 1992).

In the cable drilling technique, an impact driver (bit) is dropped from a certain height ($H \approx 1$ m) to break the ground

with its tip; water is poured into the hole from time to time and is mixed with powdered soil, transforming it into drilling mud, which is pumped out from the hole after each drilling run. There are, however, some drawbacks: incomplete cleanup with 10 to 30 cm of mud always remaining on the hole bottom, and soil loosening below the hole during the drilling process.

The boring works as a rule by employing casing (with metal strings) in two ways depending on permafrost and groundwater conditions. One way is single casing in a completely drilled hole. This is recommended for holes with provisionally stable walls that may collapse only after some elapsed time following the end of drilling. The other casing option is used for the hole walls that may break down during the installation. This employs spliced casing with several members fastened to one another successively as the hole is being drilled. The lowest unit is first placed in order to be further extended by means of electric welding; this is followed by the required number of intermediate units, and the top unit to provide for the casing retrieval.

Both single and spliced casing is made with a special cap mounted on the top by means of a drive casing shoe fixed on the drilling tool; if needed, the casing can be retrieved with a winch.

The quality of composite piling, and hence the quality of the load-bearing soil core at the foundation, is determined by the tightness of the pile-hole coupling. The coupling between the pile end and the hole bottom may loosen up because of mud remnant and soft soil, as mud is always less strong than undisturbed natural soil. The solution to this problem may consist in debris footing (Vlasov 1992).

Debris is pressed into the mud and the loosened soil by the bit, which, for this purpose, is equipped with a field replaceable nozzle resembling a round 30–50-mm-thick plate with its diameter of 1 cm less than that of the hole. Thus the compacted debris filling previously poured on the hole bottom and brought up to a required level, at least twice thicker than the mud, compresses the mud and the soil.

The compression continues until the pile refusal is no more than 2 cm for the last five impacts. The refusal total should be at least the height of the remnant mud measured prior to compaction. As a result, there forms a densely packed debris-mud pillow. This, together with the compressed soil core beneath the hole bottom, makes up the pile support that transfers vertical working loads through the composite system (consisting of the drilled-in and ferro-concrete pile elements) to the underlying soils.

After the debris-mud pillow has been created, a drilled-in concrete pole, which serves as an intermediate element of the pile system, is installed. It is of key importance for the designed foundation because the proper depth of the latter is achieved by varying the height of the drilled-in element into which the upper cast element is then embedded.

The above-foundation part of the pile is fabricated from high-class concrete (at least B-20 with water to cement ratio of 0.45 to 0.55 by mass and slump 50 to 100 mm), which is doped with NaCl admixture (2.5 to 3.5 by mass of cement) as an anti-freeze hardening accelerator. Concrete is poured into boreholes using a vertically moving tube 250 to 325 mm in diameter. Then the concrete of the required thickness is compressed with a vibratory pile driver as the

ferro-concrete pole is cast into the drilled-in pile element to be embedded into the concrete. The joint between the two elements should be no less than three hole diameters. Free space between the hole walls and the ferro-concrete pole is commonly filled with mud.

The use of mud reduces negative friction against the pile sides as the thawing soil around the pile subsides. It thus increases the total bearing capacity of the foundation that may rely upon any kind of thawed soils.

Composite piles may have either retrievable or non-retrievable casings. The latter are used when making high-quality drilled-in piles with retrievable protective casing is impossible. This usually happens in areas of landslides or thermokarst erosion. It also may happen at sites of ice-rich permafrost enclosing porous, thawed coarse-grained, or sand lenses or layers where piles may be destroyed under pressure of inter-permafrost groundwater fed from thawing soil while concrete in the lower pile is hardening.

The hardness of concrete in the drilled-in pile element is estimated with compulsory use of test samples subject to hardening in conditions similar to those expected for piles at permafrost sites. The test samples are placed in special geothermally fit boreholes. The amount of test material depends on the daily concrete placement rate.

Prior to pile grating, selected piles in the foundation have to be checked for fitting to the calculated load-bearing capacity, taking into account also the effects of negative friction from the thawing soil against the pile sides (Vlasov 1992, Torgashev 2001). The tests consist of applying the jacking static load on trial composite piles after measuring negative friction associated with thawing of soil around the piles. The measurements are performed using force gauge on the casing over the length of the cast ferro-concrete element while the space around the piles is left free. Thus the measured negative friction is to be subtracted from the limit of pile resistance after the pile has been jacked into thawed soil under static loading. The testing method and the processing of results are detailed in Vlasov (1999, 2002).

According to numerous tests at construction sites in the Magadan area, the actual load-bearing capacity of composite CIDH piles placed in holes with the diameter 450 to 530 mm and to a depth of 12 m or deeper varies from 800 to 1500 kN as a function of the thawing and thawed host soils. These piles served as foundations for about 100 five- to nine-story buildings, including the Northeastern State University in Magadan (Vlasov 1991, Vlasov & Zeeva 2004).

Conclusions

The design of composite cast-in-drilled hole (CIDH) piles and the installation and quality control follow local building regulations (BCN 1988). These specify mandatory national standards and regulations for construction under the conditions of discontinuous and warm-temperature permafrost in the Magadan area.

The composite piles have proved efficient in areas of rather thick permafrost with thawed soils that provide a solid support for structures.

The integrity of foundations is ensured because their design is based on regional pile-bearing capacity and a provision of specific negative friction, as well as correction

coefficients to these parameters that depend on the selected techniques of pile installation.

Use of CIDH piles made it possible to construct buildings at sites with thick permafrost underlain by unfrozen soil of high bearing capacity. CIDH piles provide a reliable base for building and other structures. They can be constructed of any length and diameter and can be installed precisely to design requirements.

Piles of a diameter that exceeds the maximum diameter within the length of the cast reinforced concrete element allow for estimating, with the use of casing, the actual load-bearing capacity of foundations in the field, taking into account negative friction from the thawing soil.

Structures in Magadan built on composite cast-in-drilled hole piles have been in service for many years without showing signs of deformation.

In the case of reconstruction, the serviceability of the foundations always can be checked by means of static loading tests on the constituent piles following the procedure reported by Vlasov (2004b).

References

- BCN (Branch Construction Norms) 110-010-87. 1988. Guidelines for Design and Construction of Pile Foundations in Thawed and Thawing Soils in the Magadan Region. Minvostokstroï SSSR, Moscow, 38 pp. (in Russian).
- Brattsev, L.A. & Zhukov, V.F. (eds.). 1965. *Permafrost Research for Construction: Theory and Practice (Experience in Eastern European North)*. Nauka, Moscow, 188 pp. (in Russian).
- Building Code of Russia, 2.02.04-88. 1990. Foundations on Permafrost. TsITP Gosstroï USSR, Moscow, 56 pp. (in Russian).
- Chapovsky, E.G. (ed.). 1977. *Engineering Geology of the USSR Volume 4, Far East*. Moscow University Press, Moscow, 502 pp. (in Russian).
- Eroshenko, V.N. 1972. *Pile Foundations in Plastic Frozen Soils*. Stroiizdat, Leningrad, 175 pp. (in Russian).
- Ershov, E.D. (ed.). 1989. *Geocryology of the USSR. East Siberia and Far East*. Nedra, Moscow, 515 pp. (in Russian).
- Ershov, E.D. (ed.). 1999. *Fundamentals of Geocryology. Part 5. Permafrost Engineering*. Moscow University Press, Moscow, 526 pp. (in Russian).
- Kalabin, A.I. 1960. *Permafrost and Hydrogeology of the Northeastern part of USSR*. Transactions, VNII-1, Issue 18, Magadan, 471 pp. (in Russian).
- Konash, B.E. 1977. *Pile foundations in sporadic permafrost*. Stroiizdat, Leningrad, 135 pp. (in Russian).
- Malakhaev, I.D. et al. 1974. Contained and cast-in-drilled piles: installation in complicated engineering geological conditions of Magadan. In: *Problems of Improving the Construction Performance in the North. Problems of the North*, Issue 19, Nauka, Moscow, pp. 219-225 (in Russian).
- Malinovsky, S.B. et al. 2005. Seismic risks in the Magadan region. *Kolyma* No. 1, 27-32 (in Russian).
- Rastegaev, I.K. 1992. *Development of Frozen Soils: Construction in High Latitudes*. Nauka, Novosibirsk, 351 pp. (in Russian).
- Strakhov, V.N. & Ulomov, V.M. (eds.). 2000. Seismic Risk Mapping of the Russian Federation Territory. OSR-1. Four sheets. IOFZ RAN, NNP (Tekart), Moscow.
- Torgashev, V.V. 2001. Pile Foundations in Permafrost Conditions. Permafrost Institute of the Siberian Branch of Russian Academy of Sciences Yakutsk, 234 pp. (in Russian).
- Velli, Yu.Ya., Dokuchaev, V.I., & Fedorov, N.F. (eds.). 1977. *Construction on Frozen Soils. A Handbook*. Stroiizdat, Leningrad, 552 pp. (in Russian).
- Vlasov, V.P. 1991. Installation of composite cast-in-drilled hole piles in Magadan. *Transactions, Magadan Promstroïiiproekt* Issue 1, 37-45, Magadan.
- Vlasov, V.P. 1992. Pile Foundations: Specificity of Construction in Thawing and Thawed Soils Permafrost Institute of the Siberian Branch of Russian Academy of Sciences, Yakutsk, 176 pp. (in Russian).
- Vlasov, V.P. 1994. Permafrost engineering technologies for pile foundations in zones of sporadic permafrost. *Kolyma* No. 7-8, 16-21.
- Vlasov, V.P. 1999. An efficient way of pre-construction testing of piles in thawing soils, in: *The Construction System in Russia. Problems, Prospects, and Human Resources*. Proc. Interregional Workshop. BCITY, Ulan-Ude, Book 2, pp. 3-12.
- Vlasov, V.P. 2002. Methods of static testing of trial piles in thawing and thawed soils. Proc. Fifth International Symposium on Permafrost Engineering. Permafrost Institute Press, Yakutsk. Book 1, pp. 244-248.
- Vlasov, V.P. 2004a. Problems of foundation stability in the Magadan region. *Osnovaniya, Fundamenty and Mekhanika Gruntov* No. 2, 24-29.
- Vlasov, V.P. 2004b. Management of stability of pile foundation in service. Permafrost Engineering. Proc. VI International Symposium on Permafrost Engineering. Lanzhou, China.
- Vlasov, V.P. & Konash, V.E. 1974. Static tests of piles in Magadan: data processing results. *Stroitelstvo v Raionakh Vostochnoi Sibiri and Krainego Severa*, No. 29, 68-83. Transactions, Krasnoyarsk Promstroïiiproekt, Krasnoyarsk (in Russian).
- Vlasov, V.P. & Zeeva, A.N. 2004. A new composite pile placement method for permafrost conditions in Magadan. Proc. 7-th International Symposium on Cold Region Development (ISCORD – 2004). Sept. 13-17, 2004, Sapporo, Japan. 36, D Topic in: International Association for Regions Development Studies (JACORDS). INCORD 2004, Japan – Hokkaido Organizing Committee.

Interpretation of Natural Permafrost-Related Geomorphic Processes and Landforms in the Bovanenkovo Hydrocarbon Field on the West Coast of the Yamal Peninsula

A.A. Yermak, E.A. Slagoda
Earth Cryosphere Institute, SB RAS, Tyumen, Russia

I.R. Idrisov
Tyumen State University, Tyumen, Russia

Abstract

A schematic map of the Bovanenkovo Hydrocarbon Field in the Western Yamal Peninsula was compiled at a scale of 1:50,000. The map shows the occurrence of permafrost-related geomorphic processes and landforms and determines their spatial relationships. In order to create the map, we reviewed existing maps of the west coast of the Yamal Peninsula and conducted a study of the geomorphic process classifications as well as methods and techniques of the satellite imagery and air photo interpretation of permafrost-related geomorphic processes and landforms.

Keywords: frost mounds; remote sensing; satellite imagery; thermal erosion features; coastal thermal abrasion features; thermokarst.

Introduction

Scientific exploration of the Arctic is one of Russia's main economic priorities. Identification, study, and mapping of hazardous natural processes in the Russian Arctic are important research and practical issues. For remote and poorly investigated areas, this work is conducted by using remotely sensed data. The interpretation of this data is essential not only for the design and operation of oil and gas facilities, but also to ensure environmentally sound management. The analysis of natural geomorphic process distribution in the Bovanenkovo Hydrocarbon Field region and on the Western Yamal coast is important for the development of oil and gas infrastructure.

Study Methods

Permafrost-related geomorphic processes and landforms in the Western Yamal area were interpreted using 1:50,000 scale high-resolution remote sensing data. These geomorphic features were analyzed by using the air photo database for Cape Marre-Sale, a key study site for the area (see Fig. 1). The ratio and spatial distribution of the features were determined for the study area.

The interpreted air photo data, combined with information from previously compiled geological and geomorphological small-scale maps and explanatory notes, were used to create a 1:50,000 scale schematic map showing the distribution of permafrost-related geomorphic processes within the study area. On the 1:2,500,000 scale permafrost map of the USSR, the study area is considered a part of the continuous permafrost zone; on this map, permafrost-related geomorphic processes and landforms are shown with special symbols that are not to scale (Permafrost map 1991).

On the 1:1,000,000 scale map of the natural complexes in northern West Siberia (Map of... 1991), the study area is considered a part of the marine mid-tundra province. The 3rd and 4th marine plains are the largest terrain types within the mid-tundra province. Floodplain landscapes are also prominent. These are extensively covered by wetlands and may

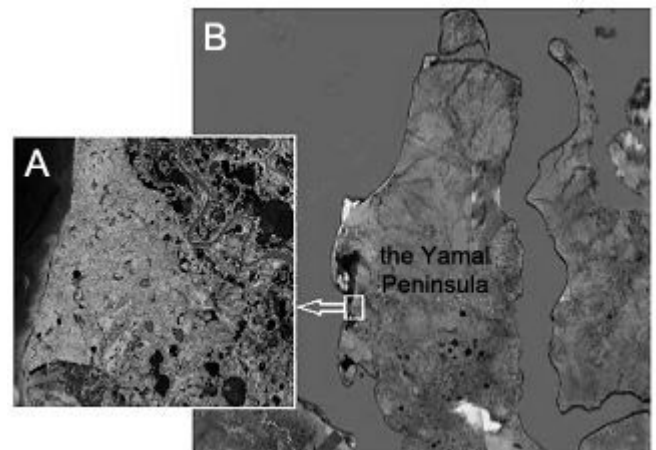



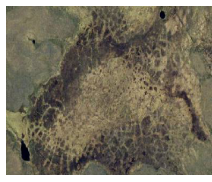

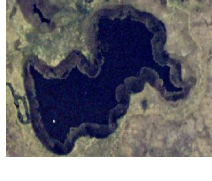


Figure 1. A – location of the study area on the Western Yamal Peninsula, for which detailed interpretation was completed (Google Earth Landsat 5 TM satellite image); B – overview satellite image of the area with the study area marked (Google Earth image).

include lakes (Melnikov 1991).

The portion of the 1:500,000 scale geocryological zoning map that covers this area gives an idea about geomorphological levels of the area pictured in the satellite image (e.g., floodplain, 1st, 2nd, and 3rd terraces), as well as about types and subtypes of permafrost (Kritsuk 2010). Some of the landforms, such as frost mounds, which are not to scale, and coastlines affected by thermal erosion, are identified on the map with symbols. The map legend provides more detailed landscape and geological descriptions of permafrost subareas which show the geomorphological levels. It also provides descriptions of relief, topography, percentage of the area covered by lakes, predominant terrain types, and types of surface deposits. Geocryological descriptions of permafrost types are also given (Kritsuk 2010). The territory described by L.N. Kritsuk is used for the description of the study area of the Western Yamal and for detailed interpretation of the satellite imagery.


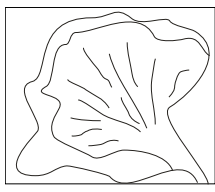



Analysis of natural process classifications according to F.P. Savarenskiy, P.N. Panyukov, V.D. Lomtadze, A.I. Sheko,

Table 1. Indicators of permafrost-related geomorphic processes.

Processes and surface expression	Description of surface expression on air photos and imagery	Satellite imagery example
Frost mounds	Round spots of lighter tone than the surrounding surface, cellular structure.	
Frost Heave area	Large spotty pattern: spots are round light in color, and are divided by dark stripes.	
Thermokarst lakes	Round shape. Spot color varies from dark gray to black.	
Thermokarst lakes, partially overgrown (25-75%)	Round shapes varying in color from dark gray to black with dark green areas on the surface.	
Alases with residual lakes with >25% of the alas area	Round shape of light green color, surrounding residual lakes.	
Alases with residual shallow lakes	Round shape of light yellow or yellow color with shallow lakelets located along the perimeter.	

and others (Savarenskiy 1937, Lomtadze 1977, Panyukov 1978, Sheko, Grechishchev 1988, Osipov et al. 1999) shows that a number of permafrost-related processes are considered hazardous, as they may have a negative impact on the area and structures located therein. The following hazardous natural geomorphic processes are typical of the Western Yamal Peninsula: frost heaving, surface frost cracking, thermokarst, thermal erosion, coastal thermal abrasion, and permafrost-related landslides. These processes produce the following: thermokarst lakes, alases, frost mounds, frost heave areas, patterned ground, coastal thermal erosion, and gully thermal erosion.

The following sources were used for the interpretation: a topographic map at a scale of 1:100,000, a geomorphological map at a scale of 1:500,000, and Quick Bird 2 satellite images with a spatial resolution of 2 m.

Alases, completely drained	Round shape, dark lobes. Dark green color, often yellow.	
Permafrost-related landslides	Complex shape with rounded contours, heterogeneous structure; down-slope orientation with swells and a superimposed alluvial fan	
Patterned ground	Intermittent network of dark lines forming a polygonal pattern..	
Thermal erosion	Linear contours, well-defined boundaries, dendritic shape.	
Thermal abrasion	Uniform structure, shape elongated along the coast, irregular contours, black color.	

Two methods of interpretation of high-resolution satellite images were used: automated and visual. The interpretation showed that the visual method is the most effective. This is because the automated method allows analysis based on only one selected parameter. Visual interpretation, on the other hand, allows the simultaneous recording of several indicators. Therefore, the following indicators provided the basis for the map: shape, color, structure, texture and association with various geomorphological levels (Table 1).

The interpretation was performed manually using ArcGIS 9.2 software. A separate interpretation layer was created for each process. All processes and landforms were mapped as individual polygons by making visual interpretations of the high-resolution imagery. A 1:50,000 scale schematic map of the study area, showing permafrost-related geomorphic processes and landforms, was compiled in this manner.

The areas of the various mapped units were calculated. The total area of the permafrost-related landforms is 136.037 km² (see Fig. 2).

The mapping reveals the areal extent of the different permafrost-related geomorphic features. The total area in the image is 411 km²; the interpretation was carried out on 35% of this area. In the remainder of the Quick Bird 2 image area, permafrost-related processes do not have distinct indicators. Therefore, no interpretation was conducted in these areas.

Frost cracking is one of the most common permafrost-related processes. It forms or has formed many of the modern and relict permafrost features in the area (Melnikov et

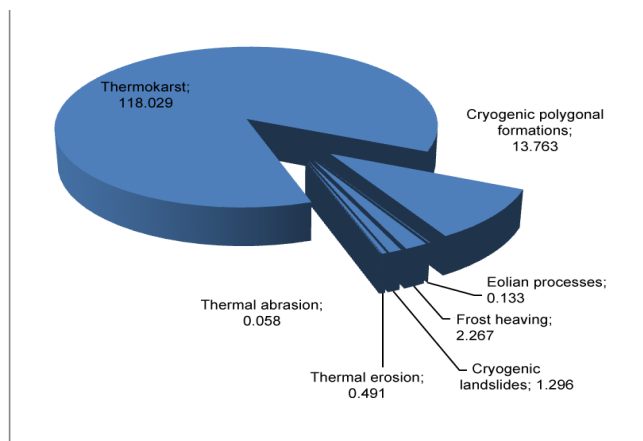


Figure 2. The distribution of permafrost-related geomorphic processes and landforms within the study area (km²).

al. 1974). Polygonal patterned ground, one form of frost cracking, is common on the 1st, 2nd, and 3rd marine terraces (Trofimov et al 1987). The polygons are morphologically pronounced, slightly waterlogged, often overlapping inter-polygonal degraded areas forming a polygonal pattern. The polygons visible in the aerial photographs are square, rectangular, trapezoidal, or polygonal in shape. The colors of the polygons range from light yellow to dark green, depending on the extent of wetland area and on the substrate. In peatlands, the polygonal grid is an indicator of the occurrence of modern ice-wedge ice. High peat content on the ground surface indicates relatively shallow seasonal thawing and creates ideal conditions for the growth and conservation of ice wedges (Baulin 2003). The polygonal grid in drained areas is associated with the degradation of ice-wedges. In some areas it is complicated by the thawing of complex massive ice deposits (Kritsuk 2010). Polygonal wedge structures cover an area of 13.763 km².

Frost heave forms mineral and composite (i.e. peat-mineral) frost mounds and frost-heave zones. Frost mounds are composed of clayey silt with high ice content, clay, and rarely silt and sand with ice and ice-ground cores and lenses. Such mounds occur mostly at low geomorphological levels (i.e. on floodplains and 1st terraces).

In frozen alases, perennial frost mounds were identified; along with individual mounds, there are also clusters of mounds that form frost heave areas (Baulin et al 2003).

Frost heave areas were identified within floodplain areas and on 1st and 2nd terraces (Trofimov et al 1987). The most characteristic form of frost heave is frost mounds with oval and round shapes.

Most of the frost mounds and frost heave areas are relict (i.e., they are not growing). Collapse of individual frost mounds was identified in some areas. Formation and growth of mineral and peat frost mounds and heave areas also occur on laidas, floodplains, and in alases (Baulin et al 2003). The area occupied by various landforms caused by frost heave is 2.267 km².

Thermokarst is widespread at all geomorphological levels, with the exception of sandy laidas. Thermokarst is represented by lakes and alases. Thermokarst lakes visible on the air photos are characterized by a wide variety of irregular round shapes. The color of thermokarst lakes is generally mostly black. There are several stages of development, from

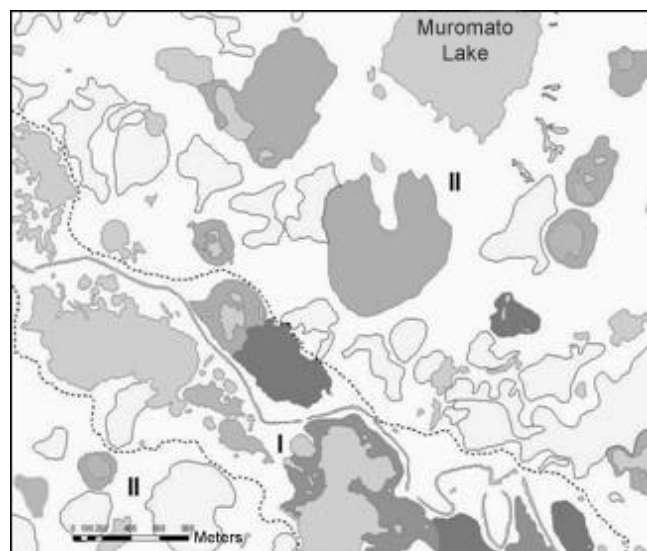


Figure 3. A portion of the 1:50,000 scale schematic map of the permafrost-related processes and landforms found in the study area. Legend. 1 - thermokarst lakes; 2 - thermokarst lakes of varying overgrowth degrees; 3 - alases with residual lakes; 4 - alases with residual shallow lakes; 5 - alases; 6 - thermal erosion; 7 - frost heaving areas; 8 - polygonal patterned ground within watersheds; 9 - areas with no processes identified within the study area. Geomorphological levels: 10 - floodplain of an unnamed river; 11 - 1st and 2nd terraces according to the map of geocryological zoning of Yamal-Gydan Region (Kritsuk 2010).

intensive lake expansion to the stage of drying out and complete overgrowth. Alases develop predominantly on 1st to 3rd level terraces (Trofimov et al. 1987). The size and shape of alases are similar to those of existing waterlogged basins. Alas bottoms are flat, sometimes with shallow lakelets, and are commonly covered with wetlands. The color of alases in the photographs varies from yellow to green, sometimes with dark spots (lakelets). The depth of the lakes was not taken into consideration for the analysis. The distribution area of various forms of thermokarst is 118.029 km².

Among the permafrost-related slope processes, solifluction, permafrost-related landslides, and liquefaction slides can be distinguished. Solifluction occurs mainly in silty-clay deposits where water content is high. These areas are associated with extensive development of shallow supra-permafrost water within the active layer (Ershov 1989). Permafrost-related landslides have developed on the terrace slopes in the areas where permafrost is found in clayey silt and clay with high ice content (including massive ice). Landslide glide surface and landslide body are distinguished in the landslide structure (Leibman & Kizyakov 2007). On the photographs, thermocirques, which are negative relief forms located on coasts and on the sides of river valleys, can be clearly identified. The shape of landslides is complex and heterogeneous, with rounded contours. The tone can vary from light to dark, depending on the degree of activity (i.e., fresh vs. overgrown). The landslides are also found in combination with alluvial fans of thermal erosional hollows, which drain the glide surface and overlay the landslide body. The landslides cover an area of 1.296 km².

Coastal thermal erosion (abrasion) within the study area is rather active. The mechanism of coastal destruction includes both mechanical abrasion and the thermal impact of sea water on the coastline. On the coast, there is an active interaction between sea water and land composed of icy permafrost (clayey silt, sand, silt, and peat). On lake shores where deposits of massive ice or polygonal wedge ice are exposed, the thermal abrasion rate is higher than in many parts of the coast that are composed of surficial deposits with low ice content. Thermal abrasion is the main reason for the formation of unstable slopes along the sea coast and along lake shores (Baulin et al 2003). The ocean coastline in the satellite images has well-defined contours, elongated irregular shapes, and a dark tone. The area covered by thermal abrasion features is 0.058 km².

The highest degree of thermal erosional gully dissection is found in areas directly adjacent to the coast, river valleys, and lake shores. Gully networks in the coastal zone are formed by gullies of different age and morphology.

Massive ice and ice-wedge ice act as catalysts for gully thermal erosion. However, gullies form in other areas as well. They can be found in weakened zones that form by frost cracking and thawing of structure-forming ice (Baulin et al 2003). On the aerial photographs, gullies have linear contours with well-defined boundaries and winding, dendritic shapes. Their color is green to dark green, often with brown shades. The area affected by thermal erosion is 0.491 km².

Aeolian processes and landforms are found locally within the study area, mostly in beach areas. They are also found on sandy terrace edges and in watersheds underlain by sandy soil. Due to the process of deflation, both negative relief forms (bulges, basins, deflation ditches) and positive relief forms (swells, mounds) have formed. On the satellite images, aeolian deposits can be identified by their elongated irregular shapes with rounded contours and whitish color. The area covered by accumulative and deflationary Aeolian forms is 0.133 km².

A portion of the 1:50,000 scale schematic map is shown in Figure 3. The processes and features described above are all mapped.

According to the interpretation in the area of the Western Yamal, both modern developing thermokarst basins and drained frozen alases prevail in the region of the Bovanenkovo Field. The area covered by thermokarst is 118.029 km², which accounts for 90% of the total study area (136.037 km²).

The areal distribution data and the schematic map will be used to direct ground-truthing. By comparing the schematic map to large-scale maps from the 1970s–80s, we plan to characterize the extent to which the study area was affected by permafrost-related processes and changes over time. These studies and the present one will allow us to update existing permafrost and terrain maps.

Acknowledgments

The work was conducted within the framework of fundamental programs IPY 2007/2008 and of the Presidium of RAS 20.7, ESD RAS-11.4.

We would like to thank Dmitry Stepanovich Drozdov for valuable advice and comments given in the process of preparing this article.

References

- Baulin, V.V., Dubikov, G.I., Aksenov, V.I. et al. 2003. *Geocryological conditions of the Kharasavey and Kruzenshtern gas fields (Yamal Peninsula)*. Moscow: GEOS, 180 pp.
- Ershov, E.D. 1989. *Geocryology of the USSR. West Siberia*. Moscow: Nedra, 454 pp.
- Kritsuk, L.N. 2010. *Ground ice in West Siberia*. Moscow: Nauchny Mir, 352 pp.
- Leibman, M.O. & Kizyakov, A.I. 2007. *Cryogenic landslides on the Yamal and the Yugorsky Peninsulas*. Moscow: Institut Kriosfery Zemli SO RAN, 206 pp.
- Lomtadze, V.D. 1977. *Engineering geology. Engineering geodynamics*. Leningrad: Nedra, 479 pp.
- Map of natural complexes of the north of West Siberia (Scale 1:1,000,000). Moscow, 1991.
- Melnikov, E.S. 1991. Explanatory note to the map of natural complexes in the north of West Siberia. Moscow: VSEGINGEO, 36 pp.
- Melnikov, E.S., Veysman, L.I., Kritsuk, L.N. et al. 1974. *Landscape indicators of engineering – geological conditions in the north of West Siberia and their indicators*. Moscow: Nedra, (VSEGINGEO). 182 pp.
- Osipov, V.I., Kutepov, V.M., Zverev, V.M. et al. 1999. *Hazardous exogenous processes*. Moscow: GEOS, 290 pp.
- Panyukov, P.N. 1978. *Engineering geology*, 2nd rev. and exp. ed., Moscow: Nedra, 296 pp.
- Permafrost map of the USSR (Scale 1:2,500,000). Moscow, 1991.
- Savarenskiy, F.P. 1937. *Engineering geology*. Moscow; Leningrad: ONTI NKTP USSR, 443 pp.
- Sheko, A.I. & Grechishchev, S.E. 1988. *Methods of study and prediction of hazardous natural processes*. Moscow: Nedra, 216 pp.
- Trofimov, V.T., Badu, Yu.B., Vasilchuk, Yu.K., Kashperuk, P.I., & Firsov, N.G. 1987. *Geocryological zoning of West Siberian plate*. Moscow: Nauka, 225 pp.

Phytoindicators of Landslide Disturbances in the Central Yamal

K.A. Yermokhina

Earth Cryosphere Institute, SB RAS, Moscow, Russia

E.G. Myalo

Lomonosov Moscow State University, Faculty of Geography, Moscow, Russia

Abstract

Research on the use of phytoindicators for monitoring and prediction of ecosystem dynamics, based on the study of the response of tundra biota to natural and anthropogenic impacts, is a critical need arising due to climate change and the development of natural resources in the Arctic. The cryogenic landslide process appears to be one of the determining factors of the transformation of ecotopes in various tundra regions, including the Central Yamal. It influences the structure and dynamics of vegetation across large areas. This paper presents the following set of phytoindicators connected with landslide age, landslide geomorphic structures, and groundwater chemistry: 1) differential species of syntaxa; 2) indicator species defined according to successional status; 3) phytomasses of the entire plant community, grayleaf willow (*Salix glauca*), and mosses; and 4) ecotypes of vascular plants. This set of phytoindicators includes physiognomic features of the plant communities that are closely connected with the indicated objects and characterized by the distinct dynamic processes, depending on the dynamics of indicated objects.

Keywords: vegetation dynamics; cryogenic landslides; phytoindicators; Yamal.

Introduction

A critical need arising due to the development of natural resources and climate change in the Arctic is research on the use of phytoindicators for monitoring and prediction of ecosystem dynamics that are based on the response of tundra vegetation to different natural and anthropogenic impacts. The dynamics of tundra vegetation are largely controlled by exogenous geological processes. The cryogenic landslide process appears to be one of the determining factors of ecological change in various tundra regions including the Central Yamal. This geological process influences the structure and dynamics of vegetation across large areas.

Here we describe the results of fieldwork carried out by K.A. Yermokhina and N.G. Ukraintseva in 1997–2002 and 2010 at Vaskiny Dachi, a long-term study site of the Earth Cryosphere Institute, SB RAS. The site was created to study cryogenic landslides in the Central Yamal region. During the field studies, a total of 165 geobotanical relevés were established. The above-ground phytomass was recorded, and plant, soil, and groundwater samples were taken. Laboratory analyses of the samples, including plant ash-content and above-ground phytomass, were conducted by specialists at the Vernadsky Institute of Geochemistry and Analytical Chemistry, RAS.

The study area is situated in the central Yamal Peninsula region (bioclimate subzone “C”) within a flat accumulative-erosional plain with two levels of structural relief. The upper level is composed of marine (Upper Pleistocene) and above-floodplain (Upper Pleistocene-Holocene) terraces, and the lower level is composed of floodplain deposits of the Sejaha and Mordyjaha rivers (Tsubulsky et al. 1995). The clayey marine deposits, widespread here, are highly saline because the permafrost of this area did not thaw during the Holocene climatic optimum (Leibman et al. 2007).

In most of the Central Yamal, shallow hillslopes occupy much more area than near-watershed, subhorizontal surfaces. Widespread cryogenic landslide processes greatly affect the structure of ecosystems here, forming undulating

topography with many dammed lakes. The area of potential landslide activity accounts for 45% of the Central Yamal (Tentyukov 1998). The area of saline marine deposits exposed by a single landslide feature can reach 100 m² or more (Ukraintseva 1997). Cryogenic landslides often transform the entire active layer (the thickness of which is about 0.5–1 m in this area). Dissolution of saline compounds contained in thawed marine deposits results in sharp increases in suprapermafrost groundwater mineralization following the landslide disturbance (Leibman et al. 2007). Landslide-affected slopes encompass a gradient of landslide structures of different age with representative geomorphic elements, including landslide shearing surfaces, landslide bodies, and landslide separation walls. As usual, the longitudinal profile of these slopes has not reached equilibrium yet. Three age categories of Yamal cryogenic landslides are distinguished in the literature (Leibman et al. 2000, Ukraintseva 1997): young (landslides occurred about 35 years ago), old (up to 300 years ago), and ancient (300–2000 years old).

A mosaic of vegetation covers the marine terrace slopes, with the component plant communities differing in spatial extent (in general, from 50 to 150 m²). In general, the spatial distribution of these communities does not depend on absolute values of altitude, slope inclination, or degree of exposure due to the generally low topographic relief. Cryogenic landslides are the only natural agents under these geomorphologic conditions responsible for abrupt differences in ecotypes of plant communities. Vegetation is represented here by the composition of dwarf birch-willow (*union Equiseto–Salicion glaucae*), dwarf birch (*association Vaccinio–Betuletum nanae*), grass-moss (*association Luzulo–Polytrichetum juniperinum*) tundras, and small patches of forb-grass meadows (*association Alopecuretum pratensis*).

Vegetation classification was carried out according to the Braun-Blanquet method. One union, integrating two associations, and three independent associations were identified. The communities of *Equiseto–Salicion glaucae* union (Table 1) are typical for the areas disturbed by the

Table 1. Prodrum of *Equiseto-Salicion glaucae* union.**Equiseto–Salicion glaucae Union**Differential species: *Salix glauca*, *Equisetum arvense* subsp. *boreale***Poo–Caricetum concolor Association**Differential species: *Carex concolor*, *Poa alpigena* subsp. *colpodea*, *Ranunculus borealis***1. Salicetosum polaris Subassociation**Differential species: *Salix polaris*, *Poa arctica*, *Dryas octopetala*, *Polytrichum juniperinum***2. Calamagrostietosum holmii Subassociation**Differential species: *Calamagrostis holmii***3. Drepanocladetosum uncinati Subassociation**Differential species: *Drepanocladus uncinatus***4. Veratretosum lobeliani Subassociation**Differential species: *Veratrum lobelianum***5. Caricetosum arctisibiricae Subassociation**Differential species: *Carex arctisibirica***6. Typicum Subassociation**Typical subassociation, faithful species: *Salix glauca*, *Equisetum arvense* subsp. *boreale*, *Carex concolor*, *Polemonium acutiflorum***7. Caricetosum lachenalii Subassociation**Differential species: *Carex lachenalii***Bistorto–Betulion nanae Association**Differential species: *Betula nana*, *Vaccinium vitis-idaea* subsp. *minus*, *Bistorta viviparum*, *Dicranum elongatum***1. Typicum Subassociation**Typical subassociation, faithful species: *Salix glauca*, *Betula nana*, *Dicranum elongatum*, *Vaccinium vitis-idaea* subsp. *minus***2. Festucetosum rubrae Subassociation**Differential species: *Alopecurus pratensis*, *Festuca rubra* subsp. *arctica*, *Ranunculus borealis***3. Peltigeretosum aphthosae Subassociation**Differential species: *Polemonium acutiflorum*, *Aulacomnium turgidum*, *Peltigera aphthosa***4. Veratretosum lobeliani Subassociation**Differential species: *Veratrum lobelianum***5. Poetosum arcticae Subassociation**Differential species: *Poa arctica*, *Carex arctisibirica***6. Eriophoretosum vaginati Subassociation**Differential species: *Nardosmia frigida*, *Eriophorum vaginatum*, *Stellaria palustris***7. Poo–Calamagrostietosum holmii Subassociation**Differential species: *Poa alpigena* subsp. *colpodea*, *Calamagrostis holmi*

Table 2. The main vegetation features on marine terrace slopes.

Vegetation syntaxa	Equiseto–Salicion glaucae Union		Vaccinio–Betuletum nanae association	Luzulo–Polytrichetum juniperinum association	Alopecuretum pratensis association
	Poo–Caricetum concolor association (1)	Bistorto–Betulion nanae association (2)			
Differential species of associations	<i>Carex concolor</i> , <i>Poa alpigena</i> subsp. <i>colpodea</i> , <i>Ranunculus borealis</i>	<i>Betula nana</i> , <i>Vaccinium vitis-idaea</i> subsp. <i>minus</i> , <i>Bistorta viviparum</i> , <i>Dicranum elongatum</i>	<i>Betula nana</i> , <i>Vaccinium vitis-idaea</i> subsp. <i>minus</i>	<i>Luzula confusa</i> , <i>Polytrichum juniperinum</i>	<i>Alopecurus pratensis</i>
RePlant community layers	shrubs, dwarf shrubs and grasses, moss-lichen layer	shrubs (frequently), dwarf shrubs and grasses, moss-lichen layer	dwarf shrubs and grasses, moss-lichen layer	grass and moss-lichen layers	grass layer and rarely moss layer
Dominant species	<i>Salix glauca</i> , <i>Equisetum arvense</i> subsp. <i>boreale</i> , <i>Carex concolor</i> , <i>Poa alpigena</i> subsp. <i>colpodea</i> , <i>Ranunculus borealis</i>	<i>Salix glauca</i> , <i>Betula nana</i> , <i>Vaccinium vitis-idaea</i> subsp. <i>minus</i> , <i>Equisetum arvense</i> subsp. <i>boreale</i> , <i>Bistorta viviparum</i> , <i>Dicranum elongatum</i>	<i>Betula nana</i> , <i>Vaccinium vitis-idaea</i> subsp. <i>minus</i>	<i>Polytrichum juniperinum</i> , <i>Polytrichum strictum</i>	polydominant grass
Projective cover (PC)	65–95%	65–90%	85%	97%	55%
Average PC of shrub layer	8–75%	0–61%	0%	0%	0%
Average PC of dwarf shrubs and grasses layer	40–64%	35–87%	50%	74%	49%
Average PC of moss component	28–80%	30–85%	84%	96%	26%
Average PC of lichen component	1–6%	0–8%	7%	2%	0%

cryogenic landslides in different extent and periods of time. Diversity of landslide ecotopes determines differences in species composition and community structure within the union. The main syntaxa features are presented in Table 2.

Landslide processes are catastrophic in relation to vegetation, according to the classification by Jurtsev (1995). Cryogenic landslides expose new substrates with diverse conditions. Considering the specifics and scale and degree of vegetation transformation, we have united “landslide” ecotopes into four types: central and peripheral parts of shearing surfaces of landslides, and central and peripheral parts of landslide bodies.

The set of syntaxa is linked to each type of ecotope (Table 3). The reliability of their relation with type of ecotope exceeds 0.70. *Poo–Caricetum concolor* association communities tend to occur in the central parts of the landslide structures, whereas *Bistorto–Betuletum nanae* association communities tend to occur in the contour parts.

Our analyses show that after the destruction of the original vegetation during the landslide event, seral changes to vegetation on newly exposed substrates depend on the newly formed landslide element (landslide body or shearing surface) and on the site position relative to the landslide movement axis (central or peripheral).

Table 3. Distribution of syntaxa by ecotope types.

Central parts of shearing surfaces	Peripheral parts of shearing surfaces	Central parts of landslide bodies	Peripheral parts of landslide bodies	Stable slopes*	Snowbeds on stable slopes
<i>Alopecuretum pratensis</i> <i>Caricetosum arctisibiricae</i> (1)** <i>typicum</i> (1) <i>Caricetosum lachenalii</i> (1)	<i>Poetosum arcticae</i> (2) <i>Eriophoretosum vaginati</i> (2) <i>Poo – Calamagrostietosum holmii</i> (2)	<i>Calamagrostietosum holmii</i> (1) <i>Drepanocladetosum uncinati</i> (1) <i>Veratretosum lobeliani</i> (1)	<i>Festucetosum rubrae</i> (2) <i>Peltigeretosum aphthosae</i> (2) <i>Veratretosum lobeliani</i> (2)	<i>Salicetosum polaris</i> (1) <i>typicum</i> (2) <i>Vaccinio–Betuletum nanae</i>	<i>Luzulo–Polytrichetum juniperinum</i>

* Stable slopes – slopes without noticeable landslide relief (the area more than 500 m²),

**here and further: (1) – subassociations of *Poo-Caricetum concolor* association, (2) – subassociations of *Bistorto-Betuletum nanae* association.

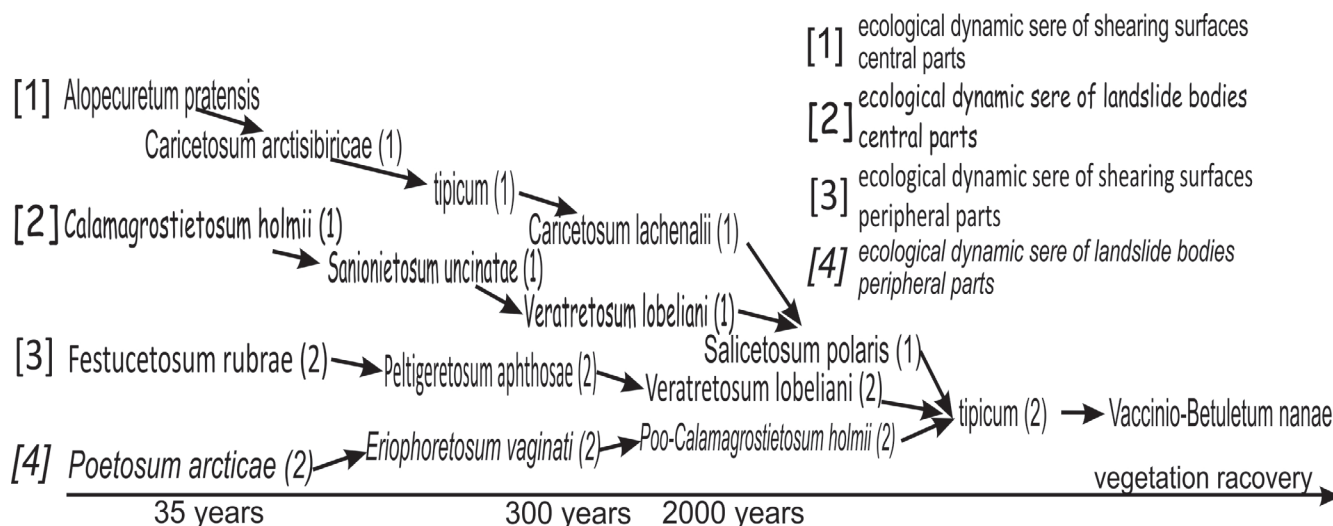


Figure 1. The successional system of vegetation for landslide slopes of marine terraces.

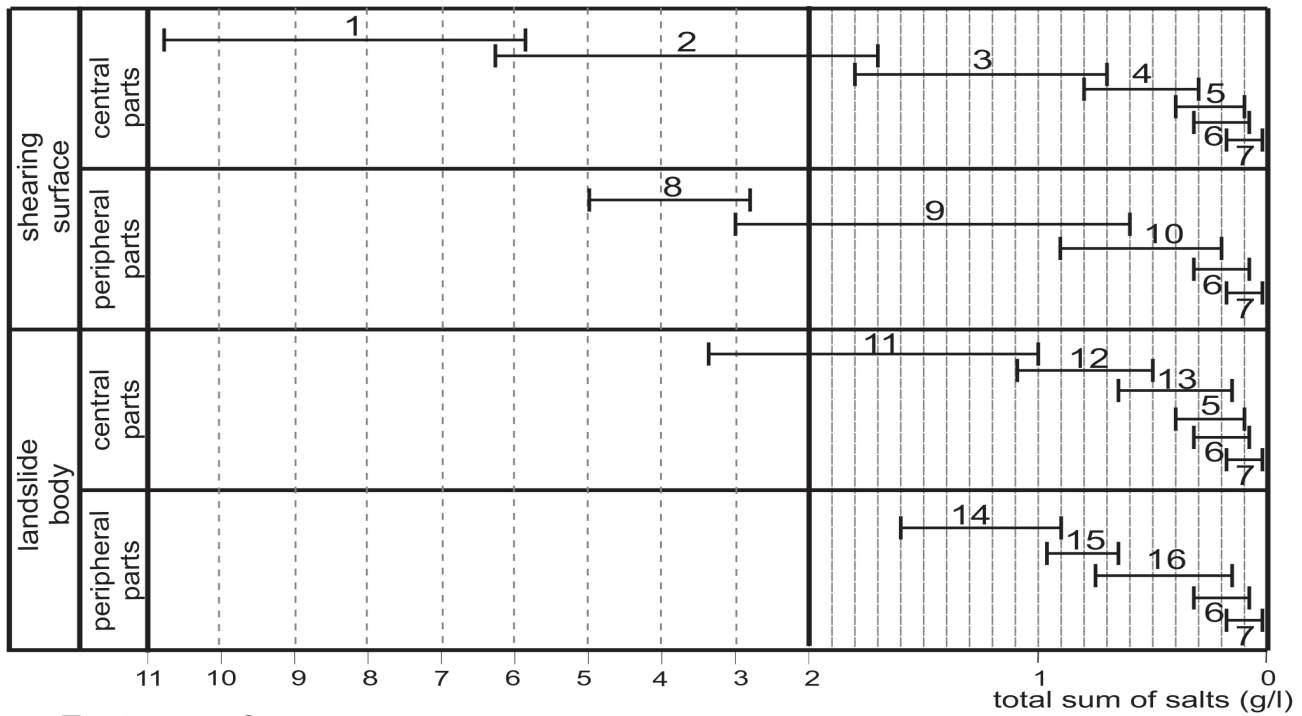
Primary succession occurs on the central parts of shearing surfaces and, on larger landslides, the central parts of colluvial deposits. Secondary succession occurs in other ecotopes because some small patches of pre-existing vegetation survive the disturbance, and these ecotopes often border on undisturbed sites. Snowbed sites occupied by *Luzulo-Polytrichetum juniperinum* association can be altered by the landslides. The denudation processes would develop in these areas according to meter-scale variability in the individual landslide. For each ecotope, the ecological dynamic series of vegetation succession during the changing ecotope process can be created.

The seral system of vegetation forming under the landslide processes on marine terrace slopes of the Central Yamal is described in Figure 1. The total duration of succession and the longevity of each ecological succession depends on the scale of transformation of the parent ecotope conditions, as caused by the cryogenic landslide. The longest successional sequence occurs on the central parts of shearing surfaces and includes the largest number of syntaxa. This observation corresponds to the fact that the most severe disturbance occurs within this part of the landslide disturbance footprint and, therefore, vegetation recovery takes the most time and the largest number of seral stages. Peripheral ecological dynamic series are the shortest and contain only five syntaxa (two are common). As vegetation recovers, convergence of the ecological dynamic series is observed, indicating the gradual homogenization of environmental conditions at ecotopes.

Canonical correspondence analysis of successional stages and environmental conditions shows that groundwater demineralization is a critical influence on succession. This factor significantly decreases as the vegetation recovers. Observations indicating parallel changes in groundwater chemistry and the accumulation of chemical elements by plants also provide evidence of the correlation between vegetation dynamics and groundwater demineralization.

The effect of groundwater demineralization is most apparent in the ecological succession of central parts of shearing surfaces, followed by the series of peripheral parts of shearing surfaces and the central parts of landslide bodies. The impact of groundwater demineralization is the least pronounced, forming on the contours of landslide bodies. The factor's manifestation is directly associated with the scale of the transformation of the parent ecotope caused by the cryogenic landslide.

In order to detect the phytoindicators of landslide age and landslide geomorphic units, we carried out a conjugated analysis of the parametric changes in the vegetation communities and their ecotopes. The parameters under study are variable, so the analysis took into account both standard deviation as well as mean values (Rosenberg 1998, McCune et al. 2002, Puzachenko 2004). Statistical analyses were conducted in the Statistica 6.0 application, and reliability estimation of the revealed relations was carried out with the Vinogradov's phytoindicator methods (Vinogradov 1964). The relationship between changes among parameter values has been specified on the basis of the correlation analysis.



Ecotopes of syntaxa:

- | | |
|--|--|
| 1 - as-tion <i>Alopecuretum pratensis</i> | 9 - subas-tion <i>Drepanocladetosum uncinati</i> (1) |
| 2 - subas-tion <i>Caricetosum arctisibiricae</i> (1) | 10 - subas-tion <i>Veratretosum lobeliani</i> (1) |
| 3 - subas-tion <i>tipicum</i> (1) | 11 - subas-tion <i>Festucetosum rubrae</i> (2) |
| 4 - subas-tion <i>Caricetosum lachenalii</i> (1) | 12 - subas-tion <i>Peltigeretosum aphthosae</i> (2) |
| 5 - subas-tion <i>Salicetosum polaris</i> (1) | 13 - subas-tion <i>Veratretosum lobeliani</i> (2) |
| 6 - subas-tion <i>tipicum</i> (2) | 14 - subas-tion <i>Poetosum arcticae</i> (2) |
| 7 - as-tion <i>Vaccinio-Betuletum nanae</i> | 15 - subas-tion <i>Eriophoretosum vaginati</i> (2) |
| 8 - subas-tion <i>Calamagrostietosum holmii</i> (1) | 16 - subas-tion <i>Poo-Calamagrostietosum holmii</i> (2) |

Figure 2. Ecological dynamic series and the change of salt content in groundwaters.

The closeness and specifics of the relations were estimated by the Pearson correlation coefficient, widely applied in geobotanical studies.

Total sum of salts and Cl, SO₄, Ca, Mg, and K contents in groundwater were estimated for ecotopes of the identified syntaxa. Distribution of these indices for the groundwater samples is approximated by the normal probability law. Seventy percent confidence intervals of the chemical indices was computed separately for every syntaxon's ecotope (Vinogradov 1964) scale having a 60% limit for the indicator. The results presented in Figure 2 clearly show how syntaxa range in the ecologic series.

The data reveal a successional mechanism in the landslide communities that proceeds parallel with the ecotope's recovery after landslide disturbance. This confirms the fact that vegetation dynamics on the marine terrace slopes is conditioned upon groundwater desalinization.

Decrease in groundwater salt content takes place as landslide structures increase in age. In general, the concentration of Cl, SO₄, Ca, Mg, and K decreases sharply on freshly exposed surfaces, with little further decrease on ancient landslide structures.

Changes in groundwater chemistry correlate with the dynamics of the community phytomass within the marine terrace slope seral system (Fig. 3).

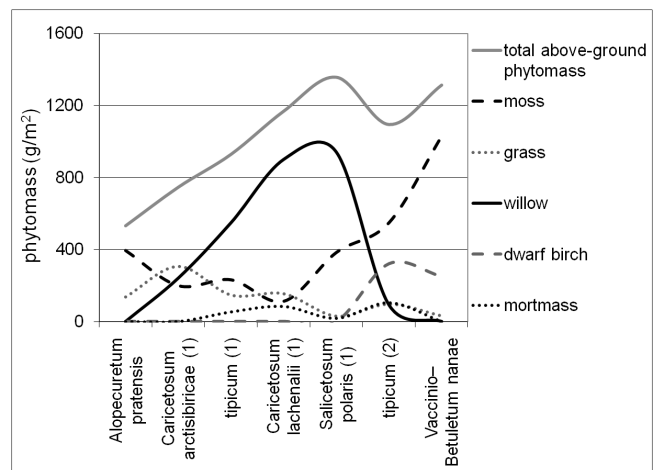


Figure 3. Change of average phytomass values in the communities of ecological dynamic succession of shearing surfaces central parts.

Phytomass increase is observed in every ecologic dynamic series up to the subclimax stage, after which the dynamics of groundwater mineralization is characterized by changing water type from fresh to ultrafresh, according to the classification of Perelman (1982). This correlation can probably be explained by plant exploitation of nutrients dissolved from marine sediments throughout early and

	young structures stage	old structures stage	ancient structures stage	subclimax stage	
shearing surfaces central parts	diff. species Alopecuretum pratensis; sp. richness - 34 total phm - 532 willow phm - 0 moss phm - 396 ecotypes of v.p.-lrpg+lbpg	diff. species Caricetosum arctisibiricae (1); sp. richness - 22 total phm - 746 willow phm - 241 moss phm - 200 ecotypes of v.p.-lrpg+lbpg	diff. species tipicum (1); sp. richness - 42 total phm - 928 willow phm - 548 moss phm - 233 ecotypes of v.p. - lrpg+srpg+rrpg	diff. species Caricetosum lachenalii (1); sp. richness - 36 total phm - 1167 willow phm - 900 moss phm - 113 ecotypes of v.p. - lrpg+rrpg+srpg	diff. species Salicetosum polaris (1); ind.species - <i>Dryas octipetala</i> sp. richness - 46 total phm - 1356 willow phm - 941 moss phm - 384 ecotypes of v.p. - lrpg diff. species tipicum (2); sp. richness - 59 total phm - 1093 willow phm - 91 moss phm - 550 ecotypes of v.p.-lrpg+hs diff. species Salicetosum polaris (1); ind.species - <i>Dryas octipetala</i> sp. richness - 46 total phm - 1356 willow phm - 941 moss phm - 384 ecotypes of v.p.-lrpg diff. species Vaccinio-Betuletum nanae; sp. richness - 30 total phm - 1312 willow phm - 0 moss phm - 1030 ecotypes of v.p. - lrpg+fbpg
shearing surfaces peripheral parts		diff. species Eriophoretosum vaginati (2); ind. species - <i>Stellaria palustris</i> sp. richness - 31 total phm - 1029 willow phm - 550 moss phm - 230 ecotypes of v.p. - lrpg+hs	diff. species Poo - Calamagrostietosum holmii (2); sp. richness - 34 total phm - 1230 willow phm - 626 moss phm - 277 ecotypes of v.p. - hs+lrpg		
landslide bodies central parts		diff. species Drepanocladetotum uncinati (1); ind. species - <i>Drepanocladus uncinatus</i> sp. richness - 38 total phm - 1329 willow phm - 1077 moss phm - 95 ecotypes of v.p. - lrpg	diff. species Veratretosum lobeliani (1); sp. richness - 27 total phm - 1386 willow phm - 1014 moss phm - 270 ecotypes of v.p. - lrpg		
landslide bodies peripheral parts		diff. species Peltigeretosum aphthosae (2); ind. species - <i>Peltigera aphthosa</i> sp. richness - 25 total phm - 1324 willow phm - 520 moss phm - 388 ecotypes of v.p. - lrpg+hs	diff. species Veratretosum lobeliani (2); sp. richness - 42 total phm - 1725 willow phm - 800 moss phm - 446 ecotypes of v.p. - lrpg+hs		
	35 years		300 years		2000 years
<i>Salix glauca</i>					

Figure 4. Indicator scheme of successional system of vegetation on landslide-affected slopes of the Central Yamal (legend: phm – phytomass (g/m^2), v.p. – vascular plants, lrpg – long-rhizome polycarpic grasses, hs – hemiprostrate shrubs, fbpg – firm-bunch polycarpic grasses, srpg – short-rhizome polycarpic grasses; rrrpg – racemose-root polycarpic grasses; lbpg – loose-bunch polycarpic grasses with short creeping roots).

intermediate successional stages. This interpretation agrees with those of Ukraintseva (1997, 2008). There is a short-term decrease in phytomass at the subclimax stage. This results from physiognomic changes as willow's phytomass (*Salix glauca*) making up about 95% in the communities decreases sharply and is largely replaced by moss. This process reflects the approach of ecotope conditions to the parent ones (i.e., before the landsliding event).

The species richness of syntaxa reaches a maximum at the pre-subclimax successional stage, while species saturation during the seral changes of vegetation remains almost the same. The early successional stages are characterized by the dominance of long-rhizome pioneer polycarpic grasses (e.g., *Dupontia fisheri*, *Equsetum arvense* subsp. *boreale*); their role gradually decreases as vegetation recovery proceeds. In the course of succession, the importance of erect dwarf shrubs (*Vaccinium vitis-idaea* subsp. *minus*) and firm-bunch grasses (*Hierochloë alpina*, *Trisetum spicatum*) increases.

The relationship between vegetation development and groundwater demineralization, as well as the already-known dependence of groundwater demineralization on landslide age, was used to build up the indicator chain "vegetation → groundwater mineralization → age of the landslide structure."

The marine terrace slopes in the Central Yamal are complex landslide systems of different ages that often

overlap one another. This fact complicates the visual identification of landslide structures in the relief. The set of vegetation indicators associated with the cryogenic landslide age, the type of formed landslide structure, and the chemical composition of groundwater were identified on the basis of analysis of vegetation dynamics, including 1) syntaxa differential species; 2) indicator species (defined according to successional status); 3) total above-ground phytomass of vegetation communities, *Salix glauca*, and moss phytomass; and 4) set of vascular plants' ecotypes. The indicator set includes physiognomic features of vegetation communities closely related to the objects of indication and characterized by the distinct dynamics depending on the dynamics of indicated objects (shown in the indication scheme, Fig. 5). To introduce age characteristics, we used the radiocarbon dating of landslide structure age carried out by Kizyakov and Leibman (2007) at this key site.

With the ungraded longitudinal slope profile, the landslide process development is possible at any stage of vegetation recovery. Nevertheless, the structure of plant communities is an important factor affecting the activation of cryogenic landslides. The ecotopes of the later recovery stages of the vegetation communities are the most resistant to the development of the landslide process. These communities have a closed shrub cover of *Salix glauca* that is often 1–1.5 m

high. At the subclimax stage, the shrub cover begins to thin and mosses begin to dominate by the phytomass. *Betula nana* in these communities is short-growing and doesn't form an independent layer. In subclimax communities, there are no plants with extensive root systems capable of stabilizing the structure of the active layer; therefore, their ecotopes are extremely non-resistant to the activation of the landslide process. On the other hand, geochemical processes proceeding in the active layer also lead to slope destabilization through slow accumulation of secondary clay minerals on the border between the active layer and the permafrost table. These clay minerals play a significant role in cryogenic landslide development (Tentyukov 1998). The physical strain in the upper horizons of the deposits, which is necessary for activation of the landslide process (Leibman et al., 2007), develops gradually over 300 years. Therefore, ecotopes where the cryogenic landslide occurred a long time ago turn out to be more susceptible to new landslides than recently disturbed ecotopes.

Yurtsev, B.A. (ed.). 1995. *Anthropogenic dynamics of vegetation cover in the Arctic and the Subarctic Regions: Principles and methods of investigation*, edited by Komarov Botanical Institute RAS, Edition 15, 185 pp.

References

- Leibman, M.O. & Kizyakov, A.I. 2007. *Landslides of Yamal and the Yugorskiy Peninsula*. Moscow: ECI SB RAS, 206 pp.
- Leibman, M.O., Kizyakov, A.I., Archegova, I.B., & Gorlanova, L.A. 2000. Landslide stages at the Yugorsky Peninsula and in Yamal. *Earth Cryosphere* 4 (no 4): 67–75.
- McCune, B., Grace, J.B., & Urban, D.L. 2002. Analysis of ecological communities. Oregon: MjM Software, Gleneden Beach, 300 pp.
- Perelman, A.I. 1982. *Natural waters geochemistry*. Moscow: Nauka, 115 pp.
- Puzachenko, Yu.G. 2004. *Mathematic methods in environmental and geographic studies*. Moscow: Akademiya, 408 pp.
- Rozenberg, G.S. 1998. *Quantitative phytoindication methods. Environmental monitoring. Biological and physical-chemical monitoring methods*. Part III. N. Novgorod, 1998, pp. 5-27.
- Tentyukov, M.P. 1998. *Landscapes geochemistry in Central Yamal*. Ekaterinburg izd-vo UrB RAS, 104 pp.
- Tsibulsky, V.R., Valeeva, E.I., Arefjev, S.P., Meltser, L.I., Moskochenko, D.V., Gashev, S.N., Brusynina, I.N., & Sharapova, T.A. 1995. *Environmental Nature of Yamal*, 2 vols., Tyumen: Institute of Northern Development, SB RAS.
- Ukrainitseva, N. 2008. Vegetation response to landslide spreading and climate Change in the West Siberian Tundra. *Proceedings of the Ninth International Conference on Permafrost*. Institute of Northern Engineering, University of Alaska Fairbanks, 2: 1793-1798.
- Ukrainitseva, N.G. 1997. *Yamal willow shrub tundra as an indicator of surface deposits salting. Basic research results for the Earth's cryosphere in the Arctic and the Subarctic Regions*. Novosibirsk: Nauka, pp. 182-187.
- Vinogradov, B.V. 1964. *Phytoindicators and their use in natural resources study*. Moscow: Vyssh.shk., 328 pp.

Changes in the State of Frozen Ground in the Course of Long-term Operation of the Yakutsk Combined Heat and Power (YCHP) Plant

S.I. Zabolotnik, P.S. Zabolotnik
Melnikov Permafrost Institute, SB RAS, Yakutsk, Russia

Abstract

Ground temperatures around and beneath the facilities of the Yakutsk Combined Heat and Power (CHP) Plant were periodically measured from 1982 to 2009. The measurements revealed that most of the ground on the plant's territory is frozen. Ground temperature at 4–10 m depth beneath the main facility is 0 to -3.5°C , while under other facilities it is from 0 to -2.5°C . Currently talik zones occur beneath all the structures built according to the passive principle. Talik thickness beneath the buildings varies from 4–5 to 15 m and more, while ground temperatures are between 0 and $+5.5^{\circ}\text{C}$. The ground adjacent to the production buildings thawed to the depth of 23–25 m, while the ground temperature increased to $+8.0$ – 11.5°C . The influence of the changes in mean annual air temperature on the ground temperature was estimated. The temperature fields of the ground mean annual temperature at the depth of 4 m are presented for 2008 and 2009.

Keywords: mean annual ground temperatures; permafrost; taliks.

Introduction

The Yakutsk Combined Heat and Power Plant (YCHP), constructed in 1937, was the first industrial facility in the USSR that used the principle of permafrost preservation in the foundation bases (passive principle). Before the plant was built, permafrost thickness at the construction site reached 180–200 m, and the ground temperature at the depth of 15 m was fluctuating between -3 and -5°C . In the first years after the plant was put into operation (1939–1943) the mean annual ground temperature at the base of the main facility's foundation (5 m depth) ranged between -4.7 and -7.4°C . Ten years later, it increased to -3.2 to -3.6°C (Tsytovich et al. 1947).

The ground around the YCHP main facility and a number of auxiliary facilities is covered with asphalt. Down to the depth of 1–4 m it is composed of fill dirt consisting of sand of different grain sizes, less often of clayey silt mixed with crushed stone, pebbles, and slag. Below, there are alluvial deposits represented by fine sand that contains inter-layers of medium and coarse sand. Soil moisture content varied from 20 to 70%, and density ranges between 1700 and 2690 kg/m^3 (Zabolotnik & Zabolotnik 2009).

Results and Discussion

During the first decades of the YCHP operation, an extensive talik zone beneath the facilities and at adjoining areas was formed. The principal causes of its formation were heat emission from the buried objects and hot industrial water leaks directly into the ground under the foundation.

In order to freeze the ground around the southern corner of the main facility in close proximity to a circulating pump station, 6 multi-pipe seasonally functioning cooling devices (SFCDD) with 500 liters of kerosene each were installed and put into operation in 1967 (Gapeev 1983). In 1973, 17 other similar devices were installed at three sides of this part of the building (Fig. 1, SFCDD Nos. 1–6 and 7–23).

The SFCDDs decreased the permafrost temperature in close proximity to the devices. However, the expected result

in freezing of the foundation bed was not fully achieved. The working radius of the devices is 2.5 m, and they were installed at a distance of 1.7–3.5 m from the building walls with an interval from 2.9–3.1 to 5–7 m (Khrustalev et al. 1983).

In 1982–1986, we precisely defined the area of talik zones for the first time. By then only two isolated plots remained from the continuous talik field presented in the reports of the Yakutsk department of KrasTGSI (1976) and Sibtekhenergo (1978).

Beneath the main facility, talik at the depth of 4.3–4.5 m was exposed in the course of drilling operations. Its lower boundary was determined only at the most distant place from the pump station (Fig. 1, brh. 17) where it rose from 6.5

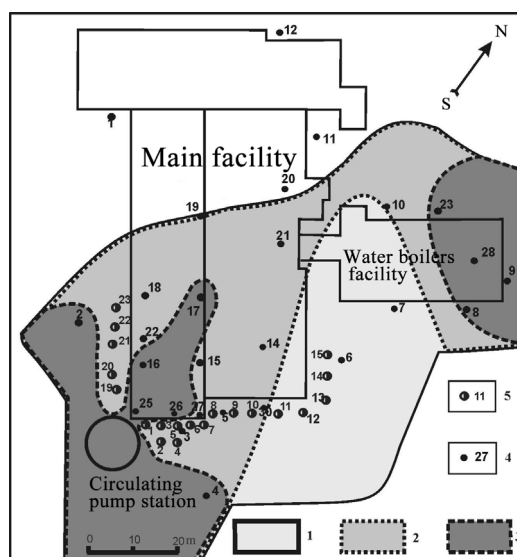


Figure 1. Changes of the talik area at the YCHP Plant site from 1976 to 1986. Talik boundaries according to the data of: 1 – the Yakutsk department of the Krasnoyarsk Trust of Geotechnical Site Investigations (KrasTGSI), 1976; 2 – the Novosibirsk Engineering Firm providing power engineering assistance services (Sibtekhenergo), 1978; 3 – the Permafrost Institute, 1986; 4 – borehole and its number; 5 – SFCDD and its number.

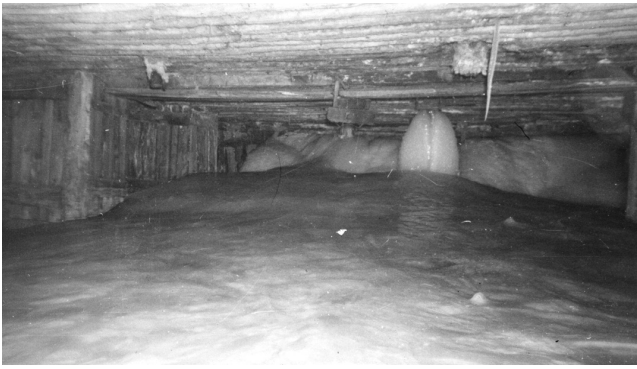


Figure 2. The cellar beneath the main facility filled up with ice. Photo by N.I. Novikov, March 27, 1986.

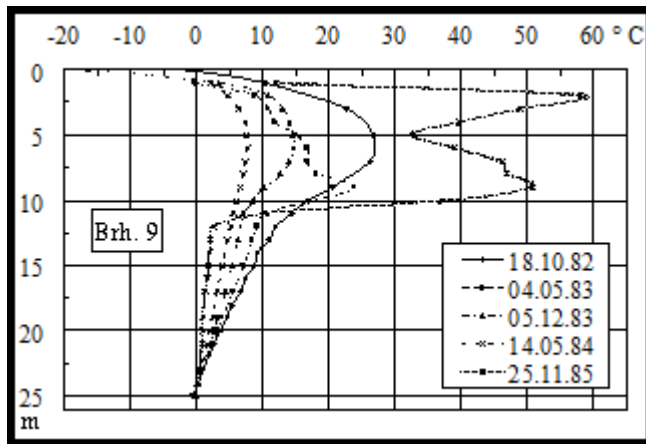


Figure 3. The influence of hot water leaks on the ground temperature.

to 6.1 m between May 1985 and January 1986. The rest of the boreholes were 4.0–5.5 m deep, which was not enough to establish the lower boundary of the talik. However, the ground temperature at the bottom of these boreholes was above zero and reached 1.4–1.8°C. The maximum talik thickness beneath the facility was not identified due to insufficient depth of the boreholes. It exceeded 17 m at the adjoining areas located outside the working radius of the SFCDs. This is indicated by the data obtained for boreholes No. 2 and No. 4 with depths of 17 and 15 m (Fig. 1). When they were drilled at the beginning of July 1982, the permafrost top was not reached. At the same time, the ground temperature at the depth of 15 m from October 1982 to December 1985 was fluctuating between values around 0.0 and 1.6–2.1°C.

The warming effect of water leaks occurred in summer and in winter because the freezing water filled the ventilated cellar. As a result, icing was formed. It functioned as insulation, preserving the foundation base from cooling by the outside cold air. On the other hand, the ice blocked up the cellar and totally prevented air circulation beneath the building. According to our observations, at the end of March 1986 the icing beneath the main facility formed a continuous field with the total ice volume exceeding 600 m³, and it almost entirely filled the ventilated cellar (Fig. 2).

Beneath a part of the water boilers facility and around it a much smaller talik area remained. Meanwhile, the ground temperature in this location was much higher and the talik was much thicker. Borehole 9 (Fig. 1), drilled to the depth

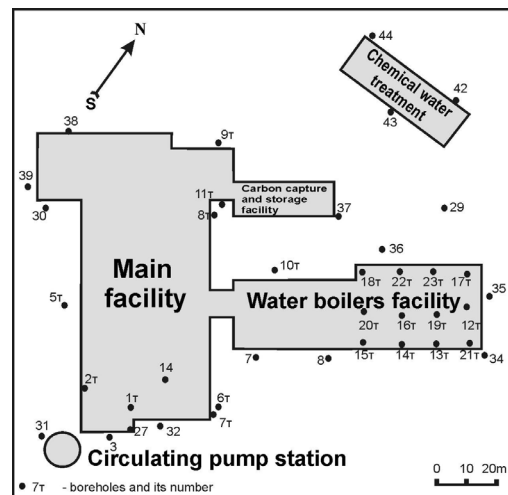


Figure 4. Disposition plan of the boreholes in which measurements were made in 2008–2009.

of 25 m beside the building in July 1982, revealed a water-saturated thick layer of sand of different grain size. Below the depth of 23 m there was a layer of weathered sandstones. In the course of drilling, we did not manage to determine whether the layer was frozen or not. However, the very first measurement of the temperature inside the borehole revealed that the permafrost top is located at the depth of 24.5 m. The cause of talik development at this location is obvious. The water leaks that periodically occurred were raising the ground temperature up to 14–27°C. The maximum temperature was registered on November 25, 1985, when it reached 58.0°C at the depth of 2 m and +50.7°C at the depth of 9 m (Fig. 3) (Zabolotnik & Novikov 1986).

By the end of April 1986, our research on the YCHP Plant's territory was completed and was not conducted again for 16 years. From 2002 to 2007 only single or short-period measurements were made. By this time the cooling devices stopped operating. As a result, a slight expansion of the area of the talik zone beneath the southern part of the main facility has occurred. The talik also occupied the territory adjacent to the southeastern wall of the facility where SFCDs Nos. 1–7 are located (see Fig. 1). It also extended beneath the annex of the water boilers facility and developed beneath the carbon capture and storage facility (CCSF). We did not manage to establish the precise boundaries of talik distribution, because 10 out of 12 boreholes were destroyed during the cleaning of ice in the cellar of the main facility. Twelve boreholes were destroyed during the repairs around the buildings.

Talik thickness exceeded 10.5 m beneath the southern corner of the main facility and 20–23 m around the pump station adjoined to it. Near the northeastern part of the water boilers facility it was fluctuating between 17.6 and 26.6 m, and between 10 and 20 m along the southeastern wall of the CCSF.

In connection with the increasing settlements of the foundations, the YCHP Plant management addressed the Permafrost Institute with the request to resume research in order to develop measures that could ensure the stability of all the structures. Consequently, from November 2007 we resumed monthly ground temperature measurements and drilled extra boreholes at the challenging points around the

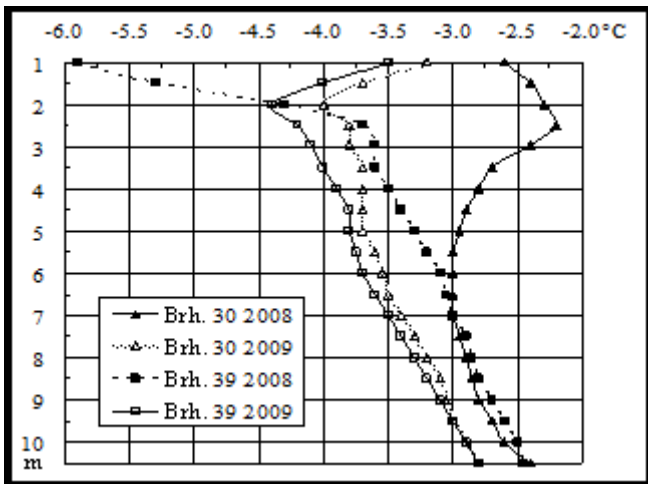


Figure 5. The mean annual ground temperature near the western corner of the main facility.

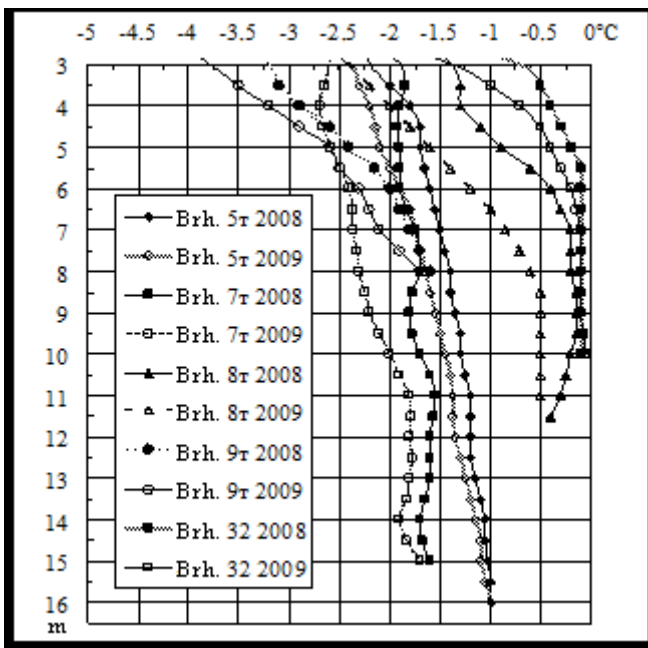


Figure 6. The mean annual ground temperature around the major part of the main facility.

structures. As a result, the number of boreholes reached 38, including 16 boreholes directly beneath the buildings (Fig. 4).

During two years of measurements (2008 and 2009), we managed to evaluate the present state of the permafrost zone on the YCHP territory and determine the particularities of changes in ground temperature regime. By the end of 2009, the frozen state of the ground was either preserved or restored on most of the plant's territory.

The lowest mean annual ground temperature was registered around the western corner of the main facility. In 2008 at the depth interval of 4–10.5 m it was fluctuating between -3.5 and -2.4°C , while in 2009 it decreased by 0.9 – 0.2°C and ranged from -3.9 to 2.8°C (Fig. 5). This indicates that the permafrost beneath and around this part of the building almost regained its initial state (i.e., the state before construction of the plant).

Such low temperatures are caused by the fact that this part of the main facility houses only administrative services and there are no devices that emit much heat. It is natural that

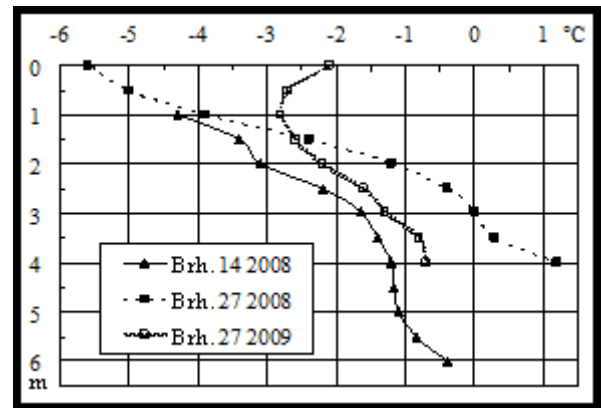


Figure 7. The mean annual ground temperature beneath the main facility near the talik zone.

at this point the influence of the building on the underlying ground is minimal. The temperature decrease during the second year is generally caused by the fact that the mean annual air temperature in 2009 was 0.7°C lower than in 2008. Around the major part of the main facility in which the major manufacturing equipment is installed, the mean annual temperature became considerably higher (Fig. 6).

Only 2 boreholes with the depth of 4–6 m remained in the frozen ground beneath the southern part of the main facility in proximity to the boundary of the talik zone. The mean annual ground temperature beneath this part of the structure is higher. At the base level of the foundation supports in 2008 it was fluctuating between -1.2 and -0.4°C (Fig. 7, brh. 14). Unfortunately, the thermistors frozen into the ground of this borehole stopped working in 2009, which did not allow us to continue the measurements. Another borehole exposed unfrozen ground at the depth of 3 m. Mean annual temperature at the depth of 4 m reached $+1.2^{\circ}\text{C}$ in 2008. In 2009 the unfrozen ground froze again and the temperature decreased to -0.7°C (Fig. 7, brh. 27).

The building of the pump station adjoins the southern corner of the main facility. Its underground part is buried deeper than 10 m. These heated buried premises present a constant heat source of great power.

The continuous heat emission thawed the grounds around the station down to a considerable depth. In July 2005, during the drilling of borehole 31 located in close proximity to the station, it was determined that the ground thawed to the depth of 23 m, while the talik zone around the station extended by at least 25 m. In 2008 and 2009, the mean annual ground temperature at the 1.5 m distance from the circulating pump station was above zero within the whole range of measurements. In the range of 4–10.5 m it was constantly higher than $+8^{\circ}\text{C}$ and reached almost $+12^{\circ}\text{C}$ (Fig. 8, brh. 31).

Beneath the southern corner of the main facility and near its outer wall the boreholes are located at the distance of 10–20 m from the pump station. It is natural that the mean annual ground temperature is not so high there as it is farther away from the heat source. In 2008, ground temperature did not exceed $+2.8^{\circ}\text{C}$, while in 2009 it was below $+2.0^{\circ}\text{C}$ (see Fig. 8, brh. 1t and 3).

The water boilers facility attached to the southeastern wall of the main facility was built in 1978. Its foundation is

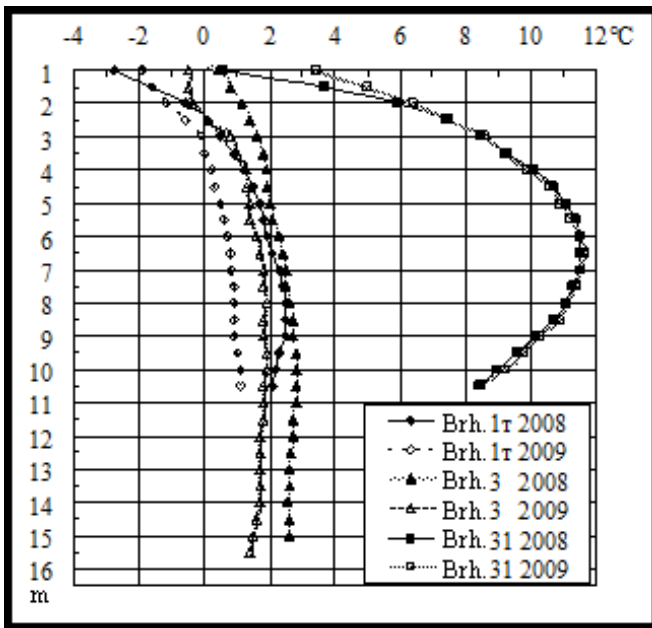


Figure 8. The mean annual ground temperature in the talik zone around the circulating pump station.

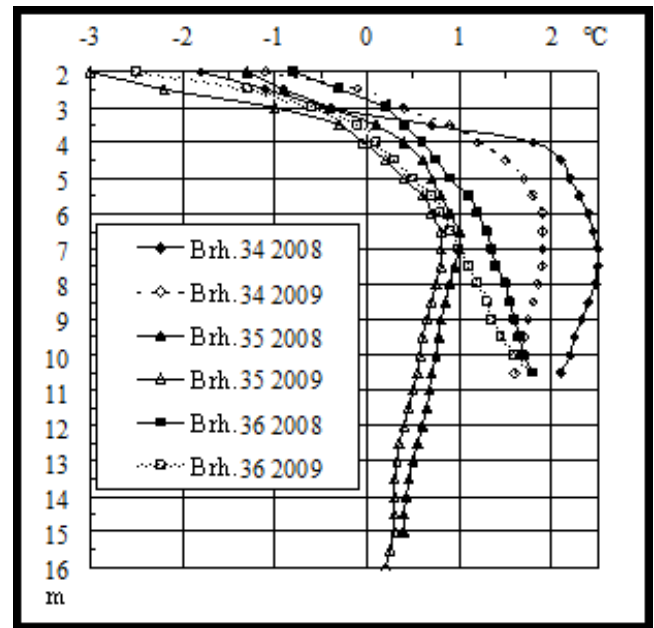


Figure 10. The mean annual ground temperature around the annex to the water boilers facility.

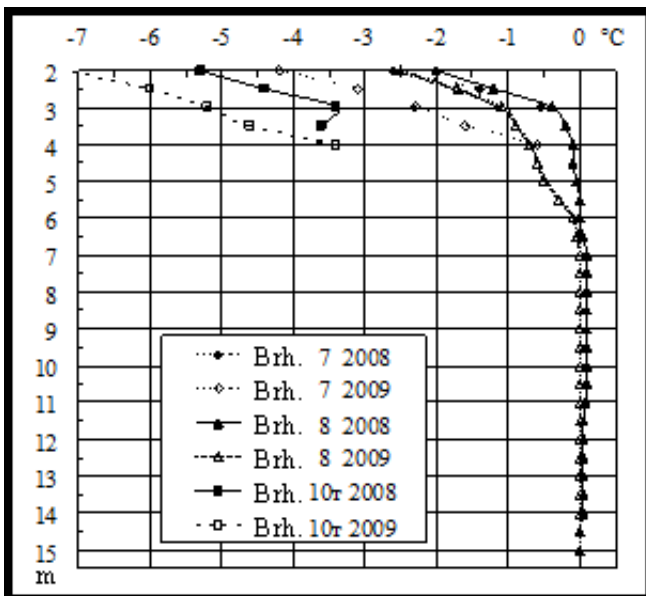


Figure 9. The mean annual ground temperature near the part of the water boilers facility that adjoins the main facility.

also located in both frozen and unfrozen ground. Presently, permafrost remained only beneath the part of the building adjacent to the main facility. Unfortunately, some blocks formed at the depth of 3-4 m and lower in boreholes 7 and 10t located near the outer walls of the facility. This made it impossible to register the temperature below the blocks. However, the two-year cycle of observations makes it possible to assess the permafrost state even at the place below the blocks' depth.

As expected, the lowest ground temperature was registered near the wall of the water boilers facility shaded from the west, south, and east. Below the seasonally thawed layer with the maximum thickness not exceeding 3 m (Zabolotnik S.I., Zabolotnik P.S. 2009) the mean annual ground temperature ranged from -3.4 to -5.2°C (Fig. 9, brh. 10t).

Near the southeastern wall of the water boilers facility

the mean annual ground temperature in close proximity to the main facility was already 2.7 – 2.9°C higher (Fig. 9, brh. 7). In 2008 at the distance of 20 m toward the part of the building attached in 1989 it remained below zero only to the depth of 5.5 m. In the range from 5.5 to 15 m the ground was thawed, but mean annual ground temperature did not exceed $+0.1^{\circ}\text{C}$. In 2009, temperature decreased by 0.5 – 0.7°C in the upper 5 m layer. The permafrost bottom lowered to 6.5 m, and below it a zero zone was formed (Fig. 9, brh. 8).

The talik was already formed beneath the aforementioned annex to the water boilers facility before its construction began. It formed due to water leaks directly into the ground of the foundation base from the part of the building that was put into operation earlier. Although the foundation pit froze in winter preceding construction of the annex, the talik has remained at this place up to now. Before this part of the facility was constructed, 12 boreholes 4 m deep were drilled under it (see Fig. 4, brh. No 12t–23t). Unfortunately, the deep 25 m borehole No. 9 was destroyed (see Fig. 1).

Around the talik zone beneath the water boilers facility the mean annual ground temperature was rather high. In 2008 at the depth of 4 m it was fluctuating between -0.2 and -0.5°C , while in 2009 it decreased to -0.4 ... -0.7°C . This indicates the gradual freezing of the talik zone from the side of the permafrost.

In the talik beneath the facility at the depth of 4 m, the mean annual ground temperature was fluctuating between 0 and $+2.9^{\circ}\text{C}$ in 2008. In 2009 it did not exceed $+2.3^{\circ}\text{C}$, while beneath the northern corner of the building it decreased to -0.1°C (see Fig. 4, brh. 12t, 17t and 23t).

The thickness of the seasonally thawed layer in the frozen grounds surrounding the thawed area did not exceed 3.1 m, while the ground inside the talik froze deeper than 4 m. Based on the fact that the mean annual ground temperature beneath the northern corner of the facility at the depth of 4 m decreased below zero in 2009, we can only state that the thickness of the seasonally frozen layer increased. Further research will show whether it will thaw the next summer.

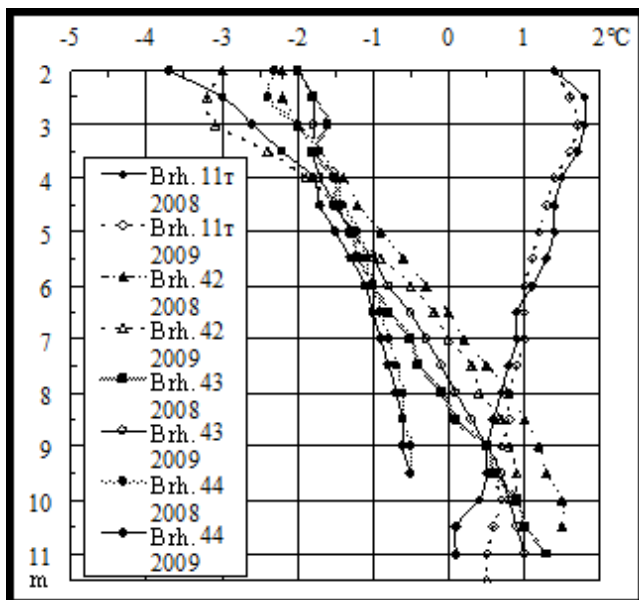


Figure 11. The mean annual ground temperature near the CCSF (borehole 11t) and around the chemical water treatment facility.

It is impossible to identify the thickness of the talik using such shallow boreholes. However, it can be inferred from 10–16-m-deep boreholes drilled by us around this part of the facility in 2005 (see Fig. 4). The measurements revealed that the maximum mean annual ground temperature at this location at the depth of 6.5–8.0 m reached $+2.5^{\circ}\text{C}$, while the talik's thickness exceeded 16 m (Fig. 10).

A narrow strip of talik extends from the water boilers facility to the carbon capture and storage facility (CCSF) and extends to its southern part.

There are no boreholes directly under the CCSF. However, two boreholes (37 and 11t) located at both sides in close proximity to its walls (see Fig. 4) were drilled in unfrozen ground.

During the drilling of borehole 37 down to the depth of 19.5 m in August 2005, a talik was exposed with the temperature ranging from $+1.0$ to $+2.0^{\circ}\text{C}$ at the depth of 8–10 m in 2005–2006. Unfortunately, in July 2006 this borehole was destroyed. At the point where the CCSF adjoins the main facility, the mean annual ground temperature in 2008 at the depth of 2–11 m was fluctuating between $+1.8$ and $+0.1^{\circ}\text{C}$. And the permafrost table was presumably found at 12 m. However, in 2009 further water leaks occurred. The ground temperature at the depth of 11–11.5 m increased up to $+0.5^{\circ}\text{C}$, and, therefore, the talik thickness increased again (Fig. 11, borehole 11t).

The chemical water treatment facility (CWTF) is set apart from the major industrial facilities. The measurements of temperature inside the three boreholes located around it indicated that continuous permafrost is found only beneath its northwestern part. However, the mean annual ground temperature at this point is rather high. Besides, it increases with depth and reaches -0.5°C at the depth of 9.5 m (Fig. 11, brh. 44).

Around the eastern part of the chemical water treatment facility in 2008 the frozen ground was found under the 2.9 m deep layer of seasonal thawing to the depth of 6.5–8.2 m. In 2009 near its northern wall the temperature of grounds

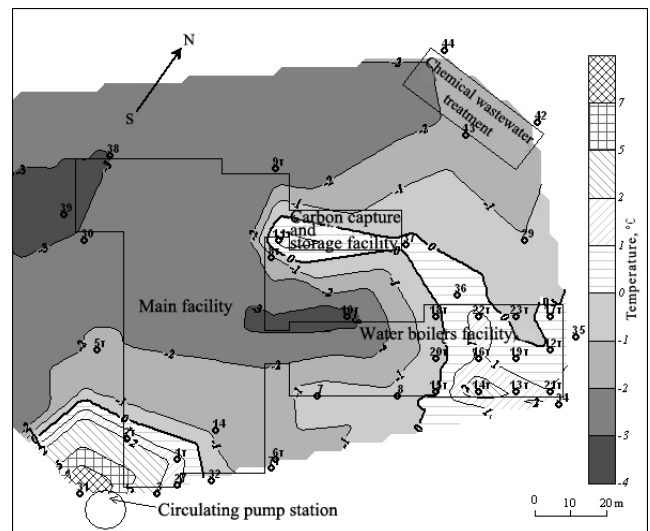


Figure 12. The mean annual ground temperature at the depth of 4 m in 2008.

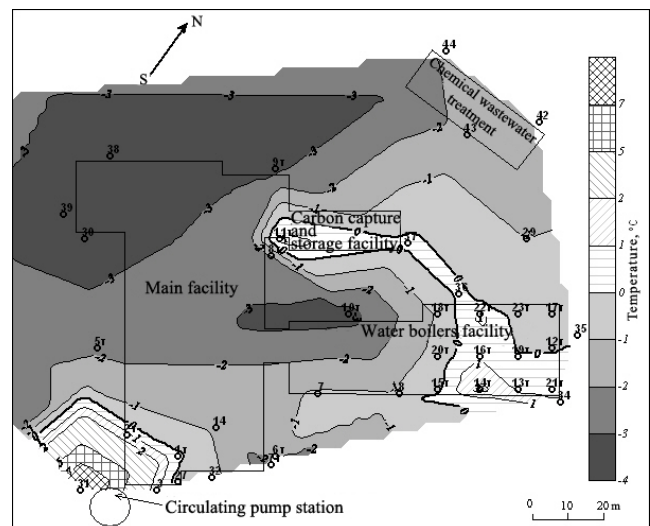


Figure 13. The mean annual ground temperature at the depth of 4 m in 2009.

decreased and the permafrost bottom lowered to the depth of 7.0 m. Near its southern wall, on the contrary, the temperature increased and the permafrost bottom went up to 7.8 m. The mean annual ground temperature reached $+1.0$ to $+1.5^{\circ}\text{C}$ (see Fig. 11, brh. 42–43).

The two-year cycle of measurements of the ground temperature made it possible to evaluate changes in the state of the permafrost zone on the YCHP Plant territory. The analysis of the mean annual ground temperature indicates that the areas of talik distribution beneath the facilities still remain rather large. In 2008, the foundations of the southern corner of the main facility, of the eastern part of the water boilers facility, and of the southeastern part of the carbon capture and storage facility rested on unfrozen ground (Fig. 12).

As mentioned above, the mean annual air temperature in 2009 decreased by 0.7°C compared to 2008. This partly influenced the change in the ground temperature regime at the foundation bases of all the facilities. Specifically, there was a decrease in the ground temperature beneath the northern part of the main facility, while beneath its southern corner there was a slight decrease in the area of the talik zone (Fig. 13).

Beneath the water boilers facility a slight decrease in the area of talik also occurred. It partly froze in the upper part at the point where it adjoins the main facility and beneath the northern corner of the facility (Fig. 13).

As for the carbon capture and storage facility, for two years there were no considerable changes registered in the temperature regime of the adjacent grounds. Most probably it is caused by periodical wastewater leaks into the grounds of the foundation.

Conclusions

The thermal state of permafrost on the territory of the Yakutsk CHP Plant experienced rather significant changes. Recent years have shown a recovery of the ground temperature regime in the foundation base of the facilities and at adjacent areas. However, it progresses very slowly and it will take many years for the ground to entirely regain the frozen state. Therefore, it is necessary to continue temperature monitoring. The results of such monitoring will allow implementation of adequate engineering solutions that will insure the stability of all the facilities.

References

- Conclusions on the inspection of the facilities and the development of a concluding monitoring cycle of the Yakutsk CHP Plant.* 1978. Gilevich, V.G., Neupokoev, G.N. Moscow-Novosibirsk "Sibtekhenergo", 37 pp. (in Russian).
- Gapeev, S.I. 1983. The experience of using cooling devices in the areas of permafrost distribution. *Control of the temperature of the foundation grounds with the help of seasonally functioning cooling devices.* Yakutsk: Izd-vo Instituta merzlotovedeniya SO AN SSSR, 41-58 (in Russian).
- Khrustalev, L.N., Yanchenko, O.M., & Naumova, L.A. 1983. The experience and prospects of using autonomous vapor-liquid cooling devices in construction on permafrost. *Control of the temperature of the foundation grounds with the help of seasonally functioning cooling devices.* Yakutsk: Izd-vo Instituta Merzlotovedeniya SO AN SSSR, 3-12 (in Russian).
- The technical report on the results of the geotechnical site investigations in the area of the Yakutsk CHP Plant's enlargement 1976. Krasnoyarsk–Yakutsk: The Association "Stroyizyskaniya" (the Association of Geotechnical Site Investigations), KrasTGSI, the Yakutsk department, 43 pp. (in Russian).
- Tsytovich, N.A., Saltykov, N.I., Zhukov, V.F., & Melnikov, P.I. 1947. *The foundations of the CHP Plant on permafrost (designing, constructing and operating experience of the Yakutsk Combined Heat and Power Plant based on the principle of permafrost preservation).* Moscow-Leningrad: Izdatelstvo Akademii nauk SSSR, 104 pp. (in Russian).
- Zabolotnik, S.I. & Novikov, N.I. 1986. *Dynamics of the temperature regime, seasonal and perennial thawing (freezing) of the grounds and the settlement of the Yakutsk CHP Plant's foundations.* – Yakutsk: Institut merzlotovedeniya SO AN SSSR, 355 pp. (in Russian).
- Zabolotnik, S.I. & Zabolotnik, P.S. 2009 Ground Temperatures beneath the Buildings of the Yakutsk CHP Plant. EISOPE 2009. *Proceedings of the Eighth International Symposium on Permafrost Engineering.* Ming Huo, Wei Ma & Fujun Niu (eds.). Lanzhou University Press: 318-323.

Evaluation of Critical Ecological Situations in the Tyumen Northern Cryolithozone under Economic Development

L.I. Zotova, S.Yu. Dedyusova
Lomonosov Moscow State University, Faculty of Geography, Russia, Moscow

Abstract

This study describes the methodological approach to formation of critical ecological situations (CES) based on the matrix account of the degree of mechanical damage (the result of the impact of engineering structures together with overexploitation during deer pasturing) and the landscape stability potential. The anthropogenic load is categorized by types and intensity of occurrence. A graphical analytical method for comparing different landscape permafrost ecological state parameters is suggested; the value of expert scores is defined; the integral coefficients of the economic development hazard are calculated.

Keywords: critical ecological situations; cryolithozone; expert evaluations; geoecology; GIS mapping; landscape stability.

Introduction

The environmental state of an area is defined by the combination of anthropogenic load and the landscape's ability to resist it. If the external load exceeds the landscape stability threshold, this causes an unfavorable ecological situation. A five-category gradation of ecological situations is defined in the standards of the Russian Ministry of Natural Resources: relatively satisfactory, tense, emergency, critical, and catastrophic. The criteria for their detection in the cryolithozone include the loss of natural resources and the impossibility of their recovery. These are supplemented by the degree of occurrence of cryogenic and deflation processes in connection with thermal and moisture content regime changes in the lithogenic landscape. The first four categories are reversible; they should be considered as the stages of formation of critical ecological situations (CES). In the cryolithozone, CES are defined by an abrupt activation of cryogenic processes and radical biota change causing a permanent negative change in natural landscape and threatening the functioning of engineering structures (Tumel et al. 2008).

The evaluation of CES formation is based on the consideration of two factors:

- the degree of mechanical damage of the topsoil cover as a result of the impact of engineering structures or overexploitation during deer pasturing;
- the potential of landscape resistance to these types of damage determined by their ability to resist the activation of cryogenic and deflation processes (Zotova et al. 2007).

The regional peculiarities of the formation of unfavorable local-level permafrost ecological situations (and the GIS version of their mapping) are discussed based on the case of the Yamburg and the Kharvuta gas-condensate fields located in the subarctic natural zone of the Tazovskiy Peninsula, underlain by continuous permafrost. Mechanical surface damages have led to an increase in mean annual ground temperature and growth of the seasonal thawing depth. As a result, the reduction of ground strength properties and activation of exogenous geological processes are most hazardous here.

The use of expert scores from various disciplines allowed us to rank these territories according to the cryogenic processes activation hazard, to the quality of domestic reindeer pasture, and to different types of ecological situations.

Methodology

All evaluation studies were carried out on the landscape scale with the help of expert scores. In the course of CES evaluation, the categories of mechanical load intensity were compared with natural landscape stability gradations through the matrix method. The anthropogenic load intensity was ranked with regard to the type of development and mechanical damages, residual deer capacity, the vegetation recovery rate, and the percentage of land disturbed (Zotova et al. 2007).

Branch-specific categories typified by three or four development risk gradations were chosen and then compared with different methods of evaluation of the ecological state of landscape permafrost. Different mathematical methods (correlation, regression, cluster analysis, etc.) were used for detection of the interrelation of factors (criteria).

The number and the spectrum of these parameters vary depending on the regional peculiarities and the research scope. The autonomous procedure of selection of branch-specific evaluation factors is well known. For example, a series of criteria directly influencing the potential activation of undesirable cryogenic processes associated with water phase changes was chosen in the course of lithocryogenic state evaluation for engineering purposes. These were permafrost ice content and temperature, seasonal thawing or freezing depth, relief, vegetation heat-insulation properties, and self-recovery rate. The parameters of food resources provision, deer pasturing density and duration, and the feeding phytocenosis self-recovery rate were chosen for environmental evaluation of the quality of domestic reindeer pastures and their digression degree. Difficulties occurred in the process of evaluating the integral express of different permafrost ecological state factors with different units of measurement.

The following quantitative evaluation criteria (indexes) were used for that: coefficients of permafrost stability

(PSC), ecological hazard (EHC), hazard (HC), and others (Tumel et al. 2008, Shpolyanskaya & Zotova 2010, Zotova & Dedyusova 2011).

The procedure of the integral evaluation of the lithocryogenic and bioresource landscape state with the help of these indexes is as follows:

- 1) selection of ecological hazard criteria (parameters) that define the activation of cryogenic processes and the resource potential of the area;
- 2) table preparation for the score interval gradation scale for their ranking by economic development risks;
- 3) assignment of a score to each landscape in accordance with the table;
- 4) ranking of all landscapes on the basis of their vulnerability to economic development with regard to gradations of calculation indexes;
- 5) evaluation mapping.

Two additional operations were conducted before ranking to account for integral index calculation:

- 3a) expert assignment of integral index values (0 to 1) to each landscape on the basis of evaluation of the actual intensity and the occurrence spectrum of the processes in addition to the bioresource value;
- 3b) analysis of the correlation with the purpose of secondary criteria sorting and production of a multiple regression equation for calculation of the “total hazard score” (for example, EHC) for each landscape.

In all cases, expert scores were used conventionally. They were simply summed up or arithmetic mean values (rarely, geometric mean values) were calculated. The calculation-statistical method of multifactorial landscape biotic and lithocryogenic basis properties correlation analysis could also be used. The score advantage consists of the possibility to numerically compare quantitative and qualitative characteristics. The disadvantage is the subjectivity of parameters selection and ranking scale development. Another disadvantage consists of the lack of any dimensionality to the scores. For more accurate evaluation, some scientists suggest defining the score dimensionality using the so-called “quality cents” accompanied by the building of the interval scale (Fig. 1).

The starting point is as follows. The quality can vary within a specific range. These variations are continuous but finite. Then the whole range of quality change can be summed to 100%, and the “quality cent” can be estimated by its division into 100 equal parts. The “quality cent” is one one-hundredth part of the total possible range of any parameter change (Simonov 1997). Since the interval scale has a measure, all scores derived from it will have a name and a corresponding dimensionality. The interval cent scale is the actual scale ruler for the determination of the distance between scores.

As of today, the method of expert evaluation of the economic development risk based on “quality cents” has been approved in the course of avalanche risk detection within the framework of small-scale GIS mapping. The graphical analytical method is suitable for evaluation studies of various scales—from minor to major review studies, especially for the comparative evaluation of territories on the basis of the same parameters. For example, dimensionality of heterogeneous factors for a cryolithozone stability map

preparation for Western Siberia was defined with the help of the cent scale (Shpolyanskaya & Zotova 2010). This method is also used in the training process due to its illustrative and laconic form.

This work estimates integral hazard coefficients for each landscape of the test sites not only with a traditional score method, but also with the “quality cent” method using the more fractional cent scale.

Research Results

Five parameters were used for the evaluation of the intensity of the cryogenic processes occurrence:

- 1) annual mean permafrost temperature (T)—the probability of hazardous processes development decreases and their recovery rate increases with temperature decrease;
- 2) total ice content (W) is characterized by ice presence in the ground surface layer to the depth of 10 m, a depth with which most of cryogenic processes are associated;
- 3) protective vegetation properties (P)—heat-insulating properties of the topsoil cover (with regard to the projective coverage and the thickness of the above-ground moss-lichenous layer, the peat horizon and the shrubs’ snow-retaining ability) and the fixing properties of the plant root system (the lichenous cover has a weak impact and the moss-peat cover has the greatest impact on processes occurrence);
- 4) ground composition (S), which the seasonally thawed layer thickness depends on; the coarser and the larger the ground composition, the greater the change in the technogenesis;
- 5) slope dissection degree and steepness (F)—an additional “regional” terrain parameter which was introduced into the evaluation scale of the Kharvuta test site for strengthening of the weight of hazardous thermo-erosional processes (earthflows) frequently occurring at this area.

The ecological biotic state of landscapes was evaluated on the basis of two parameters:

- 1) the vegetative cover self-recovery potential (V)—the slower the vegetation recovery and its projective cover growth, the higher the economic development risk;
- 2) resource potential of the territory (R)—in this case it is characterized by the productivity of domestic reindeer pastures expressed by means of the specific deer capacity (number of deer capable of feeding during 1 day within 1 ha of the pasture).

Then the selected parameters were calibrated by gradation scales (Fig. 1) where the degree of impact of each natural factor on the landscape disturbance is estimated in scores on the basis of the upper scale and in cents on the basis of the lower scale. The comparative evaluation of both regions and landscapes can be conducted based on these scales. In this work, landscapes are evaluated.

The procedure of score evaluation reference to the quality cent scale (Fig. 1) is as follows. Two scales are drawn: quality cents are displayed on the lower interval, and scores are displayed on the upper scale. Leading indicator factor scales are positioned between them. There are seven of them in this case. These factors do not correlate with each other, and

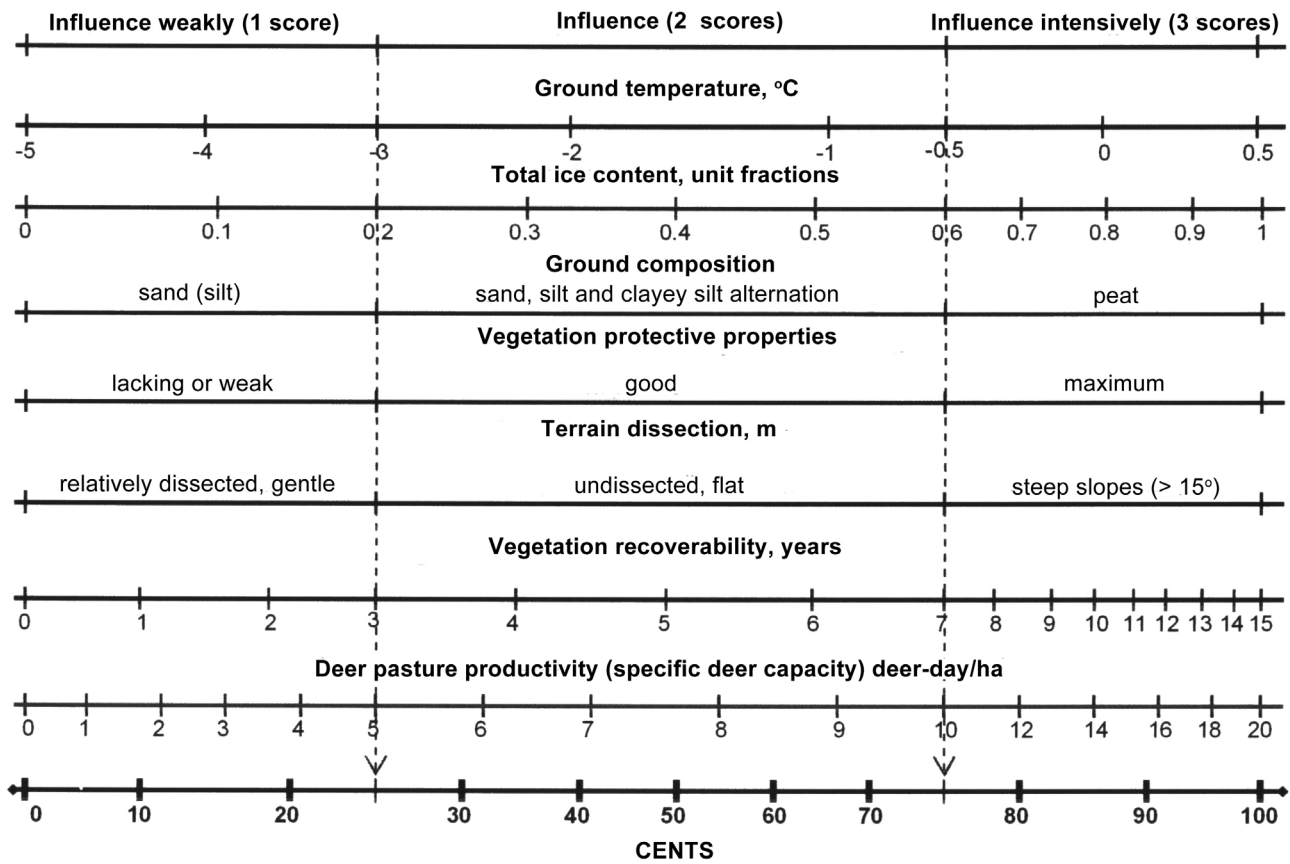


Figure 1. Correlation of evaluation scales of parameters influencing the economic development hazard in tundra.

their scales usually have a different number of gradations. The boundaries of score evaluations of the economic development hazard impact are drawn with regard to the selected factors. The projection of these boundaries onto the lower interval scale allows us to express the score evaluation of the upper scale in cents. In this case, the traditional evaluations in scores are not only preserved but are also supplemented with the evaluation of their own weight in cents within the interval from 0 (no hazard) to 100 (very hazardous).

Figure 1 shows that a high hazard of formation of exogenous processes (score 3) occurs in flat poorly dissected peated landscapes. It also occurs at steep slopes with the annual mean ground temperature close to 0°C, with ice content above 60%, with slow recoverability (more than 7–10 years), and with the maximum projective properties of the top soil cover. If these landscapes are at the same time valuable pasture lands with deer capacity above 10 deer-days/ha, then their economic development hazard grows abruptly. This is the theory. In practice, the number of these landscapes is low. Most of them tend to be classified in the middle hazard class.

Each landscape has values of seven parameters in cents attributed to it. On that basis, not only the sum but also the geometric mean value (we named it the hazard coefficient [HC]) was estimated (Zotova 2011a). The lower the HC value for this landscape, the higher its stability and, respectively, the lower the economic development hazard.

The statistical method approved on a number of deposits in the Tyumen region was used to reveal the cause-and-effect dependence between parameters. The integral development

risk index was expressed via the ecological hazard coefficient (EHC). This permitted a multifactorial correlation analysis of the landscape biotic and lithocryogenic basis properties and preparation of multiple regression equations (Zotova & Dedyusova 2011b). The EHC is essentially a quantitative measure of the degree of ecological risk varying from 0 to 1. The higher its value, the higher the possibility of cryogenic processes activation and consequent harm to deer pastures. The coefficients of parameters correlation (weighting parameters) with each other and with the EHC expert evaluation defined the spectrum of the most valuable parameters and sorted out secondary ones.

Thus it was found that the protective properties of the topsoil cover (P), the self-recovery rate (V), and the productivity of deer pastures (R)—in other words, ecological-biotic criteria—have the greatest impact on the economic development risk and the highest coefficients of correlation with the EHC of all seven parameters.

As a result, two multiple regression equations on the basis of scores (1) and “quality cents” (2) were produced for the Kharvuta key site as follows:

$$\text{EHC} = -0.433 + 0.047T + 0.028W + 0.176P + 0.021S + 0.066F + 0.098V + 0.107R \quad (1)$$

$$\text{EHC} = -0.057 + 0.002T + 0.002W + 0.003P + 0.002S + 0.001F + 0.003V + 0.002R \quad (2)$$

The group of landscape hazards, both in terms of permafrost and biotic criteria, included shrub communities

Table 1. Anthropogenic impact criteria.

Scores	Impact degree	Nature of mechanical damages, % of the area	Pasture load	Technogenic load		Visible result / loss of pastures productivity, %	Recovery period
				Types	Impact radius / also with regard to the pasturing conservation area		
1	Weak	impulse < 5%	single-time herd running	single-time transport passage; exploratory wells	> 300 m / > 1.5 km	none / 10-15%	2-3 years
2	moderate	continuous 10%	seasonal herd running	repeated transport passage, winter roads, burns	100-300 m / 1.0-1.5 km	partial vegetative cover destruction / 30%	up to 10 years
3	Significant	continuous 20%	pastures at the initial digression stage	producing wells, pipelines, mine sites, pits, fills	50-100 m / 0.3-1.5 km	topsoil removal / 50%	20 years
4	Strong	continuous 50%	excessive herd pasturing zones	permanent roads, site facilities, roadbed, ditches, trenches	< 30 m / 0.15-0.3 m	complete topsoil and snow cover removal / above 70%	> 40 years

of steep slopes and peatlands with the EHC values above 0.75 by scores and cents, and also landscapes with the HC values ≥ 2.0 by scores and ≥ 50.0 by cents. In this landscape group, anthropogenic disturbances of a mechanical nature should be completely prohibited.

The group of landscapes relatively safe for economic development, with the EHC by scores and cents below 0.45 and with the HC ≤ 1.5 by scores and ≤ 30.0 by cents, includes deflation bulges and grass-hypnum bogs as well as dry drained lichenous tundras on sands. Mechanical damage in landscapes of this group in the course of economic development is permitted, although with certain limitations.

Four evaluation maps based on different calculation options for two integral hazard indexes, the HC and the EHC, with scores and “quality cents” for each of them, were prepared on the basis of this ranking.

The calculation of the landscape areas within test sites on the basis of hazard halos showed that the method of multifactorial correlation analysis of branch-specific parameters with the development of the multiple regression equation for the EHC calculation in cents for each landscape is the most reliable (Zotova & Dedyusova 2011).

It was found that the evaluation by cents is more detailed, but in this case the spectrum of landscapes classified in the middle hazard class is extended. Therefore, the EHC occurrence evaluation in cents is underestimated as compared to the same evaluation in scores due to variation (relative scattering) of branch parameter values.

A four-category load scale in scores by the degree of the load intensity growth was developed to systematize the anthropogenic impacts of the Tyumen North gas fields (Table 1).

For example, the first stage (1 score) is the weakest impact degree; mechanical damages are of a temporary nature and make 5% of the zone area. They occur as a result of a one-time passage of track-mounted transport in summer or a one-

time deer running. The residual deep capacity constitutes 80% of the natural one. There is no visible response to the impact. It is typical of drilling pads, temporary roads, winter roads, and burns. Their relatively quick self-recovery occurs during the subsequent years.

The fourth stage (4 scores) with the highest mechanical damage gradient—up to 50%—is registered in a radius up to 500 m. The destruction includes fills, permanent roads, site facilities, roadbed, trenches with completely disrupted topsoil and removed snow cover, and zones of excessive herd pasturing (residual deer capacity below 30%). No self-recovery occurs within them. The formation of secondary phytocenoses on dumps and fills occurs extremely slowly. Even 40–50 years later, only pioneer groups with variegated species composition are observed within them.

In order to prepare the geocological situations map, the permafrost ecological state map was compared with the anthropogenic load map by means of overlaying of corresponding thematic layers (Zotova et al. 2007). The legend for the map was prepared in the form of a matrix table. Permafrost ecological state groups were given in accordance with three EHC gradations at the horizontal axis, and four categories of loads of a specific spectrum and intensity were given at the vertical axis (Table 2).

The type of a possible situation is defined based on the score sum in each matrix cell, in accordance with the expert evaluation of the exogenous process type (based on the speed of hazardous cryogenic process development and the area damaged by it). As a result, all cells are united into four groups on the basis of the score sum and form the following types of geocological situations: satisfactory, tense, emergency and critical. Each situation is characterized by a specific set of exogenous processes with different intensity.

Therefore, all the landscapes in the geocological situations map (Fig. 2) are classified into four groups on the basis of their ability to take different technogenic loads.

Table 2. Evaluation of geoeological situations formation (based on the score sum).

Degree of impact	Groups of permafrost ecological state of the EHC	Not hazardous < 0.45	Hazardous 0.45-0.75.	Very hazardous > 0.75
		1	2	3
None	1	$\sum \text{scores} = 2^*$	$\sum \text{scores} = 3$	$\sum \text{scores} = 4$
Weak	2	$\sum \text{scores} = 3$	$\sum \text{scores} = 4$	$\sum \text{scores} = 5$
Moderate	3	$\sum \text{scores} = 4$	$\sum \text{scores} = 5$	$\sum \text{scores} = 6$
Strong	4	$\sum \text{scores} = 5$	$\sum \text{scores} = 6$	$\sum \text{scores} = 7$

* – Geoeological situations: critical ($\sum = 6-7$); emergency ($\sum = 5$); tense ($\sum = 4$); satisfactory ($\sum = 2-3$).

The critical ecological situation, CES as such, happens with the occurrence of significant and poorly compensated changes in landscapes. A CES is formed in two cases: in the landscapes of the third group which are unstable in permafrost relation (gibbous hillocky and hillocky peatlands with patterned vein ice) due to a significant and strong impact, and in relatively unstable landscapes (tundras on dusty sands and low peatlands) in the zone of strong mechanical damage.

Typical processes at the CES stage are as follows:

- In peatlands: vein ice thawing, deep thermokarst in patterned-vein ice, peat block subsidence, intensive thermal erosion in cracks, ice thawing out in frost mounds, and conversion into lakes.
- In bogs with low-center polygons: progressive swamping, thermokarst, seasonal and long-term frost heave. Frost cracking—thermal erosion—is activated in cracks, and intensive deflation is developed with the formation of deflation basins in tundras on icy and ice-rich dusty sands with topsoil cover removed.

Hazardous changes were observed in the state of surface and water ecosystems, landscape in general, and its cryolithogenic basis in particular in CES halos. It is here where engineering structure accidents occur. At the same time, CES is of a reversible nature after the reduction of technogenic impacts and the completion of corresponding nature-protecting measures. The maximum intensity of processes and the maximum degree of damage caused by them in CES areas are registered during the first 3–5 years after disturbance. Their recovery is predicted after 15–20 years.

The CES stage in the Western Siberia cryolithozone was diagnosed based on the reduced geosystem contrast range and the depletion of the landscape structure. This is reflected

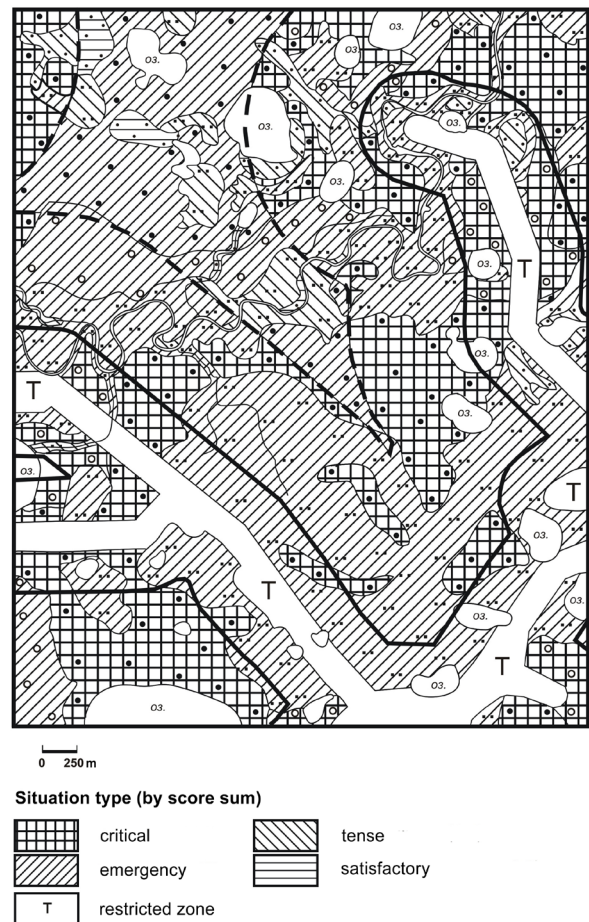


Figure 2. Fragment of the geoeological situations map for the Yamburg field.

in the development of near-dominant secondary landscapes: bog-lake swampy plain (instead of hillocky peatlands) and sandy deserted badlands (in the place of drained shrubby and lichenous tundras). And it is known that a reduced contrast range of landscapes reduces their resistance to destruction.

No more than 7% of the area of the Yamburg field and up to 4% of the area of the Kharvuta field is exposed to CES development, taking into account the technogenic load only. From the ecological point of view and taking into account the disturbance of the vegetative cover as a result of overexploitation and reduction of pasture productivity, the area of hazardous ecological situations in the Tyumen North will grow by 1.2 times.

References

Shpolyanskaya, N.A. & Zotova, L.I. 2010. North development: how to preserve balance in nature. *Ekologiya i zhizn* 11: 66-73.

Simonov, YU.G. 1997. Score evaluation in applied geographical studies and the ways of their improvement. *Vestnik Mosk. un-ta. Ser. 5. Geografiya*, 4: 7-10.

Tumel, N.V., Zotova, L.I., & Grebenets, VI. 2008. Cryogenic landscape stability concept: In *Geographical scientific schools of the Moscow University*. Edited by Academician N.S. Kasimov et al. Moscow: Izdatelskiy dom Gorodets, 139-144.

- Zotova, L.I. 2011. Theoretical and applied aspects of the expert geocological evaluation of the economic development hazard within the frames of a new educational program. *Materials of the Fourth Conference of Russia's Geocryologists*, M.V. Lomonosov Moscow State University, July 7-9, Vol. 3, Part 9, 2011: 224-231.
- Zotova, L.I. & Dedyusova, S.Yu. 2011. Complex evaluation of the lithocryogenic and bioresource state of northern geosystems. *Materials of the Fourth Conference of Russia's Geocryologists*, M.V. Lomonosov Moscow State University, July 7-9, Vol.1, Part 3, 2011: 305-312.
- Zotova, L.I., Koroleva, N.A., & Dedyusova, S.Yu. 2007. Evaluation and mapping of critical ecological situations at gas field areas within cryolithozone. *Vestnik Mosk. un-ta*, Ser. 5 Geografiya,3:54-59.

Author Index

- Ablyazina, D., 253
Abramenko, O.N., 1
Aksenov, V.I., 129
Aleksandrova, N.S., 7
Alekseev, S.V., 13
Alekseev, V.A., 19
Alekseeva, L.P., 13
Alekseeva, N.G., 19
Andreeva, M.V., 123
Antonov, V., 253
Argunov, R.N., 185
Arslanov, H.A., 293
Astakhov, A.S., 243
- Badu, Yu.B., 25
Bazhenov, A.I., 303
Beldiman, I.N., 371
Belova, N.G., 427
Berdnikov, N.M., 343
Berestyani, Yu.B., 215
Blyakharchuk, T.A., 343
Bosikov, N.P., 31
Brouchkov, A.V., 35, 153
Budantseva, N.A., 41, 51
Buldovich, S.N., 149
Bykovskiy, A., 253
- Chechin, V.A., 19
Cheverev, V.G., 47
Chizhov, A.B., 93
Chizhova, Ju.N., 51
Chizhova, Yu.N., 41
Christiansen, H.H., 41
Chuvilin, E.M., 57
- Dedyusova, S.Yu., 543
Derevyagin, A.Yu., 93
Dolgikh, G.M., 61, 297
Drozdov, D.S., 65, 463
Dubina, T.P., 329
Dubrovin, V.A., 211
Dyagileva, A.G., 71
Dzhumandzhi, V.A., 385
- Elantsev, E.M., 123
Epstein, H., 237
- Fedorov, A.N., 75, 185
Frost, G., 237
- Galanin, A.A., 81
Ganova, S.D., 329
Gavrilev, R.I., 87
Gavrilev, P.P., 75
Gavrilov, A.V., 93
Gavrilov, G., 253
- Germogenova, A.Yu., 97
Gevorkyan, S.G., 103
Glinska, E.V., 35
Golubev, V.N., 181
Gorbachev, P.A., 107, 445
Gorbatyuk, A., 253
Gorelik, J.B., 111
Gorshkov, E.I., 149
Gravis, A.G., 343
Greibenets, V.I., 117, 253
Greibenkin, S.I., 153
Griva, G.I., 35
Gubarkov, A.A., 123
Gusev, E.A., 293
- Hiyama, T., 75
- Idrisov, I.R.,
Iijima, Y., 75, 185
Iospa, A.V., 129
Isaev, V.S., 1
Isakov, V., 133
Istomin, V.A., 57, 263
Ivanova-Efimova, E.N., 137
Iwahana, G., 75
- Kapralova, V.N., 141, 517
Kaverin, D., 145
Khalilova, J.V., 381
Khilimonyuk, V.Z., 149, 153
Khimenkov, A.N., 381
Khitun, O.V., 237
Khmelnitskiy, G., 253
Khomutov, A.V., 123, 157, 237
Kislov, A.V., 117
Kiyashko, N.V., 169
Klinova, G.I., 129
Kolunin, A.V., 163
Kolunin, V.S., 163
Komarov, I.A., 1, 169
Kondratyev, V.G., 175
Konishchev, V.N., 181
Kononov, A.M., 13
Konstantinov, P.Ya., 75, 185
Kopeykin, V.V., 19
Kornienko, S.G., 189
Korobova, T.A., 463
Korostelev, Yu.V., 65, 463
Kosykh, N.P., 195
Kotov, P.I., 199
Kraev, G., 253
Kravtsova, V.I., 439
Kritsuk, L.N., 205
Krivulin, V.V., 19
Krupoderov, V.S., 211
Kudryavtsev, S.A., 215
- Kurchatova, A.N., 357, 415
Kuzmin, G.P., 221
Kuznetsova, E.P., 225
- Lavrov, I.G., 377
Lebedeva, L.S., 231, 371
Leibman, M.O., 237
Luchsheva, L.N., 19, 243
- Makaricheva, E.M., 381
Malkova, G.V., 65, 247
Mandzhiev, D., 253
Marakhtanov, V.P., 509
Maslakov, A., 253
Matyukhin, A.G., 259
Mazhitova, G., 145
Melnik, P., 253
Melnikov, V.P., 263
Melnikov, N.N., 267
Mesyats, S.P., 267
Michailin, R.G., 215
Miklyaeva, E.S., 271
Minkin, M.A., 275
Molokitina, N.S., 339
Moskalenko, N.G., 281
Motenko, R.G., 225
Myalo, E.G., 531
- Neradovskiy, L.G., 407
Nesterov, A.N., 263
- Oberman, N.G., 287
Oblogov, G.E., 293
Obzhirov, A.I., 243
Okunev, S.N., 61, 297
Opokina, O.L., 303, 415
Orehhov, P.T., 237
Orlov, T.V., 517
Osadchaya, G.G., 309, 459
Osokin, N.I., 315
Ospennikov, E.N., 149
Ostroumov, V.E., 317
Ovsyannikova, O.S., 329
- Panchenko, E., 323
Panin, V.N., 221
Pastukhov, A., 145
Pastukhov, V., 253
Pavlov, A.V., 247
Pelehan, L.G., 19
Pendin, V.V., 329
Perlshtein, G.Z., 381
Peterson, A.M., 35
Pisarev, A.D., 163
Pizhankova, E.I., 93
Podborny, E.E., 333

- Podenko, L.S., 339
Ponomareva, O.E., 343
Popova, A.A., 129
Potapova, O.A., 275
Poznanin, V.L., 349
- Radosteva, A., 253
Rekant, P.V., 499
Repin, V.E., 35
Reshetnikov, A.M., 263
Rivkin, F., 145
Rocheva, A.M., 353
Rogov, V.V., 181, 357, 415
Roman, L.T., 361
Romanyuk, S.N., 385
Rukavishnikov, V.A., 19
- Safronov, E.V., 47
Sannikov, G.S., 367
Saveleva, A., 253
Semenova, O.M., 231, 371
Serebrennikov, A.A., 377
Serebrennikov, D.A., 377
Sergeev, D.O., 381
Shavlov, A.V., 385
Shender, N.I., 481
Sheynkman, V.S., 389
- Shmelev, D.G., 117, 253, 395
Shpolyanskaya, N.A., 401
Shpuntova, A., 253
Skachkov, Yu.B., 407, 481
Skorbilin, N.A., 297
Skryabin, P.N., 411, 481
Slagoda, E.A., 303, 415
Smirnov, A., 253
Smulskiy, I.I., 421
Sokratov, S.A., 181
Soldatov, V.A., 271
Solomatin, V.I., 427
Sosnovskiy, A.V.,
Streletskaya, I.D., 259, 293, 433
Streletskiy, D.A., 253
Strizhkov, S.N., 61, 297
- Tarasenko, T.V., 439
Ter-Martirosyan, Z.G., 445
Titkov, S.N., 449
Tumel, N.V., 453, 459
- Ugarov, A.N.,
Ugarov, I.S., 185, 381
Ukraintseva, N.G., 65, 463
Urban, A.A., 469
Ustinova, E.V., 475
- Valtseva, T.Yu., 215
Varlamov, S.P., 411, 481
Vasil'chuk, A.C., 51, 487
Vasil'chuk, Yu.K., 41, 51, 487, 493
Vasilchuk, A.K., 41
Vasilev, A.A., 293, 433, 499
Vasiliev, I.S., 503
Velikotskiy, M.A., 509
Verkhoturov, A.G., 513
Viktorov, A.S., 141, 517
Vlasov, V.P., 523
- Walker, D.A., 237
- Yermak, A.A., 527
Yermokhina, K.A., 531
- Zabolotnik, S.I., 537
Zabolotnik, P.S., 537
Zemskova, A.M., 41
Zengina, T.Yu., 309
Zotova, L.I., 543

Subject Index

Volume 1

The following Subject Index was compiled from keywords given by the author of each paper.

- accuracy, 49
acoustic emission, 437
active layer depth, 267
active layer thickening, 113
active microwave, 33, 413
active rock glaciers, 215
active layer, 1, 221, 295, 377, 395, 431, 443
active-layer detachment slide, 101
aerophotogrammetry, 215
air duct foundation, 341
airborne laser scanning, 215, 49
AIRS, 277, 455
alas, 161
Alaska, 15, 155, 179, 191, 255, 271, 383, 473, 473
Alaska Highway (Alcan), 261, 283
alder, 119
alpine flora, 329
Anchorage, Alaska, 323
Andes of Patagonia, 365
Antarctica, 221
apparent cohesion, 55
arctic coastal dynamics, 425
arctic coastal erosion, 137, 97
Arctic Coastal Plain, 425
Arctic, 119, 255, 407
Argentina, 419
artesian water, 371
ASCAT Surface State flag, 85
atmospheric CH₄, 455
automatic monitoring, 267
- Barrow, 209
basal glacier ice, 107
bearing capacity, 301, 407
bedrock slopes, 131
bilateral agreements, 1
biogeochemistry, 101
biogeomorphology, 389
boreal forest, 161
borehole monitoring network, 173
borehole temperatures, 479
BTS, 365
- capacitively-coupled resistivity, 27
catchments, 185
Central Andes, 419
change detection, 125
change, 179
chilled gas pipeline, 197
China, 317
China-Russia Crude Oil Pipeline, 227
Circum-Arctic, 85
- climate, 73
climate change, 167, 203, 295, 401, 407, 485
climate data, 335
climate model, 209
climate warming, 323, 347
coastal erosion, 425
cold regions engineering, 311
Colville River, 255
communities, 395
compression, 461
compression test, 237
compressional wave, 45
connectivity, 221
consolidation effect, 237
constitutive relationship, 249
continuous permafrost, 185
creep, 311, 49, 67
crosshole, 45
CRREL, 73
cryostructure, 107, 73
- data analysis, 377
data archive, 377
deglaciation, 209
Delta, 255
design, 167
DGPS, 155, 425
direct shear, 143
discontinuous permafrost, 353
downhole, 45
dry density, 467
- eastern Siberia, 161
ecology, 221, 389
effective stresses, 55
embankment, 261
energy, 277
engineering, 167, 283, 73, 97
environmental engineering, 227
ERA-Interim reanalysis, 271
ESA DUE Permafrost, 85
evaluation of remote sensing products, 85
extreme environments, 329
- FID, 21
fill-and-spill, 449
flow velocity, 215
foundation, 67
foundation reconstruction, 341
foundation stability, 407
freeze-thaw cycles, 113, 467
freeze-thaw depth, 267
- freeze-thaw sensor, 267
freezing soil, 79
freezing temperature, 227
frost heave, 197, 79, 467
frost tube, 267, 395
frozen muskeg, 301
frozen sand, 143
frozen soil mechanics, 249
frozen soil, 461, 67
- gelisols, 485
geochemistry, 27
Geographic Information Systems, 155
geophysics, 15, 27
geotechnical investigations, 191, 353
GEOtop Model, 91, 271
GIS, 137
glacial hydrology, 359
glacier-permafrost interaction, 359
Global Positioning Systems, 155
global, 131
GLOBE, 395
GPR, 305
GRACE, 277
Greenland, 401
ground ice, 179, 283, 305, 353, 365, 473
ground movement, 113
ground temperature cables, 353
ground temperature, 243
GTN-P, 85
gullies, 125
- hazard zonation, 131
heat extraction index, 261
heat pump cooling, 341
Herschel Island, 389
high Arctic, 125
history, 1
hummock, 431
hydrology, 185, 231, 449
hysteresis, 21
- ice cohesion, 55
ice core, 371, 473
ice wedges, 125, 191, 383
ice-cemented sediment, 305
ice-wedge casts, 149
ice-wedge polygon, 431, 231
image correlation, 215
interferometric synthetic aperture radar (InSAR), 113
inventory of rock glaciers, 419

- Kotzebue, Alaska, 347
- lakes, 61, 255
- land-ocean interactions, 137
- Laptev Sea, 137
- lithals, 371
- loess, 39
- long-term monitoring, 125
- lower limit of permafrost, 243
- mapping, 125, 131
- massive ground ice, 107, 27
- massive ice, 305, 39
- MAST, 317
- Matanuska Glacier, 107
- McMurdo Dry Valleys, 305
- mean annual ground temperature, 203
- measurement assembly, 437
- methane emission, 455
- microgelivation, 437
- mining, 73
- MODIS, 85, 277, 317
- Mongolia, 173, 371, 473
- monitoring, 49
- mountain permafrost, 243, 437, 479, 55
- mountains, 131
- mudboil, 431
- new technology, 97
- N-factor, 295
- 90° pulse, 21
- non-sorted circles, 79
- Northeastern Qinghai-Tibet Plateau, 243
- Northern Alaska, 79
- Northern Yakutia, 203
- numerical modeling, 271, 359
- numerical models, 335
- oil contamination and migration, 227
- palaeoclimate, 149
- patterned ground, 119, 431
- perennial frost mound, 371
- periglacial lake, 419
- permafrost 461
- permafrost degradation, 101, 401
- permafrost evolution, 209
- permafrost mitigation technique, 261
- permafrost model, 401
- permafrost modeling, 91
- permafrost temperatures, 353
- permafrost thickness, 243
- permafrost warming, 113, 173
- permafrost, 1, 15, 27, 39, 49, 61, 107, 119, 125, 167, 179, 203, 209, 227, 277, 283, 289, 317, 323, 329, 335, 347, 359, 371, 377, 389, 395, 407, 419, 425,
- permafrost-affected soils, 485
- permanent scatterer (PS), 113
- piles, 341
- pingo, 371, 473
- P-NMR, 21
- polar regions, 377
- pore water pressure, 237
- Qinghai-Tibet Railway, 289
- Qinghai-Tibetan Plateau, 443
- rainfall, 443
- regional climate model, 401
- remote sensing, 137, 255, 317, 33, 413
- retrogressive thaw-slump, 101
- rising temperature, 55
- risk assessment, 401
- roadbed structure, 289
- roads, 283
- rock fracturing 437
- rock glacier, 479, 49, 329
- rock joints, 143
- rock slopes, 143
- Russia, 1, 413
- sampling design, 377
- sand wedges, 149
- sand-wedge infillings, 149
- satellite observation, 455
- seismic velocity, 45
- settlement source, 311
- shallow foundation, 341
- shear strength, 143, 55
- shear wave, 45
- shrub expansion, 119
- Siberia, 119, 485
- simulation, 197
- slope processes, 61
- snow depth, 155
- snow fence, 155
- soil, 467
- soil moisture content, 443
- soil moisture, 161, 33
- soil nutrients, 61
- soil organic carbon stock, 485
- soil temperature, 443
- Source area of the Yellow River, 243
- Southeast Asia, 149
- Soviet Union, 1
- spatial variability, 91
- Spitsbergen, 359
- stable isotope, 473, 305
- statistical modeled permafrost distribution, 365
- steep terrain, 131
- storage, 185
- streamflow, 449
- streams, 61
- strength and deformation, 249
- strength, 461, 67
- stress path tests, 461
- subsurface flow, 449
- surface flow, 449
- surface frost number, 317
- surface wave, 45
- survey, 15
- Svalbard, 431
- Swiss Alps, 479
- syngenetic permafrost, 191
- syngenetic, 39
- Takashi's equation, 197
- talik, 15
- talik formation, 479
- temperature difference, 295
- terrestrial laser scanner, 79
- tessellons, 149
- thaw consolidation, 311
- thaw depth, 91
- thaw settlement, 191, 383, 467
- thaw slump, 389
- thawing period, 295
- thawing permafrost, 455
- thermal conductivity, 227
- thermal orbits, 479
- thermal regime, 261
- thermal stability, 289
- thermal-erosion, 101, 125, 137, 61
- thermal-moisture process, 249
- thermokarst, 101, 161, 61
- thermokarst lake, 179, 383, 413
- time series, 33
- transpiration, 161
- tundra, 33
- tundra vegetation, 295
- tunnel, 39, 73
- unfrozen water content, 21
- urban planning, 323
- USSR, 1
- variable source area, 449
- vegetation, 389, 61
- vegetation cover, 329
- velocity, 49
- warm and ice-rich frozen soil, 237
- warming trend, 353
- water balance, 185, 231
- water content, 467
- water supply dam, 347
- water tracks, 221
- watershed, 231
- Western Canadian Arctic, 27
- wheel loads, 301
- winter roads, 407
- World War II, 283
- Wyoming, 209
- Yamal Peninsula, 413
- yedoma, 191, 383, 39
- Yukon, 15

Subject Index

Volume 2

- acidity, 509
active layer, 65, 145, 195, 231, 303, 411, 463, 481, 503
aerial imagery, 93
agglomeration, 339
air and ground temperature trends, 247
alms, 31
alkanes, 271
allochthonous, 493
allophane, 221
alluvium, 449
annual mean air temperature, 407
autochthonous, 493
- bacteria, 35
BAM, 175
bases, 275
bearing capacity, 117
biochemical reactions, 35
bioclimatic subzone, 237
biological productivity, 195
biospheric balance, 309
bogs, 459
Bovanenkovo field, 333
buried glacial ice, 427
- cartography, 463
cartometry, 367
Central Russia, 253
Central Yakutia, 75
change forecast, 7
chemical elements, 317
climate change, 281, 343, 65, 75
climate prediction, 453
climate variation, 93
climate warming, 247, 439
climate, 117, 287, 475, 481
cloud, 385
coastal thermal abrasion features, 527
composite cast-in-drilled piles, 523
compression coefficient, 199
concentration zones, 317
construction, 323
cooling device, 221
craters, 19
creep, 361
critical ecological situations, 543
cryogenic cracking, 329
cryogenic head, 469
cryogenic heaving, 253
cryogenic landslides, 531
cryogenic processes, 267, 475
cryogenic resource, 175
- cryogenic soils, 71
cryogenic stratum, 25
cryogenic structure, 271, 47
cryoglacial systems, 389
cryohydrotectonics, 205
cryolithozone, 117, 133, 149, 153, 211, 271, 287, 297, 309, 323, 353, 389, 453, 543
cryopegs, 169, 111
cryoturbations, 13
culverts, 123
- dam bases, 87
damaged land, 267
deformation structures, 13
deformations, 133, 111
deformed sediments, 303
density, 169
destruction, 103
deterministic-stochastic modeling, 371
development, 267
differential aeration, 509
discontinuous permafrost, 523
discordant contact, 427
dispersion, 339
droplet, 385
dry permafrost, 71
- eccentricity, 421
ecology, 271
ecosystem, 281
electrochemical model, 509
embankment deformation, 175
embankments, 123, 323
engineering element, 129
engineering-geocryological conditions, 329
environmental hazard, 93
environmental management limitations, 353
environmental problems, 153
equations, 421
equilibrium water content, 57
erosional-thermokarst plains, 517
erosion-control, 123
European North, 51
exogenic geological processes, 123
exogenic processes, 323, 349, 367
expert evaluations, 543
- faults, 205
fire disturbance, 281
forecast, 117, 361, 407
forest fire, 411
- forest-tundra, 195
foundation stability loss, 107, 445
foundations, 117, 275, 61
Fourier models, 407
freeze-thaw cycles, 13
freeze-thaw, 215
freezing ground, 317
freezing rate, 107
freezing temperature, 169
freezing, 111, 163, 47
frost heave, 117, 13, 445, 469
frost mounds, 343, 527
frozen ashes, 221
frozen ground, 129, 163, 259, 361
frozen soil, 103
- gas hydrates, 243, 263, 333, 57
gas pipelines, 329
gas plumes, 243
gas seeps, 499
gas-bearing structure, 25
gas-condensate field, 267
geochemical anomaly, 19
geocryological conditions, 7
geocryological hazard, 381
geocryological monitoring, 153
geocryological zonation, 459
geocryology, 513
geoecological test site, 211
geoecology, 543
geological element, 129
geological problems, 153
geological processes, 349
geosynthetics, 215
GIS mapping, 247, 543
glacial deformations, 427
glacial topography, 137
glaciers, 137, 389
ground freezing, 445, 61
ground ice content, 189
ground ice, 75, 205
ground properties, 129
ground temperature, 185, 449, 453
ground variety, 129
ground-penetrating radar, 19
grounds, 47
Gydan Bay, 293
- heat and mass transfer, 163
heat capacity, 169
heat conductivity, 221
heat flow, 199
HEAT, 199
highway, 381
HNP and VNP systems, 61

- Holocene, 415, 51
 human impact, 411
 human-induced disturbances, 281
 hydrocarbon deposits, 309
 hydrocarbon pollution, 271
 hydrochemistry, 205
 "Hydrograph" deterministic model, 371
 "Hydrograph" model, 231
 hydrolaccolith, 469
 hydrophobic particles, 339

 ice caps, 487
 ice complex, 93, 433
 ice energy, 349
 ice volume, 149
 ice wedges, 433
 ice, 163, 181, 339, 357, 57
 ice-rich permafrost, 71
 impact zone, 381
 inclination, 421
 indicators, 205
 industrial development, 459
 injection ice, 111
 insolation, 421
 interannual dynamics, 503
 intrusive ice, 415
 intrusive massive ice, 303
 involutions, 13
 irregular topography, 215
 isotope composition, 415
 isotopes, 181, 205
 isotopic composition, 433

 Kara Sea, 499
 Kolyma Upland, 81
 Kolyma Water Balance Station, 231, 371

 lake basin, 459
 lake thermokarst, 31
 lakes area, 439
 landscape, 253, 281, 353, 475, 75, 323
 landscape indicator approach, 463
 landscape map, 157
 landscape mathematical morphology, 141
 landscape stability, 543
 landslide geohazard map, 157
 landslides, 81
 Late Cenozoic, 395
 Late Pleistocene, 415
 Lena-Amga interfluve, 31
 lithology, 237, 253
 load-bearing capacity, 523
 long-term seed storage, 221

 mapping, 475
 Mars, 1
 massive ground ice, 401
 massive ice, 415, 487
 mathematical landscape morphology, 517
 mathematical models, 517
 mathematical simulation, 47
 mean annual ground temperatures, 537
 mercury, 19, 243
 metastable states, 263
 methane, 243, 333
 microelements, 71
 microorganisms, 357
 microscopy, 357
 migration, 181
 mobile forms, 317
 moistening, 31
 monitoring, 133, 211, 237, 381, 475, 481
 morphological analysis, 367
 mortmass, 195
 moss cover, 313

 natural landscape complexes, 503
 natural resource management, 309
 natural resources, 459
 natural structure, 103
 natural terrain units, 157
 natural-technical geosystems, 275
 natural-territorial complexes, 275
 negative friction, 523
 negative temperatures, 377
 Neoglacial epoch, 81
 nonclathrated water, 57
 Norilsk, 133
 Northeast European Russia, 145, 287
 northern forest tundra, 353
 numerical methods, 421

 opal, 221
 optimal temperature, 221
 orbital motion, 421

 paleoseismic-dislocations, 81
 palsa, 51
 peatlands, 459
 perennial heaving, 343
 perihelion, 421
 permafrost, 19, 35, 61, 149, 153, 175, 189, 211, 215, 221, 231, 281, 313, 333, 357, 371, 463, 475, 481, 537
 permafrost conditions, 1
 permafrost ecosystems, 195
 permafrost formation, 25, 293
 permafrost landscapes, 509
 permafrost monitoring, 247, 463
 permafrost observations, 503
 permafrost soils, 97
 permafrost table position, 499
 permafrost temperature, 287, 65
 permafrost thickness, 25
 permafrost zonation, 149
 permafrost-affected soils, 145
 permafrost-glacier interactions, 389
 permafrost-related landslides, 463
 phase composition, 169
 phase equilibrium, 263
 phytoindicators, 531
 phytomass, 195
 pile, 107, 445
 pipeline corrosion, 509
 pipeline, 381
 Pleistocene/Holocene, 433
 polar deposits, 1
 pollen spectra, 487
 polyethylene pipeline, 377
 pore solution, 317
 porous medium, 163
 precipitation variations, 439
 Primorskiy Lowlands, 395
 probability distribution, 141
 project models, 275
 protective measures, 329
 pulling force, 445
 Putorana Plateau, 137

 Quaternary deposits, 259, 293
 Quaternary history, 401

 radiation heat budget, 1
 radiation temperature, 189
 radiocarbon age, 51
 radiocarbon dating, 41
 railroad bridge, 449
 railroad, 381
 railway, 7, 175
 redox potential, 509
 regulations, 211
 reliability value, 275
 relict microorganisms, 35
 remote sensing, 141, 189, 527
 repetitive wedge ice, 469
 residual thaw layer, 453
 retrogressive thaw flow, 157
 rheology, 107
 risk assessment, 517
 risk estimates, 141
 roadbed, 123
 roads, 133, 323
 rock glaciers, 81
 rocks, 87
 runoff characteristics, 371
 runoff formation, 231
 Russian Arctic, 401
 Russian European North, 453

 Sakhalin shelf, 243
 saline permafrost, 259
 satellite imagery, 527
 satellite images, 439
 seasonal freezing, 253, 271
 seasonal thaw depth, 185, 503

- seasonal thaw, 65, 237, 253
seasonally thawed layer, 185
sediment, 57
segregated ice formation, 317
segregation ice, 111
shear viscosity, 385
short cylindrical probe, 87
Siberia, 389
snow cover, 253
sod grass cover formation, 267
soil freezing, 107
soil moisture content, 185
soil temperature, 411
soil thawing, 199
soil, 181
solifluction, 329
southern tundra, 65
specialist, 513
stability of engineering structures, 523
stability, 353
stabilizing measures, 175
stable oxygen isotopes, 41
standard, 513
Stochastic Weather Model, 371
stratigraphy, 51
strength, 361
stress intensity coefficient (SIC), 103
stress, 111, 361
stress-strain state, 215
subaquatic freezing, 25
submarine permafrost, 499
subsea permafrost zone, 401
subsurface, 211
surface temperature, 189
surface uplift, 343
Svalbard, 41
tabular massive ice, 111, 401, 427, 493
talik, 31, 449, 303, 537
tangential forces, 445
tangential frost heave stress, 107
taxonomic diversity, 35
technical concepts, 275
temperature stabilization systems, 297
temperature, 313, 361, 481
thawed soils, 523
thawing coefficient, 199
thawing, 313
thermal conductivity, 221, 313
thermal erosion features, 527
thermal erosion, 123, 267, 329, 93
thermal inertia, 189
thermal insulation, 313
thermal stabilization, 61
thermal state monitoring, 411
thermal subsidence, 343
thermal-contraction cracks, 103
thermokarst, 133, 19, 343, 527, 75
thermokarst dynamics, 141
thermokarst hazard, 93
thermokarst lakes, 367, 439
thermokarst plains, 517
thermometric monitoring, 297
thermophysical properties, 87
thixotropic, 71
total heave force, 107
transition layer, 145
trenchless technologies, 377
trends, 481
Tunguska meteorite, 19
Tunka depression, 13
underground storage, 221
unfrozen water, 57
upper permafrost, 145
urban pedogenesis, 97
urban soils, 97
urbanization, 97
vegetation dynamics, 531
vegetation, 281
vegetative cover, 237
viscosity, 103, 107
warming, 287
water balance, 75
water extract, 395
water soluble salts, 259, 395
water, 163, 181, 385
wedge ice, 303, 401, 415
Western Siberia, 7
Yakutia, 395, 407
Yamal, 41, 449, 531
Yamal Peninsula, 169